Preparation for Implementation of the Mechanistic-Empirical Pavement Design Guide in Michigan Part 3: Local Calibration and Validation of the Pavement-ME Performance Models

Final Report

Michigan Department of Transportation
Research Administration
8885 Ricks Road
Lansing, MI 48909

By

Syed Waqar Haider, Neeraj Buch, Wouter Brink,
Karim Chatti and Gilbert Baladi

Report Number: RC-1595

Michigan State University
Department of Civil and Environmental Engineering
3546 Engineering Building
East Lansing, MI 48824

November 2014

Technical Report Documentation Page

1. Report No. RC-1595	**2. Government Accession No.**	**3. MDOT Project Manager** Mike Eacker
4. Title and Subtitle Preparation for Implementation of the Mechanistic-Empirical Pavement Design Guide in Michigan Part 3: Local Calibration and Validation of Performance Models		**5. Report Date** **6. Performing Organization Code**
7. Author(s) Syed Waqar Haider, Neeraj Buch, Wouter Brink, Karim Chatti and Gilbert Baladi		**8. Performing Org. Report No.**
9. Performing Organization Name and Address Michigan State University Department of Civil and Environmental Engineering 428 S. Shaw Lane, 3546 Engineering Building East Lansing, MI 48824 Tel: (517) 355-5107, Fax: (517) 432-1827		**10. Work Unit No. (TRAIS)** **11. Contract No.** 2010 0294 **11(a). Authorization No. Z5**
12. Sponsoring Agency Name and Address Michigan Department of Transportation Research Administration 8885 Ricks Road Lansing MI 48909		**13. Type of Report & Period Covered** October 1, 2011 – October 31, 2014 **14. Sponsoring Agency Code**
15. Supplementary Notes		

16. Abstract

The main objective of Part 3 was to locally calibrate and validate the mechanistic-empirical pavement design guide (Pavement-ME) performance models to Michigan conditions. The local calibration of the performance models in the Pavement-ME is a challenging task, especially due to data limitations. A total of 108 and 20 reconstruct flexible and rigid pavement candidate projects, respectively, were selected. Similarly, a total of 33 and 8 rehabilitated pavement projects for flexible and rigid pavements, respectively were selected for the local calibration. The selection process considered pavement type, age, geographical location, and number of condition data collection cycles. The selected set of pavement section met the following data requirements (a) adequate number of sections for each performance model, (b) a wide range of inputs related to traffic, climate, design and material characterization, (c) a reasonable extent and occurrence of observed condition data over time. The national calibrated performance models were evaluated by using the data for the selected pavement sections. The results showed that the global models in the Pavement-ME don't adequately predict pavement performance for Michigan conditions. Therefore, local calibration of the models is essential. The local calibrations for all performance prediction models for flexible and rigid pavements were performed for multiple datasets (reconstruct, rehabilitation and a combination of both) and using robust statistical techniques (e.g. repeated split sampling and bootstrapping). The results of local calibration and validation of various models show that the locally calibrated model significantly improve the performance predictions for Michigan conditions. The local calibration coefficients for all performance models are documented in the report. The report also includes the recommendations on the most appropriate calibration coefficients for each of the performance models in Michigan along with the future guidelines and data needs.

17. Key Words Pavement-ME, local calibration, resampling techniques, pavement analysis and design		**18. Distribution Statement** No restrictions. This document is available to the public through the Michigan Department of Transportation.	
19. Security Classification - report Unclassified	**20. Security Classification - page** Unclassified	**21. No. of Pages**	**22. Price**

TABLE OF CONTENTS

List of Tables

List of Figures

EXECUTIVE SUMMARY

The main objectives of Part 3 were to (a) select candidate pavement projects for local calibration of performance models in Michigan, (b) evaluate the adequacy of the current global or national calibrated models for Michigan conditions, (c) calibrate the pavement performance prediction models for flexible and rigid pavements to Michigan conditions, (d) provide a catalog of calibration coefficients for each performance model for rigid and flexible pavements, (e) compare the local and global calibrated models and recommend the most representative models for Michigan conditions, and (f) recommend future local calibration guidelines and data needs.

The local calibration of the performance models in the mechanistic-empirical pavement design guide (Pavement-ME) is a challenging task, especially due to data limitations. A total of 108 (129 sections) and 20 (29 sections) reconstruct flexible and rigid pavement candidate projects, respectively, were selected. Similarly, a total of 33 (40 sections) and 8 (16 sections) rehabilitated pavement projects for flexible and rigid pavements, respectively were selected for the local calibration. The selection process considered pavement type, age, geographical location, and number of condition data collection cycles. The selected set of pavement sections met the following data requirements (a) adequate number of sections for each performance model, (b) a wide range of inputs related to traffic, climate, design and material characterization, (c) a reasonable extent and occurrence of observed condition data over time. The nationally calibrated performance models were evaluated by using the data for the selected pavement sections. The results showed that the global models in the Pavement-ME do not adequately predict pavement performance for Michigan conditions. Therefore, local calibration of the models is essential. The local calibrations for all performance prediction models for flexible and rigid pavements were performed for multiple datasets (reconstruct, rehabilitation and a combination of both) and using robust statistical techniques (e.g. repeated split sampling and bootstrapping).

The results of local calibration and validation of various models show that the calibrated models significantly improve the performance predictions for Michigan conditions. The local calibration coefficients for all performance models are documented in the report. The report also includes the recommendations on the most appropriate calibration coefficients Michigan should use for each of the performance models along with the future local calibration guidelines and data needs.

CHAPTER 1 - INTRODUCTION

1.1 PROBLEM STATEMENT

There are apprehensions on the part of State Highway Agencies (SHAs) towards the adoption of the Pavement-ME because of the (i) complex nature of the design software (numerous inputs and their hierarchical nature); (ii) perceived needs to collect more laboratory and/or field data; (iii) necessity to retool the PMS for making it compatible with the outputs of the design guide and the required inputs for the guide; (iv) need for the calibration of the performance equations to local conditions; (v) the need to employ or train pavement professionals at the regional level; and (vi) shrinking manpower and funds. The successful completion of this project will go a long way in reducing some of the uncertainties associated with the implementation of the Pavement-ME. Guidance with respect to practical ranges of significant inputs for flexible and rigid pavement designs, calibration coefficients for the transfer functions reflecting local conditions and hot mix asphalt (HMA) mixture characteristics |E*| will demonstrate to Michigan Department of Transportation (MDOT) pavement engineers the viability of implementing the Pavement-ME in the near future. An extensive test (for rehabilitation designs) of the software will add evidence on the viability and accuracy of the software. Identifying the list of input variables for rehabilitation designs that significantly impact pavement performance would assist MDOT in determining the types of new data elements needed. The technology transfer packages to be developed in this timely and significant project will serve as invaluable training tools that will enhance the capability of MDOT to analyze and design pavements by using the new M-E tools.

This research study had three distinct parts: (1) characterization of asphalt mixtures for the Pavement-ME in Michigan, (2) evaluation of the Pavement-ME for pavement rehabilitation design in Michigan, and (3) calibration and validation of the Pavement-ME performance models for Michigan conditions. Therefore, the study was divided into three separate parts. The HMA mixtures in Michigan were characterized in Part 1 and the final report was accepted by MDOT in March 2013. The evaluation of the Pavement-ME for rehabilitation design in Michigan was conducted in Part 2 and the final report was accepted by MDOT in August 2013. In Part 3, the calibration and validation of performance models was performed, and this report contains the details for this part of the study.

1.2 BACKGROUND AND SIGNIFICANCE OF WORK

The Pavement-ME is becoming the state-of-the-practice for flexible and rigid pavement designs in some states. The Pavement-ME's performance prediction models for rigid and flexible pavements were calibrated using nationwide pavement performance data. It is necessary to re-calibrate the performance models using a range of input variables typical to Michigan to minimize prediction errors (i.e., random errors and systematic bias). This study compares the predicted and observed/measured pavement performance data for the selected pavement sections in Michigan. The input and performance data were obtained from various sources within MDOT. The Pavement-ME components were examined to provide recommendations on resources required for implementing the Pavement-ME in Michigan. Detailed resource needs in terms of lab and field equipment, personnel and the needed

resources for implementation, and future recalibration of the performance models are detailed in the report.

It is important to mention that MDOT has already laid the foundation for the adoption of the Pavement-ME by supporting several studies in the last seven years. The key deliverables of these studies included: (a) critical/sensitive inputs for the design of new flexible and jointed plain concrete pavements, (b) Level 2 and 3 traffic inputs for the design of new and rehabilitated flexible and rigid pavements, (c) Catalog of level 2 inputs for coefficient of thermal expansion (CTE) of typical paving concrete mixtures, and (d) Ranges for levels 2 and 3 resilient moduli for subgrade and unbound materials. It should be noted that results from all these previous studies were utilized in Parts 2 and 3 of this study wherever applicable.

1.3 RESEARCH OBJECTIVES

The objectives of the research in Part 3 were to: (a) select candidate pavement projects for local calibration of performance models in Michigan, (b) calibrate the pavement performance prediction models for flexible and rigid pavements to Michigan conditions, (c) provide a catalog of calibration coefficients for each performance model for rigid and flexible pavements, (d) compare the local and global calibrated models and recommend the most representative models for Michigan conditions , (e) recommend future local calibration guidelines and data needs.

1.4 BENEFITS TO MDOT

The outcome of the research conducted in Part 3 of the study will have several short-term and long-term benefits by implementing the Pavement-ME in Michigan. The short-term benefits include:

- Availability of local performance models calibrated to Michigan conditions
- Justification for implementing the mechanistic-empirical pavement design methodologies in Michigan
- Improved pavement designs and performance for future pavement by using the mechanistic-empirical pavement design method.
- Availability of a set of guidelines outlining the local calibration processes for future calibration efforts

The long-term benefits will potentially include:

- An improved Pavement Management System (PMS) database which facilitates the implementation of the Pavement-ME and a feedback mechanism to evaluate the new designs in the future.
- Integration of PMS and as-constructed project information (materials, layer properties and thicknesses, costs) which can be used to support the continual use of the Pavement-ME as the pavement design procedure in Michigan.

1.5 RESEARCH PLAN

The study's objectives were accomplished by performing nine (9) subtasks. A brief description of these tasks is presented below:

1.5.1 Task 3-1: Literature Search

Several state DOTs are in the process of locally calibrating the Pavement-ME distress models as a part of their implementation efforts. For example, the states of Mississippi, Arkansas, Texas, Iowa, Washington, Arizona, North Carolina, and Oklahoma have conducted such local calibration studies. In this task, the research team reviewed all the local calibration and implementation efforts conducted by various states. The results from the review of existing efforts are summarized in this report.

1.5.2 Task 3-2: Review of MDOT's Pavement Management System

The objective of this task was to evaluate the readiness of MDOT PMS to provide the necessary data for local calibration and validation of the Pavement-ME distress models. The PMS and other data sources were evaluated to extract the following input data:

a. All performance measures predicted by the Pavement-ME for both flexible and rigid pavements were reviewed for consistency of units. The units of the measured distress data from MDOT PMS were converted to those predicted by the Pavement-ME;
b. The construction records and other sources were used to assess the pavement cross-sections. MDOT provided the information for the identified sections;
c. Traffic data as required by the Pavement-ME were obtained from MDOT (if needed). However, in the case if Level 1 data are unavailable, Levels 2 and 3 data were estimated based on completed studies conducted by the research team for the Michigan DOT; and
d. Material types used in different pavement layers were documented for the most common construction practice in Michigan. In addition, the research team investigated a sample of pavement sections, which had reached a distress index of 50 to determine relative thresholds for the distresses predicted by the Pavement-ME models. Furthermore, based on the observed pavement performance in Michigan, typical distress types (as predicted by the Pavement-ME) were identified. At the conclusion of this task, the research team highlighted any deficiencies in the PMS data collection and recommended remedies to address them.

1.5.3 Task 3-3: Project Selection

In this task, a statistically sound experimental plan for sampling the pavement sections was developed to calibrate the Pavement-ME distress and IRI prediction models based on local conditions in the State of Michigan. The local calibration NCHRP guide recommends that a local calibration factorial for each distress model should be designed to accomplish three objectives:

1. Determine local bias in the Pavement-ME global distress models;
2. Establish the cause of any bias through the local validation process; and
3. Determine the local calibration coefficients for each distress and IRI prediction model.

A two-tiered approach is recommended for the formulation of sampling template based on the agency's standard practice and specifications for common new construction and rehabilitation strategies. The primary tier factors included in the design matrix should be distress dependent, and should include design factors (i.e., pavement type, surface layer type and thickness, and subgrade soil type). The secondary tier factors should include climate, traffic, and other design features that are pavement type dependent. These are considered secondary parameters because layer thicknesses are related to traffic level and asphalt binder grade is related to climate. Furthermore, geographical regions should be considered as primary tier factor if large variations in climate are anticipated, as is the case in Michigan. The final design matrix formulated in this task was based on (a) observed performance of pavements within all seven regions in Michigan, and (b) consultation with the MDOT Research Advisory Panel (RAP).

Adequate sample size (number of pavement sections) is needed to confirm appropriateness of the global and local calibration coefficients for a specific distress prediction model from a statistical analysis standpoint. Both bias and precision are important for prediction model evaluations. The Pavement-ME assumes that all distress transfer functions are uncoupled (i.e., distress occurrence and magnitude are independent of the other distresses, with the exception of IRI empirical model). This assumption calls for a different design matrix for local calibration of each distress type. For a particular distress, the pavement sections were selected based on the magnitude (extent and severity) of the distress in the design template. Note that pavement sections selected for a distress type can be used as replicates in the design matrix for another distress type. The Pavement-ME local calibration design guidelines recommend a minimum sample size for different distress models:

Table 1-1 Minimum sample size guidelines for local calibration of distress models (38)

Distress type	Number of pavement sections
Distortion – rutting and faulting	20
Load related cracking	30
Non-load related cracking	26
Reflective cracking (HMA surfaces only)	26

The following general guidelines were considered in this research while reviewing the MDOT PMS practices for the selection of candidate pavement sections for calibration of the distress models:

- Pavement sections will be selected with the fewest number of structural layers and materials (e.g., one PCC layer, or, one/two or three HMA layers, one unbound base, and one subbase layer) to reduce the amount of input requirements for material characterization. However, care will be taken to include the types of new construction and rehabilitation strategies typically used or specified by MDOT.

- Pavement sections with and without overlays will be selected for the validation-calibration sampling template. The selection of such pavements with sufficient time-history distress data can serve the dual role as both new construction and rehabilitated pavements.
- Roadway segments that include non-conventional mixtures or layers (e.g., recycled asphalt and PCC) will be included in the experiment plan to ensure representation of such materials in the local calibration process.
- The roadway segments should have at least three condition surveys available to estimate the progression of distresses over time. The measured distress data for all pavement sections will be evaluated and checked for anomalies and outliers.
- Pavement segments should be selected based on the comparison between maximum measured distress values and the trigger values or design criteria used by MDOT for each distress type. The Pavement-ME local calibration guidelines recommend that the average maximum distress values from the sampled pavement sections should exceed 50% of the design criteria, as a minimum. This consideration becomes important when evaluating the bias and standard error terms of the prediction models in the local calibration process.

1.5.4 Task 3-4: Run designs of Pavements from the Test matrix

Once the appropriate number of pavement sections was identified in Task 3-3, all the data were extracted for determining the required inputs for the hierarchical input levels selected (refer to Task 3-2). The research team emphasized more in selecting important inputs (which significantly influence the performance predictions) for both flexible and rigid pavements as determined in the previous studies. The significant inputs for rehabilitated flexible and rigid pavements were identified in Part 2 of this study and subsequently were considered in this part. The as-built information and observed condition for the selected pavement sections in Task 3-3 were provided by MDOT. In this subtask, the Pavement-ME, with global calibrated performance models, was used to determine the performance indicators for each pavement section in the design matrix (new pavement and rehabilitated strategies). The inputs and results from the Pavement-ME outputs were stored in a separate database (Excel or Access) for all the selected pavement sections. In addition, the observed performance of the pavement sections was matched and stored in the same database for further analyses. Where inputs could not be obtained from the as-built information, reasonable assumptions were made.

1.5.5 Task 3-5: Comparison of Predicted and Measured Pavement Performance

The work executed in Task 3-4 was used as verification of the globally calibrated performance models and to further evaluate the needs for local calibration. The primary objective of model calibration is to reduce systematic bias in performance predictions. A biased model will consistently produce either over- or under-designed pavements. In addition, a secondary objective of calibration is to increase precision (or reduce standard error) of the model predictions. A less precise model is also undesirable because it leads to inconsistency in design effectiveness. The predicted distress values were compared to the measured values to determine bias and the standard error of the estimate to validate each distress prediction model for local conditions, policies, specifications and materials in the

State of Michigan. The following steps were executed to compare predicted and measured distresses:

a. Determine the bias and standard error of the estimate for the full set of data for each distress model.
b. Compare the predictions for each performance indicator to measurements and compute the residual (bias) and standard errors of the estimate for each distress prediction model. A plot of the predicted values and measured data were prepared to compare the general location of the data points to the line of equality. Figure 1-1 shows a schematic of such plots for various scenarios.
c. Evaluate the null hypothesis for the experimental factorial (developed in Task 3-3). The null hypothesis for this initial assessment is that there is no bias or no systematic difference between the measured and predicted distress values as shown by Equation(1).

$$H_o : \sum \left(y_{measured} - y_{predicted} \right) = 0 \quad (1)$$

A paired *t*-test was used for this comparison. It is possible that the above hypothesis is accepted; however, the global model still could be biased.
d. Two other model parameters (intercept and slope) will be used to fully evaluate model bias using the following fitted regression model between the measured (*y*) and predicted (*x*) values.

$$\hat{y}_i = b_o + m x_i \quad (2)$$

where; $\hat{y}_i$ = estimate of average measured value, b_o = intercept, and m =slope

The intercept and slope in Equation (2) was used to execute the following hypothesis tests:

$$H_o : b_o = 0 \text{ and } H_o : m = 1 \quad (3)$$

e. If any of the null hypotheses are rejected, the specific distress prediction model was recalibrated to the local conditions and materials.
f. If the null hypotheses are accepted (i.e., no significant bias), the standard error of the estimate for the local data set was compared to the global calibration data set to minimize the standard error of the predicted models.

In model calibration, a fitting process produces empirical model constants that are evaluated based on goodness-of-fit criteria to estimate the best set of values for the coefficients. Two methods of evaluation are generally used: (a) an analytical process for linear models, and (b) a numerical optimization technique for non-linear models. In both methods, the model constants are determined to minimize the error between measured and predicted distress values. Two types of models are used in the Pavement-ME for performance prediction: (a) structural response models, and (b) transfer functions. The former models are based on analytical solutions based on engineering mechanics (e.g., linear elastic solution to determine stress, strain and deformation for flexible pavements) while the latter models are empirical in nature and relate the pavement response or damage to distresses over time. The local calibration process deals with the transfer function for predicting distresses. Among empirical transfer functions, two different calibration approaches were required depending upon the nature of the distress being predicted: (a) model that directly calculates the

magnitude of surface distress, and (b) model that calculates the incremental damage index rather than actual distress magnitude. In the first approach, the pavement response parameter is used to compute the incremental distress in a direct relationship.

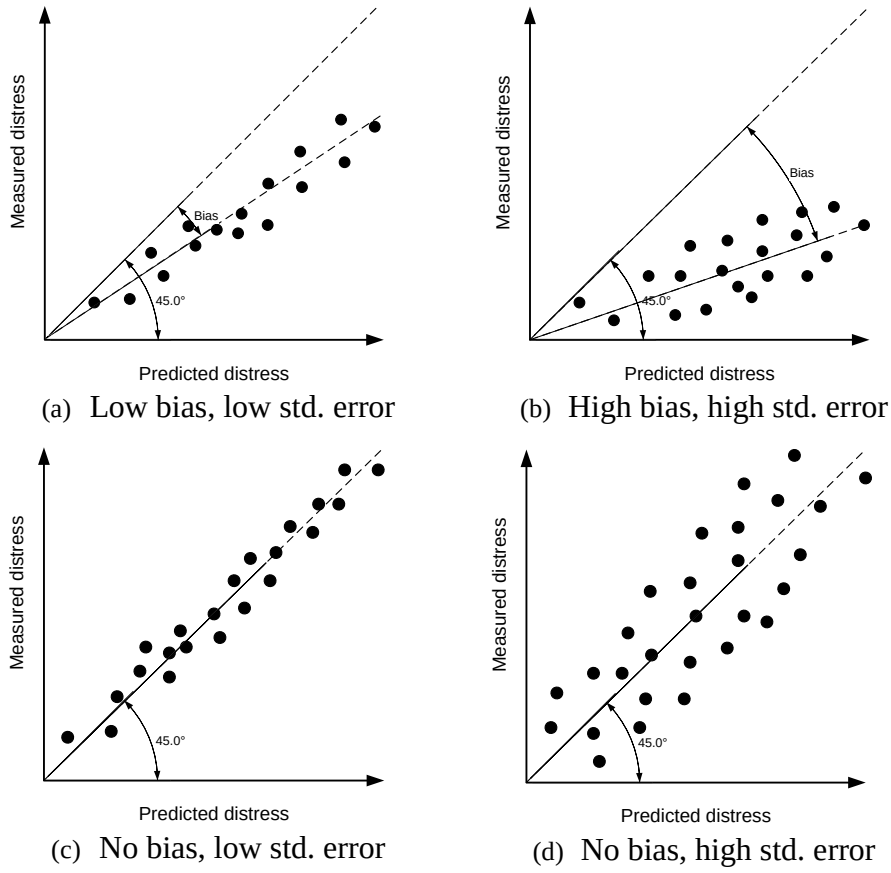

Figure 1-1 Schematic of bias and standard error (precision) for model calibration

The flexible pavement rutting model is an example within this category. The fitting of the predicted to observed distress is accomplished by minimizing the sum of squared error (ε_i) by modifying the values of the empirical calibration coefficients in the model. In the second approach, the incremental damage index is computed using a mathematical process describing the development of the distress in terms of accumulated damage. The pavement response is used to compute damage, which is then correlated to the observed distress progression. For example, Equations (4) and (5) are used to determine damage for bottom-up fatigue cracking for flexible pavements.

$$N_f = 0.0042C\beta_{f_1}k_{f_1}\left(\frac{1}{\varepsilon_t}\right)^{k_{f2}\beta_{f_2}}\left(\frac{1}{E}\right)^{k_{f3}\beta_{f3}} \quad (4)$$

where; β_{f_1} , β_{f_2} , β_{f_3} = local calibration coefficients, k_{f_1} , k_{f_2} , k_{f_3} = national calibration coefficients = 0.007566, 3.9492, 1.281, respectively. ε_t = tensile strain, and E = HMA dynamic modulus.

$$D = \sum\left(\frac{n}{N_f}\right)_{j,m,l,p,T} \quad (5)$$

Equation (6) shows the transfer function for relating pavement damage to percent fatigue cracking for flexible pavements. The model coefficients in Equations (4) and (6) were varied by using a non-linear numerical optimization to minimize the error between predicted and measured fatigue cracking. A similar approach will be adopted for all distress prediction models in the Pavement-ME for both flexible and rigid pavements.

$$FC_A = \left(\frac{6000}{1 + e^{(C_1 C_1' + C_2 C_2' \log_{10}(D))}} \right) \left(\frac{1}{60} \right) \quad (6)$$

where; C_1 , C_2 = Local calibration coefficients

1.5.6 Task 3-6: Validation of the Locally Calibrated Models

The objective of model validation is to demonstrate that calibrated models can produce robust and accurate predictions of the pavement distress for cases other than those used for model calibration. Validation typically requires an additional and independent set of in-service pavement condition data. Therefore, in this task, the research team validated the locally calibrated models by selecting an independent set of representative pavement sections (other than the calibration data set). It was anticipated that about 20 independent pavement sections were needed for models validation. Successful model validation requires that the bias and precision statistics of the model when applied to the validation data set are similar to those obtained from model calibration. The success of the validation process can be gauged based on the bias in predicted values and the standard error of the estimate (s_e). The s_e for the validation may not be equal to the s_e for calibration; generally, it is higher. Therefore, the s_e between validation and calibration data sets were compared in this task. Two types of statistical approaches were used to improve on the accuracy of the prediction models. These approaches include: (a) split-sampling, and (b) jackknifing.

1.5.7 Task 3-7: Data Recommendations

Based on the research performed from Tasks 3-1 to 3-6, the team made some recommendations related to data needs for future calibration of performance prediction models in the State of Michigan. In this regard, the recommendations address the following needs:

- Consistency between observed performance measurements and performance prediction models for rigid and flexible pavements. These recommendations include the type of distresses and measurement units as considered by the Pavement-ME.
- Format of the calibration database that can be used for similar future activities. The database structure was recommended based on the data type needs. For example, static and dynamic data elements were identified. In addition, the most practical hierarchal structure for different inputs was highlighted in the database structure.
- Compatibility between the current MDOT database systems and the one recommended for the local calibration was investigated and future modifications to address the needs for the local calibrations was recommended.
- Recommendations on data elements which could not be collected from as-constructed and other sources, but are needed.

1.5.8 Task 3-8: Plan for Future Calibration Efforts

In this task, a recommended plan for future calibration efforts is documented. Based on the findings of this study, the plan will address the following vital elements:

- Based on the findings from the literature review and the methodology adopted for local calibration in this study, the research team recommended a stepwise methodology for similar exercises in the future. The advantages and shortcomings of the recommended methodology are highlighted so that future improvements can be made, especially when more pavement sections and condition data becomes available.
- The pavement sections selected during this study will be monitored in the future before a major fix; therefore, more time series distress data will be available. Based on the results of this study and considering the trends in observed condition, the frequency of such an exercise in the future will be recommended.

1.5.9 Task 3-9: Deliverables

Several types of reports were submitted during the duration of the study—quarterly, draft final and final reports, according to the format specified in the Research & Implementation Manual. A PowerPoint presentation showing the basis and results of the study will also be submitted. In addition, implementation recommendations for adoption of the Pavement-ME analysis and design are included in the final report. A one day technology transfer class will be arranged to present the use of the M-E analysis and design process and local calibration needs to MDOT practitioners.

1.6 OUTLINE OF REPORT

This final report for Part 3 contains six (6) chapters. Chapter 1 outlines the problem statement, research objectives and brief details of various tasks performed in Part 3 of the study. Chapter 2 documents the review of literature from the previous studies related to local calibration efforts for the performance models in the Pavement-ME and implementation issues (Task 3-1). Chapter 3 discusses the data collection efforts which include a summary of the performance and input data for the selected pavement sections in Michigan for model calibrations. The work performed corresponds to Tasks 3-2 and 3-3. Chapter 4 details the local calibration methods and procedures used in this study. Chapter 5 presents the local calibration results for the various performance prediction models. This chapter corresponds to Tasks 3-4 through 3-6. Chapter 6 includes the conclusions and detailed recommendations as described in Tasks 3-7 and 3-8. Appendix A contains input data for all the pavement sections used in the local calibration of the performance models while all the local calibration results are presented in Appendix B.

CHAPTER 2 - LITERATURE REVIEW

2.1 INTRODUCTION

The mechanistic-empirical pavement analysis and design procedure to replace the empirical AASHTO 93 design method was incorporated in the Pavement-ME software (MEPDG, DARWin-ME and now Pavement-ME).The initial version of the software was made public in mid-2004. Since the release of the software, many State Highway Agencies (SHAs) have worked on exploring several aspects of the design and analysis procedures. Most of the efforts focused on (a) determining significant input variables through sensitivity studies to reduce the number of inputs, (b) evaluating local calibration needs to represent performance predictions in the local conditions (i.e., construction practices, climate, traffic, materials, and observed pavement performance), (c) performing local calibration to improve the pavement designs, and, (d) highlighting the implementation related issues such as PMS data compatibility and other data-specific needs .

The local calibration, of the Pavement-ME performance models, is a procedure that considerably relies on the available pavement cross-section, material, traffic and performance data. The NCHRP 1-40B project report (*1*) documented extensive guidelines for local calibration. The overall goal of calibration is to mathematically reduce the total error between the measured and the predicted pavement distresses and roughness (IRI). Subsequently, the calibrated models must be validated by using an independent set of projects to determine the accuracy of the pavement distress prediction models. A successful validation will produce similar or acceptable bias and precision statistics for the independent set of projects as obtained through the calibration process. The literature review is organized in two main subsections (a) local calibration process, and (b) local calibration efforts by different SHAs and most widely faced challenges while implementing the new pavement analysis and design procedure.

2.2 LOCAL CALIBRATION PROCESS

The performance prediction models in the Pavement-ME are nationally calibrated using in-service pavement material properties, pavement structure, climate and truck loading conditions, and performance data obtained from the Long-term Pavement Performance (LTPP) program (*2*). Due to the limited availability of Level 1 input properties, the nationally calibrated models are primarily based on Level 2 and Level 3 inputs (*3*). Generally, the nationally calibrated models may not perform well if the inputs and performance data used to calibrate those do not represent a state's condition. Therefore, it is recommended that each SHA conduct an evaluation to determine how well the nationally calibrated performance models predict field performance. If the predictions are not adequate, then local calibration of the Pavement-ME performance models is recommended to improve the pavement performance prediction capabilities reflecting the unique field conditions and design practices. The local calibration process is used to (a) confirm that the prediction models can predict pavement distress and smoothness without bias, and (b) determine the standard error associated with the prediction equations. The calibration process outlined in the NCHRP 1-40B final report consists of 11 steps as summarized below (*4*).

Step 1: *Select hierarchical input levels*

The hierarchical level is a policy-based decision established on the information available related to field and laboratory testing capabilities, material and construction specifications and traffic collection procedures and equipment. Different hierarchical levels for inputs can be selected based on the available data.

Step 2: *Develop experimental plan and sampling template*

The experimental plan and sampling template should represent the agencies standard specifications, construction and design practices, and construction materials. The pavement sections could represent a variety of design types, traffic levels, and climates. LTPP sections can also be included if necessary.

Step 3: *Estimate sample size for specific distress prediction models*

An adequate number of sections are required to provide statistically meaningful results. The recommended minimum number of pavement segments for each performance prediction model includes:

a. Rut depth (or faulting) – 20 roadway segments
b. Alligator and longitudinal cracking – 30 roadway segments
c. Transverse (thermal) cracking – 30 roadway segments
d. Transverse slab cracking – 26 roadway segments
e. Reflective cracking (HMA only) – 26 roadway segments

Step 4: *Select roadway segments*

Applicable roadway segments, replicate segments, and LTPP segments should be selected to populate the experimental design matrix developed in Step 2. It is recommended that the selected segments have at least 3 condition observations over an 8-10 year period.

Step 5: *Evaluate project and distress data*

The input and performance data for each project needs to be collected and verified to ensure compatibility with the requirements of the Pavement-ME. Any discrepancies between the local agency and the Pavement-ME need to be resolved to ensure compatibility. The Pavement-ME also recommends that the average condition level exceed 50% of the design criteria.

Step 6: *Conduct field testing and forensic investigation*

If any information is missing in step 5, field testing and forensic investigation are recommended to obtain the missing information.

Step 7: *Assess local bias*

Plot and compare the measured performance to the Pavement-ME predicted performance, based on the global/national models, for each pavement segment. The prediction capability and accuracy should be evaluated by performing linear regression on the predicted and measured performance, comparing the standard error of the estimate (S_e) to the nationally calibrated models and determining the bias for each performance prediction model. An R^2 value above 0.65 is considered a reasonable prediction (*5*). The bias significance is determined by performing hypothesis testing on the mean difference between the measured and predicted distresses. If the null hypothesis is rejected, then a local calibration is required. The nationally calibrated model statistics for the various performance prediction models are summarized in Table 2-1.

Table 2-1 Summary of the global models statistics

Pavement type	Performance prediction model	Model statistics		
		R-square	S_e	Number of data points, *N*
New asphalt	Alligator cracking	0.275	5.01	405
	Transverse cracking	0.344[1], 0.218, 0.057	N/A	N/A
	Rut depth	0.58	0.11	334
	IRI	0.56	18.9	1926
New JPCP	Transverse cracking	0.85	4.52	1505
	Joint faulting	0.58	0.03	1239
	IRI	0.6	17.1	163

[1] Three values correspond to levels 1, 2, and 3, respectively

Step 8: *Eliminate local bias*

If the hypothesis tests are rejected in step 7, the cause of the bias needs to be determined and removed if possible. Features to consider in removing bias include improving the accuracy and extent of traffic, climate, and material characteristics data.

Step 9: *Assess standard error of the estimate*

The S_e obtained from local calibration is compared to the nationally calibrated S_e. Reasonable S_e values are summarized in Table 2-2 (*1*, *5*).

Table 2-2 Reasonable standard error values

Pavement type	Performance prediction model	S_e
New asphalt	Alligator cracking	7
	Longitudinal cracking	600
	Transverse cracking	250
	Reflection cracking	600
	Rut depth	0.1
New JPCP	Transverse cracking	7
	Joint faulting	0.05

Step 10: *Reduce standard error of the estimate*

Determine if the standard error of each cell of the experimental matrix is dependent on other factors and adjust the local calibration coefficients to reduce the standard error. Table 2-3 summarizes the factors for eliminating bias and reducing the standard error.

Table 2-3 Factors for eliminating bias and reducing standard error (*5*)

Pavement Type	Distress	Eliminate Bias	Reduce Standard Error
Asphalt	Total rut depth	$k_{r1} = -3.35412$ $\beta_{r1} = 1$ $\beta_{s1} = 1$	$k_{r2} = 1.5606$ $k_{r3} = 0.4791$ $\beta_{r2} = 1$ $\beta_{r3} = 1$
	Alligator cracking	$k_{f1} = 0.007566$ $C_2 = 1$	$k_{f2} = 3.9492$ $k_{f3} = 1.281$ $C_1 = 1$
	Longitudinal cracking	$k_{f1} = 0.007566$ $C_2 = 3.5$	$k_{f2} = 3.9492$ $k_{f3} = 1.281$ $C_1 = 7$
	Transverse cracking	$\beta_{f3} = 1$ $k_{f3} = 1.5$	$\beta_{f3} = 1$ $k_{f3} = 1.5$
	IRI	$C_4 = 0.015$ (new) $C_4 = 0.00825$ (overlay)	$C_1 = 40$ (new) $C_1 = 40.8$ (overlay) $C_2 = 0.4$ (new) $C_2 = 0.575$ (overlay) $C_3 = 0.008$ (new) $C_3 = 0.0014$ (overlay)
Semi-Rigid Pavements	N/A	$\beta_{c1} = 1$ $C_2 = 1$	$C_1 = 1$ $C_2 = 1$ $C_4 = 1{,}000$
JPCP	Faulting	$C_1 = 1.0184$	$C_1 = 1.0184$
	Transverse cracking	$C_1 = 2$ $C_4 = 1$	$C_2 = 1.22$ $C_5 = -1.98$
	IRI—JPCP	$J_4 = 25.24$	$J_1 = 0.8203$
CRCP	Punchouts	$C_3 = 216.842$	$C_4 = 33.1579$ $C_5 = -0.58947$
	Punchouts fatigue	$C_1 = 2$	$C_2 = 1.22$
	Punchouts crack width	$C_6 = 1$	$C_6 = 1$
	IRI—CRCP	—	$C_1 = 3.15$ $C_2 = 28.35$

Step 11: *Interpretation of results*

Compare the measured and predicted distress or IRI to verify that acceptable results are obtained.

The above documented eleven (11) step process outlines the groundwork for the local calibration of the Pavement-ME performance prediction models. In each of these steps, a significant amount of work is required, especially related to the input data collection. Furthermore, some of the models require a full analysis of the software each time a calibration coefficient is adjusted which can become extremely time-consuming. The next section presents local calibration efforts and various implementation related issues reported in the literature.

2.3 LOCAL CALIBRATION EFFORTS AND CHALLENGES

The local calibration process requires a comparison between measured and predicted distress. In order to make this comparison, the SHAs first need to identify if their measured distress definitions are compatible with those predicted by the Pavement-ME. The distresses which are not compatible need conversions in order to compare the measured and predicted distresses. Recently, several SHAs have performed local calibration for both flexible and rigid pavements. Tables 2-4 and 2-5 summarize the current status for implementation along with the use of various performance models in the Pavement-ME by various SHAs for flexible and rigid pavements, respectively.

Table 2-4 Flexible pavement model calibration status (*2*)

Agency	IRI	Longitudinal cracking	Alligator cracking	Thermal cracking	Rut Depth		Reflective cracking
					Asphalt layer	Total	
Arizona	✓	-	✓	Global	✓	✓	✓
Colorado	✓	✓	✓	✓	✓	✓	✓
Hawaii	✓	Future	Future	Future	Future	Future	Future
Indiana	✓	-	✓	Global	Global	-	-
Missouri	✓	Global	Global		✓	✓	Global
New Jersey	✓	Future	Future	Future	Future	Future	Future
Oregon	✓	✓	✓	✓	✓	✓	Global

✓ Indicates model was locally calibrated
Future indicates that the model was not calibrated at the time of the report and will be calibrated in the future

Table 2-5 Rigid pavement model calibration status (*2*)

Agency	JPCP			CRCP	
	IRI	Transverse cracking	Faulting	IRI	Punchouts
Arizona	✓	✓	✓	✓	✓
Colorado	✓	✓	✓	-	-
Florida	✓	✓	✓	-	-
Indiana	✓	Global	Global	-	-
Missouri	✓	Global	Global	-	-
North Dakota	✓	Global	Global	-	-
Oregon	✓	Global	Global	✓	✓

✓ Indicates model was locally calibrated

The local calibration coefficients for the performance models adopted by various SHA's are shown in Tables 2-6 and 2-7 for rigid and flexible pavements, respectively. It can be observed from these tables that significantly different coefficients are possible in a region or state as compared to the coefficients in the global/national models.

The following issues were found to be common among all the SHAs, and should be addressed when performing local calibration to ease the way for full implementation of the Pavement-ME. These issues include:

- Number of available pavement sections
- Input data for each pavement section
- Measured condition of the selected pavement sections
- Local calibration techniques

Table 2-6 Rigid pavement local calibration efforts (*5*)

Feature	*MEPDG*	Arizona	Colorado	Florida	Missouri
Cracking					
C1	2.0	2.0	2.0	2.8389	2.0
C2	1.22	1.22	1.22	0.9647	1.22
C4	1.0	0.19	0.6	0.5640	1.0
C5	−1.98	−2.067	−2.05	−0.5946	−1.98
Std. Dev.	[1]	[4]	[7]	[1]	[1]
Faulting					
C1	1.0184	0.0355	0.5104	4.0472	1.0184
C2	0.91656	0.1147	0.00838	0.91656	0.91656
C3	0.002848	0.00436	0.00147	0.002848	0.002848
C4	0.000883739	1.1E-07	0.008345	0.000883739	0.000883739
C5	250	20000	5999	250	250
C6	0.4	2.309	0.8404	0.0790	0.4
C7	1.8331	0.189	5.9293	1.8331	1.8331
C8	400	400	[8]	400	400
Std. Dev.	[2]	[5]		[2]	[2]
Punchout					
C1	2.0	2.0			2.0
C2	1.22	1.22			1.22
C3	216.8421	85	Not applicable	Not applicable	216.8421
C4	33.15789	1.4149			33.15789
C5	−0.58947	−0.8061			−0.58947
Crack	[1]	[1]			[1]
Std. Dev.	[3]	[6]			[3]
IRI (CRCP)					
C1	3.15	3.15	Not applicable	Not applicable	3.15
C2	28.35	28.35			28.35
Std. Dev.	5.4	5.4			5.4
IRI (JPCP)					
J1	0.8203	0.6	0.8203	0.8203	0.82
J2	0.4417	3.48	0.4417	0.4417	1.17
J3	1.4929	1.22	1.4929	2.2555	1.43
J4	25.24	45.2	25.24	25.24	66.8
Std. Dev.	5.4	5.4	5.4	5.4	5.4

[1] Pow(5.3116 x CRACK,0.3903) + 2.99
[2] Pow(0.0097 x FAULT,0.05178) + 0.014
[3] 2 + 2.2593 x Pow(0.4882 x PO)
[4] Pow(9.87x CRACK,0.4012) + 0.5
[5] Pow(0.037 x FAULT,0.6532) + 0.001
[6] 1.5 + 2.9622 x Pow(PO,0.4356)
[7] Pow(57.08 x CRACK, 0.33) + 1.5
[8] 0.0831 x Pow(FAULT,0.3426) + 0.00521

Table 2-7 Flexible pavement local calibration efforts (*5*)

Feature	*MEPDG*	Arizona	Colorado	Missouri	Oregon
Cracking					
C1 Bottom	1.0	1.0	0.07	1.0	0.56
C1 Top	7.0	7.0	7.0	7.0	1.453
C2 Bottom	1.0	4.5	2.35	1.0	0.225
C2 Top	3.5	3.5	3.5	3.5	0.097
C3 Bottom	6000	6000	6000	6000	6000
C3 Top	0	0	0	0	0
C4 Top	1000	1000	1000	1000	1000
Std. Dev. Top	[1]	[1]	[1]	[1]	[1]
Std. Dev. Bottom	[2]	[2]	[12]	[2]	[2]
Fatigue					
BF1	1	249.00872	130.3674	1	1
BF2	1	1	1	1	1
BF3	1	1.23341	1.2178	1	1
Thermal Fracture					
Level 1	1.5	1.5	7.5	0.625	1.5
Level 2	0.5	0.5	0.5	0.5	0.5
Level 3	1.5	1.5	1.5	1.5	1.5
Std. Dev. (Level 1)	[3]	[3]	[3]	[3]	[3]
Std. Dev. (Level 2)	[4]	[4]	[4]	[4]	[4]
Std. Dev. (Level 3)	[5]	[5]	[5]	[5]	[5]
Rutting (asphalt)					
BR1	1.0	0.69	1.34[13]		1.48
BR2	1.0	1.0	1.0		1.0
BR3	1.0	1.0	1.0		0.9
Std. Dev.	[6]	[9]	[14]	[6]	[6]
Rutting (subgrade)					
BS1 (fine)	1.0	0.37	0.84	0.4375	1.0
Std. Dev. (fine)	[7]	[10]	[15]	[7]	[7]
BS1 (granular)	1.0	0.14	0.4	0.01	1.0
Std. Dev. (granular)	[8]	[11]	[16]	[8]	[8]
IRI					
C1 (asphalt)	40	1.2281	35	17.7	40
C2 (asphalt)	0.4	0.1175	0.3	0.975	0.4
C3 (asphalt)	0.008	0.008	0.02	0.008	0.008
C4 (asphalt)	0.015	0.028	0.019	0.01	0.015
C1 (over concrete)	40.8	40.8	40.8	40.8	40.8
C2 (over concrete)	0.575	0.575	0.575	0.575	0.575
C3 (over concrete)	0.0014	0.0014	0.0014	0.0014	0.0014
C4 (over concrete)	0.00825	0.00825	0.00825	0.00825	0.00825

[1] 200 + 2300/(1 + exp(1.072 – 2.1654 x LOG_{10} (TOP + 0.0001)))
[2] 1.13 + 13/(1 = exp(7.57 – 15.5 x LOG_{10}(BOTTOM + 0.0001)))
[3] 0.1468 x THERMAL + 65.027
[4] 0.2841 x THERMAL + 55.462
[5] 0.3972 x THERMAL + 20.422
[6] 0.24 x Pow(RUT, 0.8026) + 0.001
[7] 0.1235 x Pow(SUBRUT, 0.5012) + 0.001
[8] 0.1447 x Pow(BASERUT, 0.6711) + 0.001
[9] 0.0999 x Pow(RUT, 0.174)+0.001
[10] 0.05 x Pow(SUBRUT, 0.085) + 0.001
[11] 0.05 x Pow(BASERUT, 0.115) + 0.00110
[12] 1 + 15(1 + exp(-1.6673 – 2.4656*LOG10(BOTTOM+0.0001)))
[13] Under review
[14] 0.2052 x Pow(RUT,0.4) + 0.001
[15] 0.1822 x Pow(SUBRUT, 0.5) +0.001
[16] 0.2472 x Pow(BASERUT, 0.67) + 0.001

Several other SHAs have undertaken the local calibration process for various models within the Pavement-ME. These results were not presented in the NCHRP Synthesis 457 (*2*) and provide additional information regarding local calibration of the performance models. These

efforts performed by the various SHAs are discussed and summarized in this section. Currently, the following states have been identified:

- Arkansas
- Colorado
- FHWA
- Minnesota
- Missouri
- Montana
- New Mexico
- North Carolina
- Ohio
- Oklahoma
- Oregon
- South Carolina
- Texas
- Utah
- Washington

The review is focused on the methods used for local calibration and the significant findings in each state. Several SHAs have performed local calibration of the performance prediction models in the Pavement-ME. Table 2-8 summarizes the type of model calibrated by each SHA. Many of the States only attempted to calibrate some specific models. For example, Minnesota considered only the local calibration for transverse cracking and IRI for both flexible and rigid pavements. The local calibration was performed for the models where adequate data were available. Table 2-9 summarizes the various pavement types and the number of pavement segments considered for calibration by each state. Several States used LTPP data to increase the number of pavement sections since their local pavements did not meet the minimum recommended number of pavement segments summarized in the NCHRP 1-40B guide (*1*).

Table 2-8 Summary of local calibration efforts

State Agency	Performance Model							
	Flexible Recalibration					Rigid Recalibration		
	Alligator cracking	Longitudinal cracking	Thermal cracking	Rutting	IRI	Transverse cracking	Faulting	IRI
Arkansas	Yes	Yes	No	Yes	No	-	-	-
Colorado	Yes	-	Yes	Yes	Yes	No	No	No
Minnesota	No	No	Yes	Yes	No	Yes	No	Yes
Missouri	No	-	Yes	Yes	Yes	No	No	Yes
Montana	Yes	No	No	Yes	No	-	-	-
New Mexico	Yes	Yes	-	Yes	Yes	-	-	-
North Carolina	Yes	-	-	Yes	-	-	-	-
Ohio	No	-	No	Yes	Yes	No	No	Yes
Texas	-	-	-	Yes	-	-	-	-
Washington	Yes	Yes	-	Yes	No	Yes	No	No

"–" = model was not considered at this time
Yes = local calibration coefficients recommended
No = global calibration is sufficient or model was not calibrated

Table 2-9 Summary of calibration sections and pavement types

State Agency	Performance Model			
	Flexible Pavements		Rigid Pavements	
	Number of sections	Pavement types calibrated	Number of sections	Pavement types calibrated
Arkansas	26 total (LTPP and PMS)	New design	-	-
Colorado	95 CDOT and LTPP	New and rehab design	31 CDOT and LTPP	New and rehab design
Minnesota	13 MnROAD (rut) 14 MnROAD (TC) 12 MnROAD (LC)	New design	65 LTPP	New design
Missouri	7 MoDOT 14 LTPP 20 HMA overlays	New and rehab design	25 MoDOT 6 LTPP 5 Unbonded overlays	New and rehab design
Montana	55 LTPP and Non-LTPP	New and rehab design	-	-
New Mexico	11 LTPP 13 Non-LTPP	New design	-	-
North Carolina	22 LTPP 24 Non-LTPP	New design	-	-
Ohio	13 LTPP	New design	14 LTPP	New design
Texas	18 LTPP	New design	-	-
Washington	8 Sub-sections	New design	3 calibration 6 validation	New design

2.3.1 Local Calibration Efforts

Details regarding the local calibration of each performance model are summarized in this section. The transfer function equations are shown for each performance model for flexible and rigid pavements to highlight the local calibration coefficients.

2.3.1.1. Load related cracking in flexible pavements

Two types of load-related cracking are considered in the Pavement-ME. Alligator cracking is defined as cracks that initiate at the bottom of the HMA layers and propagate to the surface (bottom-up) with continued truck traffic in the wheel-path. Longitudinal cracking is defined as cracks that initiate at the top of the HMA surface and propagate downwards (top-down). The allowable number of axle load applications for both alligator and longitudinal cracking can be estimated using Equation (1):

$$N_{f-HMA} = k_{f1}(C)(C_H)\beta_{f1}(\varepsilon_t)^{k_{f2}\beta_{f2}}(E_{HMA})^{k_{f3}\beta_{f3}} \quad (1)$$

where:

$N_{f\text{-}HMA}$ = Allowable number of axle load applications for a flexible pavement and HMA overlays.

ε_t = Tensile strain at critical locations and calculated by the structural response model, in/in

E_{HMA} = Dynamic modulus of the HMA measured in compression, psi.

k_{f1}, k_{f2}, k_{f3} = Global field calibration parameters (from the NCHRP 1-40D re-calibration; k_{f1} = 0.007566, k_{f2} = -3.9492, and k_{f3} = -1.281).

β_{f1}, β_{f2}, β_{f3} = Local or mixture specific field calibration constants; for the global calibration effort, these constants were set to 1.0.

The C and M can be determined by using the following equations:

$$C = 10^{M} \tag{2}$$

$$M = 4.84\left(\frac{V_{be}}{V_a + V_{be}} - 0.69\right) \tag{3}$$

where:

V_{be} = Effective asphalt content by volume, percent.
V_a = Percent air voids in the HMA mixture.
C_H = Thickness correction term, dependent on type of cracking.

For bottom-up or alligator cracking, the C_H is determined by:

$$C_H = \frac{1}{0.000398 + \frac{0.003602}{1 + e^{(11.02 - 3.49 H_{HMA})}}} \tag{4}$$

For top-down or longitudinal cracking, the C_H is determined by:

$$C_H = \frac{1}{0.01 + \frac{12.00}{1 + e^{(15.676 - 2.8186 H_{HMA})}}} \tag{5}$$

The incremental damage is calculated on a grid pattern throughout the HMA layers at critical locations. The damage index is calculated by dividing the actual number of axle loads by the allowable number of axle loads. The cumulative damage is determined by summing the incremental damage over time as shown by Equation (6).

$$DI = \sum (\Delta DI)_{j,m,l,p,T} = \sum \left(\frac{n}{N_{f-HMA}}\right)_{j,m,l,p,T} \tag{6}$$

where:

n = Actual number of axle load applications within a specific time period.
j = Axle load interval.
m = Axle load type (single, tandem, tridem, quad, or special axle configuration)
l = Truck type using the truck classification groups included in the Pavement-ME.
p = Month.
T = Median temperature for the five temperature intervals or quintiles used to subdivide each month, °F.
H_{HMA} = Thickness of HMA layers (inches)
DI = Damage index

Alligator cracking transfer function

Equation (7) shows the transfer function for bottom-up fatigue cracking in the Pavement-ME and the required calibration coefficients.

$$FC_{Bottom} = \left(\frac{1}{60}\right)\left(\frac{C_4}{1+e^{C_1C_1^*+C_2C_2^*Log\left(DI_{Bottom}\bullet 100\right)}}\right) \quad (7)$$

where:

FC_{Bottom} = Area of alligator cracking that initiates at the bottom of the HMA layers, percent of total lane area.
DI_{Bottom} = Cumulative damage index at the bottom of the HMA layers.
$C_{1,2,4}$ = Transfer function regression constants; C_4 = 6,000; C_1 = 1.00; and C_2 =1.00

The C_1^* and C_2^* coefficients in Equation(7) can be determined as:

$$C_1^* = -2C_2^* \quad (8)$$

$$C_2^* = -2.40874 - 39.748\left(1+H_{HMA}\right)^{-2.856} \quad (9)$$

The local calibration of the alligator cracking model was considered by *Missouri*, *Ohio, Arkansas, Washington, Minnesota, Montana*, *New Mexico* and *Colorado*. *Missouri* used a non-statistical approach because the observed cracking was less than 5 percent for 99 percent of the test sections. The nationally calibrated model both over and under-predicted alligator cracking for the test sections. However, it was recommended that the nationally calibrated model can be used at this time and re-evaluation should be performed once more alligator cracking is observed for the selected 41 test sections (*6, 7*). The alligator cracking model was not calibrated for the state of *Ohio* due to the inability to distinguish between top-down and bottom-up cracking for the selected sections (*8*). *Arkansas* used the Excel solver add-on to optimize the local calibration coefficients by minimizing the error between the predicted and measured distress for 26 pavement sections (*9*). The state of *Washington* performed sensitivity by using an elasticity approach on the transfer functions to determine the most important calibration coefficients. Local calibration was performed on only two representative sections. The coefficients were adjusted until the error was minimized between the predicted and measured alligator cracking. The coefficients were validated using a larger set of data independent of the calibration sections. The purpose of the validation was to provide approximate field performance instead of a precise prediction for each section (*10*). The state of *Minnesota* did not observe any measured alligator cracking on the selected pavement sections for calibration. However, they compared the results from the Pavement-ME to the MnPAVE design software and determined that there is a correlation between the Pavement-ME and MnPAVE design software. They recommended changes to the fatigue damage equation by adding a direct multiplier for Minnesota conditions (*11*). The state of *Montana* calibrated the fatigue damage model instead of the alligator cracking transfer function (*12*). The state of *New Mexico* adjusted the model by running different C_1 and C_2 coefficient values in the transfer function and minimizing the error between predicted and measured alligator cracking (*13*). The local calibration of the alligator cracking model in *Colorado* used a nonlinear model optimization tool to minimize the error between the predicted and measured alligator cracking(*14*). The local calibration improved the prediction for Colorado conditions. Table 2-10 summarizes the modified local calibration coefficients among the above mentioned States.

Table 2-10 Local calibration coefficients for alligator cracking

Calibration coefficient	National coefficients	Arkansas	New Mexico	Washington	Colorado
C_1	1	0.688	0.625	1.071	0.07
C_2	1	0.294	0.25	1	2.35
C_4	6000	6000	6000	6000	6000

Longitudinal cracking transfer function

It is assumed that longitudinal cracking starts at the top of the pavement and propagates downwards. Equation (10) shows the transfer function and the calibration coefficients for top-down longitudinal cracking in the Pavement-ME.

$$FC_{Top} = 10.56\left(\frac{C_4}{1+e^{C_1-C_2 Log\left(DI_{Top}\right)}}\right) \quad (10)$$

where:

FC_{Top} = Length of longitudinal cracks that initiate at the top of the HMA layer, ft/mi.
DI_{Top} = Cumulative damage index near the top of the HMA surface
$C_{1,2,4}$ = Transfer function regression constants; C_4= 1,000; C_1=7.00; and C_2=3.5

The local calibration of the longitudinal cracking model was considered in *Arkansas, Washington, Minnesota, Montana* and *New Mexico*. The state of *Arkansas* performed local calibration on the longitudinal cracking model by changing the coefficients and minimizing the error between the predicted and measured cracking by using 26 LTPP and PMS pavement sections, while 6 sites were used for subsequent validation (*9*). *Washington* State calibrated the longitudinal cracking model using the methods described for alligator cracking (*10*). *Minnesota* did not calibrate the model due to issues with the Pavement-ME software at the time of the study (*11*). *Montana* observed a very large difference between the measured and predicted cracking and concluded that the model should not be used (*12*). *New Mexico* calibrated the longitudinal cracking model using the methods described for alligator cracking (*13*). Table 2-11 summarizes the modified local calibration coefficients in the above mentioned states.

Table 2-11 Local calibration coefficients for longitudinal cracking

Calibration coefficient	National coefficients	Arkansas	New Mexico	Washington
C1	7	3.016	3	6.42
C2	3.5	0.216	0.3	3.596
C4	1000	1000	1000	1000

2.3.1.2. Transverse (thermal) cracking model

Thermal cracking is associated with the contraction of the HMA material due to surface temperature fluctuations. The variations in temperature affect the volume changes of the material and as a consequence stresses develop due to the continual contraction of the materials, and the restrained conditions, which causes the occurrence of thermal cracks. Typically, thermal cracking in flexible pavements occur due to the temperature drop

experienced by the pavement in cold conditions. A thermal crack will initiate when the tensile stresses experienced in the HMA layers become equal to or greater than the tensile strength of the material. The initial cracks propagate through the HMA layer with more thermal cycles. The amount of crack propagation induced by a given thermal cooling cycle is predicted using the Paris law of crack propagation. Experimental results indicate that reasonable estimates of *A* and *n* can be obtained from the indirect tensile creep-compliance and strength of the HMA in accordance with Equations (11) and (12).

$$\Delta C = A\left(\Delta K\right)^{n} \tag{11}$$

where:

ΔC = Change in the crack depth due to a cooling cycle.
ΔK = Change in the stress intensity factor due to a cooling cycle.
A, n = Fracture parameters for the HMA mixture.

$$A = 10^{k_t \beta_t \left[4.389 - 2.52 Log\left(E_{HMA} \sigma_m \eta\right)\right]} \tag{12}$$

where:

η = $\eta = 0.8\left[1 + \frac{1}{m}\right]$
k_t = Coefficient determined through global calibration for each input level (Level 1 = 5.0; Level 2 = 1.5; and Level 3 = 3.0).
E_{HMA} = HMA indirect tensile modulus, psi.
σ_m = Mixture tensile strength, psi.
m = The m-value derived from the indirect tensile creep compliance curve measured in the laboratory.
β_t = Local or mixture calibration factor.

The stress intensity factor, *K*, has been incorporated in the Pavement-ME through the use of a simplified equation developed from theoretical finite element studies by using the model shown in Equation (13).

$$K = \sigma_{tip}\left(0.45 + 1.99\left(C_o\right)^{0.56}\right) \tag{13}$$

where:

σ_{tip} = Far-field stress from pavement response model at depth of crack tip, psi.
C_o = Current crack length, feet.

Equation (14) shows the transfer function for transverse cracking in the Pavement-ME.

$$TC = \beta_{t1} N\left(z\right)\left[\frac{1}{\sigma_d} Log\left(\frac{C_d}{H_{HMA}}\right)\right] \tag{14}$$

where:

TC = Observed amount of thermal cracking, ft/mi.
β_{t1} = Regression coefficient determined through global calibration (400).
$N[z]$ = Standard normal distribution evaluated at [z].
σ_d = Standard deviation of the log of the depth of cracks in the pavement (0.769), in.
C_d = Crack depth, in.
H_{HMA} = Thickness of HMA layers, in.

The transverse cracking model was considered for local calibration by *Missouri, Ohio, Arkansas, Minnesota, Montana* and *Colorado*. *Missouri* evaluated the model for both Level 1 (local creep compliance and Indirect Tensile (IDT) strength) and Level 3 (Pavement-ME defaults) inputs. It was found that the Level 1 analysis provided more accurate results. Hypothesis testing for mean difference, intercept and slope were performed to assess the bias and error in the model. The model was recalibrated and the local calibration coefficients obtained by the study were recommended for use (*6, 7*). *Ohio* used a non-statistical method to compare the measured and predicted transverse cracking. The method consists of dividing the distress magnitude into different categories and comparing the number of data points that move from one category to the next. It was concluded that the nationally calibrated model is adequate at this time (*8*). *Arkansas* did not calibrate the model because minimal observed transverse cracking due to the appropriate performance grade asphalt selection for specific climatic conditions (*9*). *Minnesota* did not calibrate the model because the current transverse cracking model was not incorporated in the Pavement-ME at the time of the study (*11*). *Montana* calibrated the model and found it to be adequate for their design practices (*12*). *Colorado* locally calibrated the transverse cracking model using Level 1 data for 12 pavement projects. The Level 1 *K* coefficient was changed between 1 and 10. It was found that a K=7.5 produced the best goodness of fit and minimal bias. Table 2-12 summarizes the modified local calibration coefficients for the various States.

Table 2-12 Local calibration coefficients for the thermal cracking model

Calibration coefficient	National coefficients	Missouri	Montana	Colorado
Level 1 K	1.5	0.625	-	7.5
Level 2 K	0.5	-	-	-
Level 3 K	1.5	-	0.25	-

2.3.1.3. Rutting model

The rutting model predicts the permanent deformation in each pavement layer/sub-layer for the entire analysis period. The rutting is predicted in absolute terms and not based on an incremental approach such as fatigue cracking. The average vertical resilient strain is computed for each analysis over the entire design life of the pavement. The rutting is predicted separately for the HMA, base, and subgrade. The total rutting predicted consists of the sum of the HMA, base, and subgrade rutting. Equation (15) shows the current rutting model for the HMA layers in the Pavement-ME. The model indicates that there are three local calibration coefficients in this function (i.e., $\beta_{r1}, \beta_{r2}\ \beta_{r3}$) Equation (16) shows the rutting model for unbound layers. This model has one calibration coefficient.

$$\Delta_{p(HMA)} = \varepsilon_{p(HMA)} h_{HMA} = \beta_{1r} k_z \varepsilon_{r(HMA)} 10^{k_{1r}} n^{k_{2r}\beta_{2r}} T^{k_{3r}\beta_{3r}} \quad (15)$$

where:

$\Delta_{p(HMA)}$	=	Accumulated permanent or plastic vertical deformation in the HMA layer/sub-layer, in.
$\varepsilon_{p(HMA)}$	=	Accumulated permanent or plastic axial strain in the HMA layer/sub-layer, in/in.
$\varepsilon_{r(HMA)}$	=	Resilient or elastic strain calculated by the structural response model at the mid-depth of each HMA sub-layer, in/in.
$h_{(HMA)}$	=	Thickness of the HMA layer/sub-layer, in.
n	=	Number of axle load repetitions.
T	=	Mix or pavement temperature, °F.

k_z = Depth confinement factor.
$k_{1r,2r,3r}$ = Global field calibration parameters (from the NCHRP 1-40D recalibration; k_{1r} = -3.35412, k_{2r} = 0.4791, k_{3r} = 1.5606).
β_{1r}, β_{2r}, β_{3r} = Local or mixture field calibration constants; for the global calibration, these constants were all set to 1.0.

$$\Delta_{p(soil)} = \beta_{s1} k_{s1} \varepsilon_v h_{soil} \left(\frac{\varepsilon_o}{\varepsilon_r} \right) e^{-\left(\frac{\rho}{n}\right)^{\beta}} \quad (16)$$

where:

$\Delta_{p(Soil)}$ = Permanent or plastic deformation for the layer/sub-layer, in.
n = Number of axle load applications.
ε_o = Intercept determined from laboratory repeated load permanent deformation tests, in/in.
ε_r = Resilient strain imposed in laboratory test to obtain material properties ε_o, β, and ρ, in/in.
ε_v = Average vertical resilient or elastic strain in the layer/sub-layer and calculated by the structural response model, in/in.
h_{Soil} = Thickness of the unbound layer/sub-layer, in.
k_{s1} = Global calibration coefficients; k_{s1}=1.673 for granular materials and 1.35 for fine-grained materials.
β_{s1} = Local calibration constant for the rutting in the unbound layers; the local calibration constant was set to 1.0 for the global calibration effort.
β = A parameter dependent on moisture content of the soil
ρ = A parameter related moisture content and resilient modulus of the soil

The total rutting is calculated based on Equation (17) below:

$$\text{Rut depth}_{Total} = \Delta_{HMA} + \Delta_{Base/subbase} + \Delta_{Subgrade} \quad (17)$$

The local calibration of the rutting model in the Pavement-ME was performed by *Arkansas, Minnesota, Missouri, Montana, New Mexico, North Carolina, Ohio, Texas, Washington* and *Colorado*. *Arkansas* calibrated the rutting model by using an iterative approach. It was found from the field observations that rutting occurred in the asphalt and the subgrade layers; therefore, the coefficient for the granular base was not changed. The model was calibrated and a reduction in error between the predicted and measured rutting was obtained (*9*). *Minnesota* performed the local calibration by investigating the contribution of each pavement layer. It was found that the global model over estimated early age rutting, especially for base and subgrade layers. Consequently, the total rutting model was adjusted by subtracting the first month predicted rutting prediction for base and subgrade layers. However, the calibration coefficients were not modified and it was observed that the adjusted rutting model predicts rutting adequately for Minnesota pavement sections (*11*). *Missouri* calibrated the rutting model by performing a series of hypothesis tests to determine the bias in the rutting model predictions. The calibration coefficients were adjusted and the error between the predicted and measured rutting was reduced (*6, 7*). *Montana* observed that the models over-predict rutting when compared with measured rut depths. The base and subgrade rutting coefficients were adjusted to reflect minimal predicted rutting to match observed rut depths in those layers. Furthermore, the HMA mix specific coefficients (*k'*s) were adjusted instead of the β coefficients. The *k* coefficients depend on the voids filled with asphalt (VFA) for each design (*12*). *New Mexico* calibrated the rutting model by changing the coefficients by minimizing the error between the predicted and measured rutting (*13*). *North Carolina* used two different methods for calibration: (a) the first method consisted of running the software

with different calibration coefficients and minimizing the error between the predicted and measured rutting, and (b) the second method used a genetic algorithm to determine the optimized coefficients (*15*). *Ohio* used a similar procedure as Missouri and used hypothesis testing to determine the model bias. The calibration coefficients were modified although some bias existed after calibration. They concluded that the modified coefficient were more reasonable than the global ones (*8*). *Texas* also used an approach that minimized the error between measured and predicted rutting. The coefficients were determined for several different regions within the State. Based on the regional coefficients, a statewide average was determined (*16*). *Washington* changed the local calibration coefficients iteratively until the error was minimized (*10*). *Colorado* calibrated the rutting model by changing the specific mixture coefficients as well as the individual layer coefficients. The local calibration slightly improved the rutting predictions for Colorado conditions when compared with the global model. The local calibration coefficients for the different States are summarized in Table 2-13.

Table 2-13 Local calibration coefficients for the rutting model

Calibration coefficient	National coefficients	AR	MO	NM	NC	OH	TX	WA	CO
β_{r1} HMA	1	1.2	1.07	1.1	13.1	0.51	2.39	1.05	1.34
β_{r2} HMA	1	1	-	1.1	0.4	-	-	1.109	1
β_{r3} HMA	1	0.8	-	0.8	1.4	-	0.856	1.1	1
β_{s1} base	1	1	0.01	0.8	0.303	0.32	-	-	0.4
β_{s1} subgrade	1	0.5	0.437	1.2	1.102	0.33	0.5	0	0.84

2.3.1.4. IRI model (flexible pavements)

Equation (18) shows the IRI performance prediction model in the Pavement-ME. There are four calibration coefficients in this model:

$$IRI = IRI_o + 0.0150(SF) + 0.400(FC_{Total}) + 0.0080(TC) + 40.0(RD) \qquad (18)$$

where:

IRI_o = Initial IRI after construction, in/mi.
SF = Site factor
FC_{Total} = Area of fatigue cracking (combined alligator, longitudinal, and reflection cracking in the wheel path), percent of total lane area. All load related cracks are combined on an area basis – length of cracks is multiplied by 1 foot to convert length into an area basis.
TC = Length of transverse cracking (including the reflection of transverse cracks in existing HMA pavements), ft/mi.
RD = Average rut depth, in.

Currently, the following equation is documented in most of the literature for the site factors (SF):

$$SF = Age\left[0.02003(PI+1) + 0.007947(Precip+1) + 0.000636(FI+1)\right] \qquad (19)$$

where:

Age	=	Pavement age, years.
PI	=	Percent plasticity index of the soil.
FI	=	Average annual freezing index, degree F days.
Precip	=	Average annual precipitation or rainfall, in.

However, during the local calibration in Michigan, it was found that the following equations were coded in the Pavement-ME analysis and design software[1]:

$$SF = (Frost + Swell) \times Age^{1.5} \quad (20)$$

$$Frost = Ln\left[(Rain + 1) \times (FI + 1) \times P_4\right] \quad (21)$$

$$Swell = Ln\left[(Rain + 1) \times (FI + 1) \times P_{200}\right] \quad (22)$$

where:

SF	=	Site factor
Age	=	Pavement age (years)
FI	=	Freezing index, °F-days.
Rain	=	Mean annual rainfall (in.)
P_4	=	Percent subgrade material passing No. 4 sieve
P_{200}	=	Percent subgrade material passing No. 200 sieve.

The IRI model was calibrated in *Missouri, Ohio, New Mexico* and *Colorado*. The IRI model was not locally calibrated in Arkansas, Minnesota, Montana and Washington. *Missouri* calibrated the IRI model after the rutting and the transverse cracking models were calibrated. The bias after calibration was deemed acceptable. *Ohio* used the same procedure as Missouri and the bias was also considered more reasonable after calibration. *New Mexico* calibrated the IRI model after calibrating the rutting and fatigue cracking models and only the site factor parameter was modified. *Colorado* calibrated the IRI model and found that the locally calibrated model improved the IRI predictions for *Colorado* conditions. The standard error of the estimate (SEE) increased slightly, and the correlation coefficient (R^2) improved significantly. The adjusted calibration coefficients for different State are presented in Table 2-14.

Table 2-14 Local calibration coefficients for the IRI model

Calibration coefficient	National coefficients	Missouri	New Mexico	Ohio	Colorado
SF	0.015	0.01	0.015	0.066	0.019
FC total	0.4	0.975	-	1.37	0.3
TC	0.008	0.008	-	0.01	0.02
RD	40	17.7	-	17.6	35

2.3.1.5. Transverse cracking model (rigid pavements)

In rigid pavements, transverse cracking is a load related distress caused by repeated loading. Under typical service conditions, transverse cracking can occur starting at either the top or bottom of the concrete slab because of slab curling. The potential for either mode of cracking is present in all slabs. Any given slab may crack either from the bottom or top of the

[1] The values were confirmed from ARA verbally.

pavement, but not both. Therefore, the predicted bottom-up and top-down cracking are not particularly meaningful by themselves, and combined cracking is reported excluding the possibility of both modes of cracking occurring on the same slab. The percentage of slabs with transverse cracks (including all severities) in a given traffic lane is used as the measure of transverse cracking and is predicted using Equation (23) for both bottom-up and top-down cracking:

$$CRK = \frac{100}{1 + C_4 \left(DI_F \right)^{C_5}} \tag{23}$$

The general expression for fatigue damage accumulations considering all critical factors (age, month, axle type, load level, temperature gradient, axle wander, and hourly traffic) for JPCP transverse cracking is as follows and referred to as Miner's hypothesis are shown in Equation (24):

$$DI_F = \sum \frac{n_{i,j,k,l,m,n,o}}{N_{i,j,k,l,m,n,o}} \tag{24}$$

where:

DI_F = Total fatigue damage (top-down or bottom-up).
$n_{i,j,k,\ldots}$ = Applied number of load applications at condition i, j, k, l, m, n.
$N_{i,j,k,\ldots}$ = Allowable number of load applications at condition i, j, k, l, m, n.
i = Age (accounts for change in PCC modulus of rupture and elasticity, slab/base contact friction, deterioration of shoulder LTE).
j = Month (accounts for change in base elastic modulus and effective dynamic modulus of subgrade reaction).
k = Axle type (single, tandem, and tridem for bottom-up cracking; short, medium, and long wheelbase for top-down cracking).
l = Load level (incremental load for each axle type).
m = Equivalent temperature difference between top and bottom PCC surfaces.
n = Traffic offset path.
o = Hourly truck traffic fraction.

The fatigue damage calculation is a process of summing damage from each damage increment. Once top-down and bottom-up damage are estimated, the corresponding total cracking is computed Equation (25).

$$TCRACK = \left(CRK_{Bottom-up} + CRK_{Top-down} - CRK_{Bottom-up} \cdot CRK_{Top-down} \right) \cdot 100\% \tag{25}$$

where:

$TCRACK$ = Total transverse cracking (percent, all severities).
$CRK_{Bottop\text{-}up}$ = Predicted amount of bottom-up transverse cracking (fraction).
$CRK_{Top\text{-}down}$ = Predicted amount of top-down transverse cracking (fraction).

The transverse cracking model was considered for local calibration in *Ohio, Minnesota, Missouri, Washington* and *Colorado*. The global model was accepted for *Ohio* and *Missouri* since there was no significant difference observed between the measured and predicted transverse cracking. Both studies recommend to revisit the local calibration of the model once more condition data becomes available for the selected projects. *Washington* calibrated the transverse cracking model and the local calibration coefficients provided a better prediction as compared to the global model. *Minnesota* used an iterative approach to locally

calibrate the transverse cracking model. The local calibration coefficients improved the transverse cracking predictions for the pavement sections in the calibration set. It should be noted that the model was calibrated on a limited dataset. *Colorado* found that their JPCP pavement sections were performing well and did not show any significant amounts of cracking. At this time, they did not locally calibrate the transverse cracking model. Table 2-15 summarizes the transverse cracking model local calibration coefficients in different states.

Table 2-15 Local calibration coefficients for the rigid transverse cracking model

Calibration coefficient	National coefficients	Missouri	Washington	Ohio	Colorado	Minnesota
C4	1	1	0.139	1	1	0.9
C5	-1.98	-1.98	-2.115	-1.98	-1.98	-2.64

2.3.1.6. Faulting model

The mean transverse joint faulting is predicted on a monthly basis using an incremental approach. A faulting increment is determined each month and the current faulting level affects the magnitude of the increment. The faulting at each month is determined as a sum of faulting increments from all previous months in the pavement life from the traffic opening date using the equations:

$$Fault_m = \sum_{i=1}^{m} \Delta Fault_i \tag{26}$$

$$\Delta Fault_i = C_{34} \times (FAULTMAX_{i-1} - Fault_{i-1})^2 \times DE_i \tag{27}$$

$$FAULTMAX_i = FAULTMAX_0 + C_7 \times \sum_{j=1}^{m} DE_j \times Log(1 + C_5 \times 5.0^{EROD})^{C_6} \tag{28}$$

$$FAULTMAX_0 = C_{12} \times \delta_{curling} \times \left[Log(1 + C_5 \times 5.0^{EROD}) \times Log(\frac{P_{200} \times WetDays}{p_s}) \right]^{C_6} \tag{29}$$

where:

$Fault_m$ = Mean joint faulting at the end of month *m*, in.
$\Delta Fault_i$ = Incremental change (monthly) in mean transverse joint faulting during month *i*, in.
$FAULTMAX_i$ = Maximum mean transverse joint faulting for month *i*, in.
$FAULTMAX_0$ = Initial maximum mean transverse joint faulting, in.
$EROD$ = Base/sub-base erodibility factor
DE_i = Differential density of energy for subgrade deformation accumulated during month *i*
$\delta_{curling}$ = Maximum mean monthly slab corner upward deflection due to temperature curling and moisture warping.
P_S = Overburden on subgrade, lb.
P_{200} = Percent subgrade material passing #200 sieve.
$WetDays$ = Average annual number of wet days (greater than 0.1 inch rainfall).
$C_{1,2,3,4,5,6,7,12,34}$ = Global calibration constants (C_1 = 1.29; C_2 = 1.1; C_3 = 0.001725; C_4 = 0.0008; C_5 = 250; C_6 = 0.4; C_7 = 1.2.

$$C_{12} = C_1 + C_2 \times FR^{0.25} \tag{30}$$

$$C_{34} = C_3 + C_4 \times FR^{0.25} \tag{31}$$

where:

FR = Base freezing index defined as percentage of time the top base temperature is below freezing (32 °F) temperature.

Several SHAs attempted to locally calibrate the faulting model. Most states accepted the global model coefficients because of limited faulting measurements. *Washington* found very different local calibration coefficients for their pavement sections included in the calibration dataset. They also determined different calibration coefficients for un-doweled and dowel-bar retrofitted (DBR) pavements. The faulting model local calibration results are summarized in Table 2-16.

Table 2-16 Local calibration coefficients for the faulting model

Calibration coefficient	National coefficients	Washington un-doweled	Washington DBR
C1	1.29	0.4	0.934
C2	1.1	0.341	0.6
C3	0.001725	0.000535	0.001725
C4	0.0008	0.000248	0.004
C5	250	77.5	250
C6	0.4	0.0064	0.4
C7	1.2	2.04	0.65
C8	400	400	400

2.3.1.7. IRI model (rigid pavements)

In the Pavement-ME, smoothness is predicted as a function of the initial as-constructed profile of the pavement and any change in the longitudinal profile over time and traffic due to distresses and foundation movements. The global IRI model was calibrated and validated using LTPP field data to assure that it would produce valid results under a variety of climatic and field conditions. The final IRI model is shown in the following equations:

$$IRI = IRI_I + C1 \times CRK + C2 \times SPALL + C3 \times TFAULT + C4 \times SF \quad (32)$$

where:

IRI = Predicted IRI, in/mi.
IRI_I = Initial smoothness measured as IRI, in/mi.
CRK = Percent slabs with transverse cracks (all severities).
SPALL = Percentage of joints with spalling (medium and high severities).
TFAULT = Total joint faulting cumulated per mi, in.
C1 = 0. 8203
C2 = 0.4417
C3 = 0.4929
C4 = 25.24
SF = Site factor.

$$SF = AGE\ (1 + 0.5556 \times FI)\ (1 + P_{200}) \times 10^{-6} \quad (33)$$

where:

AGE = Pavement age, yr.
FI = Freezing index, °F-days.
P_{200} = Percent subgrade material passing No. 200 sieve.

The transverse cracking and faulting values are obtained using the models described earlier. The transverse joint spalling is determined by Equation (34), which was calibrated using LTPP and other data.

$$SPALL = \left[\frac{AGE}{AGE + 0.01} \right] \left[\frac{100}{1 + 1.005^{(-12 \times AGE + SCF)}} \right] \quad (34)$$

where:

SPALL = Percentage joints spalled (medium- and high-severities).
AGE = Pavement age since construction, years.
SCF = Scaling factor based on site, design, and climate.

$$SCF = -1400 + 350 \times AIR\% \times (0.5 + PREFORM) + 3.4\, f'c \times 0.4 - 0.2\,(FTCYC \times AGE) + 43\, h_{PCC} - 536\, WC\_Ratio \quad (35)$$

The above model for scaling factor reported in the literature (*17*) was modified in the software as follows:

$$SCF = -1400 + 350 \times AIR\% \times (0.5 + PREFORM) + 43.4 \times f'c^{0.4} - 0.2\,(FTCYC \times AGE) + 43 \times h_{PCC} - 536 \times WC\_Ratio \quad (36)$$

where:

AIR% = PCC air content, percent.
AGE = Time since construction, years.
PREFORM = 1 if preformed sealant is present; 0 if not.
f'c = PCC compressive strength, psi.
FTCYC = Average annual number of freeze-thaw cycles.
h_{PCC} = PCC slab thickness, in.
WC_Ratio = PCC water/cement ratio.

The IRI model was considered for local calibration by *Minnesota*, *Missouri*, *Ohio*, *Washington* and *Colorado*. *Minnesota* only calibrated the IRI model with respect to the pavement age and did not change anything else. The IRI model has changed since *Minnesota* performed local calibration. *Missouri* and *Ohio* recommend the locally calibrated coefficients since those provided a better prediction with less bias compared to the global model. The global model provided adequate predictions but both States wanted to reduce bias further. *Washington* found significant differences between the global model predictions and the measured IRI. They believe that the difference between the measured and predicted IRI is attributed to the use of studded tires on *Washington* pavements. *Colorado* determined that the global model predicted IRI sufficiently and local calibration was not necessary. The IRI local calibration coefficients are summarized in Table 2-17.

Table 2-17 Local calibration coefficients for rigid IRI model

Calibration coefficient	National coefficients	Missouri	Ohio	Colorado
Cracking	0.820	0.82	0.82	0.820
Spalling	0.442	1.17	3.7	0.442
Faulting	1.493	1.43	1.711	1.493
Site Factor	25.24	66.8	5.703	25.24

2.3.2 Challenges and Lesson Learned

A survey of SHAs was conducted recently and is documented in NCHRP Synthesis 457 (*2*). The survey was sent to all the SHA's to identify their current design practices as well as their plan for the implementation of the ME-based design. The questionnaire focused on the practices, policies, and procedures that have been successfully used by the various SHA's. The challenges related to the implementation of the Pavement-ME are of particular interest. The challenges are related to the design software's complexity, availability of the needed input data, defining the most appropriate hierarchical input levels and the need for local calibration. Most SHAs are concerned with the software complexity, the training needed for the ME-based design practices, and, the operation and functionality of the software.

The availability of the necessary input data is a major concern. Most SHAs indicated that pavement condition data, existing pavement structure information, and traffic data are readily available. Very few SHA's indicated that material related data were readily available. Collecting and testing the missing information requires a significant effort by the SHAs. Selecting Level 1 inputs also requires significant effort by the agencies. The survey indicated that only site-specific vehicle classification and average annual daily truck traffic (AADTT) are likely available for the majority of SHAs. Based on the lack of available data for Level 1 inputs, regional averages or Pavement-ME default values will be used for pavement designs.

The survey respondents provided a number of challenges and lessons learned during the implementation process. As expected, one of the most common challenges reported was the lack of readily available traffic and materials data, and the large effort required to obtain the needed data. In addition, SHAs indicated that contacting the respective office or division in an agency (e.g., construction, materials, traffic or planning) early on in the implementation process is helpful. This proactive awareness and coordination among different offices will make sure that everyone understands what data are needed and why. Further, this communication will help in preparing the respective staff to conduct field sampling and testing if the needed data are not available. The survey results describe the following challenges in implementing the ME-based designs:

- District offices are resistant to change from empirical-based designs to ME-based designs. The main reason is a higher comfort level with the inputs and resulting outputs (i.e., layer thickness) with the AASHTO 1993 Guide. Therefore, making a shift to using design inputs and predicting distresses in the Pavement-ME, contrary to obtaining layer thickness as the final result, has been difficult to accept.
- Variations and changes to the pavement condition data collection procedures in different highway agencies have resulted in inconsistency with condition data measurement. These discrepancies among agencies have lowered their ability to obtain reliable pavement condition data for use in the calibration process.
- Lack of resources to conduct in-house local calibration and training of staff is another hurdle identified.
- While Pavement-ME is too complex for most practicing engineers, the adoption of the procedure may improve through training to increase the engineer's confidence in the benefits of the design procedure in the long-run.
- The procedure is evolving over time and several variations and improvement were made in last couple of years (various versions of the software). Therefore, a potential

of more work remains (i.e., recalibration of performance models), as a result of newer versions and modifications to software.

The survey (*2*) results also presented the following lessons learned in the implementation process:

- Establish realistic timelines for the calibration and validation process
- Allow sufficient time for obtaining materials and traffic data
- Ensure the data related to the existing pavement layer, materials properties, and traffic is readily available
- If necessary, develop a plan for collecting the needed data; this can require an expensive field sampling and testing effort
- Develop agency-based design inputs to avoid default or other inputs to minimize design variability
- Provide training to agency staff in ME design fundamentals, MEPDG procedures, and the Pavement-ME software

2.4 IMPLEMENTATION EFFORTS IN MICHIGAN

To support the Pavement-ME implementation process in the state of Michigan, the pavement researchers at Michigan State University (MSU) have been working with MDOT to explore the various attributes of the design and analysis software. As a result of these efforts over the last seven (7) years, the following reports have been published:

- Evaluation of the 1-37A Design Process for New and Rehabilitated JPCP and HMA Pavements (Report No. RC-1516)(*18, 19*)
- Preparation for Implementation of the Mechanistic-Empirical Pavement Design Guide in Michigan - Part 2: Rehabilitation Evaluation (Report No. RC-1594)(*20*)
- Preparation for Implementation of the Mechanistic-Empirical Pavement Design Guide in Michigan - Part 1: HMA Mixture Characterization (Report No. RC-1593)(*21*)
- Characterization of Traffic for the New M-E Pavement Design Guide in Michigan (Report No. RC-1537)(*22, 23*)
- Pavement Subgrade MR Design Values for Michigan's Seasonal Changes (Report No. RC-1531)(*24*)
- Backcalculation of Unbound Granular Layer Moduli (Report No. RC-1548)(*25*)
- Quantifying Coefficient of Thermal Expansion Values of Typical Hydraulic Cement Concrete Paving Mixtures (Report No. RC-1503)(*26*)

The results from these studies are considered throughout the local calibration process in this report. Brief findings from these works are summarized below.

2.4.1 MDOT Sensitivity Study

The MSU research team conducted a study entitled "Evaluation of the 1-37A Design Process for New and Rehabilitated JPCP and HMA pavements"(*18*). The main objectives of the study were to:

a. Evaluate the Pavement-ME pavement design procedures for Michigan conditions
b. Verify the relationship between predicted and observed pavement performance for selected pavement sections in Michigan and
c. Determine if local calibration is necessary

The report outlined the performance models for JPCP and HMA pavements. Two types of sensitivity analyses were performed namely, a preliminary one-variable-at-a-time (OAT), and a detailed analysis consisting of a full factorial design. Both analyses were conducted to reflect MDOT pavement construction, materials, and design practices. For both new rigid and flexible pavement designs, the methodology contained the following steps:

1. Determine the input variables available in the Pavement-ME and the range of values which MDOT uses in pavement design
2. Determine the practical range for each input variable based on MDOT practice and Long Term Pavement Performance (LTPP) data
3. Select a base case and perform the OAT
4. Use OAT results to design the detailed sensitivity analysis
5. Determine statistically significant input variables and two-way interactions
6. Determine practical significance of statistically significant variables
7. Draw conclusions from the results

Tables 2-18 and 2-19 show the impact of input variables on different pavement performance measures for rigid and flexible pavements, respectively.

Table 2-18 Impact of input variables on rigid pavement performance (*18*)

Design/material variable	Impact on distress/smoothness		
	Transverse joint faulting	Transverse cracking	IRI
PCC thickness	High	High	High
PCC modulus of rupture	None	High	Low
PCC coefficient of thermal expansion	High	High	High
Joint spacing	Moderate	High	Moderate
Joint load transfer efficiency	High	None	High
PCC slab width	Low	Moderate	Low
Shoulder type	Low	Moderate	Low
Permanent curl/warp	High	High	High
Base type	Moderate	Moderate	Low
Climate	Moderate	Moderate	Moderate
Subgrade type/modulus	Low	Low	Low
Truck composition	Moderate	Moderate	Moderate
Truck volume	High	High	High
Initial IRI	NA	NA	High

Table 2-19 Impact of input variables on flexible pavement performance (*18*)

Fatigue cracking	Longitudinal cracking	Transverse cracking	Rutting	IRI
HMA thickness HMA effective binder content HMA air voids Base material type Subbase material type	HMA thickness HMA air voids HMA effective binder content Base material Subbase material Subgrade material	HMA binder grade HMA thickness HMA effective binder content HMA air voids HMA aggregate gradation	HMA thickness Subgrade material Subgrade modulus HMA effective binder content HMA air voids Base material Subbase material Base thickness Subbase thickness	HMA thickness HMA aggregate gradation HMA effective binder content HMA air voids Base material type Subbase thickness Subbase material type Subgrade material type

Note: The input variables are listed in order of importance.

2.4.2 Pavement Rehabilitation Evaluation in Michigan

The study was performed to determine the sensitive inputs for the pavement rehabilitation options (*27*). Three different sensitivity analyses were performed for each rehabilitation option. The global sensitivity analysis results provided the best results. The rankings of important input variables for each rehabilitation option are summarized below:

Table 2-20 List of significant inputs — HMA over HMA

Input variables	Ranking (NSI)
Overlay air voids	1 (6)
Existing thickness	2 (5)
Overlay thickness	3 (4)
Existing pavement condition rating	4 (4)
Overlay effective binder	5 (2)
Subgrade modulus	6 (2)
Subbase modulus	7 (1)

Note: NSI = Normalized sensitivity index

Table 2-21 List of significant inputs — Composite pavement

Inputs	Ranking (NSI)
Overlay air voids	1 (9)
Overlay thickness	2 (2)
Existing PCC thickness	3 (1)

Table 2-22 List of significant inputs — Rubblized PCC pavement

Inputs	Ranking (NSI)
Overlay air voids	1 (6)
Overlay effective binder	2 (2)
Overlay thickness	3 (1)

Table 2-23 List of significant inputs — Unbonded PCC overlay

Design inputs	Ranking (NSI)
Overlay PCC thickness	1 (23)
Overlay PCC coefficient of thermal expansion (CTE)	2 (12)
Overlay PCC modulus of rupture (MOR)	3 (8)
Overlay joint spacing	4 (5)
Existing PCC elastic modulus	6 (1)
Climate	7 (1)

2.4.3 HMA Mixture Characterization in Michigan

As part of a larger MDOT study, "Preparation for Implementation of the Mechanistic-Empirical pavement Design Guide in Michigan", laboratory testing was preformed to determine HMA mixture properties for typical mixtures used in the state of Michigan. The Level 1 HMA inputs require laboratory tests to characterize a pavement in the Pavement-ME software. The most important properties obtained from this study include the following:

- Dynamic modulus (E*)
- Binder G*
- Creep compliance and,
- Indirect tensile strength (IDT)

The study determined Level 1 HMA mixture and binder characterizations for use as inputs in the Pavement-ME. Additionally, the study used artificial neural networks (ANN) for better predictions of dynamic modulus from asphalt volumetrics. The research team also reviewed the current HMA test data as part of the MDOT testing program and compared it to the data required by Pavement-ME. Standalone software, called DYNAMOD, was developed to serve as a database to obtain the necessary HMA properties in a form compatible with the Pavement-ME software.

2.4.4 Traffic Inputs in Michigan

The research team has extensively worked on the traffic characterization for the Pavement-ME in Michigan (*22*, *23*). The following traffic characteristics were investigated:

1. Monthly distribution factors
2. Hourly distribution factors
3. Truck traffic classifications
4. Axle groups per vehicle
5. Axle load distributions for different axle configurations

The data were collected from 44 Weigh-in-motion (WIM) sites distributed throughout the entire state of Michigan. The data were used to develop Level 1 (site specific) traffic inputs for the WIM locations. Cluster analysis was conducted to group sites with similar characteristics for developing Level 2 (regional) inputs. Statewide (Level 3) averages were

also determined. The inputs and their recommended input levels are summarized in Table 2-24.

Table 2-24 Conclusions and recommendations for traffic input levels

Traffic Characteristic	Impact on pavement performance		Suggested input levels (when level I data not available)	
	Rigid pavement	Flexible pavement	Rigid pavement	Flexible pavement
TTC	Significant	Moderate	Level II	
HDF	Significant	Negligible	Level II	Level III[1]
MDF	Negligible		Level III (State average)	
AGPV	Negligible		Level III (State average)	
Single ALS	Negligible		Level III (State average)	
Tandem ALS	Significant	Moderate	Level II (State average)	
Tridem ALS	Negligible	Negligible	Level III (State average)	
Quad ALS	Negligible	Moderate	Level III (State average)	

[1] Level III inputs were available for flexible pavements in the MEPDG version 1.1 and are no longer available as input in the Pavement-ME

2.4.5 Unbound Material Inputs in Michigan

Two studies to characterize unbound material in Michigan were carried out in the last few years (*24, 25*). The first study outlined the importance of the resilient modulus (MR) of the roadbed soil and how it affects pavement systems. The study focused on developing reliable methods to determine the MR of the roadbed soil for inputs in the Pavement-ME. The study divided the state of Michigan into fifteen clusters based on the similar soil characteristics. Laboratory tests were performed to determine moisture content, grain size distribution, and Atterberg limits. Furthermore, another aspect of the study was to determine the differences between lab tested MR values and back-calculated MR. Based on the analysis it was concluded that the values between laboratory MR and back-calculated MR are almost equal if the stress boundaries used in the laboratory matched those of the FWD tests. Table 2-25 summarizes the recommended MR values for design based on different roadbed types in Michigan. The study suggests that the design recommended value should be used for design.

Table 2-25 Average roadbed soil MR values (*24, 25*)

Roadbed Type		Average MR			
USCS	AASHTO	Laboratory determined (psi)	Back-calculated (psi)	Design value (psi)	Recommended design MR value (psi)
SM	A-2-4, A-4	17,028	24,764	5,290	5,200
SP1	A-1-a, A-3	28,942	27,739	7,100	7,000
SP2	A-1-b, A-3	25,685	25,113	6,500	6,500
SP-SM	A-1-b,A-2-4, A-3	21,147	20,400	7,000	7,000
SC-SM	A-2-4, A-4	23,258	20,314	5,100	5,000
SC	A-2-6, A-6,A-7-6	18,756	21,647	4,430	4,400
CL	A-4, A-6, A-7-6	37,225	15,176	4,430	4,400
ML	A-4	24,578	15,976	4,430	4,400
SC/CL/ML	A-2-6, A-4, A-6, A-7-6	26,853	17,600	4,430	4,400

The second study focused on the backcalculation of MR for unbound base and subbase materials and made the following recommendations (*25*):

1. In the design of flexible pavement sections using design Levels 2 or 3 of the Pavement-ME, the materials beneath the HMA surface layer should consist of the following two layers:
    a. Layer 1 - An aggregate base whose modulus value is 33,000 psi
    b. Layer 2 - A sand subbase whose modulus is 20,000 psi
2. In the design of rigid pavement sections using design Levels 2 or 3 of the Pavement-ME, the materials beneath the PCC slab could be either:
    a. An aggregate base layer whose modulus value is 33,000 psi supported by sand subbase whose modulus value is 20,000 psi
    b. A granular layer made up of aggregate and sand mix whose composite modulus value is 25,000 psi
    c. A sand subbase whose modulus value is 20,000 psi
3. For the design of flexible or rigid pavement sections using design Level 1 of the Pavement-ME, it is recommended that:
    - For an existing pavement structure where the PCC slabs or the HMA surface will be replaced, FWD tests be conducted every 500 feet along the project and the deflection data be used to backcalculate the moduli of the aggregate base and sand subbase or the granular layer. The modulus values to be used in the design should correspond to the 33^{rd} percentile of all values. The 33^{rd} percentile value is the same as the average value minus half the value of the standard deviation.
    - For a total reconstruction or for a new pavement section, the modulus values of the aggregate base and the sand subbase or the granular layer could be estimated as twice the average laboratory determined modulus value.
4. Additional FWD tests and backcalculation analyses should be conducted when information regarding the types of the aggregate bases under rigid and flexible pavements becomes known and no previous FWD tests were conducted.
5. MDOT should keep all information regarding the various pavement layers. The information should include the mix design parameters of the HMA and the PCC, the type, source, gradation and angularity of the aggregate and the subbase material type, source, gradation and angularity. The above information should be kept in easily searchable electronic files.

2.4.6 Coefficient of Thermal Expansion

The CTE input values were obtained from the MDOT study that determined the CTE for various aggregates available across the state of Michigan (*26*). It was decided later that the CTE values for concrete in Michigan are either 4.5 or 5.8 in/in/°F×10^{-6} depending on the location of the pavement section. For University and Metro regions, a CTE value of 5.8 in/in/°F×10^{-6} while for other regions, a value of 4.5 in/in/°F×10^{-6} should be used.

CHAPTER 3 - PROJECT SELECTION AND DATA

3.1 INTRODUCTION

The first step in a local calibration process includes the selection of an adequate number of pavement sections representing state-of-the-practice for local conditions. A subsequent, essential step is to collect the required data for the selected in-service pavement sections. The data includes the information about (a) measured pavement condition over time, and (b) several Pavement-ME inputs, for each project. The inputs directly affect the performance predictions. These predictions are compared to the measured performance of the as-constructed pavement sections. A pavement section is defined as a specific length of roadway corresponding to a construction project. A project may have up to two pavement sections (i.e. different directions on a divided highway). These sections for a project may have similar data inputs, but different measured or observed pavement performance. The predicted pavement performance in the Pavement-ME relies on the inputs used to characterize an in service pavement. Therefore, several inputs are necessary to analyze a particular pavement in the design software, especially the ones which have significant impacts on the predicted performance. This chapter describes the process for pavement section selection for local calibration and the procedures adopted to collect the necessary information for the selected pavement sections. The topics discussed in this chapter include:

1. Readily available MDOT measured condition data
2. Project selection criteria
3. Pavement cross-section information
4. Traffic inputs
5. Construction materials inputs
6. Climate inputs

3.2 AVAILABLE PMS CONDITION DATA

The first step in the data collection efforts consisted of evaluating the readiness of the MDOT Pavement Management System (PMS) database to provide the necessary data for local calibration and validation of the Pavement-ME performance models. The PMS and other data sources (construction records, previous reports, traffic monitoring information system etc.) were evaluated to extract the following input data:

a. All performance measures predicted by the Pavement-ME for both flexible and rigid pavements were evaluated for consistency of units. The units of the measured distress data from MDOT's PMS were converted to those predicted by the Pavement-ME;
b. The construction records and other sources were used to assess the pavement cross-sections, MDOT provided the information for identified sections;
c. Traffic data as required by the Pavement-ME were obtained from MDOT. In situations where Level 1 data were unavailable, Level 2 and 3 data were estimated based on the previous studies conducted by the research team in the state of Michigan; and

d. Material types used in different pavement layers were documented for the most common construction materials in Michigan.

3.2.1 Pavement Condition Measures Compatibilities

MDOT collects distress and laser based measurement (sensor) data on their pavement network every other year. The distress data in the MDOT PMS are represented by different principle distress (PD) codes. Each PD corresponds to a visually measured surface distress observed in the field. Certain distress types collected by MDOT are expressed in forms that are not compatible with the Pavement-ME performance measures; therefore, conversions were necessary to make the data comparable. The distress types collected by MDOT and the necessary conversion process are discussed in this section.

3.2.1.1. Selected distresses

The necessary distress information was identified and extracted from the MDOT PMS and sensor database. The MDOT PMS current Distress Manual was used to determine all the PDs corresponding to predicted distresses in the Pavement-ME. It should be noted that, all PDs were included since MDOT began collecting the data in 1992; the earlier versions of the PMS manual were consulted to ensure that the correct data was extracted for all years. The necessary steps for PMS data extraction include:

1. Identify the PDs that corresponds to the Pavement-ME predicted distresses,
2. Convert (if necessary) MDOT PDs to the units compatible with the Pavement-ME
3. Extract PDs, and sensor data for each project
4. Summarize time-series data for each project

The identified and extracted pavement distresses and conditions for flexible and rigid pavements are summarized in Tables 3-1 and 3-2. A detailed discussion of the conversion process is presented for both flexible and rigid pavements.

Table 3-1 Flexible pavement distresses

Flexible pavement distress	MDOT principle distresses (PDs)	MDOT units	Pavement-ME units	Conversion needed?
IRI	Directly measured	in/mile	in/mile	No
Top-down cracking	204, 205, **724, 725**	miles	ft/mile	Yes
Bottom-up cracking	234, 235, **220, 221, 730, 731**	miles	% area	Yes
Thermal cracking	**101,** 103, 104, 114, **701, 703, 704,** 110	No. of occurrences	ft/mile	Yes
Rutting	Directly measured	in	in	No
Reflective cracking	No specific PD	None	% area	N/A

Note: Bold numbers represent older PDs that are not currently in use

Table 3-2 Rigid pavement distresses

Rigid pavement distresses	MDOT principle distresses	MDOT units	Pavement-ME units	Conversion needed?
IRI	Directly measured	in/mile	in/mile	No
Faulting	Directly measured	in	in	Yes
Transverse cracking	112, 113	No. of occurrences	% slabs cracked	Yes

3.2.1.2. Pavement distress unit conversion for HMA designs

It should be noted that only the distress types predicted by the Pavement-ME were considered for the local calibration. The corresponding MDOT PDs were determined and compared with distress types predicted by the Pavement-ME to verify if any conversions were necessary. The MDOT measured pavement distresses that are related to HMA pavements are listed in Table 3-1. The conversion process (if necessary) for all distress types is as follows:

IRI: The IRI measurements in the MDOT sensor database are compatible to those in the Pavement-ME. Therefore, no conversion or adjustments were needed and the data were used directly.

Top-down cracking: Top-down cracking is defined as load related longitudinal cracking in the wheel-path. The PDs 204, 205, 724, and 725 were assumed to correspond to the top-down cracking in the MDOT PMS database because those may not have developed an interconnected pattern which indicates alligator cracking. Those cracks may show an early stage of fatigue cracking which could also be bottom-up. The PDs are recorded in miles and needs conversion to feet/mile. Data from the wheel-paths were summed into one value and divided by the total project length.

Bottom-up cracking: The bottom-up cracking is defined as alligator cracking in the wheel-path. The PDs 234, 235, 220, 221, 730 and 731 match this requirement in the MDOT PMS database. The PDs have units of miles; however, to make those compatible with the Pavement-ME alligator cracking units, conversion to percent of total area is needed. This can be achieved by using the following Equation (1):

$$\%AC_{bottom-up} = \frac{\text{Length of cracking (miles)} \times \text{width of wheelpaths (feet)}}{\text{Length of project (miles)} \times \text{Lane width (feet)}} \times 100 \qquad (1)$$

The width of each wheel path and lane width were assumed to be 3 feet and 12 feet, respectively. The typical wheelpath width of 3 feet is recommended by the LTPP distress identification manual (*1*). However, in future local calibrations MDOT associated distress can be considered to verify the width associated with alligator cracking in the wheelpath. It should be noted that the bottom-up and top-down fatigue cracking in the wheel paths (6 feet) are combined for new HMA reconstruct projects due to the difficulty determining the source (top or bottom) of the fatigue cracks observed at the surface.

Thermal cracking: Thermal cracking corresponds to transverse cracking in flexible pavements. The Pavement-ME predicts thermal cracking in feet/mile. The PDs 101, 103, 104, 114, 701, 703 and 704 were utilized to extract transverse cracking in flexible and rubblized pavements. For the composite pavement, PDs 101, 110, 114 and 701 were used. The transverse cracking is recorded as the number of occurrences. In order to convert transverse cracking into feet/mile, the number of occurrences was multiplied by the lane width for PDs 101, 103 and 104. For the PDs 114 and 701, the number of occurrences was multiplied by 3 feet because these PDs are defined as "tears" (short cracks) that are less than half the lane width. All transverse crack lengths were summed and divided by the project length to get feet/mile as shown in Equation (2).

$$TC = \frac{\sum No.\ of\ Occurences \times Lane\ Width(ft)}{Project\ Length\ (miles)} \quad (2)$$

Rutting: This is the total amount of surface rutting contributed by all the pavement layers. The average rutting (left & right wheel-paths) was determined for the entire project length. No conversion was necessary. It is assumed that the measured rutting corresponds to total surface rutting, and was compared to the total rutting predicted by the Pavement-ME.

Reflective cracking: MDOT does not have any specific PDs for reflective cracking. It is difficult to determine the difference between a thermal and a reflective crack at the surface. Therefore, the total transverse cracking observed can be compared to the total combined thermal and reflective cracking. Reflective cracking was not included in verification for this reason and due to the limitations of the prediction model in the Pavement-ME.

3.2.1.3. Pavement distress unit conversion for JPCP designs

As mentioned before, only the distresses that are predicted by the Pavement-ME were considered for the verification. The corresponding MDOT PDs were determined and necessary conversions were applied if needed. Table 3-2 summarizes the distresses related to JPCP overlays and the conversion process is discussed below:

IRI: The IRI in the MDOT sensor database does not need any conversion; the values were used directly

Faulting: Faulting is predicted as average joint faulting by the Pavement-ME. The faulting values reported in the MDOT sensor database corresponds to the average height of all faults at a discontinuity observed for an entire 0.1 mile (528 feet) section. However, the Pavement-ME faulting prediction does not distinguish between faulting at cracks or joints and only predicts faulting at the joints. Therefore, only measured average joint faulting should be compared with the predicted faulting by Pavement-ME. Because MDOT's data does not discern between faults at cracks and joints, the average joint faulting needs to be calculated. The average joint faulting is calculated using Equation (3):

$$Fault = \frac{FAULnum \times FAULi}{(528/Joint\ Spacing)} \quad (3)$$

where:

FAULnum = Number of faults in a 0.1 mile

$FAUL_i$ = Average faulting in a 0.1 mile (inches)
Joint Spacing = Joint spacing for the project

It should be noted that it may be possible that the number of faults measured exceed the number of joints in a 0.1 mile section. In this case, the faulting at cracks is included in the average faulting value. As mentioned before, such crack faulting is not predicted by the Pavement-ME. Therefore, if the number of faults is greater than the number of joints, the 0.1 mile pavement section should not be included in the calibration dataset.

Transverse cracking: The transverse cracking distress is predicted as % slabs cracked in the Pavement-ME. However, MDOT measures transverse cracking as the number of transverse cracks. The PDs 112 and 113 correspond to transverse cracking. The measured transverse cracking needs conversion to percent slabs cracked by using Equation (4).

$$\%\ \text{Slabs Cracked} = \frac{\sum PD_{112,113}}{\left(\frac{\text{Project Length(miles)} \times 5280\ ft}{\text{Joint Spacing (ft)}}\right)} \times 100 \quad (4)$$

3.2.2 Condition Database for Local Calibration

Customized PMS and sensor databases were created in order to query the selected PDs. The databases include all the distress and sensor data for multiple years in respective Microsoft Access databases. These compiled databases allowed the research team to extract condition data efficiently for any project length. The databases included measured PMS condition data from 1992 to 2011 and the sensor data from 1996 to 2011. The sensor data prior to 1996 were not in a consistent format and could not be included in the custom database. The time series condition data were extracted for each selected project. A divided highway can have an increasing and a decreasing direction to indicate north/south or east/west bounds directions. Therefore, for such projects, both directions are included in the time-series data and were considered as two sections. Distress data for undivided highways are collected in one direction only. It should be noted that a "project" corresponds to a specific job number in the construction records; however, a "section" corresponds to multiple directions in a divided highway with in a project. Therefore, the number of sections is always more than the number of projects.

3.3 PROJECT SELECTION CRITERIA

In order to locally calibrate the performance prediction models, in-service pavement sections are selected which represent Michigan pavement design, construction practices, and performance. These pavement sections should represent all current pavement types and rehabilitation types which are constructed by MDOT. The MSU research team established project selection criteria to identify and select these pavement sections. Part 2 (*2*) of the study identified and selected the various rehabilitation sections, and Part 3 focused on newly reconstructed pavements. The process for identifying and selecting pavement sections consists of the following steps:

1. Determine the minimum number of pavement sections based on the statistical requirements
2. Identify all available in-service pavement projects constructed after 1992
3. Extract all pavement distresses from the customized database for all identified projects
4. Evaluate the measured performance for all the identified projects
5. Establish a refined list of the potential projects which exhibit multiple distresses with adequate magnitude

3.3.1 Identify the Minimum Number of Required Pavement Sections

The first step for project identification and selection consists of determining the adequate number of pavement sections for local calibration based on statistical needs. The NCHRP 1-40B (*3*) suggests a method to determine the minimum number of sections for each condition measure. The minimum number of sections was calculated using Equation (5) and the results are summarized in Table 3-3 for each condition measure.

$$n = \left(\frac{Z_{\alpha/2} \times \sigma}{e_t} \right)^2 \quad (5)$$

where:

$Z_{\alpha/2}$ = The z-value from a standard normal distribution
n = Minimum number of pavement sections
σ = Performance threshold
e_t = Tolerable bias $Z_{\alpha/2} \times SEE$
SEE = Standard error of the estimate

Table 3-3 Minimum number of sections for local calibration

Performance Model	Nationally calibrated SEE	Z_{90}	Threshold	*N* (required number of sections)	Number of sections used	Total number of projects available
Flexible Pavements						
Alligator cracking (%)	5.01	1.64	20	16	121	108[2] 33[3]
Longitudinal cracking (ft/mile)	600		2000	12	165	
Thermal cracking[1]	-		-	-	169	
Rutting (in)	0.107		0.5	22	162	
IRI (in/mile)	18.9		172	83	167	
Rigid Pavements						
Transverse cracking (%)	4.52	1.64	15	11	31	20[2] 8[3]
Joint faulting (in)	0.033		0.25	57	49	
IRI (in/mile)	17.1		172	101	44	

N= minimum number of samples required for 90% confidence level
1. No *SEE*, threshold or *N* was reported for thermal cracking in the literature
2. A total of 108 and 20 projects were identified for flexible and rigid pavements, respectively, based on the construction date and PMS data availability
3. Rehabilitation projects selected from Part II of the project

3.3.2 Available In-Service Pavement Projects

The research team first identified (in consultation with MDOT) the most common pavement and rehabilitation types that are constructed throughout Michigan. The reconstruct and rehabilitation pavement types considered include:

1. HMA reconstruct
2. HMA crush & shape
3. HMA over HMA
4. HMA over rubblized PCC
5. HMA over PCC (composite)
6. JPCP reconstruct, and
7. Unbonded concrete overlay

MDOT identified and provided the rehabilitation projects (unbonded, rubblized and composite overlays) for local calibration. The research team identified the pavement sections for flexible reconstruct, crush and shape and HMA over HMA, and rigid JPCP reconstruct pavements. The pavement projects to be included in the study were selected based on the following criteria:

- *Site factors*: The site factors addressed the various regions in the state, climatic zones and subgrade soil types.
- *Traffic*: Three traffic categories were selected; less than 1000 AADTT, 1000 to 3000 AADTT; and more than 3000 AADTT. The three levels were selected based on pavement class, trunk-line routes, US routes and Interstate routes.
- *Thicknesses*: The range of constructed HMA, PCC and overlay thicknesses.
- *Open to traffic date*: The information is needed to determine the performance period.
- *As built cross-section*: Includes details of the existing structure and the overlay other than layer thickness (e.g., joint spacing, lane width, and number of lanes etc.)
- Pre-overlay repairs performed on the existing pavement (such as partial and/or full depth repairs, dowel bar retrofit).
- Material properties of both the existing and the new structure.

A procedure similar to the identification of HMA over HMA projects from the Part 2 Final Report was performed to identify projects for the calibration of reconstructed rigid and flexible pavements. For each identified pavement project, the following details were extracted from an Excel file provided by MDOT:

1. MDOT region
2. Control section number
3. Job number
4. Beginning mile point (BMP)
5. Ending mile point (EMP)
6. Year opened
7. Two way AADTT
8. Number of Distress Index (DI) points
9. Current pavement age

Initially, a total of 223 reconstruct pavement projects (job numbers) were identified based on the pavement age (constructed after 1992). Later, the measured condition data were extracted from the PMS and Sensor databases for all the 223 pavement projects. The projects that had very low levels of measured distress or no available data were excluded from the final list. Thus, there were 108 (22 flexible freeway, 63 non-freeway, and 23 crush & shape) flexible and 20 JPCP pavement projects available for the local calibration. Figures 3-1 through 3-4 show the geographical distribution of the initial and revised number of identified projects based on a measured condition evaluation for new reconstruct and crush and shape project. Details for rehabilitation projects are summarized in the Part 2 Final Report (*4*). The extracted condition data were analyzed to evaluate the following trends:

- Increasing trend (i.e., positive progression of distress over time)
- Decreasing trend (i.e., negative progression of distresses over time which may happen because of maintenance history, or measurement errors)
- Flat line (i.e., no progression over time)
- Not enough data (i.e., inadequate measured condition over time)
- No trend (i.e., high variability among different measurement cycles)

If a project showed an increasing trend for any of the condition measures it was included in the final list. Projects that had insufficient condition data, showed no time series trend, or showed a consistent flat line (no growth over time) with minimal magnitude were removed. The total number of increasing trends were determined from the final project list and compared to the minimum number of sections needed for each performance model.

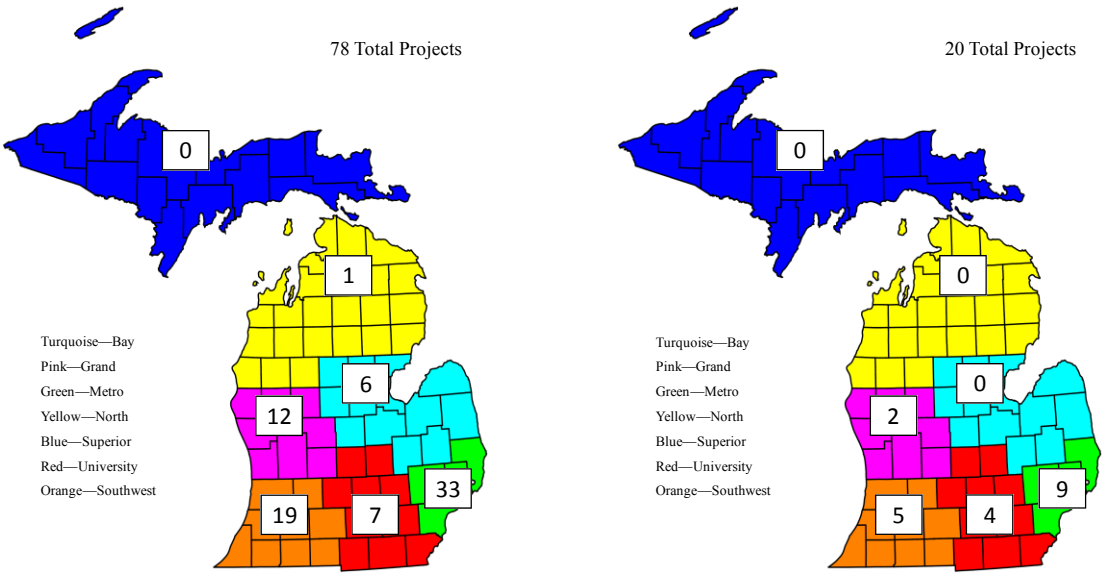

(a) Initial projects (b) Revised projects

Figure 3-1 Geographical location of identified JPCP reconstruct projects

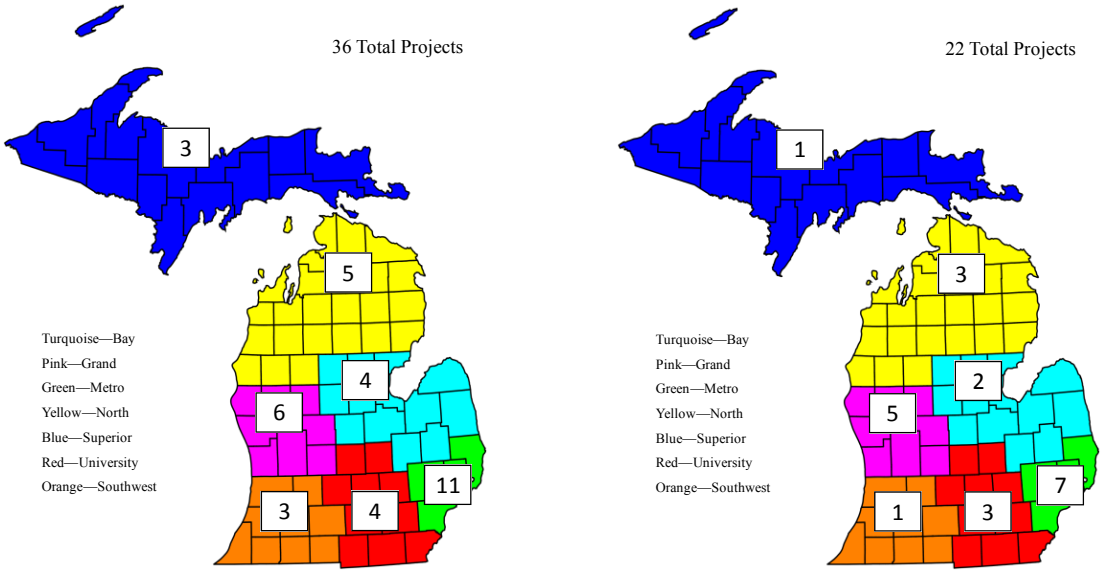

(a) Initial projects (b) Revised projects

Figure 3-2 Geographical location of identified freeway HMA reconstruct projects

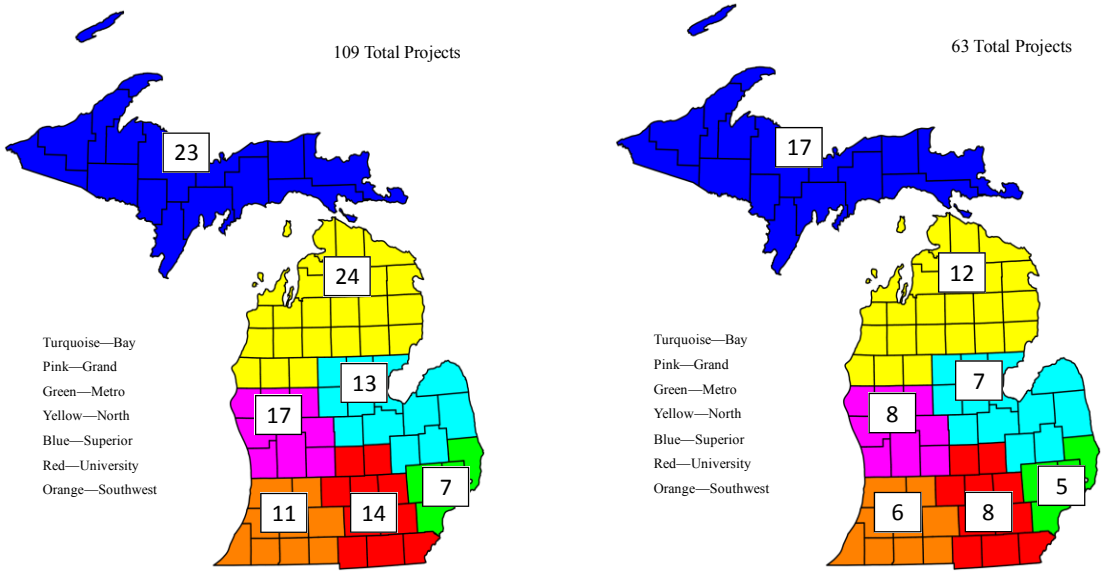

(a) Initial projects (b) Revised projects

Figure 3-3 Geographical location of identified non-freeway HMA reconstruct projects

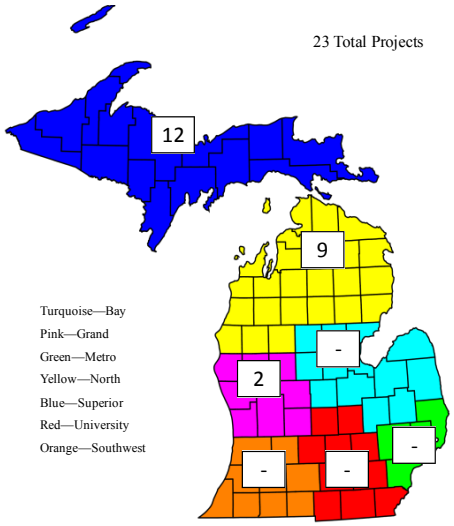

Figure 3-4 Geographical location of identified crush and shape projects

3.3.3 Summary of Selected projects

The final revised list of identified projects was sent to MDOT to acquire the necessary construction, design, and material related inputs. The research team assisted in the extraction of the requested information from the construction records. Tables 3-4 and 3-5 summarize the selected reconstruct and rehabilitation projects. Additionally, Tables 3-6 and 3-7 summarizes the selected projects based on the design matrix for reconstruct and rehabilitation projects. The crush & shape projects were analyzed as a new pavement since a specific rehabilitation option is not available in the Pavement-ME software. Therefore, those projects were included in Table 3-6 (rehabilitation) instead of Table 3-7 (reconstruct). Additional details for each selected pavement section are summarized in Appendix A.

Table 3-4 Number of reconstruct projects for each pavement type

Pavement type	MDOT region	Number of projects
Crush and Shape	Grand	2
	North	9
	Superior	12
HMA Reconstruct Freeway	Bay	2
	Grand	5
	Metro	7
	North	3
	Southwest	1
	Superior	1
	University	3
HMA Reconstruct Non-Freeway	Bay	7
	Grand	8
	Metro	5
	North	12
	Southwest	6
	Superior	17
	University	8
JPCP Reconstruct	Grand	2
	Metro	11
	Southwest	4
	University	3
Total		128

Table 3-5 Number of rehabilitation projects by MDOT region

Pavement type	MDOT region	Number of projects
Composite overlay	Bay	3
	Grand	1
	Metro	1
	North	1
	Southwest	1
HMA over HMA overlay	Bay	1
	North	5
	Southwest	7
	Superior	1
	University	1
Rubblized overlay	Grand	3
	North	4
	Southwest	1
	University	3
Unbonded overlay	Grand	1
	North	1
	Southwest	4
	University	2
Total		41

Table 3-6 Selection matrix displaying selected projects (rehabilitation sections)

Rehabilitation type	Traffic level*	Overlay thickness level*	Age (years)			Total
			<10	10 to 20	>20	
Composite overlay	1	2		1	1	7
	2	2		2	2	
	3	2			1	
HMA over HMA	1	1			7	15
		2	1	5		
	2	2	1		1	
Rubblized overlay	1	2		4	2	11
		3		2		
	2	2			1	
	3	2			1	
		3		1		
Unbonded overlay	2	2		1		8
		3		1		
	3	3	1	5		
Total			3	22	16	41

*Levels	1	2	3
Traffic (AADTT)	<1000	1000-3000	>3000
Overlay thickness (in)	<3	3-6	>6

Table 3-7 Selection matrix displaying selected projects (reconstruct sections)

Road type	Traffic level*	Thickness level*	Age Level			Total
			<10	10-15	>15	
Crush and Shape	1	1			4	4
		2		5	8	13
		3				
	2	1				
		2		1	5	6
		3				
	3	1				
		2				
		3				
HMA Reconstruct Freeway	1	1				
		2	1	3		4
		3		4	1	5
	2	1				
		2			1	1
		3		4	2	6
	3	1				
		2		1		1
		3	1	3	1	5
HMA Reconstruct Non-Freeway	1	1			1	1
		2	10	25	12	47
		3		8	1	9
	2	1				
		2	1	2	1	4
		3	1	1		2
	3	1				
		2				
		3				
JPCP Reconstruct	1	1				
		2				
		3		1		1
	2	1				
		2				
		3		1		1
	3	1				
		2				
		3	3	9	6	18
Total			17	68	43	128

*Levels	1	2	3
Traffic (AADTT)	<1000	1000-3000	>3000
Thickness (in)	<3	3-7	>7

3.4 CONDITION DATA FOR LOCAL CALIBRATION

The measured condition for each project was extracted and the necessary conversions were made to ensure compatibility with Pavement-ME predicted performance as discussed in Section 3.2.

3.4.1 Extent of Measured Condition

A thorough investigation was performed to determine the extent of distress among all pavement sections identified for the local calibration. The calibration process involves comparisons of predicted and measured performance for each selected projects. For a robust local calibration, the distress magnitudes should cover a reasonable range (i.e., above and below threshold limits for each distress type). Therefore, the distress magnitudes for all projects were summarized to determine their ranges. The initial calibration process involved 41 rehabilitation projects from Part 2. However, there was a need to include new pavements (i.e., projects which were not rehabilitated in the past) in the calibration database. Therefore, an additional 128 projects (HMA and JPCP) were selected based on the criteria discussed in Section 3.3. To further increase the calibration database, LTPP pavement sections located in Michigan and the surrounding States were considered, especially for rigid pavements.

The summary of measured performance is presented for the selected rehabilitation, reconstruction, and LTPP pavement sections. The following efforts ensure adequacy of the information needed for a robust and accurate local calibration of the performance models:

a. A total of 41 rehabilitation projects were considered in the local calibration. Thirty three projects have an HMA surface layer while 8 projects are JPCP unbonded overlays. These 33 HMA and 8 PCC unbonded overlay projects were analyzed to test the calibration procedures for different distresses in flexible and rigid pavements, respectively.

    - *HMA overlay performance data*: The magnitude and age distribution for the HMA rehabilitation projects are shown in Figures 3-5 to 3-8. The following observations can be made from results in the figures:

        - Longitudinal/top-down fatigue cracking: there is a good representation of distress above and below the threshold value of 2000 ft/mile. The age at maximum distress ranged from 8 to 20 years. It should be noted that the magnitude of bottom-up cracking predictions for rehabilitation design are always low and therefore, only longitudinal cracking is considered for such designs.
        - Rutting: Most of the projects did not exhibit significant rutting. Only one project reached the threshold value of 0.5 inches. The age distribution ranged from 6 to 20 years.
        - Transverse (thermal) cracking: The thermal cracking for the rehabilitation projects ranged from 250 to over 3000 feet/mile. The age at which the maximum thermal cracking occurred ranged from 4 to 20+ years. It should be noted that some of the thermal cracks could actually be reflective cracks. MDOT PMS does not distinguish between a reflective or transverse (thermal) crack.

- IRI: Most of the projects had IRI values less than the threshold. Three projects exceeded the threshold value of 172 inch/mile. The age at maximum IRI ranged from 4 to 20 years

- *Unbonded overlay performance data*: The magnitude and age distribution for the JPCP rehabilitation projects are shown in Figures 3-9 and 3-11. The following observations can be made from the figures:

  - Transverse cracking: None of the projects exceed the distress threshold of 15% slabs cracked. The age distribution ranges from 8 to 12 years.
  - Transverse joint faulting: None of the projects exceed the faulting threshold of 0.25 inch. The age distribution ranges from 4 to 12 years.
  - IRI: None of the unbonded overlay projects exceeded the IRI threshold of 172 in/mile. The age at maximum IRI ranges from 8 to 12 years.

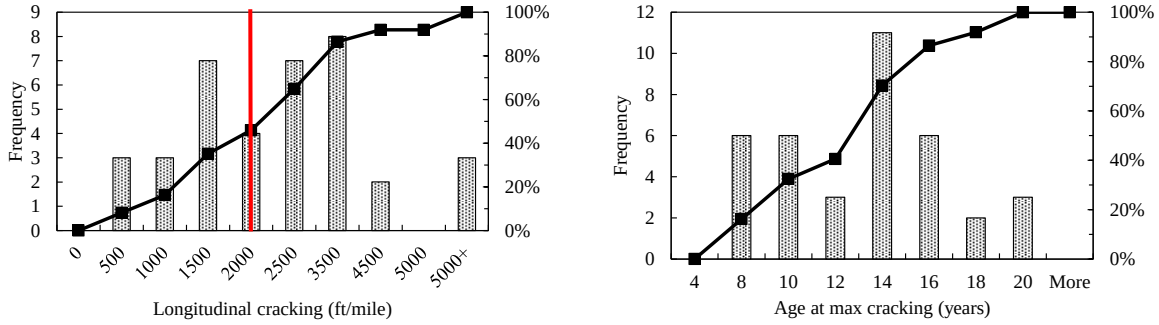

(a) Distress magnitude (b) Age distribution

Figure 3-5 Selected HMA rehabilitation sections — longitudinal cracking data

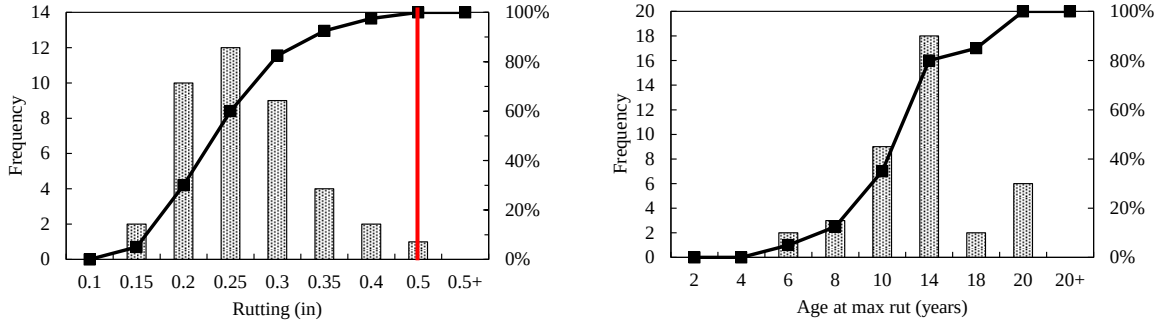

(a) Distress magnitude (b) Age distribution

Figure 3-6 Selected HMA rehabilitation sections — rutting data

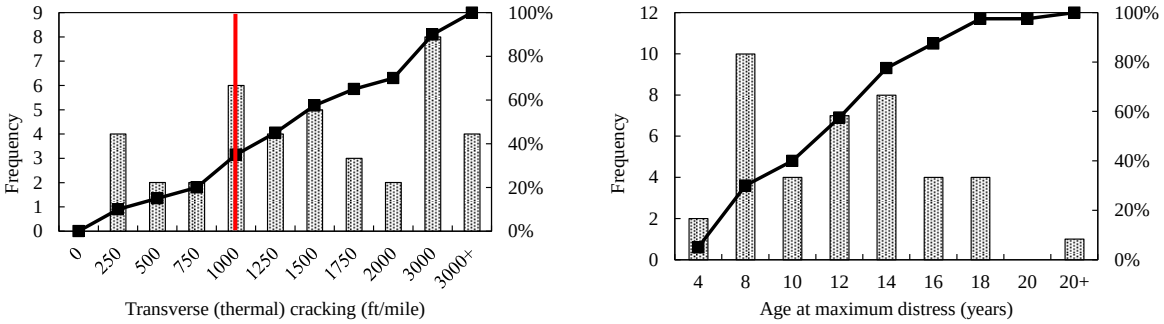

(a) Distress magnitude (b) Age distribution

Figure 3-7 Selected HMA rehabilitation sections — Transverse (thermal) cracking data

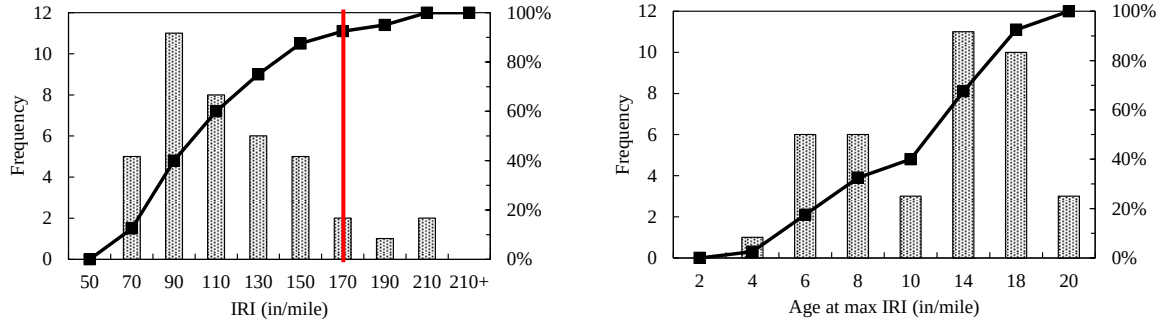

(a) Distress magnitude (b) Age distribution

Figure 3-8 Selected HMA rehabilitation sections — IRI data

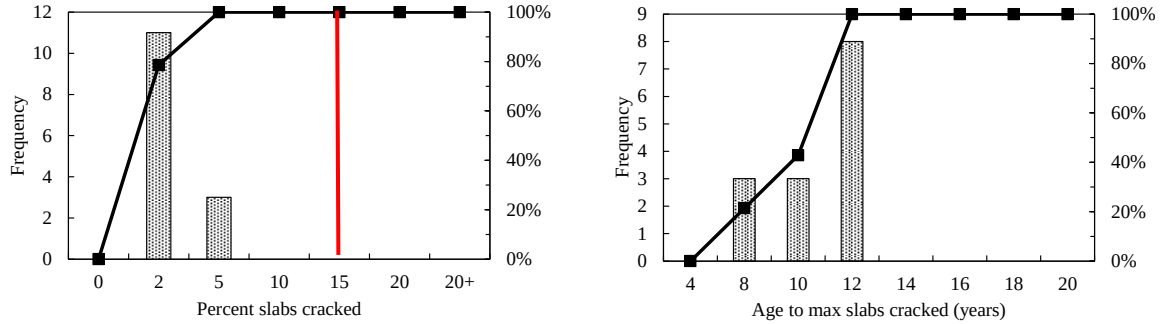

(a) Distress magnitude (b) Age distribution

Figure 3-9 Selected JPCP rehabilitation sections — cracking data

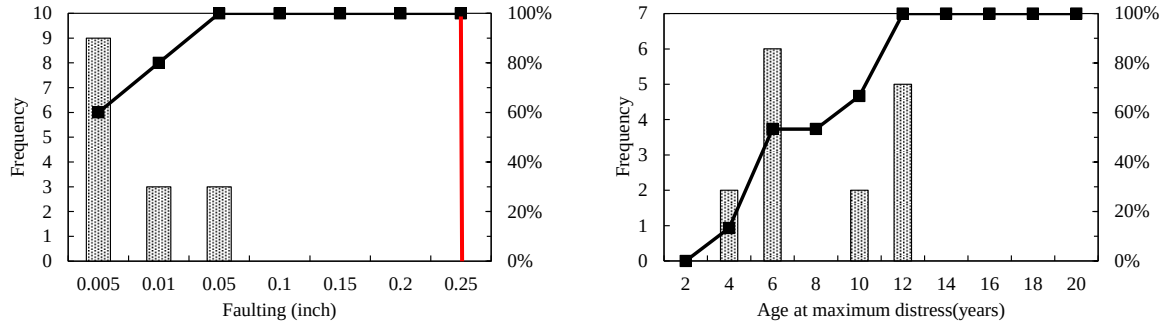

(a) Distress magnitude (b) Age distribution

Figure 3-10 Selected JPCP rehabilitation sections — joint faulting data

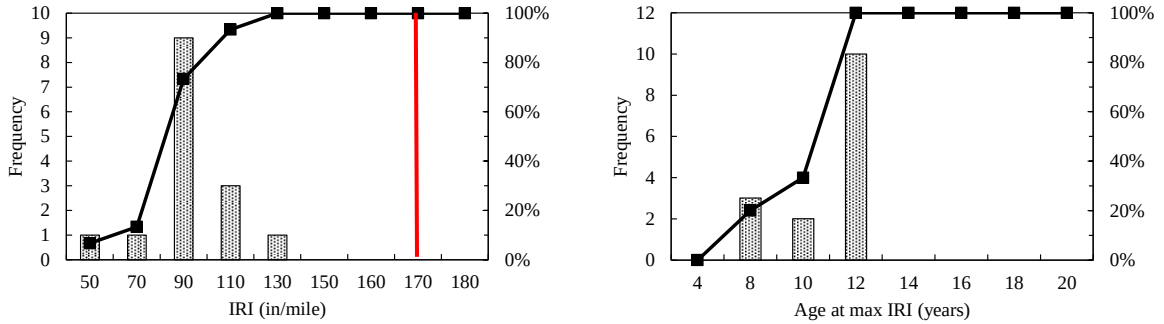

(a) Distress magnitude (b) Age distribution

Figure 3-11 Selected JPCP rehabilitation sections — IRI data

b. The research team selected 108 HMA and 20 JPCP reconstruct pavement projects in the state of Michigan.

- *Reconstruct performance data*: The magnitude and age distribution for the HMA freeway, non-freeway, crush and shape and JPCP projects are shown in Figures 3-12 to 3-29. The following observations were made:

  - HMA freeway alligator cracking: The distress magnitude ranged from 5 to 40 percent for the selected projects. Only four projects exceeded the distress threshold of 20%. The age at maximum distress ranged from 8 to 16 years.
  - HMA freeway longitudinal cracking: The distress magnitude ranged from 250 to over 3000 feet/mile for the selected projects. Only six projects exceeded the distress threshold of 2000 feet/mile. The age at maximum distress ranged from 6 to 18 years.
  - HMA freeway rutting: The rut depth ranged from 0.1 to 0.5+ inches. The rutting threshold of 0.5 was exceeded by one project. The age at maximum rutting ranged from 8 to 18 years.
  - HMA freeway thermal cracking: The thermal cracking for the selected pavement sections ranged from 50 to 1200 ft/mile. The distress threshold of 1000 ft/mile was exceeded by 9 pavement sections. The age at which the maximum distress occurred ranged from 4 to 18 years.
  - HMA freeway IRI: The observed IRI for HMA freeway projects ranges between 50 and 190+ in/mile. However, only one project exceeded the threshold value of 172 in/mile. The age at maximum IRI ranges from 4 to 18 years.
  - HMA non-freeway alligator cracking: The distress magnitude ranged from 5 to 50 percent for the selected projects. Ten projects exceeded the distress threshold of 20%. The age at maximum distress ranged from 4 to 18 years.
  - HMA non-freeway longitudinal cracking: The distress magnitude ranged from 250 to over 3000 feet/mile for the selected projects. Seven projects exceeded the distress threshold of 2000 feet/mile. The age at maximum distress ranged from 2 to 16 years.
  - HMA non-freeway rutting: The rutting distress ranged from 0.15 to 0.5 inches. The rutting threshold of 0.5 was not exceeded by any of the projects. The age at maximum rutting ranged from 4 to 18 years.

- HMA non-freeway thermal cracking: The measured thermal cracking ranged from 50 to over 1200 feet/mile. The design threshold was exceeded by 18 pavement sections. The age at the maximum distress ranged from 4 to 18 years.
- HMA non-freeway IRI: The observed IRI for HMA non-freeway projects ranged between 50 and 280 in/mile. Six projects exceeded the threshold value of 172 in/mile. The age at maximum IRI ranged from 4 to 16 years.
- HMA crush & shape alligator cracking: The measured alligator cracking ranged from 5 to 40 percent for the selected projects. The age at which the maximum distress occurred ranged between 4 and 18 years.
- HMA crush and shape longitudinal cracking: The distress magnitude ranged from 250 to 2000 feet/mile for the selected projects. None of the projects exceeded the distress threshold of 2000 feet/mile. The age at maximum distress ranged from 8 to 18 years.
- HMA crush & shape rutting: The rutting distress ranged from 0.2 to 0.5 inches. None of the sections exceeded the rutting threshold of 0.5 inch. The age at maximum rutting varied between 4 and 14 years.
- HMA crush & shape thermal cracking: The thermal cracking ranged between 50 and over 1200 feet/mile. Two pavement sections exceeded the distress threshold of 1000 feet/mile. The age at maximum distress ranged between 8 and 16 years.
- HMA crush & shape IRI: The measured IRI ranged between 70 and 130 in/mile. None of the sections exceeded the design threshold of 172 in/mile. The age at which the maximum IRI occurred ranged between 4 and 18 years.
- JPCP transverse cracking: The transverse cracking for all projects ranged from 5–80% slabs cracked. Nine projects exceeded the distress threshold of 15% slabs cracked. The age at maximum transverse cracking ranged from 4-16 years.
- Transverse joint faulting: None of the projects exceed the faulting threshold of 0.25 inch. The age distribution ranges from 2 to 16 years.
- JPCP IRI: The measured IRI ranged between 70 and 170 in/mile for all projects. None of the projects exceeded the threshold value of 172 in/mile. The age at maximum IRI ranged between 4 and 16 years.

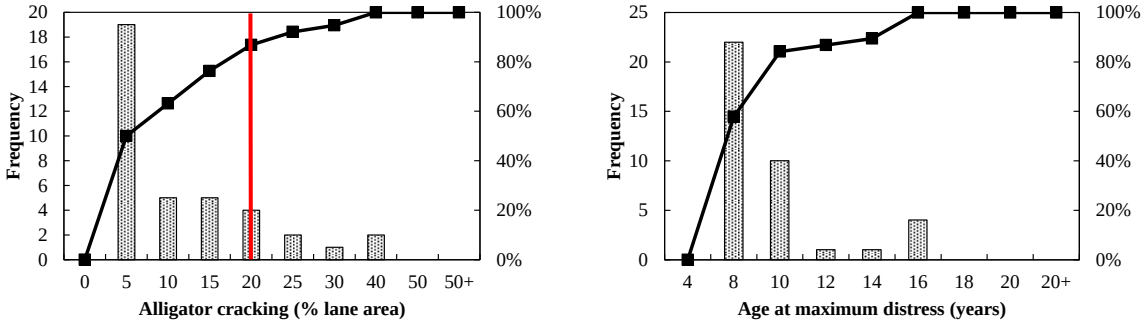

(a) Distress magnitude (b) Age distribution

Figure 3-12 Selected HMA freeway sections — alligator cracking data

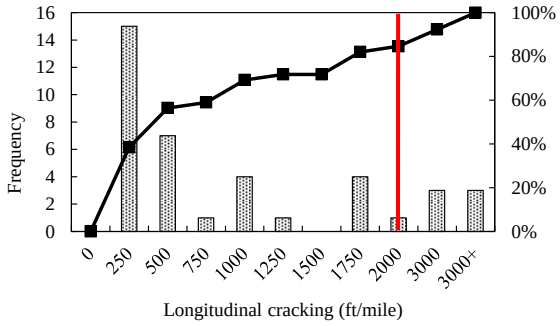

(a) Distress magnitude

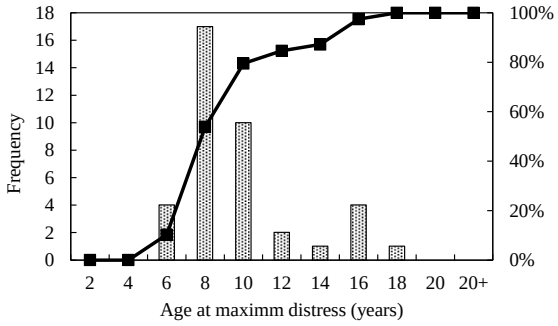

(b) Age distribution

Figure 3-13 Selected HMA freeway sections — longitudinal cracking data

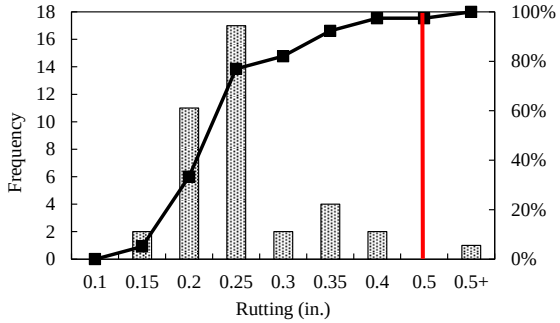

(a) Distress magnitude

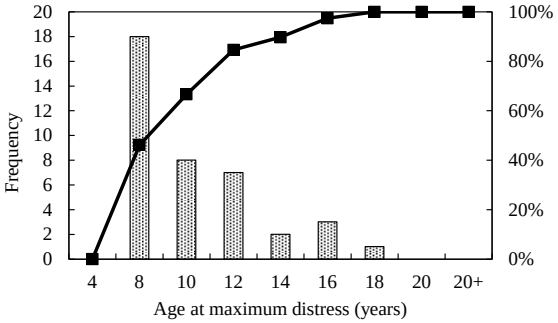

(b) Age distribution

Figure 3-14 Selected HMA freeway sections — rutting data

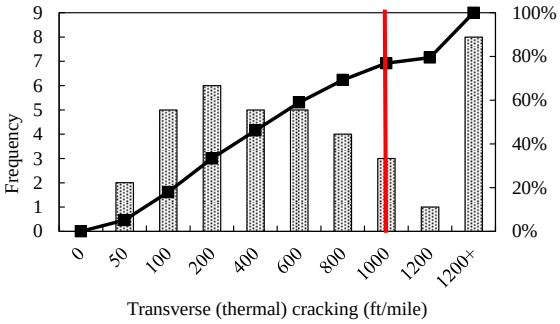

(a) Distress magnitude

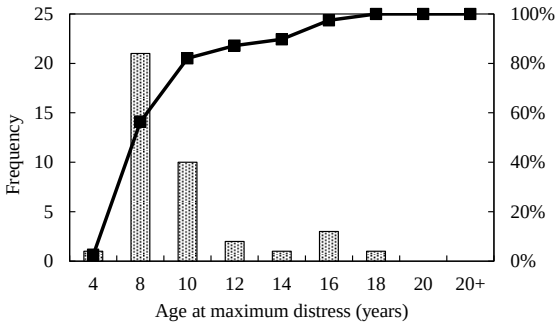

(b) Age distribution

Figure 3-15 Selected HMA freeway sections — thermal cracking data

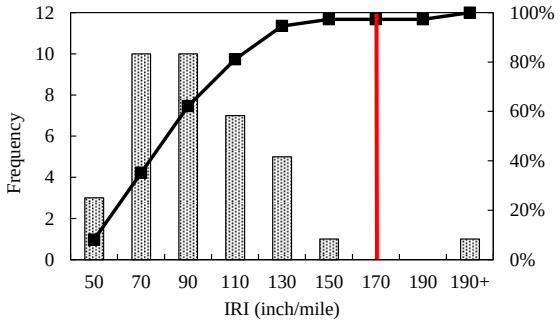

(a) Distress magnitude

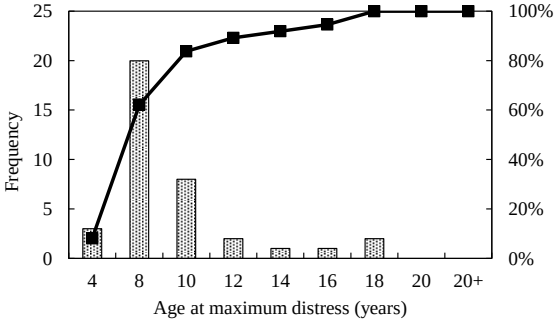

(b) Age distribution

Figure 3-16 Selected HMA freeway sections — IRI data

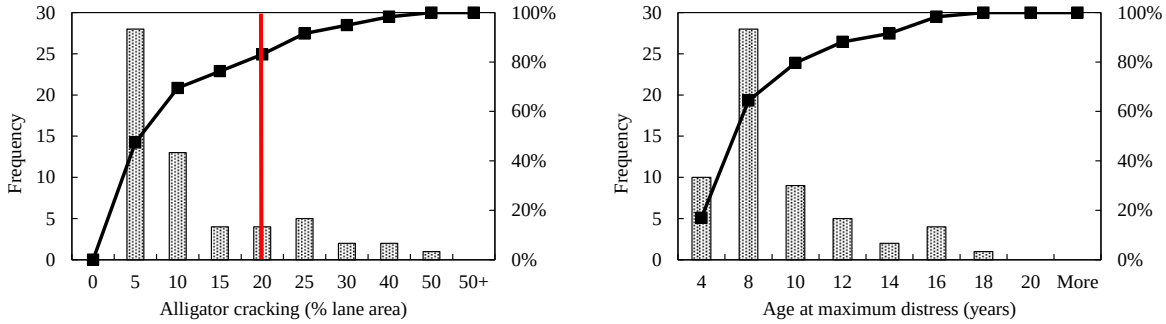

(a) Distress magnitude (b) Age distribution

Figure 3-17 Selected HMA non-freeway sections — alligator cracking data

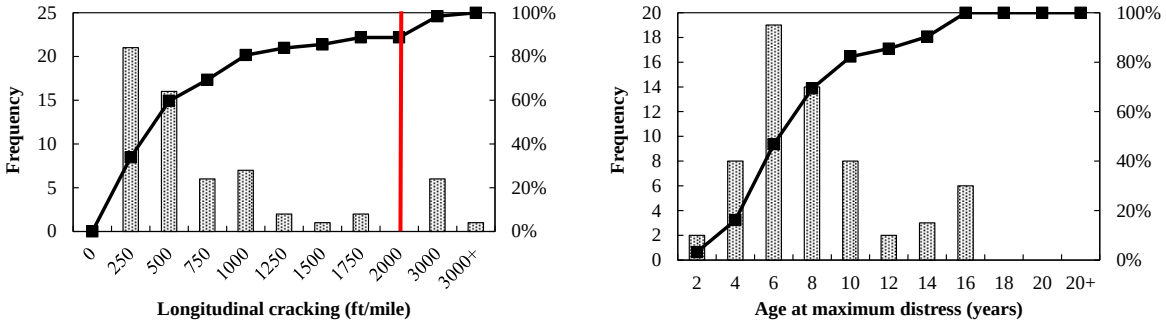

(a) Distress magnitude (b) Age distribution

Figure 3-18 Selected HMA non-freeway sections — longitudinal cracking data

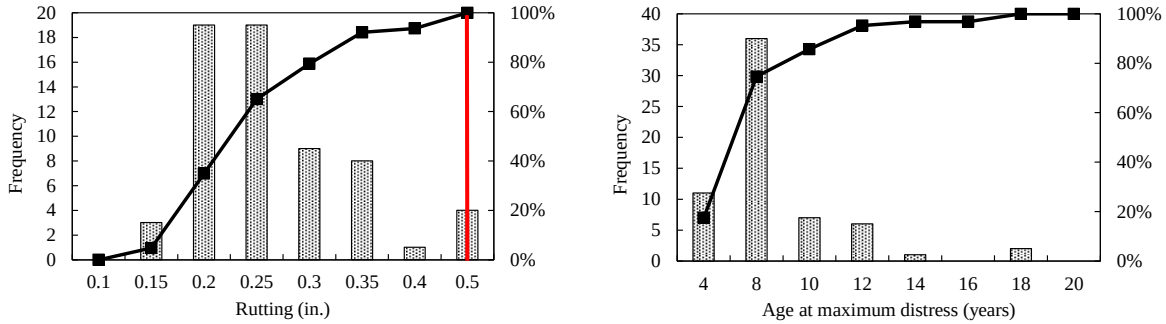

(a) Distress magnitude (b) Age distribution

Figure 3-19 Selected HMA non-freeway sections — rutting data

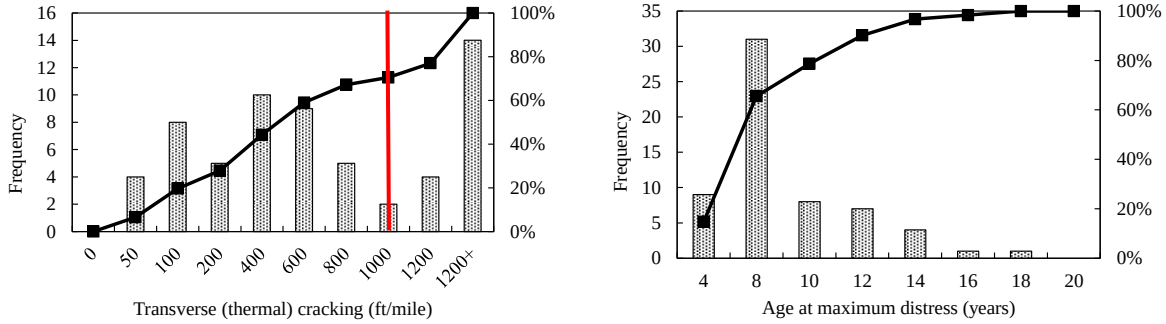

(a) Distress magnitude (b) Age distribution

Figure 3-20 Selected HMA non-freeway sections — thermal cracking data

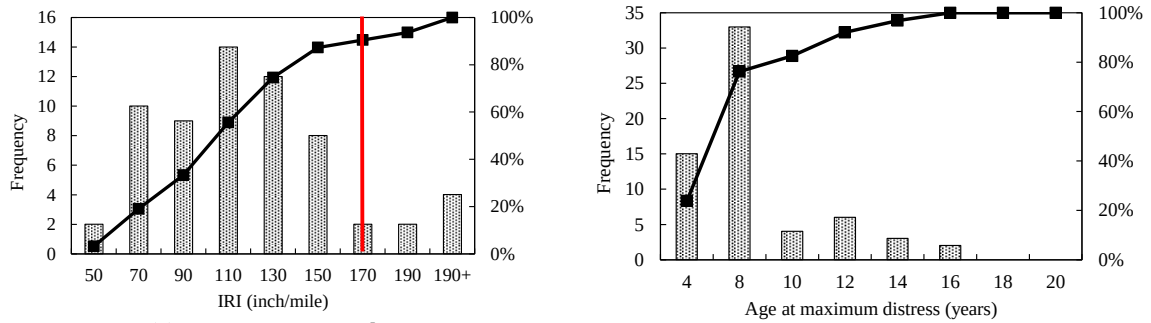

(a) Distress magnitude (b) Age distribution

Figure 3-21 Selected HMA non-freeway sections — IRI data

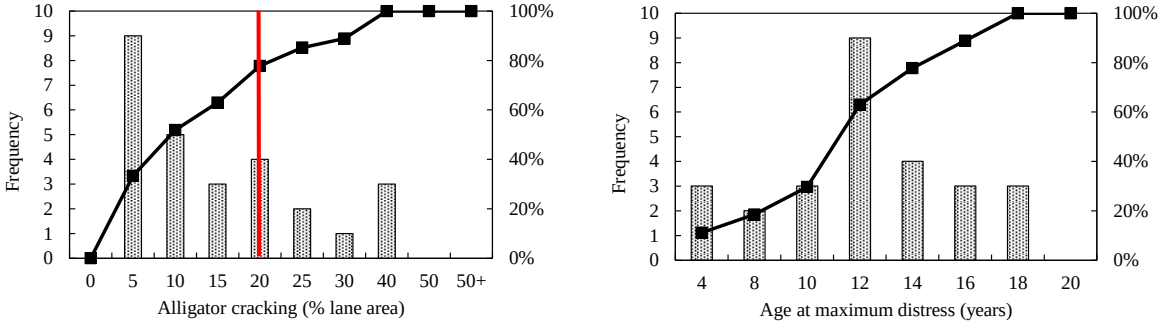

(a) Distress magnitude (b) Age distribution

Figure 3-22 Selected HMA crush and shape sections — alligator cracking data

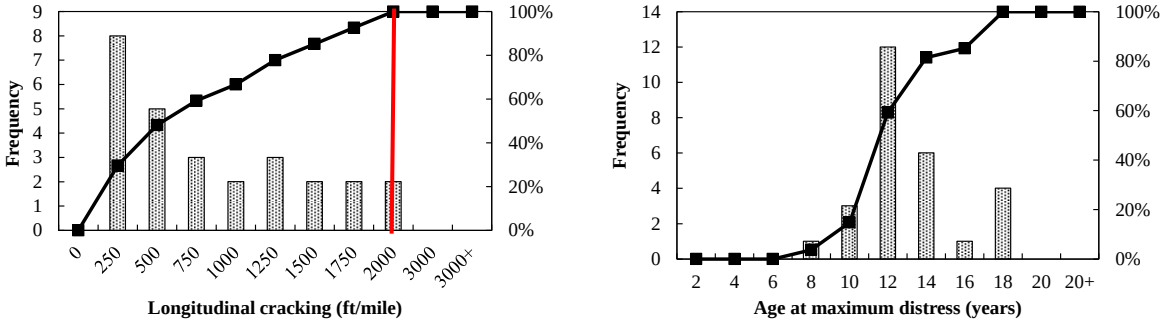

(a) Distress magnitude (b) Age distribution

Figure 3-23 Selected HMA crush and shape sections — longitudinal cracking data

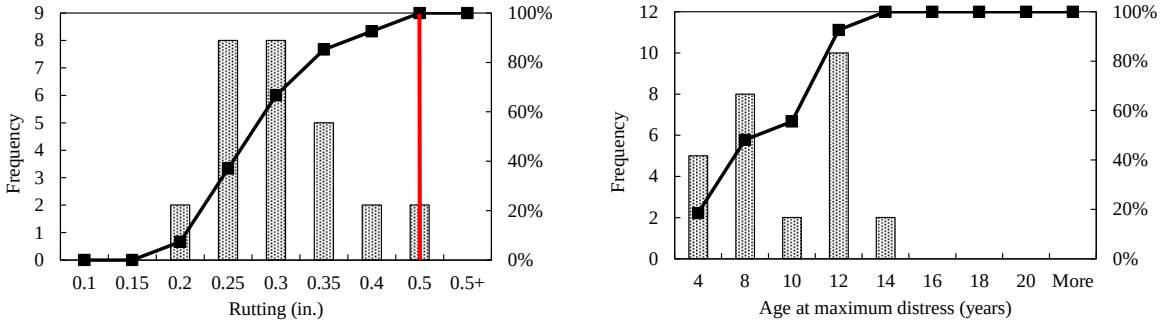

(a) Distress magnitude (b) Age distribution

Figure 3-24 Selected HMA crush and shape sections — rutting data

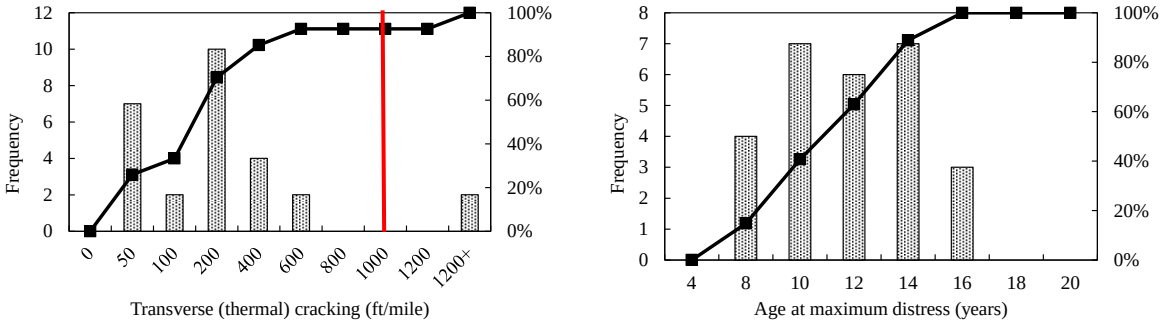

(a) Distress magnitude (b) Age distribution

Figure 3-25 Selected HMA crush and shape sections — thermal cracking data

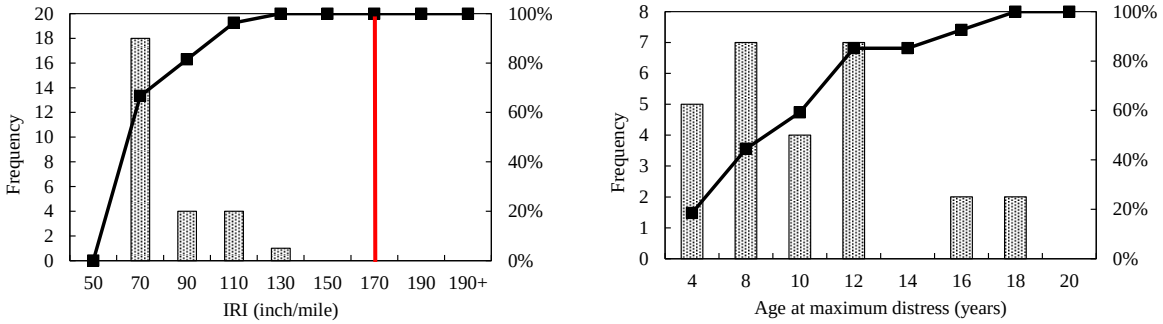

(a) Distress magnitude (b) Age distribution

Figure 3-26 Selected HMA crush and shape sections — IRI data

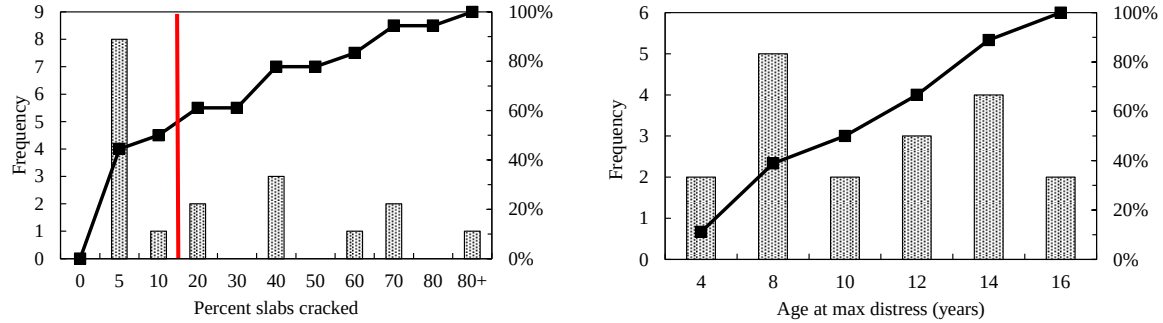

(a) Distress magnitude (b) Age distribution

Figure 3-27 Selected JPCP sections — transverse cracking data

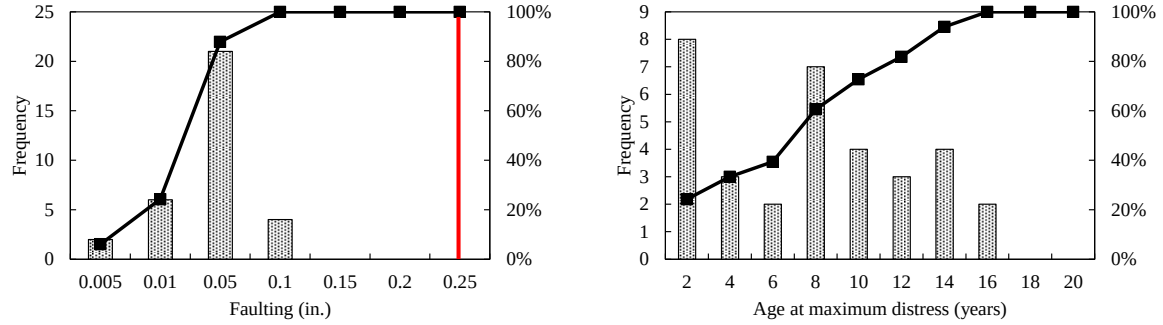

(a) Distress magnitude (b) Age distribution

Figure 3-28 Selected JPCP sections — joint faulting data

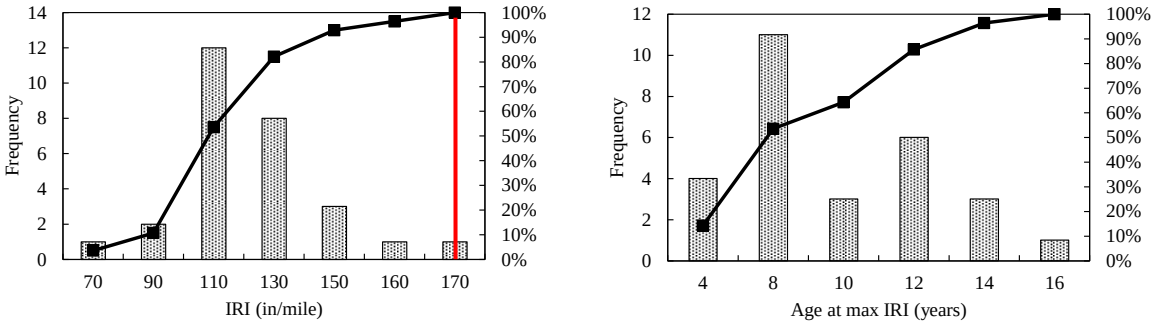

(a) Distress magnitude (b) Age distribution

Figure 3-29 Selected JPCP sections — IRI data

c. The LTPP pavement sections in Michigan and adjacent States were considered as part of the database to be used for the local calibration.

- *Flexible pavement performance data*: The magnitude of distresses and age distribution for the Michigan LTPP sections are shown in Figures 3-30 to 3-32. The performance data show that there are sufficient number of pavement sections exceeding the threshold values for cracking, rutting and IRI over time.

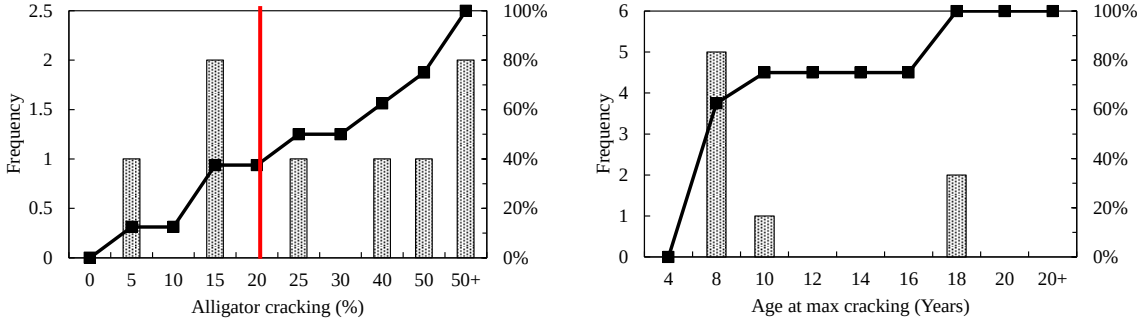

(a) Distress magnitude (b) Age distribution

Figure 3-30 Selected Michigan LTPP sections — alligator cracking data

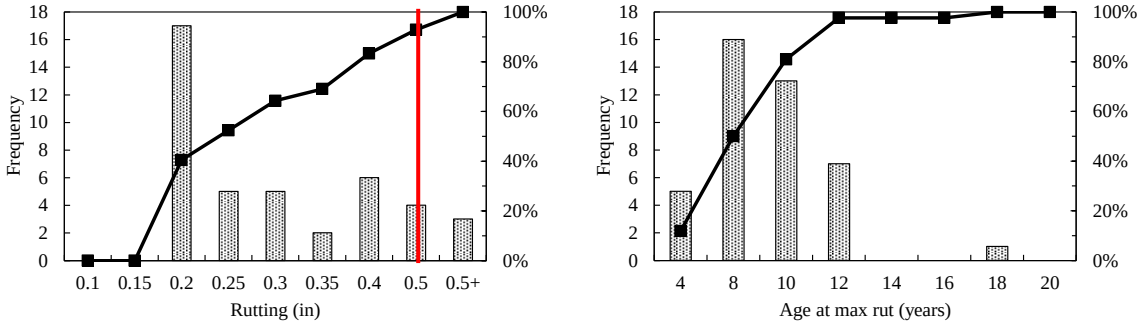

(a) Distress magnitude (b) Age distribution

Figure 3-31 Selected Michigan LTPP sections — rutting data

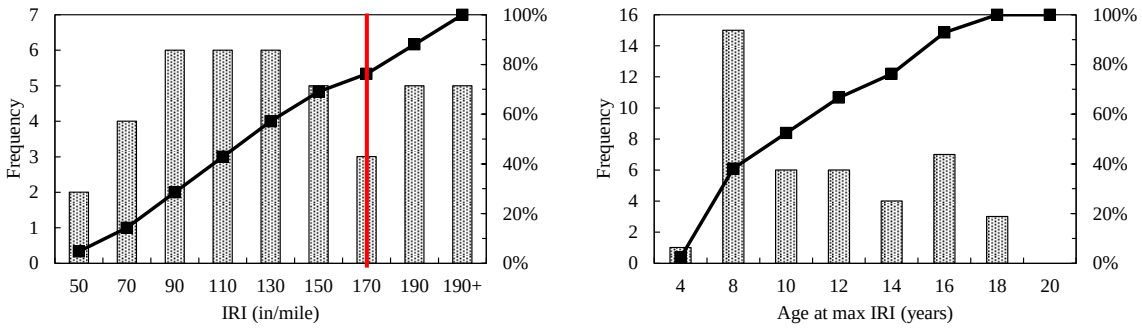

(a) Distress magnitude (b) Age distribution

Figure 3-32 Selected Michigan LTPP sections — IRI data

- *Rigid pavement performance data*: The magnitude of distresses and age distribution for the rigid LTPP sections are shown in Figures 3-33 to 3-35. The following observations were made:

  - Transverse cracking: The transverse cracking for the SPS-2 projects ranged from 10 to over 40 % slabs cracked. Three sections exceeded the distress threshold of 15% slabs cracked. The age at maximum transverse cracking ranged from 8 to18 years.
  - Faulting: None of the projects exceed the faulting threshold of 0.25 inch. The age at which maximum faulting occurred ranged from 6 to 8 years.
  - IRI: The maximum measured IRI ranged from 130 to greater than 180 in/mile for the selected SPS-2 projects. One section exceeded the threshold value of 172 in/mile. The age at maximum IRI ranged from 8 to 14 years.

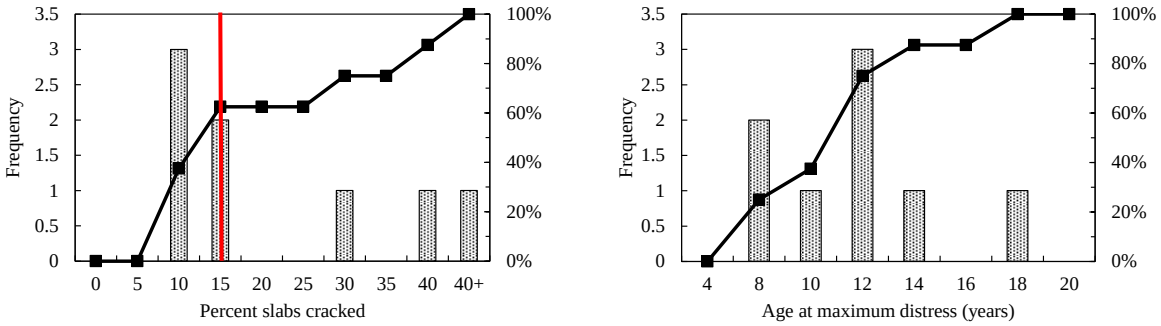

(a) Distress magnitude (b) Age distribution

Figure 3-33 Selected LTPP SPS-2 sections — transverse cracking data

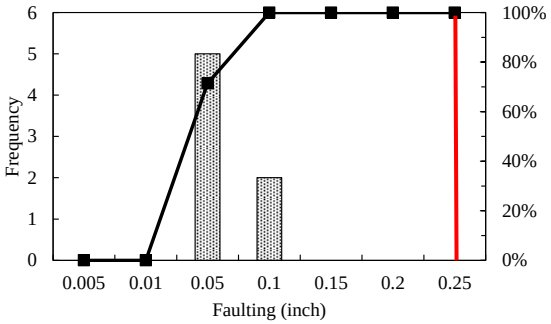

(a) Distress magnitude

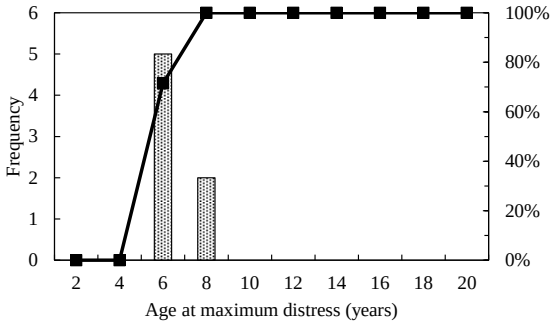

(b) Age distribution

Figure 3-34 Selected LTPP SPS-2 sections — transverse joint faulting data

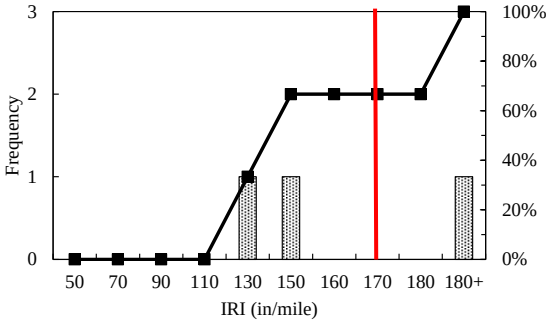

(a) Distress magnitude

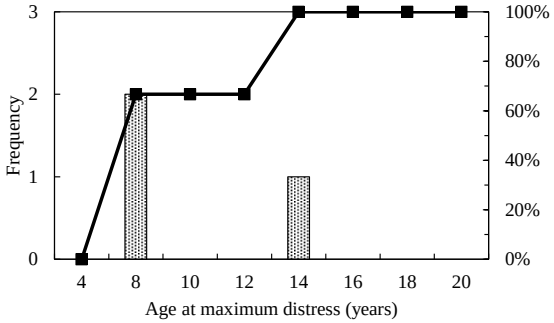

(b) Age distribution

Figure 3-35 Selected LTPP SPS-2 sections — IRI data

3.4.2 Refining the Project Section based on Performance

The measured performance data were evaluated for 20 new JPCP, and 108 new HMA projects. Normal pavement performance is based on FHWA criteria (*5*, *6*) modified to reflect Michigan distress thresholds which indicate the expected good and poor pavement performance trends for various distress types. The same criteria were used in Part 2 of the study (*4*). The measured fatigue or alligator cracking, rutting and IRI for HMA and measured transverse cracking and IRI for rigid pavements were compared with the performance criteria. The various upper and lower limits of expected performance for each distress type are shown in Figures 3-36 and 3-37 for both pavement types, respectively.

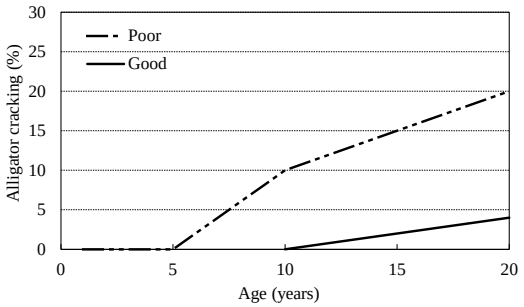

(a) Alligator cracking

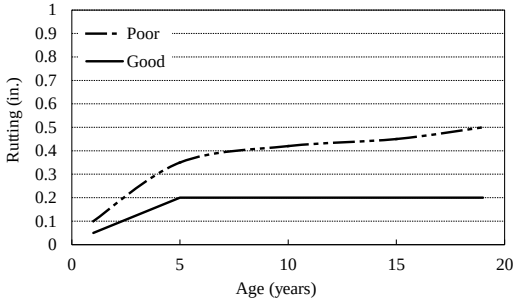

(b) Rutting

(c) IRI

Figure 3-36 Flexible pavement performance criteria

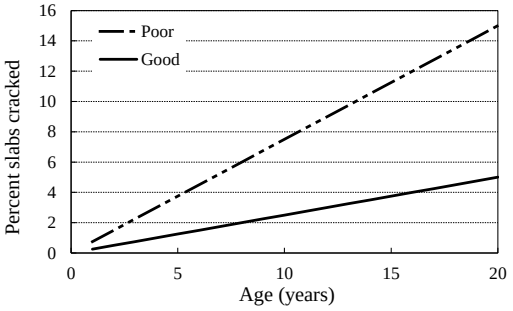

(a) Transverse cracking

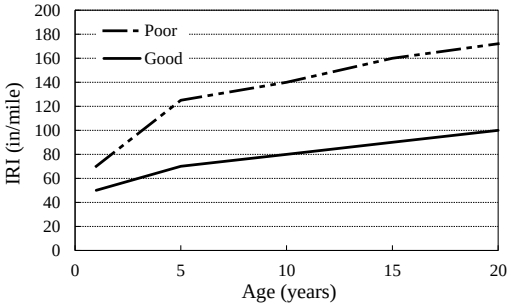

(b) IRI

Figure 3-37 Rigid pavement performance criteria

The time-series measured distresses for each project were compared to the modified FHWA criteria to identify any projects exceeding the FHWA pavement performance behavior. It is important to determine if a project exceeds the criteria for poor performance at an early age. If a pavement section exhibits an abnormal performance (i.e., premature cracking), the Pavement-ME can only account for such behavior through adjusting the critical inputs (e.g. material properties or traffic). However, a pavement section may be considered as normally performing if the distress exceeds the criteria limit beyond 10 years (which is about half of the design life). It is expected that a pavement may exceed the distress criteria at a later stage in the pavement life. The investigation was performed for the following distress types:

HMA pavements:

1. Alligator cracking
2. Rutting
3. IRI

JPCP pavements:

1. Transverse cracking
2. IRI

It should be noted that the performance criteria were not considered for thermal and longitudinal cracking. All the pavement sections were considered for the local calibration of the thermal transverse cracking model to account for the variability in the measured transverse cracking. Since the measured longitudinal cracking was combined with alligator cracking, no separate performance criterion was considered for longitudinal cracking. In addition, the performance criteria for the measured transverse joint faulting was not considered for rigid pavements (JPCP) because of low faulting magnitudes in the selected pavements sections.

Several projects exceeded the expected normal performance (indicating poor performance) based on the performance criteria. Figure 3-38 shows the measured pavement performance for all HMA projects. Several projects exceeded the alligator cracking threshold limits at an early age (i.e. above the red dashed line). However, the rutting and IRI performance followed the normal trends (i.e. between the green and red lines) and fewer projects exceeded the threshold limits. The causes for early age cracking, rutting, and IRI are important in determining whether the projects should be included in the calibration or not. Such decisions are made based on if there were any construction, or material related issues encountered at the time of construction. The pavement projects performing within the bands of the performance criteria are shown in Figure 3-39.

Figure 3-40 illustrates the measured pavement performance for the 20 JPCP projects. Several of the JPCP projects exceed the expected transverse cracking performance threshold. Based on the figure, one project shows measured transverse cracking above 80 percent slabs cracked at less than 10 years of age showing a premature failure. It is reasonable to assume that including such projects that exceed the distress threshold much earlier in their lives will give unreasonable calibration coefficients. On the other hand, the majority of the rigid pavement projects experienced expected IRI behavior. The rigid pavement projects performing within the bands of the performance criteria are shown in Figure 3-41.

Table 3-8 shows the summary of the pavement performance evaluation for all the selected sections for both pavement types. About 121 flexible pavement sections exhibited adequate performance behavior for fatigue cracking while 162 and 167 flexible pavement sections showed adequate performance for rutting and IRI, respectively. It should be noted that a project may perform poorly in cracking while rutting and IRI performance are still in the normal range. About 31 out of 33 rigid pavement sections have shown some level of cracking while 49 and 44 sections exhibited joint faulting and IRI, respectively.

Any project that exceeds the threshold performance limit is a cause for concern during the local calibration process because of the significant difference expected between predicted and measured performance. The list of projects which exceed the expected pavement performance were identified and sent to MDOT for further review. After reviewing the identified sections, it was concluded that not enough information was available to determine why these sections were performing poorly. These sections were not excluded from the local calibration at this time.

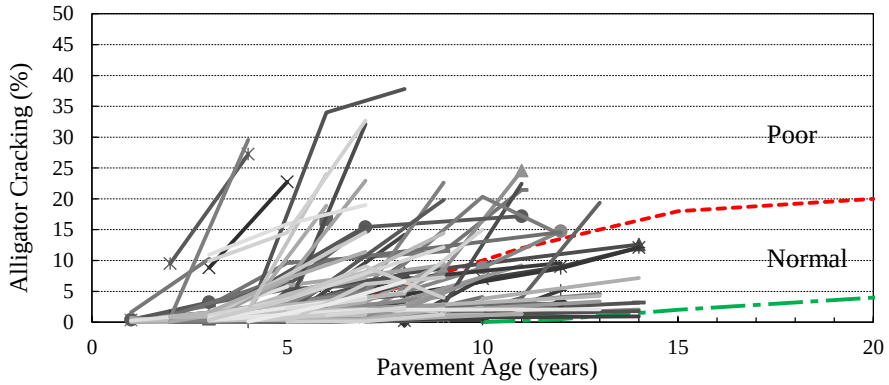

(a) Alligator cracking

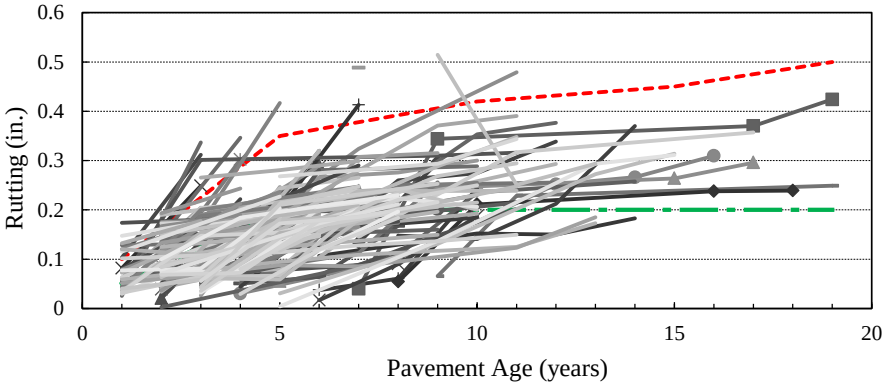

(b) Rutting

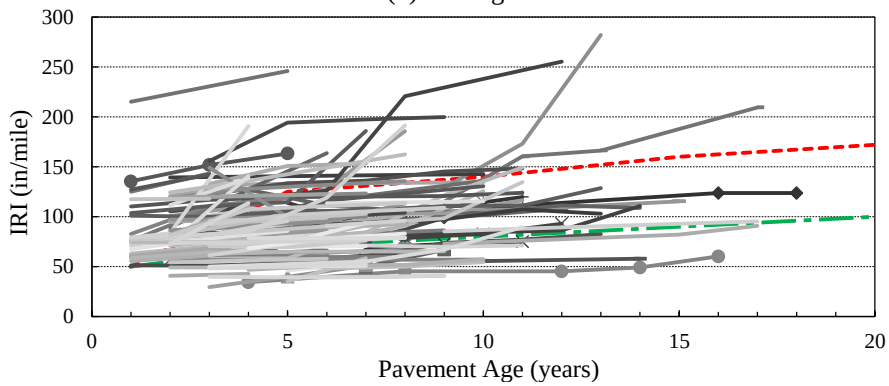

(c) IRI

Figure 3-38 Performance for all HMA projects

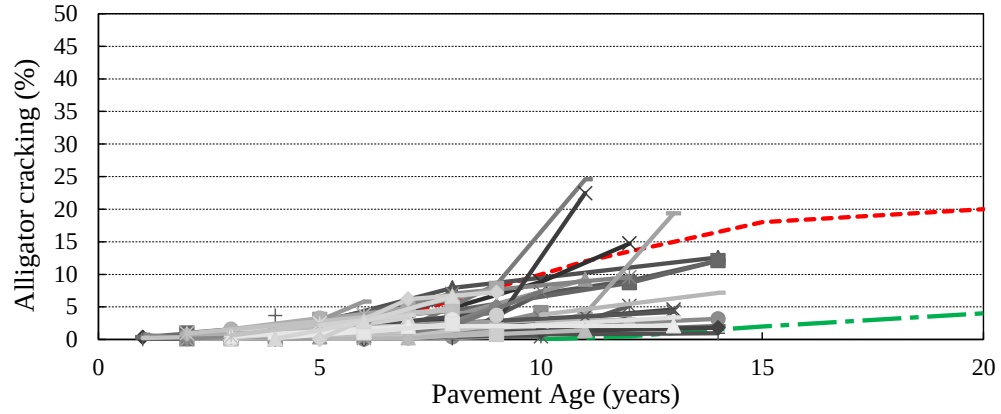

(a) Alligator cracking

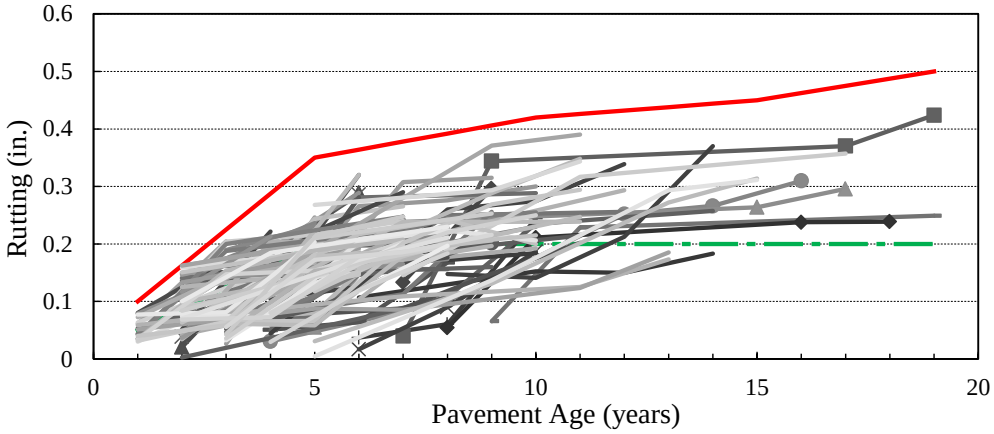

(b) Rutting

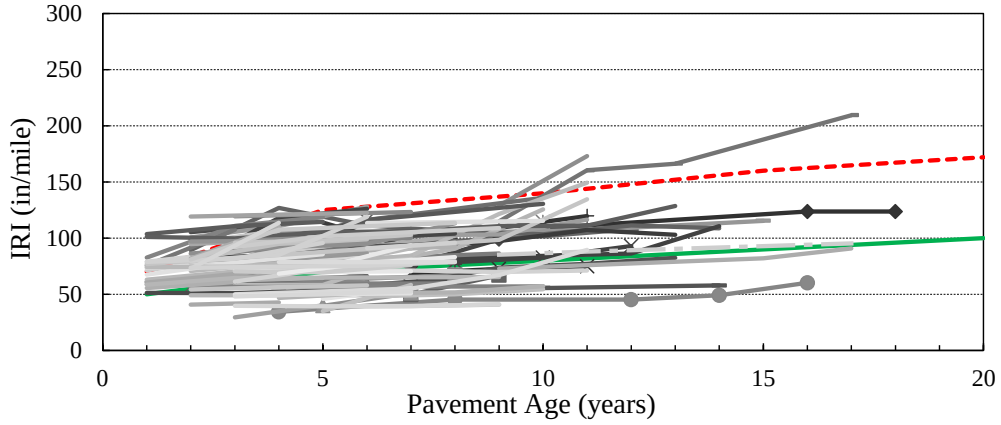

(c) IRI

Figure 3-39 Normal pavement performance for HMA projects

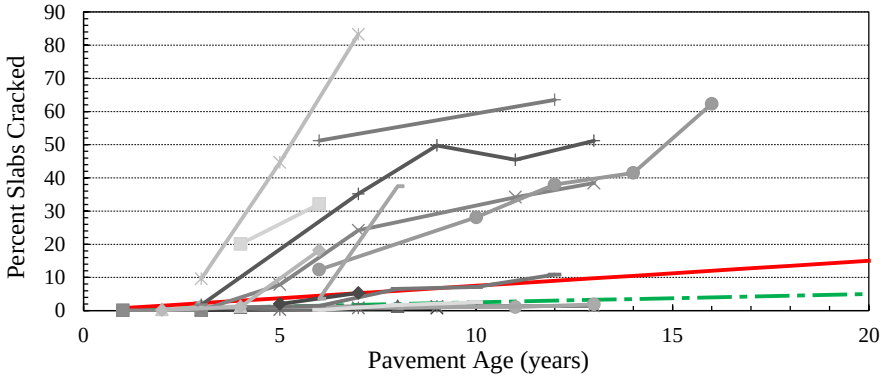

(a) Transverse cracking

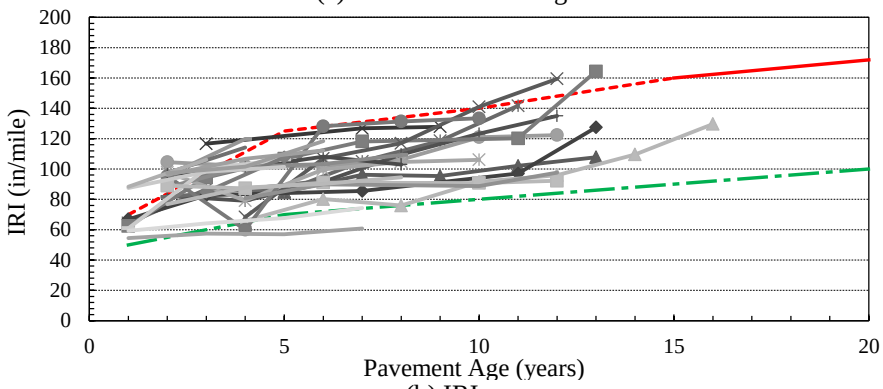

(b) IRI

Figure 3-40 Performance for all JPCP projects

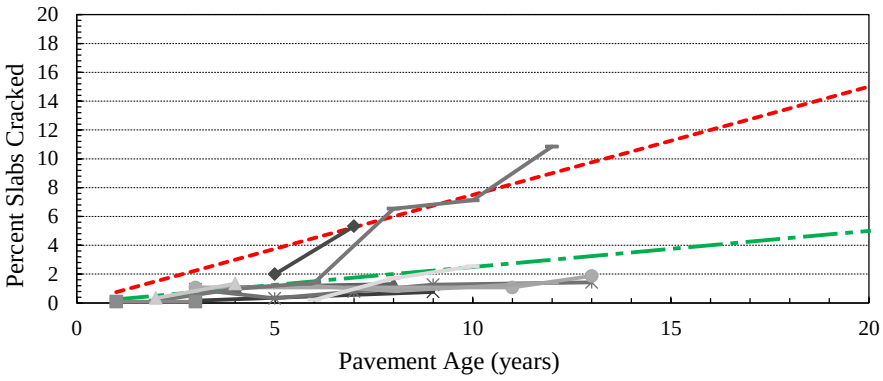

(a) Transverse cracking

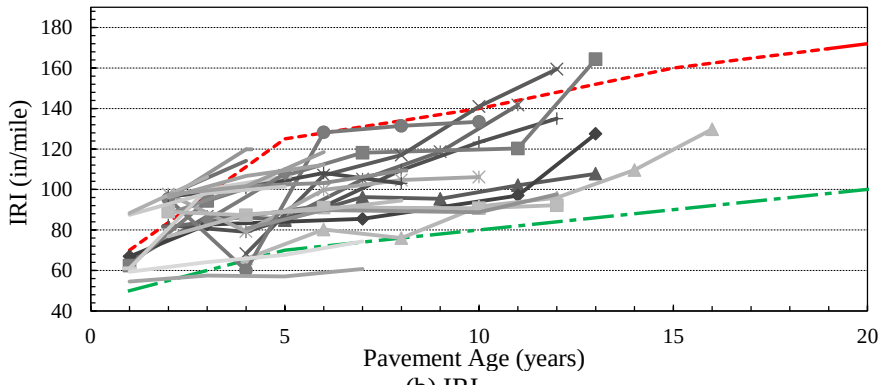

(b) IRI

Figure 3-41 Normal pavement performance for JPCP projects

Table 3-8 Projects with acceptable performance

Performance measure	Acceptable pavement sections	Total number of available sections
Flexible pavements		
Alligator cracking	121	129
Longitudinal cracking	128 (37)	129 (40)
Rutting	129 (33)	129 (40)
IRI	127 (40)	129 (40)
Rigid pavements		
Transverse cracking	18 (13)	18 (13)
Joint faulting	33 (16)	33 (16)
IRI	29 (15)	29 (15)

Note: The values in parenthesis represent number of rehabilitated pavement sections

3.5 INPUT DATA COLLECTION AND EXTENTS

The cross-sectional, traffic and material input data are needed to characterize the as-constructed pavements in the Pavement-ME software. The accuracy of the data directly impacts the performance prediction. The Pavement-ME uses a very large number of inputs to characterize a pavement. Furthermore, the hierarchical structure of the Pavement-ME provides three levels of inputs for many of the important input parameters. The input data collection efforts used to characterize a pavement in the Pavement-ME can be very time consuming. In order to reduce input data collection time, the most sensitive inputs which affect the pavement performance predictions were given priority. The sensitive inputs which affect the performance prediction for new and rehabilitation design of rigid and flexible pavements were determined by several research projects (*4, 7, 8*) as outlined in Chapter 2. Based on the results of these studies, focusing on the sensitive inputs significantly reduced the amount of time collecting input data. Additionally, the best available input level was used for the selected pavement sections. The general process for collecting the as-constructed input data, the details regarding the source of the data, issues and observations related to the data, and the final selection of the input values are discussed in this section.

3.5.1 Pavement Cross-Section and Design Feature Inputs

The pavement cross-sectional information is necessary to characterize the layer thicknesses of the various layers. The cross-sectional information was obtained from the as-constructed or as-designed drawings. These drawings were provided by MDOT for each selected project. The thickness and lane dimension information were included in these drawings. For projects where the cross-section was not available, a list of the projects with missing information was sent to MDOT. Typically, the base/subbase thicknesses were not found on the design

drawings. The missing information was obtained from MDOT. Additionally, in the case for HMA pavements, the drawings typically provided the asphalt application rate of the HMA layers which was used to determine the HMA lift thicknesses. All of the information obtained from the design drawings was used to populate the inputs necessary to characterize the in-service pavement cross-section. A summary of the design thicknesses for flexible and rigid reconstruct and rehabilitation selected pavement projects are shown in Tables 3-9 through 3-12.

Table 3-9 Average HMA reconstruct thicknesses

Types	HMA top course thickness (in.)	HMA leveling course thickness (in.)	HMA base course thickness (in.)	Base thickness (in.)	Subbase thickness (in.)
Crush and Shape	1.5	1.8	1.5	8.0	19.6
Freeway	1.6	2.2	4.7	6.6	17.6
Non-Freeway	1.5	2.1	3.3	6.3	16.4
State-wide Average	1.5	2.1	3.7	6.7	17.2

Table 3-10 Average HMA rehabilitation project thicknesses

Types	Overlay thickness (in.)	Existing pavement thickness (in.)	Base thickness (in.)	Subbase thickness (in.)
Composite	3.6	8.4	3.4	10.0
HMA over HMA	2.7	4.5	7.9	16.3
Rubblized	5.6	8.4	3.5	11.9
State-wide Average	3.9	6.7	5.9	12.9

Table 3-11 JPCP reconstruct thickness ranges

MDOT Region	Average PCC thickness (in.)	Average base thickness (in.)	Average subbase thickness (in.)
Grand	11.5	5.0	14.9
Metro	11.2	6.1	11.3
Southwest	11.7	4.0	10.7
University	11.2	6.3	9.5
State-wide Average	11.3	5.6	11.4

Table 3-12 Unbonded PCC overlay thickness ranges

Pavement type	Average PCC thickness (in.)	Average existing PCC thickness (in.)	Average base thickness (in.)	Average subbase thickness (in.)	Average asphalt interlayer thickness (in.)
Unbonded overlay	6.9	9.0	3.6	11.1	1.0

3.5.2 Traffic Inputs

The traffic data are one of the most important inputs used in the Pavement-ME pavement analysis and design procedure. The traffic inputs were obtained from various sources. The sources include:

- MDOT historical traffic counts (AADTT)
- MDOT traffic characterization study
  - Monthly distribution factors (MDF)
  - Hourly distribution factors (HDF)
  - Truck traffic classifications (TTC)
  - Axle groups per vehicle (AGPV)
  - Axle load distributions for different axle configurations (ALS)
- MDOT M-E traffic subcommittee recommendations

In order to collect the most accurate traffic inputs for the selected Michigan pavements, the traffic characterization study performed by the research team was used to determine the traffic related inputs (*9, 10*). The study identified the inputs outlined above. Furthermore, a cluster analysis was performed to group sites with similar characteristics. These clusters provide regional level inputs and are especially useful when Level 1 traffic data are not available for a particular pavement section. The most important traffic inputs were the TTC, HDF, and tandem ALS based on their impact on the predicted pavement performance. The study recommended statewide average values for all other input variables (*9*). Therefore, the results from the traffic characterization study in Michigan were utilized to characterize traffic inputs on the pavement sections included in the calibration dataset. The following inputs were collected for each pavement project:

- Average annual daily truck traffic (AADTT)
- TTC
- ALS – Tandem
- HDF

The following procedure was used to determine the cluster for each individual project:

1. Collect commodity data for each project based on MDOT GIS maps with freight data based on the roadway (see Figure 3-42).
2. Identify vehicle class 5 and 9 counts for each project from the MDOT Traffic Monitoring Information System (TMIS) from the following URL: http://mdotnetpublic.state.mi.us/tmispublic/), see Figures 3-43 to 3-44 and Table 3-13. Convert the class 5 and 9 counts to percentages for use in the discriminant analysis for project allocation to a cluster.
3. Use the MDOT commodity data, VC 5/9, AADTT, MDOT region, and road class information for input into formulas to determine the specific clusters for each project (see Figure 3-45 for the spreadsheet that identifies formula solutions to determine the clusters).

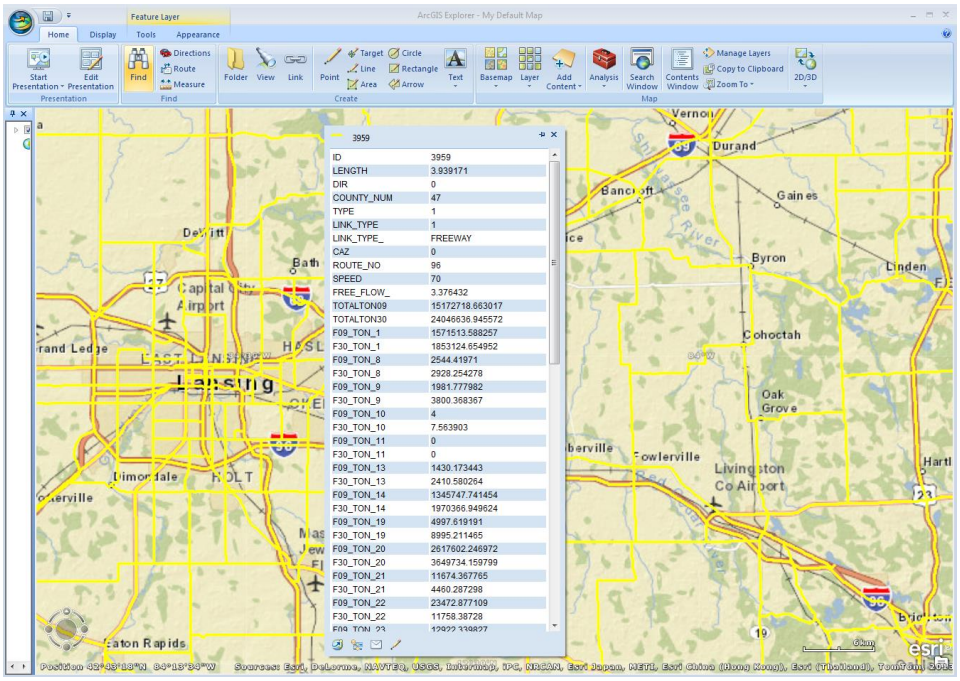

Figure 3-42 MDOT freight data

Figure 3-43 Location of classification counts

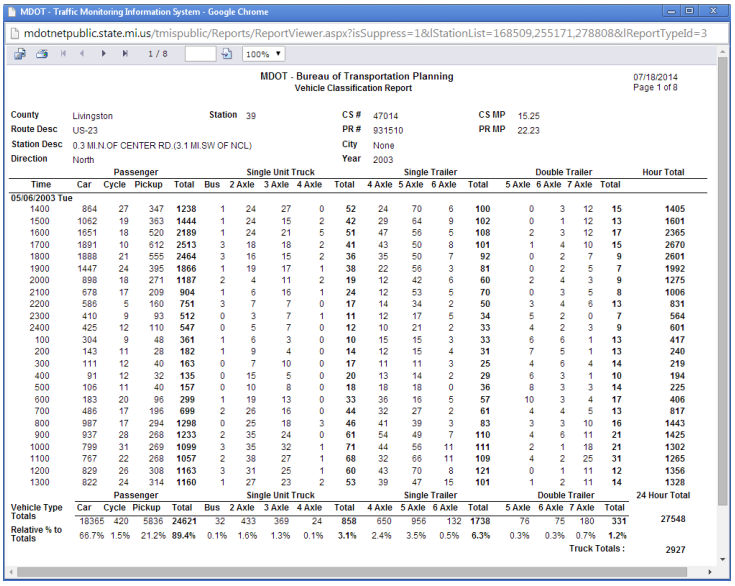

MDOT - Traffic Monitoring Information System - Google Chrome

mdotnetpublic.state.mi.us/tmispublic/Reports/ReportViewer.aspx?isSuppress=1&lStationList=168509,255171,2788088lReportTypeId=3

MDOT - Bureau of Transportation Planning
Vehicle Classification Report

07/18/2014
Page 1 of 8

County Livingston Station 39 CS # 47014 CS MP 15.25
Route Desc US-23 PR # 931510 PR MP 22.23
Station Desc 0.3 MI.N.OF CENTER RD.(3.1 MI.SW OF NCL) City None
Direction North Year 2003

Time	Passenger Car	Cycle	Pickup	Total	Single Unit Truck Bus	2 Axle	3 Axle	4 Axle	Total	Single Trailer 4 Axle	5 Axle	6 Axle	Total	Double Trailer 5 Axle	6 Axle	7 Axle	Total	Hour Total
05/06/2003 Tue																		
1400	864	27	347	**1238**	1	24	27	0	**52**	24	70	6	**100**	0	3	12	**15**	**1405**
1500	1062	19	363	**1444**	1	24	15	2	**42**	29	64	9	**102**	0	1	12	**13**	**1601**
1600	1651	18	520	**2189**	1	24	21	5	**51**	47	56	5	**108**	2	3	12	**17**	**2365**
1700	1891	10	612	**2513**	3	18	18	2	**41**	43	50	8	**101**	1	4	10	**15**	**2670**
1800	1888	21	555	**2464**	3	16	15	2	**36**	35	50	7	**92**	0	2	7	**9**	**2601**
1900	1447	24	395	**1866**	1	19	17	1	**38**	22	56	3	**81**	0	2	5	**7**	**1992**
2000	898	18	271	**1187**	2	4	11	2	**19**	12	42	6	**60**	2	4	3	**9**	**1275**
2100	678	17	209	**904**	1	6	16	1	**24**	12	53	5	**70**	0	3	5	**8**	**1006**
2200	586	5	160	**751**	3	7	7	0	**17**	14	34	2	**50**	3	4	6	**13**	**831**
2300	410	9	93	**512**	0	3	7	1	**11**	12	17	5	**34**	5	2	0	**7**	**564**
2400	425	12	110	**547**	0	5	7	0	**12**	10	21	2	**33**	4	2	3	**9**	**601**
100	304	9	48	**361**	1	6	3	0	**10**	15	15	3	**33**	6	6	1	**13**	**417**
200	143	11	28	**182**	1	9	4	0	**14**	12	15	4	**31**	7	5	1	**13**	**240**
300	111	12	40	**163**	0	7	10	0	**17**	11	11	3	**25**	4	6	4	**14**	**219**
400	91	12	32	**135**	0	15	5	0	**20**	13	14	2	**29**	6	3	1	**10**	**194**
500	106	11	40	**157**	0	10	8	0	**18**	18	18	0	**36**	8	3	3	**14**	**225**
600	183	20	96	**299**	1	19	13	0	**33**	36	16	5	**57**	10	3	4	**17**	**406**
700	486	17	196	**699**	2	26	16	0	**44**	32	27	2	**61**	4	4	5	**13**	**817**
800	987	17	294	**1298**	0	25	18	3	**46**	41	39	3	**83**	3	3	10	**16**	**1443**
900	937	28	268	**1233**	2	35	24	0	**61**	54	49	7	**110**	4	6	11	**21**	**1425**
1000	799	31	269	**1099**	3	35	32	1	**71**	44	56	11	**111**	2	1	18	**21**	**1302**
1100	767	22	268	**1057**	2	38	27	1	**68**	32	66	11	**109**	4	2	25	**31**	**1265**
1200	829	26	308	**1163**	3	31	25	1	**60**	43	70	8	**121**	0	1	11	**12**	**1356**
1300	822	24	314	**1160**	1	27	23	2	**53**	39	47	15	**101**	1	2	11	**14**	**1328**
	Passenger				**Single Unit Truck**					**Single Trailer**				**Double Trailer**				**24 Hour Total**
Vehicle Type Totals	Car	Cycle	Pickup	Total	Bus	2 Axle	3 Axle	4 Axle	Total	4 Axle	5 Axle	6 Axle	Total	5 Axle	6 Axle	7 Axle	Total	
	18365	420	5836	**24621**	32	433	369	24	**858**	650	956	132	**1738**	76	75	180	**331**	**27548**
Relative % to Totals	66.7%	1.5%	21.2%	**89.4%**	0.1%	1.6%	1.3%	0.1%	**3.1%**	2.4%	3.5%	0.5%	**6.3%**	0.3%	0.3%	0.7%	**1.2%**	
																	Truck Totals :	**2927**

Figure 3-44 Raw vehicle class counts

Table 3-13 Conversion from raw vehicle counts to vehicle class percentages

JN	CS	Direction	Year Measured / Date Measured	Bus VC 4	2 axle VC 5	3 axle VC 6	4 axle VC 7	4 axle ST VC 8	5 axle ST VC 9	6 axle ST VC 10	5 axle DT VC 11	6 axle DT VC 12	7 axle DT VC 13	Sum	VC 5	VC 9
37997	3111	-	-	-	-	-	-	-	-	-	-	-	-	0		
34120	47014	N	11/15/2011	20	256	165	32	430	1025	116	66	42	176	2328	11.0	44.0
34120	47014	N	11/16/2011	31	301	246	27	662	875	130	89	32	180	2573	11.7	34.0
34120	47014	N	11/17/2011	4	67	34	7	59	209	30	7	4	39	460	14.6	45.4
34120	47014	S	11/15/2011	35	315	171	12	495	998	114	65	49	182	2436	12.9	41.0
34120	47014	S	11/16/2011	25	377	250	17	805	718	114	93	60	165	2624	14.4	27.4
34120	47014	S	11/17/2011	4	89	52	2	156	152	17	8	12	29	521	17.1	29.2
49029	13074	N	7/22/2004	222	142	160	10	452	2768	64	2	8	205	4033	3.5	68.6
49029	13074	N	7/23/2004	205	136	138	10	472	1657	40	1	6	106	2771	4.9	59.8
49029	13074	N	7/24/2004	17	60	66	14	314	664	21	0	6	28	1190	5.0	55.8
49029	13074	N	7/25/2004	218	163	1135	16	535	1651	51	0	9	134	3912	4.2	42.2
49029	13074	N	7/26/2004	197	224	160	8	489	2342	67	0	10	169	3666	6.1	63.9
49029	13074	N	7/27/2004	219	191	175	10	533	2767	74	0	11	187	4167	4.6	66.4
49029	13074	N	7/28/2004	216	200	175	11	444	2568	66	0	10	191	3881	5.2	66.2
45591	13074-23061	N	7/22/2004	222	142	160	10	452	2768	64	2	8	205	4033	3.5	68.6
45591	13074-23061	N	7/23/2004	205	136	138	10	472	1657	40	1	6	106	2771	4.9	59.8
45591	13074-23061	N	7/24/2004	17	60	66	14	314	664	21	0	6	28	1190	5.0	55.8
45591	13074-23061	N	7/25/2004	218	163	1135	16	535	1651	51	0	9	134	3912	4.2	42.2
45591	13074-23061	N	7/26/2004	197	224	160	8	489	2342	67	0	10	169	3666	6.1	63.9
45591	13074-23061	N	7/27/2004	219	191	175	10	533	2767	74	0	11	187	4167	4.6	66.4
45591	13074-23061	N	7/28/2004	216	200	175	11	444	2568	66	0	10	191	3881	5.2	66.2
38209	41132-41133	S	11/12/2002	212	151	128	9	217	788	84	47	13	163	1812	8.3	43.5
38209	41132-41133	S	11/13/2002	200	154	117	11	281	757	83	50	15	183	1851	8.3	40.9

CLUSTER SELECTION METHODOLOGY

JN: 33007
CS: 83031, 83033
ROUTE: US-131

Variable	DATA ENTRY	*Entry Type*
Region	2	*Superior = 1, North = 2, Bay = 3, University = 4, Grand = 5, Metro = 6, Southwest = 7*
Functional Class	1	*Rural = 1, Urban = 2*
Food Product Truck %	18.63	*PERCENTAGE, (Commodity Code: 20)*
Fabricated Metal Products Truck %	2.77	*PERCENTAGE, (Commodity Code: 34)*
Machinery Truck %	1.34	*PERCENTAGE, (Commodity Code: 35)*
Rubber and Plastics Truck %	2.16	*PERCENTAGE, (Commodity Code: 30)*
Furniture and Fixtures Truck %	0.70	*PERCENTAGE, (Commodity Code: 25)*
Electrical Equipment Truck %	1.12	*PERCENTAGE, (Commodity Code: 36)*
Total Tons	1,598,444	*TONS*
VC 5 %	6.9	*PERCENTAGE*
VC 9 %	26.9	*PERCENTAGE*
AADTT	959	*NUMBER*
Misc. Manufacturing Products Truck %	0.61	*PERCENTAGE, (Commodity Code: 39)*
Road Class	2	*Interstate = 1, US Highway = 2, MI Route = 3*
Printed Matter Truck %	1.65	*PERCENTAGE, (Commodity Code: 27)*
Paper and Pulp Products Truck %	1.15	*PERCENTAGE, (Commodity Code: 26)*
Logs, Lumber, and Wood Products Truck %	7.95	*PERCENTAGE, (Commodity Code: 24)*
Transportation Equipment Truck %	2.07	*PERCENTAGE, (Commodity Code: 37)*

Truck Traffic Classification - CLUSTER NO.	3
Hourly Distribution Factor - CLUSTER NO.	2
Tandem Axle Load Spectra - CLUSTER NO.	3

Figure 3-45 Cluster selection based on steps 1 and 2

The AADTT values were determined for each project in consultation with MDOT to identify the truck volumes at the time of construction based on historical traffic records. If the historical traffic records were not available, an estimate of the AADTT for each project was based on the as-constructed project design drawings. The TTC, ALS-Tandem, and HDF clusters were used for each pavement section by following the procedure recommended in the traffic characterization study (*9*). The statewide average values were used for the MDF, AGPV, and other ALS inputs. The range and average two-way AADTT values for all reconstruct and rehabilitation projects are summarized in Table 3-14 and 3-15, respectively.

Table 3-14 Ranges of AADTT for all reconstruct projects

Road Type	REGION	Min AADTT	Max AADTT	Average AADTT
Crush and Shape	Grand	265	1986	1126
	North	91	1757	926
	Superior	60	312	178
HMA Reconstruct Freeway	Bay	313	2034	1174
	Grand	819	4315	1656
	Metro	354	6745	2434
	North	685	5722	2455
	Southwest	367	367	367
	Superior	350	350	350
	University	1220	5011	3721
HMA Reconstruct Non-Freeway	Bay	142	523	345
	Grand	367	1440	708
	Metro	152	1600	843
	North	194	880	382
	Southwest	442	996	617
	Superior	63	1096	372
	University	137	556	321
JPCP Reconstruct	Grand	3195	3499	3347
	Metro	500	16605	7883
	Southwest	7532	10578	8937
	University	5299	7498	6569
Statewide		60	16605	1859

Table 3-15 Ranges of AADTT for all rehabilitation projects

Pavement Type	Region	Minimum AADTT	Maximum AADTT	Average AADTT
Composite	Bay	512	2250	1254
	Grand	2882	2882	2882
	Metro	1380	1380	1380
	North	672	672	672
	Southwest	6064	6064	6064
HMA over HMA	Bay	200	200	200
	North	130	450	299
	Southwest	185	1564	536
	Superior	260	260	260
	University	350	350	350
Rubblized	Grand	370	575	478
	North	279	1550	696
	Southwest	856	856	856
	University	455	3707	2517
Unbonded Overlay	Grand	2744	2744	2744
	North	1458	1458	1458
	Southwest	3185	5700	4683
	University	4279	5004	4642
Statewide average		130	6064	1601

3.5.3 As-constructed Material Inputs

The as-constructed materials inputs characterize the material properties for each pavement layer at the time of construction. These inputs range from project specific values, to statewide average values. The details of material properties for each pavement structural layer are discussed in this section.

3.5.3.1. HMA layer inputs

An attempt was made to collect the HMA layer information from the construction records; however, the needed data were not available for all pavement sections. Two different input levels were identified to study the effect on HMA pavement performance. The collection process of Level 1 and Level 3 data are discussed in this section.

Level 1 HMA inputs

The level 1 HMA inputs require laboratory testing to determine several HMA mixture and binder properties. These properties include:

- Dynamic modulus (E*)
- Binder (G*)
- Creep compliance and,
- Indirect tensile strength (IDT)

The laboratory testing to determine these material properties were performed during Part 1 of this study and results are documented elsewhere (*2*). The Level 1 HMA inputs were collected for projects which had similar mixture and binder types. Since Part 1 of the study involved testing only SuperPave HMA mixtures, the test results could only be used for past projects constructed using SuperPave mixture design. Furthermore, material characterization data for only the HMA mixtures and binder types which were tested can be used (not all HMA mix/binder combinations were tested in Part 1). It should be noted that the HMA characterization data and testing results are from recently constructed projects and does not reflect the as constructed HMA materials for the selected projects. As part of the deliverables from Part 1, a software (DYNAMOD) was developed that provides easy extraction of the *E**, *G**, creep compliance and IDT values for the local materials in a format consistent with the Pavement-ME needs. Table 3-16 summarizes the number of projects which had similar HMA mixture and binder properties with tested Level 1 data.

Table 3-16 Projects with available Level 1 HMA input properties

Pavement Type	MDOT region	Number of projects with Level 1 data
Crush and Shape	North	1
HMA Reconstruct Freeway	Bay	2
	Grand	2
	Metro	4
	North	1
	University	1
HMA over HMA	Southwest	1
	University	1
HMA Reconstruct Non-Freeway	Bay	3
	Grand	7
	Metro	4
	North	5
	Southwest	5
	Superior	9
	University	8
Rubblized	Grand	1
	North	1

Level 3 HMA layer inputs

The HMA structural layers are characterized using the asphalt binder, air void content, asphalt binder content and the aggregate gradation for the asphalt mixture.

The HMA inputs were obtained from the following sources:

1. Project design drawings with typical cross-section, HMA binder type, HMA binder mix type, and application rate

2. Historical as-constructed project records which identified the HMA job mix formulas for each HMA layer. It should be noted that the historical records were not available for all projects
3. In the absence of historical records, the average aggregate gradation for each HMA mixture type was utilized.

If no historical records were available, an average gradation was determined for each HMA mixture type based on the available HMA data from the remainder of the projects in the calibration dataset. The average HMA aggregate gradation was calculated based on the values obtained from the historical records and HMA mixture characterization MDOT study (*2*). The average as-constructed percent air voids and HMA mixture inputs are summarized in Tables 3-17 through 3-20.

Table 3-17 As-constructed percent air voids

HMA mixture type	Average as-constructed air voids
GGSP	8.4
5E3	7.1
5E10	6.5
5E1	6.7
4E30	6.5
4E3	6.7
4E10	6.5
4E1	6.8
4C	5.4
4B	5.9
3E30	5.7
3E3	6.6
3E10	6.4
3E1	6.5
3C	5.5
3B	5.7
2E3	7.4
2C	5.7
13A	5.3

Table 3-18 HMA top course average aggregate gradation

HMA mixture type	Effective AC binder content	Percent passing sieve size			
		3/4	3/8	#4	#200
1100T	12.0	100.0	88.7	62.5	6.9
13 T	10.2	100.0	70.0	51.2	5.6
13A	11.7	100.0	82.8	66.0	5.4
1500T	10.4	100.0	86.0	53.4	5.2
3B	9.9	100.0	64.6	44.5	4.9
4B	11.1	100.0	89.0	60.1	5.0
4C	11.3	100.0	80.9	57.8	4.8
4C-M	11.2	100.0	86.8	51.7	4.6
4E3	11.4	100.0	90.1	67.0	6.1
4E30	12.2	100.0	85.8	52.8	4.3
5E1	11.9	100.0	96.8	76.6	5.5
5E10	12.0	100.0	98.2	75.6	5.4
5E3	11.9	100.0	97.4	74.6	5.3
GGSP	12.8	100.0	73.5	31.9	8.5
4E10 HS	10.0	100.0	85.7	65.7	4.9
5E3 HS	11.6	100.0	97.3	75.7	5.4
4E1 HS	10.8	100.0	85.8	71.4	5.4
5E1 HS	12.1	100.0	98.4	81.8	5.9
4E3 HS	10.4	100.0	86.0	65.7	5.4
5E50	11.0	100.0	99.7	77.7	6.2
5E10 HS	11.4	100.0	99.5	76.2	5.4
4E30 HS	10.0	100.0	87.1	52.3	5.5
5E30 HS	11.6	100.0	99.7	76.4	6.1

Table 3-19 HMA leveling course average aggregate gradation

HMA mixture type	Effective AC binder content	Percent passing sieve size			
		3/4	3/8	#4	#200
1100L	11.2	100.0	88.7	62.5	6.9
13 L	10.8	100.0	77.1	62.1	5.8
13A	11.7	100.0	83.6	66.4	5.5
1500L	11.4	100.0	85.0	56.1	5.5
3B	9.9	99.9	69.9	46.2	4.7
3C	10.9	100.0	72.0	49.7	5.1
3E3	10.6	100.0	78.7	46.8	3.7
3E30	10.0	98.9	83.9	66.6	4.3
4E1	11.0	100.0	86.8	68.0	4.8
4E10	10.6	100.0	87.5	58.6	4.9
4E3	10.9	100.0	87.7	88.9	4.9
4E30	11.1	100.0	86.8	64.1	5.0

Table 3-20 HMA base course average aggregate gradation

HMA mixture type	Effective AC binder content	Percent passing sieve size			
		3/4	3/8	#4	#200
700	8.5	71.5	56.0	46.9	4.5
2C	9.6	87.1	55.5	41.4	6.0
2E3	9.7	89.9	71.6	58.3	4.6
3B	9.7	99.8	62.6	40.0	4.7
3E1	11.0	100.0	71.4	48.3	4.5
3E10	10.1	99.4	75.2	47.0	4.7
3E3	10.3	99.7	79.7	58.0	4.5
3E30	11.0	99.7	76.2	55.7	5.1
4E3	11.3	100.0	85.4	68.2	5.0
3E30	9.8	100.0	77.1	57.6	4.5

3.5.3.2. PCC material inputs

The Pavement-ME transverse cracking prediction model is very sensitive to concrete strength (compressive or flexural). The PCC material related inputs were obtained from the following sources:

- Material testing results
- Typical MDOT values
- Quantifying coefficient of thermal expansion values of typical hydraulic cement concrete paving mixtures (*11*)

PCC strength:

The concrete core compressive strength (f'_c) test data were collected by MDOT. These tests represent the concrete compressive strength close to the time of construction for the selected pavement sections. These test values were used directly for each corresponding project. The in-situ strength values also represented several MDOT geographical regions. The average f'_c for each region was determined in order to represent concrete strengths for the pavement sections which did not have actual test values. The region specific average compressive strengths are summarized in Table 3-21. The transverse cracking model in the Pavement-ME directly uses modulus of rupture (MOR) to estimate damage. The MOR values were estimated based on the ACI correlation between MOR and f'_c as shown by Equation (6). Figure 3-46 shows the f'_c and estimated MOR distributions. It should be noted that the specific testing age of these cores were not available; however, all cores were tested after or at least 28 days. The Pavement-ME internally calculates the relationship between f'_c and MOR. The relationship differs slightly from Equation (6), instead of using 7.5, the software uses a value of 9.5. Since the cores were not tested at 28 days, and the actual testing dates were unknown, the lower values were assumed to better represent 28 day strengths for each pavement section.

$$MOR = 7.5 \times \sqrt{f_c'} \quad (6)$$

Table 3-21 Average values for compressive strength and MOR by MDOT region

Region/Job number	Measured compressive strength – (psi)	Calculated MOR – (psi)
All sections	5142	538
Grand	5119	537
Metro	4963	528
Southwest	5496	556
University	5165	539

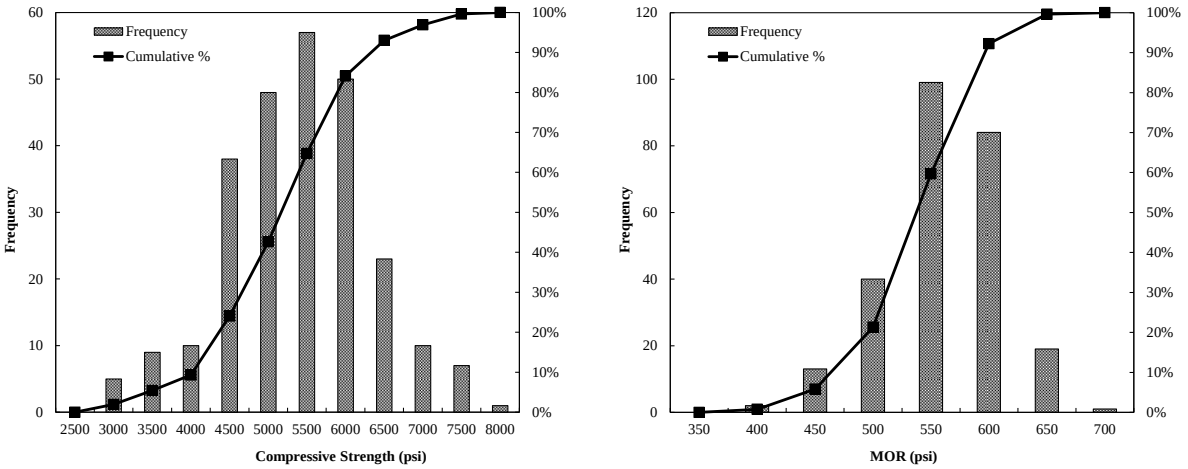

(a) Compressive strength (f'_c) (b) Modulus of rupture (MOR)

Figure 3-46 Distribution of concrete strength properties

Coefficient of thermal expansion:

The CTE input values were obtained from the MDOT study that determined the CTE for various aggregates available across the state of Michigan (*11*). The most prevalent CTE values for aggregate used in Michigan are either 4.5 or 5.8 in/in/°F×10^{-6} depending on the location of the pavement section. For University or Metro regions, a CTE value of 5.8 in/in/°F×10^{-6}, while for other regions, a value of 4.5 in/in/°F×10^{-6} was used.

3.5.3.3. Aggregate base/subbase and subgrade input values

The aggregate base/subbase and subgrade input values were obtained from the following sources:

- Backcalculation of unbound granular layer moduli (*12*)
- Pavement subgrade MR design values for Michigan's seasonal changes (*13*)

The resilient modulus (MR) values for the base and subbase material were selected based on the results from previous MDOT studies. The typical backcalculated values for base and subbase MR are 33,000 psi and 20,000 psi, respectively. These values were assumed for all projects, since in-situ MR values were not available.

The subgrade material type and resilient modulus was selected based on the Subgrade MR study (*12, 13*). The study outlined the location of specific soil types and their MR values across the entire State. There are three possible ways to incorporate the design MR (e.g.

4,400 psi — A-7-6 soil) for soils in Michigan in the Pavement-ME local calibration. These methods include:

1. Adjusted subgrade MR
2. Annual representative value (effective MR representing the entire year)
3. Design MR at specified optimum moisture content (OMC) [using typical OMC for the Michigan soils]

Method 1: Adjusted Subgrade MR

The design software internally adjusts the subgrade MR value based on the soil type and climate. Therefore, the adjustment factors were determined for each climate and soil type in the entire state. The MR values fluctuate based on the monthly climate variations for a year. The MR adjustment factors were determined from the minimum MR value over the entire 20 year design period. The adjustment factors are used to artificially adjust the MR so that the minimum value represents the MDOT recommended design MR for a particular soil (*12, 13*). For example, the following process was adopted to determine the adjustment factor and inflate the design MR values for SM soils in Lansing climate (see Table 3-22):

1. Backcalculate MR or use backcalculated MR for SM soil from previous MDOT study. The MR value in the table is 24,764 psi.
2. Run the pavement section with the backcalculated MR value obtained in step 1 and obtain the minimum MR value based on the EICM adjustments from the Pavement-ME output file.
3. Calculate the adjustment factor as shown below:

$$\text{Adjustment factor} = \frac{MR_{\min}}{MR_{backcalculated}} = \frac{17,334}{24,764} = 0.69$$

4. Determine the inflated design MR as shown below:

$$\text{Inflated MR} = \frac{MR_{design}}{\text{Adjustment factor}} = \frac{5,200}{0.69} = 7,460 \text{ psi}$$

5. Use the inflated design MR in the Pavement-ME to reflect the MDOT design MR value.

Ideally the adjusted MR value should reflect a value similar to the design MR because of the climatic variations. It should be noted that the adjustment factors were determined only for backcalculated moduli and the adjustment factors were assumed to be similar for the design MR values. However, it was also found that the adjustment factors vary depending on the magnitude of MR (i.e., backcalculated or design MR values). A summary of adjustment factors based on soil type and climate stations is shown in Table 3-22. Table 3-23 summarizes the adjusted design MR values used in the calibration process initially. The adjusted MR values are shown in Figure 3-47 for a design MR of 4400 psi.

Two concerns were identified for this method:

a. The adjustment factors were determined based on backcalculated moduli and may not accurately represent the lower design MR values.
b. The adjustment factors should have been estimated based on the design MR values for each soil type and climate.

Therefore, this method was not adopted for the final local calibration.

Method 2: Annual Representative Subgrade MR Value

Method 2 consists of directly using the design MR as an input and selecting the "annual representative value" option in the software. When this option is selected, the subgrade MR value does not fluctuate based on climatic variations over the design life. Method 2 is only applicable if the design MR represents an effective roadbed modulus (i.e., it already accounts for the moisture variations through the year). The MDOT subgrade soil characterization report (*13*) considers the design MR as effective MR. It should be noted that the backcalculated subgrade MR reflects the in-situ moisture conditions. Therefore, it is difficult to determine whether the in-situ moisture content represents optimum moisture content. Generally, a saturated soil modulus should be considered for AASHTO 93 design because those values are determined based on soaked CBR. The annual representative MR is shown in Figure 3-47. The figure shows that if this option is selected, then there is no fluctuation of the design MR. Therefore, the current local calibration of the performance models adopted this method and the design MR values for each soil type were utilized.

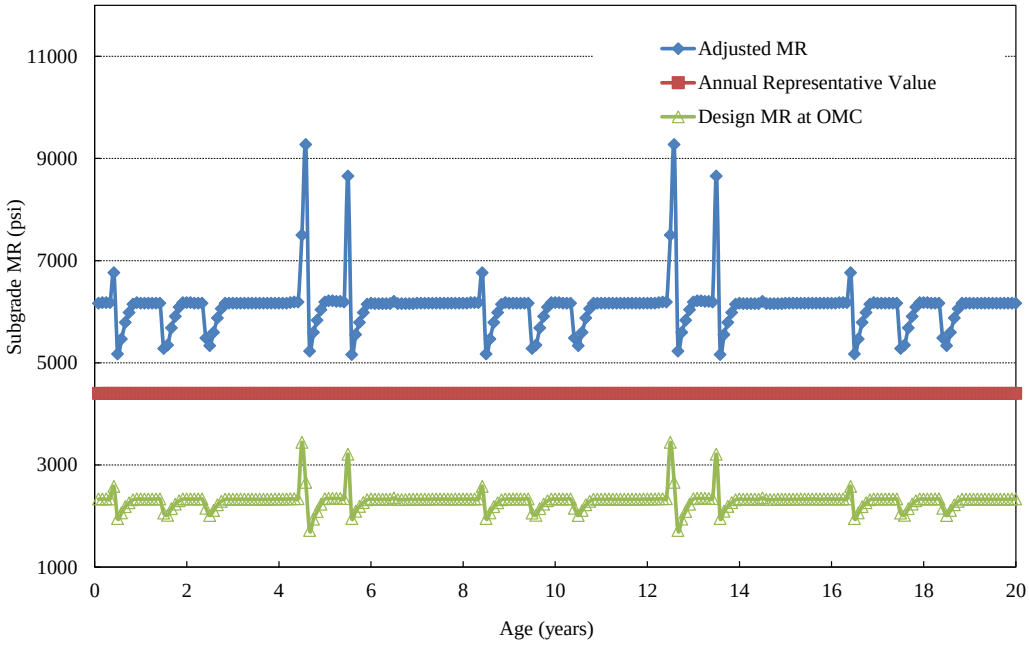

Figure 3-47 Subgrade MR over time in Lansing

Table 3-22 List of MR reduction factors for Michigan weather stations in the Pavement-ME

USCS	AASHTO	Back-calculated (psi)	Design MR value (psi)	Adrian	Ann Arbor	Battle Creek	Benton Harbor	Detroit	Flint	Gaylord	Grand Rapids	Hancock
SM	A-2-4, A-4	24,764	5,200	0.82	0.84	0.84	0.82	0.82	0.81	0.47	0.74	0.49
SP1	A-1-a, A-3	27,739	7,000	0.77	0.75	0.81	0.76	0.82	0.68	0.49	0.74	0.59
SP2	A-1-b, A-2-4, A-3	25,113	6,500	0.78	0.66	0.70	0.79	0.78	0.64	0.51	0.65	0.50
SP-SM	A-2-4, A-4	20,400	7,000	0.71	0.70	0.74	0.82	0.81	0.66	0.51	0.67	0.53
SC-SM	A-2-6, A-6, A-7-6	20,314	5,000	0.48	0.49	0.48	0.47	0.47	0.48	0.31	0.42	0.34
SC	A-4, A-6, A-7-6	21,647	4,400	0.48	0.49	0.48	0.47	0.47	0.48	0.31	0.42	0.34
CL	A-4, A-6, A-7-6	15,176	4,400	0.48	0.49	0.48	0.47	0.48	0.48	0.31	0.42	0.34
ML	A-4	15,976	4,400	0.40	0.41	0.40	0.40	0.40	0.35	0.23	0.35	0.28
SC/CL/ML	A-2-6, A-4, A-6, A-7-6	17,600	4,400	0.47	0.47	0.46	0.46	0.46	0.46	0.30	0.41	0.33

Table 3-22 List of MR reduction factors for Michigan weather stations in the Pavement-ME (cont.)

USCS	AASHTO	Back-calculated (psi)	Design MR value (psi)	Houghton Lake	Iron Mountain	Kalamazoo	Lansing	Muskegon	Pellston	Pontiac	Traverse City
SM	A-2-4, A-4	24,764	5,200	0.48	0.54	0.85	0.70	0.82	0.57	0.70	0.57
SP1	A-1-a, A-3	27,739	7,000	0.54	0.51	0.77	0.68	0.85	0.47	0.70	0.59
SP2	A-1-b, A-2-4, A-3	25,113	6,500	0.46	0.49	0.78	0.65	0.78	0.54	0.65	0.54
SP-SM	A-2-4, A-4	20,400	7,000	0.48	0.50	0.84	0.67	0.81	0.56	0.68	0.56
SC-SM	A-2-6, A-6, A-7-6	20,314	5,000	0.36	0.36	0.48	0.42	0.48	0.32	0.42	0.42
SC	A-4, A-6, A-7-6	21,647	4,400	0.36	0.36	0.48	0.42	0.48	0.32	0.42	0.41
CL	A-4, A-6, A-7-6	15,176	4,400	0.36	0.36	0.48	0.42	0.48	0.32	0.42	0.41
ML	A-4	15,976	4,400	0.24	0.26	0.40	0.34	0.40	0.26	0.35	0.28
SC/CL/ML	A-2-6, A-4, A-6, A-7-6	17,600	4,400	0.34	0.35	0.47	0.41	0.47	0.31	0.41	0.40

Table 3-23 The inflated MR values from Method 1

USCS	AASHTO	Design MR (psi)	Adrian	Ann Arbor	Battle Creek	Benton Harbor	Detroit	Flint	Gaylord	Grand Rapids	Hancock	Houghton Lake	Iron Mountain	Kalamazoo	Lansing	Muskegon	Pellston	Pontiac	Traverse City
SM	A-2-4, A-4	5,200	6,365	6,228	6,168	6,318	6,318	6,443	11,159	7,046	10,700	10,766	9,647	6,103	7,460	6,341	9,091	7,482	9,155
SP1	A-1-a, A-3	7,000	9,091	9,358	8,653	9,210	8,578	10,340	14,286	9,447	11,864	12,939	13,780	9,079	10,370	8,226	15,053	10,014	11,925
SP2	A-1-b, A-2-4, A-3	6,500	8,355	9,848	9,326	8,207	8,291	10,172	12,622	9,924	12,897	14,192	13,266	8,355	10,077	8,291	12,082	9,984	11,993
SP-SM	A-2-4, A-4	7,000	9,873	10,043	9,498	8,516	8,610	10,622	13,645	10,401	13,333	14,645	14,028	8,353	10,511	8,599	12,613	10,234	12,478
SC-SM	A-2-6, A-6, A-7-6	5,000	10,331	10,267	10,439	10,548	10,526	10,439	15,923	11,877	14,621	14,045	13,967	10,374	11,877	10,352	15,674	11,877	11,877
SC	A-4, A-6, A-7-6	4,400	9,091	9,035	9,186	9,282	9,263	9,186	14,013	10,452	12,866	12,360	12,290	9,129	10,452	9,109	13,794	10,452	10,705
CL	A-4, A-6, A-7-6	4,400	9,091	9,035	9,186	9,283	9,263	9,186	14,014	10,451	12,866	12,359	12,291	9,128	10,451	9,110	13,794	10,451	10,706
ML	A-4	4,400	10,919	10,706	10,973	10,892	10,865	12,571	18,805	12,753	15,604	17,960	17,187	11,084	13,056	11,110	16,729	12,643	15,439
SC/CL/ML	A-2-6, A-4, A-6, A-7-6	4,400	9,412	9,354	9,510	9,610	9,590	9,510	14,507	10,820	13,320	12,796	12,724	9,451	10,820	9,431	14,280	10,820	11,083

Method 3: Subgrade Design MR at OMC

Method 3 represents a case when design MR is assumed to be at the OMC for a particular soil (A-7-6) in Michigan. It should be noted that the moisture content needs to be determined for in-situ conditions when FWD testing is used to backcalculate the subgrade MR while OMC for a subgrade is required at a construction site. The OMC for a soil type obtained, from the subgrade soil characterization study in Michigan (*13*), were utilized in this method. The results show that the Pavement-ME reduced the MR from 4,400 to 2,300 psi and then it further fluctuates based on the climatic variations estimated by the Enhanced Integrated Climate Model (EICM) (see Figure 3-47).

Based on the above discussion and consultation with MDOT, method 2 was adopted for the local calibration. Consequently, the recommended design MR value corresponding to the soil type for each pavement section was utilized based on Table 3-24.

Table 3-24 Average roadbed soil MR values

Roadbed Type		Average MR			
USCS	AASHTO	Laboratory determined (psi)	Back-calculated (psi)	Design value (psi)	Recommended design MR value (psi)
SM	A-2-4, A-4	17,028	24,764	5,290	5,200
SP1	A-1-a, A-3	28,942	27,739	7,100	7,000
SP2	A-1-b, A-3	25,685	25,113	6,500	6,500
SP-SM	A-1-b,A-2-4, A-3	21,147	20,400	7,000	7,000
SC-SM	A-2-4, A-4	23,258	20,314	5,100	5,000
SC	A-2-6, A-6,A-7-6	18,756	21,647	4,430	4,400
CL	A-4, A-6, A-7-6	37,225	15,176	4,430	4,400
ML	A-4	24,578	15,976	4,430	4,400
SC/CL/ML	A-2-6, A-4, A-6, A-7-6	26,853	17,600	4,430	4,400

3.5.4 Environmental Inputs

The climate inputs were obtained from the Pavement-ME built in climate files. Each climatic station has historical weather data collected over many years. The closest weather station to each selected project was utilized. Table 3-25 summarizes the important climatic information for the stations used in the local calibration. These climate stations represent those that are available to choose as a single climate station.

Table 3-25 Michigan climate station information

Climate station	Mean annual air temperature (°F)	Mean annual rainfall or precipitation (in.)	Wet days (#)	Freezing index (°F-days	Average annual number of freeze thaw cycles
Adrian	49.4	28.9	207.0	1465.2	68.6
Ann Arbor	48.2	29.0	204.0	1771.8	76.3
Battle Creek	49.3	29.4	198.1	1479.9	58.7
Benton Harbor	49.8	28.7	189.5	1205.4	65.5
Detroit (Metro airport)	50.7	32.7	194.1	1149.9	54.5
Detroit (willow run airport)	48.8	27.8	207.5	1559.5	70
Detroit (city airport)	50.4	27.3	202.3	1157.1	47.3
Flint	48.9	26.6	197.9	1544.3	64.8
Gaylord	43.6	27.3	233.7	2346.3	63.3
Grand Rapids	49.0	30.8	206.3	1371.7	61.6
Hancock	40.8	21.5	235.3	2594.1	63.3
Houghton Lake	45.0	25.2	215.9	2152.0	75.3
Iron Mountain	42.9	22.5	205.5	2918.9	85.9
Kalamazoo	49.5	32.6	213.7	1427.3	59.6
Lansing	48.5	28.8	201.9	1658.8	70.0
Muskegon	49.1	30.5	202.8	1182.8	60.5
Pellston	43.1	30.5	233.5	2837.5	88.8
Pontiac	48.6	27.5	209.0	1520.5	58.5
Traverse City	46.6	28.0	221.5	1701.6	69.1

3.6 SUMMARY

This chapter highlights the steps necessary to select the in-service pavement sections and obtain their as-constructed input values for use in the Pavement-ME. Input data collection is one of the most important steps in the local calibration of the performance prediction models. Table 3-26 summarizes the inputs and corresponding levels for traffic, and material characterization data used for the local calibration. The complete list of projects, inputs, and measured performance are summarized in Appendix A.

Table 3-26 Summary of input levels and data source

Input			Input level	Input source
Traffic	AADTT		1	MDOT Historical Traffic counts
	TTC		2	Cluster analysis
	ALS Tandem		2	Cluster analysis
	HDF		2	Cluster analysis
	MDF		3	MDOT traffic characterization study
	AGPV		3	MDOT traffic characterization study
	ALS single, tridem, quad		3	MDOT traffic characterization study
Cross-section (new and existing)	HMA thickness		1	Project specific HMA thicknesses based on design drawings
	PCC thickness		1	Project specific PCC thicknesses based on design drawings
	Base thickness		1	Project specific base thicknesses based on design drawings
	Subbase thickness		1	Project specific subbase thicknesses based on design drawings
Construction materials	HMA	Binder type	3	Project specific binder and mixture gradation data obtained from data collection
		HMA mixture aggregate gradation	3	Project specific binder and mixture gradation data obtained from data collection
		Binder type	1	Pseudo Level 1- MDOT HMA mixture characterization study
		HMA mixture aggregate gradation	1	Pseudo Level 1- MDOT HMA mixture characterization study
	PCC	Strength (f'_c, MOR)	1	Psuedo Level 1 - project specific testing values
		CTE	2	MDOT CTE report recommendations
	Base/subbase	MR	2	Recommendations from MDOT unbound material study
	Subgrade	MR	2	Soil specific MR values - MDOT subgrade soil study
		Soil type	1	Location based soil type - MDOT subgrade soil study
Climate			1	Closest available climate station

Note:

1. Level 1 is project specific data, pseudo level 1 means that the inputs are not project specific but the material properties (lab measured) corresponds to similar materials used in the project
2. Level 2 inputs are based on regional averages in Michigan
3. Level 3 inputs are based on statewide averages in Michigan

CHAPTER 4 - LOCAL CALIBRATION PROCEDURES

4.1 INTRODUCTION

The NCHRP Project 1-40B guide documented the recommended practices for local calibration of the Pavement-ME. The guide outlines the significance of the calibration process as well as the general approach for local calibration. In general, the calibration process is used to (a) confirm that the prediction models can predict pavement distress and smoothness with minimal bias, and (b) determine the standard error associated with the prediction equations. The standard error estimates the scatter of the data around the line of equality between predicted and measured values of distress. The bias indicates if there is any consistent under or over-prediction by the prediction models. It should be noted that the local calibration process only applies to the transfer functions or statistical models in the Pavement-ME. Furthermore, the feasibility of the mechanistic or constitutive models within the Pavement-ME is assumed to be accurate and depict a correct simulation of real-world conditions. This chapter details the (a) local calibration approach and techniques used in this study for each model, (b) effect of the local calibration coefficients on the performance predictions, and, (c) need for reliability and the methods to determine the reliability equations.

4.2 CALIBRATION APPROACHES

The local calibration of the performance prediction models are performed by changing the calibration coefficients in each model. These coefficients are adjusted individually or estimated through minimizing the error between the predicted and measured distress. Table 4-1 summarizes the flexible and rigid pavement performance prediction models, their corresponding transfer functions, and model calibration coefficients. The detailed performance prediction models were summarized in Chapter 2. Two methods of closed-form model calibration are generally used: (a) an analytical process for linear models, and (b) a numerical optimization technique for non-linear models. In both methods, the model constants are determined to minimize the error between measured and predicted distress values. Two types of models are used in the Pavement-ME for performance prediction: (a) structural response models, and (b) transfer functions. The former models are based on analytical solutions based on engineering mechanics (e.g., linear elastic solution to determine stress, strain and deformation for flexible pavements) while the latter models are empirical in nature and relate the pavement response or damage over time. The local calibration process deals with the transfer function for predicting distresses. Among empirical transfer functions, two different calibration approaches may be required depending upon the nature of the distress being predicted: (a) model that directly calculates the magnitude of surface distress, and (b) model that calculates the incremental damage index rather than actual distress magnitude. In the first approach, the pavement response parameter is used to compute the incremental distress in a direct relationship. The local calibration approaches for each model are summarized in Table 4-1. Approach I indicates that the local calibration is performed without running the software each time. Alternatively, approach II requires software execution each time the coefficients are adjusted.

4.3 CALIBRATION TECHNIQUES

In model calibration, a fitting process produces empirical model constants that are evaluated based on the goodness-of-fit criteria to estimate the best set of values for the coefficients. The success of the local calibration depends on the dataset used. Different sampling techniques can improve the confidence in the local calibration coefficients. This section discusses the available local calibration procedures and sampling techniques that can be used to calibrate the performance prediction models.

The local calibration guide (*1*) suggests using statistical techniques to validate the adequacy of the performance prediction models. Traditional split sampling provides one method to calibrate the performance predictions models. Furthermore, resampling methods such as jackknifing and bootstrapping are recommended because they provide more reliable and robust assessment of the model prediction accuracy than the split sampling methods. While the traditional split sampling approach uses a two-step process for calibration and validation, advanced approaches can simultaneously consider both steps. Moreover, the goodness-of-fit statistics are based on predictions rather than on data used for fitting the model parameters. The efficiency and robustness of such approaches become more important when the sample size is small. Different methods can be used for the local calibration of the distress models including (a) traditional split sampling approach, (b) bootstrapping, and (c) jackknifing. These approaches are briefly discussed below.

4.3.1 Traditional Approach

The NCHRP Project 1-40B documented the recommended practices for local calibration of the Pavement-ME performance models (*2*). The approach is classified as traditional approach in this study and was detailed in Chapter 2 and follows the recommendations provided in the 1-40B report (*2*). The calibration-validation process depends on the number of sections selected. In addition, two calibration approaches may be necessary depending on the nature of the distress predicted through the transfer function. The first approach is used for the models that directly calculate the magnitude of the surface distress, while the second approach was used for models that calculate the incremental damage over time and related damage to distresses. Data collected from in-service pavements are used within both approaches to establish the calibration coefficients such that the overall standard error of the estimate between the predicted and observed response is minimized. The model validation procedure is used to demonstrate that the calibrated model can produce accurate predictions of pavement distress for sections other than the ones used for calibration. The success of the validation process can be determined based on the bias in the predicted values and the standard error of estimate. Statistical hypotheses tests should be performed to determine if a significant difference between the calibrated model and the model validation exists (*1, 2*).

Table 4-1 Model calibration approach (calibration outside of the software or rerunning the software)

Pavement type	Performance prediction model		Approach I	Approach II	Model transfer functions
Flexible pavements	Fatigue cracking – bottom up		✓		$FC_{Bottom} = \left(\frac{1}{60}\right)\left(\frac{6000}{1+e^{C_1 C_1^* + C_2 C_2^* Log(DI_{Bottom} \cdot 100)}}\right)$
	Fatigue cracking – top down		✓		$FC_{Top} = (10.56)\left(\frac{1000}{1+e^{C_1 - C_2 \times Log(DI_{top} \cdot 100)}}\right)$
	Rutting	HMA	✓	✓	$\Delta_{p(HMA)} = \varepsilon_{p(HMA)} h_{HMA} = \beta_{1r} k_z \varepsilon_{r(HMA)} 10^{k_{1r}} n^{k_{2r}\beta_{2r}} T^{k_{3r}\beta_{3r}}$
		Base/subgrade	✓		$\Delta_{p(soil)} = \beta_{s1} k_{s1} \varepsilon_v h_{soil} \left(\frac{\varepsilon_o}{\varepsilon_r}\right) e^{-\left(\frac{\rho}{n}\right)^{\beta}}$
	Thermal cracking			✓	$A = 10^{k_t \beta_t (4.389 - 2.52 Log(E_{HMA} \sigma_m \eta))}$
	IRI		✓		$IRI = IRI_o + C_1(RD) + C_2(FC_{Total}) + C_3(TC) + C_4(SF)$
Rigid pavements	Transverse cracking		✓		$CRK_{BU/TD} = \frac{100}{1 + C_4 (DI_F)^{C_5}}$ $TCRACK = (CRK_{Bottom-up} + CRK_{Top-down} - CRK_{Bottom-up} \cdot CRK_{Top-down}) \cdot 100\%$
	Transverse joint faulting			✓	$Fault_m = \sum_{i=1}^{m} \Delta Fault_i$ $\Delta Fault_i = C_{34} \times (FAULTMAX_{i-1} - Fault_{i-1})^2 \times DE_i$ $FAULTMAX_i = FAULTMAX_0 + C_7 \times \sum_{j=1}^{m} DE_j \times Log(1 + C_5 \times 5.0^{EROD})^{C_6}$ $FAULTMAX_0 = C_{12} \times \delta_{curling} \times \left[Log(1 + C_5 \times 5.0^{EROD}) \times Log(\frac{P_{200} \times WetDays}{p_s}) \right]^{C_6}$ $C_{12} = C_1 + C_2 \times FR^{0.25}$ $C_{34} = C_3 + C_4 \times FR^{0.25}$
	IRI		✓		$IRI = IRI_I + C_1 \times CRK + C_2 \times SPALL + C_3 \times TFAULT + C_4 \times SF$

*Red font indicates calibration coefficients

4.3.2 Bootstrapping

At its simplest, for a dataset with a sample size of *N*, *B* "bootstrap" samples of size *N* are randomly selected with replacement from the original dataset. The bootstrap is an approach used to estimate variances, confidence intervals and other statistical properties of a population from a sample. These properties are obtained by drawing samples from a sample. Each bootstrap sample typically omits several observations and has multiple copies of others. This procedure selects the new bootstrap samples "with replacement" and therefore, there is an equal chance of selecting each sample (i.e., a pavement section) multiple times. Validity of bootstrap variance estimates requires that a key analogy holds for the statistics of interest. The resampling properties of the bootstrap must be similar to the sampling properties of the population. The bootstrapped resampling can be performed using different methods: (a) resampling randomly or (b) resampling based on the residuals. The type of resampling approach for bootstrapping depends on the data structure. For example, if fixed regressors are needed for an experiment design, the bootstrapping can be performed using the residuals (error-terms). This means that the residual will correspond to the predicted value since the measured value will not change. On the other hand if the random effects of regressors are to be estimated in a regression model, random resampling can be employed in bootstrapping.

Bootstrapping based on resampling the observations is an approach that is applied when the regression models are built from data that have random regressors and responses. The procedure consists of (*3, 4*):

1. Draw an *n* sized bootstrap sample with replacement from the observations giving a *1/n* probability for each value in the sample set.
2. Calculate the ordinary least squares (OLS) coefficients from the bootstrap sample.
3. Repeat steps 1 and 2 for the total number of bootstraps desired (1000 or 10,000). Higher number of bootstraps will lead to better accuracy; however, it may not be very efficient and gain in accuracy may be not significant.
4. Obtain the probability distribution of the bootstrap estimates and use the distribution to estimate regression coefficients, variances and confidence intervals. Equation (1) shows the bootstrap regression equation:

$$\hat{Y} = X\hat{\beta}^{(b)} + \varepsilon \tag{1}$$

where,
$\hat{\beta}^{(b)}$ is an unbiased estimator of β.

Bootstraps based on resampling the residuals are used when the fixed effect of the regressors are to be considered (i.e., in an experiment design). Therefore, bootstrap resampling must preserve the data structure. The procedure based on resampling the errors is as follows (*3*):

1. Find the ordinary least squares (OLS) coefficient using the least squares regression for the sample
2. Calculate the residuals based on measured and predicted response values.
3. Draw an *n* sized bootstrap random sample with replacement from the residuals determined in Step 2.

4. Compute the bootstrap estimated values by adding the resampled residuals to the OLS regression predicted values.
5. Obtain least squares estimates from the bootstrap samples.
6. Repeat steps 3 to 5 for the total number of bootstrap samples.

Finally, the bootstrap bias, variance, and confidence intervals for regression coefficients can be estimated by using Equations (2) to (4), respectively (*3*):

$$Y^{(b)} = \hat{\beta}^{(b)} - \hat{\beta} \tag{2}$$

where:

$Y^{(b)}$ = bootstrapped bias

$\hat{\beta}^{(b)}$ = bootstrapped estimate of regression coefficient

$\hat{\beta}$ = mean estimate of regression coefficient

$$\mathrm{var}\left(\hat{\beta}^{(b)}\right) = \sum_{b=1}^{B}\left[\left(\hat{\beta}^{(br)} - \hat{\beta}^{(b)}\right)\left(\hat{\beta}^{(br)} - \hat{\beta}^{(b)}\right)'\right] \Big/ (B-1), \quad \mathrm{r} = 1,2,...,B \tag{3}$$

where:

$\mathrm{var}\left(\hat{\beta}^{(b)}\right)$ = bootstrap variance of regression coefficient

$\hat{\beta}^{(br)}$ = ordered bootstrap coefficient corresponding to B

$\hat{\beta}^{(b)}$ = unbiased estimator of β

B = number of bootstraps

$$\hat{\beta}^{(b)} - t_{n-p,\alpha/2} * S_e\left(\hat{\beta}^{(b)}\right) < \beta < \hat{\beta}^{(b)} + t_{n-p,\alpha/2} * S_e\left(\hat{\beta}^{(b)}\right) \tag{4}$$

where:

$t_{n-p,\alpha/2}$ = critical value of t with probability $\alpha/2$

$S_e\left(\hat{\beta}^{(b)}\right)$ = standard error of the $\hat{\beta}^{(b)}$

4.3.3 Jackknifing

Jackknifing is an analytical procedure for refining and confirming the calibration coefficients of a regression model. The model validation statistics are developed independently of the data used for calibration. Multiple jackknifing is used to assess the sensitivity of the validation goodness-of-fit statistics. To develop jackknife statistics from a sample of *n* sets of measured values, the data matrix is divided into two groups, one part for calibration and the other for validation. For an *n*-1 jackknife validation the procedure begins by removing one set of measurements from the data matrix and calibrating the model with the remaining *n*-1 sets of measurements. The k^{th} set of measurements that was withheld is then used to predict the criterion variable Y_k, from which the error is computed as the difference between the predicted and measured values of the criterion variable. A second set of measurements is removed while replacing the first set, and the new *n*-1 set is used to calibrate the new model. This new calibrated model is then used with the withheld set of *x* values to predict *y* and

compute 2nd error. The procedure is repeated until all *n* sets have been used for prediction. This yields *n* values of the error, from which the jackknifing goodness-of-fit statistic can be computed. The jackknifed errors are computed from measured *x* values that were not used in calibrating the model coefficients. Thus, the jackknifing goodness-of-fit statistics are considered to be independent measures of model accuracy (*5*). When comparing jackknife with bootstrap procedures, jackknife is less demanding computationally than the bootstrap method and relies on dividing the sample observations into disjoint subsets, each having the same number of observations. In addition, the jackknife takes a fundamentally different view of the possible replicates of the statistic; it treats them as a finite collection whereas bootstrap resampling assumes that the replicates are a sample from the population of infinite size. When bootstrapping is used to estimate the standard error of a statistic, it gives slightly different results when repeated on the same data, whereas the jackknife gives exactly the same result each time. The bootstrap is a more general technique and preferred to the jackknife method.

4.3.4 Summary of Resampling Techniques

The bootstrap and jackknife are nonparametric and robust resampling techniques for estimating standard errors and confidence intervals of a population parameter such as mean, median, proportion, odds ratio, or regression coefficients. The main advantage of these techniques, especially bootstrapping is estimation of parameters are possible without making distribution assumptions. In addition, the approach is valid when such assumptions are in doubt, or where parametric inference is impossible or requires very complicated formulas for the standard errors estimation. On the other hand, there are several limitations of the bootstrap method, especially when (a) using the methods for small data sets with outliers and (b) adopting bootstrapping for time series data when the independent assumption is violated. Jackknifing may be more efficient; however, it is not as powerful as bootstrapping, especially when sample size is limited. Therefore, only bootstrapping was used in the study.

4.4 PROCEDURE FOR CALIBRATION OF PERFORMANCE MODELS

The local calibration procedure for MDOT pavements follows the general guidelines provided by the NCHRP guide for local calibration (*1*) as described in Chapter 2. The first step consists of selecting the pavement sections and collecting their corresponding input data. The project selection and input data collection efforts were discussed in Chapter 3. The remaining process consists of the following steps:

1. Execute the Pavement-ME software to predict the pavement performance for each selected pavement section.
2. Extract the predicted distresses and compare with the measured distresses.
3. Test the accuracy of the global model predictions and determine if local calibration is required.
4. If local calibration is required, adjust the local calibration coefficients to eliminate bias and reduce standard error.
5. Validate the adjusted coefficients with pavement sections not included in the calibration set.
6. Adjust the reliability equations for each model.

Steps 1 and 2 do not require further explanation. Step 3 and onwards are presented next.

4.4.1 Testing the Accuracy of the Global Model Predictions

The adequacy of the global model predictions is determined through performing three hypothesis tests (step 3). The hypothesis tests provide an indication if the models are biased. Bias is defined as the consistent under- or over-prediction of distress or IRI. The bias between measured and predicted distress/IRI is determined by performing linear regression, hypothesis tests and a paired *t*-test using a significance level of 0.05. Figure 4-1 shows a representation of model bias and standard error for various conditions. The three hypothesis tests are summarized in Table 4-2. If any of these hypothesis tests are rejected (significance level greater than 0.05) for a performance model, then local calibration is recommended. The null hypothesis (H_o) represents the mean difference between predicted and measured distress is zero i.e., there is no difference between both. The alternate hypothesis (H_1) depicts that there is a difference between predicted and measured distress. Similarly, hypothesis tests were performed to test the intercept and slope differences between predicted and measured distresses.

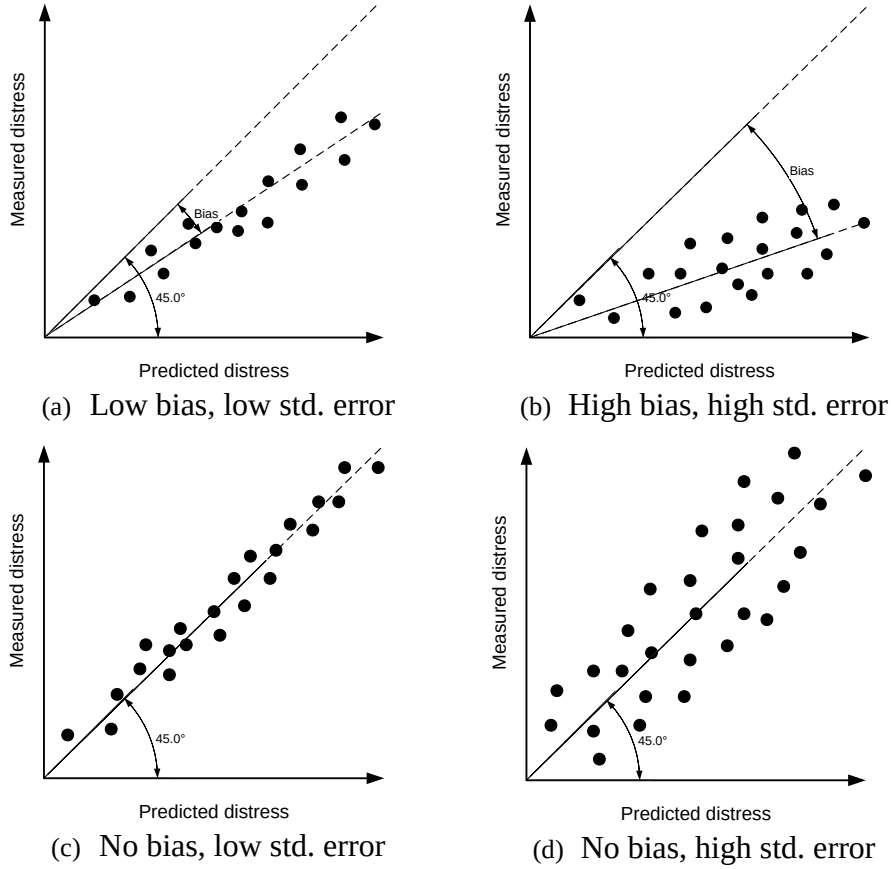

Figure 4-1 Schematic of bias and standard error for model calibration

Table 4-2 Hypothesis tests

Hypothesis test	Hypotheses
Mean difference (paired *t*-test)	$H_0 = (predicted - measured) = 0$ $H_1 = (predicted - measured) \neq 0$
Intercept	$H_0 = intercept = 0$ $H_1 = intercept \neq 0$
Slope	$H_0 = slope = 1$ $H_1 = slope \neq 1$

4.4.2 Local Calibration Coefficient Refinements

As discussed in Section 4.3, there are different procedures to locally calibrate the different performance prediction models. This section outlines the procedures used for each performance prediction model in this study (steps 4 and 5). Additionally, the various resampling techniques and datasets used for local calibration are also discussed.

4.4.2.1. Data subpopulations

The pavement performance prediction models were locally calibrated for Michigan pavements using multiple statistical sampling techniques and dataset options. The data set options are combinations of reconstruct, rehabilitation and LTPP pavement sections. The main objective for considering different subsets of all the selected pavement sections, referred as options herein, is to verify if different calibration coefficients are required for an option or an overall model calibration is adequate for different options. The options with different dataset combinations are as follows:

Option 1: MDOT reconstruct sections only
Option 2: MDOT reconstruct and rehabilitation sections
Option 3: MDOT reconstruct, rehabilitation, and LTPP sections
Option 4: MDOT rehabilitation sections only

4.4.2.2. Sampling techniques

The sampling techniques mentioned above were applied to each option (i.e., different subpopulation) for studying the effects of various sampling methods on the local calibration coefficients. The performance prediction models are locally calibrated by minimizing the sum of squared error between the measured and predicted distress for each of the following sampling techniques:

- No sampling (include all data)
- Traditional split and repeated split sampling
- Bootstrapping

The different sampling techniques are used to determine the best estimate of the local calibration coefficients and the associated standard errors. The use of these techniques is considered because of data limitations, especially due to limited sample size.

First, the entire dataset, including all the selected pavement sections, will be used to calibrate the performance prediction models. Since all of the pavement sections will be included in the calibration effort, no validation of the locally calibrated model can be performed. Second, a traditional split sampling technique will be used. In this method, 70% of the pavement sections are randomly selected for local calibration, and the remaining 30% are utilized for validation. Split sampling can indicate how well the calibrated model can predict pavement distress for pavement sections that are not included in the calibration dataset. Generally, SEE and bias from the validation should be similar to those of locally calibrated model. However, the split sampling technique might not give reasonable results when using limited sample sizes. In order to address the concerns of limited sample size, the split sampling technique was used repeatedly to estimate distributions of the calibration and validation parameters (i.e., SEE, bias, calibration coefficients). Based on these distributions, a mean value, median, and confidence intervals for each parameter is estimated. The confidence interval determined through repeated sampling provides a better indication of the variability of the calibration parameters. The final resampling technique considered will be bootstrapping. For a dataset of sample size *N*, *B* number of "bootstrap" samples of size *N* is randomly selected with replacement. The model parameters are estimated for *B* number of bootstraps. The details of bootstrapping were discussed previously. Similar to the split sampling approach, bootstrap samples are drawn from the entire dataset. The model is calibrated for each bootstrapped sample dataset and the SEE, bias, and calibration coefficient parameters are estimated. The process is repeated for *B* number of bootstraps to obtain distributions for each parameter. Figure 4-2 shows the flow diagram for the calibration process using both bootstrapping and repeated split sampling for the performance models.

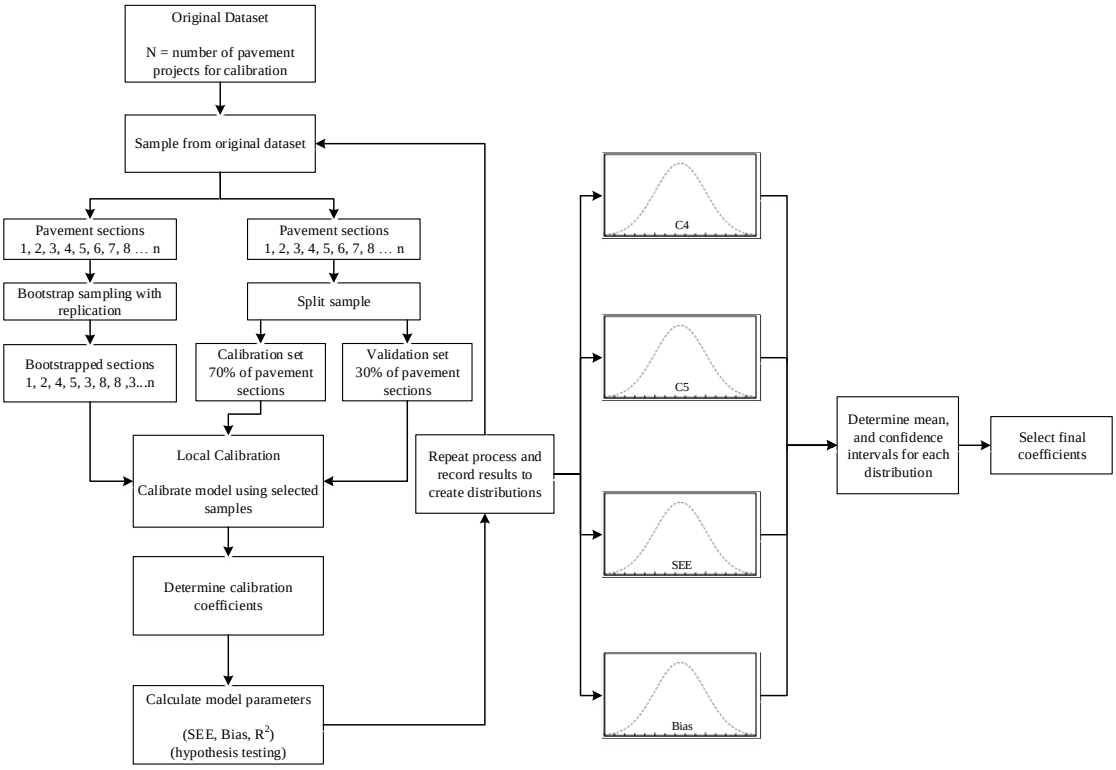

Figure 4-2 Repeated sample calibration procedure

4.5 FLEXIBLE PAVEMENT MODEL COEFFICIENTS

The flexible pavement performance prediction models include fatigue (alligator) cracking, longitudinal cracking, rutting, transverse (thermal) cracking and IRI. The impact of calibration coefficients on the predicted performance specific to each model is discussed in this section.

4.5.1 Alligator Cracking Model (bottom-up fatigue)

The alligator (bottom-up fatigue) cracking model is calibrated by changing the C_1 and C_2 coefficients (see Table 4-1). The effects of C_1 and C_2 on the predicted alligator cracking are shown in Figure 4-3. The C_1 affects the initiation or start of the alligator cracking and C_2 affects the slope of the crack propagation. In this study, two sets of calibrations are performed for the alligator cracking model (a) combined measured top-down and bottom-up cracking, and (b), bottom-up cracking only. These distresses were combined because at the surface, it is difficult to identify if the crack propagated from the top or bottom.

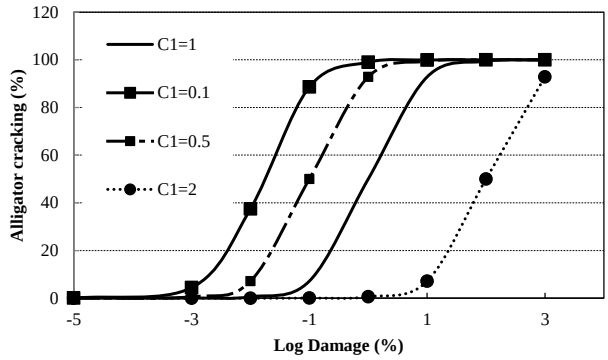

(a) Effect of C_1

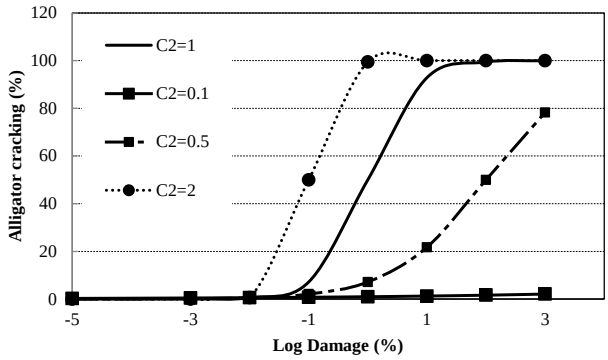

(b) Effect of C_2

Figure 4-3 Effect of calibration coefficients on alligator cracking

4.5.2 Longitudinal Cracking Model (top-down fatigue)

The longitudinal (top-down fatigue) cracking model is calibrated by changing the C_1 and C_2 coefficients (see Table 4-1). The effects of C_1 and C_2 on the predicted longitudinal cracking

are shown in Figure 4-4. The C_1 affects the initiation or start of the longitudinal cracking and C_2 affects the slope of the crack propagation.

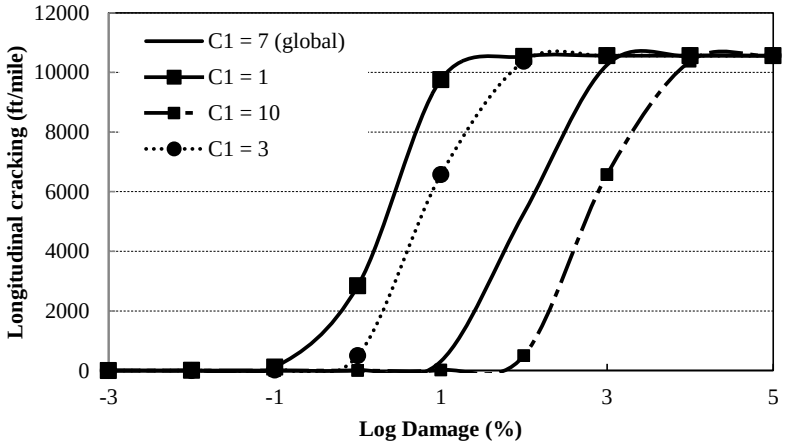

(a) Effect of C1

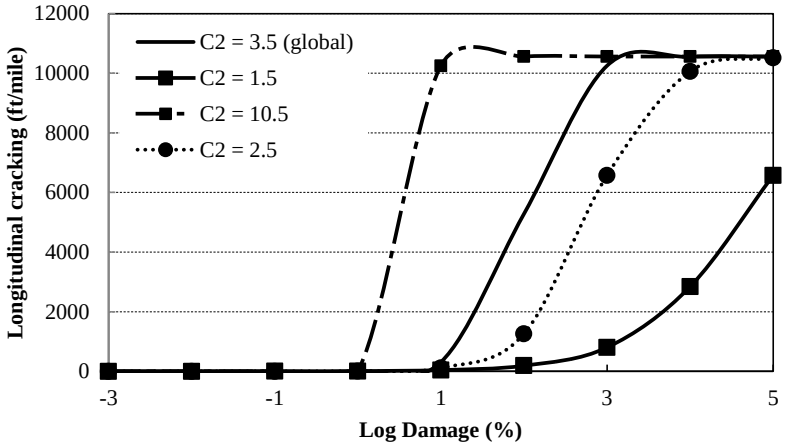

(b) Effect of C2

Figure 4-4 Effect of calibration coefficients on longitudinal cracking

4.5.3 Rutting Model

The rutting model in the Pavement-ME predicts rut depth for the HMA, base, and subgrade layers in the pavement structure. The prediction models are different for each layer and the sum of the rut depth in three layers represents the total surface rutting prediction. Since the rutting models are different for bound (HMA) and unbound layers (base, subbase, and subgrade), the measured rutting for each layer is needed for calibrating the rutting model within each. The MDOT PMS database report only total surface rutting and does not provide rutting measurements/contributions for individual layers. The transverse profiles for the selected projects were utilized to estimate the rutting in the HMA, base and subgrade layers. The HMA rutting model has three calibration coefficients as shown in Table 4-1. The local calibration coefficient (β_{r1}) is a direct multiplier and does not require rerunning of the

software every time the coefficient is adjusted. The β_{r2} and β_{r3} calibration coefficients are related to the number of load repetitions and the pavement temperature, respectively. These coefficients do require a rerunning of the software every time the coefficients are adjusted. A combination matrix was developed to determine which combination provided the lowest SEE and bias. The ranges of these coefficients values were consistent with those found in the literature as summarized in Chapter 2. Table 4-3 summarizes the β_{r2} and β_{r3} values used in the evaluation. Figure 4-5 shows the impact of the β_{r2} and β_{r3} calibration coefficients on the predicted HMA rutting. The results show that both coefficients affect the overall magnitude and rate of HMA rutting. It should be noted that the predicted rutting magnitudes will be significantly different if axle load spectra or climates are changed.

Table 4-3 HMA rutting β_{r2} and β_{r3} calibration coefficients

β_{r2} coefficients	β_{r3} coefficients
0.4	0.4
0.7	0.7
1	1
1.3	1.3

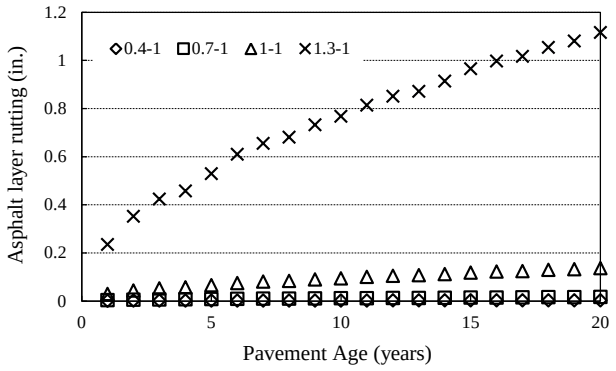

(a) β_{r2}

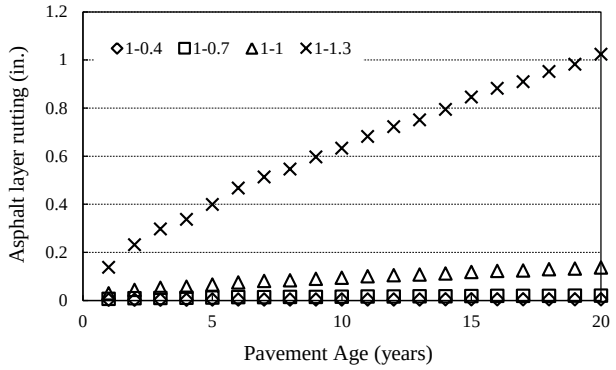

(b) β_{r3}

Figure 4-5 Effect of βr_2 and βr_3 on HMA rutting

The base and subgrade rutting models have one calibration coefficient each (β_{s1}). The coefficient is a direct multiplier in the equation and does not require rerunning of the software when the coefficient is adjusted. The total rutting is determined by summing the

HMA, base and subgrade rutting. The rutting model in the Pavement-ME was calibrated using the following two methods:

1. *Method 1: Individual layer rutting calibrations* — calibrate the rutting model by changing the individual calibration coefficient (HMA, base/subbase, and subgrade) relative to the rutting contribution of each layer by using the estimates of layer contributions from a transverse profile analysis.
2. *Method 2: Total surface rutting calibration* — calibrate the rutting model by changing the individual calibration coefficient for each layer simultaneously relative to the total surface rutting.

Transverse profile data were obtained from MDOT to estimate the layer contributions to surface rutting. The analysis of the transverse profiles for the selected flexible pavement sections could improve the rutting calibration. Analyses of transverse profiles assist in estimating the seat of rutting and the layer contributions to the total surface rutting (*Method 1*). The width and depth of the measured rut channel can be used to determine the seat of rutting. A study sponsored by the National Cooperative Highway Research Program (NCHRP) developed a procedure to determine the seat of rutting from the transverse profiles (*6*). The procedure consists of calculating the critical ratio between the total area above (positive area) and below (negative area) the profile reference line. The positive and negative areas with a reference line are shown in Figure 4-6.

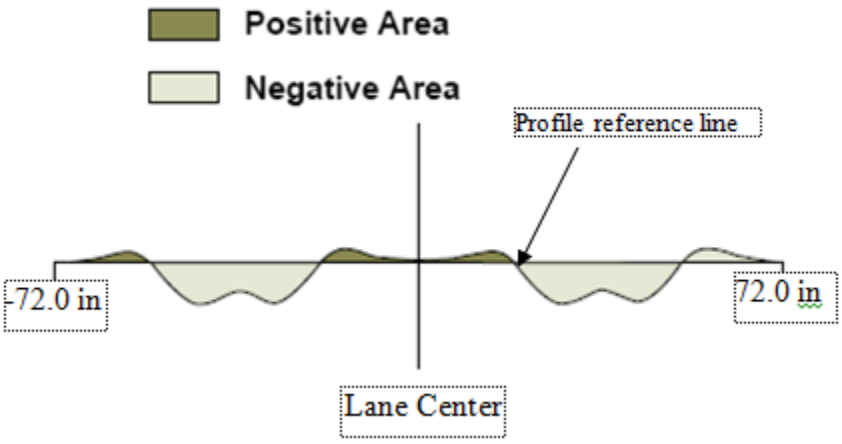

Figure 4-6 Positive and negative areas in the NCHRP procedure (*7*, *8*)

In order to determine the seat of rutting, several calculations have to be made to satisfy a set of conditions. The following calculations are needed:

$$A = Ap + An \tag{5}$$

$$R = \left| \frac{Ap}{An} \right| \tag{6}$$

$$C1 = (-858.21 \times D) + 667.58 \quad (7)$$

$$C2 = (-1509.0 \times D) - 287.78 \quad (8)$$

$$C3 = (-2120.1 \times D) - 407.95 \quad (9)$$

where,

A = Total area
Ap = Positive area
An = Negative area
R = Critical ratio
C1 = theoretical average total area for HMA failure, mm^2;
C2 = theoretical average total area for base/subbase failure, mm^2
C3 = theoretical average total area for subgrade failure, mm^2;
D = maximum rut depth, mm

Based on the above equations, the maximum rut depth is calculated by following the illustration in Figure 4-7. The total maximum rutting is the distance between the average value of the two positive peaks and the rut depth below the profile reference line. In this case, the maximum rut depth is 1.2 inches. A similar procedure was used to determine the maximum rut for all transverse profiles. The seat of rutting may occur in any of the three pavement layers (HMA, base, subgrade) and the typical failure shapes are visually represented in Figure 4-8.

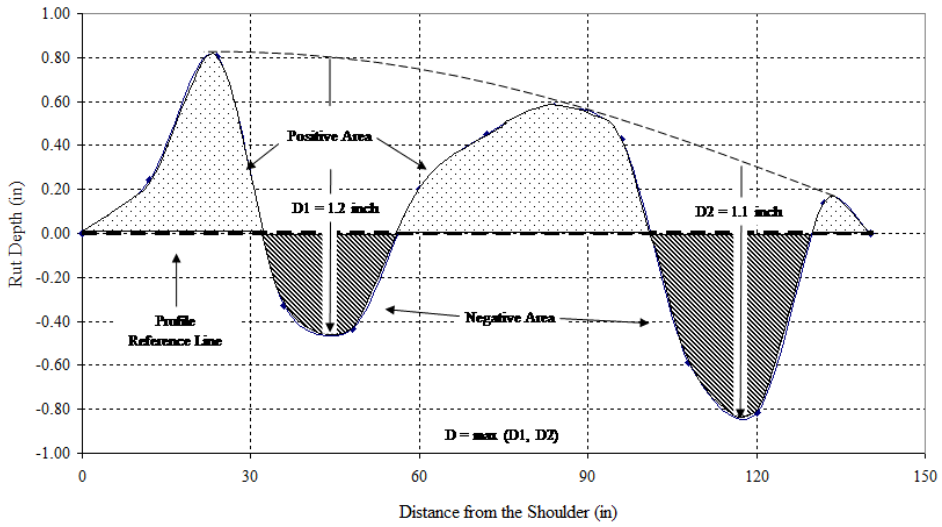

Figure 4-7 Calculation of the maximum rut depth (*7*, *8*)

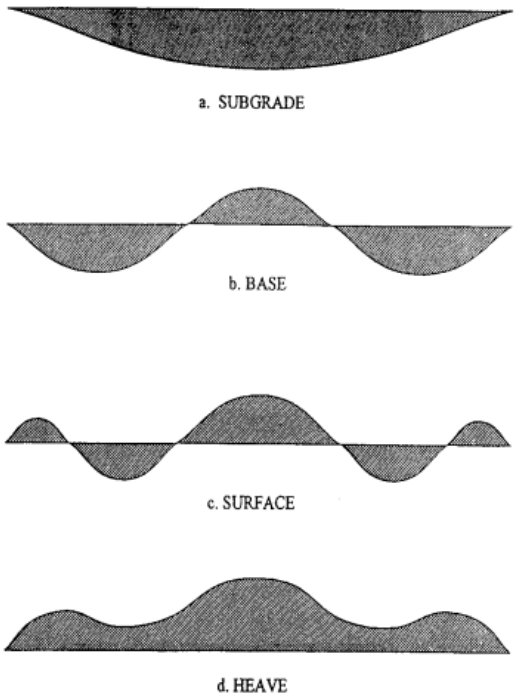

Figure 4-8 Typical seat of rutting based on transverse profile shapes (*7*, *8*)

The flow chart shown in Figure 4-9 can be used to determine the seat of rutting. Finally, Figure 4-10 can be used as an alternative to Equations (5) through (9).

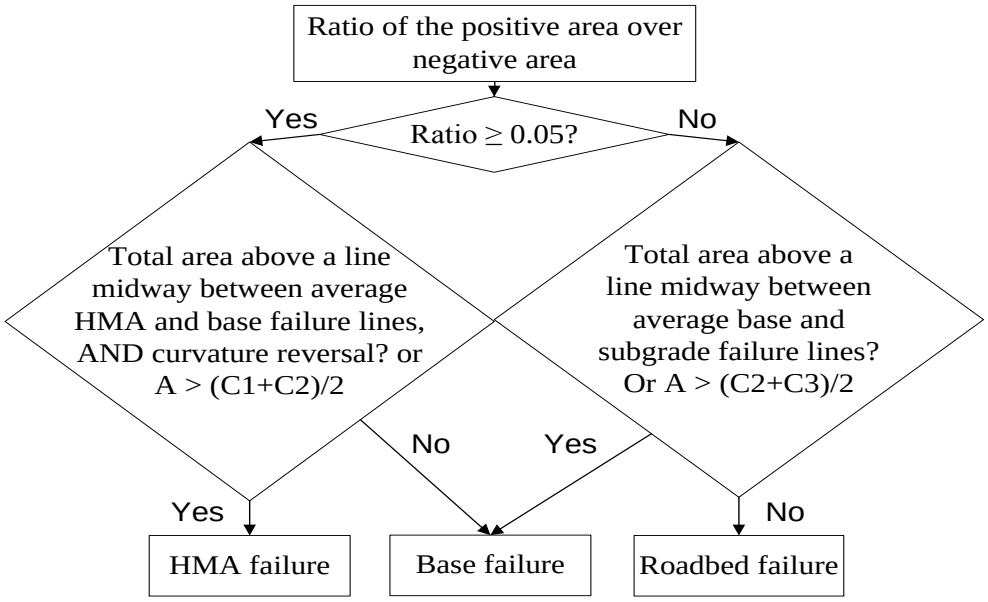

Figure 4-9 Conditions for determining the rutting seat (*7*, *8*)

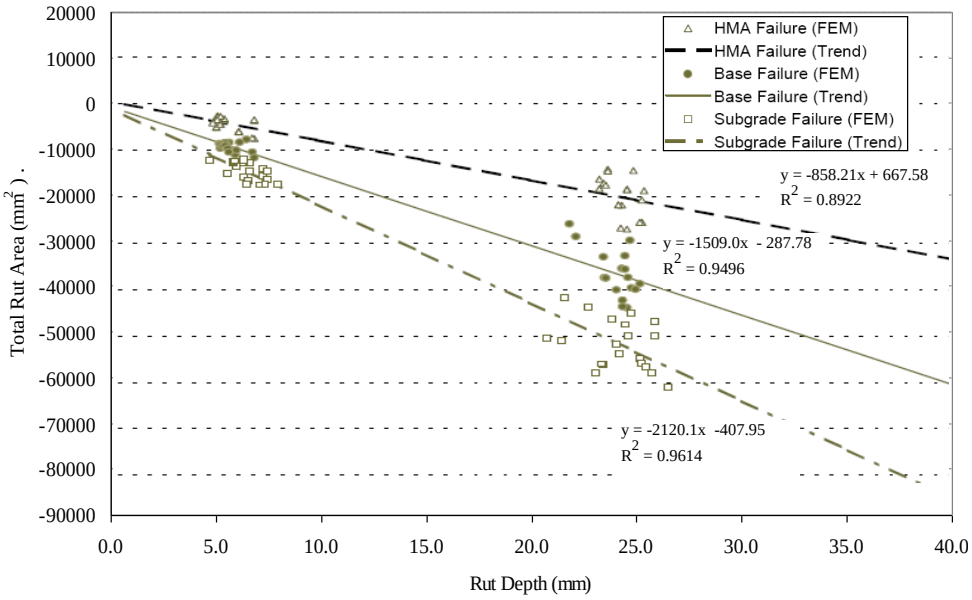

Figure 4-10 Correlation of the type of failure as a function of maximum rut depth and total rut area (*7, 8*)

The data provided by MDOT included transverse profiles approximately every six feet along the length of the entire control section and was collected in 2012 and 2013. The transverse profile data were extracted for each flexible pavement project in the calibration dataset. The transverse profiles were analyzed using the procedure described above. The research team had several discussions with the data collection vendor (M/s Fugro Roadware) regarding the methods used to calculate rutting from the raw profile data. Based on these discussions, several concerns regarding the pavement edge, and how to analyze heaving sections were clarified. The analyses were adjusted based on these clarifications. Initially, it was assumed that the first and last point in the transverse profile represents the edge of the pavement. Later, the edge was adjusted to ensure that there is no unexpected drop off because of its impact on the reference line. It should be noted that an incorrect reference line can significantly impact the seat of rutting calculations. Figure 4-11 shows the adjustment made for the pavement edge.

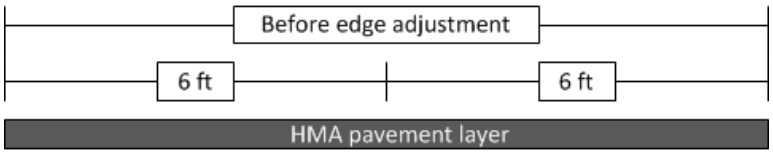

(a) Before edge adjustment

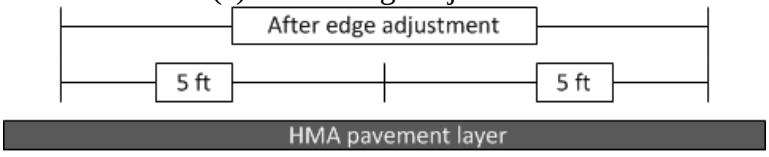

(b) After edge adjustment

Figure 4-11 Edge adjustment for transverse profile

As mentioned before, the transverse profiles were analyzed for each project. Furthermore, the transverse profile analysis results were summarized for each pavement type (new reconstruct and rehabilitation). The heave sections were excluded from the analysis because the entire transverse profile results in a positive area above the reference line. The ratio between the positive and negative area cannot be calculated for heave sections. The following process was adopted for determining the layer contributions to total surface rutting:

a. Identify and extract all the transverse profiles within a particular section (i.e., based on the beginning mile point (BMP) and ending mile point (EMP)
b. Analyze each individual transverse profile (at 6 feet interval) using the above mentioned seat of rutting NCHRP methodology
c. Determine the distribution of the seat of rutting for HMA, Base/subbase, and subgrade layers within a project
d. Calculate layer contributions to the total surface rutting based on the seat of rutting distributions
e. Repeat steps 'a' to 'd' for all selected pavement sections
f. Establish average layer contributions to total surface rutting by pavement type and MDOT regions. These averages were used for the pavement sections where transverse profile data were not available.

It should be noted that the transverse profile analyses were utilized only to determine the layer contributions (i.e., the percent) for each pavement section to total surface rutting. However, the magnitude of individual layer rutting (HMA, base/subbase, and subgrade) was determined based on the estimated percent contribution by multiplying it with the measured surface rutting over time for local calibration.

The results shown in Figure 4-12 indicate that the overwhelming majority (>70%) of rutting occurs in the HMA layer for all pavement sections. The individual percentages for each pavement section were used to determine the HMA, base and subgrade rutting from the measured rutting extracted from the MDOT sensor database. The rutting contribution from each layer is very important in the calibration of the rutting model in the Pavement-ME as mentioned later in the report.

4.5.4 Thermal Cracking Model

The transverse cracking model in the Pavement-ME has three distinct models based on the selected HMA input level. It was observed from the literature that minimal transverse (thermal) cracking was predicted for Level 3 inputs. The low prediction values were attributed to the assumption that if the appropriate asphalt binder (PG) is selected for the appropriate climatic condition, then thermal cracking should not occur. The transverse cracking model was calibrated for both Level 1 and 3 HMA inputs. All of the pavement sections in the calibration dataset had available Level 3 data. Results from Part 1 of this study were used to determine which mixture and binder types had Level 1 data. The projects with Level 1 data were also used for local calibration. It should be noted that the Level 1 data may not reflect HMA material properties at the time of construction of the selected pavement sections.

The calibration coefficients for the thermal cracking model were adjusted individually and the software requires rerunning for each project. The calibration coefficients were adjusted based on ranges obtained from the literature and are shown in Chapter 5.

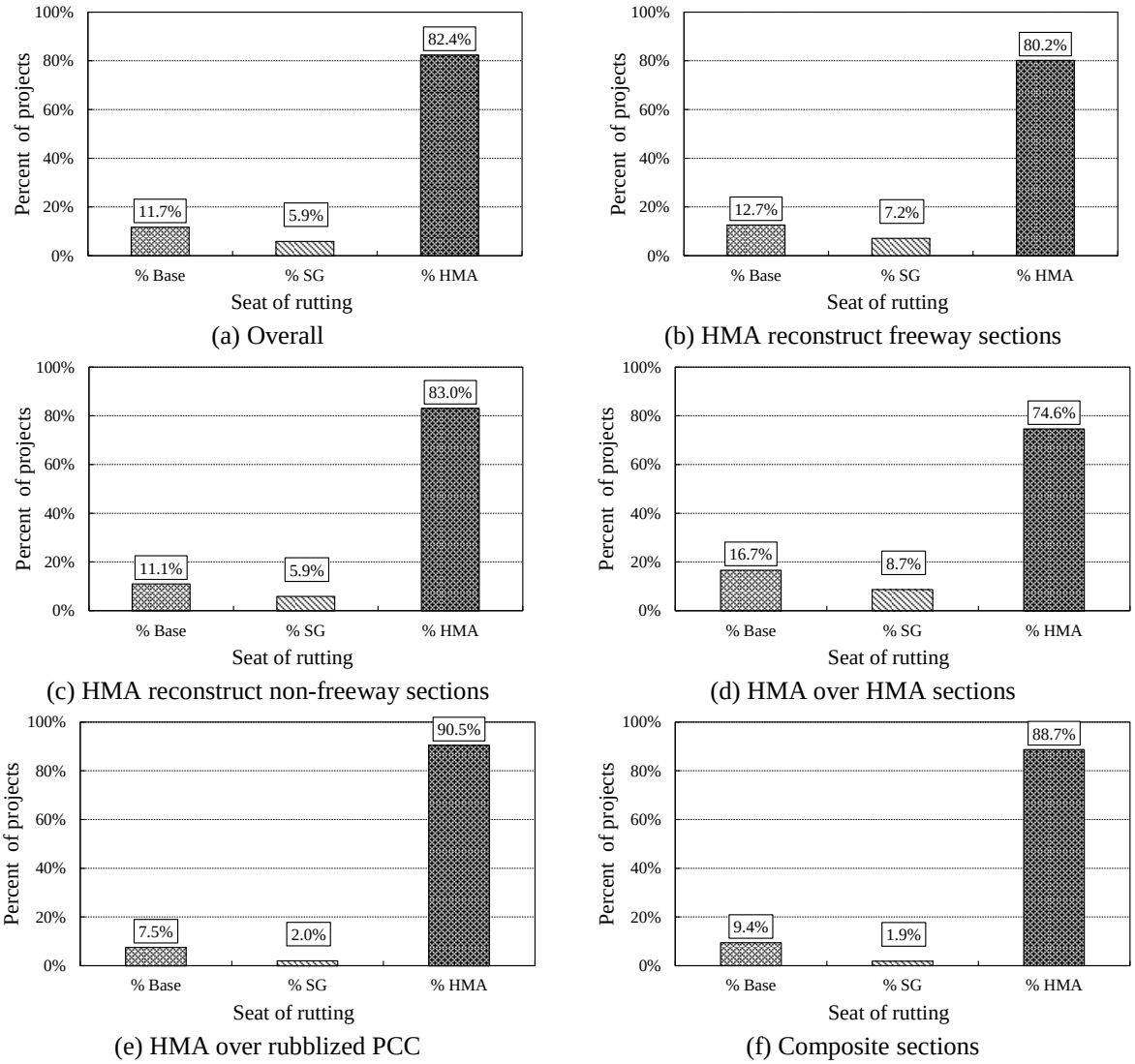

Figure 4-12 Transverse profile analysis results

4.5.5 IRI Model for Flexible Pavements

The IRI model for flexible pavements was calibrated after completing the local calibration of the fatigue; rutting and transverse cracking models. The IRI model is a function of the individual distress predictions, site factor and initial IRI (Equation 10). The regression coefficients (calibration coefficients) were adjusted to minimize the error between the predicted and measured IRI. The global model coefficients were used as seed (initial) values for the local calibration. Issues were encountered when attempting to match the IRI predictions outside the software. These predictions did not match due to errors in the site

factor (*SF*) equation found in the literature. The correct *SF* equation as coded in the Pavement-ME software is shown in Equation (10).

$$IRI = IRI_o + 40.0(RD) + 0.400(FC_{Total}) + 0.0080(TC) + 0.0150(SF) \quad (10)$$

Where;

IRI_o = Initial IRI after construction, in/mi.
SF = Site factor, refer to Equation (11)
FC_{Total} = Area of fatigue cracking (combined alligator, longitudinal, and reflection cracking in the wheel path), percent of total lane area. All load related cracks are combined on an area basis – length of cracks is multiplied by 1 foot to convert length into an area basis.
TC = Length of transverse cracking (including the reflection of transverse cracks in existing HMA pavements), ft/mi.
RD = Average rut depth, in.

$$SF = (Frost + Swell) \times Age^{1.5} \quad (11)$$

$$Frost = Ln\left[(Rain + 1) \times (FI + 1) \times P_4\right] \quad (12)$$

$$Swell = Ln\left[(Rain + 1) \times (FI + 1) \times P_{200}\right] \quad (13)$$

where;

SF = Site factor
Age = Pavement age (years)
FI = Freezing index, °F-days.
$Rain$ = Mean annual rainfall (in.)
P_4 = Percent subgrade material passing the No. 4 sieve
P_{200} = Percent subgrade material passing the No. 200 sieve.

4.6 RIGID PAVEMENT MODEL COEFFICIENTS

The rigid pavement performance prediction models include transverse cracking, faulting, and IRI. The impact of calibration coefficients on the predicted performance specific to each model is discussed in this section.

4.6.1 Transverse Cracking Model

The transverse cracking model was calibrated by adjusting the C_4 and C_5 coefficients. These coefficients affect the slope and magnitude of the transverse cracking predictions. Figure 4-13 shows the effect of changing these calibration coefficients.

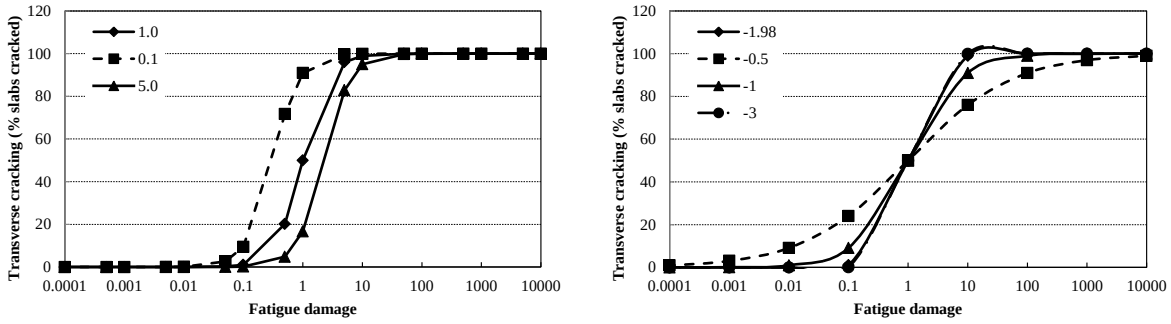

(a) C_4 (b) C_5

Figure 4-13 Effect of transverse cracking model calibration coefficients

4.6.2 Transverse Joint Faulting Model

The faulting model was calibrated by adjusting the C_1 coefficient. Only the C_1 coefficient was adjusted because the predicted faulting could not be calculated outside of the software using the model parameters due to inconsistencies in the output files and very low magnitudes of measured faulting. The magnitudes of the measured faulting for the calibration sections are extremely low (less than 0.1 inches). The C_1 coefficient directly impacts the magnitude of predicted faulting, and the software needs to be rerun every time it changes. A range of C_1 (0.4 to 1) were selected for the local calibration. The effect of the coefficient on transverse joint faulting is shown in Figure 4-14 for a range from 0.5 to 2 as an example. Increases in the coefficient increase the magnitude of the predicted faulting significantly or vice versa.

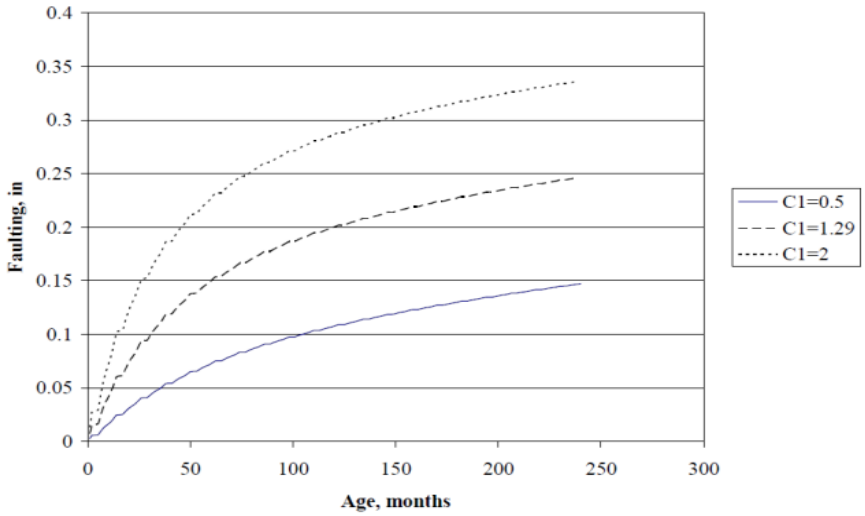

Figure 4-14 Impact of C_1 on the faulting predictions

4.6.3 IRI Model for Rigid Pavements

The rigid pavement IRI model was calibrated after the local calibration of the transverse cracking and faulting models. The IRI model is shown in Equation (14) and additional details are shown in Chapter 2. The locally calibrated transverse cracking and faulting models were used to predict IRI. The predicted and measured IRI are compared to calculate the SEE and bias. The local calibration coefficients are adjusted by performing a regression analysis. The global model calibration coefficients were used as seed values in the local calibration. It should be noted that the spalling model (coded in the software) in the global IRI model equation is not the same as reported in the literature. The spalling calculation equation found in the manual of practice (*9*) does not accurately represent the internal calculations for spalling in the software. Equation (15) shows the spalling model as documented in the literature, and Equation (16) shows the model used to calculate *SCF*. Equation (17) shows the correct model used to predict *SCF* in the software to calculate spalling. The correct model is reported in the FHWA study which determined improved performance prediction models for PCC pavements (*10*).

$$IRI = IRI_I + C1 \times CRK + C2 \times SPALL + C3 \times TFAULT + C4 \times SF \quad (14)$$

$$SPALL = \left[\frac{AGE}{AGE + 0.01} \right] \left[\frac{100}{1 + 1.005^{(-12 \times AGE + SCF)}} \right] \quad (15)$$

where:

SPALL = Percentage joints spalled (medium- and high-severities).
AGE = Pavement age since construction, years.
SCF = Scaling factor based on site, design, and climate.

$$SCF = -1400 + 350 \times AIR\% \times (0.5 + PREFORM) + 3.4 \times f'c \times 0.4 - 0.2\,(FTCYC \times AGE) + 43 \times h_{PCC} - 536 \times WC\_Ratio \quad (16)$$

where;
AIR% = PCC air content, percent.
AGE = Time since construction, years.
PREFORM = 1 if preformed sealant is present; 0 if not.
f'c = PCC compressive strength, psi.
FTCYC = Average annual number of freeze-thaw cycles.
h_{PCC} = PCC slab thickness, in.
WC_Ratio = PCC water/cement ratio.

$$SCF = -1400 + 350 \times AIR\% \times (0.5 + PREFORM) + 43.4 \times f'c^{0.4} - 0.2\,(FTCYC \times AGE) + 43 \times h_{PCC} - 536 \times WC\_Ratio \quad (17)$$

where;
AIR% = PCC air content, percent.
AGE = Time since construction, years.
PREFORM = 1 if preformed sealant is present; 0 if not.
f'c = PCC compressive strength, psi.
FTCYC = Average annual number of freeze-thaw cycles.
h_{PCC} = PCC slab thickness, in.
WC_Ratio = PCC water/cement ratio.

4.7 DESIGN RELIABILITY

Reliability has been incorporated into the Pavement-ME in a consistent and uniform fashion for all pavement types (step 6). A designer may specify the desired level of reliability for each distress type and smoothness. The level of design reliability could be based on the general consequence of reaching the terminal condition earlier than the design life. Design reliability (*R*) is defined as the probability (*P*) that the predicted distress will be less than the critical distress level over the design period (9). The design relibility for all distresses can be shown by the following equation:

$$R = P\,[\,Distress\ over\ Design\ Period < Critical\ Distress\ Level\,] \quad (18)$$

Design reliability is defined as follows for smoothness (IRI):

$$R = P\,[\,IRI\ over\ Design\ Period < Critical\ IRI\ Level\,] \quad (19)$$

This means that if 10 projects were designed and constructed using a 90 percent design reliability for fatigue cracking, one of those projects, on average, would exceed the threshold or terminal value of fatigue cracking at the end of the design period. This definition deviates from previous versions of the AASHTO 1993 Pavement Design Guide in that it considers multiple predicted distresses and IRI directly in the definition. Design reliability levels may vary by distress type and IRI or may remain constant for each. It is recommended, however, that the same reliability be used for all performance indicators(*9*).

The designer inputs critical or threshold values for each predicted distress type and IRI. The Pavement-ME procedure predicts the mean distress types and smoothness over the design life of the pavement. Figure 4-15 shows an example of average IRI prediction (solid line R = 50 %). The mean value of distresses or smoothness predicted may represent a 50 percent reliability estimate at the end of the analysis period (i.e., there is a 50 percent chance that the predicted distress or IRI will be greater than or less than the mean prediction).

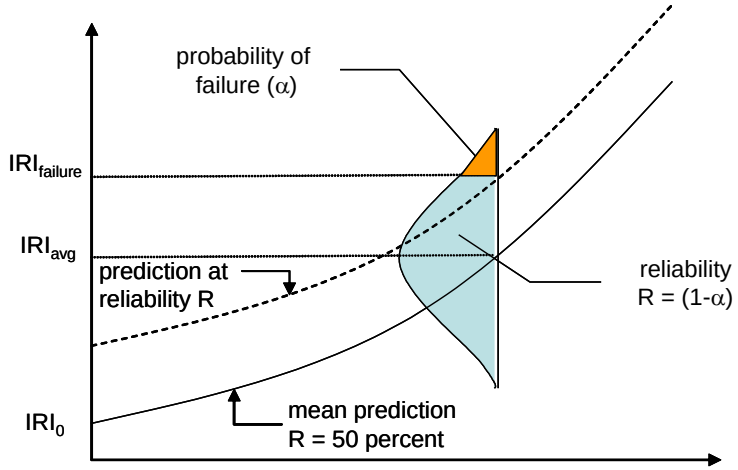

Figure 4-15 Design Reliability Concept for Smoothness (IRI)(*9*)

For all practical purposes, a designer will require a reliability higher than 50 percent.. In fact, the more important the project in terms of consequences of failure, the higher the desired design reliability. For example, the consequence of early failure on an urban freeway is far more important than the failure of a farm-to-market roadway. Some agencies typically use the level of truck traffic volume as the parameter for selecting design reliability. The dashed curve in Figure 4-15 shows the prediction at a level of reliability, *R* (e.g., 90 percent). For the design to be at least 90 percent reliable the dashed curve at reliability *R* should not cross the IRI at the threshold criteria throughout the design analysis period. If it does, the trial design should be modified to increase the reliability of the design.

The reliability of the trial design is dependent on the model prediction error (standard error) of the distress prediction equations, (see Table 4-1). In summary, the mean distress or IRI value (50 percent reliability) is increased by the number of standard errors that apply to the reliability level selected. For example, a 75 percent reliability uses a factor of 1.15 times the standard error, a 90 percent reliability uses a factor of 1.64, and a 95 percent reliability uses a value of 1.96. The calculated distresses and IRI are assumed to be approximately normally distributed over the ranges of the distress and IRI that are of interest in the design. As noted above, the standard deviation for each distress type was determined from the model

prediction error in the local calibration. Each model was globaly calibrated using LTPP and other field performance data. The prediction error was obtained as the difference of predicted and measured distress for all pavement sections included in the calibration efforts. This difference, or residual error, contains all available information on the ways in which the prediction model fails to properly explain the observed distress. The standard deviation for the IRI model was determined using a closed form variance model estimation approach.

There are two main methods to determine the design reliability for various performance models in flexible and rigid pavements:

1. *Method 1*: Reliability determined based on the relationship between the mean predicted distress and standard deviation of the measured distress.
2. *Method 2*: Reliability based on the standard error determined using the variance approach.

4.7.1 Reliability based on Method 1

The reliability of the alligator cracking model assumes that the expected percentage of fatigue cracking is approximately normally distributed. The likely variation of cracking around the expected level can be defined by the mean predicted cracking and a standard deviation. The standard deviation is a function of the error associated with the predicted cracking and the data used to calibrate the alligator cracking model. The procedure to derive the parameters of the error distribution consists of the following steps:

1. Group all the data by the level of predicted cracking. This can be accomplished by identifying the distribution bins based on the magnitude of the predicted cracking for all data.
2. Group the corresponding measured cracking data in the same distribution bins found in step 1.
3. Compute descriptive statistics for each group of data (i.e. mean and standard deviations of predicted and measured cracking).
4. Determine the relationship between the standard error of the measured cracking and predicted cracking. For example, the following equation shows the relationship between measured standard deviation and the mean (FC_{bottom}) predicted alligator cracking.

$$s_e = 1.13 + \frac{13}{1 + e^{7.57 - 15.5 \times Log(FC_{Bottom} + 0.0001)}} \quad (20)$$

5. Adjust the mean cracking for the desired reliability level by using the following relationship:

$$\hat{C} = \bar{C} + S_e \times Z_{\alpha/2} \quad (21)$$

where;

$\hat{C}$ = Predicted cracking at reliability

$\bar{C}$ = Mean predicted cracking

S_e = Standard deviation of cracking

$Z_{\alpha/2}$ = Standard normal deviate

The reliability model standard error includes the variation related to the following sources:

- Errors associated to material characterization parameters assumed or measured for design
- Errors related to assumed traffic and environmental conditions during the design period
- Model errors associated with the cracking prediction algorithms and corresponding data used

The reliability based on method 1 is used for several other distress prediction models in both flexible and rigid pavements. These performance models include:

a. Rutting model for different layers
b. Thermal cracking
c. Transverse cracking for rigid pavements
d. Transverse joint faulting

4.7.2 Reliability based on Method 2

Method 2 is only used for the flexible and rigid pavement IRI. The main reasons for a different method include: (a) availability of a closed-form solution (i.e., the regression model of IRI), and (b) known variances of the different components. In the case of the rigid IRI model, the development of the global IRI model used actual measured data for cracking, spalling and joint faulting. The global model SEE reflects measurement errors associated with the inputs along with model error, replication error and other errors. The reliability of the IRI model requires a variance analysis of the individual components. The first order second moment (FOSM) method is used to determine the standard error of the IRI model. The first step is to quantify the IRI model error through calibration. The errors include, input error, measurement error, pure error and model (lack of fit) error. The IRI standard error equations for rigid and flexible pavements are shown in Equations (22) and (23), respectively. The variance values for the different distresses are directly obtained from the locally calibrated model results.

$$s_{e(IRI-Rigid)} = \left(Var_{IRIi} + C1^2 \cdot Var_{CRK} + C2^2 \cdot Var_{Spall} + C3^2 \cdot Var_{Fault} + S_e^2\right)^{0.5} \quad (22)$$

where;

$s_{e(IRI)}$ = Standard deviation of IRI at the predicted level of mean IRI.
Var_{IRIi} = Variance of initial IRI (obtained from LTPP) = 29.16, $(in/mi)^2$.
Var_{CRK} = Variance of cracking, $(percent\ slabs)^2$.
Var_{Spall} = Variance of spalling (obtained from spalling model) = 46.24, $(percent\ joints)^2$.
Var_{Fault} = Variance of faulting, $(in/mi)^2$.
S_e^2 = Variance of overall model error = 745.3 $(in/mi)^2$.

$$s_{e(IRI-Flex)} = \left(Var_{IRIi} + C2^2 \cdot Var_{FC} + C3^2 \cdot Var_{TC} + C4^2 \cdot Var_{RutDepth} + S_e^2\right)^{0.5} \quad (23)$$

where;

$s_{e(IRI)}$ = Standard deviation of IRI at the predicted level of mean IRI.
Var_{IRIi} = Variance of initial IRI (obtained from LTPP)^2
Var_{FC} = Variance of fatigue cracking, (% lane area)^2

Var_{TC} = Variance of transverse (thermal) cracking , (ft/mile)^2.
$Var_{RutDepth}$ = Variance of rutting, (in.)^2.
S_e^2 = Variance of overall model error

4.7.3 Summary

For the globally calibrated performance prediction model, reliability standard error equations were derived based on methods 1 and 2 discussed above. The final equations for each model are summarized in Table 4-4.

Table 4-4 Reliability equations for each distress and smoothness model

Pavement Type	Pavement performance prediction model	Standard error equation
Flexible pavements	Alligator cracking	$s_{e(Alligator)} = 1.13 + \frac{13}{1 + e^{7.57 - 15.5 \times Log(FC_{Bottom} + 0.0001)}}$
	Rutting	$s_{e(HMA)} = 0.24(\Delta_{HMA})^{0.8026} + 0.001$ $s_{e(Base)} = 0.1477(\Delta_{Base})^{0.6711} + 0.001$ $s_{e(SG)} = 0.1235(\Delta_{SG})^{0.5012} + 0.001$
	Transverse cracking	$s_e(Level1) = 0.1468(TC + 65.027)$ $s_e(Level2) = 0.2841(TC + 55.462)$ $s_e(Level3) = 0.3972(TC + 20.422)$
	IRI	Estimated internally by the software
Rigid pavements	Transverse cracking	$s_{e(CRK)} = 5.3116(CRK)0.3903 + 2.99$
	Faulting	$s_{e(Fault)} = 0.0097(Fault)^{0.5178} + 0.014$
	IRI	Initial IRI S_e = 5.4 Estimated internally by the software

CHAPTER 5 - LOCAL CALIBRATION OF PERFORMANCE MODELS IN MICHIGAN

5.1 INTRODUCTION

The local calibration of the pavement performance prediction models is a challenging task that requires a significant amount of preparation. The effectiveness of local calibration depends on the input values and the measured pavement distress and roughness. Chapter 3 documented the project selection and data collection process and data synthesis for the local calibration of the performance models in Michigan. Chapter 4 presented the local calibration process and techniques used in this study. This chapter includes the results of the local calibration of the performance prediction models using different data subsets (options) and statistical techniques. The different data subsets (options) are combinations of reconstruct, rehabilitation and LTPP pavement sections. The main objective for considering different options is to verify if different calibration coefficients are required for different options. Option 3 was only included for the local calibration of rigid pavements due to a limited number of sections available. The options with different dataset combinations are as follows:

Option 1: MDOT reconstruct sections only
Option 2: MDOT reconstruct and rehabilitation sections combined
Option 3: MDOT reconstruct, rehabilitation, and LTPP sections combined
Option 4: MDOT rehabilitation sections only

The performance prediction models were locally calibrated by minimizing the sum of squared error between the measured and predicted distresses by using the following statistical techniques:

a. No sampling (include all data)
b. Traditional split sampling
c. Repeated split sampling
d. Bootstrapping
e. Bootstrapping validation

The different sampling techniques (a to d) were used to determine the best estimate of the local calibration coefficients and the associated standard errors. The use of these techniques is considered because of data limitations, especially due to limited sample size for rigid pavements, and to utilize a more robust way of quantifying model standard error and bias. The split sample bootstrapping technique (e) was used to validate the bootstrapped local calibrated performance prediction models in the Pavement-ME. The following performance models in the Pavement-ME were locally calibrated for Michigan conditions.

- Flexible pavements
    - Fatigue cracking (bottom-up)
    - Fatigue cracking (top-down)

    - Rutting
    - Transverse (thermal) cracking
    - IRI
- Rigid pavements
    - Transverse cracking
    - Faulting
    - IRI

The Pavement-ME software was executed using the as-constructed inputs for all the selected pavement sections and the predicted performance was extracted from the output files. The measured and predicted distresses over time were compared. These comparisons evaluate the adequacy of global model predictions for the measured distresses on the pavement sections. Generally, the predicted and measured performance should have a one-to-one (45 degree line of equality) relationship in the case of a good match. Otherwise, biased and/or prediction error may exist based on the spread of data around the line of equality. As a consequence, local calibration of the model is needed to reduce the bias and standard error between the predicted and measured performance. The above mentioned steps can be accomplished by performing the following process (*1*).

1. Compare the globally calibrated model predictions with measured performance.
2. Perform hypothesis tests between the measured and predicted performance (see Table 5-1). If any of the null hypotheses are rejected, follow step 3 otherwise no local calibration is needed.
3. Adjust local calibration coefficients to minimize the standard error between predicted and measured performance, and compare the measured and predicted performance.
4. Perform hypothesis testing again based on the locally calibrated coefficients and determine if the model accuracy has improved. If not, identify the possible sources of bias such as outliers in the measured performance data or improve the accuracy of input data and continue local calibration process until the standard error of the estimate is lower than the globally calibrated model.
5. Accept or reject the local calibration coefficients based on the results from step 4.

Table 5-1: Hypothesis tests

Hypothesis test	Hypotheses
Mean difference (paired *t*-test)	$H_0 = (predicted - measured) = 0$ $H_1 = (predicted - measured) \neq 0$
Intercept	$H_0 = intercept = 0$ $H_1 = intercept \neq 0$
Slope	$H_0 = slope = 1$ $H_1 = slope \neq 1$

The local calibration results are presented for both flexible and rigid pavement performance prediction models and are compared for the different statistical techniques and the data set options mentioned above.

5.2 LOCAL CALIBRATION OF FLEXIBLE PAVEMENT MODELS

The detailed results for the local calibration of the fatigue cracking, rutting, transverse (thermal) cracking and IRI models are presented in this section.

5.2.1 Fatigue Cracking Model – bottom-up

The bottom-up fatigue cracking (alligator cracking) model was calibrated by adjusting the local calibration coefficients to minimize the error between the predicted and measured fatigue cracking. The fatigue cracking model was calibrated for reconstructed pavement sections only. This is because the bottom-up cracking model did not predict any fatigue cracking on the rehabilitated pavement sections. In addition, minimal fatigue cracking was measured on the rehabilitated pavements. The fatigue cracking model was calibrated using two different methods: (a) combined measured alligator and longitudinal (AC/LC) cracking in the wheelpath, and (b) the measured alligator cracking (AC) only. In option 1a the measured alligator and longitudinal cracking in the wheelpath were combined due to difficulty in determining if an observed crack at the pavement surface propagated from the top or bottom. The guide for local calibration also recommends such a procedure (*2*). Option 1b considered only measured alligator cracking. The measured alligator cracking corresponds to specific PD's summarized in Chapter 3. The number of sections with measured alligator cracking was considerably lower than the number of sections with longitudinal cracking in the wheelpath.

5.2.1.1. Option 1a– MDOT reconstruct only (measured AC/LC combined)

The first step in the calibration process was to compare the globally calibrated model to the measured fatigue cracking. The measured and predicted fatigue cracking is shown in Figure 5-1. As seen in the figure, the global model under-predicts measured fatigue cracking. The three hypothesis tests (Table 5-2) reveal that all three tests were rejected and local calibration is needed for this model. The local calibration using different calibration techniques is discussed next.

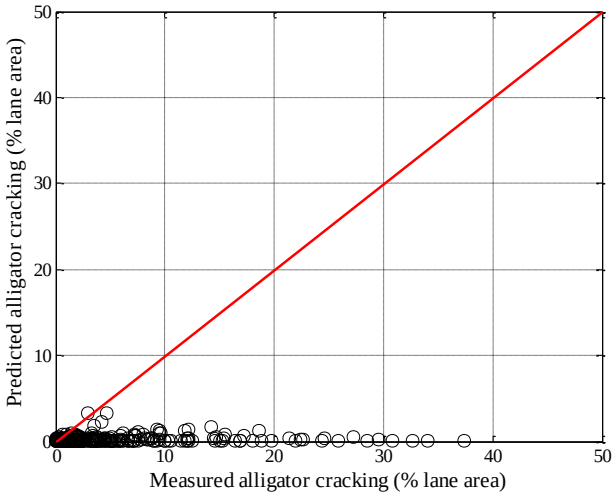

Figure 5-1 Measured versus predicted fatigue cracking

Table 5-2 Global model fatigue cracking hypothesis test results

Hypothesis test	Hypotheses	P-value
Mean difference (paired *t*-test)	H_0 = *(predicted – measured) = 0* H_1 = *(predicted – measured)* $\neq 0$	0.00
Intercept	H_0 = *intercept = 0* H_1 = *intercept* $\neq 0$	0.00
Slope	H_0 = *slope = 1* H_1 = *slope* $\neq 1$	0.00

No Sampling

The local calibration was performed using all the available pavement sections. The error was minimized between the predicted and measured fatigue cracking. Figure 5-2 shows the measured versus predicted fatigue cracking and the corresponding calibrated fatigue models with respect to fatigue damage. The local calibration results are presented in Table 5-3. The results indicate the standard error of the estimate (SEE) reduced from 7.61 percent to 6.71 percent. The bias reduced from -4.19 percent to -1.29 percent. Table 5-4 summarizes the results from the hypothesis testing and indicates that all of the hypothesis tests are still rejected. Even though the hypothesis tests are rejected, the locally calibrated model provided a better prediction of fatigue cracking for Michigan conditions based on lower SEE and bias as compared to the global model.

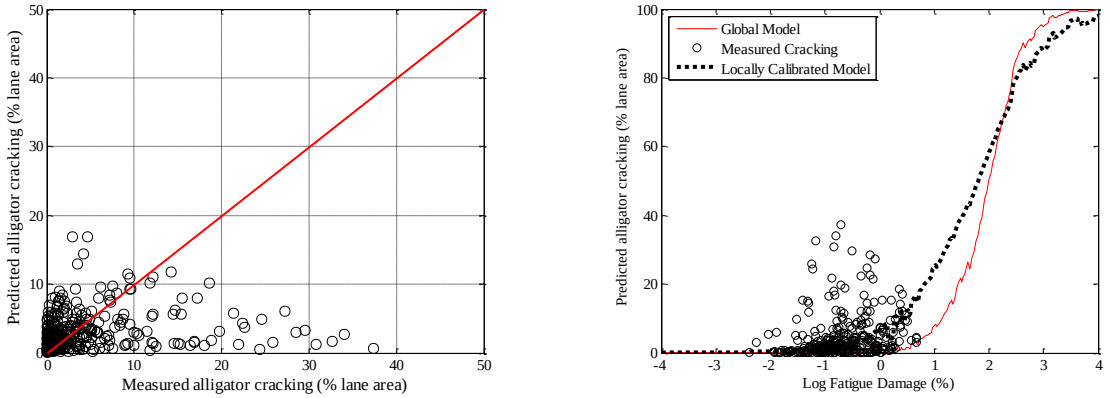

(a) Measured vs. predicted cracking (b) Fatigue damage predicted cracking

Figure 5-2 Local calibration results for fatigue cracking (full dataset)

Table 5-3 Local calibration results (full dataset)

Parameter	Global model	Local model
SEE (% total lane area)	7.64	6.71
Bias (% total lane area)	-4.19	-1.29
C_1	1.00	0.50
C_2	1.00	0.56

Table 5-4 Hypothesis testing results (full dataset)

Hypothesis test	Global model	Local model
Mean difference = 0	0.00	0.00
Intercept = 0	0.00	0.00
Slope = 1	0.00	0.00

Split Sampling

Next, the local calibration was performed using split sampling. For split sampling, seventy (70%) percent of the pavement sections were used for model calibration, and the remaining thirty (30%) percent were used for model validation. Figure 5-3 shows the measured versus predicted fatigue cracking and the corresponding calibrated and validated fatigue models with respect to fatigue damage. The results of local calibration are presented in Tables 5-5 and 5-6. The results indicate that the SEE reduced from 8.02 percent to 7.00 percent and the bias also reduced from -4.39 to -1.37 percent. The null hypothesis was rejected for all hypothesis tests which indicate that the model may still have some bias. The validation sections indicate that there is no significant difference between the measured and predicted fatigue cracking. Even though the null hypothesis tests for local calibration were rejected, the local model provides a better prediction of fatigue cracking for Michigan conditions (see Table 5-5).

Table 5-5 Local calibration results (split sampling)

Parameter	Global model	Local model	Validation
SEE (% total lane area)	8.02	7.00	6.00
Bias (% total lane area)	-4.39	-1.37	-0.78
C_1	1.00	0.50	0.50
C_2	1.00	0.56	0.56

Table 5-6 Hypothesis testing results (split sampling)

Hypothesis test	Global model	Local model	Validation
Mean difference = 0	0.00	0.00	0.20
Intercept = 0	0.00	0.00	0.00
Slope = 1	0.00	0.00	0.00

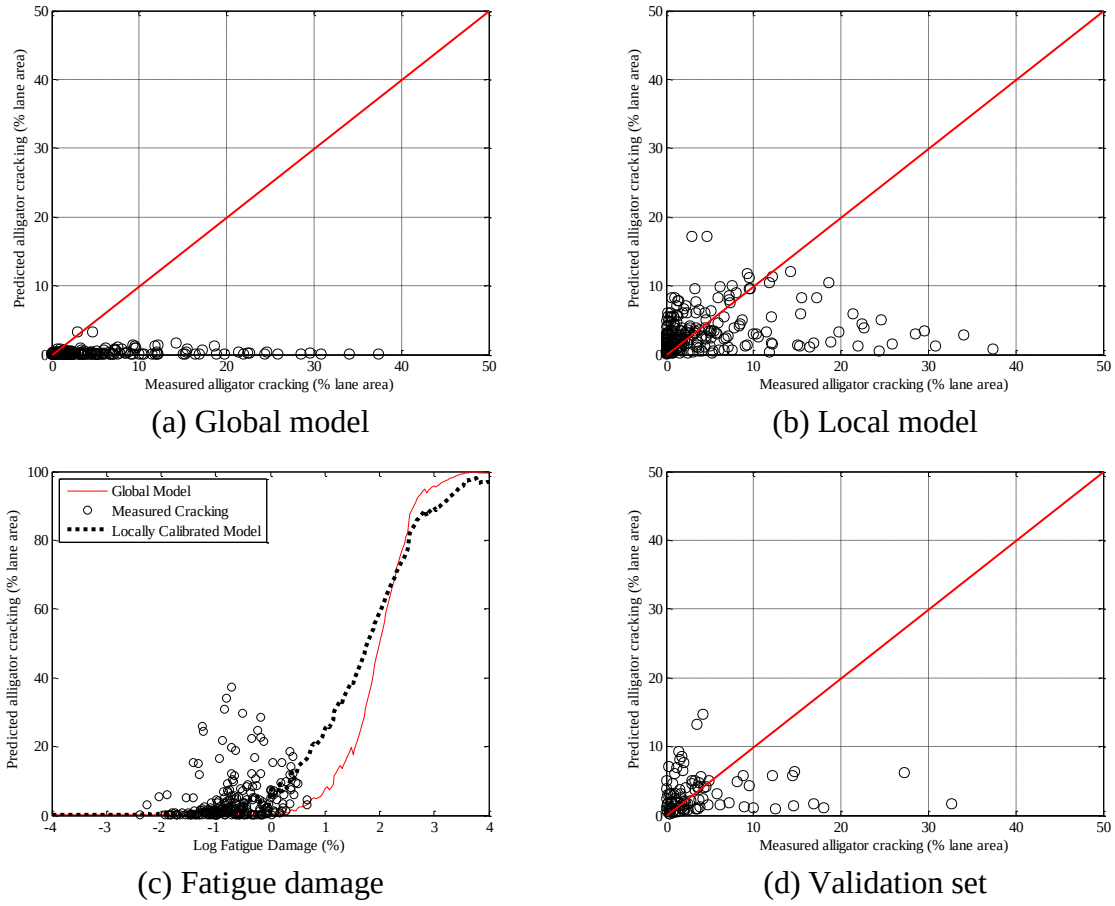

(a) Global model (b) Local model

(c) Fatigue damage (d) Validation set

Figure 5-3 Local calibration results for fatigue cracking (split sampling)

Repeated Split Sampling

The split sampling technique only considers one random selection of 70% of the pavement sections. However, if multiple split samples are taken, the SEE, bias, C_1 and C_2 values will vary for each realization. Therefore, the results of a split sample may not indicate an accurate representation of all the sections on average, especially when the sample size is limited. In order to address this limitation, split sampling was performed 1000 times to study the variability of the SEE, bias and calibration coefficients. The results of the repeated split sampling for the global and local models, as well as the validation sections are presented in Tables 5-7 to 5-9. The results indicate that the SEE and bias reduced after local calibration. Additionally, the confidence intervals (CI) for each parameter are presented. The confidence interval indicates the variability of the parameter. Figures 5-4 and 5-5 show the distribution for each parameter in the calibration and validation datasets. The SEE ranged between 5 and 8, and 4 and 9 percent for the calibration and validation subsets, respectively. The bias ranged between approximately -1.6 and -0.7, and -2.7 to 0.4 percent for the calibration and validation subsets, respectively. The C_1 and C_2 parameters did not vary much because constraints on the calibration coefficients were imposed to ensure reasonable results.

Table 5-7 Repeated split sample global model summary

Parameter	Global model mean	Global model median	Global model lower CI	Global model upper CI
SEE (% total lane area)	7.65	7.69	6.79	8.35
Bias (% total lane area)	-4.19	-4.20	-4.66	-3.66
C_1	1.00	1.00	-	-
C_2	1.00	1.00	-	-

Table 5-8 Repeated split sampling local calibration results

Parameter	Local model mean	Local model median	Local model lower CI	Local model upper CI
SEE (% total lane area)	6.71	6.76	5.84	7.39
Bias (% total lane area)	-1.22	-1.24	-1.64	-0.68
C_1	0.50	0.50	0.47	0.50
C_2	0.56	0.56	0.56	0.56

Table 5-9 Repeated split sampling validation results

Parameter	Local model mean	Local model median	Local model lower CI	Local model upper CI
SEE (% total lane area)	6.71	6.69	4.90	8.48
Bias (% total lane area)	-1.20	-1.22	-2.68	0.43
C_1	0.50	0.50	0.47	0.50
C_2	0.56	0.56	0.56	0.56

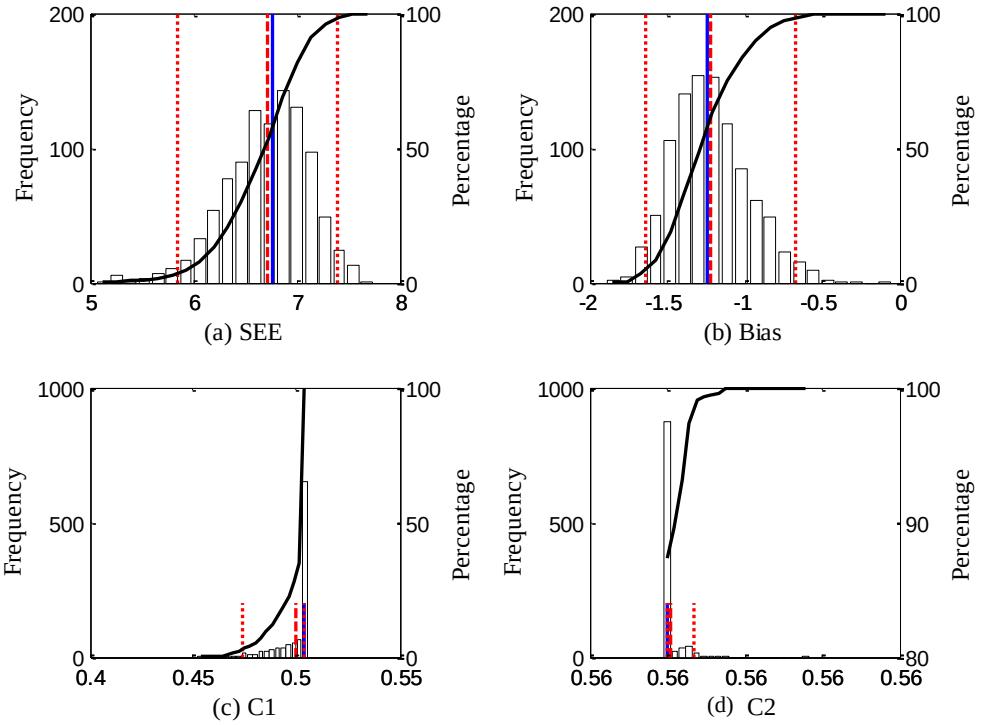

Figure 5-4 Distribution of local calibration parameters – calibration dataset (repeated split sampling)

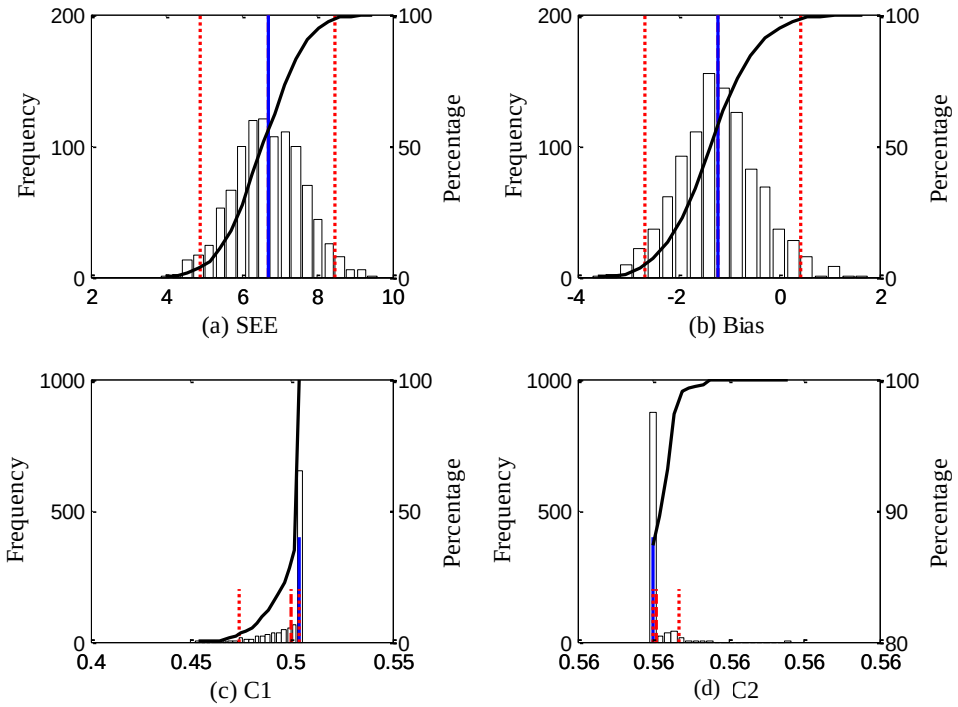

Figure 5-5 Distribution of local calibration parameters – validation dataset (repeated split sampling)

Bootstrapping

Bootstrapping is the final resampling technique considered to calibrate the fatigue cracking model. The difference between split sampling and bootstrapping is that the latter method does not split the original dataset. The bootstrap samples are selected randomly with replacement from the total number of the selected pavement sections. In this method, 1000 bootstrap samples were used to calibrate the fatigue cracking model. Tables 5-10 and 5-11 summarize the SEE, bias and calibration coefficients for the global and local calibrations. The results show that the SEE and bias reduced slightly after local calibration. Figure 5-6 shows the distribution of each parameter.

Table 5-10 Bootstrapping global model summary

Parameter	Global model mean	Global model median	Global model lower CI	Global model upper CI
SEE (% total lane area)	7.62	7.61	6.38	8.93
Bias (% total lane area)	-4.19	-4.18	-5.01	-3.45
C_1	1.00	1.00	-	-
C_2	1.00	1.00	-	-

Table 5-11 Bootstrapping local calibration results summary

Parameter	Local model mean	Local model median	Local model lower CI	Local model upper CI
SEE (% total lane area)	6.69	6.66	5.53	7.88
Bias (% total lane area)	-1.16	-1.15	-1.87	-0.43
C_1	0.50	0.50	0.46	0.50
C_2	0.56	0.56	0.56	0.56

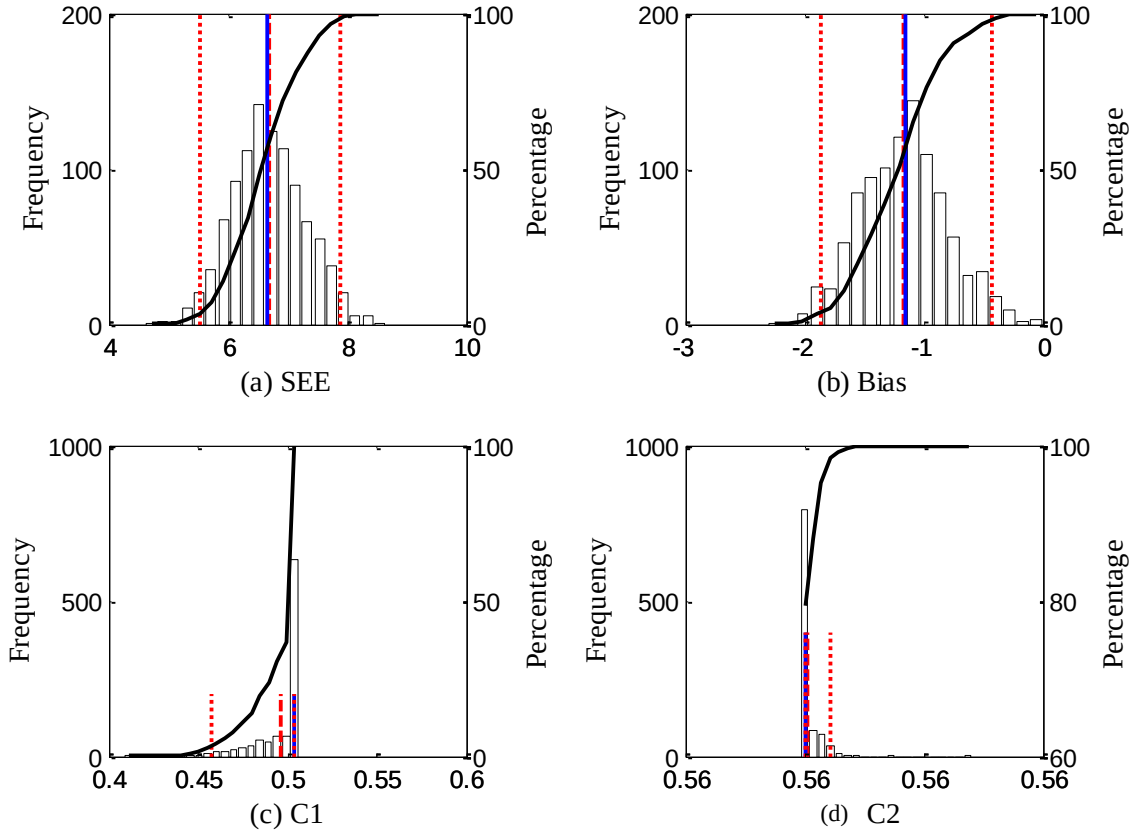

Figure 5-6 Distribution of local calibration parameters (bootstrapping)

Summary

The results for all the sampling techniques are summarized in Table 5-12. It can be seen that the repeated split sampling and bootstrapping techniques provided the lowest SEE and bias compared to the global model. Additionally, the C_1 and C_2 coefficients did not change due to the limits set to ensure reasonable comparisons between predicted and measured fatigue cracking. The constraints on the coefficients were essential because of the large differences between predicted and measured cracking. Mathematical optimization without constraints does not give rational model coefficients. Such optimization without constraints may only fit the model to the potential outlier (if any).

Table 5-12 Summary of results for all sampling techniques (option 1a)

Sampling technique	SEE	Bias	C_1	C_2
No sampling	6.71	-1.29	0.50	0.56
Split sampling	7.00	-1.37	0.50	0.56
Repeated split sampling	6.71	-1.22	0.50	0.56
Bootstrapping	6.69	-1.16	0.50	0.56

5.2.1.2. Option 1b– MDOT reconstruct only (measured AC only)

Similar procedures were used to calibrate the fatigue cracking model for MDOT reconstruct sections using only measured alligator cracking instead of the combined AC/LC (option 1a). The summary of results for all sampling techniques is presented in Table 5-13 with additional information in Appendix B.

Table 5-13 Summary of results for all sampling techniques (option 1b)

Sampling Technique	SEE	Bias	C_1	C_2
No sampling	3.67	-0.75	0.68	0.56
Split sampling	4.02	-0.84	0.68	0.56
Repeated split sampling	3.66	-0.73	0.68	0.56
Bootstrapping	3.60	-0.69	0.67	0.56

Although the SEE and bias are reduced for the Option 1b model calibration, the number of pavement sections and the magnitude of the measured alligator cracking were reduced significantly. In addition, it is difficult to distinguish the difference between alligator and longitudinal cracking from the PMS data. Given these limitations, the models for options 1a and 1b can be selected based on the confidence in the measured data. Therefore, Option 1a calibration coefficients should be the preferred values if the longitudinal cracking model is not considered.

5.2.1.3. Reliability for the alligator cracking model

The standard error of the calibrated fatigue cracking models were used to establish the relationship between the standard deviation of the measured cracking and mean predicted cracking as explained in Chapter 4. These relationships are used to calculate the cracking for a specific reliability. Tables 5-14 and 5-15 summarize these relations for the options considered for fatigue cracking.

Table 5-14 Reliability summary for Option 1a

Sampling technique	Global model equation	Local model equation
No Sampling	$s_{e(Alligator)} = 1.13 + \frac{13}{1+e^{7.57-15.5\times log(D)}}$	$s_{e(Alligator)} = 2.3988 + \frac{15.676}{1+e^{0.1475-0.4641\times log(D)}}$
Split Sampling		$s_{e(Alligator)} = 0.6 + \frac{24}{1+e^{0.1-0.5\times log(D)}}$
Repeated split sampling		$s_{e(Alligator)} = 0.9919 + \frac{17.093}{1+e^{0.1103-0.4361\times log(D)}}$
Bootstrapping		$s_{e(Alligator)} = 0.7874 + \frac{17.817}{1+e^{0.0699-0.4559\times log(D)}}$

Table 5-15 Reliability summary for Option 1b

Sampling technique	Global model equation	Local model equation
No Sampling	$s_{e(Alligator)} = 1.13 + \frac{13}{1+e^{7.57-15.5\times log(D)}}$	$s_{e(Alligator)} = 0.01 + \frac{22.074}{1+e^{1.00-0.5328\times log(D)}}$
Split Sampling		$s_{e(Alligator)} = 0.01 + \frac{24.715}{1+e^{1.00-0.6448\times log(D)}}$
Repeated split sampling		$s_{e(Alligator)} = 0.01 + \frac{33.088}{1+e^{1.397-0.5985\times log(D)}}$
Bootstrapping		$s_{e(Alligator)} = 0.01 + \frac{32.913}{1+e^{1.3972-0.5976\times log(D)}}$

5.2.2 Fatigue Cracking Model – top-down

Similar to the alligator cracking (bottom-up) model, the longitudinal cracking (top-down) model was calibrated by minimizing the sum of squared error between the measured and predicted cracking.

5.2.2.1. Option 1 MDOT reconstruct pavements only

The first step in the calibration process was to compare the globally calibrated longitudinal cracking model to the measured top down fatigue cracking. The measured and predicted top-down fatigue cracking is shown in Figure 5-7. As seen in the figure, the global model under-predicts measured top-down fatigue cracking. The three hypothesis tests (Table 5-16) reveals that all three tests were rejected and local calibration is needed for this model. The local calibration using different calibration techniques is discussed next.

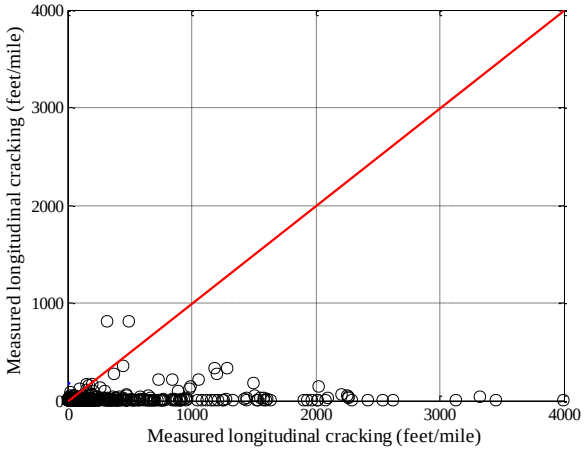

Figure 5-7 Measured versus predicted fatigue cracking

Table 5-16 Global model fatigue cracking hypothesis test results

Hypothesis test	Hypotheses	P-value
Mean difference (paired *t*-test)	H_0 = *(predicted – measured) = 0* H_1 = *(predicted – measured)* $\neq 0$	0.00
Intercept	H_0 = *intercept = 0* H_1 = *intercept* $\neq 0$	0.00
Slope	H_0 = *slope = 1* H_1 = *slope* $\neq 1$	0.00

No Sampling

The local calibration was performed using all the available pavement sections. The error was minimized between the predicted and measured fatigue cracking. Figure 5-8 shows the measured versus predicted fatigue cracking and the corresponding calibrated fatigue models with respect to fatigue damage. The local calibration results are presented in Table 5-17. The results indicate the standard error of the estimate (SEE) reduced from 741.21 ft/mile to 644.47 ft/mile. The bias reduced from -409.32 ft/mile to -125.44 ft/mile. Table 5-4 summarizes the results from the hypothesis testing and indicates that all of the hypothesis tests are still rejected. Even though the hypothesis tests are rejected, the locally calibrated model provided a better prediction of fatigue cracking for the Michigan conditions.

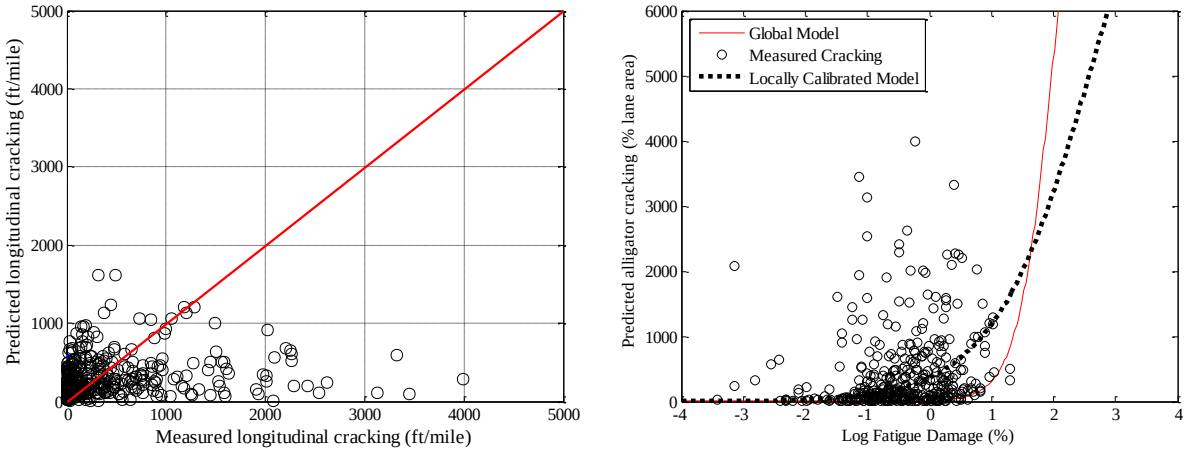

(a) Measured vs. predicted cracking (b) Fatigue damage predicted cracking

Figure 5-8 Local calibration results for fatigue cracking (full dataset)

Table 5-17 Local calibration results (full dataset)

Parameter	Global model	Local model
SEE (ft/mile)	741.21	644.47
Bias (ft/mile)	-409.32	-125.44
C_1	7.00	3.32
C_2	3.50	1.25

Table 5-18 Hypothesis testing results (full dataset)

Hypothesis test	Global model	Local model
Mean difference = 0	0.00	0.00
Intercept = 0	0.00	0.00
Slope = 1	0.00	0.00

Split Sampling

Next, the local calibration was performed using split sampling. Figure 5-9 shows the measured versus predicted fatigue cracking and the corresponding calibrated and validated fatigue models with respect to fatigue damage. The results of local calibration are presented in Tables 5-19 and 5-20. The results indicate that the SEE reduced from 807.52 to 700.71 ft/mile and the bias also reduced from -453.48 to -141.54 ft/mile. The null hypothesis was rejected for all hypothesis tests which indicate that the model may still have some bias. The validation sections indicate that there is no significant difference between the measured and predicted fatigue cracking. Even though the hypothesis tests were significantly different than the null, the local model provides a better prediction of fatigue cracking for Michigan conditions.

Table 5-19 Local calibration results (split sampling)

Parameter	Global model	Local model	Validation
SEE (ft/mile)	807.52	700.71	494.75
Bias (ft/mile)	-453.48	-141.54	-68.73
C_1	7.00	3.30	3.30
C_2	7.00	1.25	1.25

Table 5-20 Hypothesis testing results (split sampling)

Hypothesis test	Global model	Local model	Validation
Mean difference = 0	0.00	0.00	0.13
Intercept = 0	0.00	0.00	0.00
Slope = 1	0.00	0.00	0.00

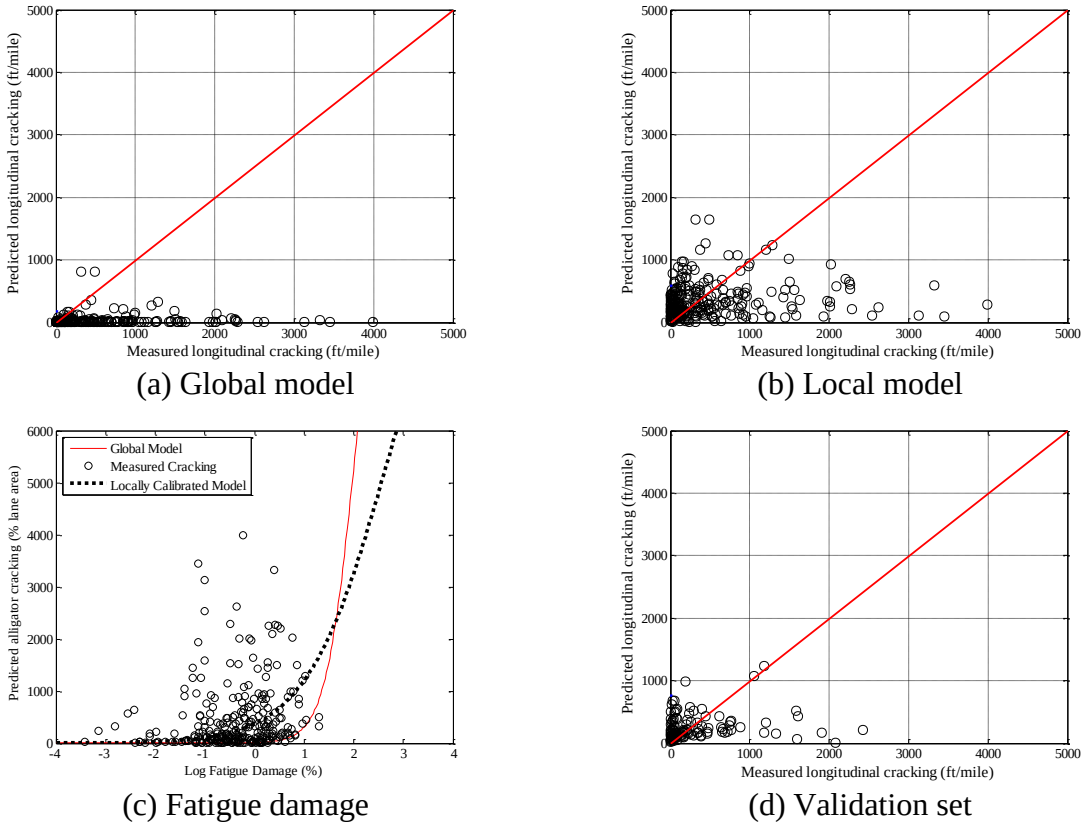

(a) Global model (b) Local model

(c) Fatigue damage (d) Validation set

Figure 5-9 Local calibration results for fatigue cracking (split sampling)

Repeated Split Sampling

The split sampling technique only considers one random selection of 70% of the pavement sections. However, if multiple split samples are taken, the SEE, bias, C_1 and C_2 values will vary for each realization. Therefore, the results of a split sample may not indicate an accurate representation of all the sections on average, especially when the sample size is limited. In order to address this limitation the split sampling was performed 1000 times to study the variability of the SEE, bias and calibration coefficients. The results of the repeated split sampling for the global and local models, as well as the validation sections are presented in Tables 5-21 to 5-23. The results indicate that the SEE and bias reduced after local calibration. Additionally, the confidence intervals for each parameter are presented. The confidence interval indicates the variability of the parameter. Figures 5-10 and 5-11 show the distribution for each parameter in the calibration and validation datasets. The C_1 and C_2 parameters did not vary much because constraints on the calibration coefficients were imposed to ensure reasonable results.

Table 5-21 Repeated split sample global model summary

Parameter	Global model mean	Global model median	Global model lower CI	Global model upper CI
SEE (ft/mile)	739.96	742.34	642.99	818.50
Bias (ft/mile)	-408.56	-408.06	-460.33	-353.78
C_1	1.00	1.00	-	-
C_2	1.00	1.00	-	-

Table 5-22 Repeated split sampling local calibration results

Parameter	Local model mean	Local model median	Local model lower CI	Local model upper CI
SEE (ft/mile)	642.53	645.28	555.83	710.83
Bias (ft/mile)	-124.58	-124.76	-157.32	-90.77
C_1	3.32	3.32	3.16	3.52
C_2	1.25	1.25	1.25	1.25

Table 5-23 Repeated split sampling validation results

Parameter	Local model mean	Local model median	Local model lower CI	Local model upper CI
SEE (ft/mile)	648.70	650.68	466.25	830.75
Bias (ft/mile)	-124.93	-128.32	-308.60	64.65
C_1	3.32	3.32	3.16	3.52
C_2	1.25	1.25	1.25	1.25

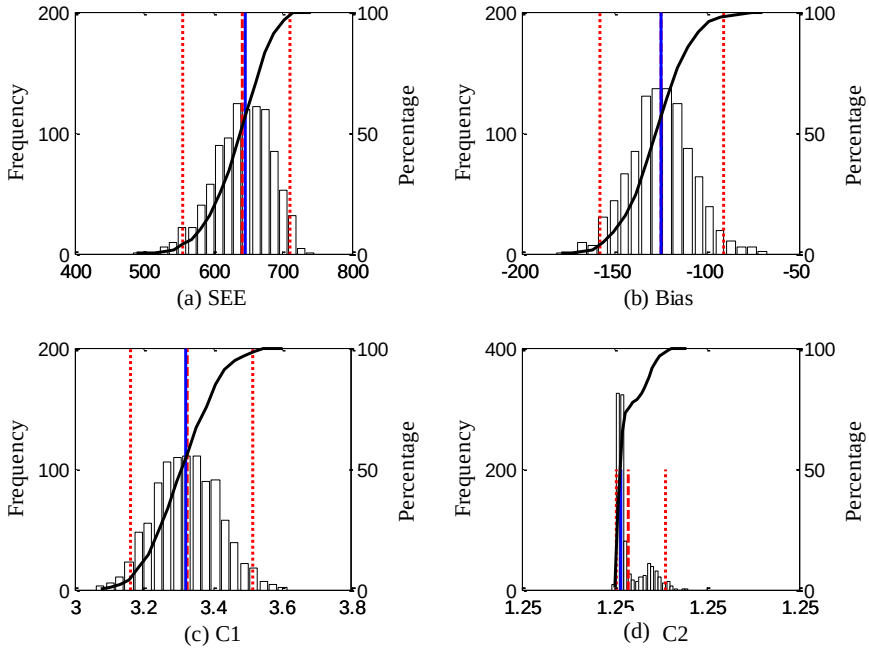

Figure 5-10 Distribution of local calibration parameters – calibration dataset (repeated split sampling)

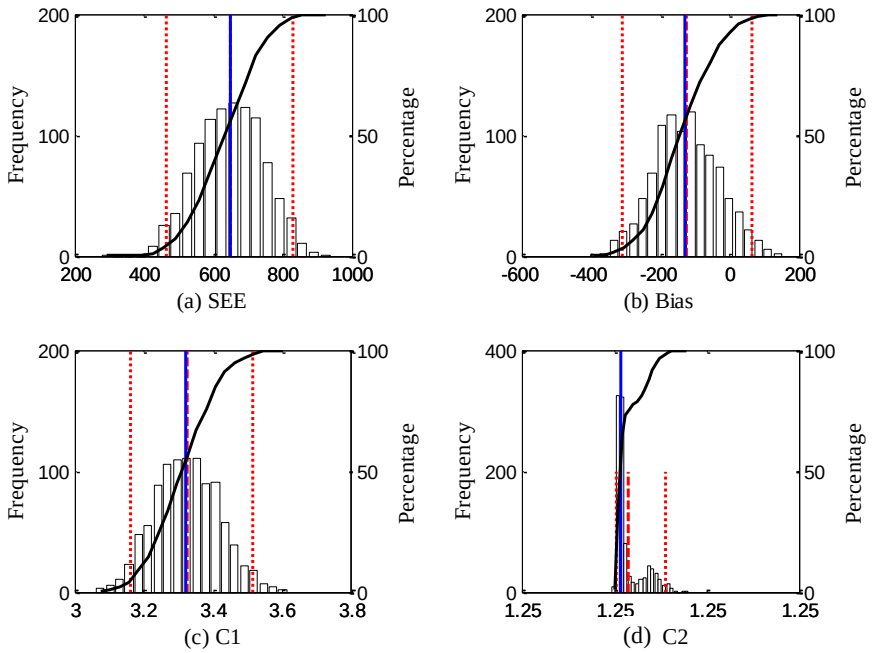

Figure 5-11 Distribution of local calibration parameters – validation dataset (repeated split sampling)

Bootstrapping

Bootstrapping is the final resampling technique considered to recalibrate the top-down fatigue cracking model. In this method, 1000 bootstrap samples were used to recalibrate the fatigue cracking model. Tables 5-24 and 5-25 summarize the SEE, bias and calibration coefficients for the global and local calibrations. The results show that the SEE and bias reduced slightly after local calibration. Figure 5-12 shows the distribution of each parameter.

Table 5-24 Bootstrapping global model summary

Parameter	Global model mean	Global model median	Global model lower CI	Global model upper CI
SEE (ft/mile)	741.41	738.34	614.64	871.40
Bias (ft/mile)	-411.36	-409.36	-495.00	-335.23
C_1	1.00	1.00	-	-
C_2	1.00	1.00	-	-

Table 5-25 Bootstrapping local calibration results summary

Parameter	Local model mean	Local model median	Local model lower CI	Local model upper CI
SEE (ft/mile)	641.44	640.16	526.91	759.87
Bias (ft/mile)	-122.72	-121.44	-175.87	-73.53
C_1	3.32	3.32	3.04	3.58
C_2	1.25	1.25	1.25	1.25

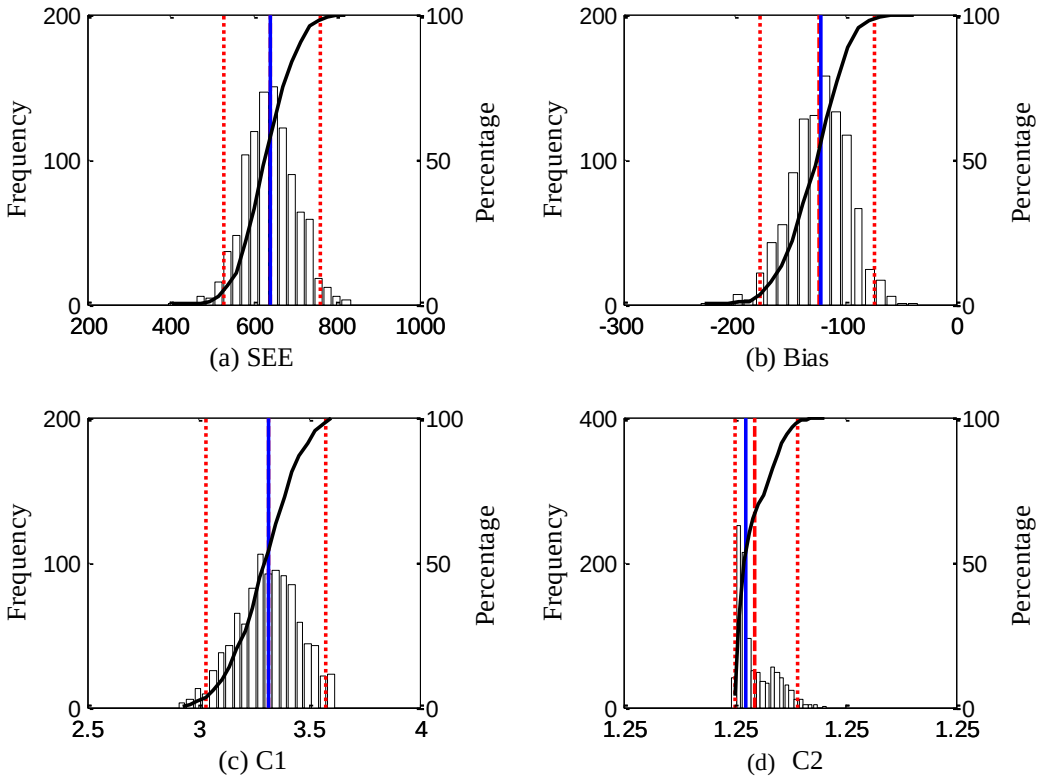

Figure 5-12 Distribution of local calibration parameters (bootstrapping)

5.2.2.2. Summary

The results for all the sampling techniques are summarized in Table 5-26. It can be seen that the repeated split sampling and bootstrapping techniques provided the lowest SEE and bias compared to the global model. Additionally, the C_1 and C_2 coefficients did not change due to the limits set to ensure reasonable comparisons between predicted and measured fatigue cracking.

Table 5-26 Summary of results for all sampling techniques (option 1)

Sampling technique	SEE	Bias	C_1	C_2
No sampling	644.47	-125.44	3.32	1.25
Split sampling	700.71	-141.54	3.30	1.25
Repeated split sampling	642.53	-124.58	3.32	1.25
Bootstrapping	641.44	-122.72	3.32	1.25

Similar procedures were used to calibrate the top-down fatigue cracking model for MDOT reconstruct sections by combining the reconstruct and rehabilitation pavement sections (option 2). The summary of results for all sampling techniques is presented in Table 5-27.

Table 5-27 Summary of results for all sampling techniques (option 2)

Sampling technique	SEE	Bias	C_1	C_2
No sampling	856.06	-185.37	2.97	1.2
Split sampling	858.43	-177.72	2.93	1.2
Repeated split sampling	853.26	-184.74	2.98	1.2
Bootstrapping	850.44	-181.97	2.97	1.2

The summary of results for all sampling techniques using Option 4 (rehabilitation sections only) is presented in Table 5-28. The results indicate that the bootstrap provided the lowest SEE and bias compared to all other sampling techniques

Table 5-28 Summary of results for all sampling techniques (option 4)

Sampling technique	SEE	Bias	C_1	C_2
No sampling	1213.53	-382.7	2.36	1.2
Split sampling	1193.07	-310.6	2.37	1.2
Repeated split sampling	1200.63	-322.87	2.27	1.2
Bootstrapping	1189.44	-283.96	2.23	1.2

5.2.2.3. Reliability for longitudinal cracking model

The standard errors of the calibrated top-down fatigue cracking models were used to establish the relationship between the standard deviation of the measured cracking and mean predicted cracking as explained in Chapter 4. These relationships are used to calculate the cracking for a specific reliability. Tables 5-29 and 5-31 summarize these relations for the options considered for top-down fatigue cracking.

Table 5-29 Reliability summary for Option 1

Sampling technique	Global model equation	Local model equation
No Sampling	$s_{e(Longitudinal)} = 200 + \frac{2300}{1+e^{1.07-2.165\times log(D_{td}+0.0001)}}$	$s_{e(Longitudinal)} = 150 + \frac{2300}{1+e^{2-0.6\times log(D_{td}+0.0001)}}$
Split Sampling		$s_{e(Longitudinal)} = 150 + \frac{2300}{1+e^{2.1-0.4\times log(D_{td}+0.0001)}}$
Repeated split sampling		$s_{e(Longitudinal)} = 150 + \frac{2300}{1+e^{2.2-0.61\times log(D_{td}+0.0001)}}$
Bootstrapping		$s_{e(Longitudinal)} = 150 + \frac{2300}{1+e^{1.9-0.6\times log(D_{td}+0.0001)}}$

Table 5-30 Reliability summary for Option 2

Sampling technique	Global model equation	Local model equation
No Sampling	$s_{e(Longitudinal)} = 200 + \frac{2300}{1+e^{1.07-2.165\times log(D_{td}+0.0001)}}$	$s_{e(Longitudinal)} = 300 + \frac{3000}{1+e^{1.8-0.61\times log(D_{td}+0.0001)}}$
Split Sampling		$s_{e(Longitudinal)} = 250 + \frac{3000}{1+e^{1.9677-1.2723\times log(D_{td}+0.0001)}}$
Repeated split sampling		$s_{e(Longitudinal)} = 300 + \frac{3000}{1+e^{1.8-0.61\times log(D_{td}+0.0001)}}$
Bootstrapping		$s_{e(Longitudinal)} = 300 + \frac{3000}{1+e^{1.8-0.61\times log(D_{td}+0.0001)}}$

Table 5-31 Reliability summary for Option 4

Sampling technique	Global model equation	Local model equation
No Sampling	$s_{e(Longitudinal)} = 200 + \frac{2300}{1+e^{1.07-2.165\times log(D_{td}+0.0001)}}$	$s_{e(Longitudinal)} = 700 + \frac{3000}{1+e^{1.0-0.8\times log(D_{td}+0.0001)}}$
Split Sampling		$s_{e(Longitudinal)} = 700 + \frac{3000}{1+e^{0.5-1.0\times log(D_{td}+0.0001)}}$
Repeated split sampling		$s_{e(Longitudinal)} = 700 + \frac{3000}{1+e^{1.1-0.9\times log(D_{td}+0.0001)}}$
Bootstrapping		$s_{e(Longitudinal)} = 700 + \frac{3000}{1+e^{1.1-1.0\times log(D_{td}+0.0001)}}$

5.2.3 Rutting Model

As mentioned in Chapter 4, the rutting model in the Pavement-ME was calibrated using two methods:

1. *Method 1*: Individual rutting layer calibration (i.e., calibrate the rutting model by changing the individual calibration coefficients (HMA, base/subbase, and subgrade) relative to rutting contribution of each layer by using the estimates from the transverse profile analysis).
2. *Method 2*: Total rutting calibration (i.e., calibrate the rutting model by changing the individual calibration coefficient for each layer simultaneously relative to the total rutting).

Figure 5-13 shows the global rutting models (before calibration) for the flexible reconstruct pavement sections in Michigan. The results show that the global model significantly over predicts the total rutting for Michigan conditions. The over prediction in the total rutting is mainly contributed by the predicted base/subbase and subgrade rutting. The individual layer contribution to total rutting was estimated by using the transverse profiles for each pavement section, based on the transverse profile analysis presented in Chapter 4. It should be noted that only total rutting measured on the pavement surface is stored in the MDOT PMS. However, individual layer rutting was estimated based on the relative proportions determined from the transverse profile analyses. The relative proportion were utilized to estimate the individual layers rutting contribution (i.e., HMA, base/subbase and subgrade layers) .

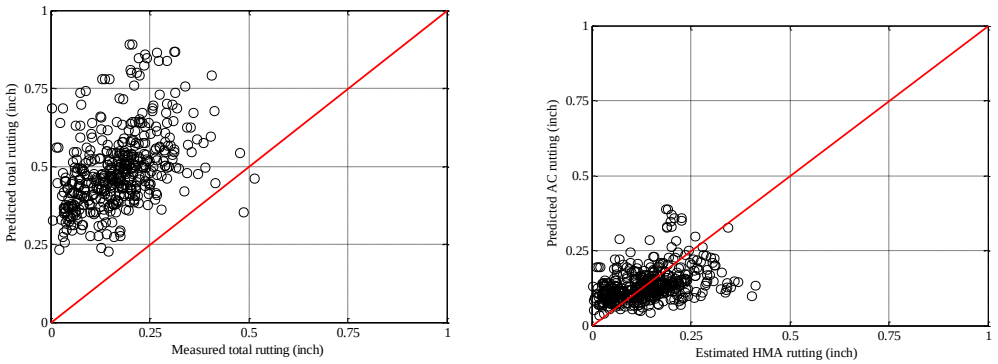

(a) Global model total rutting

(b) HMA rutting

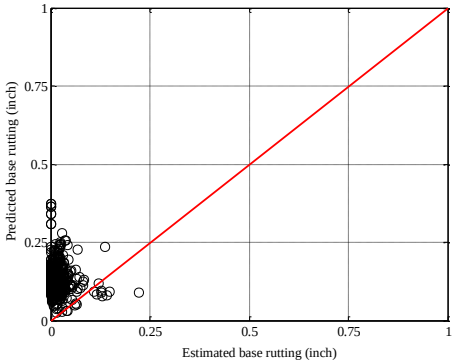

(c) Base rutting

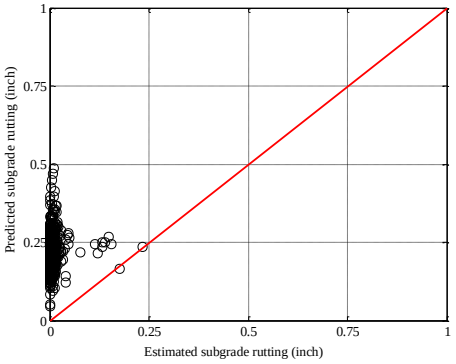

(d) Subgrade rutting

Figure 5-13 Global rutting model verification

Tables 5-32 and 5-33 summarize the SEE, bias, and hypothesis testing results for the global rutting model. The results indicate that there is not a significant difference between the measured and predicted HMA rutting. The hypothesis tests for base, subgrade and total rutting were all rejected and a significant difference between the measured and predicted rutting was found. Therefore, local calibration for the rutting model is needed in Michigan. Only options 1, 2 and 4 were considered for the rutting model calibration. Option 3 (LTPP pavement sections) was not included because an adequate number of MDOT pavement sections were available.

Table 5-32 Global model SEE and bias

Layer	SEE (in.)	Bias (in.)
HMA rut	0.0786	-0.0037
Base rut	0.1267	0.1111
Subgrade	0.2242	0.2143
Total rut	0.3431	0.3217

Table 5-33 Global model hypothesis testing results

Layer	t-test *p*-value	Intercept *p*-value	Slope = 1 *p*-value
HMA rut	0.3220	0.0000	0.0000
Base rut	0.0000	0.0000	0.0000
Subgrade	0.0000	0.0000	0.0000
Total rut	0.0000	0.0000	0.0000

5.2.3.1. Option 1: Method 1– MDOT reconstruct pavements only

No Sampling

Since the majority of the hypothesis tests were rejected (see Table 5-33), local calibration of the rutting model is required. First, the rutting model was calibrated by adjusting the individual layer (HMA, base, subgrade) calibration coefficients. The PMS data from MDOT provided the measured total rutting for each pavement section. The individual layer rutting was determined by using the transverse profile analysis results as discussed in Chapter 4. The calibration was performed by minimizing the error between the measured and predicted rutting for each pavement layer. It is not meaningful to evaluate individual pavement layer rutting by itself because those were only estimated; therefore, the SEE and bias of the locally calibrated model was determined based on the total rutting. Figure 5-14 shows the comparison between measured and predicted rutting for total, HMA, base and subgrade rutting for the locally calibrated model using the Method 1. Tables 5-34 to 5-36 summarize the local calibration results. The results show that overall, the SEE and bias were reduced for all pavement layers. The local calibration of the base and the subgrade rutting models had the largest impact on the total rutting. The hypothesis tests reveal that there is no significant difference between the measured and predicted base, and subgrade rutting. The HMA and total rutting still indicates a significant difference. The intercept and slope hypothesis tests were rejected for all pavement layers.

Table 5-34 Local model SEE and bias

Layer	SEE	Bias
HMA	0.0783	-0.0094
Base	0.0262	-0.0034
Subgrade	0.0228	-0.0003
Total	0.0869	-0.0132

Table 5-35 Local model hypothesis tests

Layer	*t*-test *p*-value	Intercept *p*-value	Slope = 1 *p*-value
HMA	0.0110	0.0000	0.0000
Base	0.0054	0.0000	0.0000
Subgrade	0.7695	0.0000	0.0000
Total	0.0013	0.0000	0.0000

Table 5-36 Local model calibration coefficients

Calibration coefficient	Global model	Local model
HMA rutting (br1)	1.0000	0.9580
Base rutting (bs1)	1.0000	0.1181
Subgrade rutting (bsg1)	1.0000	0.0410

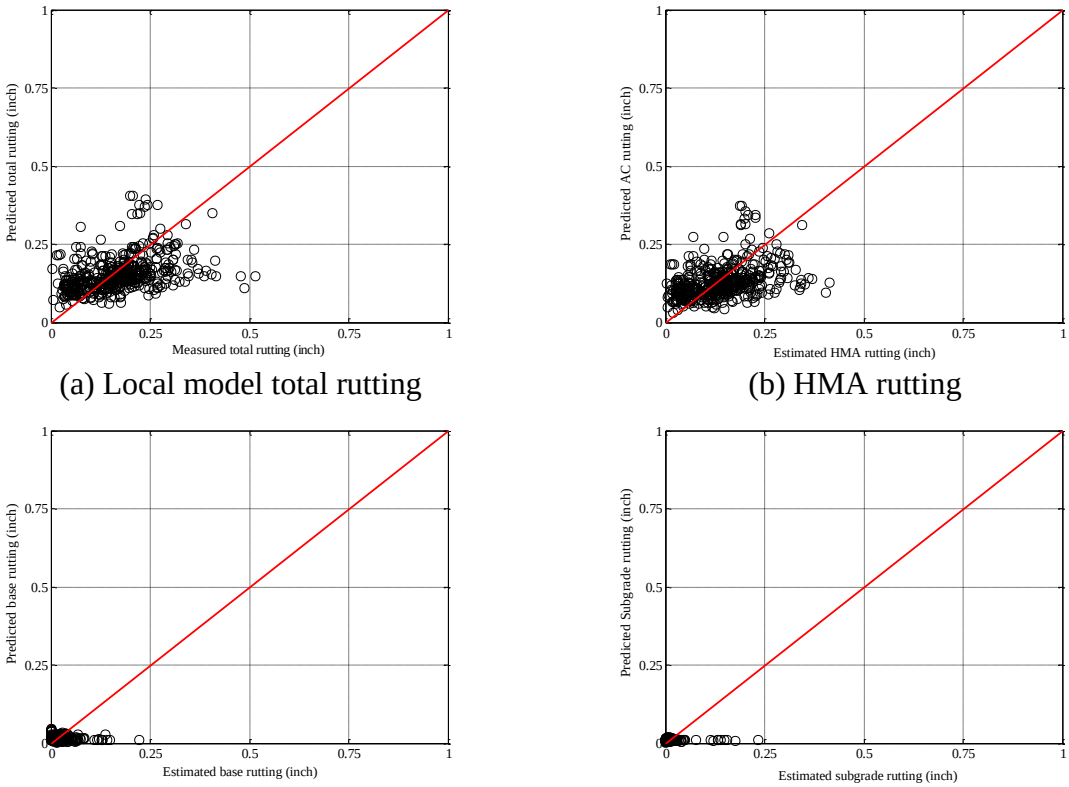

(a) Local model total rutting (b) HMA rutting

(c) Base rutting (d) Subgrade rutting

Figure 5-14 Rutting model local calibration measured versus predicted – Individual layer calibration

Split Sampling

Split sampling was performed to study how well the calibrated model can predict rutting for sections not included in the calibration set. The global model results are shown in Table 5-37. The results show that there is a significant difference between the predicted and measured rutting except for HMA rutting. Local calibration and validation were performed and the results are summarized in Tables 5-38 and 5-39. The results show that the SEE and bias was reduced for base, subgrade and total rutting. The HMA rutting results are almost identical to the global model.

Table 5-37 Global model parameters

Layer	SEE	Bias	t-test p-value	Intercept p-value	Slope = 1 p-value
HMA	0.0769	0.0034	0.4496	0.0000	0.0000
Base	0.1313	0.1134	0.0000	0.0000	0.0000
Subgrade	0.2243	0.2139	0.0000	0.0000	0.0000
Total	0.3534	0.3306	0.0000	0.0000	0.0000

Table 5-38 Local model parameters (split sampling)

Layer	SEE	Bias	t-test p-value	Intercept p-value	Slope = 1 p-value
HMA	0.0759	-0.0080	0.0674	0.0000	0.0000
Base	0.0268	-0.0040	0.0086	0.0000	0.0000
Subgrade	0.0236	-0.0004	0.7433	0.0000	0.0000
Total	0.0853	-0.0125	0.0109	0.0000	0.0000

Table 5-39 Local model validation parameters (split sampling)

Layer	SEE	Bias	t-test p-value	Intercept p-value	Slope = 1 p-value
HMA	0.0841	-0.0281	0.0000	0.0000	0.0000
Base	0.0250	-0.0011	0.5941	0.0000	0.0000
Subgrade	0.0210	0.0017	0.3416	0.0000	0.0000
Total	0.0913	-0.0276	0.0002	0.0000	0.0000

Repeated Split Sampling

Repeated split sampling was performed to study the variability of the data and the calibration statistics. The global model results are summarized in Table 5-40. The locally calibrated model results from calibration and validation are shown in Tables 5-41 and 5-42. The results indicate that the SEE and bias are reduced for all pavement layers after the local calibration. The distributions showing the mean, median and 95th percentile values of the model coefficients for calibration and validation are shown in Figures 5-15 and 5-16, respectively.

Table 5-40 Global model results (repeated split sampling)

Layer	Average SEE	SEE Lower CI	SEE Upper CI	Average bias (in.)	Bias Lower CI	Bias Upper CI
HMA	0.0785	0.0729	0.0836	-0.0037	-0.0113	0.0037
Base	0.1268	0.1170	0.1342	0.1111	0.1041	0.1182
Subgrade	0.2245	0.2168	0.2318	0.2144	0.2072	0.2216
Total	0.3435	0.3270	0.3573	0.3218	0.3083	0.3339

Table 5-41 Local model calibration results (repeated split sampling)

Statistics	HMA rutting	Base rutting	Subgrade rutting	Total rutting
Average SEE	0.0781	0.0260	0.0224	0.0867
SEE Lower CI	0.0726	0.0193	0.0133	0.0796
SEE Upper CI	0.0830	0.0298	0.0270	0.0926
Average bias (in.)	-0.0092	-0.0034	-0.0003	-0.0130
Bias Lower CI	-0.0126	-0.0047	-0.0006	-0.0165
Bias Upper CI	-0.0050	-0.0020	0.0000	-0.0087
Average calibration coefficient	0.9603	0.1185	0.0410	N/A
Calibration coefficient Lower CI	0.9049	0.1005	0.0307	N/A
Calibration coefficient Upper CI	1.0346	0.1407	0.0497	N/A

Table 5-42 Local model validation results (repeated split sampling)

Statistics	HMA rutting	Base rutting	Subgrade rutting	Total rutting
Average SEE	0.0797	0.0257	0.0216	0.0882
SEE Lower CI	0.0669	0.0151	0.0080	0.0730
SEE Upper CI	0.0920	0.0378	0.0364	0.1032
Average bias (in.)	-0.0090	-0.0033	-0.0004	-0.0127
Bias Lower CI	-0.0331	-0.0120	-0.0083	-0.0377
Bias Upper CI	0.0177	0.0051	0.0060	0.0168
Average calibration coefficient	0.9603	0.1185	0.0410	N/A
Calibration coefficient Lower CI	0.9049	0.1005	0.0307	N/A
Calibration coefficient Upper CI	1.0346	0.1407	0.0497	N/A

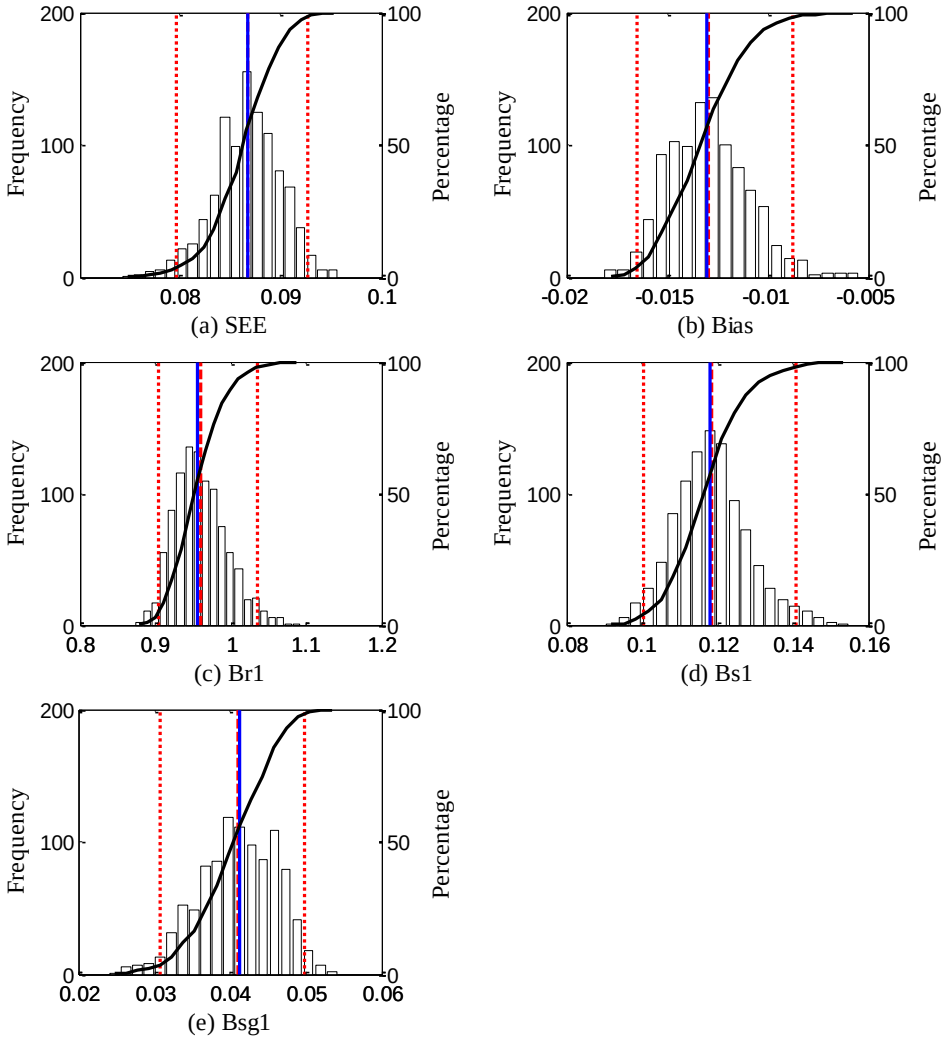

Figure 5-15 Distribution of calibration parameters - calibration (repeated split sampling)

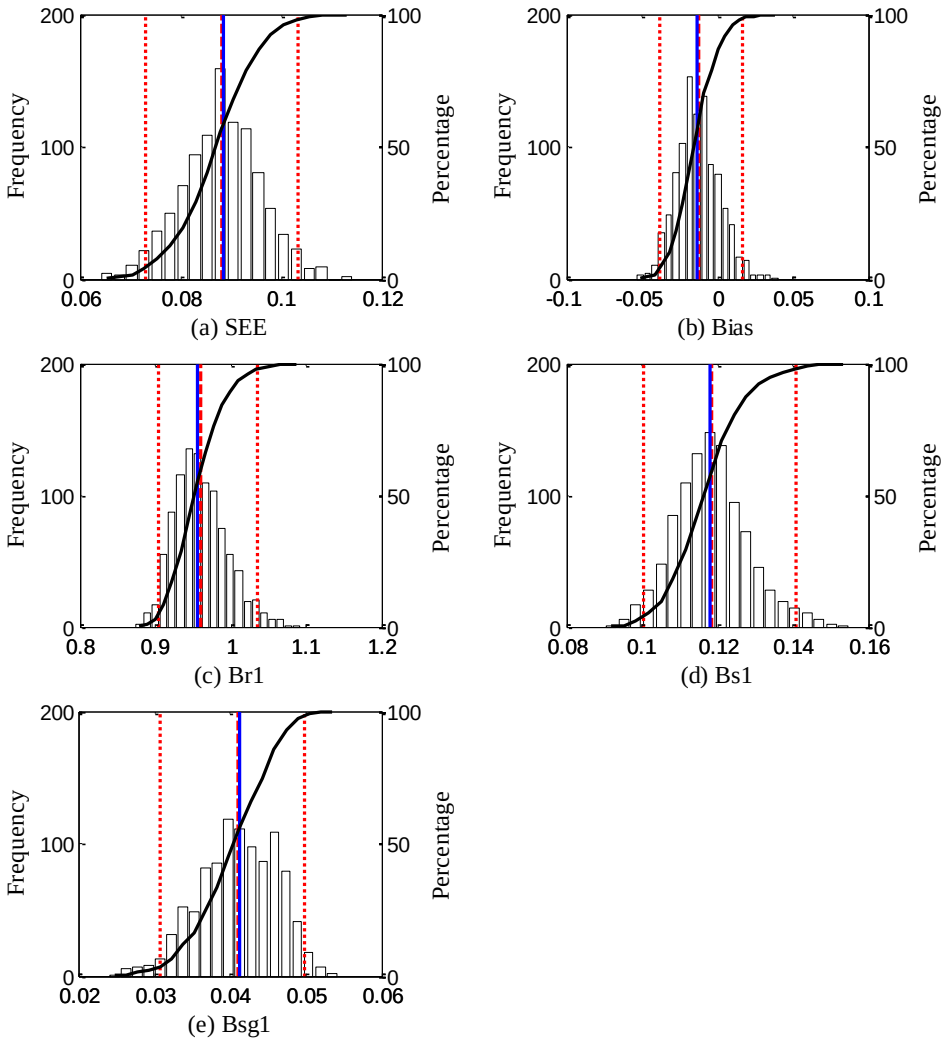

Figure 5-16 Distribution of calibration parameters - validation (repeated split sampling)

Bootstrapping

Bootstrapping was performed by randomly selecting pavement sections with replacement as explained in Chapter 4. The global model results are summarized in Table 5-43 and the locally calibrated model results are shown in Table 5-44. The SEE and bias are reduced after local calibration. The distributions of model statistics based on 1000 bootstraps are shown in Figure 5-17.

Table 5-43 Global rutting model

Layer type	Average SEE	SEE Lower CI	SEE Upper CI	Average bias (in.)	Bias Lower CI	Bias Upper CI
HMA	0.0785	0.0706	0.0870	-0.0039	-0.0148	0.0068
Base	0.1264	0.1146	0.1401	0.1110	0.1010	0.1219
Subgrade	0.2240	0.2122	0.2360	0.2142	0.2031	0.2253
Total	0.3425	0.3223	0.3654	0.3213	0.3026	0.3417

Table 5-44 Local rutting model

Statistics	HMA rutting	Base rutting	Subgrade rutting	Total rutting
Average SEE	0.0780	0.0258	0.0221	0.0865
SEE Lower CI	0.0702	0.0187	0.0092	0.0772
SEE Upper CI	0.0865	0.0333	0.0318	0.0962
Average bias (in.)	-0.0091	-0.0034	-0.0003	-0.0128
Bias Lower CI	-0.0152	-0.0056	-0.0008	-0.0188
Bias Upper CI	-0.0038	-0.0015	0.0001	-0.0073
Average calibration coefficient	0.9628	0.1190	0.0411	N/A
Calibration coefficient Lower CI	0.8721	0.0927	0.0277	N/A
Calibration coefficient Upper CI	1.0628	0.1479	0.0577	N/A

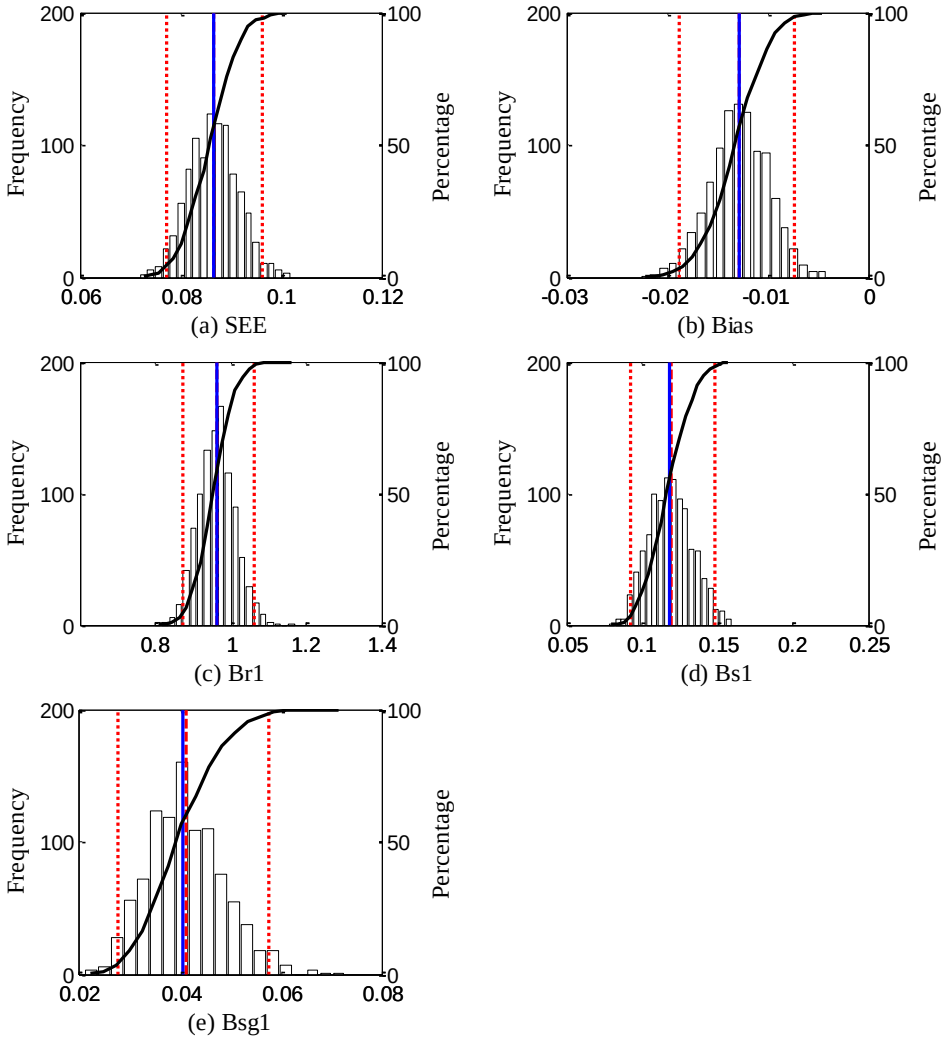

Figure 5-17 Distribution of calibration parameters (bootstrapping)

Summary

The rutting model local calibration results for all sampling techniques for Method 1are summarized in Table 5-45. The overall results show that the bootstrap model coefficients have the lowest SEE for the rutting model in option 1.

Table 5-45 Rutting model calibration results summary – Option 1 Method 1

Sampling Technique	Pavement layer rutting	SEE	Bias	Calibration coefficient
No sampling	HMA	0.0783	-0.0094	0.9580
	Base	0.0262	-0.0034	0.1181
	Subgrade	0.0228	-0.0003	0.0410
	Total	0.0869	-0.0132	-
Split sampling	HMA	0.0759	-0.0080	0.9204
	Base	0.0268	-0.0040	0.1209
	Subgrade	0.0236	-0.0004	0.0435
	Total	0.0853	-0.0125	-
Repeated split sampling	HMA	0.0781	-0.0092	0.9603
	Base	0.026	-0.0034	0.1185
	Subgrade	0.0224	-0.0003	0.041
	Total	0.0867	-0.013	-
Bootstrapping	HMA	0.078	-0.0091	0.9628
	Base	0.0258	-0.0034	0.119
	Subgrade	0.0221	-0.0003	0.0411
	Total	0.0865	-0.0128	-

5.2.3.2. Option 1: Method 2 – MDOT reconstruct pavements only

For Method 2, the rutting model was calibrated using the same dataset as for Method 1. The calibration coefficients were changed simultaneously to minimize the error between the total measured and predicted rutting without considering the rutting in the individual pavement layers (see details in Chapter 4). The adequacy of the global model was tested to determine if local calibration is necessary. The global model's SEE, bias and hypothesis test results are summarized in Table 5-46. Figure 5-18 shows the comparison between measured and predicted rutting for all layers. The results indicate that there is a significant difference between measured and predicted base, subgrade and total rutting.

Table 5-46 Global rutting model SEE, bias and hypothesis testing results

Layer	SEE	Bias	t-test p-value	Intercept p-value	Slope = 1 p-value
HMA	0.0786	-0.0037	0.3220	0.0000	0.0000
Base	0.1267	0.1111	0.0000	0.0000	0.0000
Subgrade	0.2242	0.2143	0.0000	0.0000	0.0000
Total	0.3431	0.3217	0.0000	0.0000	0.0000

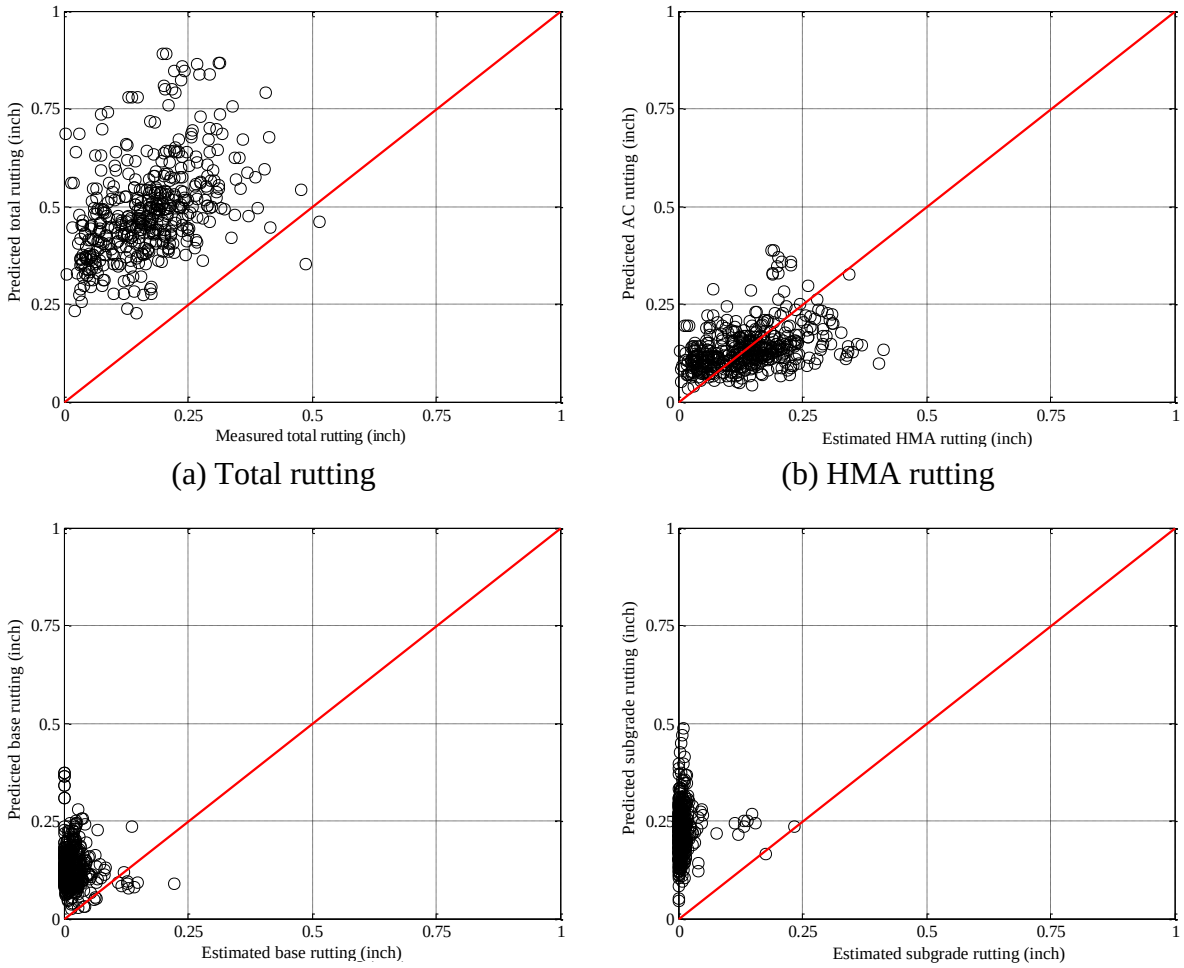

(a) Total rutting (b) HMA rutting

(c) Base rutting (d) Subgrade rutting

Figure 5-18 Global rutting model - measured versus predicted

The local calibration results for the Method 2 are summarized in Table 5-47. The results show that the SEE and bias reduced for base, subgrade and total rutting but not for AC rutting. The total rutting mean difference between the measured and predicted values were not significantly different from each other. Table 5-48 shows the locally calibrated layer coefficient values. All other hypothesis tests were rejected. Figure 5-19 shows the comparison between measured and predicted rutting for all layers using the locally calibrated model.

Table 5-47 Rutting model Local calibration results

Layer	Global Model		Local Model				
	SEE	Bias	SEE	Bias	t-test p-value	Intercept p-value	Slope = 1 p-value
HMA	0.0786	-0.0037	0.1167	-0.0892	0.0000	0.0000	0.0000
Base	0.1267	0.1111	0.0304	0.0109	0.0000	0.0000	0.0000
Subgrade	0.2242	0.2143	0.0840	0.0775	0.0000	0.0000	0.0000
Total	0.3431	0.3217	0.0812	-0.0009	0.8142	0.0000	0.0000

Table 5-48 Local calibration coefficients

Layer coefficient	Global model	Local model
HMA rutting (br1)	1.0000	0.3738
Base rutting (bs1)	1.0000	0.2283
Subgrade rutting (bsg1)	1.0000	0.3886

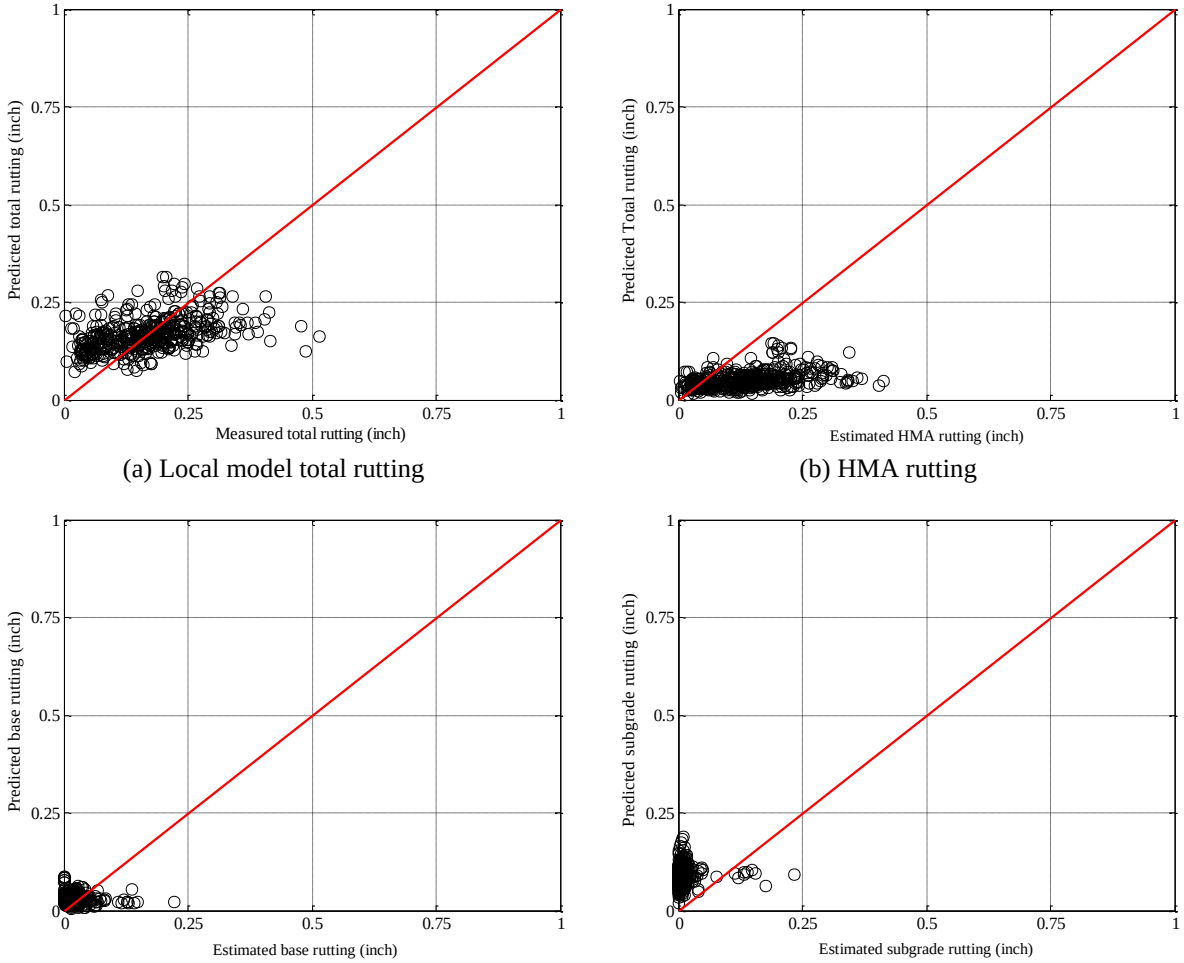

(a) Local model total rutting

(b) HMA rutting

(c) Base rutting

(d) Subgrade rutting

Figure 5-19 Local calibration results

Summary

Similar procedures as shown for Method 1 (i.e., split sampling, repeated split sampling and bootstrapping) were performed for Method 2. Table 5-49 summarizes the results for all four sampling techniques for Method 2. Overall, the SEE and bias did not change significantly between the various sampling techniques. The detailed results are presented in Appendix B.

Table 5-49 Summary results for all sampling techniques

Sampling Technique	Pavement layer rutting	SEE	Bias	Calibration coefficient
No sampling	HMA	0.1167	-0.0892	0.3738
	Base	0.0304	0.0109	0.2283
	Subgrade	0.0840	0.0775	0.3886
	Total	0.0812	-0.0009	-
Split sampling	HMA	0.1050	-0.0758	0.4383
	Base	0.0350	0.0199	0.2832
	Subgrade	0.0630	0.0543	0.2930
	Total	0.0806	-0.0016	-
Repeated split sampling	HMA	0.1161	-0.0881	0.382
	Base	0.0314	0.0113	0.2324
	Subgrade	0.0827	0.076	0.3824
	Total	0.081	-0.0008	-
Bootstrapping	HMA	0.1151	-0.0866	0.3932
	Base	0.0314	0.0098	0.2216
	Subgrade	0.0828	0.0762	0.3833
	Total	0.0804	-0.0007	-

5.2.3.3. Option 2: Method 1– MDOT reconstruct and rehabilitated pavements

The results for the Option 2 – Method 1 are presented in Table 5-50. The detailed results for each sampling technique are summarized in the Appendix B.

Table 5-50 Summary of results for all sampling techniques

Sampling technique	Pavement layer rutting	SEE	Bias	Calibration coefficient
No sampling	HMA	0.0774	-0.0099	0.9422
	Base	0.0258	-0.0051	0.0974
	Subgrade	0.0205	-0.0006	0.0367
	Total	0.0865	-0.0155	-
Split sampling	HMA	0.0746	-0.0086	0.9372
	Base	0.0277	-0.0049	0.1014
	Subgrade	0.0200	-0.0004	0.0348
	Total	0.0843	-0.0140	-
Repeated split sampling	HMA	0.0783	-0.009	0.9451
	Base	0.0254	-0.0048	0.0982
	Subgrade	0.0192	-0.0004	0.0368
	Total	0.0872	-0.0143	-
Bootstrapping	HMA	0.0772	-0.0096	0.9453
	Base	0.0256	-0.005	0.0985
	Subgrade	0.02	-0.0005	0.0367
	Total	0.0862	-0.0152	-

5.2.3.4. Option 2: Method 2– MDOT reconstruct and rehabilitated pavements

The results for the Option 2 – Method 2 are presented in Table 5-51. The detailed results for each sampling technique are summarized in the Appendix B.

Table 5-51 Option 2 – Method 2

Sampling Technique	Pavement layer rutting	SEE	Bias	Calibration coefficient
No sampling	HMA	0.0906	-0.0533	0.6251
	Base	0.0279	-0.0144	0.0276
	Subgrade	0.0695	0.0623	0.3241
	Total	0.0830	-0.0055	-
Split sampling	HMA	0.0971	-0.0646	0.5100
	Base	0.0256	-0.0063	0.1006
	Subgrade	0.0728	0.0666	0.3367
	Total	0.0813	-0.0042	-
Repeated split sampling	HMA	0.0915	-0.0542	0.6193
	Base	0.0275	-0.0131	0.0377
	Subgrade	0.0693	0.0619	0.3224
	Total	0.0829	-0.0054	-
Bootstrapping	HMA	0.0919	-0.0543	0.6201
	Base	0.0271	-0.012	0.0449
	Subgrade	0.0684	0.0611	0.3184
	Total	0.0823	-0.0051	-

5.2.3.5. Option 4: Method 1 – MDOT rehabilitated pavements only

The results for the Option 4 – Method 1 are presented in Table 5-52. The detailed results for each sampling technique are summarized in Appendix B

Table 5-52 Option 4 – Method 1

Sampling Technique	Pavement layer rutting	SEE	Bias	Calibration coefficient
No sampling	HMA	0.0746	-0.0113	0.8909
	Base	0.0231	-0.0072	0.0597
	Subgrade	0.0096	-0.0012	0.0216
	Total	0.0828	-0.0197	-
Split sampling	HMA	0.0780	-0.0118	0.9108
	Base	0.0263	-0.0082	0.0678
	Subgrade	0.0112	-0.0018	0.0223
	Total	0.0877	-0.0218	-
Repeated split sampling	HMA	0.0742	-0.011	0.8979
	Base	0.0228	-0.0072	0.0601
	Subgrade	0.0094	-0.0011	0.0217
	Total	0.0823	-0.0193	-
Bootstrapping	HMA	0.0737	-0.0109	0.9032
	Base	0.0225	-0.0071	0.0612
	Subgrade	0.0092	-0.0011	0.0216
	Total	0.0817	-0.0191	-

5.2.3.6. Option 4: Method 2 – MDOT rehabilitated pavements only

The results for the Option 4 – Method 2 are presented in Table 5-53. The detailed results for each sampling technique are summarized in Appendix B.

Table 5-53 Option 4 – Method 2

Sampling Technique	Pavement layer rutting	SEE	Bias	Calibration coefficient
No sampling	HMA	0.0746	-0.0116	0.8888
	Base	0.0249	-0.0146	0.0100
	Subgrade	0.0211	0.0154	0.1040
	Total	0.0814	-0.0108	-
Split sampling	HMA	0.0769	0.0010	0.9277
	Base	0.0258	-0.0134	0.0100
	Subgrade	0.0123	0.0032	0.0506
	Total	0.0800	-0.0092	-
Repeated split sampling	HMA	0.076	-0.012	0.8898
	Base	0.0247	-0.0144	0.0105
	Subgrade	0.0237	0.0162	0.1065
	Total	0.0807	-0.0102	-
Bootstrapping	HMA	0.0758	-0.011	0.9042
	Base	0.0245	-0.0141	0.0129
	Subgrade	0.0236	0.0153	0.1011
	Total	0.0796	-0.0098	-

5.2.3.7. Rutting model summary

The local calibration based on total rutting for Method 2 show lower SEE and bias as compared to the global and are somewhat lower than those from the Method 1. However, Method 2 has some practical discrepancies as discussed below:

- The local calibration based on Method 2 doesn't minimize the sum of squared error for each pavement layer. As a consequence, some of those coefficients can be zero which is not realistic.
- Method 2 is not representative of the actual field observed rutting phenomenon because it can mask the rutting contributions for unbound layers.

Tables 5-50 and 5-51 (bootstrapping technique) show the results for SEE and bias for individual layers for Methods 1 and 2, respectively. Further, Figures 5-20 and 5-21 show examples of the residual plots for Option 1 for Methods 1 and 2, respectively. The residual plots show a random scatter for Method 1 while a systematic error can be observed for HMA, base and subgrade layers for Method 2.

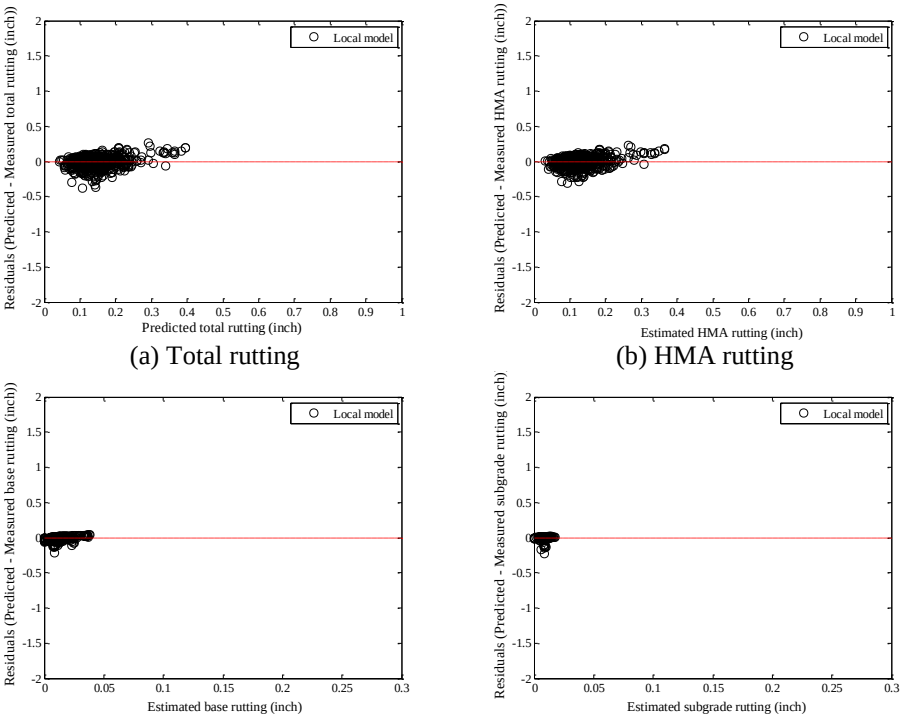

(a) Total rutting (b) HMA rutting

(c) Base/subbase rutting (d) Subgrade

Figure 5-20 Residual versus predicted rutting for Method 1

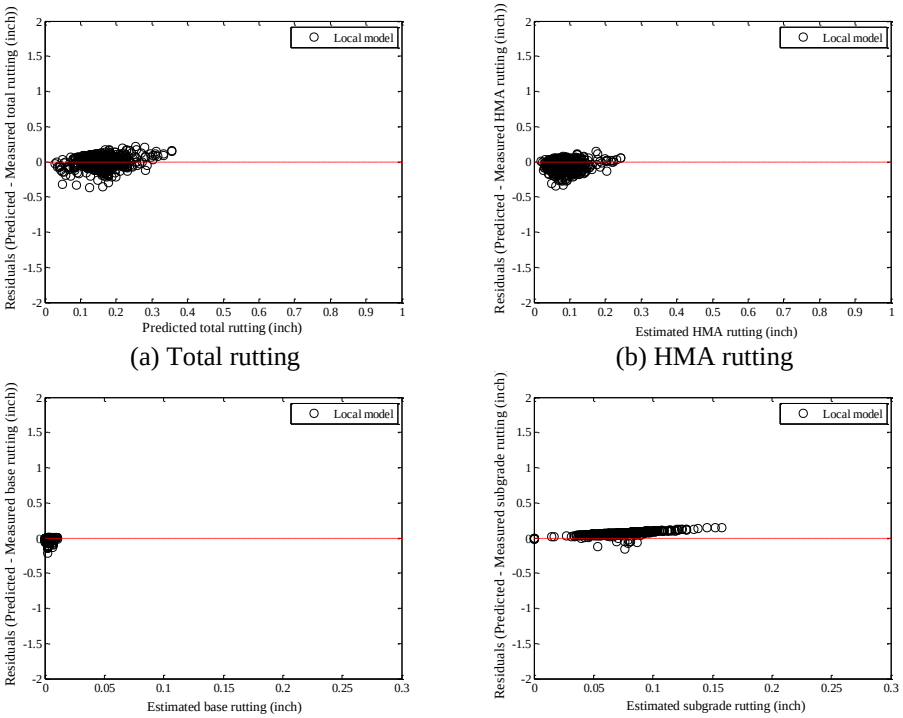

(a) Total rutting (b) HMA rutting

(c) Base/subbase rutting (d) Subgrade

Figure 5-21 Residual versus predicted rutting for Method 2

5.2.3.8. Reliability for the rutting model

The standard error of the calibrated rutting models were used to establish the relationship between the standard deviation of the measured rutting and mean predicted rutting as explained in Chapter 4. These relationships are used to calculate the rutting for a specific reliability. Tables 5-54 to 5-59 summarize these relations for the options considered for the rutting models using the bootstrapping technique. The details for the other techniques can be found in Appendix B.

Table 5-54 Rutting model reliability for Option 1 – Method 1 - Bootstrap

Pavement layer	Global model equation	Local model equation
HMA rutting	$s_{e(HMA)} = 0.24\left(Rut_{HMA}\right)^{0.8026} + 0.001$	$s_{e(HMA)} = 0.107\left(Rut_{HMA}\right)^{0.2}$
Base rutting	$s_{e(base)} = 0.1477\left(Rut_{base}\right)^{0.6711} + 0.001$	$s_{e(base)} = 0.0925\left(Rut_{subgrade}\right)^{0.3599}$
Subgrade	$s_{e(subgrade)} = 0.1235\left(Rut_{subgrade}\right)^{0.5012} + 0.001$	$s_{e(subgrade)} = 1.5969\left(Rut_{subgrade}\right)^{0.9134}$

Table 5-55 Rutting model reliability for Option 1 – Method 2 - Bootstrap

Pavement layer	Global model equation	Local model equation
HMA rutting	$s_{e(HMA)} = 0.24\left(Rut_{HMA}\right)^{0.8026} + 0.001$	$s_{e(HMA)} = 0.0727\left(Rut_{HMA}\right)^{0.014}$
Base rutting	$s_{e(base)} = 0.1477\left(Rut_{base}\right)^{0.6711} + 0.001$	$s_{e(base)} = 0.0306\left(Rut_{subgrade}\right)^{0.0284}$
Subgrade	$s_{e(subgrade)} = 0.1235\left(Rut_{subgrade}\right)^{0.5012} + 0.001$	$s_{e(subgrade)} = 0.0866\left(Rut_{subgrade}\right)^{0.5416}$

Table 5-56 Rutting model reliability for Option 2 – Method 1 - Bootstrap

Pavement layer	Global model equation	Local model equation
HMA rutting	$s_{e(HMA)} = 0.24\left(Rut_{HMA}\right)^{0.8026} + 0.001$	$s_{e(HMA)} = 0.1126\left(Rut_{HMA}\right)^{0.2352}$
Base rutting	$s_{e(base)} = 0.1477\left(Rut_{base}\right)^{0.6711} + 0.001$	$s_{e(base)} = 0.1145\left(Rut_{base}\right)^{0.3907}$
Subgrade	$s_{e(subgrade)} = 0.1235\left(Rut_{subgrade}\right)^{0.5012} + 0.001$	$s_{e(subgrade)} = 3.6118\left(Rut_{subgrade}\right)^{1.0951}$

Table 5-57 Rutting model reliability for Option 2 – Method 2 - Bootstrap

Pavement layer	Global model equation	Local model equation
HMA rutting	$s_{e(HMA)} = 0.24\left(Rut_{HMA}\right)^{0.8026} + 0.001$	$s_{e(HMA)} = 0.9348\left(Rut_{HMA}\right)^{1.0122}$
Base rutting	$s_{e(base)} = 0.1477\left(Rut_{base}\right)^{0.6711} + 0.001$	$s_{e(base)} = 0.0229\left(Rut_{base}\right)^{0.0057}$
Subgrade	$s_{e(subgrade)} = 0.1235\left(Rut_{subgrade}\right)^{0.5012} + 0.001$	$s_{e(subgrade)} = 0.0668\left(Rut_{subgrade}\right)^{0.4202}$

Table 5-58 Rutting model reliability for Option 4 – Method 1 - Bootstrap

Pavement layer	Global model equation	Local model equation
HMA rutting	$s_{e(HMA)} = 0.24\left(Rut_{HMA}\right)^{0.8026} + 0.001$	$s_{e(HMA)} = 0.2333\left(Rut_{HMA}\right)^{0.5824}$
Base rutting	$s_{e(base)} = 0.1477\left(Rut_{base}\right)^{0.6711} + 0.001$	$s_{e(base)} = 0.0776\left(Rut_{base}\right)^{0.3212}$
Subgrade	$s_{e(subgrade)} = 0.1235\left(Rut_{subgrade}\right)^{0.5012} + 0.001$	$s_{e(subgrade)} = 0.0546\left(Rut_{subgrade}\right)^{0.3143}$

Table 5-59 Rutting model reliability for Option 4 – Method 2 - Bootstrap

Pavement layer	Global model equation	Local model equation
HMA rutting	$s_{e(HMA)} = 0.24\left(Rut_{HMA}\right)^{0.8026} + 0.001$	$s_{e(HMA)} = 0.0789\left(Rut_{HMA}\right)^{0.1078}$
Base rutting	$s_{e(base)} = 0.1477\left(Rut_{base}\right)^{0.6711} + 0.001$	$s_{e(base)} = 0.0454\left(Rut_{base}\right)^{0.2154}$
Subgrade	$s_{e(subgrade)} = 0.1235\left(Rut_{subgrade}\right)^{0.5012} + 0.001$	$s_{e(subgrade)} = 0.0119\left(Rut_{subgrade}\right)^{0.0455}$

5.2.4 Transverse (thermal) Cracking Model

The transverse thermal cracking model was calibrated by changing the K coefficient in the Pavement-ME software. Each time the *K* coefficient is modified, the software needs to be rerun to obtain the thermal cracking predictions. Since, thermal cracking is significantly impacted by the HMA layer characterization, the local calibration was also performed for Level 1 and 3 HMA mixture characteristics.

5.2.4.1. Level 1 HMA layer characterization

The Level 1 analyses for all options are summarized in Tables 5-60 and 5-61. The calibration coefficient increments were selected based on the literature. The results show that a *K* value of 0.75 provided the best result for Michigan conditions (i.e., lowest SEE and bias). For Option 1, the SEE reduced from 1343.58 to 753.24 ft/mile and the bias also reduced from 903.06 to -70.40 ft/mile, when compared with the current global thermal cracking mode. For Option 2, a $K = 0.75$ combination also yielded the best results with an SEE and bias of 732.1 and -73.8 ft/mile. Figures 5-22 and 5-23 show the measured versus predicted thermal cracking results after local calibration for both Options. Options 3 and 4 were not considered for the level 1 transverse cracking model due to a limited number of LTPP and MDOT rehabilitation sections with Level 1 HMA data.

Table 5-60 Transverse thermal cracking results – Option 1

Parameter	SEE	Bias
Global model Level 1	1343.58	903.06
K = 0.5 Level 1	767.05	-217.64
K = 0.75 Level 1	753.24	-70.40
K = 1 Level 1	943.39	246.75
K = 1.1 Level 1	1019.15	369.83
K = 1.2 Level 1	1094.84	492.97
K = 1.3 Level 1	1176.40	630.50
K = 1.4 Level 1	1277.75	783.51
K = 1.7 Level 1	1459.76	1109.90
K = 2 Level 1	1560.47	1310.64
K = 2.5 Level 1	1692.66	1553.99

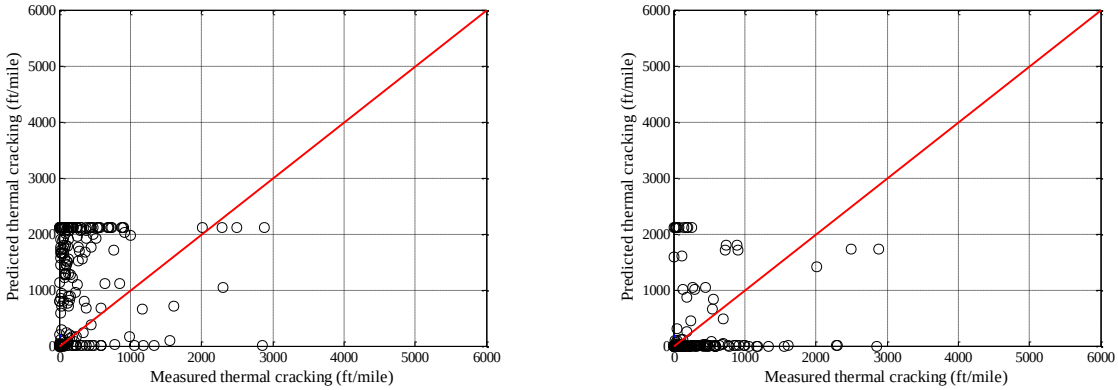

(a) Global model (b) Local model

Figure 5-22 Option 1 measured versus predicted transverse (thermal) cracking

Table 5-61 Transverse thermal cracking results – Option 2

Parameter	SEE	Bias
Global model Level 1	1306.5	854.7
K = 0.5 Level 1	745.5	-212.6
K = 0.75 Level 1	732.1	-73.8
K = 1 Level 1	916.4	225.1
K = 1.1 Level 1	989.9	341.2
K = 1.2 Level 1	1063.2	457.5
K = 1.3 Level 1	1142.3	588.4
K = 1.4 Level 1	1241.0	736.0
K = 1.7 Level 1	1425.3	1064.9
K = 2 Level 1	1529.4	1271.1
K = 2.5 Level 1	1667.5	1524.3

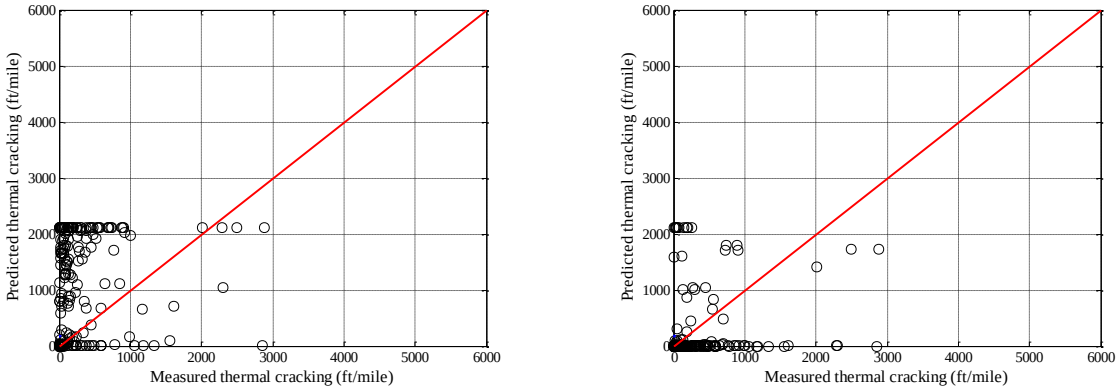

(a) Global model (b) Local model

Figure 5-23 Option 2 measured versus predicted transverse (thermal) cracking

5.2.4.2. Level 3 HMA layer characterization

The Level 3 analysis followed a similar procedure as for Level 1 and the results are summarized in Tables 5-62 through 5-64. Option 1 showed that K = 3 had the best overall bias, even though the SEE is slightly higher than the global model. Figure 5-24 shows the measured versus predicted results for both global and local models. Alternatively, for the Option 2, K = 4 provided the lowest bias compared to all other options. Option 3 was not performed for Level 3 due to a limited number of SPS-1 sections available. Option 4 only considers rehabilitation pavements and a K = 5 provided the best results.

Table 5-62 Transverse thermal cracking Level 3 results – Option 1

Parameter	SEE	Bias
Global model Level 3	754.6	-318.5
K = 2 Level 3	785.5	-249.7
K = 3 Level 3	867.2	-23.2
K = 4 Level 3	978.2	233.9
K = 5 Level 3	1107.2	494.5

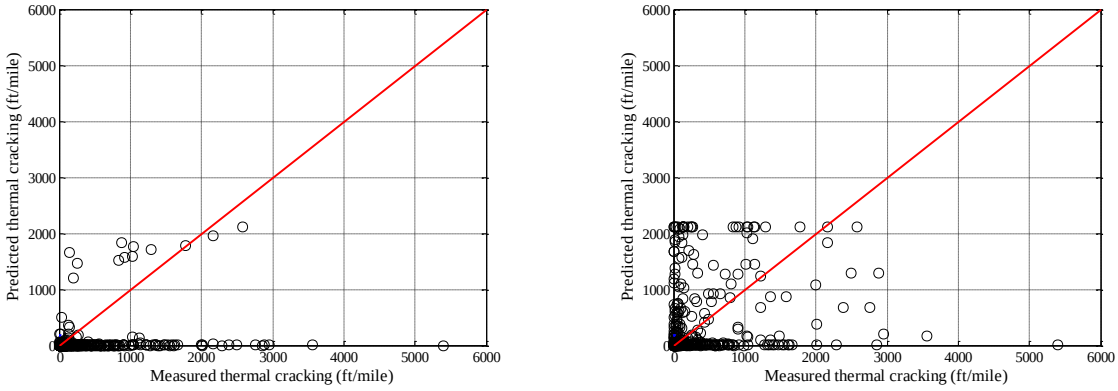

(a) Global model (b) Local model

Figure 5-24 Measured versus predicted TC for Option 1

Table 5-63 Transverse thermal cracking Level 3 results – Option 2

Parameter	SEE	Bias
Global model Level 3	945.0	-489.0
K = 2 Level 3	965.6	-416.2
K = 3 Level 3	1022.4	-209.6
K = 4 Level 3	1057.7	35.3
K = 5 Level 3	1121.8	289.6

Table 5-64 Transverse thermal cracking Level 3 results – Option4

Parameter	SEE	Bias
Global model Level 3	1304.7	-906.6
K = 2 Level 3	1312.1	-824.0
K = 3 Level 3	1334.6	-666.1
K = 4 Level 3	1237.6	-451.0
K = 5 Level 3	1163.8	-212.0

5.2.4.3. Reliability for thermal cracking model

The standard error of the calibrated thermal cracking models were used to establish the relationship between the standard deviation of the measured cracking and mean predicted cracking as explained in Chapter 4. These relationships are used to calculate thermal cracking for a specific reliability. Tables 5-65 and 5-66 summarize these relations for the options considered for the thermal cracking models using the no sampling technique. The other details can be found in Appendix B.

Table 5-65 Reliability summary for Level 1

Data set option	Global model equation	Local model equation
Option 1	$s_e(Level1) = 0.1468(TC) + 65.027$	$s_e(Level1) = 0.4203(TC) + 216.94$
Option 2	$s_e(Level1) = 0.1468(TC) + 65.027$	$s_e(Level1) = 0.4258(TC) + 210.08$

Table 5-66 Reliability summary for Level 3

Data set option	Global model equation	Local model equation
Option 1	$s_e(Level3) = 0.3972(TC) + 20.422$	$s_e(Level3) = 0.142(TC) + 670.28$
Option 2	$s_e(Level3) = 0.3972(TC) + 20.422$	$s_e(Level3) = 0.7737(TC) + 622.92$
Option 4	$s_e(Level3) = 0.3972(TC) + 20.422$	$s_e(Level3) = 0.7039(TC) + 324.26$

5.2.5 Flexible Pavement Roughness (IRI) Model

The IRI model was calibrated after the local calibration of the fatigue and transverse cracking, and rutting models were completed. These distresses are considered directly in the IRI model along with the site factor. Option 3 was not considered for IRI model calibration because a sufficient number of MDOT pavement sections were available. Figure 5-25 shows the predicted and measured IRI for the global model for only reconstructed pavement sections. It can be seen that the global IRI model coefficient with locally calibrated distresses predicts the measured IRI reasonably.

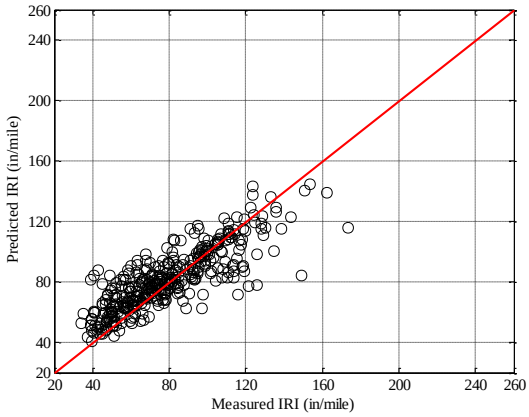

Figure 5-25 Flexible IRI global model calibration measured versus predicted – no sampling

Tables 5-67 and 5-68 show the global model coefficients and statistics, and hypothesis tests results, respectively. The results of hypothesis tests show the need for local calibration of the IRI model for Michigan conditions. The details of the local calibration are included in Appendix B. Tables 5-69 to 5-71 show the summary results for the Options 1, 2 and 4, respectively. The following observations can be made through these results:

- The locally calibrated model using the reconstructed pavements (Option 1) show the minimum SEE among all options but bias may vary by option.
- The locally calibrated model using the rehabilitated pavements (Option 4) show the highest SEE because of the following reasons:
  - smaller sample size,
  - lower extents of observed IRI,
  - lower rutting and absence of predicted alligator cracking on the rehabilitated pavements.
- The bootstrapping resampling technique gives the lowest SEE for all data subsets (options) considered in the analysis.

Table 5-67 Global IRI model calibration parameters

Parameter	Global
SEE (in/mile)	14.8261
Bias (in/mile)	2.7552
C1	40.0000
C2	0.4000
C3	0.0080
C4	0.0150

Table 5-68 Global model hypothesis testing results

Hypothesis test	Hypotheses	P-value
Mean difference (paired *t*-test)	H_0 = *(predicted – measured) = 0* H_1 = *(predicted – measured)* $\neq 0$	0.0003
Intercept	H_0 = *intercept = 0* H_1 = *intercept* $\neq 0$	0.0000
Slope	H_0 = *slope = 1* H_1= *slope* $\neq 1$	0.0000

Table 5-69 Flexible IRI local calibration – Option 1

Sampling Technique	Parameter	SEE	Bias	C1	C2	C3	C4
No Sampling	Global model	14.8261	2.7552	40.0000	0.4000	0.0080	0.0150
	Local model	14.1044	0.0070	48.5626	0.4781	0.0064	0.0072
Split sampling	Global model	14.9090	2.4035	40.0000	0.4000	0.0080	0.0150
	Local model calibration	14.1483	0.0973	52.8662	0.3535	0.0064	0.0071
	Local model validation	14.1497	0.5702	52.8662	0.3535	0.0064	0.0071
Repeated split sampling	Global Model Mean	14.8176	2.7282	40.0000	0.4000	0.0080	0.0150
	Global Model Median	14.8629	2.7679	40.0000	0.4000	0.0080	0.0150
	Global model lower CI	13.3900	1.0972	-	-	-	-
	Global model upper CI	15.9512	4.2236	-	-	-	-
	Local Model Mean	14.0562	0.0294	50.8200	0.4088	0.0064	0.0070
	Local Model Median	14.1138	0.0213	50.8000	0.4693	0.0064	0.0072
	Local model lower CI	12.3621	-0.4797	41.8300	0.3200	0.0064	0.0053
	Local model upper CI	15.3295	0.6616	57.8000	0.4800	0.0070	0.0072
	Local Model Mean - validation	14.2948	0.1403	50.8200	0.4088	0.0064	0.0070
	Local Model Median - validation	14.3197	0.1667	50.8000	0.4693	0.0064	0.0072
	Local model lower CI	10.9564	-4.5686	41.8300	0.3200	0.0064	0.0053
	Local model upper CI	17.7144	4.9868	57.8000	0.4800	0.0070	0.0072
Bootstrapping	Global Model Mean	14.7738	2.7817	40.0000	0.4000	0.0080	0.0150
	Global Model Median	14.7500	2.7779	40.0000	0.4000	0.0080	0.0150
	Global model lower CI	12.9187	0.4205	-	-	-	-
	Global model upper CI	16.6746	5.0187	-	-	-	-
	Local Model Mean	13.9428	-0.0391	50.3720	0.4102	0.0066	0.0068
	Local Model Median	13.9428	-0.0160	51.1021	0.4800	0.0064	0.0072
	Local model lower CI	11.8322	-0.9072	38.5371	0.3200	0.0064	0.0048
	Local model upper CI	16.2173	0.8145	57.8050	0.4800	0.0084	0.0072

Table 5-70 Flexible IRI local calibration – Option 2

Sampling Technique	Parameter	SEE	Bias	C1	C2	C3	C4
No Sampling	Global model	16.0659	0.2456	40.0000	0.4000	0.0080	0.0150
	Local model	15.8267	0.0564	32.0602	0.3200	0.0064	0.0180
Split sampling	Global model	16.6468	-0.2285	40.0000	0.4000	0.0080	0.0150
	Local model calibration	16.3668	-0.2634	33.4400	0.3200	0.0064	0.0180
	Local model validation	14.7618	1.3524	33.4400	0.3200	0.0064	0.0180
Repeated split sampling	Global Model Mean	16.1000	0.2126	40.0000	0.4000	0.0080	0.0150
	Global Model Median	16.1383	0.2346	40.0000	0.4000	0.0080	0.0150
	Global model lower CI	14.8243	-1.2712	-	-	-	-
	Global model upper CI	17.2964	1.7130	-	-	-	-
	Local Model Mean	15.8346	-0.2411	32.1854	0.3428	0.0064	0.0175
	Local Model Median	15.8684	-0.1812	33.4400	0.3200	0.0064	0.0180
	Local model lower CI	14.5452	-1.1543	25.6184	0.3200	0.0064	0.0149
	Local model upper CI	17.0303	0.3264	33.4400	0.4800	0.0064	0.0180
	Local Model Mean - validation	15.8973	-0.1664	32.1854	0.3428	0.0064	0.0175
	Local Model Median - validation	15.9040	0.0272	33.4400	0.3200	0.0064	0.0180
	Local model lower CI	12.8664	-4.8854	25.6184	0.3200	0.0064	0.0149
	Local model upper CI	18.7973	3.8174	33.4400	0.4800	0.0064	0.0180
Bootstrapping	Global Model Mean	16.0256	0.2779	40.0000	0.4000	0.0080	0.0150
	Global Model Median	16.0372	0.2614	40.0000	0.4000	0.0080	0.0150
	Global model lower CI	13.9711	-1.9643	-	-	-	-
	Global model upper CI	17.9502	2.5374	-	-	-	-
	Local Model Mean	15.7316	-0.3810	31.6450	0.3613	0.0065	0.0172
	Local Model Median	15.7544	-0.3082	33.4400	0.3200	0.0064	0.0180
	Local model lower CI	13.6244	-1.6554	22.2960	0.3200	0.0064	0.0137
	Local model upper CI	17.6772	0.4516	33.4400	0.4800	0.0071	0.0180

Table 5-71 Flexible IRI local calibration results – Option 4

Sampling Technique	Parameter	SEE	Bias	C1	C2	C3	C4
No Sampling	Global model	20.6944	-5.9035	40.0000	0.4000	0.0080	0.0150
	Local model	17.9586	0.3185	20.8000	0.1600	0.0048	0.0277
Split sampling	Global model	22.6387	-5.8644	40.0000	0.4000	0.0080	0.0150
	Local model calibration	19.9658	0.8658	20.8000	0.1600	0.0048	0.0282
	Local model validation	13.6126	0.7417	20.8000	0.1600	0.0048	0.0282
Repeated split sampling	Global Model Mean	20.7012	-5.8767	40.0000	0.4000	0.0080	0.0150
	Global Model Median	20.9912	-5.9631	40.0000	0.4000	0.0080	0.0150
	Global model lower CI	16.4997	-9.3455	-	-	-	-
	Global model upper CI	23.8782	-2.0099	-	-	-	-
	Local Model Mean	17.8550	0.2396	20.8988	0.1600	0.0048	0.0275
	Local Model Median	18.0194	0.2738	20.8000	0.1600	0.0048	0.0277
	Local model lower CI	14.7366	-0.9799	20.8000	0.1600	0.0048	0.0232
	Local model upper CI	20.2766	1.3002	21.6186	0.1600	0.0048	0.0300
	Local Model Mean - validation	18.7280	-0.0133	20.8988	0.1600	0.0048	0.0275
	Local Model Median - validation	18.7737	0.2452	20.8000	0.1600	0.0048	0.0277
	Local model lower CI	11.7677	-11.4828	20.8000	0.1600	0.0048	0.0232
	Local model upper CI	25.7248	8.9161	21.6186	0.1600	0.0048	0.0300
Bootstrapping	Global Model Mean	20.4800	-5.8312	40.0000	0.4000	0.0080	0.0150
	Global Model Median	20.6428	-5.9656	40.0000	0.4000	0.0080	0.0150
	Global model lower CI	14.9401	-11.3979	-	-	-	-
	Global model upper CI	25.4311	0.1292	-	-	-	-
	Local Model Mean	17.5260	0.1290	21.4303	0.1600	0.0049	0.0271
	Local Model Median	17.6062	0.1613	20.8000	0.1600	0.0048	0.0276
	Local model lower CI	13.2472	-1.4172	20.8000	0.1600	0.0048	0.0208
	Local model upper CI	21.3238	1.5613	31.2000	0.1600	0.0071	0.0300

5.3 LOCAL CALIBRATION OF RIGID PAVEMENT MODELS

The rigid pavement performance prediction models were locally calibrated using the typical designs and construction materials specific to Michigan. The transverse cracking, faulting and IRI models were locally calibrated. The local calibration results are discussed below.

5.3.1 Transverse Cracking Model

The globally calibrated transverse cracking model was verified by comparing the predicted and measured cracking. The model adequacy was tested by comparing the standard error of the estimate (SEE) and bias of the global model and by performing the three hypothesis tests mentioned before. The first hypothesis test determines if there was a statistically significant difference between the predicted and measured cracking. The second and third hypothesis tests indicates if the intercept and slope of the linear line between measured and predicted performance is similar to zero and one, respectively. A zero intercept and slope of one indicate that no bias exists between the predicted and measured performance. Similar verification procedures were performed by various SHA's (*3-5*). Figure 5-26 shows the comparison between the measured and predicted transverse cracking using the global cracking model. Based on the results, the global cracking model significantly under-predicts measured cracking. The hypothesis tests revealed that there is a significant difference between the predicted and measured transverse cracking (see Table 5-72). While the intercept of the global model was not significantly different than zero before calibration, the slope of regression line was significantly different than one. Since two of the three hypothesis tests were rejected the transverse cracking model needs calibration.

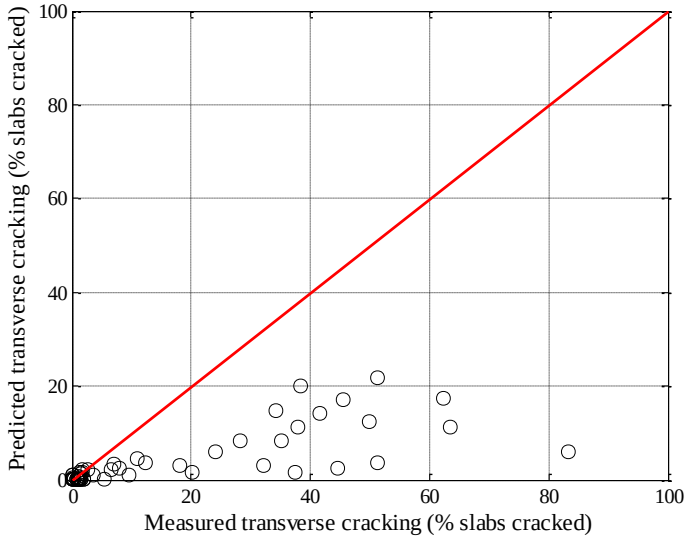

Figure 5-26 Comparison between measured and predicted transverse cracking (global model)

Table 5-72 Global model hypothesis testing results

Hypothesis test	Hypotheses	P-value
Mean difference (paired *t*-test)	H_0 = *(predicted – measured) = 0* H_1 = *(predicted – measured)* $\neq 0$	0.00
Intercept	H_0 = *intercept = 0* H_1 = *intercept* $\neq 0$	0.36
Slope	H_0 = *slope = 1* H_1 = *slope* $\neq 1$	0.00

The local calibration of the transverse cracking model aims to minimize the error between the measured and predicted cracking. The tranverse cracking model was calibrated using all of the selected MDOT JPCP pavement sections. The various resampling techniques outlined in Chapter 4 and presented for flexible pavements above are presented for the cracking model. The emphasis of this demonstration is to outline the differences between various methods and how it affects the calibration coefficient and associated variability when using a limited number of pavement sections for local calibration. The local calibration was performed using different sets of data. These datasets include different sets of pavement sections as given below:

1. Option 1: All newly constructed JPCP pavement sections
2. Option 2: Option 1 and MDOT unbonded overlay pavement sections
3. Option 3: The pavement sections in Option 2 and MDOT unbonded overlay pavement sections and SPS-2 sections in Michigan and Ohio
4. Option 4: MDOT unbonded overlay pavement sections

The results of the local calibration effort for rigid pavements is presented in detail for Option 1 to show the approach. The summary results for the other options are presented in this section while details can be found in Appendix B.

5.3.1.1. Option 1 – MDOT reconstruct only

No Sampling

In this procedure, the transverse cracking model was calibrated using all of the available MDOT JPCP pavement sections. Figure 5-27 shows the comparison between the measured and predicted transverse cracking, and a comparison of the transfer function for the global and locally calibrated models. The SEE, bias, and model coefficients (C_4 and C_5) are summarized in Table 5-73. Based on the results, SEE reduced from 21.10 to 12.30 percent slabs cracked, and the bias reduced from -11.86 to 0.17 percent slabs cracked. The C_4 and C_5 coefficients were changed from 1 and -1.98 to 0.27 and -1.56, respectively.

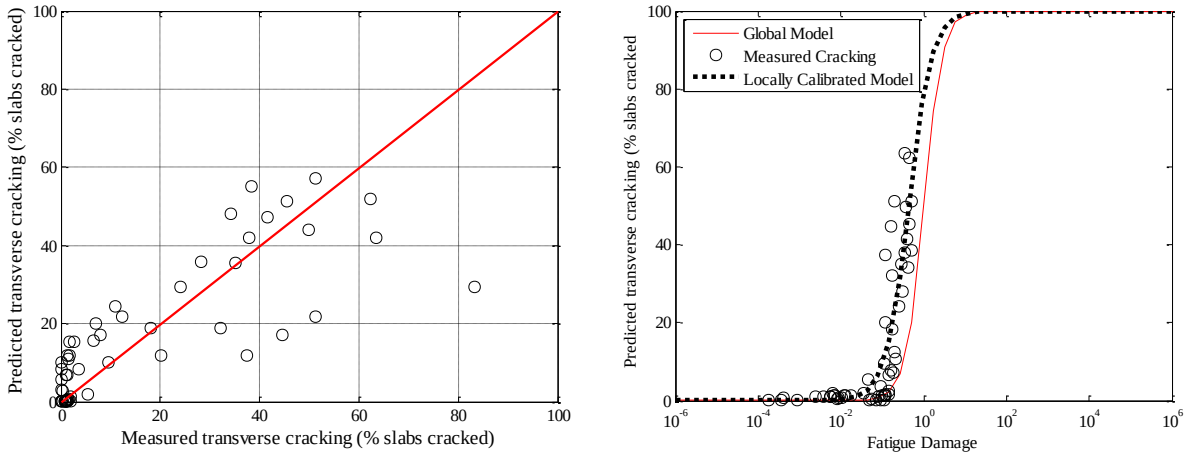

(a) Measured vs. predicted cracking (b) Fatigue damage predicted cracking

Figure 5-27 Local calibration results using entire dataset

Table 5-73 Local calibration results using entire dataset

Parameter	Global model	Local model
SEE (% slabs cracked)	21.10	12.30
Bias (% slabs cracked)	-11.86	0.17
C_4	1.00	0.27
C_5	-1.98	-1.56

Hypothesis testing was performed to determine the adequacy of the calibrated cracking model. Results in Table 5-74 show that there is no significant difference between predicted and measured cracking (i.e. fail to reject the null hypothesis). In addition, the intercept and slope hypothesis tests indicates that these parameters are significantly different from 0 and 1, respectively. Although two of the hypothesis tests were rejected, the overall SEE and bias were reduced significantly for practical purposes.

Table 5-74 No sampling hypothesis test results (p-value)

Hypothesis test	Global model	Local model
Mean difference = 0	0.00	0.92
Intercept = 0	0.36	0.00
Slope = 1	0.00	0.00

Split sampling and repeated split sampling

The split sampling technique was utilized to calibrate the transverse cracking model. Seventy (70%) percent of the pavement sections were used for calibration, and the remaining thirty (30%) percent were used for model validation. The model parameters are summarized in Table 5-75. The comparison between measured and predicted transverse cracking is summarized in Figure 5-28.The results show that the calibrated model SEE reduced from

24.09 to 13.05 percent slabs cracked and the model bias reduced from -14.59 to -0.14 percent slabs cracked when compared with the global model. The C_4 and C_5 coefficients were adjusted to 0.35 and -1.28 as a result of the local calibration. The model validation results show that the SEE is slightly higher and bias is much higher than the calibrated model. Generally, the calibration and validation SEE, and bias should be similar in magnitude when calibrated models are developed based a larger sample size.

Table 5-75 Split sampling calibration results

Parameter	Global model	Local model	Validation
SEE (% slabs cracked)	24.09	13.05	12.24
Bias (% slabs cracked)	-14.59	0.14	8.13
C_4	1.00	0.35	0.35
C_5	-1.98	-1.28	-1.28

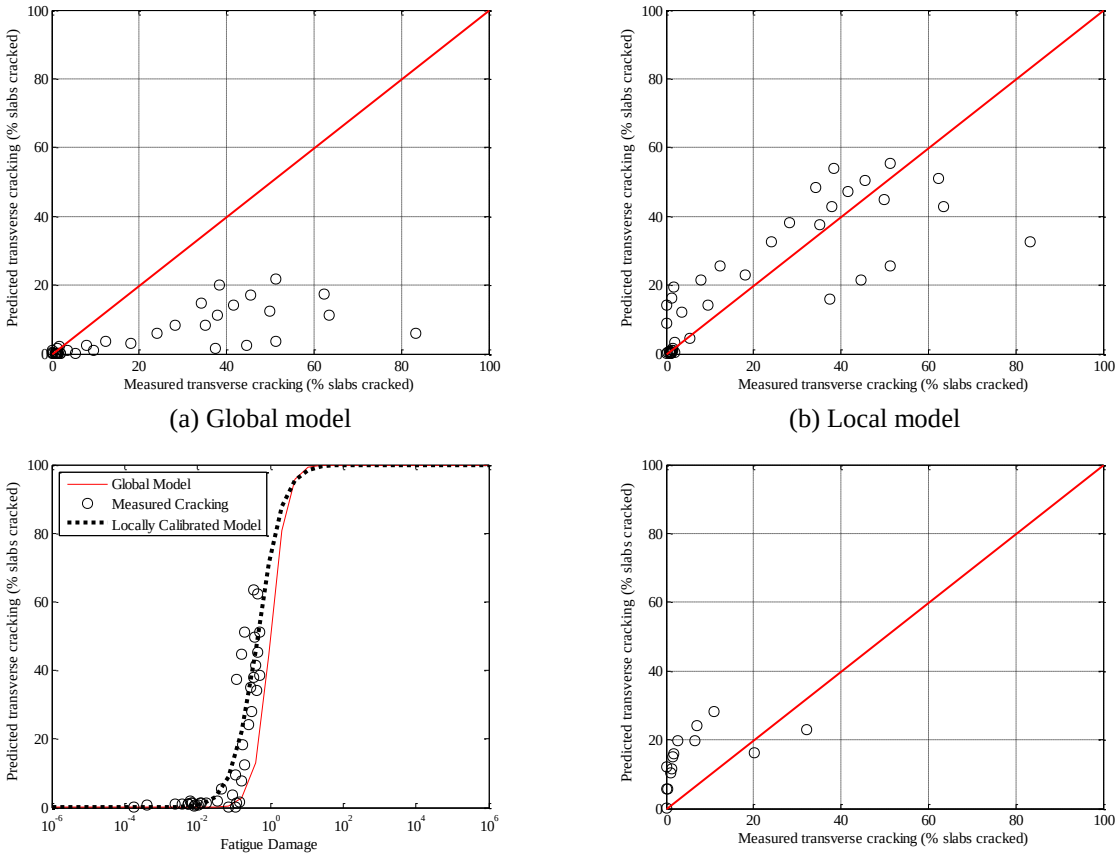

(a) Global model

(b) Local model

(c) Fatigue damage

(d) Validation set

Figure 5-28 Split sampling local calibration results

Table 5-76 shows the results of the hypothesis tests. These results indicate that there is no significant difference between the measured and predicted cracking for the calibrated model and the intercept is not significantly different than zero. The hypothesis test for slope indicates it is significantly different than 1 for the local model and the validation set.

Table 5-76 Split sample hypothesis test results (p-value)

Hypothesis test	Global model	Local model	Validation
Mean difference = 0	0.00	0.94	0.00
Intercept = 0	0.50	0.01	0.00
Slope = 1	0.00	0.00	0.04

The split sampling technique only considers a random selection of 70 percent of the pavement sections. However, if multiple split samples are taken, the SEE, bias, C_4 and C_5 values will vary for each realization. Therefore, the results of a split sample may not indicate an accurate representation of all the sections on average, especially when the sample size is limited. In order to determine a better estimate of the calibration coefficients, SEE and bias, the split sampling technique was performed 1000 times and named repeated split sampling. The results of the local calibration using repeated split sampling are shown in Figure 5-29 while the validation results are shown in Figure 5-30. The frequency distributions for SEE, bias, C_4 and C_5 indicate the variability for each parameter due to repeated split sampling. Average SEE and bias, and 95% confidence intervals based on the results are summarized in Table 5-77 for calibration and Table 5-78 for validation datasets. The validation results showed a slightly higher SEE and less bias than the calibration dataset; however, these values are much lower than for the case of a single split sample, especially for bias.

Table 5-77 Repeated split sampling results for calibration set

Parameter	Local model mean	Local model median	Local model lower CI	Local model upper CI
SEE (percent slabs cracked)	11.92	12.71	7.04	14.33
Bias (percent slabs cracked)	0.15	0.17	-0.37	0.52
C_4	0.26	0.27	0.14	0.36
C_5	-1.63	-1.59	-1.98	-1.31

Table 5-78 Repeated split sampling results for validation set

Parameter	Local model mean	Local model median	Local model lower CI	Local model upper CI
SEE (percent slabs cracked)	14.10	13.02	5.30	26.35
Bias (percent slabs cracked)	0.04	0.06	-13.69	12.30
C_4	0.26	0.27	0.14	0.36
C_5	-1.63	-1.59	-1.98	-1.31

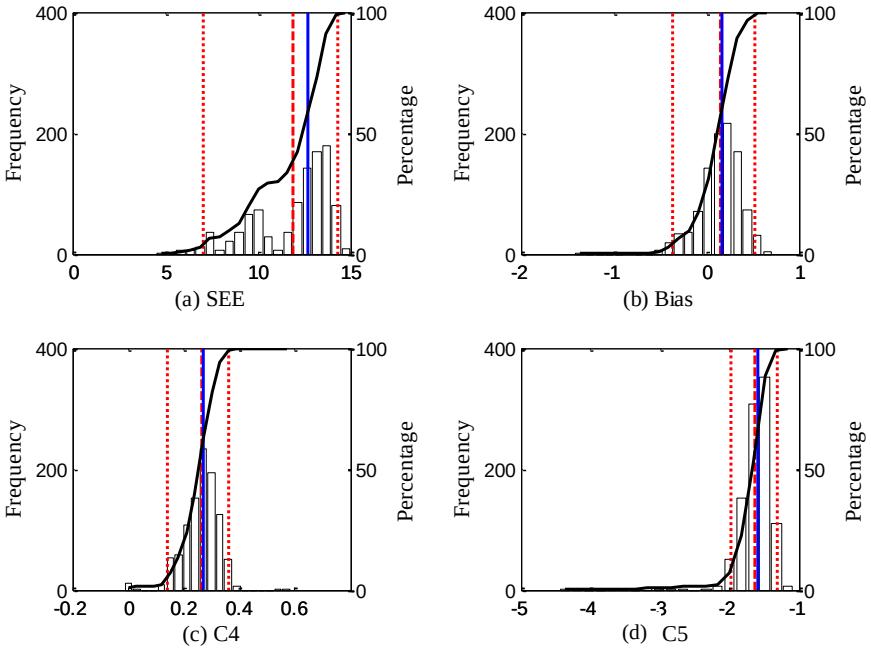

Figure 5-29 Repeated split sampling frequency distributions – calibration set

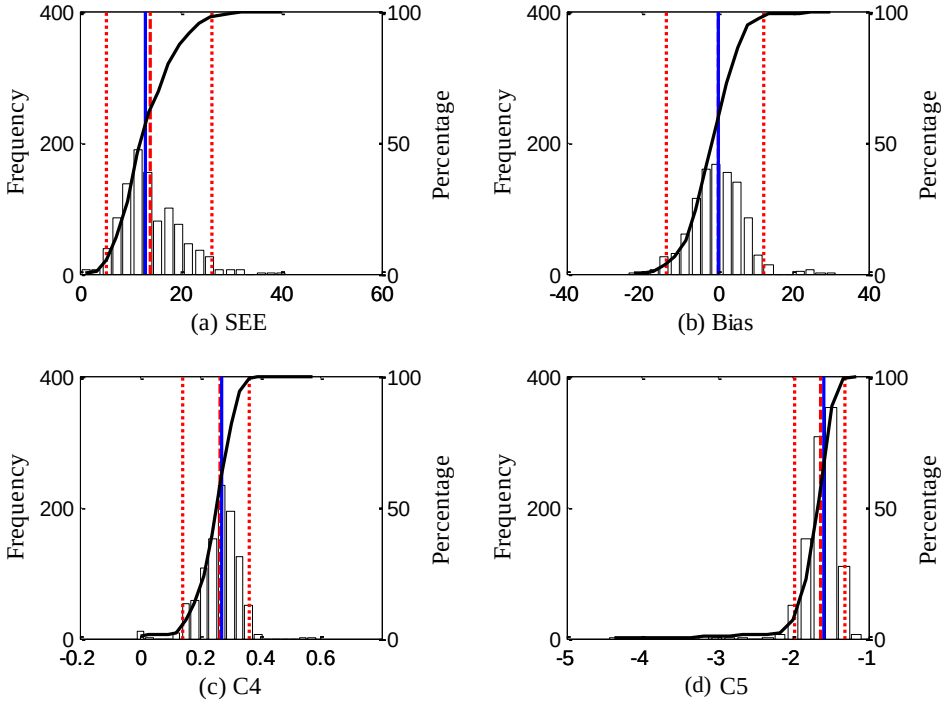

Figure 5-30 Repeated split sampling frequency distributions – validation set

Bootstrapping

Bootstrapping is the final resampling technique considered to recalibrate the transverse cracking model. The difference between split sampling and bootstrapping is that the latter method does not split the original dataset. The bootstrap samples are selected randomly with replacement from the total number of the selected pavement sections. In this method, 1000 bootstrap samples were used to recalibrate the cracking model. Figure 5-31 shows an example of the predicted and measured cracking for the calibration datasets for 1000 bootstrap samples. Figure 5-32 illustrates the parameter distributions for the 1000 bootstrap calibrations. The average values and the 95% confidence intervals for SEE, bias, C_4 and C_5 are summarized in Table 5-79. These results show that the SEE is slightly lower while bias is slightly higher than repeated split sampling calibration.

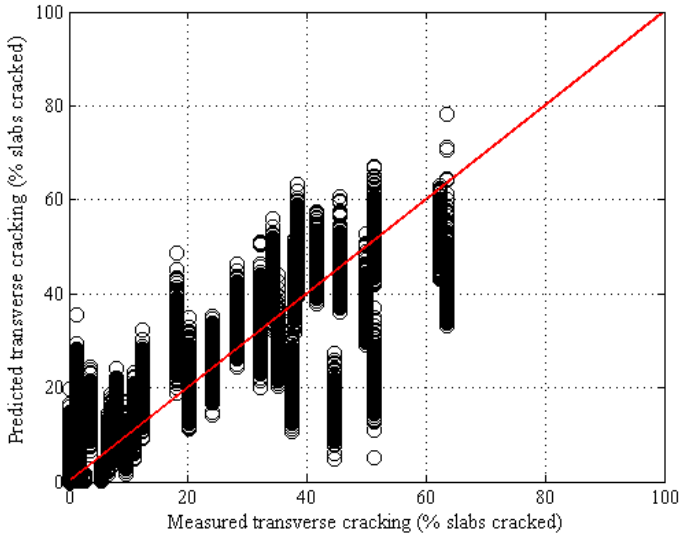

Figure 5-31 Bootstrap sampling measured versus predicted results (1000 bootstraps)

Table 5-79 Bootstrap sampling calibration results summary (1000 bootstraps)

Parameter	Local Model Mean	Local Model Median	Local model lower CI	Local model upper CI
SEE (percent slabs cracked)	11.37	11.65	5.21	16.21
Bias (percent slabs cracked)	0.13	0.15	-0.54	0.68
C4	0.25	0.26	0.02	0.44
C5	-1.71	-1.63	-2.95	-1.21

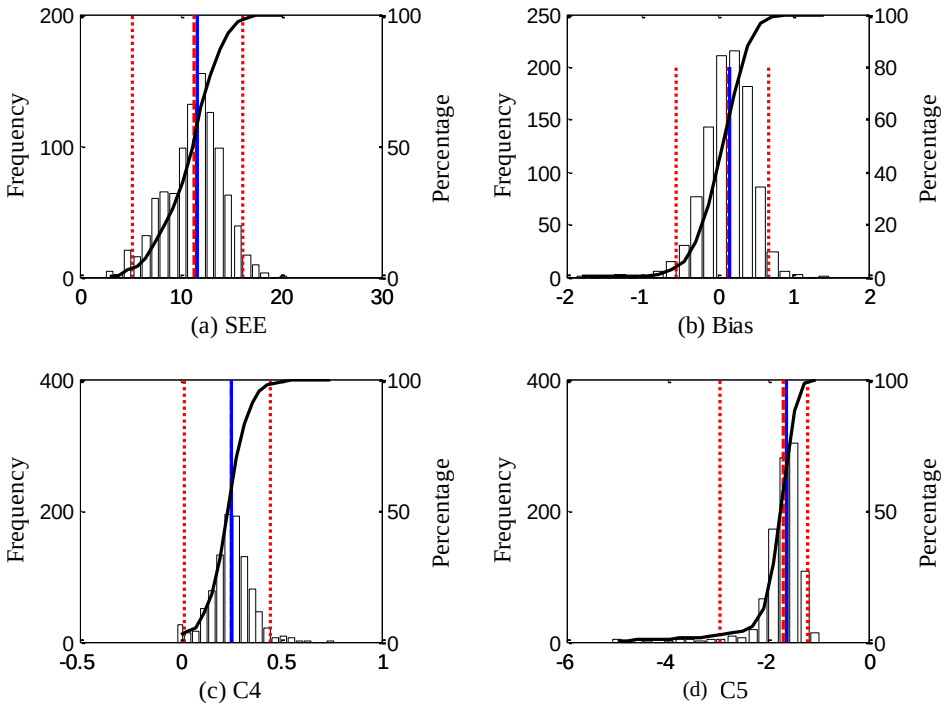

Figure 5-32: Bootstrap sampling calibration results (1000 bootstraps)

Summary

This section summarized the local calibration of the transverse cracking model in the Pavement-ME. The local calibration process includes several sequential steps as described in the Chapter 4. Table 5-80 shows the summary results for the various resampling techniques. The following is a summary of the findings:

- The SEE and bias for the global model is much higher as compared to the locally calibrated model using all the selected pavement sections (i.e., the entire dataset).
- Calibrating with a single split sample also reduced the SEE and bias; however, such a method will be more useful in case of a larger sample size.
- The main advantage of using repeated sampling is to quantify the variability (i.e., confidence interval) associated with the model predictions and parameters. In addition, for a limited data set these techniques will help in reducing the SEE and bias for the calibrated model.
- The quantification of the variability will also help in determining a more robust design reliability in the Pavement-ME.

Table 5-80 Results summary of all sampling technique

Sampling technique	Parameter	SEE	Bias	C4	C5
No Sampling	Global model	21.10	-11.86	1.00	0.27
	Local model	12.30	0.17	-1.98	-1.56
Split sampling	Global model	24.09	-14.59	1.00	-1.98
	Local model calibration	13.05	0.14	0.35	-1.28
	Local model validation	12.24	8.13	0.35	-1.28
Repeated split sampling	Global Model Mean	21.03	-11.83	1.00	-1.98
	Global Model Median	21.03	-11.83	1.00	-1.98
	Global model lower CI	14.59	-15.71	-	-
	Global model upper CI	25.06	-7.48	-	-
	Local Model Mean	11.92	0.15	0.26	-1.63
	Local Model Median	12.71	0.17	0.27	-1.59
	Local model lower CI	7.04	-0.37	0.14	-1.98
	Local model upper CI	14.33	0.52	-1.98	-1.31
	Local Model Mean - validation	14.10	0.04	0.26	-1.63
	Local Model Median - validation	13.02	0.06	0.27	-1.59
	Local model lower CI	5.30	-13.69	0.14	-1.98
	Local model upper CI	26.35	12.30	-1.98	-1.31
Bootstrapping	Global Model Mean	20.62	-11.74	1.00	-1.98
	Global Model Median	20.68	-11.55	1.00	-1.98
	Global model lower CI	12.05	-18.69	-	-
	Global model upper CI	28.91	-5.54	-	-
	Local Model Mean	**11.37**	**0.13**	**0.25**	**-1.71**
	Local Model Median	11.65	0.15	0.26	-1.63
	Local model lower CI	5.21	-0.54	0.02	-2.95
	Local model upper CI	16.21	0.68	-2.95	-1.21

5.3.1.2. Summary of other options

The procedures for the local calibration adopted for Options 2, 3 and 4 are similar to Option 1. Tables 5-81 to 5-83 show the summary results for these options, respectively. The detailed results can be found in the Appendix B. The following is a summary of the findings:

- The SEE and bias for global model is much higher as compared to the locally calibrated model using different datasets.
- The bootstrapping showed the minimum SEE among all sampling techniques among the three options.
- Although SEE for the Option 4 is lowest, there are only eight (8) unbonded overlay projects, with a limited magnitude of cracking. Therefore, such model coefficients are not very reliable.

Table 5-81 Summary of Option 2 local calibration – Transverse cracking model

Sampling technique	Parameter	SEE	Bias	C4	C5
No Sampling	Global model	14.30	-5.83	1.00	-1.98
	Local model	8.43	0.37	0.24	-1.67
Split sampling	Global model	12.18	-4.60	1.00	-1.98
	Local model calibration	6.74	0.06	0.19	-1.81
	Local model validation	11.18	0.84	0.19	-1.81
Repeated split sampling	Global model mean	14.19	-5.83	1.00	-1.98
	Global model median	14.19	-5.83	1.00	-1.98
	Global model lower CI	9.56	-8.11	-	-
	Global model upper CI	17.28	-3.35	-	-
	Local model mean	8.16	0.33	0.23	-1.74
	Local model median	8.76	0.37	0.24	-1.69
	Local model lower CI	4.30	-0.24	0.12	-2.17
	Local model upper CI	10.09	0.70	-2.17	-1.50
	Local model mean - validation	9.22	0.49	0.23	-1.74
	Local model median - validation	8.42	0.59	0.24	-1.69
	Local model lower CI - validation	2.41	-5.98	0.12	-2.17
	Local model upper CI - validation	18.22	7.36	-2.17	-1.50
Bootstrapping	Global Model mean	13.86	-5.79	1.00	-1.98
	Global Model median	13.76	-5.59	1.00	-1.98
	Global model lower CI	7.15	-9.79	-	-
	Global model upper CI	19.80	-2.40	-	-
	Local Model mean	**7.81**	**0.30**	**0.23**	**-1.80**
	Local Model median	7.92	0.31	0.23	-1.71
	Local model lower CI	3.53	-0.45	0.02	-3.03
	Local model upper CI	11.78	0.84	-3.03	-1.43

Table 5-82 Summary of Option 3 local calibration – Transverse cracking model

Sampling technique	Parameter	SEE	Bias	C4	C5
No Sampling	Global model	16.94	-4.46	1.00	-1.98
	Local model	13.79	1.76	2.16	-0.58
Split sampling	Global model	18.92	-4.36	1.00	-1.98
	Local model calibration	14.96	2.44	2.56	-0.48
	Local model validation	11.13	2.60	2.56	-0.48
Repeated split sampling	Global Model Mean	16.98	-4.44	1.00	-1.98
	Global Model Median	16.98	-4.44	1.00	-1.98
	Global model lower CI	12.69	-7.56	-	-
	Global model upper CI	19.95	-1.76	-	-
	Local Model Mean	13.62	1.70	2.15	-0.61
	Local Model Median	13.78	1.78	2.23	-0.56
	Local model lower CI	10.25	0.43	0.81	-1.01
	Local model upper CI	15.91	2.63	-1.01	-0.45
	Local Model Mean - validation	14.95	2.03	2.15	-0.61
	Local Model Median - validation	14.50	2.16	2.23	-0.56
	Local model lower CI - validation	9.69	-6.38	0.81	-1.01
	Local model upper CI - validation	21.89	9.29	-1.01	-0.45
Bootstrapping	Global Model Mean	16.77	-4.45	1.00	-1.98
	Global Model Median	16.86	-4.52	1.00	-1.98
	Global model lower CI	11.19	-8.86	-	-
	Global model upper CI	22.09	0.03	-	-
	Local Model Mean	**13.24**	**1.65**	**2.14**	**-0.64**
	Local Model Median	13.42	1.67	2.16	-0.59
	Local model lower CI	8.56	-0.26	0.50	-1.25
	Local model upper CI	17.11	3.41	-1.25	-0.37

Table 5-83 Summary of Option 4 local calibration – Transverse cracking model

Sampling Technique	Parameter	SEE	Bias	C4	C5
No Sampling	Global model	0.92	-0.55	1.00	-1.98
	Local model	0.72	-0.04	5.00	-1.00
Split sampling	Global model	0.80	-0.48	1.00	-1.98
	Local model calibration	0.63	-0.05	5.00	-1.04
	Local model validation	0.95	-0.29	5.00	-1.04
Repeated split sampling	Global Model Mean	0.91	-0.55	1.00	-1.98
	Global Model Median	0.91	-0.55	1.00	-1.98
	Global model lower CI	0.57	-0.73	-	-
	Global model upper CI	1.10	-0.31	-	-
	Local Model Mean	0.70	-0.04	5.00	-1.00
	Local Model Median	0.74	-0.04	5.00	-0.99
	Local model lower CI	0.43	-0.07	5.00	-1.13
	Local model upper CI	0.83	0.00	-1.13	-0.90
	Local Model Mean - validation	0.78	-0.02	5.00	-1.00
	Local Model Median - validation	0.76	-0.01	5.00	-0.99
	Local model lower CI - validation	0.38	-0.78	5.00	-1.13
	Local model upper CI - validation	1.24	0.66	-1.13	-0.90
Bootstrapping	Global Model Mean	0.88	-0.54	1.00	-1.98
	Global Model Median	0.89	-0.54	1.00	-1.98
	Global model lower CI	0.44	-0.87	-	-
	Global model upper CI	1.26	-0.25	-	-
	Local Model Mean	**0.67**	**-0.04**	**4.96**	**-1.01**
	Local Model Median	0.69	-0.04	5.00	-1.00
	Local model lower CI	0.35	-0.09	4.63	-1.20
	Local model upper CI	0.90	0.01	-1.20	-0.86

5.3.1.3. Reliability for the transverse cracking model

The standard error of the calibrated cracking models were used to establish the relationship between the standard deviation of the measured cracking and mean predicted cracking as explained in Chapter 4. These relationships are used to calculate the cracking for a specific reliability. Tables 5-84 to 5-87 summarize these relations for the options considered for the cracking model. The details for the other options can be found in Appendix B.

Table 5-84 Transverse cracking reliability – Option 1

Sampling technique	Global model equation	Local model equation
No Sampling	$s_{e(CRK)} = 5.3116(CRK)^{0.3903} + 2.99$	$s_{e(CRK)} = 1.4355(CRK)^{0.7612}$
Split Sampling		$s_{e(CRK)} = 1.2486(CRK)^{0.8515}$
Repeated split sampling		$s_{e(CRK)} = 1.6722(CRK)^{0.6927}$
Bootstrapping		$s_{e(CRK)} = 1.8631(CRK)^{0.6467}$

Table 5-85 Transverse cracking reliability – Option 2

Sampling technique	Global model equation	Local model equation
No Sampling	$s_{e(CRK)} = 5.3116(CRK)^{0.3903} + 2.99$	$s_{e(CRK)} = 0.8271(CRK)^{0.8191}$
Split Sampling		$s_{e(CRK)} = 0.7493(CRK)^{0.92}$
Repeated split sampling		$s_{e(CRK)} = 1.2571(CRK)^{0.6745}$
Bootstrapping		$s_{e(CRK)} = 1.34(CRK)^{0.6593}$

Table 5-86 Transverse cracking reliability – Option 3

Sampling technique	Global model equation	Local model equation
No Sampling	$s_{e(CRK)} = 5.3116(CRK)^{0.3903} + 2.99$	$s_{e(CRK)} = 3.2396(CRK)^{0.5495}$
Split Sampling		$s_{e(CRK)} = 2.8915(CRK)^{0.5425}$
Repeated split sampling		$s_{e(CRK)} = 5.1702(CRK)^{0.3036}$
Bootstrapping		$s_{e(CRK)} = 5.6178(CRK)^{0.2763}$

Table 5-87 Transverse cracking reliability – Option 4

Sampling technique	Global model equation	Local model equation
No Sampling	$s_{e(CRK)} = 5.3116(CRK)^{0.3903} + 2.99$	$s_{e(CRK)} = 0.7639(CRK)^{0.724}$
Split Sampling		$s_{e(CRK)} = 0.828(CRK)^{0.7029}$
Repeated split sampling		$s_{e(CRK)} = 0.803(CRK)^{0.4802}$
Bootstrapping		$s_{e(CRK)} = 0.6819(CRK)^{0.2867}$

5.3.2 Faulting Model

The local calibration of the faulting model was performed by changing the C_1 coefficient as explained in Chapter 4. The results for local calibration for the faulting model are shown in Table 5-88. It can be seen that C_1=0.4 gives the lowest SEE and bias for all but the Option 4. A C_1 value of 0.85 for Option 4 gives the lowest SEE and bias. This option is not recommended due to the limited number of unbonded overlay pavement sections and low magnitude of measured faulting.

Table 5-88 Summary of Option 1 local calibration – Faulting model

Parameter	Option 1		Option 2		Option 3		Option 4	
	SEE	Bias	SEE	Bias	SEE	Bias	SEE	Bias
Global model	0.059	0.035	0.051	0.026	0.049	0.023	0.005	-0.002
$C_1 = 0.4$	0.024	0.007	0.021	0.004	0.022	0.002	0.005	-0.003
$C_1 = 0.5$	0.029	0.011	0.025	0.008	0.025	0.005	0.005	-0.002
$C_1 = 0.6$	0.034	0.015	0.029	0.011	0.029	0.008	0.005	-0.002
$C_1 = 0.65$	0.036	0.017	0.032	0.013	0.031	0.010	0.005	-0.002
$C_1 = 0.7$	0.039	0.020	0.034	0.015	0.033	0.012	0.005	-0.002
$C_1 = 0.75$	0.042	0.022	0.037	0.016	0.035	0.014	0.005	-0.002
$C_1 = 0.8$	0.045	0.025	0.039	0.018	0.038	0.015	0.004	-0.002
$C_1 = 0.85$	0.048	0.027	0.042	0.020	0.040	0.017	0.004	-0.001
$C_1 = 0.9$	0.045	0.025	0.039	0.018	0.038	0.015	0.004	-0.002

5.3.2.1. Reliability for faulting model

The standard errors of the calibrated faulting models were used to establish the relationship between the standard deviation of the measured faulting and mean predicted faulting as explained in Chapter 4. These relationships are used to calculate faulting for a specific reliability. Table 5-89 summarizes these relations for the options considered for the faulting model. It should be noted that the changes in the faulting model reliability are not correctly accounted in the predictions; therefore, the global model reliability standard error is recommended until this issue is resolved in a future software update.

Table 5-89 Faulting model reliability

Data option	Global model equation	Local model equation
Option 1	$s_{e(Fault)} = 0.0097(Fault)^{0.5178} + 0.014$	$s_{e(Fault)} = 0.042(Fault)^{0.25}$
Option 2		$s_{e(Fault)} = 0.0442(Fault)^{0.2698}$
Option 3		$s_{e(Fault)} = 0.0335(Fault)^{0.1754}$
Option 4		$s_{e(Fault)} = 0.0253(Fault)^{0.2378}$

5.3.3 Rigid Pavement Roughness (IRI) Model

The IRI model was calibrated after the local calibration of the transverse cracking, and faulting models were completed. These distresses are considered directly in the IRI model along with the site factor and spalling predictions. All the Options were considered for the local calibration of the rigid pavement IRI model. Figure 5-33 shows the predicted and measured IRI for the global model for JPCP sections. It can be seen that the global IRI model coefficient with locally calibrated distresses predicts the measured IRI reasonably. Figures 5-34 and 5-35 show the similar plots for the local calibrated models using no sampling and split sampling techniques, respectively for Option 1. The figures show that the local calibration improves the IRI predictions for JPCP sections.

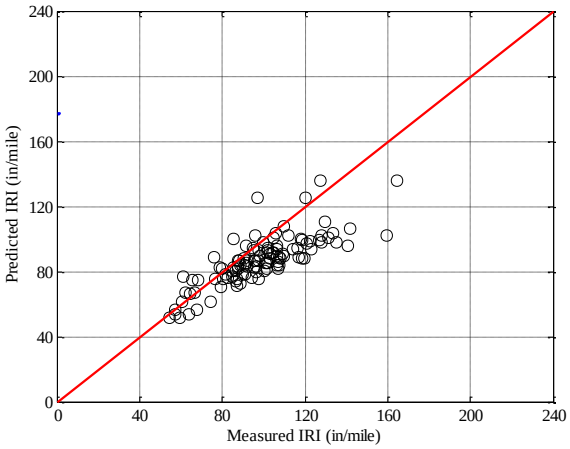

Figure 5-33 Global IRI model measured versus predicted IRI

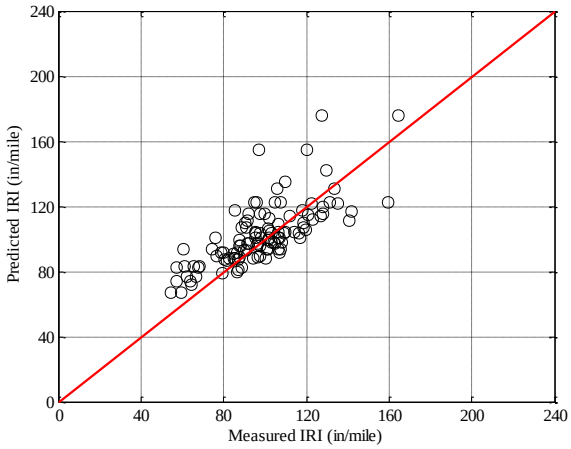

Figure 5-34 IRI local calibration measured versus predicted – no sampling

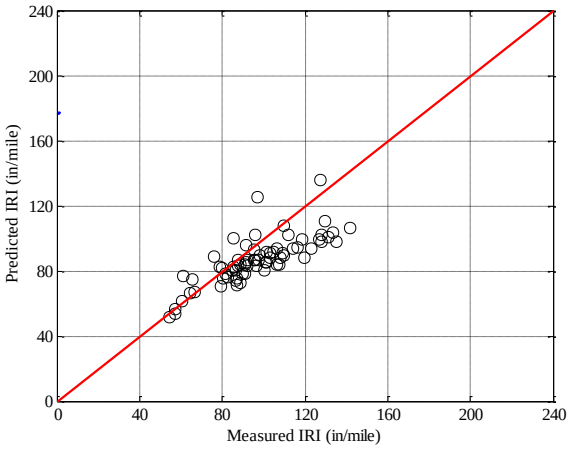

(a) Global model

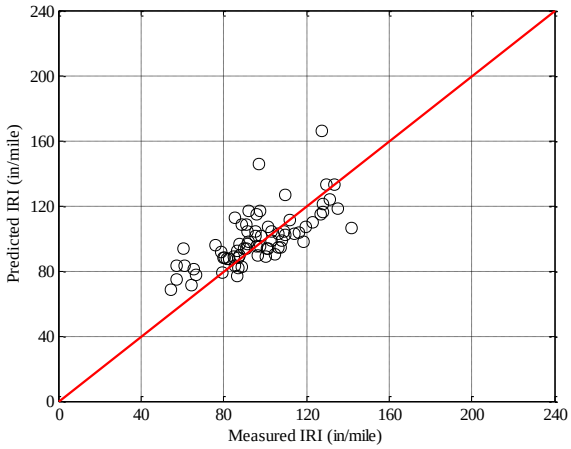

(b) Local model

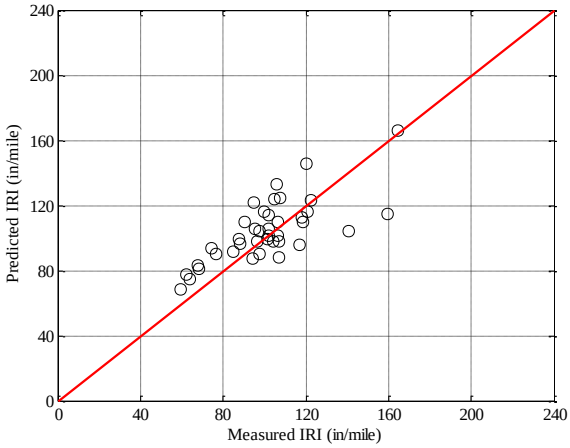

(c) Local model validation

Figure 5-35 Option 1 IRI local calibration measured versus predicted – split sampling

Tables 5-90 through 5-93 show the summary results for the Options 1 to 4, respectively. The details of the local calibration are included in Appendix B. The following observations can be made from these results:

- The locally calibrated models using the reconstructed pavements (Option 1) and reconstruct and rehabilitated pavement (Option 2) show similar SEE and bias.
- The locally calibrated model using only the rehabilitated pavements (Option 4) show the similar SEE to the Options 1 and 2.
- The bootstrapping resampling technique gives the lowest SEE for all data subsets (options) considered in the analysis.

Table 5-90 Summary of Option 1 local calibration – Rigid IRI model

Sampling technique	Parameter	SEE	Bias	C1	C2	C3	C4
No sampling	Global model	17.314	-11.398	0.820	0.442	1.493	25.240
	Local model	15.564	4.215	0.586	11.833	1.493	25.240
Split sampling	Global model	16.263	-10.020	0.820	0.442	1.493	25.240
	Local model	14.999	3.070	0.342	12.599	1.493	25.240
	Validation	16.341	3.401	0.342	12.599	1.493	25.240
Repeated split sampling	Global model	17.330	-11.410	0.820	0.442	1.492	25.240
	Local model mean	15.263	4.314	0.603	11.840	1.493	25.240
	Local model median	15.406	4.341	0.604	11.721	1.493	25.240
	Local model lower CI	12.163	2.710	0.161	9.757	1.493	25.240
	Local model upper CI	17.195	5.766	1.051	14.422	1.493	25.240
Bootstrapping	Global model	17.239	-11.466	0.820	0.442	1.492	25.240
	Local model mean	14.899	4.417	0.584	12.068	1.493	25.240
	Local model median	14.833	4.395	0.590	12.023	1.493	25.240
	Local model lower CI	11.651	2.673	0.035	8.754	1.493	25.240
	Local model upper CI	18.350	6.422	1.159	15.396	1.493	25.240

Table 5-91 Summary of Option 2 local calibration – Rigid IRI model

Sampling technique	Parameter	SEE	Bias	C1	C2	C3	C4
No sampling	Global model	15.474	-10.026	0.820	0.442	1.493	25.240
	Local model	13.792	-0.498	1.182	3.465	1.493	25.240
Split sampling	Global model	16.433	-10.745	0.820	0.442	1.493	25.240
	Local model	14.847	-1.109	1.301	3.202	1.493	25.240
	Validation	12.641	1.212	1.301	3.202	1.493	25.240
Repeated split sampling	Global model	15.508	-10.038	0.820	0.442	1.492	25.240
	Local model mean	13.648	-0.415	1.192	3.512	1.493	25.240
	Local model median	13.714	-0.399	1.175	3.467	1.493	25.240
	Local model lower CI	11.501	-1.543	0.920	2.701	1.493	25.240
	Local model upper CI	15.181	0.704	1.604	4.610	1.493	25.240
Bootstrapping	Global model	15.390	-10.024	0.820	0.442	1.492	25.240
	Local model mean	13.424	-0.382	1.198	3.570	1.493	25.240
	Local model median	13.451	-0.407	1.171	3.517	1.493	25.240
	Local model lower CI	10.963	-2.056	0.829	2.323	1.493	25.240
	Local model upper CI	15.932	1.423	1.686	5.234	1.493	25.240

Table 5-92 Summary of Option 3 local calibration – Rigid IRI model

Sampling technique	Parameter	SEE	Bias	C1	C2	C3	C4
No sampling	Global model	23.056	-9.862	0.820	0.442	1.493	25.240
	Local model	21.471	0.770	1.781	2.028	1.493	25.240
Split sampling	Global model	24.611	-8.805	0.820	0.442	1.493	25.240
	Local model	23.889	0.365	1.562	1.760	1.493	25.240
	Validation	14.764	-4.996	1.562	1.760	1.493	25.240
Repeated split sampling	Global model	22.844	-9.897	0.820	0.442	1.492	25.240
	Local model mean	21.096	0.863	1.834	1.993	1.493	25.240
	Local model median	23.226	0.912	1.709	2.027	1.493	25.240
	Local model lower CI	13.031	-0.883	1.354	0.292	1.493	25.240
	Local model upper CI	24.773	2.445	2.611	3.670	1.493	25.240
Bootstrapping	Global model	21.999	-9.799	0.820	0.442	1.492	25.240
	Local model mean	20.099	0.996	1.855	1.980	1.493	25.240
	Local model median	20.566	0.939	1.799	1.965	1.493	25.240
	Local model lower CI	12.371	-1.343	1.096	0.000	1.493	25.240
	Local model upper CI	31.016	3.343	2.785	4.327	1.493	25.240

Table 5-93 Summary of Option 4 local calibration – Rigid IRI model

Sampling technique	Parameter	SEE	Bias	C1	C2	C3	C4
No sampling	Global model	11.339	-7.555	0.820	0.442	1.493	25.240
	Local model	7.949	0.268	0.001	2.541	1.493	25.240
Split sampling	Global model	10.872	-7.494	0.820	0.442	1.493	25.240
	Local model	7.128	0.302	0.001	2.601	1.493	25.240
	Validation	10.483	1.055	0.001	2.601	1.493	25.240
Repeated split sampling	Global model	11.395	-7.575	0.820	0.442	1.492	25.240
	Local model mean	7.901	0.280	0.001	2.554	1.493	25.240
	Local model median	7.984	0.265	0.000	2.551	1.493	25.240
	Local model lower CI	6.419	-0.085	0.000	2.003	1.493	25.240
	Local model upper CI	8.931	0.686	0.000	3.164	1.493	25.240
Bootstrapping	Global model	11.179	-7.539	0.820	0.442	1.492	25.240
	Local model mean	7.602	0.295	0.041	2.540	1.493	25.240
	Local model median	7.613	0.281	0.000	2.559	1.493	25.240
	Local model lower CI	5.470	-0.250	0.000	1.577	1.493	25.240
	Local model upper CI	9.510	0.881	0.000	3.513	1.493	25.240

5.4 VALIDATION OF LOCAL CALIBRATED MODELS

The local calibration of the performance models presented above should be able to predict pavement performance for the projects which were not part of the calibration. This process is necessary to validate the robustness, accuracy and adequacy of the model predictions. As mentioned above, the local calibration of the performance models were performed for different subsets of the selected pavement sections and with multiple statistical techniques. The above results indicate that the local models calibrated using bootstrapping consistently showed the lowest SEE and bias for the different dataset options. While local calibration for all the performance models were performed initially using the complete dataset within each option, the model coefficients still needed validation with pavement sections not included in the calibration. Therefore, considering the robustness and efficiency of bootstrapping, the original dataset, for each option, was divided into two subsets. While 80% of the pavement sections were used to calibrate the models, 20% were later utilized for validation. It should be noted that bootstrap validation was only performed for the following models:

Flexible pavements

- Fatigue cracking (bottom-up)
- Fatigue cracking (top-down)
- Rutting
- Thermal cracking
- IRI

Rigid Pavements

- Transverse cracking
- Faulting
- IRI

The thermal cracking and faulting models require rerunning of the Pavement-ME software every time the local coefficients are modified. Therefore, only the no sampling technique was utilized for the local calibration of those models and no repeated resampling validation can be performed for independent pavement sections. The model validation results using the bootstrap split sampling are presented next by pavement type.

5.4.1 Flexible Pavements

Tables 5-94 and 5-95 show a comparison of the alligator and longitudinal cracking model statistics between the global and local models along with the validation of the locally calibrated model. The results indicate that the validation and local model SEE and bias are similar. This shows that the locally calibrated alligator cracking model accurately predicts the cracking for pavement sections not included in the local calibrations dataset. The longitudinal cracking validation results indicate that the locally calibrated model can accurately predict longitudinal cracking for pavement sections not included in the calibration when comparing Option 1. Option 2 and 4 did not yield similar results. Figure 5-36 and 5-37 shows the

goodness-of-fit for the local model validation for both alligator and longitudinal cracking and verifies the model coefficients.

Table 5-94 Flexible pavement alligator cracking model validation

Parameter	Global model	Local model	Local model validation
SEE	7.447	6.269	6.946
Bias	-4.282	-0.716	-1.952

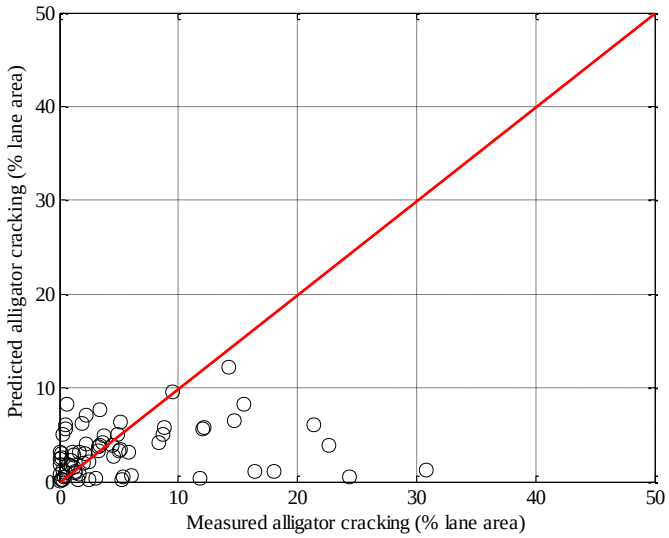

Figure 5-36 Measured versus predicted — Alligator cracking model validation (Flexible)

Table 5-95 Flexible pavement longitudinal cracking model validation

Options	SEE			Bias		
	Global Model	Local model	Validation	Global Model	Local model	Validation
1	817.4715	696.8328	631.5130	-466.8421	-136.9143	-21.3558
2	729.1168	627.0209	892.3061	-405.5257	-111.3998	-439.1413
4	1549.0513	1177.1581	629.3458	-1086.5433	-226.3333	201.7576

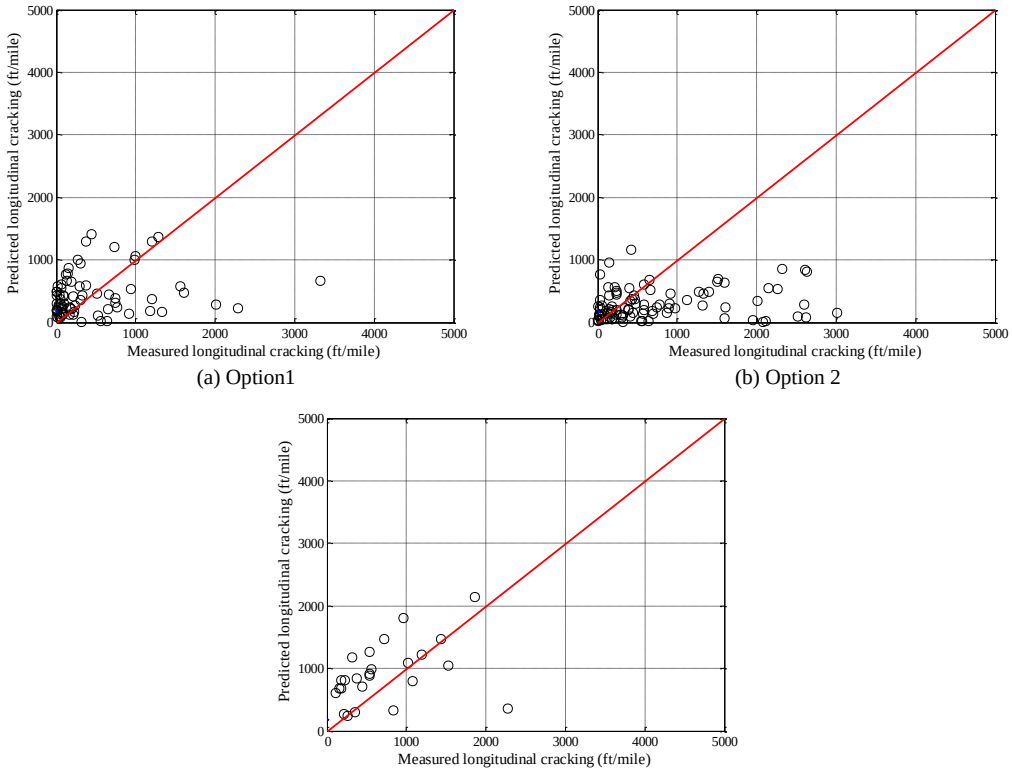

(a) Option1

(b) Option 2

(c) Option 4

Figure 5-37 Measured versus predicted — Longitudinal cracking model validation (Flexible)

Table 5-96 shows a comparison of the rutting model statistics between the global and local models along with the validation of the locally calibrated model. The validation was performed within each dataset considered for the rutting model. The results indicate that the validation and local model SEE and bias are similar. This shows that the locally calibrated rutting model accurately predicts total rutting for pavement sections not included in the local calibration dataset. Figure 5-38 shows the goodness-of-fit for the local model validation and verifies the model coefficients. Tables 5-97 and 5-98 summarize the calibration and validation results for the levels 1 and 3 thermal cracking model. The validation was performed using a single split sample to compare the SEE and bias. Figures 5-39 and 5-40 show the comparison between the measured and predicted thermal cracking model validation. It should be noted that bootstrap validation of the thermal cracking model cannot be performed because of the limitations discussed in Chapter 4. Similarly, Table 5-99 shows the validation results for the locally calibrated IRI model. The results indicate that the validation and local model SEE and bias are practically similar. This shows that the locally calibrated IRI model accurately predicts IRI for pavement sections not included in the local calibration dataset. Figure 5-41 shows the goodness-of-fit for the local IRI model validation and verifies the model coefficients.

Table 5-96 Flexible pavement rutting model validation

Options	SEE (inch)			Bias (inch)		
	Global Model	Local model	Validation	Global Model	Local model	Validation
1	0.3369	0.0849	0.1102	0.3139	-0.0111	-0.0155
2	0.3567	0.0858	0.0853	0.3180	-0.0151	-0.0306
4	0.3666	0.0865	0.1072	0.2833	-0.0224	-0.0546

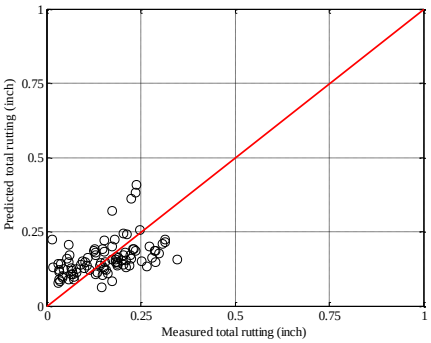

(a) Option1

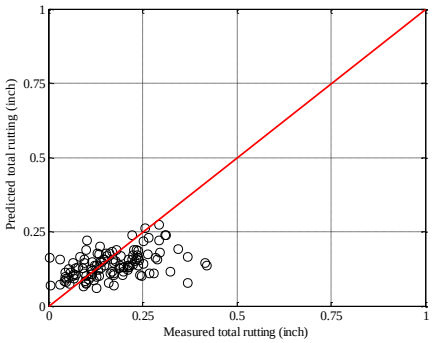

(b) Option 2

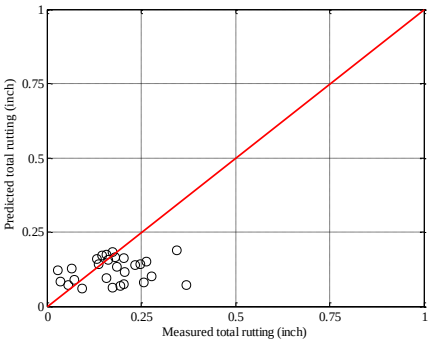

(c) Option 4

Figure 5-38 Measured versus predicted — Rutting model validation (Flexible)

Table 5-97 Flexible pavement thermal cracking model validation – Level 1

Options	SEE (ft/mile)			Bias (ft/mile)		
	Global Model	Local model	Validation	Global Model	Local model	Validation
1	1319.34	786.42	685.73	873.37	-67.01	-78.10
2	1314.89	737.18	733.34	-861.89	-127.76	46.93

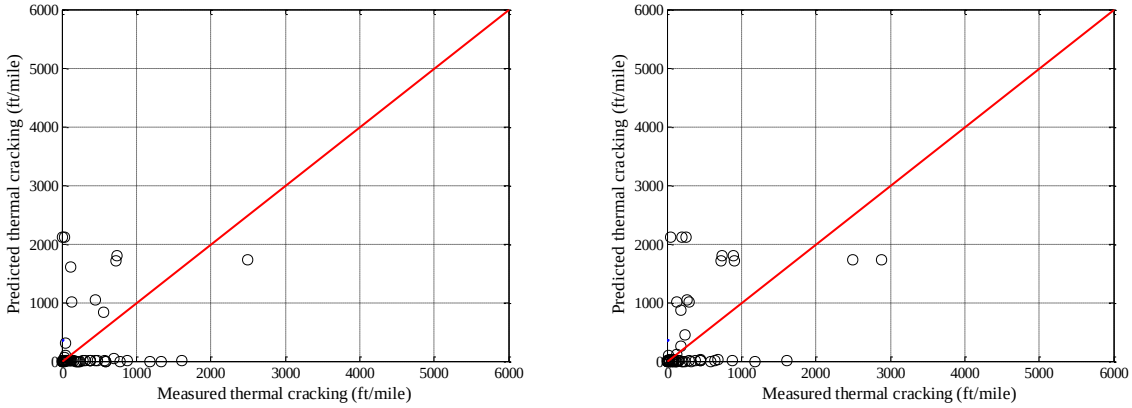

(a) Option 1 (b) Option 2

Figure 5-39 Measured versus predicted — Thermal cracking model validation (Flexible)

Table 5-98 Flexible pavement thermal cracking model validation – Level 3

Options	SEE (ft/mile)			Bias (ft/mile)		
	Global Model	Local model	Validation	Global Model	Local model	Validation
1	823.51	867.22	837.49	-349.97	-23.21	63.54
2	1009.53	1029.43	1122.42	-537.31	-61.91	245.33
4	1322.81	1263.64	933.05	-930.48	-125.38	-400.12

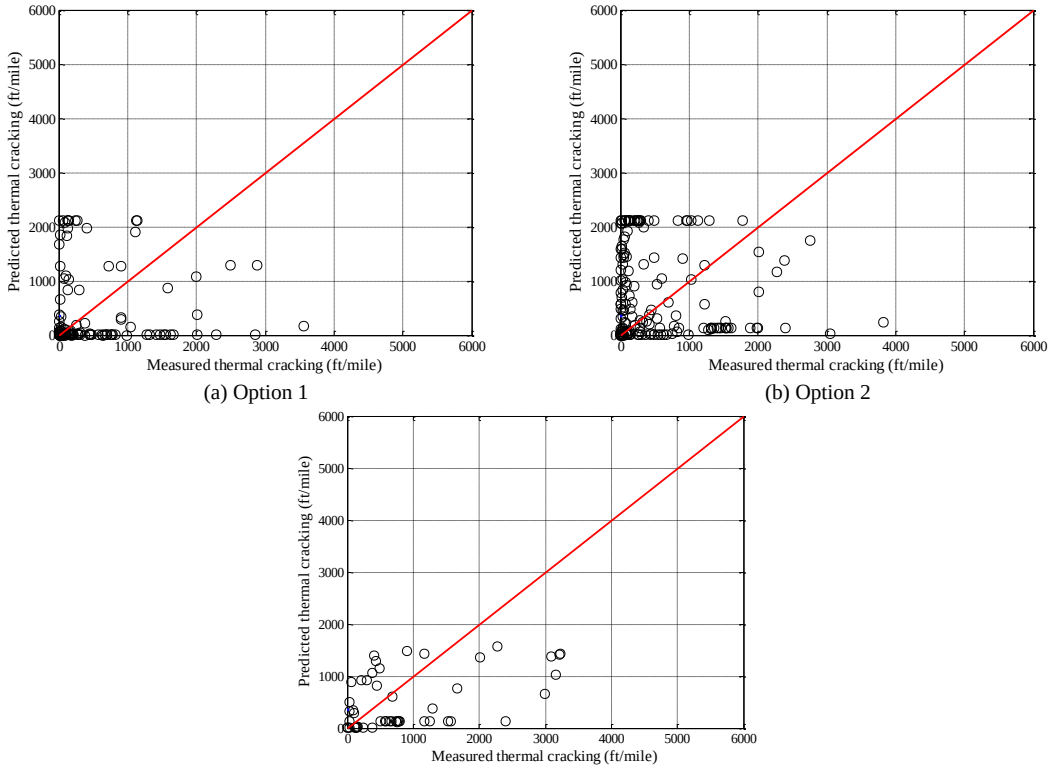

(a) Option 1 (b) Option 2

(c) Option 4

Figure 5-40 Measured versus predicted — Level 3 thermal cracking model validation (Flexible)

Table 5-99 Flexible pavement IRI model validation

Options	SEE			Bias		
	Global Model	Local model	Validation	Global Model	Local model	Validation
1	15.2543	15.1863	10.9135	0.6137	-0.7226	1.0022
2	15.2846	14.9275	18.2064	0.8357	-0.4715	0.0887
4	22.6132	17.5204	14.0299	-9.4328	-0.4048	-1.8670

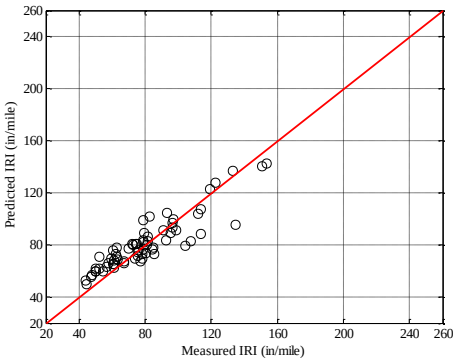

(a) Option1

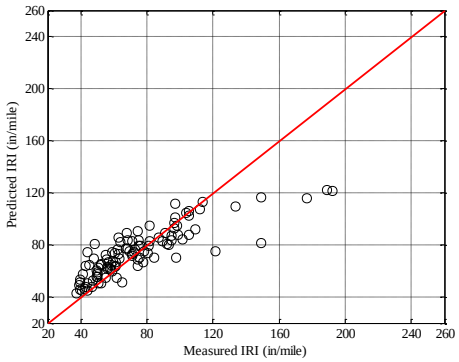

(b) Option 2

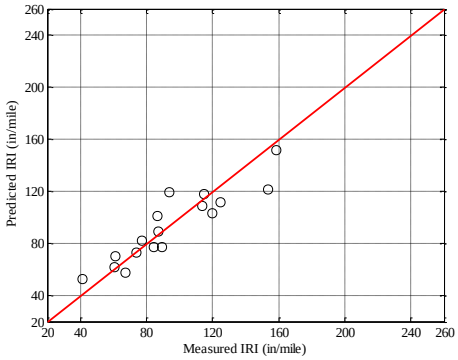

(c) Option 4

Figure 5-41 Measured versus predicted — IRI model validation (Flexible)

5.4.2 Rigid Pavements

Table 5-100 shows the comparison of cracking model statistics between the global and local models along with the validation of the locally calibrated model for rigid pavement. The validation was performed within each dataset considered for the cracking model. The results indicate that the validation and local model SEE and bias are not similar. This is mainly because of the smaller sample size and low extent of cracking within some options. However, the locally calibrated cracking model is much better than the global model. Figure 5-42 shows the goodness-of-fit for the local model validation and verifies the model coefficients.

Table 5-100 Rigid pavement transverse cracking model validation

Options	SEE			Bias		
	Global Model	Local model	Validation	Global Model	Local model	Validation
1	22.8853	12.6026	22.4378	-13.9244	0.3197	-8.9434
2	16.0455	8.9093	12.2402	-7.5017	0.2667	-4.2322
3	14.0377	7.8001	13.7216	-5.9053	0.2924	-2.8180
4	0.9947	0.7029	0.5744	-0.6707	-0.0251	0.0776

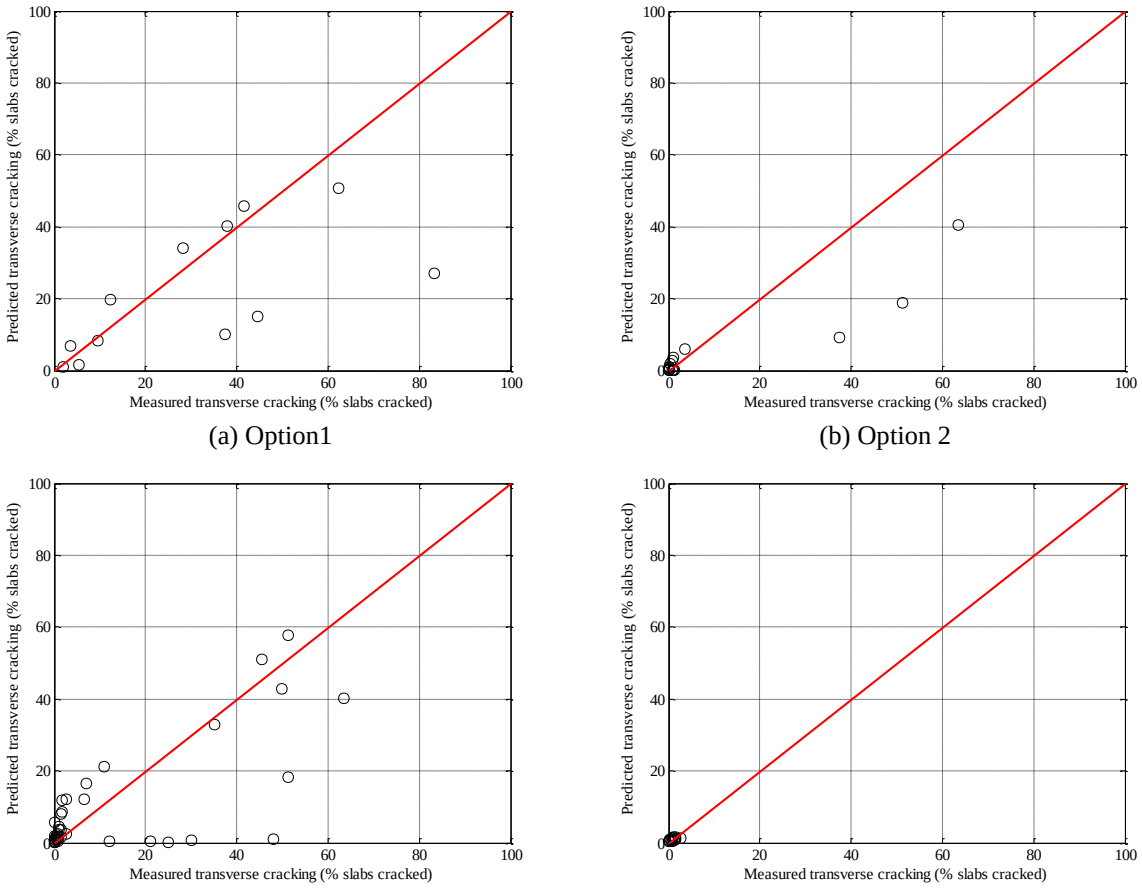

(a) Option1 (b) Option 2

(c) Option 3 (d) Option 4

Figure 5-42 Measured versus predicted — Transverse cracking model validation (Rigid)

Table 5-101 summarizes the validation results for the faulting model. The results show that the model can accurately predict faulting for pavement sections that were not included in the calibration. Figure 5-43 shows the validation results for all the options.

Table 5-101 Rigid pavement faulting model validation

Options	SEE (inch)			Bias (inch)		
	Global Model	Local model	Validation	Global Model	Local model	Validation
1	0.059	0.023	0.029	0.039	0.008	0.007
2	0.058	0.024	0.015	0.033	0.008	-0.001
3	0.055	0.024	0.019	0.029	0.005	0.000
4	0.057	0.047	0.028	0.031	0.024	0.012

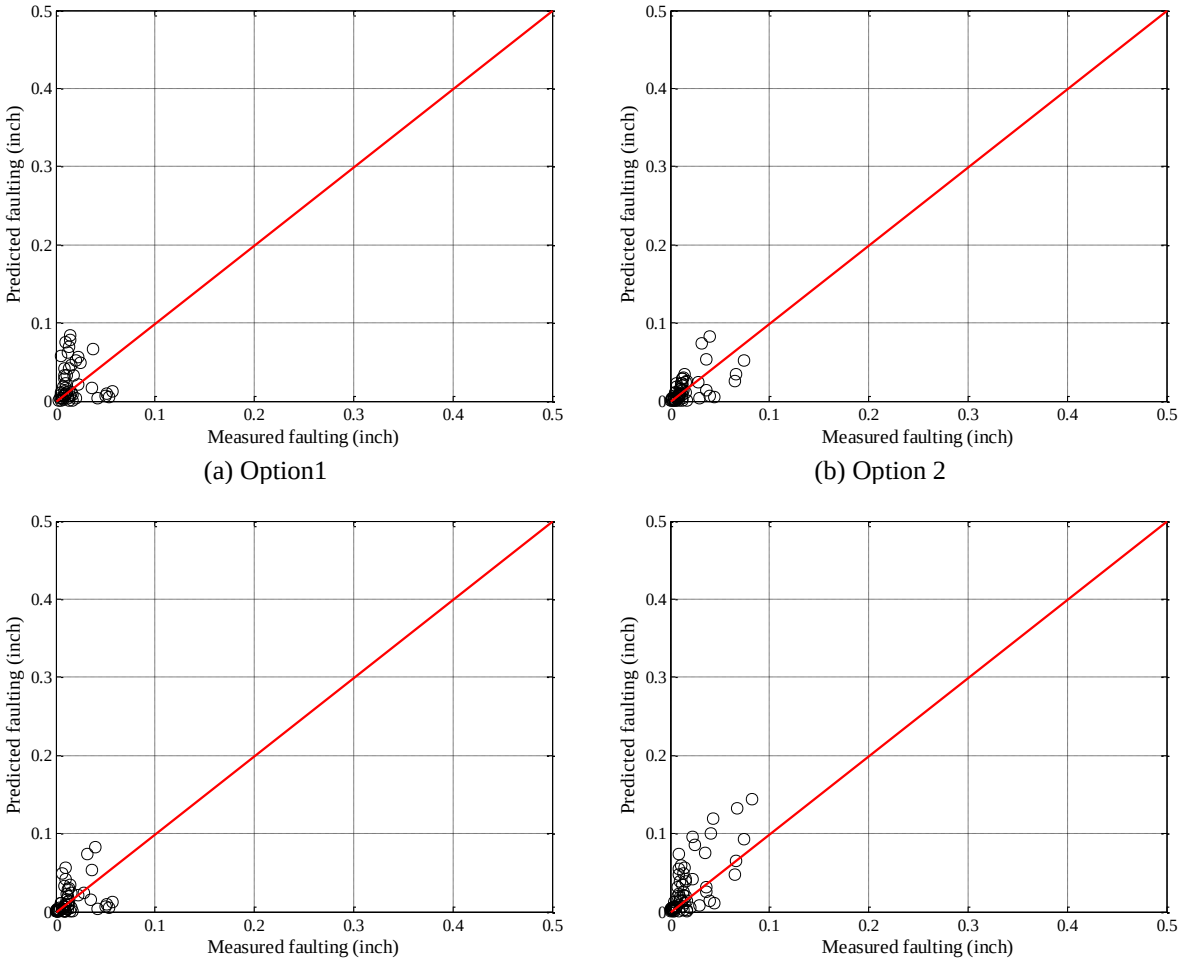

(a) Option1 (b) Option 2

(c) Option 3 (d) Option 4

Figure 5-43 Measured versus predicted — Faulting model validation (Rigid)

Similarly, Table 5-102 shows the validation results for the locally calibrated rigid pavement IRI model. These results indicate that the validation and local model SEE and bias are practically similar. This shows that the locally calibrated IRI model accurately predicts IRI for pavement sections not included in the local calibration datasets. Figure 5-44 shows the goodness-of-fit for the local model validation and verifies the model coefficients.

Table 5-102 Rigid pavement IRI model validation

Options	SEE			Bias		
	Global Model	Local model	Validation	Global Model	Local model	Validation
1	17.476	15.250	12.444	-11.426	4.393	-2.404
2	16.322	14.755	14.467	-10.544	0.480	7.522
3	17.446	14.226	14.343	-10.382	2.090	2.788
4	10.548	7.294	6.432	-7.127	0.207	-1.539

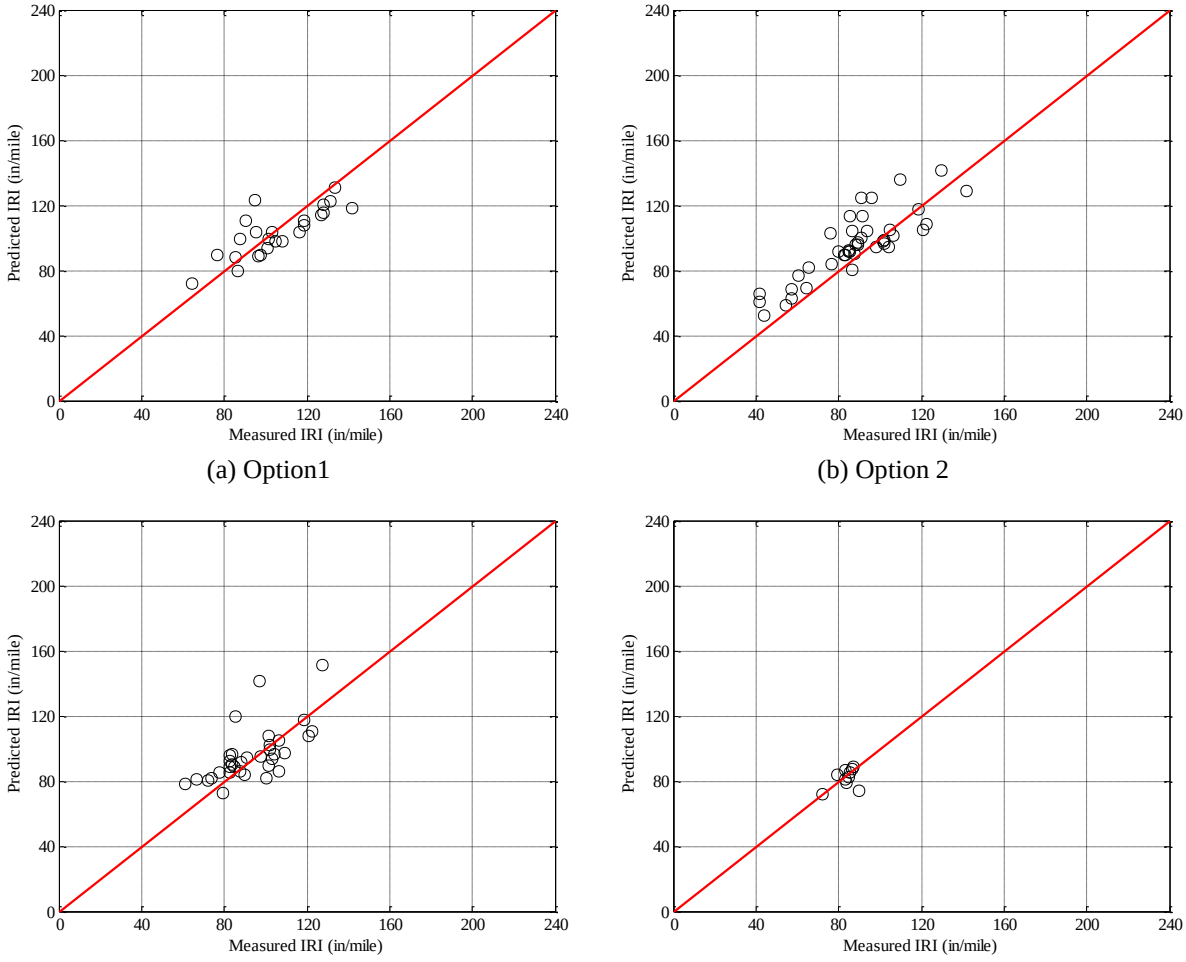

(a) Option1 (b) Option 2

(c) Option 3 (d) Option 4

Figure 5-44 Measured versus predicted — IRI model validation (Rigid)

5.5 SUMMARY OF FINDINGS

Once all the models are locally calibrated and validated, the final model statistics and coefficients need to be summarized for each model within the different data subsets and by each pavement type considered in the study. The following are the final results for the locally calibrated models for Michigan conditions.

5.5.1 Flexible Pavements

Tables 5-103 to 5-107 summarize the comparison between the global and locally calibrated model coefficients for each of the flexible pavement performance models considered in this study within each data subset (or option). The local models SEE, bias and coefficients are highlighted in grey.

Table 5-103 Locally calibrated model coefficients — Alligator cracking (Flexible)

Option	Model type	SEE	Bias	C_1	C_2
Option 1a	Global model	7.64	-4.19	1	1
	Local model	6.69	-1.16	0.50	0.56

Table 5-104 Locally calibrated model coefficients — Longitudinal cracking (Flexible)

Option	Model type	SEE	Bias	C_1	C_2
Option 2	Global model	996.20	-580.85	7	3.5
	Local model	850.44	-181.97	2.97	1.20

Table 5-105 Locally calibrated model coefficients — Rutting (Flexible)

Option	Model type	SEE	Bias	Br1	Bs1	Bsg1
Option 1	Global model	0.3425	0.3213	1	1	1
	Local model	0.0865	0.0772	0.9628	0.119	0.0411
Option 2	Global model	0.3572	0.3241	1	1	1
	Local model	0.0862	-0.0152	0.9453	0.0985	0.0367
Option 4	Global model	0.4029	0.3313	1	1	1
	Local model	0.0817	-0.0191	0.9032	0.0612	0.0216

Table 5-106 Locally calibrated model coefficients — Thermal cracking (Flexible)

Level	Option	Model type	SEE	Bias	K
Level 1	Option 1	Global model	1343.58	903.06	1.5
		Local Model	753.24	-70.40	0.75
	Option 2	Global model	1306.50	854.70	1.5
		Local Model	732.10	-73.80	0.75
Level 3	Option 1	Global model	1343.58	903.06	1.5
		Local Model	867.20	-23.20	3
	Option 2	Global model	945.00	-489.00	1.5
		Local Model	1057.70	35.30	4
	Option 4	Global model	1304.70	-906.60	1.5
		Local Model	1163.80	-212.00	5

Table 5-107 Locally calibrated model coefficients — IRI (Flexible)

Options	Model type	SEE	Bias	C_1	C_2	C_3	C_4
Option 1	Global model	14.7738	2.7817	40.0000	0.4000	0.0080	0.0150
	Local model	13.9428	-0.0391	50.3720	0.4102	0.0066	0.0068
Option 2	Global model	16.0256	0.2779	40.0000	0.4000	0.0080	0.0150
	Local model	15.7316	-0.3810	31.6450	0.3613	0.0065	0.0172
Option 4	Global model	20.4800	-5.8312	40.0000	0.4000	0.0080	0.0150
	Local model	17.5260	0.1290	21.4303	0.1600	0.0049	0.0271

Figure 5-45 shows an example of Pavement-ME performance prediction for a flexible reconstruct pavement section using the Option 1 bootstrap local calibration coefficients and its corresponding reliability relationships for each distress type. The results show that the total rutting predictions by local models are much lower as compared to the global models. All of the locally calibrated models show better predictions when compared with the measured performance on this particular pavement section.

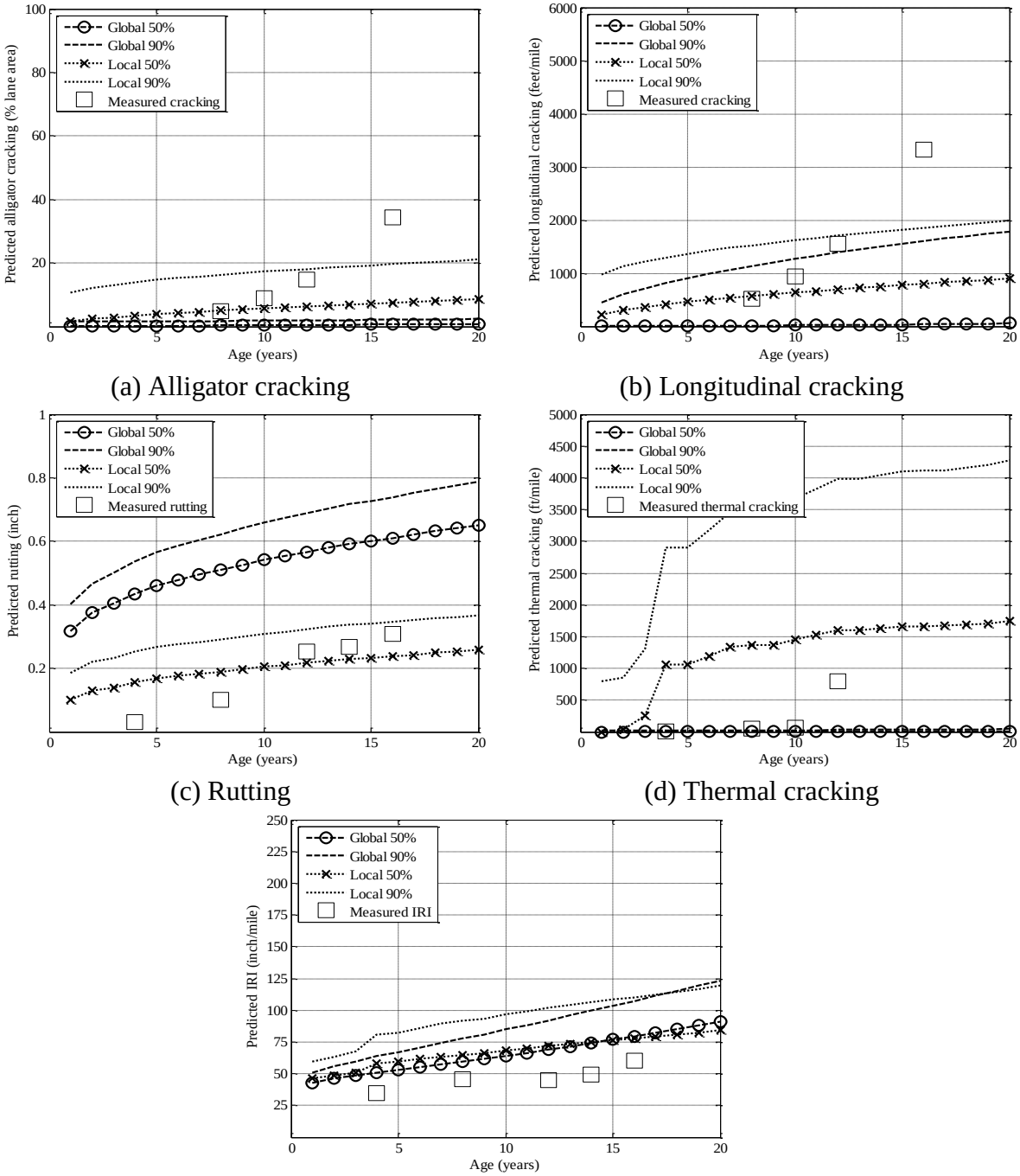

(a) Alligator cracking

(b) Longitudinal cracking

(c) Rutting

(d) Thermal cracking

(e) IRI

Figure 5-45 Comparison between global and local models— JN20046 (Flexible)

5.5.2 Rigid Pavements

Tables 5-108 to 5-110 summarize the comparison between the global and locally calibrated model coefficients for each of the rigid pavement performance models considered in this study within each data subset (or option). The local models SEE, bias and coefficients are highlighted in grey.

Table 5-108 Locally calibrated model coefficients — Transverse cracking (Rigid)

Options	Model type	SEE	Bias	C_4	C_5
Option 1	Global model	20.62	-11.74	1	-1.98
	Local model	11.37	0.13	0.25	-1.71
Option 2	Global model	13.86	-5.79	1	-1.98
	Local model	7.81	0.3	0.23	-1.8
Option 3	Global model	16.77	-4.45	1	-1.98
	Local model	13.24	1.65	2.14	-0.64
Option 4	Global model	0.88	-0.54	1	-1.98
	Local model	0.67	-0.04	4.96	-1.01

Table 5-109 Locally calibrated model coefficients — Faulting (Rigid)

Option	Model type	SEE	Bias	C_1
Option 1	Global model	0.059	0.035	1.29
	Local model	0.024	0.007	0.4
Option 2	Global model	0.051	0.026	1.29
	Local model	0.021	0.004	0.4
Option 3	Global model	0.049	0.023	1.29
	Local model	0.022	0.002	0.4
Option 4	Global model	0.005	-0.002	1.29
	Local model	0.004	-0.001	0.85

Table 5-110 Locally calibrated model coefficients — IRI (Rigid)

Option	Model type	SEE	Bias	C_1	C_2	C_3	C_4
Option 1	Global model	17.239	-11.466	0.820	0.442	1.492	25.240
	Local model	14.899	4.417	0.584	12.068	1.493	25.240
Option 2	Global model	15.390	-10.024	0.820	0.442	1.492	25.240
	Local model	13.424	-0.382	1.198	3.570	1.493	25.240
Option 3	Global model	21.999	-9.799	0.820	0.442	1.492	25.240
	Local model	20.099	0.996	1.855	1.980	1.493	25.240
Option 4	Global model	11.179	-7.539	0.820	0.442	1.492	25.240
	Local model	7.602	0.295	0.041	2.540	1.493	25.240

Figure 5-46 shows an example of Pavement-ME performance prediction for a rigid reconstruct pavement section using the Option 1 bootstrap local calibration coefficients and its corresponding reliability relationships for each distress type. The results show that all of the locally calibrated models show better predictions when compared with the measured performance on this particular pavement section.

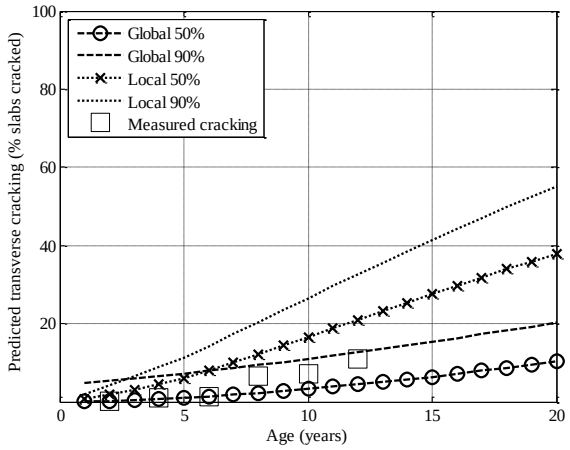

(a) Transverse cracking

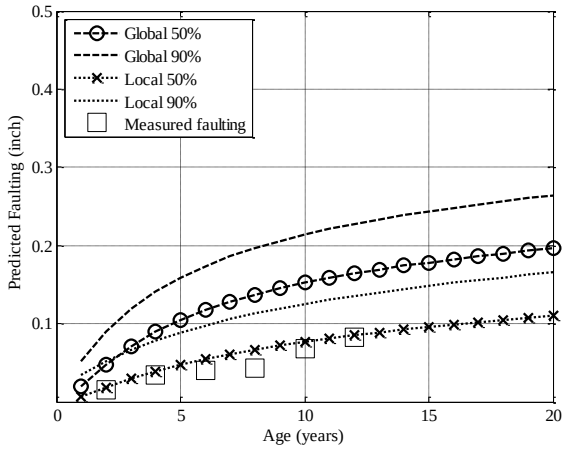

(b) Faulting

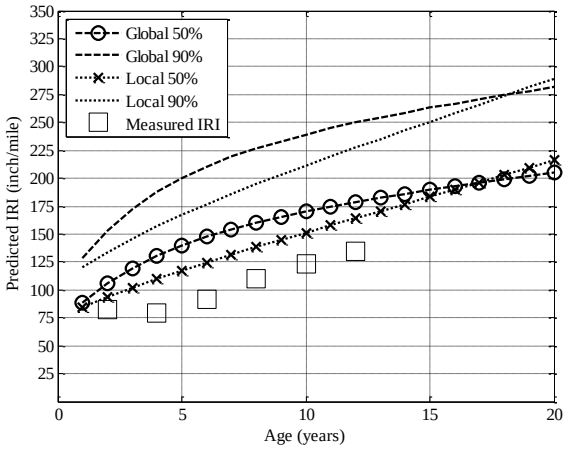

(c) IRI

Figure 5-46 Comparison between global and local models— JN45855 (Rigid)

CHAPTER 6 - CONCLUSIONS AND RECOMMENDATIONS

6.1 SUMMARY

The main objectives for Part 3 of this research project were to (a) select candidate pavement projects for the local calibration of performance models in Michigan, (b) evaluate the adequacy of the current global or national calibrated models for Michigan conditions, (c) calibrate the pavement performance prediction models for flexible and rigid pavements to Michigan conditions, (d) provide a catalog of calibration coefficients for each performance model for rigid and flexible pavements, (e) compare the local and globally calibrated models and recommend the most representative models for Michigan conditions , (f) recommend future local calibration guidelines and data needs.

The local calibration of the performance models in the mechanistic-empirical pavement design guide (Pavement-ME) is a challenging task, especially due to data limitations. A total of 108 (129 sections) and 20 (29 sections) reconstruct flexible and rigid pavement candidate projects, respectively, were selected. Similarly, a total of 33 (40 sections) and 8 (16 sections) rehabilitated pavement projects for flexible and rigid pavements, respectively were selected for the local calibration. The selection process considered pavement type, age, geographical location, and number of condition data collection cycles. The selected set of pavement sections met the following data requirements (a) adequate number of sections for each performance model, (b) a wide range of inputs related to traffic, climate, design and material characterization, (c) a reasonable extent and occurrence of observed condition data over time. The nationally calibrated performance models were evaluated by using data from the selected pavement sections. The results showed that the global models in the Pavement-ME don't adequately predict pavement performance for Michigan conditions. Therefore, a local calibration of the models was essential. The local calibration for all performance prediction models for flexible and rigid pavements were performed for multiple datasets (reconstruct, rehabilitation and a combination of both) and using robust statistical techniques (e.g. repeated split sampling and bootstrapping). The results of the local calibration and validation of various models show that the calibrated model significantly improves the performance predictions for Michigan conditions. The local calibration coefficients for all performance models are documented in the report. The report also includes recommendations on the most appropriate calibration coefficients for each of the performance models in Michigan, along with future local calibration guidelines and data needs.

6.2 LOCAL CALIBRATION FINDINGS

Based on the results of the analyses performed in Part 3 tasks, various conclusions were drawn. These conclusions can be divided into the following three broad topics:

- Data collection for the selected pavement sections
- Local calibration process
- Catalog of the local calibration coefficients

6.2.1 Data Needs for Local Calibration

The first step in the local calibration process includes the selection of an adequate number of pavement sections representing state-of-the-practice for the local conditions. Subsequently, an essential step is to collect the required data for the selected pavement sections. The data includes information about (a) measured pavement condition, and (b) many Pavement-ME inputs, for each project. Chapter 3 describes the process for pavement section selection for local calibration and the procedures adopted to collect the necessary information for the selected pavement sections. The data needs for the local calibration are:

1. Readily available MDOT measured condition data
2. Project selection criteria
3. Pavement cross-section information
4. Traffic inputs
5. Construction materials inputs
6. Climate inputs

Table 6-1 summarizes the inputs and corresponding levels for the available data.

Table 6-1 Summary of input levels and data source

Input			Input level	Input source
Traffic	AADTT		1	Historical traffic counts
	TTC		2	Clusters from previous traffic study
	ALS Tandem		2	Clusters from previous traffic study
	HDF		2	Clusters from previous traffic study
	MDF		3	Traffic characterization study
	AGPV		3	Traffic characterization study
	ALS single, tridem, quad		3	Traffic characterization study
Cross-section (new and existing)	HMA thickness		1	Design drawings
	PCC thickness		1	Design drawings
	Base thickness		1	Design drawings
	Subbase thickness		1	Design drawings
Construction materials	HMA	Binder type	3	Project specific binder and mixture gradation data obtained from data collection
		HMA mixture aggregate gradation	3	Project specific binder and mixture gradation data obtained from historical record
		Binder type	1	Pseudo Level 1- MDOT HMA mixture characterization study
		HMA mixture aggregate gradation	1	Pseudo Level 1- MDOT HMA mixture characterization study
	PCC	Strength (f'_c, MOR)	1	Psuedo Level 1(Project specific QC/QA)
		CTE	3	CTE study
	Base/subbase	MR	2	Unbound MR study
	Subgrade	MR	2	Subgrade MR study
		Soil type	1	Subgrade MR study
Climate			1	Closest available climate station (Pavement-ME)

Note: Level 1 is project specific data, pseudo level 1 means that the inputs are not project specific but the material properties (lab measured) corresponds to similar materials used in the project. Level 2 inputs are based on regional averages in Michigan. Level 3 inputs are based on statewide averages in Michigan

6.2.2 Process for Local Calibration

The NCHRP Project 1-40B documented the recommended practices for local calibration of the Pavement-ME. The guide outlines the significance of the calibration process and the general approach for local calibration. In general, the calibration process is used to:

a. Confirm that the performance models can predict pavement distress and smoothness with minimal bias, and
b. Determine the standard error associated with the prediction equations.

The standard error estimates the scatter of the data around the line of equality between predicted and measured values of distress. The bias indicates if there is any consistent under or over-prediction by the prediction models. In general the local calibration of the performance models involve the following steps:

1. Select the appropriate number of pavement sections based on the selection criteria documented in Chapter 3 for each performance model. The final list of candidate pavement sections should be refined based on the magnitude and extent of the measured performance.
2. Collect traffic, climate, pavement cross-section, and materials data for all the selected pavement sections.
3. Execute the Pavement-ME software to predict the pavement performance for each selected pavement section.
4. Extract the predicted distresses and compare with the measured distresses.
5. Test the accuracy of the global model predictions and determine if local calibration is required.
6. Adjust the local calibration coefficients to minimize bias and standard error by using different sampling and resampling techniques, if local calibration is required. It should be noted that different subsets of data representing reconstruct and rehab can be analyzed separately to determine the need for distinct calibration coefficients.
7. Validate the adjusted coefficients with pavement sections not included in the calibration set.
8. Modify the reliability equations for each performance model based on the final calibrated models.

6.2.3 Coefficients for the Locally Calibrated Models

Based on the local calibration of the performance models by following the above mentioned process, the following conclusions can be made:

- Bootstrapping consistently showed the lowest SEE and bias for different dataset options for alligator cracking, rutting, transverse cracking, and IRI models.
- Thermal cracking and faulting models require rerunning of the Pavement-ME software every time the local coefficients are modified. Therefore, only the no-sampling technique was utilized for the local calibration of those models.

- For each performance prediction model, the following options (data subsets) provided the most rational results:

    - Alligator cracking: Option 1a provided the most realistic model because more pavement sections and measured cracking data were available. Option 1b is not recommended because only a limited number of pavement sections exhibited alligator cracking based on the corresponding PDs in the MDOT PMS database.
    - Longitudinal cracking: Option 1 showed the lowest SEE and bias. Therefore, these model coefficients should be used for reconstruct designs. However, it should be noted that if option 1a is adopted for alligator cracking, longitudinal cracking model should not be used because such measured cracking is already included in Option 1a. Model coefficient based on Option 2 should be used for rehabilitation designs because more pavement sections were available for the local calibration.
    - Rutting: Individual layer calibration provided the best results. Option 2 (combination of reconstruct and rehabilitation) gave the most realistic results for the rutting model.
    - Thermal cracking: Level 1 calibration coefficients for Option 2 showed the best results. For level 3, Option 2 provided the most practical results.
    - IRI (flexible): The options provided varying results and, Options 1 and 4 showed the most appropriate results for reconstruct and rehabilitated pavement section, respectively.
    - Rigid transverse cracking: Option 2 provided the most practical results and contains more pavement sections. Therefore, the model coefficients based on Option 2 are recommended for both reconstruct and rehabilitation.
    - Faulting: Even though the magnitude of the measured faulting in the selected pavement sections was low, Option 2 provided the best results.
    - IRI (rigid): Option 2 provided the best results. It should be noted that the faulting coefficient in the IRI model is set to the global model coefficient because of the low levels of measured faulting due to dowelled joints in Michigan.

Based on the above findings, the local calibration coefficients and standard error equations for reliability for each performance model within flexible and rigid pavements are presented in Tables 6-2 to 6-5, respectively. The tables also contain the recommended options (dataset used for calibration) for each performance model. If option 1 is recommended, then use that model coefficients for only reconstruct pavement designs. On the other hand, if option 4 is recommended, the model should only be used for rehabilitation design. In the cases where only option 2 is recommended, use those models for both rehabilitation and reconstruct pavement designs.

Table 6-2 Summary of flexible pavement performance models with local coefficients in Michigan

Pavement type	Data Subset	Performance prediction model		Performance models and transfer functions	Local coefficient
Flexible pavements	Option 1a	Fatigue cracking – Bottom-up		$FC_{Bottom} = \left(\frac{1}{60}\right)\left(\frac{6000}{1+e^{C_1C_1^*+C_2C_2^*Log(DI_{Bottom}\cdot 100)}}\right)$	$C_1 = 0.50$ $C_2 = 0.56$
	Option 1b				$C_1 = 0.67$ $C_2 = 0.56$
	Option 1	Fatigue cracking – top-down		$FC_{Top} = (10.56)\left(\frac{1000}{1+e^{C_1-C_2\times Log(DI_{top}\cdot 100)}}\right)$	$C_1 = 3.32$ $C_2 = 1.25$
	Option 2				$C_1 = 2.97$ $C_2 = 1.2$
	Option 2	Rutting	HMA	$\Delta_{p(HMA)} = \varepsilon_{p(HMA)}h_{HMA} = \beta_{1r}k_z\varepsilon_{r(HMA)}10^{k_{1r}}n^{k_{2r}\beta_{2r}}T^{k_{3r}\beta_{3r}}$	$\beta_{1r} = 0.9453$ $\beta_{2r} = 1.3$ $\beta_{3r} = 0.7$
			Base/subgrade	$\Delta_{p(soil)} = \beta_{s1}k_{s1}\varepsilon_v h_{soil}\left(\frac{\varepsilon_o}{\varepsilon_r}\right)e^{-\left(\frac{\rho}{n}\right)^{\beta}}$	$\beta_{s1} = 0.0985$ $\beta_{sg1} = 0.0367$
	Option 2	Thermal cracking		$A = 10^{k_t\beta_t(4.389-2.52Log(E_{HMA}\sigma_m\eta))}$	$K = 0.75$ (Level 1) $K = 4$ (Level 3)
	Option 1	IRI		$IRI = IRI_o + C_1(RD) + C_2(FC_{Total}) + C_3(TC) + C_4(SF)$	$C_1 = 50.3720,\ C_2 = 0.4102$ $C_3 = 0.0066,\ C_4 = 0.0068$
	Option 4				$C_1 = 21.4303,\ C_2 = 0.1600$ $C_3 = 0.0049,\ C_4 = 0.0271$

Note: Option 1 = Reconstruct pavements, Option 2 = Combined reconstruct and rehabilitated pavements, Option 4 = Rehabilitated pavements. The model coefficients in red color show the local calibrated new coefficients. Option 1a uses both alligator and longitudinal cracking; therefore, if Option 1a is used longitudinal model should not be used.

Table 6-3 Summary of flexible pavement performance model coefficients and standard errors

Pavement type	Data Subset	Performance prediction model		Local coefficient	Standard error
Flexible pavements	Option 1a	Fatigue cracking – bottom-up		$C_1 = 0.50$ $C_2 = 0.56$	$s_{e(Alligator)} = 0.7874 + \frac{17.817}{1+e^{0.0699-0.4559\times log(D)}}$
	Option 1b			$C_1 = 0.67$ $C_2 = 0.56$	$s_{e(Alligator)} = 0.01 + \frac{32.913}{1+e^{1.3972-0.5976\times log(D)}}$
	Option 1	Fatigue cracking – top-down		$C_1 = 3.32$ $C_2 = 1.25$	$s_{e(Longitudinal)} = 150 + \frac{2300}{1+e^{1.9-0.6\times log(D_{td}+0.0001)}}$
	Option 2			$C_1 = 2.97$ $C_2 = 1.2$	$s_{e(Longitudinal)} = 300 + \frac{3000}{1+e^{1.8-0.61\times log(D_{td}+0.0001)}}$
	Option 2	Rutting	HMA	$\beta_{1r} = 0.9453$ $\beta_{2r} = 1.3$ $\beta_{3r} = 0.7$	$s_{e(HMA)} = 0.1126\left(Rut_{HMA}\right)^{0.2352}$
			Base/subgrade	$\beta_{s1} = 0.0985$ $\beta_{sg1} = 0.0367$	$s_{e(base)} = 0.1145\left(Rut_{base}\right)^{0.3907}$ $s_{e(subgrade)} = 3.6118\left(Rut_{subgrade}\right)^{1.0951}$
	Option 2	Thermal cracking		$K = 0.75$ (Level 1) $K = 4$ (Level 3)	$s_e(Level1) = 0.4258(TC) + 210.08$ $s_e(Level3) = 0.7737(TC) + 622.92$
	Option 1	IRI		$C_1 = 50.3720,\ C_2 = 0.4102$ $C_3 = 0.0066,\ C_4 = 0.0068$	Internally determined by the software
	Option 4			$C_1 = 21.4303,\ C_2 = 0.1600$ $C_3 = 0.0049,\ C_4 = 0.0271$	

Table 6-4 Summary of rigid pavement performance models with local coefficients in Michigan

Pavement type	Data Subset	Performance prediction model	Performance models and transfer functions	Local coefficient
Rigid pavements	Option 2	Transverse cracking	$CRK_{BU/TD} = \frac{100}{1 + C_4 \left(DI_F\right)^{C_5}}$	$C_4 = 0.23$ $C_5 = -1.80$
	Option 2	Transverse joint faulting	$Fault_m = \sum_{i=1}^{m} \Delta Fault_i$ $\Delta Fault_i = C_{34} \times (FAULTMAX_{i-1} - Fault_{i-1})^2 \times DE_i$ $FAULTMAX_i = FAULTMAX_0 + C_7 \times \sum_{j=1}^{m} DE_j \times Log(1 + C_5 \times 5.0^{EROD})^{C_6}$ $FAULTMAX_0 = C_{12} \times \delta_{curling} \times \left[Log(1 + C_5 \times 5.0^{EROD}) \times Log(\frac{P_{200} \times WetDays}{p_s}) \right]^{C_6}$ $C_{12} = C_1 + C_2 \times FR^{0.25}$ $C_{34} = C_3 + C_4 \times FR^{0.25}$	$C_1 = 0.4$ $C_2 = 0.91656$ $C_3 = 0.0021848$ $C_4 = 0.000883739$ $C_5 = 250$ $C_6 = 0.4$ $C_7 = 1.83312$ $C_8 = 400$
	Option 2	IRI	$IRI = IRI_I + C_1 \times CRK + C_2 \times SPALL + C_3 \times TFAULT + C_4 \times SF$	$C_1 = 1.198$ $C_2 = 3.570$ $C_3 = 1.4929$ $C_4 = 25.24$

Note: Option 1 = Reconstruct pavements, Option 2 = Combined reconstruct and rehabilitated pavements, Option 4 = Rehabilitated pavements. The model coefficients in red color show the local calibrated new coefficients.

Table 6-5 Summary of rigid pavement performance model coefficients and standard errors

Pavement type	Data Subset	Performance prediction model	Local coefficient	Reliability
Rigid pavements	Option 2	Transverse cracking	$C_4 = 0.23$ $C_5 = -1.80$	$s_{e(CRK)} = 1.34(CRK)^{0.6593}$
	Option 2	Transverse joint faulting	$C_1 = 0.4$ $C_2 = 0.91656$ $C_3 = 0.0021848$ $C_4 = 0.000883739$ $C_5 = 250$ $C_6 = 0.4$ $C_7 = 1.83312$ $C_8 = 400$	$s_{e(Fault)} = 0.0442(Fault)^{0.2698}$
	Option 2	IRI	$C_1 = 1.198$ $C_2 = 3.570$ $C_3 = 1.4929$ $C_4 = 25.24$	Internally determined by the software

Note: For reliability, the SE models mentioned in this table corresponds to the local calibration; however, the global faulting model is recommended due to software issues.

6.3 RECOMMENDATIONS

The following are the recommendations based on the findings from Part 3 of this study:

1. The IRI measurements in the MDOT sensor database are compatible to those in the Pavement-ME. Therefore, no conversion or adjustments were needed and the data was used directly.
2. Top-down cracking is defined as load related longitudinal cracking in the wheel-path. The PDs 204, 205, 724, and 725 in the MDOT PMS were used to represent the top-down cracking. The PDs are recorded in miles and needs conversion to feet/mile. Data from the wheel-paths can be summed into one value and divided by the total project length for the unit conversions.
3. Bottom-up cracking is defined as alligator cracking in the wheel-path. The PDs 234, 235, 220, 221, 730 and 731 match this requirement in the MDOT PMS database. The PDs have units of miles; however, to make those compatible with the Pavement-ME alligator cracking units, conversion to percent of total area is needed. This can be achieved by using the following Equation (1):

$$\%AC_{bottom-up} = \frac{\text{Length of cracking (miles)} \times \text{width of wheelpaths (feet)}}{\text{Length of project (miles)} \times \text{Lane width (feet)}} \times 100 \quad (1)$$

4. The bottom-up and top-down fatigue cracking in the wheel-paths are combined for new HMA reconstruct projects due to the difficulty determining the initiation (top or bottom) of the fatigue cracks observed at the surface. However, for rehabilitation design only longitudinal cracking data can be used.
5. Thermal cracking corresponds to transverse cracking in flexible pavements. The Pavement-ME predicts thermal cracking in feet/mile. The PDs 101, 103, 104, 114, 701, 703 and 704 were utilized to extract transverse cracking in flexible and rubblized pavements. For the composite pavement, PDs 101, 110, 114 and 701 were used. The transverse cracking is recorded as the number of occurrences. In order to convert transverse cracking in feet/mile, the number of occurrences was multiplied by the lane width for PDs 101, 103 and 104. For the PDs 114 and 701, the number of occurrences was multiplied by 3 feet because these PDs are defined as “tears” (short cracks) that are less than half the lane width. All transverse crack lengths can be summed and divided by the project length to get feet/mile as shown in Equation (2).

$$TC = \frac{\sum No.\ of\ Occurences \times Lane\ Width(ft)}{Project\ Length\ (miles)} \quad (2)$$

6. The average surface rutting (left & right wheel-paths) was determined for the entire project length. No conversion is necessary.
7. MDOT does not have any specific PDs for reflective cracking. It is difficult to determine the difference between a thermal and a reflective crack at the surface. A separate measurement for reflective cracking is recommended if the reflective cracking model is to be locally calibrated in the future.
8. The faulting values reported in the MDOT sensor database corresponds to the average height of all faults at a discontinuity (crack or joint) observed for an entire 0.1 mile section. However, the Pavement-ME faulting prediction does not distinguish between

faulting at cracks or joints and only predicts faulting at the joints. Therefore, only measured average joint faulting should be compared with the predicted faulting by Pavement-ME. Because MDOT's data does not discern between faults at cracks and joints, the average joint faulting needs to be calculated. The average joint faulting is calculated using Equation (3) as mentioned in chapter 3:

$$Fault = \frac{FAULnum \times FAULi}{(528/Joint\ Spacing)} \tag{3}$$

9. The transverse cracking distress is predicted as % slabs cracked in the Pavement-ME. However, MDOT measures transverse cracking as the number of transverse cracks. The PDs 112 and 113 correspond to transverse cracking. The measured transverse cracking needs conversion to percent slabs cracked by using Equation (4).

$$\%\ \text{Slabs Cracked} = \frac{\sum PD_{112,113}}{\left(\frac{\text{Project Length(miles)} \times 5280\ ft}{\text{Joint Spacing (ft)}}\right)} \times 100 \tag{4}$$

10. It is strongly recommended that all new flexible and rigid pavement rehabilitation or reconstruct projects be considered for future calibrations. Therefore, the most accurate as-constructed input data (traffic, and material properties for HMA and PCC layers) should be collected and stored in a database for future local calibrations.
11. The number of pavement projects and sections shortlisted in the study should be increased by adding pavement projects constructed after 2006 (since the local calibration was performed by using projects constructed until 2006), especially for rigid pavements. It is strongly recommended to include all the new projects where level 1 HMA data were obtained in Part 1 of this study.
12. A separate database including all the input data should be created and maintained along with linkage (project specific information, e.g. control section, BMP and EMP) with the PMS database. The database should be updated as more projects become available as mentioned in step 11.
13. It would be very useful to collect condition data on the selected projects (during this round of calibration) every other year.
14. The process adopted for the local calibration of the performance models in this study is also recommended for the future calibrations. The recommended options for each model should be used for future calibration. Resampling technique like bootstrapping is strongly recommended for future calibration; however, when additional pavement sections are available then traditional split-sampling can be used for models calibration and validation.
15. The local calibration model coefficients shown in Tables 6-2 and 6-4 are recommended to replace the global/national models coefficients in Michigan. However, these coefficients need to be re-evaluated and modified when more pavement sections with higher levels of distress, become available, especially for rehabilitated pavements with two or more cycles of distress measurements.
16. It is recommended that the local calibrations should be performed every six years. In six years, both the existing and new pavement sections will have three additional performance data points for the local calibration.

17. The input data for additional pavement sections should be collected at the time of construction to populate the local calibration database before the next calibration cycle.
18. It is strongly recommended to characterize pavement materials in the laboratory for the additional pavement sections and the data should be added to the local calibration database.

6.4 IMPLEMENTATION

Based on the conclusions and recommendations of Part 3 of this study, the following are recommendations for the implementation of the Pavement-ME in the state of Michigan:

- Increased use of FWD for backcalculation of layer moduli to characterize existing pavement conditions for all the rehabilitation options adopted in Michigan is warranted, especially for high traffic volume roads.
- PMS distress data and unit conversion is also necessary to ensure compatibility between MDOT measured and Pavement-ME predicted distresses in the long-term for implementation of the new design methodology (see Tables 6-6 and 6-7). The units can be converted by using the equations mentioned above. The results of conversion should be stored separately in the database for the selected PDs. Sensor data (IRI, rut depth) do not need any further conversion because of their current compatibility with Pavement-ME.

Table 6-6 Flexible pavement distresses

Flexible pavement distresses	MDOT principle distresses	MDOT units	Pavement-ME units	Conversion needed?
IRI	Directly measured	in/mile	in/mile	No
Top-down cracking	204, 205, **724, 725**	miles	ft/mile	Yes
Bottom-up cracking	234, 235, **220, 221, 730, 731**	miles	% area	Yes
Thermal cracking	**101,** 103, 104, 114, **701, 703, 704,** 110	No. of occurrences	ft/mile	Yes
Rutting	Directly measured	in	in	No
Reflective cracking	No specific PD	None	% area	N/A

Note: Bold numbers represent older PDs that are not currently in use

Table 6-7 Rigid pavement distresses

Rigid pavement distresses	MDOT principle distresses	MDOT units	Pavement-ME units	Conversion needed?
IRI	Directly measured	in/mile	in/mile	No
Faulting	Directly measured	in	in	Yes
Transverse cracking	112, 113	No. of occurrences	% slabs cracked	Yes

- The significant input variables that are related to the various reconstruct and rehabilitation types summarized in Chapter 3 should be an integral part of a database for construction and material related information. Such information will be beneficial for future design projects and local calibration of the performance models in the Pavement-ME. Table 6-8 summarizes the testing requirements for the significant input variables needed for the local calibration.

Table 6-8 Testing requirements for significant input variables for rehabilitation

Pavement layer type	Significant input variables	Lab test[1]	Field test
Reconstruct and Overlay	HMA air voids	Yes	
	HMA effective binder	Yes	
	HMA binder and mixture characterization (*G**, *E** etc.)	Yes	
	PCC CTE (per °F x 10-6)	Yes	
	PCC MOR (psi)	Yes	
Existing	HMA thickness		Extract core
	Pavement condition rating		Distress survey
	Subgrade modulus		FWD testing
	Subbase modulus		FWD testing
	PCC thickness		Extract core
	Existing PCC elastic modulus (psi)		FWD

[1] Either use current practice or AASHTO test methods

REFERENCES

CHAPTER 2

1. NCHRP Project 1-40B, "Local Calibration Guidance for the Recommended Guide for Mechanistic-Empirical Pavement Design of New and Rehabilitated Pavement Structures," Final NCHRP Report 2009.
2. Fick, S. B., "Evaluation of the AASHTO Empirical and Mechanistic-Empirical Pavement Design Procedures using the AASHO Road Test," Civil Engineering Department, University of Maryland, College Park, 2010.
3. AASHTO, "Mechanistic-Empirical Pavement Design Guide: A Manual of Practice: Interim Edition," American Association of State Highway and Transportation Officials 2008.
4. Quintus, H. L. V., M. I. Darter, and J. Mallela, "Local Calibration Guidance for the Recommended Guide for Mechanistic-Empirical Design of New and Rehabilitated Pavement Structures," 2004.
5. Pierce, L. M. and G. McGovern, "Implementation of the AASHTO Mechanistic-Empirical Pavement Design Guide and Software," NCHRP Synthesis 457 2014.
6. Mallela, J., L. Titus-Glover, H. V. Quintus, M. I. Darter, M. Stanley, and C. Rao, "Implementing the AASHTO Mechanistic-Empirical Pavement Design Guide in Missouri Volume II: MEPDG Model Validation and Calibration," Missouri Department of Transportation 2009.
7. Mallela, J., L. Titus-Glover, H. V. Quintus, M. I. Darter, M. Stanley, C. Rao, and S. Sadasivam, "Implementing the AASHTO Mechanistic-Empirical Pavement Design Guide in Missouri Volume I: Study Findings, Conclusions, and Recommendations," Missouri Department of Transportation 2009.
8. Glover, L. T. and J. Mallela, "Guidelines for Implementing NCHRP 1-37A M-E Design Procedures in Ohio: Volume 4 - MEPDG Models Validation & Recalibration," Ohio Department of Transportation 2009.
9. Hall, K. D., D. X. Xiao, and K. C. P. Wang, "Calibration of the MEPDG for Flexible Pavement Design in Arkansas," Transportation Research Record, 2010.
10. Li, J., L. M. Pierce, and J. Uhlmeyer, "Calibration of the Flexible Pavement Portion of the Mechanistic-Empirical Pavement Design Guide for the Washington State Department of Transportation," Transportation Research Record, 2008.
11. Velasquez, R., K. Hoegh, I. Yut, N. Funk, GeorgeCochran, M. Marasteanu, and L. Khazanovich, "Implementation of the MEPDG for New and Rehabilitated Pavement Structures for Design of Concrete and Asphalt Pavements in Minnesota," Minnesota Department of Transportation 2009.
12. Quintus, H. V. and J. S. Moulthrop, "Mechanistic-Empirical Pavement Design Guide Flexible Pavement Performance Prediction Models for Montana: Volume I Executive Research Summary," The State of Montana Department of Transportation, FHWA/MT-07-008/8158-1, 2007.
13. FHWA, "Local Calibration of the MEPDG Using Pavement Management Systems," FHWA HIF-11-026, 2010.

14. Mallela, J., L. Titus-Glover, S. Sadasivam, B. Bhattacharya, M. I. Darter, and H. L. V. Quintus, "Implementation of the AASHTO Mechanistic-Empirical Pavement Design Guide for Colorado," Colorado Department of Transportation 2013.
15. Chatti, K., M. Kutay, and L. Lei, "Relationships between Laboratory-Measured and Field-Derived Properties of Pavement Layers," 2011.
16. Banerjee, A., J. P. Aguiar-Moya, and J. A. Prozzi, "Texas Experience using LTPP for Calibration of the MEPDG Permanent Deformation Models," Transportation Research Record, 2009.
17. Hoerner, T. E., M. I. Darter, L. Khazanovich, and L. Titus-Glover, "Improved Prediction Models for PCC Pavement Performance-Related Specifications," Federal Highway Administration, FHWA-RD-00-130, 2000.
18. Buch, N., K. Chatti, S. W. Haider, and A. Manik, "Evaluation of the 1-37A Design Process for New and Rehabilitated JPCP and HMA Pavements, Final Report," Michigan Department of Transportation, Construction and Technology Division, P.O. Box 30049, Lansing, MI 48909, Lansing, Research Report RC-1516, 2008.
19. Haider, S. W., N. Buch, and K. Chatti, "Evaluation of M-E PDG for Rigid Pavements—Incorporating the State-of-the-Practice in Michigan," presented at the 9th International Conference on Concrete Pavements San Francisco, California, USA, 2008, pp.
20. Kutay, E. and A. Jamrah, "Preparation for Implementation of the Mechanistic-Empirical Pavement Design Guide in Michigan: Part 1 - HMA Mixture Characterization," Michigan Department of Transportation, 425 West Ottawa, P.O. Box 30050 Lansing, MI 48909, Lansing, Research Report ORBP OR10-022, 2012.
21. Kutay, M. E. and A. Jamrah, "Preparation for Implementaiton of the Mechanistic-Empirical pavement Design Guide in Michigan Part 1: HMA Mixture Characterization," Michigan Department of Transportation RC-1593, 2013.
22. Buch, N., S. W. Haider, J. Brown, and K. Chatti, "Characterization of Truck Traffic in Michigan for the New Mechanistic Empirical Pavemnet Design Guide, Final Report," Michigan Department of Transportation, Construction and Technology Division, P.O. Box 30049, Lansing, MI 48909, Lansing, Research Report RC-1537, 2009.
23. Haider, S. W., N. Buch, K. Chatti, and J. Brown, "Development of Traffic Inputs for Mechanistic-Empirical Pavement Design Guide in Michigan," Transportation Research Record, vol. 2256, pp. 179-190, 2011.
24. Baladi, G. Y., T. Dawson, and C. Sessions, "Pavement Subgrade MR Design Values for Michigan's Seasonal Changes, Final Report," Michigan Department of Transportation, Construction and Technology Division, P.O. Box 30049, Lansing, MI 48909, Lansing, Research Report RC-1531, 2009.
25. Baladi, G. Y., K. A. Thottempudi, and T. Dawson, "Backcalculation of Unbound Granular Layer Moduli, Final Report," Michigan Department of Transportation, Construction and Technology Division, P.O. Box 30049, Lansing, MI 48909, Lansing, 2010.
26. Buch, N. and S. Jahangirnejad, "Quantifying Coefficient of Thermal Expansion Values of Typical Hydraulic Cement Concrete Paving Mixtures, Final Report," Michigan Department of Transportation, Construction and Technology Division, P.O. Box 30049, Lansing, MI 48909, Lansing, Research Report RC-1503, 2008.

27. Buch, N., S. W. Haider, K. Chatti, G. Y. Baladi, W. Brink, and I. Harsini, "Preparation for Implementation of the Mechanistic-Empirical Pavement Design Guide in Michigan - Part 2: Rehabilitation Evaluation," Michigan Department of Transportation 2013.

CHAPTER 3

1. Miller, J. S. and W. Y. Bellinger, "Distress Identification Manual," FHWA-RD-03-031 2003.
2. Kutay, M. E. and A. Jamrah, "Preparation for Implementaiton of the Mechanistic-Empirical pavement Design Guide in Michigan Part 1: HMA Mixture Characterization," Michigan Department of Transportation RC-1593, 2013.
3. NCHRP Project 1-40B, "Local Calibration Guidance for the Recommended Guide for Mechanistic-Empirical Pavement Design of New and Rehabilitated Pavement Structures," Final NCHRP Report 2009.
4. Buch, N., S. W. Haider, K. Chatti, G. Y. Baladi, W. Brink, and I. Harsini, "Preparation for Implementation of the Mechanistic-Empirical Pavement Design Guide in Michigan - Part 2: Rehabilitation Evaluation," Michigan Department of Transportation 2013.
5. Rauhut, J. B., A. Eltahan, and A. L. Simpson, "Common Characteristics of Good and Poorly Performing AC Pavements," Federal Highway Administration, FHWA-RD-99-193, December 1999.
6. Khazanovich, L., D. M, B. R, and M. T, "Common Characteristics of Good and Poorly Performing PCC Pavements," Federal Highway Administration, FHWA-RD-97-131, 1998.
7. Buch, N., K. Chatti, S. W. Haider, and A. Manik, "Evaluation of the 1-37A Design Process for New and Rehabilitated JPCP and HMA Pavements, Final Report," Michigan Department of Transportation, Construction and Technology Division, P.O. Box 30049, Lansing, MI 48909, Lansing, Research Report RC-1516, 2008.
8. Schwartz, C. W., R. Li, S. Kim, H. Ceylan, and R. Gopalakrishnan, "Sensitivity Evaluation of MEPDG Performance Prediction," NCHRP 1-47 Final Report, 2011.
9. Buch, N., S. W. Haider, J. Brown, and K. Chatti, "Characterization of Truck Traffic in Michigan for the New Mechanistic Empirical Pavemnet Design Guide, Final Report," Michigan Department of Transportation, Construction and Technology Division, P.O. Box 30049, Lansing, MI 48909, Lansing, Research Report RC-1537, 2009.
10. Haider, S. W., N. Buch, K. Chatti, and J. Brown, "Development of Traffic Inputs for Mechanistic-Empirical Pavement Design Guide in Michigan," Transportation Research Record, vol. 2256, pp. 179-190, 2011.
11. Buch, N. and S. Jahangirnejad, "Quantifying Coefficient of Thermal Expansion Values of Typical Hydraulic Cement Concrete Paving Mixtures, Final Report," Michigan Department of Transportation, Construction and Technology Division, P.O. Box 30049, Lansing, MI 48909, Lansing, Research Report RC-1503, 2008.
12. Baladi, G. Y., K. A. Thottempudi, and T. Dawson, "Backcalculation of Unbound Granular Layer Moduli, Final Report," Michigan Department of Transportation,

Construction and Technology Division, P.O. Box 30049, Lansing, MI 48909, Lansing, 2010.
13. Baladi, G. Y., T. Dawson, and C. Sessions, "Pavement Subgrade MR Design Values for Michigan's Seasonal Changes, Final Report," Michigan Department of Transportation, Construction and Technology Division, P.O. Box 30049, Lansing, MI 48909, Lansing, Research Report RC-1531, 2009.

CHAPTER 4

1. NCHRP Project 1-40B, "User Manual and Local Calibration Guide for the Mechanistic-Empirical Pavement Design Guide and Software " NCHRP In Progress, 2007.
2. NCHRP Project 1-40B, "Local Calibration Guidance for the Recommended Guide for Mechanistic-Empirical Pavement Design of New and Rehabilitated Pavement Structures," Final NCHRP Report 2009.
3. Sahinler, S. and D. Topuz, "Bootstrap and Jakknife Resampling Algorithms for Estimation of Regression Parameters," Journal of Applied Quantitative Methods, vol. 2, pp. 188-199, 2007.
4. Fox, J., "Bootstrapping regression models," An R and S-PLUS Companion to Applied Regression: A Web Appendix to the Book. Sage, Thousand Oaks, CA. URL http://cran. r-project. org/doc/contrib/Fox-Companion/appendix-bootstrapping. pdf, 2002.
5. Quintus, H. V., C. Schwartz, R. H. McCuen, and D. Andrei, "Jackknife Testing - An Experiment Approach to Refine Model Calibration and Validation," Research Results Digest 283, National Cooperative Highway Research Program Research Results Digest 283, 2003.
6. White, T. D., E. H. John, J. T. H. Adam, and F. Hongbing, "Contribution of Pavement Structural Layers to Rutting of Hot Mix Asphalt Pavements," NCHRP, Washington, DC. Report 468, 2002.
7. White, T. D., J. E. Haddock, A. J. T. Hand, and H. Fang, "Contributions of pavement structural layers to rutting of hot mix asphalt pavements," Transportation Research Board NCHRP Report No. 468, 2002.
8. Haddock, J. E., J. T. H. Adam, F. Hongbing, and T. D. White, "Determining Layer Contributions to Rutting by Surface Profile Analysis," ASCE Journal of Transportation Engineering, vol. Vol. 131, pp. 131-139, 2005.
9. AASHTO, "Mechanistic-Empirical Pavement Design Guide: A Manual of Practice: Interim Edition," American Association of State Highway and Transportation Officials 2008.
10. Hoerner, T. E., M. I. Darter, L. Khazanovich, L. Titus-Glover, and K. L. Smith, "Improved prediction Models for PCC Pavement Performance-Related Specifications - Volume 1: Final Report," Federal Highway Administration FHWA-RD-00-130, 2000.

CHAPTER 5

1. Quintus, H. L. V., M. I. Darter, and J. Mallela, "Local Calibration Guidance for the Recommended Guide for Mechanistic-Empirical Design of New and Rehabilitated Pavement Structures," 2004.
2. NCHRP Project 1-40B, "Local Calibration Guidance for the Recommended Guide for Mechanistic-Empirical Pavement Design of New and Rehabilitated Pavement Structures," Final NCHRP Report 2009.
3. Mallela, J., L. Titus-Glover, H. V. Quintus, M. I. Darter, M. Stanley, and C. Rao, "Implementing the AASHTO Mechanistic-Empirical Pavement Design Guide in Missouri Volume II: MEPDG model Validation and Calibration," Missouri Department of Transportation 2009.
4. Glover, L. T. and J. Mallela, "Guidelines for Implementing NCHRP 1-37A M-E Design Procedures in Ohio: Volume 4 - MEPDG models Validation & Recalibration," Ohio Department of Transportation 2009.
5. Mallela, J., L. Titus-Glover, S. Sadasivam, B. Bhattacharya, M. I. Darter, and H. L. V. Quintus, "Implementation of the AASHTO Mechanistic-Empirical Pavement Design Guide for Colorado," Colorado Department of Transportation 2013.

APPENDIX A - INPUT DATA

Table of Contents

List of Tables

A.1 HMA NON-FREEWAY PROJECT INPUTS

A.1.1 Inventory and Traffic Inputs

Table A-1 Inventory and traffic inputs for HMA non-freeway projects

JN	REGION	OPENED	Roadway	AADTT 2-Way MDOT Confirmed	Percent trucks in Design dir	Percent trucks in Design lane	MDOT TTC Cluster	HDF Cluster	ALS Tandem	MDF Cluster	AGPV Cluster Single	AGPV Cluster Tridem	AGPV Cluster Quad	ALS Single	ALS Tandem	ALS Tridem	ALS Quad	Initial IRI	Climate
34096	Southwest	2000	M-63	683	51	90	S-A	S-A	S-A	S-A	S-A	S-A	S-A	S-A	S-A	S-A	S-A	85	Benton Harbor
59881	Metro	2005	US-12	1304	51	90	S-A	S-A	S-A	S-A	S-A	S-A	S-A	S-A	S-A	S-A	S-A	87	Detroit
58344	North	2004	M-42	201	51	90	2	2	3	S-A	S-A	S-A	S-A	S-A	S-A	S-A	S-A	75	Traverse City
59933	Superior	2005	M-28	280	51	90	3	2	3	S-A	S-A	S-A	S-A	S-A	S-A	S-A	S-A	72	Marquette
33263	Superior	2006	M-38	120	51	90	S-A	S-A	S-A	S-A	S-A	S-A	S-A	S-A	S-A	S-A	S-A	65	Iron Mountain
60346	North	2007	US-131/M-66	880	51	90	2	2	3	S-A	S-A	S-A	S-A	S-A	S-A	S-A	S-A	40	Traverse City
74862	North	2008	US-23	194	51	90	2	3	1	S-A	S-A	S-A	S-A	S-A	S-A	S-A	S-A	73	Houghton Lake
32341	Grand	2002	M-46	588	51	90	3	2	5	S-A	S-A	S-A	S-A	S-A	S-A	S-A	S-A	95	Grand rapids
52746	Superior	2001	US-2/US-141	1033	51	90	3	2	3	S-A	S-A	S-A	S-A	S-A	S-A	S-A	S-A	65	Iron Mountain
32303	Superior	1996	US-2	109	51	90	2	2	3	S-A	S-A	S-A	S-A	S-A	S-A	S-A	S-A	60	Iron Mountain
48270	Bay	2002	M-84	308	51	90	S-A	S-A	S-A	S-A	S-A	S-A	S-A	S-A	S-A	S-A	S-A	82	Flint
46573	Bay	2003	US-127 BR	276	51	90	3	3	1	S-A	S-A	S-A	S-A	S-A	S-A	S-A	S-A	70	Flint
45707	Metro	2000	Old M-14	260	51	90	S-A	S-A	S-A	S-A	S-A	S-A	S-A	S-A	S-A	S-A	S-A	98	Detroit
45835	Southwest	2001	Bus I-94	500	51	90	S-A	S-A	S-A	S-A	S-A	S-A	S-A	S-A	S-A	S-A	S-A	85	Battle Creek
47064	Metro	2004	US-12	1600	51	90	S-A	S-A	S-A	S-A	S-A	S-A	S-A	S-A	S-A	S-A	S-A	87	Detroit
26620	Superior	1992	US-41	160	51	90	2	2	3	S-A	S-A	S-A	S-A	S-A	S-A	S-A	S-A	85	Iron Mountain
31009	North	1995	M-55	391	51	90	2	2	3	S-A	S-A	S-A	S-A	S-A	S-A	S-A	S-A	70	Houghton Lake
44934	Superior	1999	US-2	550	51	90	2	2	3	S-A	S-A	S-A	S-A	S-A	S-A	S-A	S-A	73	Iron Mountain
45791	Grand	2001	M-57	794	51	90	3	2	5	S-A	S-A	S-A	S-A	S-A	S-A	S-A	S-A	71	Grand Rapids
41124	Southwest	2001	US-12	996	51	90	2	3	3	S-A	S-A	S-A	S-A	S-A	S-A	S-A	S-A	85	Battle Creek
6767	Grand	2002	M-45	859	51	90	S-A	S-A	S-A	S-A	S-A	S-A	S-A	S-A	S-A	S-A	S-A	55	Grand Rapids

Table A-1 Inventory and traffic inputs for HMA non-freeway projects (continued)

JN	REGION	OPENED	Roadway	AADTT 2-Way MDOT Confirmed	Percent trucks in Design dir	Percent trucks in Design lane	MDOT TTC Cluster	HDF Cluster	ALS Tandem	MDF Cluster	AGPV Cluster Single	AGPV Cluster Tridem	AGPV Cluster Quad	ALS Single	ALS Tandem	ALS Tridem	ALS Quad	Initial IRI	Climate
45441	Bay	1999	M-13	523	51	90	3	3	3	S-A	S-A	S-A	S-A	S-A	S-A	S-A	S-A	73	Flint
38178	Grand	1998	I-196 BL	1440	51	90	S-A	S-A	S-A	S-A	S-A	S-A	S-A	S-A	S-A	S-A	S-A	50	Grand Rapids
45642	University	2001	M-50	556	51	90	3	2	3	S-A	S-A	S-A	S-A	S-A	S-A	S-A	S-A	68	Detroit
55181	North	2003	US-10	276	51	90	3	3	3	S-A	S-A	S-A	S-A	S-A	S-A	S-A	S-A	75	Muskegon
48547	Southwest	2003	M-51	554	51	90	3	2	5	S-A	S-A	S-A	S-A	S-A	S-A	S-A	S-A	70	Kalamazoo
46031	Grand	2003	M-44	370	51	90	2	2	1	S-A	S-A	S-A	S-A	S-A	S-A	S-A	S-A	71	Grand Rapids
49037	North	2004	M-65	367	51	90	2	2	3	S-A	S-A	S-A	S-A	S-A	S-A	S-A	S-A	58	Houghton Lake
53767	Grand	2004	M-20	367	51	90	3	2	5	S-A	S-A	S-A	S-A	S-A	S-A	S-A	S-A	70	Muskegon
50617	Bay	2004	M-25	142	51	90	3	2	5	S-A	S-A	S-A	S-A	S-A	S-A	S-A	S-A	60	Flint
50530	Metro	2004	M-29	152	51	90	S-A	S-A	S-A	S-A	S-A	S-A	S-A	S-A	S-A	S-A	S-A	96	Pontiac
45594	University	2005	Conn 81 EB	158	51	90	S-A	S-A	S-A	S-A	S-A	S-A	S-A	S-A	S-A	S-A	S-A	70	Lansing
45857	Grand	2004	M-50	423	51	90	S-A	S-A	S-A	S-A	S-A	S-A	S-A	S-A	S-A	S-A	S-A	90	Grand Rapids
75176	University	2004	US-223 BR	180	51	90	3	3	3	S-A	S-A	S-A	S-A	S-A	S-A	S-A	S-A	70	Adrian
32331	North	1999	M-32	460	51	90	2	2	1	S-A	S-A	S-A	S-A	S-A	S-A	S-A	S-A	72	Gaylord
38464	North	1998	US-10	521	51	90	3	3	3	S-A	S-A	S-A	S-A	S-A	S-A	S-A	S-A	54	Houghton Lake
36171	Bay	1997	M-20	388	51	90	3	3	1	S-A	S-A	S-A	S-A	S-A	S-A	S-A	S-A	56	Houghton Lake
36170	Bay	1996	M-20	388	51	90	3	3	4	S-A	S-A	S-A	S-A	S-A	S-A	S-A	S-A	58	Houghton Lake
34039	Superior	1995	M-95	179	51	90	2	2	1	S-A	S-A	S-A	S-A	S-A	S-A	S-A	S-A	50	Iron Mountain
36190	Superior	1995	US-41/M-28	521	51	90	3	2	3	S-A	S-A	S-A	S-A	S-A	S-A	S-A	S-A	65	Hancock
35139	Bay	1994	M-20	388	51	90	3	3	1	S-A	S-A	S-A	S-A	S-A	S-A	S-A	S-A	40	Flint
27576	Superior	1992	M-183	63	51	90	S-A	S-A	S-A	S-A	S-A	S-A	S-A	S-A	S-A	S-A	S-A	70	Iron Mountain
50768	Southwest	2006	US-12	442	51	90	S-A	S-A	S-A	S-A	S-A	S-A	S-A	S-A	S-A	S-A	S-A	85	Kalamzoo
79903	Superior	2006	M-203	100	51	90	S-A	S-A	S-A	S-A	S-A	S-A	S-A	S-A	S-A	S-A	S-A	63	Hancock
45009	Superior	2000	US-2	126	51	90	2	2	3	S-A	S-A	S-A	S-A	S-A	S-A	S-A	S-A	55	Hancock
55775	Superior	2005	US-2	1086	51	90	3	2	3	S-A	S-A	S-A	S-A	S-A	S-A	S-A	S-A	73	Iron Mountain

Table A-1 Inventory and traffic inputs for HMA non-freeway projects (continued)

JN	REGION	OPENED	Roadway	AADTT 2-Way MDOT Confirmed	Percent trucks in Design dir	Percent trucks in Design lane	MDOT TTC Cluster	HDF Cluster	ALS Tandem	MDF Cluster	AGPV Cluster Single	AGPV Cluster Tridem	AGPV Cluster Quad	ALS Single	ALS Tandem	ALS Tridem	ALS Quad	Initial IRI	Climate
60292	Superior	2005	US-2	283	51	90	2	2	3	S-A	S-A	S-A	S-A	S-A	S-A	S-A	S-A	52	Iron Mountain
80158	Superior	2006	M-28	363	51	90	2	2	3	S-A	S-A	S-A	S-A	S-A	S-A	S-A	S-A	58	Hancock
53244	Superior	2006	M-26	121	51	90	2	2	1	S-A	S-A	S-A	S-A	S-A	S-A	S-A	S-A	61	Hancock
45798	Grand	2003	M-45	819	51	90	S-A	S-A	S-A	S-A	S-A	S-A	S-A	S-A	S-A	S-A	S-A	67	Grand Rapids
51598	University	2002	M-49	137	51	90	S-A	S-A	S-A	S-A	S-A	S-A	S-A	S-A	S-A	S-A	S-A	77	Battle Creek
50933	Superior	2002	M-94	131	51	90	S-A	S-A	S-A	S-A	S-A	S-A	S-A	S-A	S-A	S-A	S-A	61	Hancock
50719	North	2002	M-65	363	51	90	2	2	3	S-A	S-A	S-A	S-A	S-A	S-A	S-A	S-A	49	Houghton Lake
31328	University	2002	M-43	319	51	90	S-A	S-A	S-A	S-A	S-A	S-A	S-A	S-A	S-A	S-A	S-A	54	Lansing
45641	University	2002	M-43	319	51	90	S-A	S-A	S-A	S-A	S-A	S-A	S-A	S-A	S-A	S-A	S-A	88	Lansing
26668	North	1994	US-31	353	51	90	3	3	4	S-A	S-A	S-A	S-A	S-A	S-A	S-A	S-A	30	Muskegon
31050	Southwest	1994	US-12	529	51	90	3	2	3	S-A	S-A	S-A	S-A	S-A	S-A	S-A	S-A	85	Battle Creek
31045	North	1995	US-23	360	51	90	2	3	1	S-A	S-A	S-A	S-A	S-A	S-A	S-A	S-A	56	Houghton Lake
49401	Metro	2002	Old M-14	900	51	90	S-A	S-A	S-A	S-A	S-A	S-A	S-A	S-A	S-A	S-A	S-A	68	Detroit
52745	Superior	2004	US-2/US-141/M-95	1096	51	90	3	2	3	S-A	S-A	S-A	S-A	S-A	S-A	S-A	S-A	81	Iron Mountain
46565	University	2002	M-21	465	51	90	3	3	1	S-A	S-A	S-A	S-A	S-A	S-A	S-A	S-A	70	Lansing
21218	North	1992	M-32	221	51	90	2	2	1	S-A	S-A	S-A	S-A	S-A	S-A	S-A	S-A	63	Gaylord
45672	University	2001	M-71	430	51	90	S-A	S-A	S-A	S-A	S-A	S-A	S-A	S-A	S-A	S-A	S-A	63	Flint

A.1.2 HMA Layer inputs

Table A-2 HMA top layer inputs for non-freeway projects

JN	HMA Top Thickness (in)	HMA Top Binder Type	HMA Top Aggregate Gradation	HMA Top Effective Binder Content	HMA Top Air Voids (as constructed)	HMA Top Percent Passing 3/4	HMA Top Percent Passing 3/8	HMA Top Percent Passing #4	HMA Top Percent Passing 200
34096	2.0	PG 64-28	4E3	11.4	6.7	100	90.1	67.0	6.1
59881	2.0	70-22p	4E10	10.0	6.5	100	85.7	65.7	4.9
58344	1.8	70-28P	4E3	11.0	6.3	100	85.2	68.8	6.0
59933	1.5	58-34	5E3	12.0	7.1	100	94.9	75.8	6.6
33263	1.5	58-34	5E1	11.9	6.7	100	96.8	76.6	5.5
60346	2.0	64-28	4E3	10.9	6.7	100	88.9	72.3	5.3
74862	1.5	70-28P	5E3	11.2	7.1	100	93.3	78.6	4.9
32341	1.5	70-28	5E3	11.6	7.1	100	93.4	67.7	4.8
52746	1.5	64-34	5E3	11.2	7.1	100	99.9	65.4	4.7
32303	1.5	200-250	13A	11.7	5.3	100	82.8	66.0	5.4
48270	1.5	64-28/70-28	5E3	11.2	7.1	100	93.3	83.8	6.1
46573	1.5	64-28	5E3	12.0	7.1	100	99.5	80.5	4.3
45707	1.5	70-22	5E3	11.0	6.5	100	96.7	59.1	4.7
45835	1.5	64-28	5E3	11.9	7.1	100	97.4	74.6	5.3
47064	2.0	70-22P	5E10	12.0	6.5	100	98.2	75.6	5.4
26620	1.0	85-100	1500T	10.4	7.0	100	86.0	53.4	5.2
31009	1.5	120-150	4B	11.1	5.9	100	89.0	60.1	5.0
44934	1.5	52-28	4C	11.3	5.4	100	80.9	57.8	4.8
45791	1.5	70-28	5E3	11.8	7.1	100	97.4	74.6	5.3
41124	2.0	64-28	5E3	11.9	7.1	100	97.4	74.6	5.3
6767	1.5	64-28	5E3	11.9	7.1	100	97.4	74.6	5.3
45441	1.5	58-28	4C	11.3	5.4	100	80.9	57.8	4.8

Table A-2 HMA top layer inputs for non-freeway projects (continued)

JN	HMA Top Thickness (in)	HMA Top Binder Type	HMA Top Aggregate Gradation	HMA Top Effective Binder Content	HMA Top Air Voids (as constructed)	HMA Top Percent Passing 3/4	HMA Top Percent Passing 3/8	HMA Top Percent Passing #4	HMA Top Percent Passing 200
38178	1.5	58-28	4E10	10.0	6.5	100	85.7	65.7	4.9
45642	1.5	64-28	5E3	11.9	7.1	100	97.4	74.6	5.3
55181	1.6	70-28P	5E3	11.9	7.1	100	97.4	74.6	5.3
48547	2.0	64-28	4E3	11.0	6.7	100	97.4	74.6	5.3
46031	1.5	70-28	5E3	11.7	6.3	100	99.8	77.6	4.9
49037	1.5	64-28	5E3	11.0	8.8	100	97.4	74.6	5.3
53767	1.5	70-28P	5E3	11.9	7.1	100	97.4	74.6	5.3
50617	1.5	64-28	5E3	12.0	7.1	100	97.2	76.5	6.0
50530	1.5	58-22	5E1	12.2	6.7	100	99.1	64.3	5.0
45594	1.5	64-28	5E1	12.2	6.4	100	98.8	79.5	5.4
45857	1.5	70-28P	5E3	12.0	8.3	100	98.2	77.9	5.5
75176	1.5	58-28	5E1	11.9	6.7	100	96.8	76.6	5.5
32331	1.7	58-28	5E3	11.9	7.1	100	97.4	74.6	5.3
38464	1.5	58-28	4B	11.1	5.9	100	89.0	60.1	5.0
36171	1.5	58-28	4B	11.5	5.6	100	91.8	64.2	3.1
36170	1.4	AC-5	4B	11.1	6.0	100	94.3	67.3	3.9
34039	1.2	85-100	4B	10.7	7.1	100	90.0	51.3	6.0
36190	1.5	120-150	13A	11.7	5.3	100	82.8	66.0	5.4
35139	1.3	120-150	4B	11.1	5.9	100	89.0	60.1	5.0
27576	1.3	120-150	1100	12.0	7.0	100	88.7	62.5	6.9
50768	1.5	64-28	5E3	11.7	6.3	100	97.4	66.5	4.7
79903	1.5	52-34	5E1	12.4	7.5	100	95.4	75.4	4.5
45009	1.5	58-28	5E1	12.4	7.1	100	93.5	75.2	5.1
55775	1.5	64-34P	5E3	11.6	7.1	100	93.6	77.0	5.1
60292	1.5	58-34	5E1	11.9	6.7	100	96.8	76.6	5.5

Table A-2 HMA top layer inputs for non-freeway projects (continued)

JN	HMA Top Thickness (in)	HMA Top Binder Type	HMA Top Aggregate Gradation	HMA Top Effective Binder Content	HMA Top Air Voids (as constructed)	HMA Top Percent Passing 3/4	HMA Top Percent Passing 3/8	HMA Top Percent Passing #4	HMA Top Percent Passing 200
80158	1.5	58-34	5E3	11.9	7.1	100	97.4	74.6	5.3
53244	1.5	58-34	5E1	11.9	6.7	100	95.2	73.7	5.2
45798	1.5	64-28	5E3	12.2	7.1	100	99.9	75.0	4.6
51598	2.0	64-28	4E3	13.2	6.7	100	99.2	70.6	4.7
50933	1.5	58-34	5E1	11.7	6.7	100	99.4	83.0	6.0
50719	1.5	58-28	5E1 5E3	11.6	7.0	100	91.6	75.0	6.0
31328	1.5	70-28	5E3	12.4	5.8	100	98.2	64.6	5.1
45641	1.5	70-28	5E3	12.4	7.1	100	99.3	76.9	4.2
26668	1.0	120-150	4B	10.6	5.9	100	89.8	64.7	6.2
31050	1.5	85-100	4B	11.1	5.9	100	89.0	60.1	5.0
31045	1.5	120-150	4B	11.1	5.9	100	89.0	60.1	5.0
49401	1.5	70-22	5E3	11.9	7.1	100	97.4	74.6	5.3
52745	1.5	64-34P	5E3	11.8	7.0	100	99.3	77.2	6.8
46565	1.5	70-28	5E3	12.4	7.3	100	98.4	82.2	5.3
21218	1.3	120-150	1100T 20AA	12.0	7.0	100	88.7	62.5	6.9
45672	1.5	58-28	5E3	11.9	7.1	100	97.4	74.6	5.3

Table A-3 HMA leveling layer inputs for non-freeway projects

JN	HMA Leveling Thickness (in)	HMA Leveling Binder Type	HMA Leveling Aggregate Gradation	HMA Leveling Effective Binder Content	HMA Leveling Air Voids (as constructed)	HMA Leveling Percent Passing 3/4	HMA Leveling Percent Passing 3/8	HMA Leveling Percent Passing #4	HMA Leveling Percent Passing 200
34096	3.8	PG 58-28	3E3	10.6	6.6	100	78.7	46.8	3.7
59881	2.5	70-22p	4E10	10.6	6.5	100	87.5	58.6	4.9
58344	2.5	70-28P	4E3	11.0	6.7	100	85.2	68.8	6.0
59933	4.0	58-34	4E3	10.2	6.7	100	83.4	66.4	5.9
33263	2.0	58-34	4E1	11.0	6.8	100	86.8	68.0	4.8
60346	2.0	64-28	4E3	10.9	6.7	100	88.9	72.3	5.3
74862	2.0	70-28P	4E3	10.9	6.7	100	89.7	75.0	5.0
32341	2.3	70-28	4E3	11.2	6.7	100	89.4	52.3	3.5
52746	2.0	64-34	4E3	10.0	6.7	100	88.5	59.9	5.6
32303	1.5	200-250	13A	11.7	5.3	100	83.6	66.4	5.5
48270	2.0	64-28/70-28	4E3	10.0	6.7	100	86.4	66.9	4.1
46573	2.0	64-28	4E3	11.2	6.7	100	89.4	52.3	3.5
45707	2.0	70-22	4E3	10.1	6.2	100	83.4	45.7	4.3
45835	2.0	64-28	4E3	10.9	6.7	100	87.7	88.9	4.9
47064	2.5	70-22P	4E10	10.6	6.5	100	87.5	58.6	4.9
26620	1.5	85-100	1500L	11.4	7.0	100	85.0	56.1	5.5
31009	1.5	120-150	3B	9.9	5.7	100	69.9	46.2	4.7
44934	2.0	52-28	3C	10.9	5.5	100	72.0	49.7	5.1
45791	2.5	70-28	4E3	10.9	6.7	100	87.7	88.9	4.9
41124	3.0	64-28	4E3	10.9	6.7	100	87.7	88.9	4.9
6767	1.5	64-28	4E3	10.9	6.7	100	87.7	88.9	4.9
45441	2.0	58-28	3C	10.9	5.5	100	72.0	49.7	5.1
38178	2.0	58-28	3E10	8.2	6.4	99	75.2	47.0	4.7
45642	2.0	64-28	4E3	10.9	6.7	100	87.7	88.9	4.9

Table A-3 HMA leveling layer inputs for non-freeway projects (continued)

JN	HMA Leveling Thickness (in)	HMA Leveling Binder Type	HMA Leveling Aggregate Gradation	HMA Leveling Effective Binder Content	HMA Leveling Air Voids (as constructed)	HMA Leveling Percent Passing 3/4	HMA Leveling Percent Passing 3/8	HMA Leveling Percent Passing #4	HMA Leveling Percent Passing 200
55181	2.0	70-28P	4E3	10.9	6.7	100	87.7	88.9	4.9
48547	3.0	64-28	3E3	10.6	6.6	100	78.7	46.8	3.7
46031	2.0	70-28	4E3	11.5	6.2	100	90.4	73.4	5.9
49037	2.0	64-28	4E3	10.6	7.1	100	79.4	60.2	4.1
53767	2.0	70-28P	4E3	10.9	6.7	100	87.7	88.9	4.9
50617	2.0	64-28	4E3	12.2	6.7	100	84.6	76.7	5.3
50530	2.0	58-22	4E1	12.0	6.4	100	85.7	51.2	4.1
45594	2.0	64-28	4E1	11.0	6.8	100	88.4	72.7	5.8
45857	2.0	70-28P	4E3	11.0	6.7	100	86.3	711.0	5.1
75176	2.0	58-28	4E1	11.0	6.8	100	86.8	68.0	4.8
32331	2.3	58-28	3E3	10.6	6.6	100	78.7	46.8	3.7
38464	2.5	58-28	3B	9.9	5.7	100	69.9	46.2	4.7
36171	3.5	58-28	3B	9.7	6.3	100	71.9	38.4	4.1
36170	1.5	120-150	3B	9.9	6.5	100	75.4	41.6	5.7
34039	1.5	85-100	3B	9.7	6.8	100	35.4	24.6	3.7
36190	1.5	120-150	13A	11.7	5.3	100	83.6	66.4	5.5
35139	1.7	120-150	3B	9.9	5.7	100	69.9	46.2	4.7
27576	1.2	120-150	1100	11.2	7.0	100	88.7	62.5	6.9
50768	2.0	64-28	4E3	11.1	6.7	100	88.5	56.5	4.5
79903	2.0	52-34	4E1	11.9	8.1	100	88.1	69.4	4.4
45009	2.0	58-28	4E 1	10.5	6.1	100	86.8	68.1	4.6
55775	2.0	64-34P	4E3	10.2	6.7	100	89.9	68.0	5.3
60292	2.0	58-34	4E1	11.0	6.8	100	86.8	68.0	4.8
80158	3.0	58-34	3E3	10.9	6.6	100	78.7	46.8	3.7
53244	2.0	58-34	4E1	11.2	6.8	100	86.3	68.2	4.5

Table A-3 HMA leveling layer inputs for non-freeway projects (continued)

JN	HMA Leveling Thickness (in)	HMA Leveling Binder Type	HMA Leveling Aggregate Gradation	HMA Leveling Effective Binder Content	HMA Leveling Air Voids (as constructed)	HMA Leveling Percent Passing 3/4	HMA Leveling Percent Passing 3/8	HMA Leveling Percent Passing #4	HMA Leveling Percent Passing 200
45798	2.0	64-28	4E3	11.0	6.7	100	89.9	52.5	4.5
51598	2.0	64-28	4E3	13.2	6.7	100	99.2	70.6	4.7
50933	2.5	58-34	4E1	10.2	5.9	100	89.7	72.5	4.7
50719	2.0	58-28	4E1	10.8	6.8	100	79.6	67.2	5.5
31328	2.0	70-28	4E3	11.4	6.0	100	86.9	46.1	4.0
45641	2.0	70-28	4E3	11.8	6.7	100	88.2	57.0	5.2
26668	1.5	120-150	3B	9.1	5.7	100	75.0	50.8	5.2
31050	1.5	85-100	3B	9.9	5.7	100	69.9	46.2	4.7
31045	4.0	120-150	3B	9.9	5.7	100	69.9	46.2	4.7
49401	2.0	70-22	4E3	10.9	6.7	100	87.7	88.9	4.9
52745	2.0	64-34P	4E3	9.8	6.7	100	88.1	70.3	5.6
46565	2.0	70-28	4E3	10.6	7.7	100	89.4	80.9	4.0
21218	1.3	120-150	1100L 20AA	11.2	7.0	100	88.7	62.5	6.9
45672	2.0	58-28	4E3	10.9	6.7	100	87.7	88.9	4.9

Table A-4 HMA base layer inputs for non-freeway projects

JN	HMA Base Thickness (in)	HMA Base Binder Type	HMA Base Aggregate Gradation	HMA Base Effective Binder Content	HMA Base Air Voids (as constructed)	HMA Base Mixture Percent Passing 3/4	HMA Base Mixture Percent Passing 3/8	HMA Base Mixture Percent Passing #4	HMA Base Mixture Percent Passing 200
34096	5.0	58-28	2E3	9.7	7.4	89.9	71.6	58.3	4.6
59881	4.0	58-28	3E10	10.1	6.4	99.4	75.2	47.0	4.7
58344	-	-	-	-	-	-	-	-	-
59933	-	-	-	-	-	-	-	-	-
33263	2.0	58-28	4E1	10.4	6.8	100.0	86.8	68.0	4.8
60346	3.0	58-28	3E3	10.3	6.6	100.0	84.7	65.3	4.8
74862	3.0	58-28	3E3	10.5	6.6	100.0	81.6	59.9	4.3
32341	3.0	58-22	3E3	9.6	6.6	100.0	83.7	63.3	3.8
52746	3.0	58-28	3E3	10.0	6.6	100.0	88.5	59.9	5.6
32303	-	-	-		-	-	-	-	-
48270	3.0	58-22	3E3	9.6	6.6	100.0	71.8	65.5	4.4
46573	3.0	58-22	3E3	9.6	6.6	100.0	83.7	63.3	3.8
45707	3.8	64-22	3E3	9.9	5.1	99.2	73.9	38.3	4.2
45835	5.5	58-28	2E3	9.7	7.4	89.9	71.6	58.3	4.6
47064	4.0	58-22	3E10	10.1	6.4	99.4	75.2	47.0	4.7
26620	4.0	85-100	700	9.2	7.0	71.4	52.5	45.2	4.1
31009	-	-	-	-	-	-	-	-	-
44934	3.0	52-28	3C	10.9	5.5	100.0	72.0	49.7	5.1
45791	-	-	-	-	-	-	-	-	-
41124	4.0	58-28	3E3	9.4	6.6	99.7	79.7	58.0	4.5
6767	2.5	58-28	3E3	9.4	6.6	99.7	79.7	58.0	4.5
45441	2.0	58-28	2C	9.6	5.7	87.1	55.5	41.4	6.0
38178	3.0	58-28	2E10	9.0	7.0	89.9	71.6	58.3	4.6
45642	3.0	58-22	3E3	9.4	6.6	99.7	79.7	58.0	4.5

Table A-4 HMA base layer inputs for non-freeway projects (continued)

JN	HMA Base Thickness (in)	HMA Base Binder Type	HMA Base Aggregate Gradation	HMA Base Effective Binder Content	HMA Base Air Voids (as constructed)	HMA Base Mixture Percent Passing 3/4	HMA Base Mixture Percent Passing 3/8	HMA Base Mixture Percent Passing #4	HMA Base Mixture Percent Passing 200
55181	3.0	58-28	3E3	9.4	6.6	99.7	79.7	58.0	4.5
48547	4.0	58-22	2E3	9.7	7.4	89.9	71.6	58.3	4.6
46031	2.0	58-22	4E3	11.5	6.2	100.0	90.4	73.4	5.9
49037	2.0	64-28	4E3	10.6	6.7	100.0	79.4	60.2	4.1
53767	3.0	58-22	3E3	9.4	6.6	99.7	79.7	58.0	4.5
50617	3.0	58-22	3E3	11.6	6.6	97.4	77.1	65.8	4.5
50530	3.5	58-22	3E1	11.4	6.5	100.0	59.9	37.9	4.0
45594	3.0	58-22	3E1	11.2	7.1	99.9	76.3	45.4	4.3
45857	2.0	58-22	4E3	11.8	6.7	100.0	86.3	71.1	5.1
75176	3.0	58-22	3E1	11.0	6.5	100.0	71.4	48.3	4.5
32331	-	-	-	-	-	-	-	-	-
38464	-	-	-	-	-	-	-	-	-
36171	-	-	-	-	-	-	-	-	-
36170	2.0	120-150	3B	9.9	6.5	99.7	75.4	41.6	5.7
34039	3.0	85-100	3B	9.7	6.8	99.6	35.4	24.6	3.7
36190	1.5	120-150	13A	11.7	5.3	100.0	83.6	66.4	5.5
35139	3.5	120-150	11A	10.8	7.0	100.0	77.1	62.1	5.8
27576	-	-	-	-	-	-	-	-	-
50768	3.0	58-22	3E3	10.4	6.6	100.0	82.4	64.0	4.6
79903	-	-	-	-	-	-	-	-	-
45009	-	-	-	-	-	-	-	-	-
55775	3.0	58-28	3E3	9.8	6.6	100.0	76.8	59.5	3.4
60292	-	58-34	4E1	10.4	6.8	100.0	86.8	68.0	4.8
80158	-	-	-	-	-	-	-	-	-
53244	-	-	-	-	-	-	-	-	-

Table A-4 HMA base layer inputs for non-freeway projects (continued)

JN	HMA Base Thickness (in)	HMA Base Binder Type	HMA Base Aggregate Gradation	HMA Base Effective Binder Content	HMA Base Air Voids (as constructed)	HMA Base Mixture Percent Passing 3/4	HMA Base Mixture Percent Passing 3/8	HMA Base Mixture Percent Passing #4	HMA Base Mixture Percent Passing 200
45798	3.0	58-22	3E3	10.2	6.6	98.3	85.7	74.0	4.1
51598	3.0	58-22	3E3	10.8	6.6	99.8	72.6	36.6	4.7
50933	-	-	-	-	-	-	-	-	-
50719	3.0	58-28	3E1	10.4	6.5	100.0	77.9	61.6	5.1
31328	3.0	58-22	3E3	10.3	5.8	100.0	74.8	37.6	4.7
45641	3.0	58-22	3E3	11.4	6.6	100.0	72.3	51.1	5.2
26668	3.0	120-150	11A	10.8	7.0	100.0	77.1	62.1	5.8
31050	8.9	85-100	11A	10.8	7.0	100.0	77.1	62.1	5.8
31045	-	-	-	-	-	-	-	-	-
49401	4.0	58-28	3E3	9.4	6.6	99.7	79.7	58.0	4.5
52745	3.0	58-28	3E3	9.6	5.8	100.0	89.3	58.6	5.4
46565	4.5	58-22	2E3	9.6	7.4	89.8	73.5	59.1	4.8
21218	2.0	120-150	500 20C	10.8	7.0	100.0	77.1	62.1	5.8
45672	6.0	58-28	2E3	9.7	7.4	89.9	71.6	58.3	4.6

A.1.3 Aggregate Base and Subgrade Soil Inputs

Table A-5 Aggregate base, subbase and subgrade material inputs for HMA non-freeway projects

JN	Aggregate Base Thickness (in)	Aggregate Base Material type	Aggregate Base Resilient Modulus (psi)	Aggregate Subbase Thickness (in)	Aggregate Subbase Material type	Aggregate Subbase Modulus (psi)	Subgrade Material type	Subgrade Resilient Modulus (psi) (backcalc- Baladi project)	Subgrade Resilient Modulus (psi) (Design- Baladi project)	Subgrade Resilient Modulus (psi) (Inflated design value)	AASHTO
34096	6.3	Crushed Gravel	33000	12	A-3 Sand Subbase	20000	SP-SM	20400	7000	10448	A-2-4, A-4
59881	6.0	Crushed Gravel	33000	18	A-3 Sand Subbase	20000	CL	15176	4400	10476	A-4, A-6, A-7-6
58344	6.0	Crushed Gravel	33000	12	A-3 Sand Subbase	20000	SP-1	27739	7000	10294	A-1-a, A-3
59933	8.0	Crushed Gravel	33000	18	A-3 Sand Subbase	20000	ML	15976	4400	12941	A-4
33263	8.0	Crushed Gravel	33000	18	A-3 Sand Subbase	20000	CL	15176	4400	10476	A-4, A-6, A-7-6
60346	6.0	Crushed Gravel	33000	14	A-3 Sand Subbase	20000	SP-1	27739	7000	10294	A-1-a, A-3
74862	6.0	Crushed Gravel	33000	18	A-3 Sand Subbase	20000	SC-SM	20314	5000	11905	A-2-6, A-6, A-7-6
32341	6.0	Crushed Gravel	33000	18	A-3 Sand Subbase	20000	SP-1	27739	7000	10294	A-1-a, A-3
52746	6.0	Crushed Gravel	33000	18	A-3 Sand Subbase	20000	SM	24764	5200	7429	A-2-4, A-4
32303	6.0	Crushed Gravel	33000	20	A-3 Sand Subbase	20000	SM	24764	5200	7429	A-2-4, A-4
48270	6.0	Crushed Gravel	33000	18	A-3 Sand Subbase	20000	SC	21647	4400	10476	A-4, A-6, A-7-6
46573	6.0	Crushed Gravel	33000	14	A-3 Sand Subbase	20000	SC	21647	4400	10476	A-4, A-6, A-7-6
45707	6.0	Crushed Gravel	33000	18	A-3 Sand Subbase	20000	CL	15176	4400	10476	A-4, A-6, A-7-6
45835	8.0	Crushed Gravel	33000	12	A-3 Sand Subbase	20000	SP-1	27739	7000	10294	A-1-a, A-3
47064	6.0	Crushed Gravel	33000	18	A-3 Sand Subbase	20000	CL	15176	4400	10476	A-4, A-6, A-7-6
26620	6.0	Crushed Gravel	33000	15	A-3 Sand Subbase	20000	CL	15176	4400	10476	A-4, A-6, A-7-6
31009	8.0	Crushed Gravel	33000	12	A-3 Sand Subbase	20000	SP-2	25113	6500	10000	A-1-b, A-2-4, A-3
44934	8.0	Crushed Gravel	33000	18	A-3 Sand Subbase	20000	SM	24764	5200	7429	A-2-4, A-4
45791	6.0	Crushed Gravel	33000	18	A-3 Sand Subbase	20000	SP-1	27739	7000	10294	A-1-a, A-3
41124	6.0	Crushed Gravel	33000	15	A-3 Sand Subbase	20000	SP-1	27739	7000	10294	A-1-a, A-3
6767	6.0	Crushed Gravel	33000	18	A-3 Sand Subbase	20000	SP-SM	20400	7000	10448	A-2-4, A-4
45441	4.0	Crushed Gravel	33000	12	A-3 Sand Subbase	20000	SC	21647	4400	10476	A-4, A-6, A-7-6

Table A-5 Aggregate base, subbase and subgrade material inputs for HMA non-freeway projects (continued)

JN	Aggregate Base Thickness (in)	Aggregate Base Material type	Aggregate Base Resilient Modulus (psi)	Aggregate Subbase Thickness (in)	Aggregate Subbase Material type	Aggregate Subbase Modulus (psi)	Subgrade Material type	Subgrade Resilient Modulus (psi) (backcalc- Baladi project)	Subgrade Resilient Modulus (psi) (Design- Baladi project)	Subgrade Resilient Modulus (psi) (Inflated design value)	AASHTO
38178	9.0	Crushed Gravel	33000	12	A-3 Sand Subbase	20000	SP-1	27739	7000	10294	A-1-a, A-3
45642	6.0	Crushed Gravel	33000	18	A-3 Sand Subbase	20000	SC	21647	4400	10476	A-4, A-6, A-7-6
55181	6.0	Crushed Gravel	33000	18	A-3 Sand Subbase	20000	SP-1	27739	7000	10294	A-1-a, A-3
48547	6.0	Crushed Gravel	33000	-	-	-	SM	24764	5200	7429	A-2-4, A-4
46031	6.0	Crushed Gravel	33000	18	A-3 Sand Subbase	20000	SM	24764	5200	7429	A-2-4, A-4
49037	6.0	Crushed Gravel	33000	18	A-3 Sand Subbase	20000	SC-SM	20314	5000	11905	A-2-6, A-6, A-7-6
53767	6.0	Crushed Gravel	33000	-	-	-	SP-1	27739	7000	10294	A-1-a, A-3
50617	6.0	Crushed Gravel	33000	18	A-3 Sand Subbase	20000	SC	21647	4400	10476	A-4, A-6, A-7-6
50530	6.0	Crushed Gravel	33000	18	A-3 Sand Subbase	20000	CL	15176	4400	10476	A-4, A-6, A-7-6
45594	6.0	Crushed Gravel	33000	18	A-3 Sand Subbase	20000	SC	21647	4400	10476	A-4, A-6, A-7-6
45857	6.0	Crushed Gravel	33000	18	A-3 Sand Subbase	20000	SM	24764	5200	7429	A-2-4, A-4
75176	6.0	Crushed Gravel	33000	18	A-3 Sand Subbase	20000	SM	24764	5200	7429	A-2-4, A-4
32331	4.0	Crushed Gravel	33000	12	A-3 Sand Subbase	20000	SP-1	27739	7000	10294	A-1-a, A-3
38464	6.0	Crushed Gravel	33000	4	A-3 Sand Subbase	20000	SM	24764	5200	7429	A-2-4, A-4
36171	6.0	Crushed Gravel	33000	18	A-3 Sand Subbase	20000	CL	15176	4400	10476	A-4, A-6, A-7-6
36170	6.0	Crushed Gravel	33000	18	A-3 Sand Subbase	20000	SC	21647	4400	10476	A-4, A-6, A-7-6
34039	6.0	Crushed Gravel	33000	12	A-3 Sand Subbase	20000	SM	24764	5200	7429	A-2-4, A-4
36190	6.0	Crushed Gravel	33000	18	A-3 Sand Subbase	20000	SP-SM	20400	7000	10448	A-2-4, A-4
35139	8.0	Crushed Gravel	33000	18	A-3 Sand Subbase	20000	CL	15176	4400	10476	A-4, A-6, A-7-6
27576	6.0	Crushed Gravel	33000	18	A-3 Sand Subbase	20000				#N/A	#N/A
50768	6.0	Crushed Gravel	33000	18	A-3 Sand Subbase	20000	SP-1	27739	7000	10294	A-1-a, A-3
79903	8.0	Crushed Gravel	33000	12	A-3 Sand Subbase	20000	CL	15176	4400	10476	A-4, A-6, A-7-6
45009	8.0	Crushed Gravel	33000	18	A-3 Sand Subbase	20000	SM	24764	5200	7429	A-2-4, A-4
55775	6.0	Crushed Gravel	33000	18	A-3 Sand Subbase	20000	SM	24764	5200	7429	A-2-4, A-4
60292	8.0	Crushed Gravel	33000	18	A-3 Sand Subbase	20000	SM	24764	5200	7429	A-2-4, A-4
80158	8.0	Crushed Gravel	33000	18	A-3 Sand Subbase	20000	ML	15976	4400	12941	A-4

Table A-5 Aggregate base, subbase and subgrade material inputs for HMA non-freeway projects (continued)

JN	Aggregate Base Thickness (in)	Aggregate Base Material type	Aggregate Base Resilient Modulus (psi)	Aggregate Subbase Thickness (in)	Aggregate Subbase Material type	Aggregate Subbase Modulus (psi)	Subgrade Material type	Subgrade Resilient Modulus (psi) (backcalc- Baladi project)	Subgrade Resilient Modulus (psi) (Design- Baladi project)	Subgrade Resilient Modulus (psi) (Inflated design value)	AASHTO
53244	8.0	Crushed Gravel	33000	18	A-3 Sand Subbase	20000	CL	15176	4400	10476	A-4, A-6, A-7-6
45798	6.0	Crushed Gravel	33000	18	A-3 Sand Subbase	20000	SP-SM	20400	7000	10448	A-2-4, A-4
51598	6.0	Crushed Gravel	33000	18	A-3 Sand Subbase	20000	SC-SM	20314	5000	11905	A-2-6, A-6, A-7-6
50933	8.0	Crushed Gravel	33000	12	A-3 Sand Subbase	20000	SP-SM	20400	7000	10448	A-2-4, A-4
50719	8.0	Crushed Gravel	33000	12	A-3 Sand Subbase	20000	SC-SM	20314	5000	11905	A-2-6, A-6, A-7-6
31328	6.0	Crushed Gravel	33000	18	A-3 Sand Subbase	20000	SC	21647	4400	10476	A-4, A-6, A-7-6
45641	6.0	Crushed Gravel	33000	18	A-3 Sand Subbase	20000	SC	21647	4400	10476	A-4, A-6, A-7-6
26668	6.0	Crushed Gravel	33000	19	A-3 Sand Subbase	20000	SP-1	27739	7000	10294	A-1-a, A-3
31050	4.0	Crushed Gravel	33000	18	A-3 Sand Subbase	20000	SP-1	27739	7000	10294	A-1-a, A-3
31045	6.0	Crushed Gravel	33000	18	A-3 Sand Subbase	20000	SC-SM	20314	5000	11905	A-2-6, A-6, A-7-6
49401	6.0	Crushed Gravel	33000	18	A-3 Sand Subbase	20000	CL	15176	4400	10476	A-4, A-6, A-7-6
52745	6.0	Crushed Gravel	33000	18	A-3 Sand Subbase	20000	SM	24764	5200	7429	A-2-4, A-4
46565	6.0	Crushed Gravel	33000	18	A-3 Sand Subbase	20000	SM	24764	5200	7429	A-2-4, A-4
21218	4.0	Crushed Gravel	33000	18	A-3 Sand Subbase	20000	SP-1	27739	7000	10294	A-1-a, A-3
45672	6.0	Crushed Gravel	33000	12	A-3 Sand Subbase	20000	SM	24764	5200	7429	A-2-4, A-4

A.2 HMA FREEWAY PROJECT INPUTS

A.2.1 Inventory and Traffic Inputs

Table A-6 Inventory and traffic inputs for HMA freeway projects

JN	REGION	OPENED	Roadway	AADTT 2-Way MDOT Confirmed	Percent trucks in Design direction	Percent trucks in Design lane	MDOT TTC Cluster	HDF Cluster	ALS Tandem	MDF Cluster	AGPV Cluster Single	AGPV Cluster Tridem	AGPV Cluster Quad	ALS Single	ALS Tandem	ALS Tridem	ALS Quad	Initial IRI	Climate
33007	North	2000	US-131	959	51	90	3	2	3	S-A	S-A	S-A	S-A	S-A	S-A	S-A	S-A	55	Traverse city
34695	Grand	1997	M-37	1119	51	90	3	3	1	S-A	S-A	S-A	S-A	S-A	S-A	S-A	S-A	70	Grand Rapids
25745	Grand	1991	M-44	908	51	90	S-A	S-A	S-A	S-A	S-A	S-A	S-A	S-A	S-A	S-A	S-A	70	Grand Rapids
52803	Metro	2005	I-96	6745	51	90	1	3	4	S-A	S-A	S-A	S-A	S-A	S-A	S-A	S-A	76	Detroit
46273	Metro	2004	M-53	2065	51	90	3	3	3	S-A	S-A	S-A	S-A	S-A	S-A	S-A	S-A	50	Detroit
53932	Superior	2002	I-75	350	51	90	3	3	4	S-A	S-A	S-A	S-A	S-A	S-A	S-A	S-A	50	Pellston
47050	Metro	2001	BL-I-94	354	51	90	S-A	S-A	S-A	S-A	S-A	S-A	S-A	S-A	S-A	S-A	S-A	95	Pontiac
31804	Bay	2005	M-84	313	51	90	S-A	S-A	S-A	S-A	S-A	S-A	S-A	S-A	S-A	S-A	S-A	60	Flint
45693	Metro	2002	US-24	640	51	90	S-A	S-A	S-A	S-A	S-A	S-A	S-A	S-A	S-A	S-A	S-A	90	Detroit
47085	Metro	2002	I-375	1000	51	90	S-A	S-A	S-A	S-A	S-A	S-A	S-A	S-A	S-A	S-A	S-A	78	Detroit
34519	University	2004	US-23	5011	51	90	3	3	4	S-A	S-A	S-A	S-A	S-A	S-A	S-A	S-A	73	Ann Arbor
43893	Bay	2000	US-127	2034	51	90	3	2	3	S-A	S-A	S-A	S-A	S-A	S-A	S-A	S-A	48	Lansing
20046	University	1995	US-127	1220	51	90	3	2	3	S-A	S-A	S-A	S-A	S-A	S-A	S-A	S-A	40	Lansing
48388	Southwest	2000	M-66/I-194	367	51	90	3	2	5	S-A	S-A	S-A	S-A	S-A	S-A	S-A	S-A	75	Battle creek
47840	Grand	2001	M-45	819	51	90	S-A	S-A	S-A	S-A	S-A	S-A	S-A	S-A	S-A	S-A	S-A	65	Grand Rapids
26748	Metro	1998	US-12	1130	51	90	S-A	S-A	S-A	S-A	S-A	S-A	S-A	S-A	S-A	S-A	S-A	60	Detroit
34693	Grand	2001	M-37	1119	51	90	3	3	1	S-A	S-A	S-A	S-A	S-A	S-A	S-A	S-A	70	Grand Rapids
33008	North	2001	US-131	5722	51	90	1	3	3	S-A	S-A	S-A	S-A	S-A	S-A	S-A	S-A	45	Traverse City
34682/34683	North	2002	US-131	685	51	90	1	3	3	S-A	S-A	S-A	S-A	S-A	S-A	S-A	S-A	39	Traverse City
53326	Metro	2003	I-94	5106	51	90	1	3	4	S-A	S-A	S-A	S-A	S-A	S-A	S-A	S-A	72	Detroit
53508	Grand	2001	M-6	4315	51	90	3	2	5	S-A	S-A	S-A	S-A	S-A	S-A	S-A	S-A	62	Grand Rapids
29581	University	1994	I-96	4933	51	90	3	3	4	S-A	S-A	S-A	S-A	S-A	S-A	S-A	S-A	40	Lansing

A.2.2 HMA Layer Inputs

Table A-7 HMA top layer inputs for freeway projects

JN	HMA Top Thickness (in)	HMA Top Binder Type	HMA Top Aggregate Gradation	HMA Top Effective Binder Content	HMA Top Air Voids (as constructed)	HMA Top Percent Passing 3/4	HMA Top Percent Passing 3/8	HMA Top Percent Passing #4	HMA Top Percent Passing 200
33007	1.2	58-28	5E3	12.2	6.9	100	98.5	73.8	5.0
34695	1.5	85-100	4C	11.3	5.4	100	80.9	57.8	4.8
25745	1.5	85-100 (AC-10)	13 T	10.2	7.0	100	70.0	51.2	5.6
52803	1.5	76-22P	GGSP	12.8	8.4	100	73.5	31.9	8.5
46273	2.0	70-22P	4E30	12.2	6.5	100	85.8	52.8	4.3
53932	2.0	58-34	5E10	12.0	6.5	100	98.2	75.6	5.4
47050	2.0	64-22	4E3	11.4	6.7	100	90.1	67.0	6.1
31804	1.5	PG 70-28P	5E3	11.0	7.1	100	97.4	74.6	5.3
45693	2.0	PG 70-22P	5E10	13.0	6.5	100	99.7	60.8	4.5
47085	2.0	PG 70-28P	5E10	12.0	6.5	100	98.5	71.8	5.8
34519	2.0	PG 70-28P	4E30	12.2	6.5	100	85.8	52.8	4.3
43893	1.5	PG 64-28	5E10	11.6	5.9	100	99.8	80.4	5.3
20046	1.3	PEN 120-150	4C	11.2	5.4	100	86.8	51.7	4.6
48388	1.5	PG 70-22	5E10	12.5	6.5	100	100.0	55.0	4.3
47840	1.5	PG 64-28	5E3	12.0	7.1	100	97.4	74.6	5.3
26748	1.5	PEN 85-100	4C	11.3	6.3	100	84.4	65.0	5.3
34693	1.5	PG 70-22	5E10	12.0	6.5	100	98.2	75.6	5.4
33008	1.5	PG 58-28	5E3	12.0	7.1	100	97.4	74.6	5.3
34682/34683	1.5	PG 64-28	5E3	12.0	7.1	100	97.4	74.6	5.3
53326	2.0	PG 70-22	4E30	12.2	6.5	100	85.8	52.8	4.3
53508	2.0	PG 70-28	4E30	12.2	6.5	100	85.8	52.8	4.3
29581	1.3	PEN 85-100	4C	11.2	5.7	100	84.1	51.1	4.7

Table A-8 HMA leveling layer inputs for freeway projects

JN	HMA Top Thickness (in)	HMA Top Binder Type	HMA Top Aggregate Gradation	HMA Top Effective Binder Content	HMA Top Air Voids (as constructed)	HMA Top Percent Passing 3/4	HMA Top Percent Passing 3/8	HMA Top Percent Passing #4	HMA Top Percent Passing 200
33007	1.8	58-28	4E3	11.3	6.5	100.0	86.5	69.8	5.2
34695	1.5	85-100	3C	10.9	5.5	100.0	72.0	49.7	5.1
25745	1.5	85-100 (AC-10)	13L	10.8	7.0	100.0	77.1	62.1	5.8
52803	2.5	76-22P	4E30	11.6	6.5	100.0	87.1	66.6	5.3
46273	3.0	70-22P	3E30	10.0	6.7	98.9	83.9	66.6	4.3
53932	2.5	58-34	4E10	10.6	6.5	100.0	87.5	58.6	4.9
47050	3.0	64-22	3E3	10.6	6.6	100.0	78.7	46.8	3.7
31804	2.0	PG 70-28P	4E3	10.3	6.7	100.0	87.7	88.9	4.9
45693	2.5	PG 70-22P	4E10	11.6	6.5	100.0	87.0	57.1	4.6
47085	2.5	PG 70-28P	4E10	10.6	6.5	100.0	79.1	42.8	5.0
34519	2.5	PG 70-28P	4E30	12.2	6.5	100.0	85.8	52.8	4.3
43893	2.0	PG 64-28	4E10	9.8	5.7	100.0	80.0	36.9	3.9
20046	1.2	PEN 120-150	3C	10.8	5.5	100.0	72.7	44.8	5.2
48388	2.0	PG 70-22	4E10	11.0	6.5	100.0	92.9	43.5	5.0
47840	2.0	PG 64-28	4E3	10.9	6.7	100.0	87.7	88.9	4.9
26748	1.5	PEN 85-100	3C	10.8	6.0	100.0	65.7	48.2	5.7
34693	2.0	PG 70-22	4E10	10.6	6.5	100.0	87.5	58.6	4.9
33008	2.0	PG 58-28	4E3	10.9	6.7	100.0	87.7	88.9	4.9
34682/34683	2.0	PG 64-28	4E3	10.9	6.7	100.0	87.7	88.9	4.9
53326	3.0	PG 70-22	3E30	10.0	5.7	98.9	83.9	66.6	4.3
53508	2.9	PG 70-28	3E30	10.0	5.7	98.9	83.9	66.6	4.3
29581	2.0	PEN 85-100	3C	10.9	5.0	100.0	67.8	41.3	4.6

Table A-9 HMA base layer inputs for freeway projects

JN	HMA Top Thickness (in)	HMA Top Binder Type	HMA Top Aggregate Gradation	HMA Top Effective Binder Content	HMA Top Air Voids (as constructed)	HMA Top Percent Passing 3/4	HMA Top Percent Passing 3/8	HMA Top Percent Passing #4	HMA Top Percent Passing 200
33007	2.5	58-28	3E3	10.7	6.6	100.0	81.7	62.0	5.3
34695	6.0	85-100	2C	9.6	5.7	87.1	55.5	41.4	6.0
25745	5.0	85-100 (AC-10)	7	7.8	7.0	71.6	59.4	48.6	4.9
52803	10.0	70-22P	3E30	11.8	4.7	100.0	74.0	53.5	5.0
46273	5.9	64-22P	3E30	10.0	6.7	98.9	83.9	66.6	4.3
53932	3.5	58-28	3E10	10.1	6.4	99.4	75.2	47.0	4.7
47050	3.0	58-22	3E3	10.3	6.6	99.7	79.7	58.0	4.5
31804	3.0	PG 58-22	3E3	9.4	6.6	99.7	79.7	58.0	4.5
45693	4.0	PG 58-28P	3E10	10.4	6.4	100.0	77.1	43.8	5.3
47085	4.0	PG 58-22	3E10	9.6	6.4	99.9	67.3	37.1	5.0
34519	6.5	PG 64-22	3E30	12.2	5.7	99.9	74.5	55.2	5.9
43893	4.5	PG 58-28	3E10	10.5	6.8	98.1	65.0	26.7	3.5
20046	4.0	PEN 120-150	2C	9.3	5.7	86.3	55.6	39.8	4.7
48388	6.0	PG 58-28	3E10	9.1	6.4	100.0	77.1	41.0	4.4
47840	3.0	PG 58-28	3E3	10.3	6.6	99.7	79.7	58.0	4.5
26748	4.5	PEN 85-100	2C	10.1	5.8	88.2	58.0	45.7	8.2
34693	4.0	PG 58-28	3E10	10.1	6.4	99.4	75.2	47.0	4.7
33008	3.0	PG 58-28	3E3	10.3	6.6	99.7	79.7	58.0	4.5
34682/34683	3.0	PG 58-28	2E3	9.7	7.4	89.9	71.6	58.3	4.6
53326	7.0	PG 70-22	2E30	9.7	7.0	89.9	71.6	58.3	4.6
53508	5.9	PG 64-22	3E30	11.0	5.7	99.7	76.2	55.7	5.1
29581	5.0	PEN 85-100	2C	9.4	5.5	86.8	53.0	38.6	5.1

A.2.3 Aggregate Base and Subgrade Soil Inputs

Table A-10 Aggregate base, subbase and subgrade material inputs for HMA freeway projects

JN	Aggregate Base Thickness (in)	Aggregate Base Material type	Aggregate Base Resilient Modulus (psi)	Aggregate Subbase Thickness (in)	Aggregate Subbase Material type	Aggregate Subbase Modulus (psi)	Subgrade Material type	Subgrade Resilient Modulus (psi) (backcalc- Baladi project)	Subgrade Resilient Modulus (psi) (Design- Baladi project)	Subgrade Resilient Modulus (psi) (Inflated design value)	AASHTO
33007	6.0	Crushed Gravel	33000	18.0	Sand Subbase	20000	SP-1	27739	7000	10294.1	A-1-a, A-3
34695	6.0	Crushed Gravel	33000	18.0	Sand Subbase	20000	SP-1	27739	7000	10294.1	A-1-a, A-3
25745	4.0	Crushed Gravel	33000	21.0	Sand Subbase	20000	SP-1	27739	7000	10294.1	A-1-a, A-3
52803	16.0	Crushed Gravel	33000	8.0	Sand Subbase	20000	CL	15176	4400	10476.2	A-4, A-6, A-7-6
46273	6.3	Crushed Gravel	33000	18.1	Sand Subbase	20000	SP-1	27739	7000	10294.1	A-1-a, A-3
53932	7.9	Crushed Gravel	33000	21.0	Sand Subbase	20000	SP-1	27739	7000	10294.1	A-1-a, A-3
47050	4.0	Crushed Gravel	33000	18.1	Sand Subbase	20000	CL	15176	4400	10476.2	A-4, A-6, A-7-6
31804	6.3	Crushed Gravel	33000	18.1	Sand Subbase	20000	SC	21647	4400	10476.2	A-4, A-6, A-7-6
45693	6.3	Crushed Gravel	33000	18.1	Sand Subbase	20000	CL	15176	4400	10476.2	A-4, A-6, A-7-6
47085	10.2	Crushed Gravel	33000	14.0	Sand Subbase	20000	CL	15176	4400	10476.2	A-4, A-6, A-7-6
34519	6.0	Crushed Gravel	33000	18.0	Sand Subbase	20000	SC	21647	4400	10476.2	A-4, A-6, A-7-6
43893	6.3	Crushed Gravel	33000	18.1	Sand Subbase	20000	SC	21647	4400	10476.2	A-4, A-6, A-7-6
20046	4.0	Crushed Gravel	33000	24.0	Sand Subbase	20000	SC	21647	4400	10476.2	A-4, A-6, A-7-6
48388	7.9	Crushed Gravel	33000	15.0	Sand Subbase	20000	SP-1	27739	7000	10294.1	A-1-a, A-3
47840	6.3	Crushed Gravel	33000	17.7	Sand Subbase	20000	SP-SM	20400	7000	10447.8	A-2-4, A-4
26748	6.0	Crushed Gravel	33000	18.0	Sand Subbase	20000	CL	15176	4400	10476.2	A-4, A-6, A-7-6
34693	6.3	Crushed Gravel	33000	18.1	Sand Subbase	20000	SP-1	27739	7000	10294.1	A-1-a, A-3
33008	6.0	Crushed Gravel	33000	18.0	Sand Subbase	20000	SP-1	27739	7000	10294.1	A-1-a, A-3
34682/34683	6.3	Crushed Gravel	33000	18.1	Sand Subbase	20000	SP-1	27739	7000	10294.1	A-1-a, A-3
53326	6.3	Crushed Gravel	33000	18.1	Sand Subbase	20000	CL	15176	4400	10476.2	A-4, A-6, A-7-6
53508	5.9	Crushed Gravel	33000	17.7	Sand Subbase	20000	SP-1	27739	7000	10294.1	A-1-a, A-3
29581	4.0	Crushed Gravel	33000	14.0	Sand Subbase	20000	SC	21647	4400	10476.2	A-4, A-6, A-7-6

A.3 HMA CRUSH AND SHAPE Project Inputs

A.3.1 Inventory and Traffic Inputs

Table A-11 Inventory and traffic inputs for HMA crush and shape projects

JN	REGION	OPENED	Roadway	AADTT 2-Way MDOT Confirmed	Percent trucks in Design dir	Percent trucks in Design lane	MDOT TTC Cluster	HDF Cluster	ALS Tandem	MDF Cluster	AGPV Cluster Single	AGPV Cluster Tridem	AGPV Cluster Quad	ALS Single	ALS Tandem	ALS Tridem	ALS Quad	Initial IRI	Climate
28121	Grand	1993	US-131 NB	1986	51	90	3	3	3	S-A	S-A	S-A	S-A	S-A	S-A	S-A	S-A	42	Muskegon
30728	North	1994	I-75 NB	1111	51	90	3	3	4	S-A	S-A	S-A	S-A	S-A	S-A	S-A	S-A	40	Gaylord
32510	North	1997	I-75 NB	1208	51	90	3	3	4	S-A	S-A	S-A	S-A	S-A	S-A	S-A	S-A	40	Gaylord
34066	North	1997	I-75 NB	1431	51	90	3	3	4	S-A	S-A	S-A	S-A	S-A	S-A	S-A	S-A	40	Houghton Lake
44827	North	1997	I-75 NB	1730	51	90	3	3	4	S-A	S-A	S-A	S-A	S-A	S-A	S-A	S-A	40	Houghton Lake
50699	North	2004	US-131 NB	1757	51	90	3	3	3	S-A	S-A	S-A	S-A	S-A	S-A	S-A	S-A	42	Houghton Lake
29704	Superior	1999	M-203	216	51	90	S-A	S-A	S-A	S-A	S-A	S-A	S-A	S-A	S-A	S-A	S-A	70	Hancock
31085	Superior	1997	M-28	285	51	90	3	3	1	S-A	S-A	S-A	S-A	S-A	S-A	S-A	S-A	55	Pellston
32262	Superior	1992	M-26	161	51	90	2	2	1	S-A	S-A	S-A	S-A	S-A	S-A	S-A	S-A	60	Hancock
32310	North	1995	M-66	180	51	90	2	2	1	S-A	S-A	S-A	S-A	S-A	S-A	S-A	S-A	62	Traverse City
32327	North	1998	M-72	555	51	90	3	2	4	S-A	S-A	S-A	S-A	S-A	S-A	S-A	S-A	45	Gaylord
32337	North	2001	M-18	268.8	51	90	2	3	1	S-A	S-A	S-A	S-A	S-A	S-A	S-A	S-A	65	Houghton Lake
32340	Grand	1996	M-66	265	51	90	3	2	5	S-A	S-A	S-A	S-A	S-A	S-A	S-A	S-A	55	Grand Rapids
34038	Superior	1998	M-38	157	51	90	2	2	1	S-A	S-A	S-A	S-A	S-A	S-A	S-A	S-A	85	Hancock
34043	Superior	1997	M-95	203	51	90	3	2	3	S-A	S-A	S-A	S-A	S-A	S-A	S-A	S-A	55	Hancock
34045	Superior	1999	M-64	60	51	90	S-A	S-A	S-A	S-A	S-A	S-A	S-A	S-A	S-A	S-A	S-A	43	Hancock
34056	Superior	1998	M-117	203	51	90	3	3	1	S-A	S-A	S-A	S-A	S-A	S-A	S-A	S-A	55	Pellston
35983	Superior	1998	US-2	132	51	90	2	2	1	S-A	S-A	S-A	S-A	S-A	S-A	S-A	S-A	52	Hancock
36524	Superior	1995	M-77	74	51	90	S-A	S-A	S-A	S-A	S-A	S-A	S-A	S-A	S-A	S-A	S-A	43	Pellston
37910	North	1998	M-22	91	51	90	S-A	S-A	S-A	S-A	S-A	S-A	S-A	S-A	S-A	S-A	S-A	65	Traverse City
38007	Superior	1999	M-35	147	51	90	S-A	S-A	S-A	S-A	S-A	S-A	S-A	S-A	S-A	S-A	S-A	42	Iron Mountain
38019	Superior	2000	M-28	312	51	90	3	3	4	S-A	S-A	S-A	S-A	S-A	S-A	S-A	S-A	44	Pellston
38061	Superior	1996	M-64	191	51	90	S-A	S-A	S-A	S-A	S-A	S-A	S-A	S-A	S-A	S-A	S-A	35	Hancock

A.3.2 HMA Layer Inputs

Table A-12 HMA top layer inputs for crush and shape projects

JN	HMA Top Thickness (in)	HMA Top Binder Type	HMA Top Aggregate Gradation	HMA Top Effective Binder Content	HMA Top Air Voids (as constructed)	HMA Top Percent Passing 3/4	HMA Top Percent Passing 3/8	HMA Top Percent Passing #4	HMA Top Percent Passing 200
28121	1.5	85-100	3B	9.9	5.3	100.0	64.6	44.5	4.9
30728	1.5	AC-2.5	4B	11.6	5.3	100.0	89.8	64.0	5.0
32510	1.5	120-150	4C	11.3	5.4	100.0	80.9	57.8	4.8
34066	1.5	52-28	4B	11.2	6.0	100.0	85.8	57.8	4.4
44827	1.5	58-28	4B	10.7	5.9	100.0	82.6	54.1	4.3
50699	1.5	64-28	5E10	12.0	7.5	100.0	99.9	65.5	5.5
29704	1.5	52-28	4C	11.4	5.4	100.0	69.5	48.5	4.5
31085	1.5	52-28	4B	11.4	6.1	100.0	89.6	62.9	5.7
32262	1.0	120-150	4B	10.6	5.9	100.0	85.4	45.7	6.3
32310	1.3	AC-5	13A	11.8	5.3	100.0	79.2	62.0	5.8
32327	1.4	58-28	4B	11.2	5.9	100.0	88.3	60.6	4.1
32337	1.5	64-28	4C	11.2	5.4	100.0	85.7	66.7	4.8
32340	1.5	AC-5	13A	11.8	5.7	100.0	88.9	78.6	5.0
34038	1.5	52-28	4B	11.4	5.9	100.0	86.5	63.3	5.8
34043	1.3	120-150	4B	11.1	5.9	100.0	89.0	60.1	5.0
34045	1.3	58-28	13A	12.6	4.4	100.0	79.2	63.8	4.8
34056	1.5	52-28	4E3	10.6	6.4	100.0	86.9	56.3	8.3
35983	1.5	52-28	13A	10.5	5.0	100.0	83.8	59.5	5.8
36524	2.5	AC 2.5	4B	10.8	5.4	100.0	94.5	65.8	5.1
37910	1.5	58-28	5E3	12.7	7.8	100.0	98.6	72.5	4.4
38007	1.5	52-28	4E1	10.8	6.8	100.0	85.8	71.4	5.4
38019	1.5	58-28	5E1	10.6	6.7	100.0	96.8	76.6	5.5
38061	1.5	200-250	13A	11.7	5.3	100.0	82.8	66.0	5.4

Table A-13 HMA leveling layer inputs for crush and shape projects

JN	HMA Leveling Thickness (in)	HMA Leveling Binder Type	HMA Leveling Aggregate Gradation	HMA Leveling Effective Binder Content	HMA Leveling Air Voids (as constructed)	HMA Leveling Percent Passing 3/4	HMA Leveling Percent Passing 3/8	HMA Leveling Percent Passing #4	HMA Leveling Percent Passing 200
28121	1.5	AC-10	3B	9.5	5.3	100.0	77.1	53.9	4.6
30728	1.5	AC-2.5	3B	9.4	5.9	100.0	71.8	50.4	4.6
32510	2.0	120-150	3C	10.9	5.5	100.0	72.0	49.7	5.1
34066	2.0	52-28	3B	10.2	5.7	100.0	77.1	51.6	4.0
44827	2.0	58-28	3B	10.3	5.7	100.0	72.1	47.8	4.6
50699	2.0	64-28	4E10	9.6	7.8	100.0	94.3	79.0	6.1
29704	2.0	52-28	3C	12.0	5.5	100.0	83.7	59.8	5.8
31085	2.0	52-28	3B	9.5	5.5	100.0	80.0	52.0	6.1
32262	1.5	120-150	3B	10.6	5.7	100.0	53.4	35.9	4.8
32310	1.3	AC-5	13A	11.8	5.3	100.0	82.4	63.6	6.5
32327	1.6	58-28	3B	10.0	5.7	100.0	78.9	53.0	4.2
32337	2.0	58-28	3C	10.2	5.5	100.0	70.4	54.4	4.3
32340	1.5	AC-5	13A	11.8	5.7	100.0	88.9	78.6	5.0
34038	2.0	52-28	3B	10.8	5.7	100.0	71.1	54.0	5.3
34043	1.5	120-150	3B	9.9	5.7	99.9	69.9	46.2	4.7
34045	2.0	58-28	13A	12.6	5.7	100.0	79.2	63.8	4.8
34056	1.7	52-28	3E3	10.6	6.6	100.0	78.7	46.8	3.7
35983	1.5	52-28	13A	10.5	5.0	100.0	83.8	59.5	5.8
36524	-	-	-	0.0					
37910	2.0	58-28	3E3	10.6	8.2	100.0	78.7	46.8	3.7
38007	2.5	52-28	3E1	11.0	6.5	100.0	71.4	48.3	4.5
38019	2.5	58-28	4E1	11.0	6.8	100.0	86.8	68.0	4.8
38061	1.5	200-250	13A	11.7	5.3	100.0	83.6	66.4	5.5

Table A-14 HMA base layer inputs for crush and shape projects

JN	HMA Base Thickness (in)	HMA Base Binder Type	HMA Base Aggregate Gradation	HMA Base Effective Binder Content	HMA Base Air Voids (as constructed)	HMA Base Mixture Percent Passing 3/4	HMA Base Mixture Percent Passing 3/8	HMA Base Mixture Percent Passing #4	HMA Base Mixture Percent Passing 200
28121	1.5	AC-10	3B	9.5	5.3	100.0	77.1	53.9	4.6
30728	-	-	-			-	-	-	-
32510	-	-	-			-	-	-	-
34066	-	-	-			-	-	-	-
44827	-	-	-			-	-	-	-
50699	-	-	-			-	-	-	-
29704	-	-	-			-	-	-	-
31085	-	-	-			-	-	-	-
32262	-	-	-			-	-	-	-
32310	-	-	-			-	-	-	-
32327	-	-	-			-	-	-	-
32337	-	-	-			-	-	-	-
32340	-	-	-			-	-	-	-
34038	-	-	-			-	-	-	-
34043	-	-	-			-	-	-	-
34045	-	-	-			-	-	-	-
34056	-	-	-			-	-	-	-
35983	-	-	-			-	-	-	-
36524	-	-	-			-	-	-	-
37910	-	-	-			-	-	-	-
38007	-	-	-			-	-	-	-
38019	-	-	-			-	-	-	-
38061	-	-	-			-	-	-	-

A.3.3 Aggregate Base and Subgrade Soil Inputs

Table A-15 Aggregate base, subbase and subgrade material inputs for HMA crush and shape projects

JN	HMA Crushed Layer Thickness	HMA Crushed Layer Modulus	Aggregate Base Thickness (in)	Aggregate Base Material type	Aggregate Base Resilient Modulus (psi)	Aggregate Subbase Thickness (in)	Aggregate Subbase Material type	Aggregate Subbase Modulus (psi)	Subgrade Material type	Subgrade Resilient Modulus (psi) (backcalc- Baladi project)	Subgrade Resilient Modulus (psi) (Design- Baladi project)	Subgrade Resilient Modulus (psi) (Inflated design value)	AASHTO
28121	2.8	70000	4	Crushed Gravel	33000	18	Sand Subbase	20000	SP-1	27739	7000	10294	A-1-a, A-3
30728	3.5	70000	8	Crushed Gravel	33000	28	Sand Subbase	20000	SP-1	27739	7000	10294	A-1-a, A-3
32510	4.8	70000	8	Crushed Gravel	33000	28	Sand Subbase	20000	SP-1	27739	7000	10294	A-1-a, A-3
34066	4.5	70000	8	Crushed Gravel	33000	28	Sand Subbase	20000	SP-2	25113	6500	10000	A-1-b, A-2-4, A-3
44827	2.5	70000	8	Crushed Gravel	33000	28	Sand Subbase	20000	SP-1	27739	7000	10294	A-1-a, A-3
50699	7.3	70000	4	Crushed Gravel	33000	18	Sand Subbase	20000	SM	24764	5200	7429	A-2-4, A-4
29704	3.0	70000	8.5	Crushed Gravel	33000	21	Sand Subbase	20000	ML	15976	4400	12941	A-4
31085	7.0	70000	8	Crushed Gravel	33000	26	Sand Subbase	20000	SP-SM	20400	7000	10448	A-2-4, A-4
32262	2.3	70000	10	Crushed Gravel	33000	15	Sand Subbase	20000	ML	15976	4400	12941	A-4
32310	2.3	70000	8	Crushed Gravel	33000	-	Sand Subbase	20000	SP-1	27739	7000	10294	A-1-a, A-3
32327	3.5	70000	7	Crushed Gravel	33000	-	Sand Subbase	20000	SP-1	27739	7000	10294	A-1-a, A-3
32337	6.0	70000	2.4	Crushed Gravel	33000	-	Sand Subbase	20000	SP-2	25113	6500	10000	A-1-b, A-2-4, A-3
32340	4.0	70000	8	Crushed Gravel	33000	21	Sand Subbase	20000	SP-1	27739	7000	10294	A-1-a, A-3
34038	3.3	70000	7	Crushed Gravel	33000	12	Sand Subbase	20000	ML	15976	4400	12941	A-4
34043	2.5	70000	5	Crushed Gravel	33000	6	Sand Subbase	20000	SP-SM	20400	7000	10448	A-2-4, A-4
34045	2.3	70000	6	Crushed Gravel	33000	18	Sand Subbase	20000	CL	15176	4400	10476	A-4, A-6, A-7-6
34056	5.5	70000	8.5	Crushed Gravel	33000	18	Sand Subbase	20000	SP-SM	20400	7000	10448	A-2-4, A-4
35983	4.0	70000	15	Crushed Gravel	33000	-	Sand Subbase	20000	SM	24764	5200	7429	A-2-4, A-4
36524	2.5	70000	11.5	Crushed Gravel	33000	15	Sand Subbase	20000	CL	15176	4400	10476	A-4, A-6, A-7-6
37910	4.0	70000	10	Crushed Gravel	33000	-	Sand Subbase	20000	SP-1	27739	7000	10294	A-1-a, A-3
38007	4.0	70000	11	Crushed Gravel	33000	-	Sand Subbase	20000	SP-SM	20400	7000	10448	A-2-4, A-4
38019	6.3	70000	7.75	Crushed Gravel	33000	-	Sand Subbase	20000	SP-1	27739	7000	10294	A-1-a, A-3
38061	2.0	70000	11.25	Crushed Gravel	33000	14	Sand Subbase	20000	CL	15176	4400	10476	A-4, A-6, A-7-6

A.4 JPCP PROJECT INPUTS

A.4.1 Inventory and Traffic Inputs

Table A-16 Inventory and traffic inputs for JPCP projects

Job Number	Control Section	Region	Opened	AADTT 2-Way MDOT Confirmed	Percent trucks in Design dir	Percent trucks in Design lane	MDOT TTC Cluster	HDF Cluster	ALS Cluster Tandem	MDF Cluster	AGPV Cluster Single	AGPV Cluster Tandem	AGPV Cluster Tridem	AGPV Cluster Quad	ALS Cluster Single	ALS Cluster Tridem	ALS Cluster Quad	Climate	Initial IRI
36003	63191	Metro	1995	10000	51	90	1	3	4	S-A	S-A	S-A	S-A	S-A	S-A	S-A	S-A	Detroit	63
32516	11017	Southwest	1995	7735	51	90	1	1	4	S-A	S-A	S-A	S-A	S-A	S-A	S-A	S-A	Benton Harbor	63
28215	47065	University	1997	5299	51	90	1	2	4	S-A	S-A	S-A	S-A	S-A	S-A	S-A	S-A	Ann Arbor	63
38063	82061	Metro	1998	4825	51	90	S-A	S-A	S-A	S-A	S-A	S-A	S-A	S-A	S-A	S-A	S-A	Detroit	75
36005	82194	Metro	1998	12030	51	90	1	3	1	S-A	S-A	S-A	S-A	S-A	S-A	S-A	S-A	Detroit	70
38094	11017	Southwest	1998	9903	51	90	1	1	4	S-A	S-A	S-A	S-A	S-A	S-A	S-A	S-A	Benton Harbor	63
38100	82194	Metro	1999	12030	51	90	1	3	1	S-A	S-A	S-A	S-A	S-A	S-A	S-A	S-A	Detroit	70
45752	82125	Metro	1999	14755	51	90	1	3	1	S-A	S-A	S-A	S-A	S-A	S-A	S-A	S-A	Detroit	75
45855	80023	Southwest	1999	10578	51	90	1	3	4	S-A	S-A	S-A	S-A	S-A	S-A	S-A	S-A	Benton Harbor	77
44603	81076	University	1999	7498	51	90	1	3	4	S-A	S-A	S-A	S-A	S-A	S-A	S-A	S-A	Ann Arbor	75
33337	41064	Grand	2001	3499	51	90	3	2	5	S-A	S-A	S-A	S-A	S-A	S-A	S-A	S-A	Grand Rapids	75
54361	70025	Grand	2004	3195	51	90	3	2	5	S-A	S-A	S-A	S-A	S-A	S-A	S-A	S-A	Grand Rapids	75
34963	63192	Metro	2002	500	51	90	S-A	S-A	S-A	S-A	S-A	S-A	S-A	S-A	S-A	S-A	S-A	Pontiac	75
34014	82022	Metro	2003	16605	51	90	1	3	4	S-A	S-A	S-A	S-A	S-A	S-A	S-A	S-A	Detroit	75
48611	58033	University	2004	6911	51	90	1	1	4	S-A	S-A	S-A	S-A	S-A	S-A	S-A	S-A	Adrian	50
59066	82052	Metro	2003	3020	51	90	S-A	S-A	S-A	S-A	S-A	S-A	S-A	S-A	S-A	S-A	S-A	Detroit	70
47197	50011	Metro	2005	3250	51	90	3	3	3	S-A	S-A	S-A	S-A	S-A	S-A	S-A	S-A	Pontiac	75
53168	82192	Metro	2004	2758	51	90	S-A	S-A	S-A	S-A	S-A	S-A	S-A	S-A	S-A	S-A	S-A	Detroit	63
60077	82124	Metro	2005	6939	51	90	1	3	4	S-A	S-A	S-A	S-A	S-A	S-A	S-A	S-A	Detroit	75
60488/79085	13083	Southwest	2007	7532	51	90	1	1	4	S-A	S-A	S-A	S-A	S-A	S-A	S-A	S-A	Battle Creek	70

A.4.2 JPCP Layer Inputs

Table A-17 PCC layer inputs for all JPCP projects

Job Number	Joint Spacing (ft)	Dowel Diameter (in)	Lane Width (ft)	Shoulder type	PCC Thickness (in)	PCC Compressive Strength from Cores (psi)	PCC MOR (calculated from cores)	PCC CTE	Cement content	Water cement ratio	Aggregate type	Job Number
36003	15	1.5	12	Tied	11.7	5334	548	5.8	526	0.45	Limestone	36003
32516	16	1.5	14	Tied	12.6	4892	525	5.7	564	0.45	Limestone	32516
28215	15	1.25	12	Tied	10.1	5412	552	5.7	526	0.45	Limestone	28215
38063	13	1.25	12	Tied	9.9	6498	605	5.8	526	0.45	Limestone	38063
36005	16	1.5	12	Tied	12.2	4765	518	5.8	526	0.45	Limestone	36005
38094	16	1.25	14	No	11.4	5958	579	4.5	526	0.45	Limestone	38094
38100	16	1.5	12	Tied	12.4	4799	520	5.8	526	0.45	Limestone	38100
45752	16	1.5	12	Tied	11.3	5105	536	5.8	526	0.45	Limestone	45752
45855	13.5	1.25	12	Tied	11.3	5607	562	4.5	526	0.45	Limestone	45855
44603	15	1.25	12	Tied	12.0	6121	587	5.8	526	0.45	Limestone	44603
33337	15	1.25	12	No	11.2	5120	537	4.5	526	0.45	Limestone	33337
54361	15	1.25	12	No	11.7	4961	528	4.5	526	0.45	Limestone	54361
34963	15	1.25	12	Tied	10.8	6398	600	5.8	526	0.45	Limestone	34963
34014	16	1.5	12	Tied	12.4	5765	569	5.8	526	0.45	Limestone	34014
48611	15	1.25	14	No, except tied from Milepoint 13.185 to 13.583	11.4	3871	467	5.8	526	0.45	Limestone	48611
59066	15	1.25	12	Tied	9.0	-	560	5.8	526	0.45	Limestone	59066
47197	15	1.25	12	Tied	9.5	5263	544	5.8	526	0.45	Limestone	47197
53168	15	1.25	11	Tied	9.5	4735	516	5.8	526	0.45	Limestone	53168
60077	15	1.5	12	Tied	12.4	4901	525	5.8	526	0.45	Limestone	60077
60488/79085	14	1.25	14	Tied	11.5	5619	562	4.5	526	0.45	Limestone	60488/79085

A.4.3 Aggregate Base and Subgrade Soil Inputs

Table A-18 Aggregate base, subbase and subgrade layer inputs for all JPCP projects

Job Number	Base Thickness (in)	Base Material type	Base Modulus (psi)	Subbase Thickness (in)	Subbase Material type	Subbase Modulus (psi)	Subgrade Material type (by loc.)	Subgrade Modulus (psi) (backcalc /design- Baladi project)	Subgrade Modulus (psi) (Inflated design)	AASHTO
36003	4.0	Crushed Gravel	33000	10.0	A-3	20000	SC/CL/ML	17600/4400	10732	A-2-6, A-4, A-6, A-7-6
32516	4.0	Crushed Gravel	33000	8.0	A-3	20000	SP-SM	20400/7000	10448	A-2-4, A-4
28215	7.0	Crushed Gravel	33000	9.0	A-3	20000	SC/CL/ML	17600/4400	10732	A-2-6, A-4, A-6, A-7-6
38063	3.9	Crushed Gravel	33000	10.0	A-3	20000	SC/CL/ML	17600/4400	10732	A-2-6, A-4, A-6, A-7-6
36005	3.9	Crushed Gravel	33000	10.0	A-3	20000	SC/CL/ML	17600/4400	10732	A-2-6, A-4, A-6, A-7-6
38094	4.0	Crushed Gravel	33000	12.0	A-3	20000	SP1	27739/7000	10294	A-1-a, A-3
38100	3.9	Crushed Gravel	33000	11.8	A-3	20000	SC/CL/ML	17600/4400	10732	A-2-6, A-4, A-6, A-7-6
45752	3.9	Crushed Gravel	33000	12.0	A-3	20000	SC/CL/ML	17600/4400	10732	A-2-6, A-4, A-6, A-7-6
45855	4.0	Crushed Gravel	33000	10*	A-3	20000	SP1	27739/7000	10294	A-1-a, A-3
44603	4.0	Crushed Gravel	33000	10.0	A-3	20000	SP-SM	20400/7000	10448	A-2-4, A-4
33337	4.0	Crushed Gravel	33000	12.0	A-3	20000	SC-SM	20314/5000	11905	A-2-6, A-6, A-7-6
54361	5.9	Crushed Gravel	33000	17.7	A-3	20000	SC-SM	20314/5000	11905	A-2-6, A-6, A-7-6
34963	4.0	Crushed Gravel	33000	12.0	A-3	20000	SC/CL/ML	17600/4400	10732	A-2-6, A-4, A-6, A-7-6
34014	15.7	Crushed Gravel	33000	-			SC/CL/ML	17600/4400	10732	A-2-6, A-4, A-6, A-7-6
48611	8.0	Crushed Gravel	33000	10	A-3	20000	SP-SM	20400/7000	10448	A-2-4, A-4
59066	4.0	Crushed Gravel	33000	12.0	A-3	20000	SC/CL/ML	17600/4400	10732	A-2-6, A-4, A-6, A-7-6
47197	4.0	Crushed Gravel	33000	12.0	A-3	20000	SP2	25113/6500	10000	A-1-b, A-2-4, A-3
53168	4.0	Crushed Gravel	33000	12.0	A-3	20000	SC/CL/ML	17600/4400	10732	A-2-6, A-4, A-6, A-7-6
60077	16.0	Crushed Gravel	33000	-			SC/CL/ML	17600/4400	10732	A-2-6, A-4, A-6, A-7-6
60488/79085	4.0	Crushed Gravel	33000	12.0	A-3	20000	SP1	27739/7000	10294	A-1-a, A-3

A.5 HMA over HMA

A.5.1 Inventory and Traffic Inputs

Table A-19 Inventory and traffic inputs for HMA over HMA projects

Project Number	Control section	Route	Year opened	Two way AADTT	Percent trucks in Design dir	Percent trucks in Design lane	MDOT TTC Cluster	HDF Cluster	ALS Tandem	Climate
33534	67015/83031	US-131	1992	450	51	90	3	2	3	Houghton Lake
33550	80012	I-196	1992	1564	51	90	3	2	5	Kalamazoo
28155	80111	M-40	1991	185	51	90	3	2	3	Kalamazoo
26658	28021	M-113	1992	130	51	90	3	2	4	Traverse City
29755	80072	M-40	1994	185	51	90	3	2	5	Traverse City
30701	14041	US-12	1994	408	51	90	2	2	3	Kalamazoo
31047	2042	M-28	1996	260	51	90	2	2	3	Iron Mountain
32361	32092	M-25	1997	200	51	90	S-A	S-A	S-A	Flint
45875	14042	US-12	2002	805	51	90	3	3	4	Benton Harbor
50715	30041	M-34	2005	350	51	90	S-A	S-A	S-A	Battle Creek
20313	45021	M-72	1983	300	51	90	S-A	S-A	S-A	Traverse City
12802	10041	M-115	1984	300	51	90	S-A	S-A	S-A	Traverse City
24621	13092	M-99	1987	238	51	90	S-A	S-A	S-A	Battle Creek
25515	83021/83052	M-115/M-55	1989	315	51	90	3	2	5	Gaylord
30702	14041	US-12	1990	365	51	90	2	2	3	Benton Harbor

A.5.2 HMA Layer Inputs

Table A-20 HMA top layer inputs for HMA over HMA projects

Project Number	HMA Top Thickness (in)	HMA Top Binder Type	HMA Top Aggregate Gradation	HMA Top Air Voids (as constructed)	HMA Top Effective Binder Content	HMA Top Percent Passing 3/4	HMA Top Percent Passing 3/8	HMA Top Percent Passing #4	HMA Top Percent Passing 200
33534	1.25	120-150	4B	5.74	10.4	100	85.5	50	5.9
33550	1.5	85-100	4C	5.52	11.8	100	89.7	58.6	5.7
28155	1.25	120-150	1100T	7	11.8	100	88.7	62.5	6.9
26658	2.5	120-150	1100T	7	12	100	81.4	59.6	5.4
29755	3	120-150	1100T	7	12	100	88.7	62.5	6.9
30701	1.5	85-100	4C	5.4	11.8	100	81	58	5
31047	1.5	120-150	1100T	7	12	100	88.7	62.5	6.9
32361	1.5	120-150	1100T	7	12	100	88.7	62.5	6.9
45875	2	PG 64-28	5E3	7.05	12	100	97.5	67.2	5.4
50715	1	PG 64-28	5E3	7.05	12.1	100	97.5	67.2	5.4
20313	1	120-150	1100T	7	12	100	84.6	67.1	7.4
12802	2.5	120-150	1100L	7	11.2	100	85	64	6.4
24621	1.25	120-150	1100T	7	11.2	100	85.8	63.6	6.9
25515	1.25	120-150	1100T	7	11	100	89.8	61.6	5.6
30702	1.25	85-100	1500T	7	11.2	100	88.8	67.8	6

Table A-21 HMA leveling layer inputs for HMA over HMA projects

Project Number	HMA Leveling Thickness (in)	HMA Leveling Binder Type	HMA Leveling Aggregate Gradation	HMA Leveling Air Voids (as constructed)	HMA Leveling Effective Binder Content	HMA Leveling Percent Passing 3/4	HMA Leveling Percent Passing 3/8	HMA Leveling Percent Passing #4	HMA Leveling Percent Passing 200
33534	1.25	120-150	3B	5.74	9.4	100	71.4	49.8	4.8
33550	1.5	85-100	3C	5.52	10	100	64	54.4	6.5
28155	1.25	120-150	1100L	7	11	100	88.7	62.5	6.9
26658	2.5	120-150	1100T	7	11.4	100	82.7	62.6	5.7
29755	3	120-150	1100L	7	12	100	88.7	62.5	6.9
30701	1.5	85-100	3C	5.2	10	100	72	50	5
31047	1.5	120-150	1100L	7	12	100	88.7	62.5	6.9
32361	1.5	120-150	1100L	7	12	100	88.7	62.5	6.9
45875	2	PG 64-28	4E3	7.05	12	100.0	87.7	88.9	4.9
50715	2.5	PG 64-28	5E3	7.05	12.4	100	64.9	35.4	4.6
20313	1.25	120-150	1100T	7	10.4	100	86.6	62.5	5.8
12802	-	-	-	-	-	-	-	-	-
24621	1.25	120-150	1100L	7	10.4	100	86.7	65.9	8.5
25515	1.25	120-150	1100L	7	10.4	100	88	64.8	5.6
30702	-	-	-	-	-	-	-	-	-

Table A-22 HMA base layer inputs for HMA over HMA projects

Project Number	Existing HMA Thickness (in)	Existing HMA binder type	Existing HMA aggregate Gradation	Existing HMA Air Voids (as constructed)	Existing HMA Effective binder content (%)	Existing HMA Existing Percent Passing 3/4	Existing HMA Existing Percent Passing 3/8	Existing HMA Existing Percent Passing #4	Existing HMA Existing Percent Passing 200
33534	3.25	85-100	3B	7	11.6	100	71.4	49.8	4.8
33550	4.5	85-100	3C	7	12	100	64	54.4	6.5
28155	5.2	120-150	1100L	7	11	100	89.4	68.5	5.4
26658	N/A	120-150	1100L	7	11.4	100	81.4	59.6	5.4
29755	4-5.5	120-150	1100L	7	11	100	82.7	62.6	5.7
30701	4.5	85-100	3C	7	11	100	64	54.4	6.5
31047	3	120-150	1100L	7	11	100	82.7	62.6	5.7
32361	3.7	120-150		7	11	100	82.7	62.6	5.7
45875	4.5	PG 64-28	4E3	7	11	100	86.8	64.9	4.6
50715	7.5	PG 64-28	4E3	7	11	100	86.8	64.9	4.6
20313	1.5	120-150		7	11	100	86.6	63	5.8
12802	4.75	120-150	1100L	7	11	100	85	64	6.4
24621	3.75	120-150		7	11	100	86.7	65.9	8.5
25515	2.25	120-150		7	11	100	88	64.8	5.6
30702	7.1	85-100		7	11	100	88.8	67.8	6

A.5.3 Aggregate Base and Subbase Layer Inputs

Table A-23 Aggregate base, subbase and subgrade layer inputs for all HMA over HMA projects

Project Number	Base Thickness (in)	Base Material type	Base Modulus (psi)	Subbase Thickness (in)	Subbase Material type	Subbase Modulus (psi)	Subgrade Material type	Subgrade Modulus (psi) (backcalc/design - Baladi project)	SubgradeMR Inflated -Location Based	Subgrade Modulus (psi) (Inflated design)
33534	11	Crushed Stone	33000	25	A-3	20000	SP1- A3	27739/ 7000	12939	10294
33550	8	Crushed Stone	33000	28	A-3	20000	SP1-A-3	27739/ 7000	9079	10294
28155	7	Crushed Stone	33000	12	A-3	20000	SP1-A-3	27739/ 7000	9079	10294
26658	N/A	Crushed Stone	33000	N/A	A-3	20000	SP1-A-3	27739/ 7000	11925	10294
29755	4/5 stabilized						SP1-A-3	27739/ 7000	11925	10294
30701	7	Crushed Stone	33000	15	A-3	20000	SP1-A-3	27739/ 7000	9079	10294
31047	10	Crushed Stone	33000	18	A-3	20000	SP-SM	20400/ 7000	14028	10448
32361	7	Crushed Stone	33000	13.7	A-3	20000	SM - A-4	24764/ 5200	6443	7429
45875	11	Crushed Stone	33000	15	A-3	20000	SP1-A-3	27739/ 7000	9210	10294
50715	6	Crushed Stone	33000	8	A-3	20000	SP-SM	20400/ 7000	9498	10448
20313	5	Crushed Stone	33000				SP1-A-3	27739/ 7000	11925	10294
12802	7	Crushed Stone	33000	0 or 12	A-3	20000	SP1-A-3	27739/ 7000	11925	10294
24621	8	Crushed Stone	33000				SP1- A-3	27739/ 7000	8653	10294
25515	10	Crushed Stone	33000				SP1-A-3	27739/ 7000	14286	10294
30702	5	Crushed Stone	33000				SP1-A-3	27739/ 7000	9210	10294

A.6 Rubblized

A.6.1 Inventory and Traffic Inputs

Table A-24 Inventory and traffic inputs for rubblized projects

Project Number	Control Section	Route	Year opened	Two way AADTT	Percent trucks in Design dir	Percent trucks in Design lane	MDOT TTC Cluster	HDF Cluster	ALS Tandem	Climate
28115	34031/34032	M-66	1989	490/340	51	90	3	2	5	Grand Rapids
26755	20014	I-75	1990	1550	51	90	3	3	4	Houghton Lake
29768	47013/47014	US-23	1992	3390	51	90	3	2	4	Ann Arbor
29670	13033	I-194	1993	856	51	90	2	3	3	Battle Creek
29581	33084/33083	I-96	1994	3707	51	90	3	2	4	Lansing
28111	24021/16021	M-68	1990	280	51	90	3	3	1	Pellston
29729	74012	M-53	1995	370	51	90	3	2	3	Flint
45053	67021/ 67022	US-10	1999	675	51	90	3	2	3	Houghton Lake
44109	5011	US-31	1999	279	51	90	2	2	3	Traverse City
38190	41033/61171	M-37	2000	575	51	90	3	2	5	Muskegon
32388	46082	M-50	1997	455	51	90	2	2	3	Adrian

A.6.2 HMA Layer Inputs

Table A-25 HMA layer inputs for rubblized projects

Project Number	HMA Thickness (in)	HMA binder type	Mixture Air Voids (as const)	HMA Effective binder	Cumulative % Retained 3/4	Cumulative % Retained 3/8	Cumulative % Retained #4	% Passing 200
28115	5	Pen 120-150	7	10.8	79.6	67.7	59	3.1
26755	4.25	Pen 120-150	7	11.4	100	86.1	62.8	5.1
29768	5.25	Pen 85-100	7	10	100	86.9	59.1	7.1
29670	6.25	Pen 85-100	7	12	100	99.7	80.1	5.8
29581	7.5	Pen 85-100	7	12.4	100	84	63.1	4.9
28111	4	Pen 200-300	7	10.8	100	84	61.2	5.7
29729	5 Edge, 7.2 Center Line	Pen 120-150	7	10.4	100	61.7	47.8	5.6
45053	5.5	PG 64-28	7	12	100	83.3	43.8	4.1
44109	7.5	PG 58-28	7	13	100	98	66.1	4.5
38190	5.5	PG 58-28	7	10.4	100	83.5	66.3	4.9
32388	6CL, 7E	Pen 85-100	7	10.2	100	61.3	44.6	5

A.6.3 Existing Pavement, Aggregate Base and Subbase Layer Inputs

Table A-26 Aggregate base, subbase and subgrade layer inputs for rubblized projects

Project Number	PCC Thickness (in)	PCC Fractured Elastic Modulus (psi)	Base Thickness (in)	Base Material type	Base Modulus (psi)	Subbase Thickness (in)	Subbase Material type	Subbase Modulus (psi)	Material Type	Modulus (psi) (backcalc/design - Baladi project)	SubgradeMR Inflated -Location Based	Modulus (psi) (inflated design)
28115	9	70000	3	Crushed Stone	33000	9	A-3	20000	ML	20314/ 5000	12753	11905
26755	8	70000	0			0			SP-2	25113/ 6500	14192	10000
29768	9	70000	4	Crushed Stone	33000	14	A-3	20000	SP-2	25113/ 6500	9848	10000
29670	9	70000	3	Crushed Stone	33000	9	A-3	20000	SP-1	27739/ 7000	8653	10294
29581	9	70000	4	Crushed Stone	33000	10	A-3	20000	CL	17600/ 4400	10451	10732
28111	9	70000	N/A			0			SP-1	27739/ 7000	15053	10294
29729	9	70000	N/A			18	A-3	20000	SM	24764/ 5200	6443	7429
45053	9	70000	3	Crushed Stone	33000	12	A-3	20000	SP-1	27739/ 7000	12939	10294
44109	8	70000	0			9	A-3	20000	SP-1	27739/ 7000	11925	10294
38190	9	70000	4	Crushed Stone	33000	14	A-3	20000	SP-1	27739/ 7000	8226	10294
32388	8	70000	0			12	A-3	20000	CL	17600/ 4400	9091	10732

A.7 Composite pavements

A.7.1 Inventory and Traffic Inputs

Table A-27 Inventory and traffic inputs for composite projects

Project Number	Control section	Route	Year opened	Two way AADTT	Percent trucks in Design dir	Percent trucks in Design lane	MDOT TTC Cluster	HDF Cluster	ALS Tandem	Climate
25543	25131	I-75	1987	2250	51	90	3	3	1	Flint
24252	80024/39024	I-96	1988	6064	51	90	3	1	4	Kalamazoo
29586	41026/70063	I-96	1990	2882	51	90	3	2	3	Grand Rapids
29716	67051/83051	M-115	1992	672	51	90	3	2	5	Houghton Lake
33812	50031	M-97	1995	1380	51	90	S-A	S-A	S-A	Detroit
33924	9032	M-13	1996	1000	51	90	S-A	S-A	S-A	Flint
45443	32011	M-25	2000	512	51	90	3	3	3	Flint

A.7.2 HMA Layer Inputs

Table A-28 HMA layer inputs for composite projects

Project Number	HMA Thickness (in)	HMA binder type	HMA as constructed air voids	HMA effective binder content	Cumulative % Retained 3/4	Cumulative % Retained 3/8	Cumulative % Retained #4	% Passing 200
25543	4	85-100	7	12.2	100	88.6	68.3	6.5
24252	4.5	85-100	7	11.2	100	88	68.1	5.4
29586	3	85-100	7	12	100	88.4	63.8	6.5
29716	3.75	120-150	7	12	100	87	60	6
33812	3	85-100	7	10.6	100	61.7	44	5.6
33924	4	120-150	7	11	100	85.6	48.5	5.4
45443	3.5	PG 64-28	7	13	100	98	79.1	5.9

A.7.3 Existing Pavement, Aggregate Base and Subbase Layer Inputs

Table A-29 Existing pavement, aggregate base, and subbase layer inputs for composite projects

Project Number	Existing PCC Thickness (in)	PCC Compressive Strength (psi)	Base Thickness (in)	Base Material type	Base Modulus (psi)	Subbase Thickness (in)	Subbase Material type	Subbase Modulus (psi)	Subgrade Material type	Subgrade Modulus (psi) (backcalc/design - Baladi project)	SubgradeMR Inflated - Location Based	Subgrade Modulus (psi) (inflated design)
25543	9	5000	4	Crushed Stone	33000	10	A-3	20000	SM - A-4	24764/ 5200	6443	7429
24252	9	5000	3	Crushed Stone	33000	9	A-3	20000	SP1-A-3	27739/ 7000	9079	10294
29586	9	5000	3	Crushed Stone	33000	12	A-3	20000	A-4	20314/ 5000	12753	11905
29716	9	5000	0			0			SP1- A-3	27739/ 7000	12939	10294
33812	9	5000	3	Crushed Stone	33000	14	A-3	20000	SP1-A-3	27739/ 7000	8578	10294
33924	8	5000	4	Crushed Stone	33000	10	A-3	20000	SC - A-6	17600/ 4400	9186	10732
45443	8	5000	0			15	A-3	20000	SC - A-6	17600/ 4400	9186	10732

A.8 JPCP Unbonded Overlay Pavements

A.8.1 Inventory and Traffic Inputs

Table A-30 Inventory and traffic inputs for JPCP unbonded overlays

Project Number	Control Section	Region	Roadway	Year opened	Two way AADTT	Percent trucks in Design dir	Percent trucks in Design lane	MDOT TTC Cluster	HDF Cluster	ALS Tandem	Climate
37997	3111	Southwest	US-131 NB, SB	1998	4250	50	90	3	3	3	Kalamazoo
34120	47014	University	US-23 NB, SB	1999	4279	50	90	3	2	4	Ann Arbor
49029	13074	Southwest	I-69 NB, SB	1999	5700	50	90	3	1	4	Kalamazoo
45591	13074-23061	Southwest	I-69 NB, SB	2000	5595	50	90	3	1	4	Battle Creek
38209	41132-41133	Grand	US-131 NB, SB	2000	2744	50	90	3	2	3	Grand Rapids
43499	47014	University	US-23 NB, SB	2001	5004	50	90	3	2	4	Ann Arbor
73873	65041	North	I-75 NB	2003	1458	50	90	3	3	4	Houghton Lake
50763	39014, 3111	Southwest	US-131 NB, SB	2004	3185	50	90	3	2	3	Kalamazoo

A.8.2 PCC Layer Inputs

Table A-31 PCC layer inputs for JPCP unbonded overlay projects

Project Number	PCC Thickness (in)	PCC Modulus of Rupture (psi)	PCC Compressive Strength (psi)	Joint Spacing (ft)	Dowel Diameter (in.)	PCC CTE	Cement Content	Water Cement Ratio
37997	7.1	555	5496	13	1.25	5.7	526	0.45
34120	7.9	536	5165	13	1.25	5.7	526	0.45
49029	7.1	555	5496	13	1.25	5.7	526	0.45
45591	7.1	555	5496	13	1.25	5.7	526	0.45
38209	6.3	536	5142	13	1.25	4.5	526	0.45
43499	7.1	536	5165	13	1.25	5.7	526	0.45
73873	6	536	5142	13	1.25	5.7	526	0.45
50763	6.5	555	5496	13	1.25	5.7	526	0.45

A.8.3 Existing Pavement Inputs

Table A-32 Existing pavement inputs for JPCP unbonded overlay projects

Project Number	Asphalt Interlayer Thickness (in)	Asphalt Interlayer Binder Type	Existing PCC Thickness (in)	Existing PCC Elastic Modulus (ksi)	Base thickness (in)	Base material type	Base Modulus (psi)	Subbase Thickness (in)	Subbase Material type	Subbase Modulus (psi)	Subgrade Material type (by loc.)	Subgrade Modulus (psi) (backcalc /design- Baladi project)	Subgrade MR (psi) (Inflated Design value) By climate	Subgrade MR (psi) (Inflated Design value)
37997	1	PG 58-28	9	3000	3	Crushed Stone	33000	11	A-3	20000	SP1-A-3	27739/ 7000	9079	10294
34120	1	PG 58-28	9	3000	3	Crushed Stone	33000	14	A-3	20000	SP2-A-3	25113/ 6500	9848	10000
49029	1	PG 58-28	9	3000	4	Crushed Stone	33000	10	A-3	20000	SP1-A-3	27739/ 7000	9079	10294
45591	1	PG 58-28	9	3000	4	Crushed Stone	33000	10	A-3	20000	SP1-A-3	27739/ 7000	8653	10294
38209	1	PG 58-28	9	3000	4	Crushed Stone	33000	10	A-3	20000	A-4	20314/ 5000	12753	11905
43499	1	PG 70-28	9	3000	3	Crushed Stone	33000	14	A-3	20000	SP2-A-3	25113/ 6500	9848	10000
73873	1	PG 64-28	9	3000	4	Crushed Stone	33000	10	A-3	20000	SP2-A-3	25113/ 6500	14192	10000
50763	1	PG 58-28	9	3000	4	Crushed Stone	33000	10	A-3	20000	SP1-A-3	27739/ 7000	9079	10294

APPENDIX B – LOCAL CALIBRATION RESULTS

Table of Contents

List of Tables

List of Figures

B.1 Flexible Pavement Performance Prediction Models

B.1.1 Fatigue Cracking Model – Bottom-up

B.1.1.1 Option 1a

No sampling

Table B-1 Option 1a local calibration results – no sampling

Parameter	Global model	Local model
SEE	7.64	6.71
Bias	-4.19	-1.29
R^2	0.01	0.02
t-test pvalue	0.00	0.00
Intercept = 0	0.00	0.00
Slope = 1	0.00	0.00
C1	1.00	0.50
C2	1.00	0.56

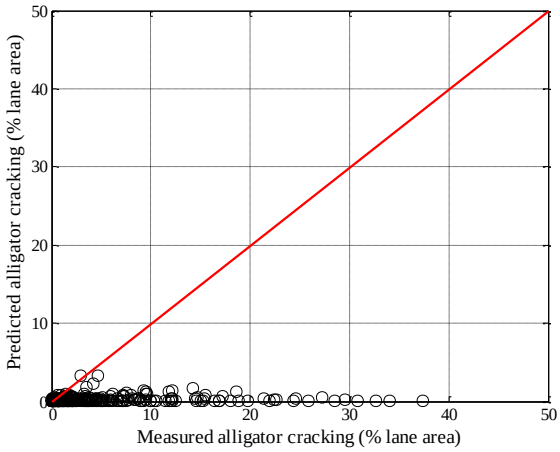

Figure B-1 Option 1a measured versus predicted fatigue cracking – no sampling

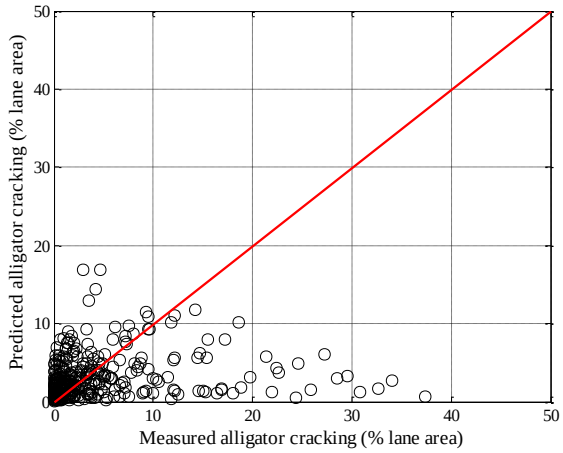

(a) Measured vs. predicted cracking

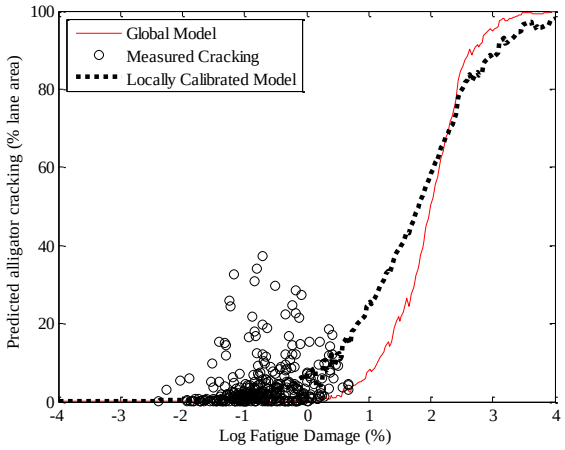

(b) Fatigue damage predicted cracking

Figure B-2 Option 1a local calibration results - no sampling

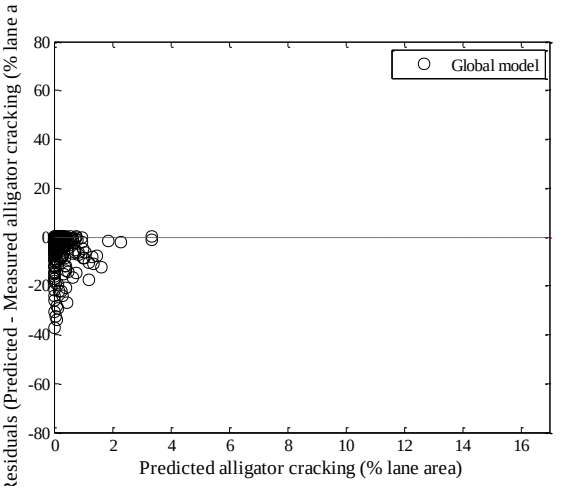

(a) Measured vs. predicted cracking

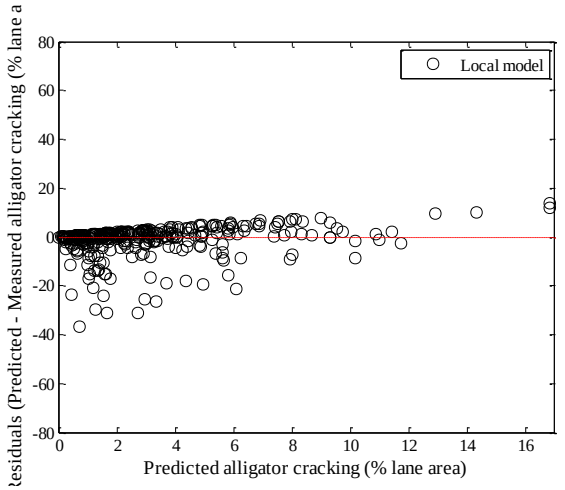

(b) Fatigue damage predicted cracking

Figure B-3 Option 1a local calibration residual plots - no sampling

Reliability

Table B-2 Option 1a global and local alligator cracking model reliability – no sampling

Global model reliability equation	Local model reliability equation
$s_{e(Alligator)} = 1.13 + \frac{13}{1+e^{7.57-15.5\times log(D)}}$	$s_{e(Alligator)} = 2.3988 + \frac{15.676}{1+e^{0.1475-0.4641\times log(D)}}$

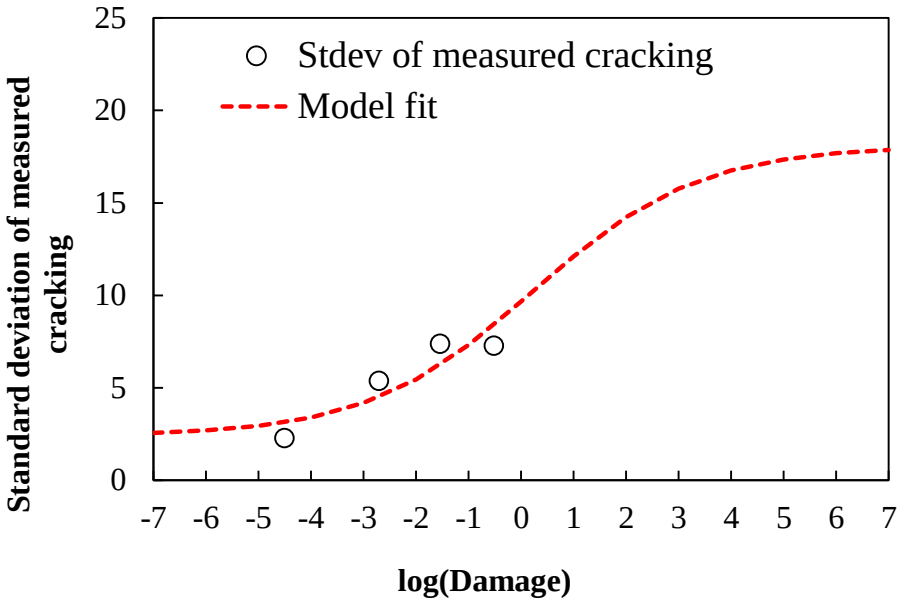

Figure B-4 Option 1a fitted reliability model after local calibration –no sampling

Split sampling

Table B-3 Option 1a local calibration results – split sampling

Parameter	Global model	Local model calibration	Local model validation
SEE	8.02	7.00	6.00
Bias	-4.39	-1.37	-0.78
R^2	0.02	0.03	0.01
t-test pvalue	0.00	0.00	0.20
Intercept = 0	0.00	0.00	0.00
Slope = 1	0.00	0.00	0.00
C1	1.00	0.50	0.50
C2	1.00	0.56	0.56

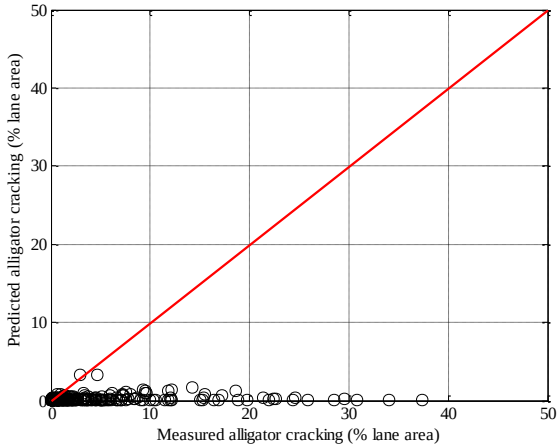

(a) Global model

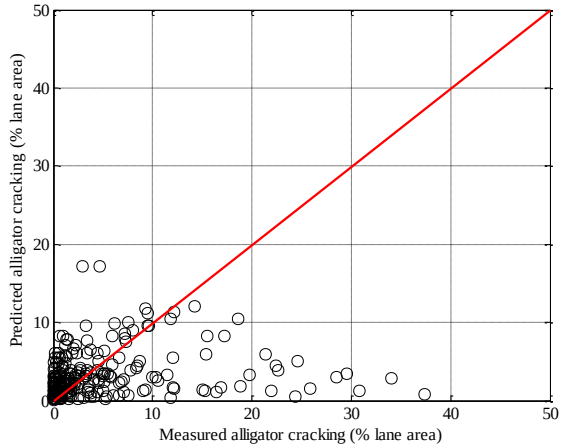

(b) Local model

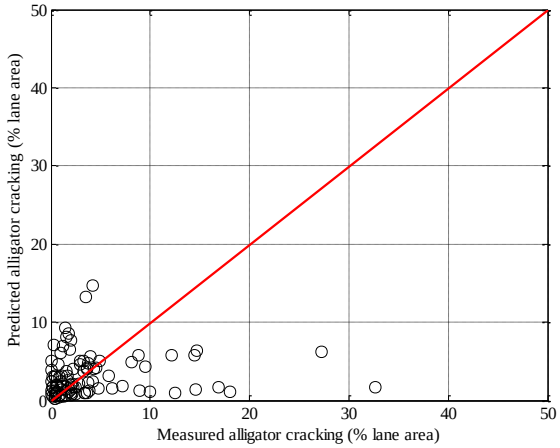

(c) Local model validation

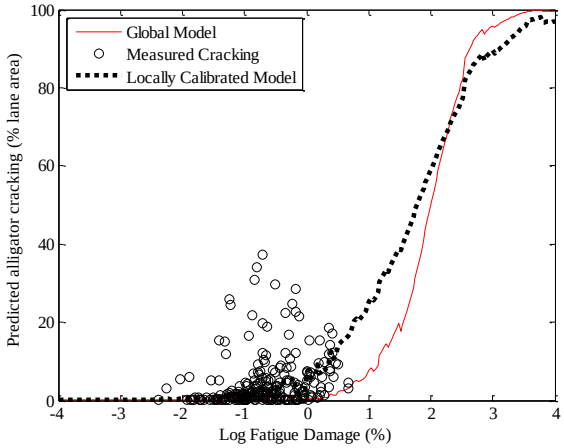

(d) Fatigue damage predicted cracking

Figure B-5 Option 1a local calibration results - split sampling

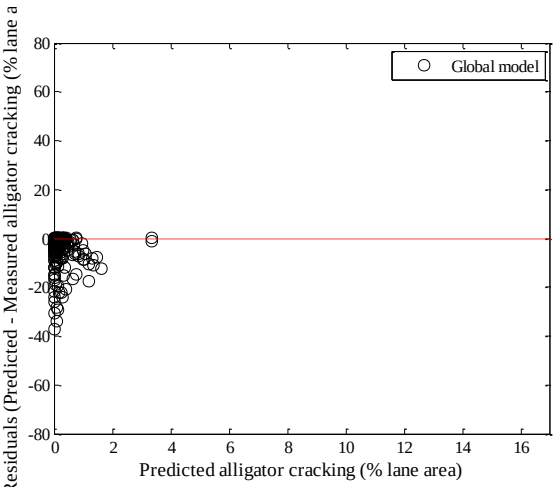

(a) Global model

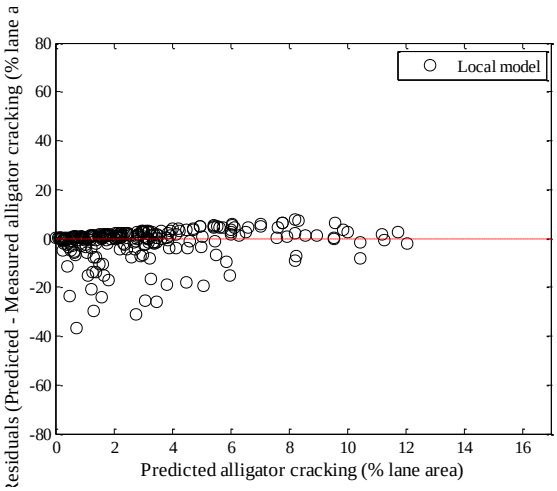

(b) Local model

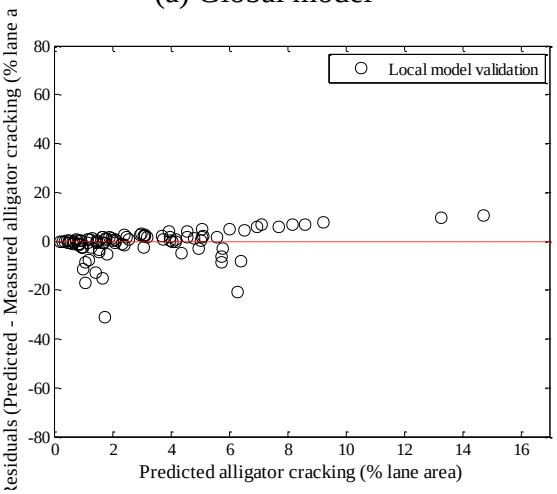

(c) Local model validation

Figure B-6 Option 1a local calibration residual plots - split sampling

Reliability

Table B-4 Option 1a global and local alligator cracking model reliability – split sampling

Global model reliability equation	Local model reliability equation
$s_{e(Alligator)} = 1.13 + \frac{13}{1+e^{7.57-15.5\times log(D)}}$	$s_{e(Alligator)} = 0.6 + \frac{24}{1+e^{0.1-0.5\times log(D)}}$

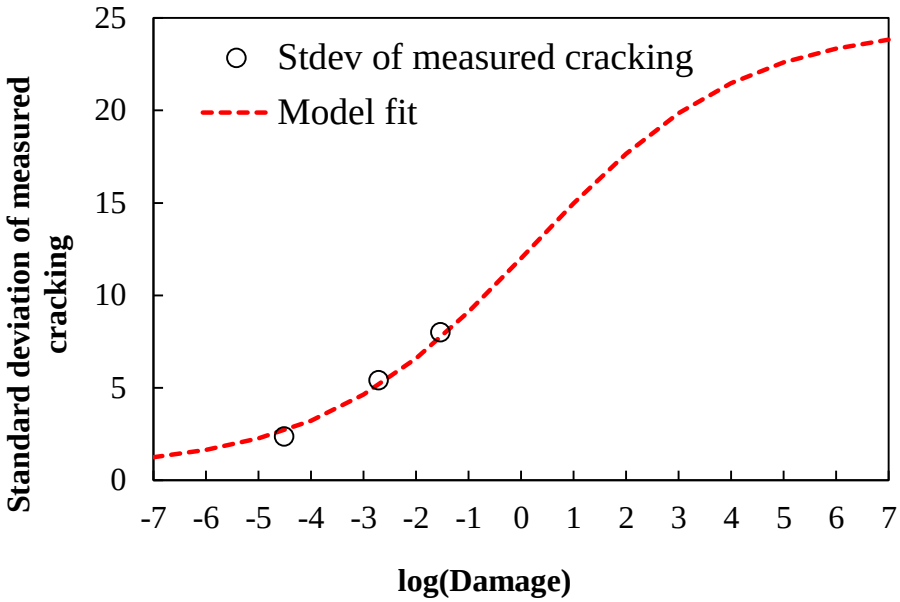

Figure B-7 Option 1a fitted reliability model after local calibration – split sampling

Repeated split sampling

Table B-5 Option 1a local calibration results – repeated split sampling

Global Model				
Parameter	Global Model Mean	Global Model Median	Global model lower CI	Global model upper CI
SEE	7.65	7.69	6.79	8.35
Bias	-4.19	-4.20	-4.66	-3.66
C1	1.00	1.00	-	-
C2	1.00	1.00	-	-
Local Model				
Parameter	Local Model Mean	Local Model Median	Local model lower CI	Local model upper CI
SEE	6.71	6.76	5.84	7.39
Bias	-1.22	-1.24	-1.64	-0.68
C1	0.50	0.50	0.47	0.50
C2	0.56	0.56	0.56	0.56
Local Model Validation				
Parameter	Local Model Mean	Local Model Median	Local model lower CI	Local model upper CI
SEE	6.71	6.69	4.90	8.48
Bias	-1.20	-1.22	-2.68	0.43
C1	0.50	0.50	0.47	0.50
C2	0.56	0.56	0.56	0.56

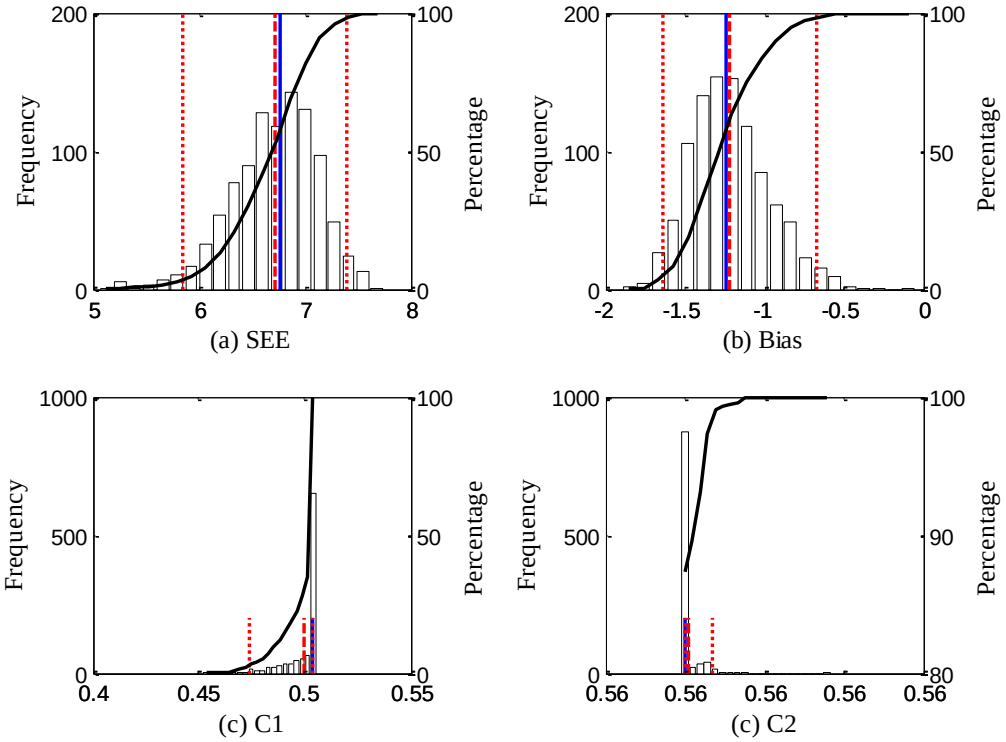

Figure B-8 Option 1a repeated split sampling frequency distributions – calibration

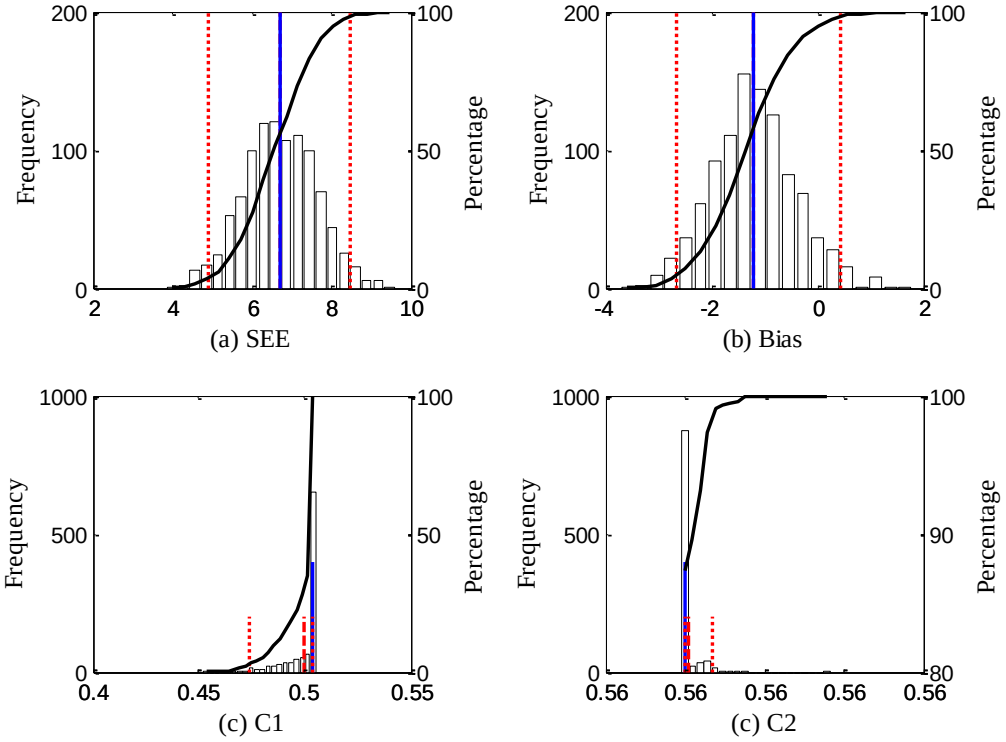

Figure B-9 Option 1a repeated split sampling frequency distributions – validation

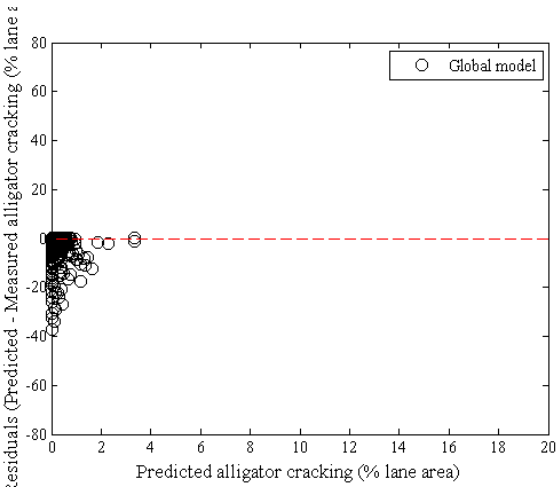

(a) Global model

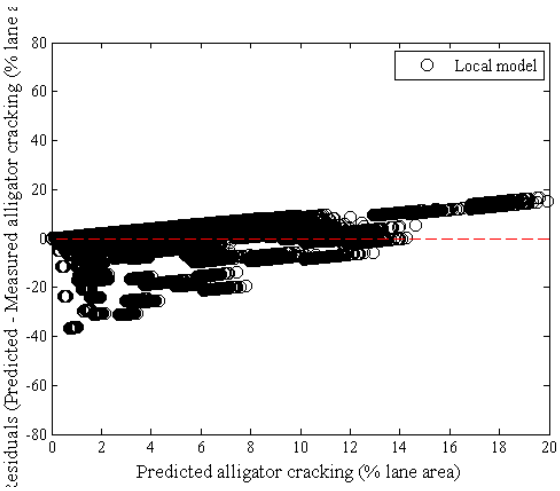

(b) Local model

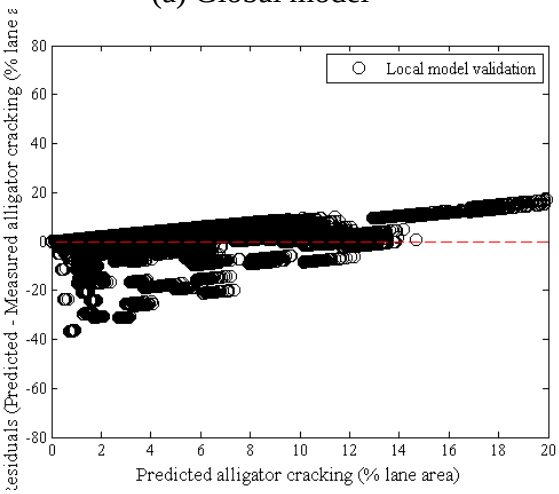

(c) Local model validation

Figure B-10 Option 1a local calibration residual plots – repeated split sampling

Reliability

Table B-6 Option 1a global and local alligator cracking model reliability – repeated split sampling

Global model reliability equation	Local model reliability equation
$s_{e(Alligator)} = 1.13 + \frac{13}{1+e^{7.57-15.5\times log(D)}}$	$s_{e(Alligator)} = 0.9919 + \frac{17.093}{1+e^{0.1103-0.4361\times log(D)}}$

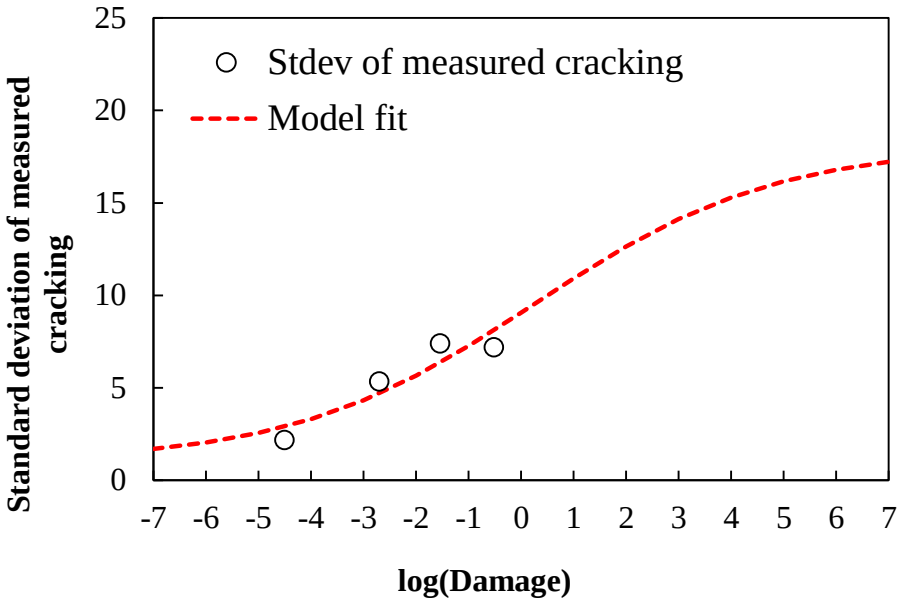

Figure B-11 Option 1a fitted reliability model after local calibration – repeated split sampling

Bootstrapping

Table B-7 Option 1a local calibration results – bootstrapping

Global Model				
Parameter	Global Model Mean	Global Model Median	Global model lower CI	Global model upper CI
SEE	7.62	7.61	6.38	8.93
Bias	-4.19	-4.18	-5.01	-3.45
C1	1.00	1.00	-	-
C2	1.00	1.00	-	-
Local Model				
Parameter	Local Model Mean	Local Model Median	Local model lower CI	Local model upper CI
SEE	6.69	6.66	5.53	7.88
Bias	-1.16	-1.15	-1.87	-0.43
C1	0.50	0.50	0.46	0.50
C2	0.56	0.56	0.56	0.56

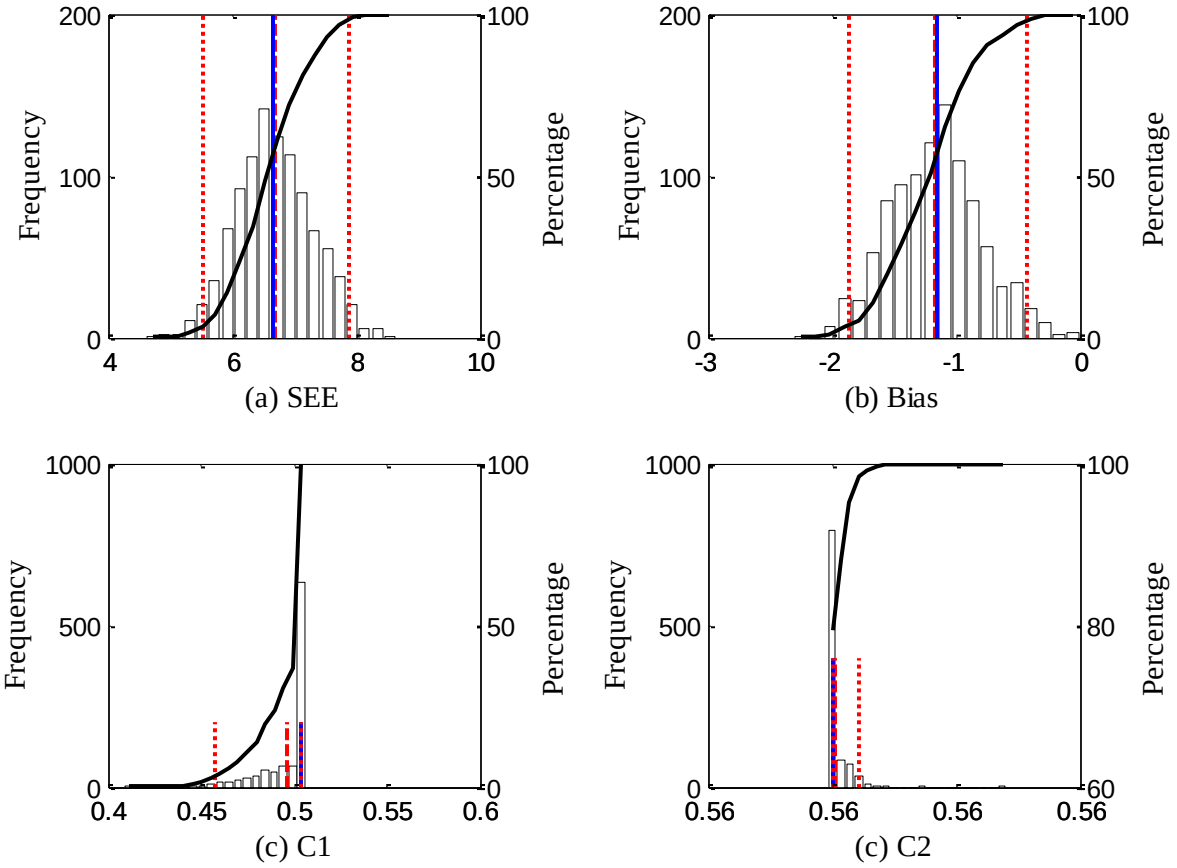

Figure B-12 Option 1a bootstrapping frequency distributions

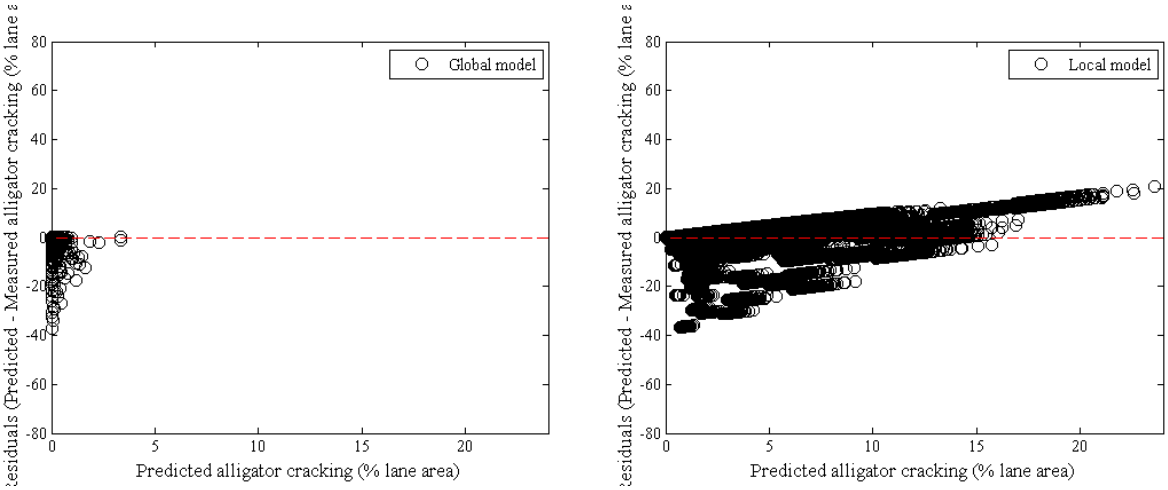

Figure B-13 Option 1a local calibration residual plots – bootstrapping

Reliability

Table B-8 Option 1a global and local alligator cracking model reliability – bootstrapping

Global model reliability equation	Local model reliability equation
$s_{e(Alligator)} = 1.13 + \frac{13}{1 + e^{7.57 - 15.5 \times log(D)}}$	$s_{e(Alligator)} = 0.7874 + \frac{17.817}{1 + e^{0.0699 - 0.4559 \times log(D)}}$

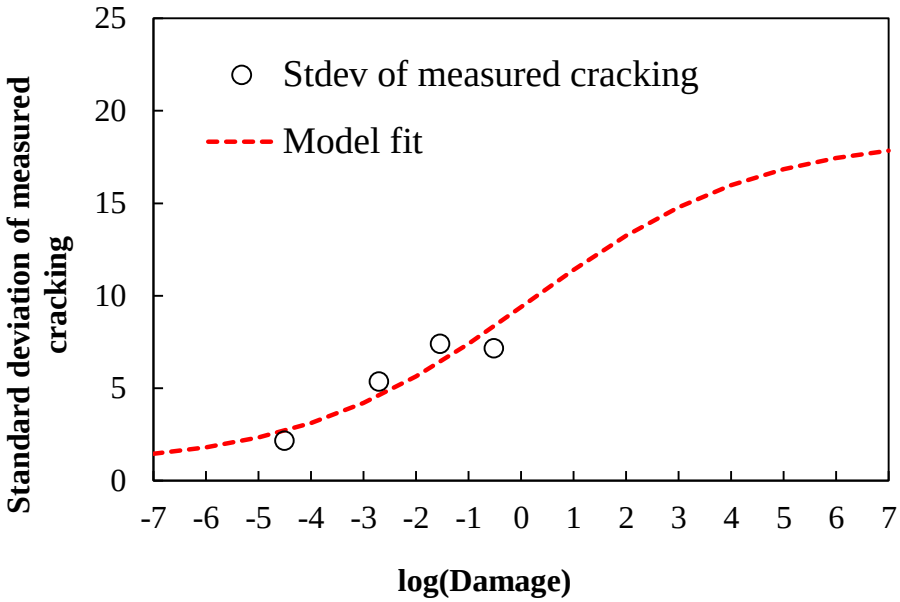

Figure B-14 Option 1a fitted reliability model after local calibration – bootstrapping

B.1.1.2 Option 1b

No sampling

Table B-9 Option 1a local calibration results – no sampling

Parameter	Global model	Local model
SEE	4.02	3.67
Bias	-2.00	-0.75
R^2	0.00	0.00
t-test pvalue	0.00	0.09
Intercept = 0	0.00	0.00
Slope = 1	0.00	0.00
C1	1.00	0.68
C2	1.00	0.56

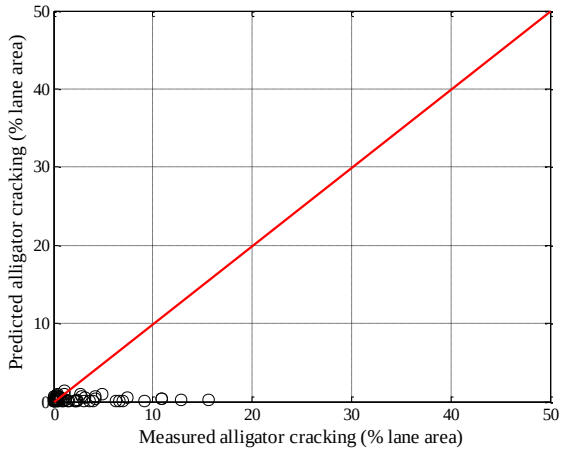

Global model

Figure B-15 Option 1b measured versus predicted fatigue cracking – no sampling

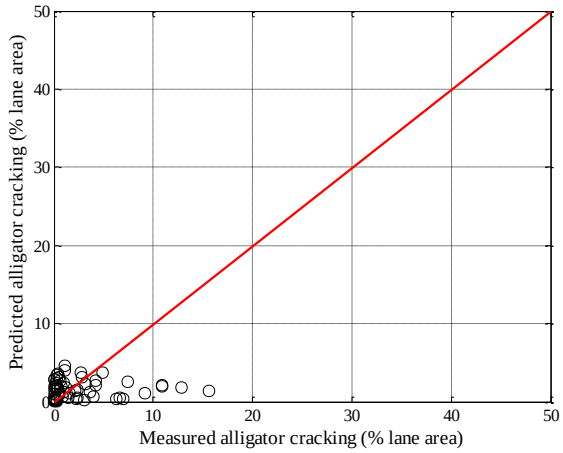

(a) Measured vs. predicted cracking

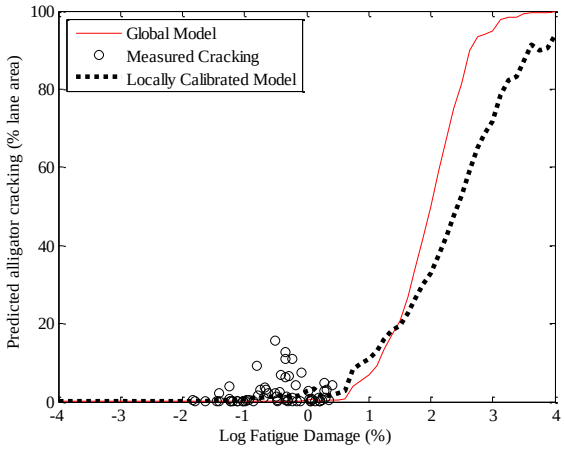

(b) Fatigue damage predicted cracking

Figure B-16 Option 1b local calibration results – no sampling

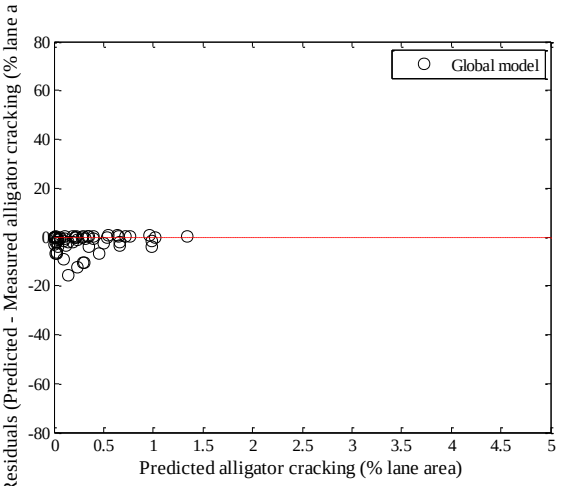

(a) Global model

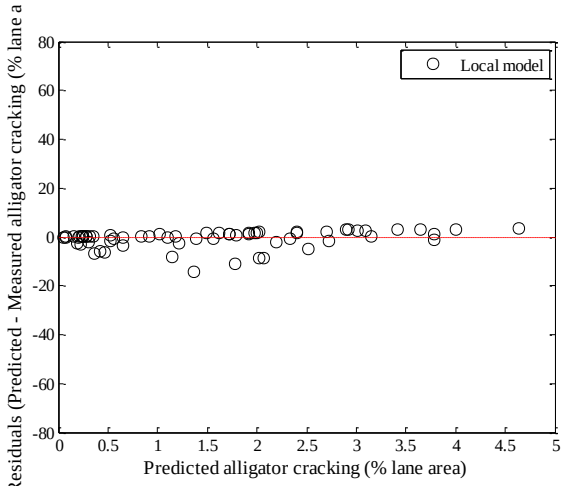

(b) Local model

Figure B-17 Option 1b local calibration residual plots – no sampling

Reliability

Table B-10 Option 1b global and local alligator cracking model reliability – no sampling

Global model reliability equation	Local model reliability equation
$s_{e(Alligator)} = 1.13 + \frac{13}{1+e^{7.57-15.5\times log(D)}}$	$s_{e(Alligator)} = 0.01 + \frac{22.074}{1+e^{1.00-0.5328\times log(D)}}$

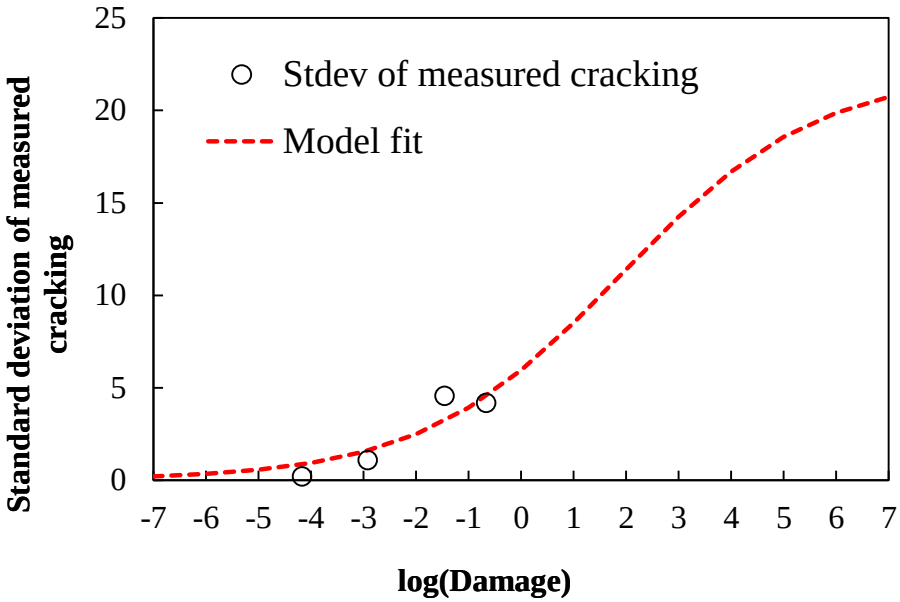

Figure B-18 Option 1b fitted reliability model after local calibration –no sampling

Split sampling

Table B-11 Option 1b local calibration results – split sampling

Parameter	Global model	Local model calibration	Local model validation
SEE	4.40	4.02	2.64
Bias	-2.22	-0.84	-0.34
R^2	0.00	0.00	0.02
t-test pvalue	0.00	0.14	0.59
Intercept = 0	0.00	0.00	0.00
Slope = 1	0.00	0.00	0.00
C1	1.00	0.68	0.68
C2	1.00	0.56	0.56

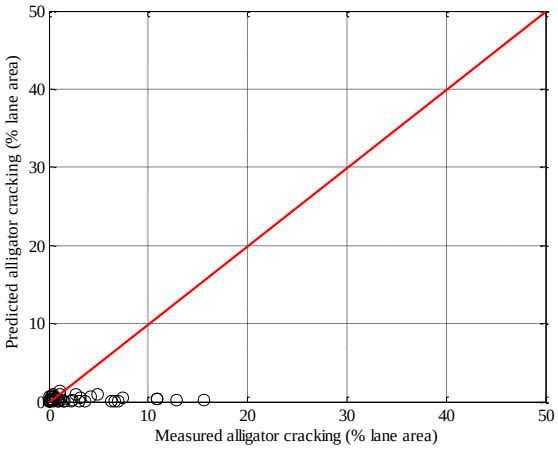

(a) Global model

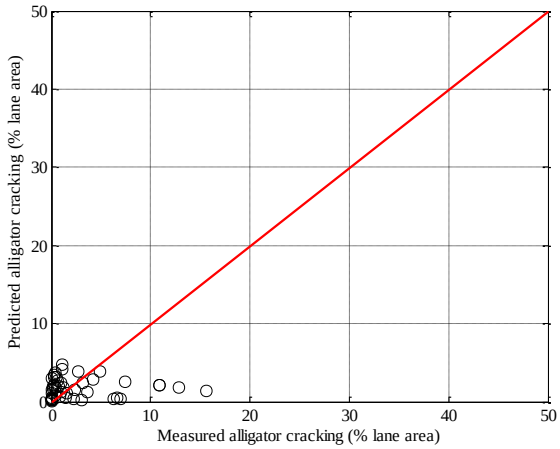

(b) Local model

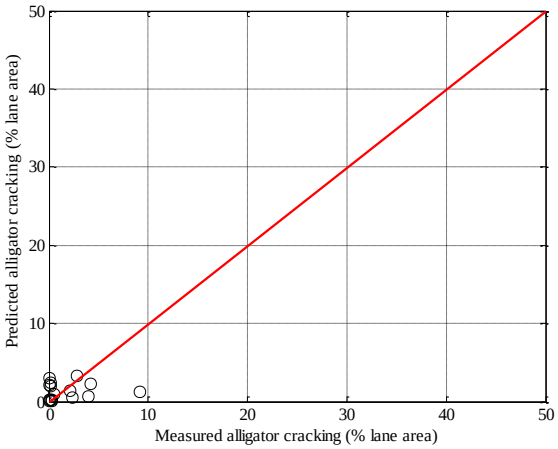

(c) Local model validation

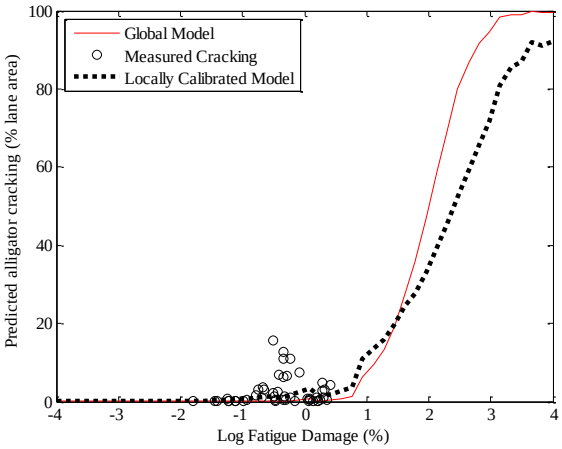

(d) Fatigue damage predicted cracking

Figure B-19 Option 1b local calibration results - split sampling

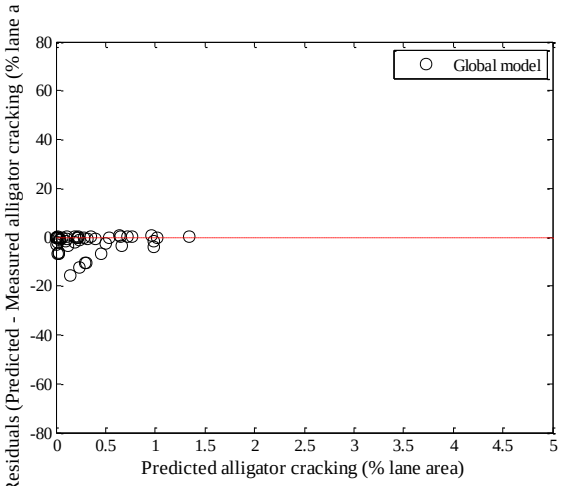

(a) Global model

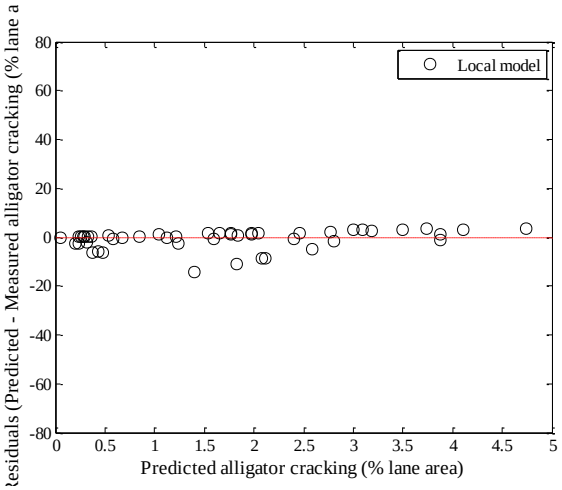

(b) Local model

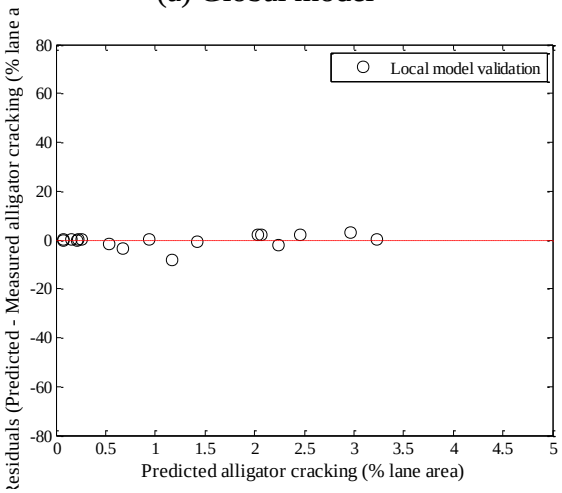

(c) Local model validation

Figure B-20 Option 1b local calibration residual plots - split sampling

Reliability

Table B-12 Option 1b global and local alligator cracking model reliability – split sampling

Global model reliability equation	Local model reliability equation
$s_{e(Alligator)} = 1.13 + \frac{13}{1 + e^{7.57 - 15.5 \times log(D)}}$	$s_{e(Alligator)} = 0.01 + \frac{24.715}{1 + e^{1.00 - 0.6448 \times log(D)}}$

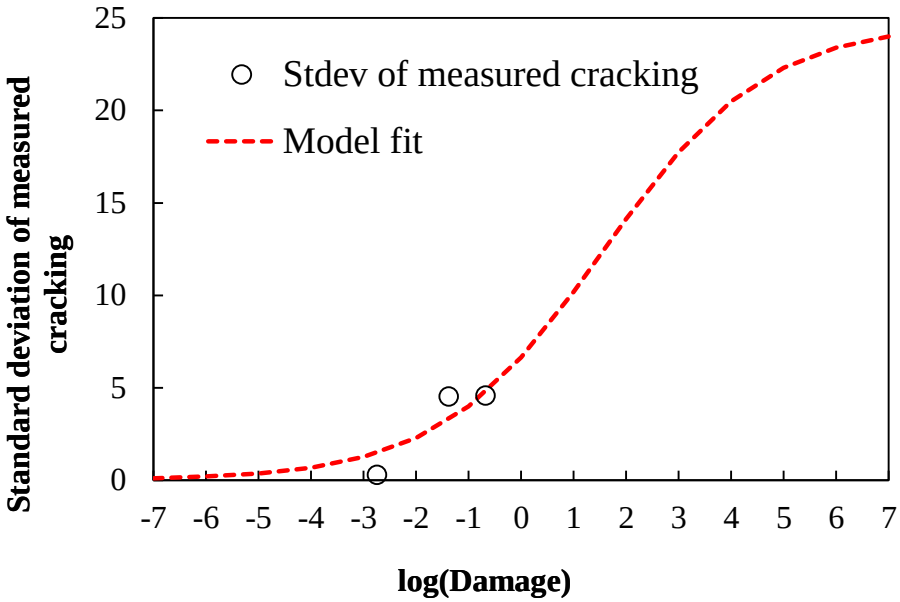

Figure B-21 Option 1b fitted reliability model after local calibration – split sampling

Repeated split sampling

Table B-13 Option 1b local calibration results – repeated split sampling

Global Model				
Parameter	Global Model Mean	Global Model Median	Global model lower CI	Global model upper CI
SEE	4.03	4.10	3.03	4.74
Bias	-2.01	-2.03	-2.56	-1.41
C1	1.00	1.00	-	-
C2	1.00	1.00	-	-
Local Model				
Parameter	Local Model Mean	Local Model Median	Local model lower CI	Local model upper CI
SEE	3.66	3.72	2.77	4.27
Bias	-0.73	-0.76	-1.04	-0.32
C1	0.68	0.68	0.61	0.72
C2	0.56	0.56	0.56	0.56
Local Model Validation				
Parameter	Local Model Mean	Local Model Median	Local model lower CI	Local model upper CI
SEE	3.77	3.76	1.87	5.41
Bias	-0.63	-0.69	-2.37	1.54
C1	0.68	0.68	0.61	0.72
C2	0.56	0.56	0.56	0.56

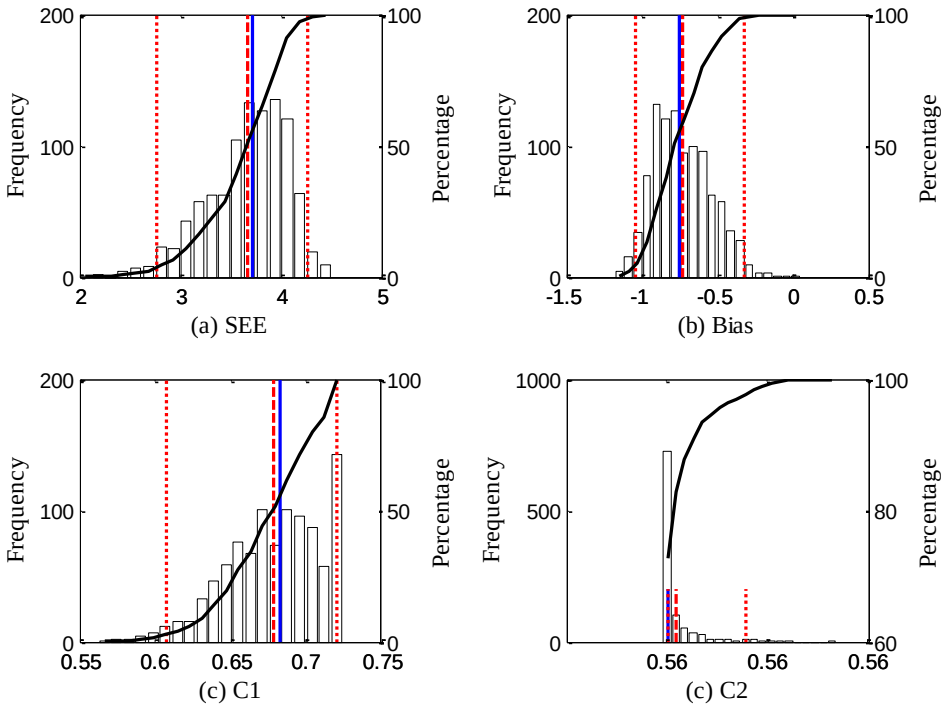

Figure B-22 Option 1b repeated split sampling frequency distributions – calibration

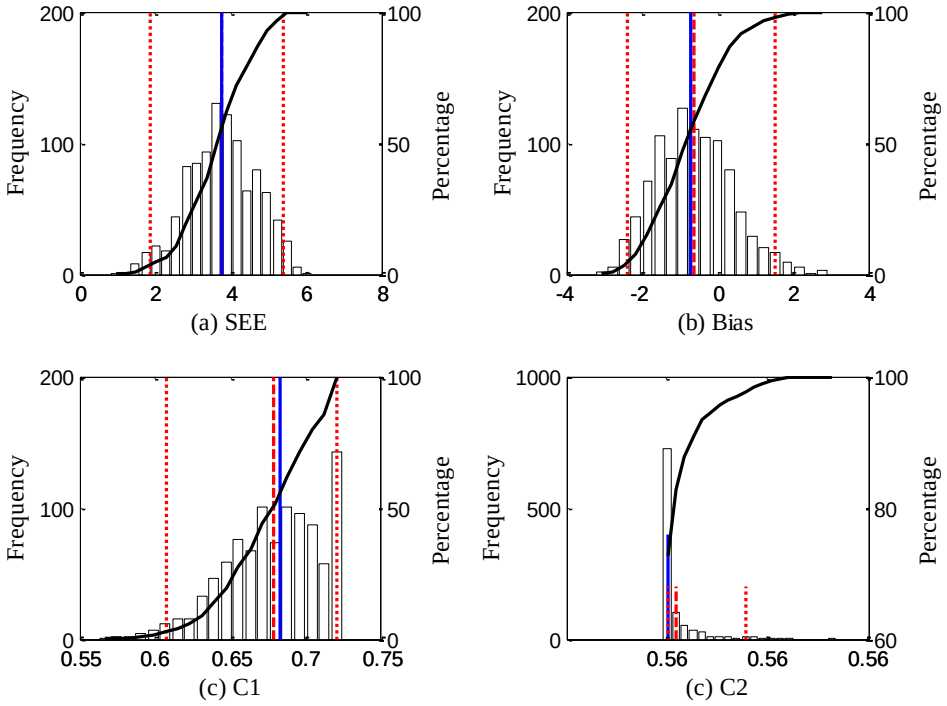

Figure B-23 Option 1b repeated split sampling frequency distributions – validation

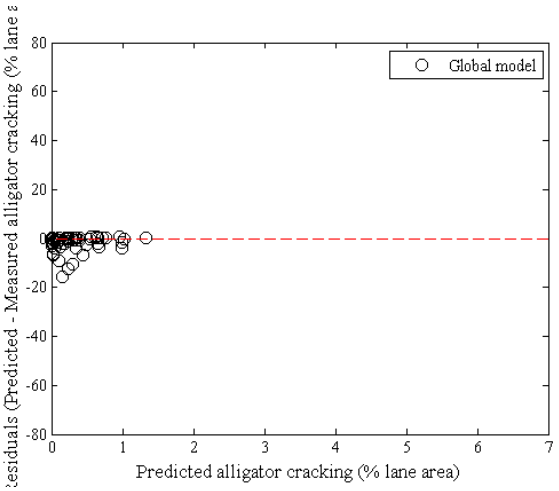

(a) Global model

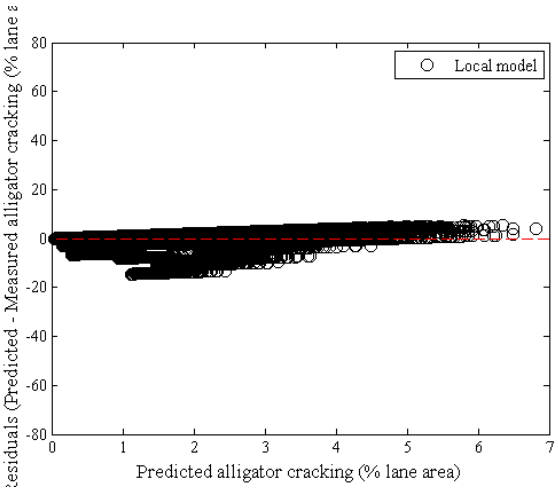

(b) Local model

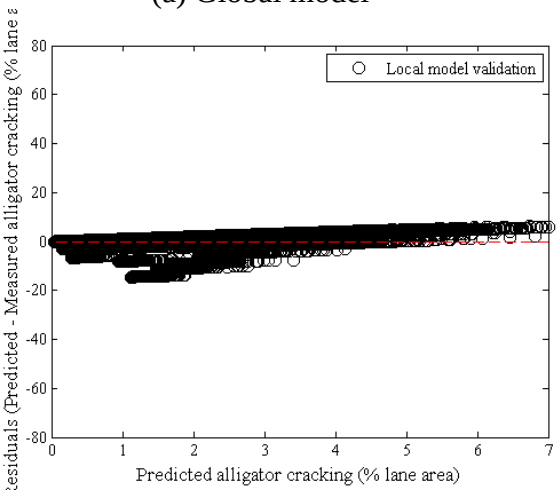

(c) Local model validation

Figure B-24 Option 1b local calibration residual plots – repeated split sampling

Reliability

Table B-14 Option 1b global and local alligator cracking model reliability – repeated split sampling

Global model reliability equation	Local model reliability equation
$s_{e(Alligator)} = 1.13 + \frac{13}{1+e^{7.57-15.5\times log(D)}}$	$s_{e(Alligator)} = 0.01 + \frac{33.088}{1+e^{1.397-0.5985\times log(D)}}$

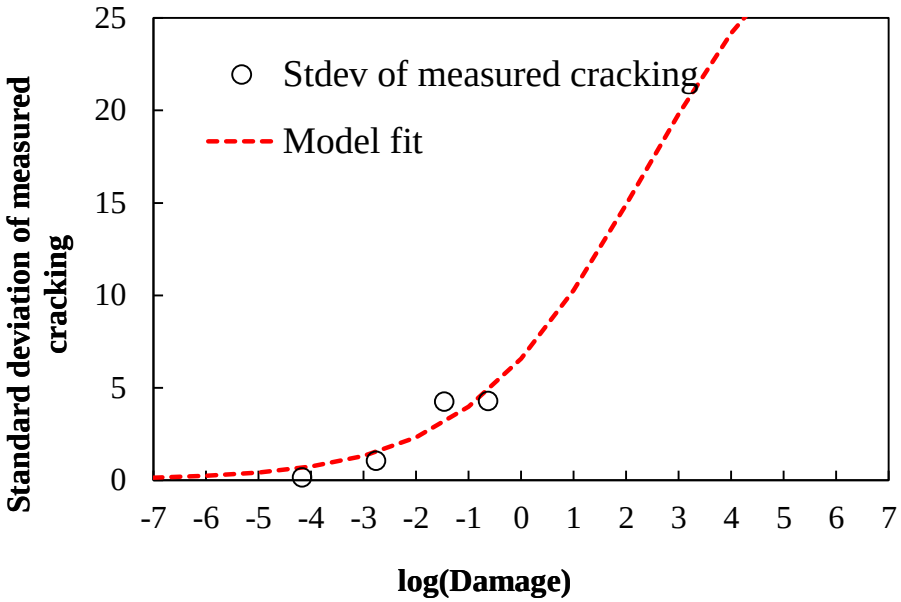

Figure B-25 Option 1b fitted reliability model after local calibration – repeated split sampling

Bootstrapping

Table B-15 Option 1b local calibration results – bootstrapping

Global Model				
Parameter	Global Model Mean	Global Model Median	Global model lower CI	Global model upper CI
SEE	3.97	3.98	2.70	5.33
Bias	-2.01	-2.00	-2.95	-1.19
C1	1.00	1.00	-	-
C2	1.00	1.00	-	-
Local Model				
Parameter	Local Model Mean	Local Model Median	Local model lower CI	Local model upper CI
SEE	3.60	3.62	2.50	4.75
Bias	-0.69	-0.69	-1.26	-0.15
C1	0.67	0.68	0.59	0.72
C2	0.56	0.56	0.56	0.56

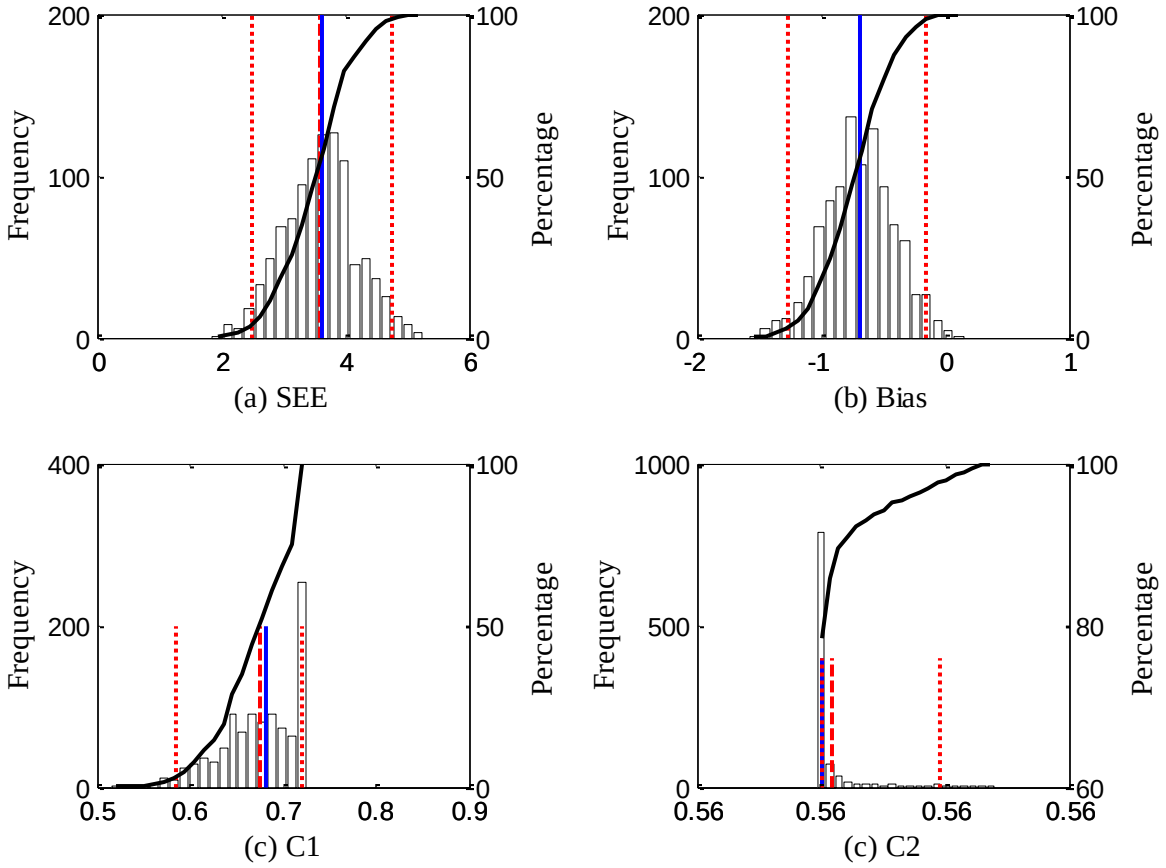

Figure B-26 Option 1b bootstrapping frequency distributions

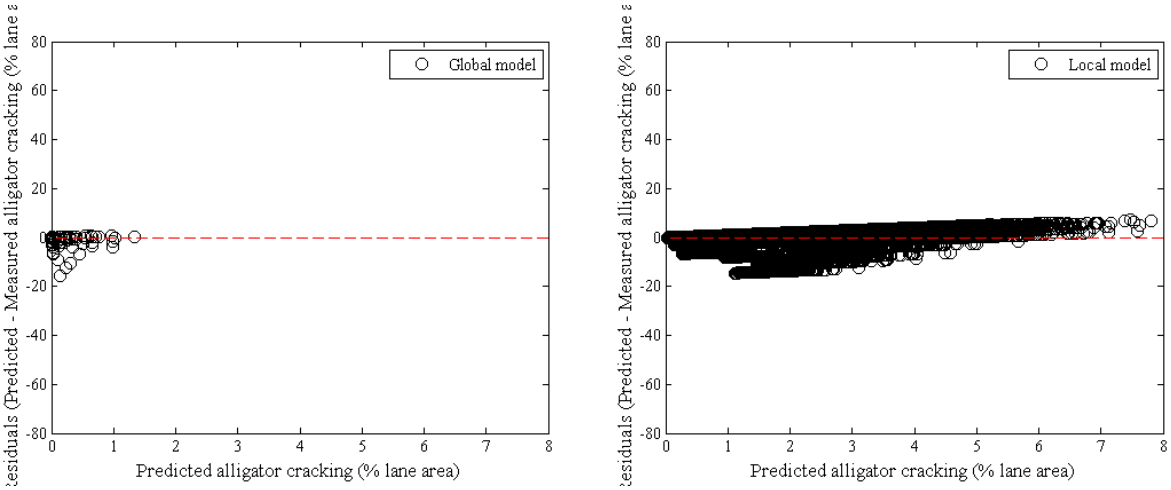

Figure B-27 Option 1b local calibration residual plots – bootstrapping

Reliability

Table B-16 Option 1b global and local alligator cracking model reliability – bootstrapping

Global model reliability equation	Local model reliability equation
$s_{e(Alligator)} = 1.13 + \frac{13}{1+e^{7.57-15.5\times log(D)}}$	$s_{e(Alligator)} = 0.01 + \frac{32.913}{1+e^{1.3972-0.5976\times log(D)}}$

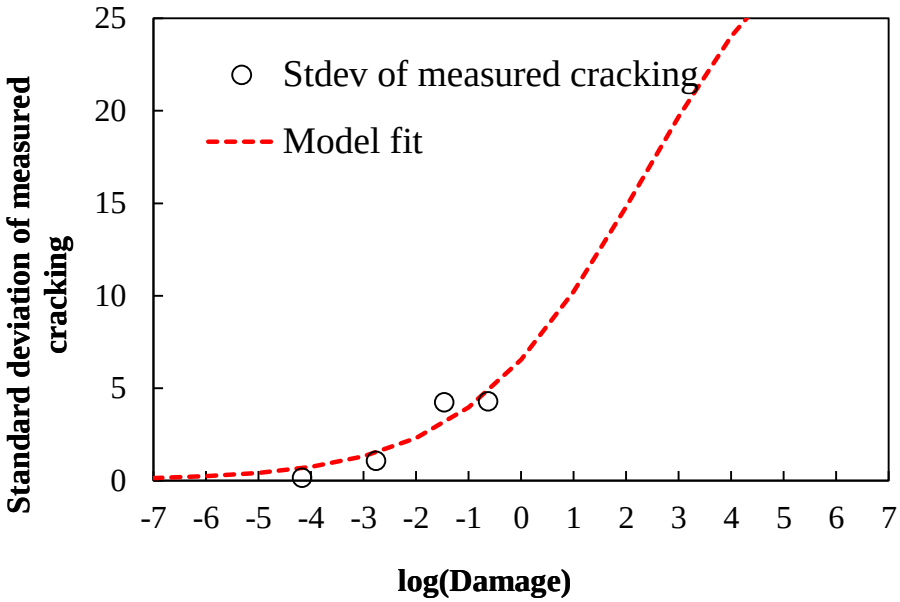

Figure B-28 Option 1b fitted reliability model after local calibration – bootstrapping

B.1.2 Fatigue Cracking Model – Top-down

B.1.2.1 Option 1

No sampling

Table B-17 Option 1 local calibration results – no sampling

Parameter	Global model	Local model
SEE	741.21	644.47
Bias	-409.32	-125.44
R^2	0.01	0.03
t-test pvalue	0.00	0.00
Intercept = 0	0.00	0.00
Slope = 1	0.00	0.00
C1	7.00	3.32
C2	3.50	1.25

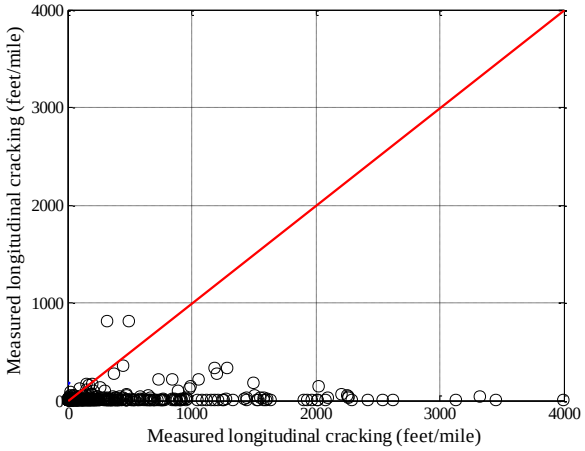

Figure B-29 Option 1 measured versus predicted fatigue cracking – no sampling

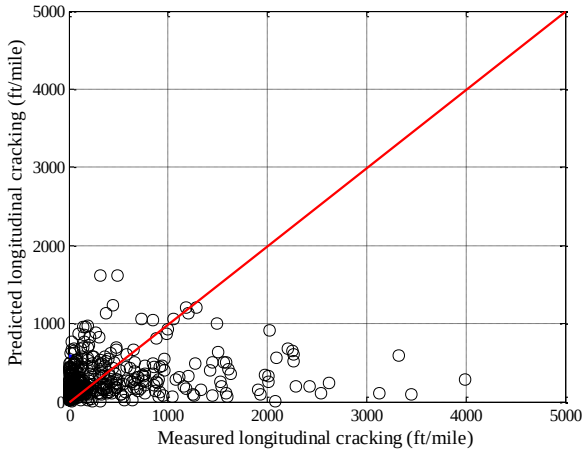

(a) Measured vs. predicted cracking

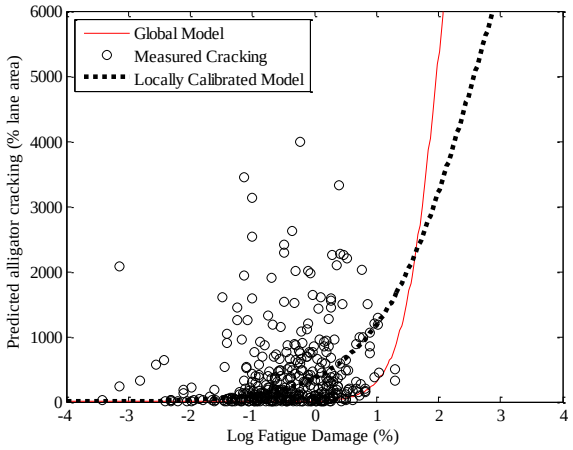

(b) Fatigue damage predicted cracking

Figure B-30 Option 1 local calibration results - no sampling

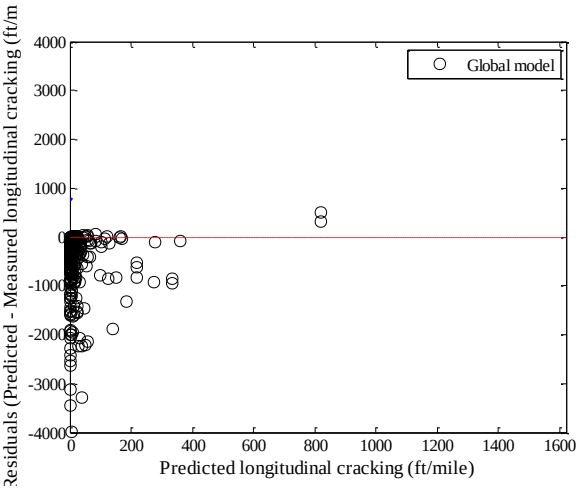

(a) Global model

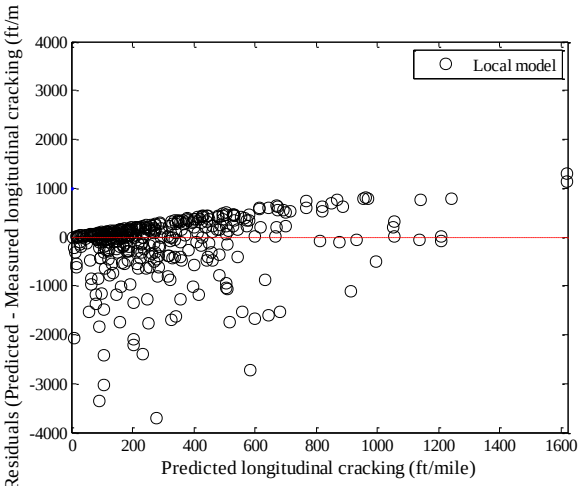

(b) Local model

Figure B-31 Option 1 local calibration residual plots - no sampling

Reliability

Table B-18 Option 1 global and local alligator cracking model reliability – no sampling

Global model reliability equation	Local model reliability equation
$s_{e(Longitudinal)} = 200 + \frac{2300}{1+e^{1.07-2.165\times log(D_{td}+0.0001)}}$	$s_{e(Longitudinal)} = 150 + \frac{2300}{1+e^{2-0.6\times log(D_{td}+0.0001)}}$

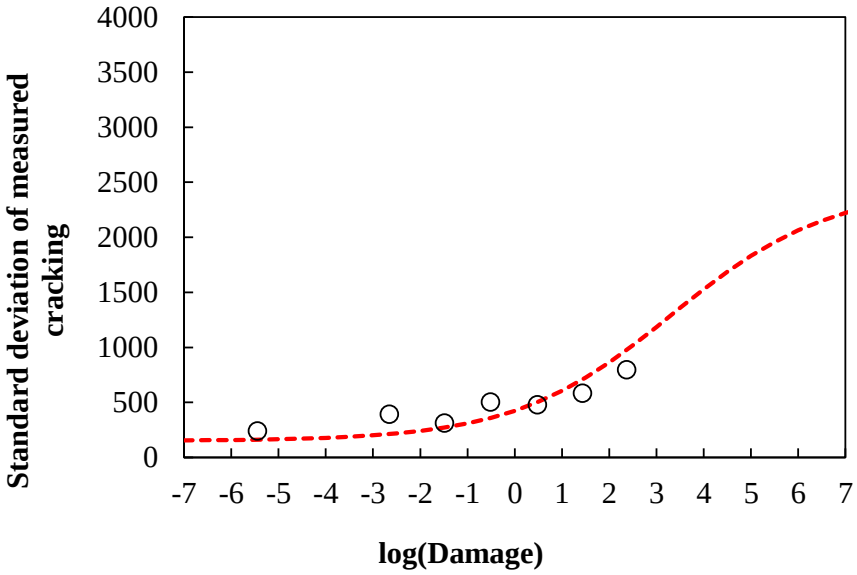

Figure B-32 Option 1 fitted reliability model after local calibration –no sampling

Split sampling

Table B-19 Option 1 local calibration results – split sampling

Parameter	Global model	Local model calibration	Local model validation
SEE	807.52	700.71	494.75
Bias	-453.48	-141.54	-68.73
R^2	0.00	0.02	0.02
t-test pvalue	0.00	0.00	0.13
Intercept = 0	0.00	0.00	0.00
Slope = 1	0.00	0.00	0.00
C1	7.00	3.30	3.30
C2	3.5	1.25	1.25

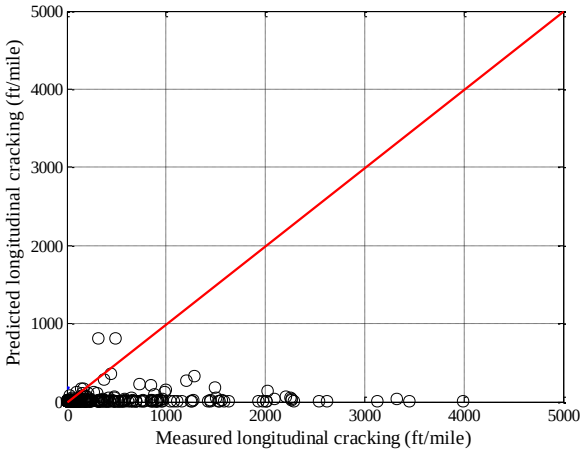

(a) Global model

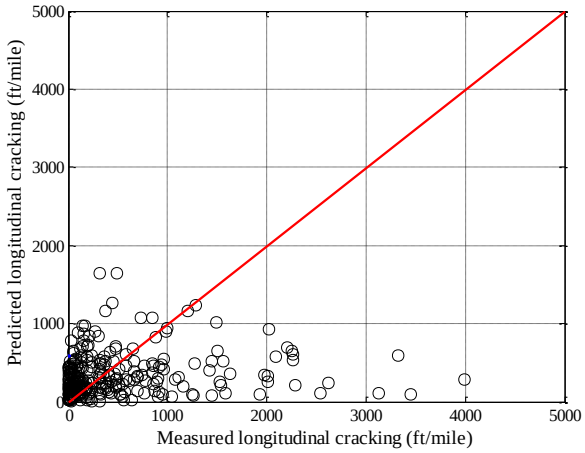

(b) Local model

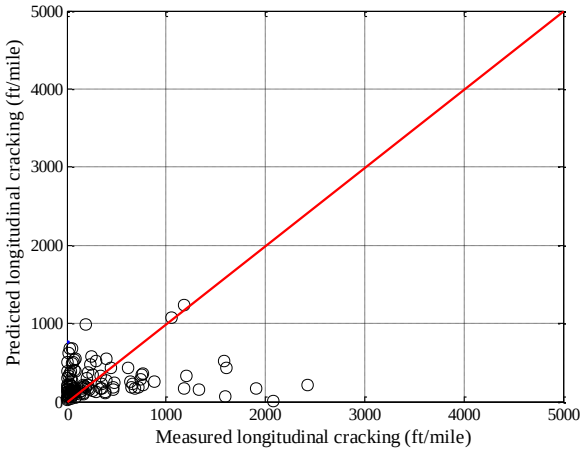

(c) Local model validation

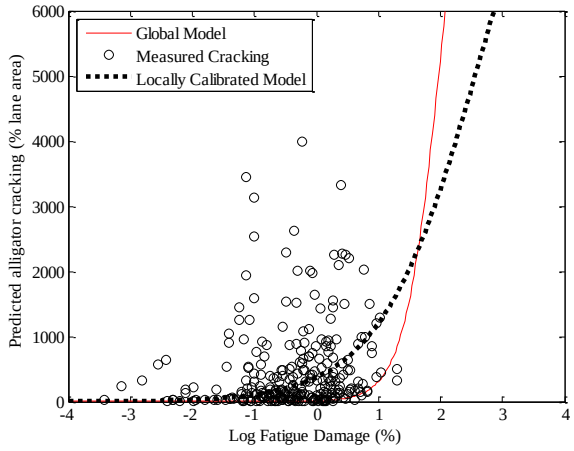

(d) Fatigue damage predicted cracking

Figure B-33 Option 1 local calibration results - split sampling

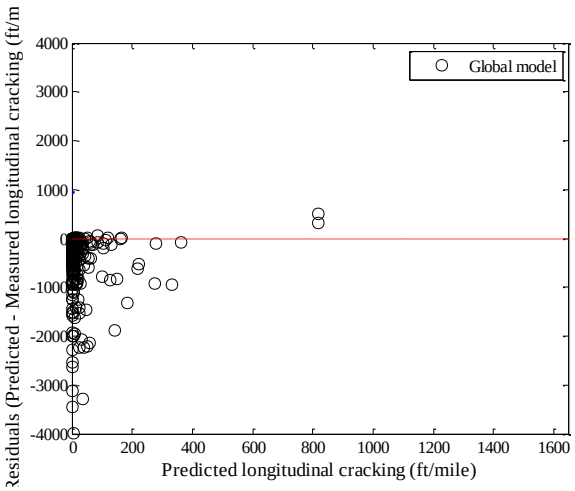

(a) Global model

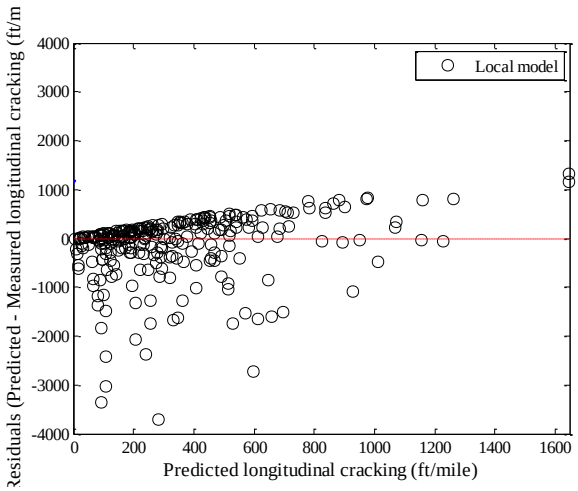

(b) Local model

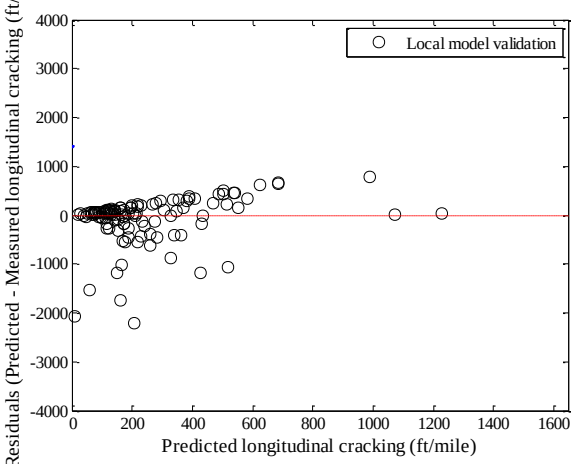

(c) Local model validation

Figure B-34 Option 1 local calibration residual plots - split sampling

Reliability

Table B-20 Option 1 global and local alligator cracking model reliability – split sampling

Global model reliability equation	Local model reliability equation
$s_{e(Longitudinal)} = 200 + \frac{2300}{1+e^{1.07-2.165\times log(D_{td}+0.0001)}}$	$s_{e(Longitudinal)} = 150 + \frac{2300}{1+e^{2.1-0.4\times log(D_{td}+0.0001)}}$

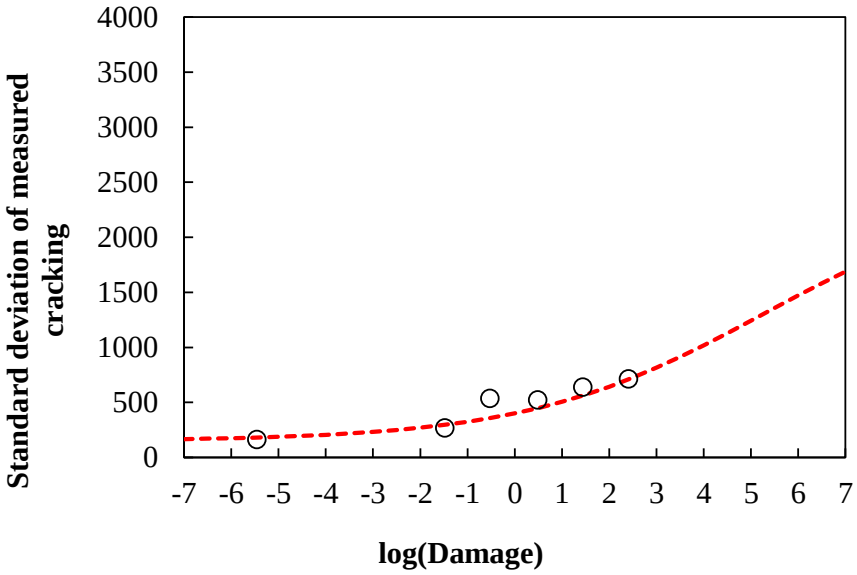

Figure B-35 Option 1 fitted reliability model after local calibration – split sampling

Repeated split sampling

Table B-21 Option 1 local calibration results – repeated split sampling

Global Model				
Parameter	Global Model Mean	Global Model Median	Global model lower CI	Global model upper CI
SEE	739.96	742.34	642.99	818.50
Bias	-408.56	-408.06	-460.33	-353.78
C1	7.00	7.00	-	-
C2	3.50	3.50	-	-
Local Model				
Parameter	Local Model Mean	Local Model Median	Local model lower CI	Local model upper CI
SEE	642.53	645.28	555.83	710.83
Bias	-124.58	-124.76	-157.32	-90.77
C1	3.32	3.32	3.16	3.52
C2	1.25	1.25	1.25	1.25
Local Model Validation				
Parameter	Local Model Mean	Local Model Median	Local model lower CI	Local model upper CI
SEE	648.70	650.68	466.25	830.75
Bias	-124.93	-128.32	-308.60	64.65
C1	3.32	3.32	3.16	3.52
C2	1.25	1.25	1.25	1.25

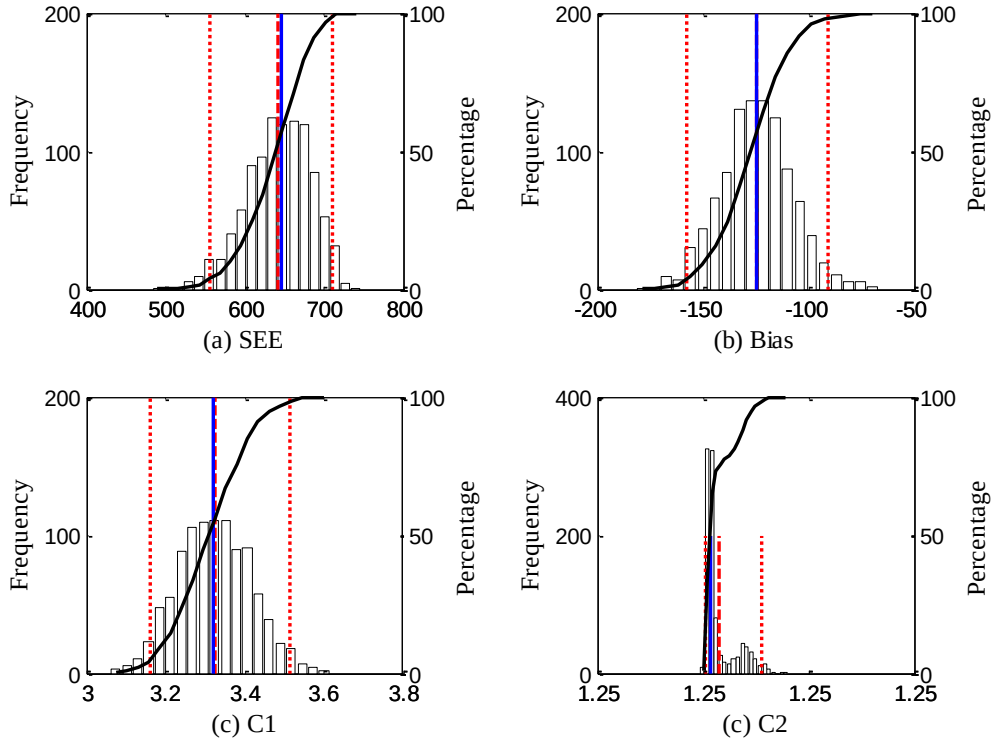

Figure B-36 Option 1 repeated split sampling frequency distributions – calibration

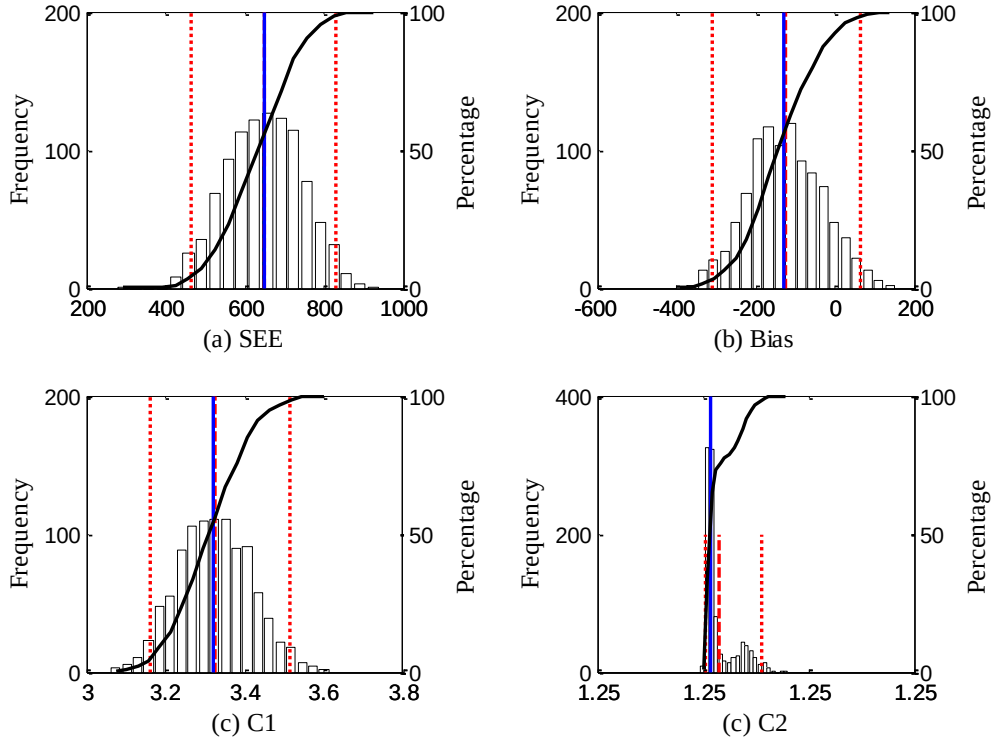

Figure B-37 Option 1 repeated split sampling frequency distributions – validation

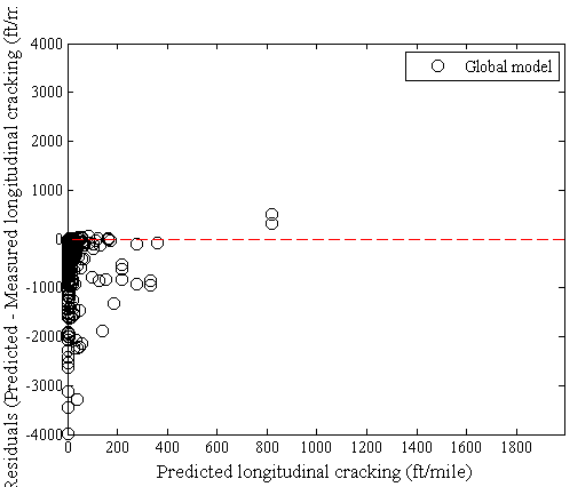

(a) Global model

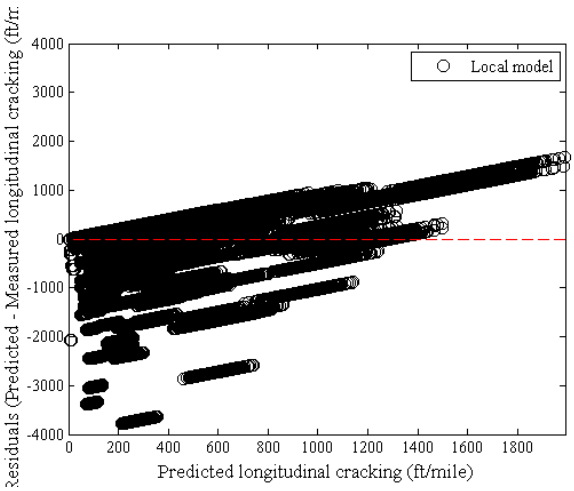

(b) Local model

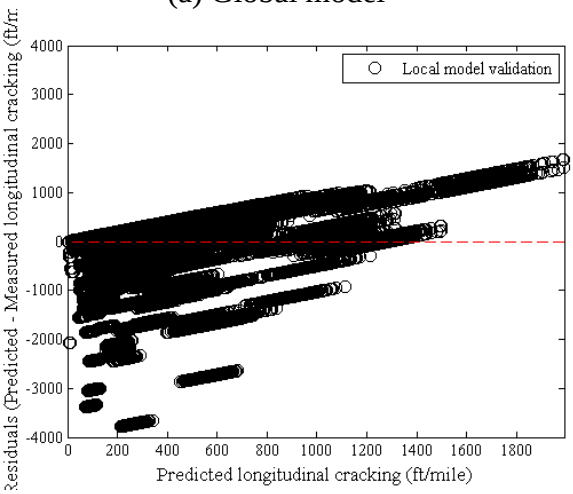

(c) Local model validation

Figure B-38 Option 1 local calibration residual plots – repeated split sampling

Reliability

Table B-22 Option 1 global and local alligator cracking model reliability – repeated split sampling

Global model reliability equation	Local model reliability equation
$s_{e(Longitudinal)} = 200 + \frac{2300}{1+e^{1.07-2.165\times log(D_{td}+0.0001)}}$	$s_{e(Longitudinal)} = 150 + \frac{2300}{1+e^{2.2-0.61\times log(D_{td}+0.0001)}}$

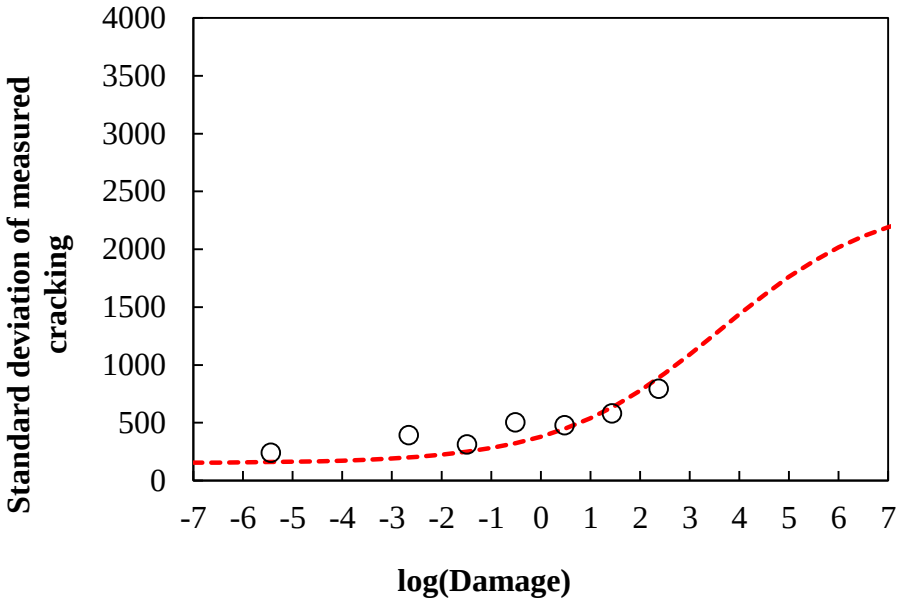

Figure B-39 Option 1 fitted reliability model after local calibration – repeated split sampling

Bootstrapping

Table B-23 Option 1 local calibration results – bootstrapping

Global Model				
Parameter	Global Model Mean	Global Model Median	Global model lower CI	Global model upper CI
SEE	741.41	738.34	614.64	871.40
Bias	-411.36	-409.36	-495.00	-335.23
C1	7.00	7.00	-	-
C2	3.50	3.50	-	-
Local Model				
Parameter	Local Model Mean	Local Model Median	Local model lower CI	Local model upper CI
SEE	641.44	640.16	526.91	759.87
Bias	-122.72	-121.44	-175.87	-73.53
C1	3.32	3.32	3.04	3.58
C2	1.25	1.25	1.25	1.25

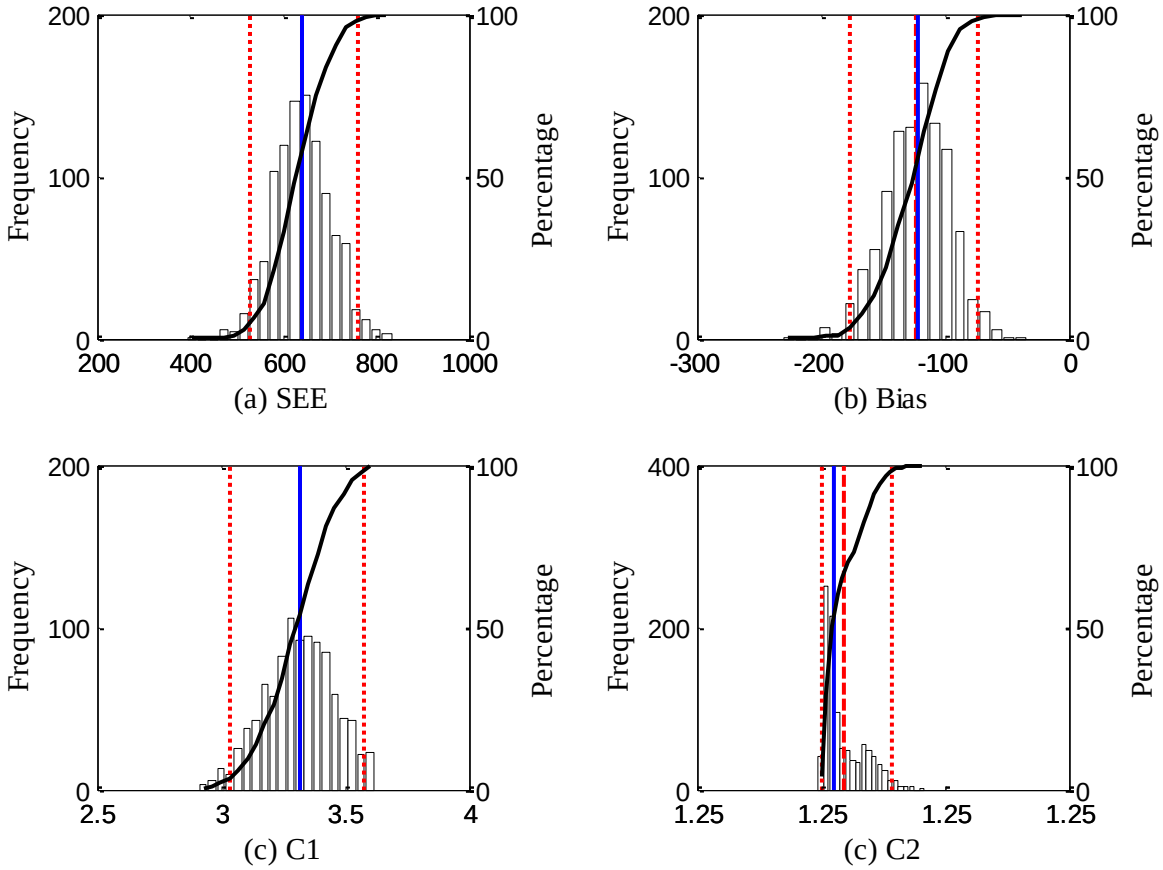

Figure B-40 Option 1 bootstrapping frequency distributions

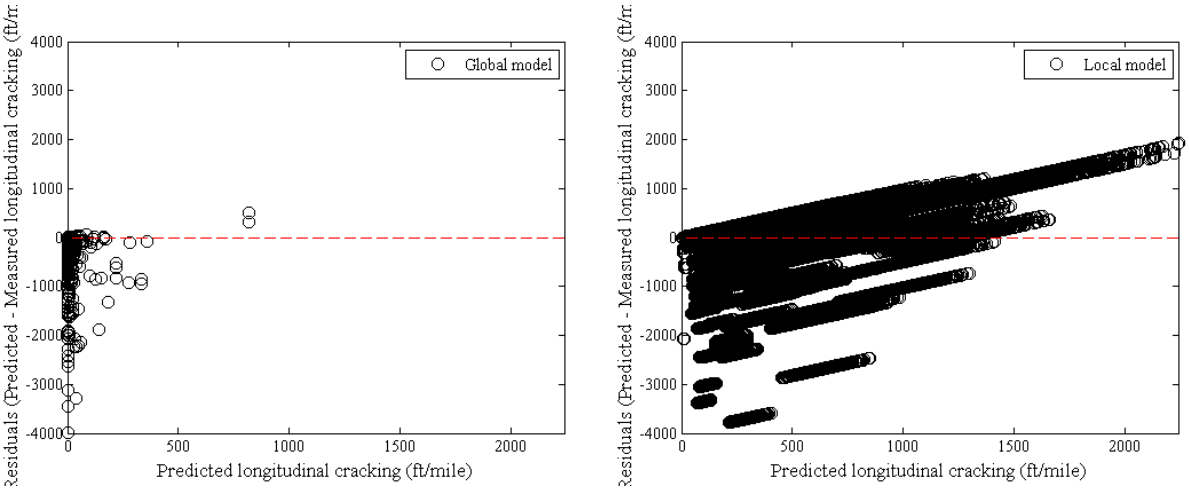

(a) Global model (b) Local model

Figure B-41 Option 1 local calibration residual plots – bootstrapping

Reliability

Table B-24 Option 1 global and local alligator cracking model reliability – bootstrapping

Global model reliability equation	Local model reliability equation
$s_{e(Longitudinal)} = 200 + \frac{2300}{1+e^{1.07-2.165\times log(D_{td}+0.0001)}}$	$s_{e(Longitudinal)} = 150 + \frac{2300}{1+e^{1.9-0.6\times log(D_{td}+0.0001)}}$

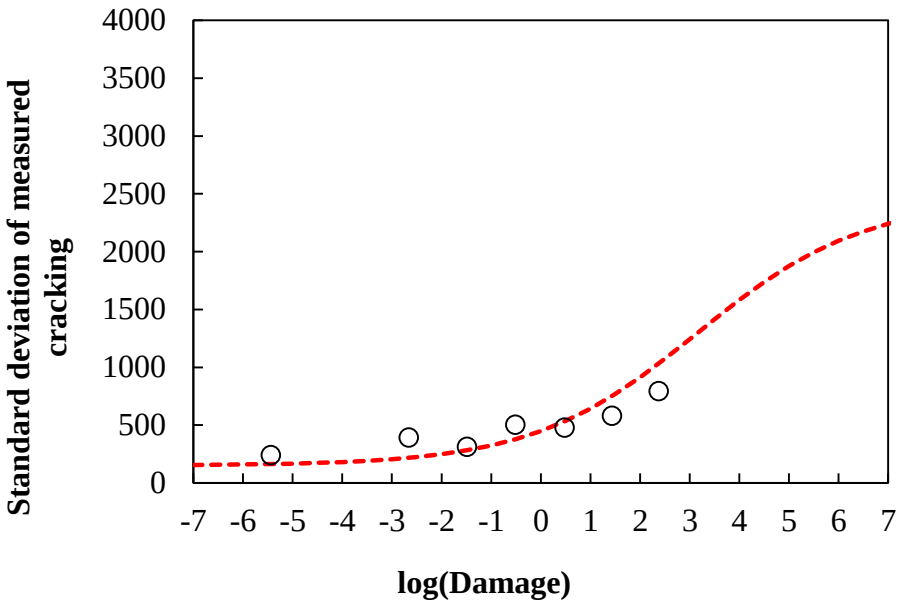

Figure B-42 Option 1 fitted reliability model after local calibration – bootstrapping

B.1.2.2 Option 2

No sampling

Table B-25 Option 2 local calibration results – no sampling

Parameter	Global model	Local model
SEE	998.85	856.06
Bias	-580.99	-185.37
R^2	0.01	0.03
t-test pvalue	0.00	0.00
Intercept = 0	0.00	0.00
Slope = 1	0.00	0.00
C1	7.00	2.97
C2	3.50	1.20

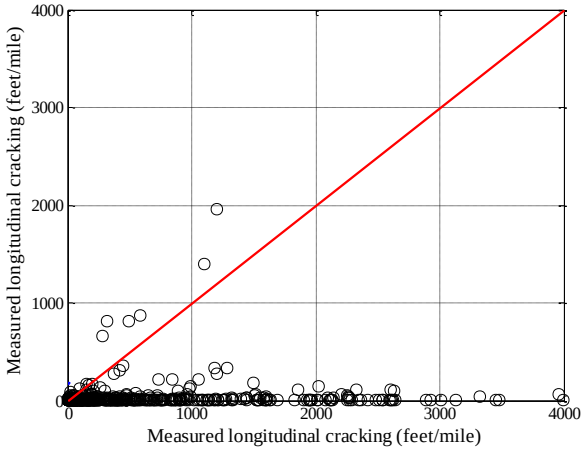

Global model

Figure B-43 Option 2 measured versus predicted fatigue cracking – no sampling

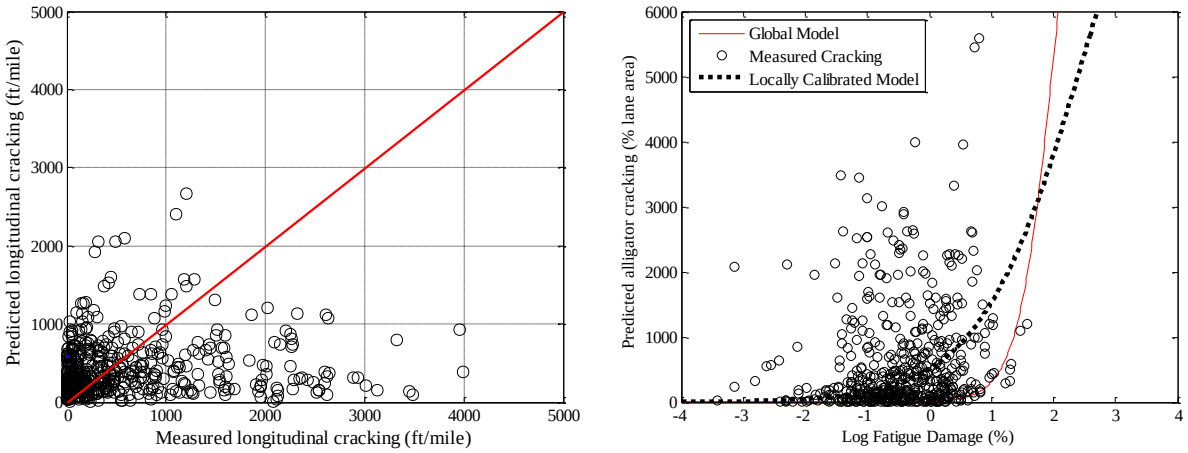

(a) Measured vs. predicted cracking (b) Fatigue damage predicted cracking

Figure B-44 Option 2 local calibration results – no sampling

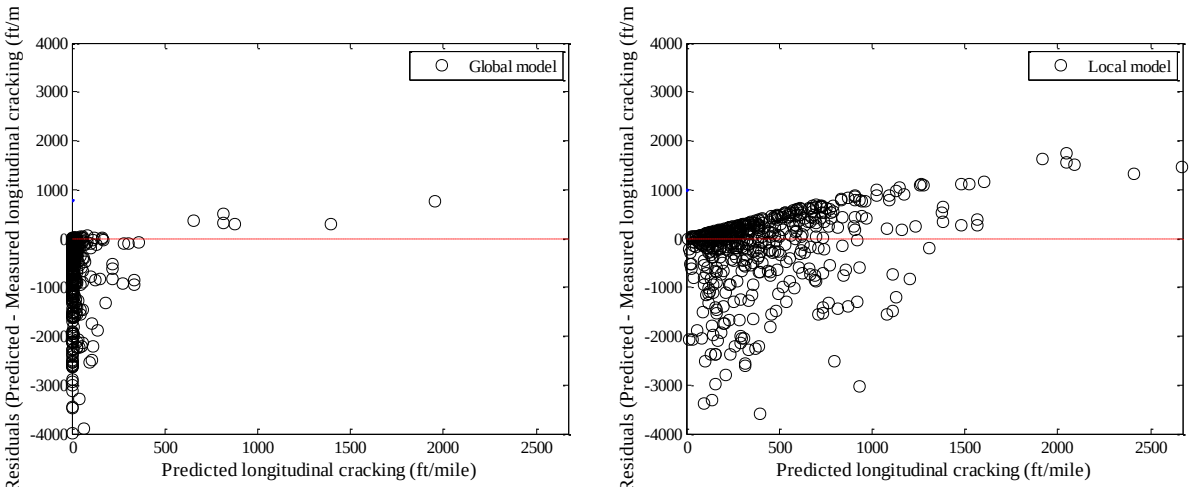

(a) Global model (b) Local model

Figure B-45 Option 2 local calibration residual plots – no sampling

Reliability

Table B-26 Option 2 global and local alligator cracking model reliability – no sampling

Global model reliability equation	Local model reliability equation
$s_{e(Longitudinal)} = 200 + \frac{2300}{1+e^{1.07-2.165\times log(D_{td}+0.0001)}}$	$s_{e(Longitudinal)} = 300 + \frac{3000}{1+e^{1.8-0.61\times log(D_{td}+0.0001)}}$

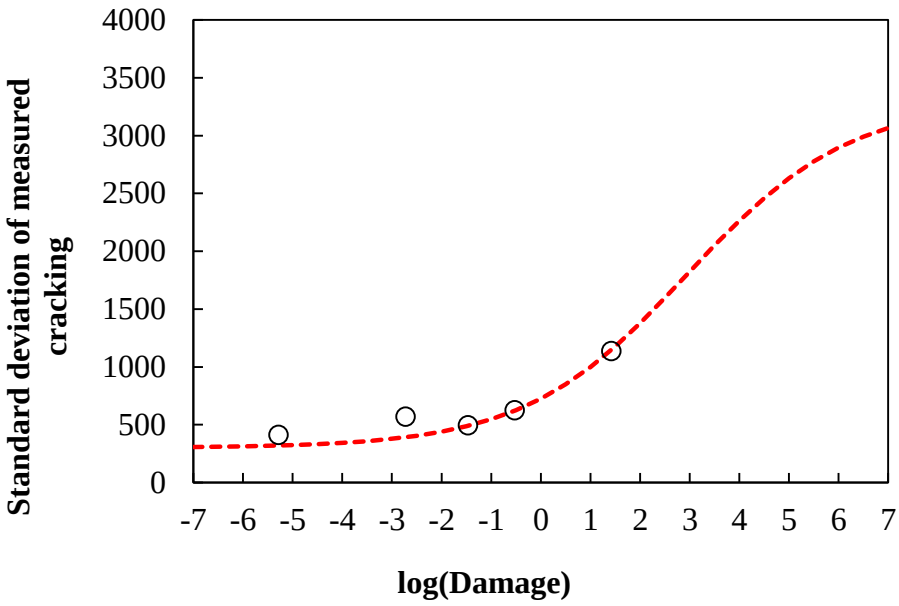

Figure B-46 Option 2 fitted reliability model after local calibration –no sampling

Split sampling

Table B-27 Option 2 local calibration results – split sampling

Parameter	Global model	Local model calibration	Local model validation
SEE	997.83	858.43	856.74
Bias	-563.66	-177.72	-148.71
R^2	0.01	0.03	0.01
t-test pvalue	0.00	0.00	0.03
Intercept = 0	0.03	0.00	0.00
Slope = 1	0.00	0.00	0.00
C1	7.00	2.93	2.93
C2	3.50	1.20	1.20

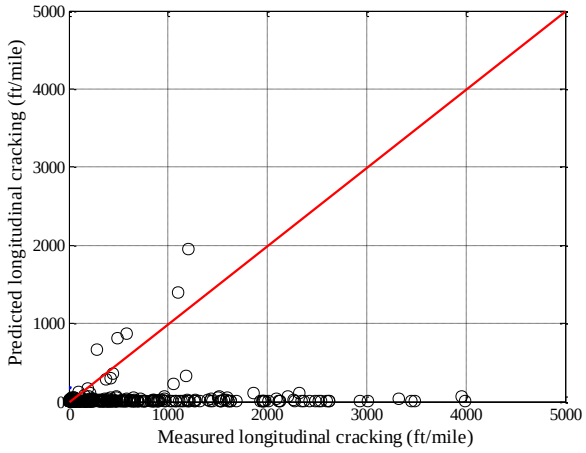

(a) Global model

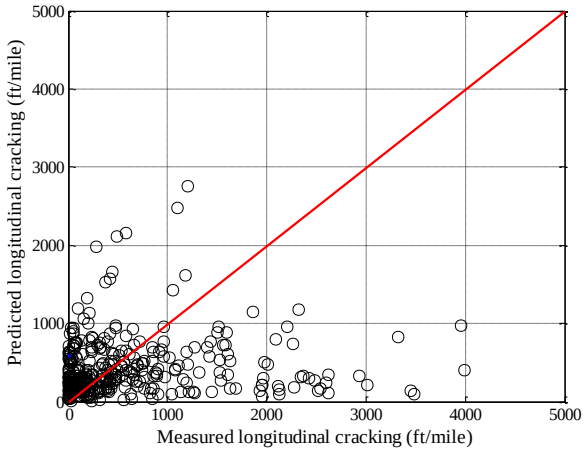

(b) Local model

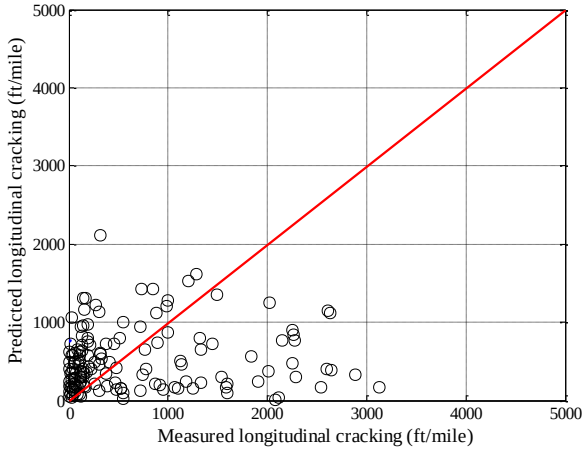

(c) Local model validation

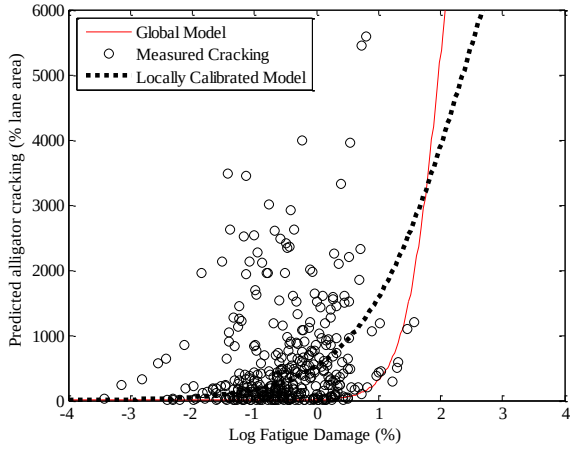

(d) Fatigue damage predicted cracking

Figure B-47 Option 2 local calibration results - split sampling

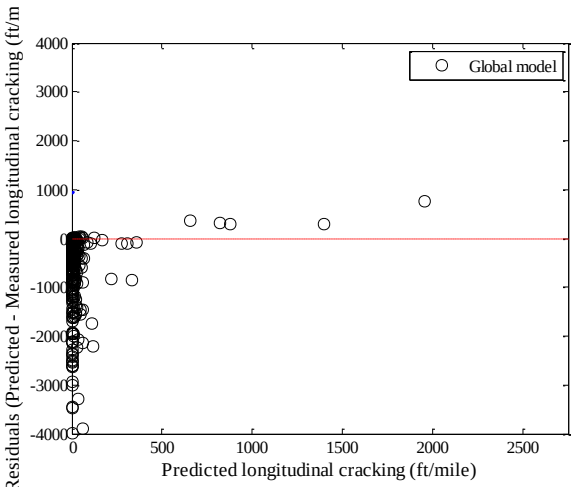

(a) Global model

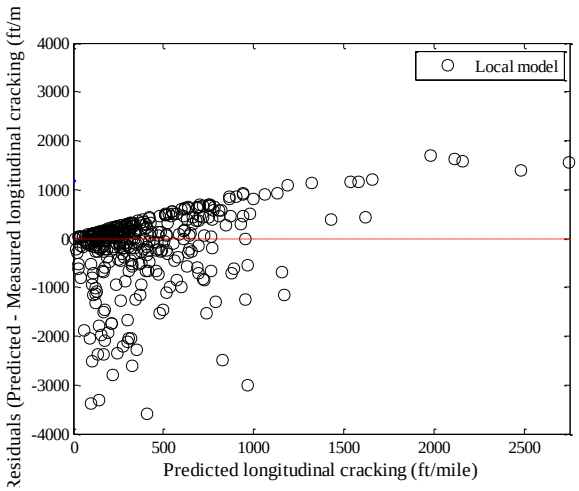

(b) Local model

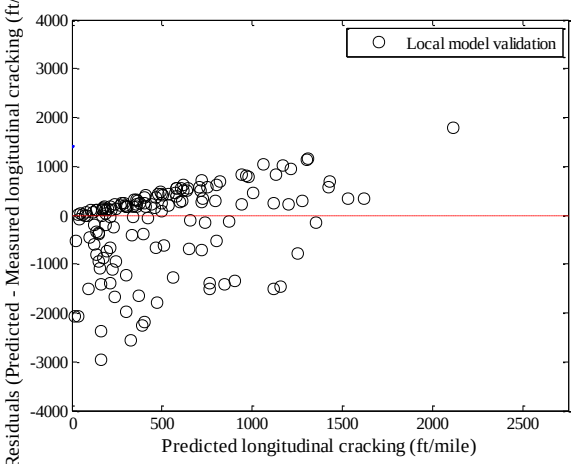

(c) Local model validation

Figure B-48 Option 2 local calibration residual plots - split sampling

Reliability

Table B-28 Option 2 global and local alligator cracking model reliability – split sampling

Global model reliability equation	Local model reliability equation
$s_{e(Longitudinal)} = 200 + \frac{2300}{1+e^{1.07-2.165\times log(D_{td}+0.0001)}}$	$s_{e(Longitudinal)} = 250 + \frac{3000}{1+e^{1.9677-1.2723\times log(D_{td}+0.0001)}}$

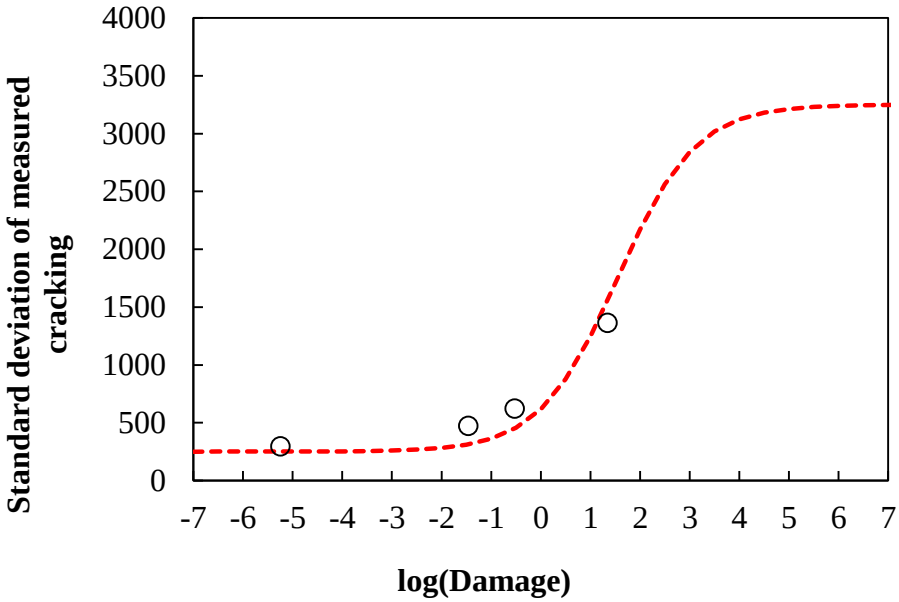

Figure B-49 Option 2 fitted reliability model after local calibration – split sampling

Repeated split sampling

Table B-29 Option 2 local calibration results – repeated split sampling

Global Model				
Parameter	Global Model Mean	Global Model Median	Global model lower CI	Global model upper CI
SEE	997.60	1007.73	865.75	1092.97
Bias	-581.11	-583.28	-646.35	-509.97
C1	7.00	7.00	-	-
C2	3.50	3.50	-	-
Local Model				
Parameter	Local Model Mean	Local Model Median	Local model lower CI	Local model upper CI
SEE	853.26	857.89	748.64	935.63
Bias	-184.74	-184.62	-237.16	-128.13
C1	2.98	2.98	2.75	3.20
C2	1.20	1.20	1.20	1.20
Local Model Validation				
Parameter	Local Model Mean	Local Model Median	Local model lower CI	Local model upper CI
SEE	864.65	861.78	648.52	1084.79
Bias	-180.99	-182.84	-417.00	93.67
C1	2.98	2.98	2.75	3.20
C2	1.20	1.20	1.20	1.20

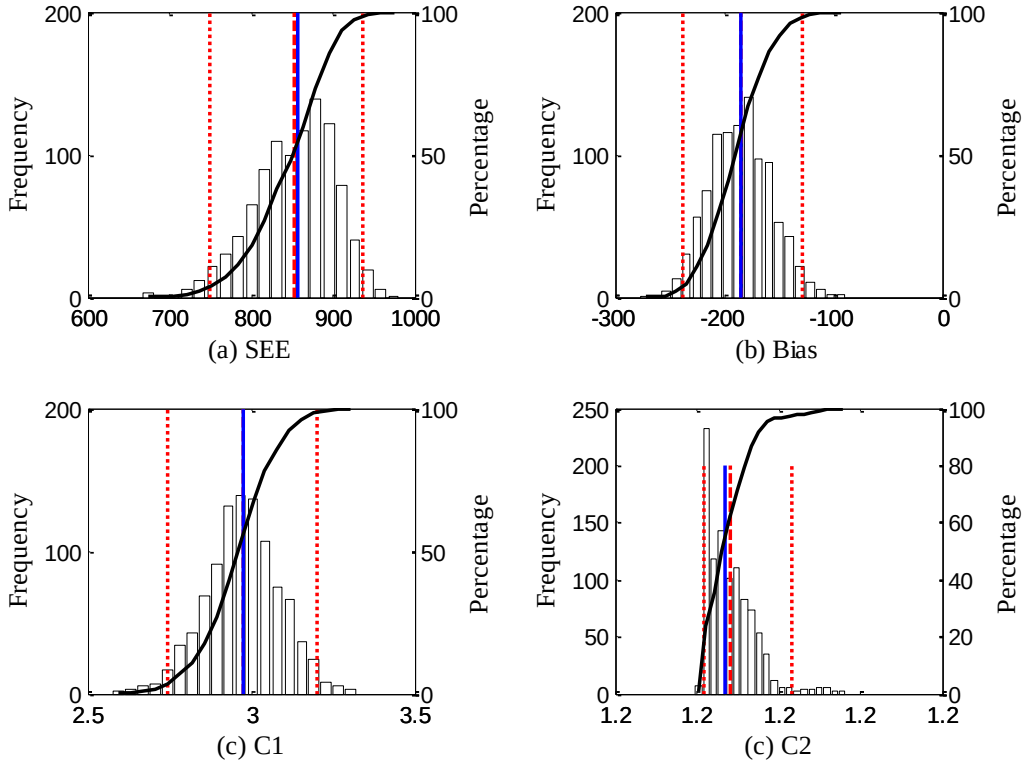

Figure B-50 Option 2 repeated split sampling frequency distributions – calibration

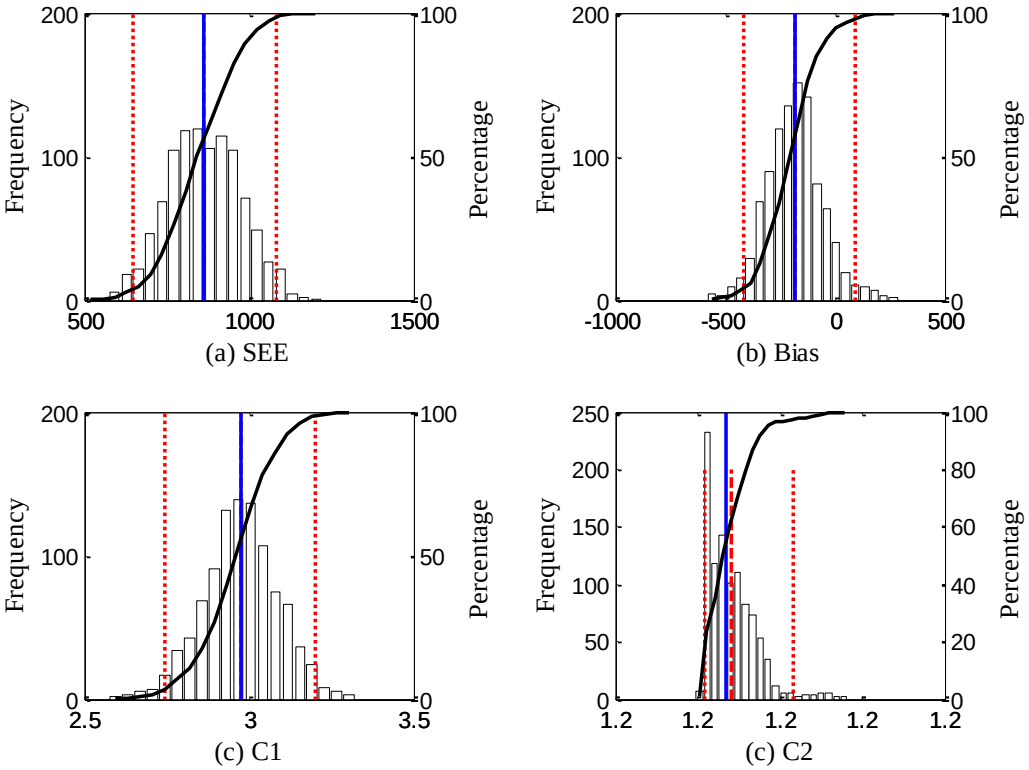

Figure B-51 Option 2 repeated split sampling frequency distributions – validation

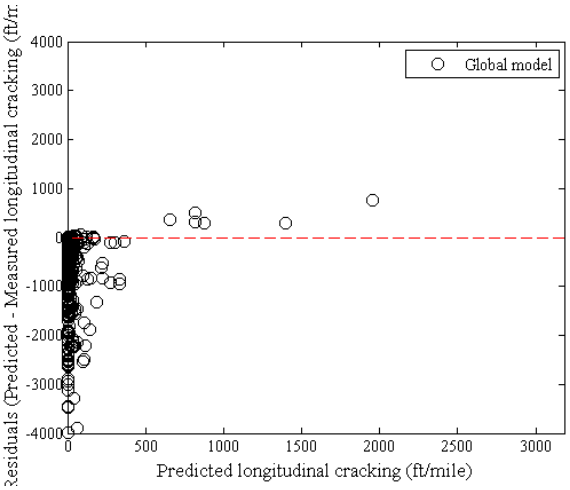

(a) Global model

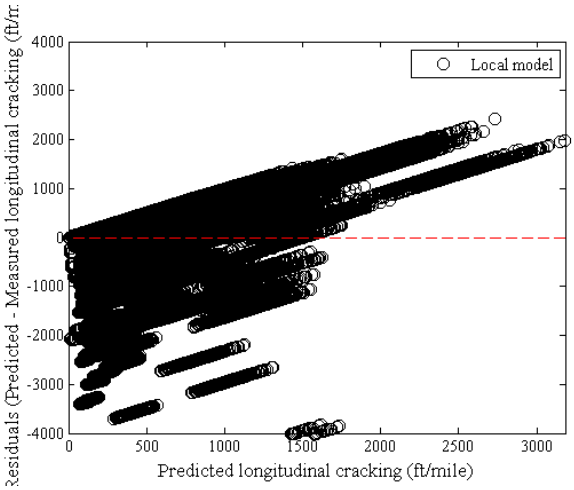

(b) Local model

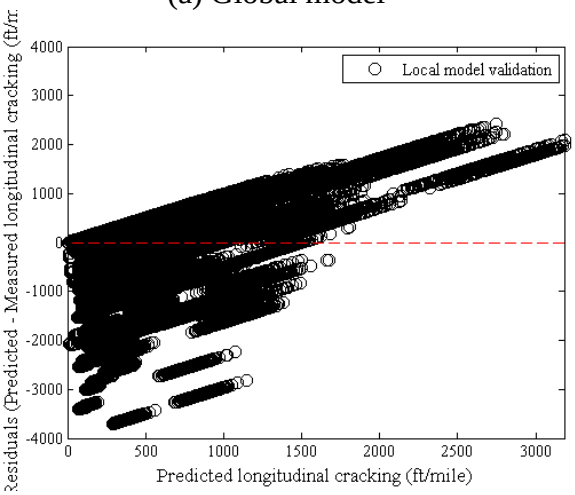

(c) Local model validation

Figure B-52 Option 2 local calibration residual plots – repeated split sampling

Reliability

Table B-30 Option 2 global and local alligator cracking model reliability – repeated split sampling

Global model reliability equation	Local model reliability equation
$s_{e(Longitudinal)} = 200 + \frac{2300}{1+e^{1.07-2.165\times log(D_{td}+0.0001)}}$	$s_{e(Longitudinal)} = 300 + \frac{3000}{1+e^{1.8-0.61\times log(D_{td}+0.0001)}}$

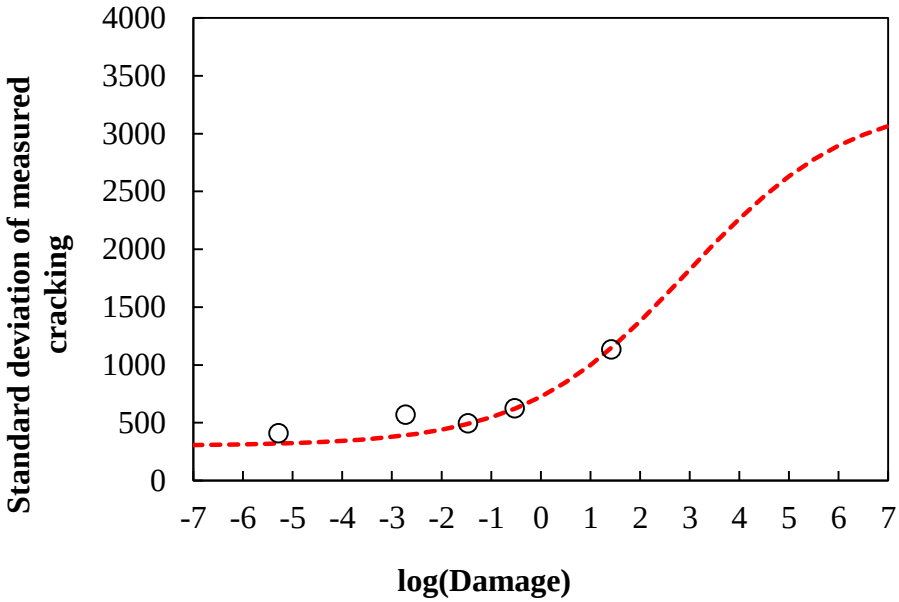

Figure B-53 Option 2 fitted reliability model after local calibration – repeated split sampling

Bootstrapping

Table B-31 Option 2 local calibration results – bootstrapping

Global Model				
Parameter	Global Model Mean	Global Model Median	Global model lower CI	Global model upper CI
SEE	996.20	992.28	831.70	1200.25
Bias	-580.85	-580.61	-691.15	-480.97
C1	7.00	7.00	-	-
C2	3.50	3.50	-	-
Local Model				
Parameter	Local Model Mean	Local Model Median	Local model lower CI	Local model upper CI
SEE	850.44	847.03	717.48	1018.32
Bias	-181.97	-180.66	-264.64	-105.74
C1	2.97	2.98	2.64	3.29
C2	1.20	1.20	1.20	1.20

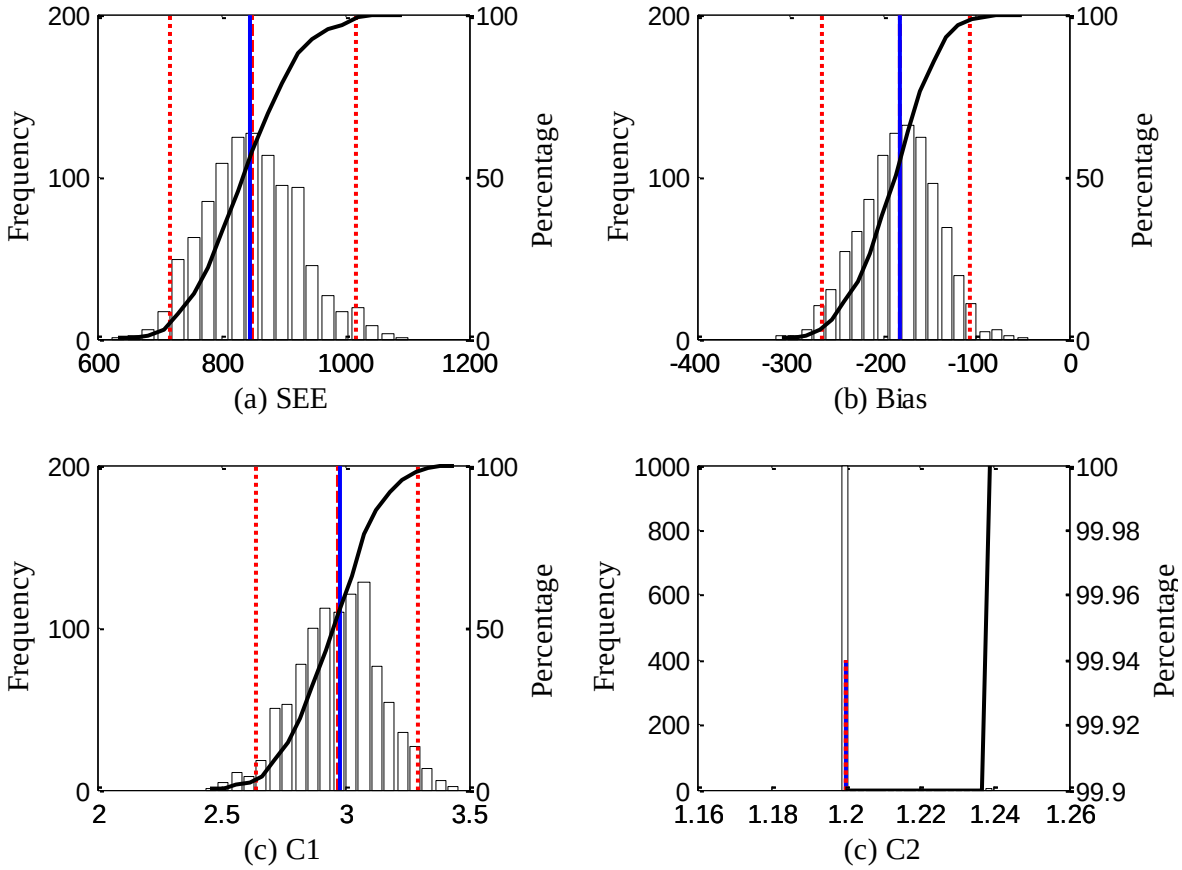

Figure B-54 Option 2 bootstrapping frequency distributions

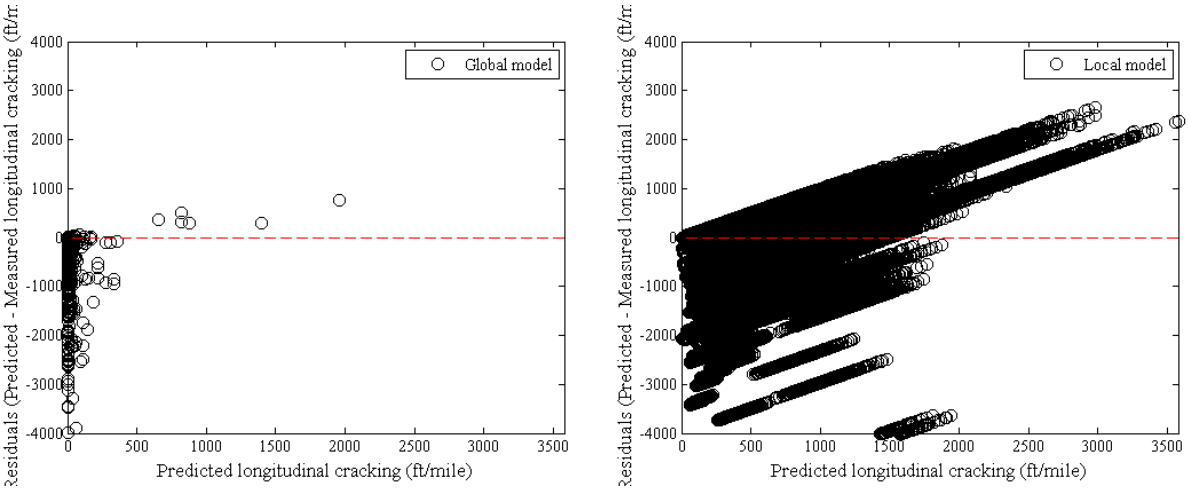

Figure B-55 Option 2 local calibration residual plots – bootstrapping

Reliability

Table B-32 Option 2 global and local alligator cracking model reliability – bootstrapping

Global model reliability equation	Local model reliability equation
$s_{e(Longitudinal)} = 200 + \frac{2300}{1+e^{1.07-2.165\times log(D_{td}+0.0001)}}$	$s_{e(Longitudinal)} = 300 + \frac{3000}{1+e^{1.8-0.61\times log(D_{td}+0.0001)}}$

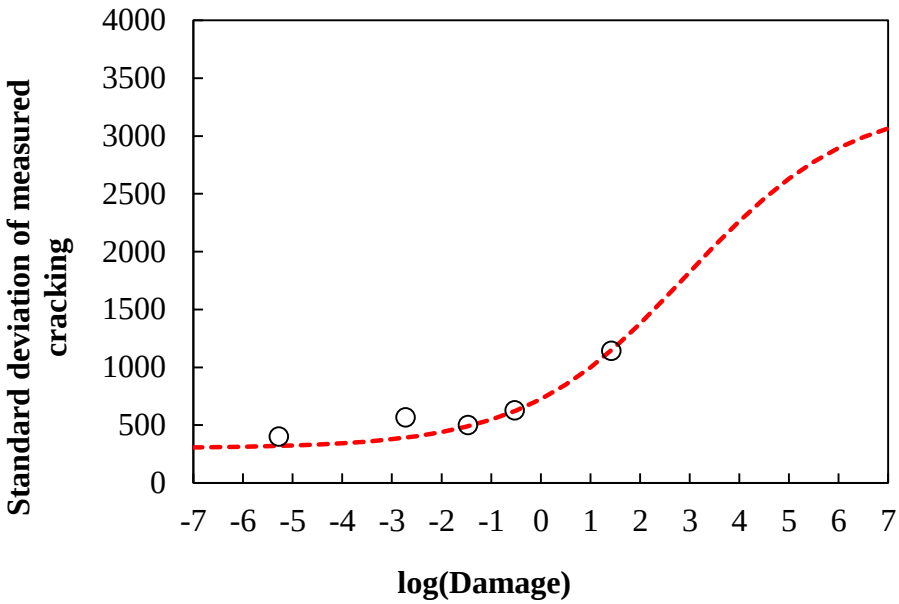

Figure B-56 Option 2 fitted reliability model after local calibration – bootstrapping

B.1.2.3 Option 4

No sampling

Table B-33 Option 4 local calibration results – no sampling

Parameter	Global model	Local model
SEE	1518.82	1213.53
Bias	-1071.64	-382.70
R^2	0.00	0.04
t-test pvalue	0.00	0.00
Intercept = 0	0.12	0.00
Slope = 1	0.00	0.00
C1	7.00	2.36
C2	3.50	1.20

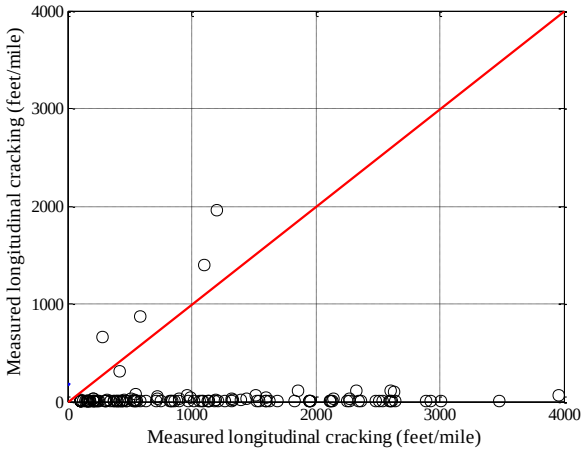

Global model

Figure B-57 Option 4 measured versus predicted fatigue cracking – no sampling

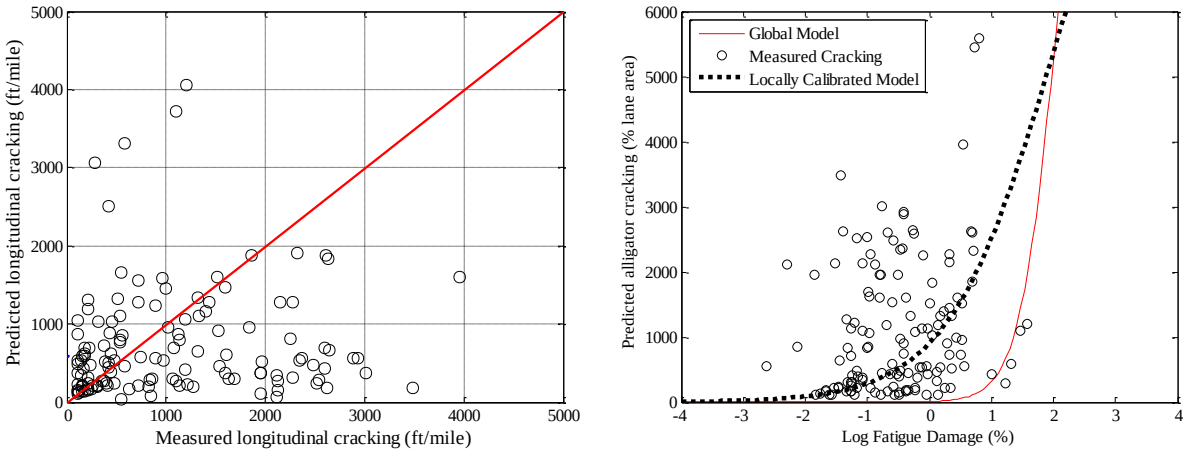

(a) Measured vs. predicted cracking (b) Fatigue damage predicted cracking

Figure B-58 Option 4 local calibration results – no sampling

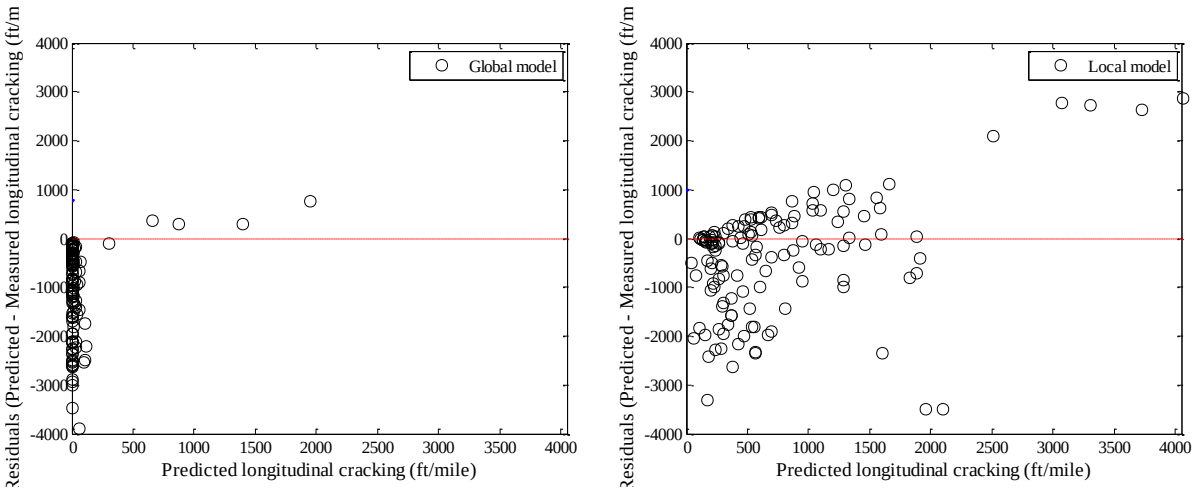

(a) Global model (b) Local model

Figure B-59 Option 4 local calibration residual plots – no sampling

Reliability

Table B-34 Option 4 global and local alligator cracking model reliability – no sampling

Global model reliability equation	Local model reliability equation
$s_{e(Longitudinal)} = 200 + \frac{2300}{1+e^{1.07-2.165\times log(D_{td}+0.0001)}}$	$s_{e(Longitudinal)} = 700 + \frac{3000}{1+e^{1.0-0.8\times log(D_{td}+0.0001)}}$

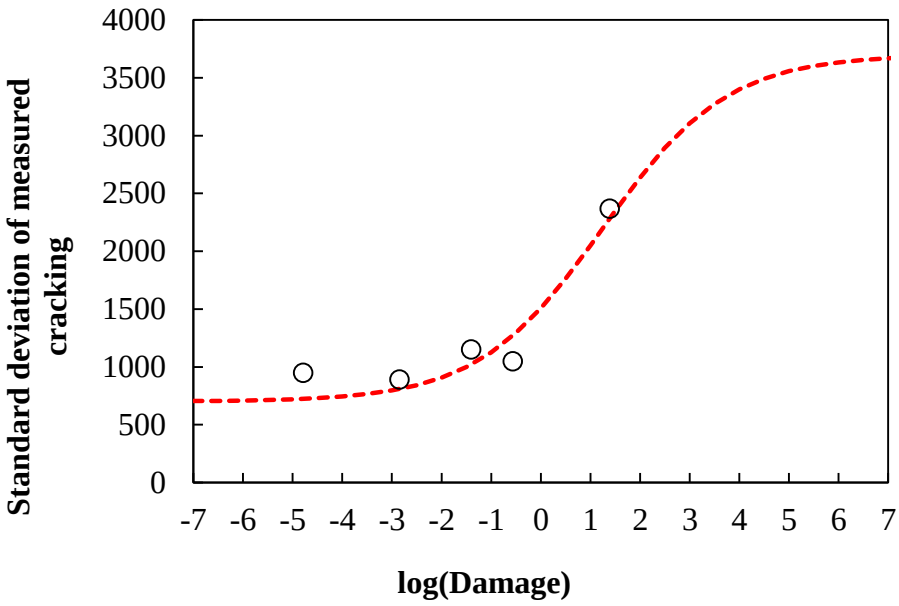

Figure B-60 Option 4 fitted reliability model after local calibration –no sampling

Split sampling

Table B-35 Option 4 local calibration results – split sampling

Parameter	Global model	Local model calibration	Local model validation
SEE	1537.23	1193.07	1313.41
Bias	-1040.89	-310.60	-618.73
R^2	0.00	0.08	0.07
t-test pvalue	0.00	0.01	0.00
Intercept = 0	0.14	0.00	0.00
Slope = 1	0.00	0.00	0.00
C1	7.00	2.37	2.37
C2	3.50	1.20	1.20

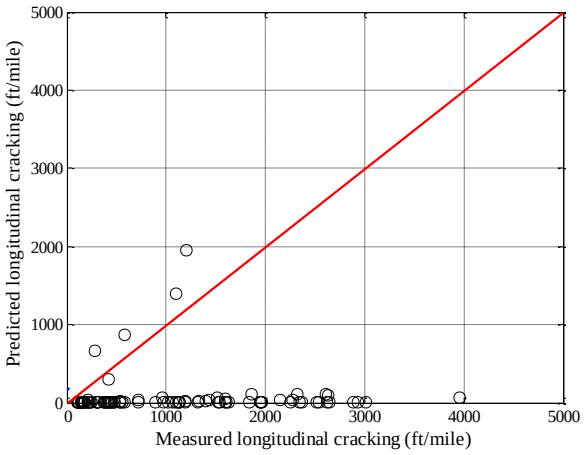

(a) Global model

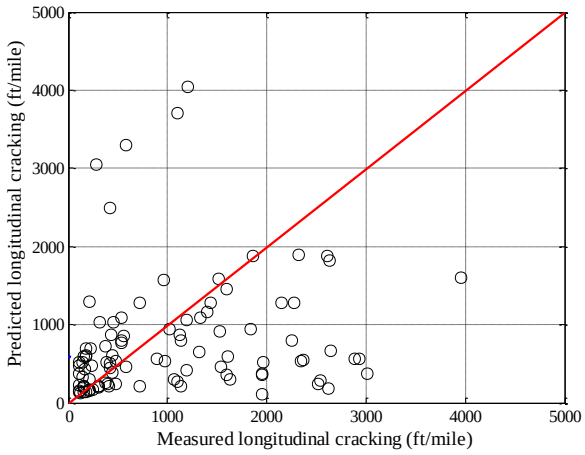

(b) Local model

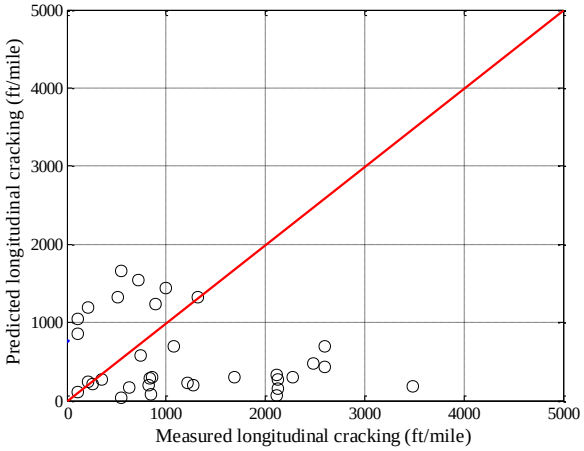

(c) Local model validation

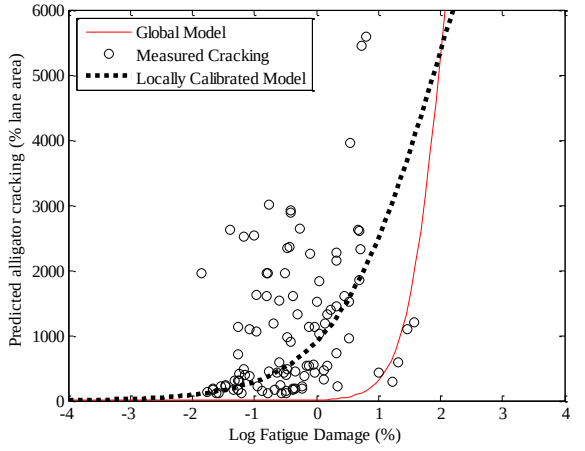

(d) Fatigue damage predicted cracking

Figure B-61 Option 4 local calibration results - split sampling

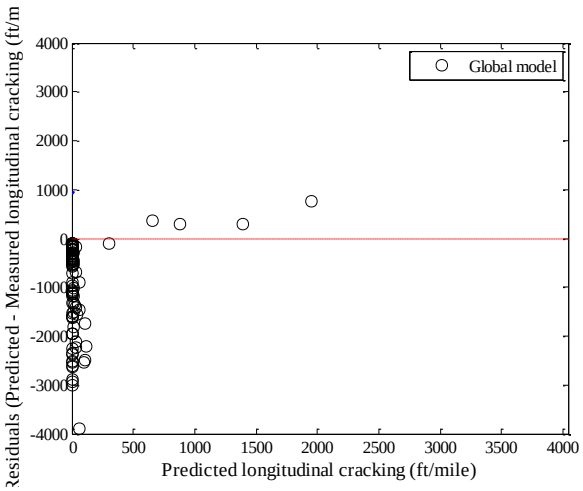

(a) Global model

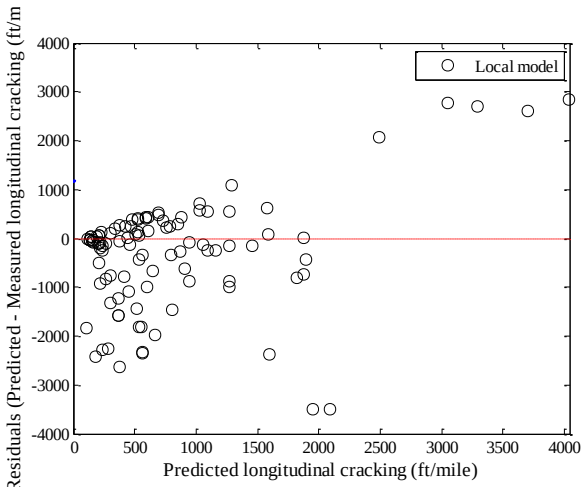

(b) Local model

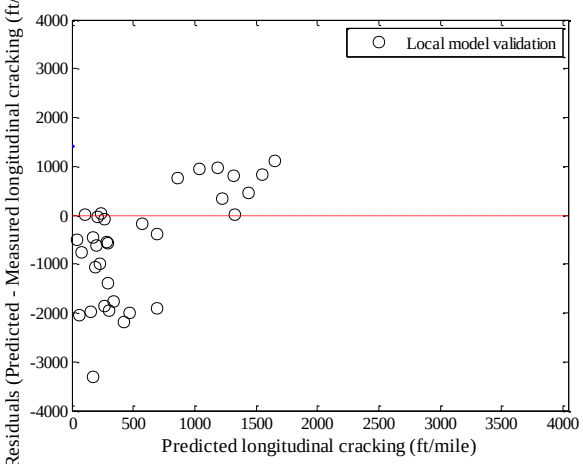

(c) Local model validation

Figure B-62 Option 4 local calibration residual plots - split sampling

Reliability

Table B-36 Option 4 global and local alligator cracking model reliability – split sampling

Global model reliability equation	Local model reliability equation
$s_{e(Longitudinal)} = 200 + \frac{2300}{1+e^{1.07-2.165\times log(D_{td}+0.0001)}}$	$s_{e(Longitudinal)} = 700 + \frac{3000}{1+e^{0.5-1.0\times log(D_{td}+0.0001)}}$

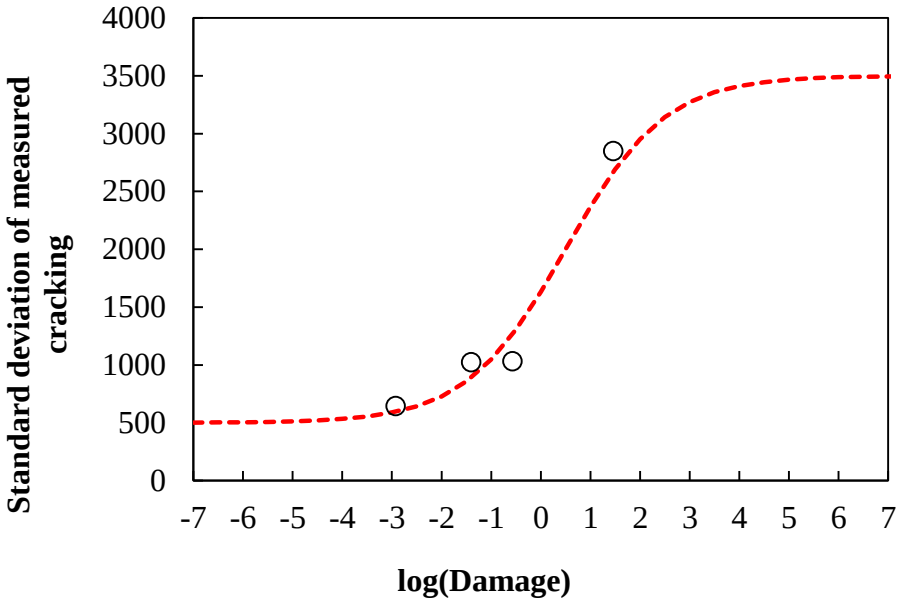

Figure B-63 Option 4 fitted reliability model after local calibration – split sampling

Repeated split sampling

Table B-37 Option 4 local calibration results – repeated split sampling

Global Model				
Parameter	Global Model Mean	Global Model Median	Global model lower CI	Global model upper CI
SEE	1526.24	1566.61	1262.97	1704.61
Bias	-1077.40	-1082.03	-1243.48	-898.41
C1	7.00	7.00	-	-
C2	3.50	3.50	-	-
Local Model				
Parameter	Local Model Mean	Local Model Median	Local model lower CI	Local model upper CI
SEE	1200.63	1208.68	973.63	1378.28
Bias	-322.87	-321.70	-485.94	-159.86
C1	2.27	2.39	1.79	2.40
C2	1.20	1.20	1.20	1.20
Local Model Validation				
Parameter	Local Model Mean	Local Model Median	Local model lower CI	Local model upper CI
SEE	1283.29	1268.41	777.59	1800.53
Bias	-287.20	-364.11	-900.44	719.47
C1	2.27	2.39	1.79	2.40
C2	1.20	1.20	1.20	1.20

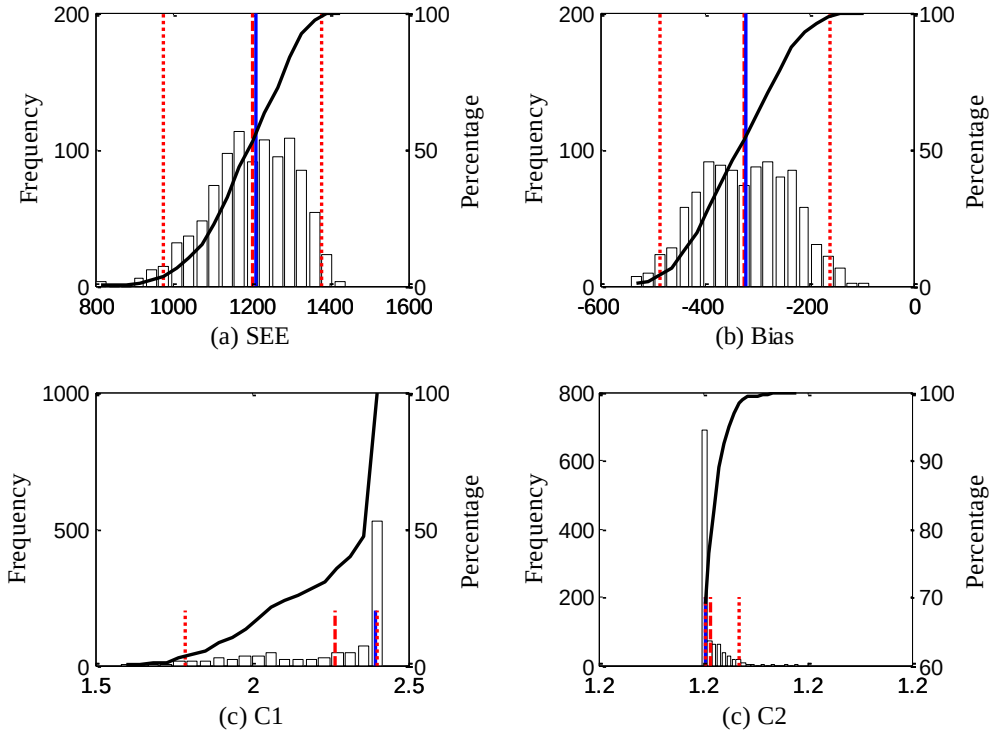

Figure B-64 Option 4 repeated split sampling frequency distributions – calibration

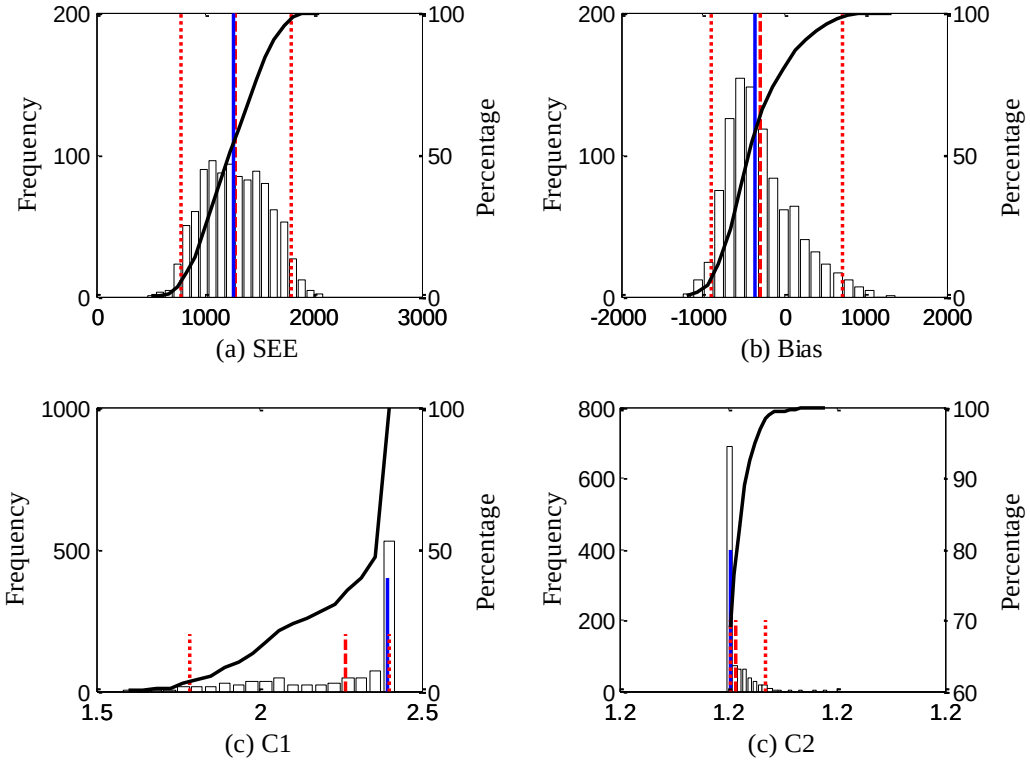

Figure B-65 Option 4 repeated split sampling frequency distributions – validation

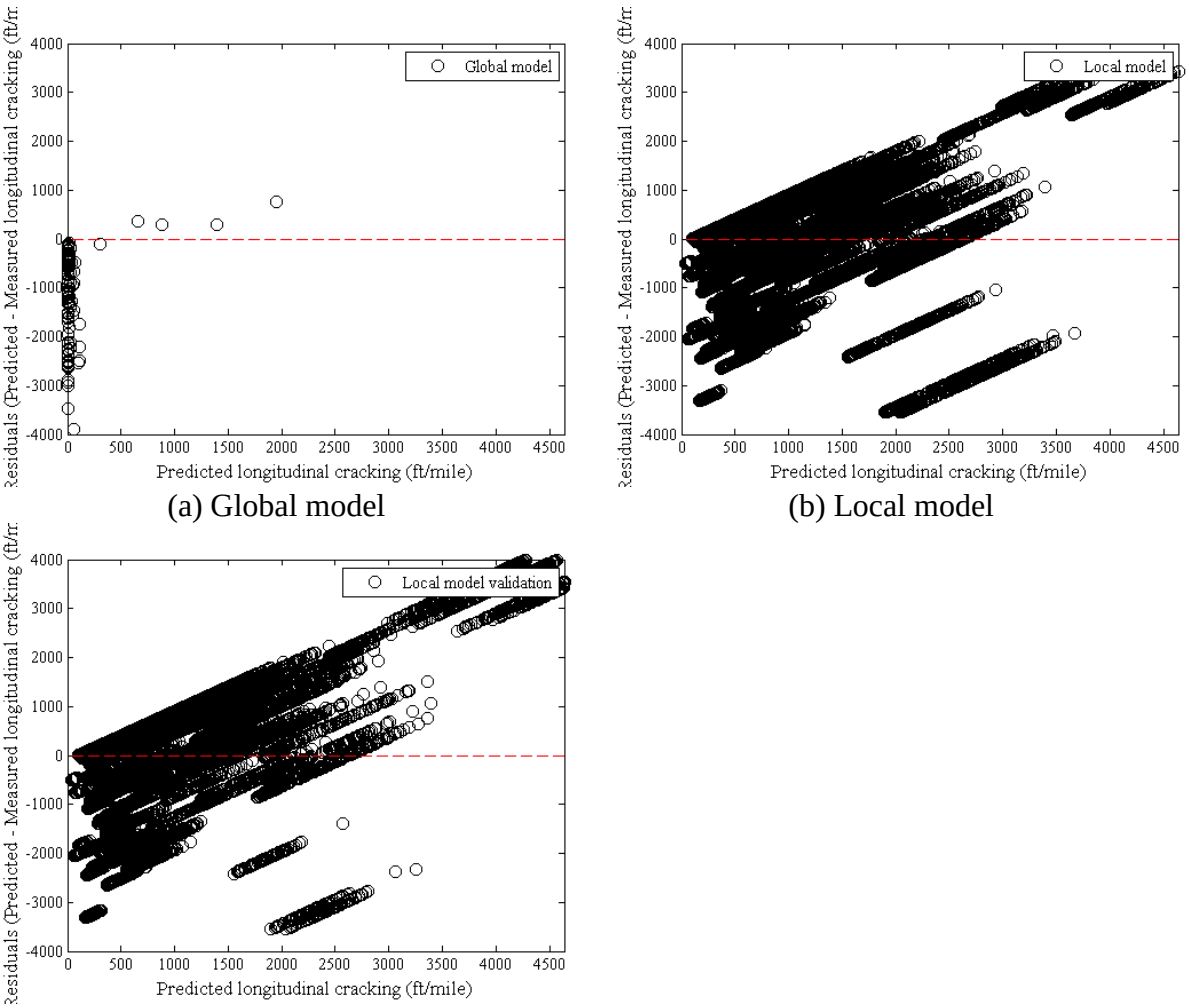

(a) Global model

(b) Local model

(c) Local model validation

Figure B-66 Option 4 local calibration residual plots – repeated split sampling

Reliability

Table B-38 Option 4 global and local alligator cracking model reliability – repeated split sampling

Global model reliability equation	Local model reliability equation
$s_{e(Longitudinal)} = 200 + \frac{2300}{1+e^{1.07-2.165\times log(D_{td}+0.0001)}}$	$s_{e(Longitudinal)} = 700 + \frac{3000}{1+e^{1.1-0.9\times log(D_{td}+0.0001)}}$

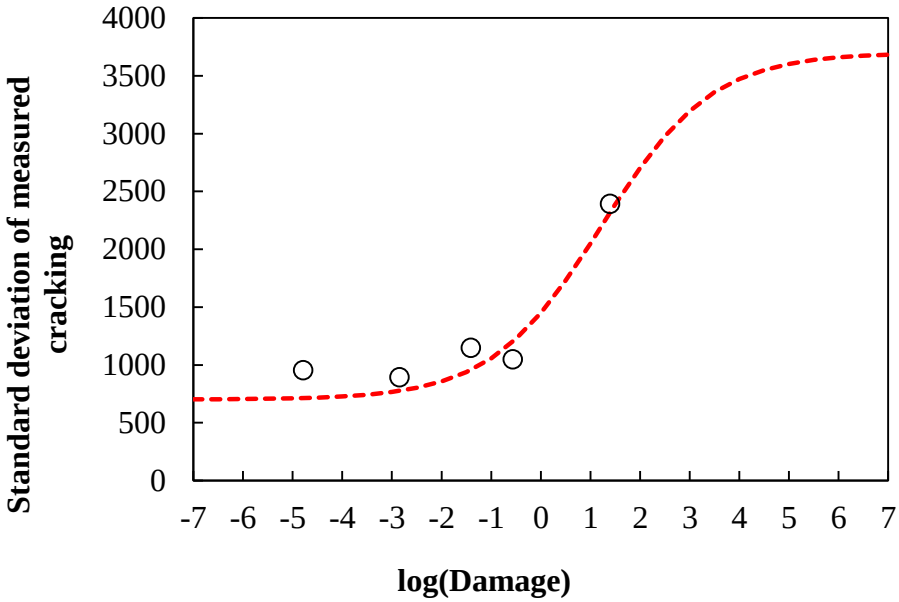

Figure B-67 Option 4 fitted reliability model after local calibration – repeated split sampling

Bootstrapping

Table B-39 Option 4 local calibration results – bootstrapping

Global Model				
Parameter	Global Model Mean	Global Model Median	Global model lower CI	Global model upper CI
SEE	1512.27	1501.86	1169.60	1930.76
Bias	-1072.23	-1060.70	-1385.29	-807.29
C1	7.00	7.00	-	-
C2	3.50	3.50	-	-
Local Model				
Parameter	Local Model Mean	Local Model Median	Local model lower CI	Local model upper CI
SEE	1189.44	1187.05	898.51	1488.09
Bias	-283.96	-282.67	-507.09	-67.54
C1	2.23	2.36	1.69	2.40
C2	1.20	1.20	1.20	1.20

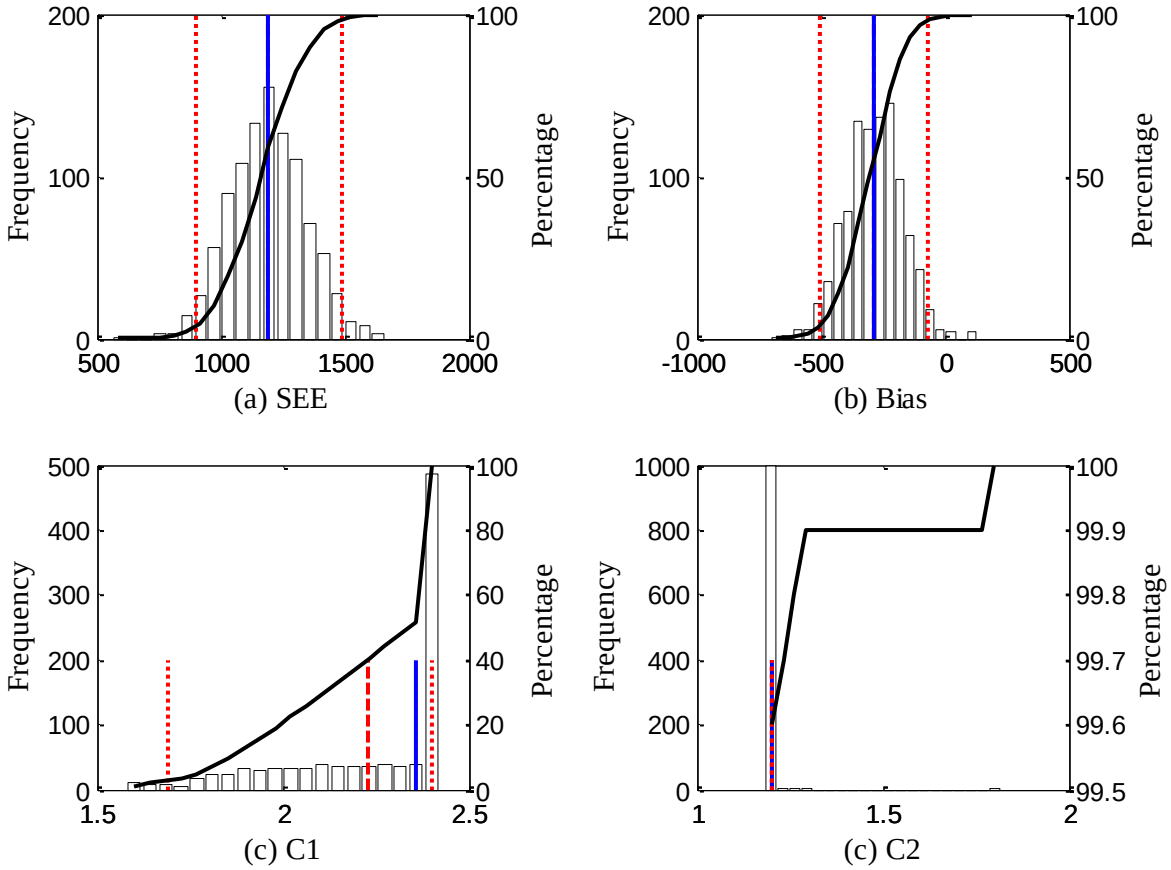

Figure B-68 Option 4 bootstrapping frequency distributions

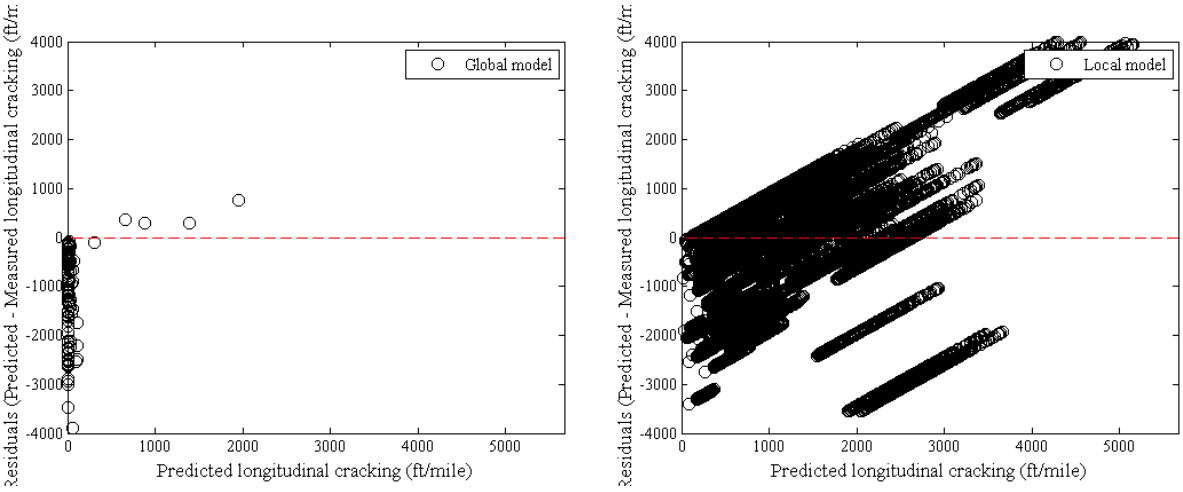

Figure B-69 Option 4 local calibration residual plots – bootstrapping

Reliability

Table B-40 Option 4 global and local alligator cracking model reliability – bootstrapping

Global model reliability equation	Local model reliability equation
$s_{e(Longitudinal)} = 200 + \frac{2300}{1+e^{1.07-2.165\times log(D_{td}+0.0001)}}$	$s_{e(Longitudinal)} = 700 + \frac{3000}{1+e^{1.1-1.0\times log(D_{td}+0.0001)}}$

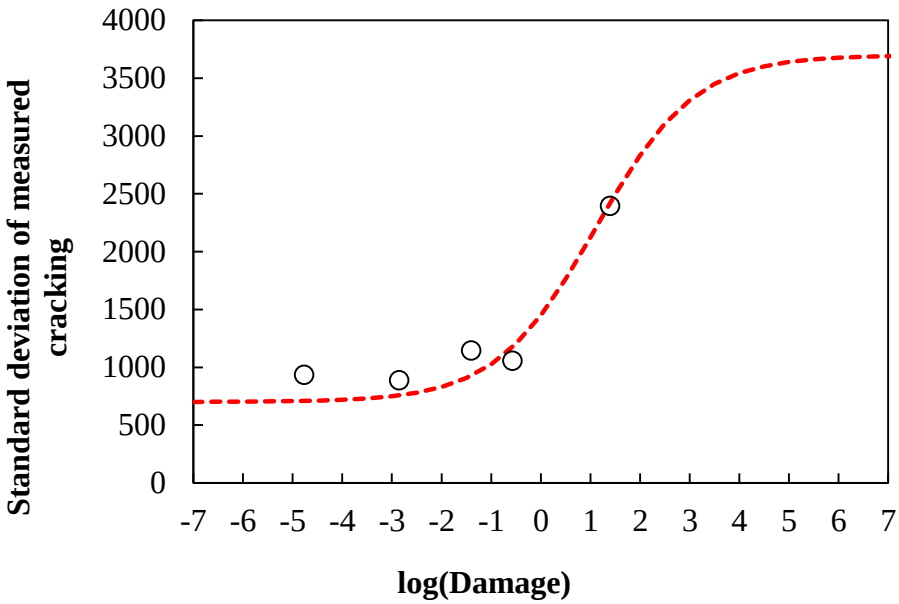

Figure B-70 Option 4 fitted reliability model after local calibration – bootstrapping

B.1.3 Rutting Model

B.1.3.1 Option 1 – Method 1

No sampling

Table B-41 Option 1: Method 1 – Global model goodness of fit – no sampling

HMA layer	SEE (in.)	Bias (in.)
AC rut	0.0786	-0.0037
Base rut	0.1267	0.1111
Subgrade	0.2242	0.2143
Total rut	0.3431	0.3217

Table B-42 Option 1: Method 1 – Global model *p*-values

HMA layer	t-test p-value	Intercept p-value	Slope = 1 p-value
AC rut	0.3220	0.0000	0.0000
Base rut	0.0000	0.0000	0.0000
Subgrade	0.0000	0.0000	0.0000
Total rut	0.0000	0.0000	0.0000

Table B-43 Option 1: Method 1 – Local model goodness of fit– no sampling

HMA layer	SEE	Bias
AC rut	0.0783	-0.0094
Base rut	0.0262	-0.0034
Subgrade	0.0228	-0.0003
Total rut	0.0869	-0.0132

Table B-44 Option 1: Method 1 – Local model *p*-values– no sampling

HMA layer	t-test p-value	Intercept p-value	Slope = 1 p-value
AC rut	0.0110	0.0000	0.0000
Base rut	0.0054	0.0000	0.0000
Subgrade	0.7695	0.0000	0.0000
Total rut	0.0013	0.0000	0.0000

Table B-45 Option 1: Method 1 – Local model *p*-values– no sampling

Calibration Coefficient	Global model	Local model
HMA rutting (br1)	1.0000	0.9580
Base rutting (bs1)	1.0000	0.1181
Subgrade rutting (bsg1)	1.0000	0.0410

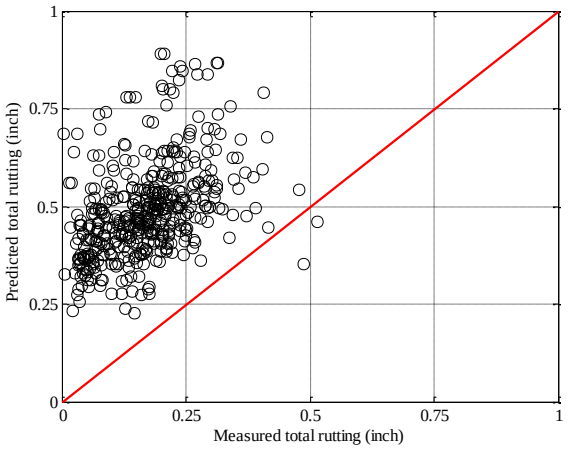

(a) Global model

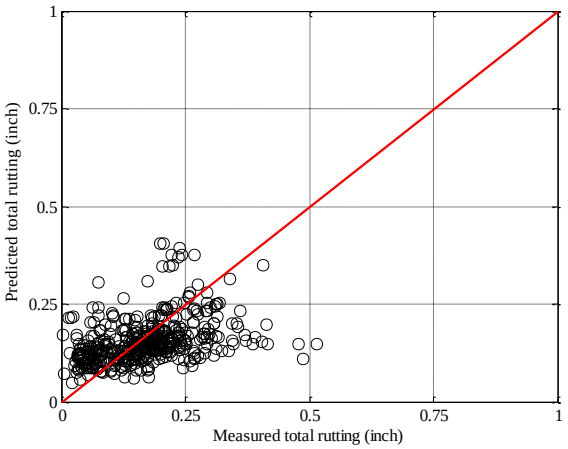

(b) Local model

Figure B-71 Option 1: Method 1 Total rutting local calibration results - no sampling

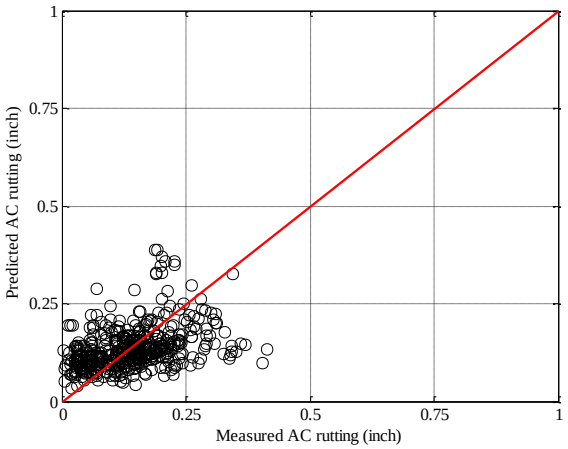

(a) Global model

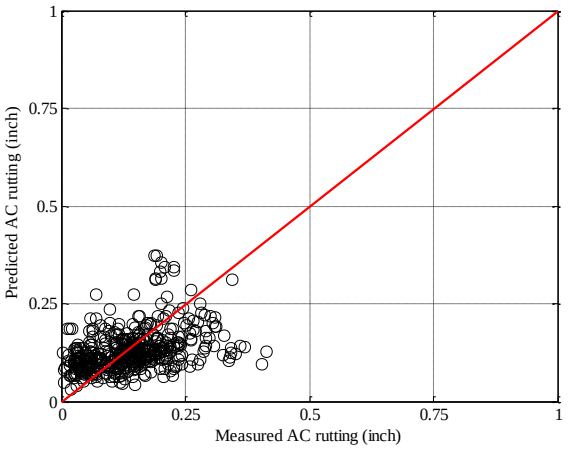

(b) Local model

Figure B-72 Option 1: Method 1 HMA rutting local calibration results - no sampling

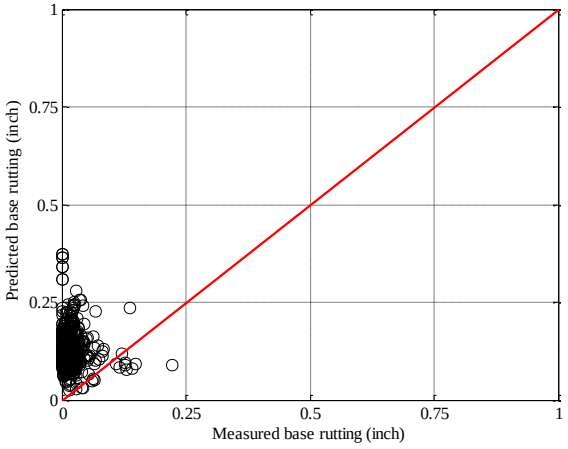

(a) Global model

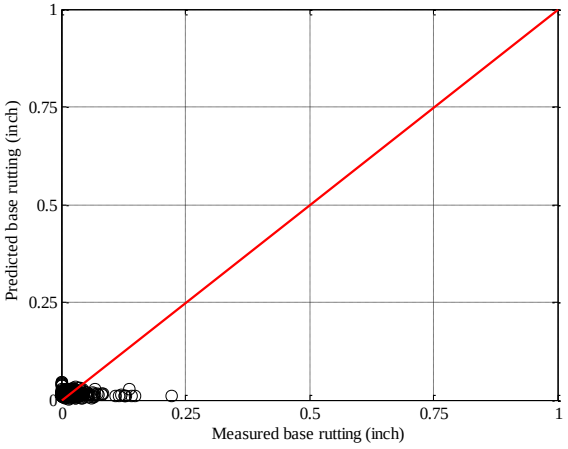

(b) Local model

Figure B-73 Option 1: Method 1 Base rutting local calibration results - no sampling

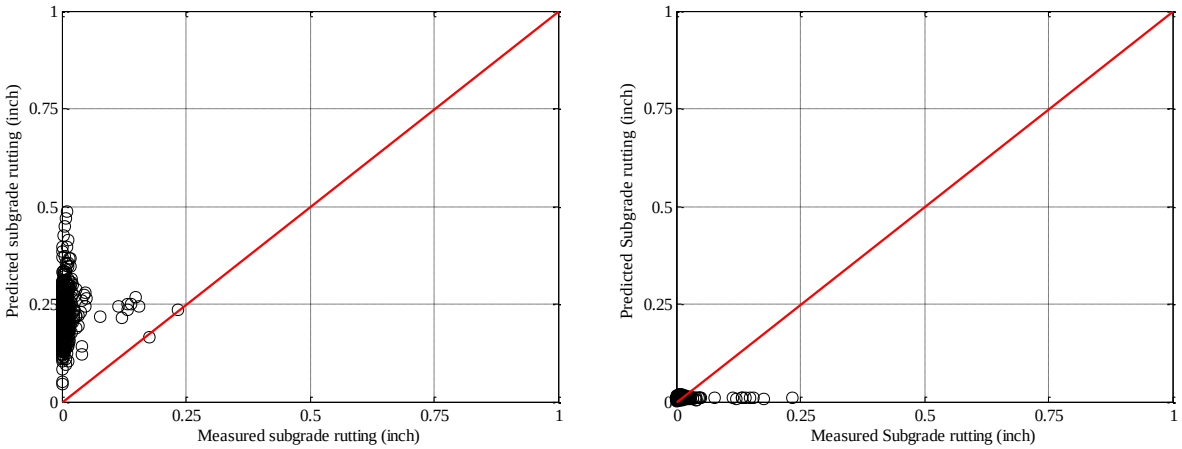

(a) Global model (b) Local model

Figure B-74 Option 1: Method 1 Subgrade rutting local calibration results - no sampling

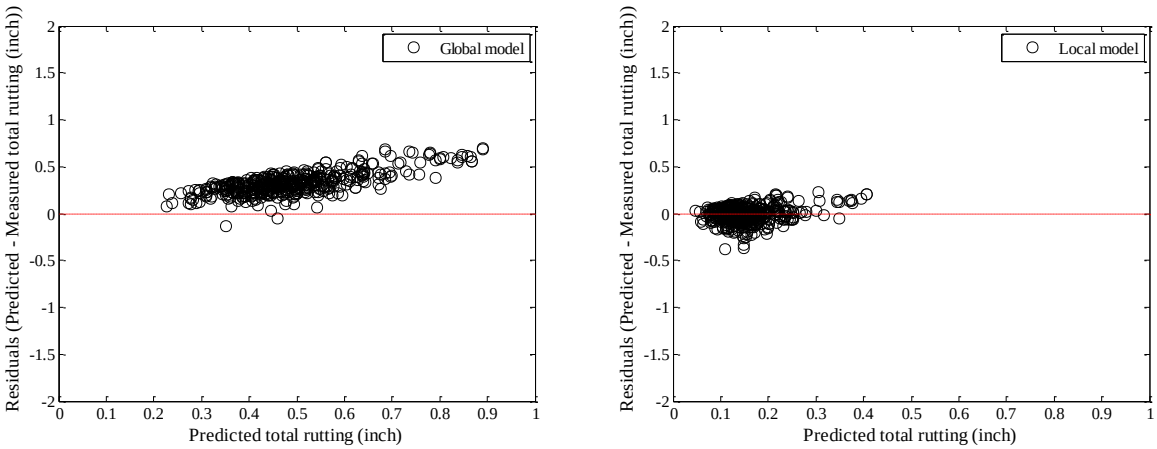

(a) Global model (b) Local model

Figure B-75 Option 1: Method 1 Total rutting residual plots - no sampling

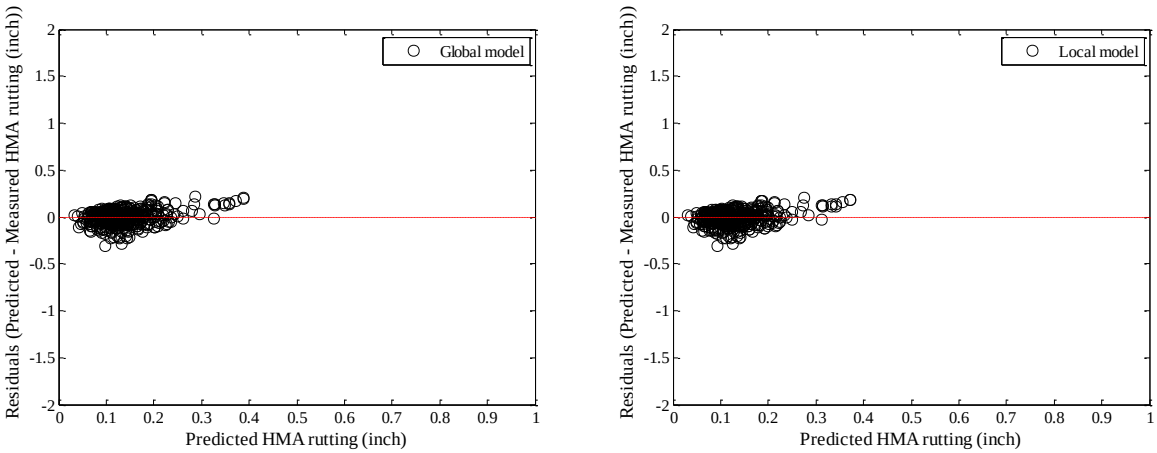

(a) Global model (b) Local model

Figure B-76 Option 1: Method 1 HMA rutting residual plots - no sampling

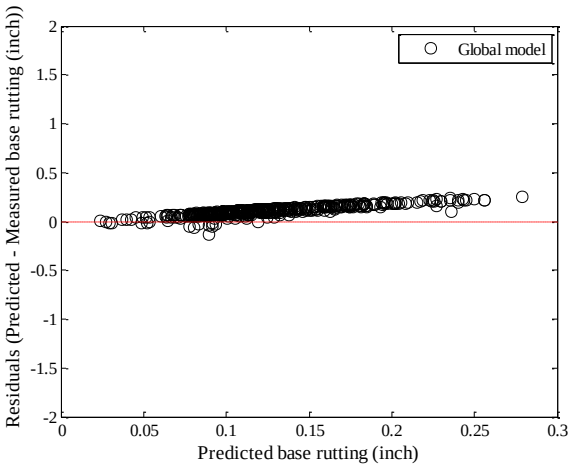

(a) Global model

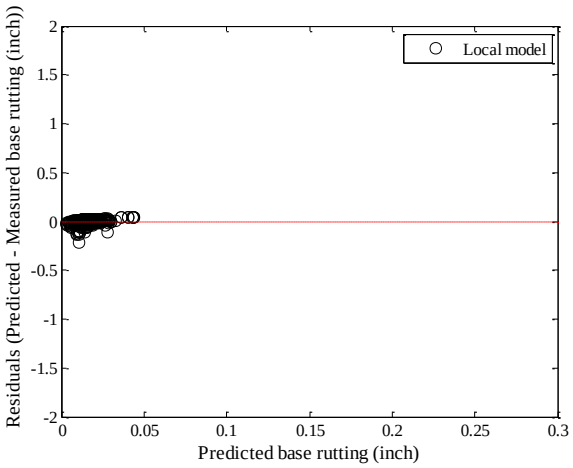

(b) Local model

Figure B-77 Option 1: Method 1 Base rutting residual plots - no sampling

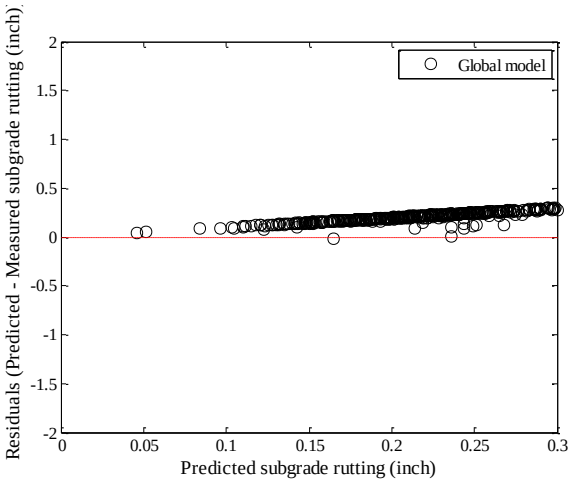

(a) Global model

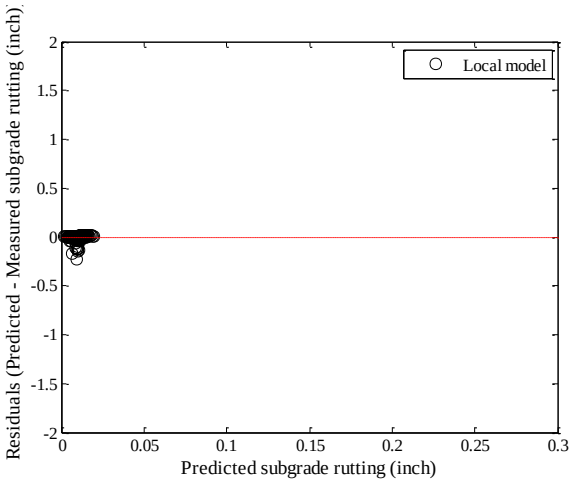

(b) Local model

Figure B-78 Option 1: Method 1 Subgrade rutting residual plots - no sampling

Reliability

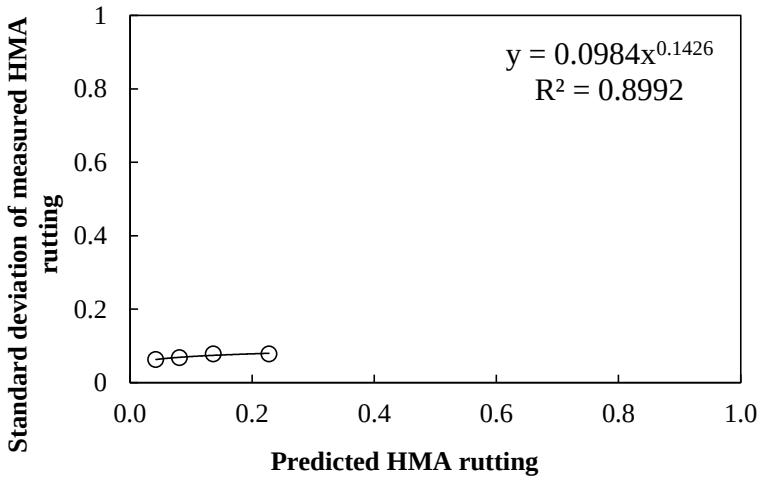

(a) HMA rutting reliability

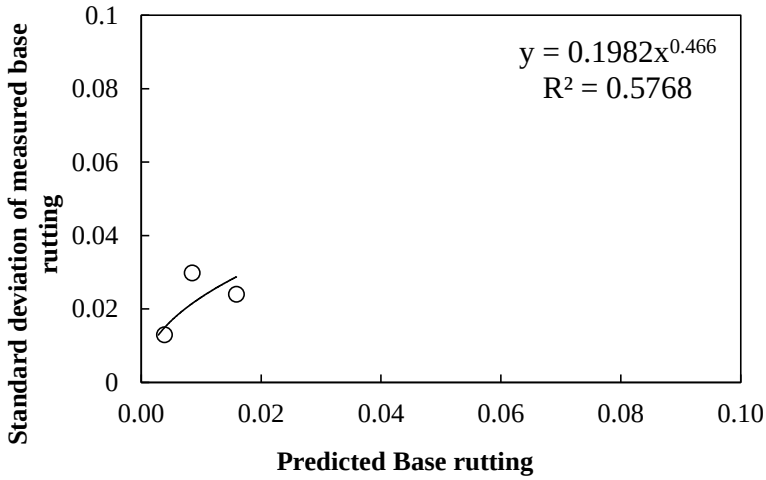

(b) Base rutting reliability

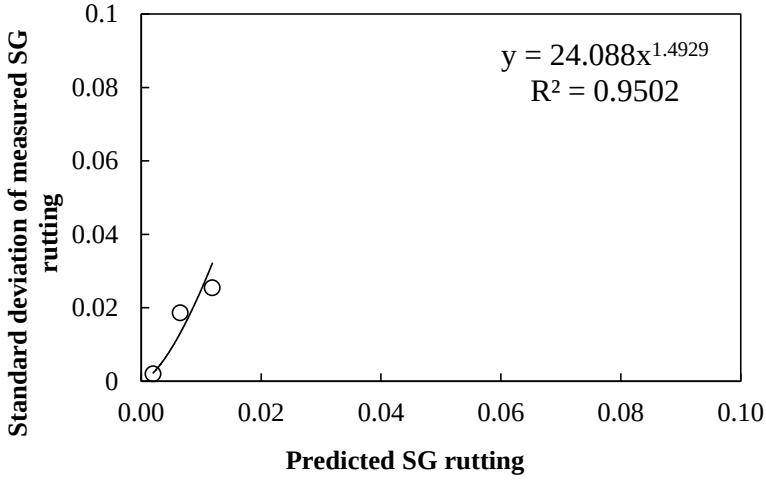

(c) Subgrade rutting reliability

Figure B-79 Rutting model reliability equations – option 1 method 1 – no sampling

Split sampling

Table B-46 Option 1: Method 1 – Global model goodness of fit – split sampling

HMA layer	SEE (in.)	Bias (in.)
AC rut	0.0769	0.0034
Base rut	0.1313	0.1134
Subgrade	0.2243	0.2139
Total rut	0.3534	0.3306

Table B-47 Option 1: Method 1 – Global model *p*-values - split sampling

HMA layer	t-test p-value	Intercept p-value	Slope = 1 p-value
AC rut	0.4496	0.0000	0.0000
Base rut	0.0000	0.0000	0.0000
Subgrade	0.0000	0.0000	0.0000
Total rut	0.0000	0.0000	0.0000

Table B-48 Option 1: Method 1 – Local model goodness of fit– split sampling

HMA layer	SEE	Bias
AC rut	0.0759	-0.0080
Base rut	0.0268	-0.0040
Subgrade	0.0236	-0.0004
Total rut	0.0853	-0.0125

Table B-49 Option 1: Method 1 – Local model *p*-values– split sampling

HMA layer	t-test p-value	Intercept p-value	Slope = 1 p-value
AC rut	0.0674	0.0000	0.0000
Base rut	0.0086	0.0000	0.0000
Subgrade	0.7433	0.0000	0.0000
Total rut	0.0109	0.0000	0.0000

Table B-50 Option 1: Method 1 – Local model *p*-values – split sampling

Calibration Coefficient	Global model	Local model
HMA rutting (br1)	1.0000	0.9204
Base rutting (bs1)	1.0000	0.1209
Subgrade rutting (bsg1)	1.0000	0.0435

Table B-51 Option 1: Method 1 – Local model validation p-values – split sampling

HMA layer	t-test p-value	Intercept p-value	Slope = 1 p-value
AC rut	0.0000	0.0000	0.0000
Base rut	0.5941	0.0000	0.0000
Subgrade	0.3416	0.0000	0.0000
Total rut	0.0002	0.0000	0.0000

Table B-52 Option 1: Method 1 – Local model validation SEE and bias – split sampling

HMA layer	SEE	Bias
AC rut	0.0841	-0.0281
Base rut	0.0250	-0.0011
Subgrade	0.0210	0.0017
Total rut	0.0913	-0.0276

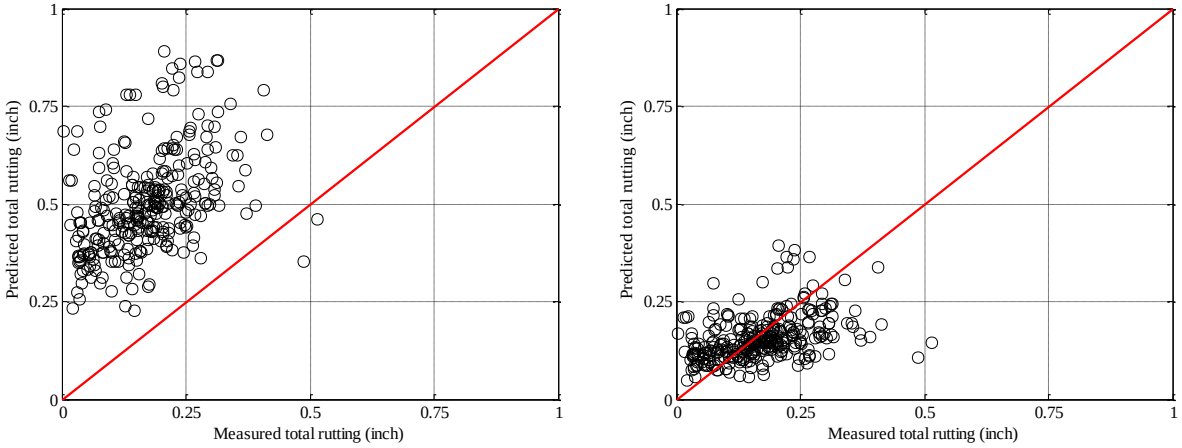

(a) Global model (b) Local model

Figure B-80 Option 1: Method 1 Total rutting local calibration results - split sampling

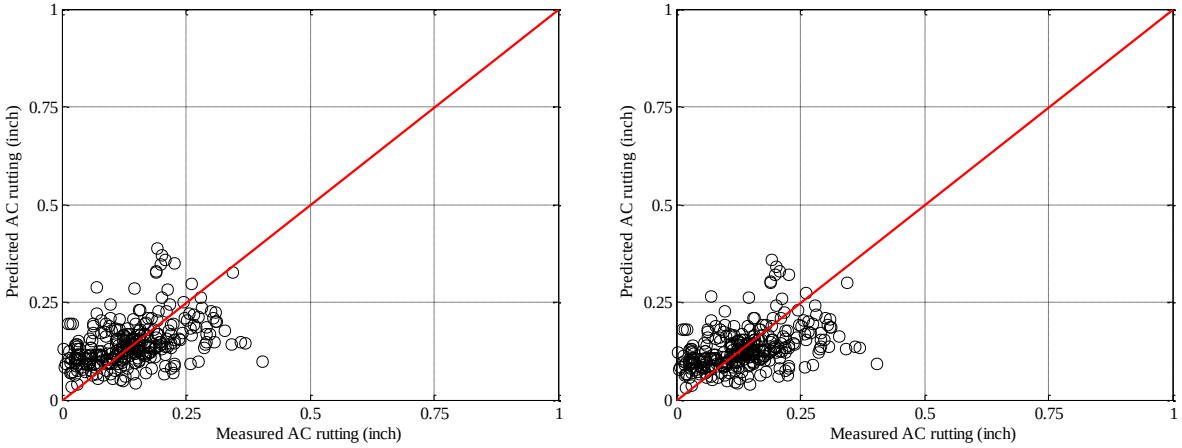

(a) Global model (b) Local model

Figure B-81 Option 1: Method 1 HMA rutting local calibration results - split sampling

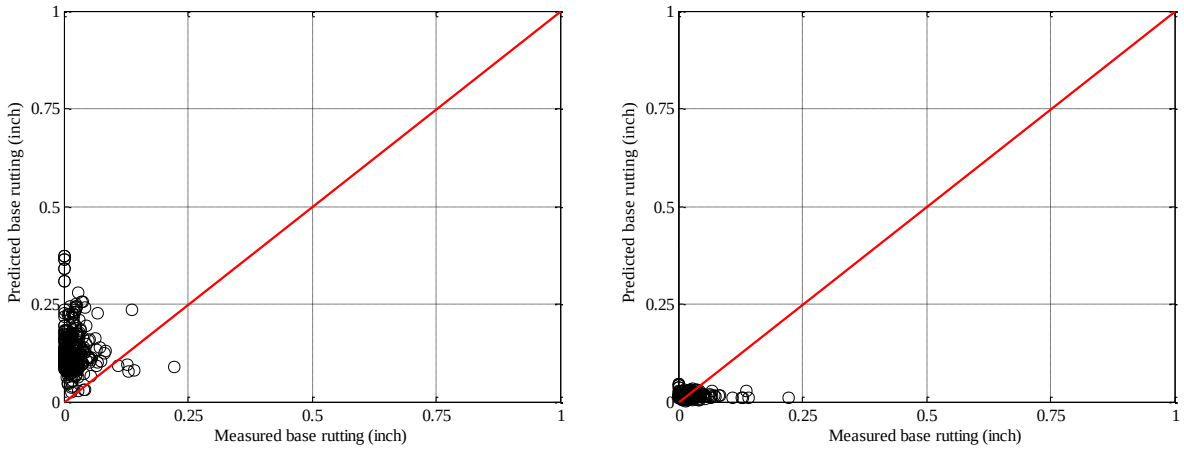

(a) Global model (b) Local model

Figure B-82 Option 1: Method 1 Base rutting local calibration results - split sampling

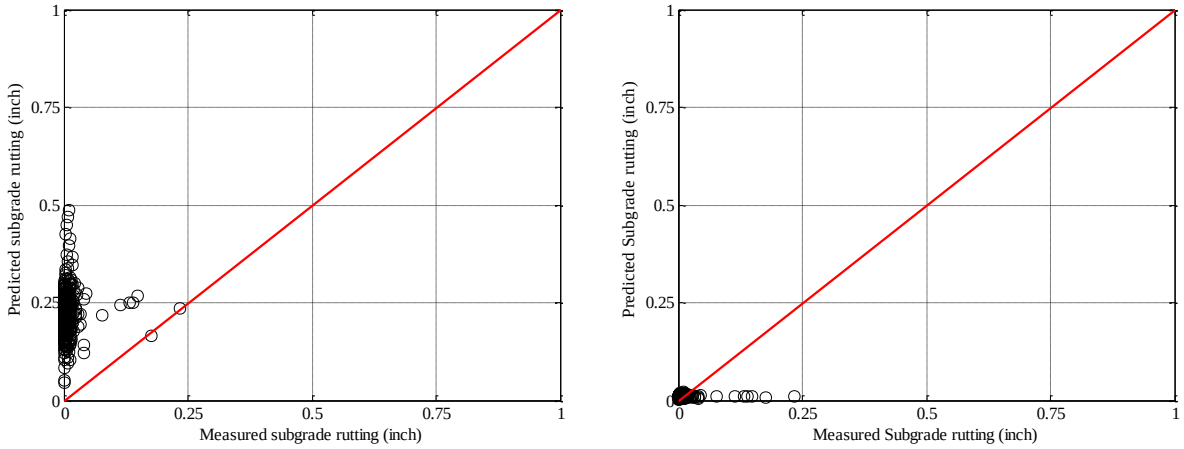

(a) Global model (b) Local model

Figure B-83 Option 1: Method 1 Subgrade rutting local calibration results - split sampling

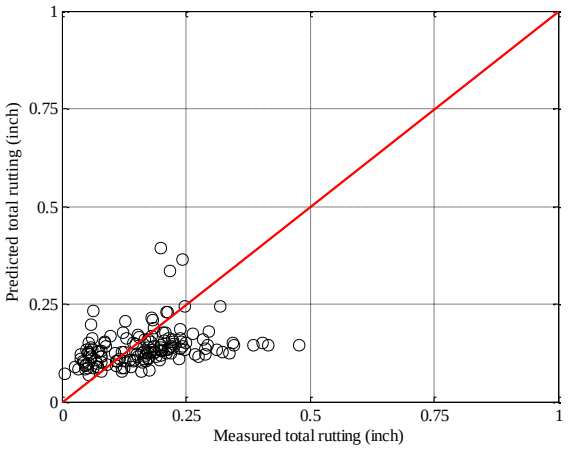

(a) Total rutting

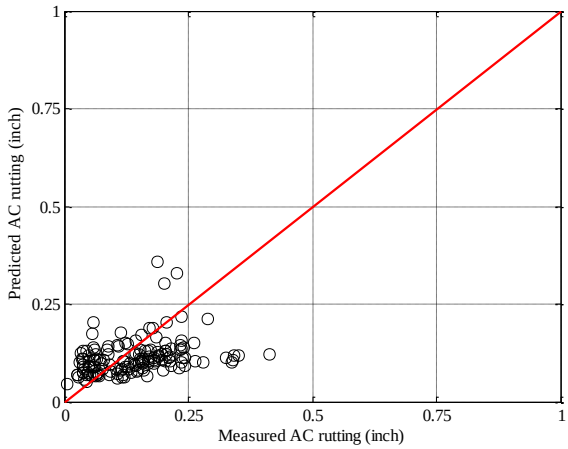

(b) HMA rutting

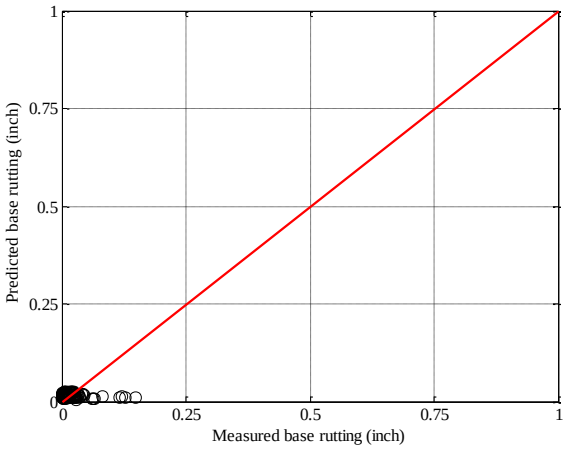

(c) Base rutting

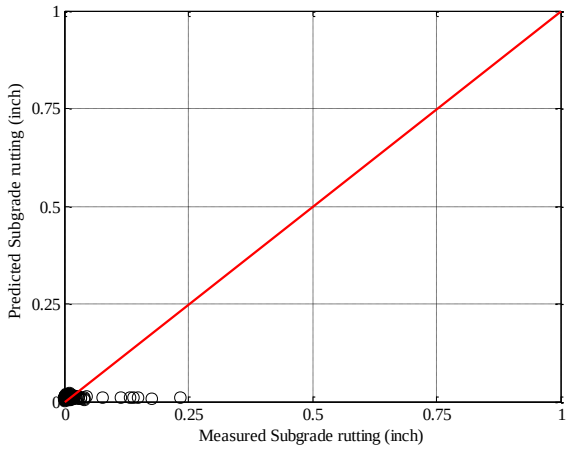

(d) Subgrade rutting

Figure B-84 Option 1: Method 1 Rutting model validation – split sampling

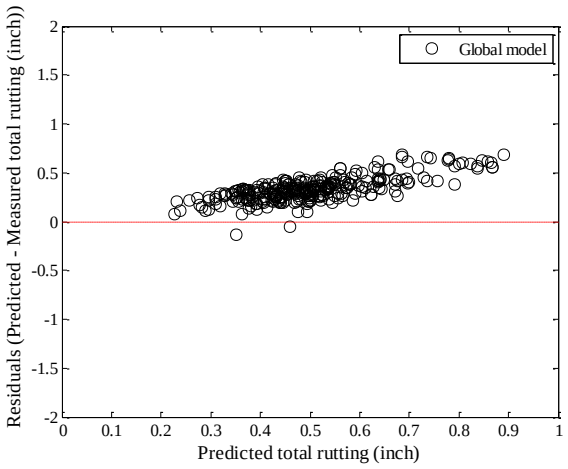

(a) Global model

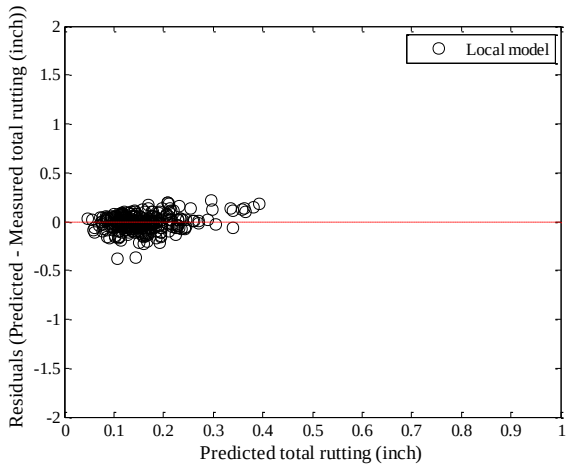

(b) Local model

Figure B-85 Option 1: Method 1 Total rutting residual plots - split sampling

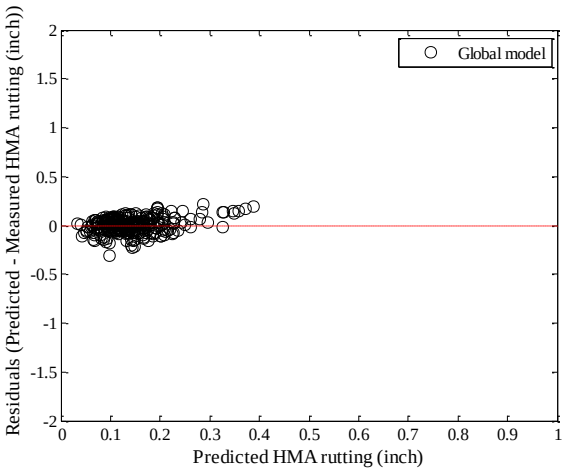

(a) Global model

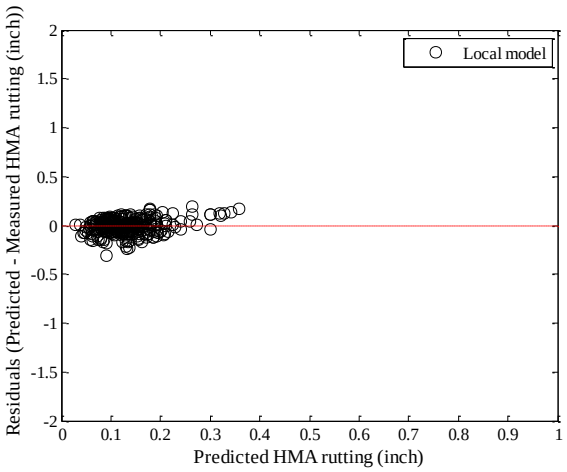

(b) Local model

Figure B-86 Option 1: Method 1 HMA rutting residual plots - split sampling

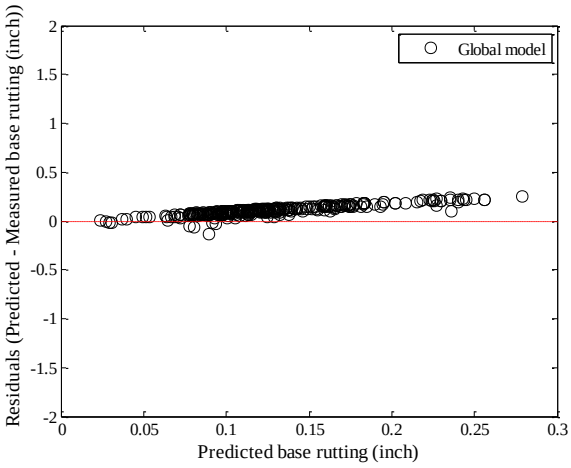

(a) Global model

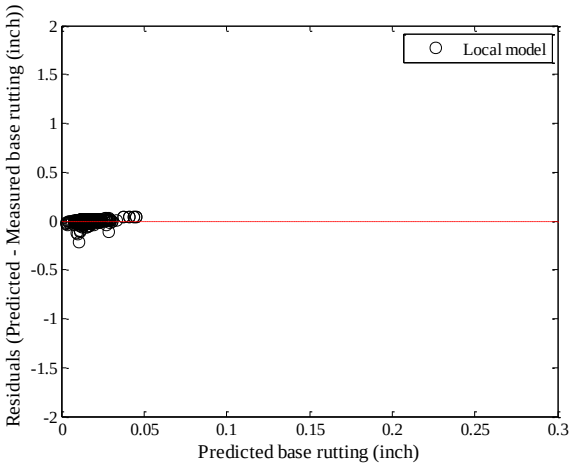

(b) Local model

Figure B-87 Option 1: Method 1 Base rutting residual plots - split sampling

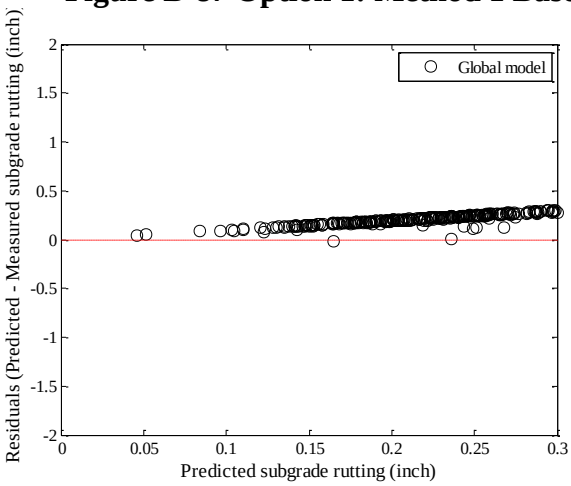

(a) Global model

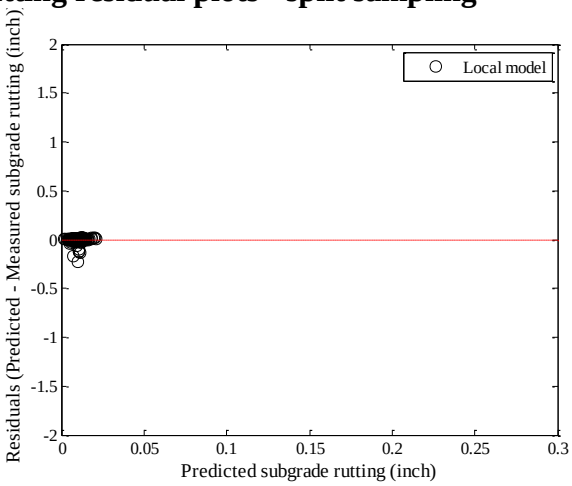

(b) Local model

Figure B-88 Option 1: Method 1 Subgrade rutting residual plots - split sampling

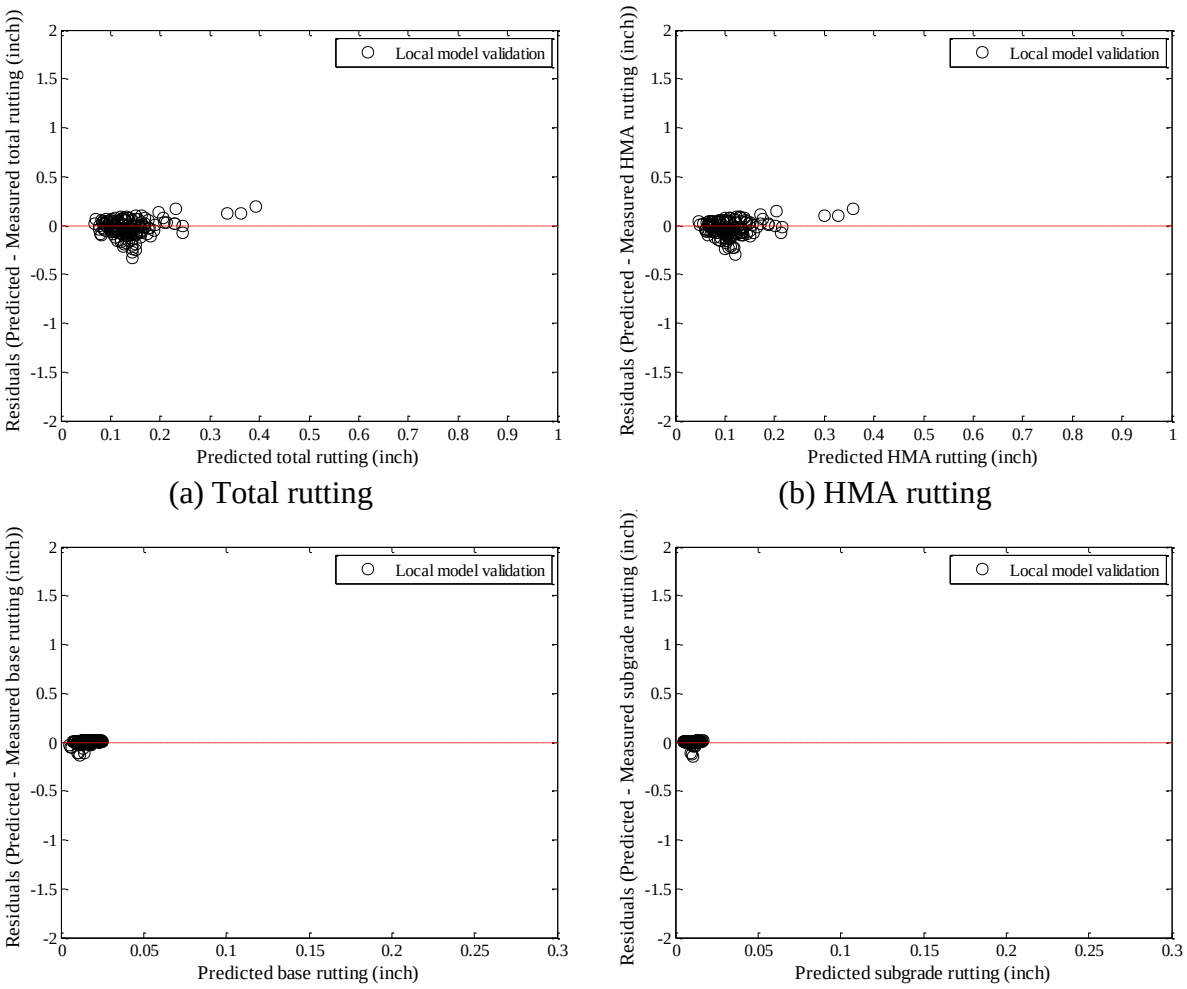

(a) Total rutting (b) HMA rutting

(c) Base rutting (d) Subgrade rutting

Figure B-89 Option 1: Method 1 Rutting model validation residual plots – split sampling

Reliability

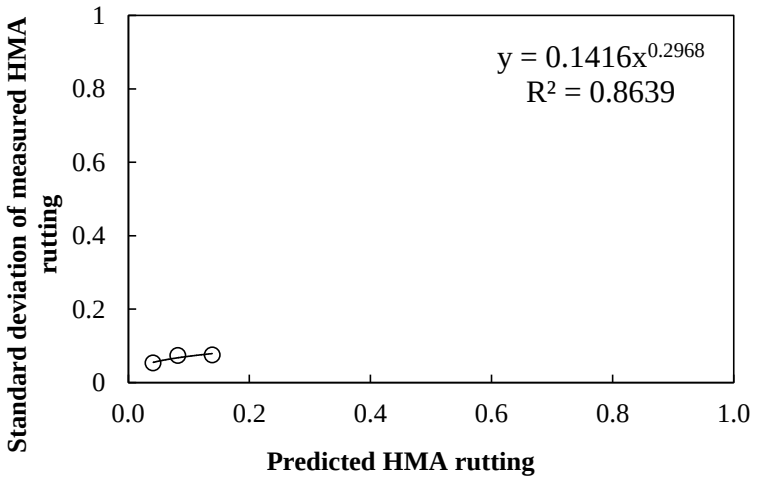

(a) HMA rutting reliability

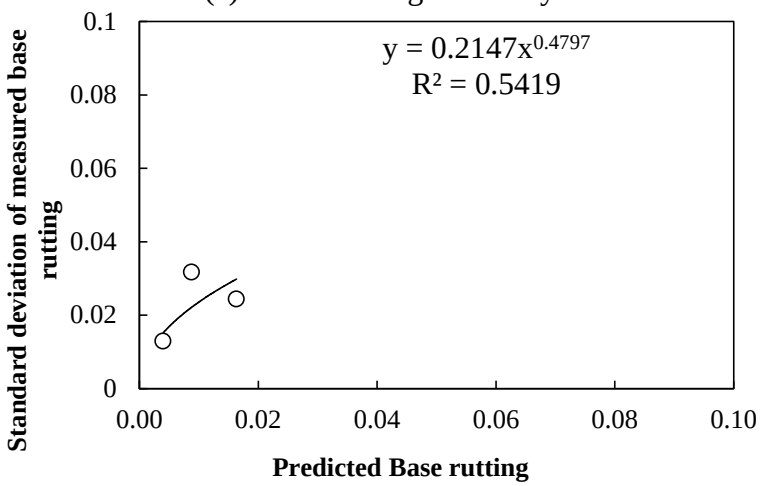

(b) Base rutting reliability

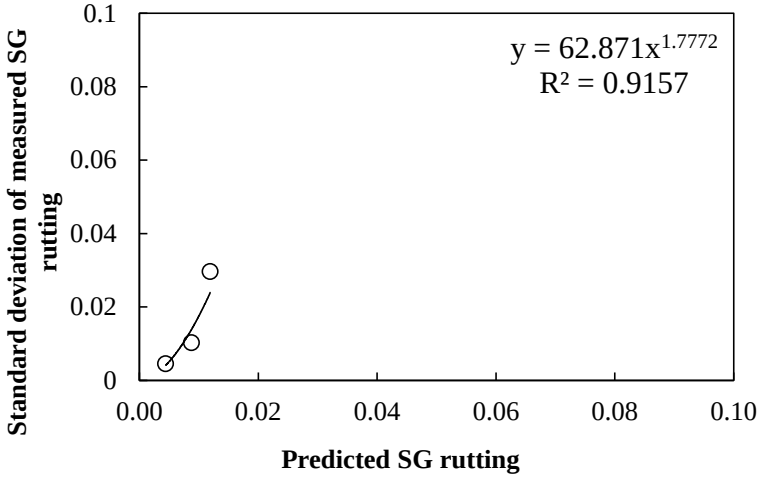

(c) Subgrade rutting reliability

Figure B-90 Rutting model reliability equations – option 1 method 1 – split sampling

Repeated split sampling

Table B-53 Option 1: Method 1 – Global model SEE and bias – repeated split sampling

Global Model	Average SEE	SEE Lower CI	SEE Upper CI	Average bias (in.)	Bias Lower CI	Bias Upper CI
AC rutting	0.0785	0.0729	0.0836	-0.0037	-0.0113	0.0037
Base rutting	0.1268	0.1170	0.1342	0.1111	0.1041	0.1182
Subgrade rutting	0.2245	0.2168	0.2318	0.2144	0.2072	0.2216
Total rutting	0.3435	0.3270	0.3573	0.3218	0.3083	0.3339

Table B-54 Option 1: Method 1 – Local model SEE and bias – repeated split sampling

Calibration set	AC rutting	Base rutting	Subgrade rutting	Total rutting
Average SEE	0.0781	0.0260	0.0224	0.0867
SEE Lower CI	0.0726	0.0193	0.0133	0.0796
SEE Upper CI	0.0830	0.0298	0.0270	0.0926
Average bias (in.)	-0.0092	-0.0034	-0.0003	-0.0130
Bias Lower CI	-0.0126	-0.0047	-0.0006	-0.0165
Bias Upper CI	-0.0050	-0.0020	0.0000	-0.0087
Average calibration coefficient	0.9603	0.1185	0.0410	N/A
Calibration coefficient Lower CI	0.9049	0.1005	0.0307	N/A
Calibration coefficient Upper CI	1.0346	0.1407	0.0497	N/A

Table B-55 Option 1: Method 1 – Local model validation SEE and bias – repeated split sampling

Validation set	AC rutting	Base rutting	Subgrade rutting	Total rutting
Average SEE	0.0797	0.0257	0.0216	0.0882
SEE Lower CI	0.0669	0.0151	0.0080	0.0730
SEE Upper CI	0.0920	0.0378	0.0364	0.1032
Average bias (in.)	-0.0090	-0.0033	-0.0004	-0.0127
Bias Lower CI	-0.0331	-0.0120	-0.0083	-0.0377
Bias Upper CI	0.0177	0.0051	0.0060	0.0168
Average calibration coefficient	0.9603	0.1185	0.0410	N/A
Calibration coefficient Lower CI	0.9049	0.1005	0.0307	N/A
Calibration coefficient Upper CI	1.0346	0.1407	0.0497	N/A

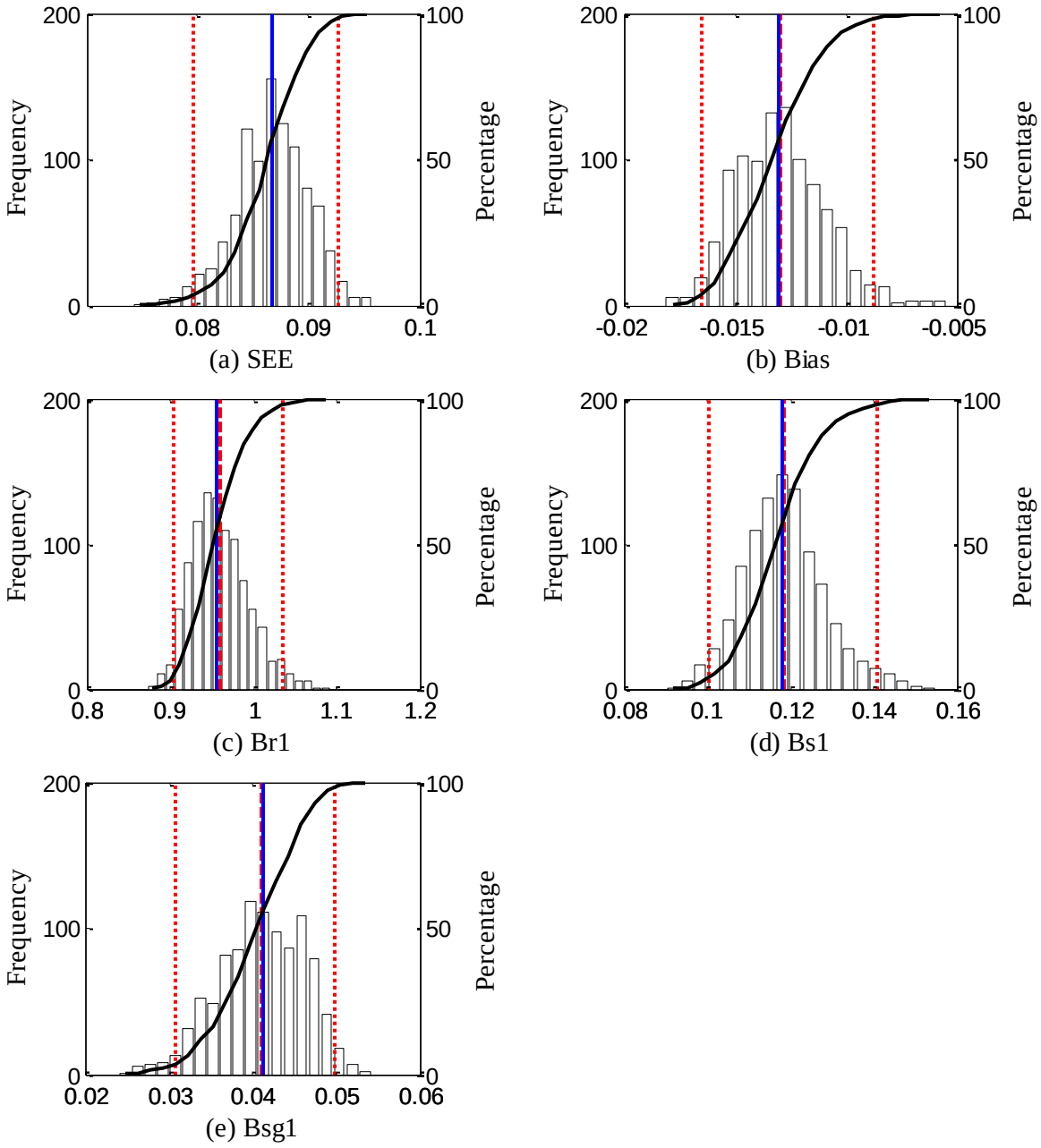

Figure B-91 Option 1: Method 1 repeated split sampling total rutting frequency distributions – calibration

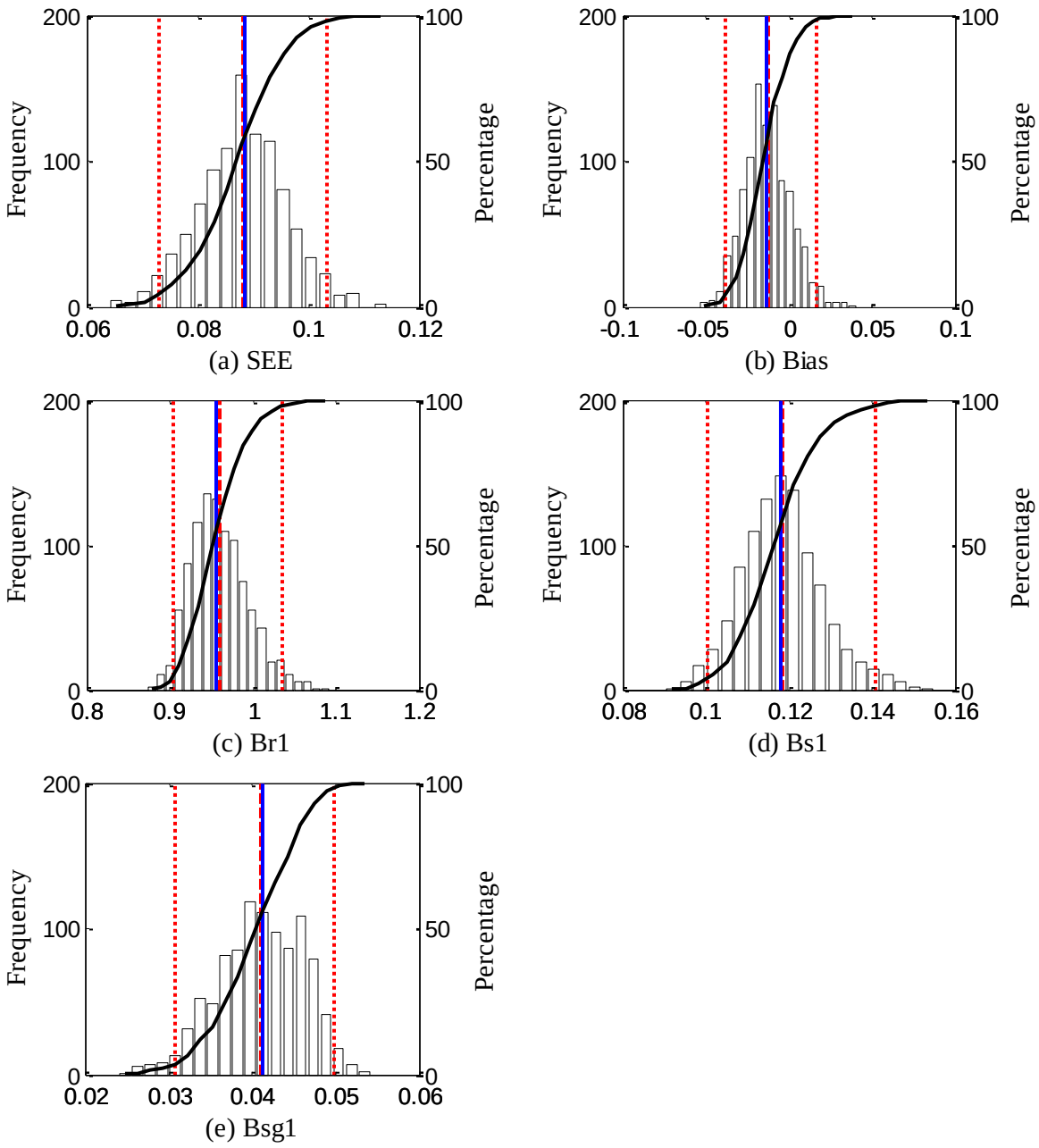

Figure B-92 Option 1: Method 1 repeated split sampling total rutting frequency distributions – validation

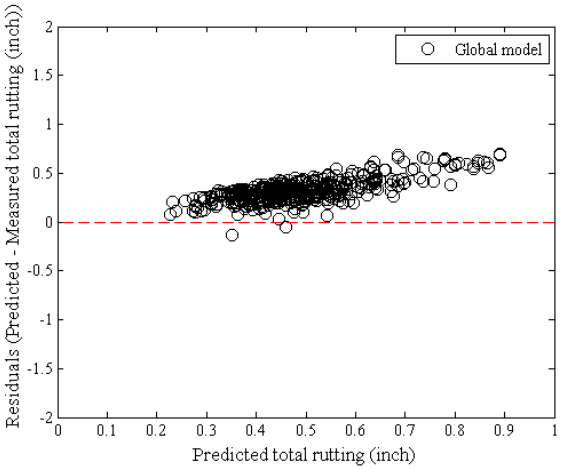

(a) Global model

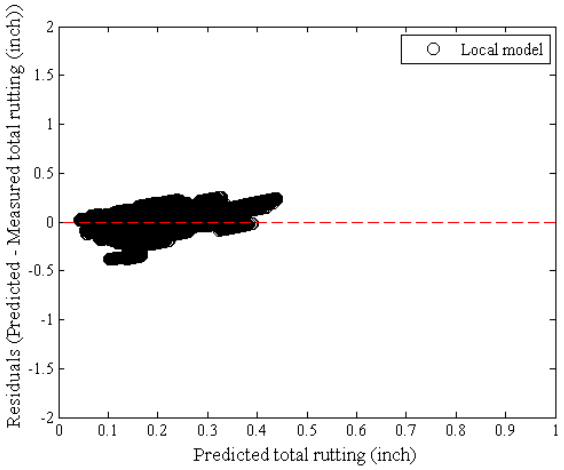

(b) Local model

Figure B-93 Option 1: Method 1 Total rutting residual plots - repeated split sampling

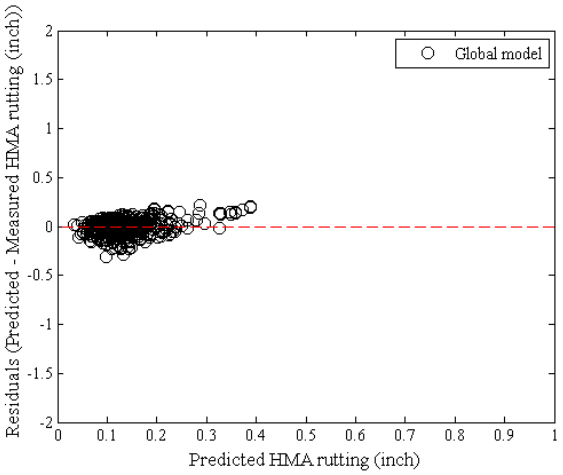

(a) Global model

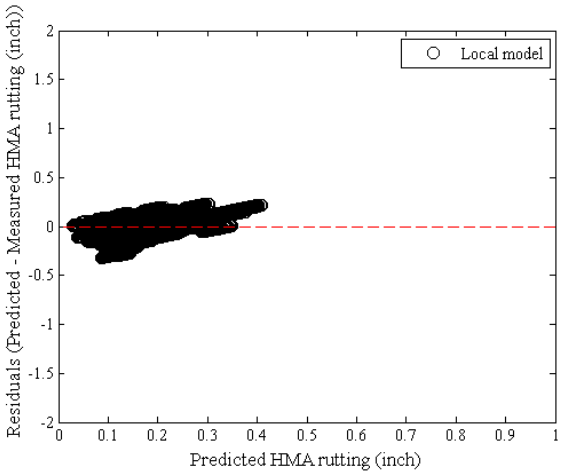

(b) Local model

Figure B-94 Option 1: Method 1 HMA rutting residual plots - repeated split sampling

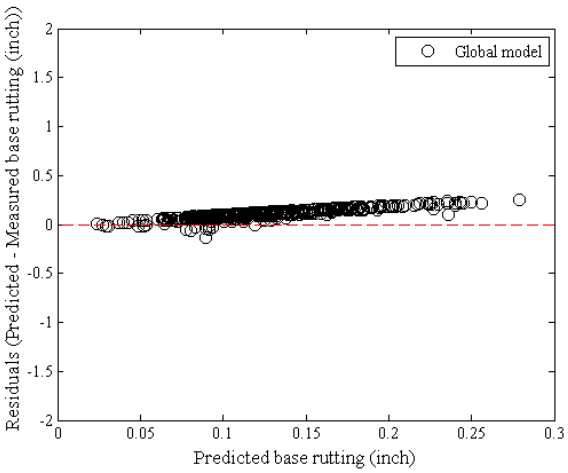

(a) Global model

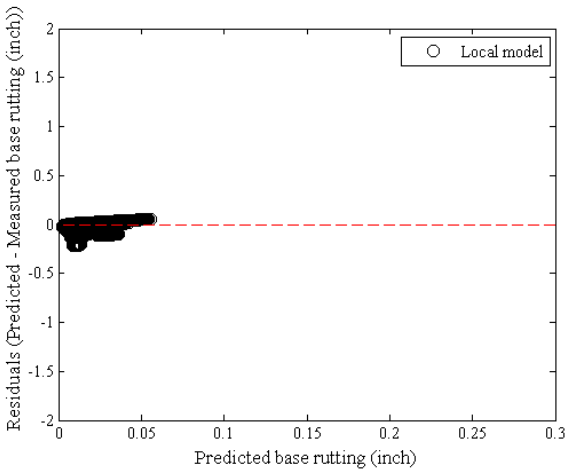

(b) Local model

Figure B-95 Option 1: Method 1 Base rutting residual plots - repeated split sampling

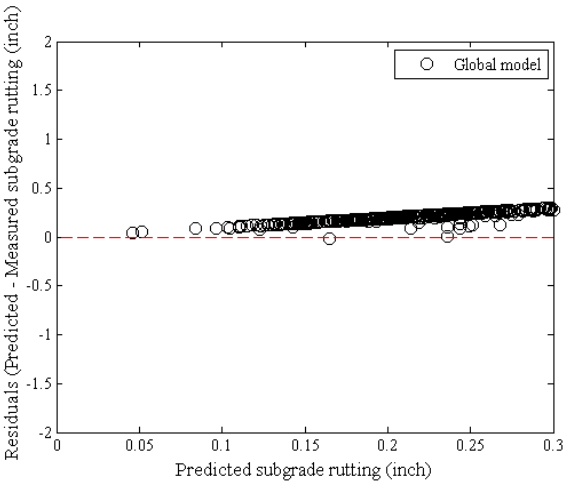

(a) Global model

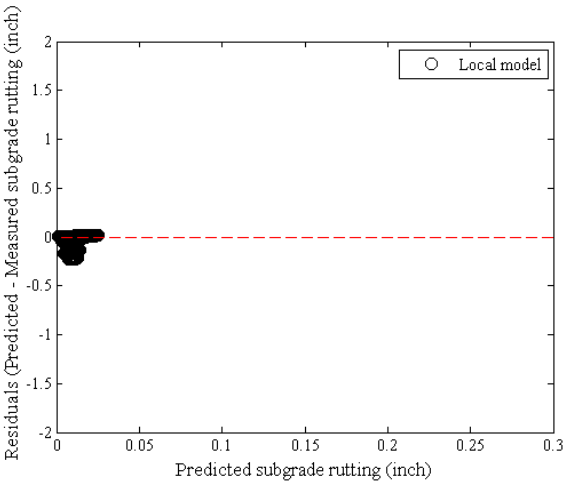

(b) Local model

Figure B-96 Option 1: Method 1 Subgrade rutting residual plots - repeated split sampling

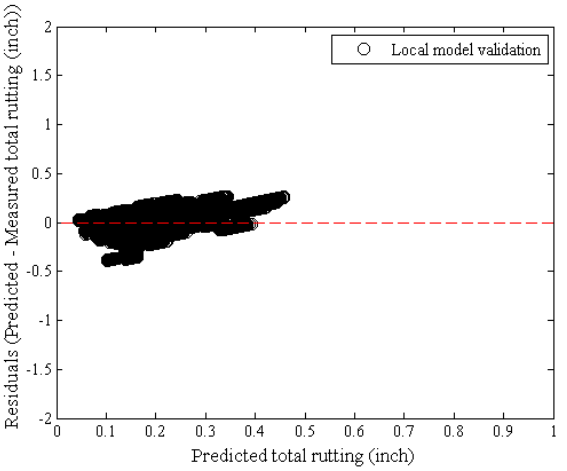

(a) Total rutting

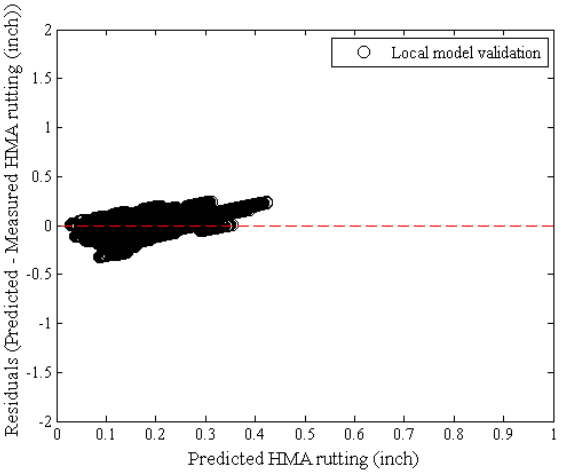

(b) HMA rutting

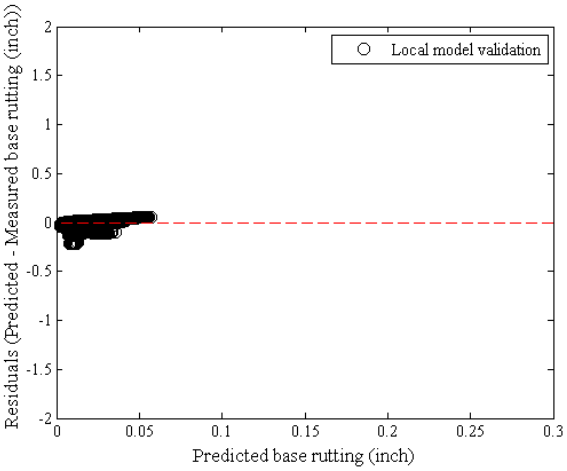

(c) Base rutting

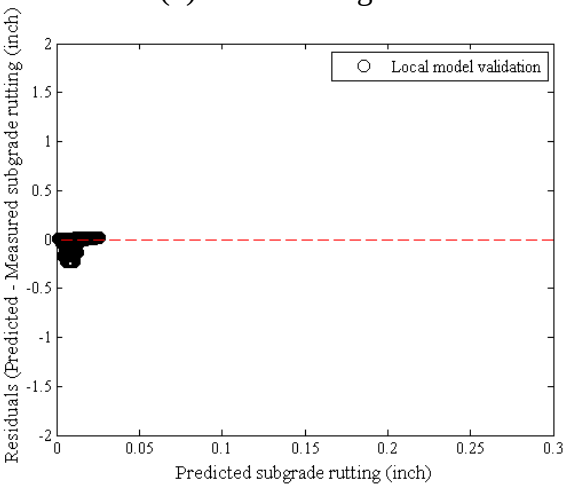

(d) Subgrade rutting

Figure B-97 Option 1: Method 1 Rutting model validation residual plots – repeated split sampling

Reliability

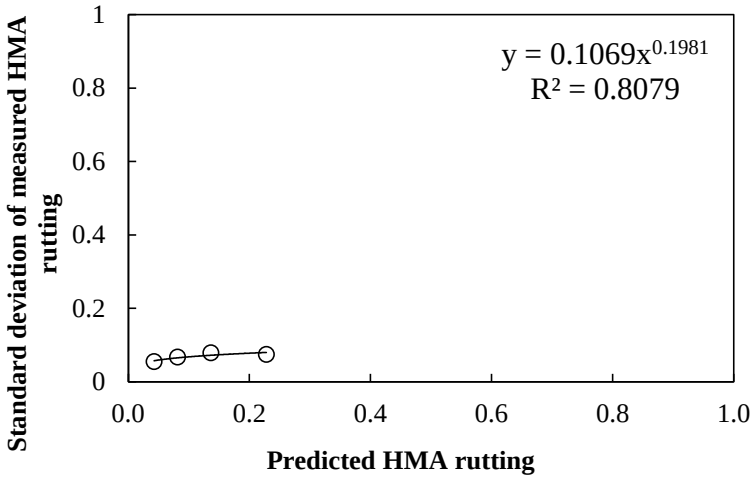

(a) HMA rutting reliability

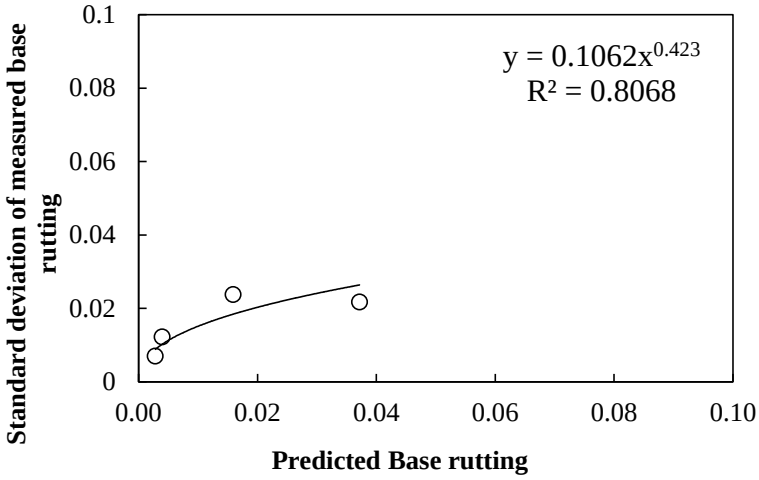

(b) Base rutting reliability

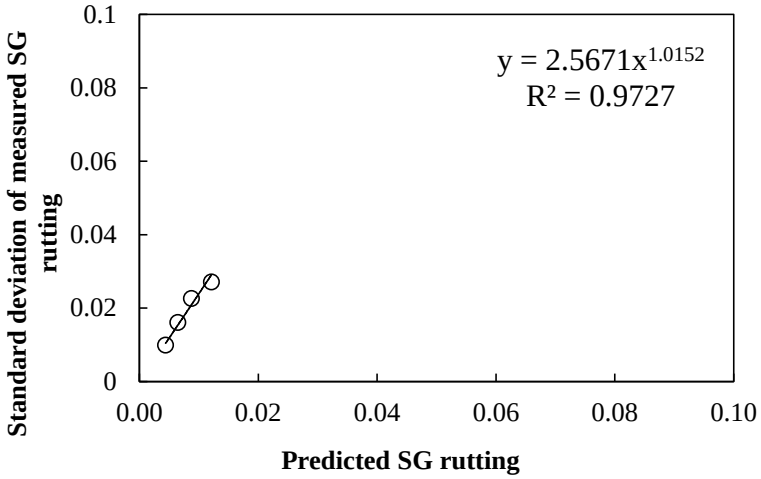

(c) Subgrade rutting reliability

Figure B-98 Rutting model reliability – option 1 method 1 – repeated split sampling

Bootstrapping

Table B-56 Option 1: Method 1 – Global model SEE and bias – bootstrapping

Calibration set	Average SEE	SEE Lower CI	SEE Upper CI	Average bias (in.)	Bias Lower CI	Bias Upper CI
AC rutting	0.0785	0.0706	0.0870	-0.0039	-0.0148	0.0068
Base rutting	0.1264	0.1146	0.1401	0.1110	0.1010	0.1219
Subgrade rutting	0.2240	0.2122	0.2360	0.2142	0.2031	0.2253
Total rutting	0.3425	0.3223	0.3654	0.3213	0.3026	0.3417

Table B-57 Option 1: Method 1 – Local model SEE and bias – bootstrapping

Calibration set	AC rutting	Base rutting	Subgrade rutting	Total rutting
Average SEE	0.0780	0.0258	0.0221	0.0865
SEE Lower CI	0.0702	0.0187	0.0092	0.0772
SEE Upper CI	0.0865	0.0333	0.0318	0.0962
Average bias (in.)	-0.0091	-0.0034	-0.0003	-0.0128
Bias Lower CI	-0.0152	-0.0056	-0.0008	-0.0188
Bias Upper CI	-0.0038	-0.0015	0.0001	-0.0073
Average calibration coefficient	0.9628	0.1190	0.0411	N/A
Calibration coefficient Lower CI	0.8721	0.0927	0.0277	N/A
Calibration coefficient Upper CI	1.0628	0.1479	0.0577	N/A

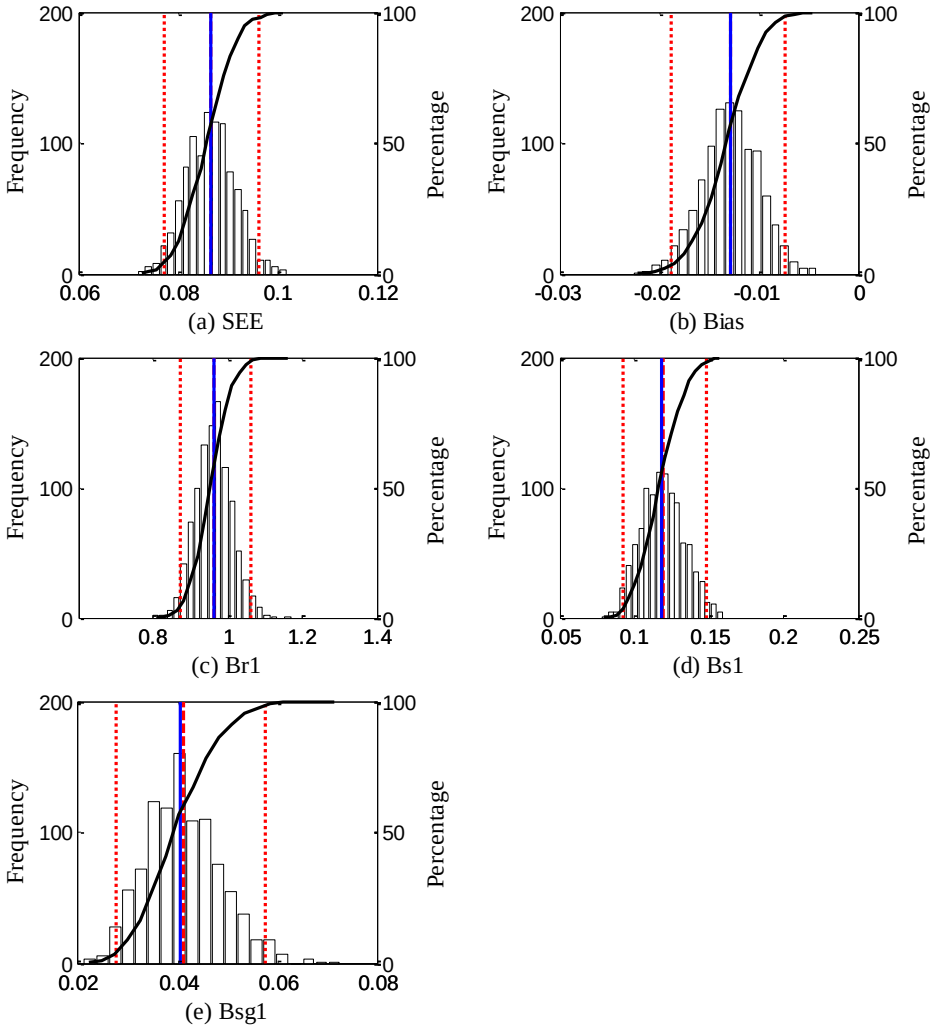

Figure B-99 Option 1: Method 1 bootstrapping total rutting frequency distributions – calibration

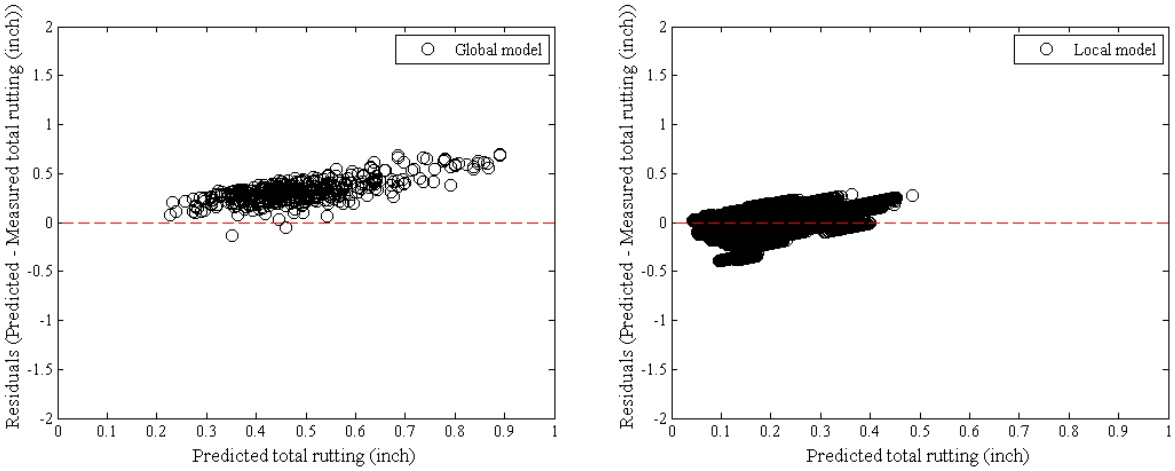

Figure B-100 Option 1: Method 1 Total rutting residual plots - bootstrapping

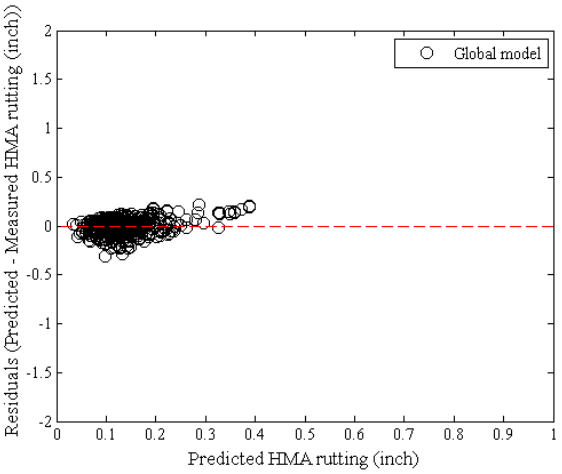

(a) Global model

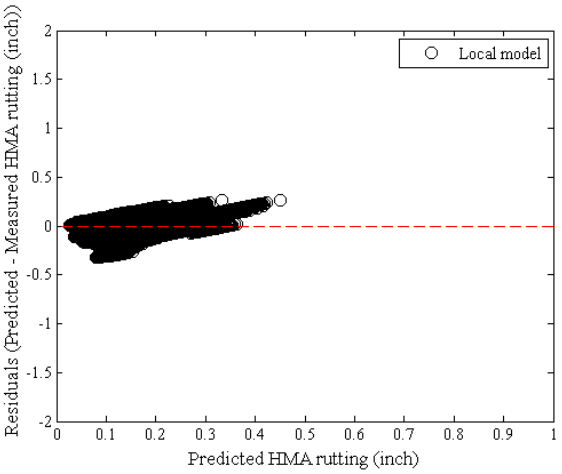

(b) Local model

Figure B-101 Option 1: Method 1 HMA rutting residual plots - bootstrapping

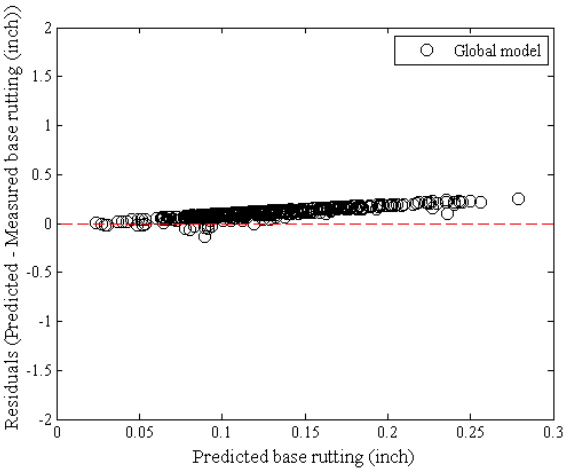

(a) Global model

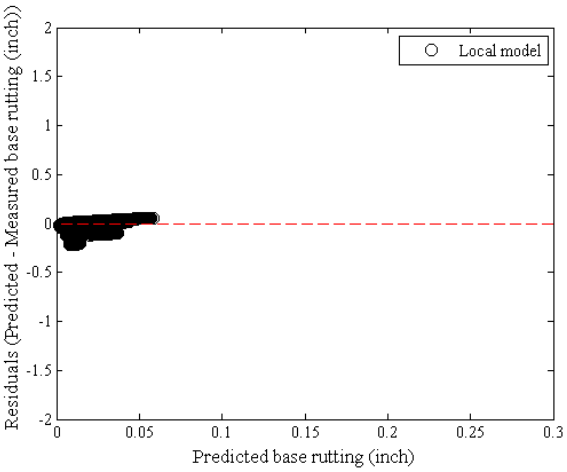

(b) Local model

Figure B-102 Option 1: Method 1 Base rutting residual plots - bootstrapping

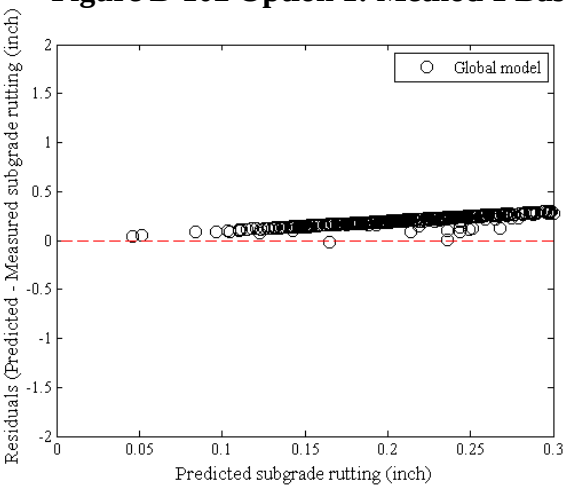

(a) Global model

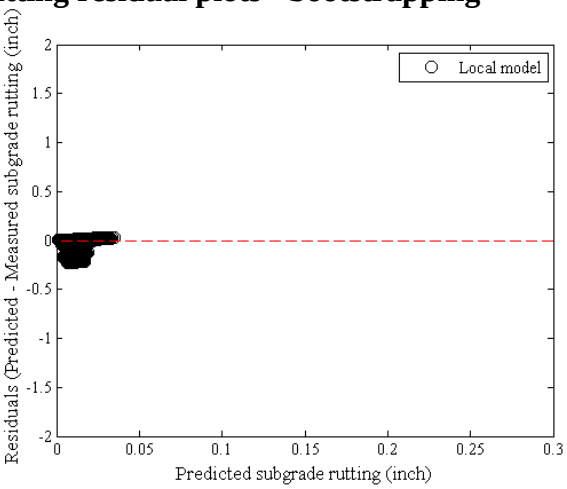

(b) Local model

Figure B-103 Option 1: Method 1 Subgrade rutting residual plots - bootstrapping

Reliability

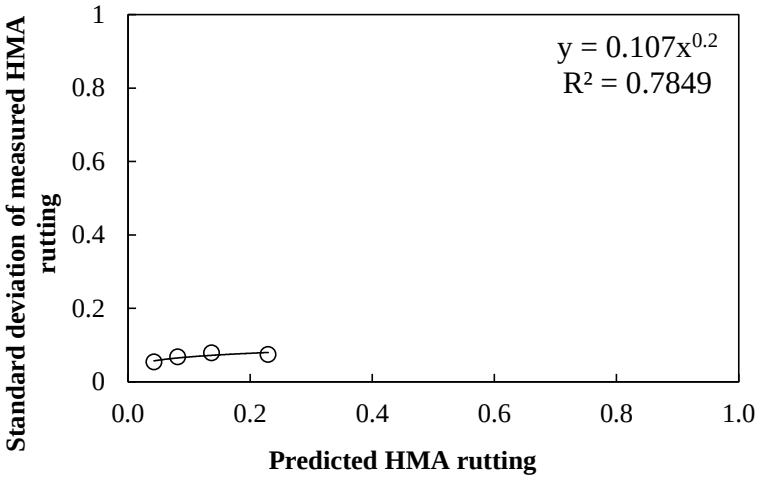

(a) HMA rutting reliability

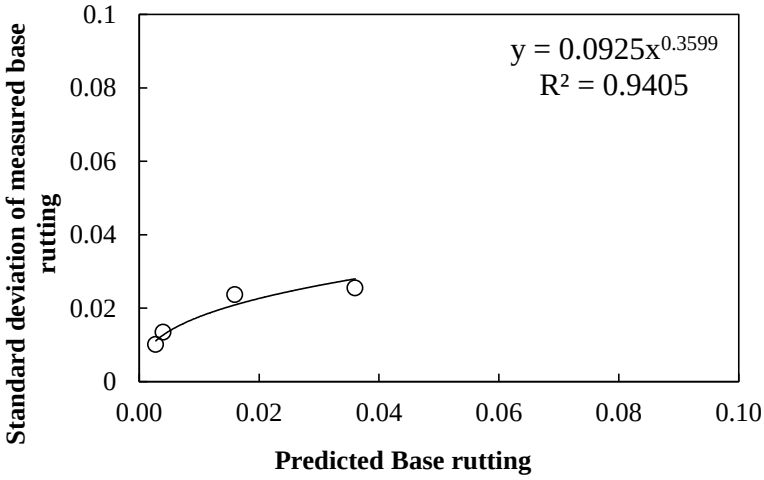

(b) Base rutting reliability

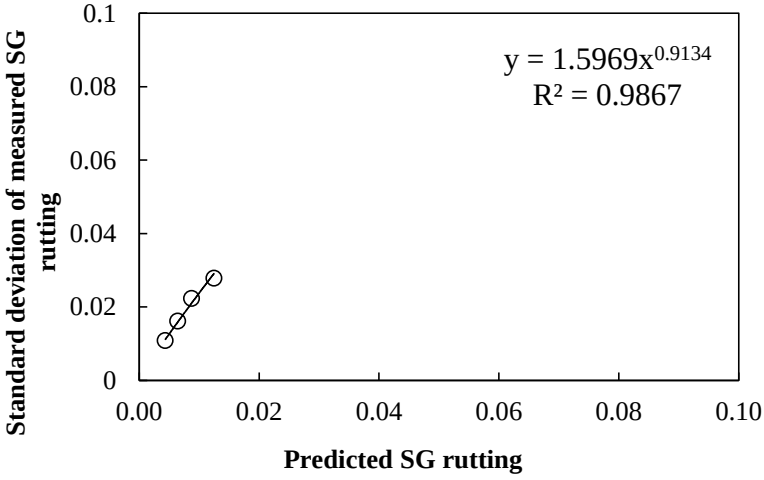

(c) Subgrade rutting reliability

Figure B-104 Rutting model reliability – option 1 method 1 - bootstrapping

B.1.3.2 Option 1 – Method 2

No sampling

Table B-58 Option 1: Method 2 – Global model goodness of fit – no sampling

HMA layer	SEE (in.)	Bias (in.)
AC rut	0.0786	-0.0037
Base rut	0.1267	0.1111
Subgrade	0.2242	0.2143
Total rut	0.3431	0.3217

Table B-59 Option 1: Method 2 – Global model *p*-values

HMA layer	t-test p-value	Intercept p-value	Slope = 1 p-value
AC rut	0.3220	0.0000	0.0000
Base rut	0.0000	0.0000	0.0000
Subgrade	0.0000	0.0000	0.0000
Total rut	0.0000	0.0000	0.0000

Table B-60 Option 1: Method 2 – Local model goodness of fit– no sampling

HMA layer	SEE	Bias
AC rut	0.1167	-0.0892
Base rut	0.0304	0.0109
Subgrade	0.0840	0.0775
Total rut	0.0812	-0.0009

Table B-61 Option 1: Method 2 – Local model *p*-values– no sampling

HMA layer	t-test p-value	Intercept p-value	Slope = 1 p-value
AC rut	0.0000	0.0000	0.0000
Base rut	0.0000	0.0000	0.0000
Subgrade	0.0000	0.0000	0.0000
Total rut	0.8142	0.0000	0.0000

Table B-62 Option 1: Method 2 – Local model *p*-values– no sampling

Calibration Coefficient	Global model	Local model
HMA rutting (br1)	1.0000	0.3738
Base rutting (bs1)	1.0000	0.2283
Subgrade rutting (bsg1)	1.0000	0.3886

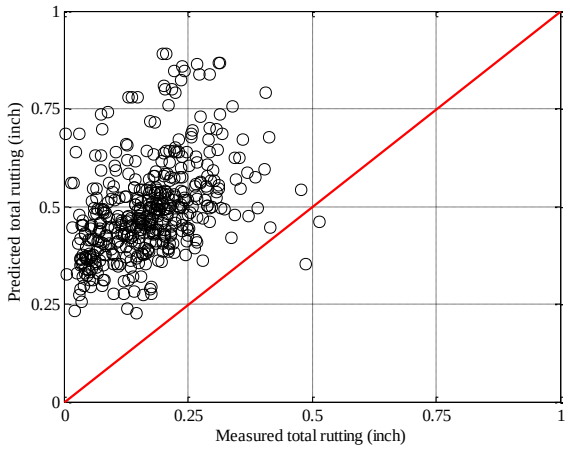

(a) Global model

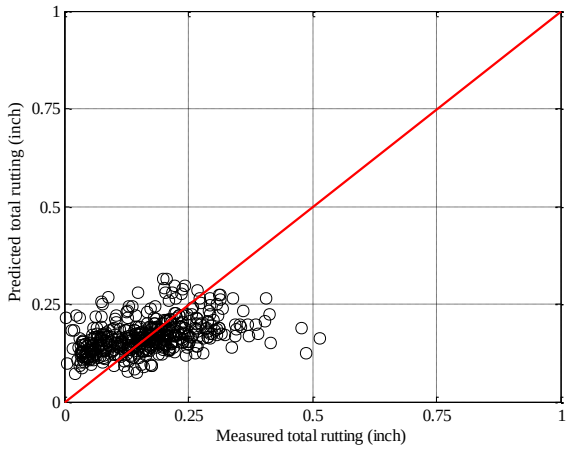

(b) Local model

Figure B-105 Option 1: Method 2 Total rutting local calibration results - no sampling

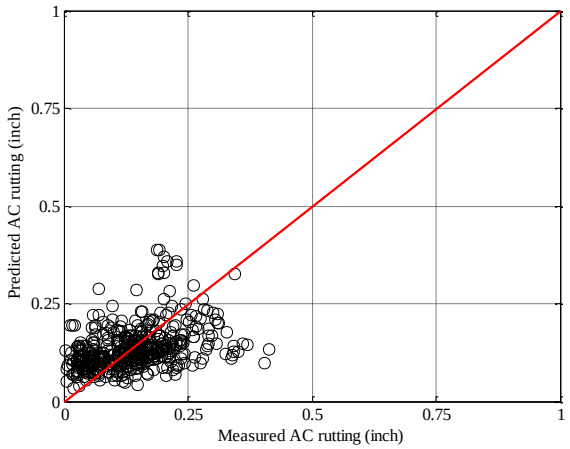

(a) Global model

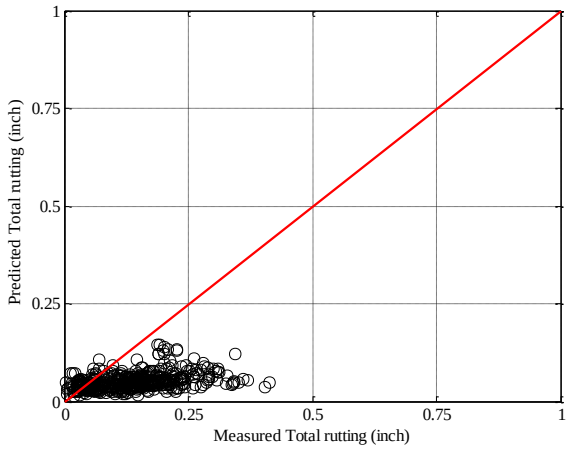

(b) Local model

Figure B-106 Option 1: Method 2 HMA rutting local calibration results - no sampling

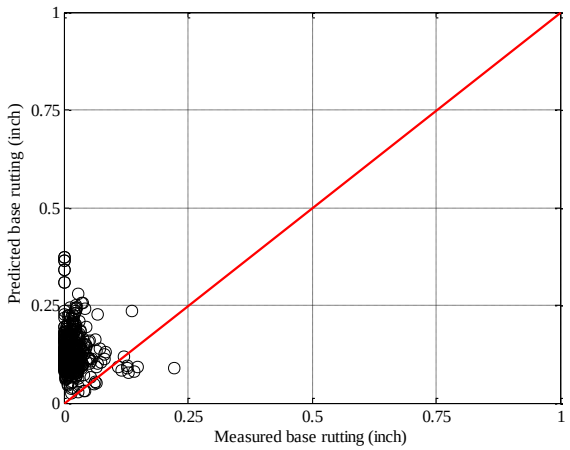

(a) Global model

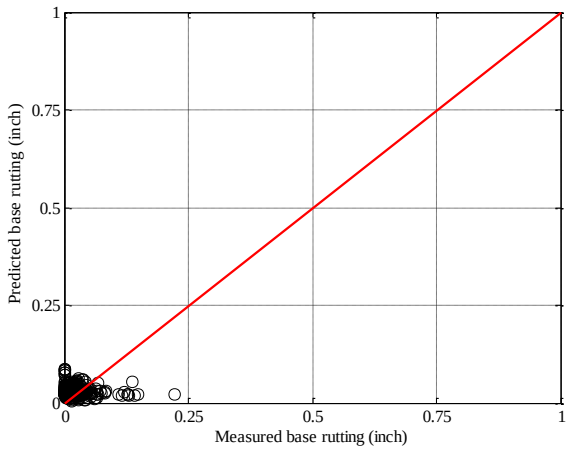

(b) Local model

Figure B-107 Option 1: Method 2 Base rutting local calibration results - no sampling

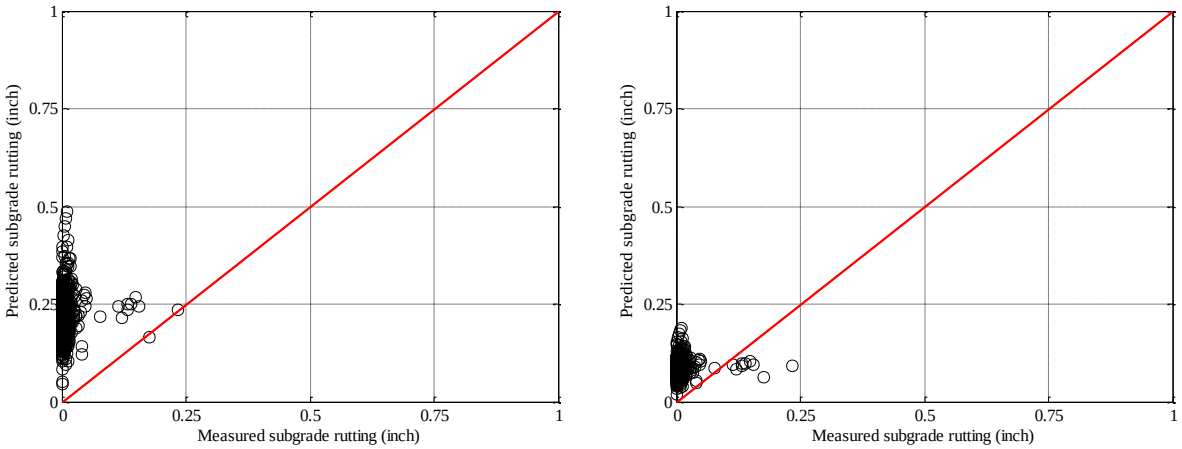

(a) Global model (b) Local model

Figure B-108 Option 1: Method 2 Subgrade rutting local calibration results - no sampling

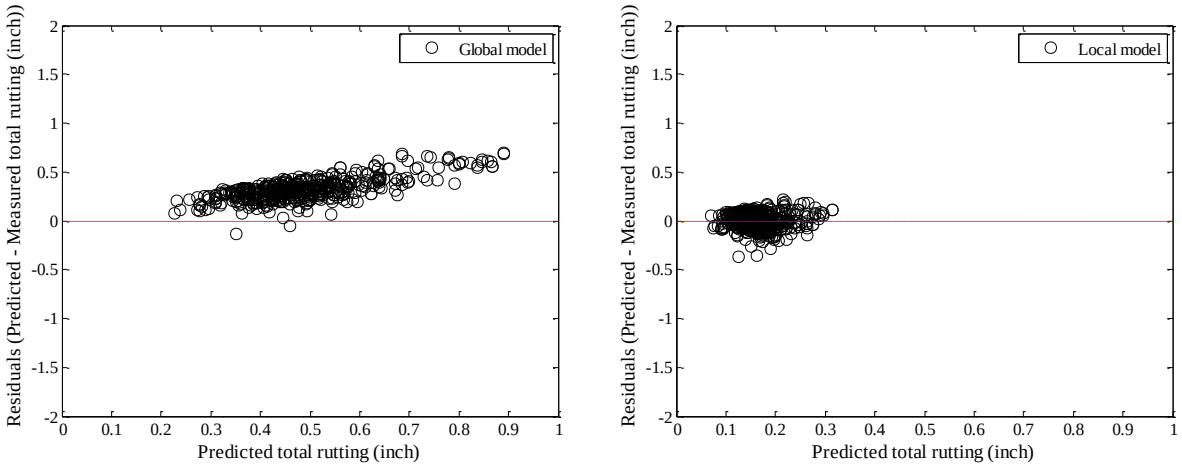

(a) Global model (b) Local model

Figure B-109 Option 1: Method 2 Total rutting residual plots - no sampling

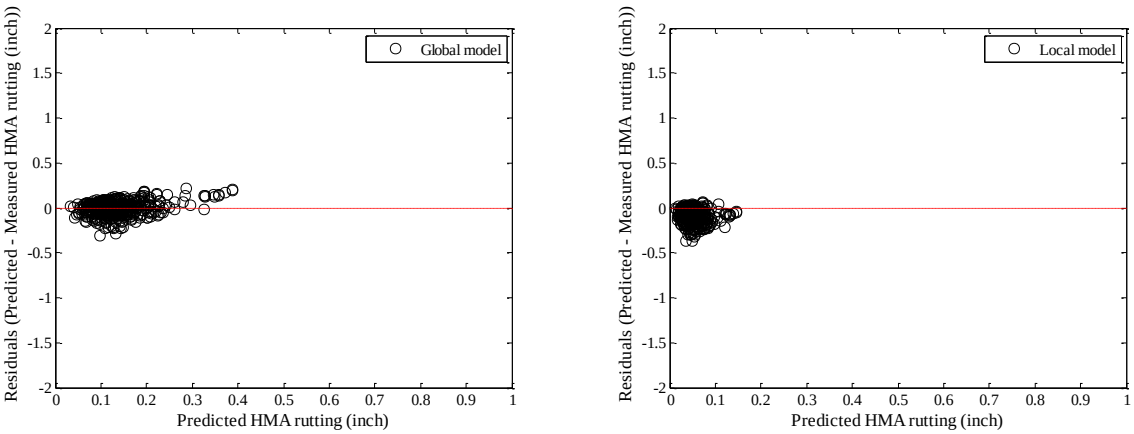

(a) Global model (b) Local model

Figure B-110 Option 1: Method 2 HMA rutting residual plots - no sampling

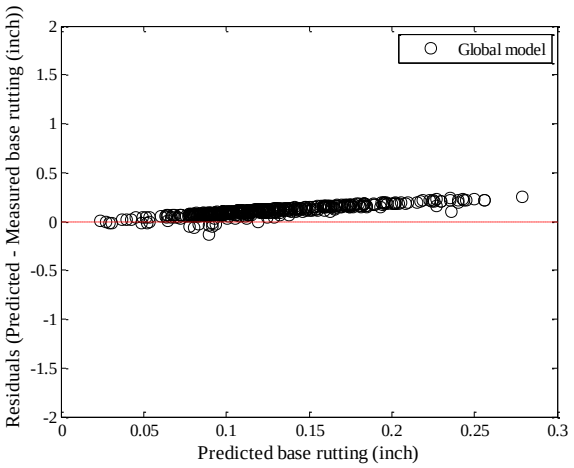

(a) Global model

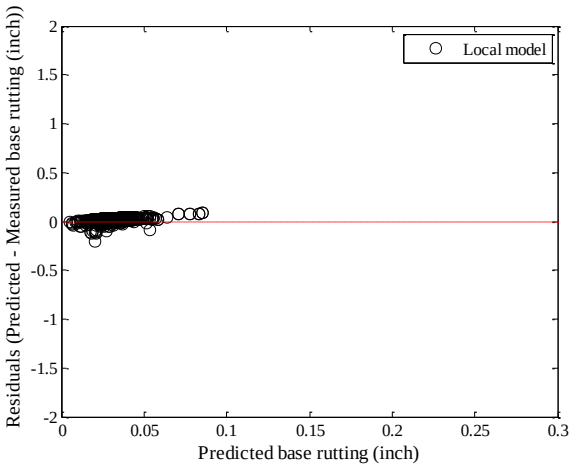

(b) Local model

Figure B-111 Option 1: Method 2 Base rutting residual plots - no sampling

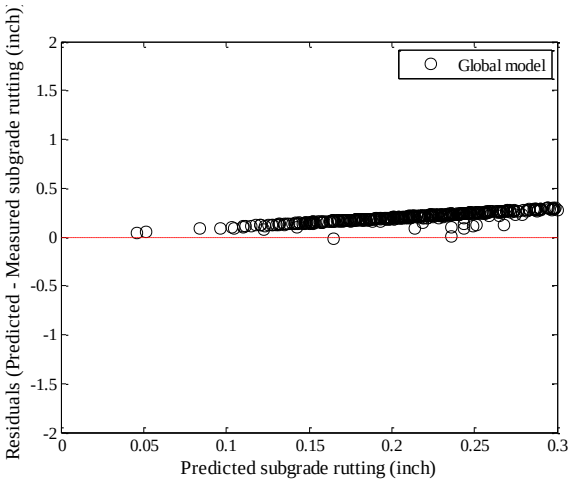

(a) Global model

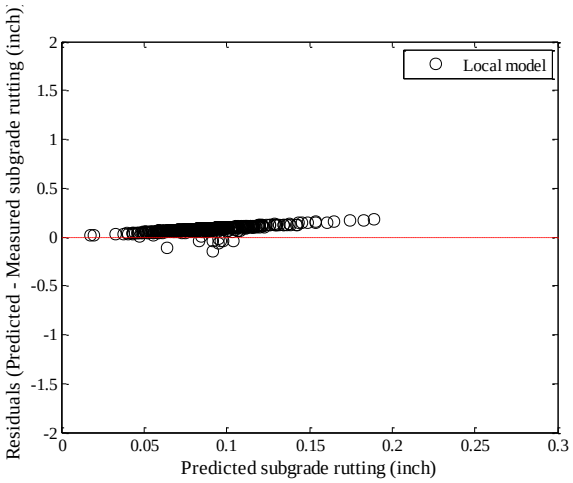

(b) Local model

Figure B-112 Option 1: Method 2 Subgrade rutting residual plots - no sampling

Reliability

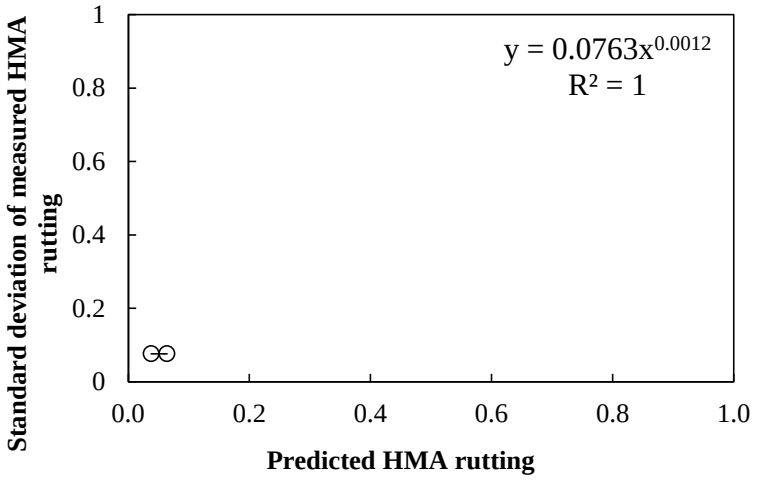

(a) HMA rutting reliability

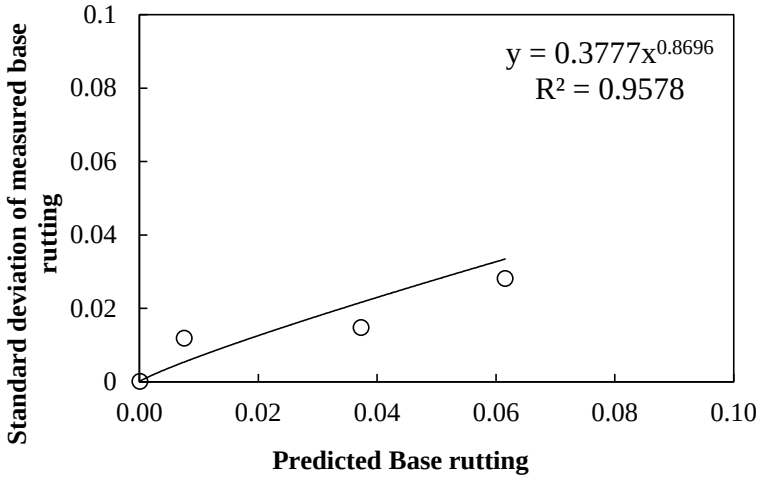

(b) Base rutting reliability

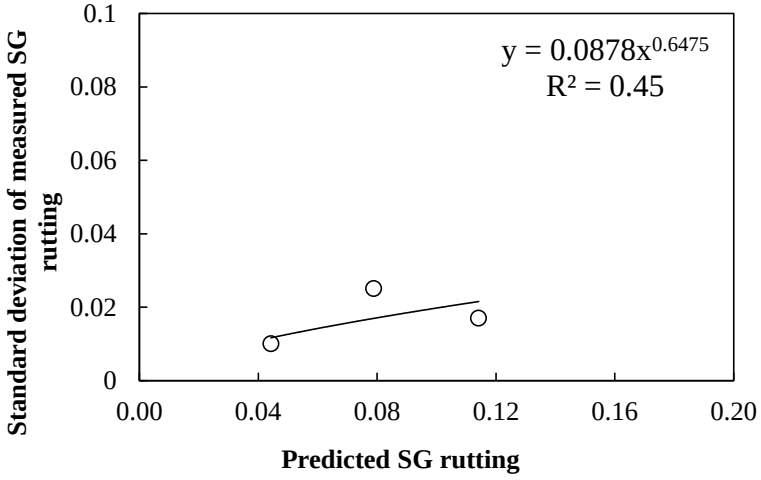

(c) Subgrade rutting reliability

Figure B-113 Rutting model reliability equations – option 1 method 2 – no sampling

Split sampling

Table B-63 Option 1: Method 2 – Global model goodness of fit – split sampling

HMA layer	SEE (in.)	Bias (in.)
AC rut	0.0768	0.0003
Base rut	0.1293	0.1150
Subgrade	0.2220	0.2106
Total rut	0.3478	0.3259

Table B-64 Option 1: Method 2 – Global model *p*-values - split sampling

HMA layer	t-test p-value	Intercept p-value	Slope = 1 p-value
AC rut	0.9481	0.0000	0.0000
Base rut	0.0000	0.0000	0.0000
Subgrade	0.0000	0.0000	0.0000
Total rut	0.0000	0.0000	0.0000

Table B-65 Option 1: Method 2 – Local model goodness of fit– split sampling

HMA layer	SEE	Bias
AC rut	0.1050	-0.0758
Base rut	0.0350	0.0199
Subgrade	0.0630	0.0543
Total rut	0.0806	-0.0016

Table B-66 Option 1: Method 2 – Local model *p*-values– split sampling

HMA layer	t-test p-value	Intercept p-value	Slope = 1 p-value
AC rut	0.0000	0.0000	0.0000
Base rut	0.0000	0.0000	0.0000
Subgrade	0.0000	0.0000	0.0000
Total rut	0.7277	0.0000	0.0000

Table B-67 Option 1: Method 2 – Local model *p*-values – split sampling

Calibration Coefficient	Global model	Local model
HMA rutting (br1)	1.0000	0.4383
Base rutting (bs1)	1.0000	0.2832
Subgrade rutting (bsg1)	1.0000	0.2930

Table B-68 Option 1: Method 2 – Local model validation p-values – split sampling

HMA layer	t-test p-value	Intercept p-value	Slope = 1 p-value
AC rut	0.0000	0.0000	0.0000
Base rut	0.0000	0.0000	0.0000
Subgrade	0.0000	0.0000	0.0000
Total rut	0.0170	0.0000	0.0000

Table B-69 Option 1: Method 2 – Local model validation SEE and bias – split sampling

HMA layer	SEE	Bias
AC rut	0.1210	-0.0908
Base rut	0.0352	0.0135
Subgrade	0.0630	0.0601
Total rut	0.0846	-0.0172

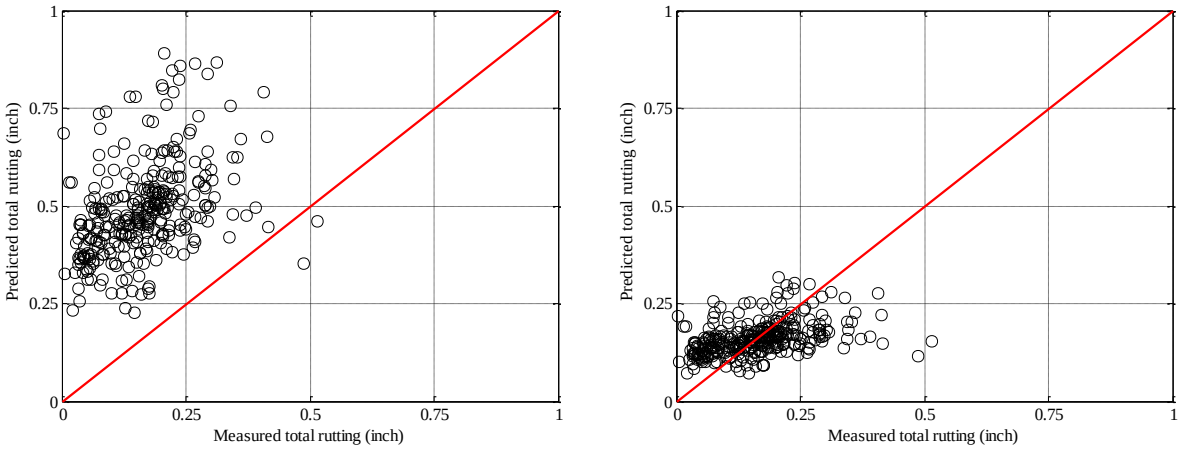

(a) Global model (b) Local model

Figure B-114 Option 1: Method 2 Total rutting local calibration results - split sampling

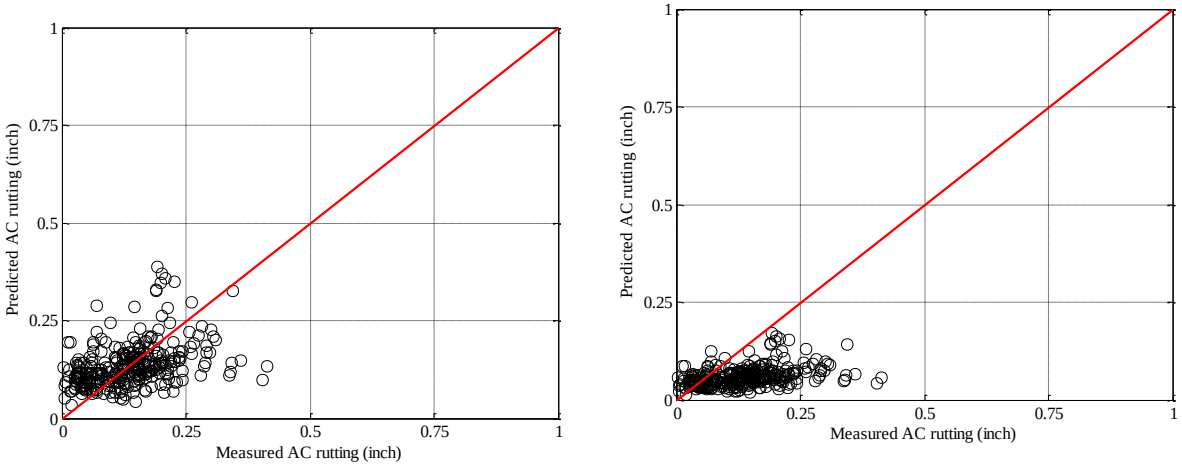

(a) Global model

(b) Local model

Figure B-115 Option 1: Method 2 HMA rutting local calibration results - split sampling

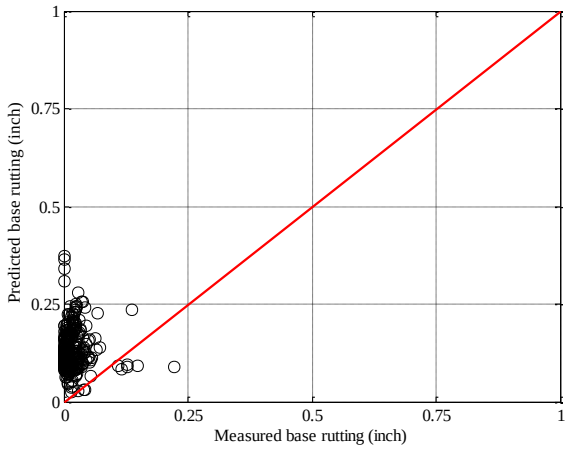

(a) Global model

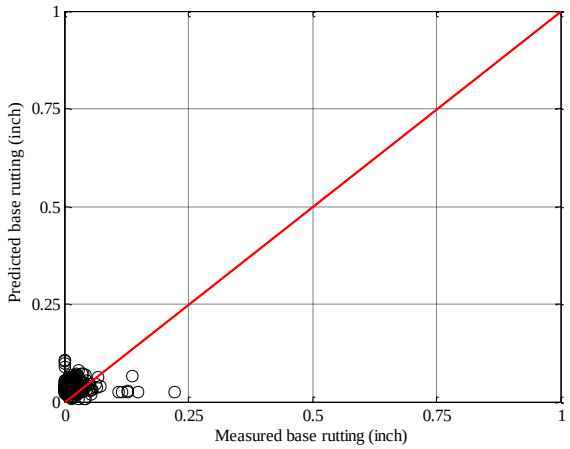

(b) Local model

Figure B-116 Option 1: Method 2 Base rutting local calibration results - split sampling

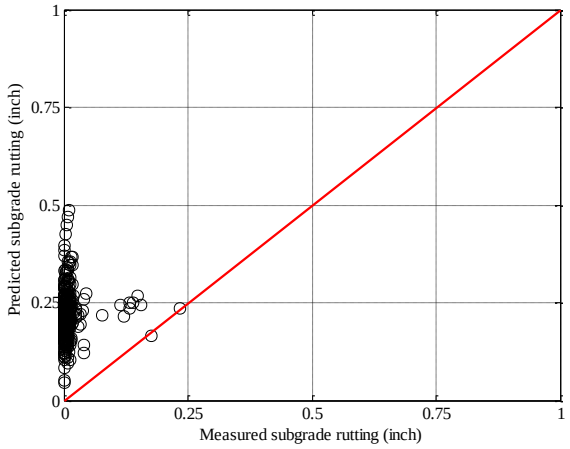

(a) Global model

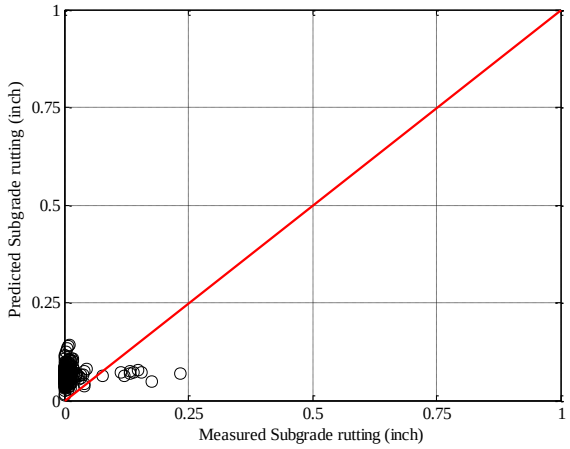

(b) Local model

Figure B-117 Option 1: Method 2 Subgrade rutting local calibration results - split sampling

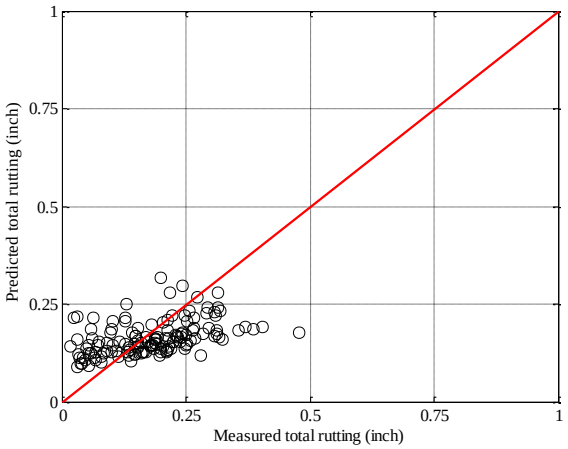

(a) Total rutting

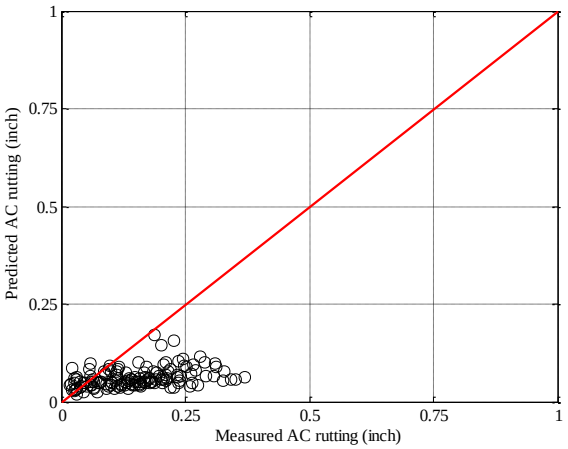

(b) HMA rutting

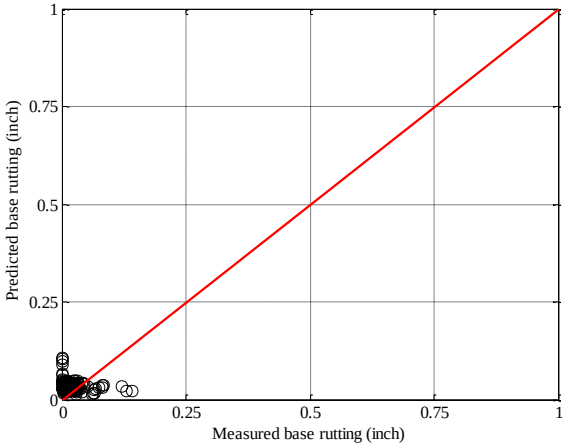

(c) Base rutting

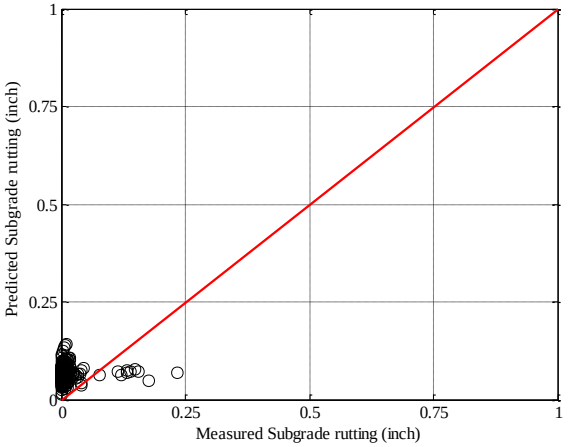

(d) Subgrade rutting

Figure B-118 Option 1: Method 1 Rutting model validation – split sampling

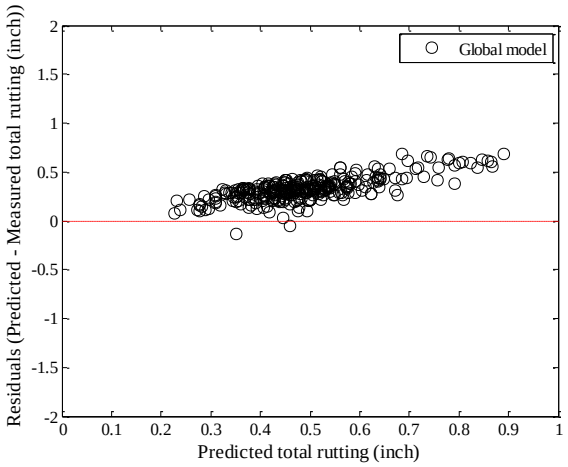

(a) Global model

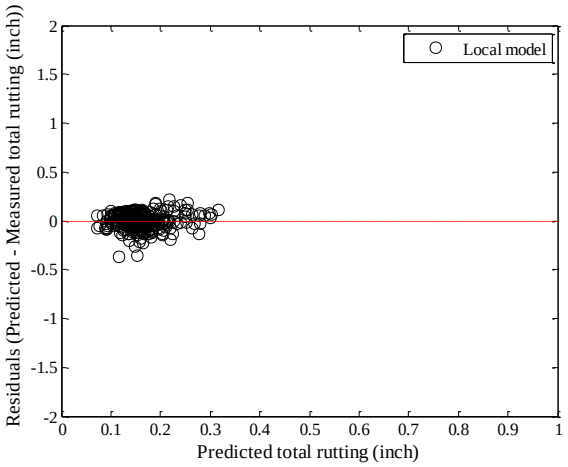

(b) Local model

Figure B-119 Option 1: Method 2 Total rutting local calibration residual plots - split sampling

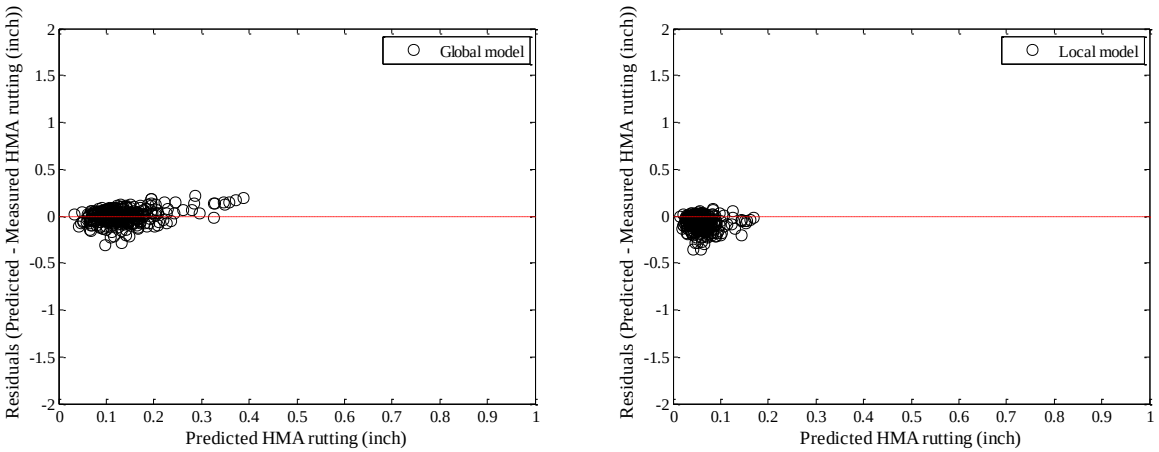

(a) Global model (b) Local model

Figure B-120 Option 1: Method 2 HMA rutting local calibration residual plots - split sampling

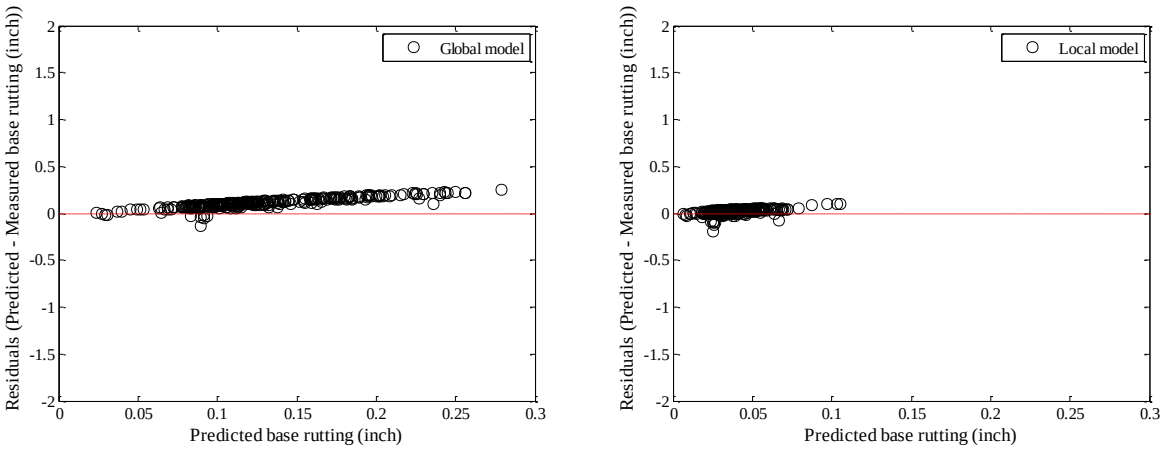

(a) Global model (b) Local model

Figure B-121 Option 1: Method 2 Base rutting local calibration residual plots - split sampling

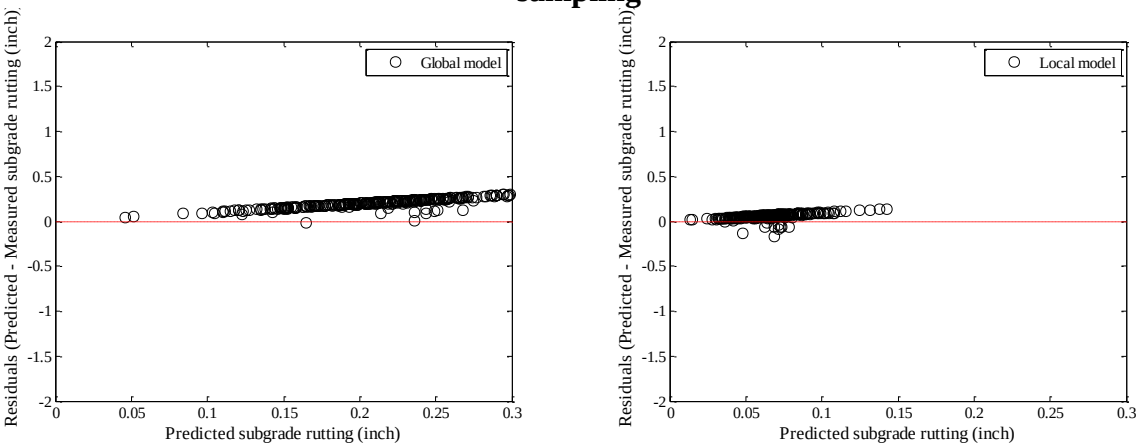

(a) Global model (b) Local model

Figure B-122 Option 1: Method 2 Subgrade rutting local calibration residual plots - split sampling

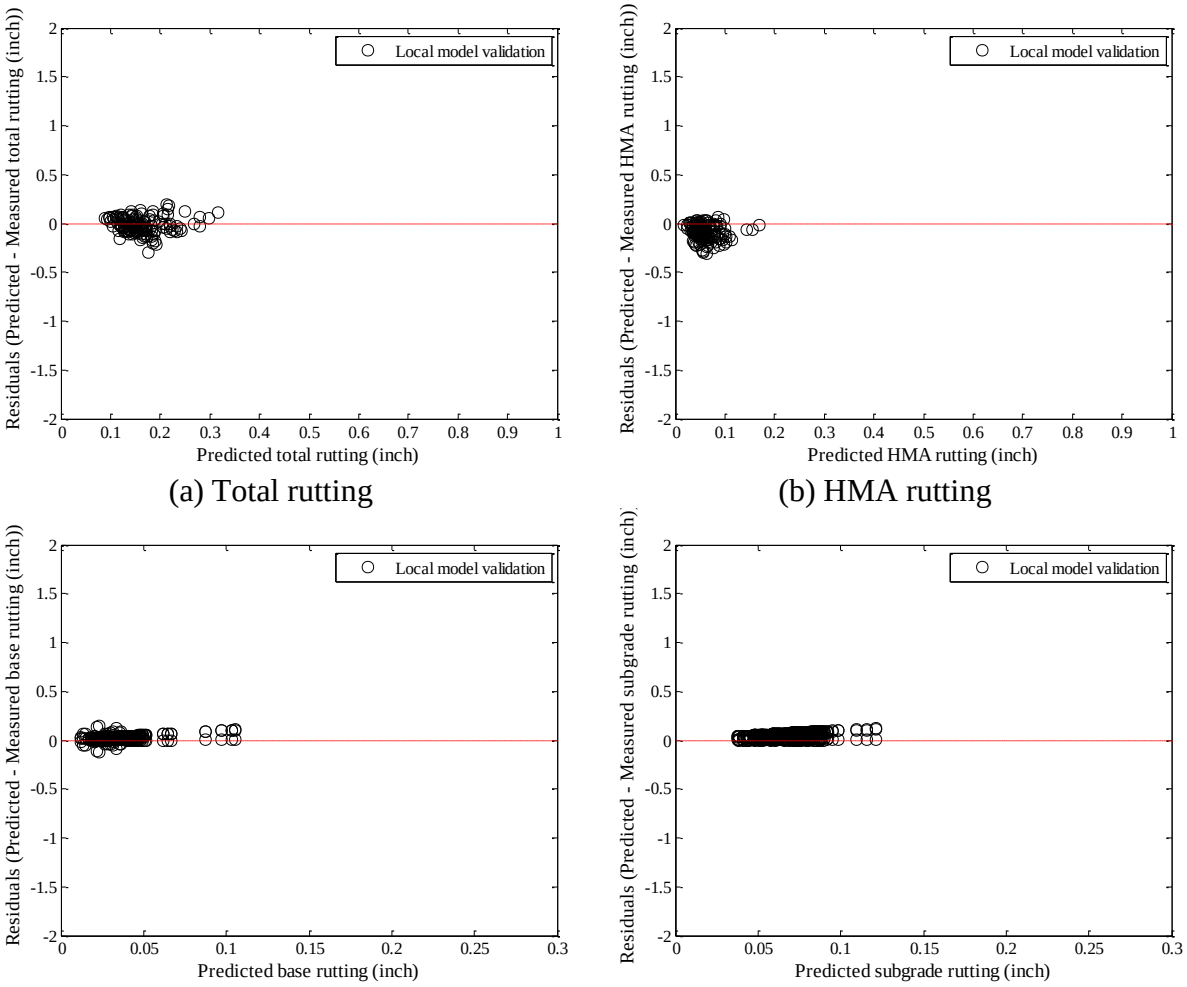

(a) Total rutting (b) HMA rutting

(c) Base rutting (d) Subgrade rutting

Figure B-123 Option 1: Method 2 Rutting model validation residual plots – split sampling

Reliability

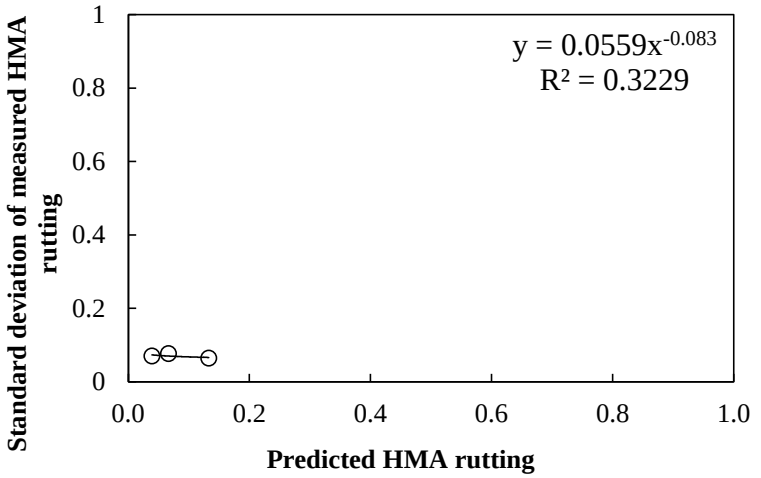

(a) HMA rutting reliability

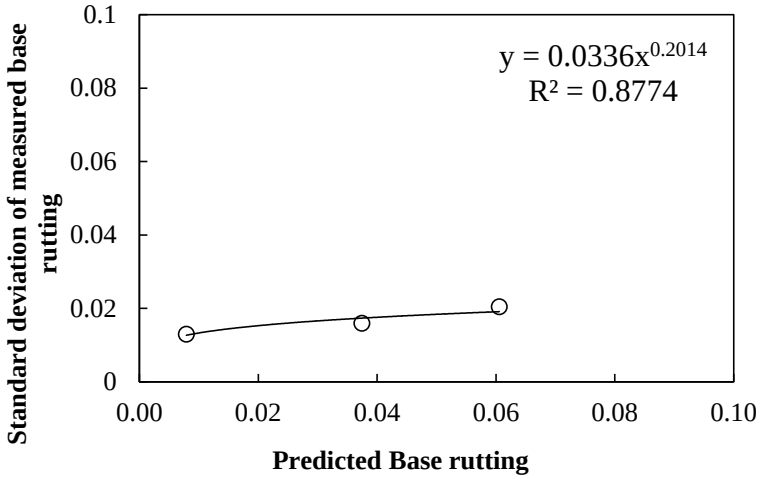

(b) Base rutting reliability

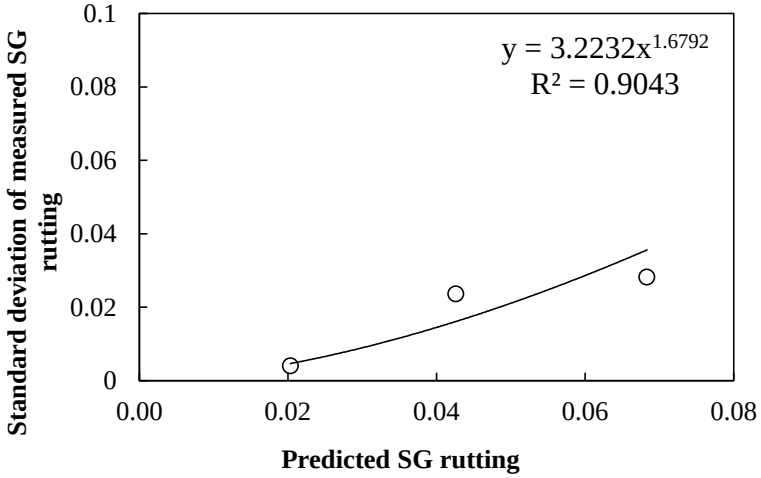

(c) Subgrade rutting reliability

Figure B-124 Rutting model reliability equations – option 1 method 2 – split sampling

Repeated split sampling

Table B-70 Option 1: Method 2 – Global model SEE and bias – repeated split sampling

Global Model	Average SEE	SEE Lower CI	SEE Upper CI	Average bias (in.)	Bias Lower CI	Bias Upper CI
AC rutting	0.0785	0.0730	0.0832	-0.0036	-0.0105	0.0033
Base rutting	0.1266	0.1171	0.1340	0.1109	0.1035	0.1181
Subgrade rutting	0.2244	0.2159	0.2311	0.2142	0.2069	0.2206
Total rutting	0.3433	0.3286	0.3567	0.3215	0.3090	0.3343

Table B-71 Option 1: Method 2 – Local model SEE and bias – repeated split sampling

Calibration set	AC rutting	Base rutting	Subgrade rutting	Total rutting
Average SEE	0.1161	0.0314	0.0827	0.0810
SEE Lower CI	0.0947	0.0246	0.0599	0.0751
SEE Upper CI	0.1339	0.0407	0.1065	0.0857
Average bias (in.)	-0.0881	0.0113	0.0760	-0.0008
Bias Lower CI	-0.1088	-0.0042	0.0533	-0.0024
Bias Upper CI	-0.0603	0.0271	0.1010	0.0008
Average calibration coefficient	0.3820	0.2324	0.3824	N/A
Calibration coefficient Lower CI	0.2364	0.1122	0.2795	N/A
Calibration coefficient Upper CI	0.5922	0.3594	0.4970	N/A

Table B-72 Option 1: Method 2 – Local model validation SEE and bias – repeated split sampling

Validation set	AC rutting	Base rutting	Subgrade rutting	Total rutting
Average SEE	0.1171	0.0316	0.0832	0.0829
SEE Lower CI	0.0925	0.0173	0.0592	0.0711
SEE Upper CI	0.1380	0.0495	0.1148	0.0960
Average bias (in.)	-0.0881	0.0117	0.0762	-0.0003
Bias Lower CI	-0.1106	-0.0047	0.0516	-0.0217
Bias Upper CI	-0.0547	0.0319	0.1070	0.0206
Average calibration coefficient	0.3820	0.2324	0.3824	N/A
Calibration coefficient Lower CI	0.2364	0.1122	0.2795	N/A
Calibration coefficient Upper CI	0.5922	0.3594	0.4970	N/A

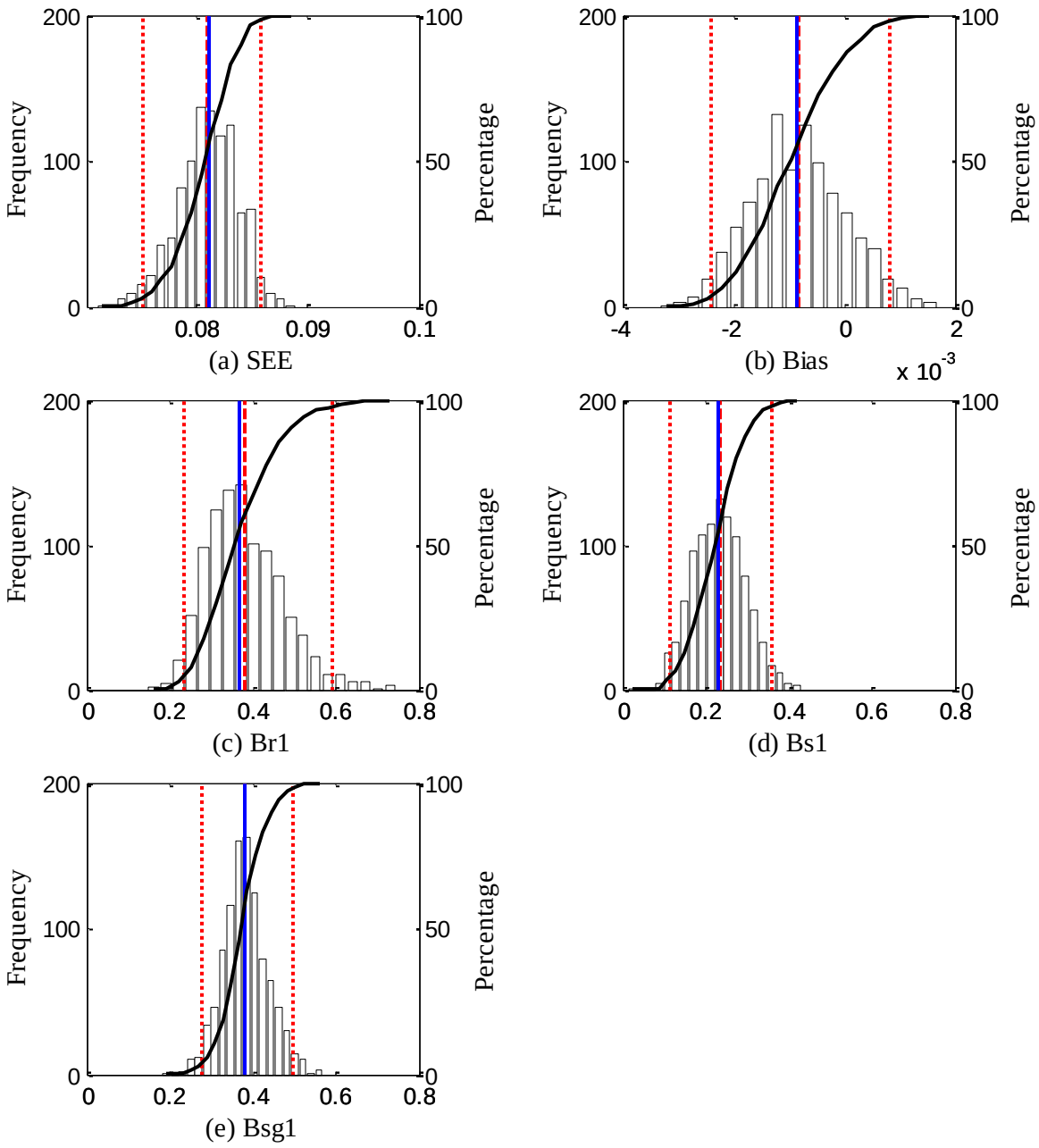

Figure B-125 Option 1: Method 2 repeated split sampling total rutting frequency distributions – calibration

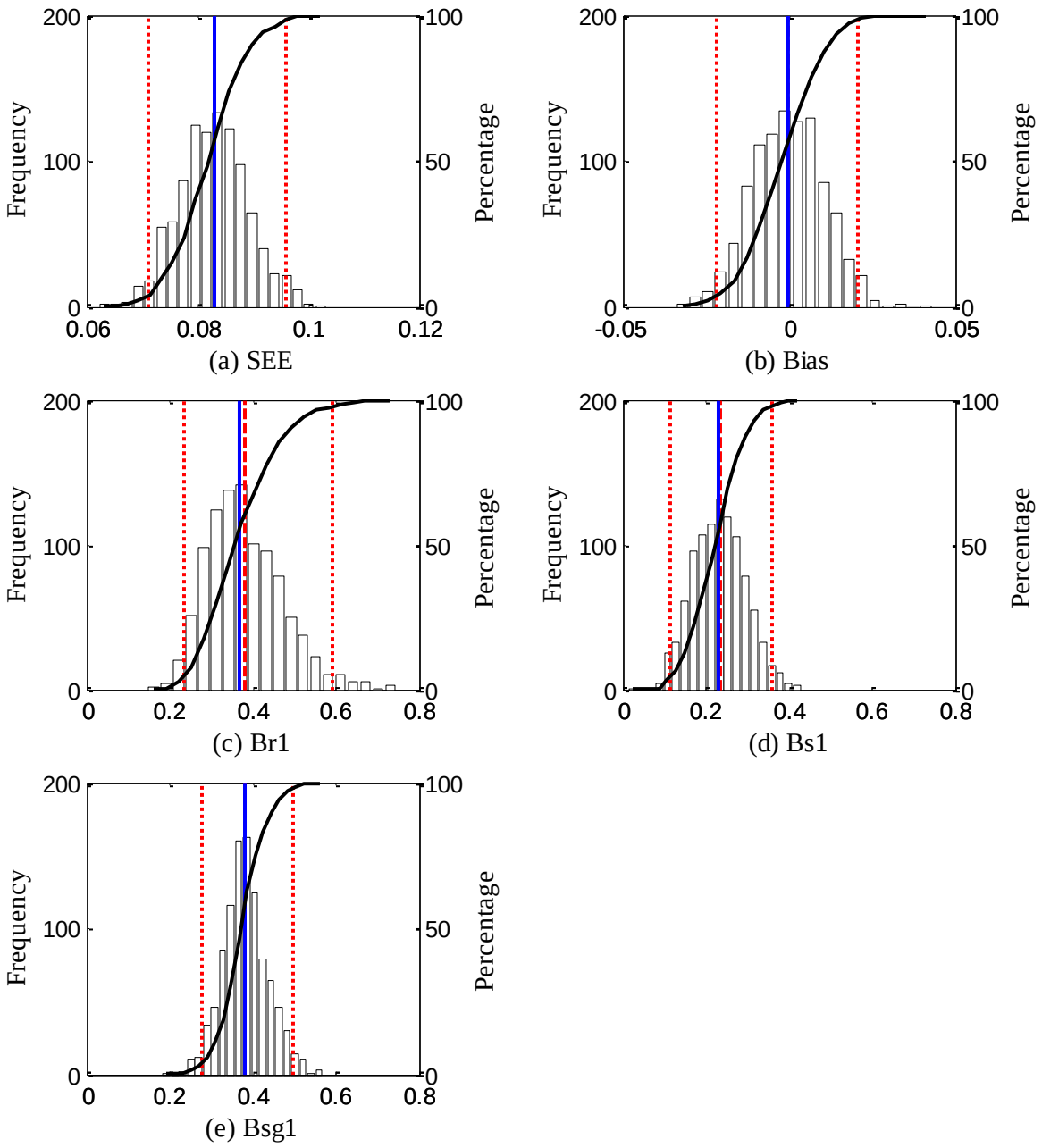

Figure B-126 Option 1: Method 2 repeated split sampling total rutting frequency distributions – validation

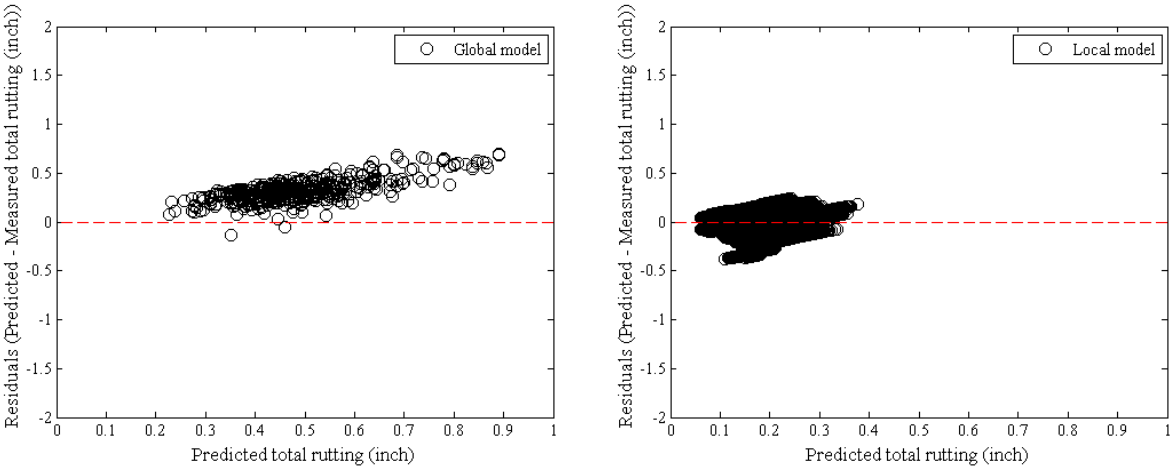

(a) Global model (b) Local model

Figure B-127 Option 1: Method 2 Total rutting local calibration residual plots - repeated split sampling

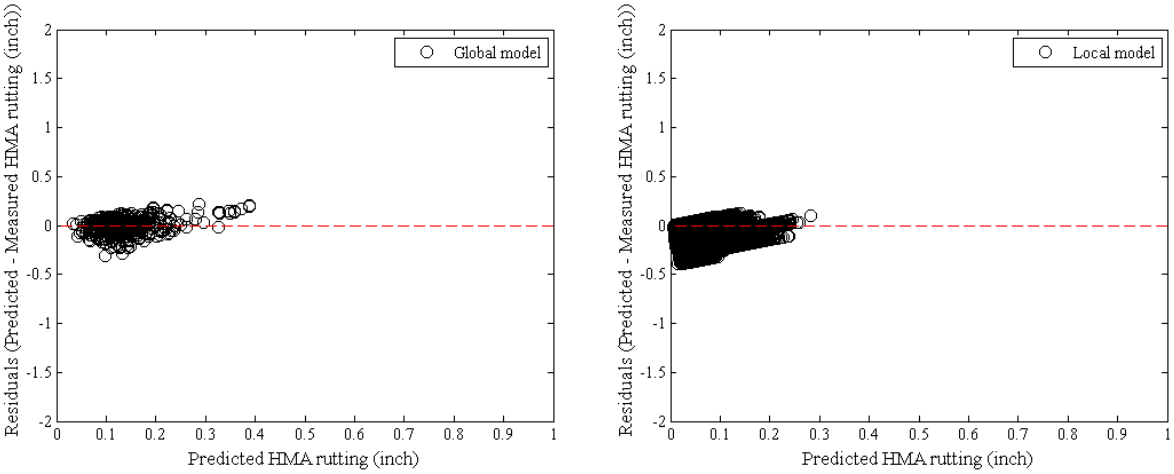

(a) Global model (b) Local model

Figure B-128 Option 1: Method 2 HMA rutting local calibration residual plots - repeated split sampling

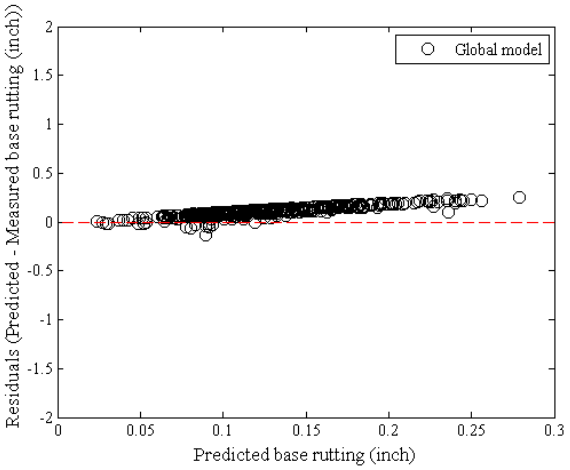

(a) Global model

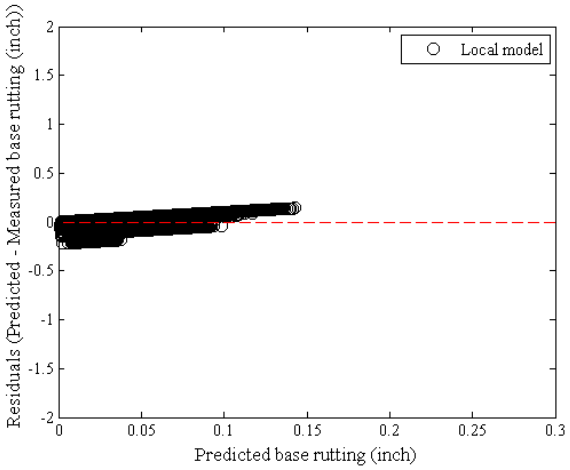

(b) Local model

Figure B-129 Option 1: Method 2 Base rutting local calibration residual plots - repeated split sampling

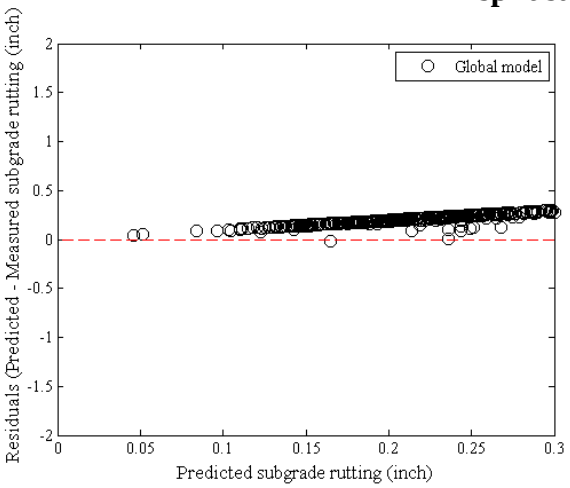

(a) Global model

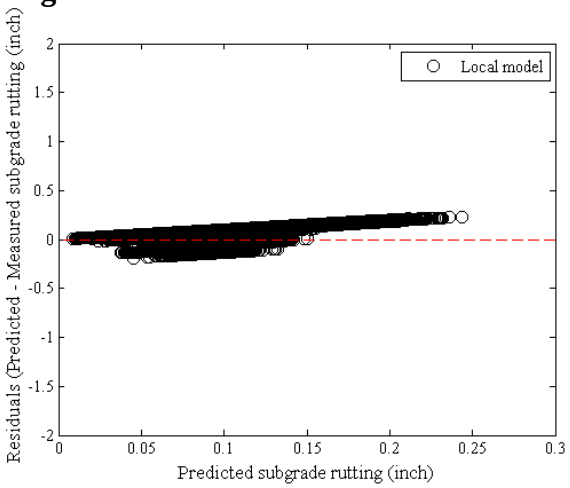

(b) Local model

Figure B-130 Option 1: Method 2 Subgrade rutting local calibration residual plots - repeated split sampling

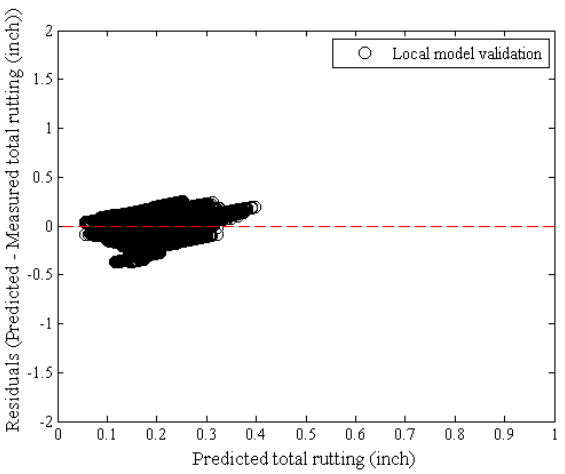

(a) Total rutting

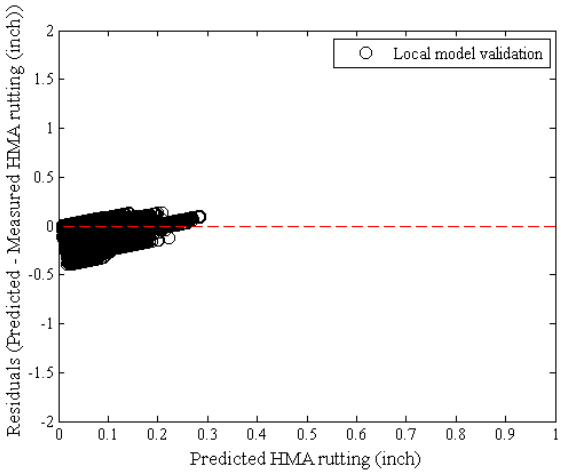

(b) HMA rutting

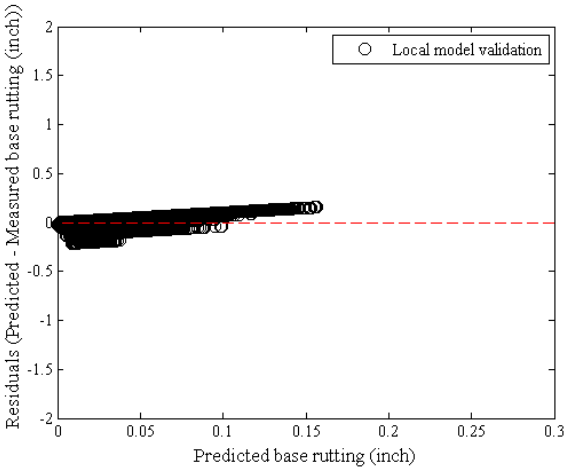

(c) Base rutting

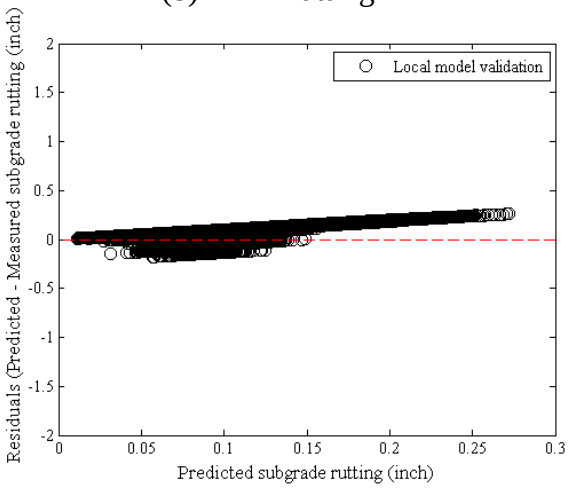

(d) Subgrade rutting

Figure B-131 Option 1: Method 2 Rutting model validation residual plots – repeated split sampling

Reliability

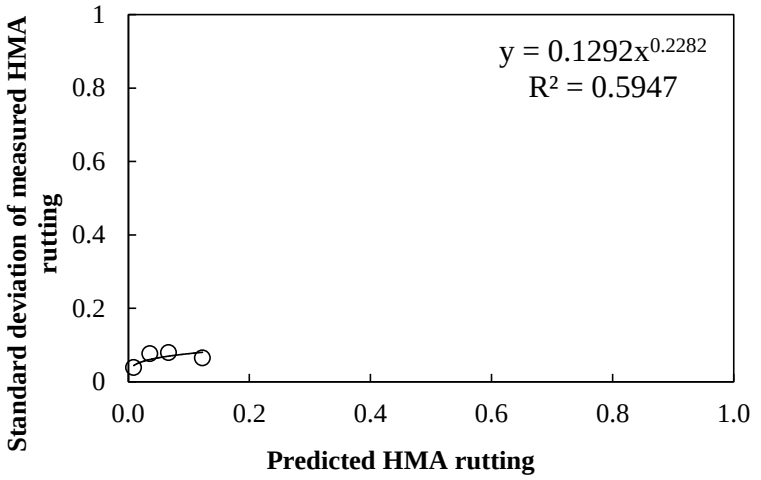

(a) HMA rutting reliability

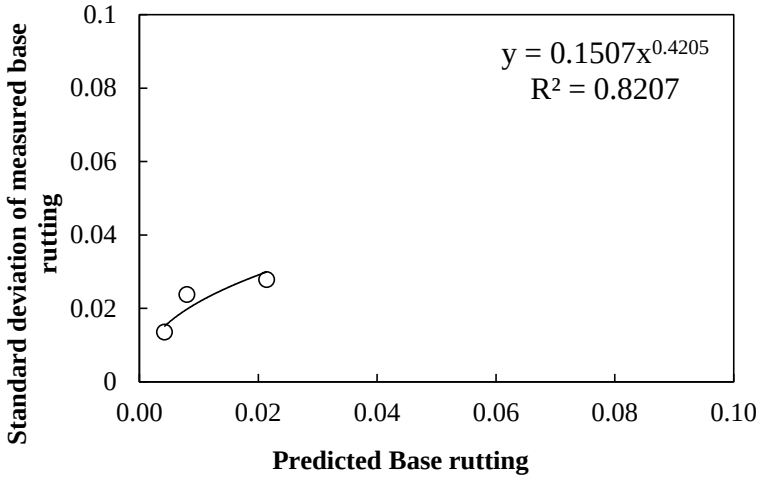

(b) Base rutting reliability

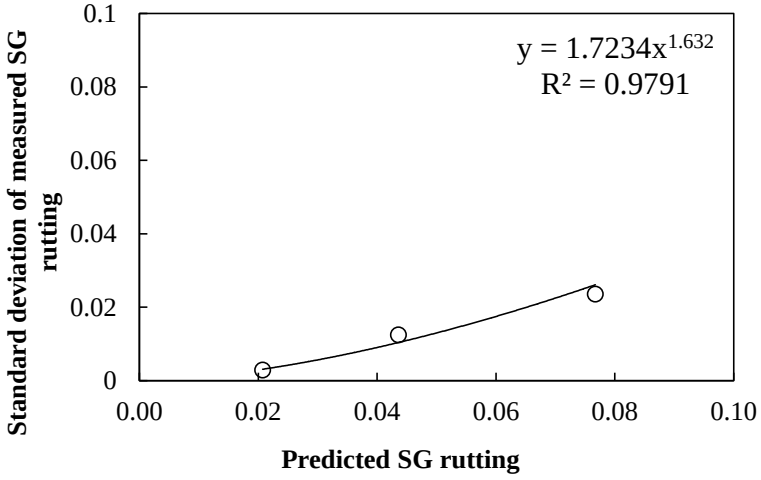

(c) Subgrade rutting reliability

Figure B-132 Rutting model reliability equations – option 1 method 2 – repeated split sampling

Bootstrapping

Table B-73 Option 1: Method 2 – Global model SEE and bias – bootstrapping

Calibration set	Average SEE	SEE Lower CI	SEE Upper CI	Average bias (in.)	Bias Lower CI	Bias Upper CI
AC rutting	0.0783	0.0706	0.0870	-0.0035	-0.0148	0.0076
Base rutting	0.1265	0.1146	0.1397	0.1110	0.1008	0.1217
Subgrade rutting	0.2242	0.2130	0.2365	0.2143	0.2040	0.2258
Total rutting	0.3431	0.3211	0.3651	0.3218	0.3029	0.3414

Table B-74 Option 1: Method 2 – Local model SEE and bias – bootstrapping

Calibration set	AC rutting	Base rutting	Subgrade rutting	Total rutting
Average SEE	0.1151	0.0314	0.0828	0.0804
SEE Lower CI	0.0853	0.0218	0.0484	0.0723
SEE Upper CI	0.1442	0.0457	0.1151	0.0890
Average bias (in.)	-0.0866	0.0098	0.0762	-0.0007
Bias Lower CI	-0.1206	-0.0112	0.0414	-0.0031
Bias Upper CI	-0.0458	0.0337	0.1085	0.0015
Average calibration coefficient	0.3932	0.2216	0.3833	N/A
Calibration coefficient Lower CI	0.1510	0.0654	0.2218	N/A
Calibration coefficient Upper CI	0.7001	0.4041	0.5354	N/A

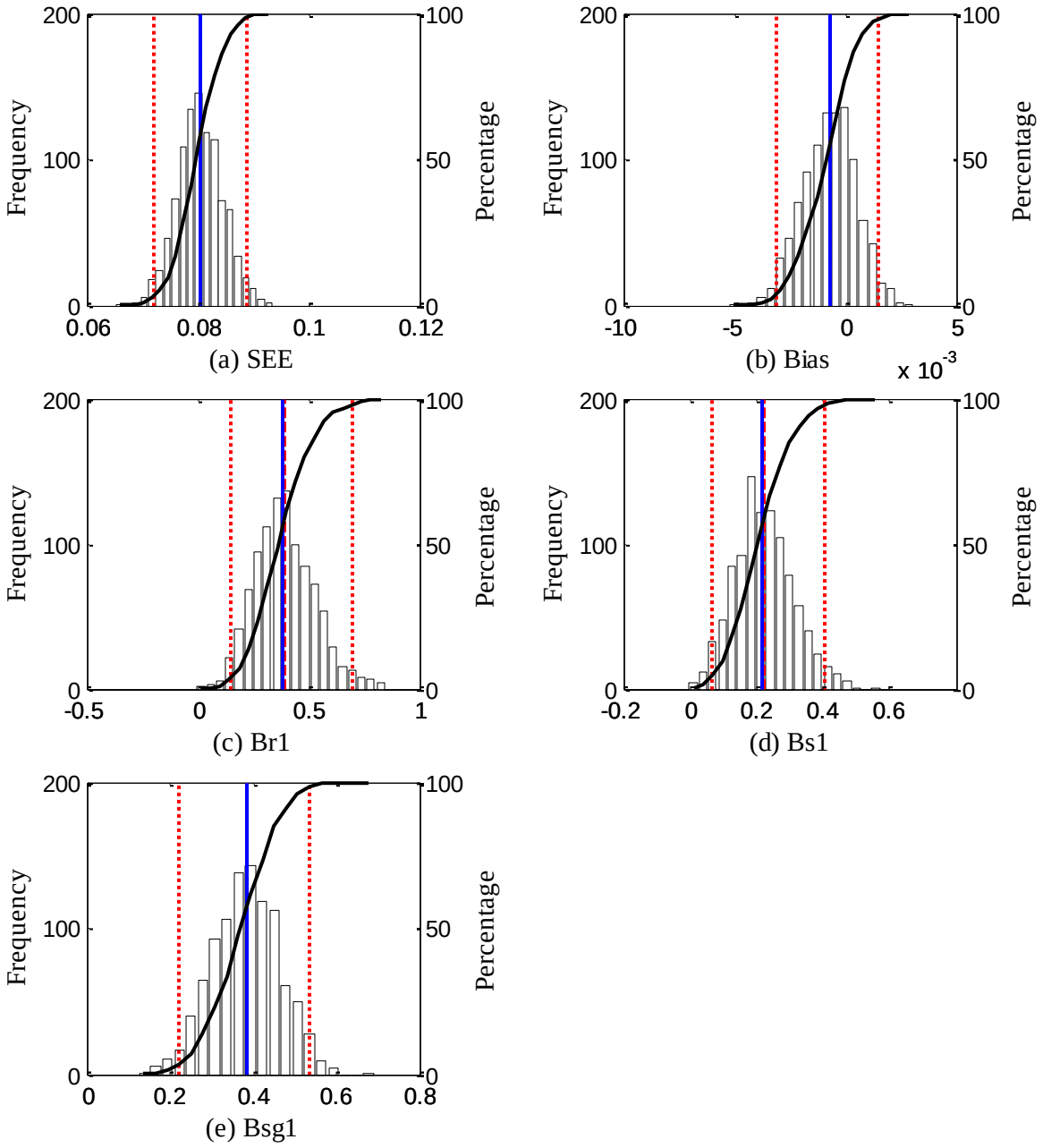

Figure B-133 Option 1: Method 2 bootstrapping total rutting frequency distributions – calibration

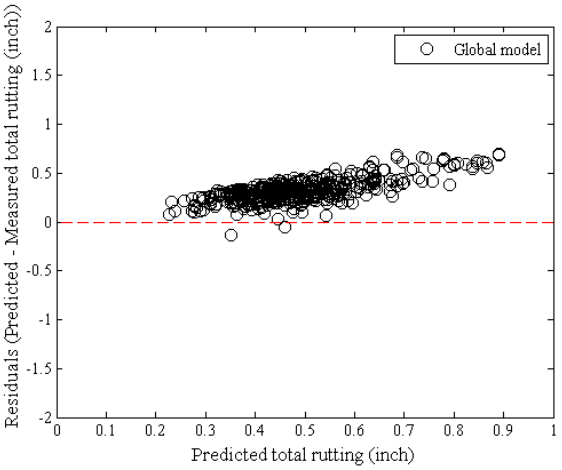

(a) Global model

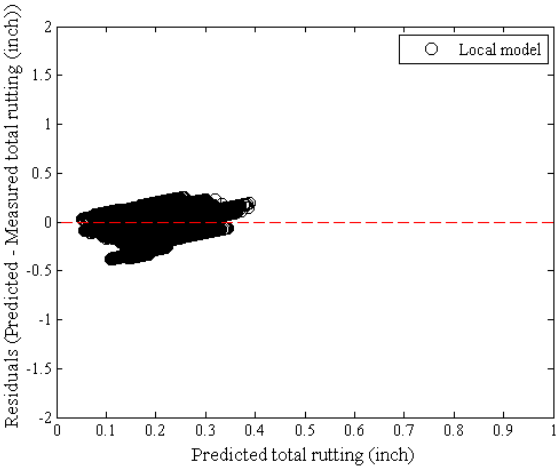

(b) Local model

Figure B-134 Option 1: Method 2 Total rutting local calibration residual plots - bootstrapping

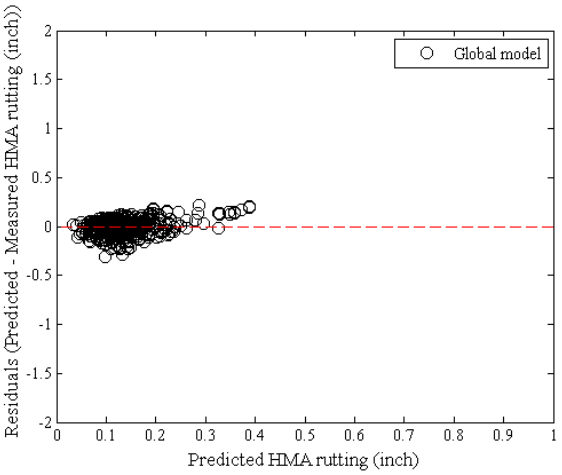

(a) Global model

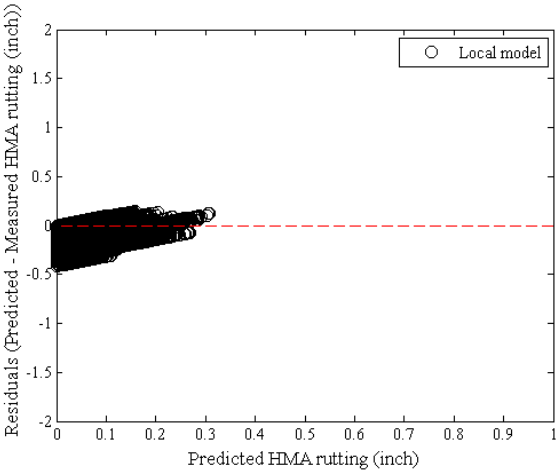

(b) Local model

Figure B-135 Option 1: Method 2 HMA rutting local calibration residual plots - bootstrapping

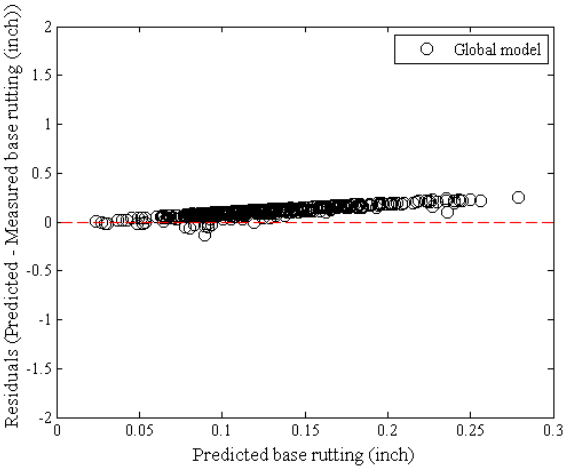

(a) Global model

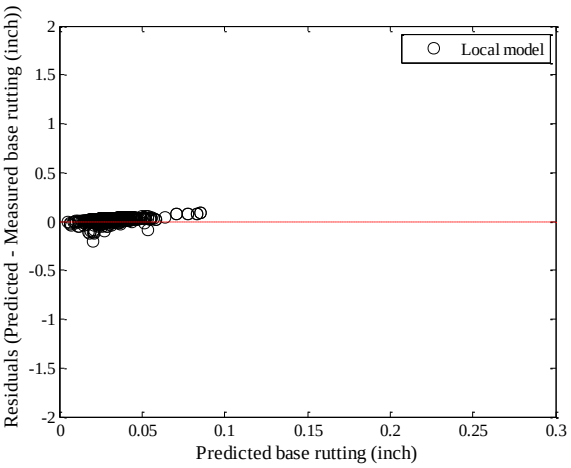

(b) Local model

Figure B-136 Option 1: Method 2 Base rutting local calibration residual plots - bootstrapping

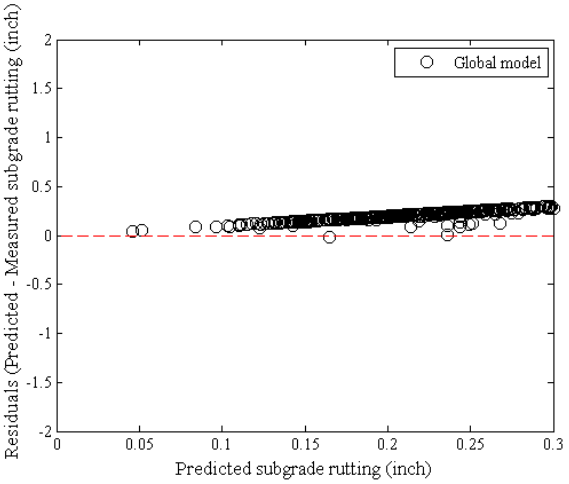

(a) Global model

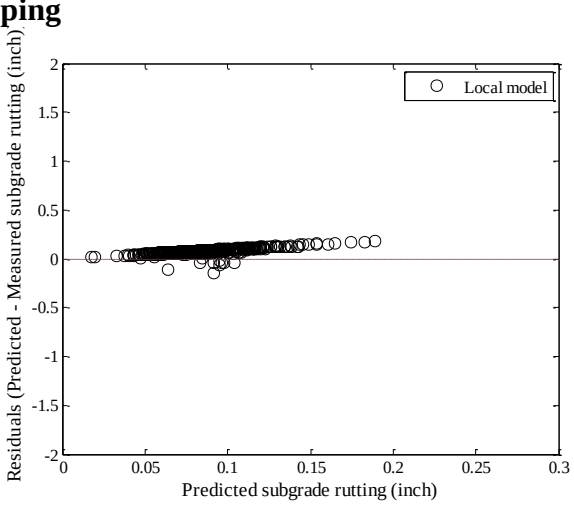

(b) Local model

Figure B-137 Option 1: Method 2 Subgrade rutting local calibration residual plots - bootstrapping

Reliability

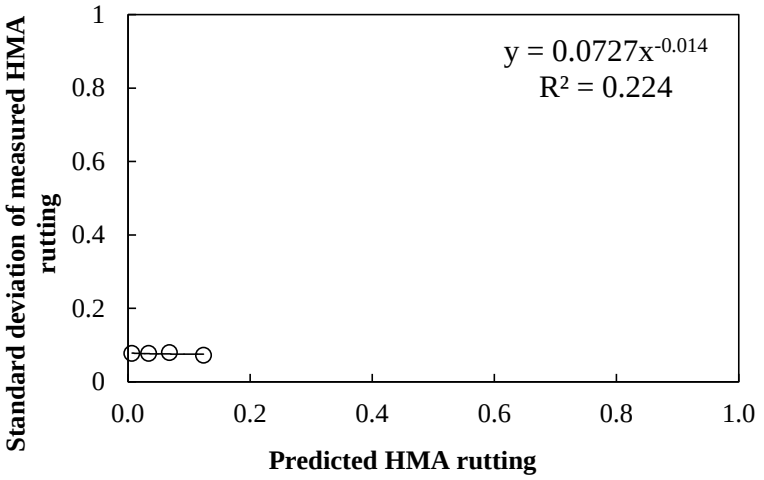

(a) HMA rutting reliability

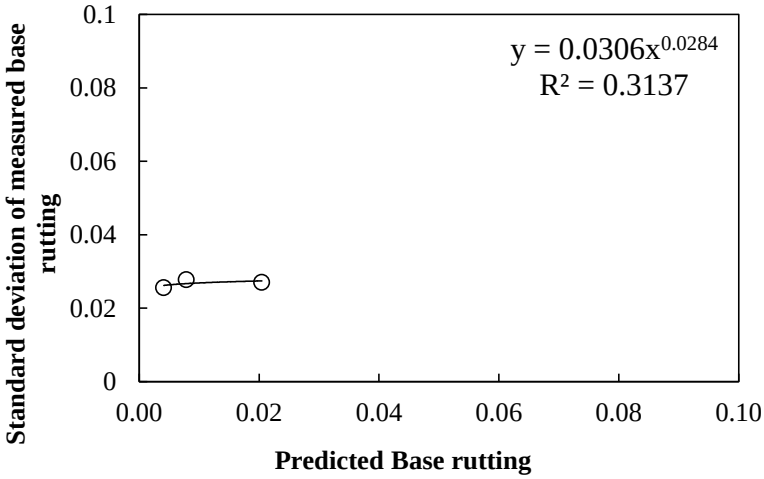

(b) Base rutting reliability

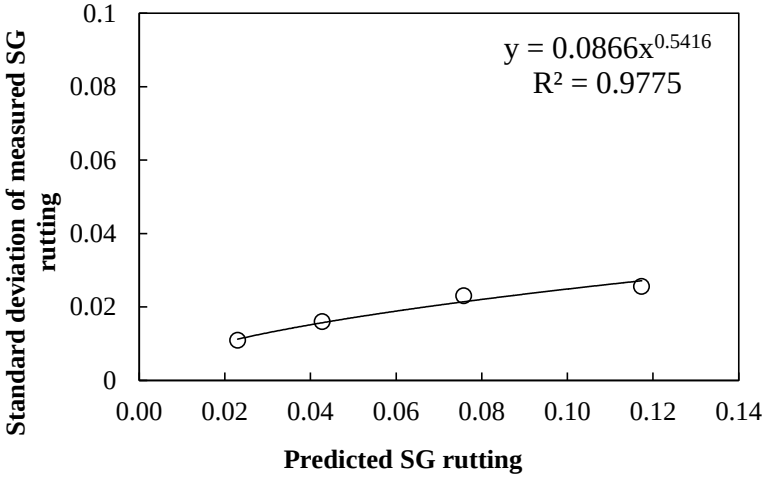

(c) Subgrade rutting reliability

Figure B-138 Rutting model reliability equations – option 1 method 2 – bootstrapping

B.1.3.3 Option 2 – Method 1

No sampling

Table B-75 Option 2: Method 1 – Global model goodness of fit – no sampling

HMA layer	SEE (in.)	Bias (in.)
AC rut	0.0779	-0.0019
Base rut	0.1405	0.1160
Subgrade	0.2235	0.2100
Total rut	0.3574	0.3241

Table B-76 Option 2: Method 1 – Global model *p*-values

HMA layer	t-test p-value	Intercept p-value	Slope = 1 p-value
AC rut	0.5505	0.0000	0.0000
Base rut	0.0000	0.0000	0.0000
Subgrade	0.0000	0.0000	0.0000
Total rut	0.0000	0.0000	0.0000

Table B-77 Option 2: Method 1 – Local model goodness of fit– no sampling

HMA layer	SEE	Bias
AC rut	0.0774	-0.0099
Base rut	0.0258	-0.0051
Subgrade	0.0205	-0.0006
Total rut	0.0865	-0.0155

Table B-78 Option 2: Method 1 – Local model *p*-values– no sampling

HMA layer	t-test p-value	Intercept p-value	Slope = 1 p-value
AC rut	0.0021	0.0000	0.0000
Base rut	0.0000	0.0000	0.0000
Subgrade	0.5188	0.0000	0.0000
Total rut	0.0000	0.0000	0.0000

Table B-79 Option 2: Method 1 – Local model *p*-values– no sampling

Calibration Coefficient	Global model	Local model
HMA rutting (br1)	1.0000	0.9422
Base rutting (bs1)	1.0000	0.0974
Subgrade rutting (bsg1)	1.0000	0.0367

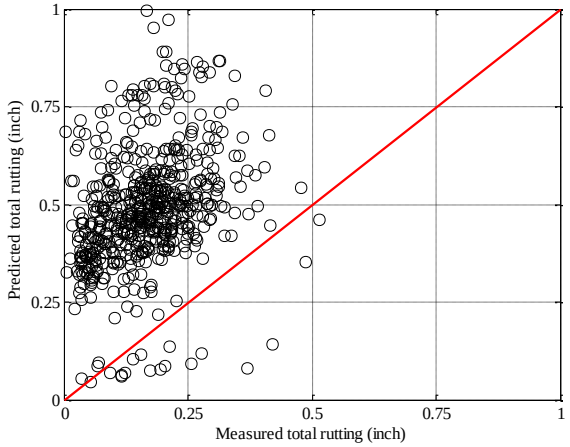

(a) Global model

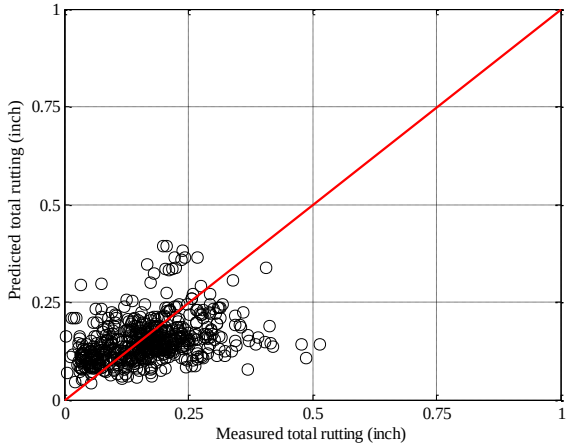

(b) Local model

Figure B-139 Option 2: Method 1 – Total rutting local calibration results - no sampling

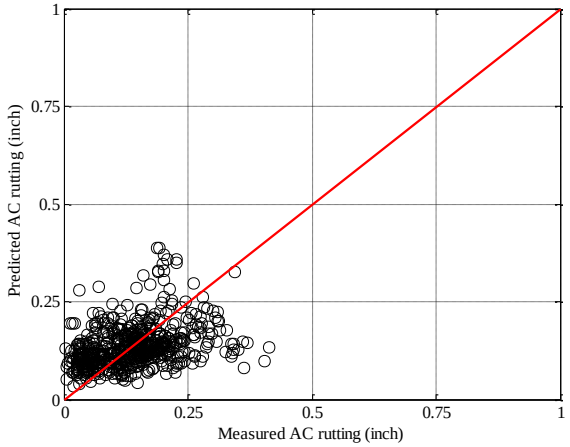

(a) Global model

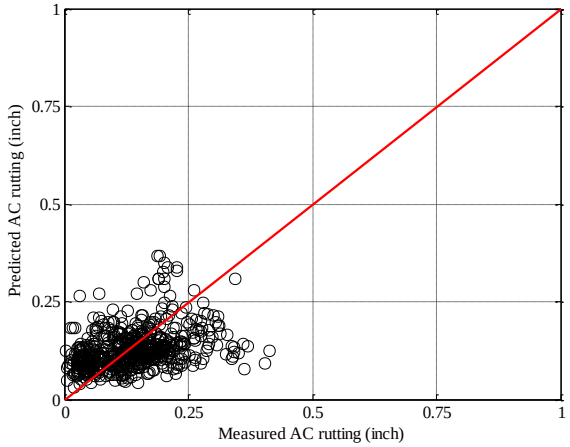

(b) Local model

Figure B-140 Option 2: Method 1 – HMA rutting local calibration results - no sampling

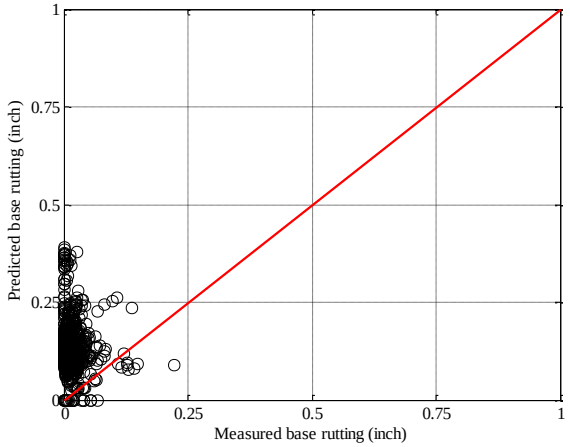

(a) Global model

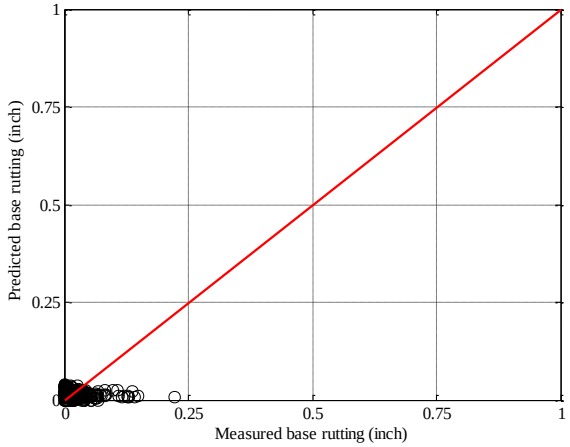

(b) Local model

Figure B-141 Option 2: Method 1 – Base rutting local calibration results - no sampling

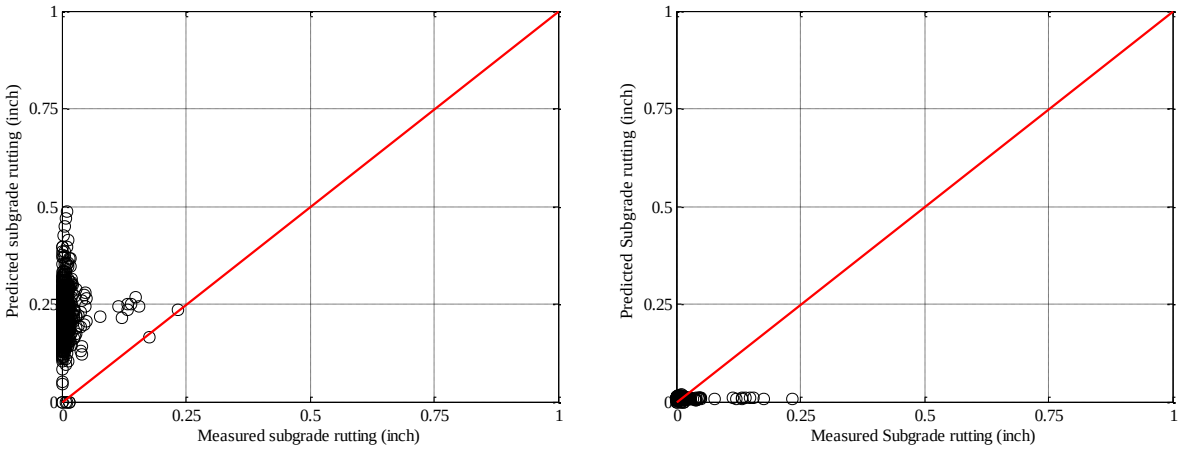

(a) Global model (b) Local model

Figure B-142 Option 2: Method 1 – Subgrade rutting local calibration results - no sampling

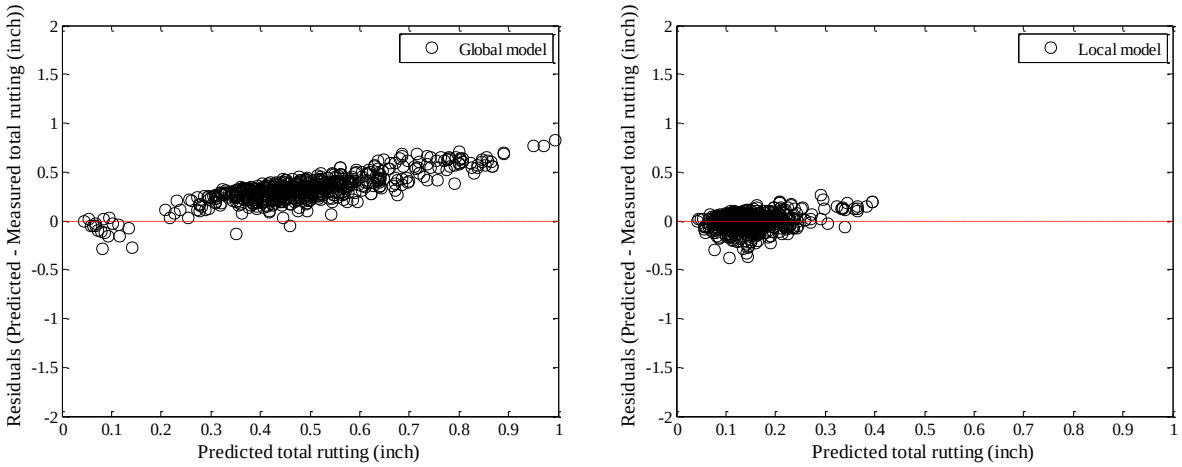

(a) Global model (b) Local model

Figure B-143 Option 2: Method 1 – Total rutting residual plots - no sampling

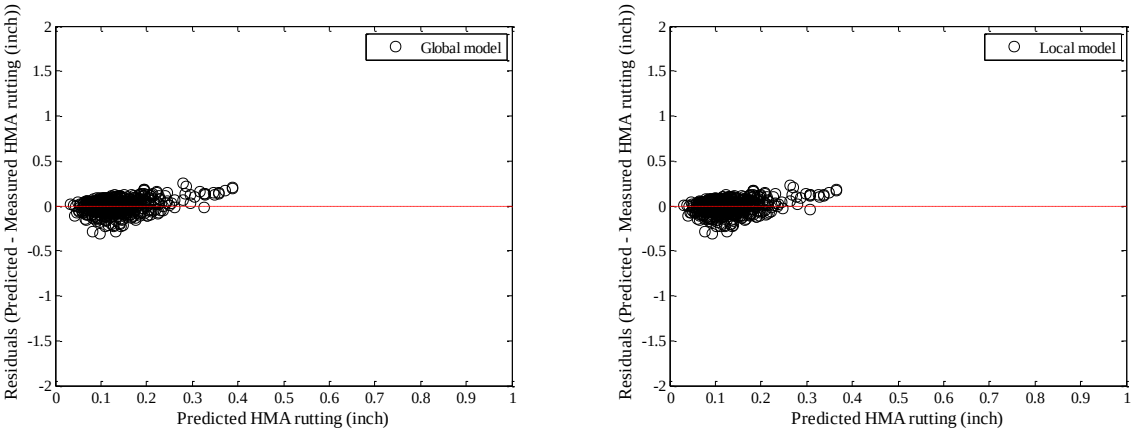

(a) Global model (b) Local model

Figure B-144 Option 2: Method 1 – HMA rutting residual plots - no sampling

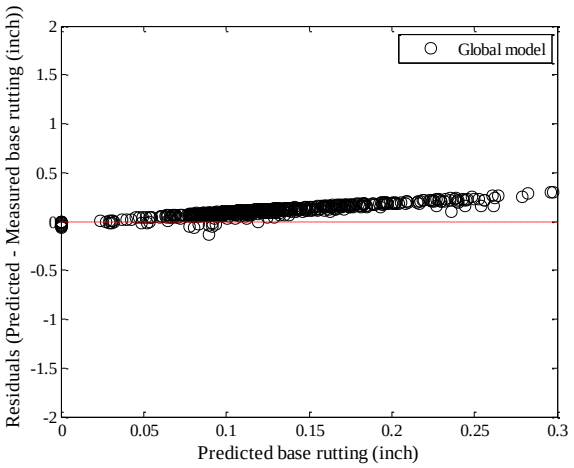

(a) Global model

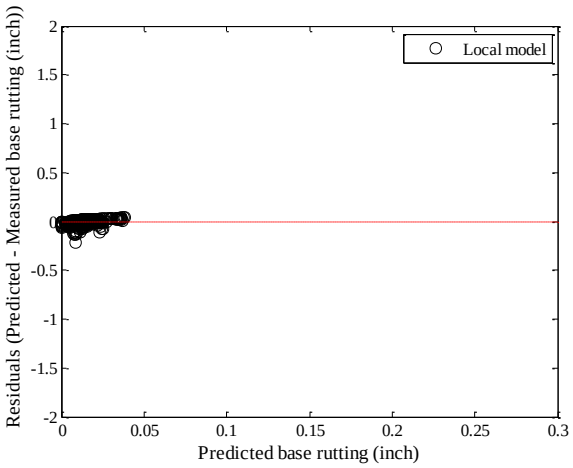

(b) Local model

Figure B-145 Option 2: Method 1 – Base rutting residual plots - no sampling

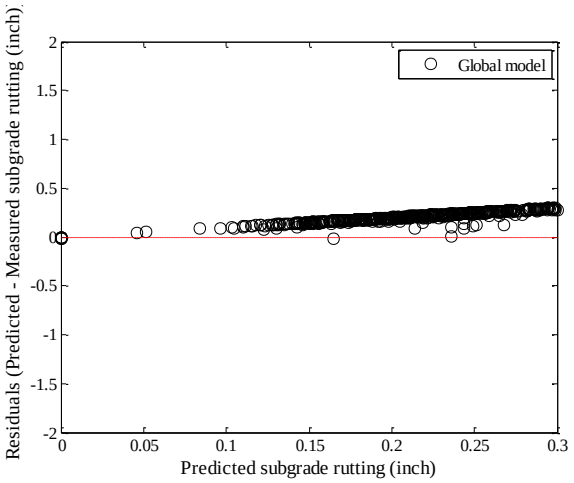

(a) Global model

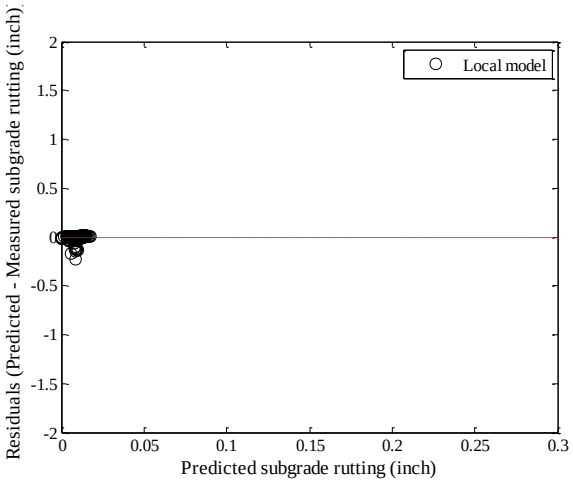

(b) Local model

Figure B-146 Option 2: Method 1 – Subgrade rutting residual plots ts - no sampling

Reliability

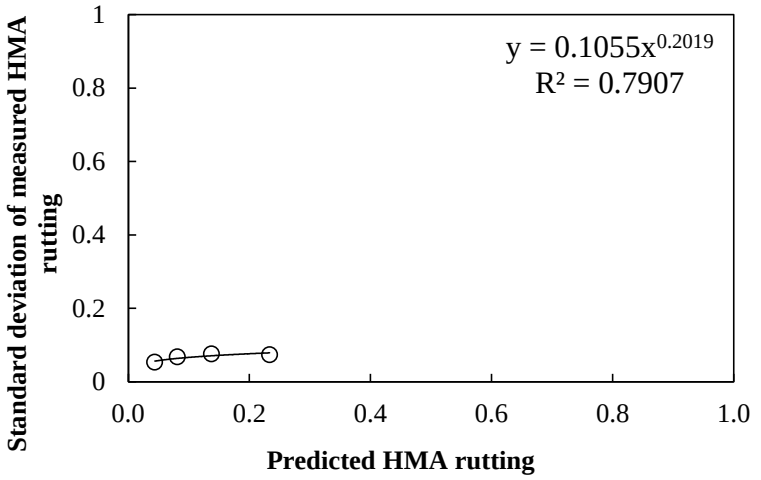

(a) HMA rutting reliability

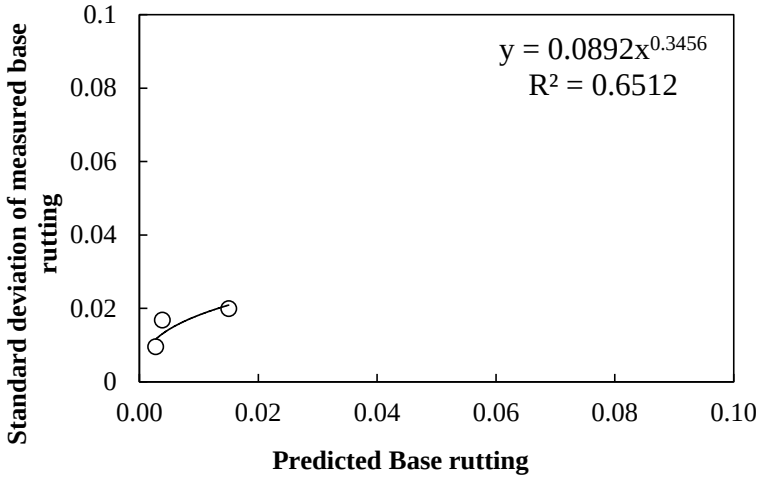

(b) Base rutting reliability

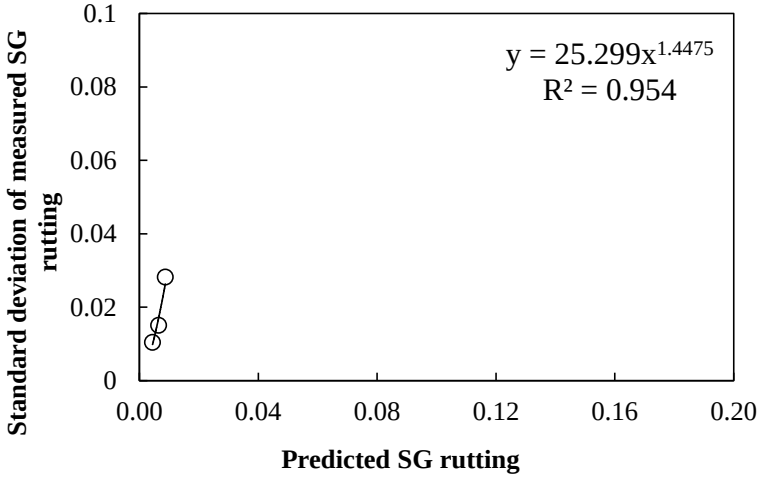

(c) Subgrade rutting reliability

Figure B-147 Rutting model reliability equations – option 2 method 1 – no sampling

Split sampling

Table B-80 Option 2: Method 1 – Global model goodness of fit – split sampling

HMA layer	SEE (in.)	Bias (in.)
AC rut	0.0752	0.0002
Base rut	0.1391	0.1140
Subgrade	0.2275	0.2121
Total rut	0.3617	0.3264

Table B-81 Option 2: Method 1 – Global model *p*-values - split sampling

HMA layer	t-test p-value	Intercept p-value	Slope = 1 p-value
AC rut	0.9510	0.0000	0.0000
Base rut	0.0000	0.0000	0.0000
Subgrade	0.0000	0.0000	0.0003
Total rut	0.0000	0.0000	0.0000

Table B-82 Option 2: Method 1 – Local model goodness of fit– split sampling

HMA layer	SEE	Bias
AC rut	0.0746	-0.0086
Base rut	0.0277	-0.0049
Subgrade	0.0200	-0.0004
Total rut	0.0843	-0.0140

Table B-83 Option 2: Method 1 – Local model *p*-values– split sampling

HMA layer	t-test p-value	Intercept p-value	Slope = 1 p-value
AC rut	0.0207	0.0000	0.0000
Base rut	0.0003	0.0000	0.0000
Subgrade	0.6594	0.0000	0.0000
Total rut	0.0008	0.0000	0.0000

Table B-84 Option 2: Method 1 – Local model *p*-values – split sampling

Calibration Coefficient	Global model	Local model
HMA rutting (br1)	1.0000	0.9372
Base rutting (bs1)	1.0000	0.1014
Subgrade rutting (bsg1)	1.0000	0.0348

Table B-85 Option 2: Method 1 – Local model validation p-values – split sampling

HMA layer	t-test p-value	Intercept p-value	Slope = 1 p-value
AC rut	0.0166	0.0000	0.0000
Base rut	0.0200	0.0000	0.0000
Subgrade	0.1916	0.0000	0.0000
Total rut	0.0024	0.0000	0.0000

Table B-86 Option 2: Method 1 – Local model validation SEE and bias – split sampling

HMA layer	SEE	Bias
AC rut	0.0842	-0.0151
Base rut	0.0208	-0.0036
Subgrade	0.0219	-0.0021
Total rut	0.0921	-0.0209

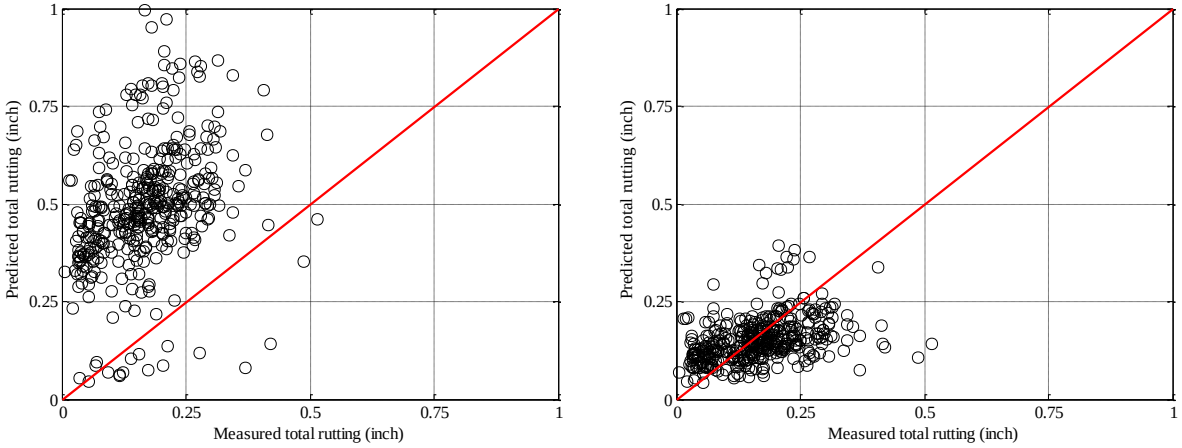

(a) Global model (b) Local model

Figure B-148 Option 2 Method 1 Total rutting local calibration results - split sampling

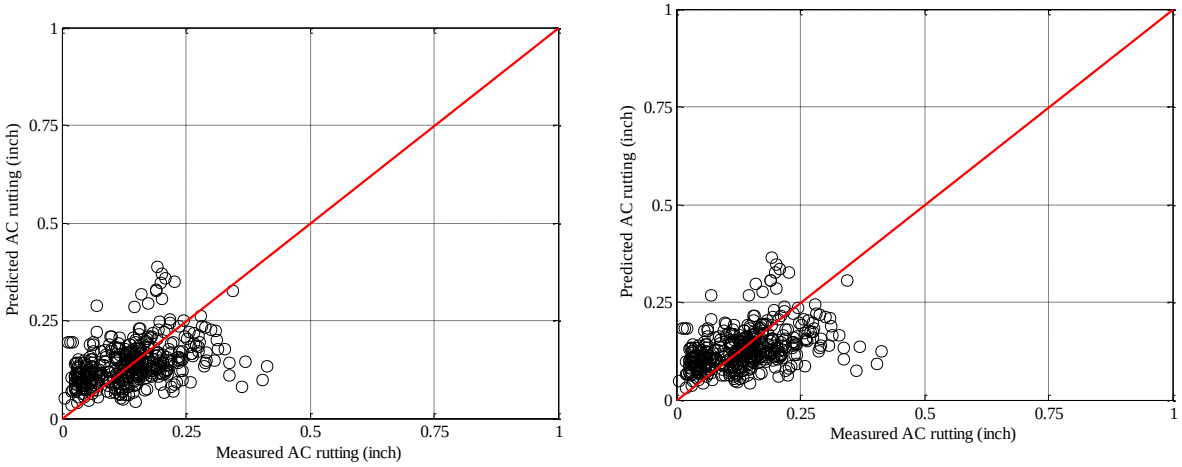

(a) Global model

(b) Local model

Figure B-149 Option 2: Method 1 HMA rutting local calibration results - split sampling

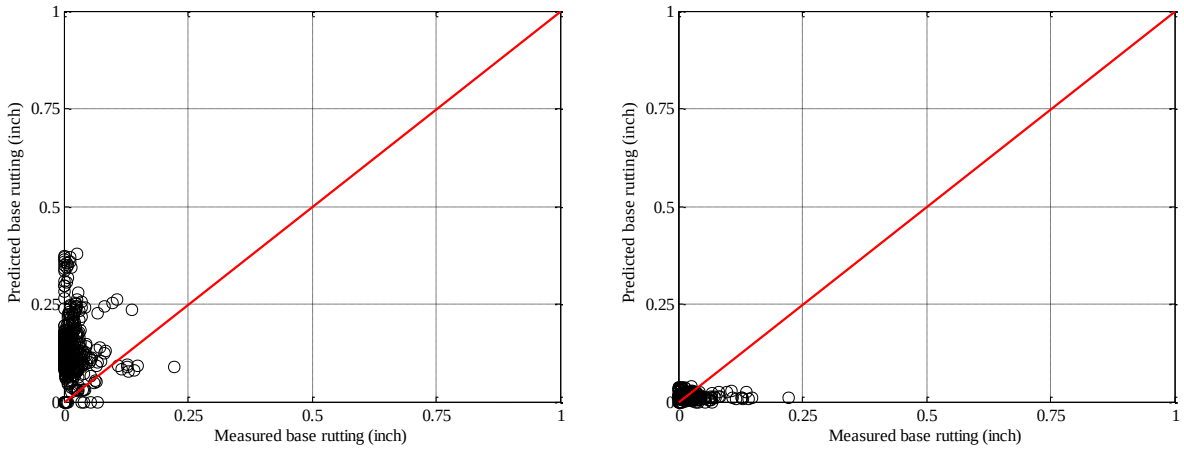

(a) Global model (b) Local model

Figure B-150 Option 2: Method 1 Base rutting local calibration results - split sampling

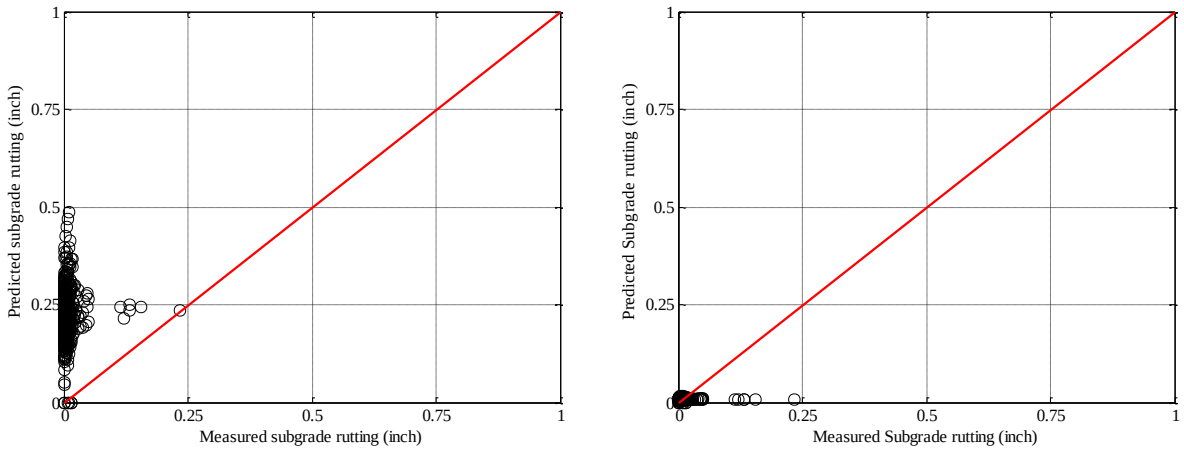

(a) Global model (b) Local model

Figure B-151 Option 2 Method 1 Subgrade rutting local calibration results - split sampling

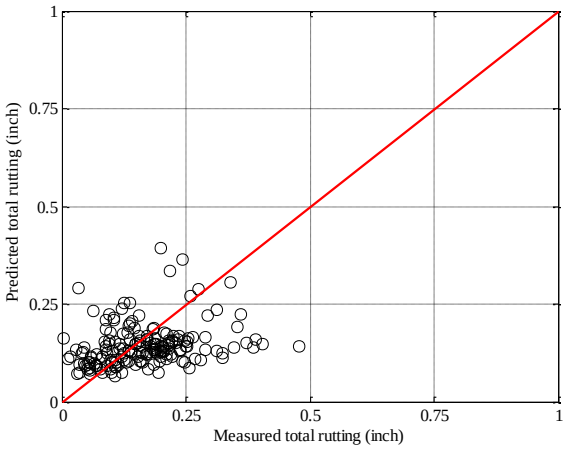

(a) Total rutting

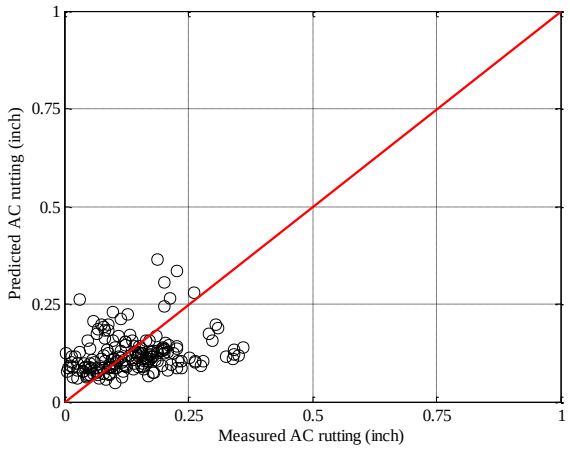

(b) HMA rutting

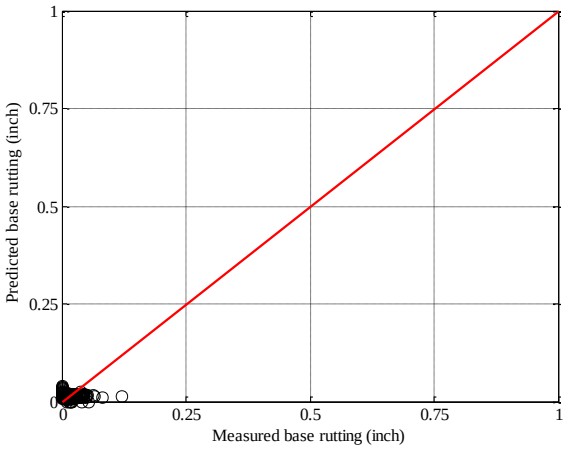

(c) Base rutting

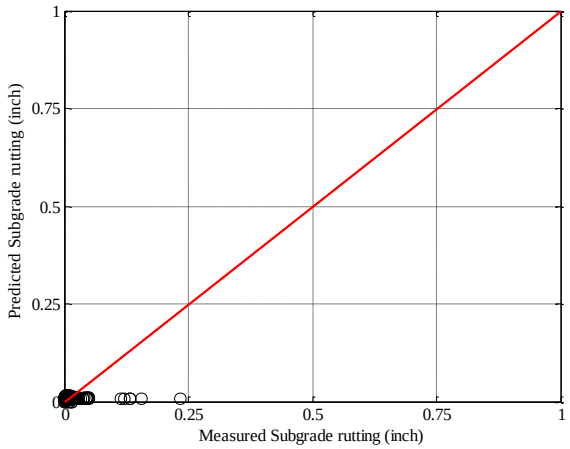

(d) Subgrade rutting

Figure B-152 Option 2: Method 1 – Rutting model validation – split sampling

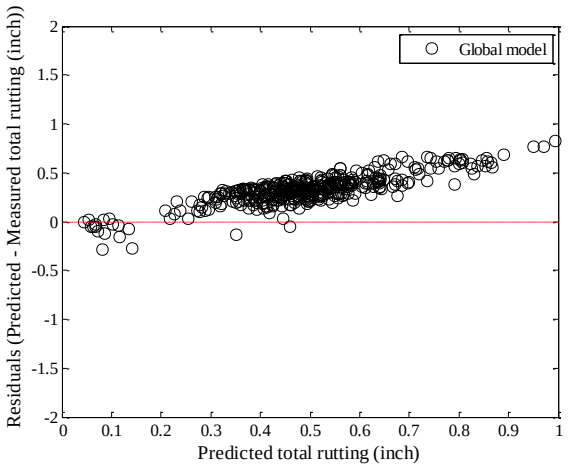

(a) Global model

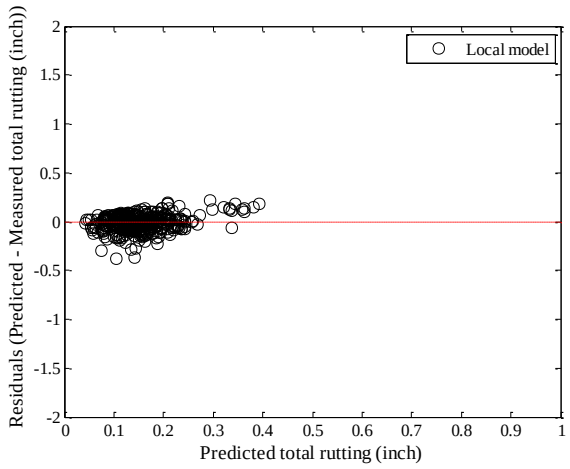

(b) Local model

Figure B-153 Option 2 Method 1 Total rutting residual plots - split sampling

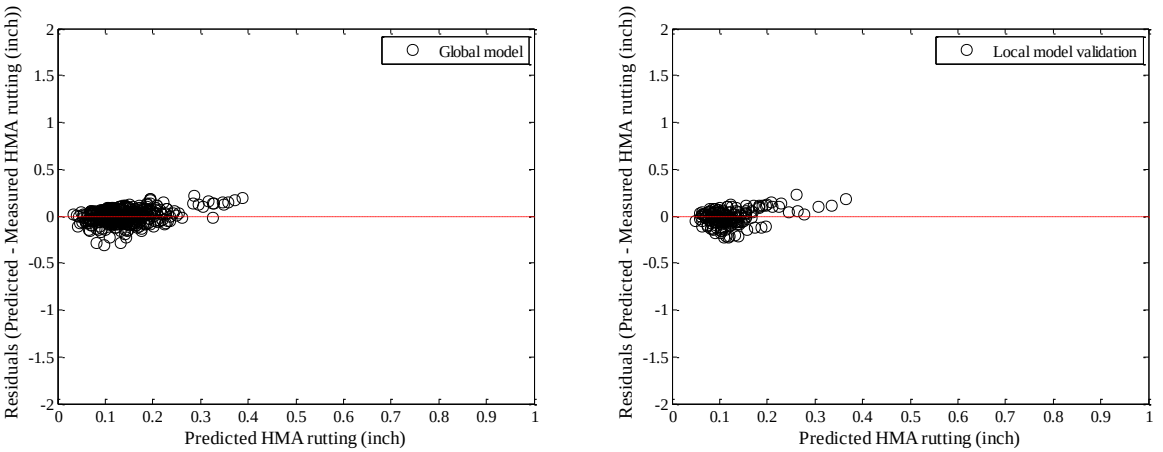

(a) Global model (b) Local model

Figure B-154 Option 2: Method 1 HMA rutting residual plots - split sampling

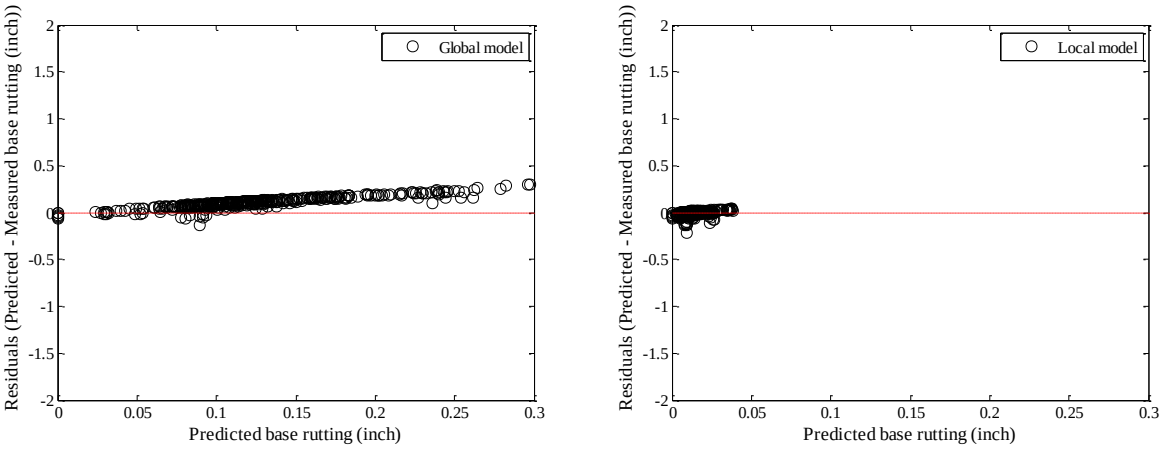

(a) Global model (b) Local model

Figure B-155 Option 2: Method 1 Base rutting residual plots - split sampling

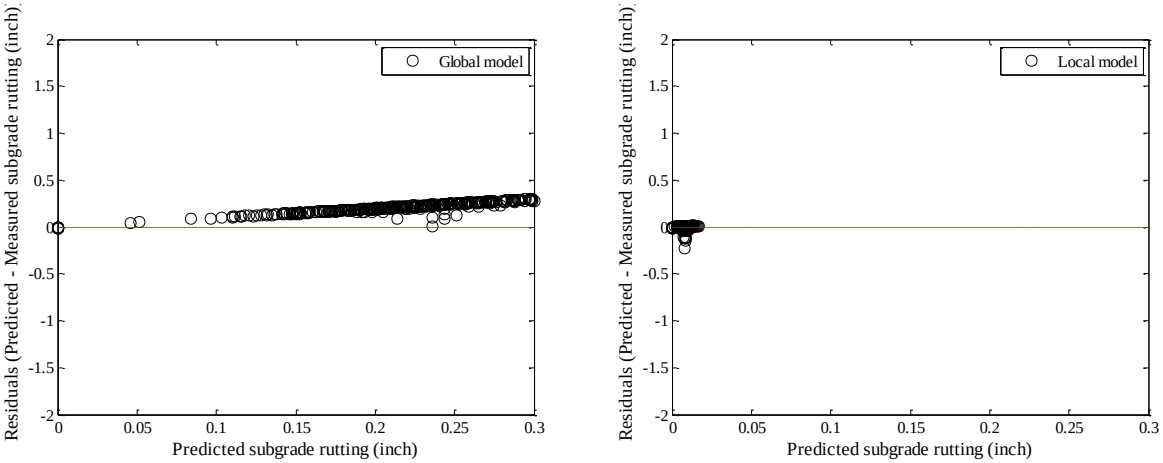

(a) Global model (b) Local model

Figure B-156 Option 2 Method 1 Subgrade rutting residual plots - split sampling

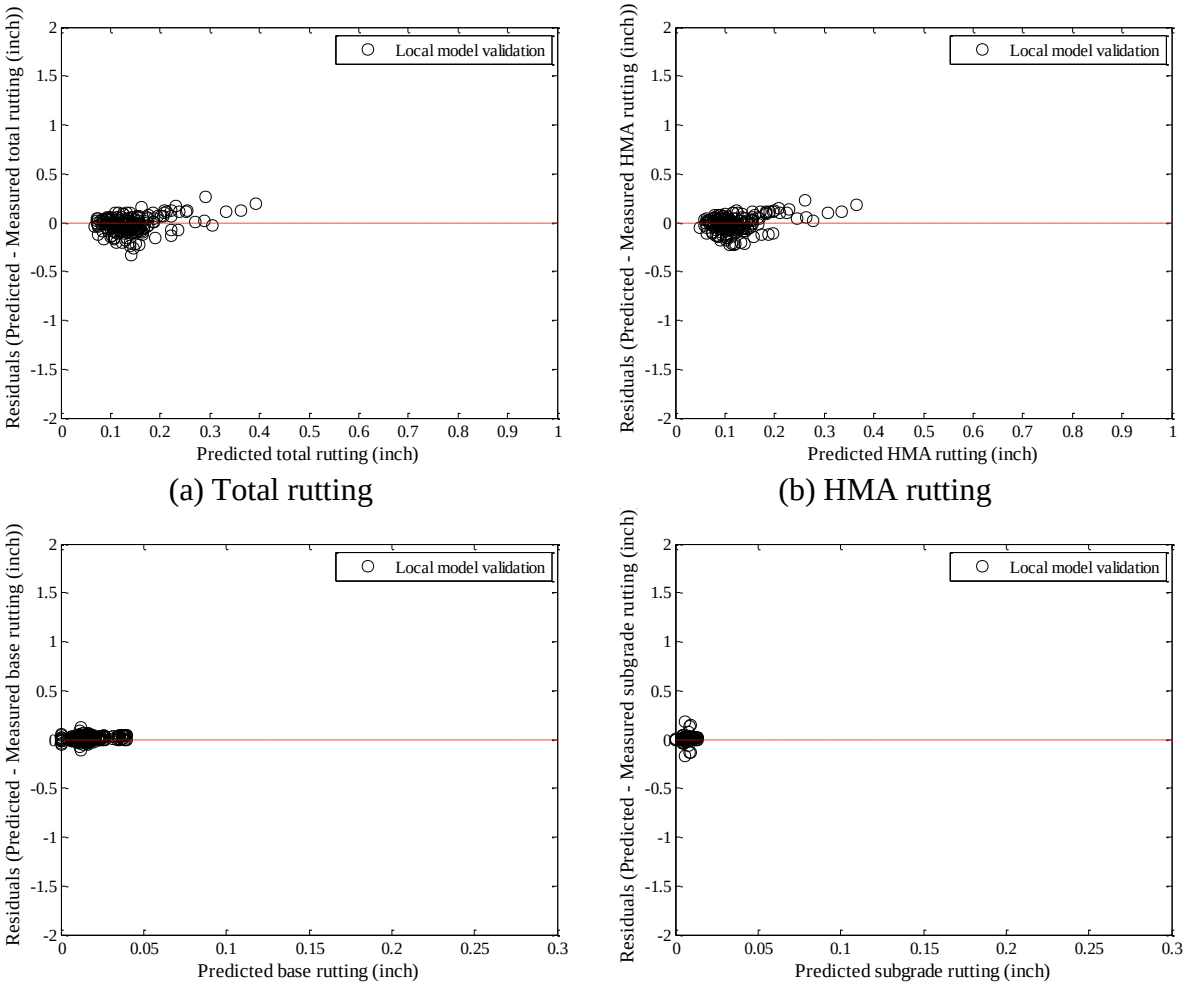

(a) Total rutting (b) HMA rutting

(c) Base rutting (d) Subgrade rutting

Figure B-157 Option 2: Method 1 – Rutting model validation residual plots – split sampling

Reliability

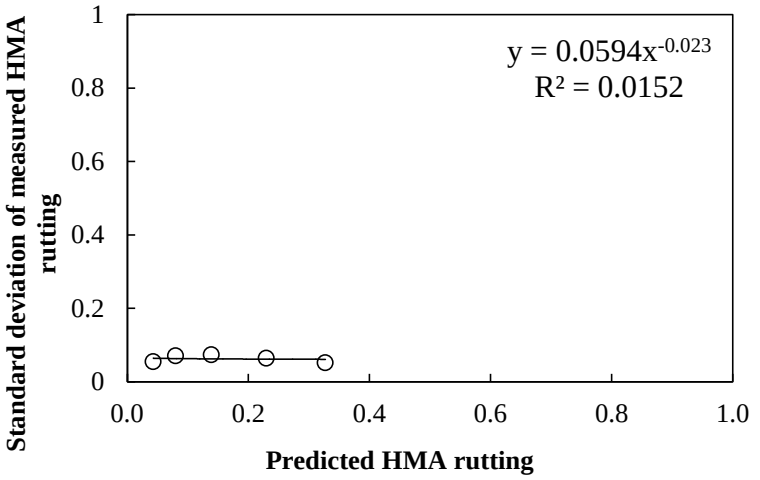

(a) HMA rutting reliability

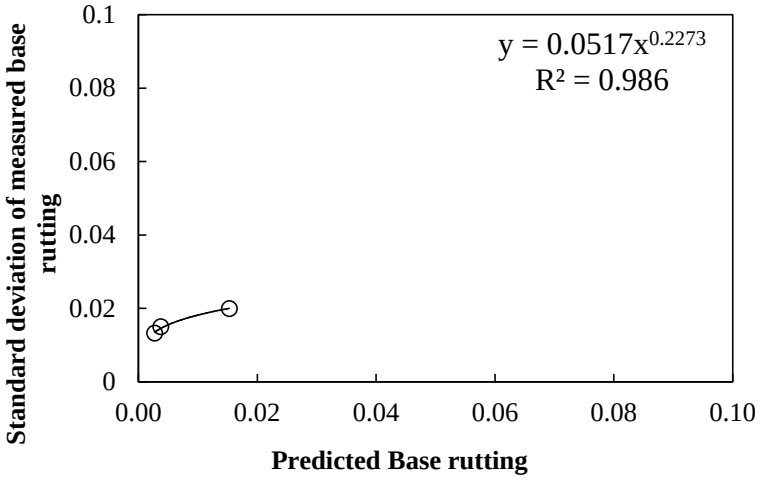

(b) Base rutting reliability

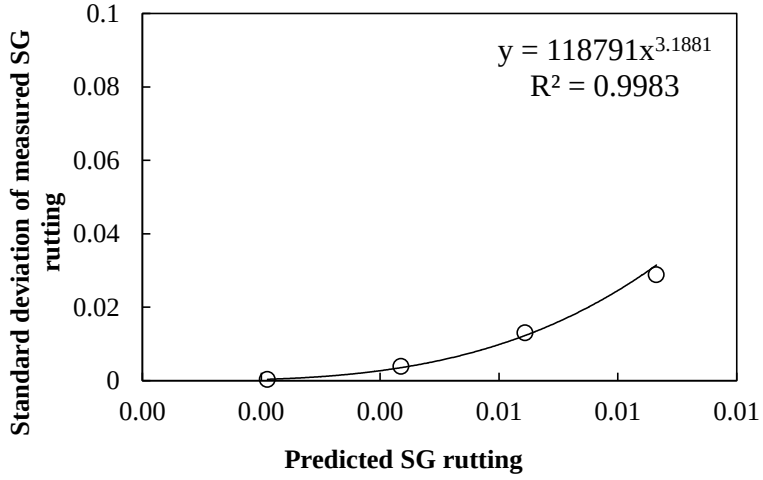

(c) Subgrade rutting reliability

Figure B-158 Rutting model reliability equations – option 2 method 1 – split sampling

Repeated split sampling

Table B-87 Option 2: Method 1 – Global model SEE and bias – repeated split sampling

Global Model	Average SEE	SEE Lower CI	SEE Upper CI	Average bias (in.)	Bias Lower CI	Bias Upper CI
AC rutting	0.0779	0.0726	0.0822	-0.0021	-0.0088	0.0046
Base rutting	0.1403	0.1297	0.1499	0.1158	0.1079	0.1243
Subgrade rutting	0.2237	0.2168	0.2303	0.2100	0.2027	0.2174
Total rutting	0.3572	0.3419	0.3713	0.3237	0.3096	0.3382

Table B-88 Option 2: Method 1 – Local model SEE and bias – repeated split sampling

Calibration set	AC rutting	Base rutting	Subgrade rutting	Total rutting
Average SEE	0.0773	0.0258	0.0205	0.0864
SEE Lower CI	0.0723	0.0206	0.0132	0.0800
SEE Upper CI	0.0816	0.0290	0.0242	0.0916
Average bias (in.)	-0.0097	-0.0051	-0.0006	-0.0153
Bias Lower CI	-0.0124	-0.0063	-0.0008	-0.0184
Bias Upper CI	-0.0063	-0.0037	-0.0003	-0.0117
Average calibration coefficient	0.9451	0.0982	0.0368	N/A
Calibration coefficient Lower CI	0.8935	0.0822	0.0286	N/A
Calibration coefficient Upper CI	1.0084	0.1159	0.0443	N/A

Table B-89 Option 2: Method 1 – Local model validation SEE and bias – repeated split sampling

Validation set	AC rutting	Base rutting	Subgrade rutting	Total rutting
Average SEE	0.0783	0.0254	0.0192	0.0872
SEE Lower CI	0.0676	0.0168	0.0082	0.0741
SEE Upper CI	0.0895	0.0352	0.0316	0.1007
Average bias (in.)	-0.0090	-0.0048	-0.0004	-0.0143
Bias Lower CI	-0.0301	-0.0123	-0.0065	-0.0367
Bias Upper CI	0.0135	0.0019	0.0049	0.0109
Average calibration coefficient	0.9451	0.0982	0.0368	N/A
Calibration coefficient Lower CI	0.8935	0.0822	0.0286	N/A
Calibration coefficient Upper CI	1.0084	0.1159	0.0443	N/A

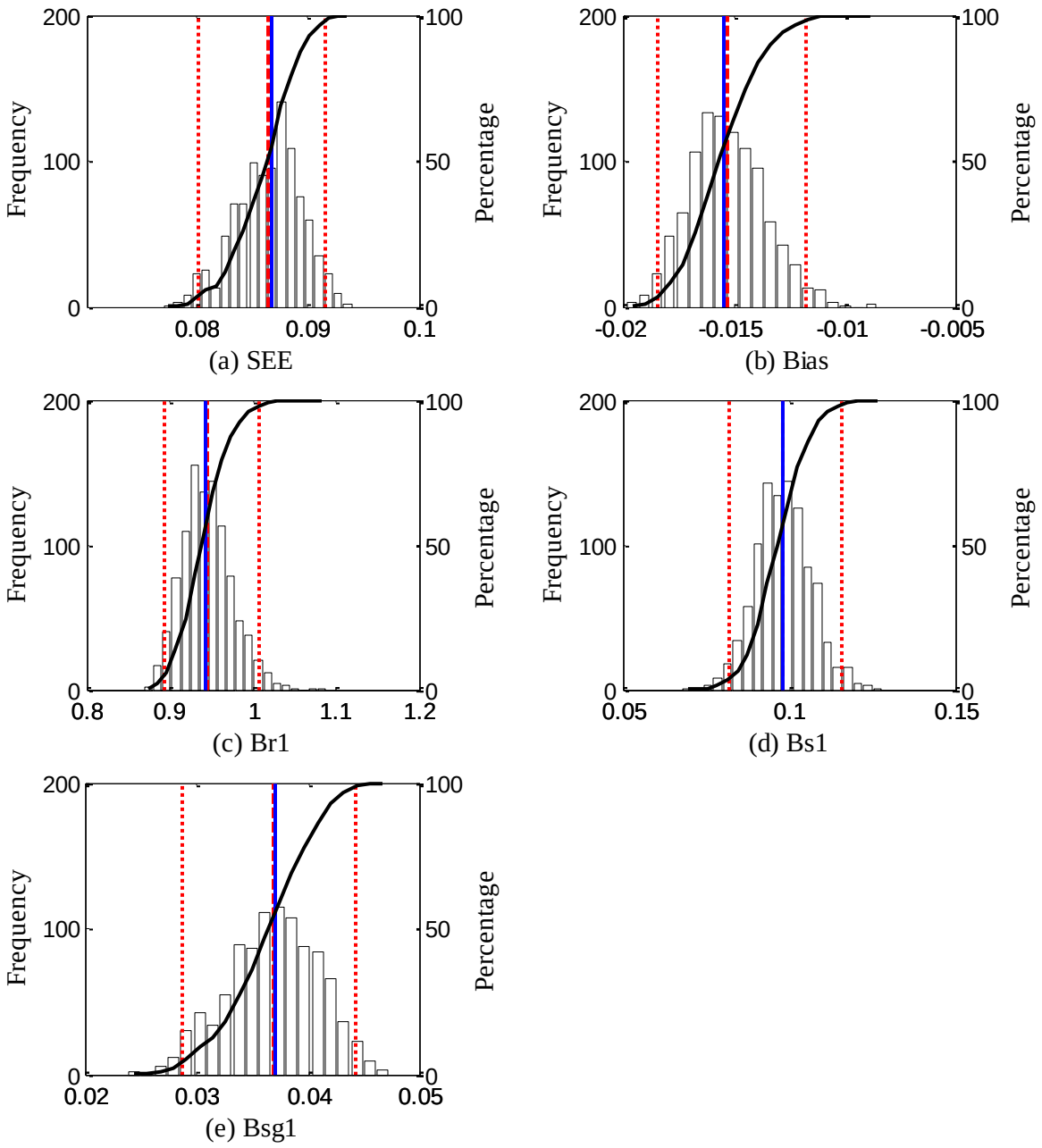

Figure B-159 Option 2: Method 1 – repeated split sampling total rutting frequency distributions – calibration

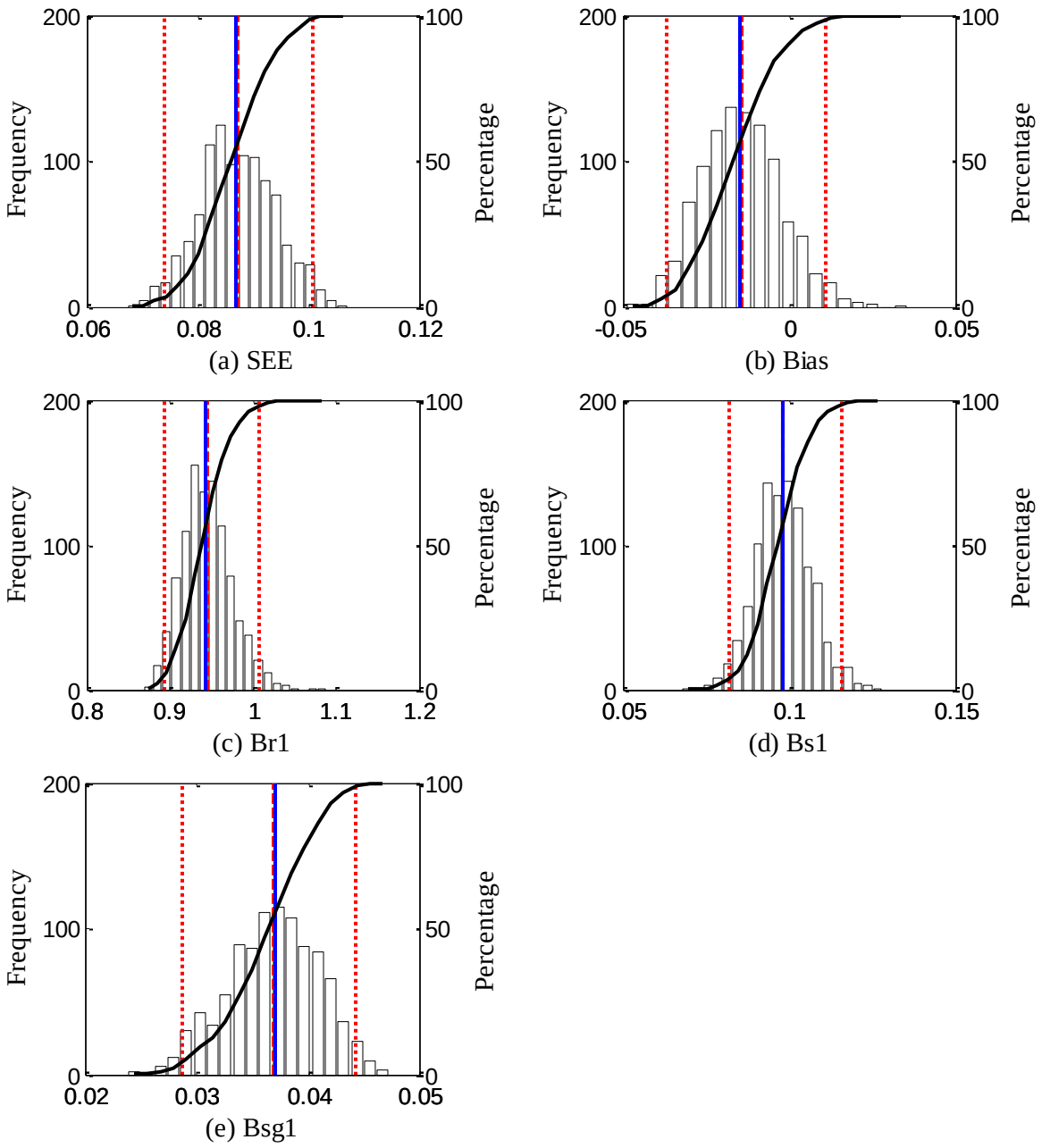

Figure B-160 Option 2: Method 1 – repeated split sampling total rutting frequency distributions – validation

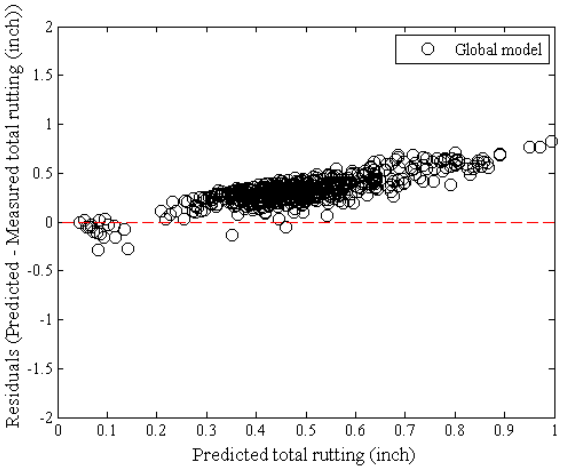

(a) Global model

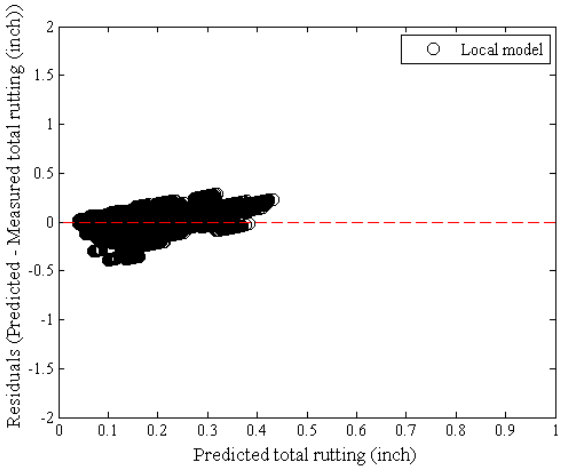

(b) Local model

Figure B-161 Option 2 Method 1 Total rutting residual plots - repeated split sampling

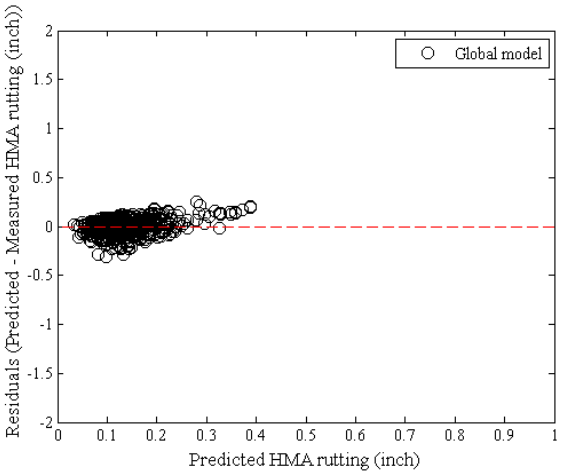

(a) Global model

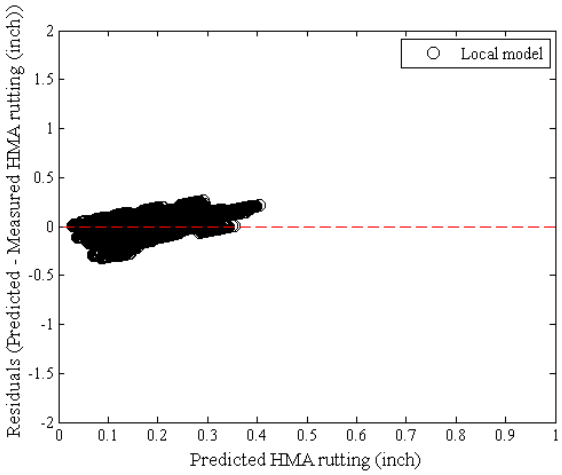

(b) Local model

Figure B-162 Option 2: Method 1 HMA rutting residual plots - repeated split sampling

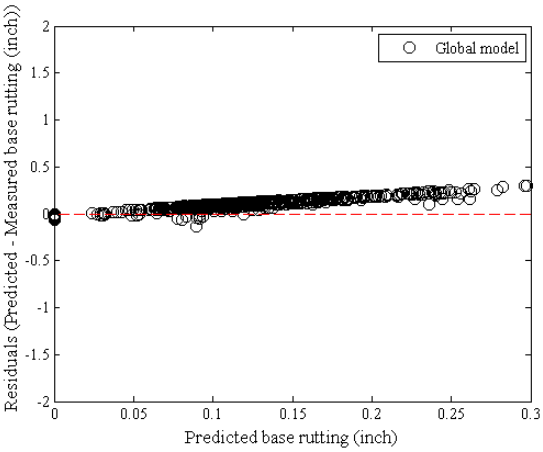

(a) Global model

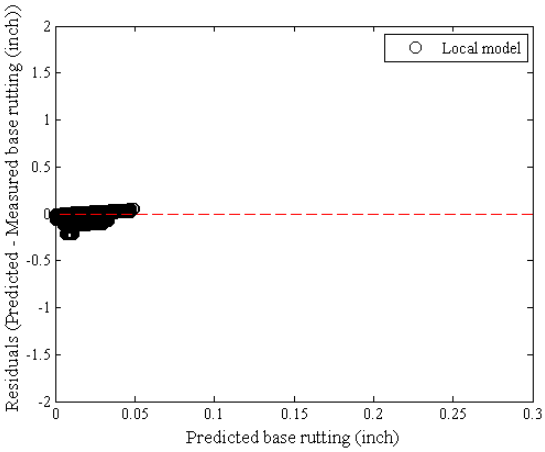

(b) Local model

Figure B-163 Option 2: Method 1 Base rutting residual plots - repeated split sampling

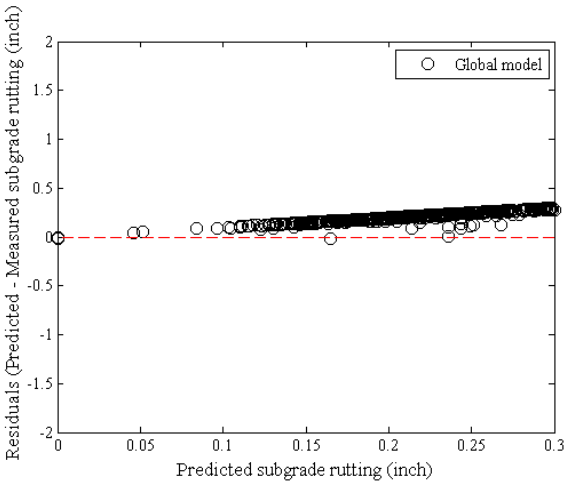

(a) Global model

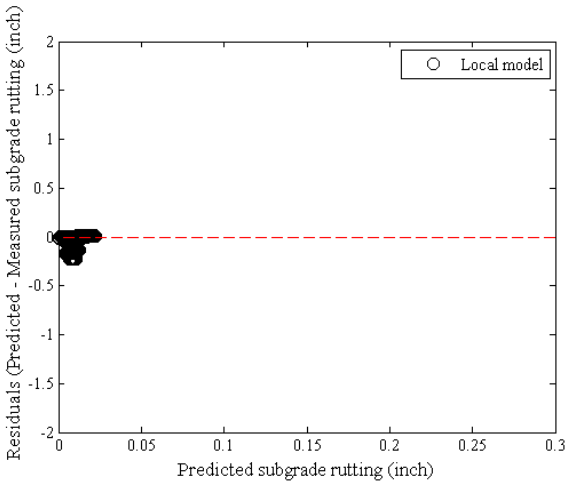

(b) Local model

Figure B-164 Option 2 Method 1 Subgrade rutting residual plots - repeated split sampling

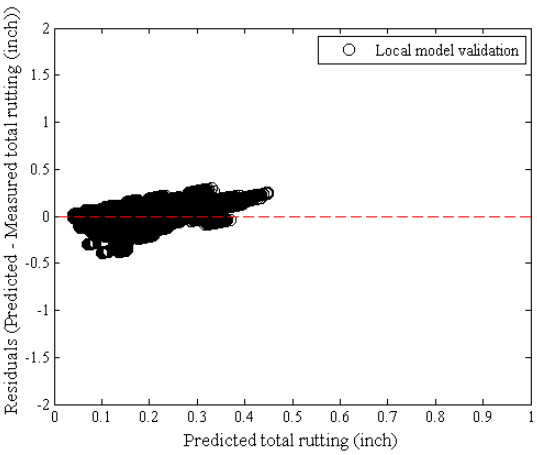

(a) Total rutting

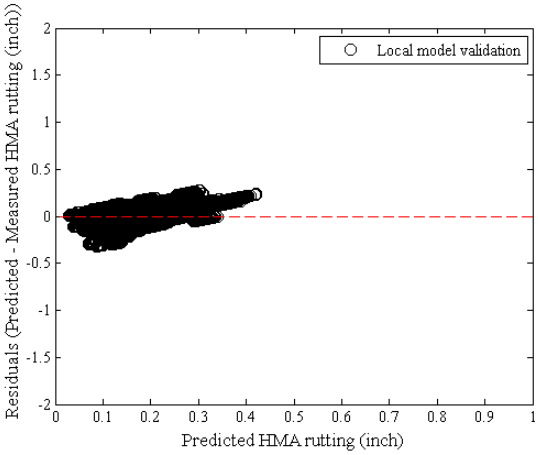

(b) HMA rutting

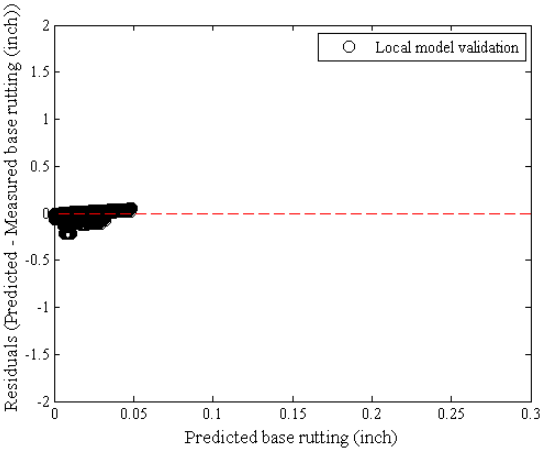

(c) Base rutting

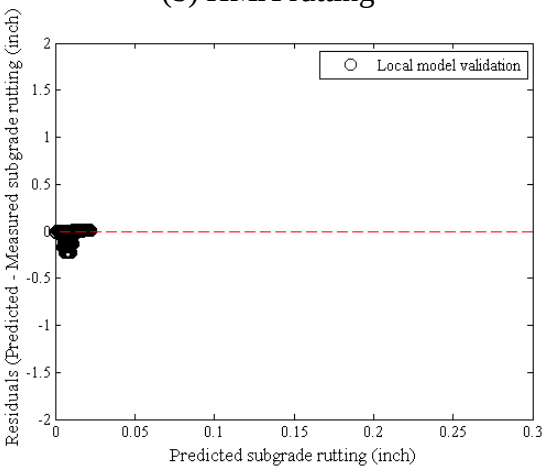

(d) Subgrade rutting

Figure B-165 Option 2: Method 1 – Rutting model validation residual plots – repeated split sampling

Reliability

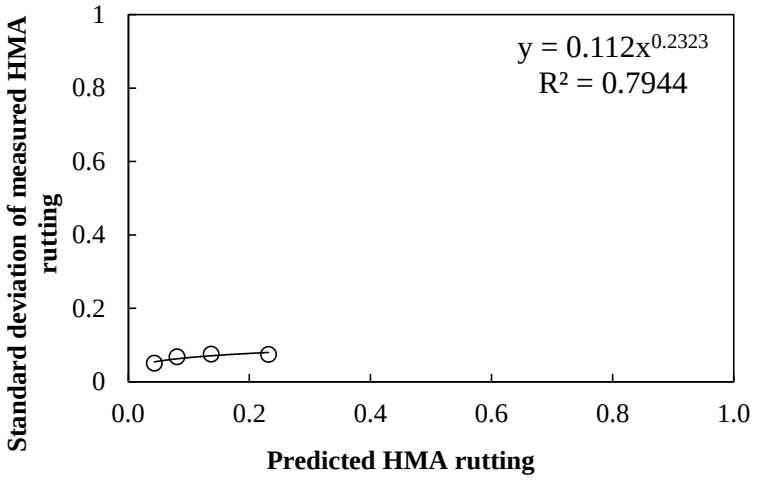

(a) HMA rutting reliability

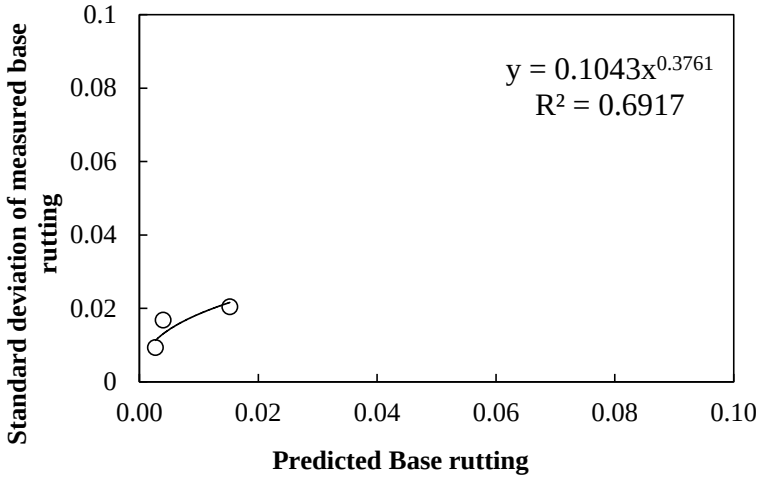

(b) Base rutting reliability

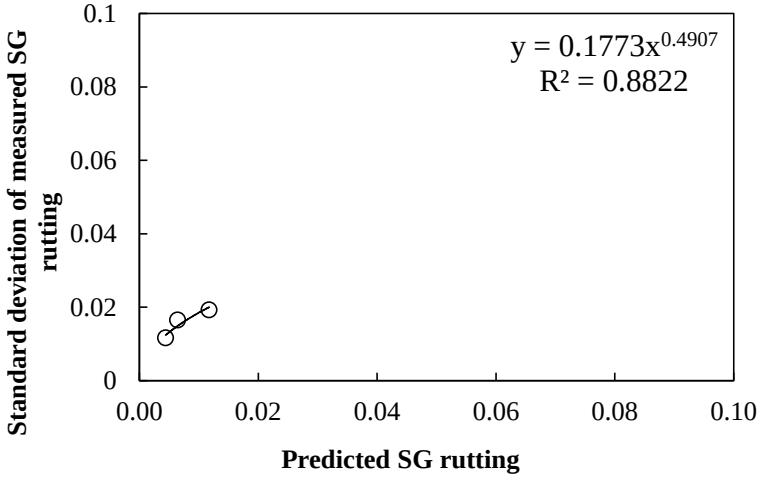

(c) Subgrade rutting reliability

Figure B-166 Rutting model reliability equations – option 2 method 1 – repeated split sampling

Bootstrapping

Table B-90 Option 2: Method 1 – Global model SEE and bias – bootstrapping

Calibration set	Average SEE	SEE Lower CI	SEE Upper CI	Average bias (in.)	Bias Lower CI	Bias Upper CI
AC rutting	0.0779	0.0708	0.0855	-0.0020	-0.0113	0.0082
Base rutting	0.1402	0.1253	0.1563	0.1160	0.1027	0.1294
Subgrade rutting	0.2236	0.2127	0.2349	0.2101	0.1981	0.2221
Total rutting	0.3572	0.3338	0.3815	0.3241	0.3010	0.3466

Table B-91 Option 2: Method 1 – Local model SEE and bias – bootstrapping

Calibration set	AC rutting	Base rutting	Subgrade rutting	Total rutting
Average SEE	0.0772	0.0256	0.0200	0.0862
SEE Lower CI	0.0703	0.0198	0.0107	0.0774
SEE Upper CI	0.0845	0.0319	0.0287	0.0952
Average bias (in.)	-0.0096	-0.0050	-0.0005	-0.0152
Bias Lower CI	-0.0144	-0.0068	-0.0010	-0.0200
Bias Upper CI	-0.0054	-0.0032	-0.0002	-0.0106
Average calibration coefficient	0.9453	0.0985	0.0367	N/A
Calibration coefficient Lower CI	0.8655	0.0746	0.0252	N/A
Calibration coefficient Upper CI	1.0262	0.1257	0.0506	N/A

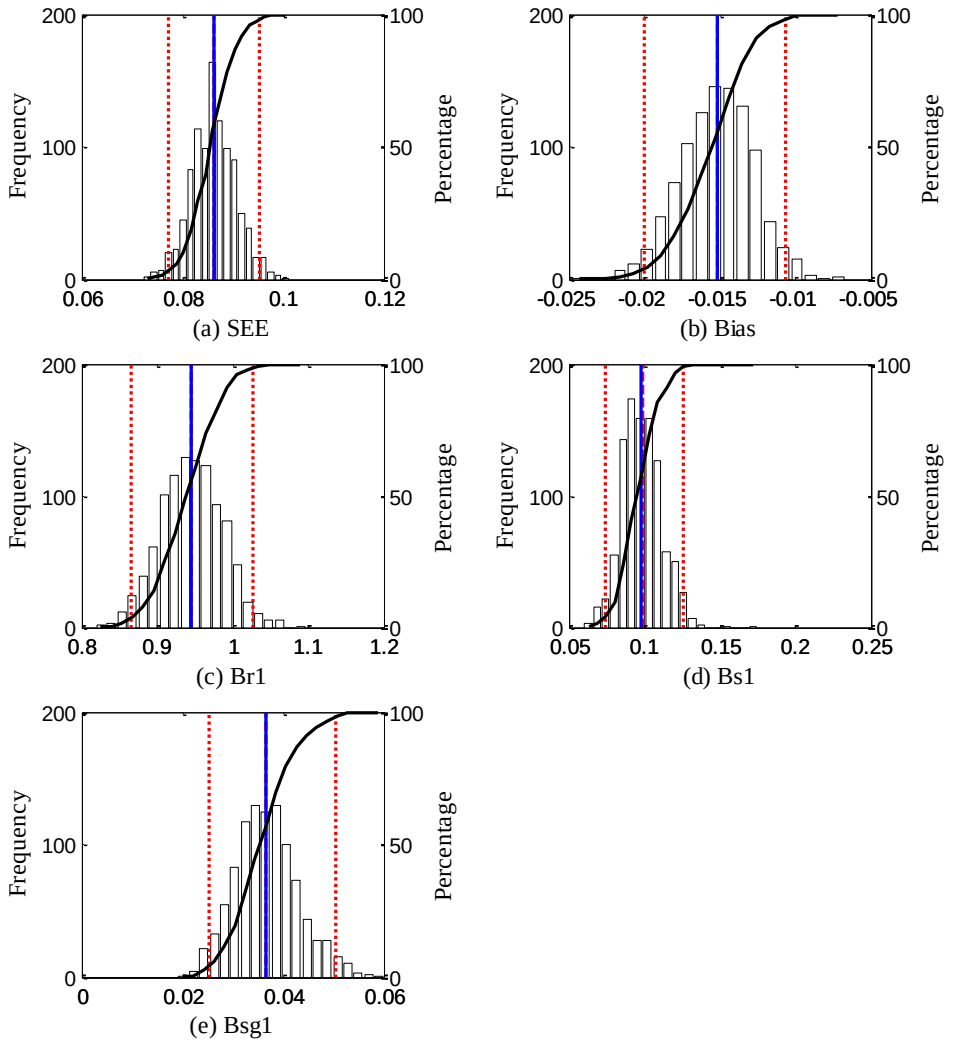

Figure B-167 Option 2: Method 1 – bootstrapping total rutting frequency distributions –calibration

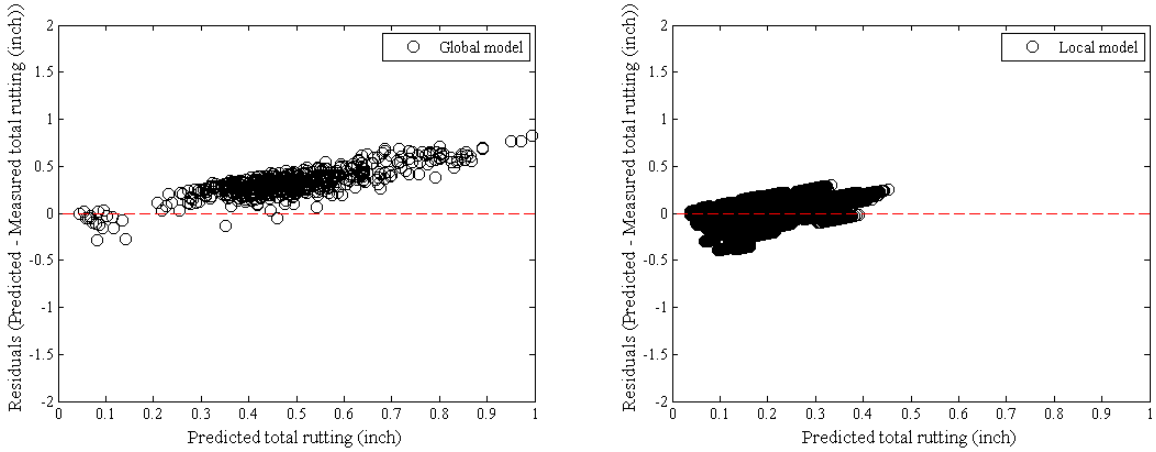

(a) Global model (b) Local model

Figure B-168 Option 2 Method 1 Total rutting residual plots - bootstrapping

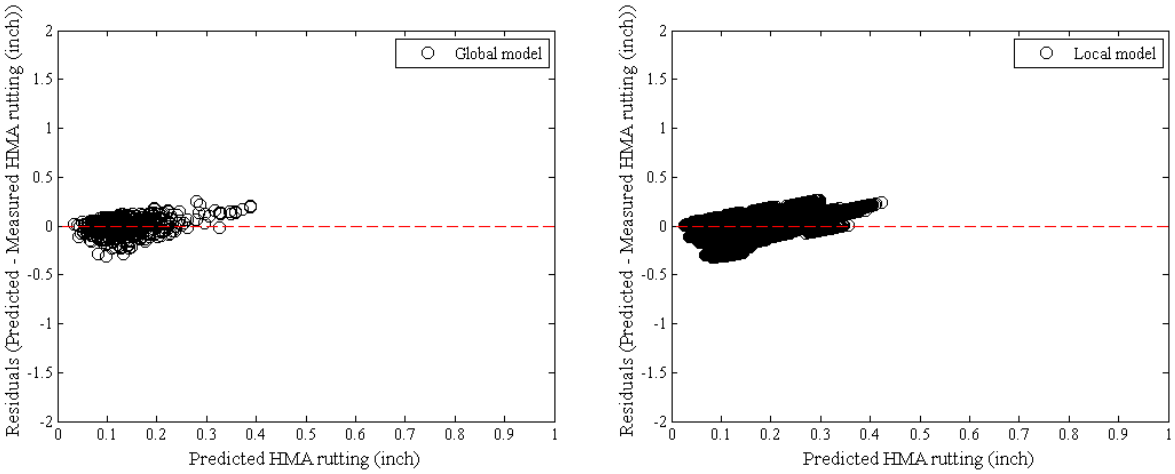

(a) Global model (b) Local model

Figure B-169 Option 2: Method 1 HMA rutting residual plots - bootstrapping

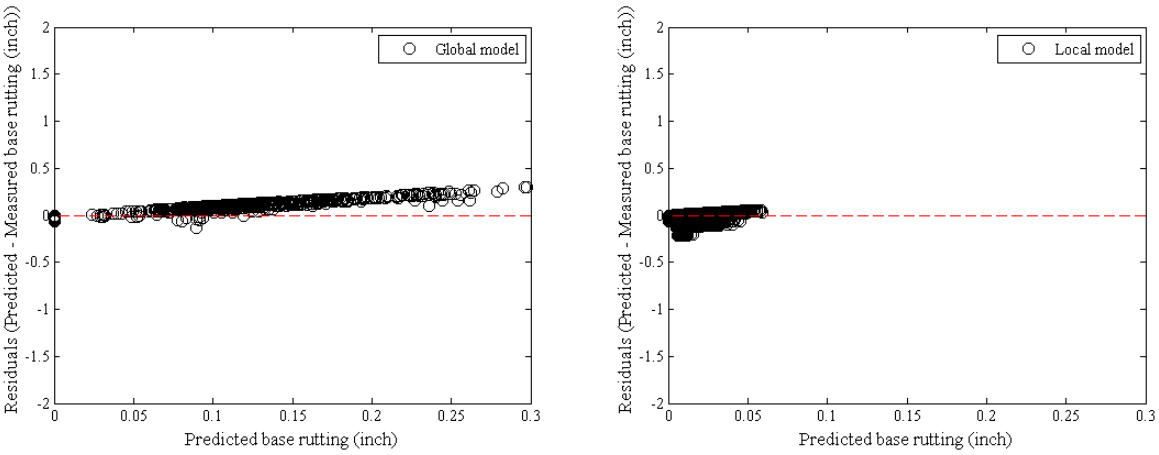

(a) Global model (b) Local model

Figure B-170 Option 2: Method 1 Base rutting residual plots - bootstrapping

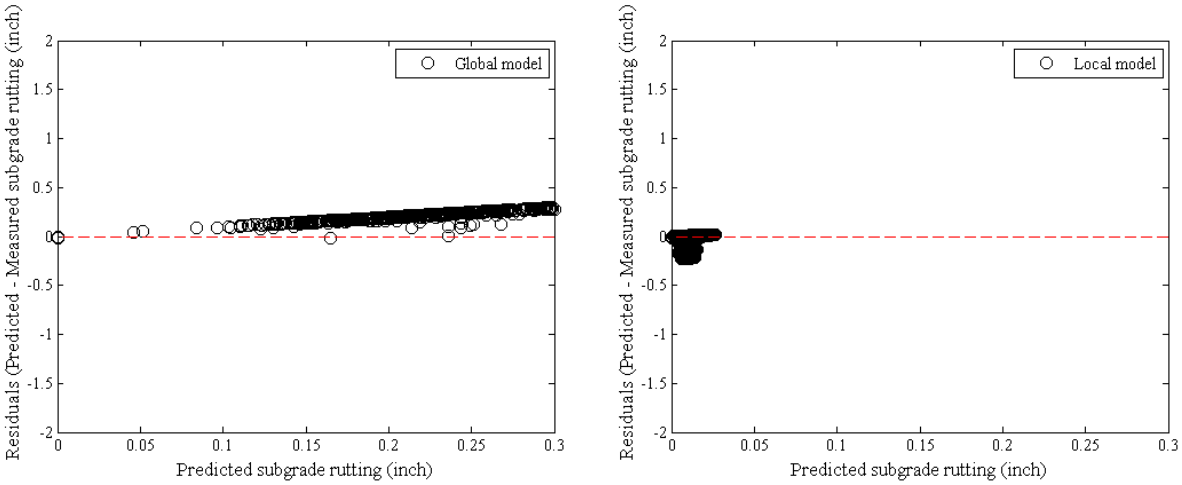

(a) Global model (b) Local model

Figure B-171 Option 2 Method 1 Subgrade rutting residual plots - bootstrapping

Reliability

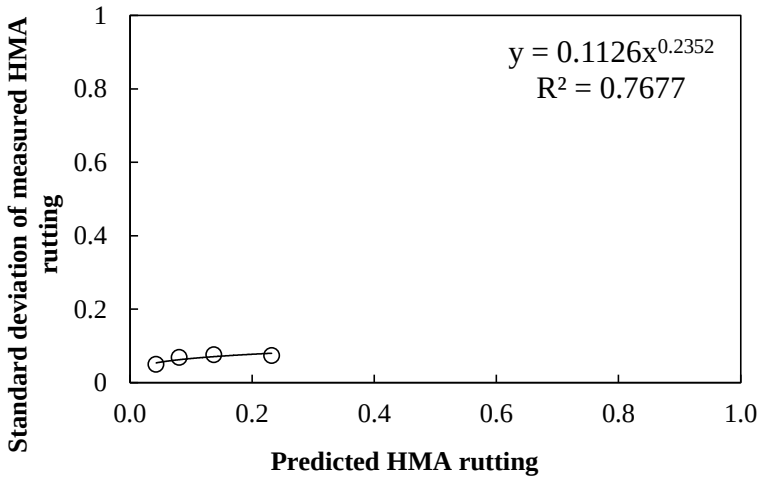

(a) HMA rutting reliability

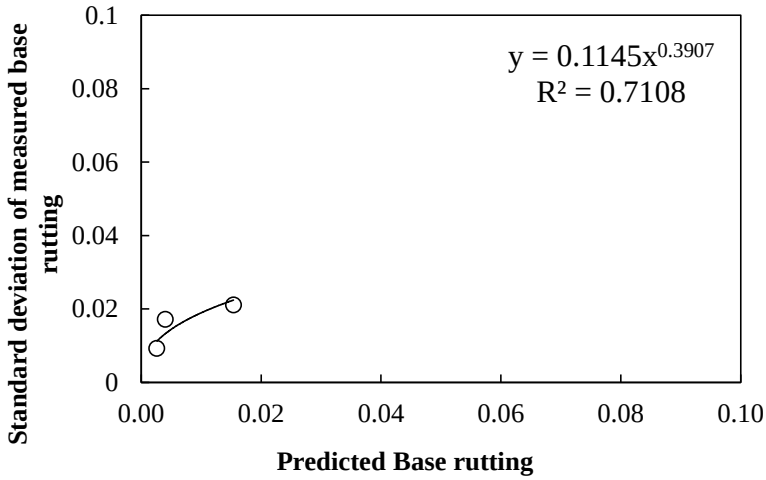

(b) Base rutting reliability

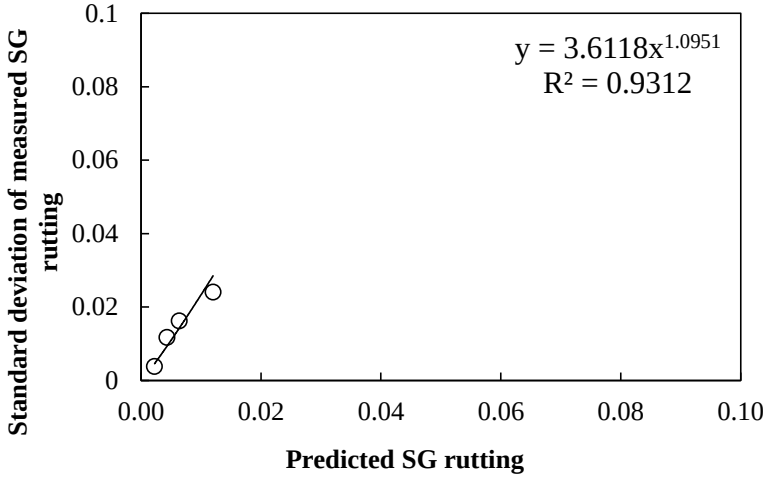

(c) Subgrade rutting reliability

Figure B-172 Rutting model reliability equations – option 2 method 1 – bootstrapping

B.1.3.4 Option 2 – Method 2

No sampling

Table B-92 Option 2: Method 2 – Global model goodness of fit – no sampling

HMA layer	SEE (in.)	Bias (in.)
AC rut	0.0779	-0.0019
Base rut	0.1405	0.1160
Subgrade	0.2235	0.2100
Total rut	0.3574	0.3241

Table B-93 Option 2: Method 2 – Global model *p*-values

HMA layer	t-test p-value	Intercept p-value	Slope = 1 p-value
AC rut	0.5505	0.0000	0.0000
Base rut	0.0000	0.0000	0.0000
Subgrade	0.0000	0.0000	0.0000
Total rut	0.0000	0.0000	0.0000

Table B-94 Option 2: Method 2 – Local model goodness of fit– no sampling

HMA layer	SEE	Bias
AC rut	0.0906	-0.0533
Base rut	0.0279	-0.0144
Subgrade	0.0695	0.0623
Total rut	0.0830	-0.0055

Table B-95 Option 2: Method 2 – Local model *p*-values– no sampling

HMA layer	t-test p-value	Intercept p-value	Slope = 1 p-value
AC rut	0.0000	0.0000	0.0000
Base rut	0.0000	0.0000	0.0000
Subgrade	0.0000	0.0000	0.0000
Total rut	0.1103	0.0000	0.0000

Table B-96 Option 2: Method 2 – Local model *p*-values– no sampling

Calibration Coefficient	Global model	Local model
HMA rutting (br1)	1.0000	0.6251
Base rutting (bs1)	1.0000	0.0276
Subgrade rutting (bsg1)	1.0000	0.3241

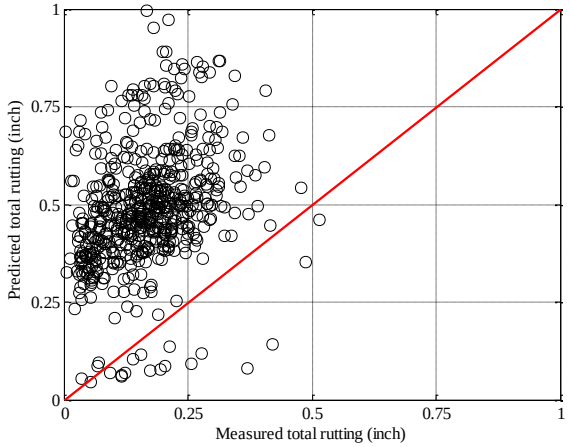

(a) Global model

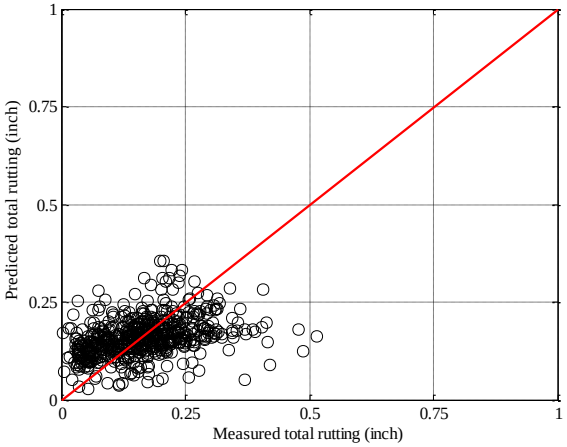

(b) Local model

Figure B-173 Option 2: Method 2 – Total rutting local calibration results - no sampling

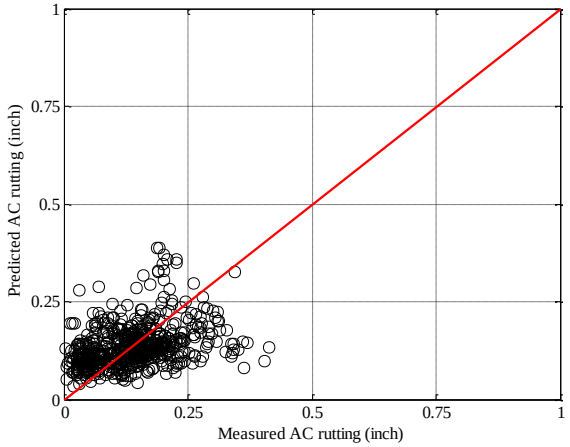

(a) Global model

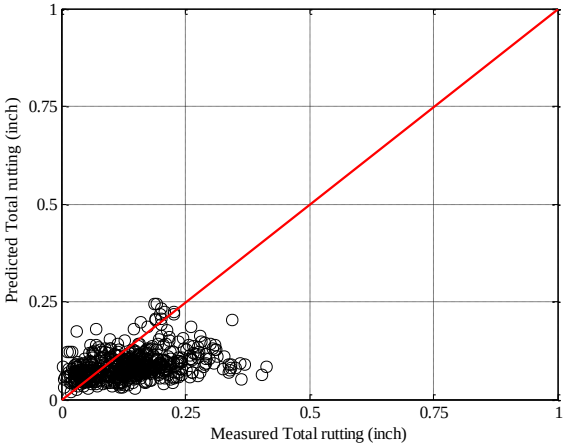

(b) Local model

Figure B-174 Option 2: Method 2 – HMA rutting local calibration results - no sampling

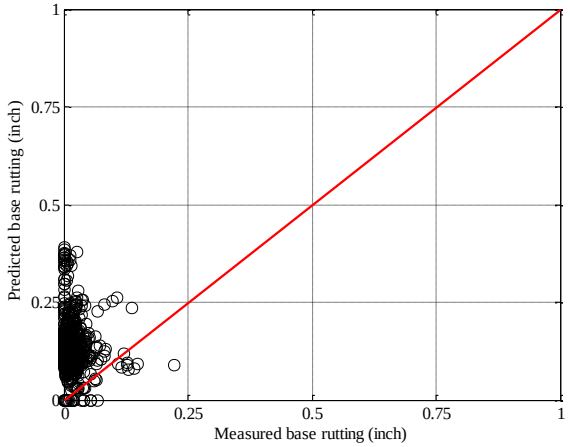

(a) Global model

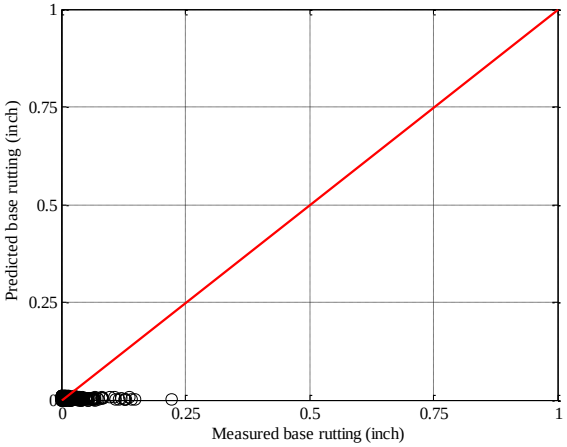

(b) Local model

Figure B-175 Option 2: Method 2 – Base rutting local calibration results - no sampling

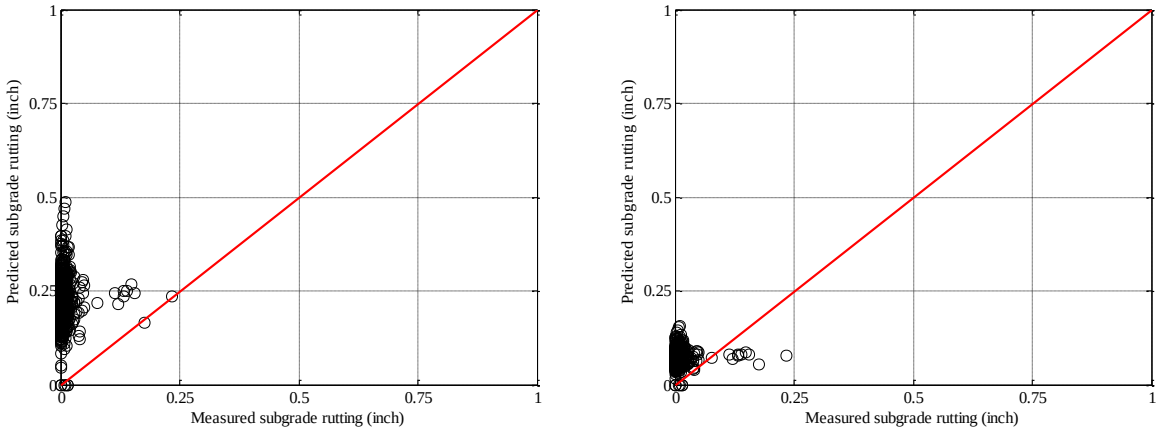

(a) Global model (b) Local model

Figure B-176 Option 2: Method 2 – Subgrade rutting local calibration results - no sampling

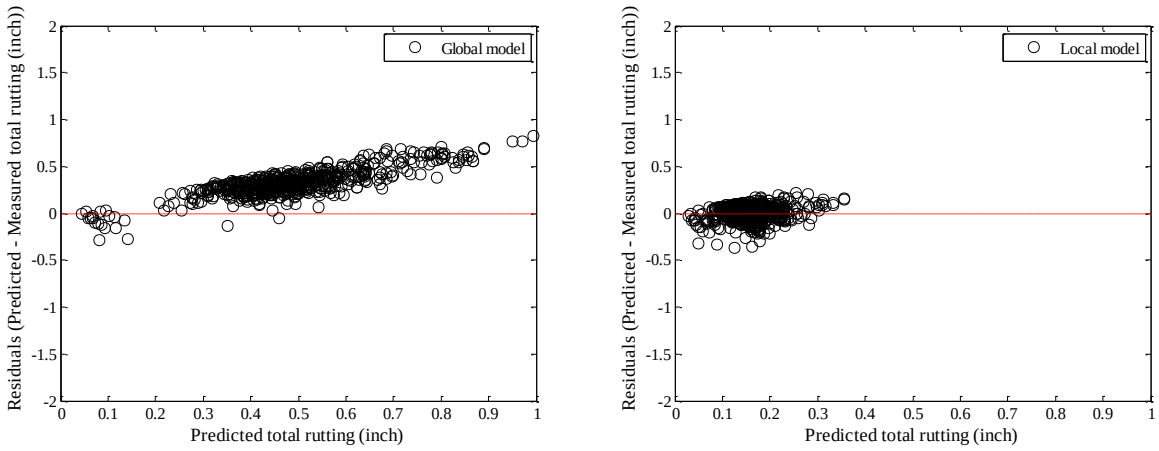

(a) Global model (b) Local model

Figure B-177 Option 2: Method 2 – Total rutting residual plots - no sampling

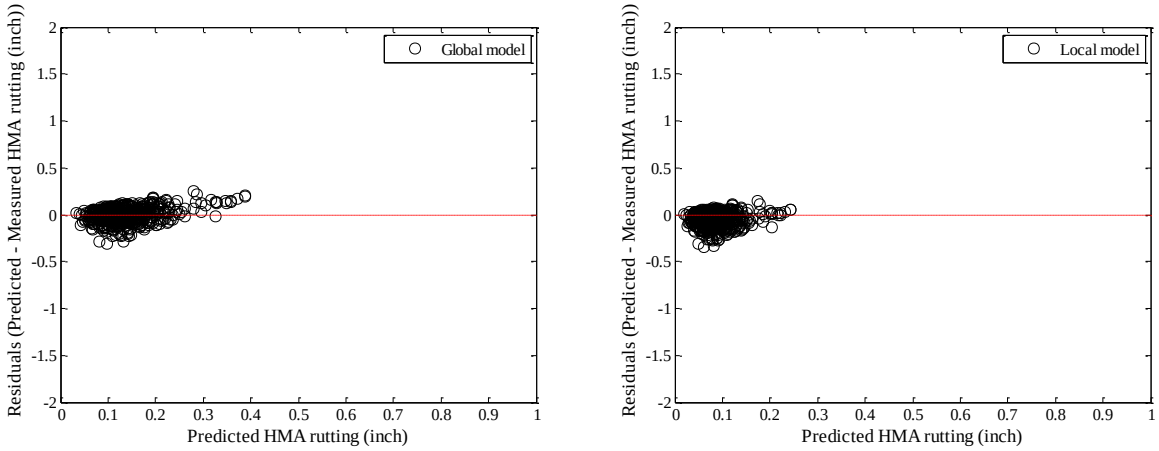

(a) Global model (b) Local model

Figure B-178 Option 2: Method 2 – HMA rutting residual plots - no sampling

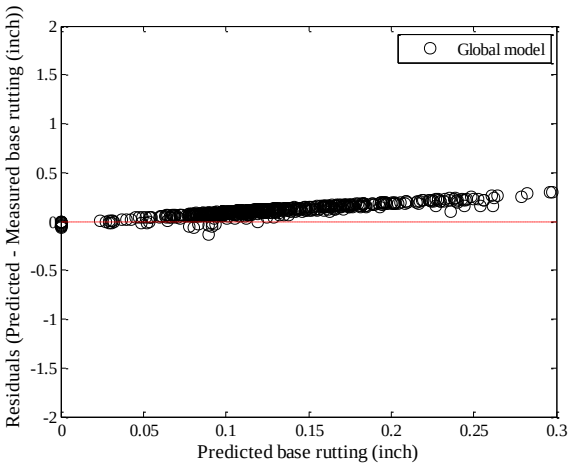

(a) Global model

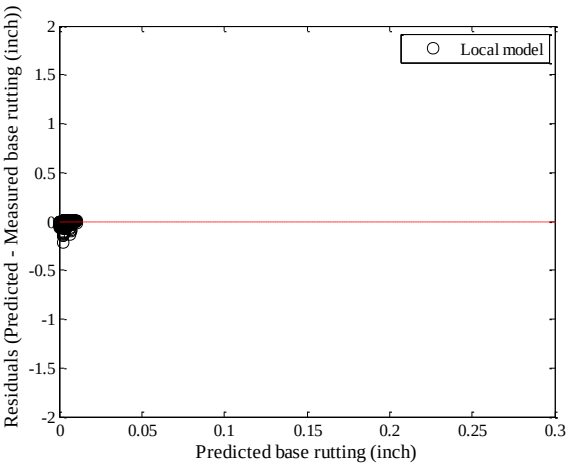

(b) Local model

Figure B-179 Option 2: Method 2 – Base rutting residual plots - no sampling

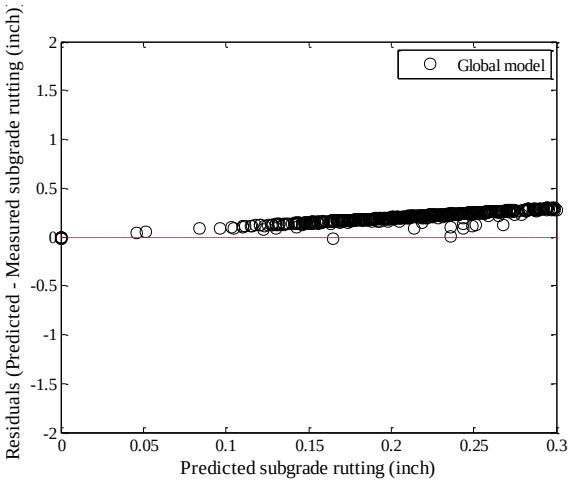

(a) Global model

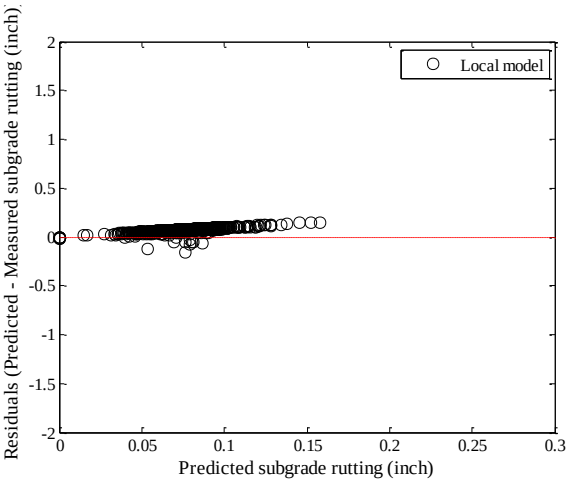

(b) Local model

Figure B-180 Option 2: Method 2 – Subgrade rutting residual plots - no sampling

Reliability

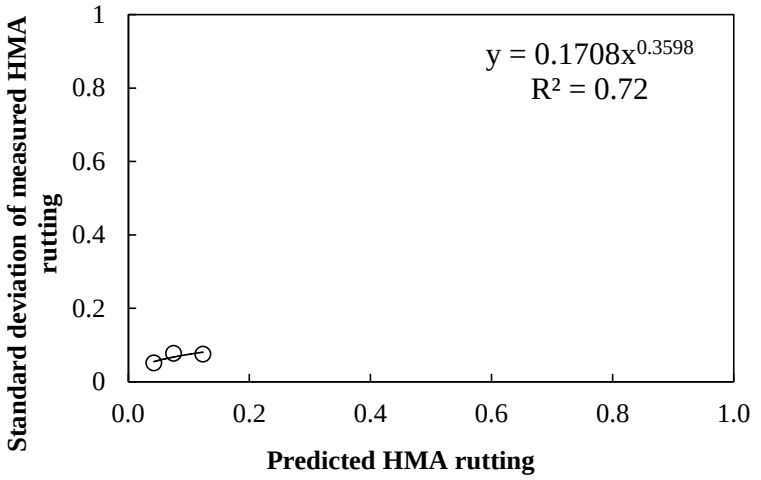

(a) HMA rutting reliability

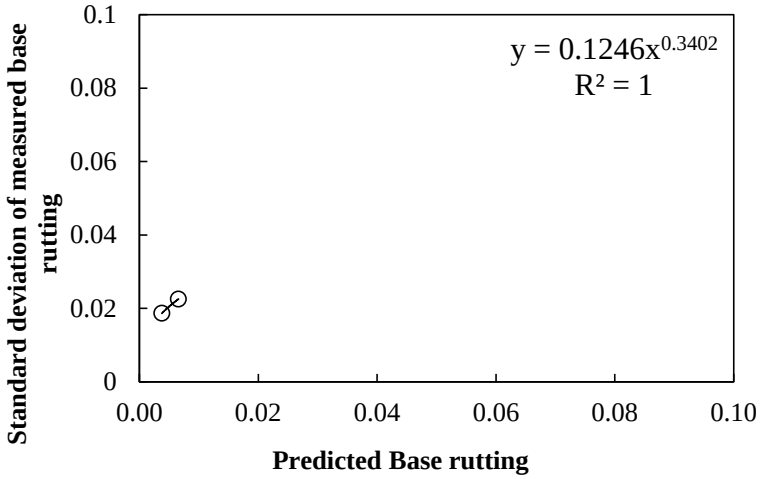

(b) Base rutting reliability

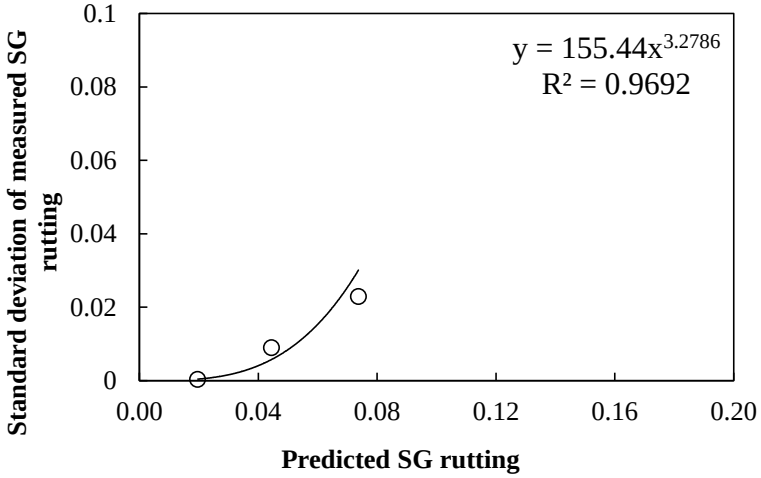

(c) Subgrade rutting reliability

Figure B-181 Rutting model reliability equations – option 2 method 2 – no sampling

Split sampling

Table B-97 Option 2: Method 2 – Global model goodness of fit – split sampling

HMA layer	SEE (in.)	Bias (in.)
AC rut	0.0786	0.0028
Base rut	0.1335	0.1111
Subgrade	0.2271	0.2146
Total rut	0.3573	0.3285

Table B-98 Option 2: Method 2 – Global model *p*-values - split sampling

HMA layer	t-test p-value	Intercept p-value	Slope = 1 p-value
AC rut	0.4768	0.0000	0.0000
Base rut	0.0000	0.0000	0.0000
Subgrade	0.0000	0.0000	0.0000
Total rut	0.0000	0.0000	0.0000

Table B-99 Option 2: Method 2 – Local model goodness of fit– split sampling

HMA layer	SEE	Bias
AC rut	0.0971	-0.0646
Base rut	0.0256	-0.0063
Subgrade	0.0728	0.0666
Total rut	0.0813	-0.0042

Table B-100 Option 2: Method 2 – Local model *p*-values– split sampling

HMA layer	t-test p-value	Intercept p-value	Slope = 1 p-value
AC rut	0.0000	0.0000	0.0000
Base rut	0.0000	0.0000	0.0000
Subgrade	0.0000	0.0000	0.0000
Total rut	0.2936	0.0000	0.0000

Table B-101 Option 2: Method 2 – Local model *p*-values – split sampling

Calibration Coefficient	Global model	Local model
HMA rutting (br1)	1.0000	0.5100
Base rutting (bs1)	1.0000	0.1006
Subgrade rutting (bsg1)	1.0000	0.3367

Table B-102 Option 2: Method 2 – Local model validation p-values – split sampling

HMA layer	t-test p-value	Intercept p-value	Slope = 1 p-value
AC rut	0.0000	0.0000	0.0000
Base rut	0.7072	0.0000	0.0000
Subgrade	0.0000	0.0000	0.0000
Total rut	0.0036	0.0000	0.0000

Table B-103 Option 2: Method 2 – Local model validation SEE and bias – split sampling

HMA layer	SEE	Bias
AC rut	0.1086	-0.0798
Base rut	0.0264	-0.0008
Subgrade	0.0716	0.0612
Total rut	0.0886	-0.0194

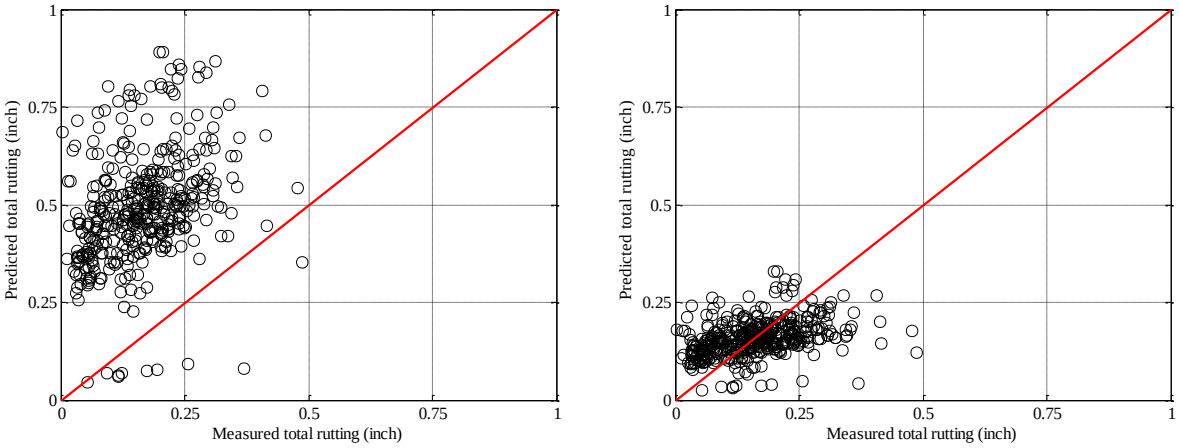

(a) Global model (b) Local model

Figure B-182 Option 2: Method 2 – Total rutting local calibration results - split sampling

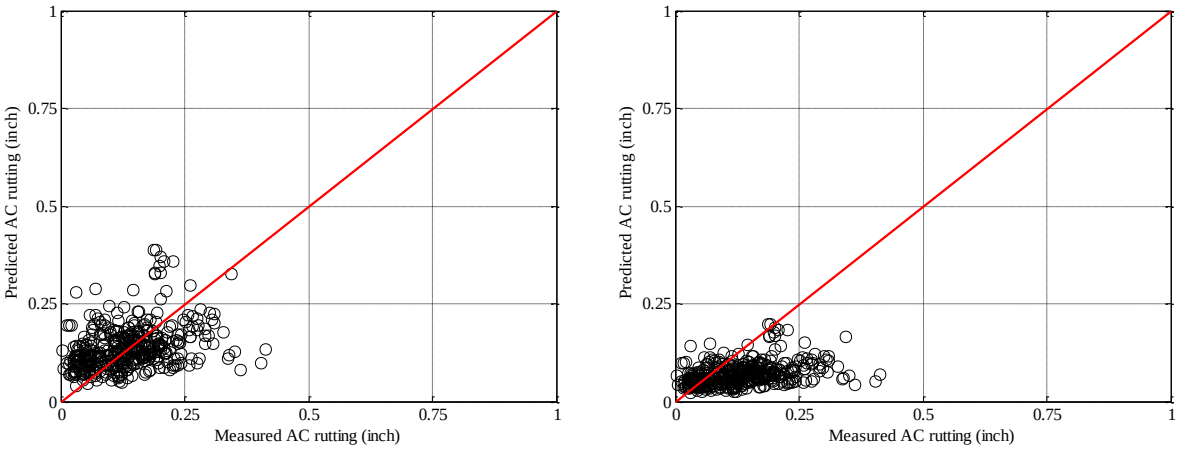

(a) Global model (b) Local model

Figure B-183 Option 2: Method 2 – HMA rutting local calibration results - split sampling

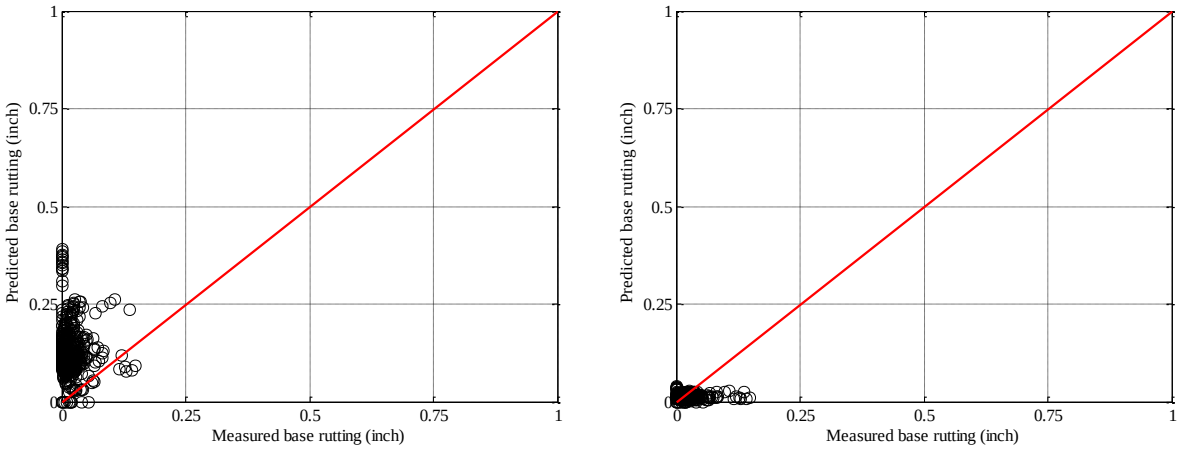

(a) Global model (b) Local model

Figure B-184 Option 2: Method 2 – Base rutting local calibration results - split sampling

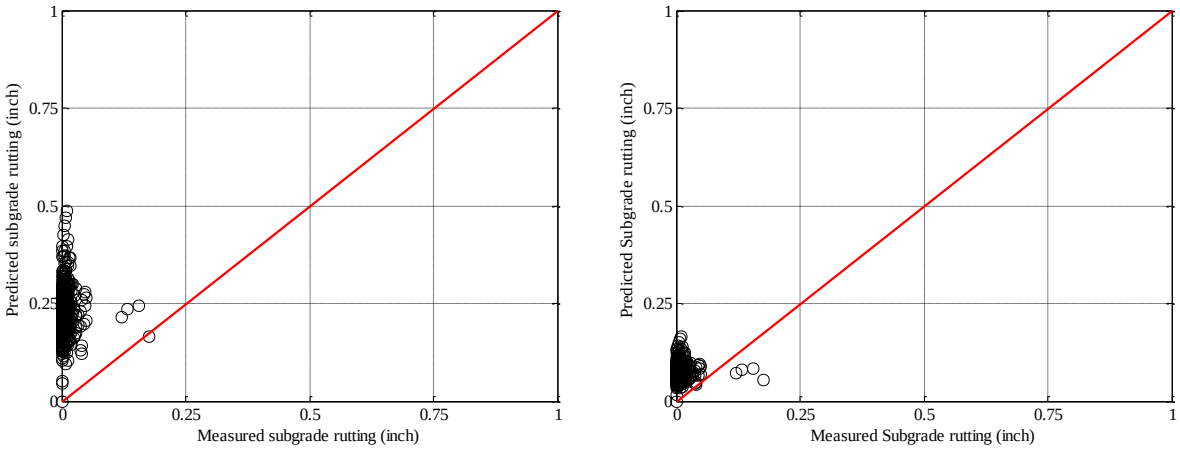

(a) Global model (b) Local model

Figure B-185 Option 2: Method 2 – Subgrade rutting local calibration results - split sampling

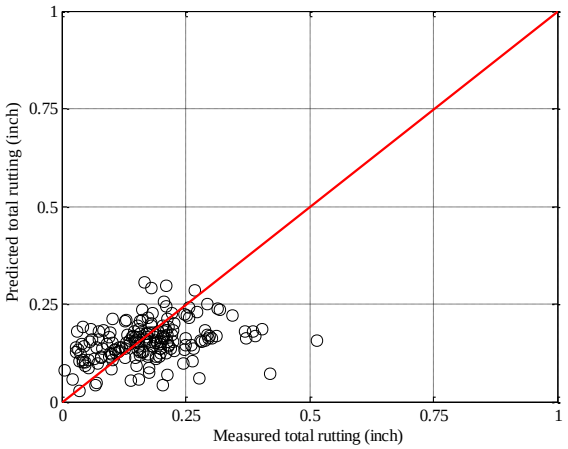

(a) Total rutting

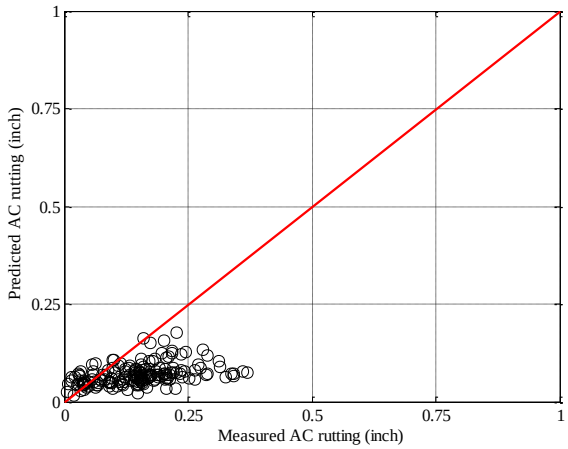

(b) HMA rutting

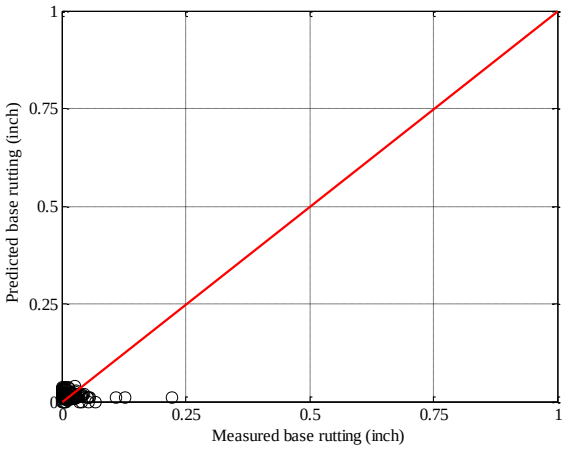

(c) Base rutting

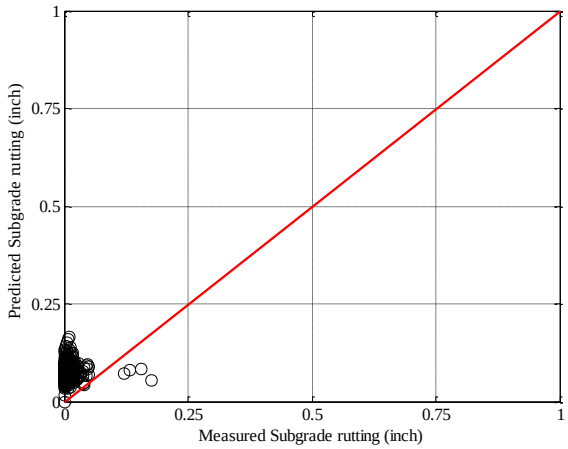

(d) Subgrade rutting

Figure B-186 Option 2: Method 2 – Rutting model validation – split sampling

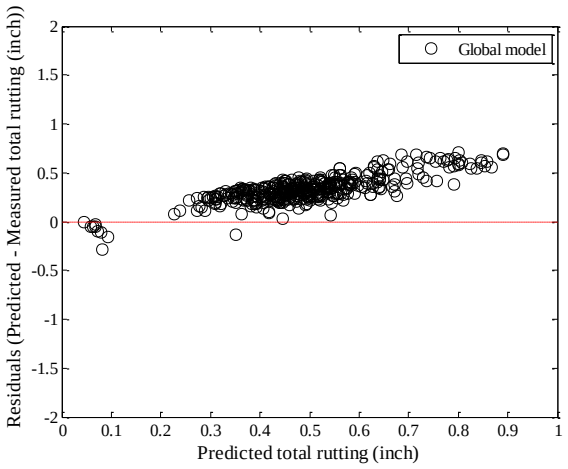

(a) Global model

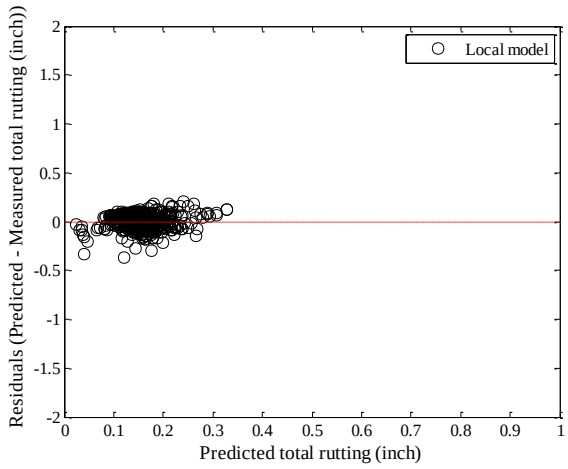

(b) Local model

Figure B-187 Option 2: Method 2 – Total rutting residual plots - split sampling

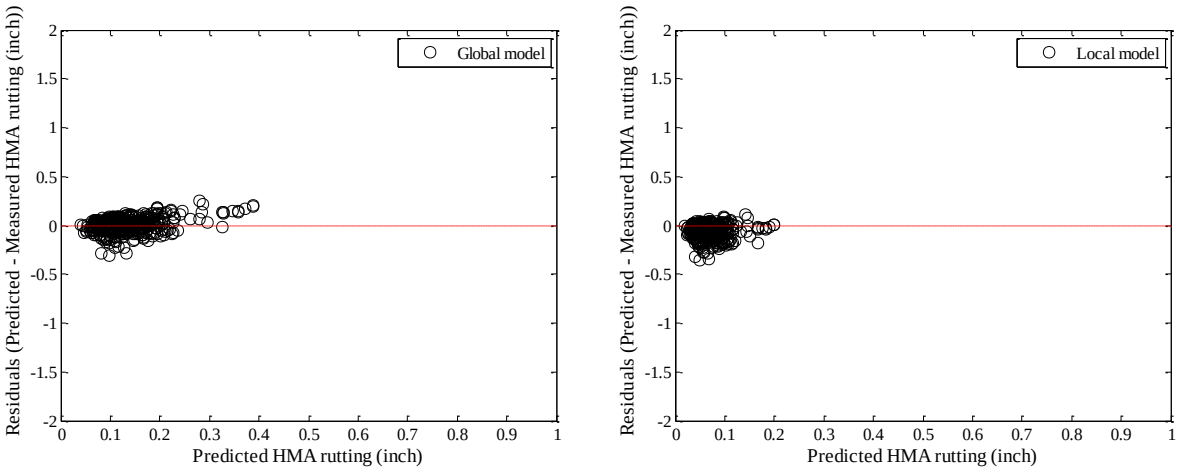

(a) Global model (b) Local model

Figure B-188 Option 2: Method 2 – HMA rutting residual plots - split sampling

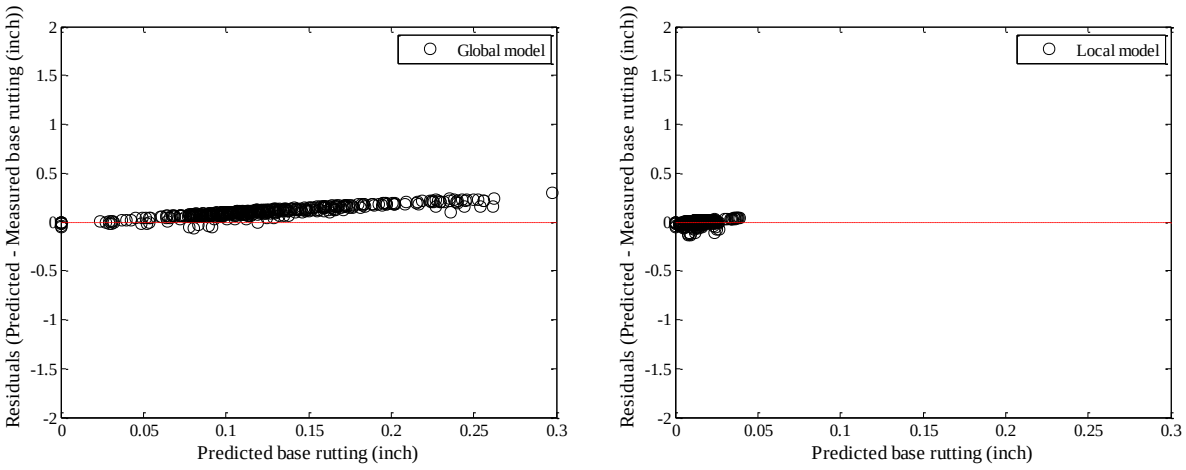

(a) Global model (b) Local model

Figure B-189 Option 2: Method 2 – Base rutting residual plots - split sampling

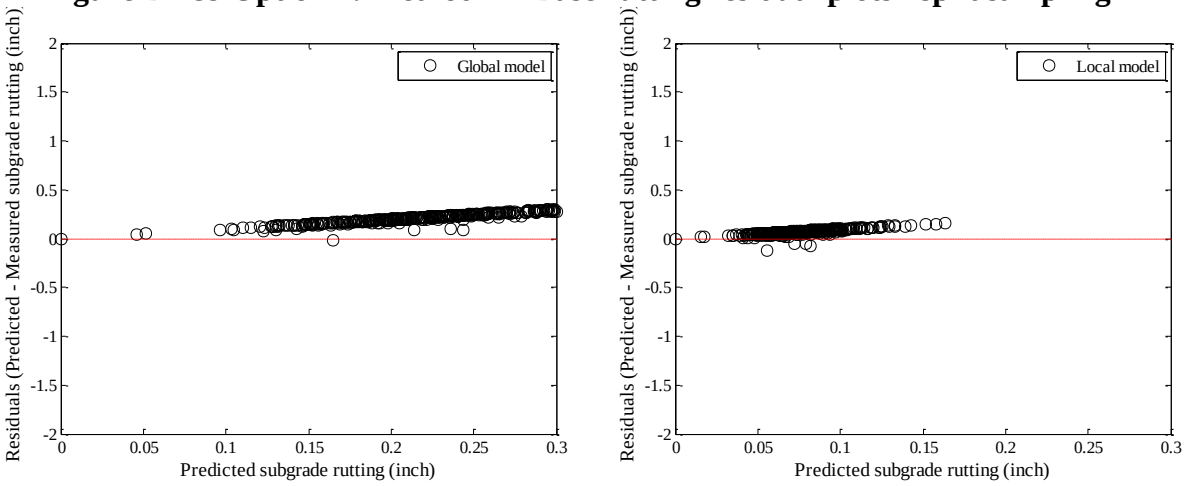

(a) Global model (b) Local model

Figure B-190 Option 2: Method 2 – Subgrade rutting residual plots - split sampling

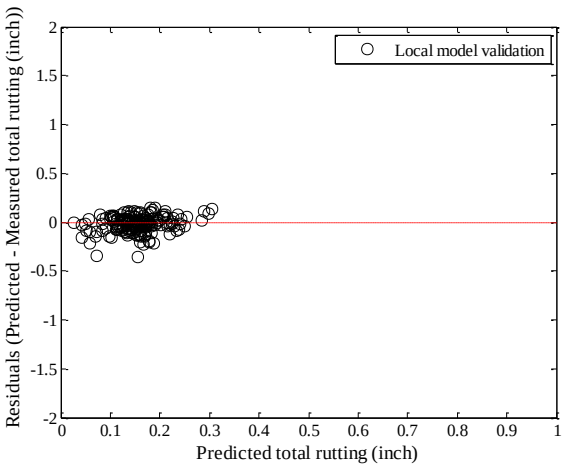

(a) Total rutting

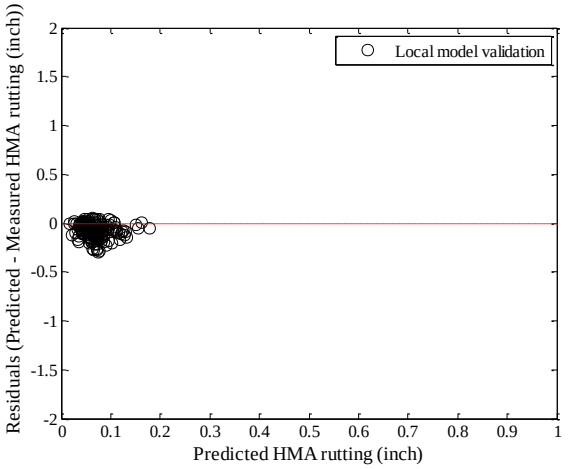

(b) HMA rutting

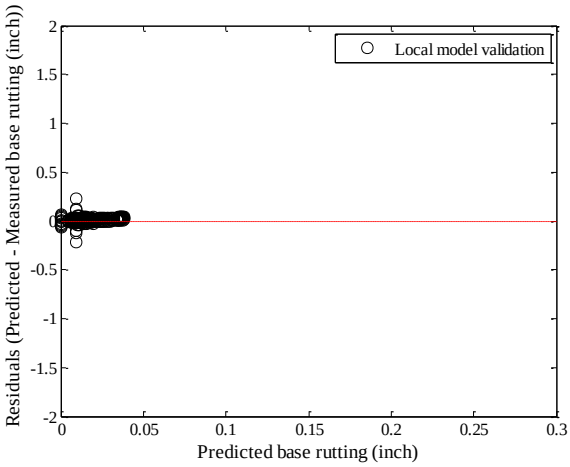

(c) Base rutting

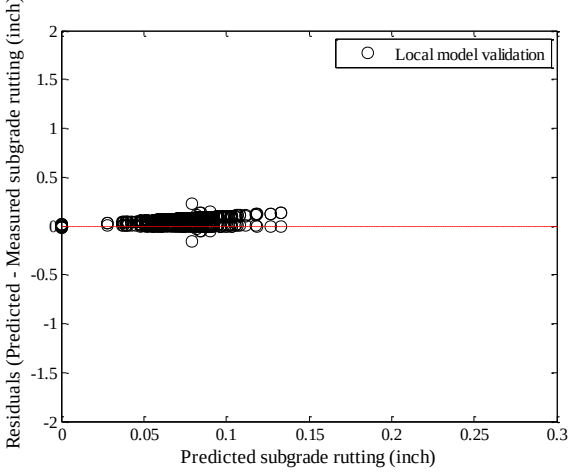

(d) Subgrade rutting

Figure B-191 Option 2: Method 2 – Rutting model validation residual plots – split sampling

Reliability

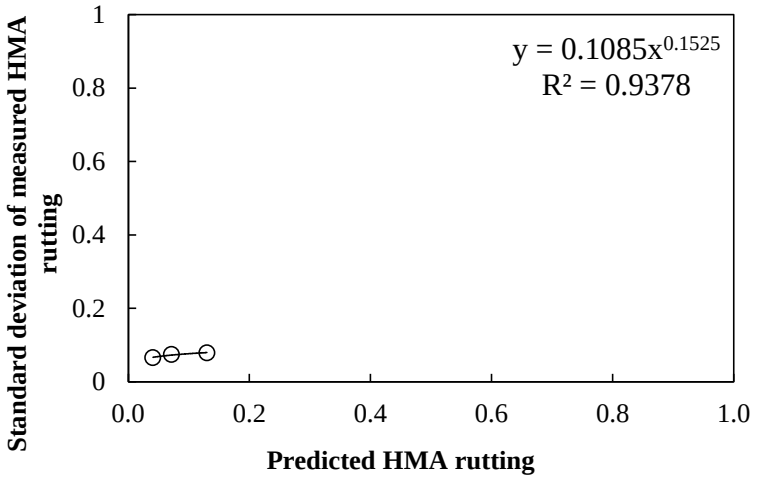

(a) HMA rutting reliability

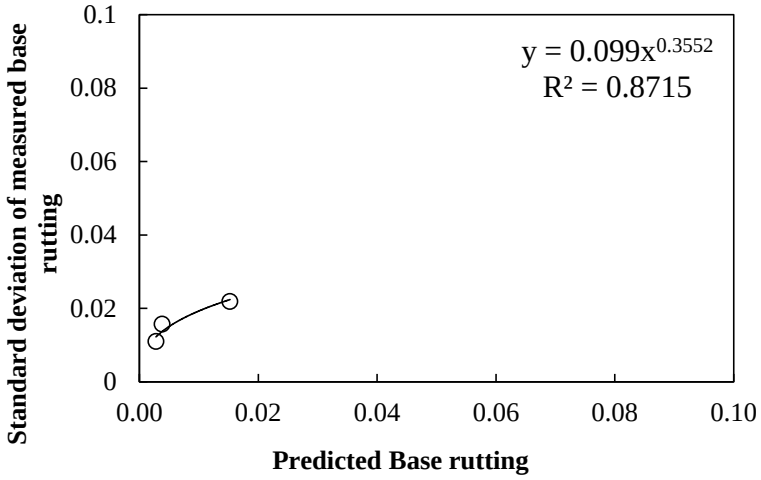

(b) Base rutting reliability

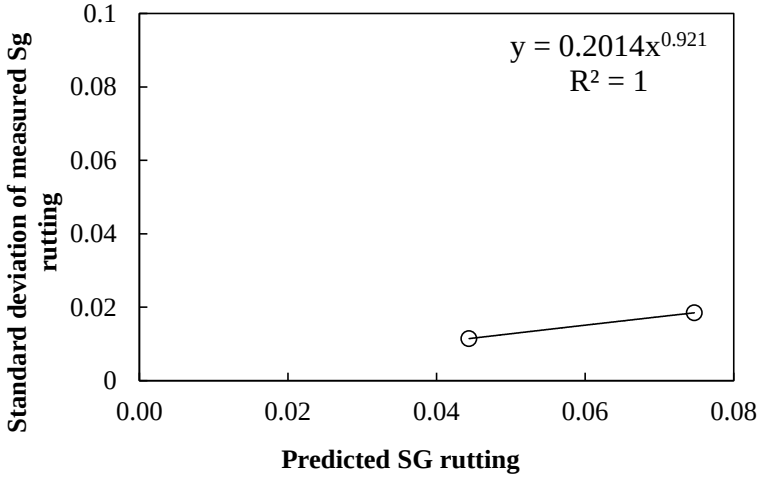

(c) Subgrade rutting reliability

Figure B-192 Rutting model reliability equations – option 2 method 2 – split sampling

Repeated split sampling

Table B-104 Option 2: Method 2 – Global model SEE and bias – repeated split sampling

Global Model	Average SEE	SEE Lower CI	SEE Upper CI	Average bias (in.)	Bias Lower CI	Bias Upper CI
AC rutting	0.0781	0.0731	0.0825	-0.0018	-0.0083	0.0048
Base rutting	0.1405	0.1293	0.1498	0.1161	0.1072	0.1242
Subgrade rutting	0.2237	0.2162	0.2307	0.2100	0.2026	0.2178
Total rutting	0.3578	0.3420	0.3726	0.3243	0.3088	0.3392

Table B-105 Option 2: Method 2 – Local model SEE and bias – repeated split sampling

Calibration set	AC rutting	Base rutting	Subgrade rutting	Total rutting
Average SEE	0.0915	0.0275	0.0693	0.0829
SEE Lower CI	0.0789	0.0215	0.0476	0.0776
SEE Upper CI	0.1055	0.0320	0.0904	0.0876
Average bias (in.)	-0.0542	-0.0131	0.0619	-0.0054
Bias Lower CI	-0.0746	-0.0184	0.0387	-0.0075
Bias Upper CI	-0.0308	-0.0033	0.0832	-0.0030
Average calibration coefficient	0.6193	0.0377	0.3224	N/A
Calibration coefficient Lower CI	0.4725	0.0100	0.2204	N/A
Calibration coefficient Upper CI	0.8116	0.1068	0.4164	N/A

Table B-106 Option 2: Method 2 – Local model validation SEE and bias – repeated split sampling

Validation set	AC rutting	Base rutting	Subgrade rutting	Total rutting
Average SEE	0.0923	0.0276	0.0695	0.0844
SEE Lower CI	0.0770	0.0185	0.0467	0.0725
SEE Upper CI	0.1096	0.0374	0.0936	0.0964
Average bias (in.)	-0.0540	-0.0131	0.0618	-0.0054
Bias Lower CI	-0.0793	-0.0209	0.0398	-0.0259
Bias Upper CI	-0.0197	-0.0020	0.0843	0.0161
Average calibration coefficient	0.6193	0.0377	0.3224	N/A
Calibration coefficient Lower CI	0.4725	0.0100	0.2204	N/A
Calibration coefficient Upper CI	0.8116	0.1068	0.4164	N/A

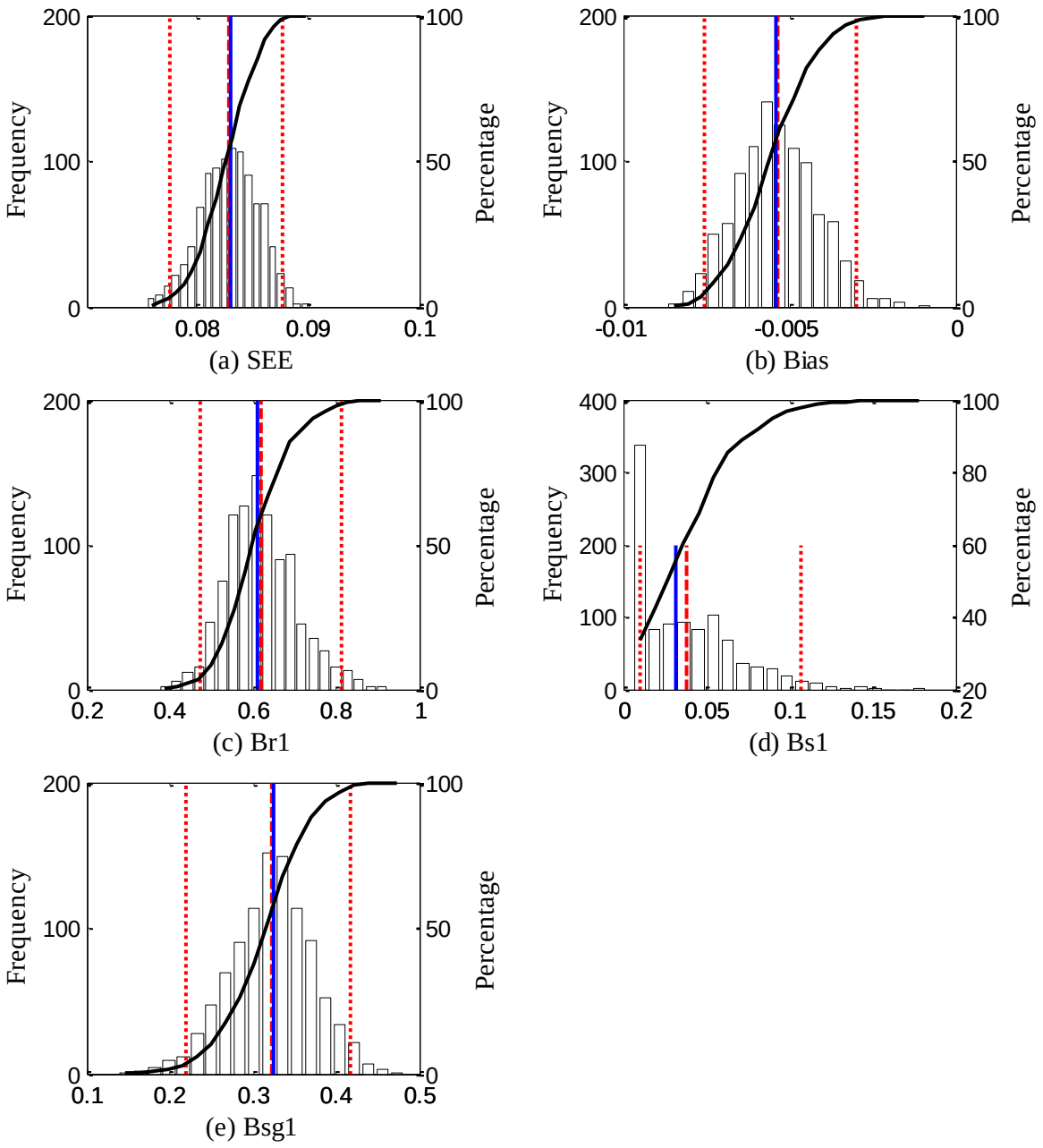

Figure B-193 Option 2: Method 2 – repeated split sampling total rutting frequency distributions – calibration

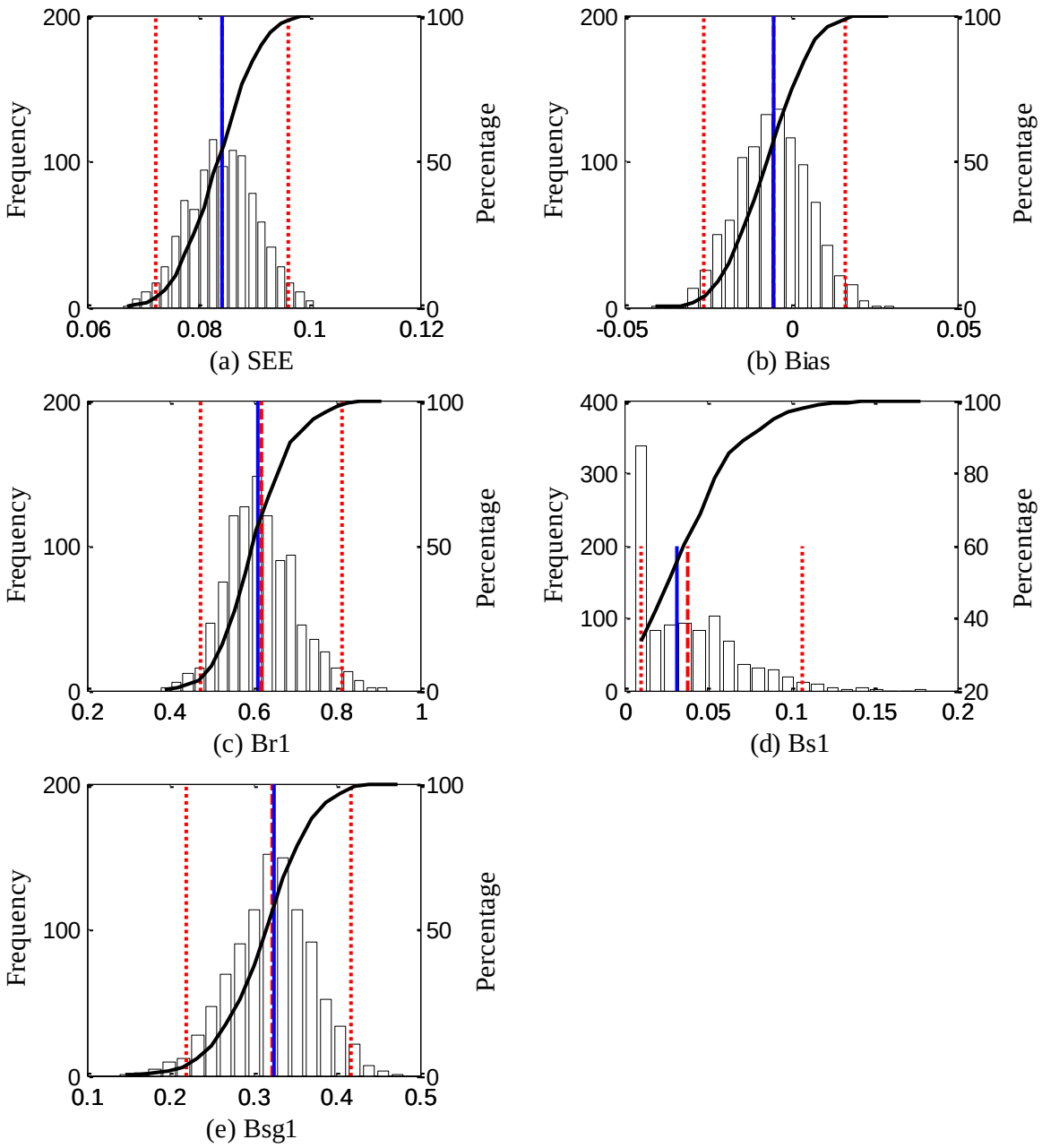

Figure B-194 Option 2: Method 2 – repeated split sampling total rutting frequency distributions – validation

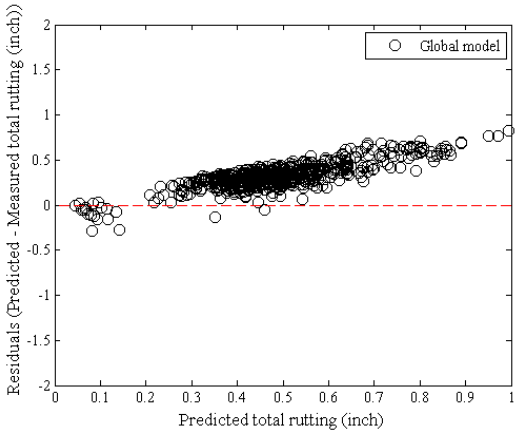

(a) Global model

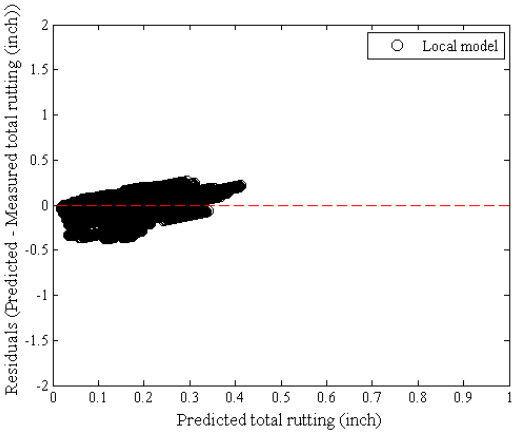

(b) Local model

Figure B-195 Option 2: Method 2 – Total rutting residual plots – repeated split sampling

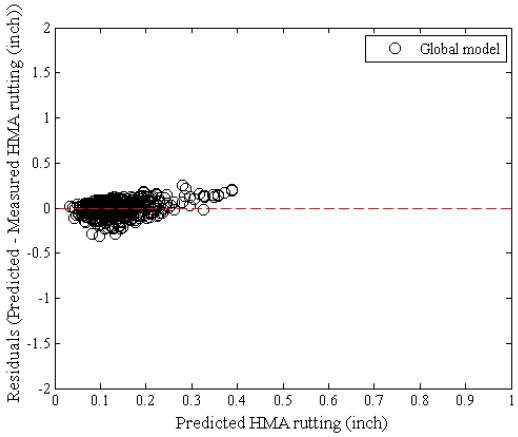

(a) Global model

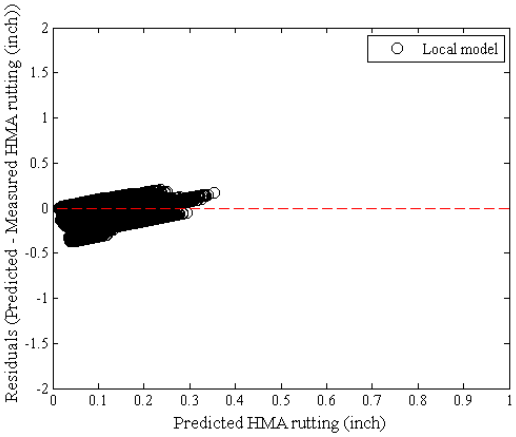

(b) Local model

Figure B-196 Option 2: Method 2 – HMA rutting residual plots - repeated split sampling

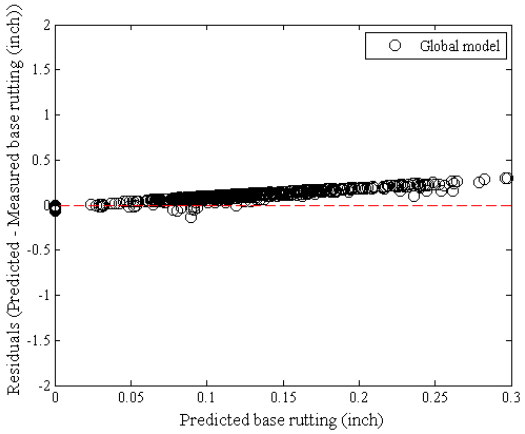

(a) Global model

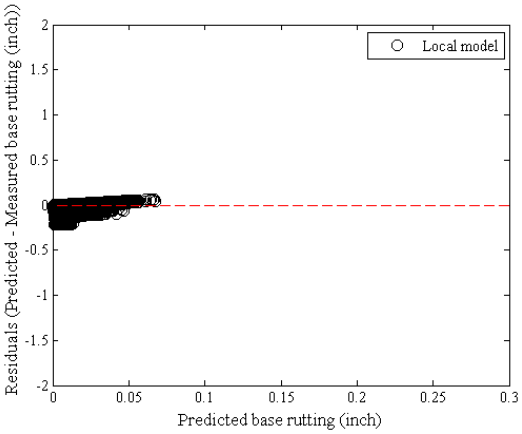

(b) Local model

Figure B-197 Option 2: Method 2 – Base rutting residual plots - repeated split sampling

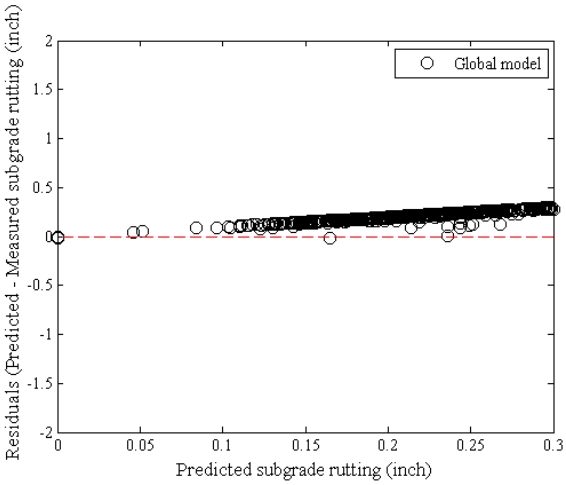

(a) Global model

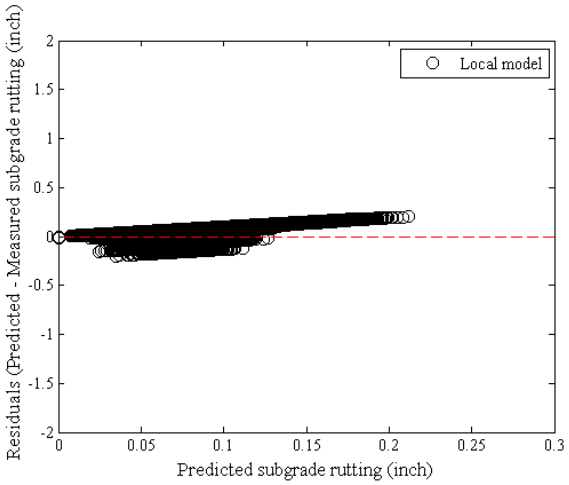

(b) Local model

Figure B-198 Option 2: Method 2 – Subgrade rutting residual plots - repeated split sampling

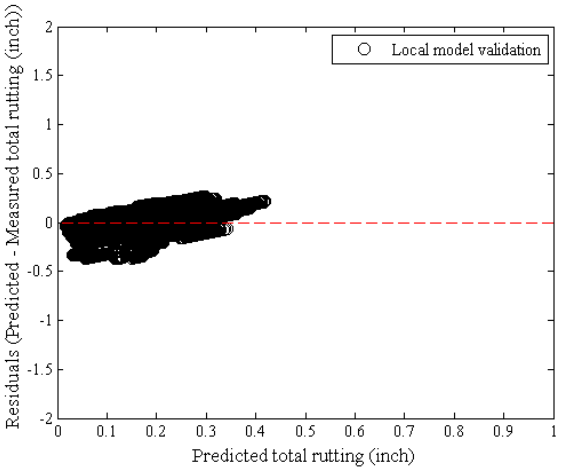

(a) Total rutting

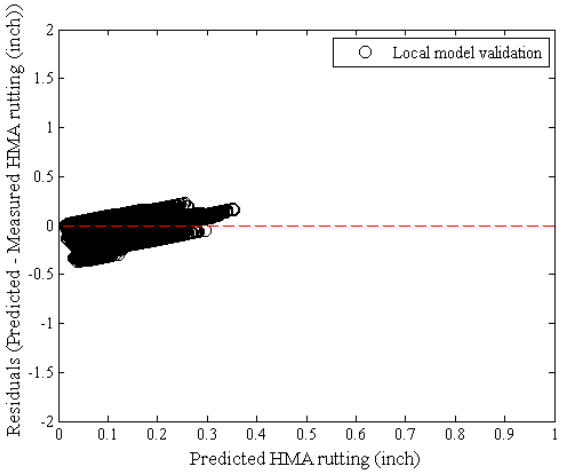

(b) HMA rutting

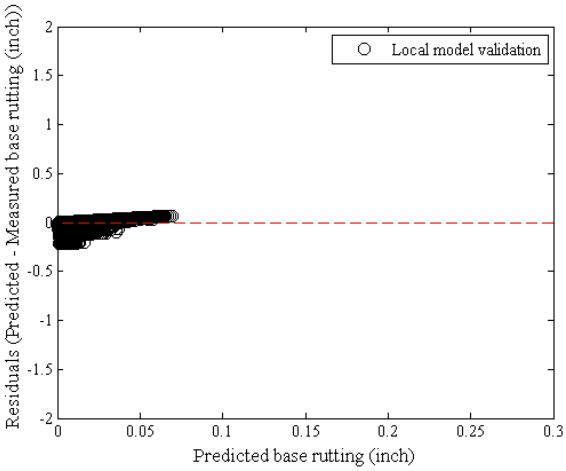

(c) Base rutting

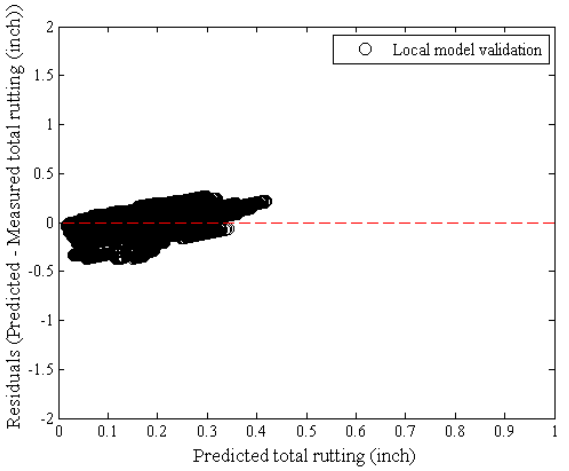

(d) Subgrade rutting

Figure B-199 Option 2: Method 2 – Rutting model validation residual plots – repeated split sampling

Reliability

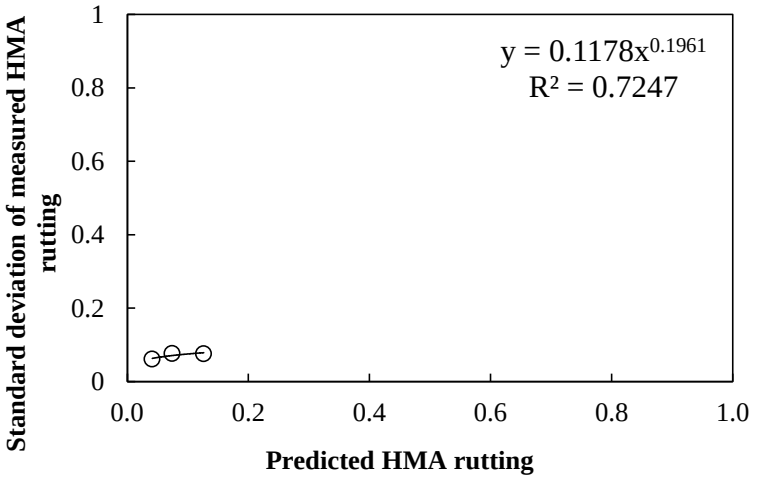

(a) HMA rutting reliability

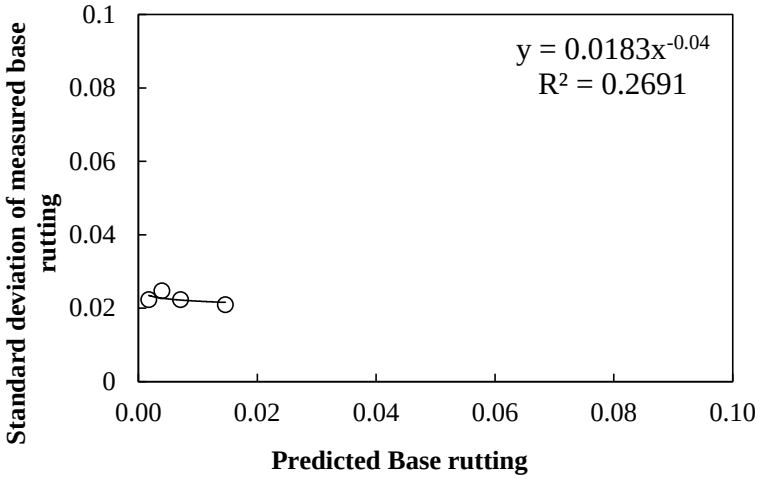

(b) Base rutting reliability

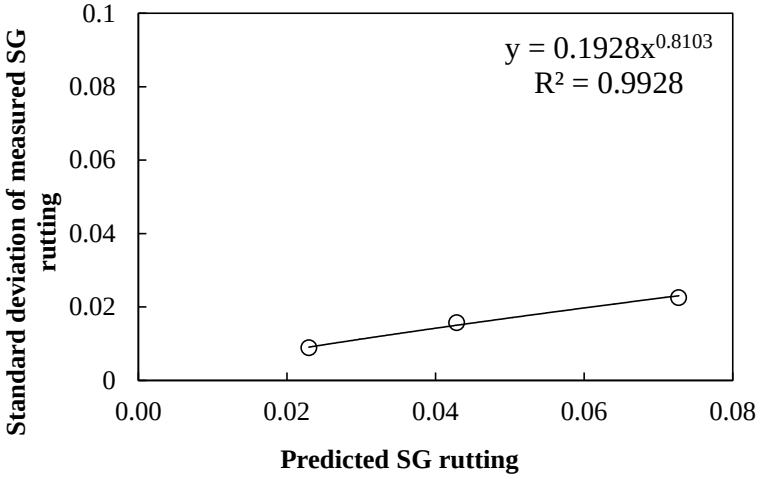

(c) Subgrade rutting reliability

Figure B-200 Rutting model reliability equations – option 2 method 2 – repeated split sampling

Bootstrapping

Table B-107 Option 2: Method 2 – Global model SEE and bias – bootstrapping

Calibration set	Average SEE	SEE Lower CI	SEE Upper CI	Average bias (in.)	Bias Lower CI	Bias Upper CI
AC rutting	0.0779	0.0709	0.0852	-0.0019	-0.0116	0.0079
Base rutting	0.1403	0.1241	0.1577	0.1163	0.1034	0.1305
Subgrade rutting	0.2234	0.2125	0.2351	0.2100	0.1982	0.2220
Total rutting	0.3574	0.3344	0.3799	0.3244	0.3011	0.3479

Table B-108 Option 2: Method 2 – Local model SEE and bias – bootstrapping

Calibration set	AC rutting	Base rutting	Subgrade rutting	Total rutting
Average SEE	0.0919	0.0271	0.0684	0.0823
SEE Lower CI	0.0743	0.0205	0.0364	0.0749
SEE Upper CI	0.1125	0.0344	0.0959	0.0902
Average bias (in.)	-0.0543	-0.0120	0.0611	-0.0051
Bias Lower CI	-0.0838	-0.0195	0.0289	-0.0086
Bias Upper CI	-0.0204	0.0025	0.0885	-0.0021
Average calibration coefficient	0.6201	0.0449	0.3184	N/A
Calibration coefficient Lower CI	0.4031	0.0100	0.1729	N/A
Calibration coefficient Upper CI	0.8857	0.1538	0.4424	N/A

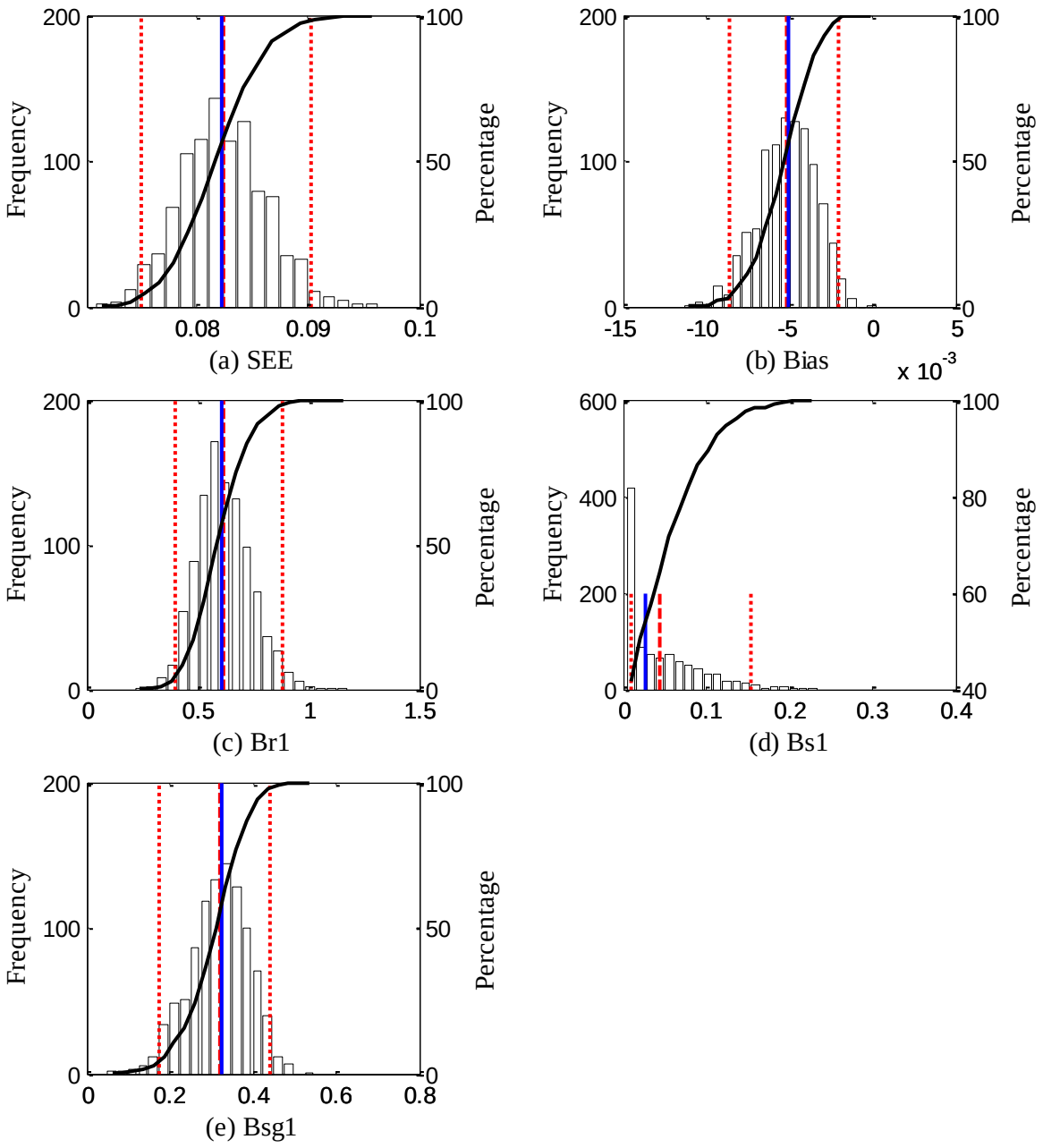

Figure B-201 Option 2: Method 2 – bootstrapping total rutting frequency distributions –calibration

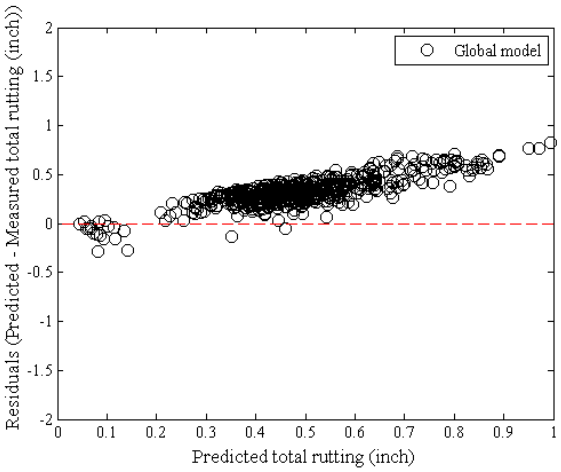

(a) Global model

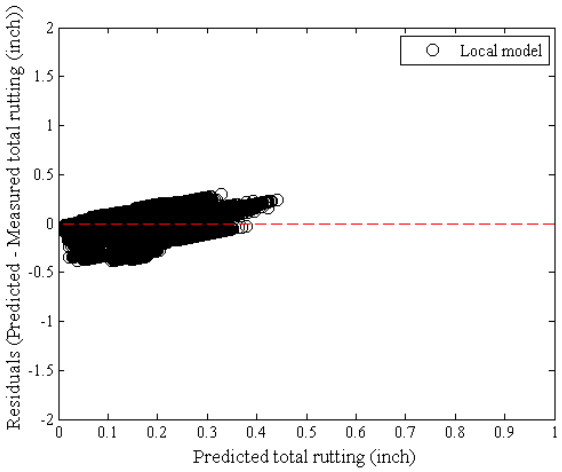

(b) Local model

Figure B-202 Option 2: Method 2 – Total rutting residual plots – bootstrapping

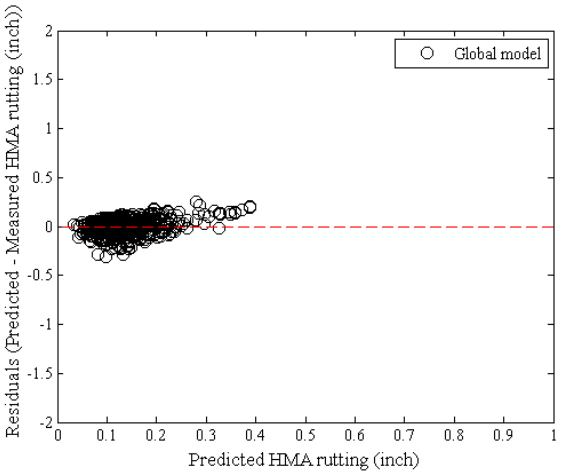

(a) Global model

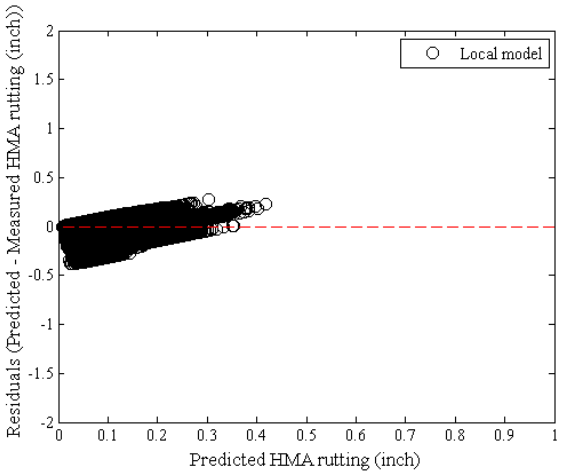

(b) Local model

Figure B-203 Option 2: Method 2 – HMA rutting residual plots - bootstrapping

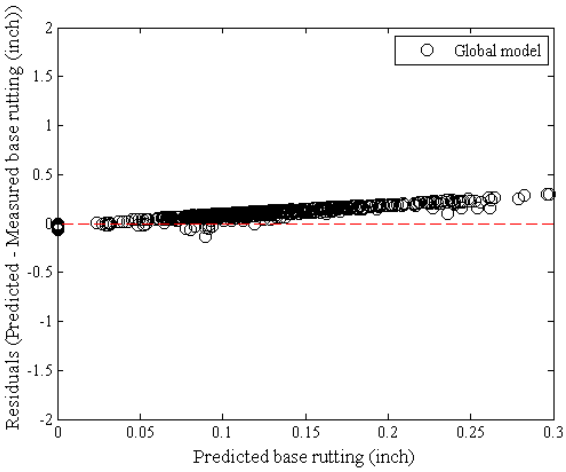

(a) Global model

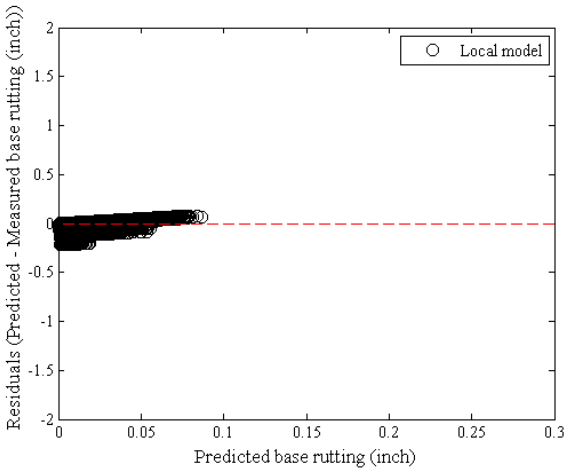

(b) Local model

Figure B-204 Option 2: Method 2 – Base rutting residual plots - bootstrapping

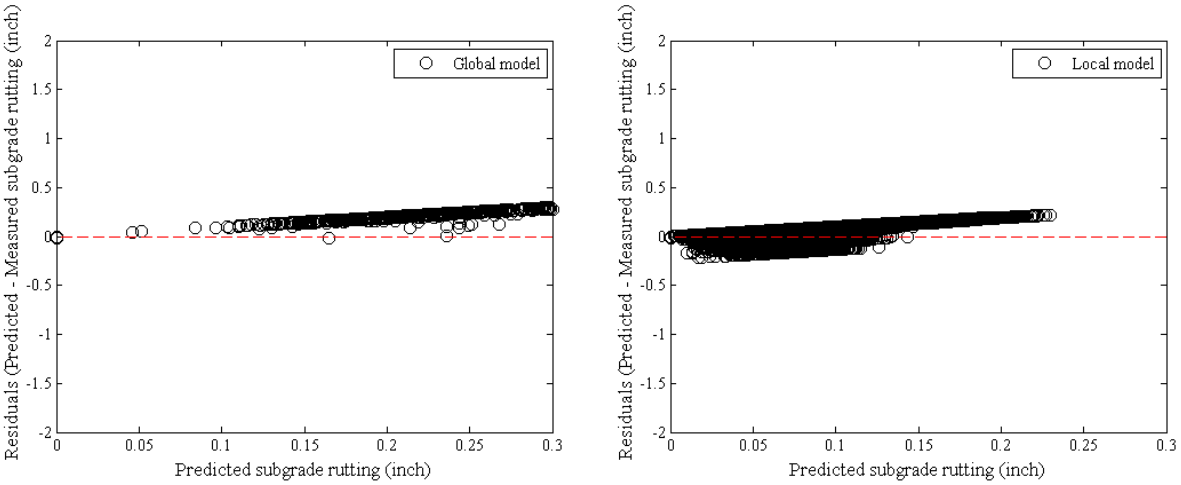

(a) Global model (b) Local model

Figure B-205 Option 2: Method 2 – Subgrade rutting residual plots - bootstrapping

Reliability

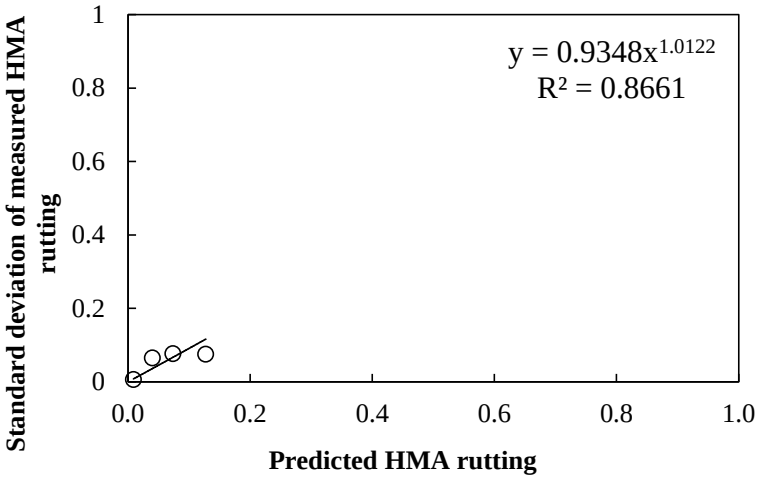

(a) HMA rutting reliability

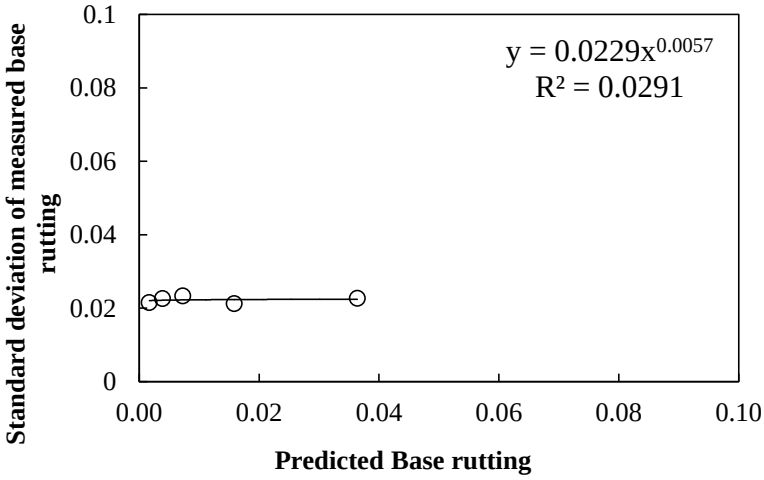

(b) Base rutting reliability

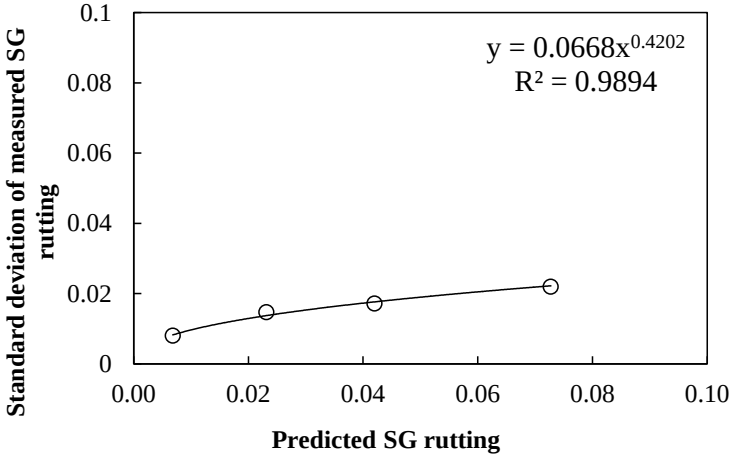

(c) Subgrade rutting reliability

Figure B-206 Rutting model reliability equations – option 2 method 2 – bootstrapping

B.1.3.5 Option 4 – Method 1

No sampling

Table B-109 Option 4: Method 1 – Global model goodness of fit – no sampling

HMA layer	SEE (in.)	Bias (in.)
AC rut	0.0763	0.0038
Base rut	0.1797	0.1323
Subgrade	0.2230	0.1959
Total rut	0.4035	0.3320

Table B-110 Option 4: Method 1 – Global model *p*-values

HMA layer	t-test p-value	Intercept p-value	Slope = 1 p-value
AC rut	0.5589	0.0000	0.0000
Base rut	0.0000	0.0000	0.0005
Subgrade	0.0000	0.0000	0.1369
Total rut	0.0000	0.0000	0.0039

Table B-111 Option 4: Method 1 – Local model goodness of fit– no sampling

HMA layer	SEE	Bias
AC rut	0.0746	-0.0113
Base rut	0.0231	-0.0072
Subgrade	0.0096	-0.0012
Total rut	0.0828	-0.0197

Table B-112 Option 4: Method 1 – Local model *p*-values– no sampling

HMA layer	t-test p-value	Intercept p-value	Slope = 1 p-value
AC rut	0.0756	0.0000	0.0000
Base rut	0.0002	0.0000	0.0000
Subgrade	0.1610	0.0000	0.0000
Total rut	0.0050	0.0000	0.0000

Table B-113 Option 4: Method 1 – Local model *p*-values– no sampling

Calibration Coefficient	Global model	Local model
HMA rutting (br1)	1.0000	0.8909
Base rutting (bs1)	1.0000	0.0597
Subgrade rutting (bsg1)	1.0000	0.0216

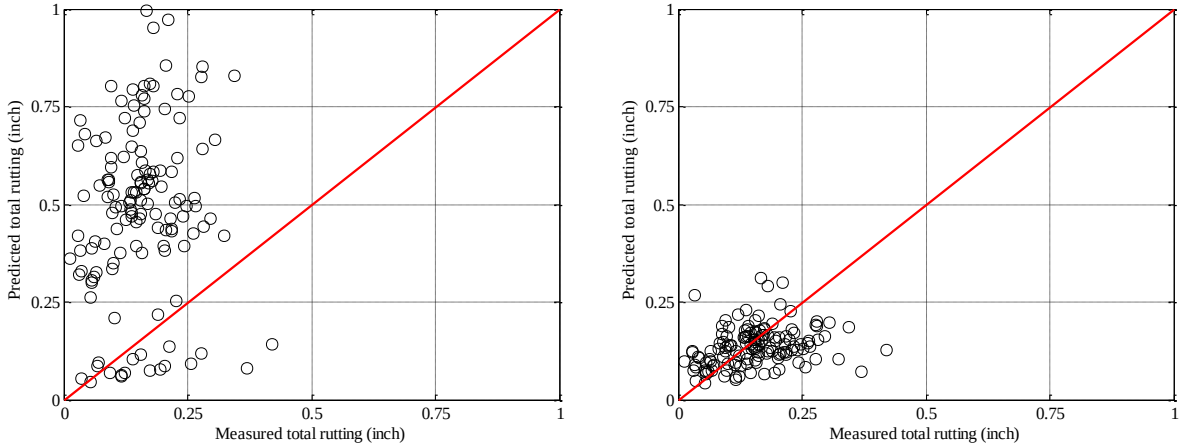

(a) Global model (b) Local model

Figure B-207 Option 4: Method 1 – Total rutting local calibration results - no sampling

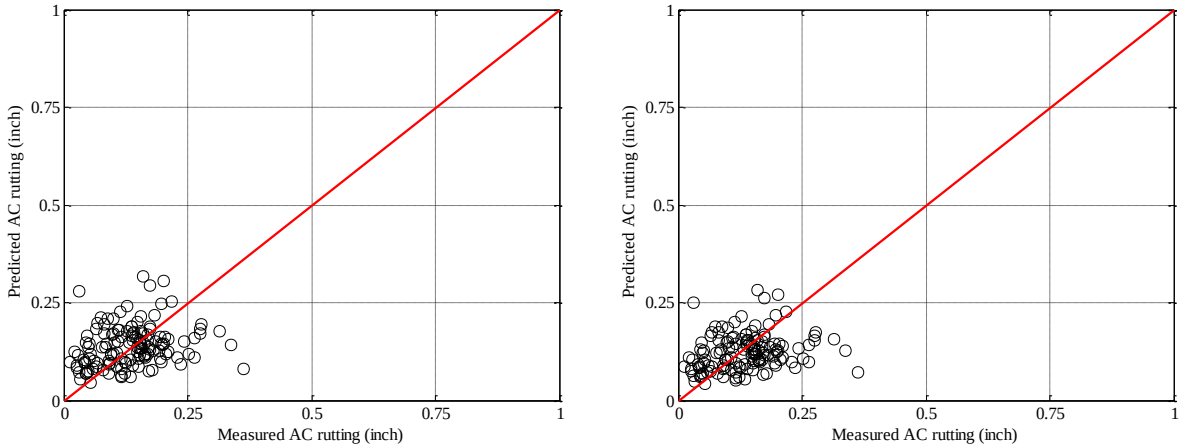

(a) Global model (b) Local model

Figure B-208 Option 4: Method 1 – HMA rutting local calibration results - no sampling

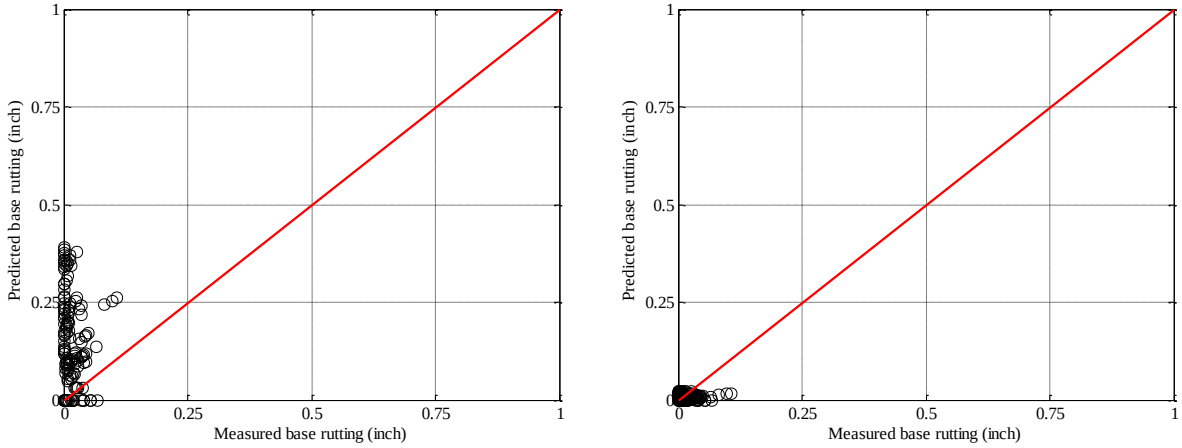

(a) Global model (b) Local model

Figure B-209 Option 4: Method 1 – Base rutting local calibration results - no sampling

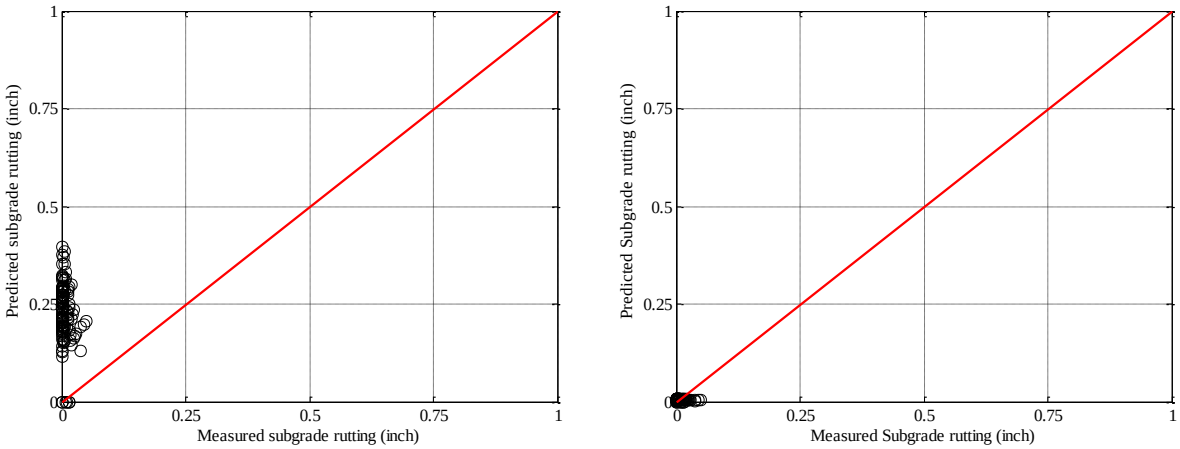

(a) Global model (b) Local model

Figure B-210 Option 4: Method 1 – Subgrade rutting local calibration results - no sampling

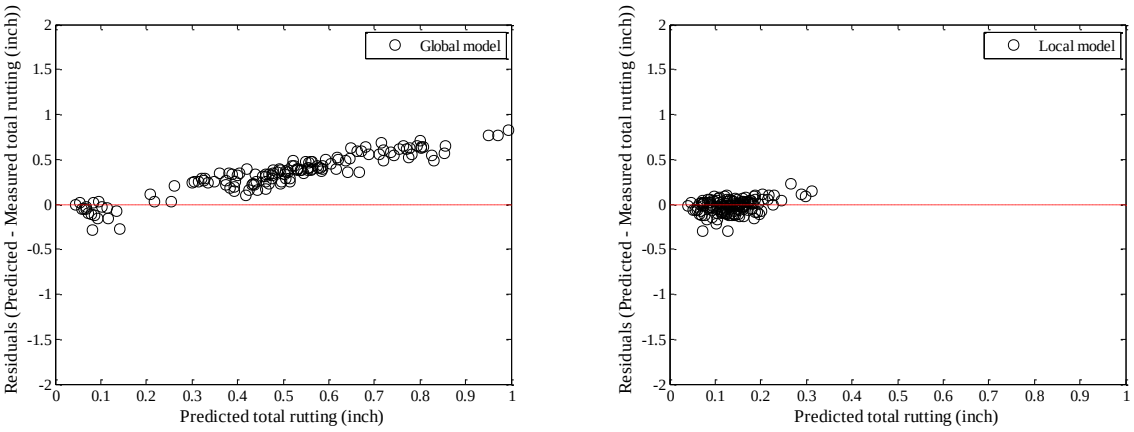

(a) Global model (b) Local model

Figure B-211 Option 4: Method 1 – Total rutting residual plots - no sampling

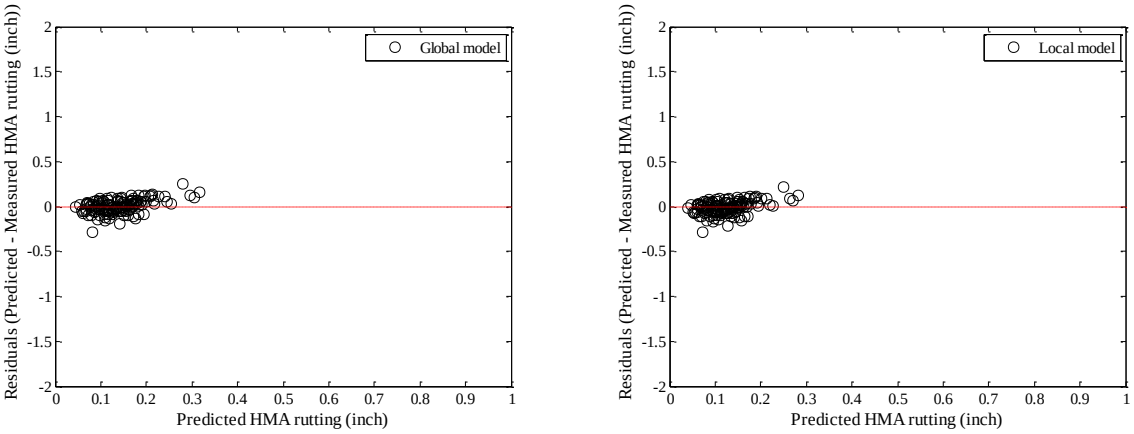

(a) Global model (b) Local model

Figure B-212 Option 4: Method 1 – HMA rutting residual plots - no sampling

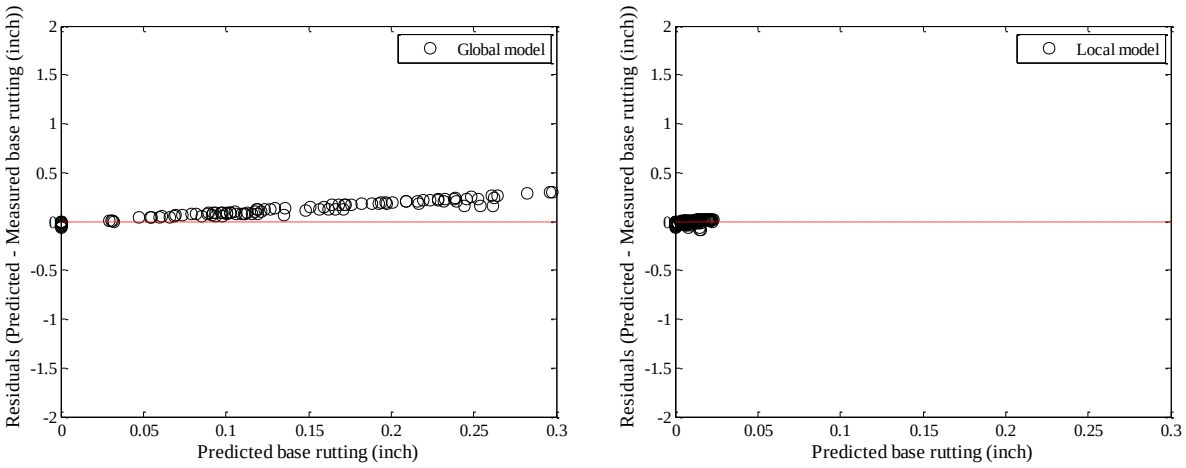

(a) Global model (b) Local model

Figure B-213 Option 4: Method 1 – Base rutting residual plots - no sampling

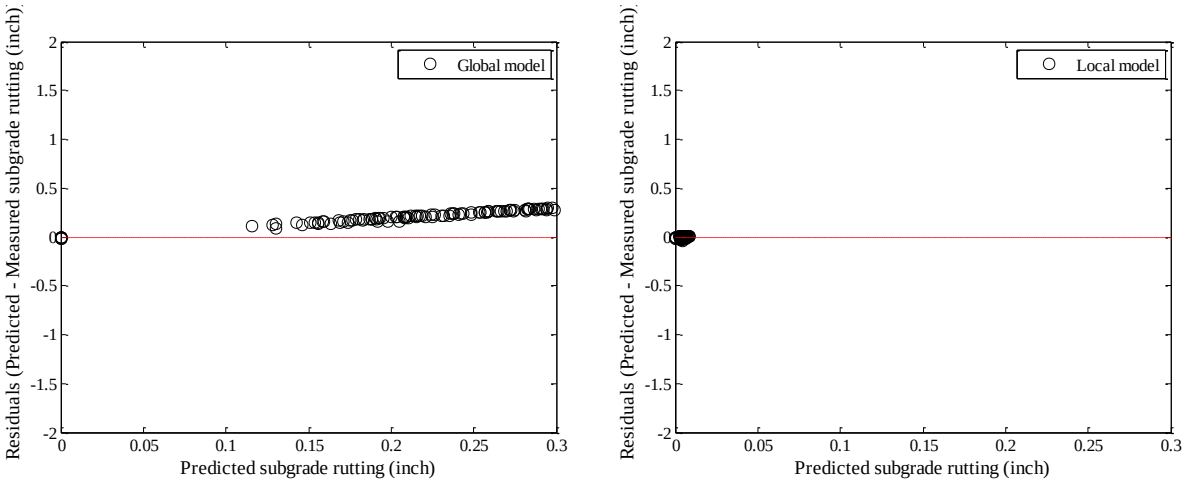

(a) Global model (b) Local model

Figure B-214 Option 4: Method 1 – Subgrade rutting residual plots - no sampling

Reliability

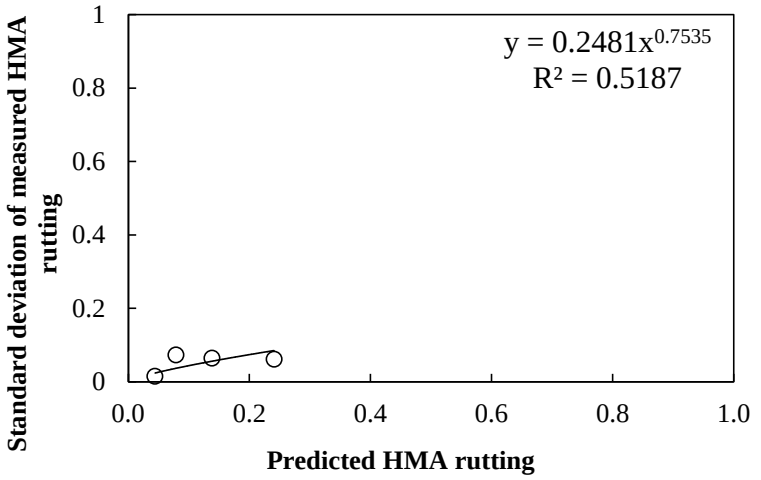

(a) HMA rutting reliability

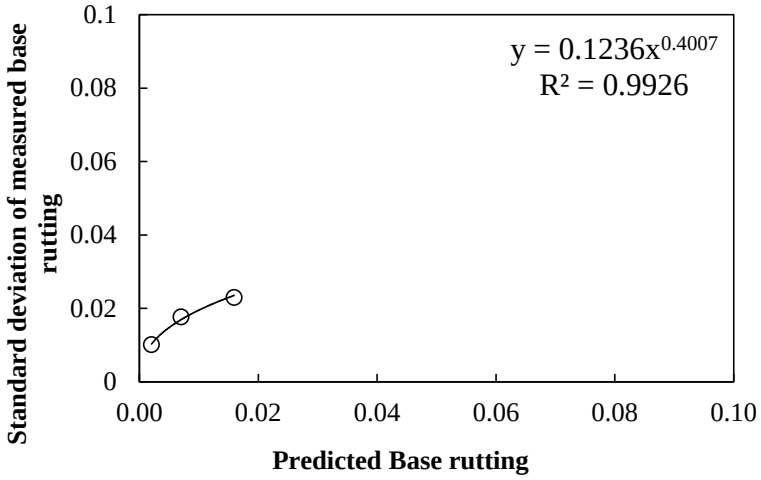

(b) Base rutting reliability

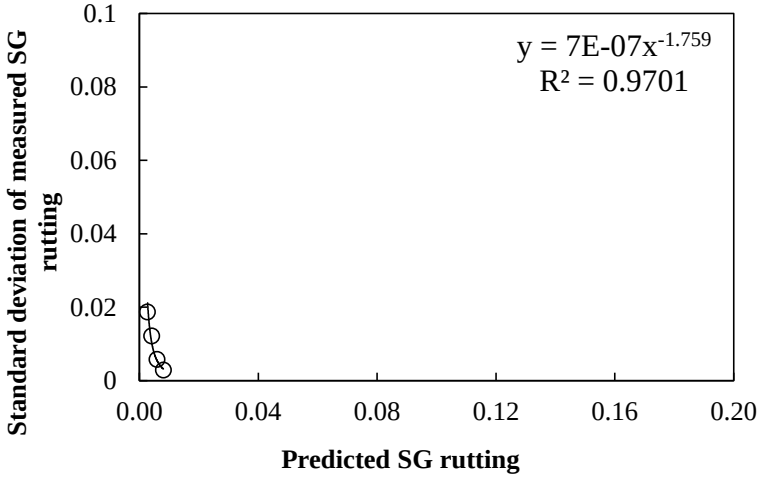

(c) Subgrade rutting reliability

Figure B-215 Rutting model reliability equations – option 4 method 1 – no sampling

Split sampling

Table B-114 Option 4: Method 1 – Global model goodness of fit – split sampling

HMA layer	SEE (in.)	Bias (in.)
AC rut	0.0791	0.0004
Base rut	0.1873	0.1356
Subgrade	0.2236	0.1915
Total rut	0.4145	0.3275

Table B-115 Option 4: Method 1 – Global model *p*-values - split sampling

HMA layer	t-test p-value	Intercept p-value	Slope = 1 p-value
AC rut	0.9591	0.0000	0.0000
Base rut	0.0000	0.0000	0.0056
Subgrade	0.0000	0.0000	0.0446
Total rut	0.0000	0.0000	0.0030

Table B-116 Option 4: Method 1 – Local model goodness of fit– split sampling

HMA layer	SEE	Bias
AC rut	0.0780	-0.0118
Base rut	0.0263	-0.0082
Subgrade	0.0112	-0.0018
Total rut	0.0877	-0.0218

Table B-117 Option 4: Method 1 – Local model *p*-values– split sampling

HMA layer	t-test p-value	Intercept p-value	Slope = 1 p-value
AC rut	0.1472	0.0000	0.0000
Base rut	0.0025	0.0000	0.0000
Subgrade	0.1161	0.0000	0.0000
Total rut	0.0161	0.0000	0.0000

Table B-118 Option 4: Method 1 – Local model *p*-values – split sampling

Calibration Coefficient	Global model	Local model
HMA rutting (br1)	1.0000	0.9108
Base rutting (bs1)	1.0000	0.0678
Subgrade rutting (bsg1)	1.0000	0.0223

Table B-119 Option 4: Method 1 – Local model validation p-values – split sampling

HMA layer	t-test p-value	Intercept p-value	Slope = 1 p-value
AC rut	0.8408	0.0000	0.0000
Base rut	0.4581	0.0000	0.0000
Subgrade	0.4242	0.0000	0.0000
Total rut	0.7720	0.0000	0.0000

Table B-120 Option 4: Method 1 – Local model validation SEE and bias – split sampling

HMA layer	SEE	Bias
AC rut	0.0691	-0.0021
Base rut	0.0156	-0.0017
Subgrade	0.0053	0.0006
Total rut	0.0731	-0.0031

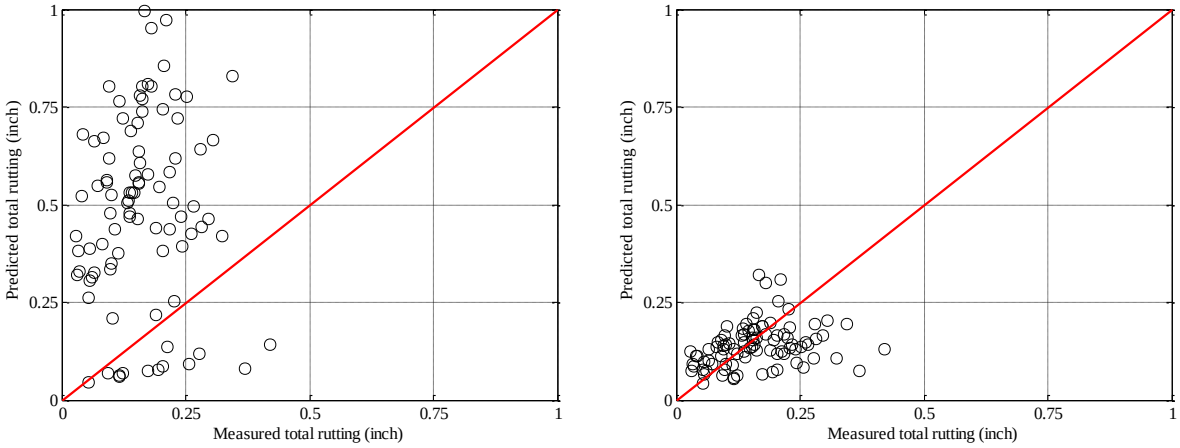

(a) Global model (b) Local model

Figure B-216 Option 4: Method 1 – Total rutting local calibration results - split sampling

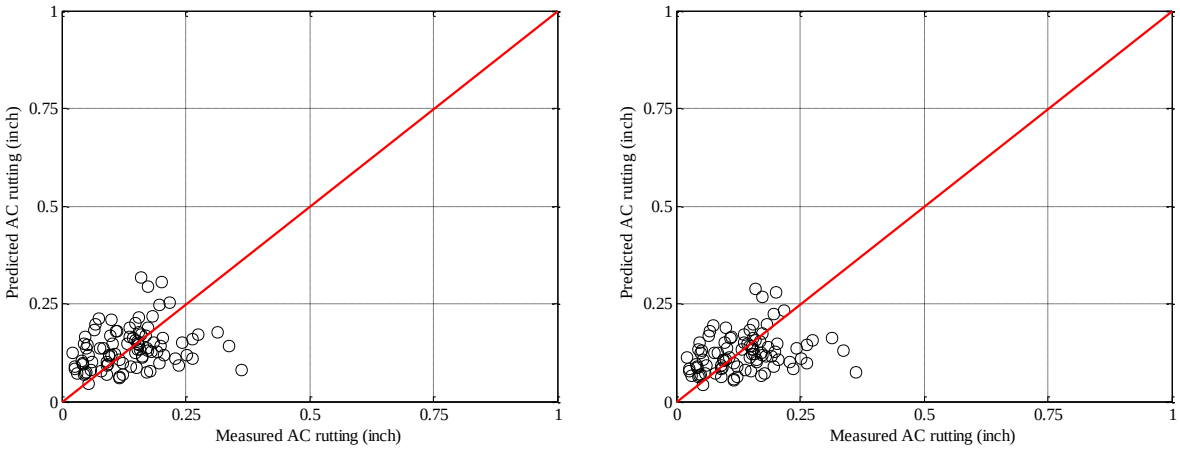

(a) Global model (b) Local model

Figure B-217 Option 4: Method 1 – HMA rutting local calibration results - split sampling

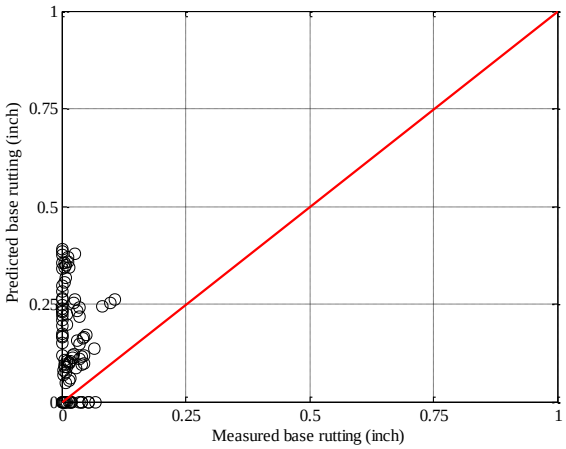

(a) Global model

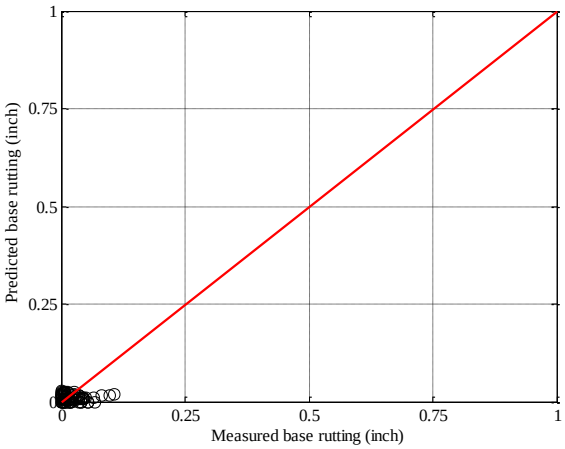

(b) Local model

Figure B-218 Option 4: Method 1 – Base rutting local calibration results - split sampling

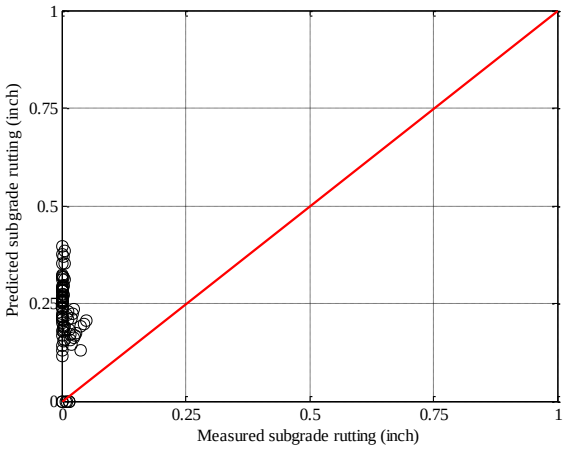

(a) Global model

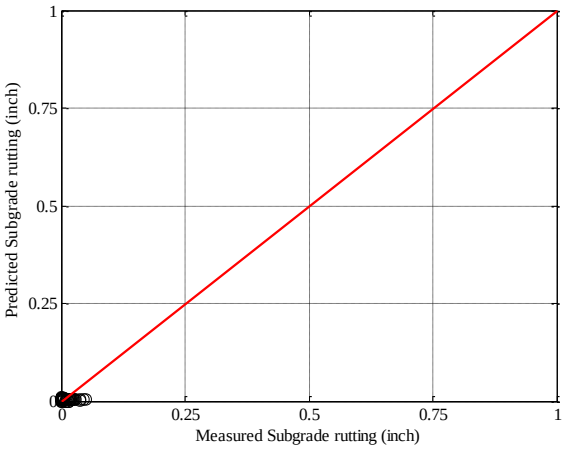

(b) Local model

Figure B-219 Option 4: Method 1 – Subgrade rutting local calibration results - split sampling

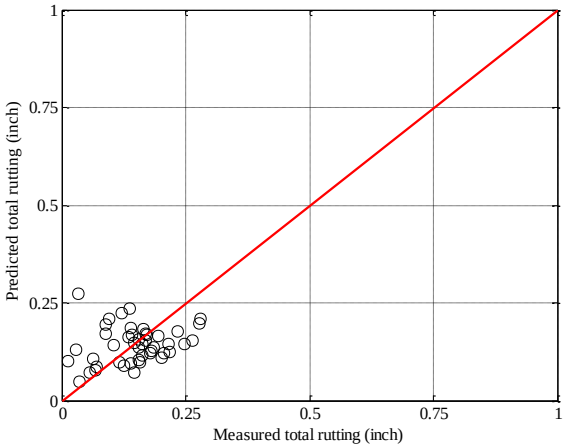

(a) Total rutting

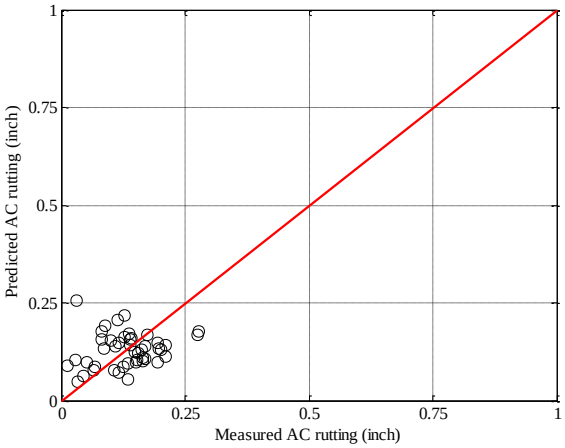

(b) HMA rutting

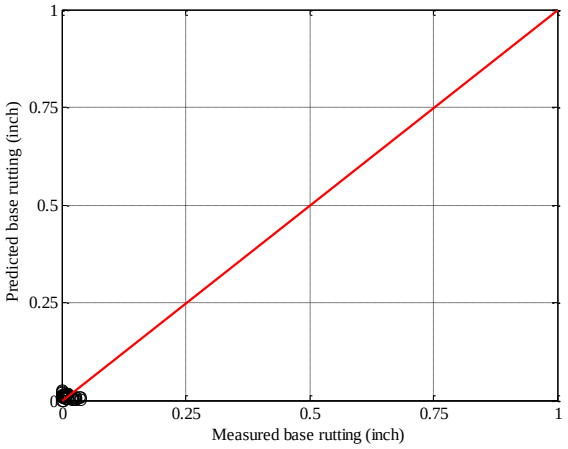

(c) Base rutting

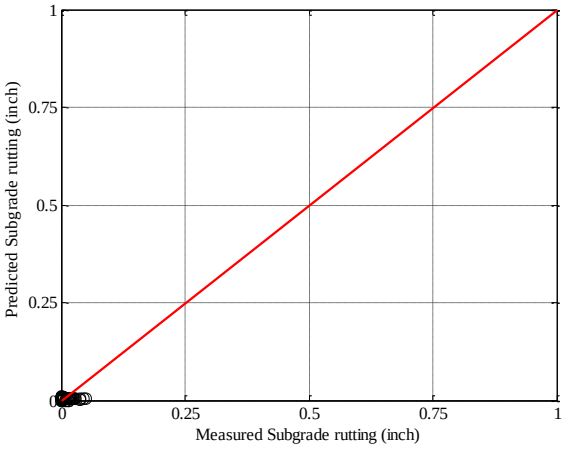

(d) Subgrade rutting

Figure B-220 Option 4: Method 1 – Rutting model validation – split sampling

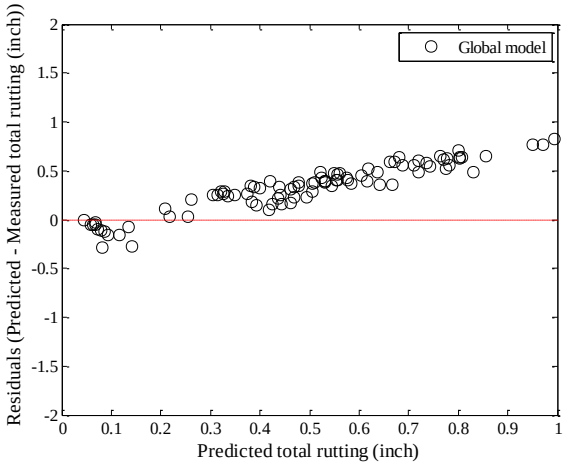

(a) Global model

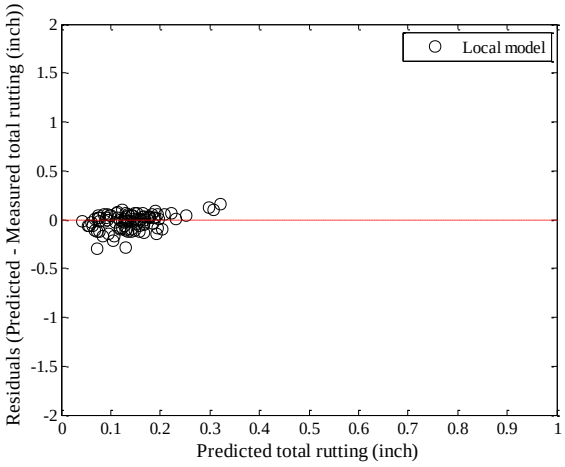

(b) Local model

Figure B-221 Option 4: Method 1 – Total rutting residual plots - split sampling

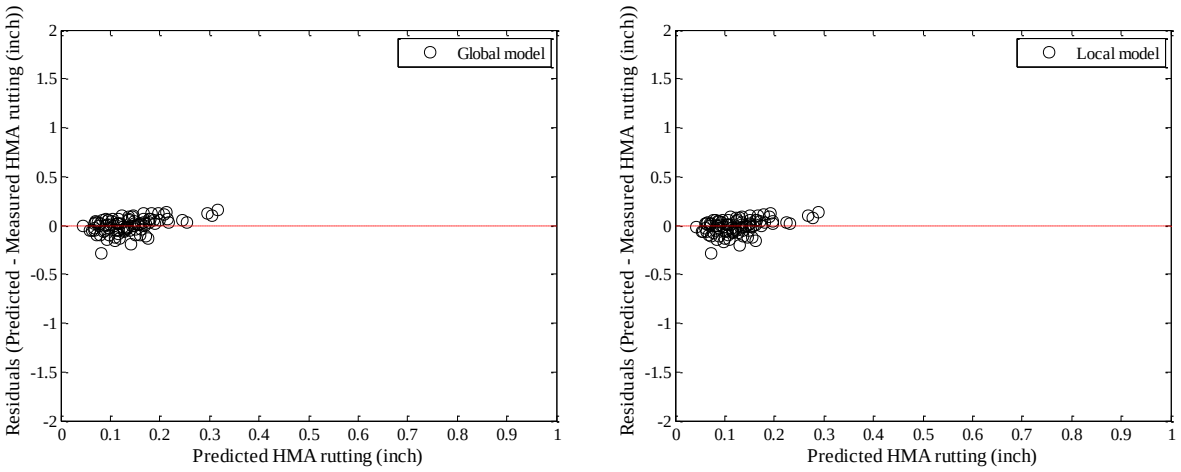

(a) Global model (b) Local model

Figure B-222 Option 4: Method 1 – HMA rutting residual plots - split sampling

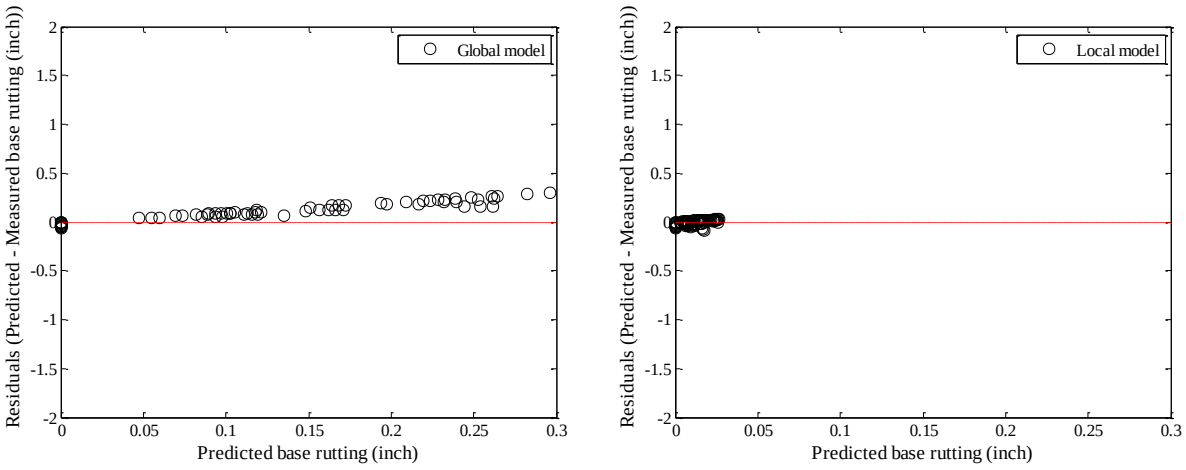

(a) Global model (b) Local model

Figure B-223 Option 4: Method 1 – Base rutting residual plots - split sampling

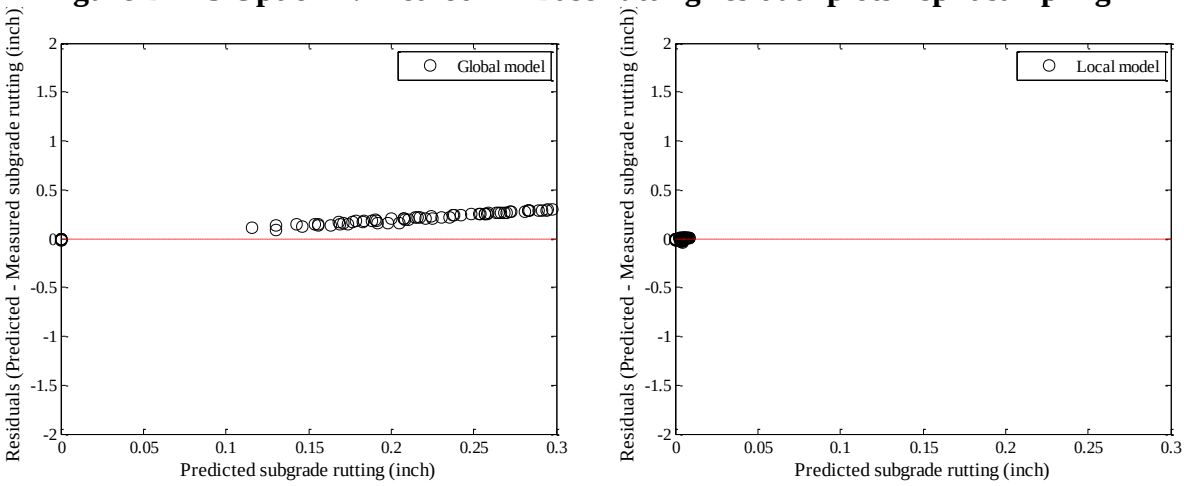

(a) Global model (b) Local model

Figure B-224 Option 4: Method 1 – Subgrade rutting residual plots - split sampling

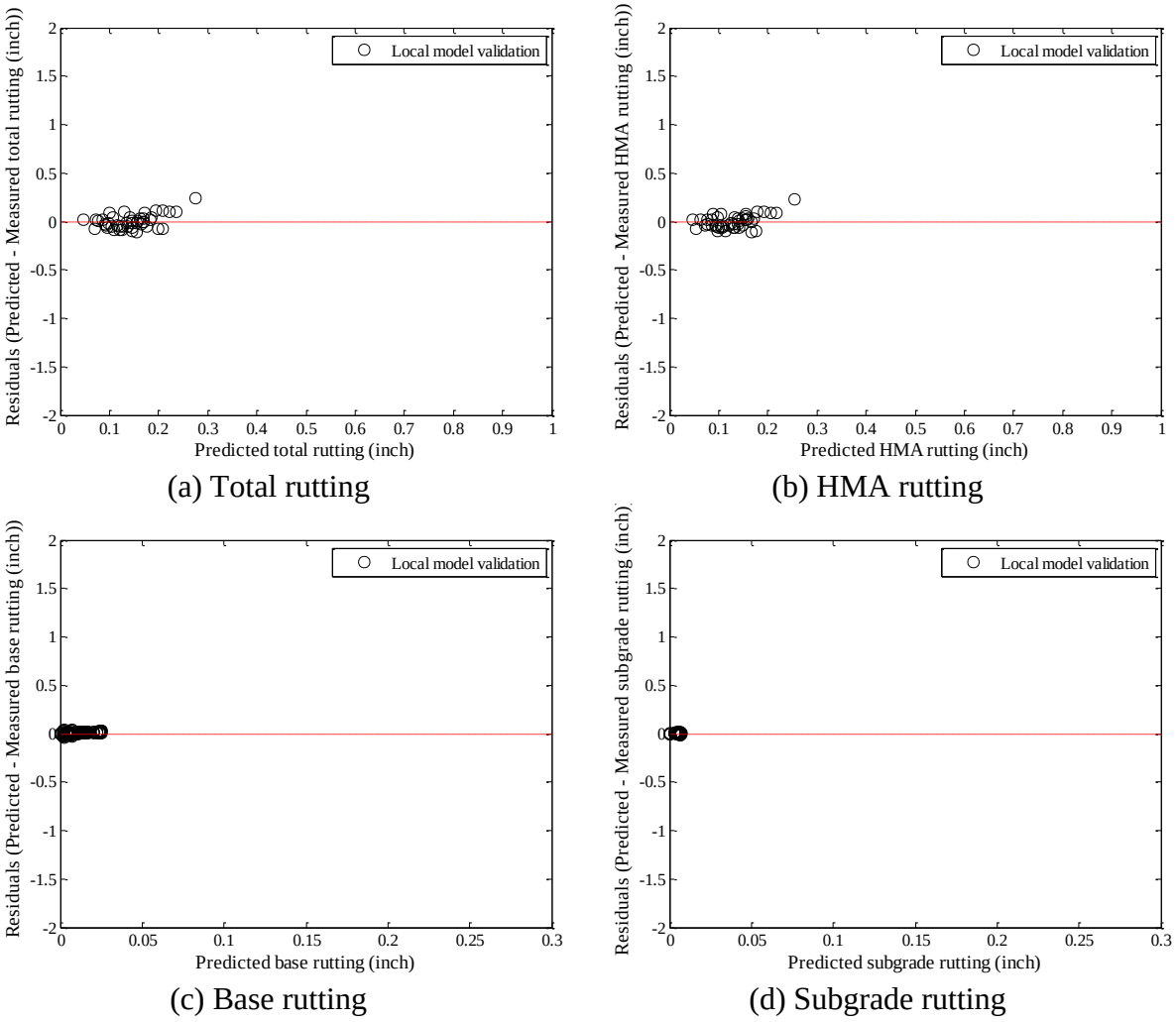

(a) Total rutting (b) HMA rutting

(c) Base rutting (d) Subgrade rutting

Figure B-225 Option 4: Method 1 – Rutting model validation residual plots – split sampling

Reliability

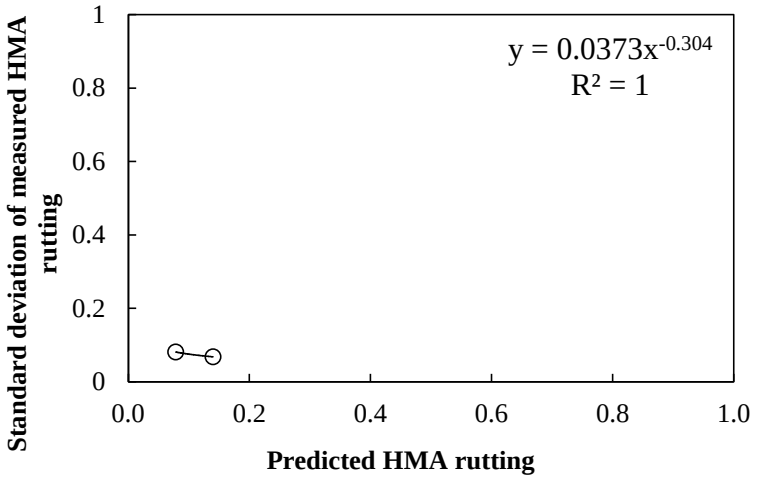

(a) HMA rutting reliability

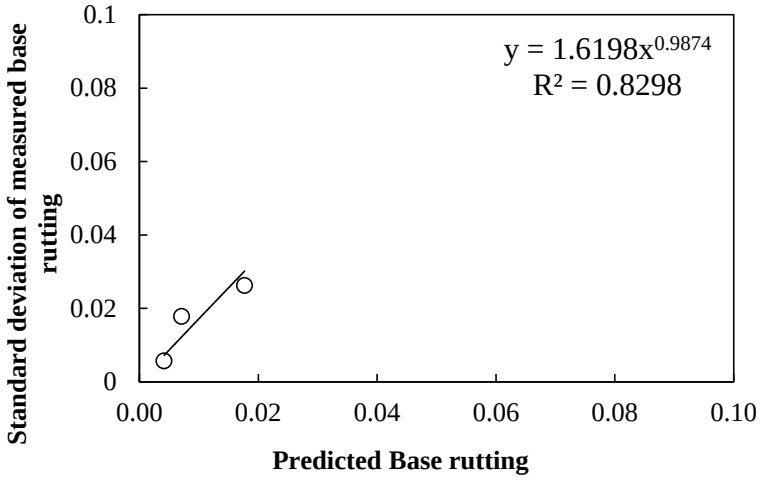

(b) Base rutting reliability

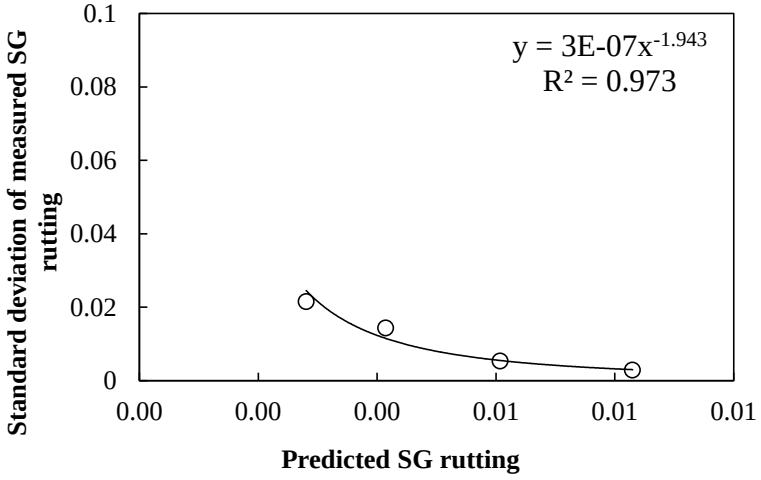

(c) Subgrade rutting reliability

Figure B-226 Rutting model reliability equations – option 4 method 1 – split sampling

Repeated split sampling

Table B-121 Option 4: Method 1 – Global model SEE and bias – repeated split sampling

Global Model	Average SEE	SEE Lower CI	SEE Upper CI	Average bias (in.)	Bias Lower CI	Bias Upper CI
AC rutting	0.0764	0.0657	0.0850	0.0034	-0.0117	0.0163
Base rutting	0.1801	0.1485	0.2054	0.1325	0.1027	0.1600
Subgrade rutting	0.2234	0.2053	0.2401	0.1957	0.1744	0.2180
Total rutting	0.4042	0.3560	0.4415	0.3317	0.2811	0.3808

Table B-122 Option 4: Method 1 – Local model SEE and bias – repeated split sampling

Calibration set	AC rutting	Base rutting	Subgrade rutting	Total rutting
Average SEE	0.0742	0.0228	0.0094	0.0823
SEE Lower CI	0.0650	0.0170	0.0052	0.0708
SEE Upper CI	0.0821	0.0265	0.0114	0.0921
Average bias (in.)	-0.0110	-0.0072	-0.0011	-0.0193
Bias Lower CI	-0.0155	-0.0095	-0.0018	-0.0247
Bias Upper CI	-0.0050	-0.0048	-0.0004	-0.0135
Average calibration coefficient	0.8979	0.0601	0.0217	N/A
Calibration coefficient Lower CI	0.8091	0.0313	0.0121	N/A
Calibration coefficient Upper CI	1.0260	0.0909	0.0299	N/A

Table B-123 Option 4: Method 1 – Local model validation SEE and bias – repeated split sampling

Validation set	AC rutting	Base rutting	Subgrade rutting	Total rutting
Average SEE	0.0780	0.0239	0.0094	0.0862
SEE Lower CI	0.0559	0.0133	0.0047	0.0604
SEE Upper CI	0.0991	0.0350	0.0163	0.1109
Average bias (in.)	-0.0099	-0.0072	-0.0011	-0.0183
Bias Lower CI	-0.0532	-0.0222	-0.0083	-0.0614
Bias Upper CI	0.0391	0.0085	0.0049	0.0321
Average calibration coefficient	0.8979	0.0601	0.0217	N/A
Calibration coefficient Lower CI	0.8091	0.0313	0.0121	N/A
Calibration coefficient Upper CI	1.0260	0.0909	0.0299	N/A

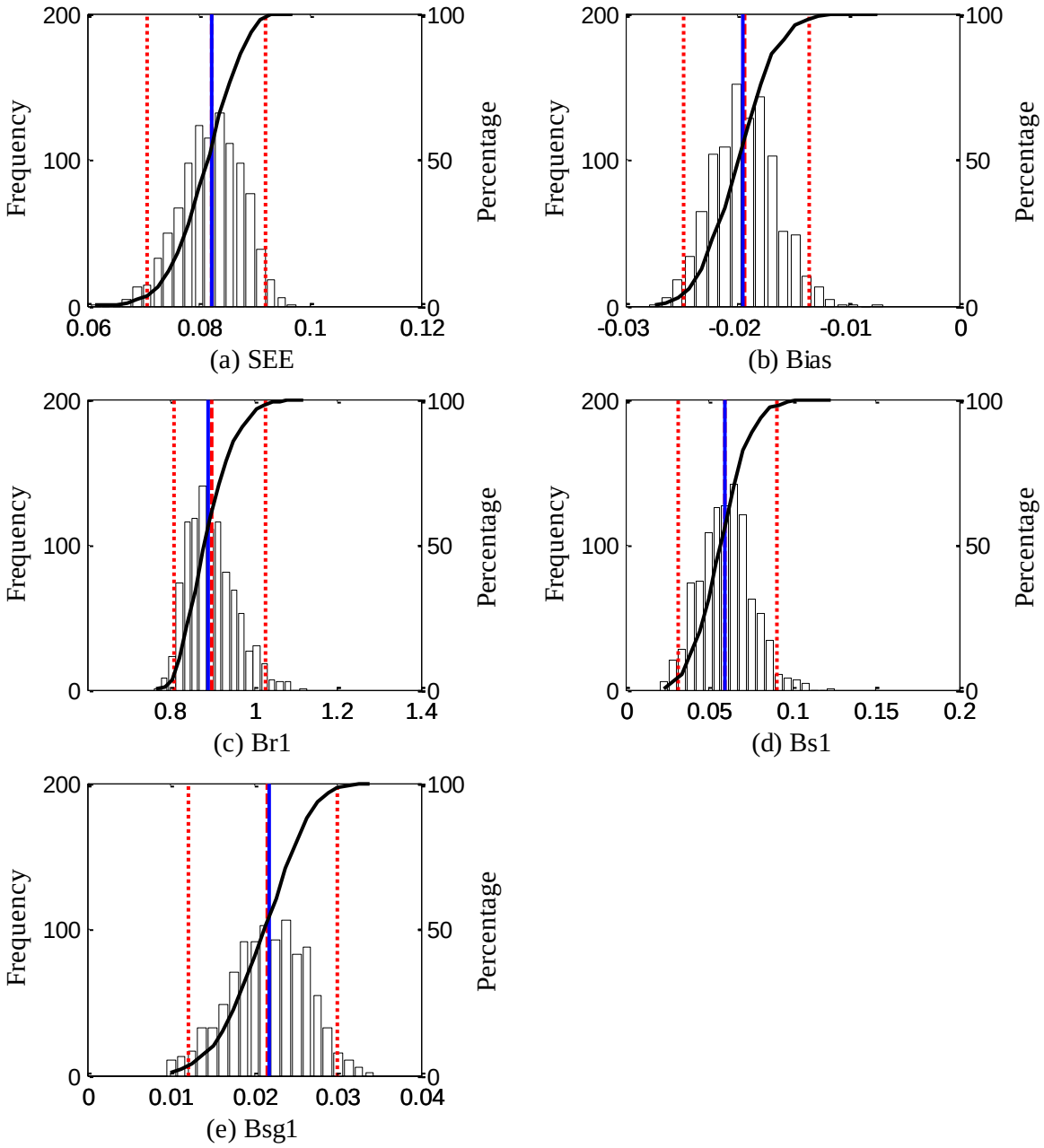

Figure B-227 Option 4: Method 1 – repeated split sampling total rutting frequency distributions – calibration

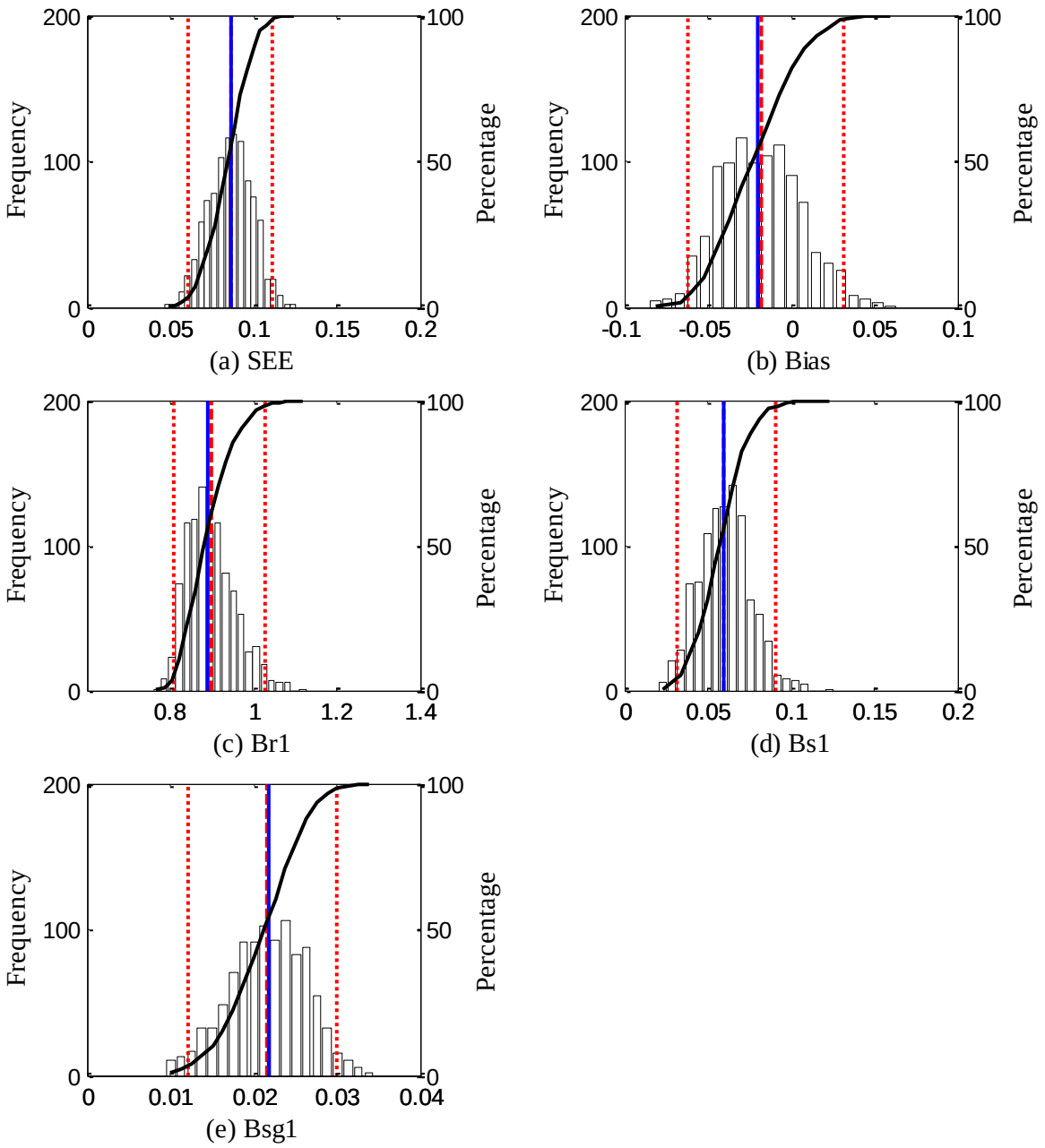

Figure B-228 Option 4: Method 1 – repeated split sampling total rutting frequency distributions – validation

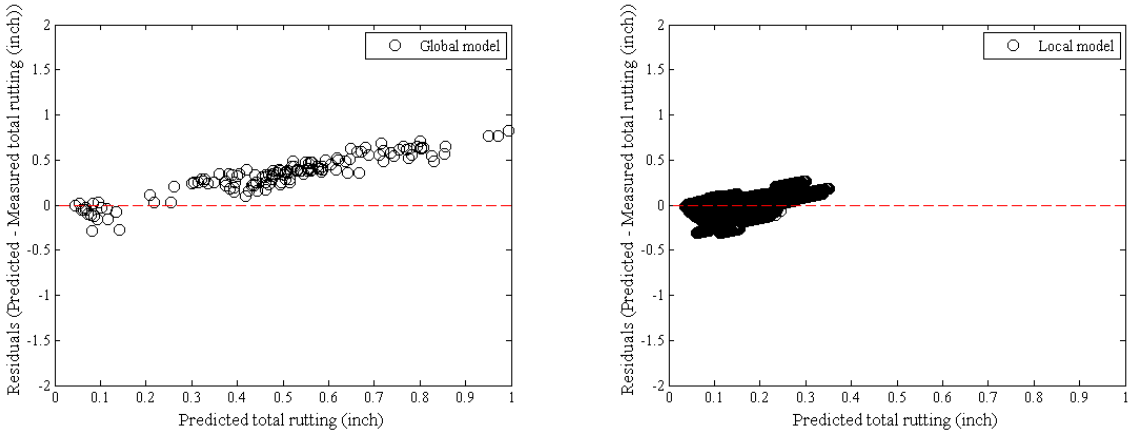

(a) Global model (b) Local model

Figure B-229 Option 4: Method 1 – Total rutting residual plots – repeated split sampling

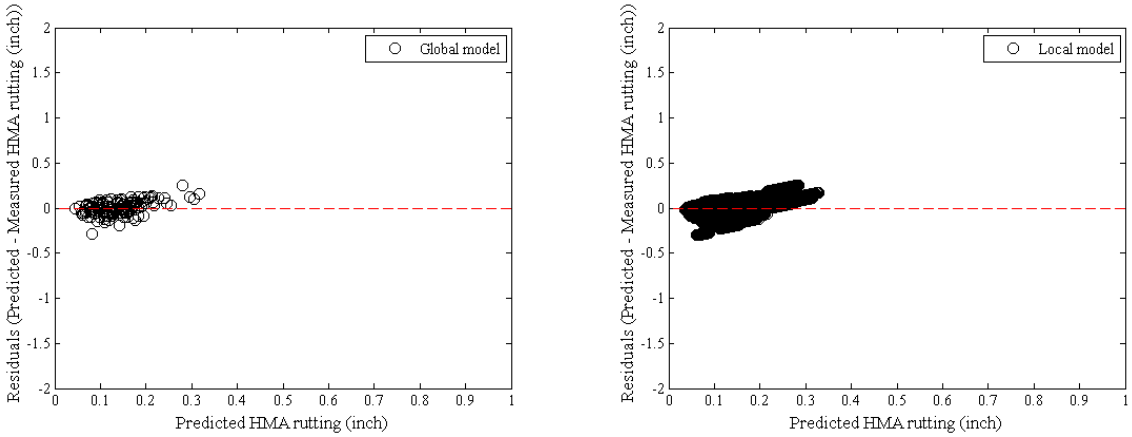

(a) Global model (b) Local model

Figure B-230 Option 4: Method 1 – HMA rutting residual plots - repeated split sampling

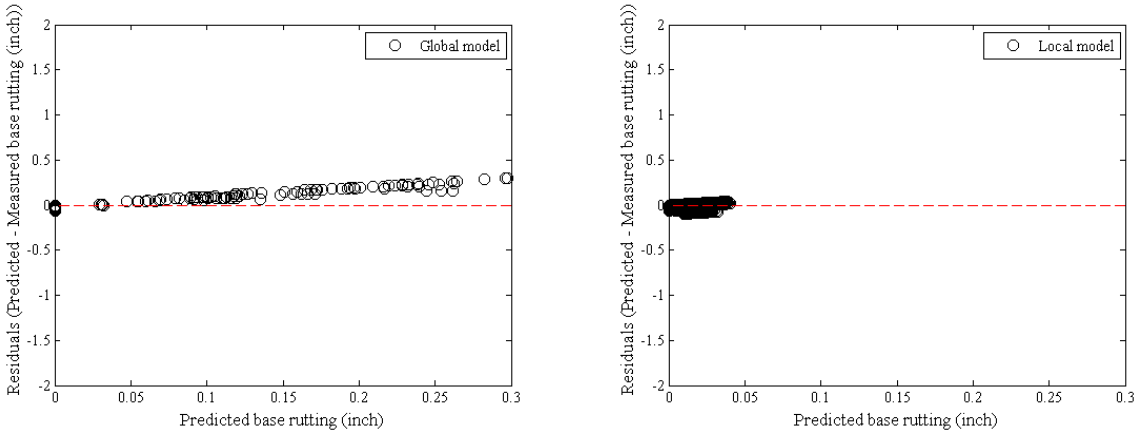

(a) Global model (b) Local model

Figure B-231 Option 4: Method 1 – Base rutting residual plots - repeated split sampling

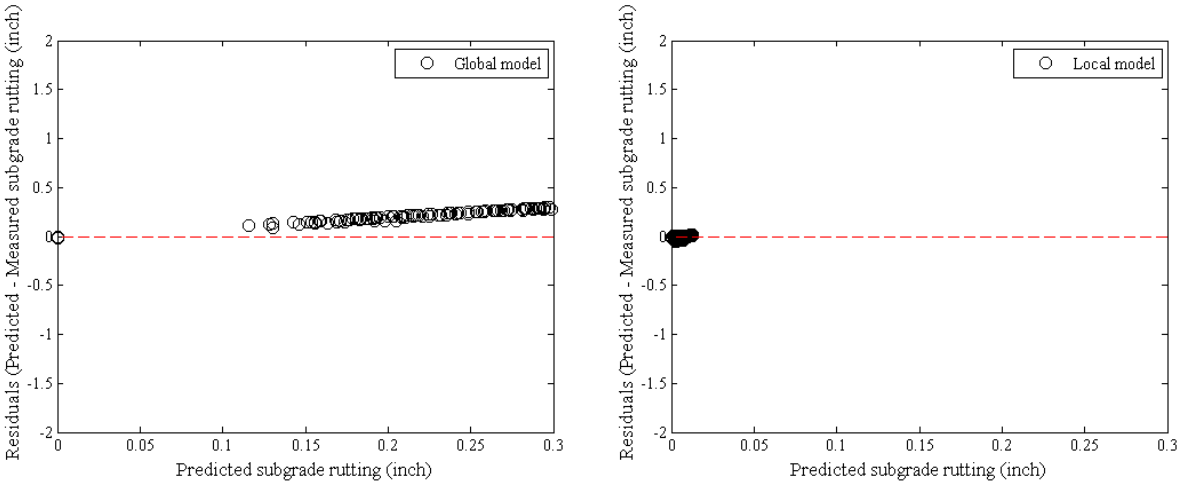

(a) Global model (b) Local model

Figure B-232 Option 4: Method 1 – Subgrade rutting residual plots - repeated split sampling

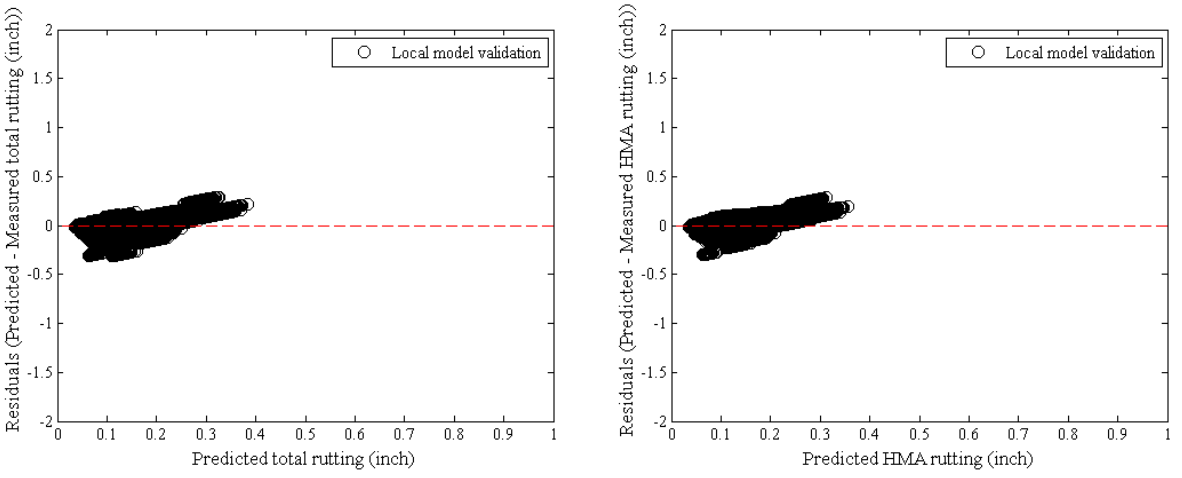

(a) Total rutting (b) HMA rutting

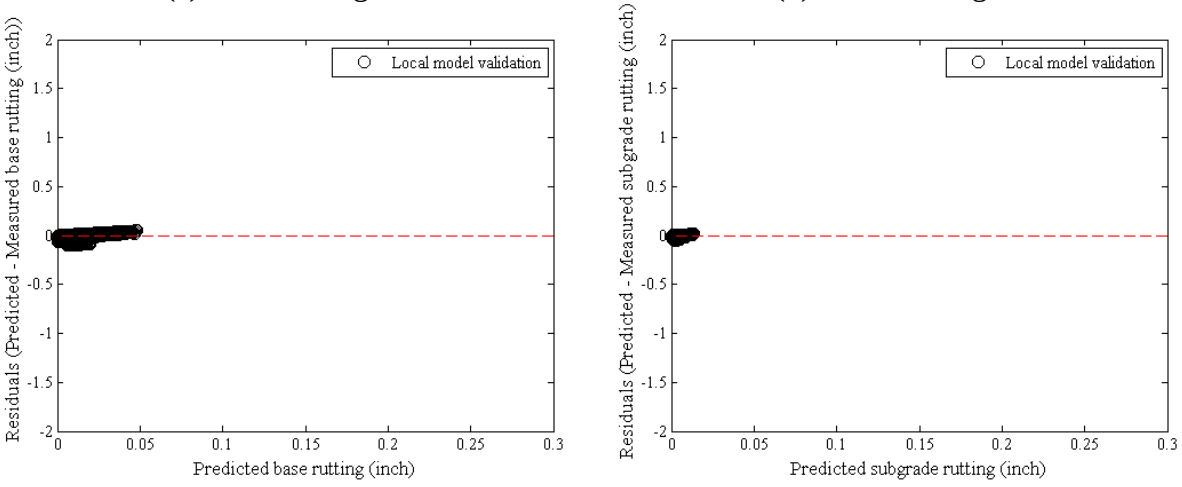

(c) Base rutting (d) Subgrade rutting

Figure B-233 Option 4: Method 1 – Rutting model validation residual plots – repeated split sampling

Reliability

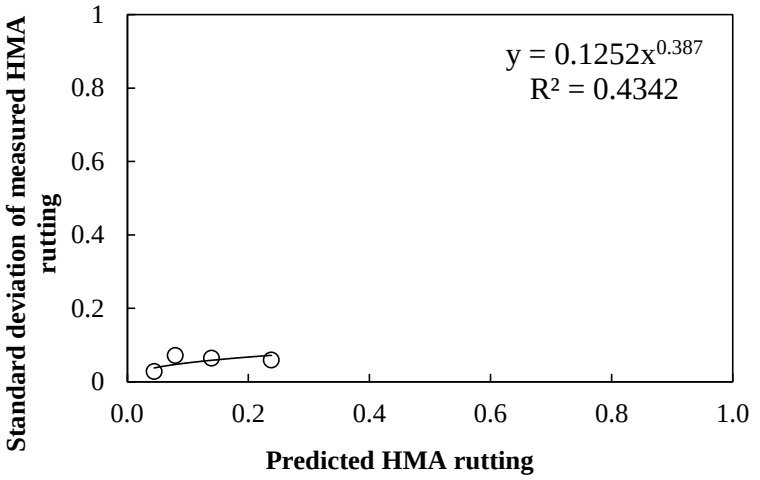

(a) HMA rutting reliability

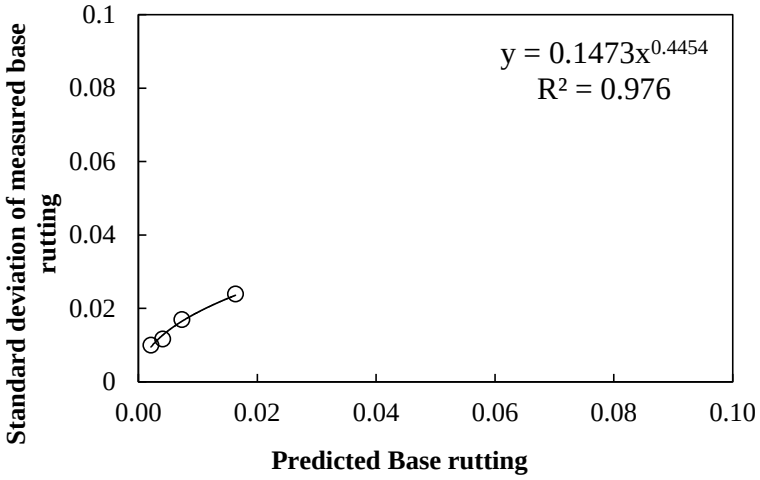

(b) Base rutting reliability

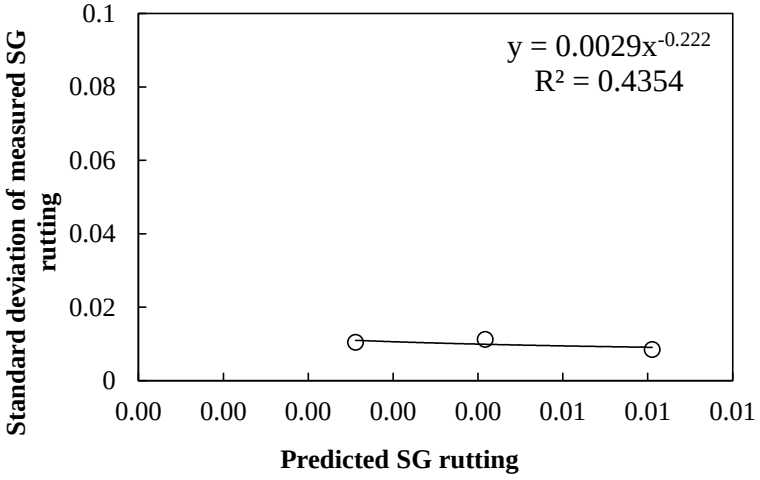

(c) Subgrade rutting reliability

Figure B-234 Rutting model reliability equations – option 4 method 1 – repeated split sampling

Bootstrapping

Table B-124 Option 4: Method 1 – Global model SEE and bias – bootstrapping

Calibration set	Average SEE	SEE Lower CI	SEE Upper CI	Average bias (in.)	Bias Lower CI	Bias Upper CI
AC rutting	0.0762	0.0624	0.0912	0.0030	-0.0176	0.0253
Base rutting	0.1789	0.1350	0.2213	0.1324	0.0886	0.1766
Subgrade rutting	0.2228	0.1964	0.2502	0.1958	0.1635	0.2305
Total rutting	0.4029	0.3402	0.4669	0.3313	0.2559	0.4090

Table B-125 Option 4: Method 1 – Local model SEE and bias – bootstrapping

Calibration set	AC rutting	Base rutting	Subgrade rutting	Total rutting
Average SEE	0.0737	0.0225	0.0092	0.0817
SEE Lower CI	0.0609	0.0157	0.0046	0.0657
SEE Upper CI	0.0885	0.0293	0.0134	0.0979
Average bias (in.)	-0.0109	-0.0071	-0.0011	-0.0191
Bias Lower CI	-0.0179	-0.0109	-0.0021	-0.0276
Bias Upper CI	-0.0032	-0.0037	-0.0002	-0.0110
Average calibration coefficient	0.9032	0.0612	0.0216	N/A
Calibration coefficient Lower CI	0.7529	0.0273	0.0107	N/A
Calibration coefficient Upper CI	1.0876	0.1114	0.0352	N/A

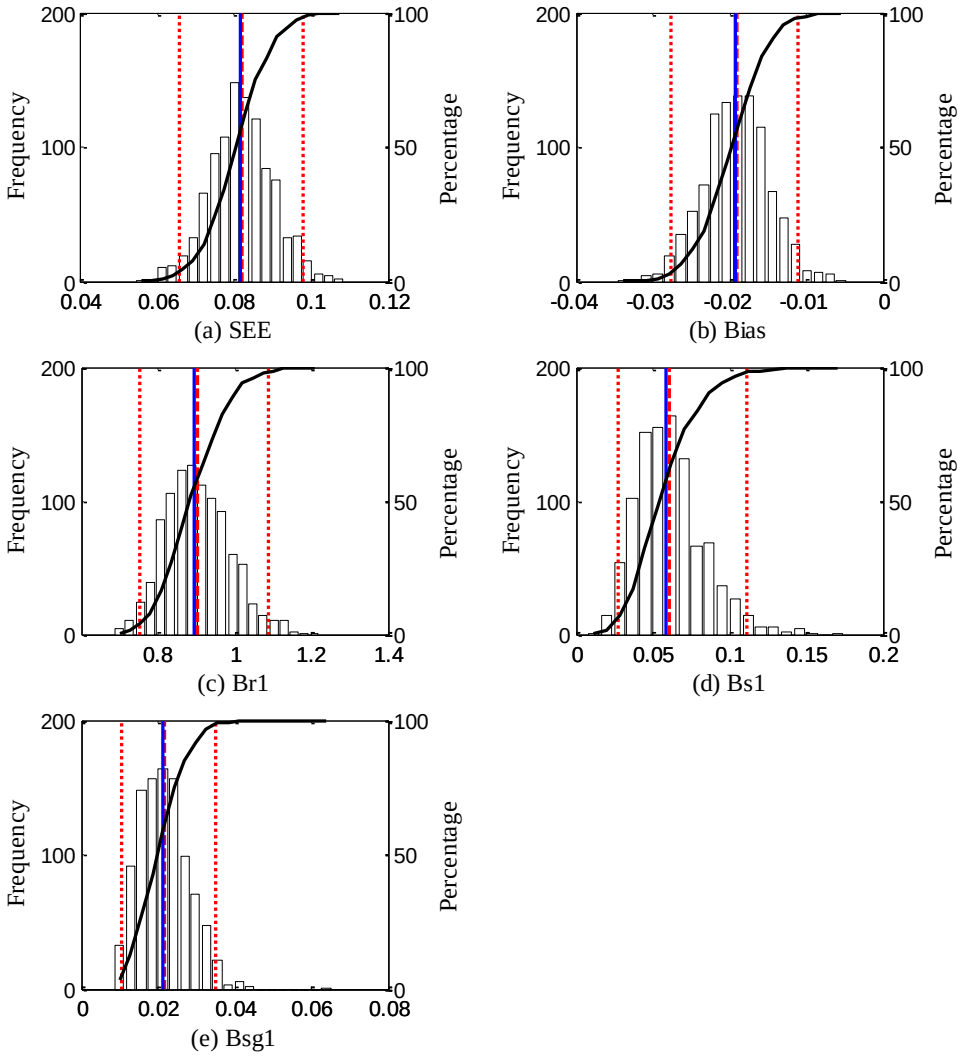

Figure B-235 Option 4: Method 1 – bootstrapping total rutting frequency distributions –calibration

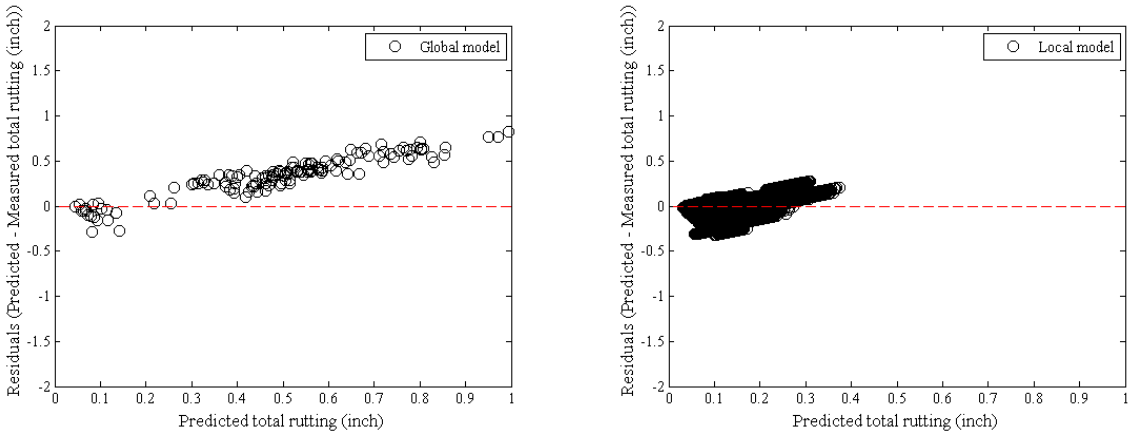

Figure B-236 Option 4: Method 1 – Total rutting residual plots – bootstrapping

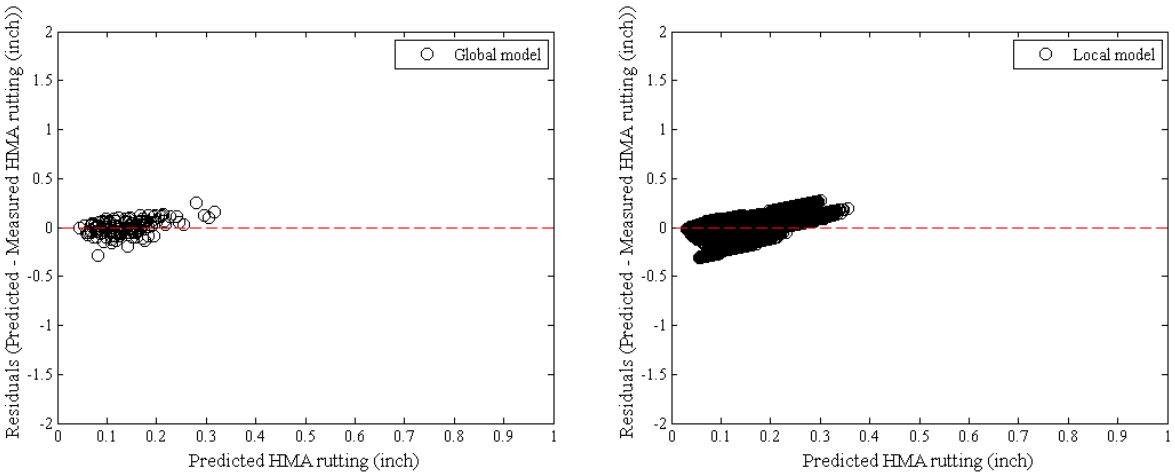

(a) Global model (b) Local model

Figure B-237 Option 4: Method 1 – HMA rutting residual plots - bootstrapping

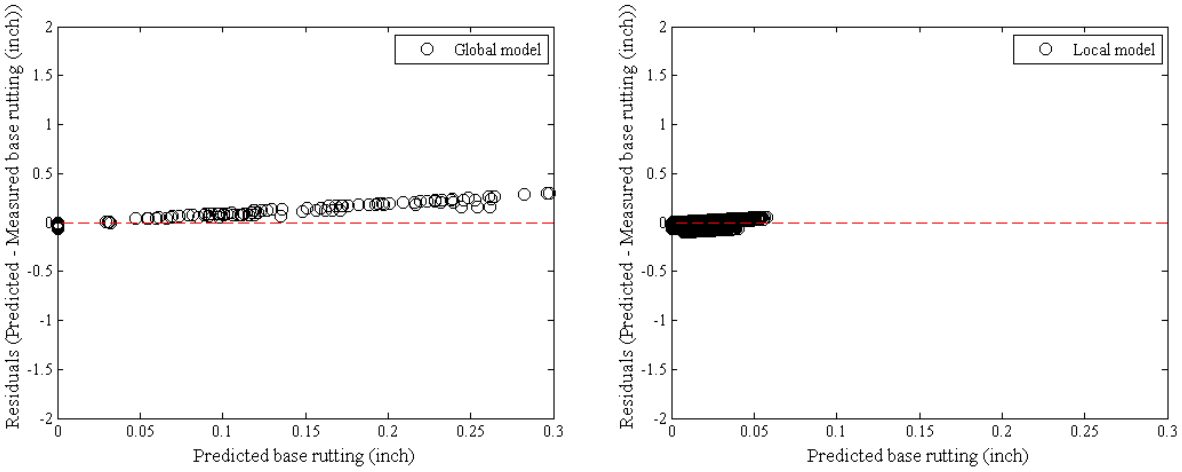

(a) Global model (b) Local model

Figure B-238 Option 4: Method 1 – Base rutting residual plots - bootstrapping

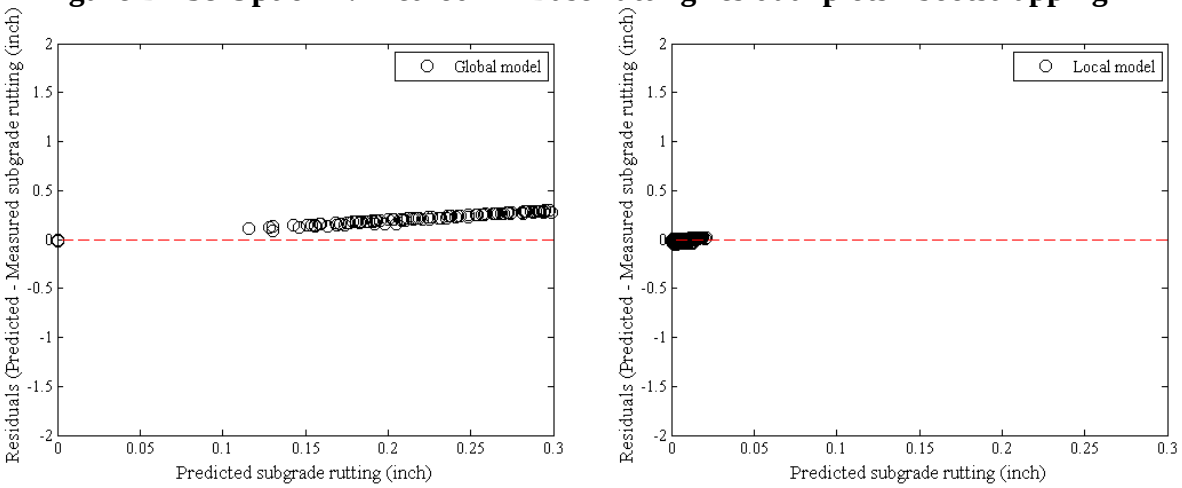

(a) Global model (b) Local model

Figure B-239 Option 4: Method 1 – Subgrade rutting residual plots - bootstrapping

Reliability

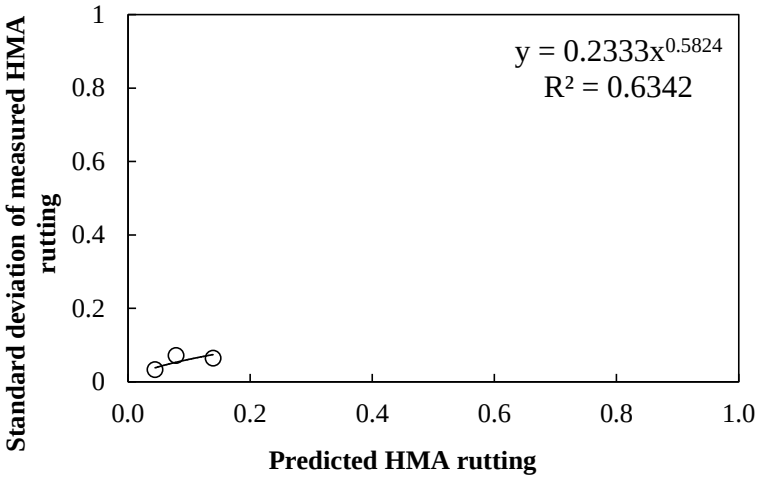

(a) HMA rutting reliability

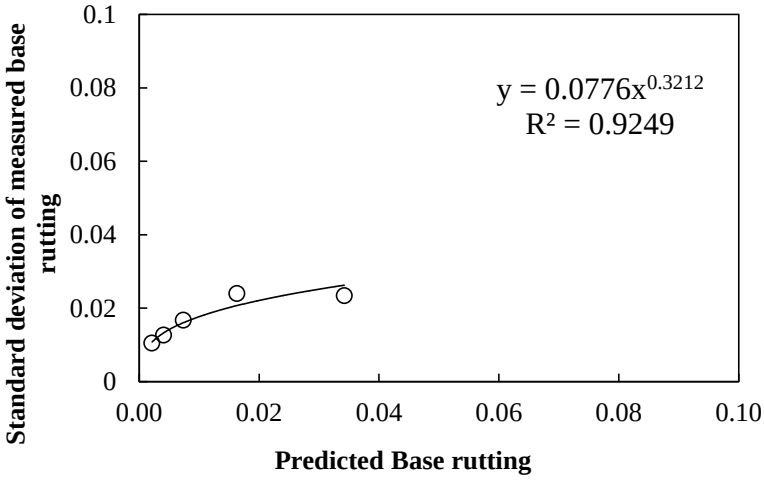

(b) Base rutting reliability

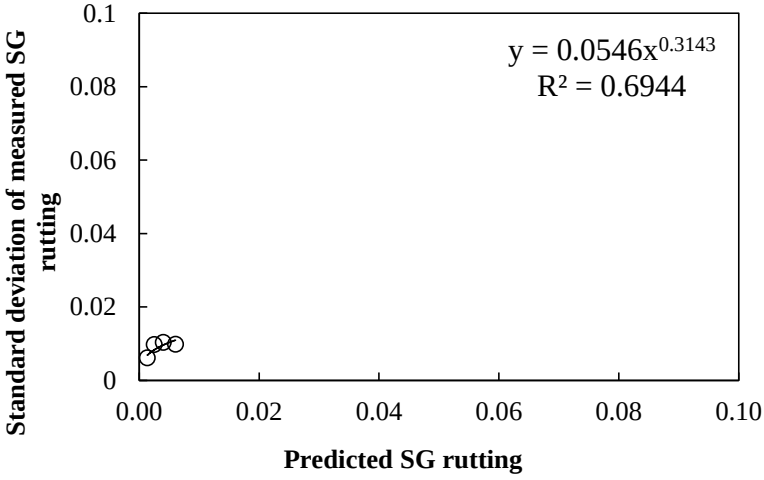

(c) Subgrade rutting reliability

Figure B-240 Rutting model reliability equations – option 4 method 1 – bootstrapping

B.1.3.6 Option 4 – Method 2

No sampling

Table B-126 Option 4: Method 2 – Global model goodness of fit – no sampling

HMA layer	SEE (in.)	Bias (in.)
AC rut	0.0763	0.0038
Base rut	0.1797	0.1323
Subgrade	0.2230	0.1959
Total rut	0.4035	0.3320

Table B-127 Option 4: Method 2 – Global model *p*-values

HMA layer	t-test p-value	Intercept p-value	Slope = 1 p-value
AC rut	0.5589	0.0000	0.0000
Base rut	0.0000	0.0000	0.0005
Subgrade	0.0000	0.0000	0.1369
Total rut	0.0000	0.0000	0.0039

Table B-128 Option 4: Method 2 – Local model goodness of fit– no sampling

HMA layer	SEE	Bias
AC rut	0.0746	-0.0116
Base rut	0.0249	-0.0146
Subgrade	0.0211	0.0154
Total rut	0.0814	-0.0108

Table B-129 Option 4: Method 2 – Local model *p*-values– no sampling

HMA layer	t-test p-value	Intercept p-value	Slope = 1 p-value
AC rut	0.0684	0.0000	0.0000
Base rut	0.0000	0.0000	0.0000
Subgrade	0.0000	0.0000	0.0000
Total rut	0.1225	0.0000	0.0000

Table B-130 Option 4: Method 2 – Local model *p*-values– no sampling

Calibration Coefficient	Global model	Local model
HMA rutting (br1)	1.0000	0.8888
Base rutting (bs1)	1.0000	0.0100
Subgrade rutting (bsg1)	1.0000	0.1040

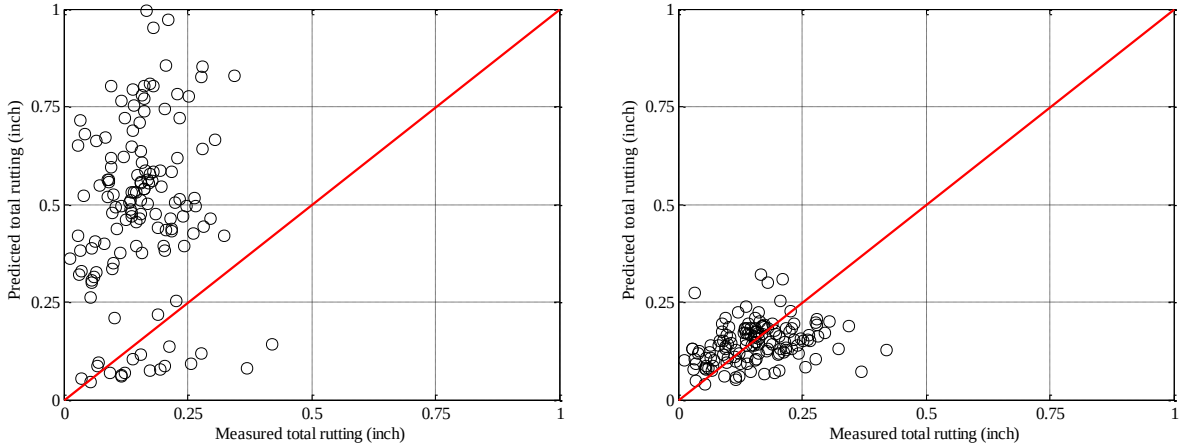

(a) Global model (b) Local model

Figure B-241 Option 4: Method 2 – Total rutting local calibration results - no sampling

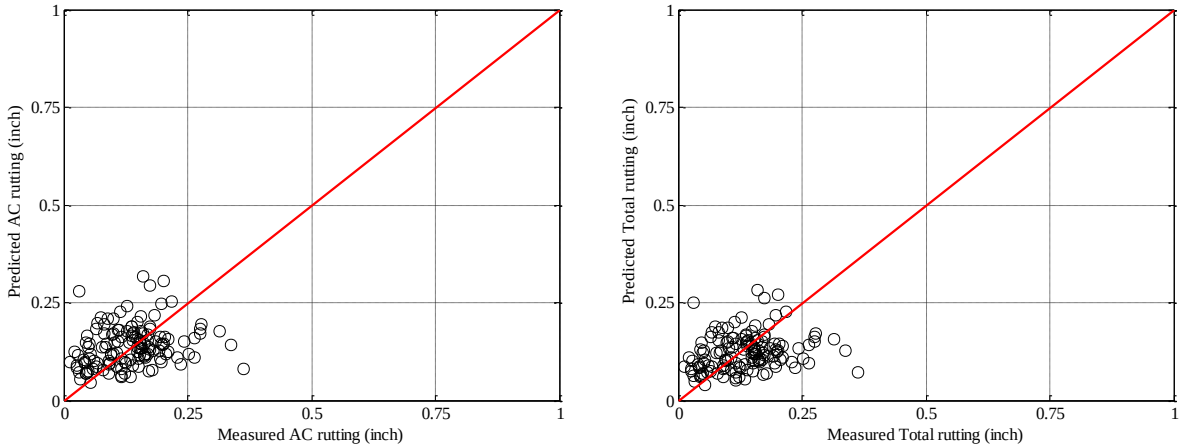

(a) Global model (b) Local model

Figure B-242 Option 4: Method 2 – HMA rutting local calibration results - no sampling

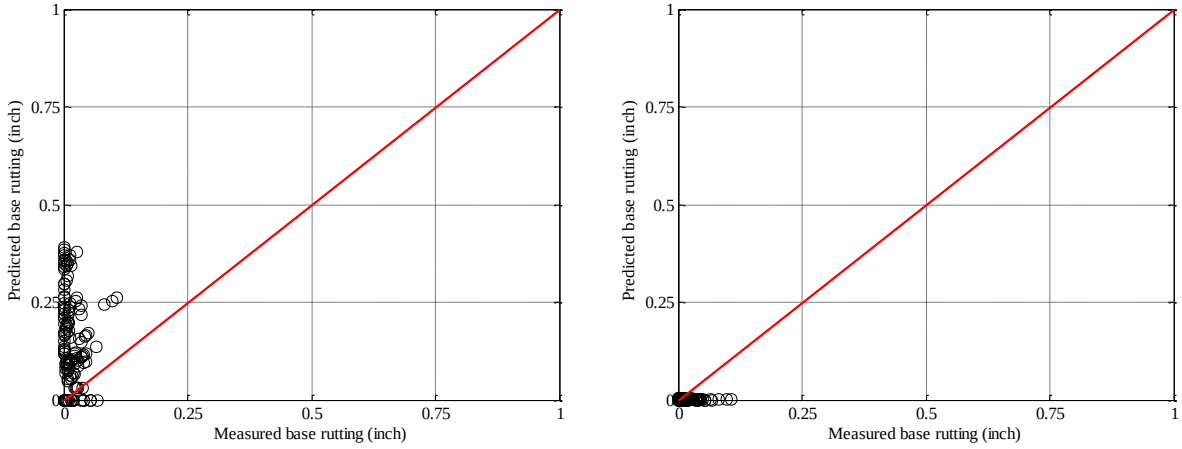

(a) Global model (b) Local model

Figure B-243 Option 4: Method 2 – Base rutting local calibration results - no sampling

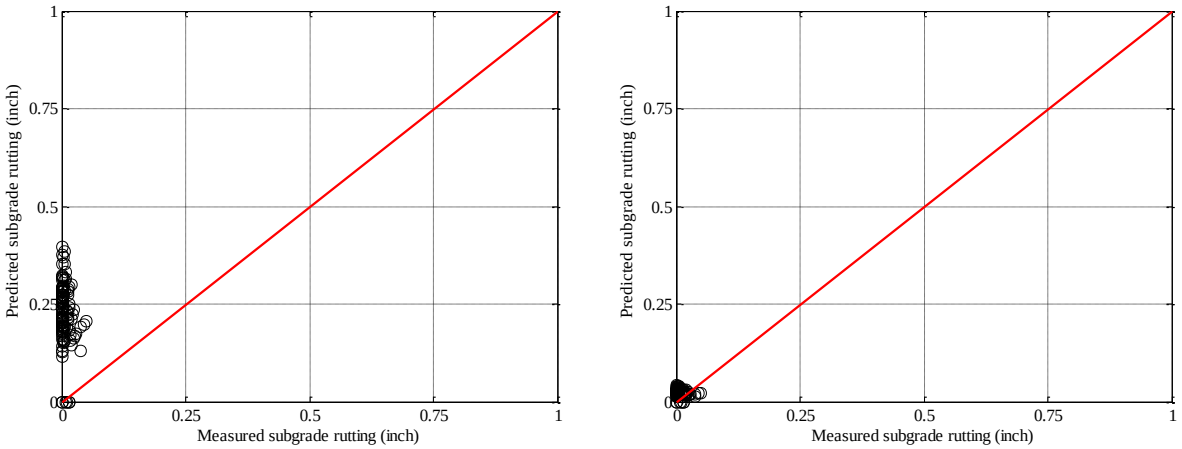

(a) Global model (b) Local model

Figure B-244 Option 4: Method 2 – Subgrade rutting local calibration results - no sampling

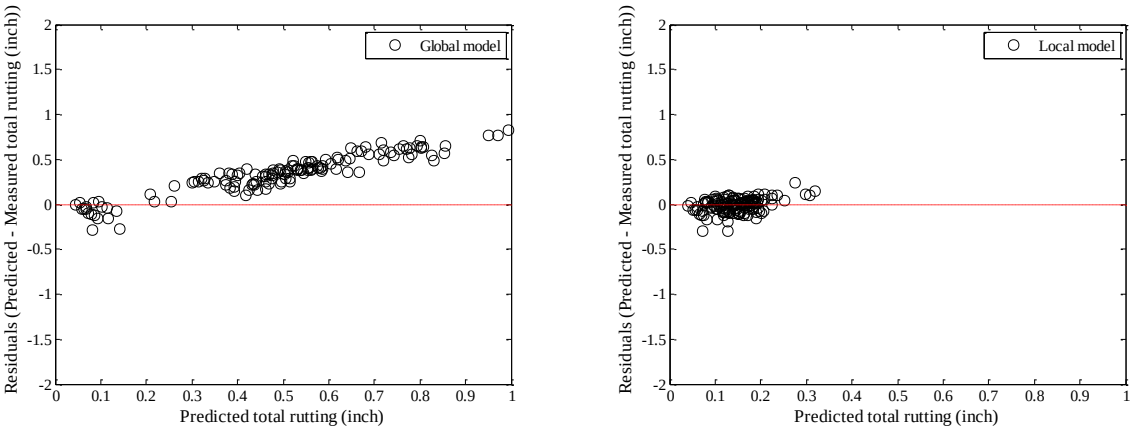

(a) Global model (b) Local model

Figure B-245 Option 4: Method 2 – Total rutting residual plots - no sampling

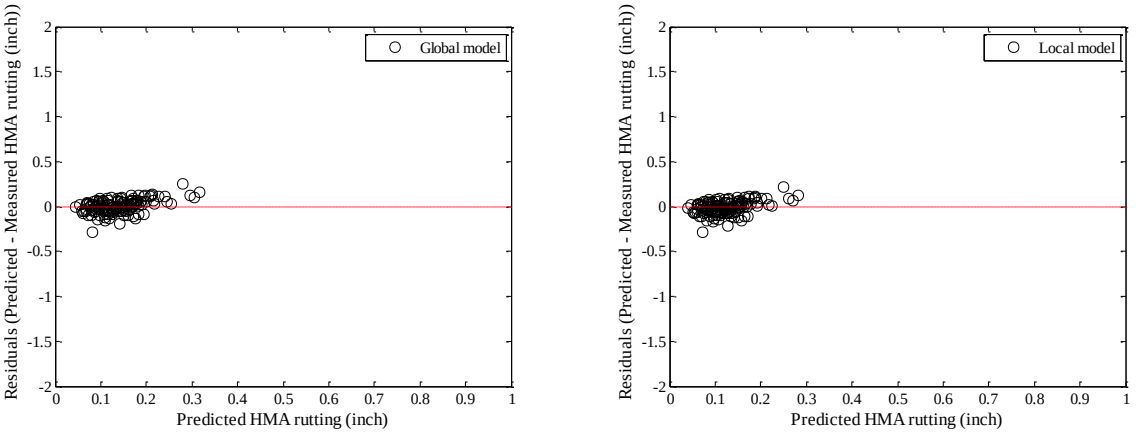

(a) Global model (b) Local model

Figure B-246 Option 4: Method 2 – HMA rutting residual plots - no sampling

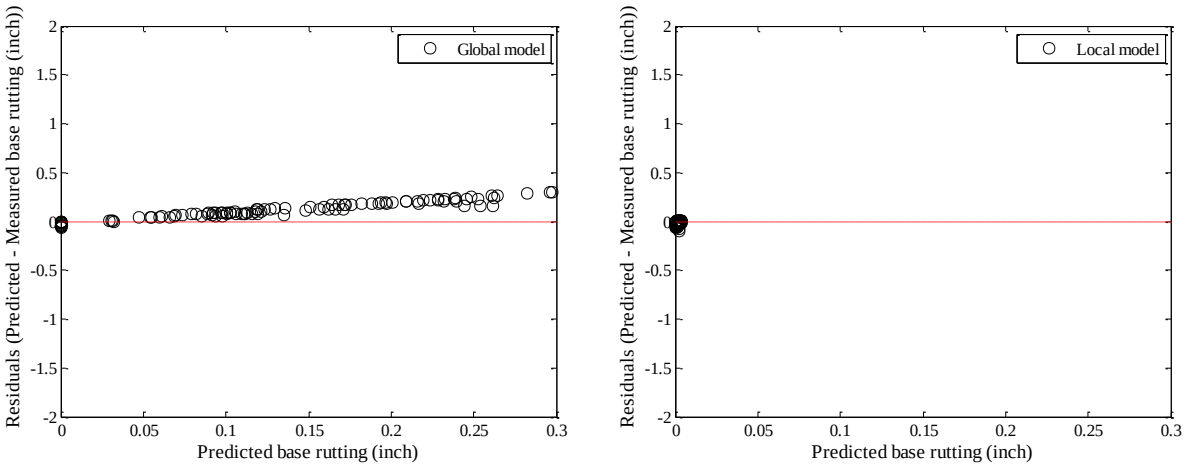

(a) Global model (b) Local model

Figure B-247 Option 4: Method 2 – Base rutting residual plots - no sampling

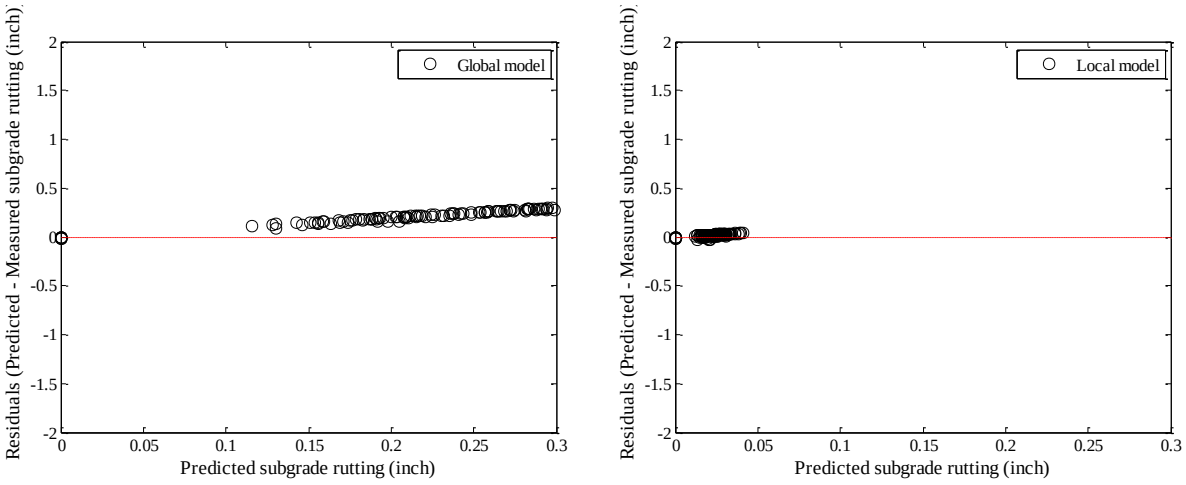

(a) Global model (b) Local model

Figure B-248 Option 4: Method 2 – Subgrade rutting residual plots - no sampling

Reliability

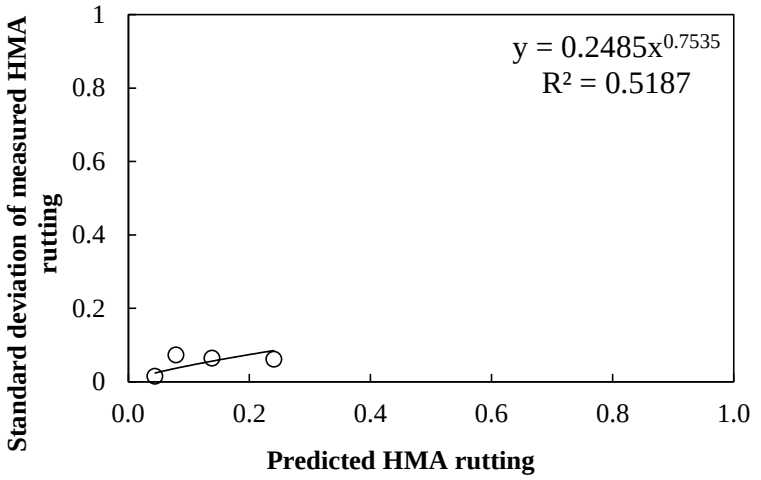

(a) HMA rutting reliability

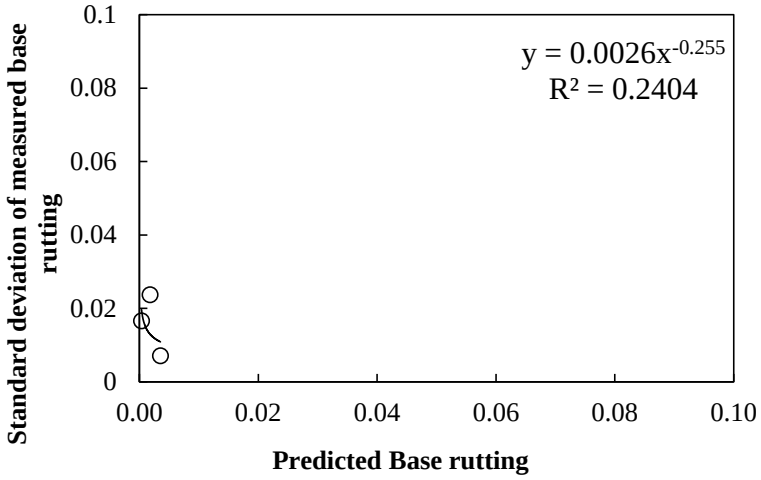

(b) Base rutting reliability

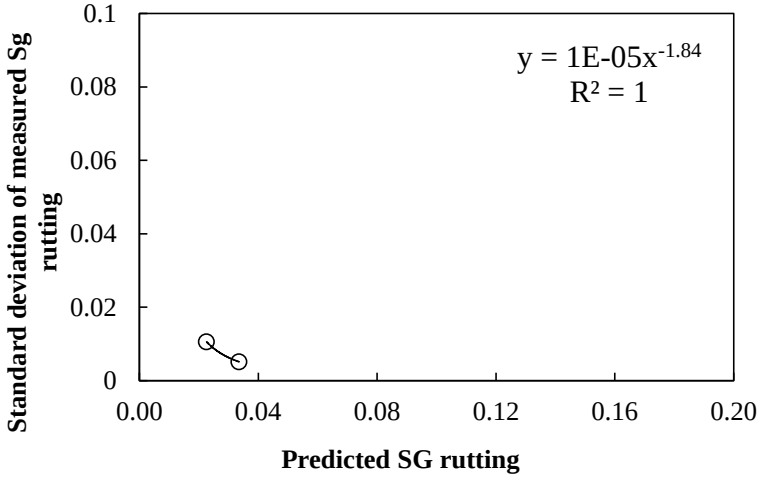

(c) Subgrade rutting reliability

Figure B-249 Rutting model reliability equations – option 4 method 2 – no sampling

Split sampling

Table B-131 Option 4: Method 2 – Global model goodness of fit – split sampling

HMA layer	SEE (in.)	Bias (in.)
AC rut	0.0793	0.0109
Base rut	0.1691	0.1240
Subgrade	0.2055	0.1730
Total rut	0.3852	0.3079

Table B-132 Option 4: Method 2 – Global model *p*-values - split sampling

HMA layer	t-test p-value	Intercept p-value	Slope = 1 p-value
AC rut	0.1860	0.0000	0.0000
Base rut	0.0000	0.0000	0.0377
Subgrade	0.0000	0.0000	0.2417
Total rut	0.0000	0.0000	0.0127

Table B-133 Option 4: Method 2 – Local model goodness of fit– split sampling

HMA layer	SEE	Bias
AC rut	0.0769	0.0010
Base rut	0.0258	-0.0134
Subgrade	0.0123	0.0032
Total rut	0.0800	-0.0092

Table B-134 Option 4: Method 2 – Local model *p*-values– split sampling

HMA layer	t-test p-value	Intercept p-value	Slope = 1 p-value
AC rut	0.9021	0.0000	0.0000
Base rut	0.0000	0.0000	0.0000
Subgrade	0.0109	0.0000	0.0000
Total rut	0.2707	0.0000	0.0000

Table B-135 Option 4: Method 2 – Local model *p*-values – split sampling

Calibration Coefficient	Global model	Local model
HMA rutting (br1)	1.0000	0.9277
Base rutting (bs1)	1.0000	0.0100
Subgrade rutting (bsg1)	1.0000	0.0506

Table B-136 Option 4: Method 2 – Local model validation p-values – split sampling

HMA layer	t-test p-value	Intercept p-value	Slope = 1 p-value
AC rut	0.0448	0.0002	0.0000
Base rut	0.0000	0.0000	0.0000
Subgrade	0.0000	0.0000	0.0000
Total rut	0.0160	0.0000	0.0000

Table B-137 Option 4: Method 2 – Local model validation SEE and bias – split sampling

HMA layer	SEE	Bias
AC rut	0.0718	-0.0211
Base rut	0.0237	-0.0171
Subgrade	0.0106	0.0077
Total rut	0.0873	-0.0305

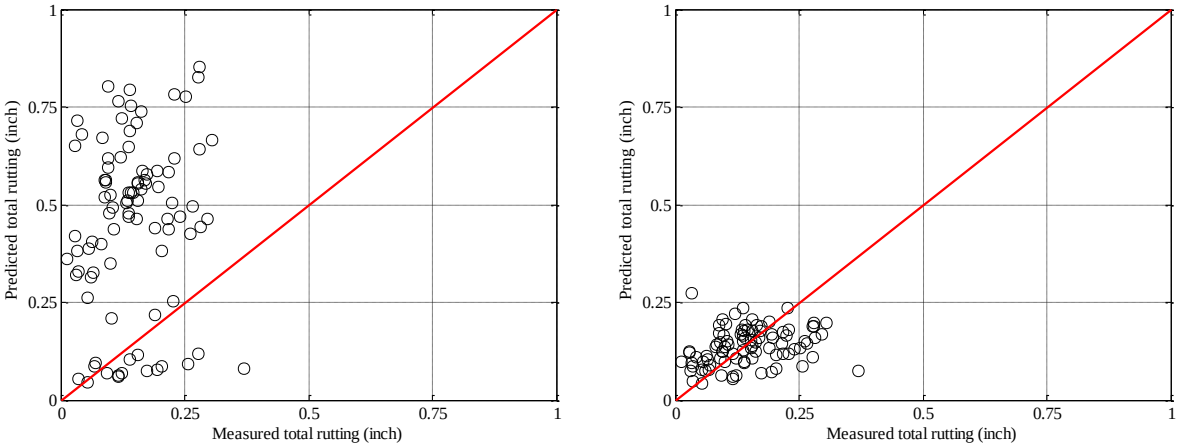

(a) Global model (b) Local model

Figure B-250 Option 4: Method 2 – Total rutting local calibration results - split sampling

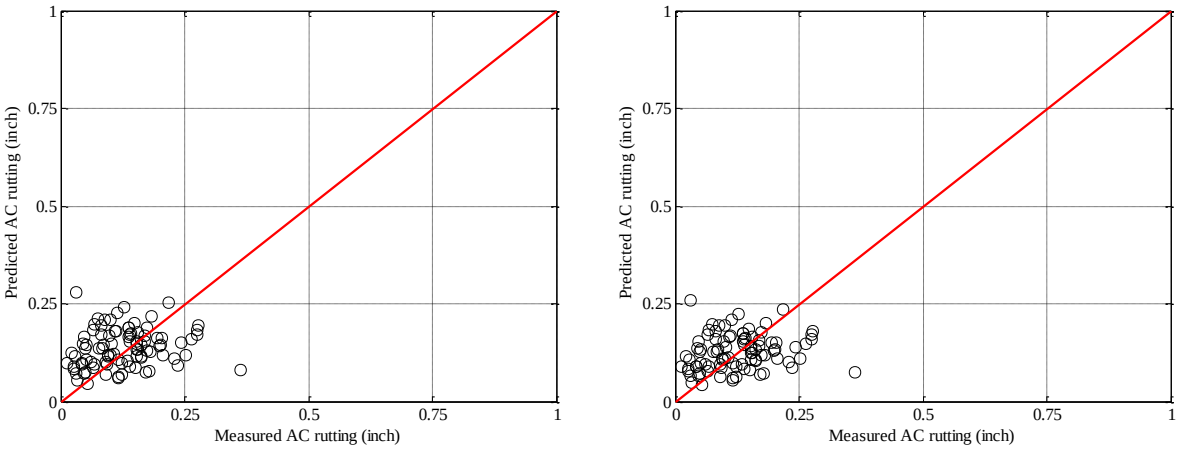

(a) Global model (b) Local model

Figure B-251 Option 4: Method 2 – HMA rutting local calibration results - split sampling

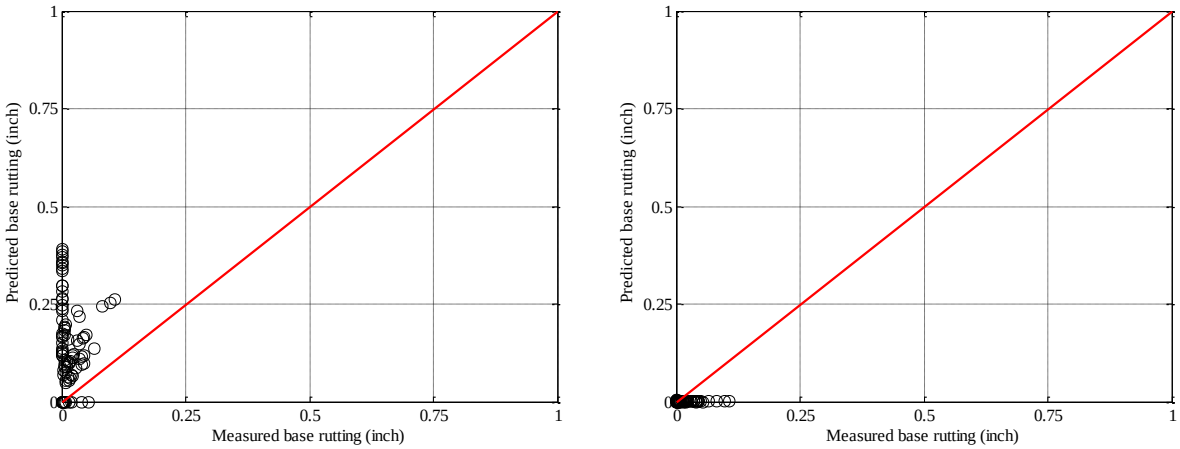

(a) Global model (b) Local model

Figure B-252 Option 4: Method 2 – Base rutting local calibration results - split sampling

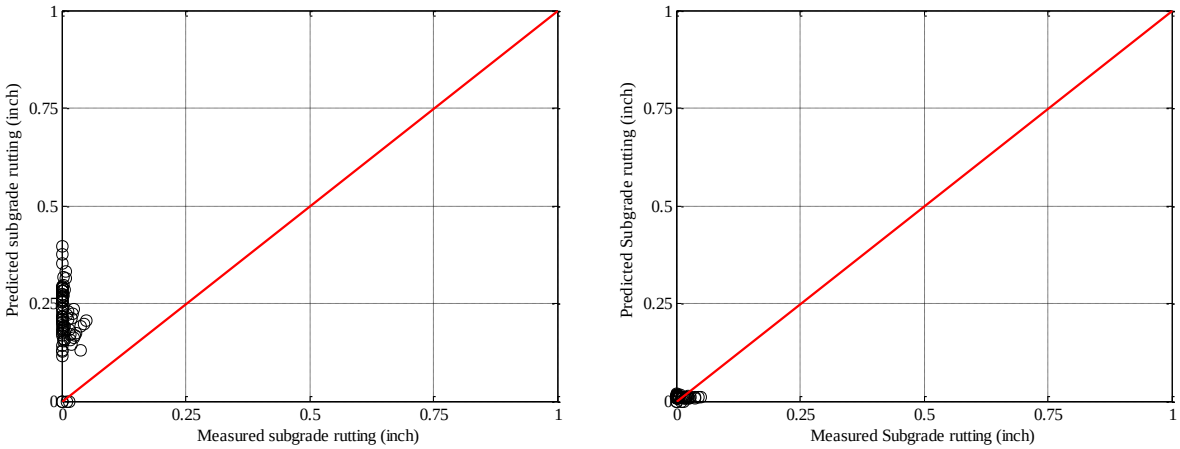

(a) Global model (b) Local model

Figure B-253 Option 4: Method 2 – Subgrade rutting local calibration results - split sampling

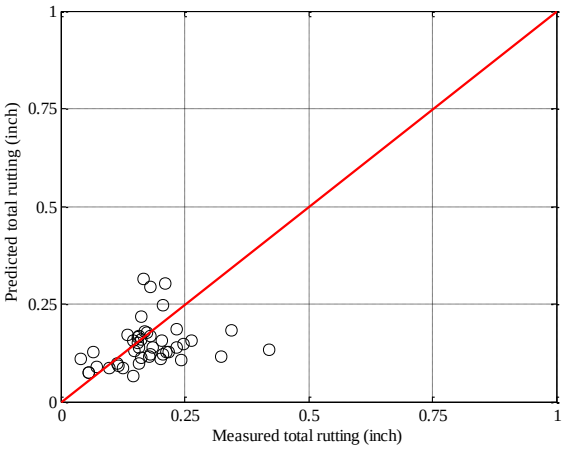

(a) Total rutting

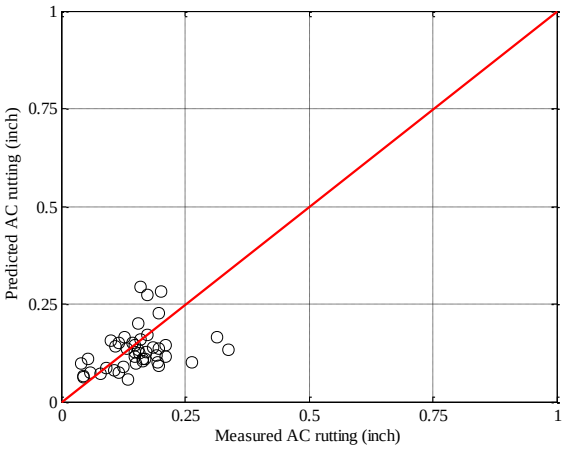

(b) HMA rutting

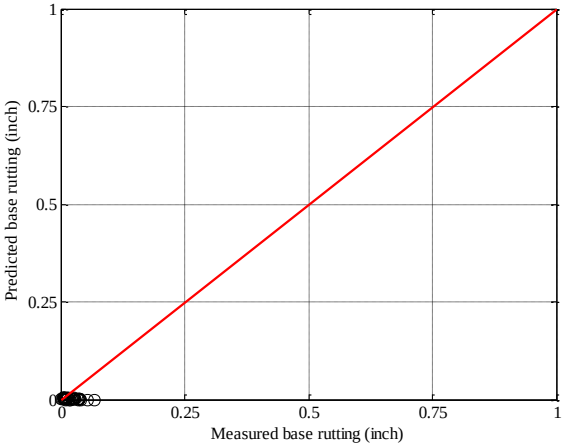

(c) Base rutting

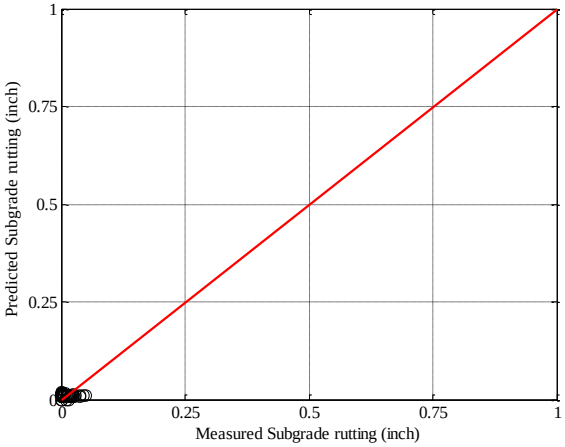

(d) Subgrade rutting

Figure B-254 Option 4: Method 2 – Rutting model validation – split sampling

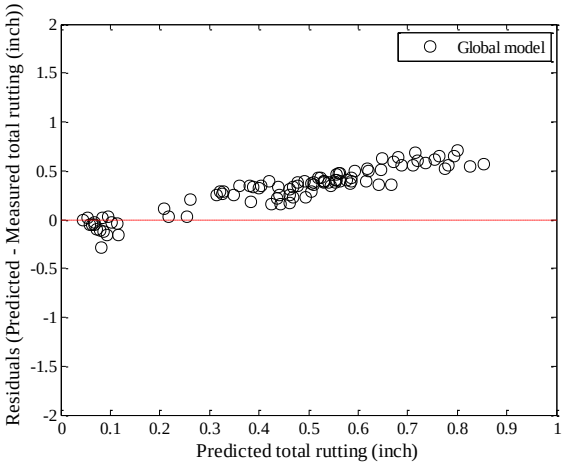

(a) Global model

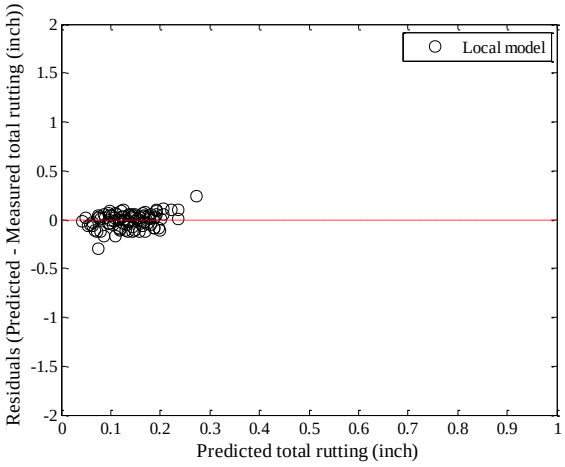

(b) Local model

Figure B-255 Option 4: Method 2 – Total rutting residual plots - split sampling

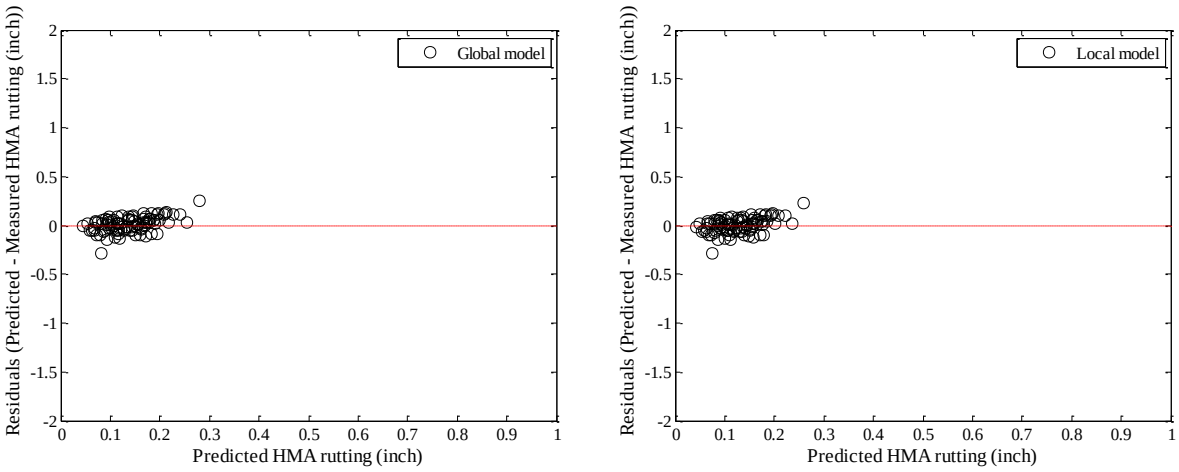

(a) Global model (b) Local model

Figure B-256 Option 4: Method 2 – HMA rutting residual plots - split sampling

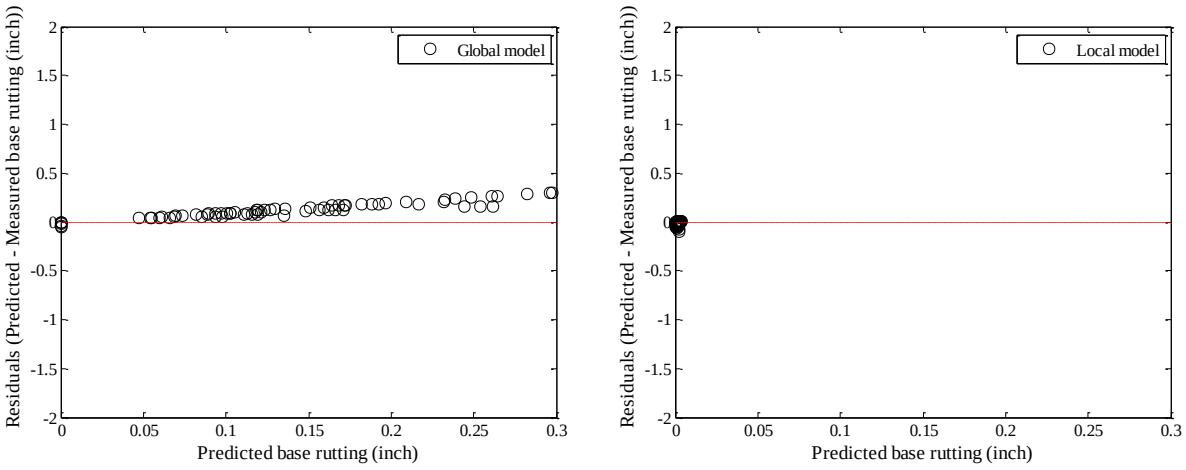

(a) Global model (b) Local model

Figure B-257 Option 4: Method 2 – Base rutting residual plots - split sampling

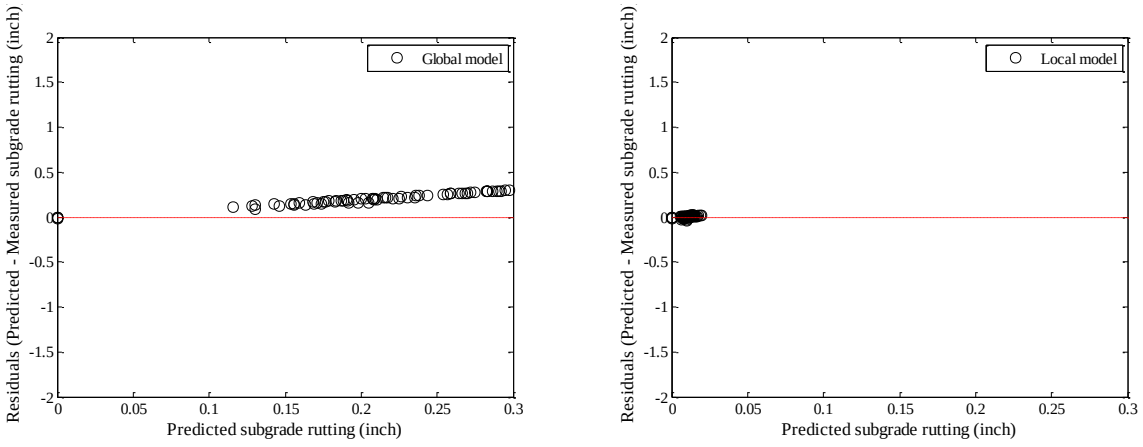

(a) Global model (b) Local model

Figure B-258 Option 4: Method 2 – Subgrade rutting residual plots - split sampling

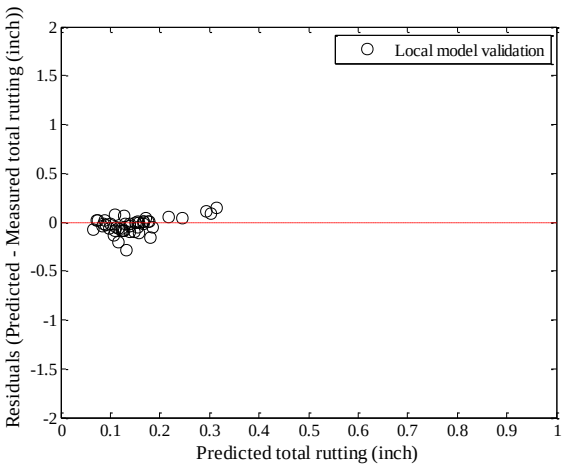

(a) Total rutting

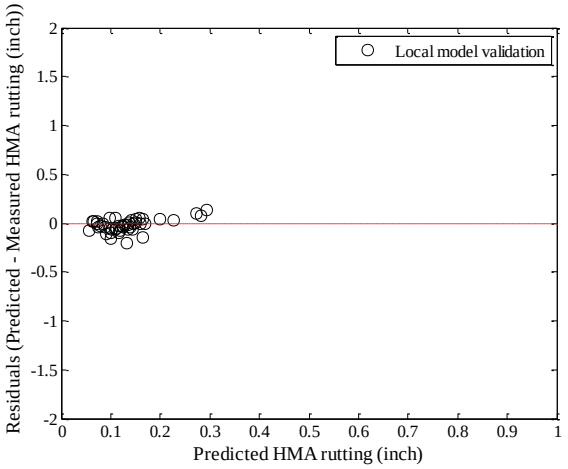

(b) HMA rutting

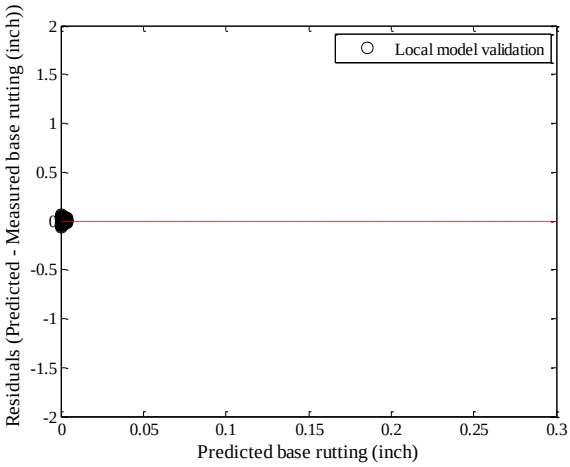

(c) Base rutting

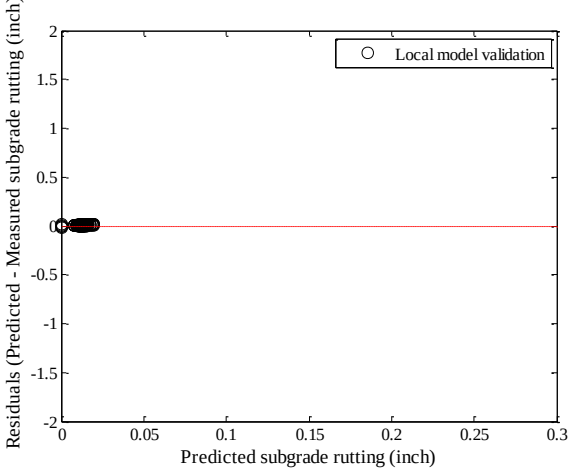

(d) Subgrade rutting

Figure B-259 Option 4: Method 2 – Rutting model validation residual plots – split sampling

Reliability

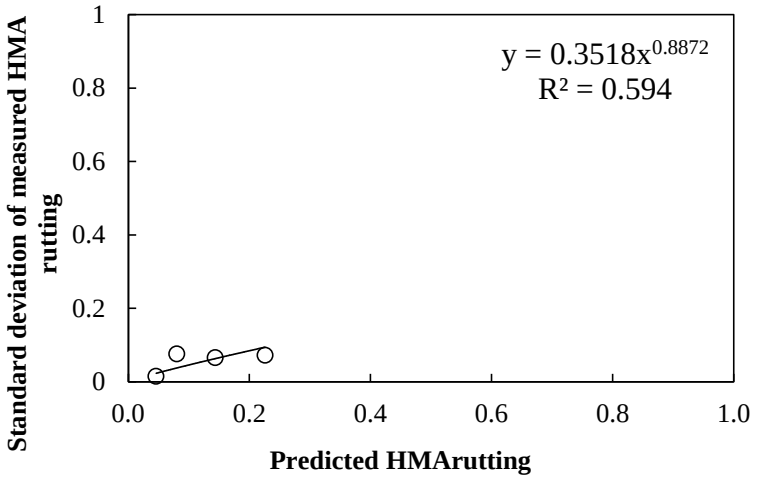

(a) HMA rutting reliability

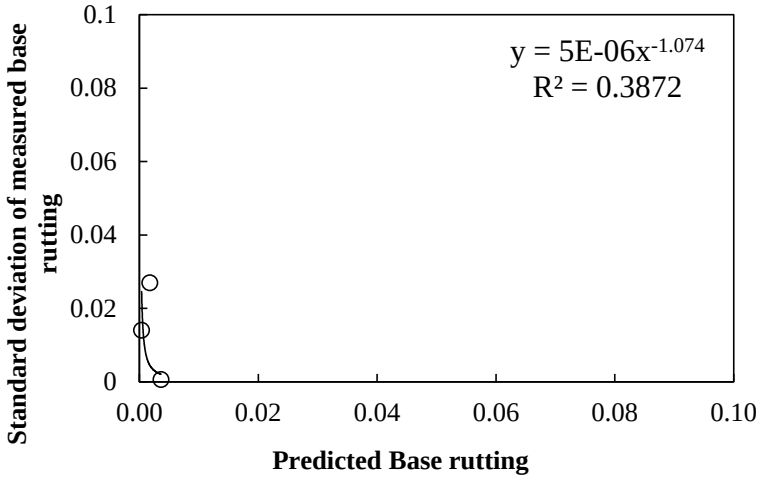

(b) Base rutting reliability

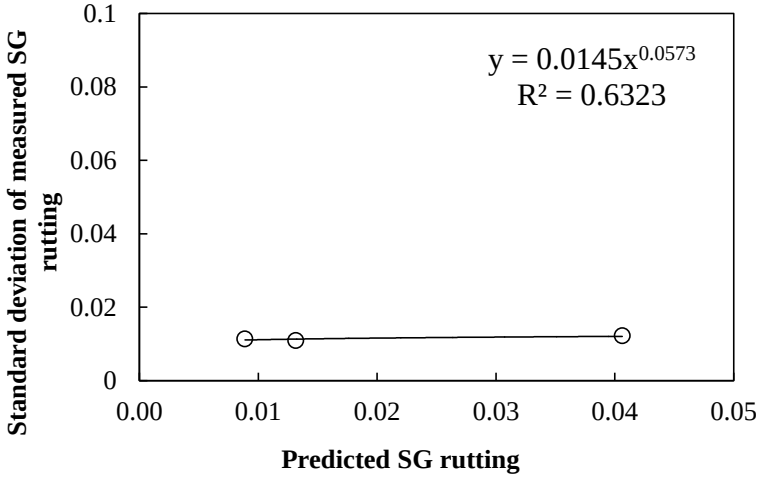

(c) Subgrade rutting reliability

Figure B-260 Rutting model reliability equations – option 4 method 2 – split sampling

Repeated split sampling

Table B-138 Option 4: Method 2 – Global model SEE and bias – repeated split sampling

Global Model	Average SEE	SEE Lower CI	SEE Upper CI	Average bias (in.)	Bias Lower CI	Bias Upper CI
AC rutting	0.0767	0.0651	0.0849	0.0038	-0.0123	0.0171
Base rutting	0.1802	0.1475	0.2045	0.1325	0.1027	0.1588
Subgrade rutting	0.2236	0.2060	0.2408	0.1959	0.1745	0.2192
Total rutting	0.4047	0.3592	0.4422	0.3322	0.2838	0.3802

Table B-139 Option 4: Method 2 – Local model SEE and bias – repeated split sampling

Calibration set	AC rutting	Base rutting	Subgrade rutting	Total rutting
Average SEE	0.0760	0.0247	0.0237	0.0807
SEE Lower CI	0.0660	0.0177	0.0084	0.0683
SEE Upper CI	0.0832	0.0293	0.0500	0.0908
Average bias (in.)	-0.0120	-0.0144	0.0162	-0.0102
Bias Lower CI	-0.0410	-0.0186	-0.0050	-0.0160
Bias Upper CI	0.0164	-0.0095	0.0440	-0.0034
Average calibration coefficient	0.8898	0.0105	0.1065	N/A
Calibration coefficient Lower CI	0.6397	0.0100	0.0100	N/A
Calibration coefficient Upper CI	1.1789	0.0133	0.2331	N/A

Table B-140 Option 4: Method 2 – Local model validation SEE and bias – repeated split sampling

Validation set	AC rutting	Base rutting	Subgrade rutting	Total rutting
Average SEE	0.0810	0.0244	0.0231	0.0865
SEE Lower CI	0.0566	0.0120	0.0040	0.0580
SEE Upper CI	0.1121	0.0375	0.0499	0.1150
Average bias (in.)	-0.0112	-0.0147	0.0152	-0.0106
Bias Lower CI	-0.0649	-0.0250	-0.0053	-0.0538
Bias Upper CI	0.0599	-0.0055	0.0390	0.0484
Average calibration coefficient	0.8898	0.0105	0.1065	N/A
Calibration coefficient Lower CI	0.6397	0.0100	0.0100	N/A
Calibration coefficient Upper CI	1.1789	0.0133	0.2331	N/A

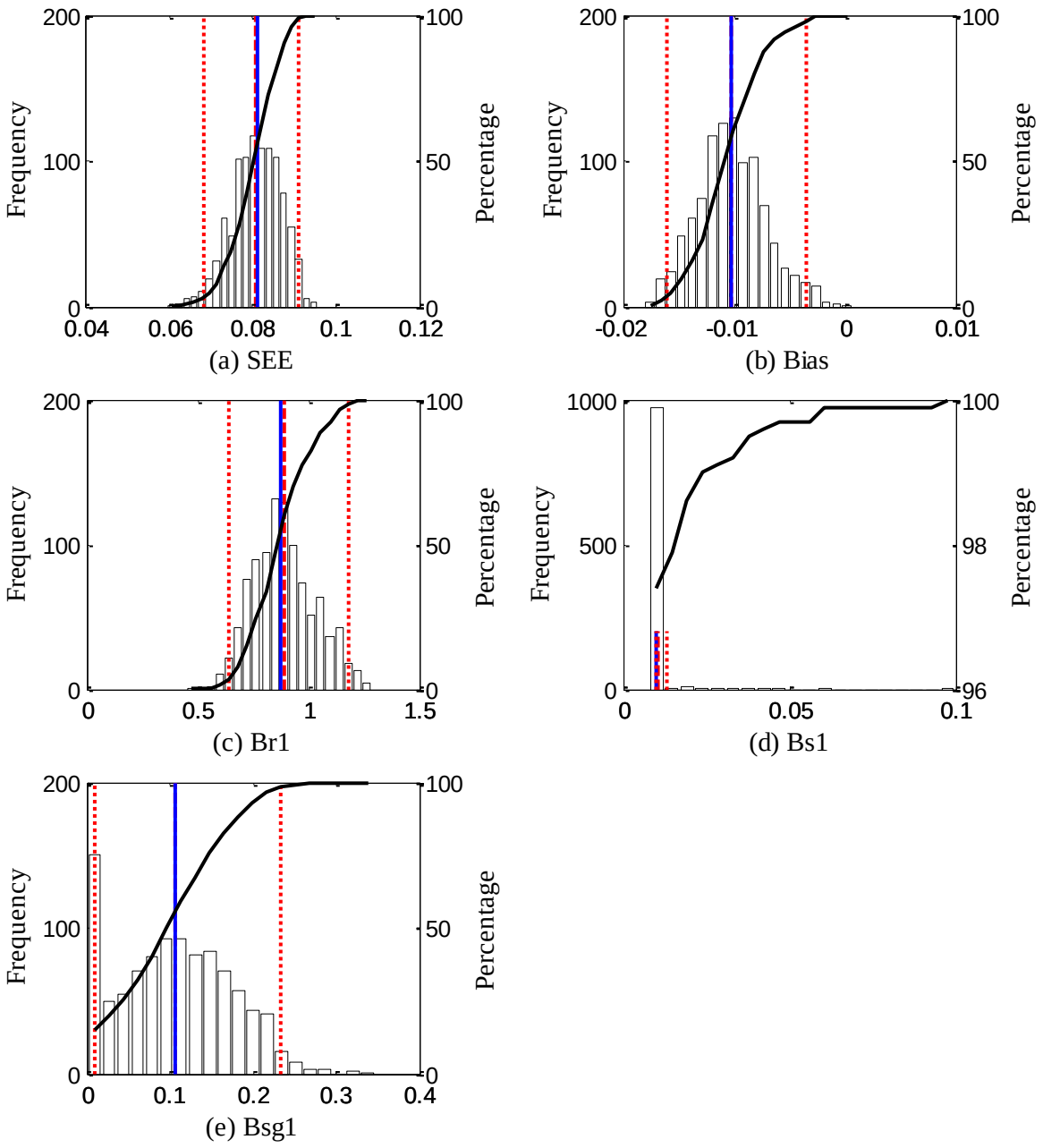

Figure B-261 Option 4: Method 2 – repeated split sampling total rutting frequency distributions – calibration

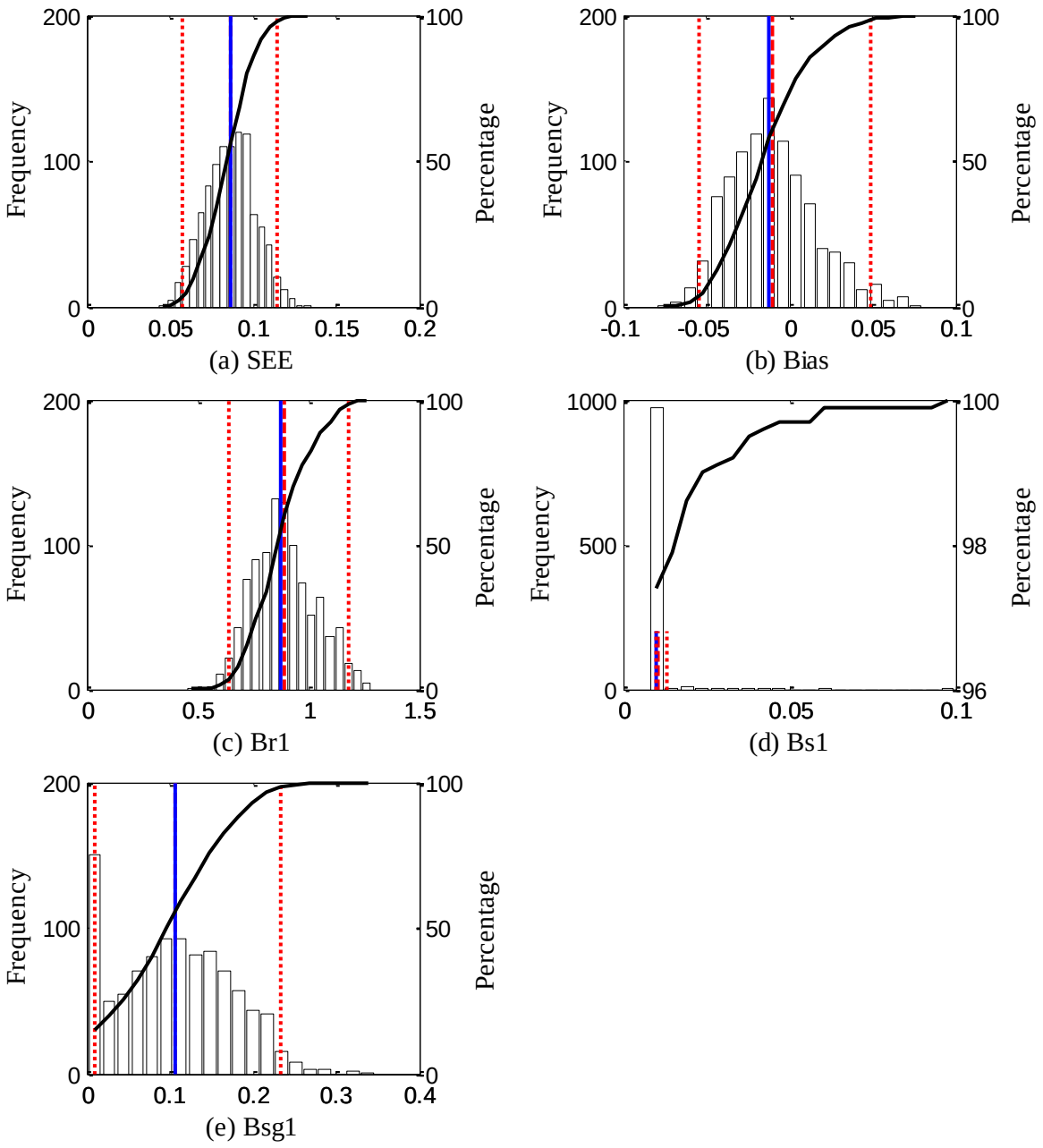

Figure B-262 Option 4: Method 2 – repeated split sampling total rutting frequency distributions – validation

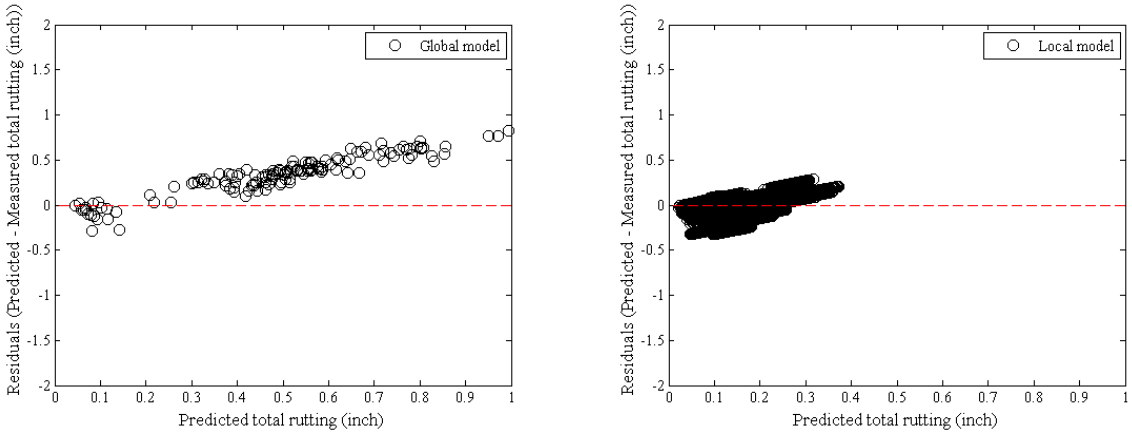

(a) Global model (b) Local model

Figure B-263 Option 4: Method 2 – Total rutting residual plots – repeated split sampling

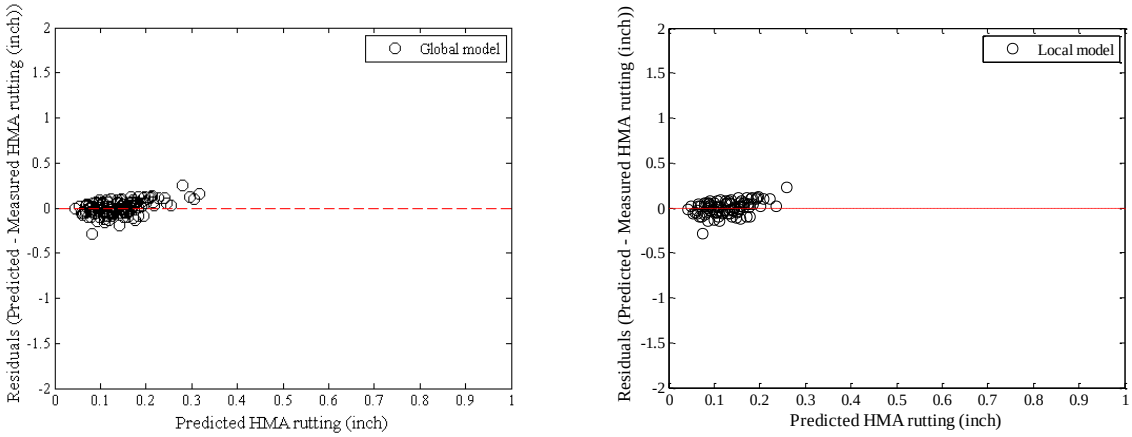

(a) Global model (b) Local model

Figure B-264 Option 4: Method 2 – HMA rutting residual plots - repeated split sampling

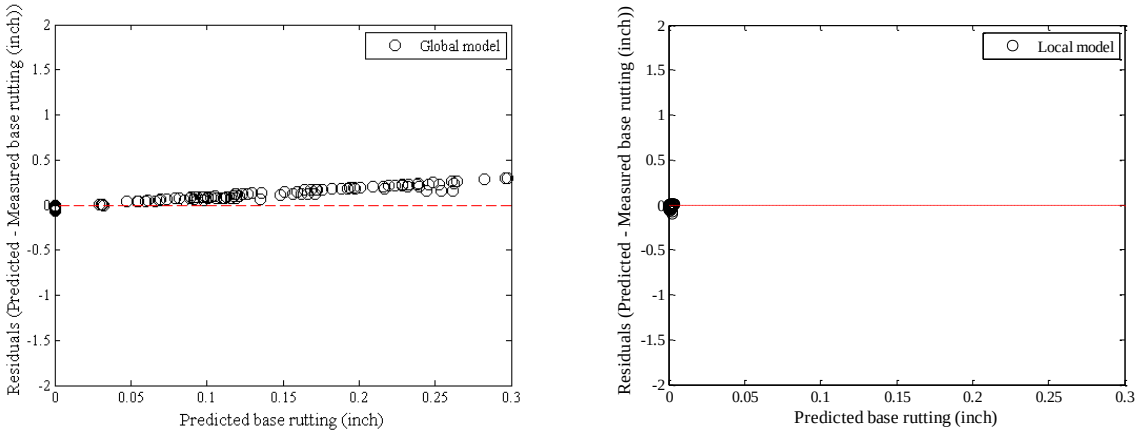

(a) Global model (b) Local model

Figure B-265 Option 4: Method 2 – Base rutting residual plots - repeated split sampling

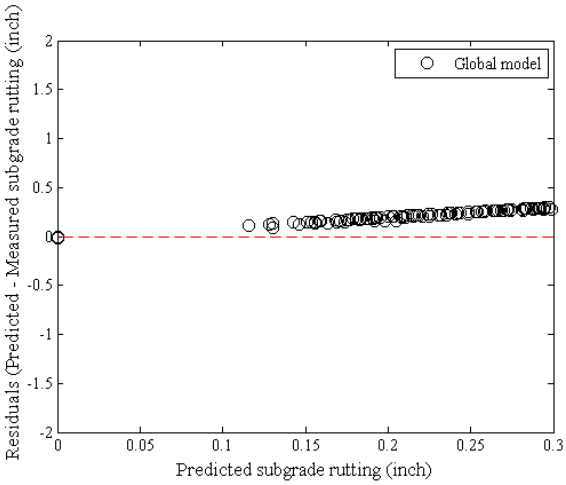

(a) Global model

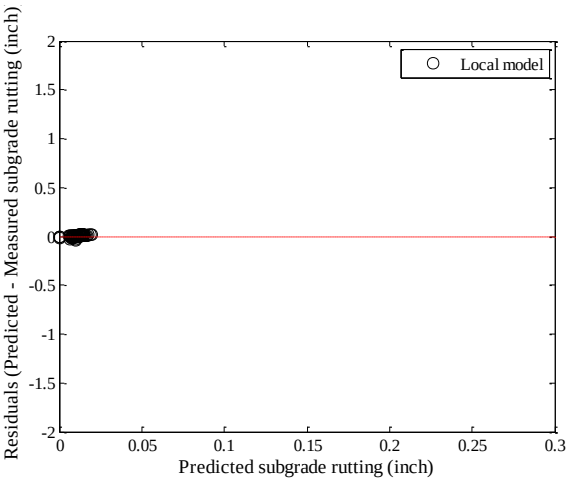

(b) Local model

Figure B-266 Option 4: Method 2 – Subgrade rutting residual plots - repeated split sampling

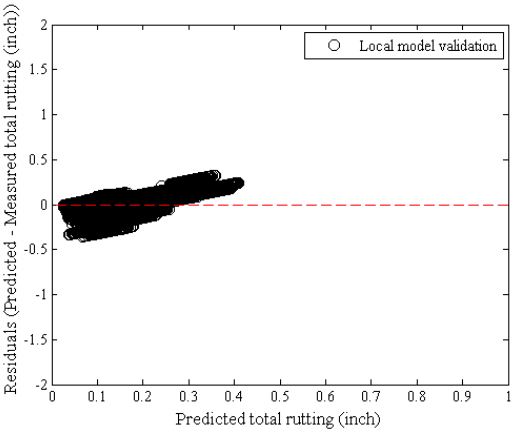

(a) Total rutting

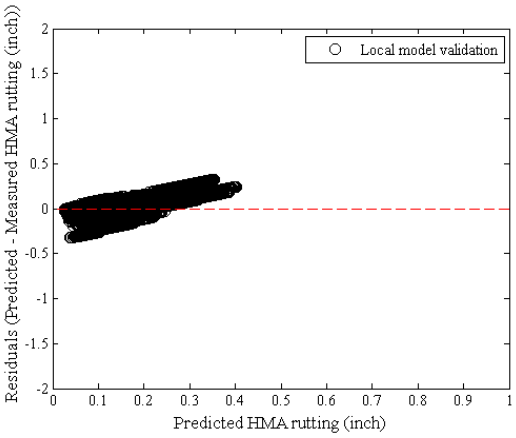

(b) HMA rutting

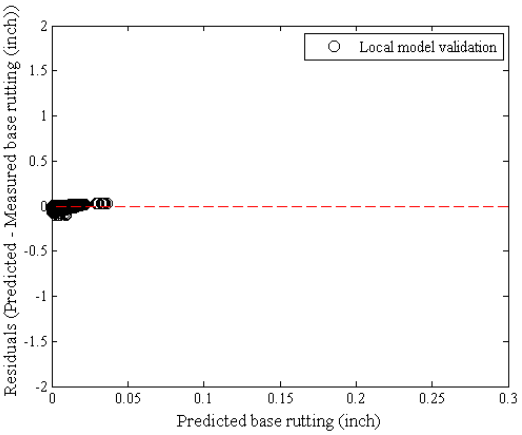

(c) Base rutting

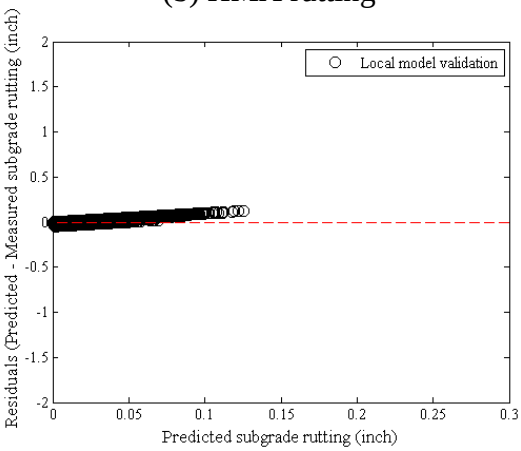

(d) Subgrade rutting

Figure B-267 Option 4: Method 2 – Rutting model validation residual plots – repeated split sampling

Reliability

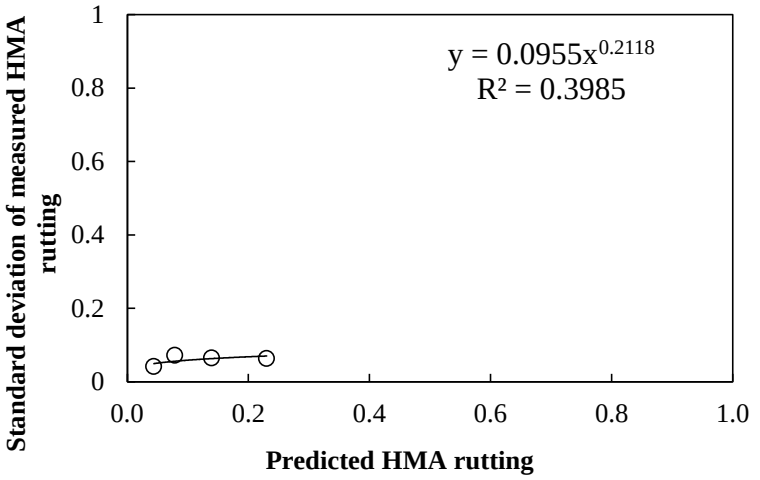

(a) HMA rutting reliability

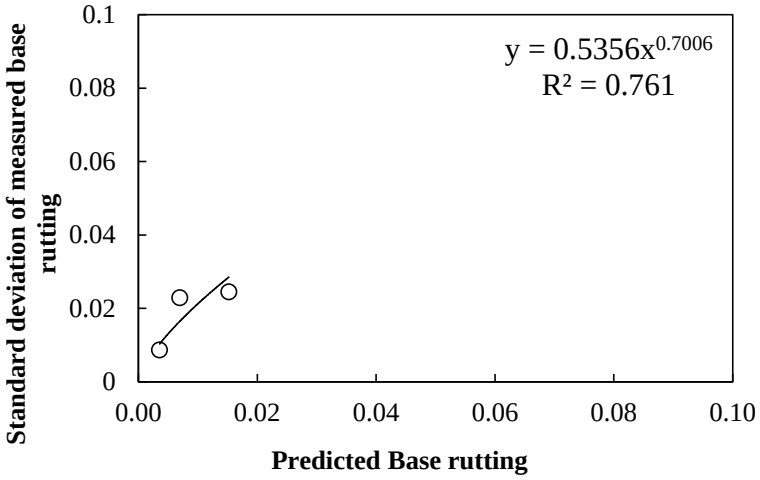

(b) Base rutting reliability

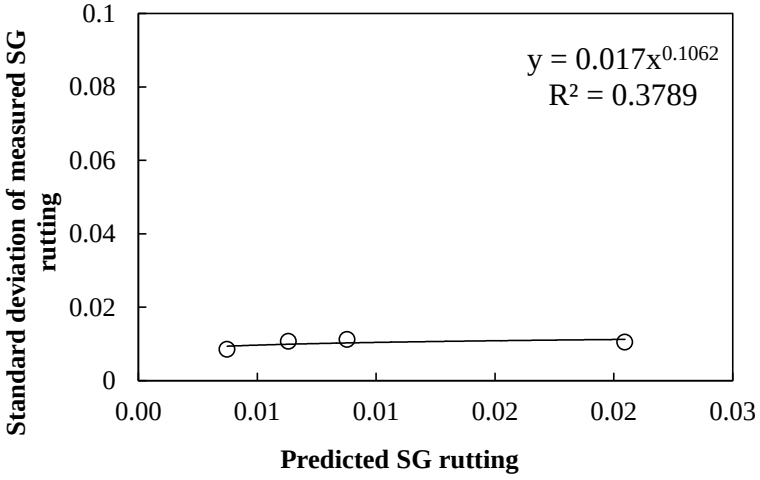

(c) Subgrade rutting reliability

Figure B-268 Rutting model reliability equations – option 4 method 2 – repeated split sampling

Bootstrapping

Table B-141 Option 4: Method 2 – Global model SEE and bias – bootstrapping

Calibration set	Average SEE	SEE Lower CI	SEE Upper CI	Average bias (in.)	Bias Lower CI	Bias Upper CI
AC rutting	0.0760	0.0612	0.0904	0.0032	-0.0187	0.0259
Base rutting	0.1788	0.1342	0.2189	0.1327	0.0901	0.1740
Subgrade rutting	0.2221	0.1943	0.2514	0.1954	0.1607	0.2316
Total rutting	0.4021	0.3390	0.4609	0.3313	0.2551	0.4031

Table B-142 Option 4: Method 2 – Local model SEE and bias – bootstrapping

Calibration set	AC rutting	Base rutting	Subgrade rutting	Total rutting
Average SEE	0.0758	0.0245	0.0236	0.0796
SEE Lower CI	0.0614	0.0163	0.0060	0.0644
SEE Upper CI	0.0905	0.0336	0.0628	0.0963
Average bias (in.)	-0.0110	-0.0141	0.0153	-0.0098
Bias Lower CI	-0.0538	-0.0214	-0.0058	-0.0181
Bias Upper CI	0.0173	-0.0067	0.0571	-0.0019
Average calibration coefficient	0.9042	0.0129	0.1011	N/A
Calibration coefficient Lower CI	0.5475	0.0100	0.0100	N/A
Calibration coefficient Upper CI	1.2275	0.0520	0.2866	N/A

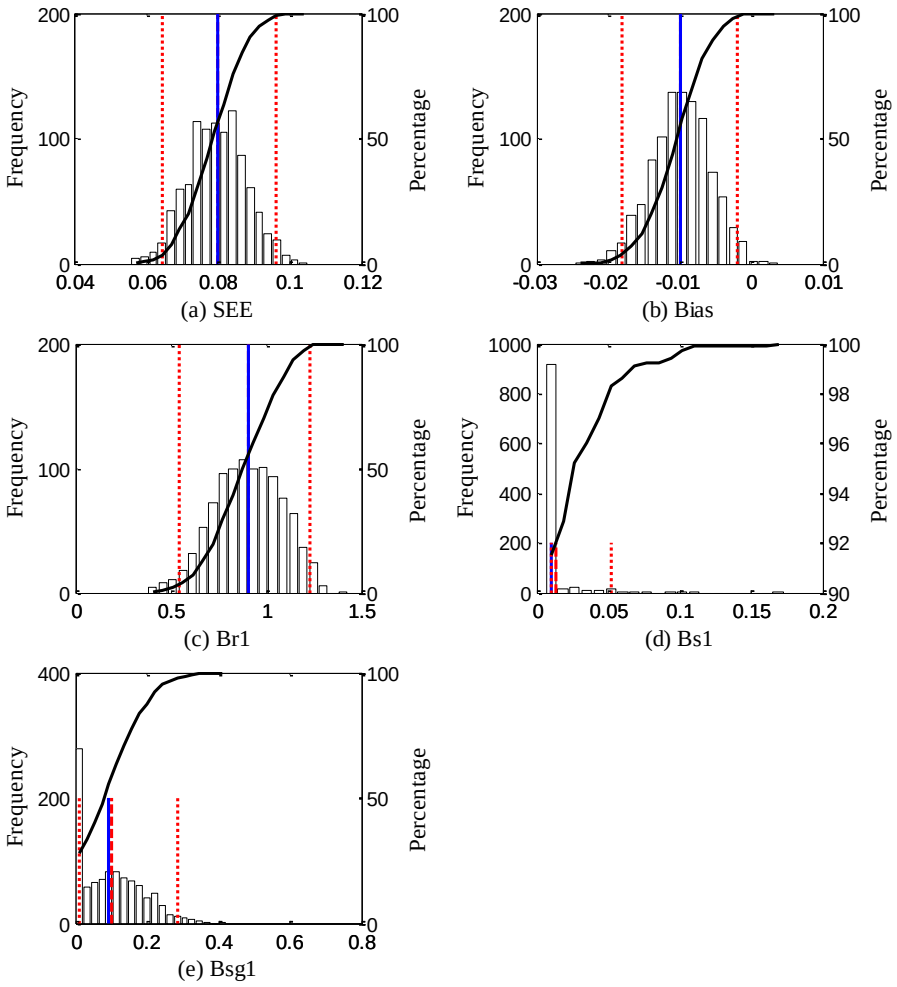

Figure B-269 Option 4: Method 2 – bootstrapping total rutting frequency distributions –calibration

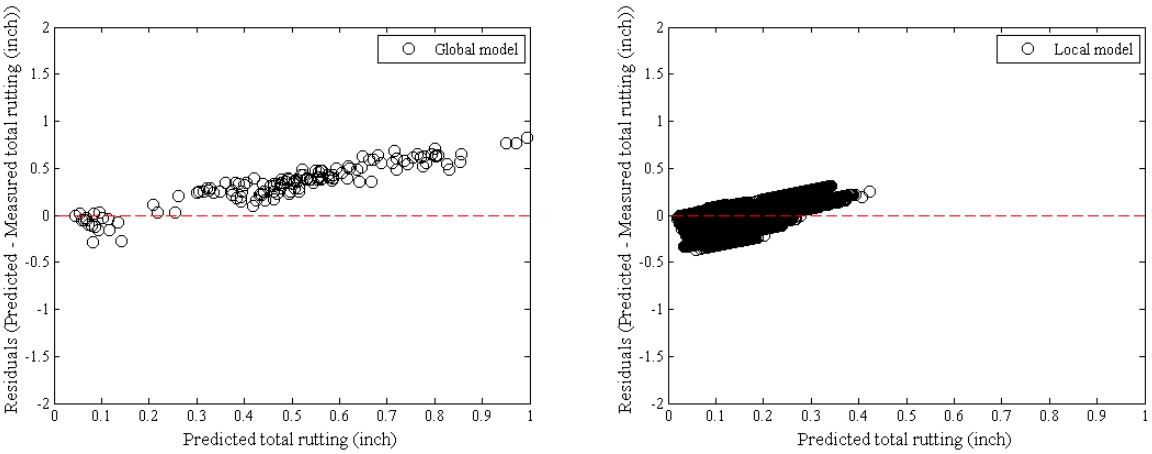

(a) Global model (b) Local model

Figure B-270 Option 4: Method 2 – Total rutting residual plots - bootstrapping

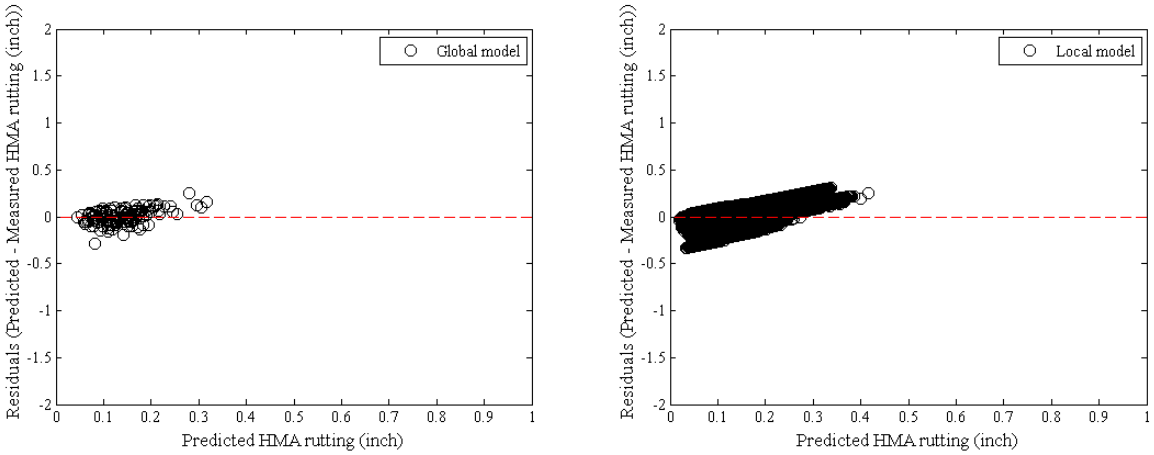

(a) Global model (b) Local model

Figure B-271 Option 4: Method 2 – HMA rutting residual plots - bootstrapping

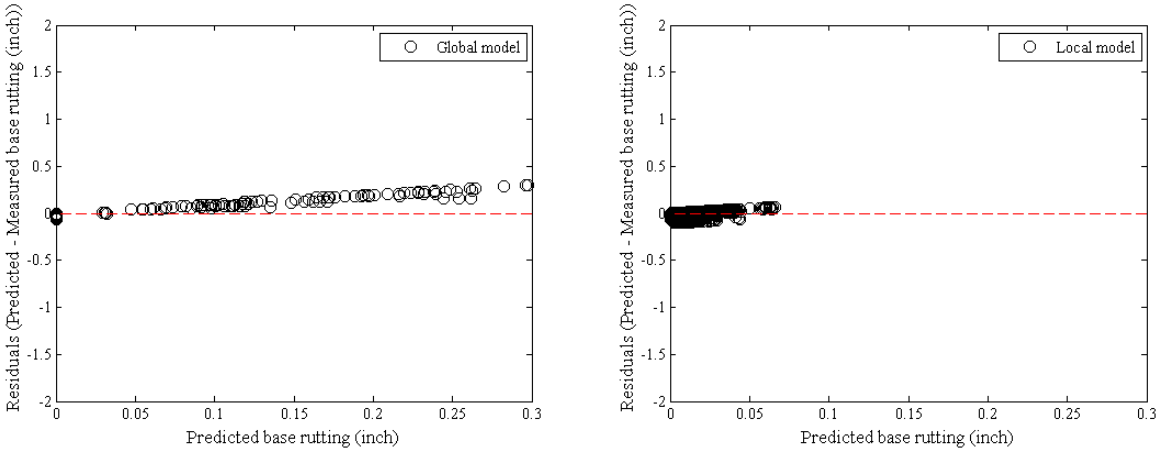

(a) Global model (b) Local model

Figure B-272 Option 4: Method 2 – Base rutting residual plots - bootstrapping

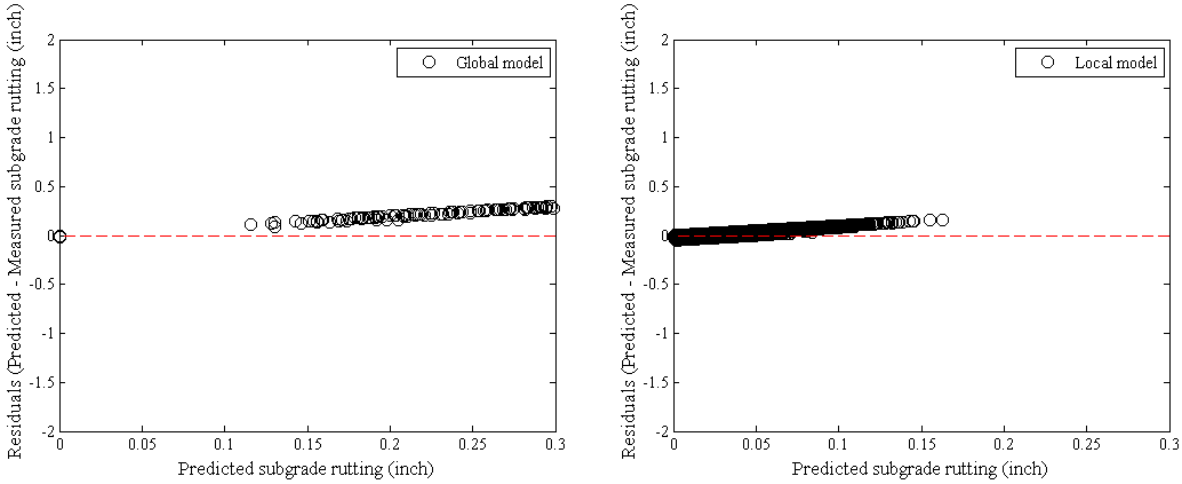

(a) Global model (b) Local model

Figure B-273 Option 4: Method 2 – Subgrade rutting residual plots - bootstrapping

Reliability

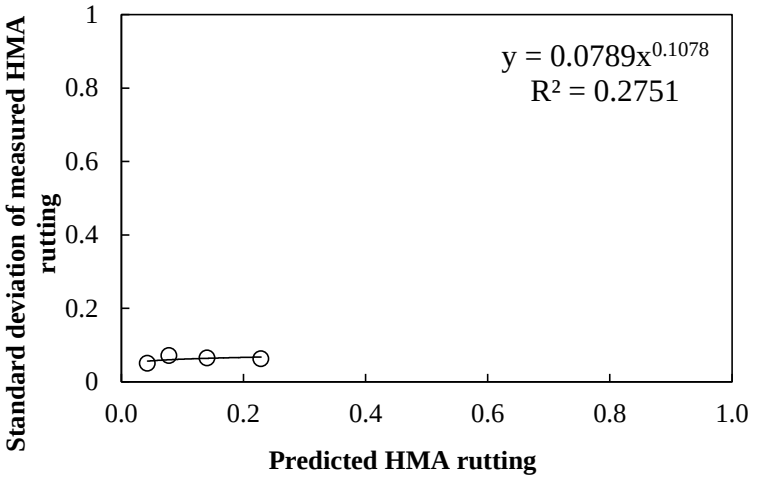

(a) HMA rutting reliability

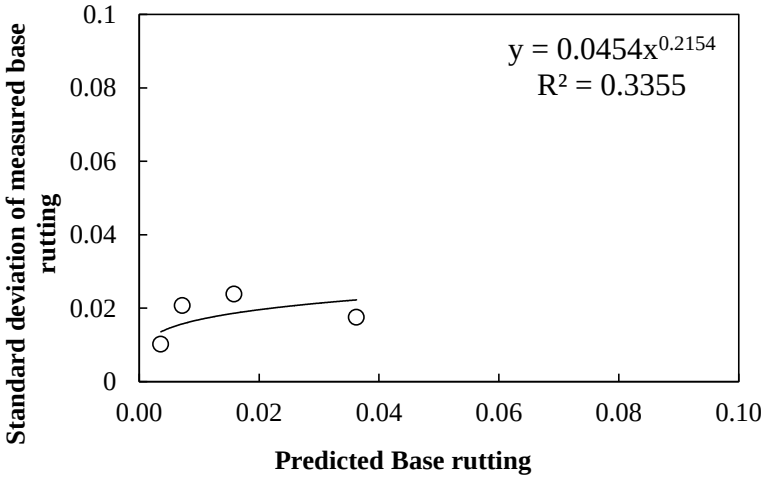

(b) Base rutting reliability

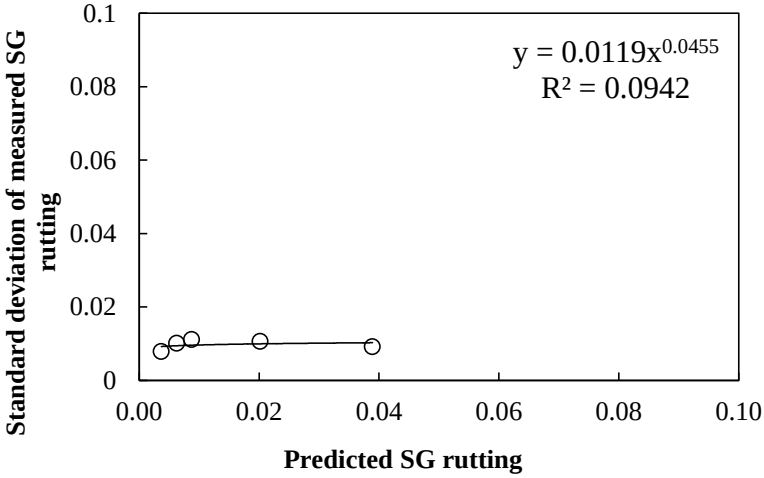

(c) Subgrade rutting reliability

Figure B-274 Rutting model reliability equations – option 4 method 2 – bootstrapping

B.1.4 Transverse Cracking Model

B.1.4.1 Level 1

Option 1

Table B-143 Level 1 Option 1 thermal cracking results

Parameter	SEE	Bias
Global model Level 1	1343.58	903.06
K = 0.5 Level 1	767.05	-217.64
K = 0.75 Level 1	753.24	-70.40
K = 1 Level 1	943.39	246.75
K = 1.1 Level 1	1019.15	369.83
K = 1.2 Level 1	1094.84	492.97
K = 1.3 Level 1	1176.40	630.50
K = 1.4 Level 1	1277.75	783.51
K = 1.7 Level 1	1459.76	1109.90
K = 2 Level 1	1560.47	1310.64
K = 2.5 Level 1	1692.66	1553.99

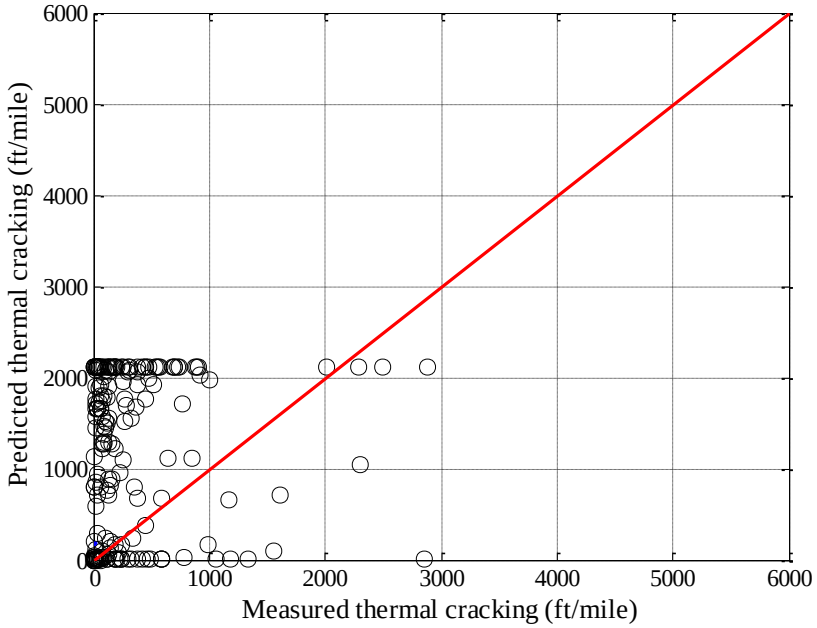

Figure B-275 Level 1 thermal cracking global model – option 1

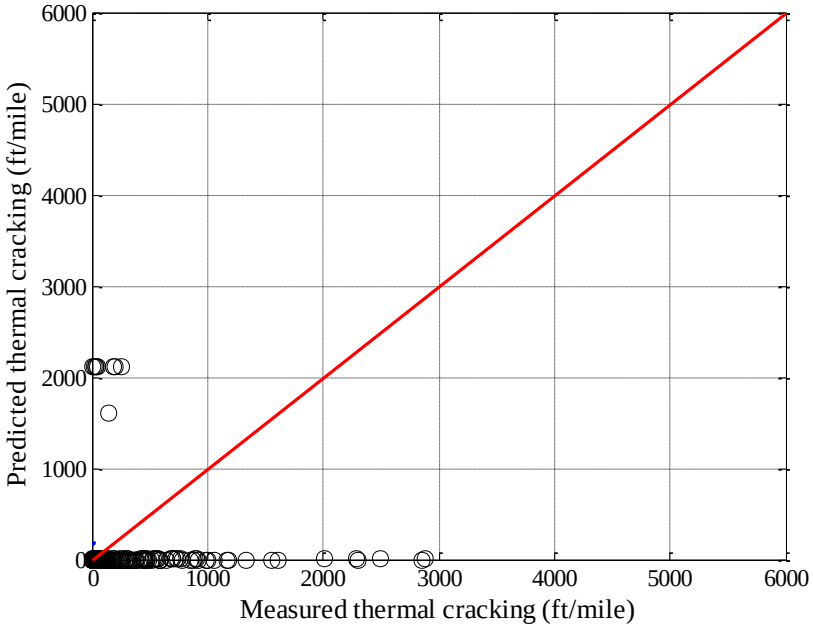

Figure B-276 Level 1 thermal cracking local model K = 0.5 – option 1

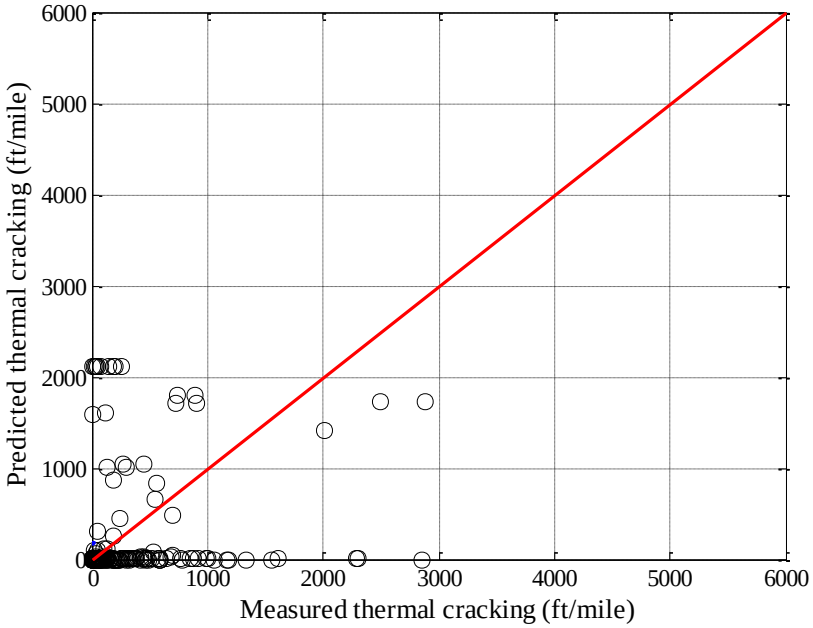

Figure B-277 Level 1 thermal cracking local model K = 0.75 – option 1

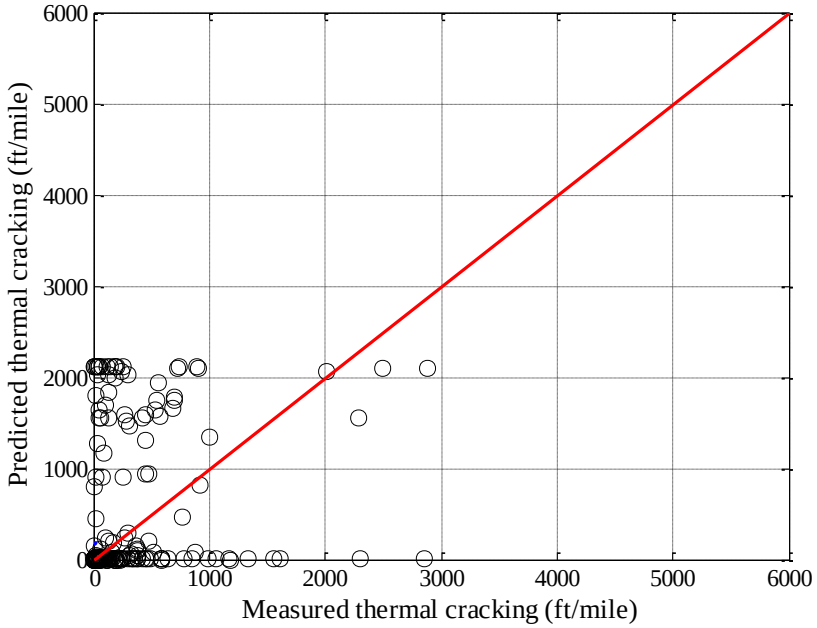

Figure B-278 Level 1 thermal cracking local model K = 1 – option 1

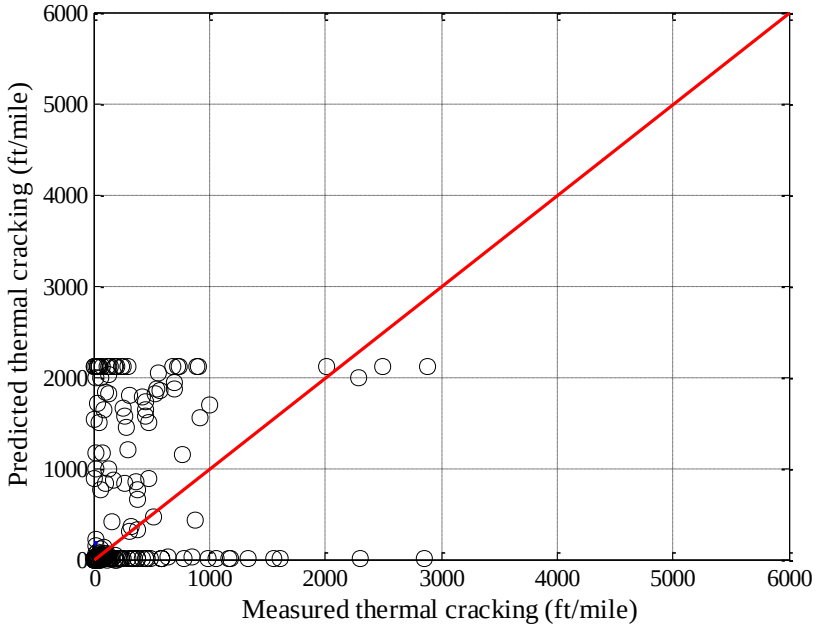

Figure B-279 Level 1 thermal cracking local model K = 1.1 – option 1

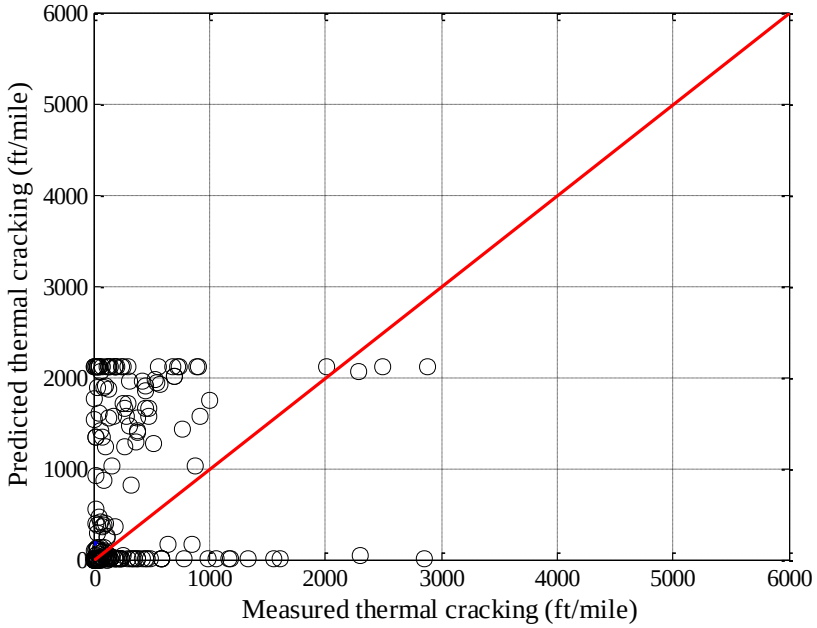

Figure B-280 Level 1 thermal cracking local model K = 1.2 – option 1

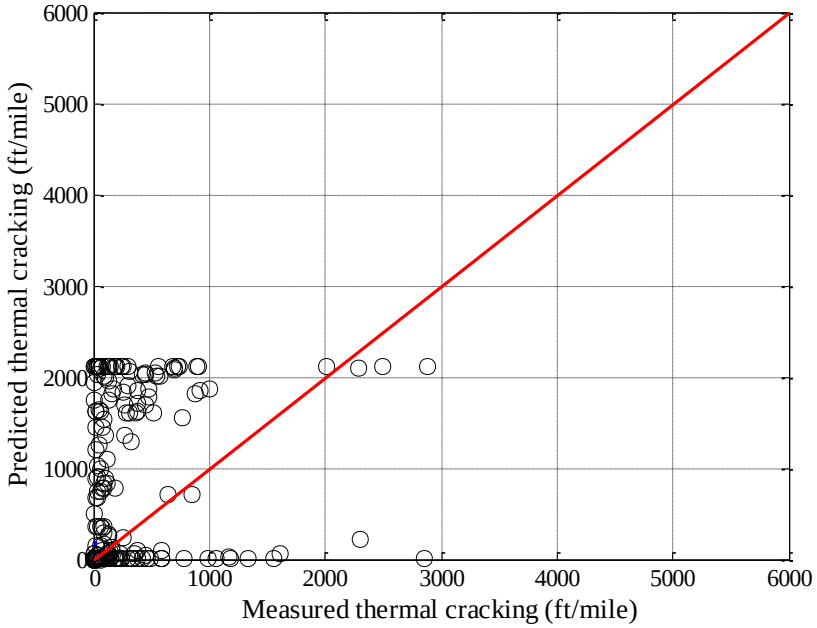

Figure B-281 Level 1 thermal cracking local model K = 1.3 – option 1

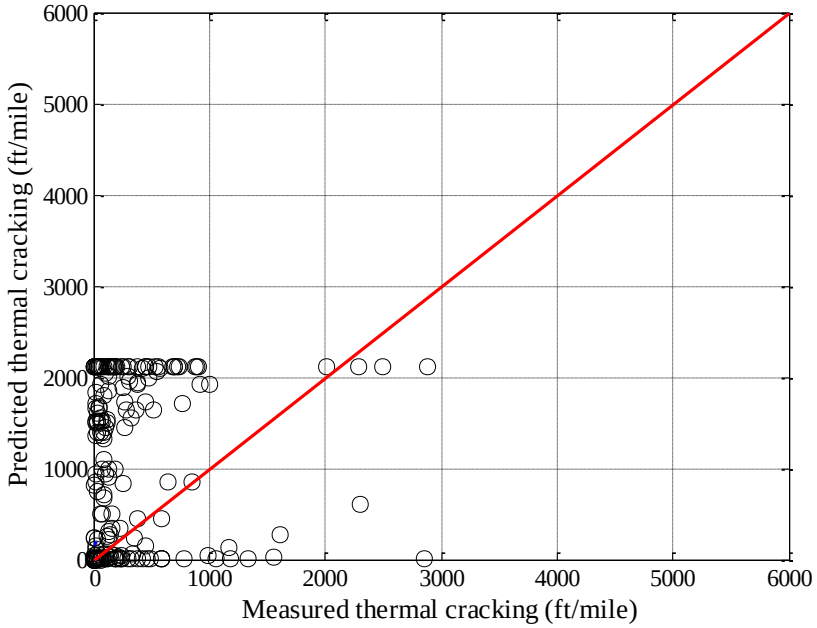

Figure B-282 Level 1 thermal cracking local model K = 1.4 – option 1

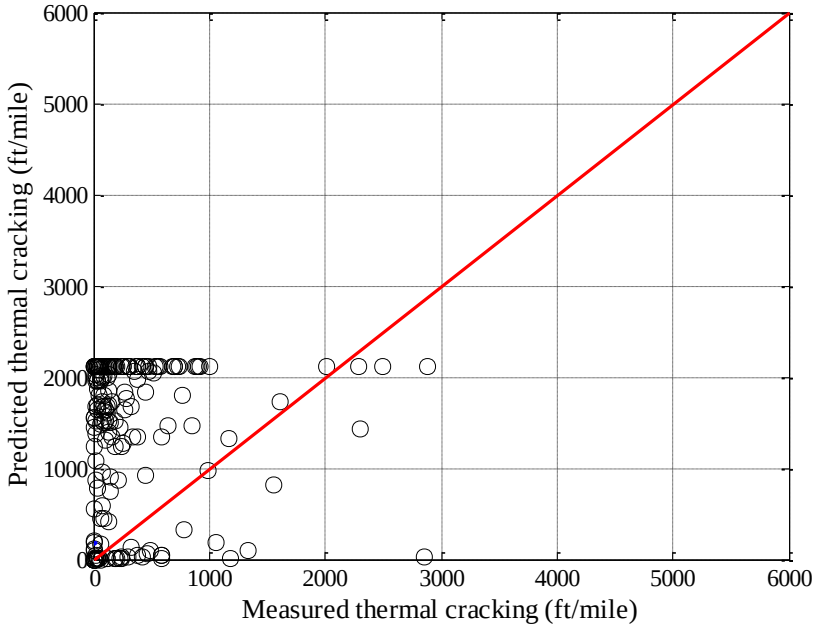

Figure B-283 Level 1 thermal cracking local model K = 1.7 – option 1

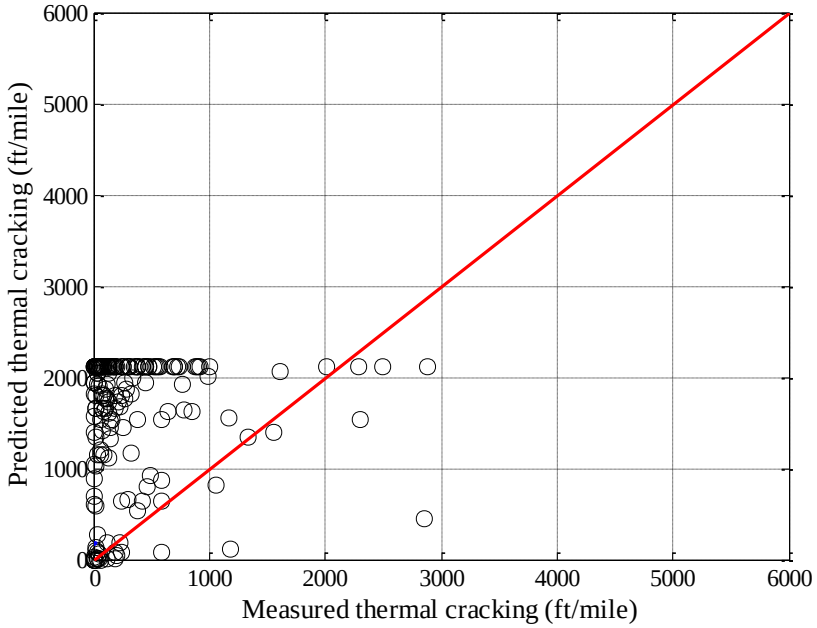

Figure B-284 Level 1 thermal cracking local model K = 2 – option 1

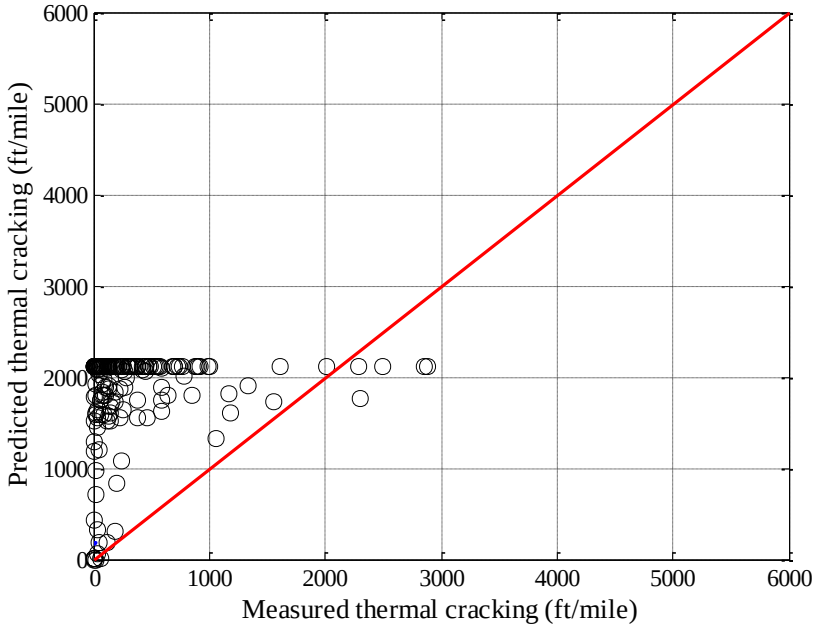

Figure B-285 Level 1 thermal cracking local model K = 2.5– option 1

Reliability

Table B-144 Level 1 Option 1 reliability equation

Data set option	Global model equation	Local model equation
Option 1	$s_e(Level1) = 0.1468(TC) + 65.027$	$s_e(Level1) = 0.4203(TC) + 216.94$

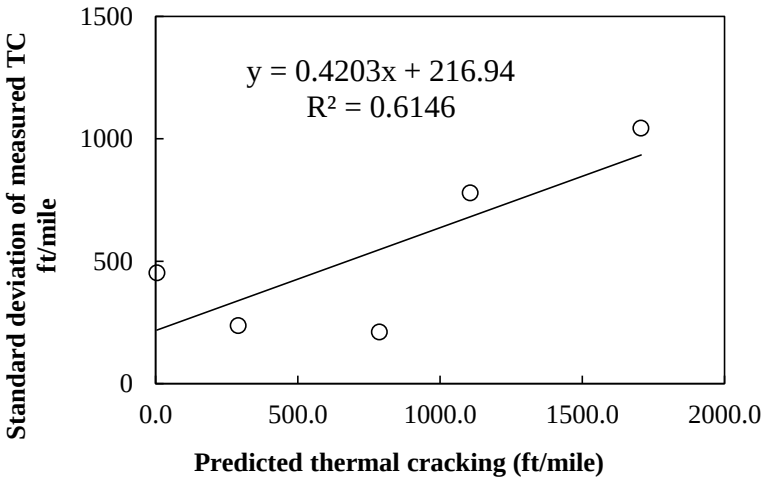

Figure B-286 Level 1 Option 1 thermal cracking fitted reliability model

Option 2

Table B-145 Level 1 Option 2 thermal cracking results

Parameter	SEE	Bias
Global model Level 1	1306.5	854.7
K = 0.5 Level 1	745.5	-212.6
K = 0.75 Level 1	732.1	-73.8
K = 1 Level 1	916.4	225.1
K = 1.1 Level 1	989.9	341.2
K = 1.2 Level 1	1063.2	457.5
K = 1.3 Level 1	1142.3	588.4
K = 1.4 Level 1	1241.0	736.0
K = 1.7 Level 1	1425.3	1064.9
K = 2 Level 1	1529.4	1271.1
K = 2.5 Level 1	1667.5	1524.3

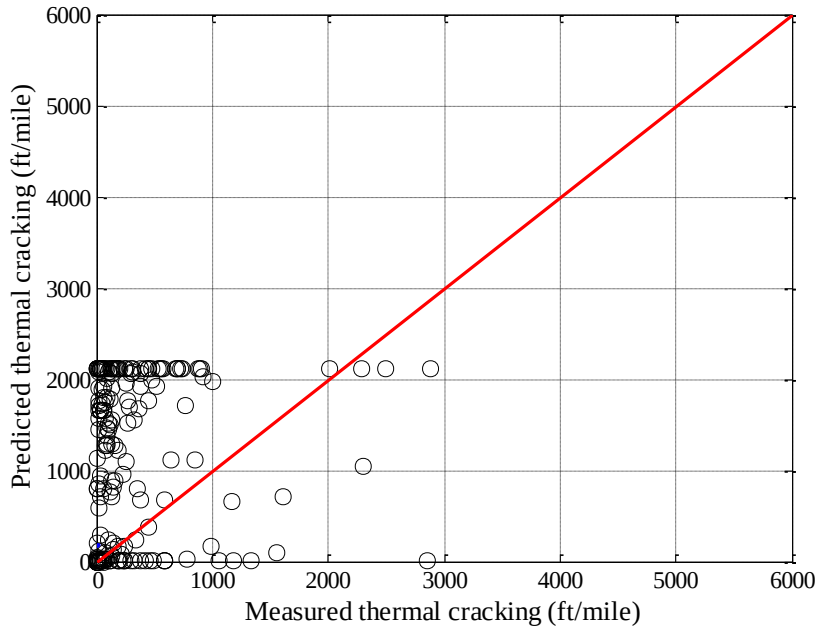

Figure B-287 Level 1 thermal cracking global model – option 2

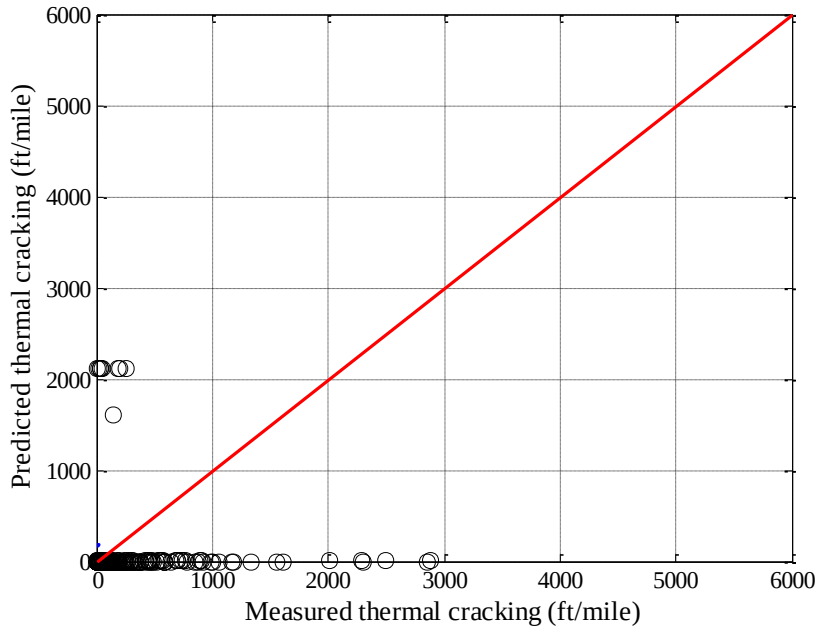

Figure B-288 Level 1 thermal cracking local model K = 0.5 – option 2

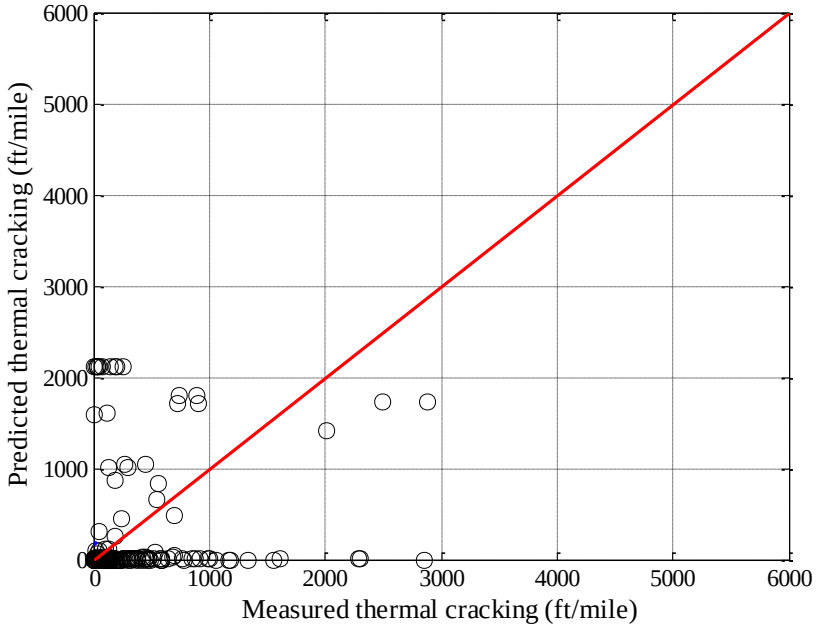

Figure B-289 Level 1 thermal cracking local model K = 0.75 – option 2

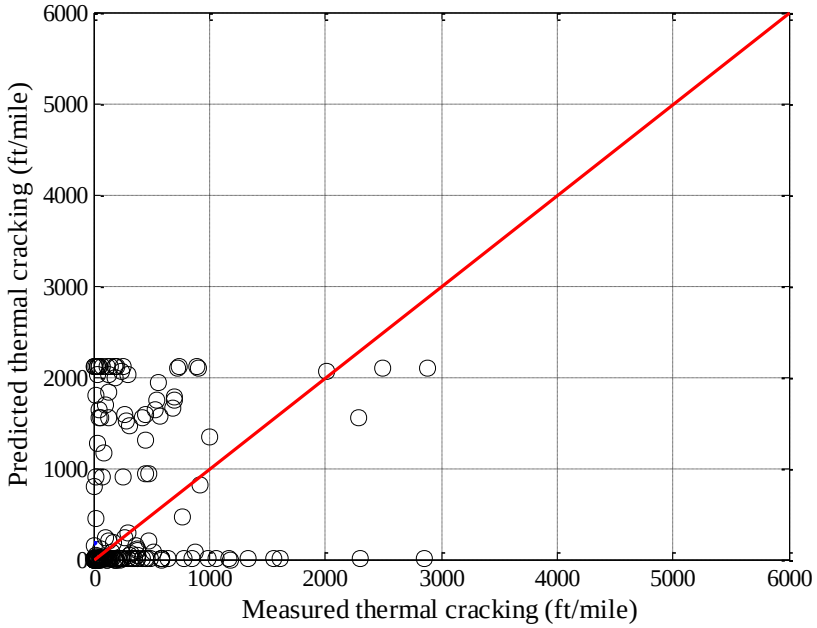

Figure B-290 Level 1 thermal cracking local model K = 1 – option 2

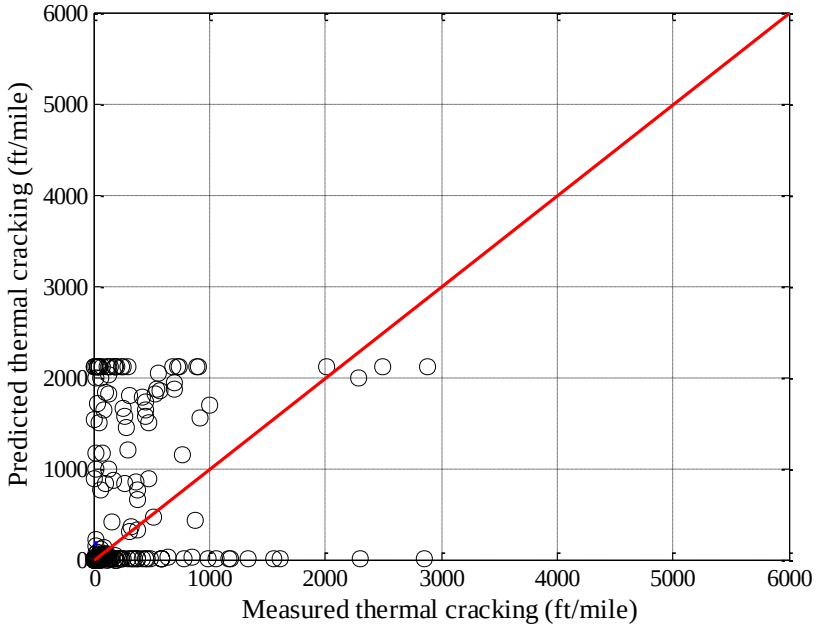

Figure B-291 Level 1 thermal cracking local model K = 1.1 – option 2

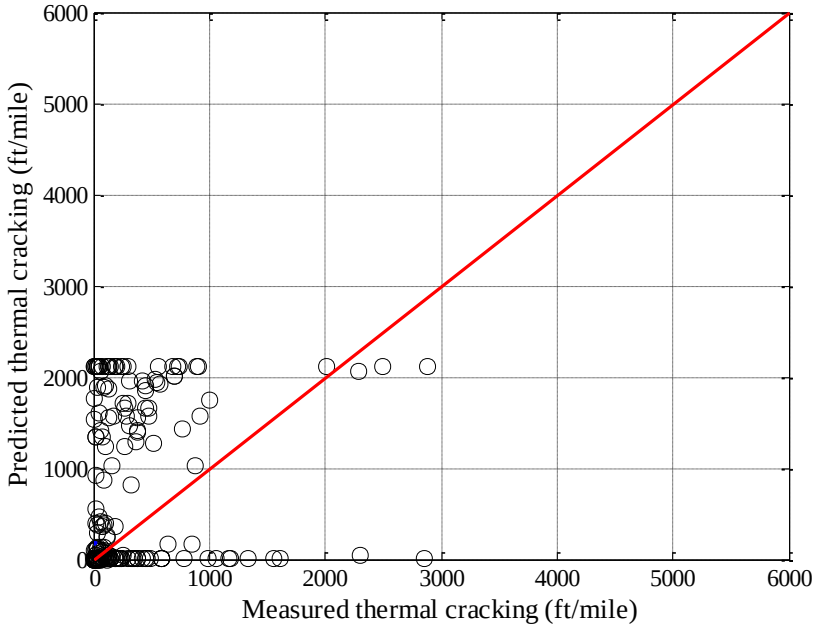

Figure B-292 Level 1 thermal cracking local model K = 1.2 – option 2

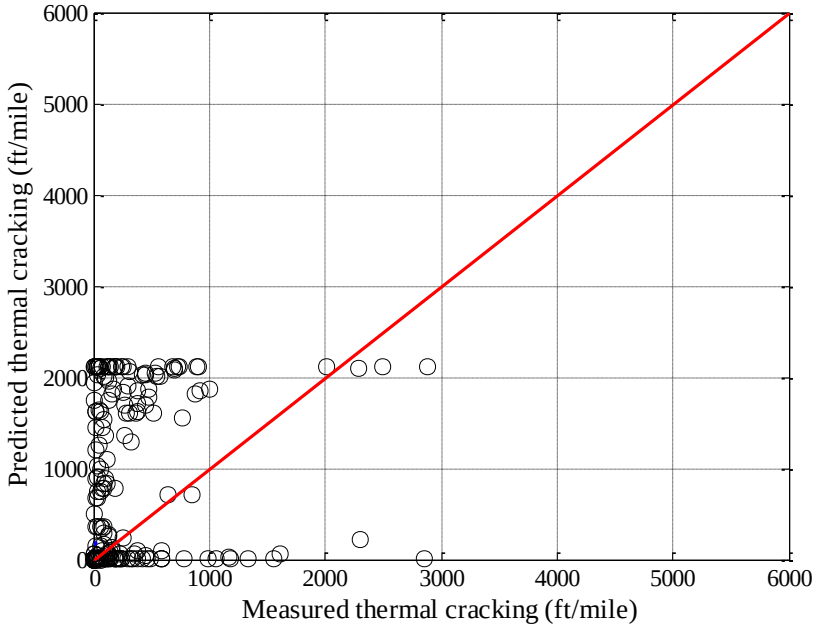

Figure B-293 Level 1 thermal cracking local model K = 1.3 – option 2

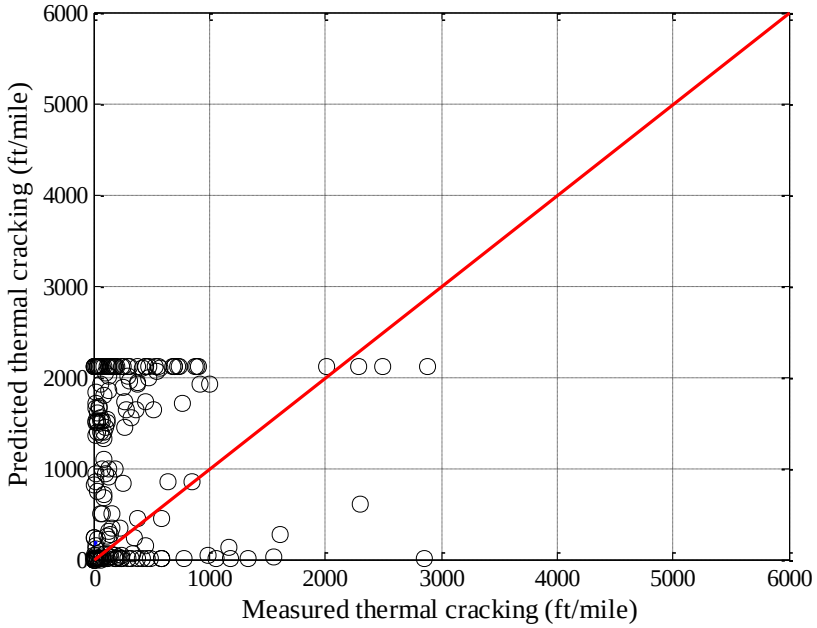

Figure B-294 Level 1 thermal cracking local model K = 1.4 – option 2

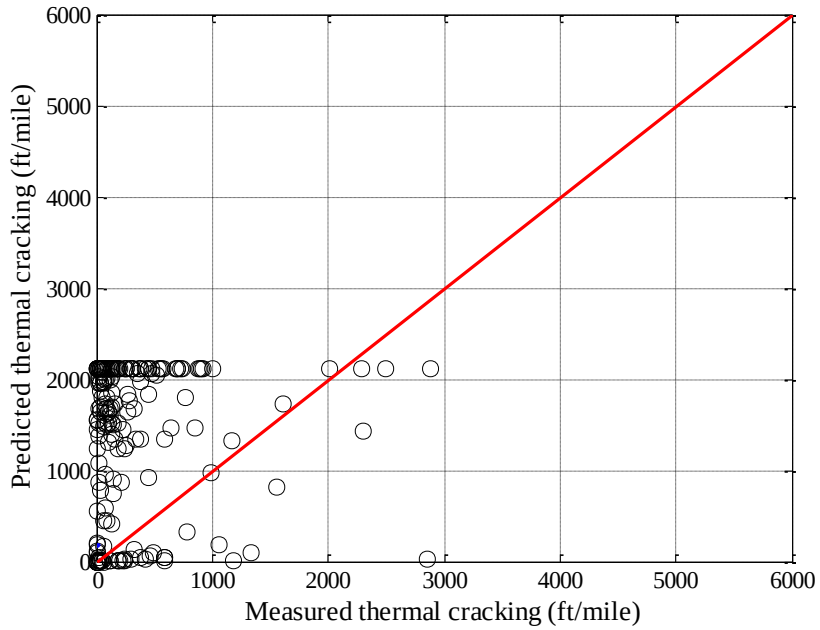

Figure B-295 Level 1 thermal cracking local model K = 1.7 – option 2

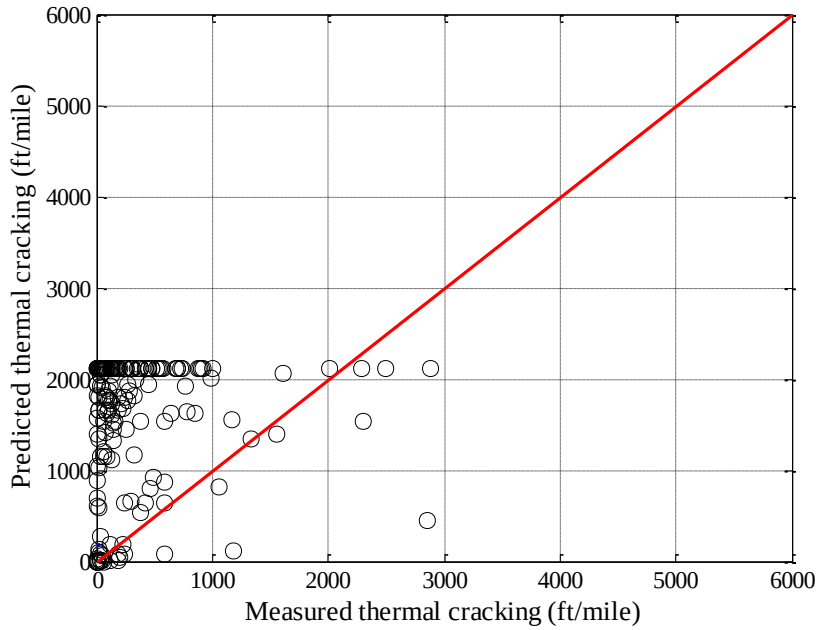

Figure B-296 Level 1 thermal cracking local model K = 2 – option 2

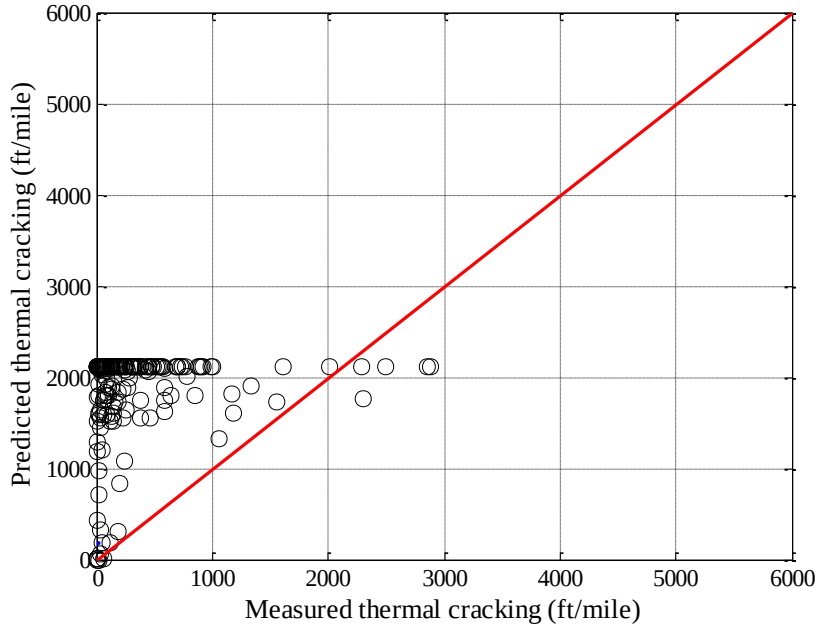

Figure B-297 Level 1 thermal cracking local model K = 2.5 – option 2

Reliability

Table B-146 Level 1 Option 2 reliability equation

Data set option	Global model equation	Local model equation
Option 2	$s_e(Level1) = 0.1468(TC) + 65.027$	$s_e(Level1) = 0.4258(TC) + 210.08$

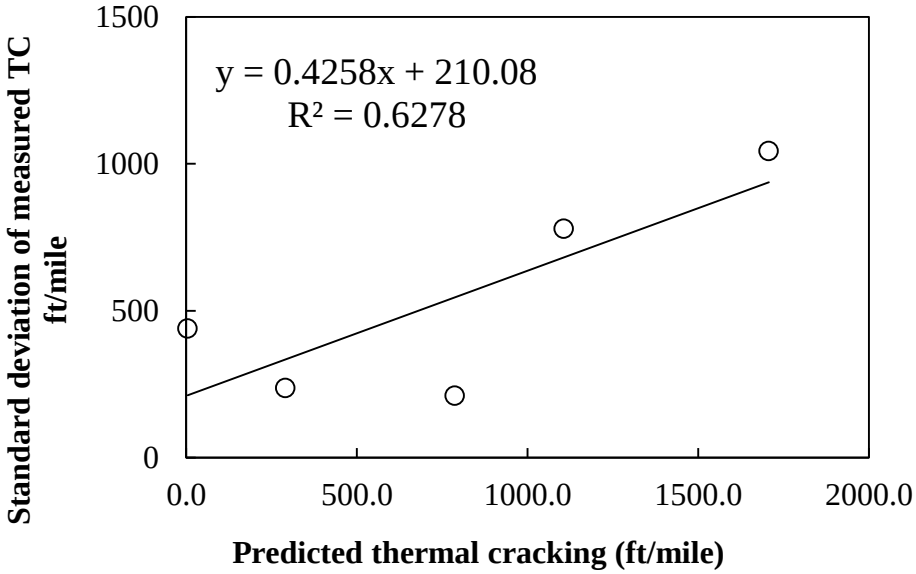

Figure B-298 Level 1 Option 2 thermal cracking fitted reliability model

B.1.4.2 Level 3

Option 1

Table B-147 Level 3 Option 1 thermal cracking results

Parameter	SEE	Bias
Global model K = 1.5	754.6	-318.5
K = 2 Level 3	785.5	-249.7
K = 3 Level 3	867.2	-23.2
K = 4 Level 3	978.2	233.9
K = 5 Level 3	1107.2	494.5

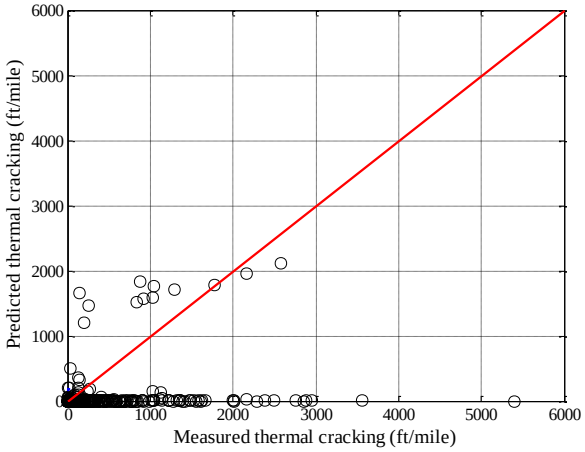

Figure B-299 Level 3 thermal cracking global model – option 1

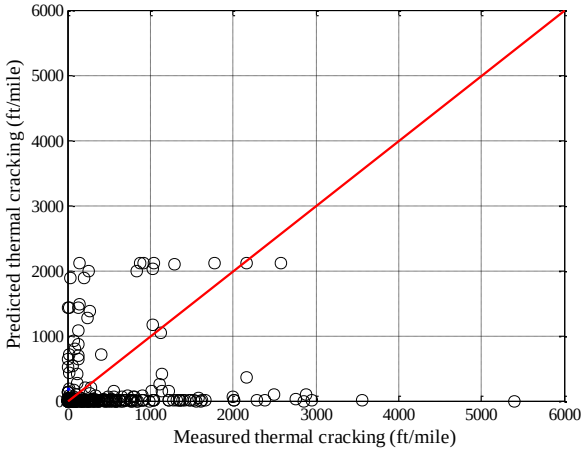

Figure B-300 Level 3 thermal cracking local model K = 2 – option 1

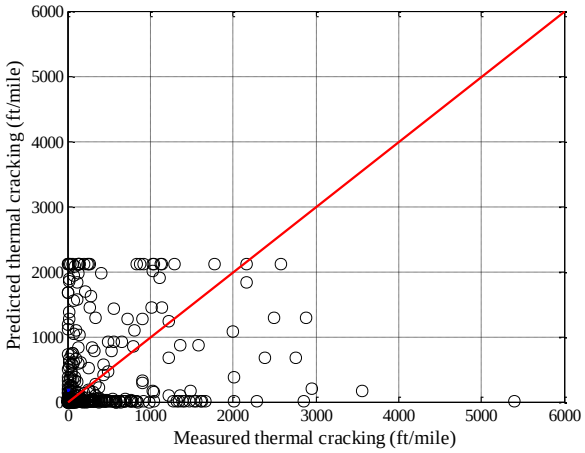

Figure B-301 Level 3 thermal cracking local model K = 3 – option 1

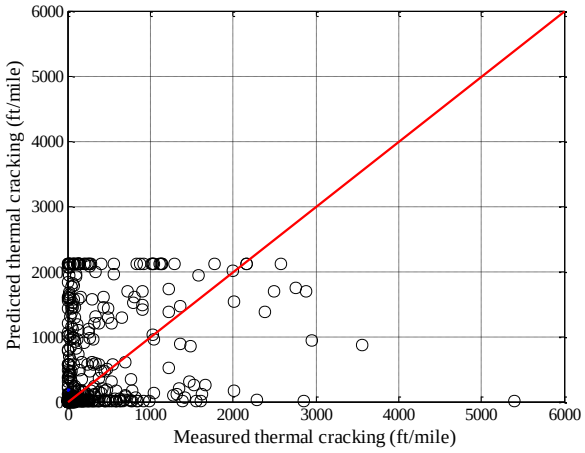

Figure B-302 Level 3 thermal cracking local model K =4 – option 1

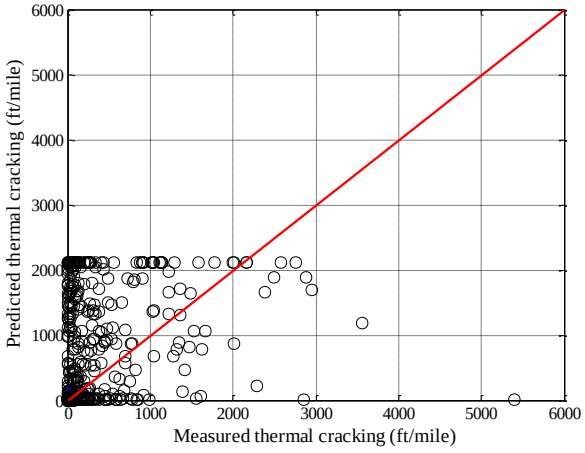

Figure B-303 Level 3 thermal cracking local model K = 5 – option 1

Reliability

Table B-148 Level 3 Option 1 reliability equation

Data set option	Global model equation	Local model equation
Option 1	$s_e(Level3) = 0.3972(TC) + 20.422$	$s_e(Level3) = 0.142(TC) + 670.28$

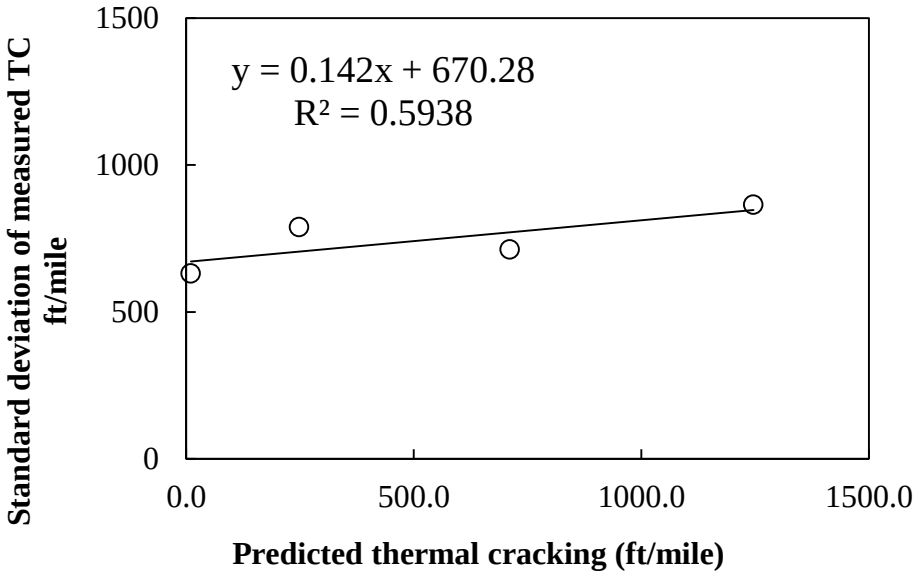

Figure B-304 Level 3 Option 1 thermal cracking fitted reliability model

Option 2

Table B-149 Level 3 Option 2 thermal cracking results

Parameter	SEE	Bias
Global model Level 3	945.0	-489.0
K = 2 Level 3	965.6	-416.2
K = 3 Level 3	1022.4	-209.6
K = 4 Level 3	1057.7	35.3
K = 5 Level 3	1121.8	289.6

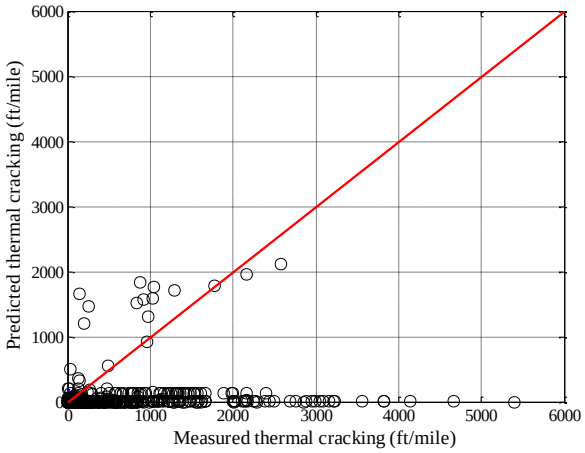

Figure B-305 Level 3 thermal cracking global model – option 2

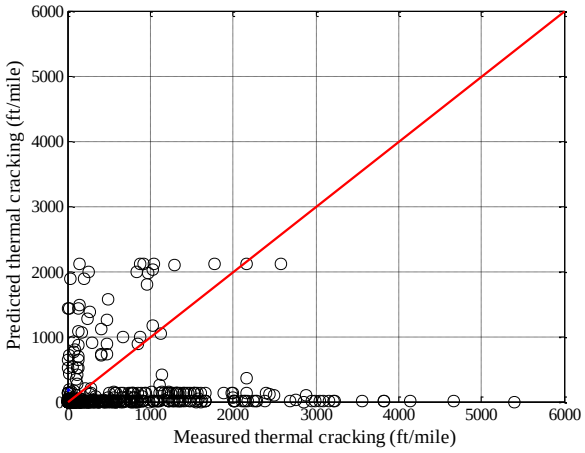

Figure B-306 Level 3 thermal cracking local model K = 2 – option 2

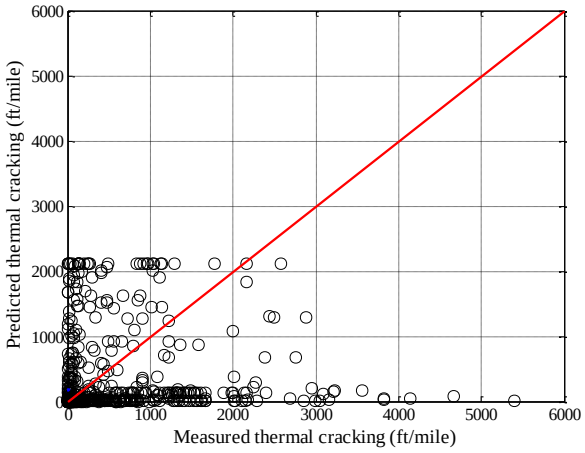

Figure B-307 Level 3 thermal cracking local model K = 3 – option 2

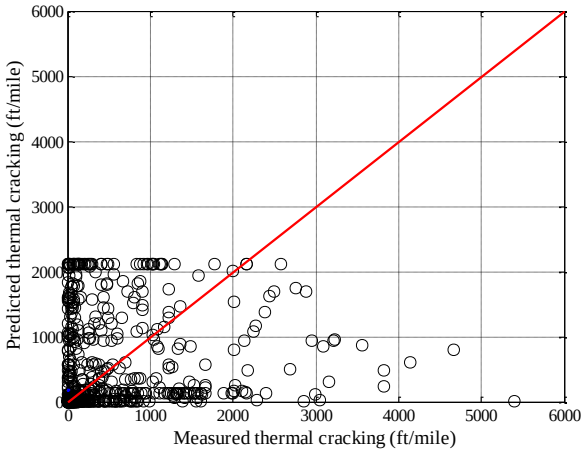

Figure B-308 Level 3 thermal cracking local model K =4 – option 2

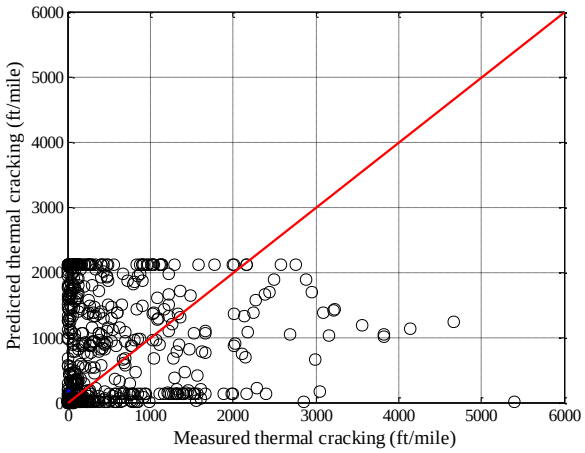

Figure B-309 Level 3 thermal cracking local model K = 5 – option 2

Reliability

Table B-150 Level 3 Option 2 reliability equation

Data set option	Global model equation	Local model equation
Option 2	$s_e(Level3) = 0.3972(TC) + 20.422$	$s_e(Level3) = 0.7737(TC) + 622.92$

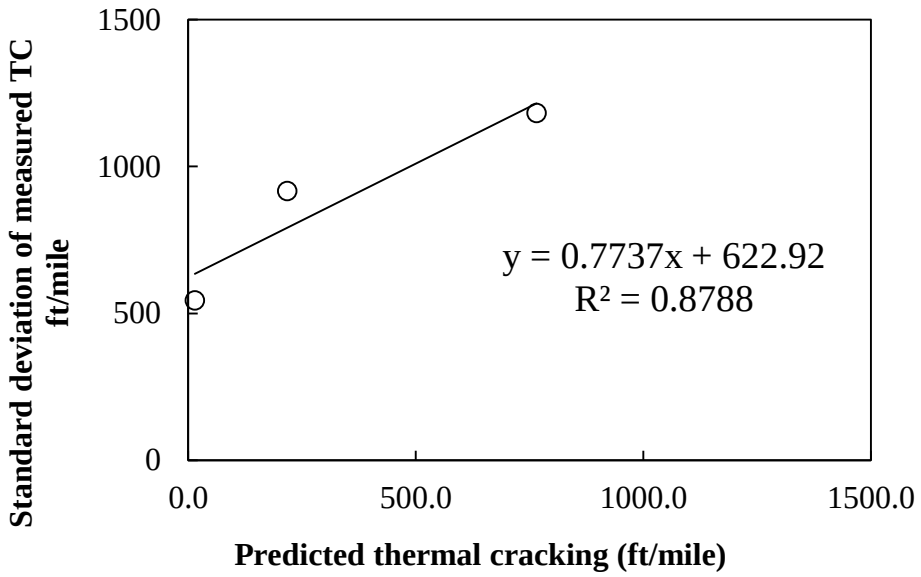

Figure B-310 Level 3 Option 2 thermal cracking fitted reliability model

Option 4

Table B-151 Level 3 Option 4 thermal cracking results

Parameter	SEE	Bias
Global model Level 3	1304.7	-906.6
K = 2 Level 3	1312.1	-824.0
K = 3 Level 3	1334.6	-666.1
K = 4 Level 3	1237.6	-451.0
K = 5 Level 3	1163.8	-212.0

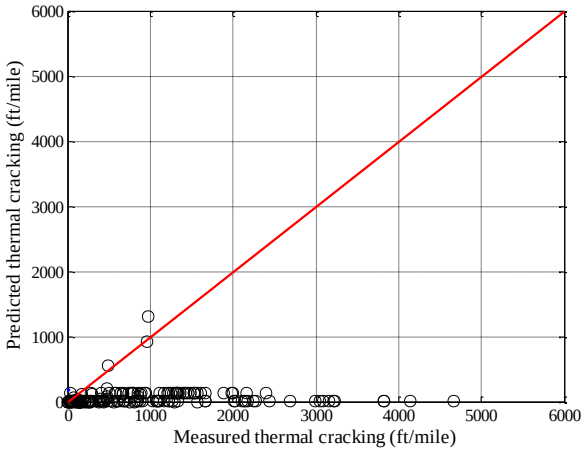

Figure B-311 Level 3 thermal cracking global model – option 3

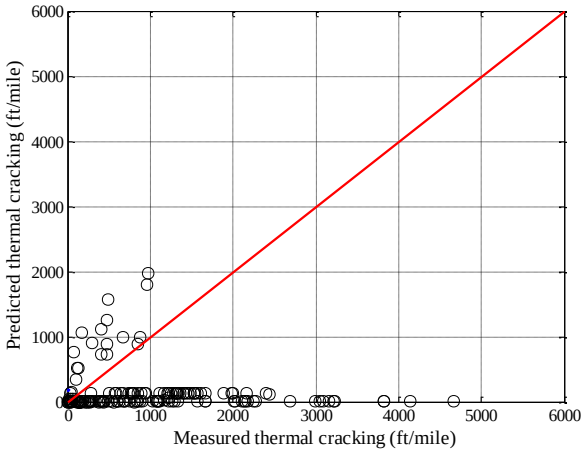

Figure B-312 Level 3 thermal cracking local model K = 2 – option 3

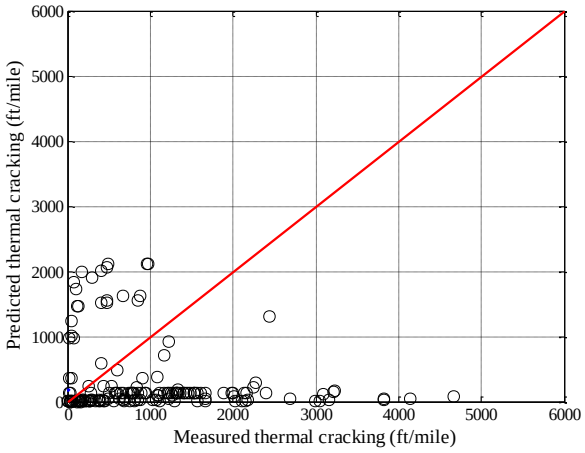

Figure B-313 Level 3 thermal cracking local model K = 3 – option 3

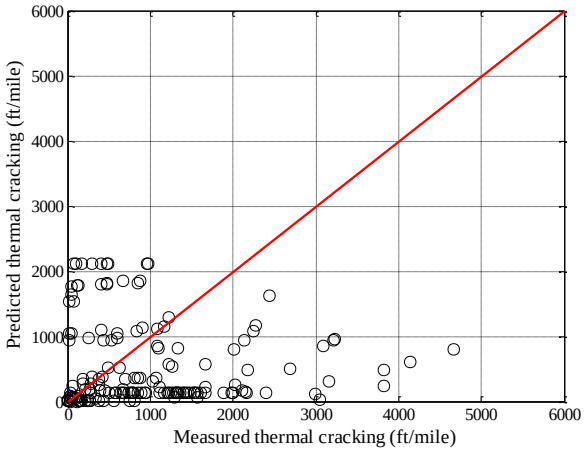

Figure B-314 Level 3 thermal cracking local model K =4 – option 3

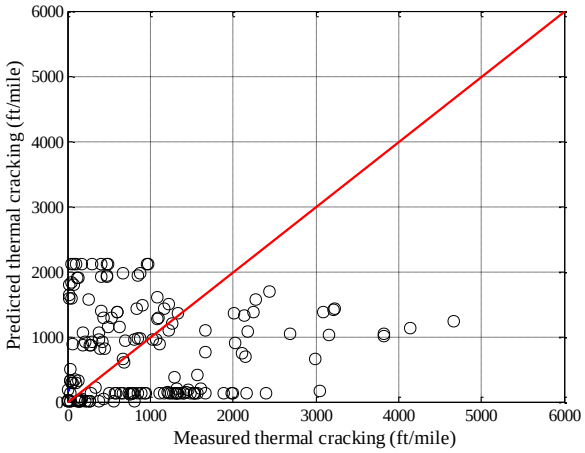

Figure B-315 Level 3 thermal cracking local model K = 5 – option 3

Reliability

Table B-152 Level 3 Option 4 reliability equation

Data set option	Global model equation	Local model equation
Option 4	$s_e(Level3) = 0.3972(TC) + 20.422$	$s_e(Level3) = 0.7039(TC) + 324.26$

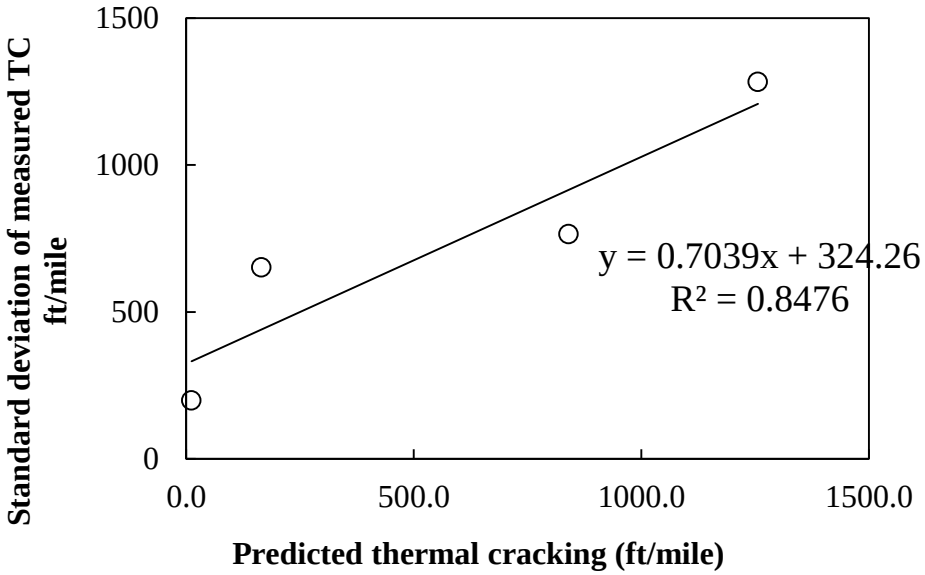

Figure B-316 Level 3 Option 4 thermal cracking fitted reliability model

B.1.5 Pavement Roughness (IRI)

B.1.5.1 Option 1

No sampling

Table B-153 Option 1 IRI local calibration results – no sampling

Parameter	Global	Local
SEE	14.8261	14.1044
Bias	2.7552	0.0070
R^2	0.6922	0.7228
t-test pvalue	0.0003	0.9923
Intercept = 0	0.0000	0.0000
Slope = 1	0.0000	0.0000
C1	40.0000	48.5626
C2	0.4000	0.4781
C3	0.0080	0.0064
C4	0.0150	0.0072

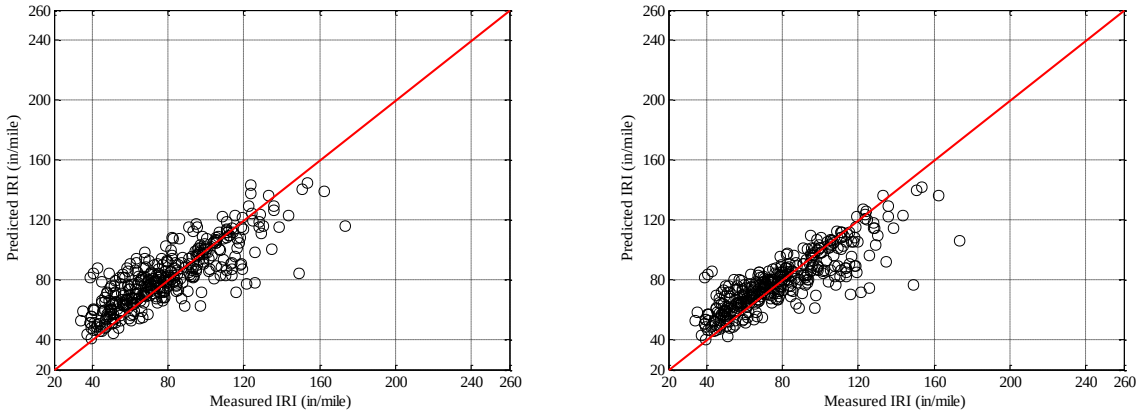

(a) Global model (b) Local model

Figure B-317 Option 1 IRI local calibration measured versus predicted – no sampling

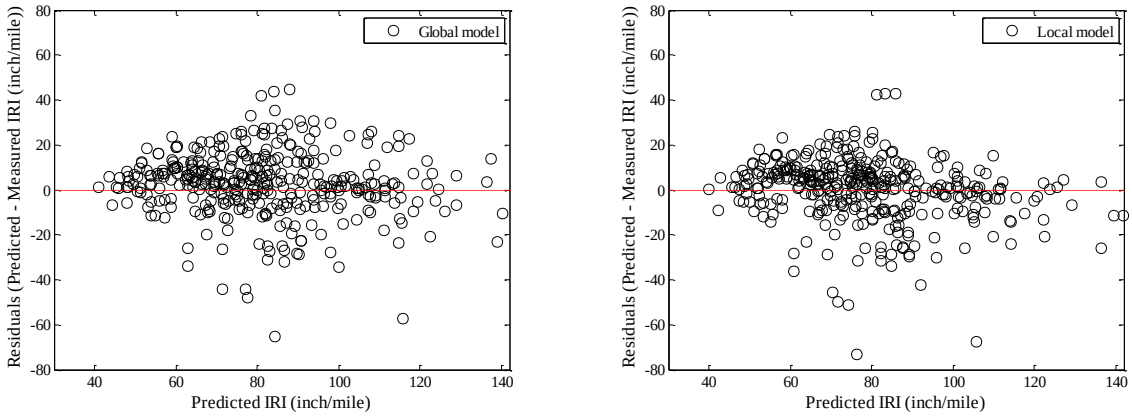

(a) Global model (b) Local model

Figure B-318 Option 1 IRI local calibration residual plots – no sampling

Reliability

The IRI reliability is internally estimated by the software.

Split sampling

Table B-154 Option 1 IRI local calibration results – split sampling

Parameter	Global model	Local model	Validation
SEE	14.9090	14.1483	14.1497
Bias	2.4035	0.0973	0.5702
R^2	0.6945	0.7280	0.7129
t-test pvalue	0.0108	0.9140	0.6515
Intercept = 0	0.0000	0.0000	0.0000
Slope = 1	0.0000	0.0000	0.0000
C1	40.0000	52.8662	52.8662
C2	0.4000	0.3535	0.3535
C3	0.0080	0.0064	0.0064
C4	0.0150	0.0071	0.0071

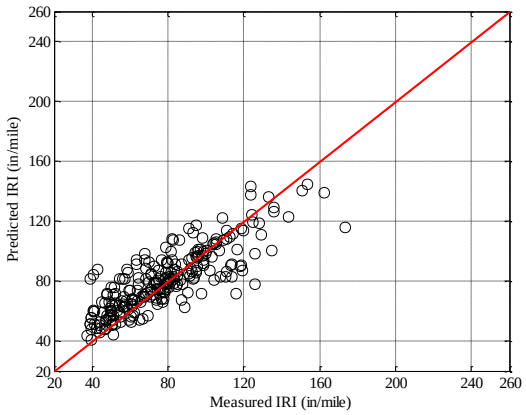

(a) Global model

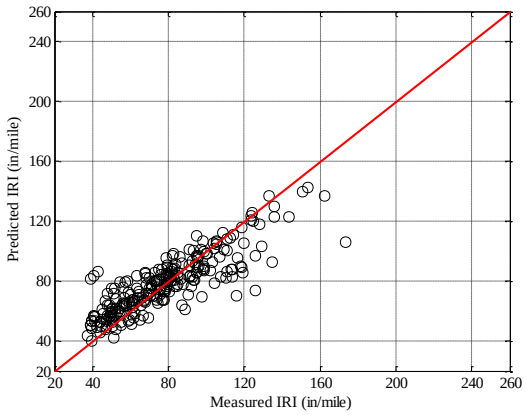

(b) Local model

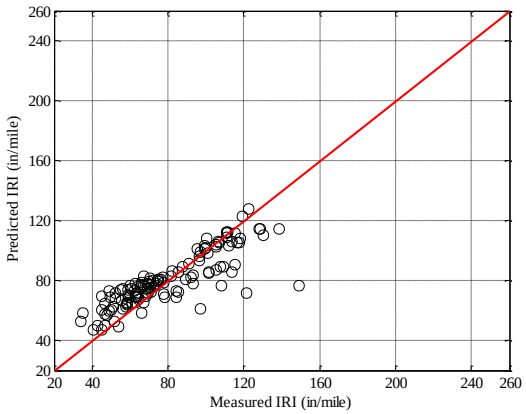

(c) Local model validation

Figure B-319 Option 1 IRI local calibration measured versus predicted – split sampling

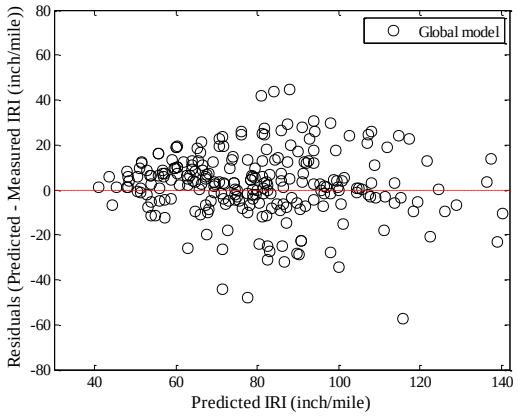

(a) Global model

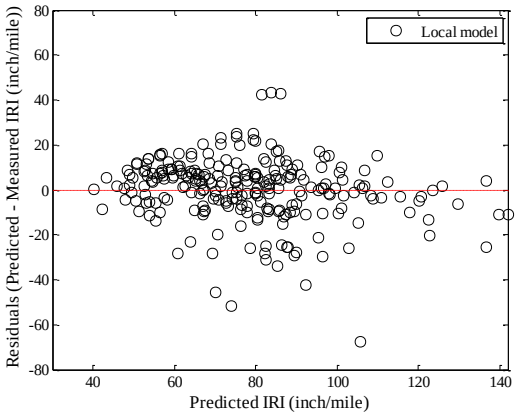

(b) Local model

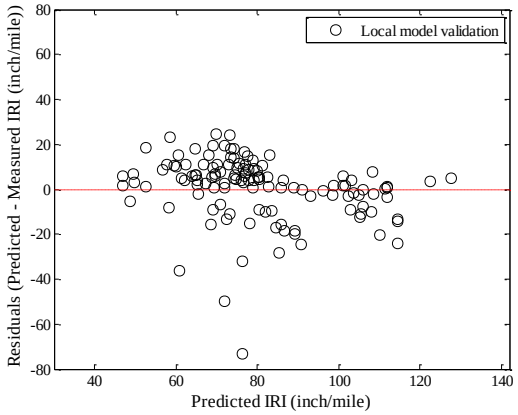

(c) Local model validation

Figure B-320 Option 1 IRI local calibration residual plots – split sampling

Reliability

The IRI reliability is internally estimated by the software.

Repeated split sampling

Table B-155 Option 1 IRI local calibration results – repeated split sampling

Global Model				
Parameter	Global Model Mean	Global Model Median	Global model lower CI	Global model upper CI
SEE	14.8176	14.8629	13.3900	15.9512
Bias	2.7282	2.7679	1.0972	4.2236
C1	40.0000	40.0000	-	-
C2	0.4000	0.4000	-	-
C3	0.0080	0.0080	-	-
C4	0.0150	0.0150	-	-
Local Model				
Parameter	Local Model Mean	Local Model Median	Local model lower CI	Local model upper CI
SEE	14.0562	14.1138	12.3621	15.3295
Bias	0.0294	0.0213	-0.4797	0.6616
C1	50.8200	50.8000	41.8300	57.8000
C2	0.4088	0.4693	0.3200	0.4800
C3	0.0064	0.0064	0.0064	0.0070
C4	0.0070	0.0072	0.0053	0.0072
Local Model validation				
Parameter	Local Model Mean	Local Model Median	Local model lower CI	Local model upper CI
SEE	14.2948	14.3197	10.9564	17.7144
Bias	0.1403	0.1667	-4.5686	4.9868
C1	50.8200	50.8000	41.8300	57.8000
C2	0.4088	0.4693	0.3200	0.4800
C3	0.0064	0.0064	0.0064	0.0070
C4	0.0070	0.0072	0.0053	0.0072

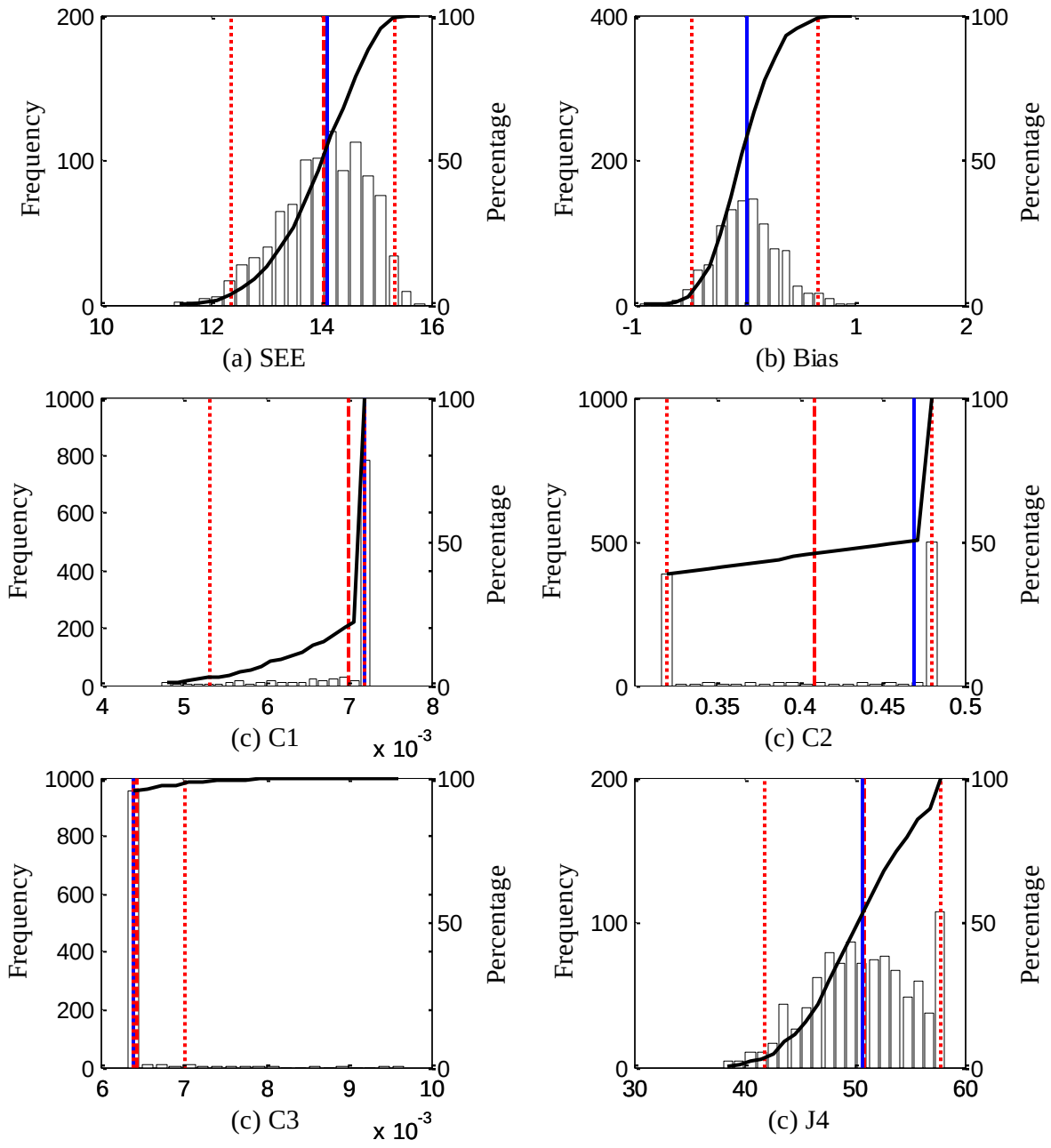

Figure B-321 Option 1 IRI repeated split sampling frequency distributions – calibration

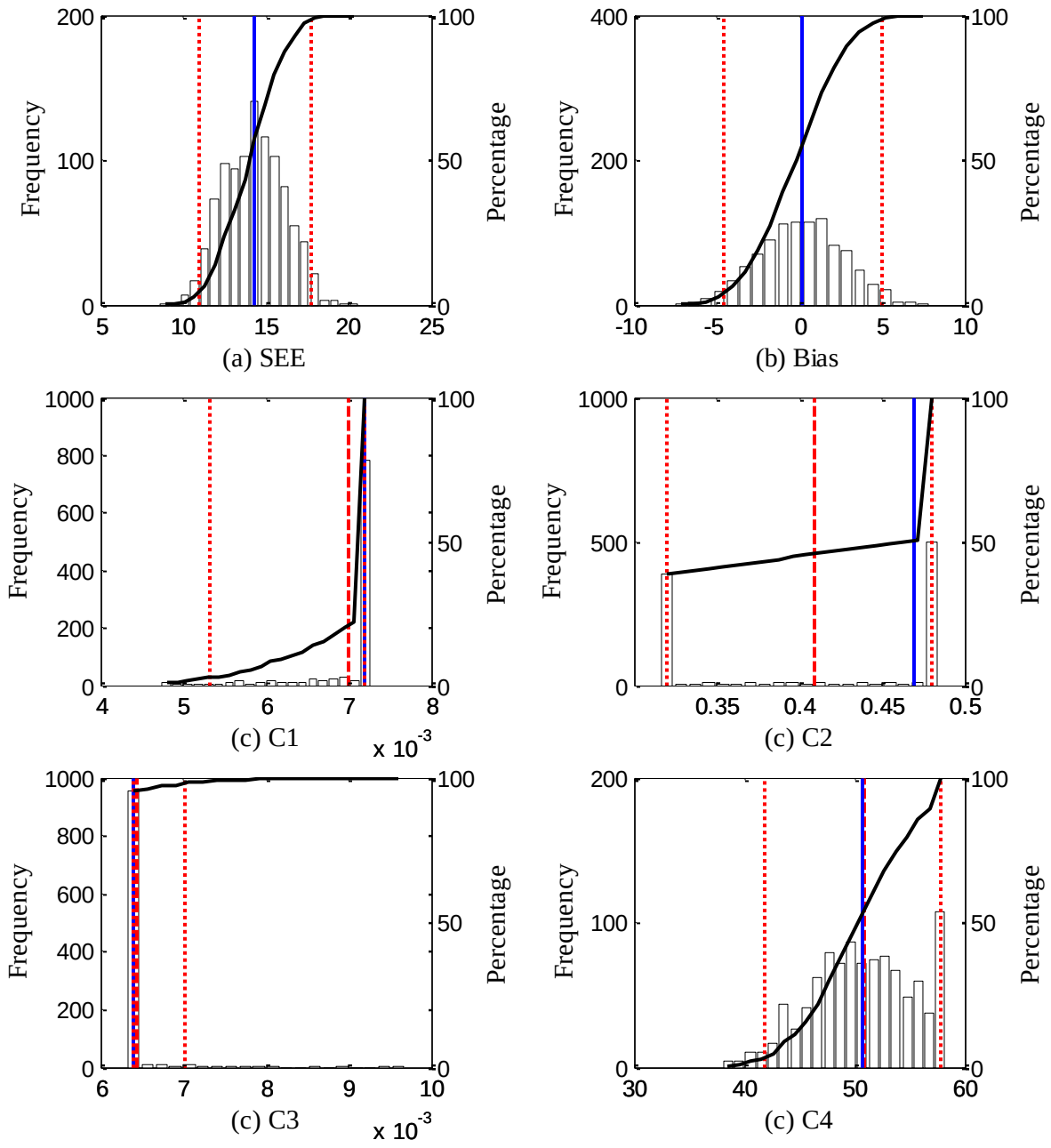

Figure B-322 Option 1 IRI repeated split sampling frequency distributions – validation

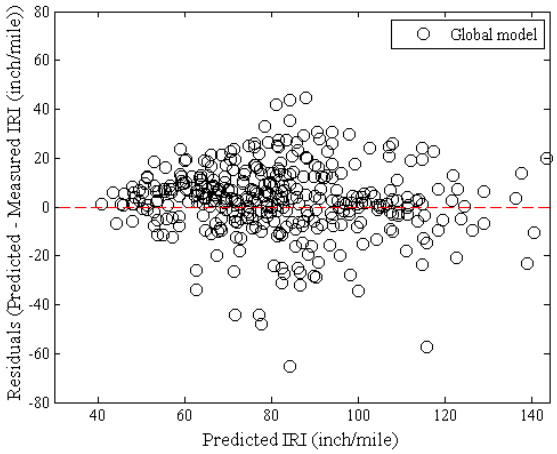

(a) Global model

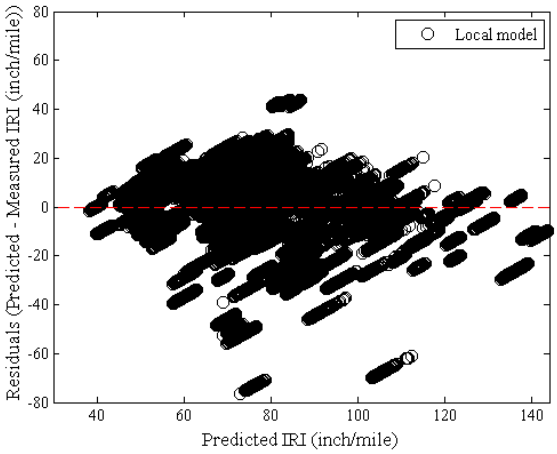

(b) Local model

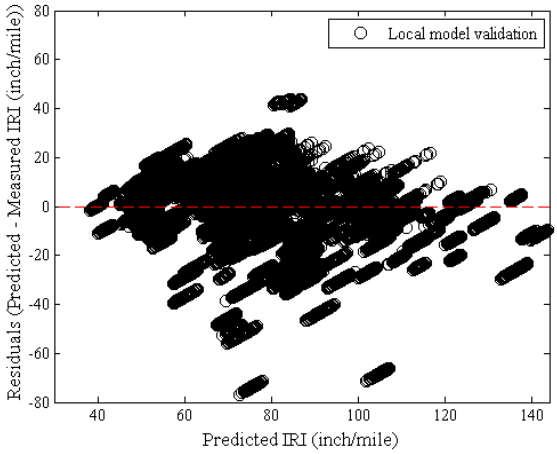

(c) Local model validation

Figure B-323 Option 1 IRI local calibration residual plots – repeated split sampling

Reliability

The IRI reliability is internally estimated by the software.

Bootstrapping

Table B-156 Option 1 IRI local calibration results – bootstrapping

Global Model				
Parameter	Global Model Mean	Global Model Median	Global model lower CI	Global model upper CI
SEE	14.7738	14.7500	12.9187	16.6746
Bias	2.7817	2.7779	0.4205	5.0187
C1	40.0000	40.0000	-	-
C2	0.4000	0.4000	-	-
C3	0.0080	0.0080	-	-
C4	0.0150	0.0150	-	-
Local Model				
Parameter	Local Model Mean	Local Model Median	Local model lower CI	Local model upper CI
SEE	13.9428	13.9428	11.8322	16.2173
Bias	-0.0391	-0.0160	-0.9072	0.8145
C1	50.3720	51.1021	38.5371	57.8050
C2	0.4102	0.4800	0.3200	0.4800
C3	0.0066	0.0064	0.0064	0.0084
C4	0.0068	0.0072	0.0048	0.0072

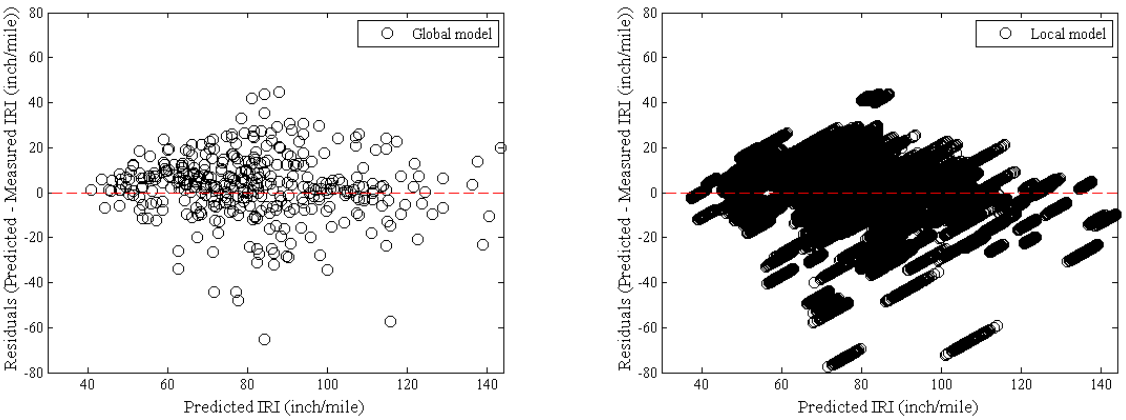

(a) Global model (b) Local model

Figure B-324 Option 1 IRI local calibration residual plots – bootstrapping

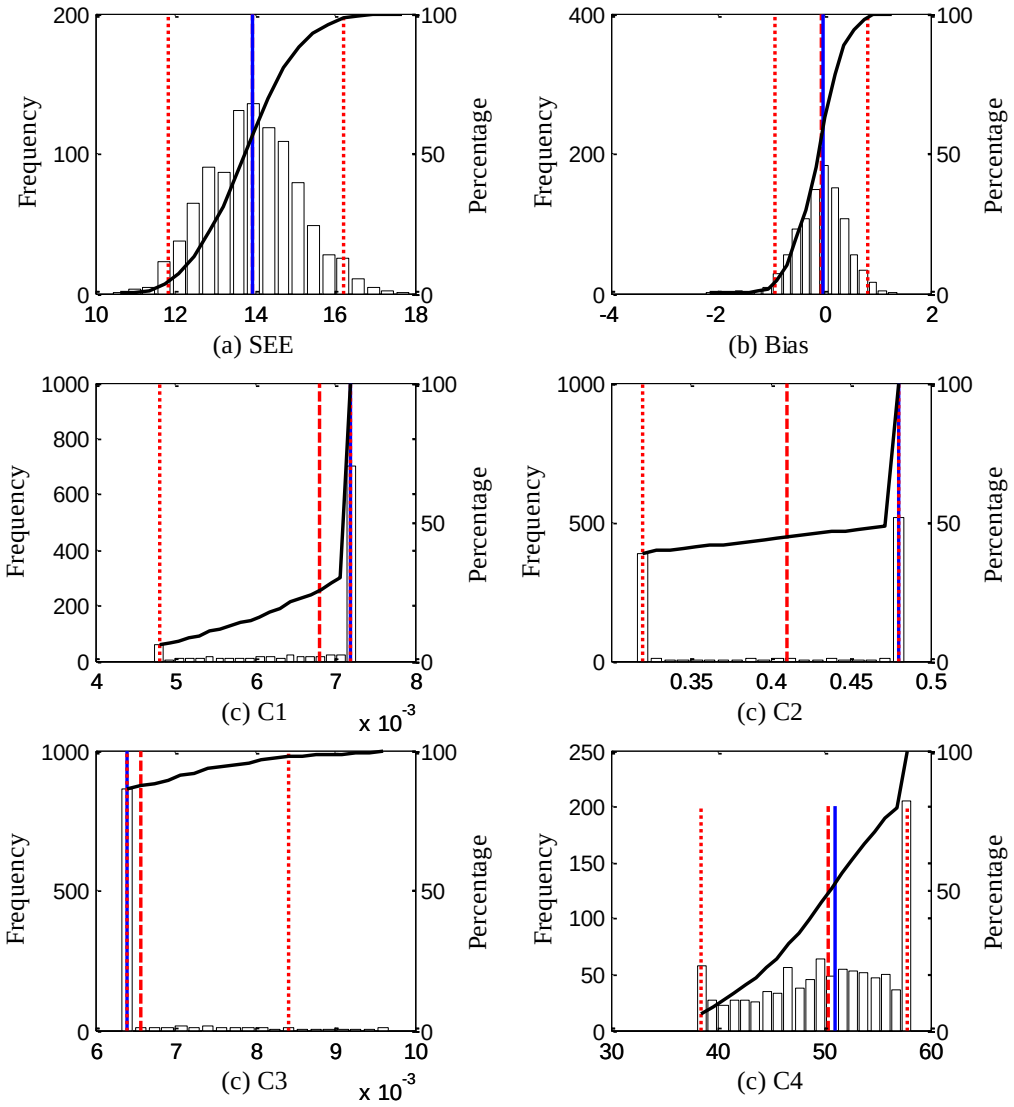

Figure B-325 Option 1 IRI bootstrapping frequency distributions

Reliability

The IRI reliability is internally estimated by the software.

B.1.5.2 Option 2

No sampling

Table B-157 Option 2 IRI local calibration results – no sampling

Parameter	Global	Local
SEE	16.0659	15.8267
Bias	0.2456	0.0564
R^2	0.6857	0.6936
t-test pvalue	0.7407	0.9385
Intercept = 0	0.0000	0.0000
Slope = 1	0.0000	0.0000
C1	40.0000	32.0602
C2	0.4000	0.3200
C3	0.0080	0.0064
C4	0.0150	0.0180

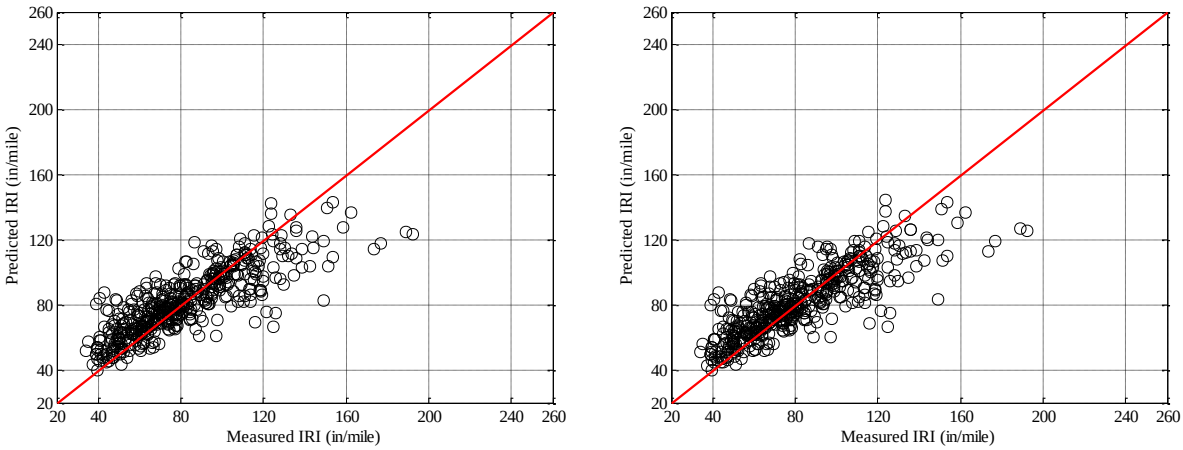

(a) Global model (b) Local model

Figure B-326 Option 2 IRI local calibration measured versus predicted – no sampling

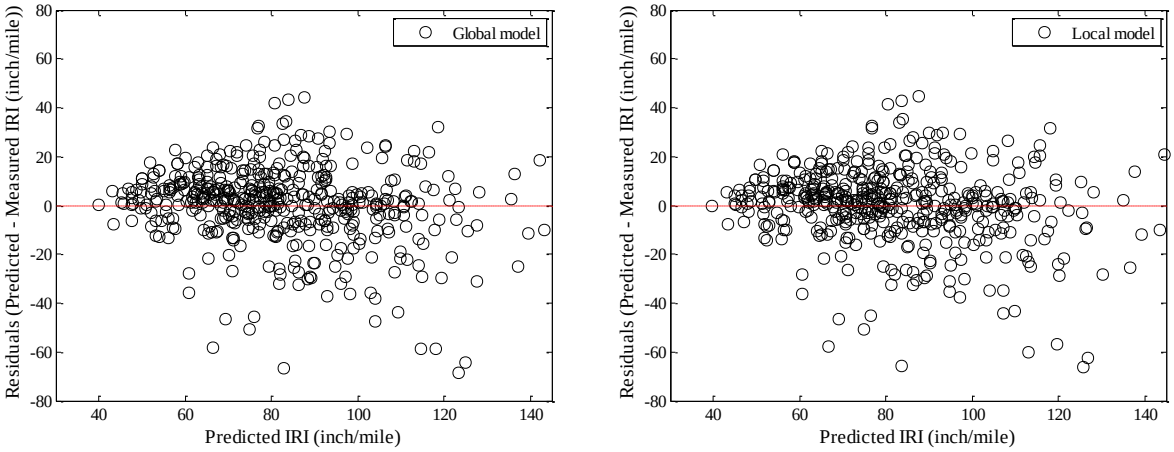

(a) Global model (b) Local model

Figure B-327 Option 2 IRI local calibration residual plots – no sampling

Reliability

The IRI reliability is internally estimated by the software.

Split sampling

Table B-158 Option 2 IRI local calibration results – split sampling

Parameter	Global model	Local model	Validation
SEE	16.6468	16.3668	14.7618
Bias	-0.2285	-0.2634	1.3524
R^2	0.6991	0.7091	0.6549
t-test pvalue	0.8074	0.7749	0.2553
Intercept = 0	0.0000	0.0000	0.0000
Slope = 1	0.0000	0.0000	0.0000
C1	40.0000	33.4400	33.4400
C2	0.4000	0.3200	0.3200
C3	0.0080	0.0064	0.0064
C4	0.0150	0.0180	0.0180

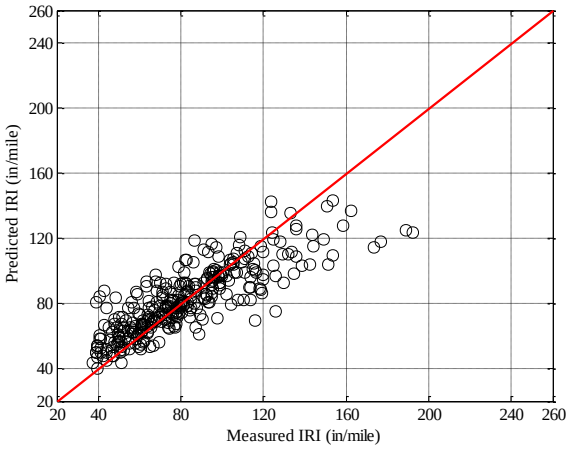

(a) Global model

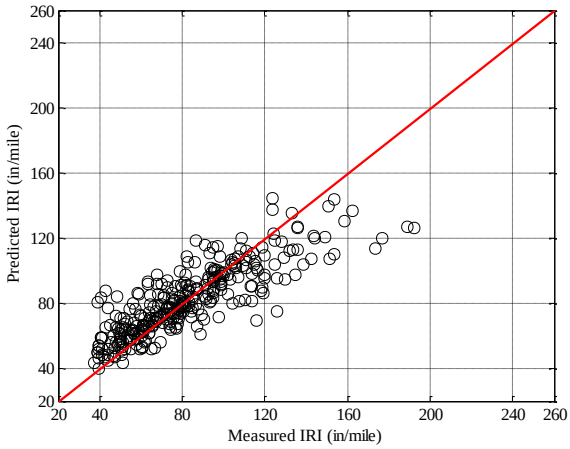

(b) Local model

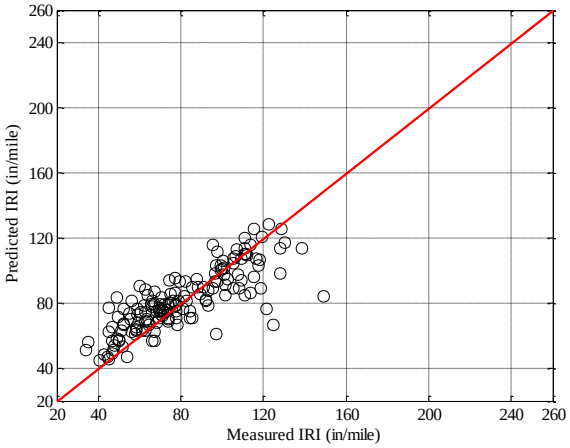

(c) Local model validation

Figure B-328 Option 2 IRI local calibration measured versus predicted – split sampling

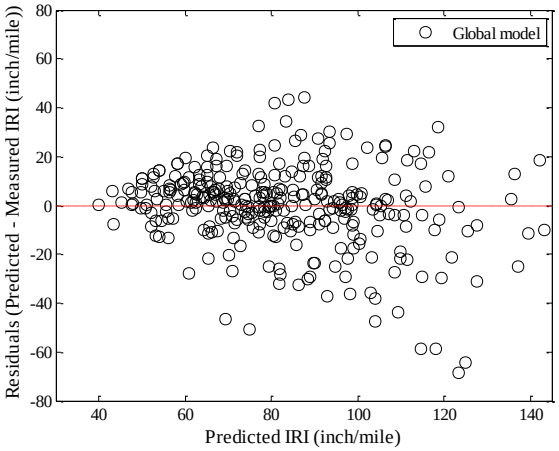

(a) Global model

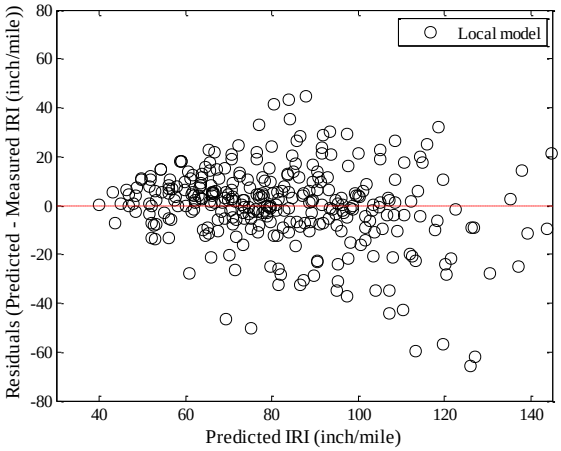

(b) Local model

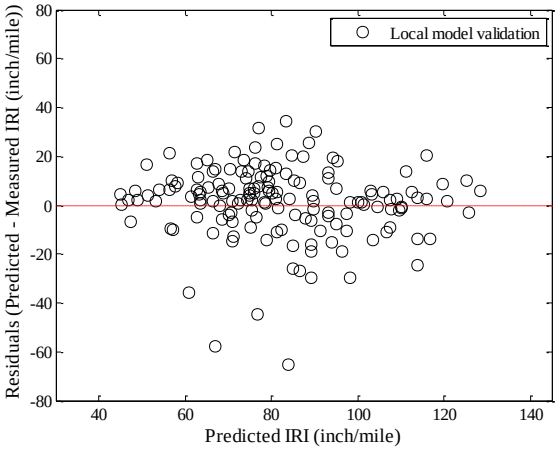

(c) Local model validation

Figure B-329 Option 2 IRI local calibration residual plots – split sampling

Reliability

The IRI reliability is internally estimated by the software.

Repeated split sampling

Table B-159 Option 2 IRI local calibration results – repeated split sampling

Global Model				
Parameter	Global Model Mean	Global Model Median	Global model lower CI	Global model upper CI
SEE	16.1000	16.1383	14.8243	17.2964
Bias	0.2126	0.2346	-1.2712	1.7130
C1	40.0000	40.0000	-	-
C2	0.4000	0.4000	-	-
C3	0.0080	0.0080	-	-
C4	0.0150	0.0150	-	-
Local Model				
Parameter	Local Model Mean	Local Model Median	Local model lower CI	Local model upper CI
SEE	15.8346	15.8684	14.5452	17.0303
Bias	-0.2411	-0.1812	-1.1543	0.3264
C1	32.1854	33.4400	25.6184	33.4400
C2	0.3428	0.3200	0.3200	0.4800
C3	0.0064	0.0064	0.0064	0.0064
C4	0.0175	0.0180	0.0149	0.0180
Local Model validation				
Parameter	Local Model Mean	Local Model Median	Local model lower CI	Local model upper CI
SEE	15.8973	15.9040	12.8664	18.7973
Bias	-0.1664	0.0272	-4.8854	3.8174
C1	32.1854	33.4400	25.6184	33.4400
C2	0.3428	0.3200	0.3200	0.4800
C3	0.0064	0.0064	0.0064	0.0064
C4	0.0175	0.0180	0.0149	0.0180

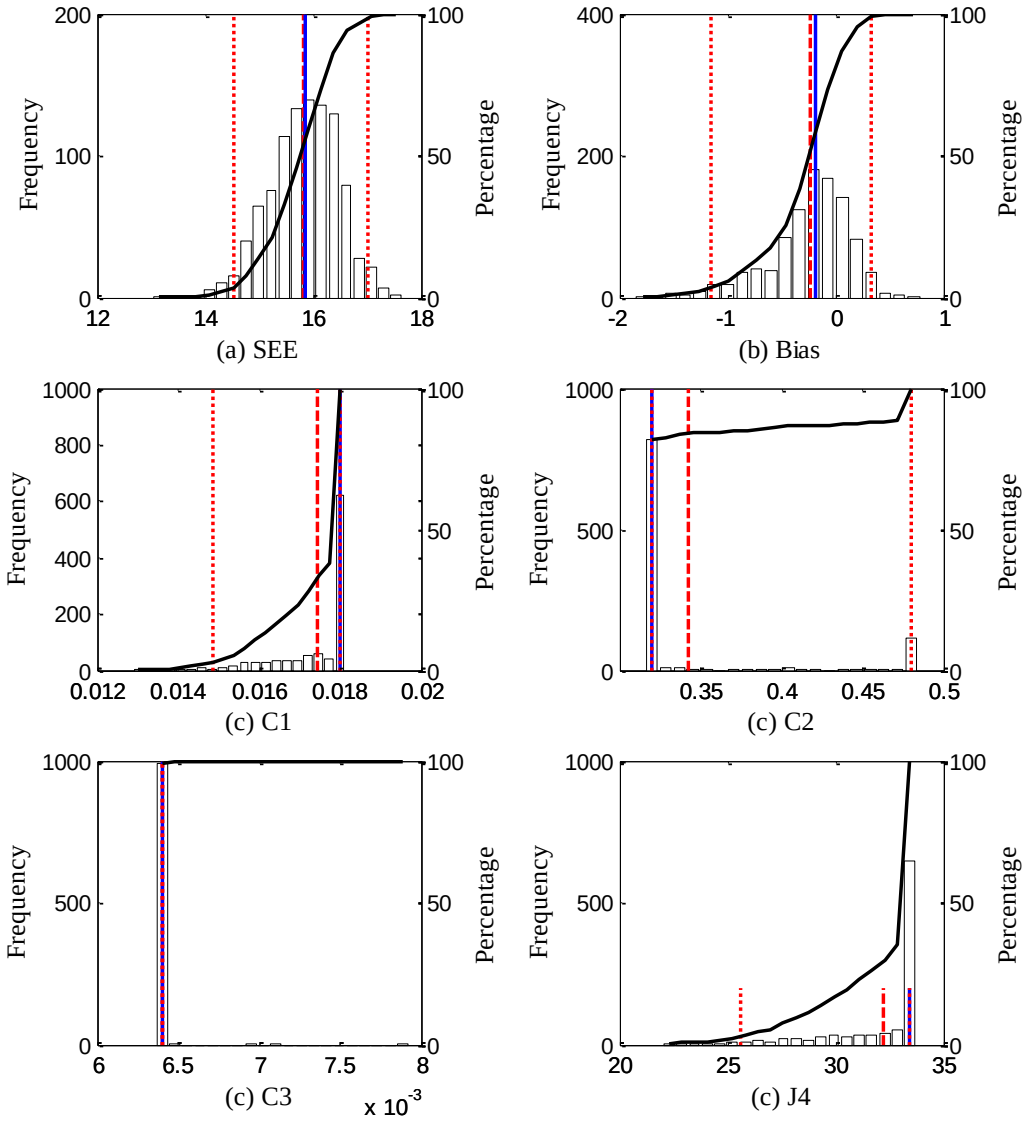

Figure B-330 Option 2 IRI repeated split sampling frequency distributions – calibration

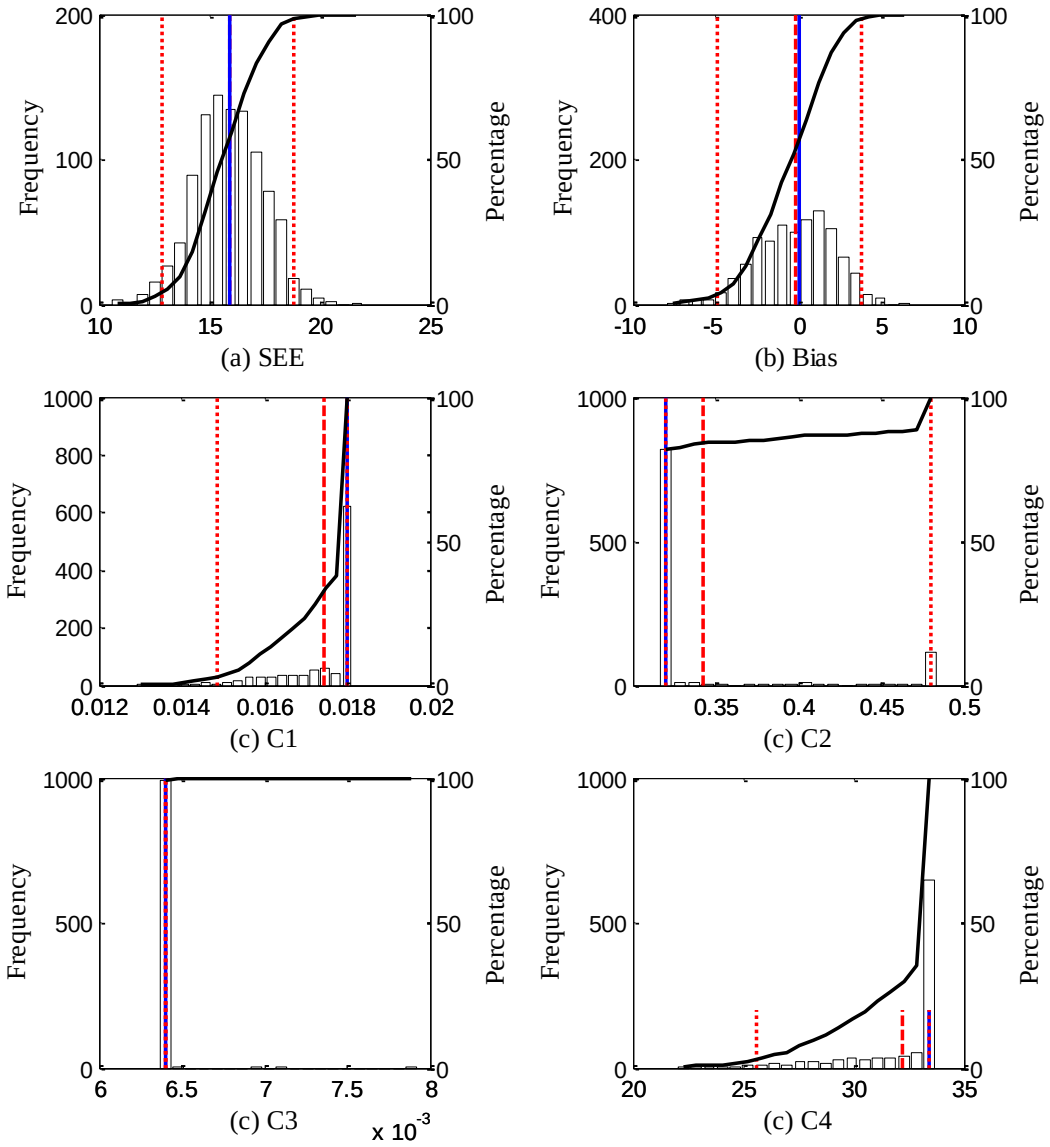

Figure B-331 Option 2 IRI repeated split sampling frequency distributions – validation

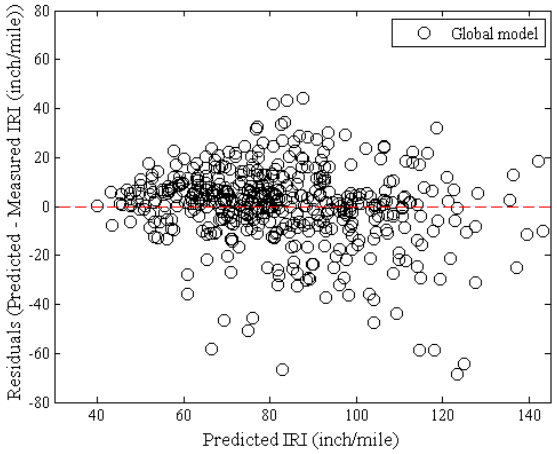

(a) Global model

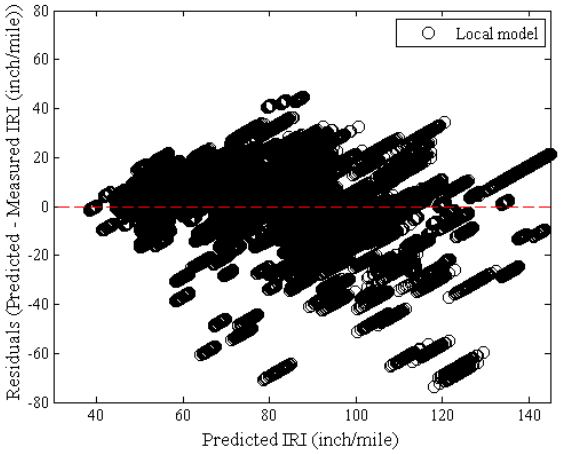

(b) Local model

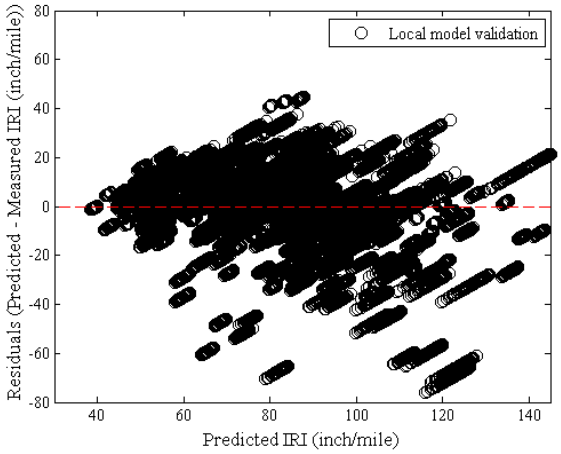

(c) Local model validation

Figure B-332 Option 2 IRI local calibration residual plots – repeated split sampling

Reliability

The IRI reliability is internally estimated by the software.

Bootstrapping

Table B-160 Option 2 IRI local calibration results – bootstrapping

Global Model				
Parameter	Global Model Mean	Global Model Median	Global model lower CI	Global model upper CI
SEE	16.0256	16.0372	13.9711	17.9502
Bias	0.2779	0.2614	-1.9643	2.5374
C1	40.0000	40.0000	-	-
C2	0.4000	0.4000	-	-
C3	0.0080	0.0080	-	-
C4	0.0150	0.0150	-	-
Local Model				
Parameter	Local Model Mean	Local Model Median	Local model lower CI	Local model upper CI
SEE	15.7316	15.7544	13.6244	17.6772
Bias	-0.3810	-0.3082	-1.6554	0.4516
C1	31.6450	33.4400	22.2960	33.4400
C2	0.3613	0.3200	0.3200	0.4800
C3	0.0065	0.0064	0.0064	0.0071
C4	0.0172	0.0180	0.0137	0.0180

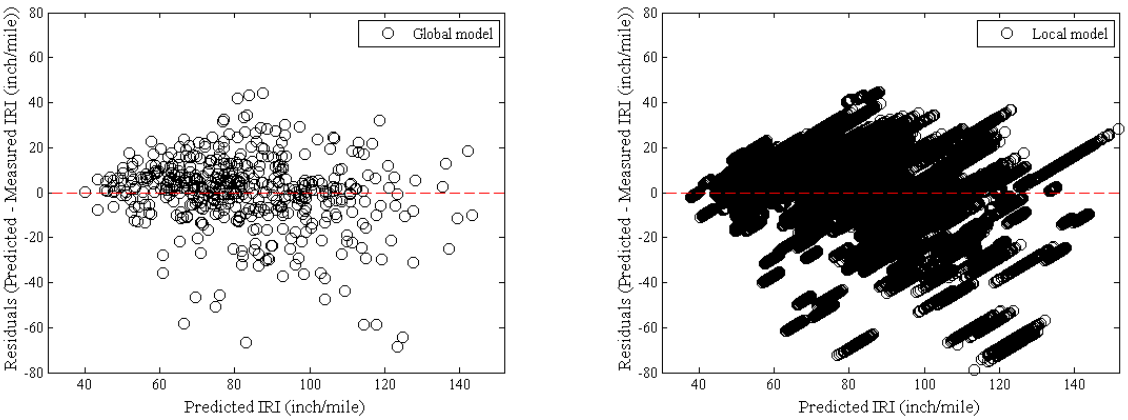

(a) Global model (b) Local model

Figure B-333 Option 2 IRI local calibration residual plots – repeated split sampling

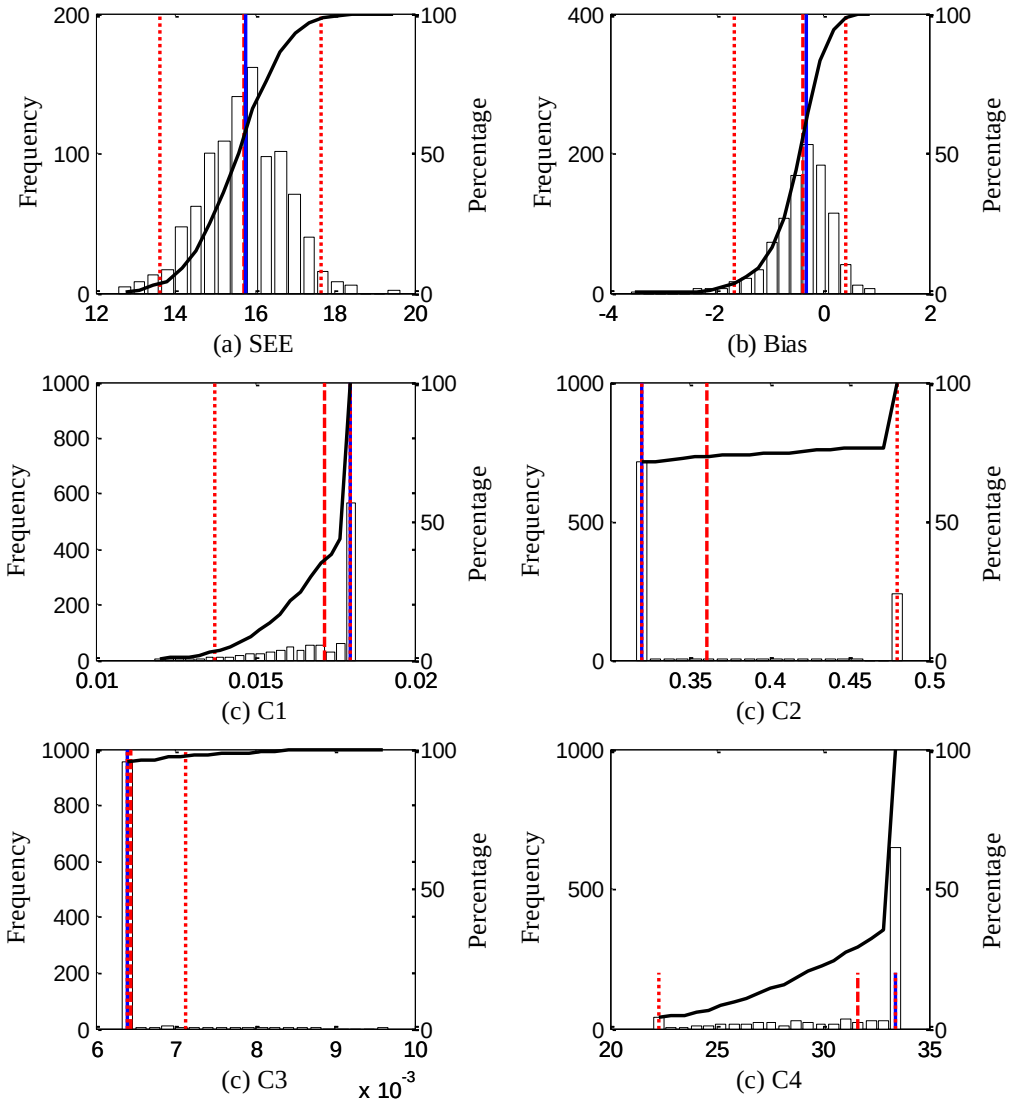

Figure B-334 Option 2 IRI bootstrapping frequency distributions

Reliability

The IRI reliability is internally estimated by the software.

B.1.5.3 Option 4

No sampling

Table B-161 Option 4 IRI local calibration results – no sampling

Parameter	Global	Local
SEE	20.6944	17.9586
Bias	-5.9035	0.3185
R^2	0.6884	0.7006
t-test pvalue	0.0040	0.8610
Intercept = 0	0.0000	0.0000
Slope = 1	0.0000	0.0000
C1	40.0000	20.8000
C2	0.4000	0.1600
C3	0.0080	0.0048
C4	0.0150	0.0277

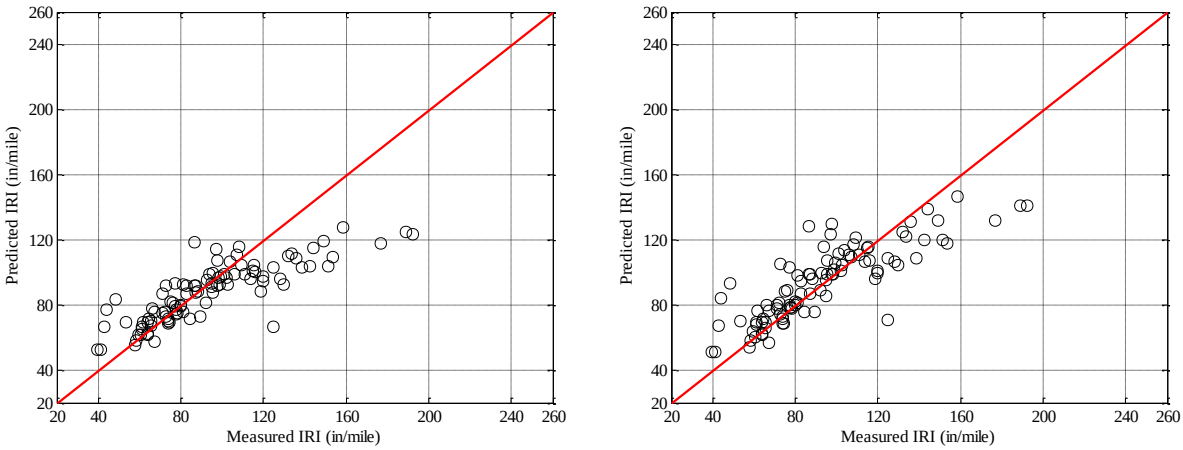

(a) Global model (b) Local model

Figure B-335 Option 4 IRI local calibration measured versus predicted – no sampling

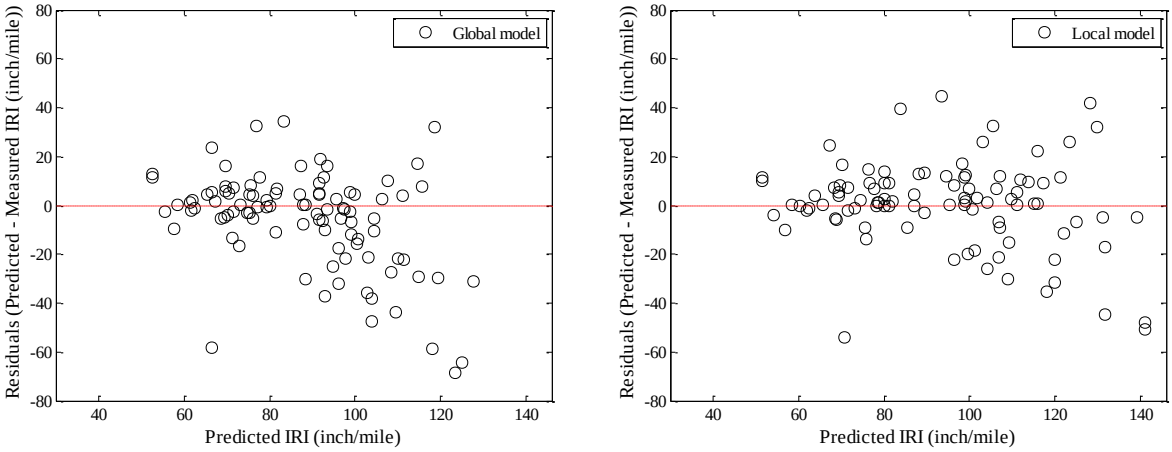

(a) Global model (b) Local model

Figure B-336 Option 4 IRI local calibration residual plots – no sampling

Reliability

The IRI reliability is internally estimated by the software.

Split sampling

Table B-162 Option 4 IRI local calibration results – split sampling

Parameter	Global model	Local model	Validation
SEE	22.6387	19.9658	13.6126
Bias	-5.8644	0.8658	0.7417
R^2	0.6798	0.6814	0.7711
t-test pvalue	0.0328	0.7255	0.7558
Intercept = 0	0.0000	0.0000	0.0037
Slope = 1	0.0000	0.0000	0.0035
C1	40.0000	20.8000	20.8000
C2	0.4000	0.1600	0.1600
C3	0.0080	0.0048	0.0048
C4	0.0150	0.0282	0.0282

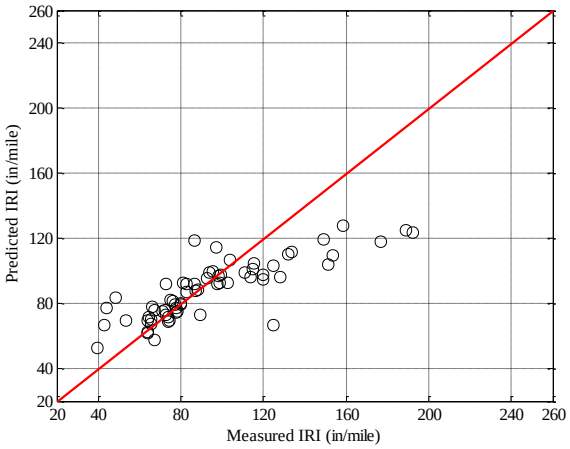

(a) Global model

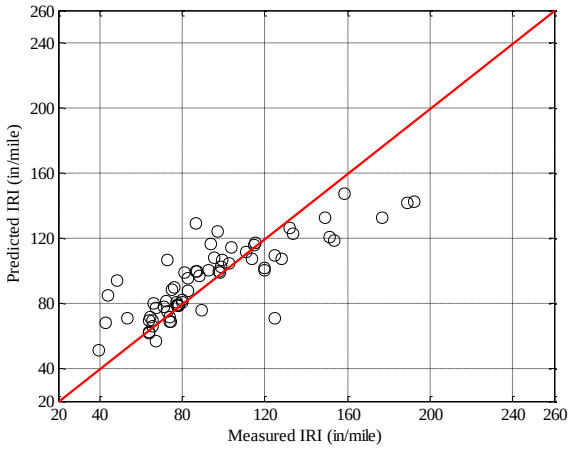

(b) Local model

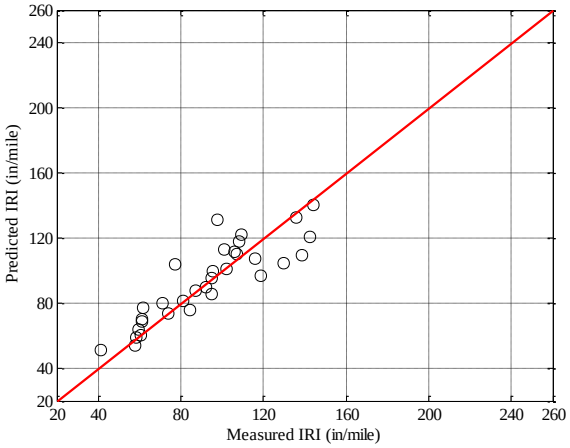

(c) Local model validation

Figure B-337 Option 4 IRI local calibration measured versus predicted – split sampling

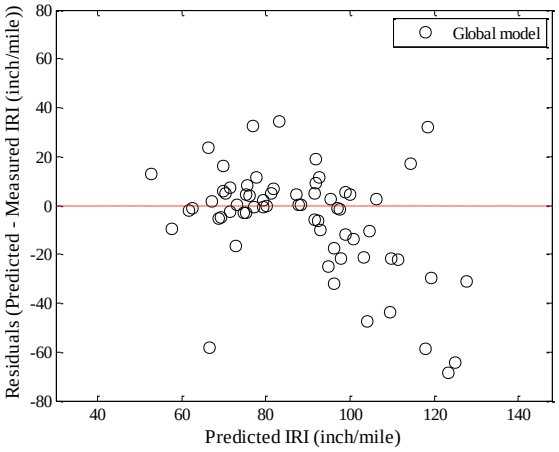

(a) Global model

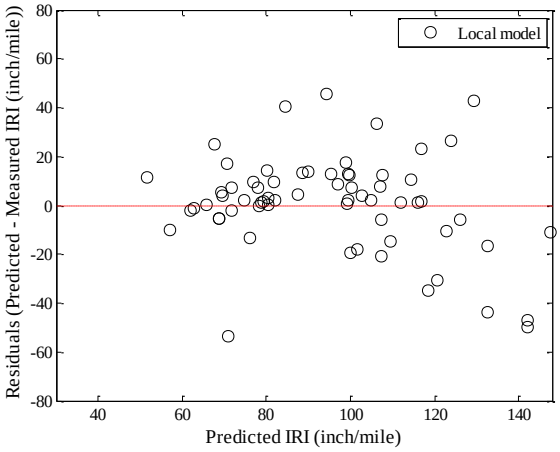

(b) Local model

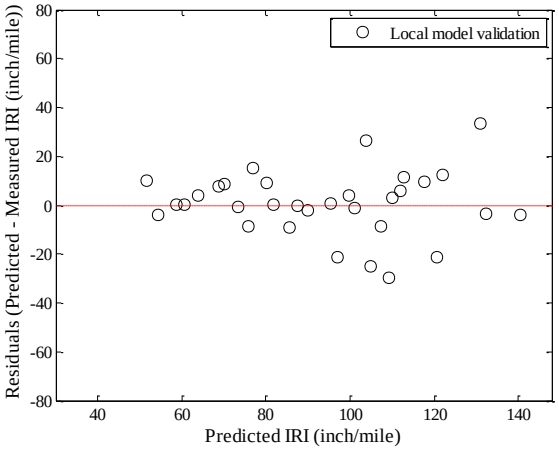

(c) Local model validation

Figure B-338 Option 4 IRI local calibration residual plots – split sampling

Reliability

The IRI reliability is internally estimated by the software.

Repeated split sampling

Table B-163 Option 4 IRI local calibration results – repeated split sampling

Global Model				
Parameter	Global Model Mean	Global Model Median	Global model lower CI	Global model upper CI
SEE	20.7012	20.9912	16.4997	23.8782
Bias	-5.8767	-5.9631	-9.3455	-2.0099
C1	40.0000	40.0000	-	-
C2	0.4000	0.4000	-	-
C3	0.0080	0.0080	-	-
C4	0.0150	0.0150	-	-
Local Model				
Parameter	Local Model Mean	Local Model Median	Local model lower CI	Local model upper CI
SEE	17.8550	18.0194	14.7366	20.2766
Bias	0.2396	0.2738	-0.9799	1.3002
C1	20.8988	20.8000	20.8000	21.6186
C2	0.1600	0.1600	0.1600	0.1600
C3	0.0048	0.0048	0.0048	0.0048
C4	0.0275	0.0277	0.0232	0.0300
Local Model validation				
Parameter	Local Model Mean	Local Model Median	Local model lower CI	Local model upper CI
SEE	18.7280	18.7737	11.7677	25.7248
Bias	-0.0133	0.2452	-11.4828	8.9161
C1	20.8988	20.8000	20.8000	21.6186
C2	0.1600	0.1600	0.1600	0.1600
C3	0.0048	0.0048	0.0048	0.0048
C4	0.0275	0.0277	0.0232	0.0300

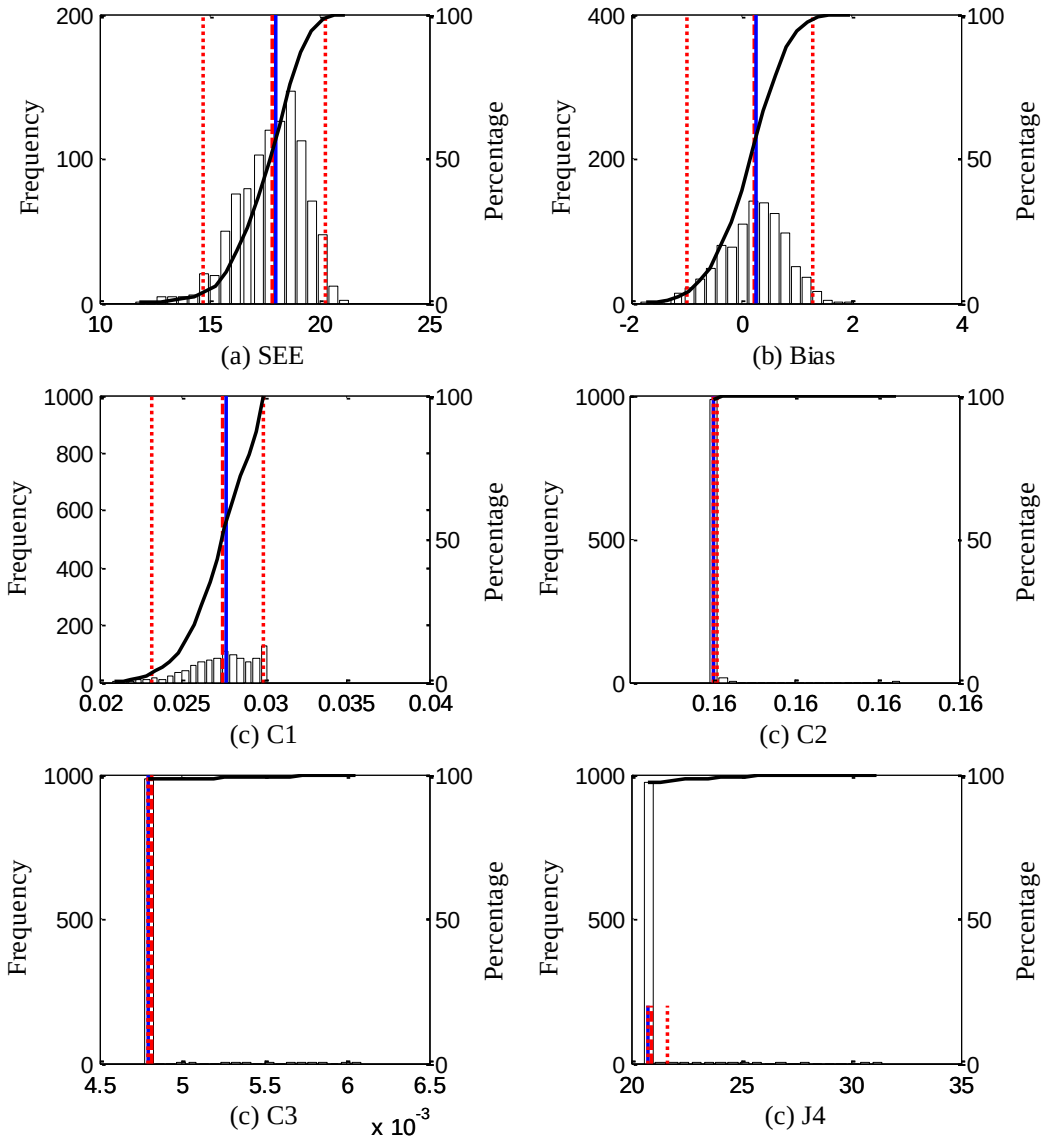

Figure B-339 Option 4 IRI repeated split sampling frequency distributions – calibration

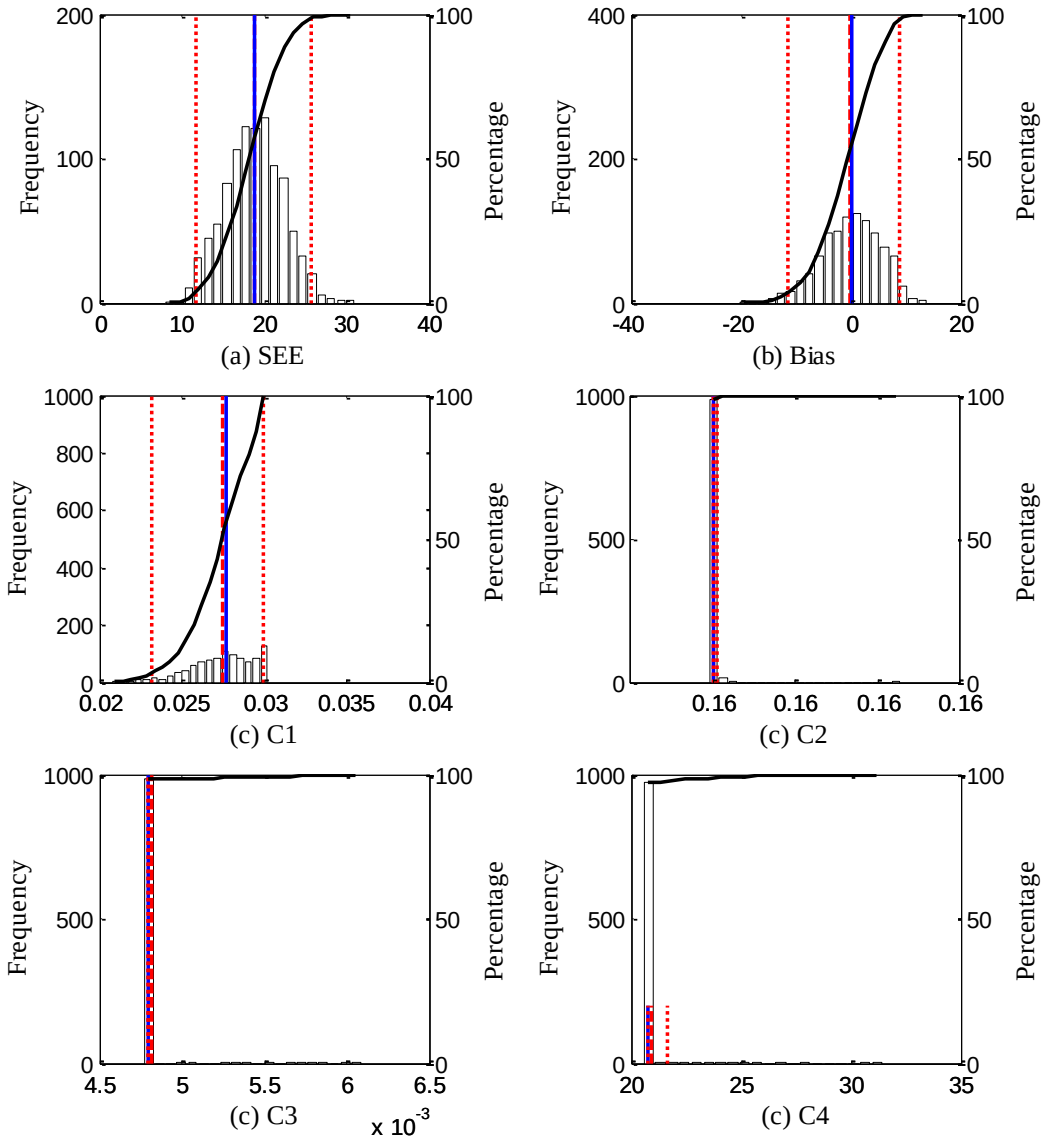

Figure B-340 Option 4 IRI repeated split sampling frequency distributions – validation

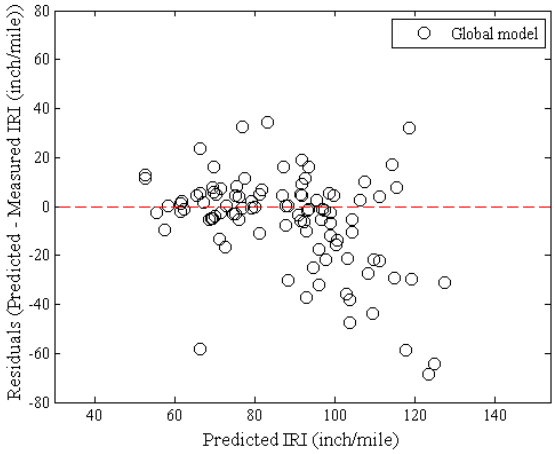

(a) Global model

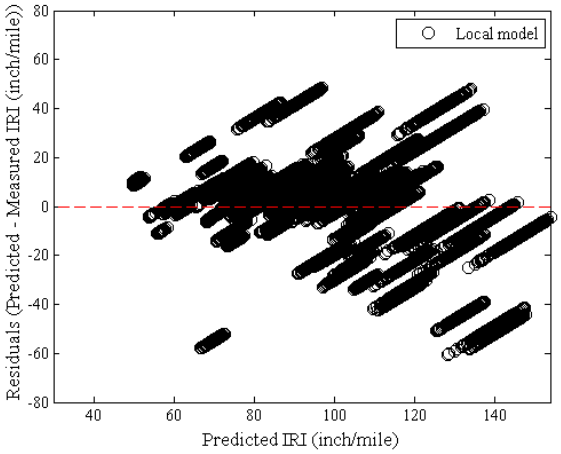

(b) Local model

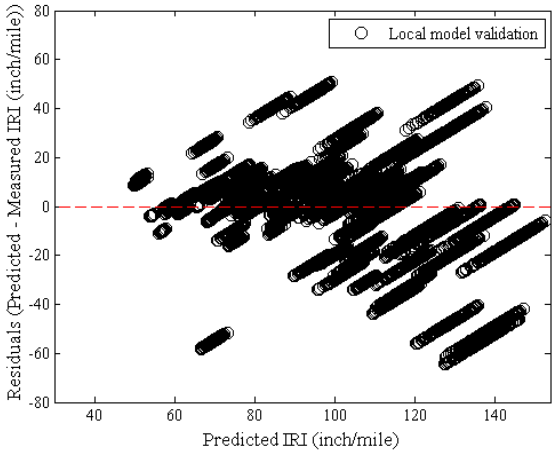

(c) Local model validation

Figure B-341 Option 4 IRI local calibration residual plots – repeated split sampling

Reliability

The IRI reliability is internally estimated by the software.

Bootstrapping

Table B-164 Option 4 IRI local calibration results – bootstrapping

Global Model				
Parameter	Global Model Mean	Global Model Median	Global model lower CI	Global model upper CI
SEE	20.4800	20.6428	14.9401	25.4311
Bias	-5.8312	-5.9656	-11.3979	0.1292
C1	40.0000	40.0000	-	-
C2	0.4000	0.4000	-	-
C3	0.0080	0.0080	-	-
C4	0.0150	0.0150	-	-
Local Model				
Parameter	Local Model Mean	Local Model Median	Local model lower CI	Local model upper CI
SEE	17.5260	17.6062	13.2472	21.3238
Bias	0.1290	0.1613	-1.4172	1.5613
C1	21.4303	20.8000	20.8000	31.2000
C2	0.1600	0.1600	0.1600	0.1600
C3	0.0049	0.0048	0.0048	0.0071
C4	0.0271	0.0276	0.0208	0.0300

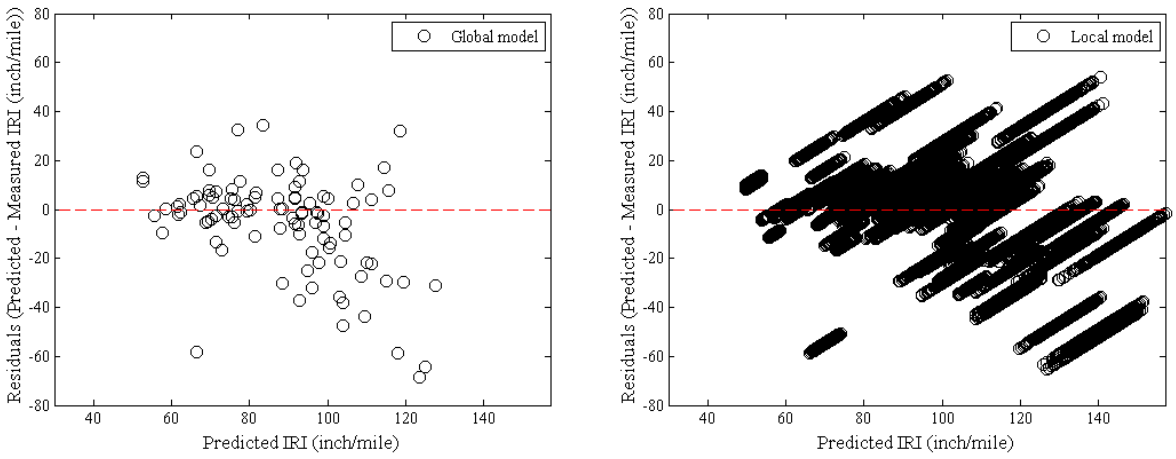

(a) Global model (b) Local model

Figure B-342 Option 4 IRI local calibration residual plots – bootstrapping

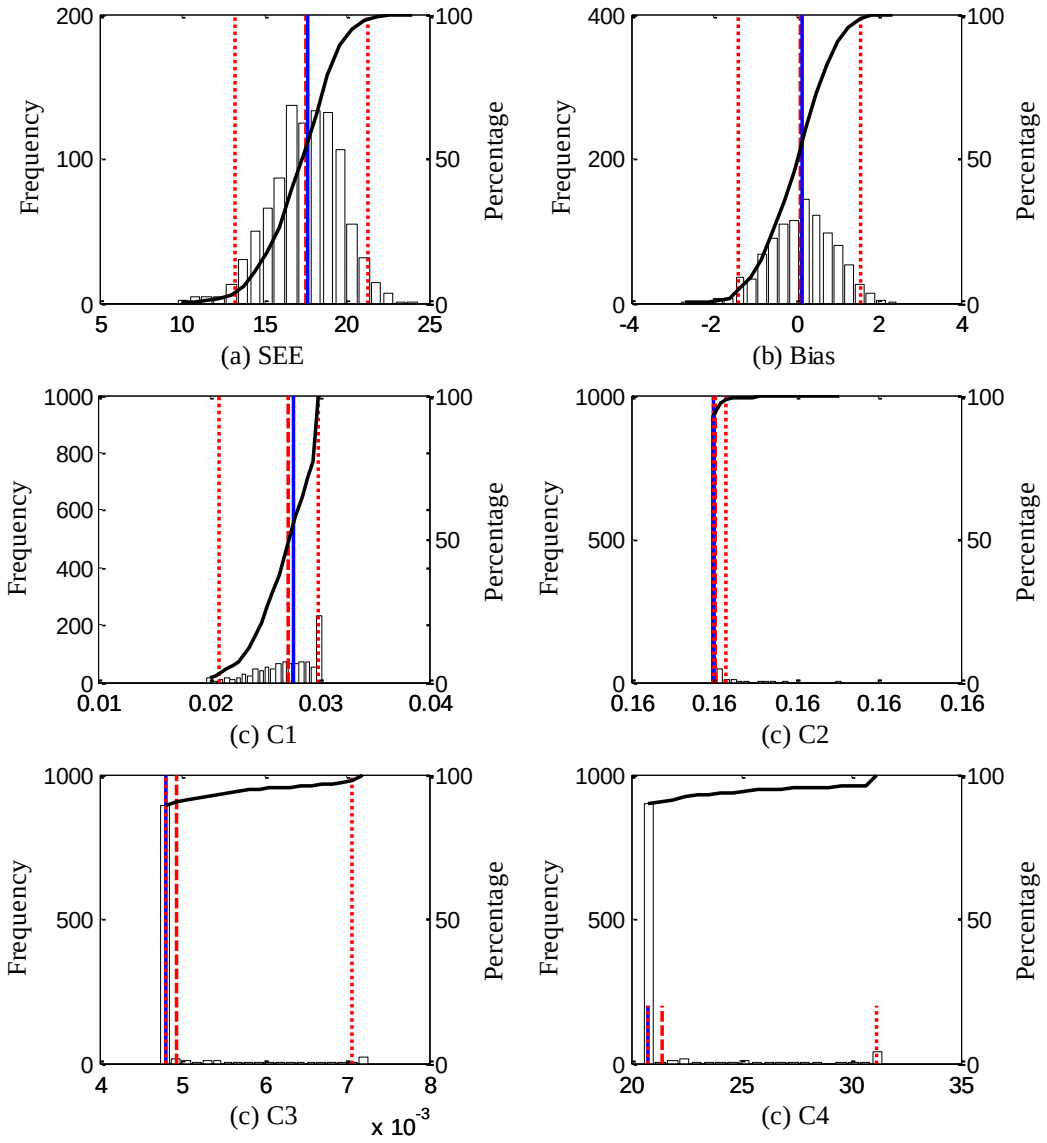

Figure B-343 Option 2 IRI bootstrapping frequency distributions

Reliability

The IRI reliability is internally estimated by the software.

B.2 Rigid Pavement Performance Prediction Models

B.2.1 Transverse cracking

B.2.1.1 Option 1

No sampling

Table B-165 Option 1 transverse cracking local calibration results – no sampling

Parameter	Global model	Local model
SEE	21.10	12.30
Bias	-11.86	0.17
R^2	0.58	0.67
t-test pvalue	0.00	0.92
Intercept = 0	0.36	0.00
Slope = 1	0.00	0.00
C4	1.00	0.27
C5	-1.98	-1.56

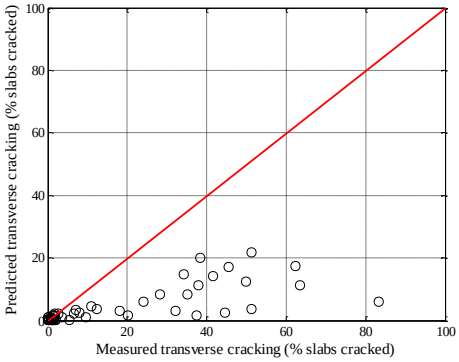

(a) Global model

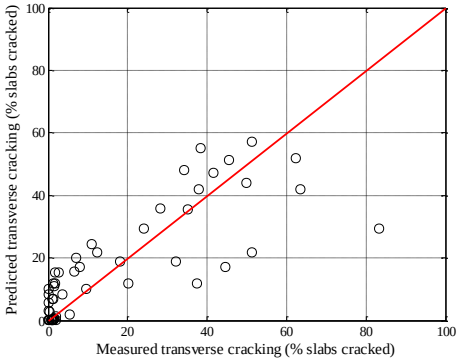

(b) Local model

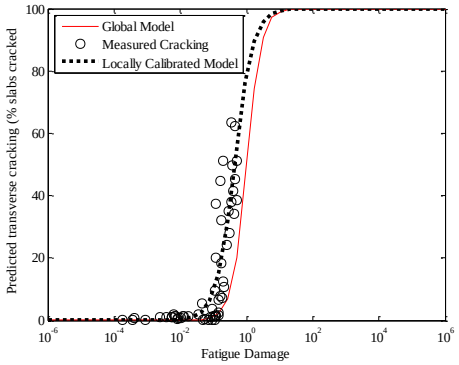

(c) Fatigue damage predicted cracking

Figure B-344 Option 1 transverse cracking local calibration measured vs. predicted – no sampling

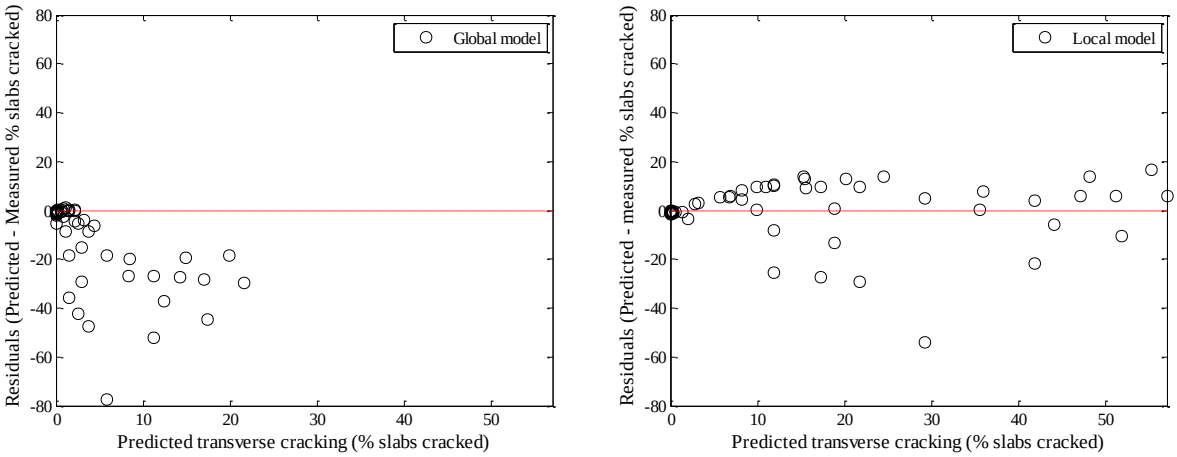

(a) Global model (b) Local model

Figure B-345 Option 1 transverse cracking residual plots – no sampling

Reliability

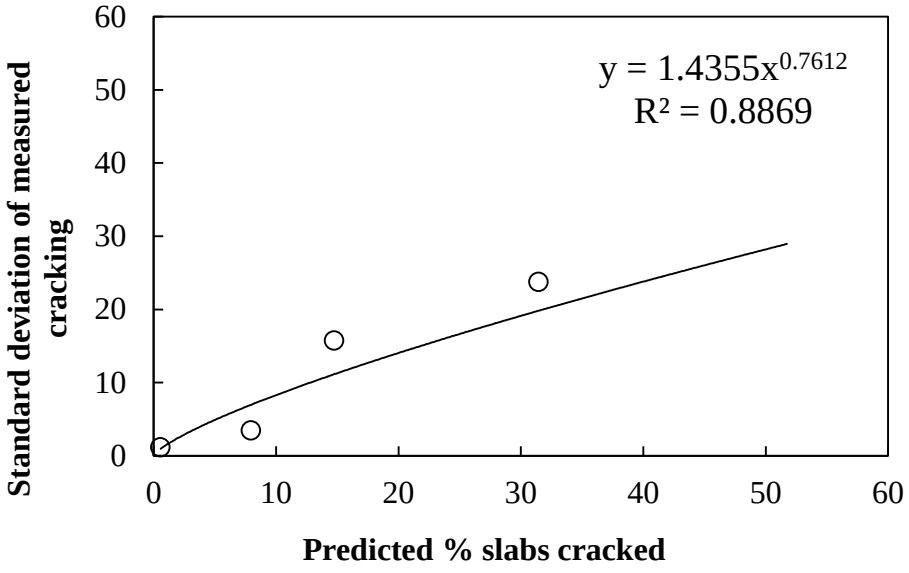

Figure B-346 Option 1 Transverse cracking reliability model fitting – no sampling

Split sampling

Table B-166 Option 1 transverse cracking local calibration results – split sampling

Parameter	Global model	Local model calibration	Local model validation
SEE	24.09	13.05	12.24
Bias	-14.59	0.14	8.13
R^2	0.57	0.69	0.32
t-test pvalue	0.00	0.94	0.00
Intercept = 0	0.50	0.01	0.00
Slope = 1	0.00	0.00	0.04
C4	1.00	0.35	0.35
C5	-1.98	-1.28	-1.28

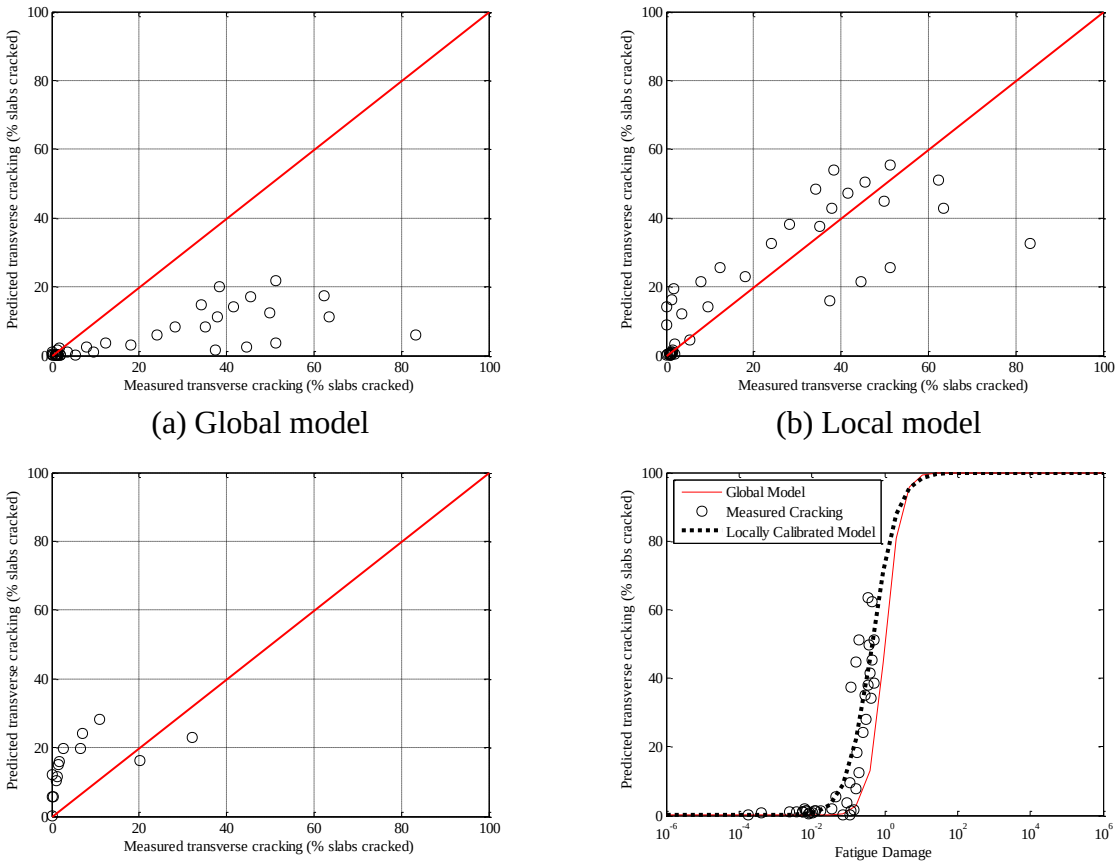

(a) Global model

(b) Local model

(c) Local model validation

(d) Fatigue damage predicted cracking

Figure B-347 Option 1 transverse cracking local calibration measured vs. predicted – split sampling

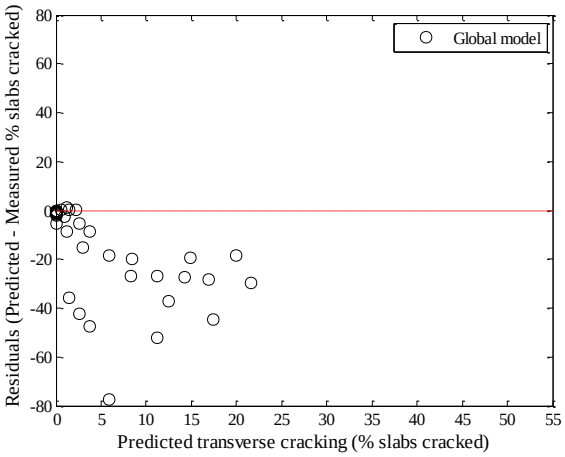

(a) Global model

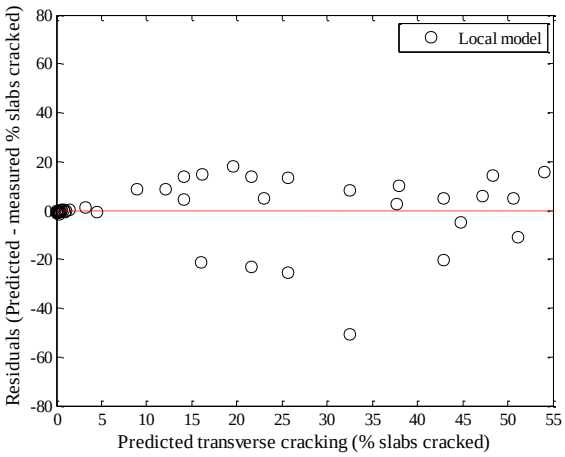

(b) Local model

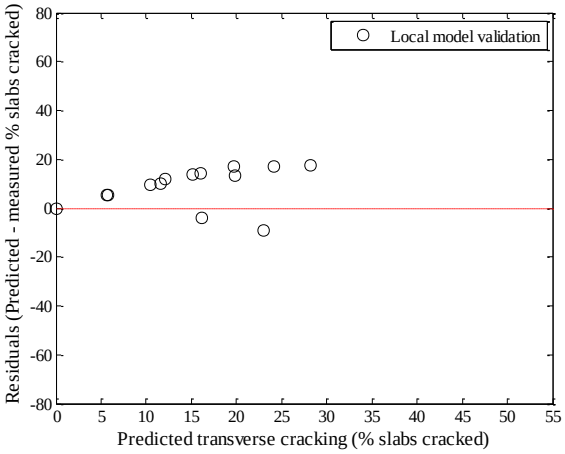

(c) Local model validation

Figure B-348 Option 1 transverse cracking residual plots – split sampling

Reliability

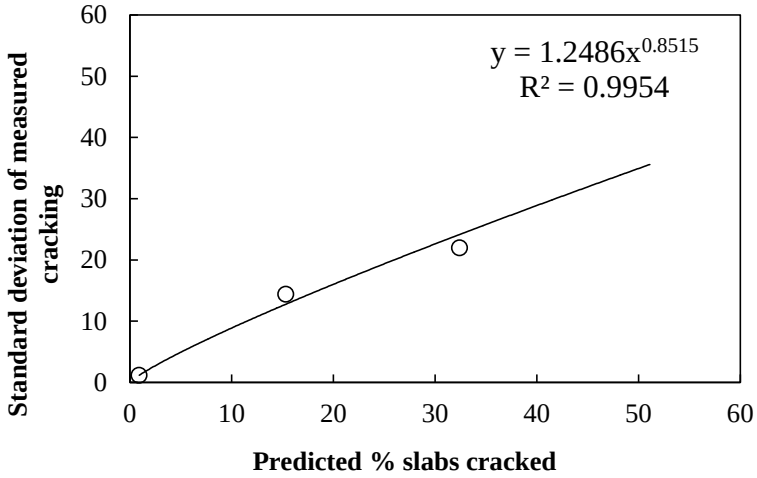

Figure B-349 Option 1 Transverse cracking reliability model fitting – split sampling

Repeated split sampling

Table B-167 Option 1 transverse cracking local calibration results – repeated split sampling

Parameter	Global Model Mean	Global Model Median	Global model lower CI	Global model upper CI
SEE	21.03	21.03	14.59	25.06
Bias	-11.83	-11.83	-15.71	-7.48
C4	1.00	1.00	-	-
C5	-1.98	-1.98	-	-
Parameter	Local Model Mean	Local Model Median	Local model lower CI	Local model upper CI
SEE	11.92	12.71	7.04	14.33
Bias	0.15	0.17	-0.37	0.52
C4	0.26	0.27	0.14	0.36
C5	-1.63	-1.59	-1.98	-1.31
Parameter	Local Model Mean	Local Model Median	Local model lower CI	Local model upper CI
SEE	14.10	13.02	5.30	26.35
Bias	0.04	0.06	-13.69	12.30
C4	0.26	0.27	0.14	0.36
C5	-1.63	-1.59	-1.98	-1.31

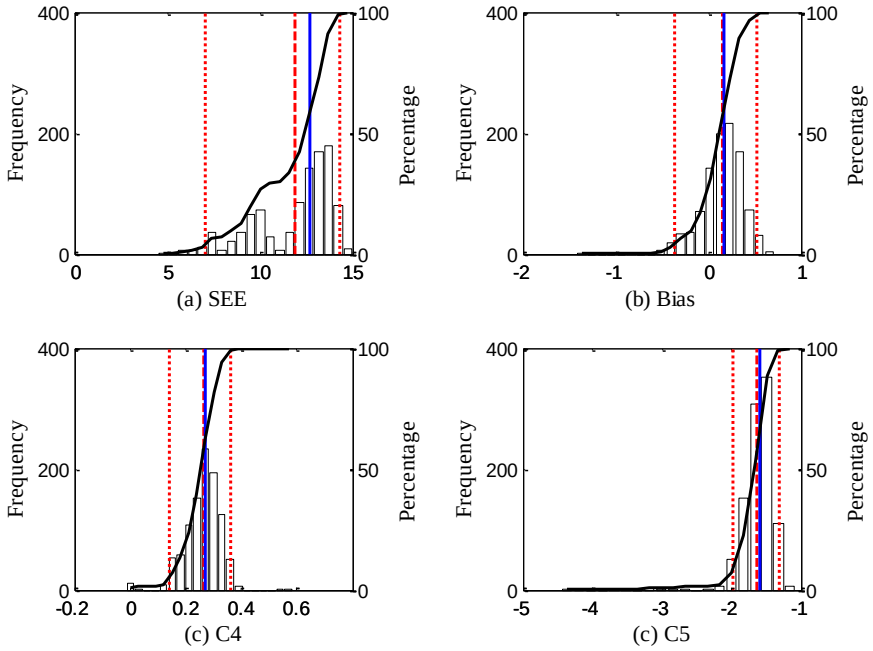

Figure B-350 Option 1 – Distribution of calibration parameters – repeated split sampling - Calibration

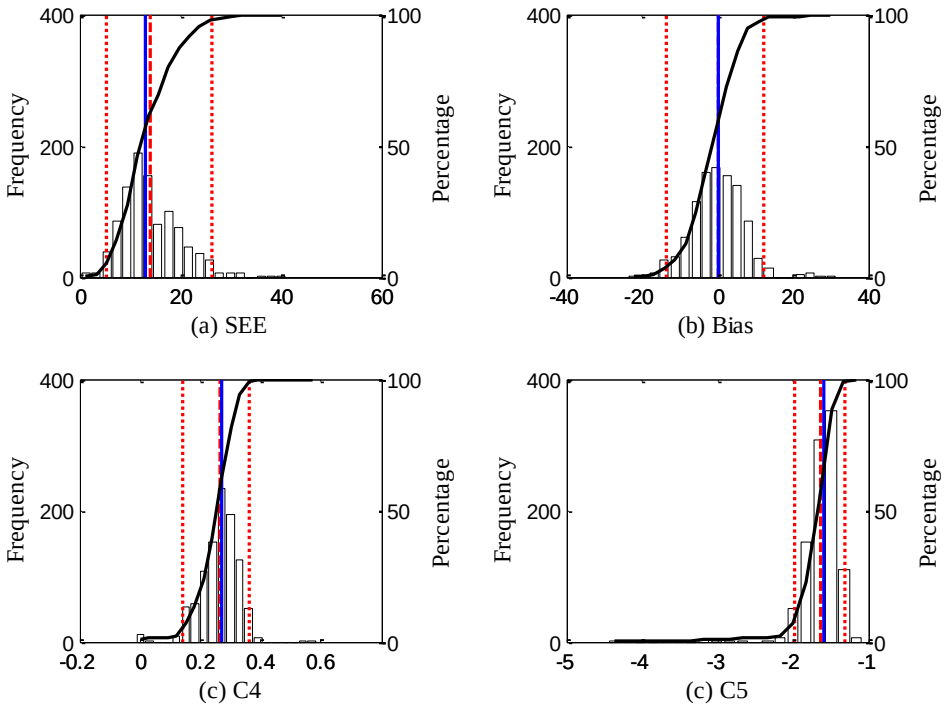

Figure B-351 Option 1 – Distribution of calibration parameters – repeated split sampling - Validation

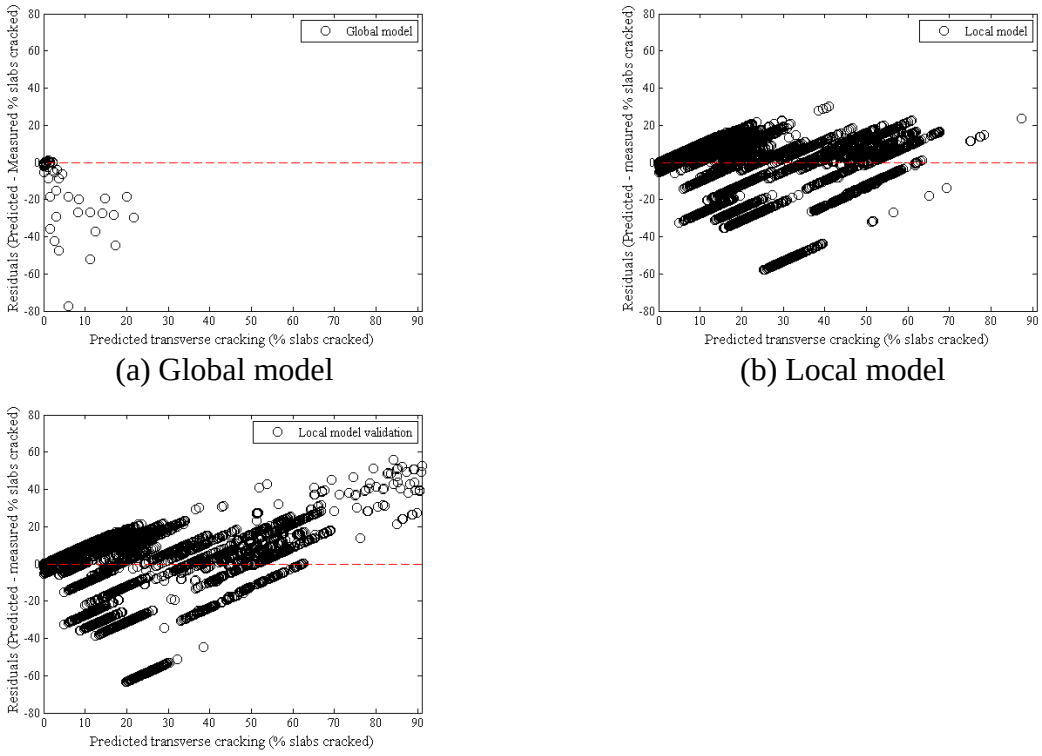

Figure B-352 Option 1 transverse cracking residual plots – repeated split sampling

Reliability

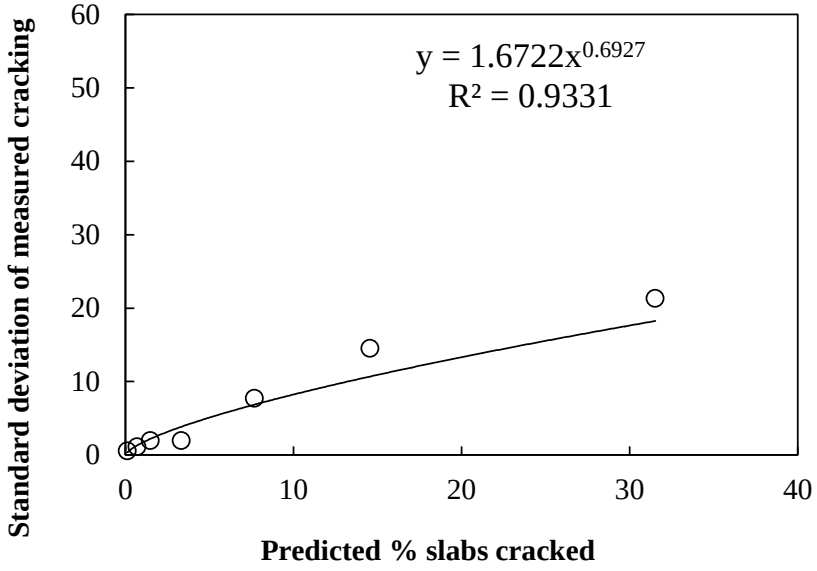

Figure B-353 Option 1 Transverse cracking reliability model fitting – repeated split sampling

Bootstrapping

Table B-168 Option 1 transverse cracking local calibration results – bootstrapping

Parameter	Global Model Mean	Global Model Median	Global model lower CI	Global model upper CI
SEE	20.62	20.68	12.05	28.91
Bias	-11.74	-11.55	-18.69	-5.54
C4	1.00	1.00	-	-
C5	-1.98	-1.98	-	-
Parameter	Local Model Mean	Local Model Median	Local model lower CI	Local model upper CI
SEE	11.37	11.65	5.21	16.21
Bias	0.13	0.15	-0.54	0.68
C4	0.25	0.26	0.02	0.44
C5	-1.71	-1.63	-2.95	-1.21

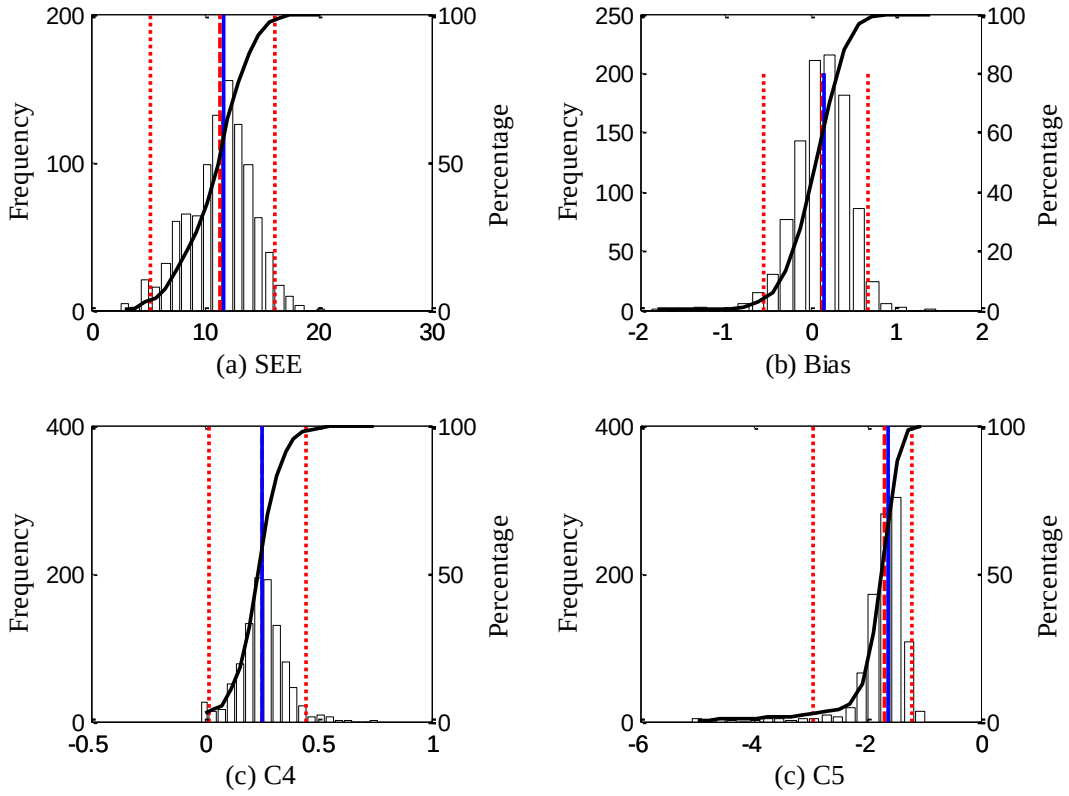

Figure B-354 Option 1 – Distribution of calibration parameters – bootstrapping

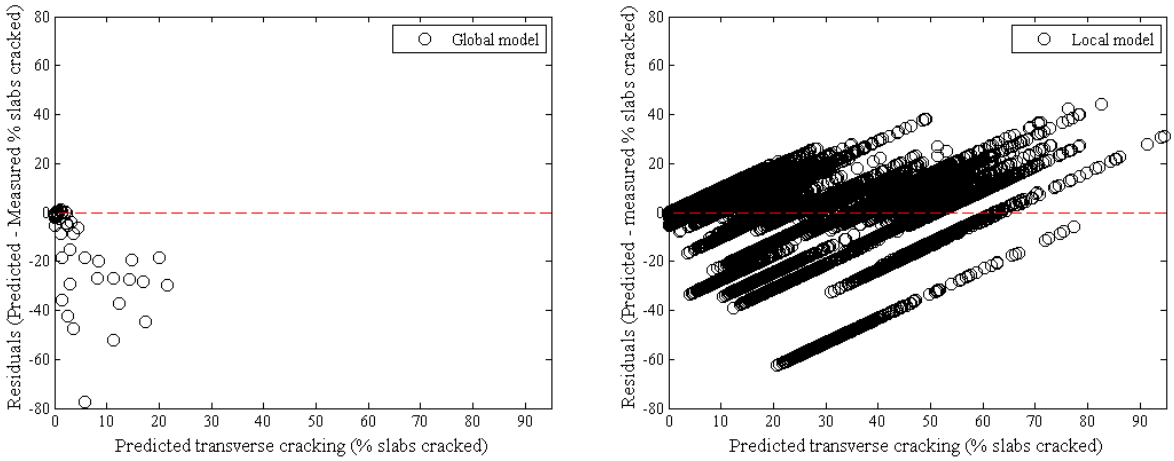

Figure B-355 Option 1 transverse cracking residual plots – bootstrapping

Reliability

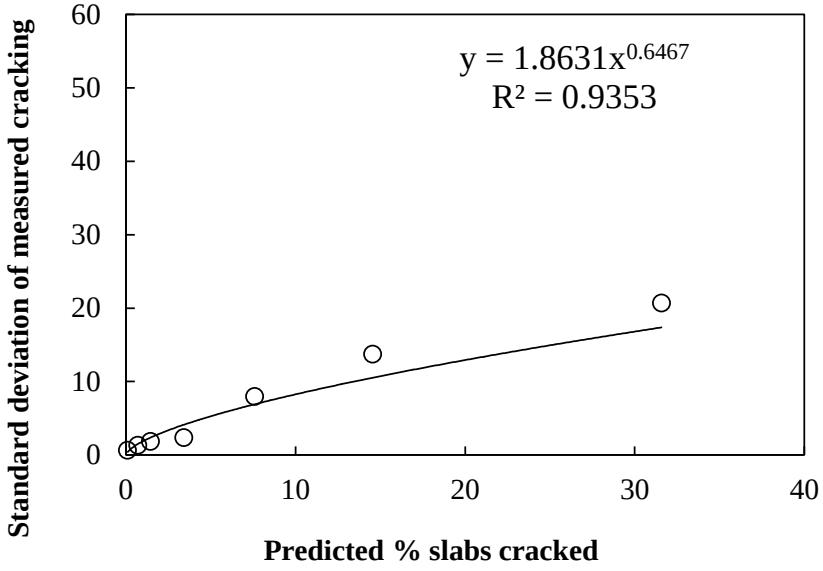

Figure B-356 Option 1 Transverse cracking reliability model fitting – bootstrapping

B.2.1.2 Option 2

No sampling

Table B-169 Option 2 transverse cracking local calibration results – no sampling

Parameter	Global model	Local model
SEE	14.30	8.43
Bias	-5.83	0.37
R^2	0.65	0.73
t-test pvalue	0.00	0.63
Intercept = 0	0.42	0.00
Slope = 1	0.00	0.00
C4	1.00	0.24
C5	-1.98	-1.67

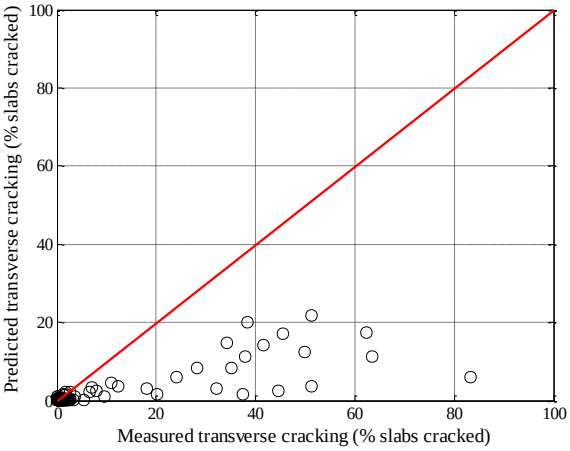

(a) Global model

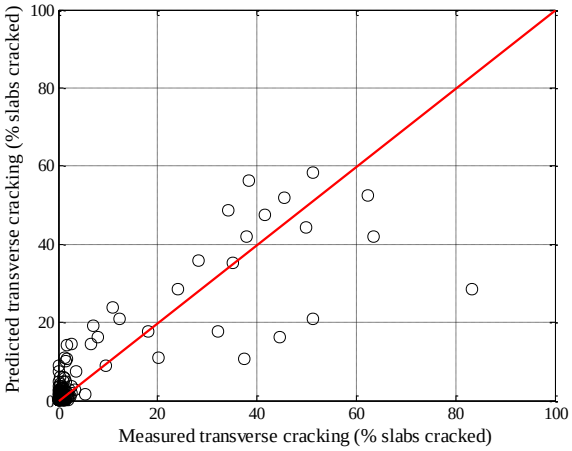

(b) Local model

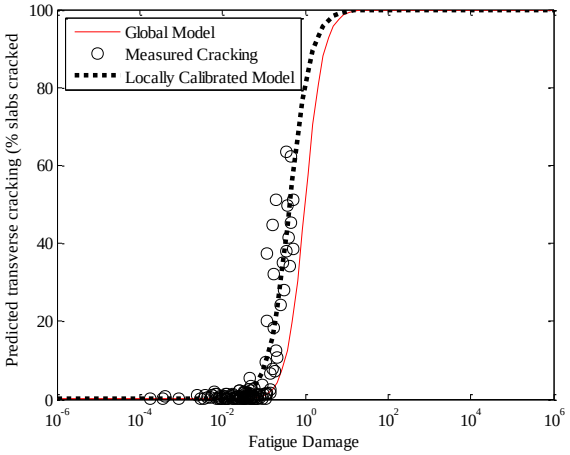

(c) Fatigue damage predicted cracking

Figure B-357 Option 2 transverse cracking local calibration measured vs. predicted – no sampling

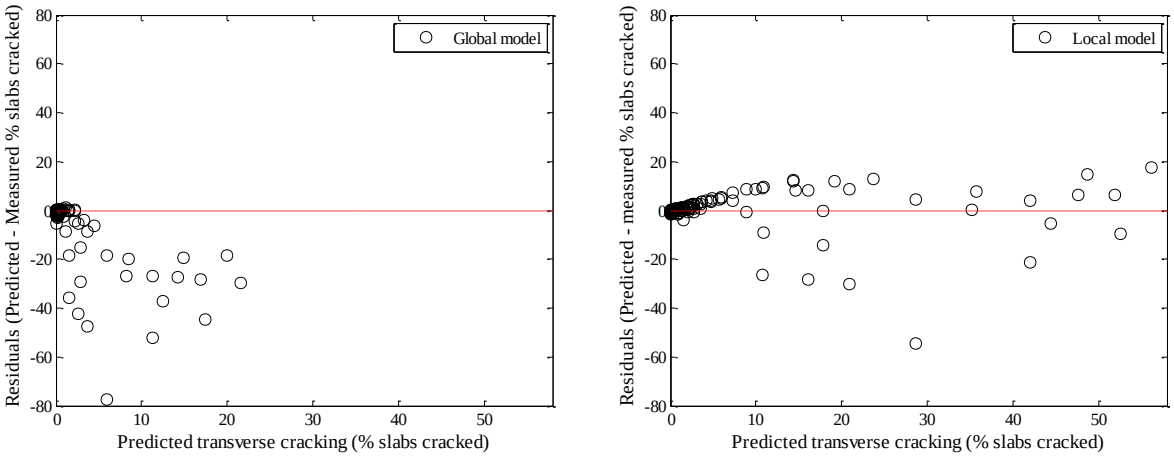

(a) Global model (b) Local model

Figure B-358 Option 2 transverse cracking residual plots – no sampling

Reliability

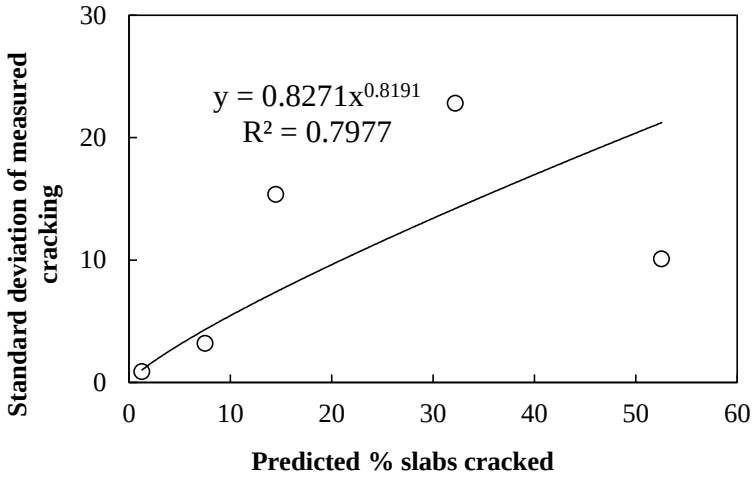

Figure B-359 Option 2 Transverse cracking reliability model fitting – no sampling

Split sampling

Table B-170 Option 2 transverse cracking local calibration results – split sampling

Parameter	Global model	Local model calibration	Local model validation
SEE	12.18	6.74	11.18
Bias	-4.60	0.06	0.84
R^2	0.70	0.77	0.68
t-test pvalue	0.00	0.94	0.62
Intercept = 0	0.87	0.07	0.04
Slope = 1	0.00	0.00	0.00
C4	1.00	0.19	0.19
C5	-1.98	-1.81	-1.81

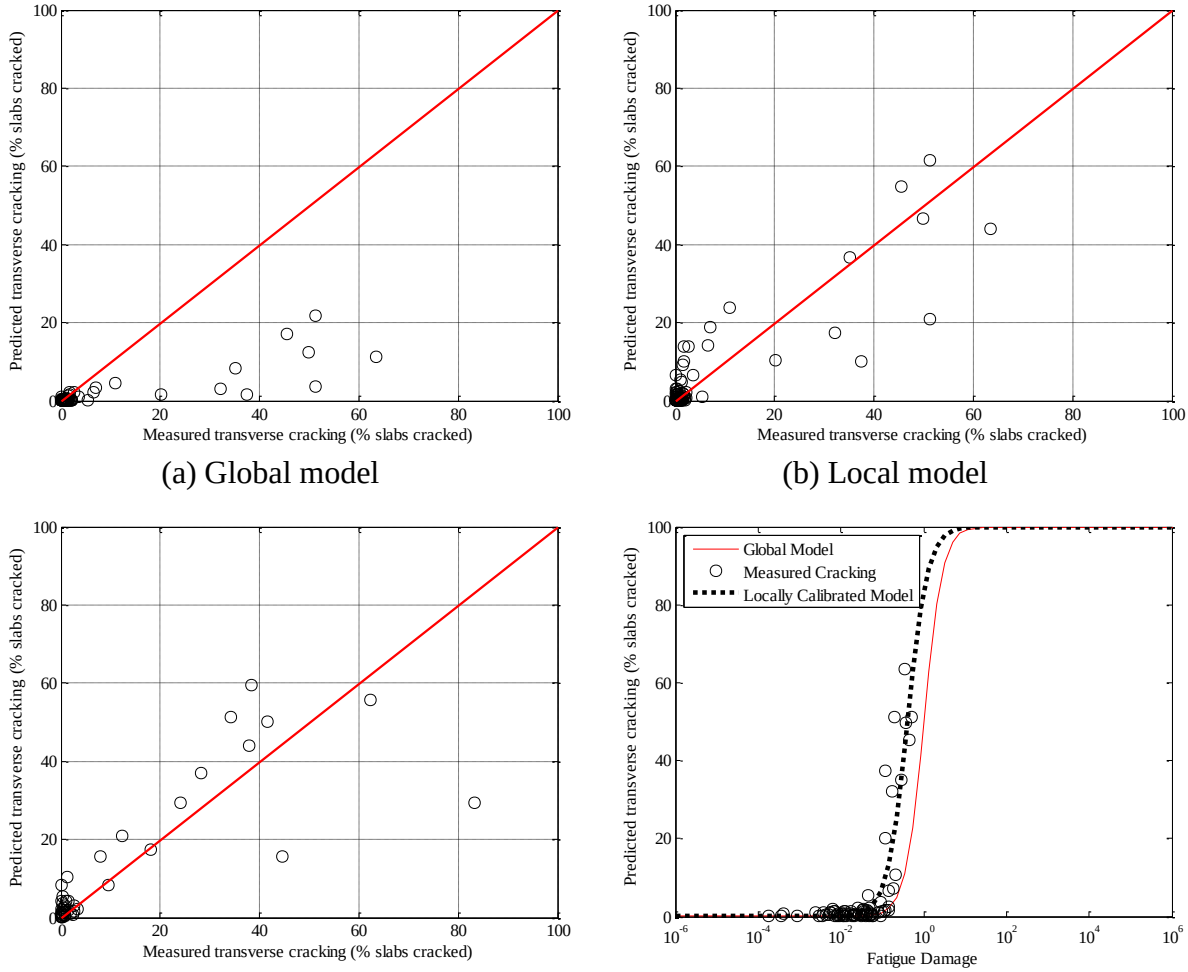

(a) Global model

(b) Local model

(c) Local model validation

(d) Fatigue damage predicted cracking

Figure B-360 Option 2 transverse cracking local calibration measured vs. predicted – split sampling

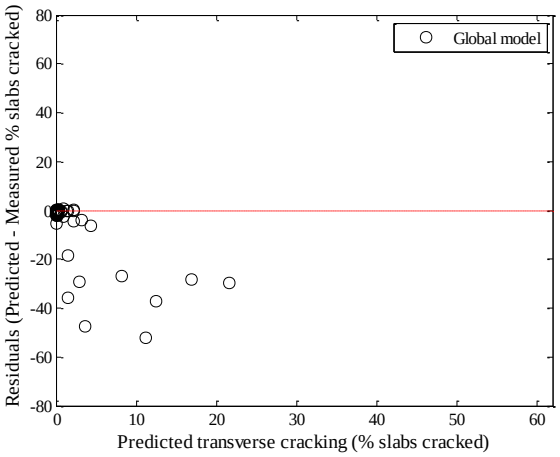

(a) Global model

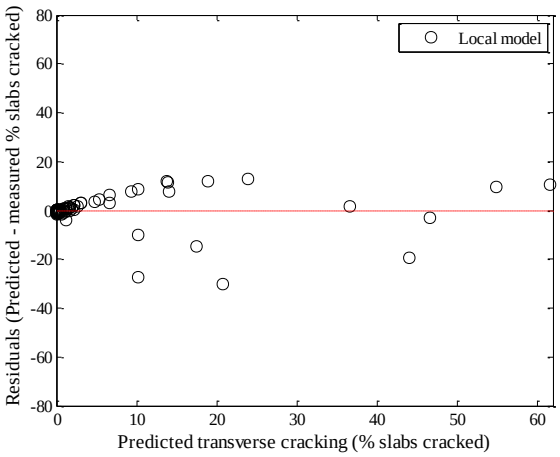

(b) Local model

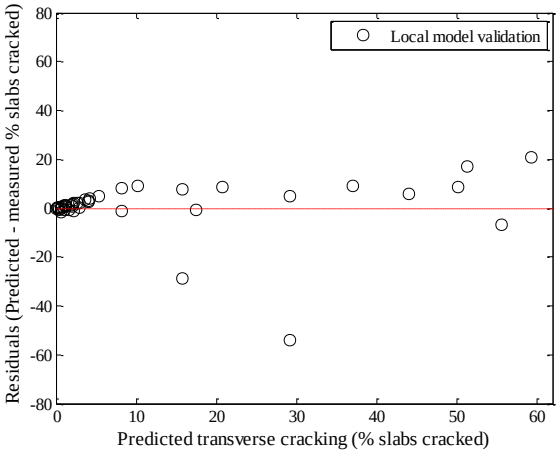

(c) Local model validation

Figure B-361 Option 2 transverse cracking residual plots – split sampling

Reliability

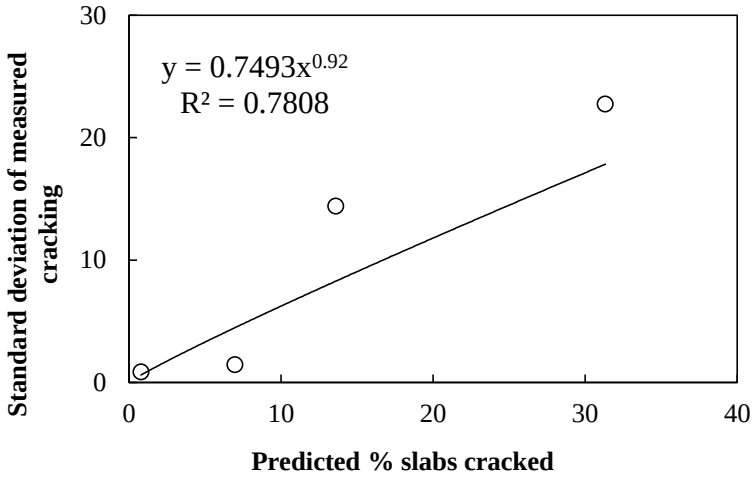

Figure B-362 Option 2 Reliability model fitting – split sampling

Repeated split sampling

Table B-171 Option 2 transverse cracking local calibration results – repeated split sampling

Parameter	Global Model Mean	Global Model Median	Global model lower CI	Global model upper CI
SEE	14.19	14.19	9.56	17.28
Bias	-5.83	-5.83	-8.11	-3.35
C4	1.00	1.00	-	-
C5	-1.98	-1.98	-	-
Parameter	Local Model Mean	Local Model Median	Local model lower CI	Local model upper CI
SEE	8.16	8.76	4.30	10.09
Bias	0.33	0.37	-0.24	0.70
C4	0.23	0.24	0.12	0.31
C5	-1.74	-1.69	-2.17	-1.50
Parameter	Local Model Mean	Local Model Median	Local model lower CI	Local model upper CI
SEE	9.22	8.42	2.41	18.22
Bias	0.49	0.59	-5.98	7.36
C4	0.23	0.24	0.12	0.31
C5	-1.74	-1.69	-2.17	-1.50

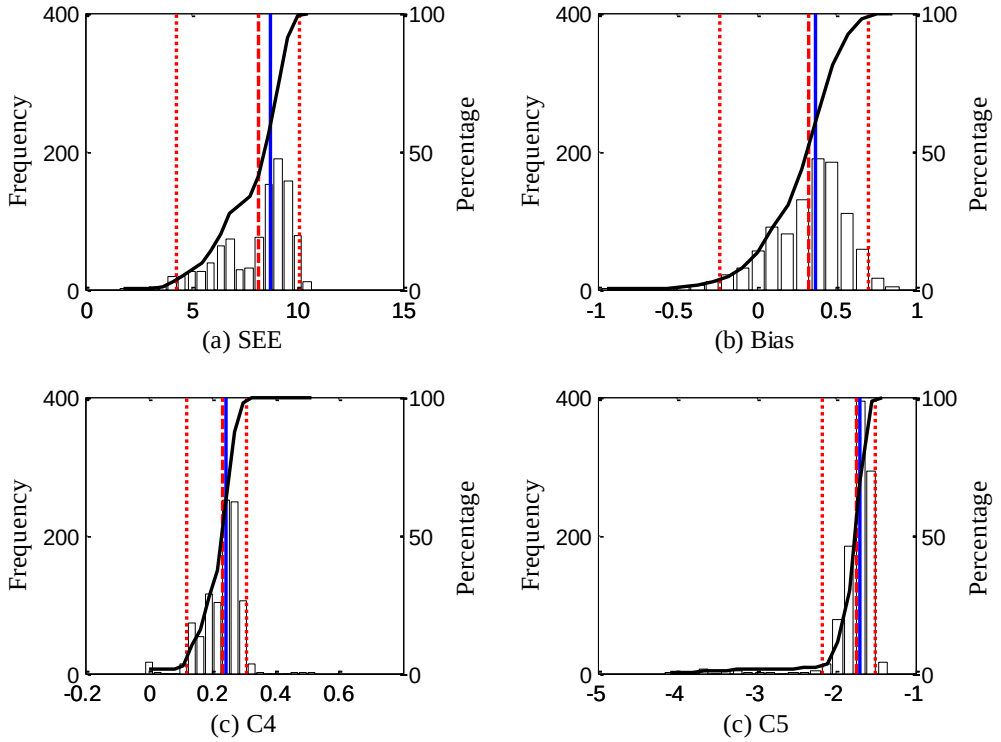

Figure B-363 Option 2 – Distribution of calibration parameters – repeated split sampling - Calibration

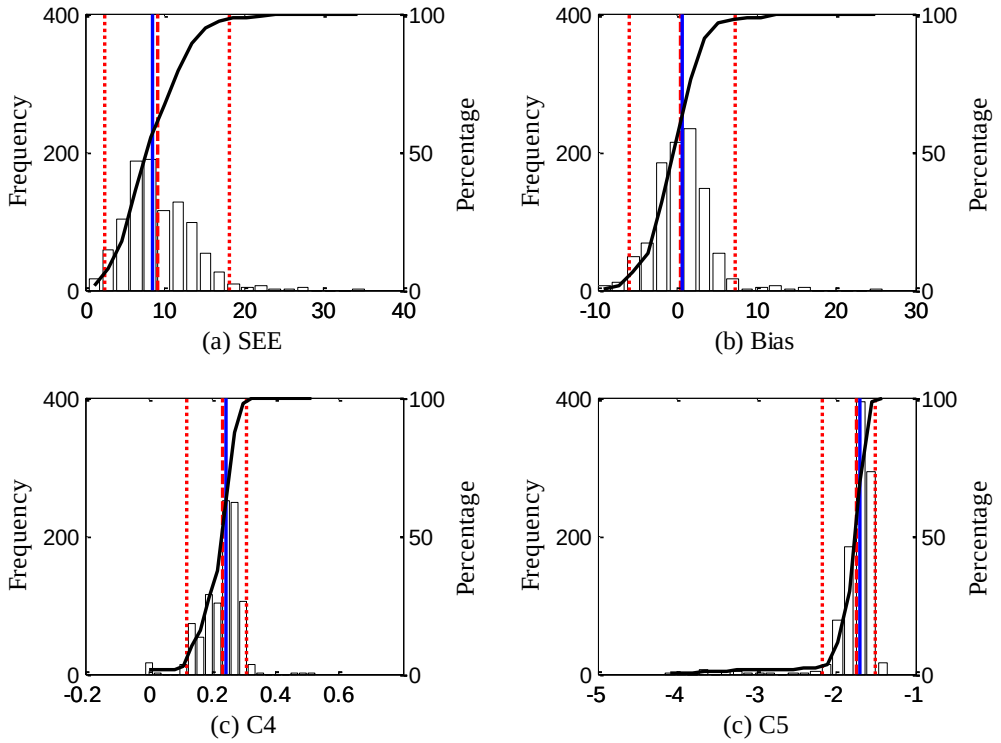

Figure B-364 Option 2 – Distribution of calibration parameters – repeated split sampling - Validation

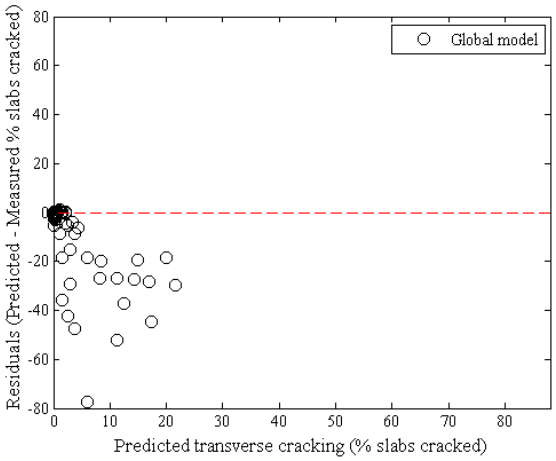

(a) Global model

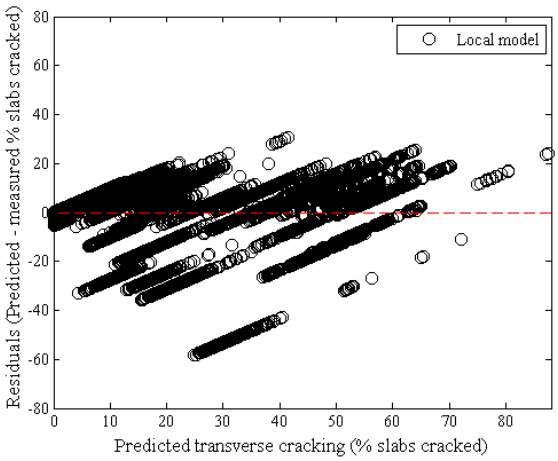

(b) Local model

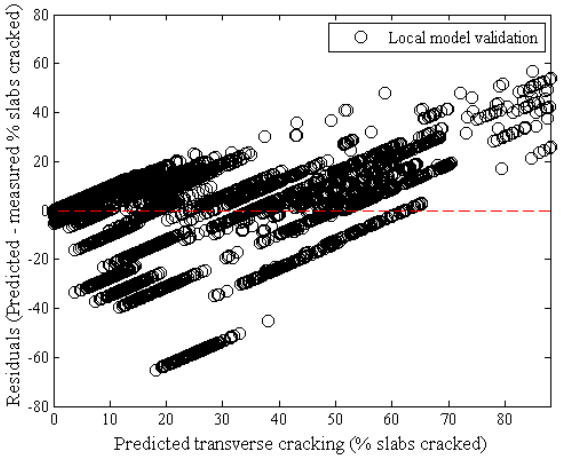

(c) Local model validation

Figure B-365 Option 2 transverse cracking residual plots – repeated split sampling

Reliability

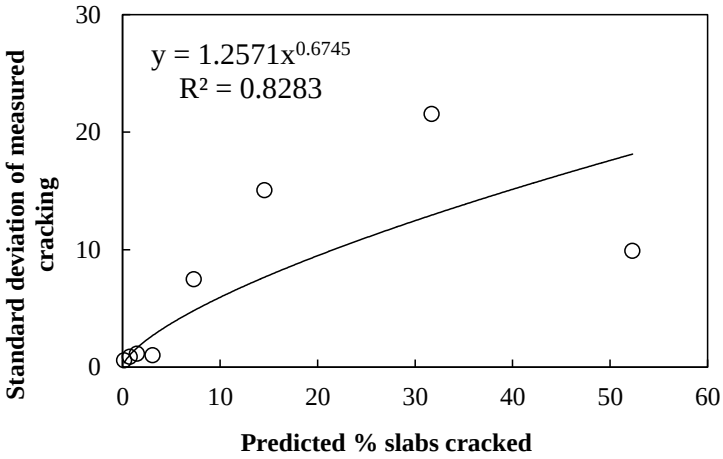

Figure B-366 Option 2 Transverse cracking reliability model fitting – repeated split sampling

Bootstrapping

Table B-172 Option 2 transverse cracking local calibration results – bootstrapping

Parameter	Global Model Mean	Global Model Median	Global model lower CI	Global model upper CI
SEE	13.86	13.76	7.15	19.80
Bias	-5.79	-5.59	-9.79	-2.40
C4	1.00	1.00	-	-
C5	-1.98	-1.98	-	-
Parameter	Local Model Mean	Local Model Median	Local model lower CI	Local model upper CI
SEE	7.81	7.92	3.53	11.78
Bias	0.30	0.31	-0.45	0.84
C4	0.23	0.23	0.02	0.42
C5	-1.80	-1.71	-3.03	-1.43

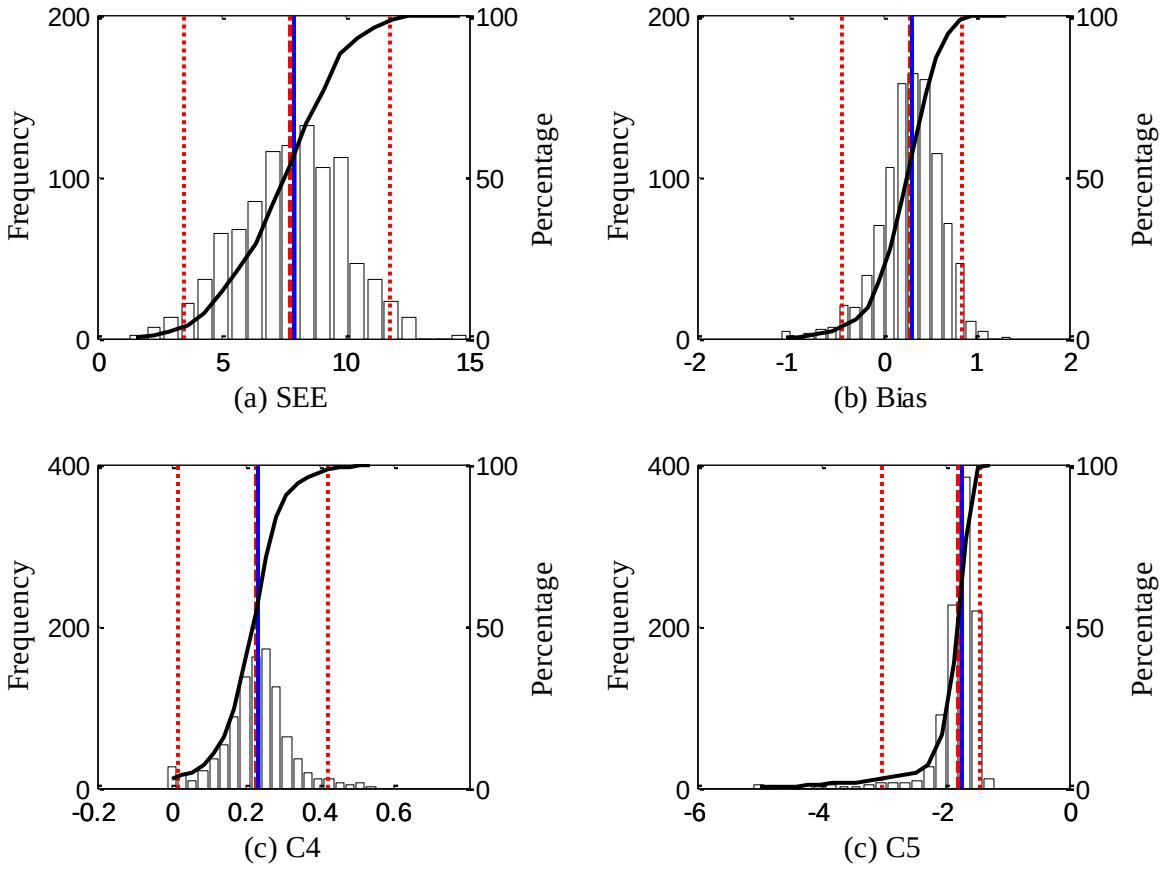

Figure B-367 Option 2 – Distribution of calibration parameters – bootstrapping

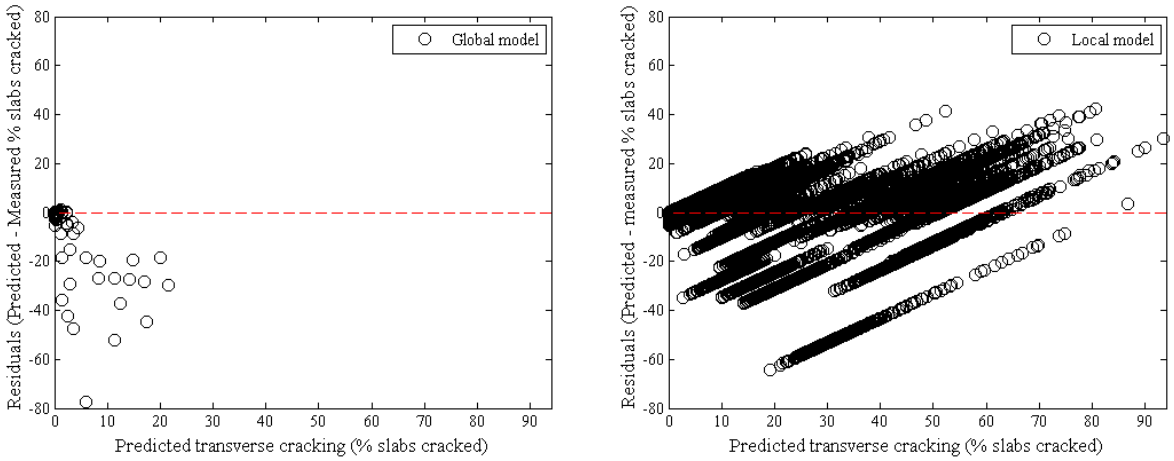

(a) Global model (b) Local model

Figure B-368 Option 2 transverse cracking residual plots – bootstrapping

Reliability

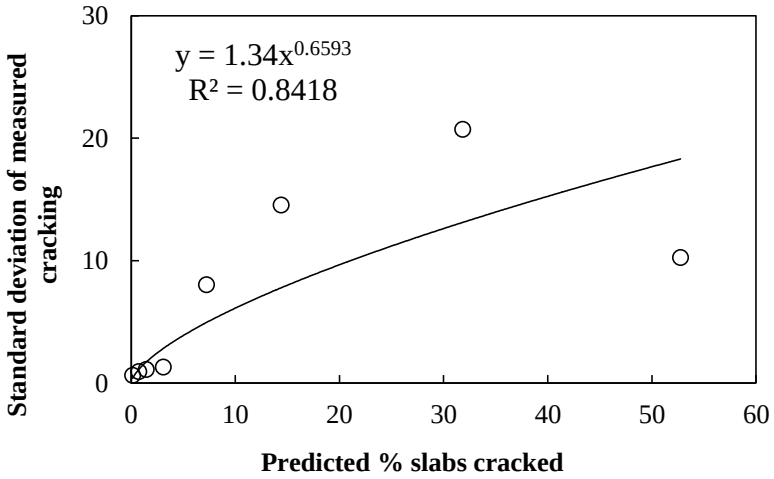

Figure B-369 Option 2 Transverse cracking reliability model fitting – bootstrapping

B.2.1.3 Option 3

No sampling

Table B-173 Option 3 transverse cracking local calibration results – no sampling

Parameter	Global model	Local model
SEE	16.94	13.79
Bias	-4.46	1.76
R^2	0.13	0.26
t-test pvalue	0.00	0.11
Intercept = 0	0.04	0.00
Slope = 1	0.00	0.00
C4	1.00	2.16
C5	-1.98	-0.58

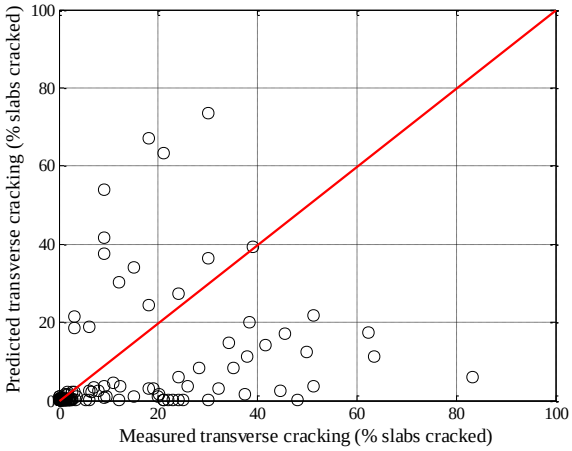

(a) Global model

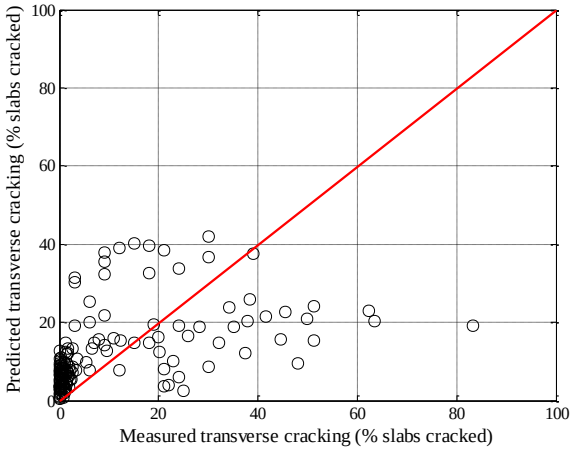

(b) Local model

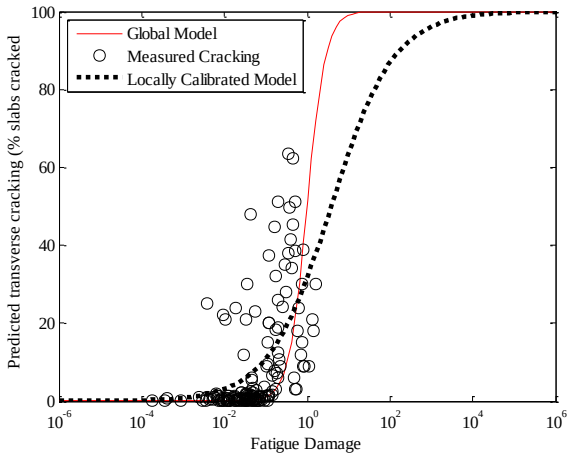

(c) Fatigue damage predicted cracking

Figure B-370 Option 3 transverse cracking local calibration measured vs. predicted – no sampling

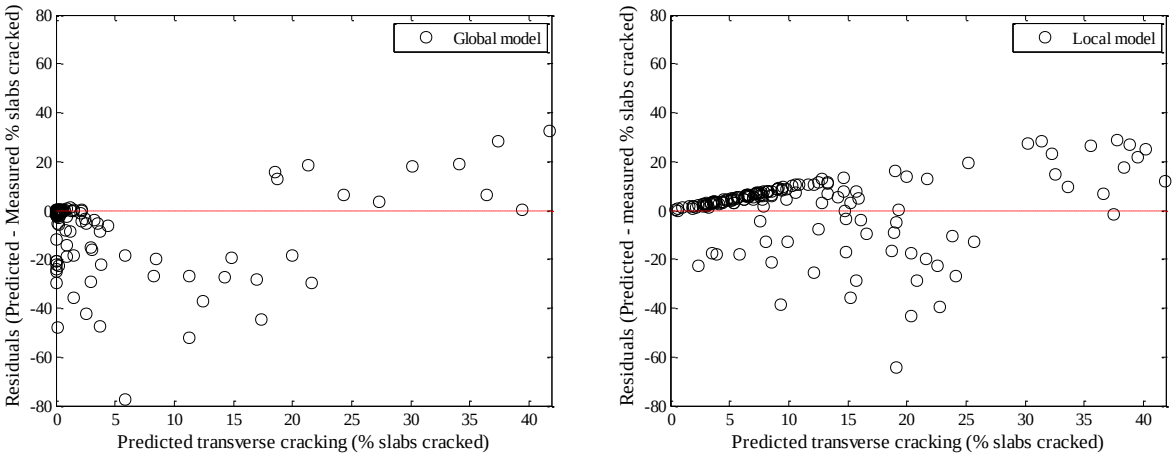

(a) Global model (b) Local model

Figure B-371 Option 3 transverse cracking residual plots – no sampling

Reliability

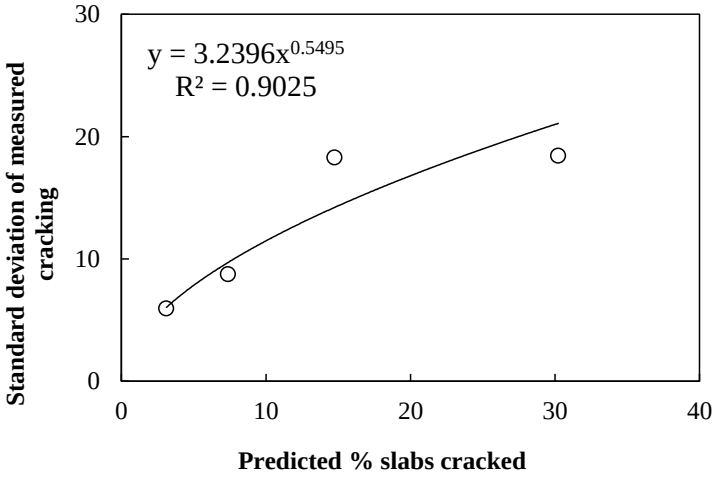

Figure B-372 Option 3 Transverse cracking reliability model fitting – no sampling

Split sampling

Table B-174 Option 3 transverse cracking local calibration results – split sampling

Parameter	Global model	Local model calibration	Local model validation
SEE	18.92	14.96	11.13
Bias	-4.36	2.44	2.60
R^2	0.10	0.20	0.59
t-test pvalue	0.01	0.09	0.11
Intercept = 0	0.03	0.00	0.00
Slope = 1	0.00	0.00	0.00
C4	1.00	2.56	2.56
C5	-1.98	-0.48	-0.48

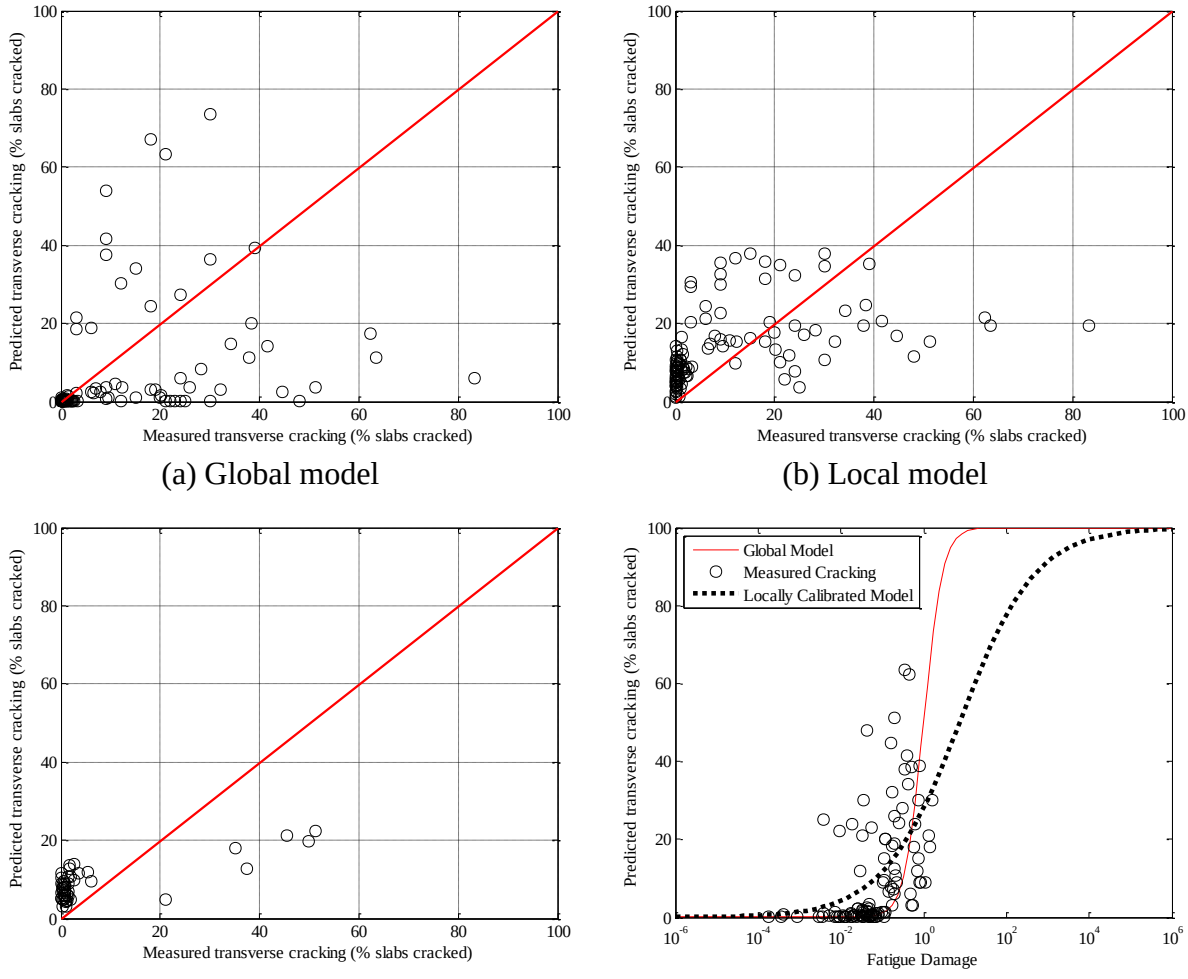

(a) Global model

(b) Local model

(c) Local model validation

(d) Fatigue damage predicted cracking

Figure B-373 Option 3 transverse cracking local calibration measured vs. predicted – split sampling

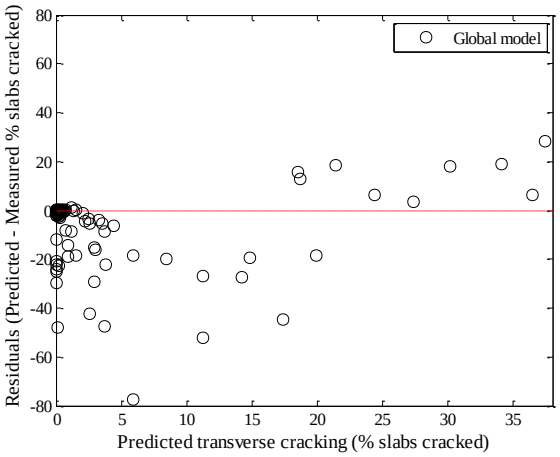

(a) Global model

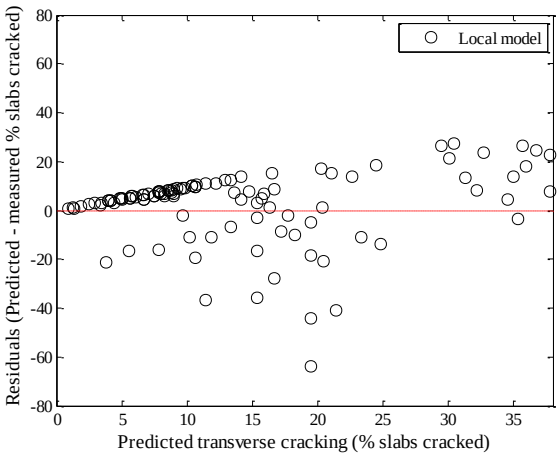

(b) Local model

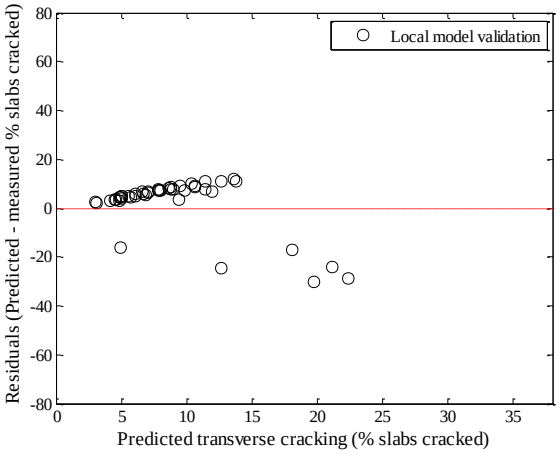

(c) Local model validation

Figure B-374 Option 3 transverse cracking residual plots – split sampling

Reliability

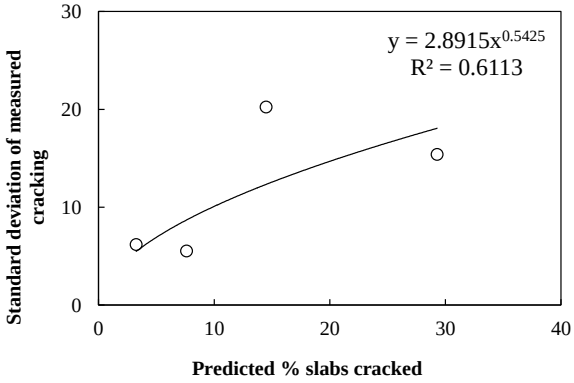

Figure B-375 Option 3 Transverse cracking reliability model fitting – split sampling

Repeated split sampling

Table B-175 Option 3 transverse cracking local calibration results – repeatedsplit sampling

Parameter	Global Model Mean	Global Model Median	Global model lower CI	Global model upper CI
SEE	16.98	16.98	12.69	19.95
Bias	-4.44	-4.44	-7.56	-1.76
C4	1.00	1.00	-	-
C5	-1.98	-1.98	-	-
Parameter	Local Model Mean	Local Model Median	Local model lower CI	Local model upper CI
SEE	13.62	13.78	10.25	15.91
Bias	1.70	1.78	0.43	2.63
C4	2.15	2.23	0.81	3.33
C5	-0.61	-0.56	-1.01	-0.45
Parameter	Local Model Mean	Local Model Median	Local model lower CI	Local model upper CI
SEE	14.95	14.50	9.69	21.89
Bias	2.03	2.16	-6.38	9.29
C4	2.15	2.23	0.81	3.33
C5	-0.61	-0.56	-1.01	-0.45

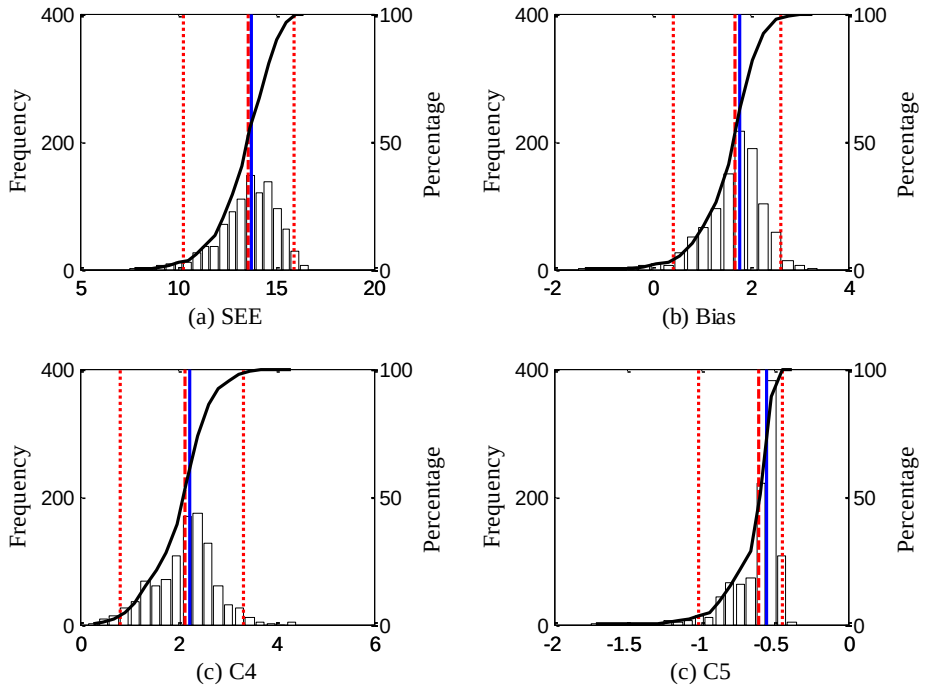

Figure B-376 Option 3 – Distribution of calibration parameters – repeated split sampling - Calibration

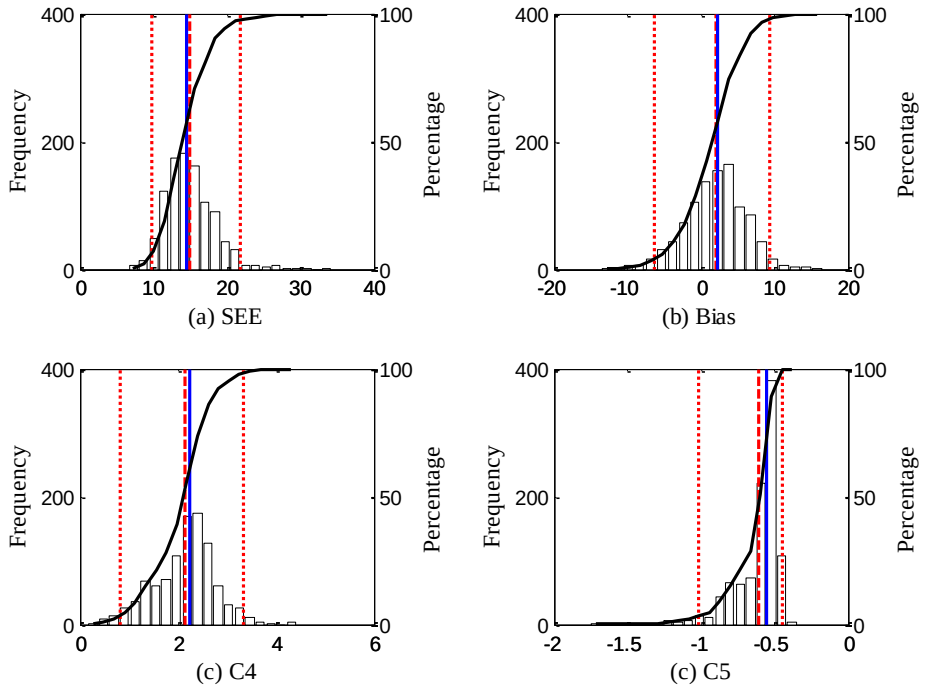

Figure B-377 Option 3 – Distribution of calibration parameters – repeated split sampling – Validation

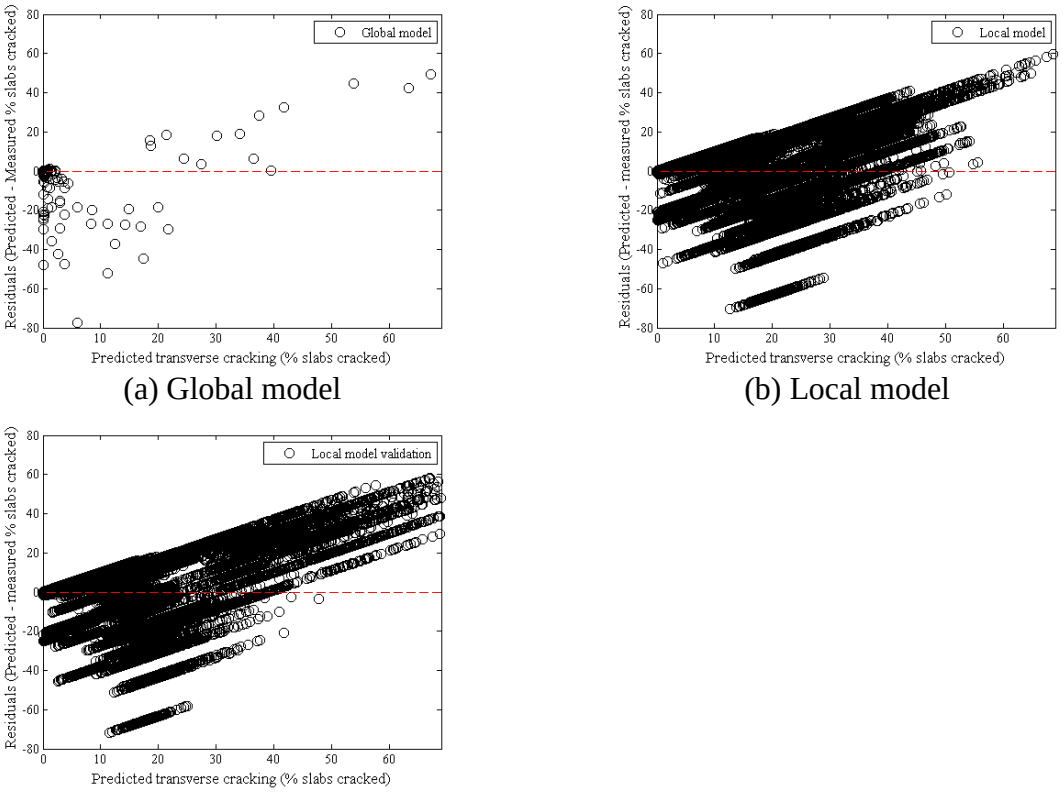

Figure B-378 Option 3 transverse cracking residual plots – repeated split sampling

Reliability

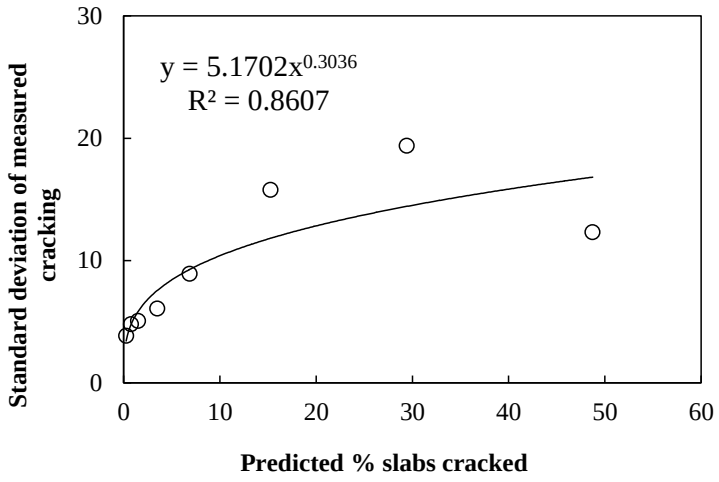

Figure B-379 Option 3 Transverse cracking reliability model fitting – repeated split sampling

Bootstrapping

Table B-176 Option 3 transverse cracking local calibration results – bootstrapping

Parameter	Global Model Mean	Global Model Median	Global model lower CI	Global model upper CI
SEE	16.77	16.86	11.19	22.09
Bias	-4.45	-4.52	-8.86	0.03
C4	1.00	1.00	-	-
C5	-1.98	-1.98	-	-
Parameter	Local Model Mean	Local Model Median	Local model lower CI	Local model upper CI
SEE	13.24	13.42	8.56	17.11
Bias	1.65	1.67	-0.26	3.41
C4	2.14	2.16	0.50	3.69
C5	-0.64	-0.59	-1.25	-0.37

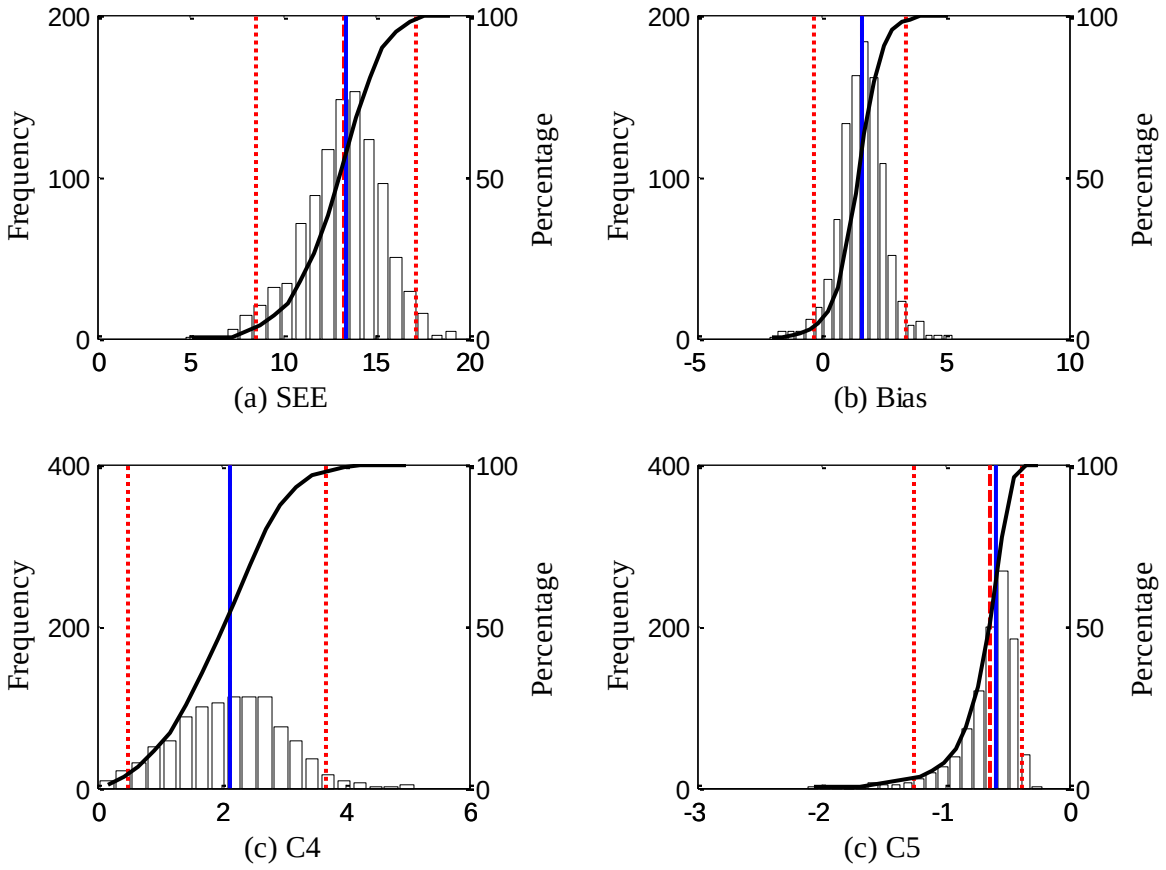

Figure B-380 Option 3 – Distribution of calibration parameters – bootstrapping

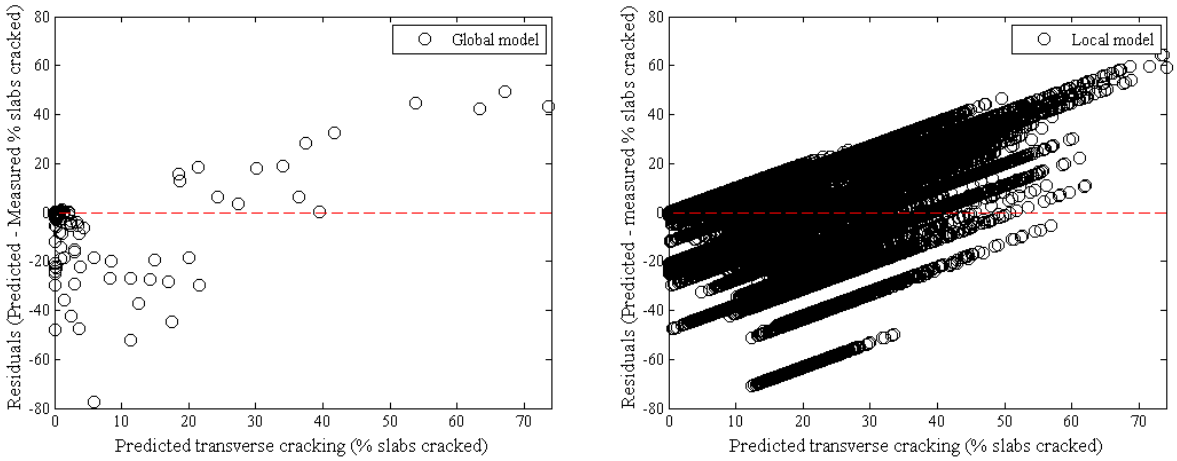

(a) Global model (b) Local model

Figure B-381 Option 3 transverse cracking residual plots – bootstrapping

Reliability

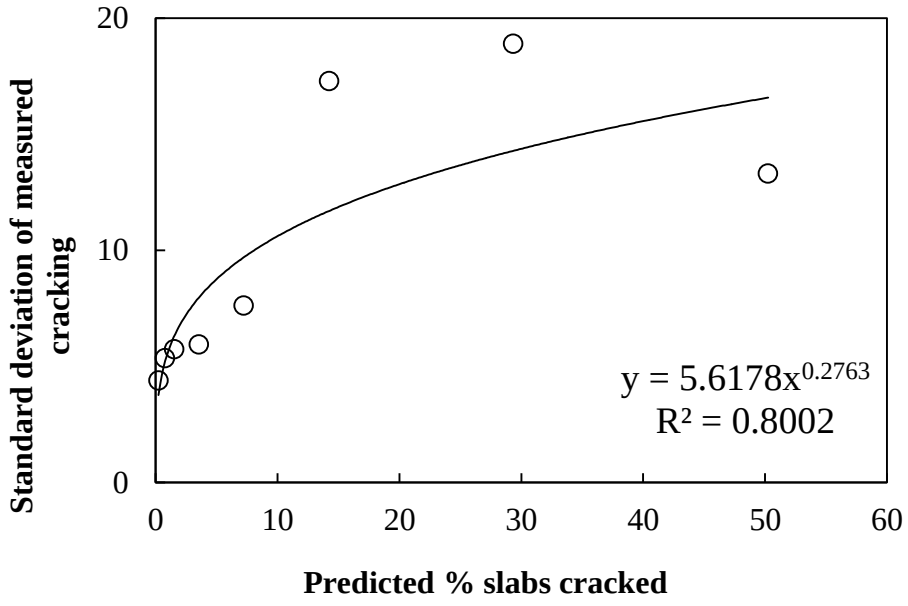

Figure B-382 Option 3 Transverse cracking reliability model fitting – bootstrapping

B.2.1.4 Option 4

No sampling

Table B-177 Option 4 transverse cracking local calibration results – no sampling

Parameter	Global model	Local model
SEE	0.92	0.72
Bias	-0.55	-0.04
R^2	0.07	0.12
t-test pvalue	0.00	0.65
Intercept = 0	0.00	0.00
Slope = 1	0.00	0.00
C4	1.00	5.00
C5	-1.98	-1.00

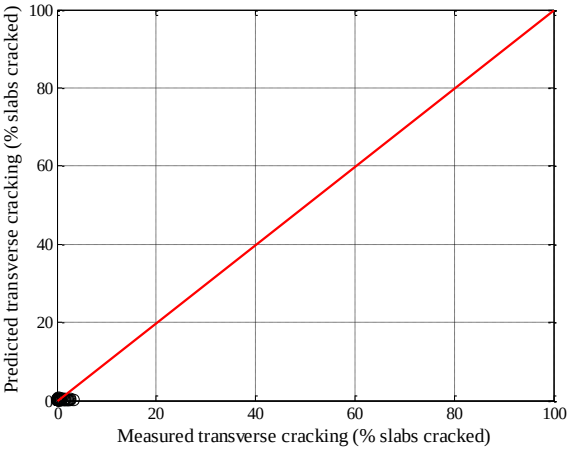

(a) Global model

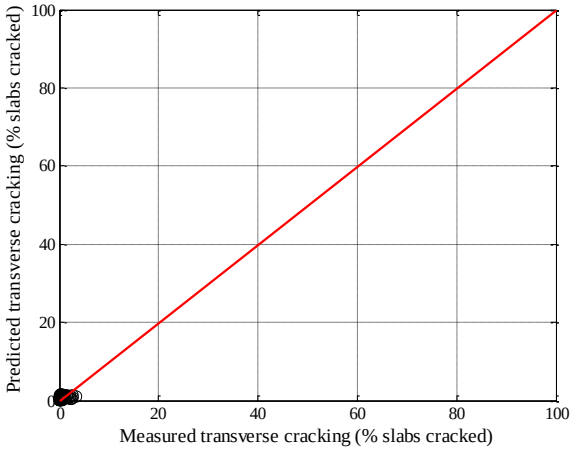

(b) Local model

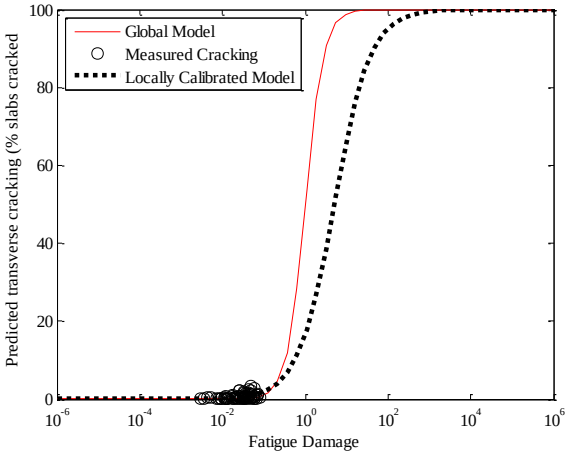

(c) Fatigue damage predicted cracking

Figure B-383 Option 4 transverse cracking local calibration measured vs. predicted – no sampling

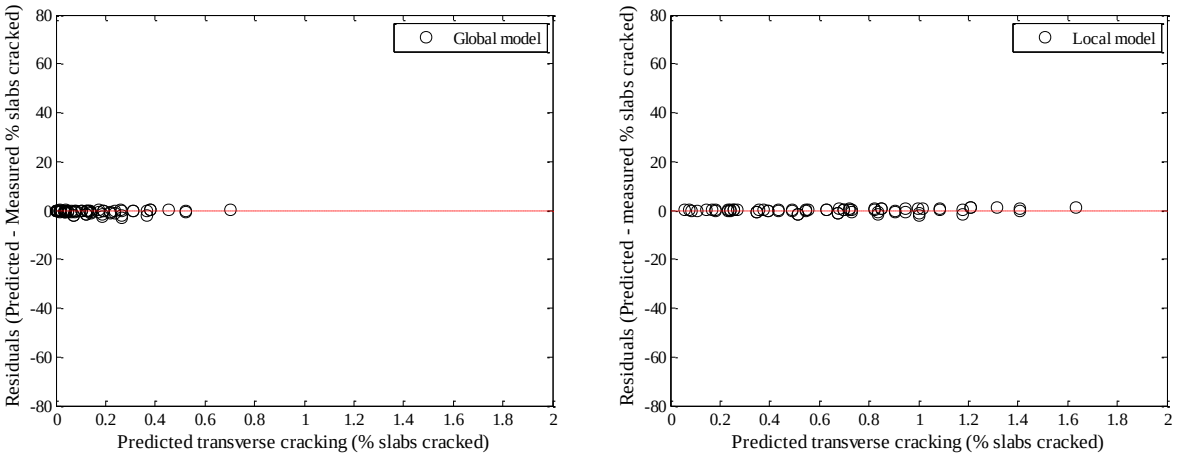

(a) Global model (b) Local model

Figure B-384 Option 4 transverse cracking residual plots – no sampling

Reliability

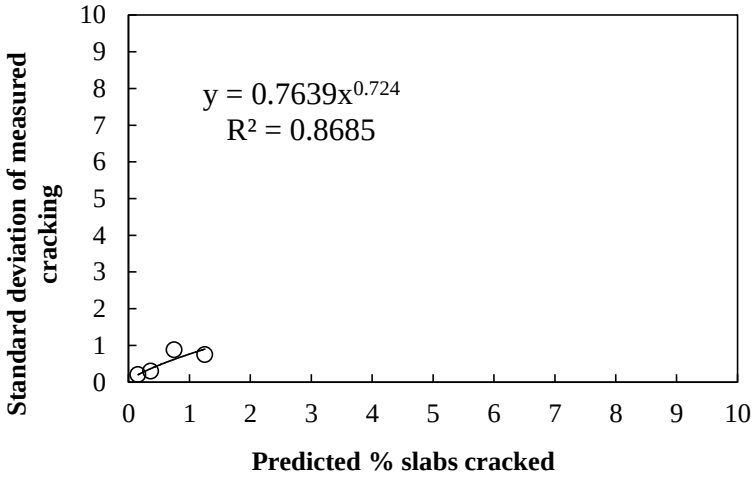

Figure B-385 Option 4 Transverse cracking reliability model fitting – no sampling

Split sampling

Table B-178 Option 4 transverse cracking local calibration results – split sampling

Parameter	Global model	Local model calibration	Local model validation
SEE	0.80	0.63	0.95
Bias	-0.48	-0.05	-0.29
R^2	0.09	0.14	0.13
t-test pvalue	0.00	0.63	0.16
Intercept = 0	0.00	0.00	0.00
Slope = 1	0.00	0.00	0.00
C4	1.00	5.00	5.00
C5	-1.98	-1.04	-1.04

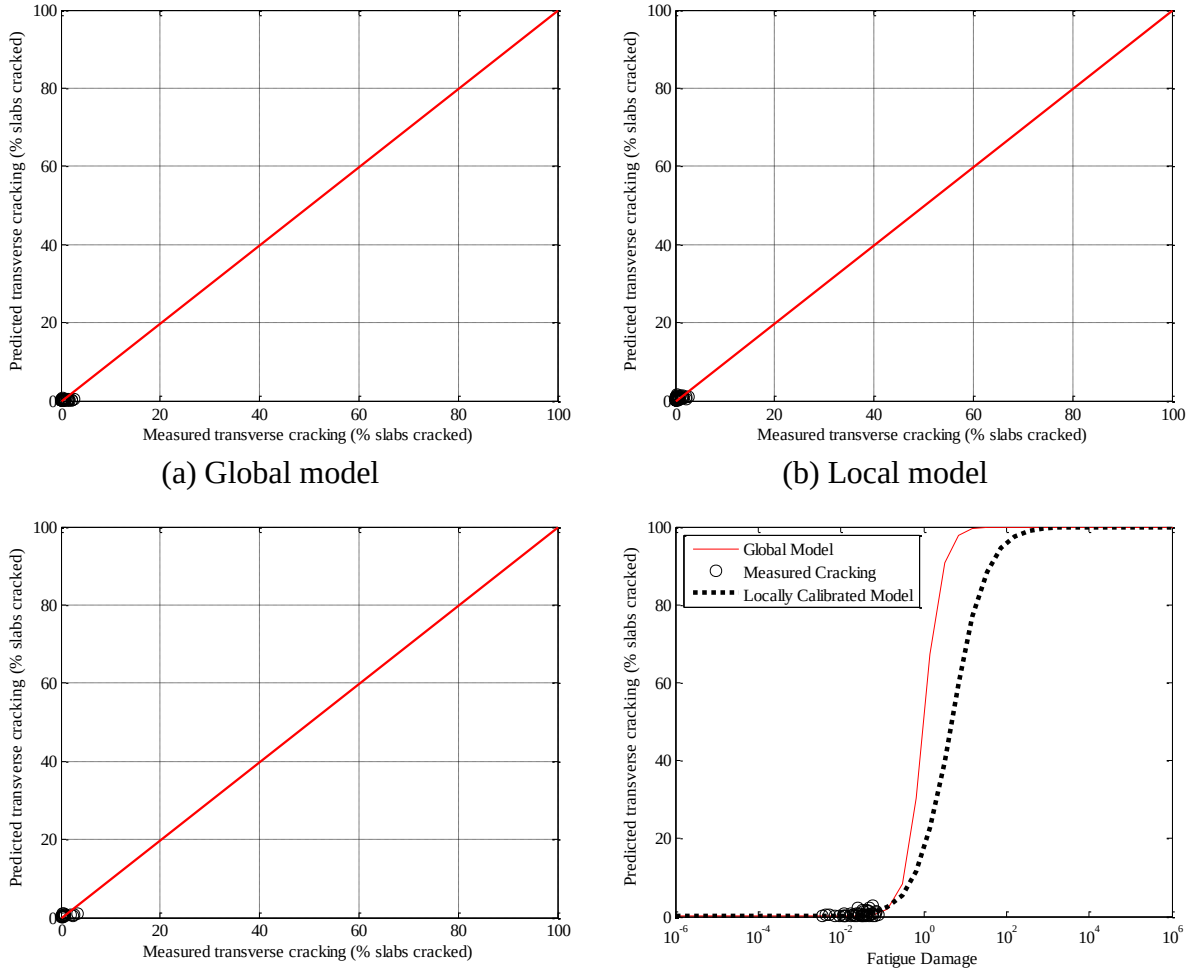

(a) Global model

(b) Local model

(c) Local model validation

(d) Fatigue damage predicted cracking

Figure B-386 Option 4 transverse cracking local calibration measured vs. predicted – split sampling

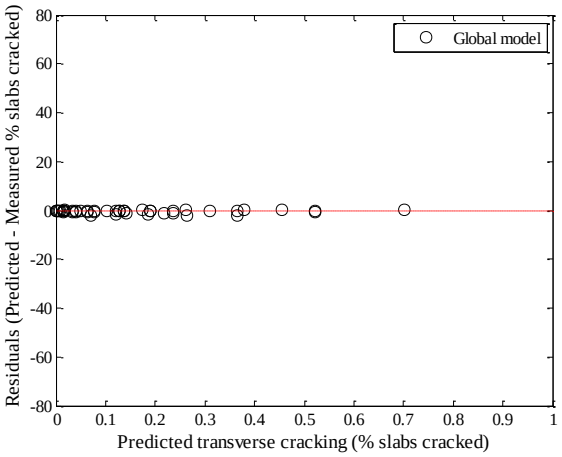

(a) Global model

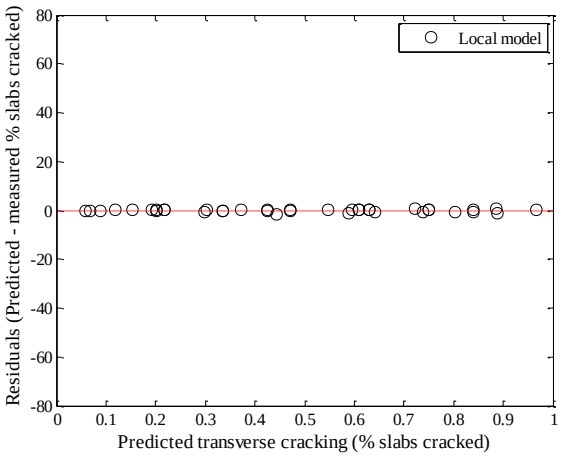

(b) Local model

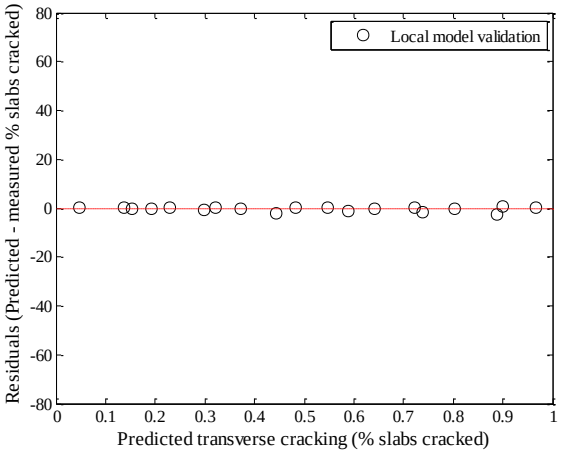

(c) Local model validation

Figure B-387 Option 4 transverse cracking residual plots – split sampling

Reliability

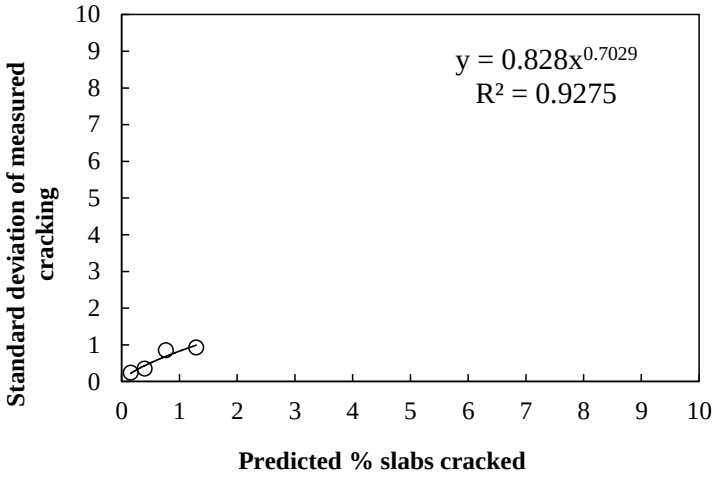

Figure B-388 Option 4 Transverse cracking reliability model fitting – split sampling

Repeated split sampling

Table B-179 Option 4 transverse cracking local calibration results – repeated split sampling

Parameter	Global Model Mean	Global Model Median	Global model lower CI	Global model upper CI
SEE	0.91	0.91	0.57	1.10
Bias	-0.55	-0.55	-0.73	-0.31
C4	1.00	1.00	-	-
C5	-1.98	-1.98	-	-
Parameter	Local Model Mean	Local Model Median	Local model lower CI	Local model upper CI
SEE	0.70	0.74	0.43	0.83
Bias	-0.04	-0.04	-0.07	0.00
C4	5.00	5.00	5.00	5.00
C5	-1.00	-0.99	-1.13	-0.90
Parameter	Local Model Mean	Local Model Median	Local model lower CI	Local model upper CI
SEE	0.78	0.76	0.38	1.24
Bias	-0.02	-0.01	-0.78	0.66
C4	5.00	5.00	5.00	5.00
C5	-1.00	-0.99	-1.13	-0.90

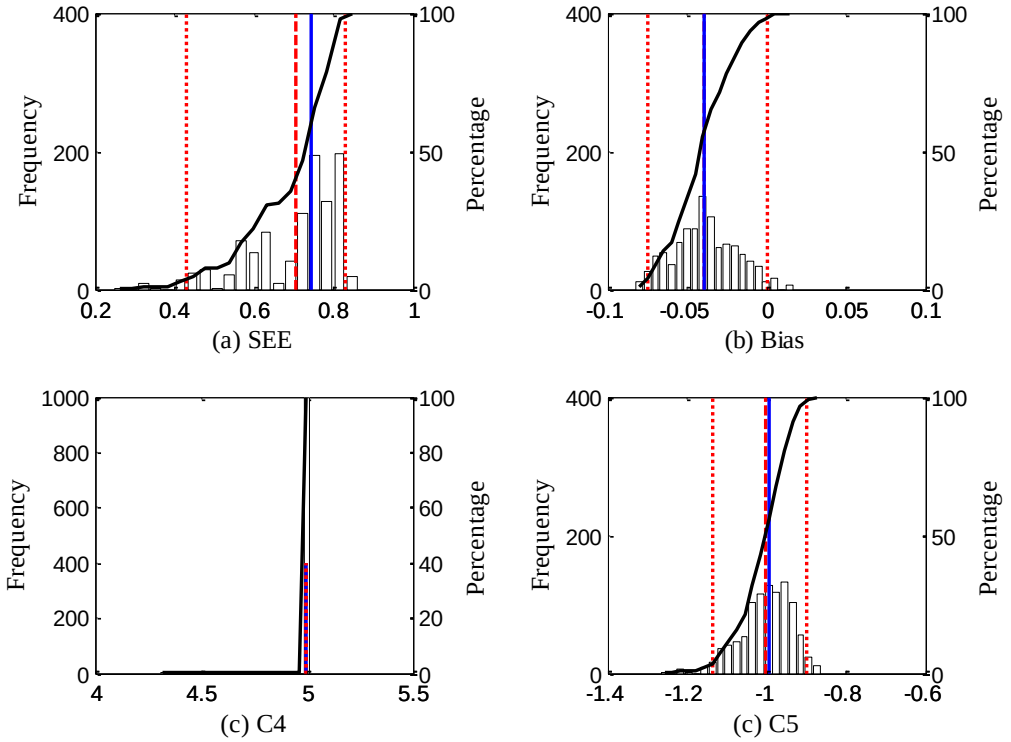

Figure B-389 Option 4 – Distribution of calibration parameters – repeated split sampling - Calibration

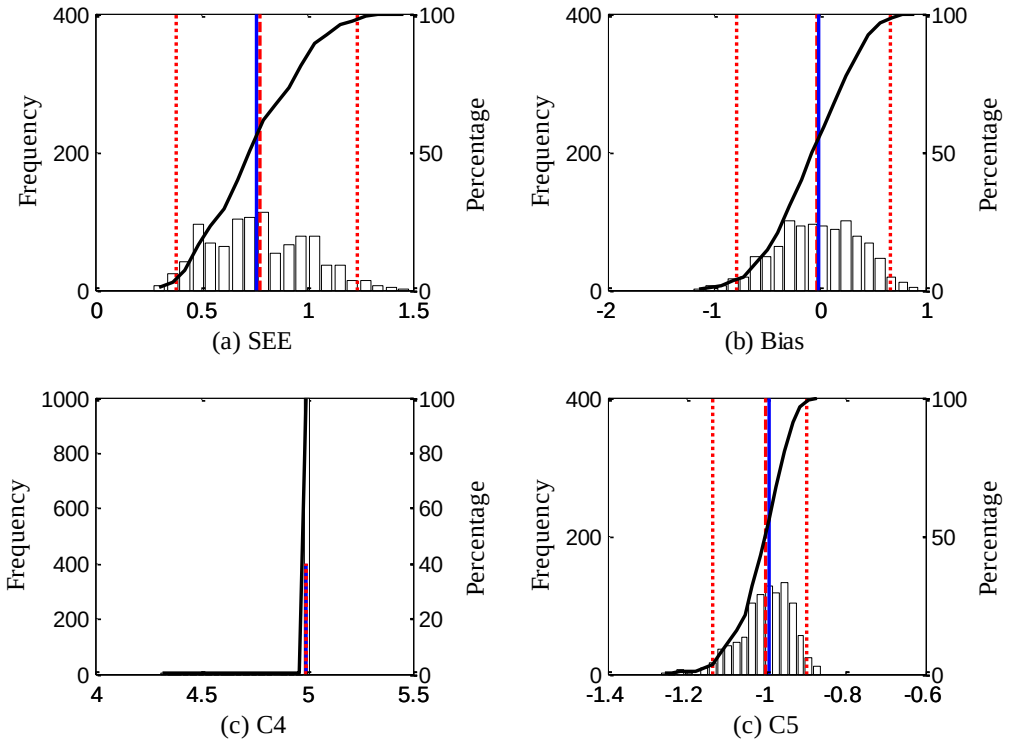

Figure B-390 Option 4 – Distribution of calibration parameters – repeated split sampling - Validation

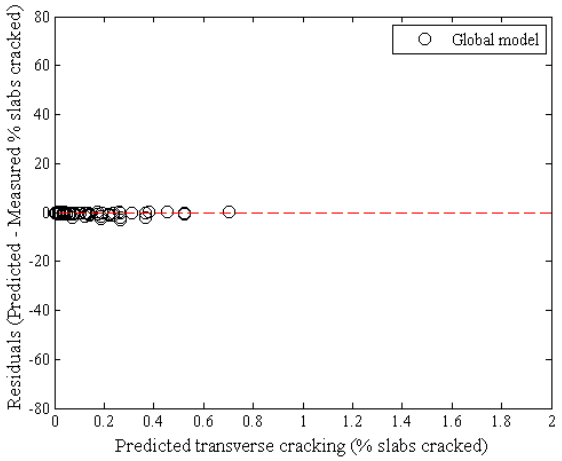

(a) Global model

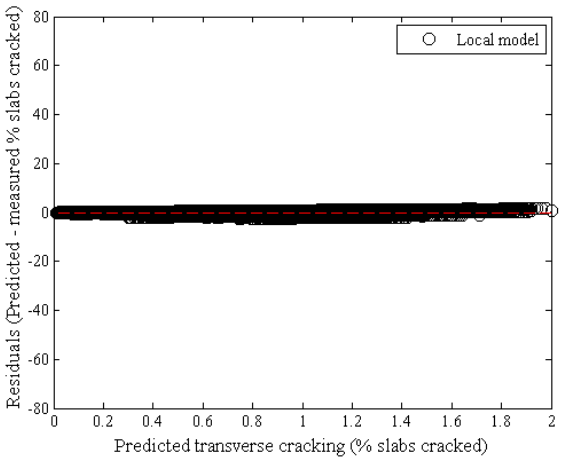

(b) Local model

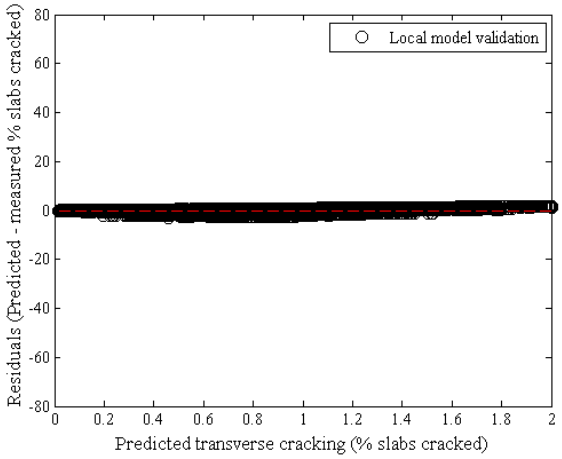

(c) Local model validation

Figure B-391 Option 4 transverse cracking residual plots – repeated split sampling

Reliability

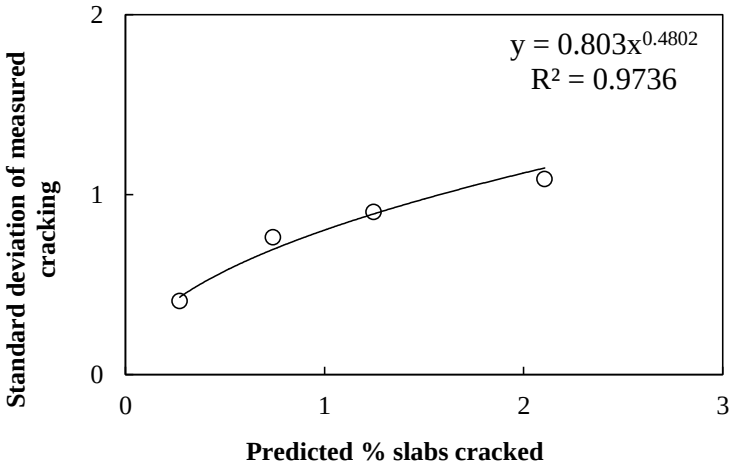

Figure B-392 Option 4 Transverse cracking reliability model fitting – repeated split sampling

Bootstrapping

Table B-180 Option 4 transverse cracking local calibration results – bootstrapping

Parameter	Global Model Mean	Global Model Median	Global model lower CI	Global model upper CI
SEE	0.88	0.89	0.44	1.26
Bias	-0.54	-0.54	-0.87	-0.25
C4	1.00	1.00	-	-
C5	-1.98	-1.98	-	-
Parameter	Local Model Mean	Local Model Median	Local model lower CI	Local model upper CI
SEE	0.67	0.69	0.35	0.90
Bias	-0.04	-0.04	-0.09	0.01
C4	4.96	5.00	4.63	5.00
C5	-1.01	-1.00	-1.20	-0.86

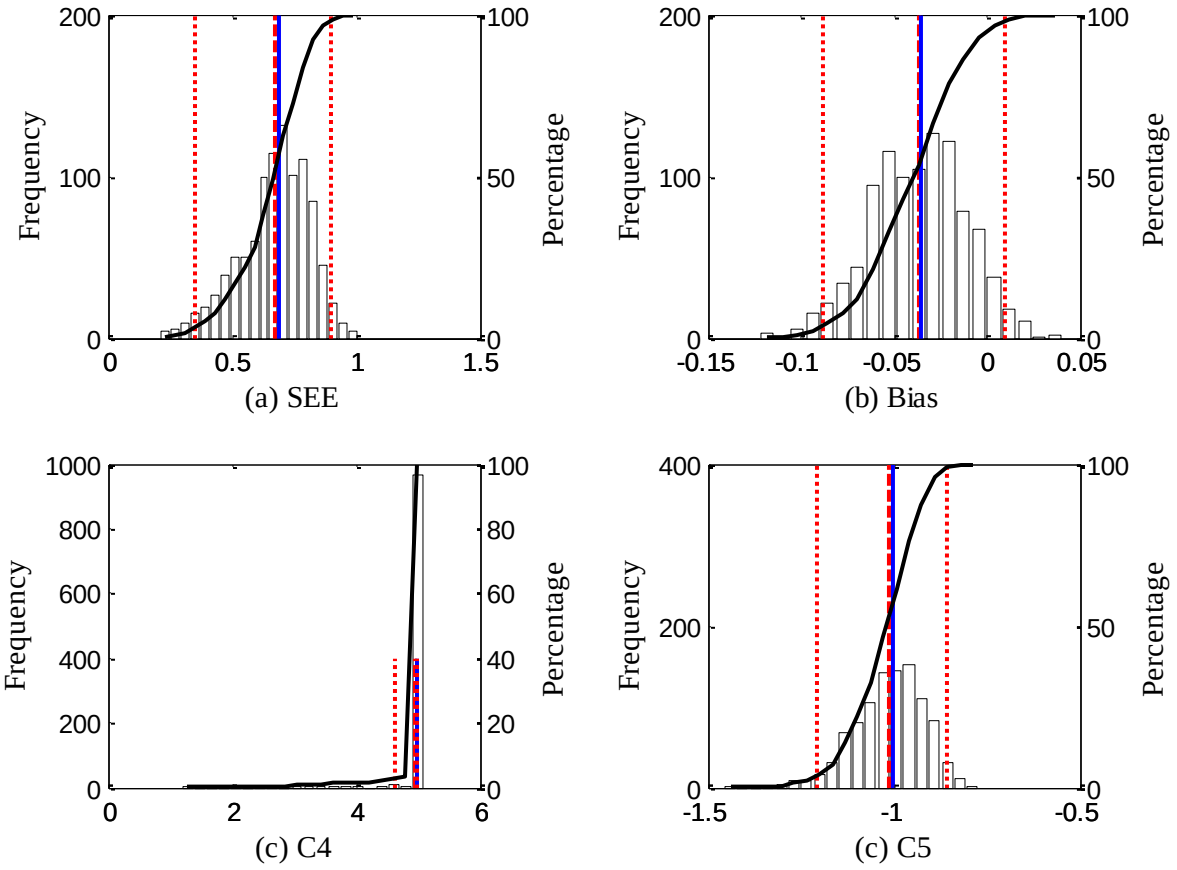

Figure B-393 Option 4 – Distribution of calibration parameters – bootstrapping

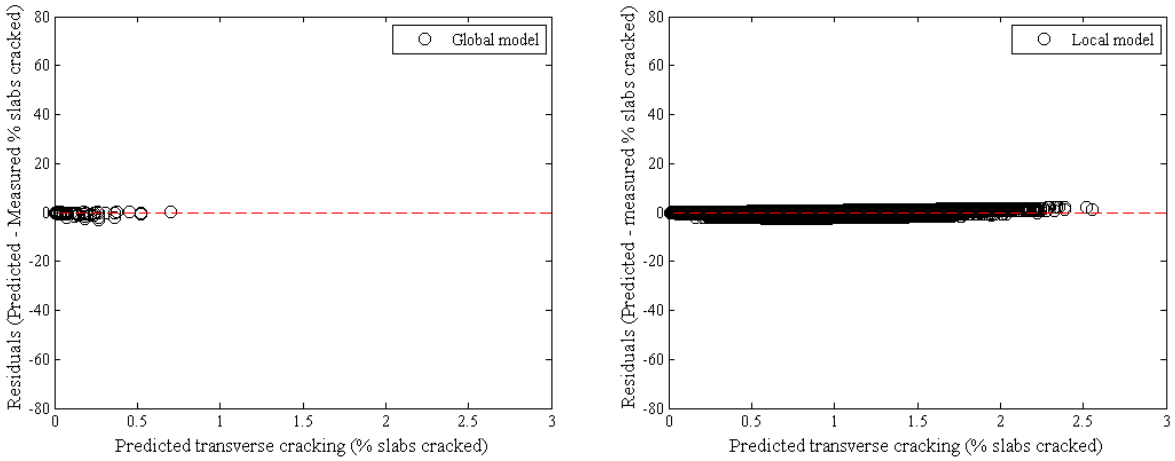

(a) Global model (b) Local model

Figure B-394 Option 3 transverse cracking residual plots – bootstrapping

Reliability

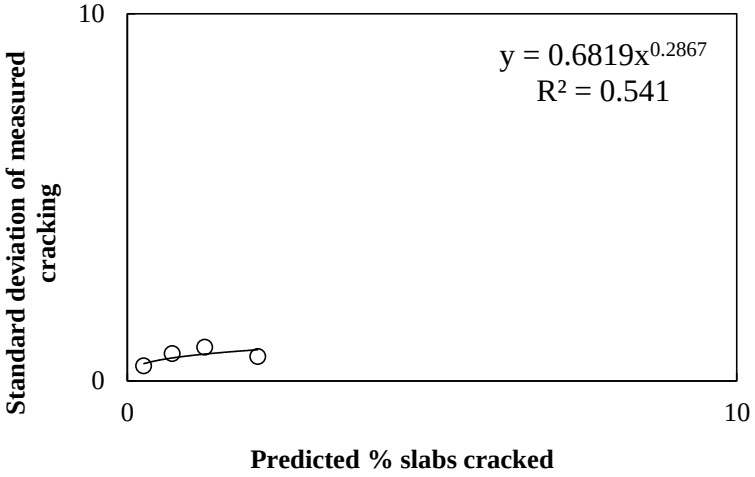

Figure B-395 Option 4 Transverse cracking reliability model fitting – bootstrapping

B.2.2 Faulting

B.2.2.1 Option 1

Table B-181 Option 1 faulting model local calibration results

Parameter	SEE	Bias
Global model	0.059	0.035
C1 = 0.4	0.024	0.007
C1 = 0.5	0.029	0.011
C1 = 0.6	0.034	0.015
C1 = 0.65	0.036	0.017
C1 = 0.7	0.039	0.020
C1 = 0.75	0.042	0.022
C1 = 0.8	0.045	0.025
C1 = 0.85	0.048	0.027
C1 = 0.9	0.045	0.025

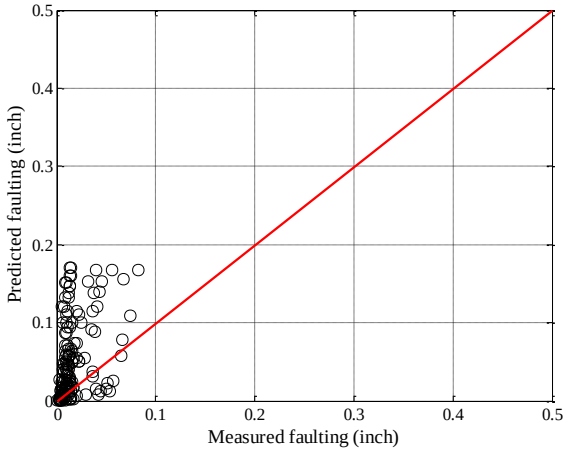

Figure B-396 Option 1 – Global faulting model

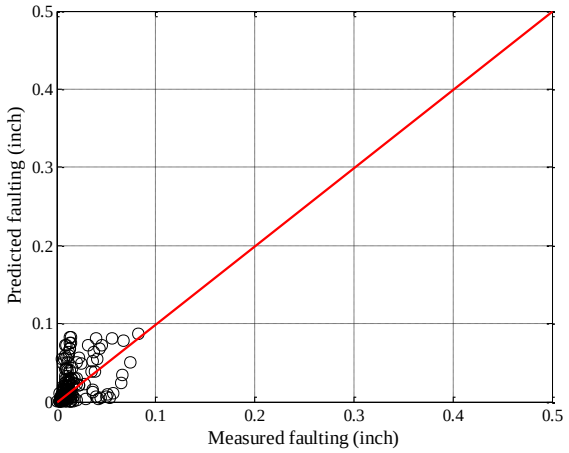

Figure B-397 Option 1 – C1 = 0.4

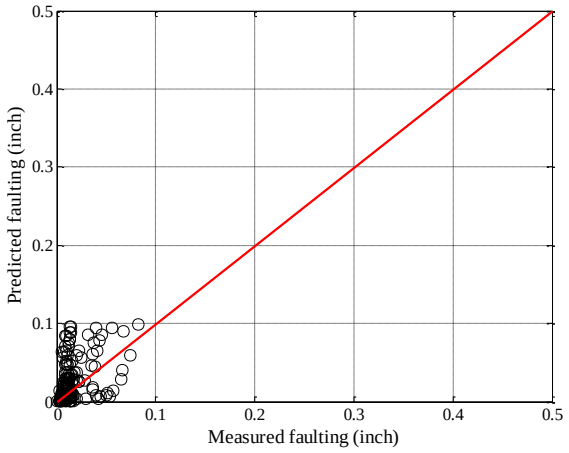

Figure B-398 Option 1 – C1 = 0.5

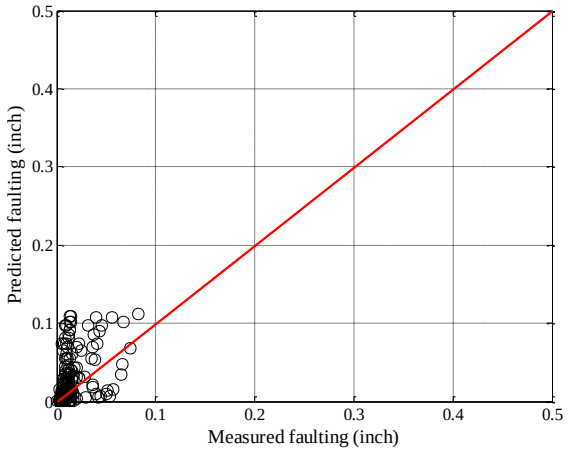

Figure B-399 Option 1 – C1 = 0.6

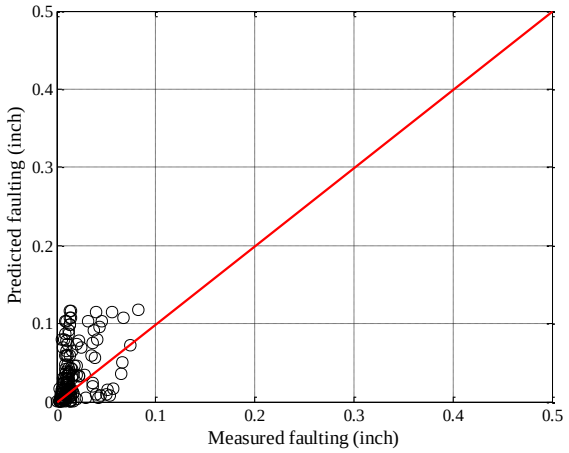

Figure B-400 Option 1 – C1 = 0.65

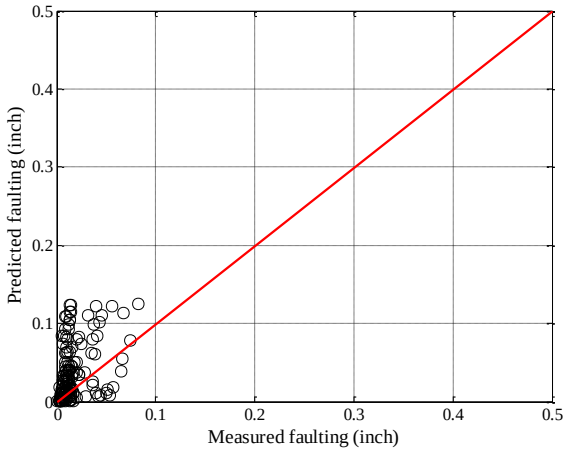

Figure B-401 Option 1 – C1 = 0.7

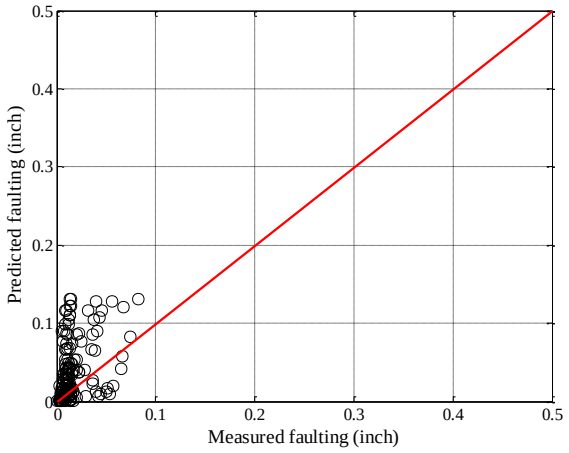

Figure B-402 Option 1 – C1 = 0.75

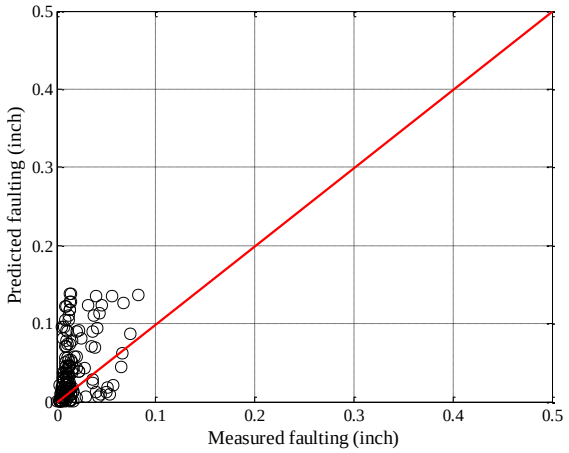

Figure B-403 Option 1 – C1 = 0.8

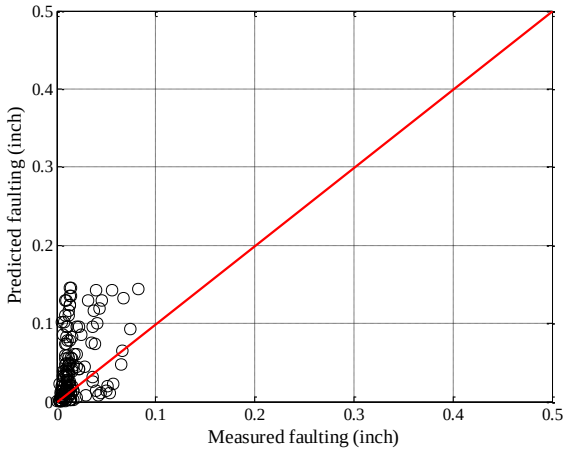

Figure B-404 Option 1 – C1 = 0.85

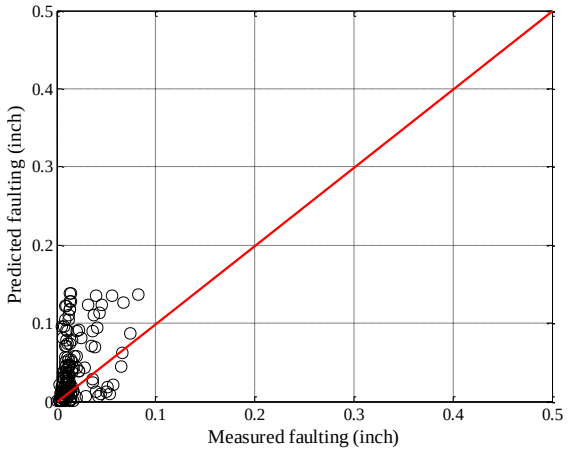

Figure B-405 Option 1 – C1 = 0.9

Reliability

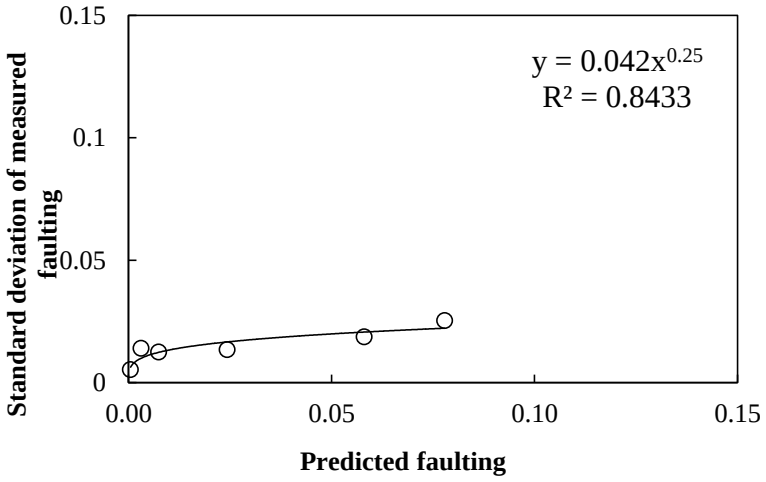

Figure B-406 Option 1 faulting model reliability equation

B.2.2.2 Option 2

Table B-182 Option 2 faulting model local calibration results

Parameter	SEE	Bias
Global model	0.051	0.026
C1 = 0.4	0.021	0.004
C1 = 0.5	0.025	0.008
C1 = 0.6	0.029	0.011
C1 = 0.65	0.032	0.013
C1 = 0.7	0.034	0.015
C1 = 0.75	0.037	0.016
C1 = 0.8	0.039	0.018
C1 = 0.85	0.042	0.020
C1 = 0.9	0.039	0.018

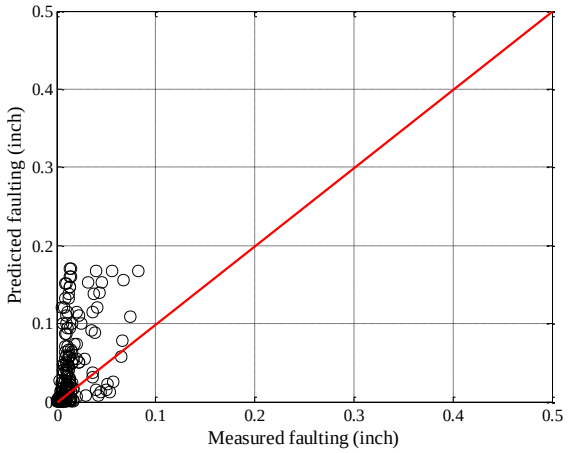

Figure B-407 Option 2 – Global faulting model

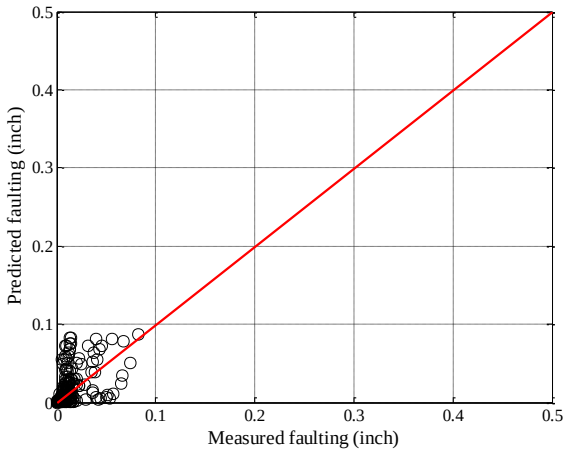

Figure B-408 Option 2 – C1 = 0.4

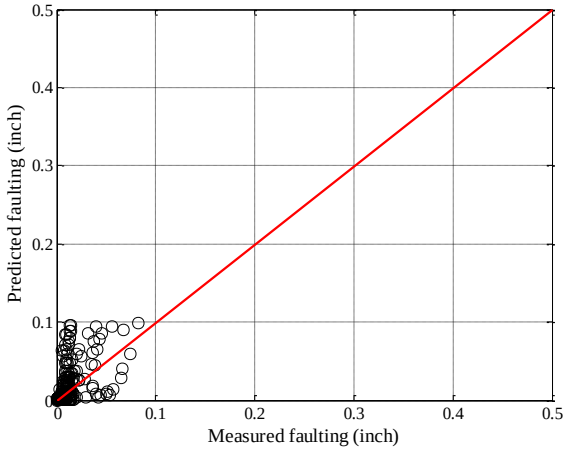

Figure B-409 Option 2 – C1 = 0.5

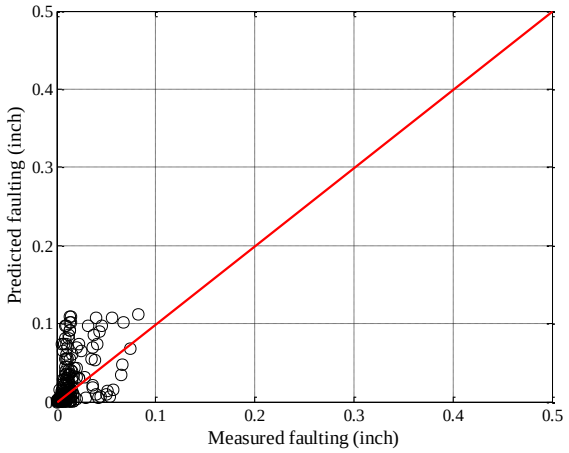

Figure B-410 Option 2 – C1 = 0.6

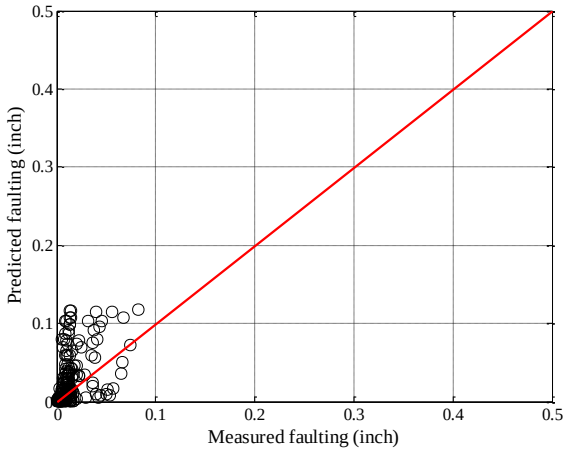

Figure B-411 Option 2 – C1 = 0.65

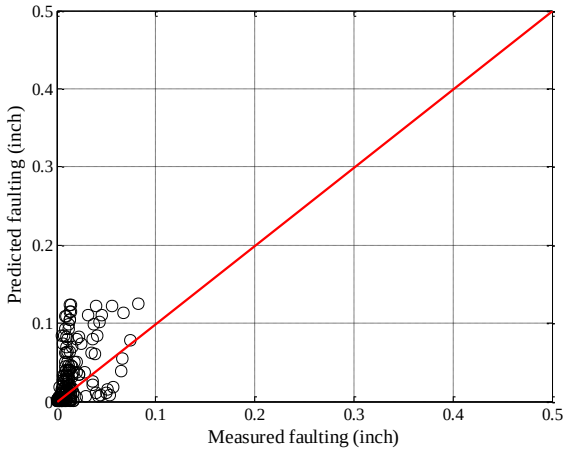

Figure B-412 Option 2 – C1 = 0.7

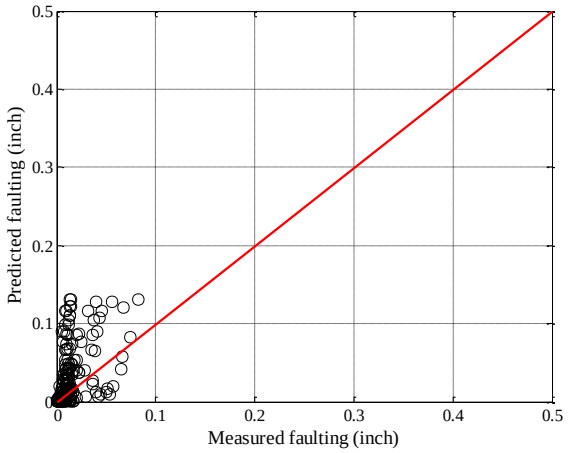

Figure B-413 Option 2 – C1 = 0.75

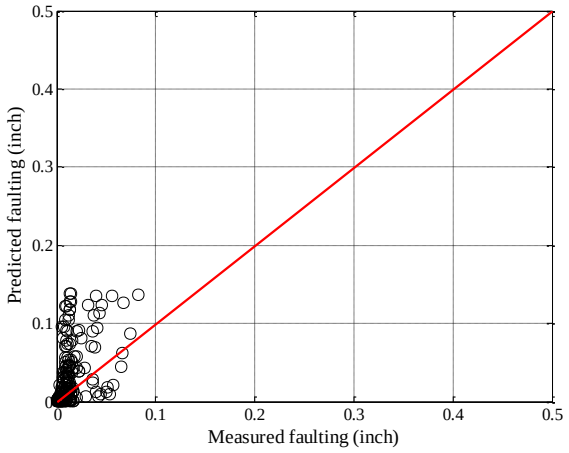

Figure B-414 Option 2 – C1 = 0.8

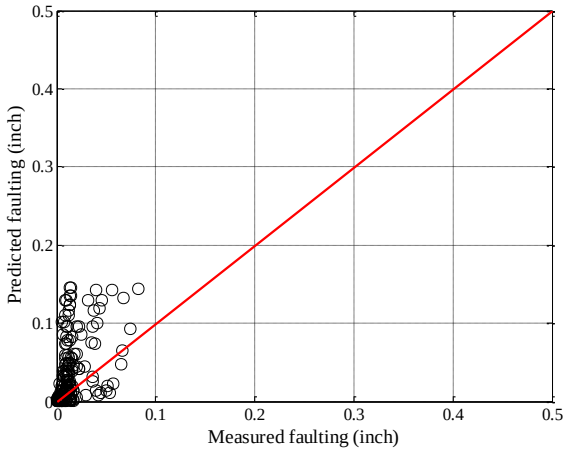

Figure B-415 Option 2 – C1 = 0.85

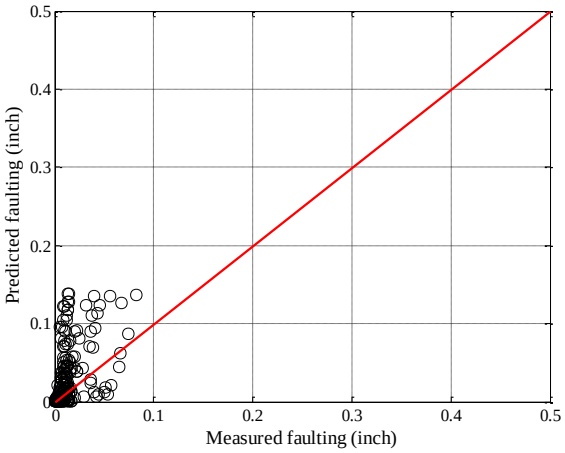

Figure B-416 Option 2 – C1 = 0.9

Reliability

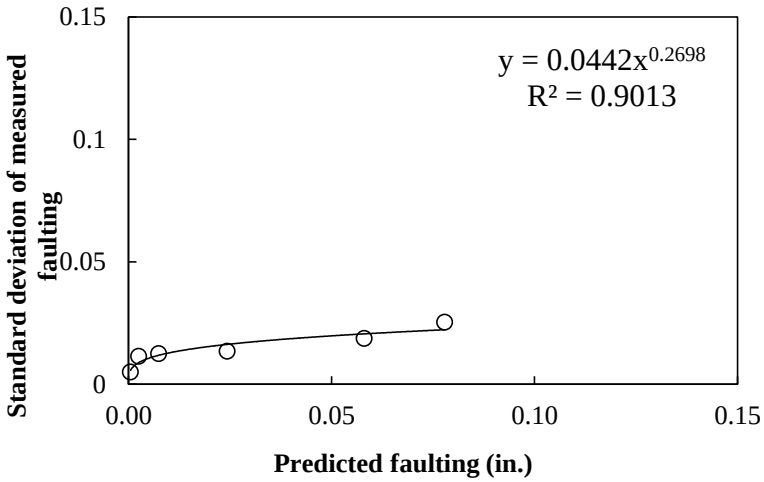

Figure B-417 Option 2 faulting model reliability equation

B.2.2.3 Option 3

Table B-183 Option 3 faulting model local calibration results

Parameter	SEE	Bias
Global model	0.049	0.023
C1 = 0.4	0.022	0.002
C1 = 0.5	0.025	0.005
C1 = 0.6	0.029	0.008
C1 = 0.65	0.031	0.010
C1 = 0.7	0.033	0.012
C1 = 0.75	0.035	0.014
C1 = 0.8	0.038	0.015
C1 = 0.85	0.040	0.017
C1 = 0.9	0.038	0.015

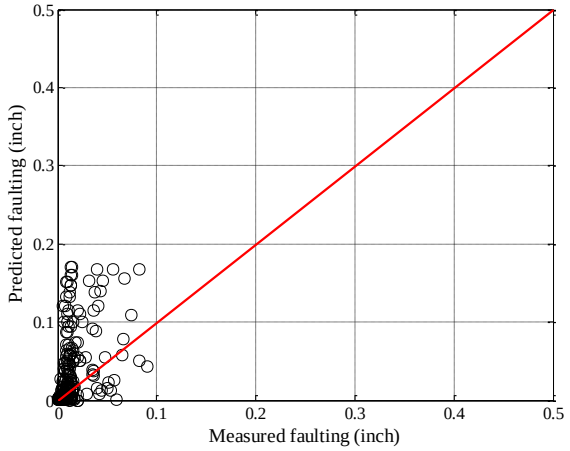

Figure B-418 Option 3 - Global faulting model

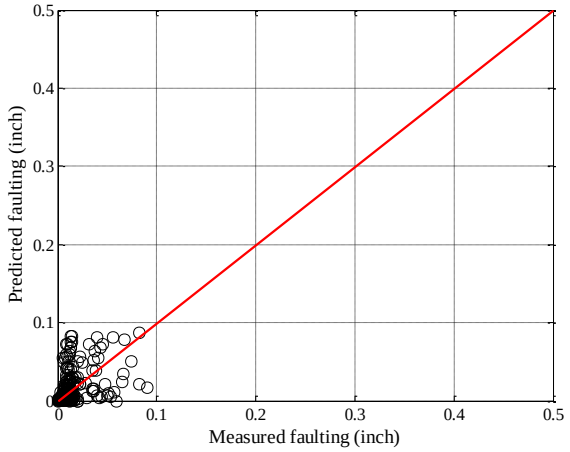

Figure B-419 Option 3 - C1 = 0.4

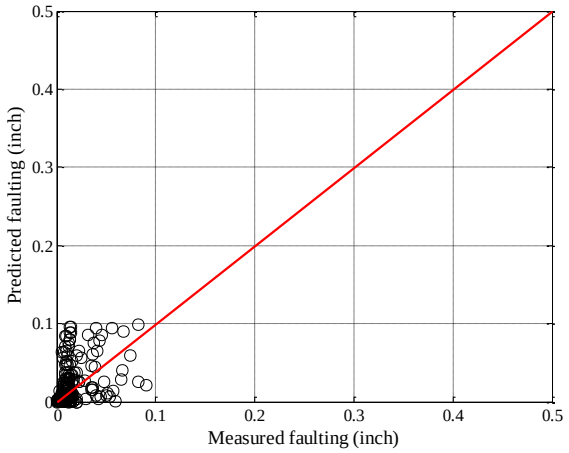

Figure B-420 Option 3 - C1 = 0.5

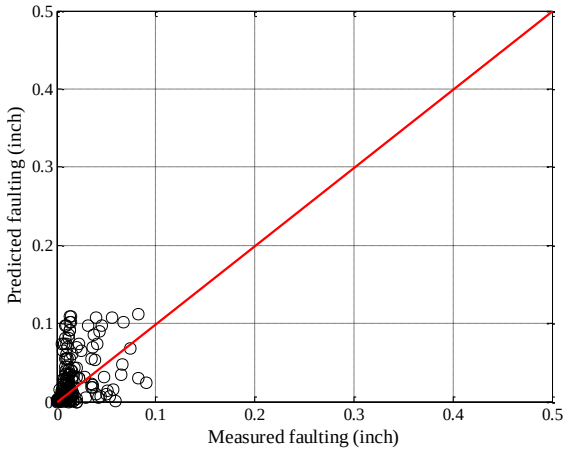

Figure B-421 Option 3 - C1 = 0.6

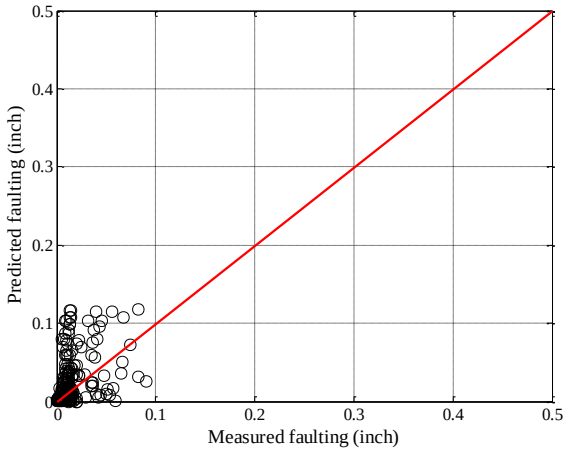

Figure B-422 Option 3 - C1 = 0.65

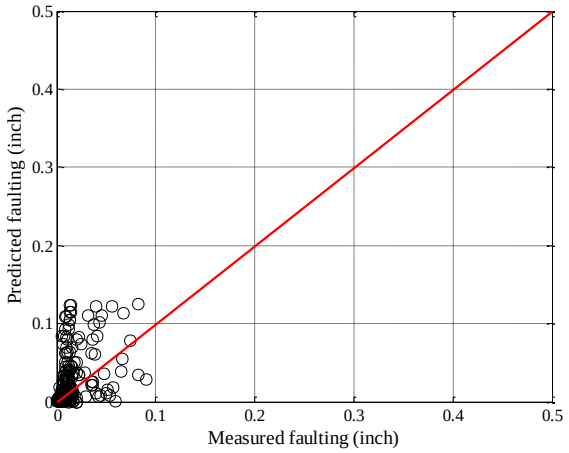

Figure B-423 Option 3 - C1 = 0.7

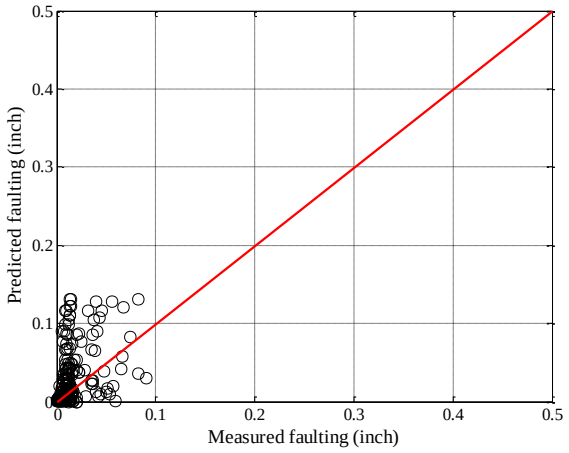

Figure B-424 Option 3 - C1 = 0.75

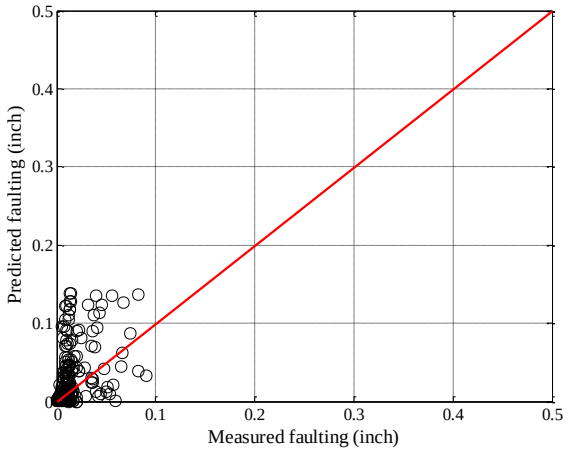

Figure B-425 Option 3 - C1 = 0.8

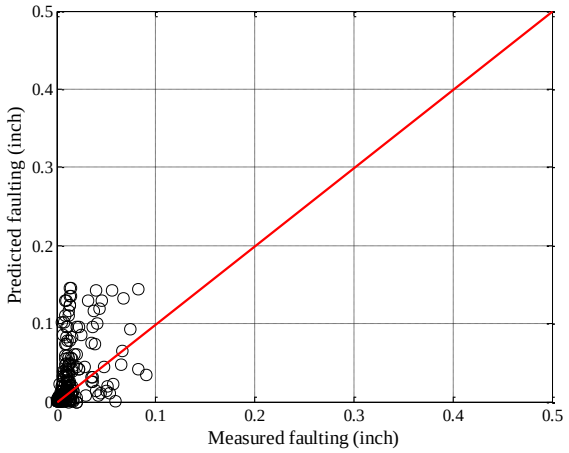

Figure B-426 Option 3 - C1 = 0.85

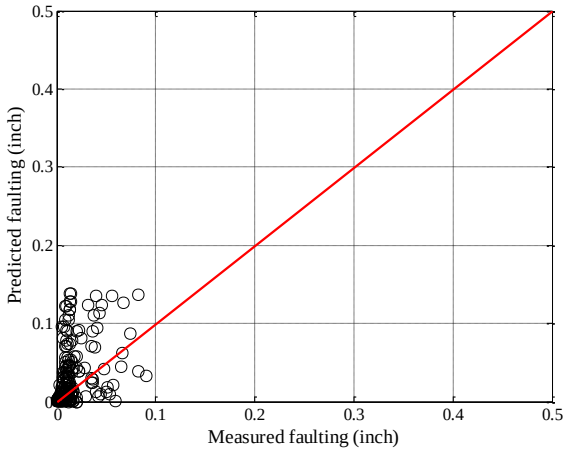

Figure B-427 Option 3 - C1 = 0.9

Reliability

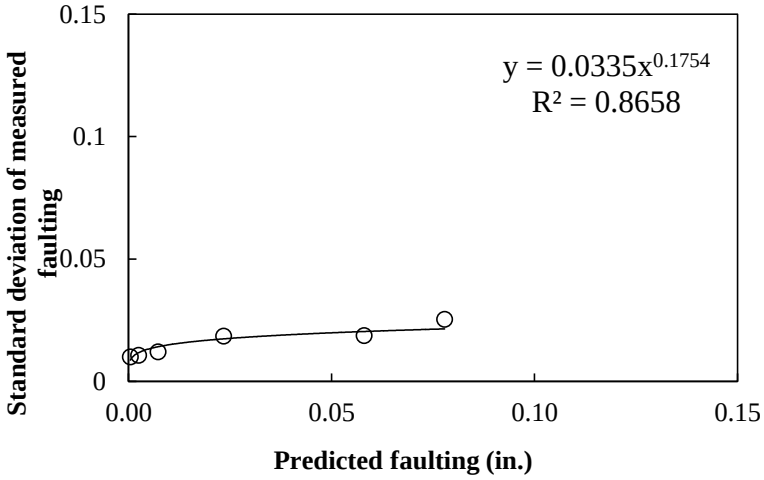

Figure B-428 Option 3 faulting model reliability equation

B.2.2.4 Option 4

Table B-184 Option 4 faulting model local calibration results

Parameter	SEE	Bias
Global model	0.005	-0.002
C1 = 0.4	0.005	-0.003
C1 = 0.5	0.005	-0.002
C1 = 0.6	0.005	-0.002
C1 = 0.65	0.005	-0.002
C1 = 0.7	0.005	-0.002
C1 = 0.75	0.005	-0.002
C1 = 0.8	0.004	-0.002
C1 = 0.85	0.004	-0.001
C1 = 0.9	0.004	-0.002

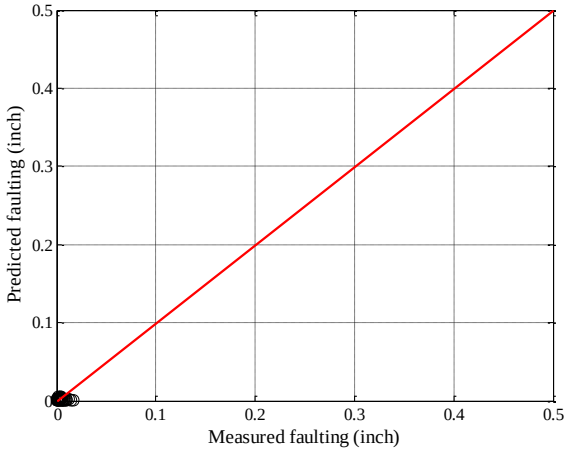

Figure B-429 Option 4 - Global faulting model

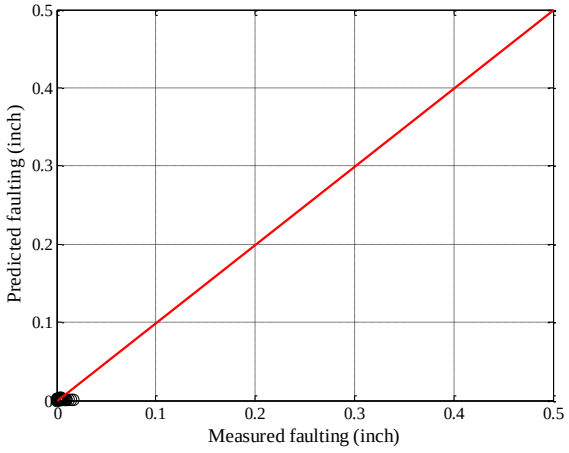

Figure B-430 Option 4 - C1 = 0.4

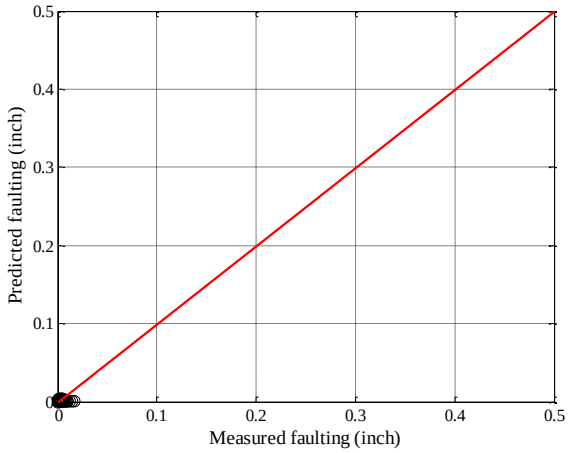

Figure B-431 Option 4 - C1 = 0.5

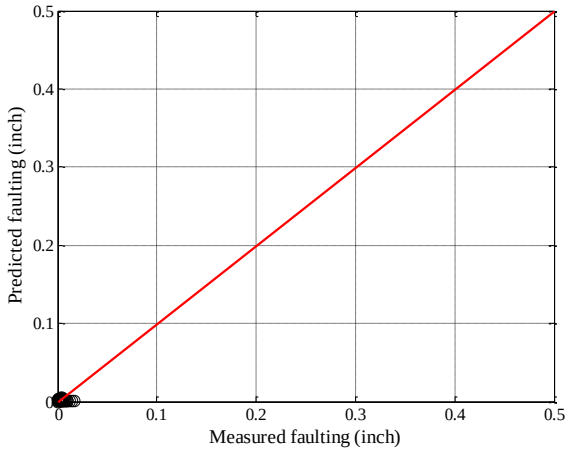

Figure B-432 Option 4 - C1 = 0.6

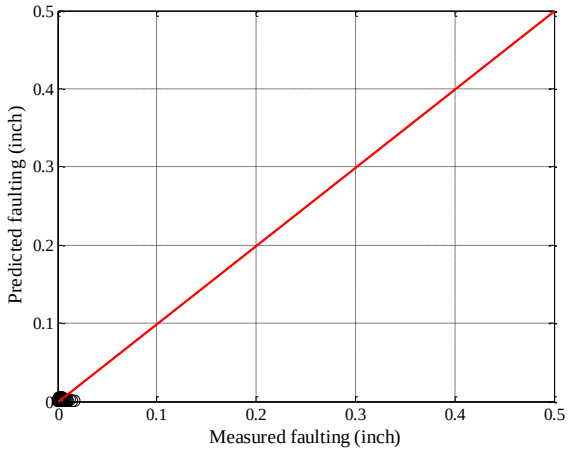

Figure B-433 Option 4 - C1 = 0.65

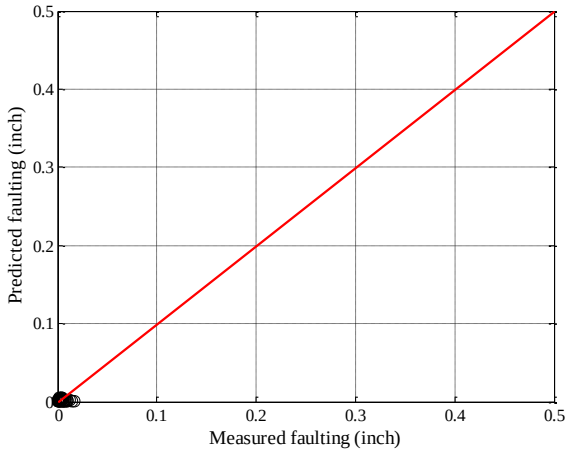

Figure B-434 Option 4 - C1 = 0.7

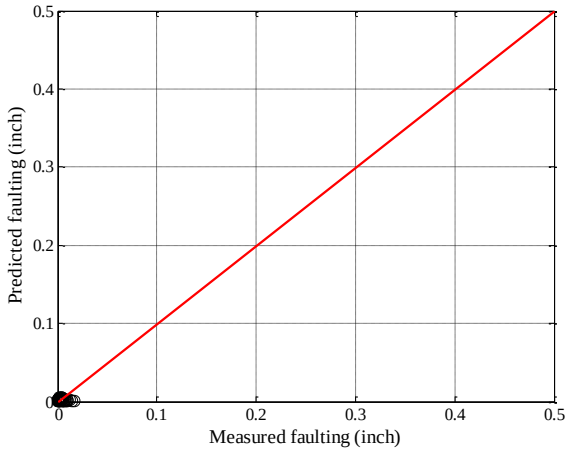

Figure B-435 Option 4 - C1 = 0.75

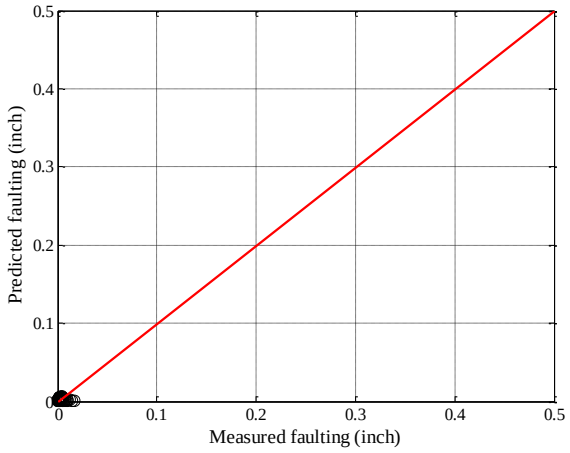

Figure B-436 Option 4 - C1 = 0.8

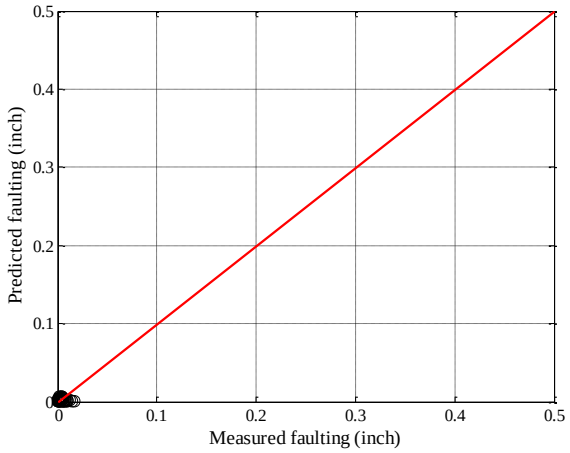

Figure B-437 Option 4 - C1 = 0.85

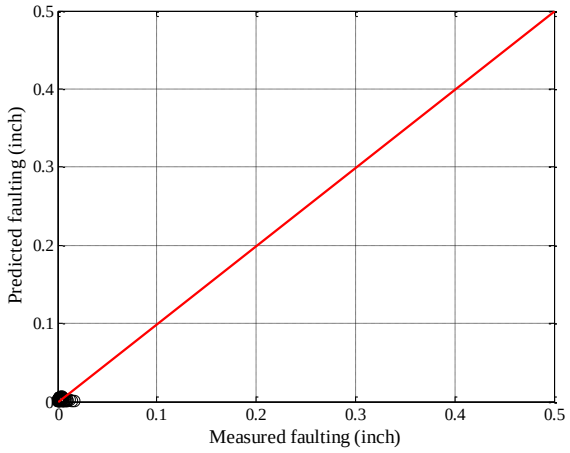

Figure B-438 Option 4 - C1 = 0.9

Reliability

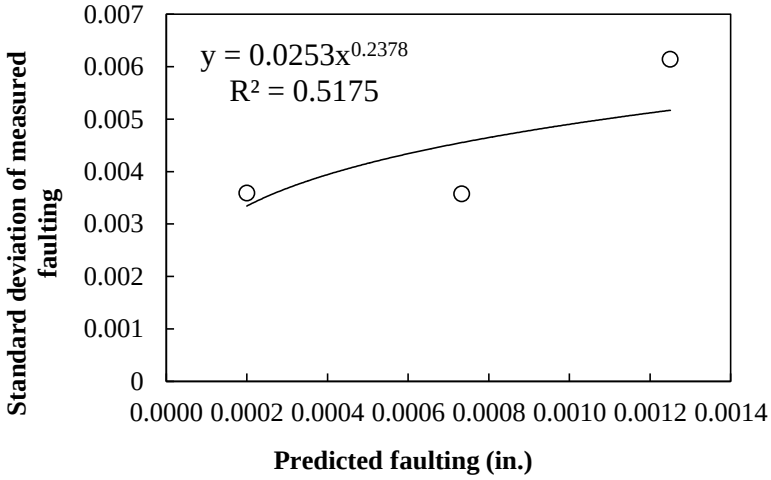

Figure B-439 Option 4 faulting model reliability equation

B.2.3 Pavement Roughness (IRI)

B.2.3.1 Option 1

No sampling

Table B-185 Option 1 IRI local calibration results – no sampling

Parameter	Global	Local
SEE	17.314	15.564
Bias	-11.398	4.215
R^2	0.640	0.538
t-test pvalue	0.000	0.004
Intercept = 0	0.000	0.000
Slope = 1	0.000	0.000
C1	0.820	0.586
C2	0.442	11.833
C3	1.493	1.493
C4	25.240	25.240

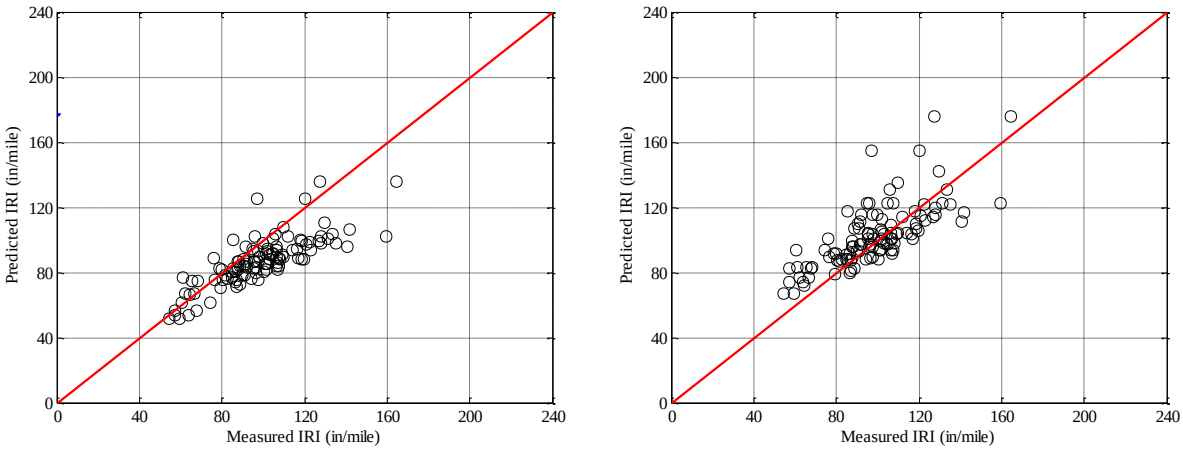

(a) Global model (b) Local model

Figure B-440 Option 1 IRI local calibration measured versus predicted – no sampling

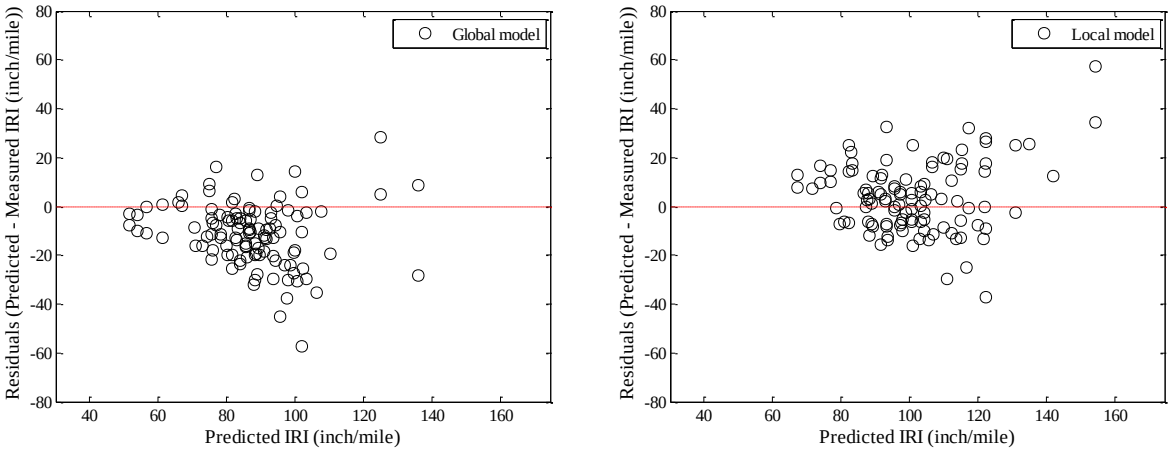

(a) Global model (b) Local model

Figure B-441 Option 1 IRI local calibration residual plots – no sampling

Reliability

The IRI reliability is internally estimated by the software, and uses an initial IRI standard deviation of 5.4 inch/mile.

Split sampling

Table B-186 Option 1 IRI local calibration results – split sampling

Parameter	Global model	Local model	Validation
SEE	16.263	14.999	16.341
Bias	-10.020	3.070	3.401
R^2	0.614	0.497	0.543
t-test pvalue	0.000	0.080	0.186
Intercept = 0	0.000	0.000	0.000
Slope = 1	0.000	0.000	0.000
C1	0.820	0.342	0.342
C2	0.442	12.599	12.599
C3	1.493	1.493	1.493
C4	25.240	25.240	25.240

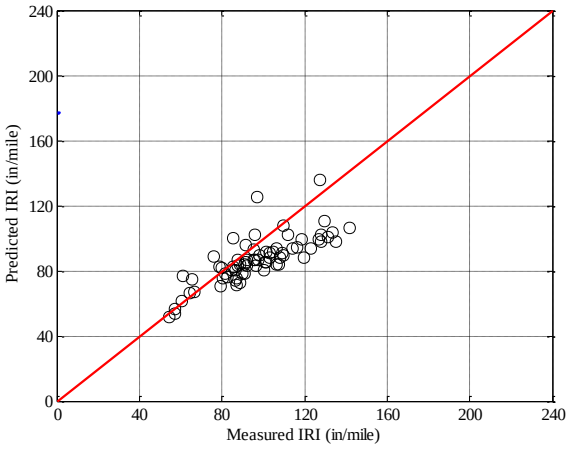

(a) Global model

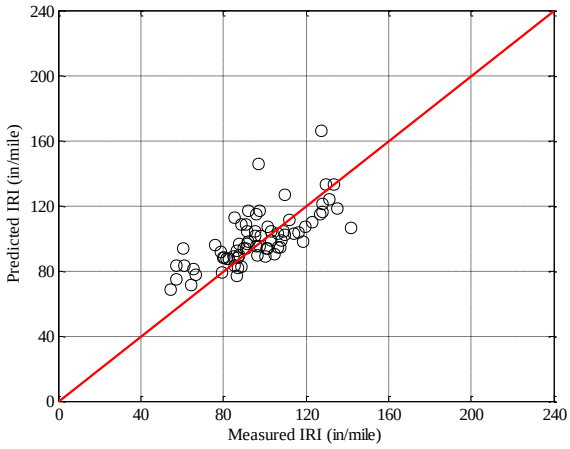

(b) Local model

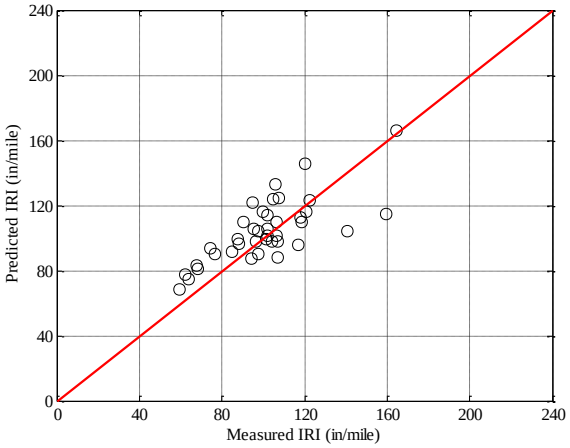

(c) Local model validation

Figure B-442 Option 1 IRI local calibration measured versus predicted – split sampling

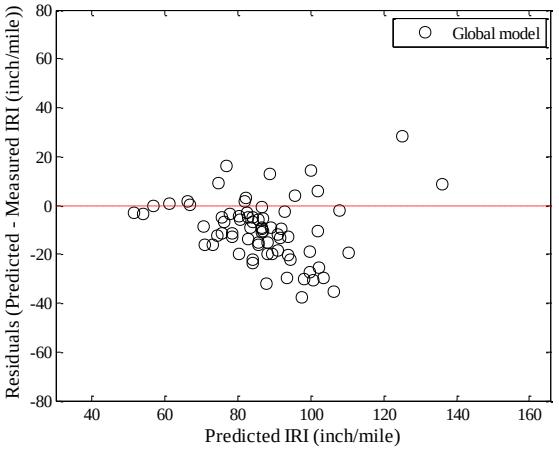

(a) Global model

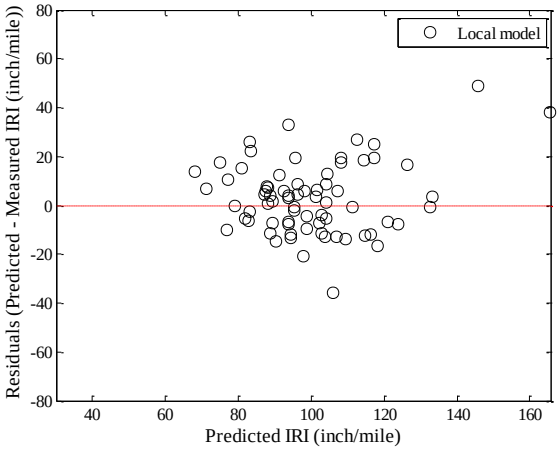

(b) Local model

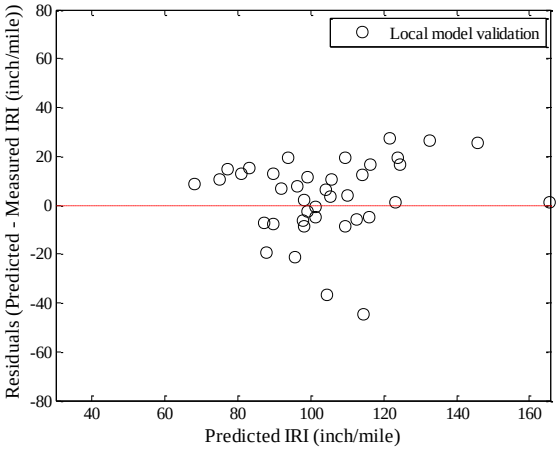

(c) Local model validation

Figure B-443 Option 1 IRI local calibration residual plots – split sampling

Reliability

The IRI reliability is internally estimated by the software, and uses an initial IRI standard deviation of 5.4 inch/mile.

Repeated split sampling

Table B-187 Option 1 IRI local calibration results – repeated split sampling

Global Model				
Parameter	Global Model Mean	Global Model Median	Global model lower CI	Global model upper CI
SEE	17.330	17.658	14.491	19.182
Bias	-11.410	-11.393	-14.018	-9.028
C1	0.820	0.820	-	-
C2	0.442	0.442	-	-
C3	1.492	1.492	-	-
C4	25.240	25.240	-	-
Local Model				
Parameter	Local Model Mean	Local Model Median	Local model lower CI	Local model upper CI
SEE	15.263	15.406	12.163	17.195
Bias	4.314	4.341	2.710	5.766
C1	0.603	0.604	0.161	1.051
C2	11.840	11.721	9.757	14.422
C3	1.493	1.493	1.493	1.493
C4	25.240	25.240	25.240	25.240
Local Model validation				
Parameter	Local Model Mean	Local Model Median	Local model lower CI	Local model upper CI
SEE	17.109	16.515	10.052	29.205
Bias	4.383	4.166	-6.031	17.373
C1	0.603	0.604	0.161	1.051
C2	11.840	11.721	9.757	14.422
C3	1.493	1.493	1.493	1.493
C4	25.240	25.240	25.240	25.240

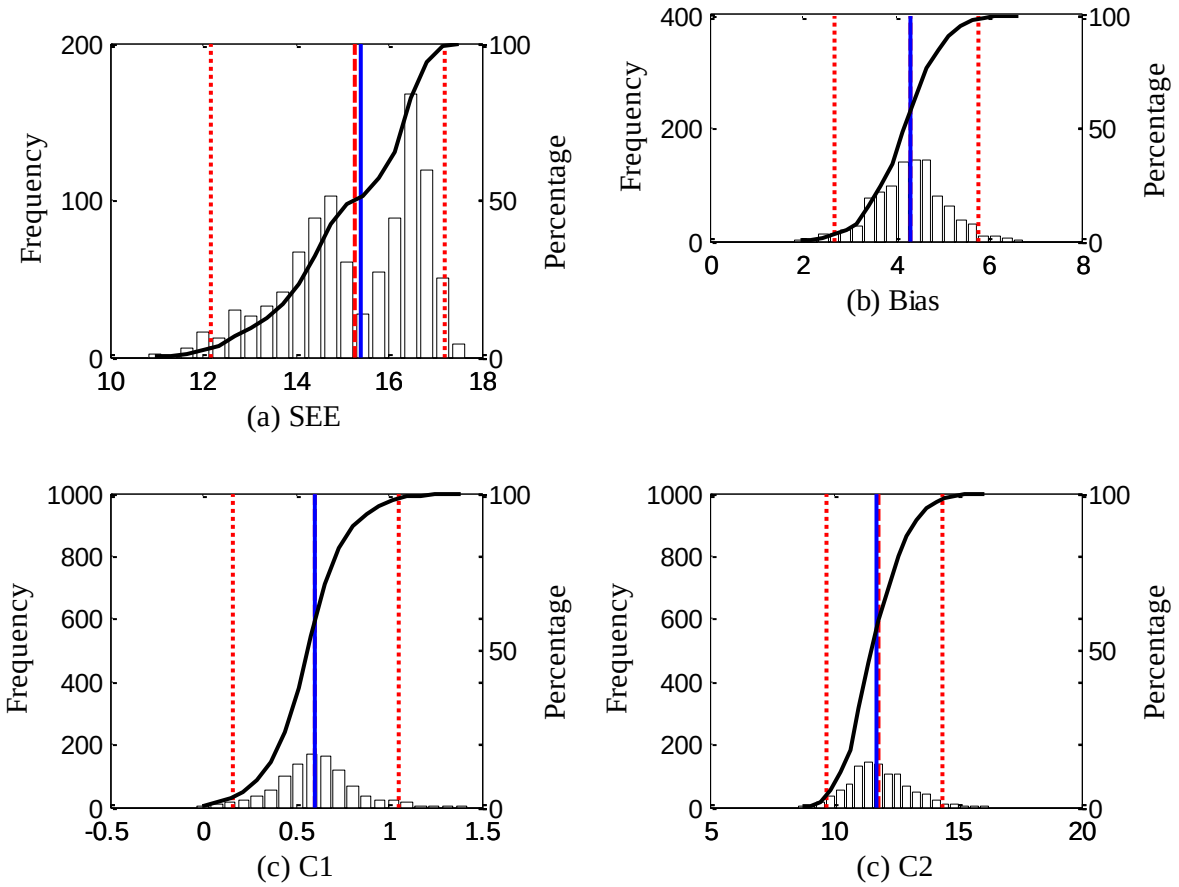

Figure B-444 Option 1 IRI repeated split sampling frequency distributions – calibration

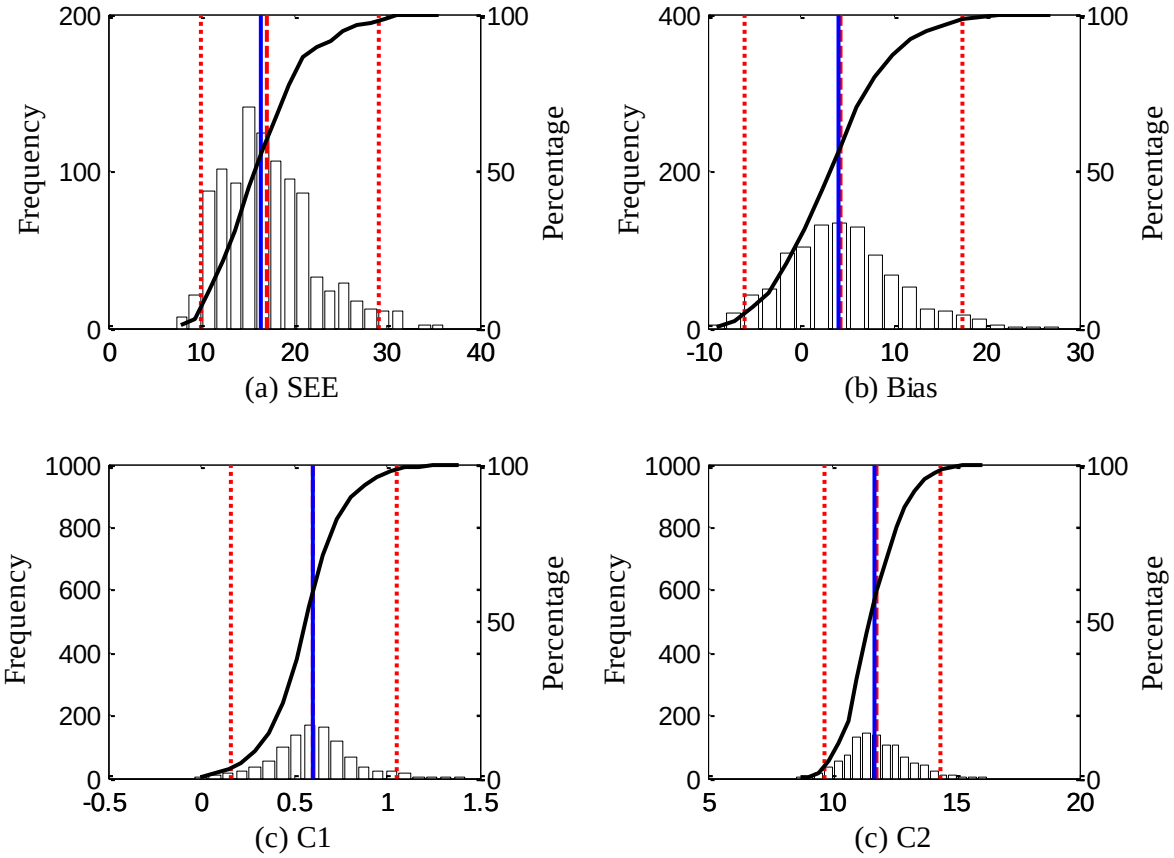

Figure B-445 Option 1 IRI repeated split sampling frequency distributions – validation

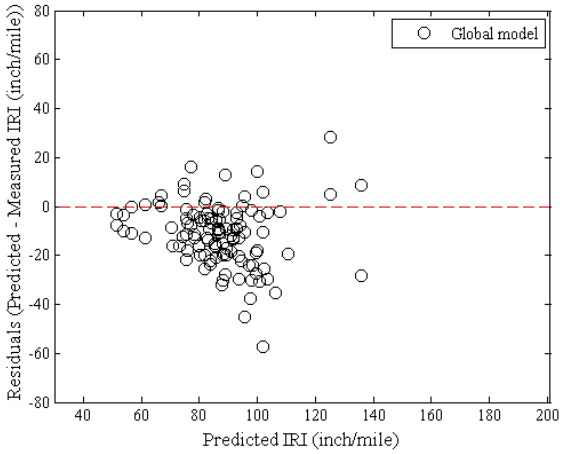

(a) Global model

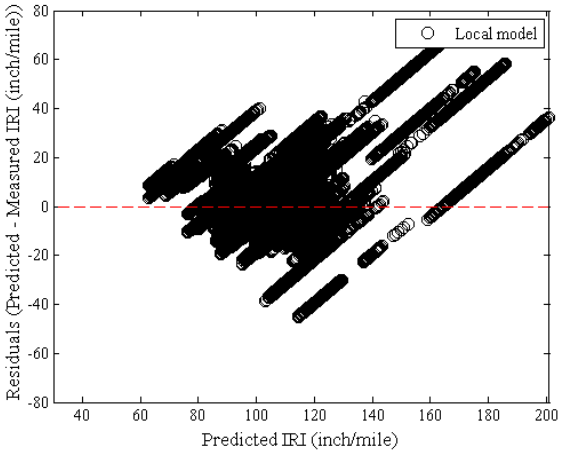

(b) Local model

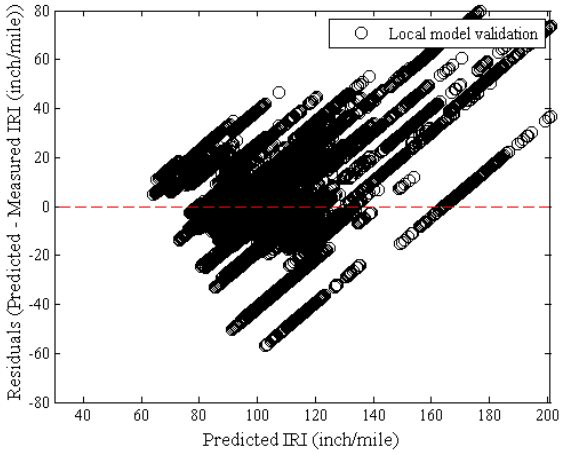

(c) Local model validation

Figure B-446 Option 1 IRI local calibration residual plots – repeated split sampling

Reliability

The IRI reliability is internally estimated by the software, and uses an initial IRI standard deviation of 5.4 inch/mile.

Bootstrapping

Table B-188 Option 1 IRI local calibration results – bootstrapping

Global Model				
Parameter	Global Model Mean	Global Model Median	Global model lower CI	Global model upper CI
SEE	17.239	17.085	13.847	21.179
Bias	-11.466	-11.462	-14.950	-7.870
C1	0.820	0.820	-	-
C2	0.442	0.442	-	-
C3	1.492	1.492	-	-
C4	25.240	25.240	-	-
Local Model				
Parameter	Local Model Mean	Local Model Median	Local model lower CI	Local model upper CI
SEE	14.899	14.833	11.651	18.350
Bias	4.417	4.395	2.673	6.422
C1	0.584	0.590	0.035	1.159
C2	12.068	12.023	8.754	15.396
C3	1.493	1.493	1.493	1.493
C4	25.240	25.240	25.240	25.240

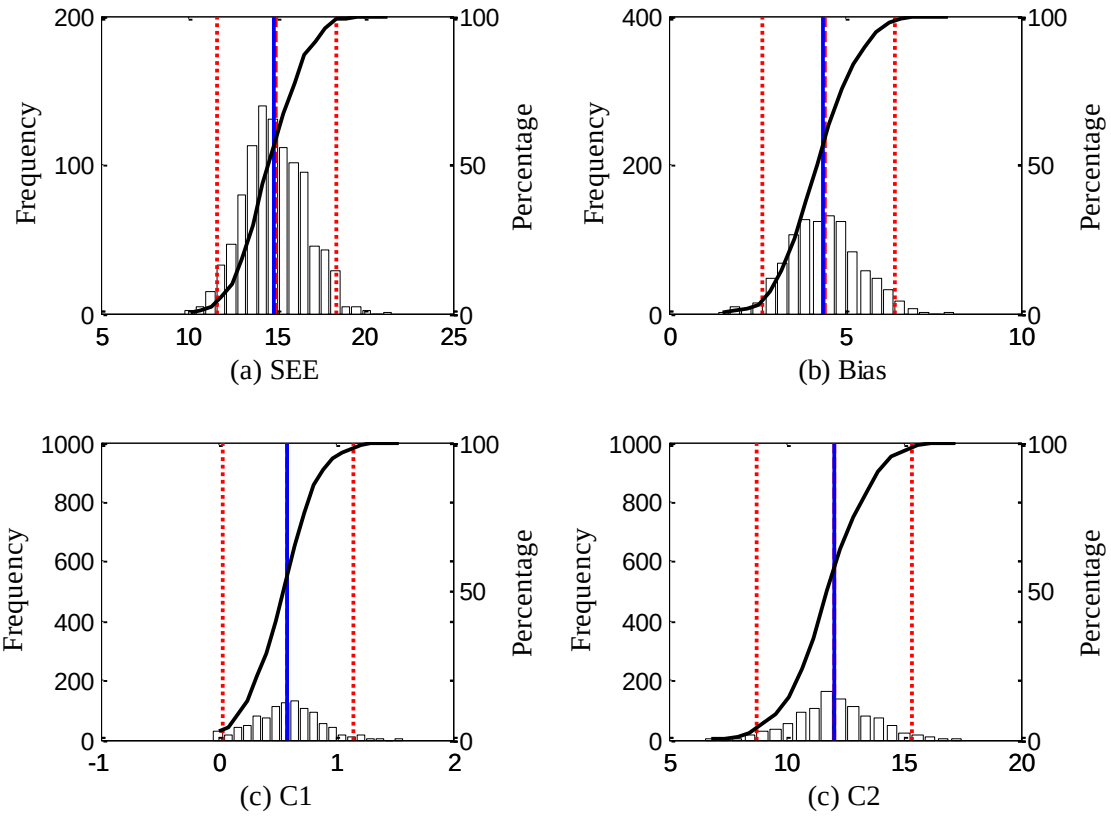

Figure B-447 Option 1 IRI bootstrapping frequency distributions

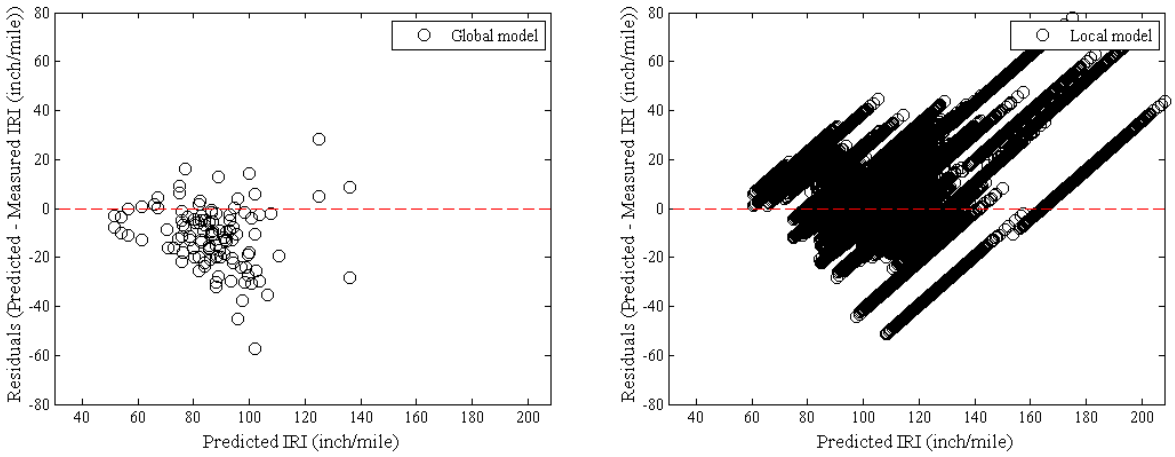

(a) Global model (b) Local model

Figure B-448 Option 1 IRI local calibration residual plots – repeated split sampling

Reliability

The IRI reliability is internally estimated by the software, and uses an initial IRI standard deviation of 5.4 inch/mile.

B.2.3.2 Option 2

No sampling

Table B-189 Option 2 IRI local calibration results – no sampling

Parameter	Global	Local
SEE	15.474	13.792
Bias	-10.026	-0.498
R^2	0.722	0.614
t-test pvalue	0.000	0.638
Intercept = 0	0.000	0.000
Slope = 1	0.000	0.000
C1	0.820	1.182
C2	0.442	3.465
C3	1.493	1.493
C4	25.240	25.240

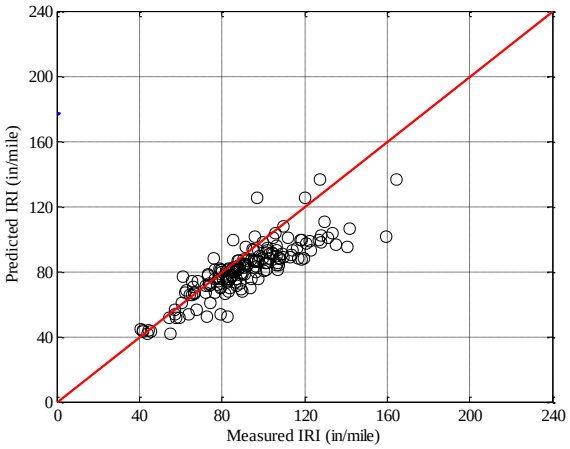

(a) Global model

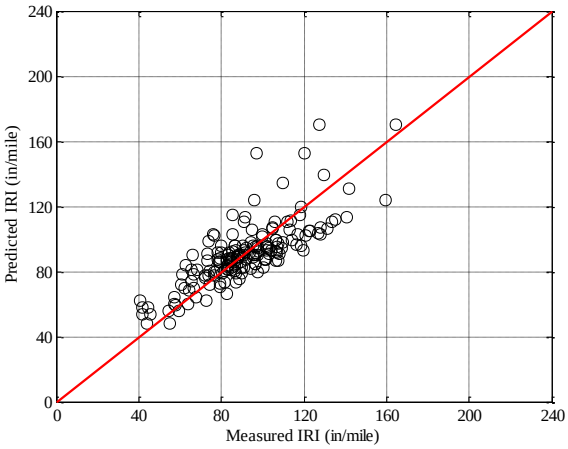

(b) Local model

Figure B-449 Option 2 IRI local calibration measured versus predicted – no sampling

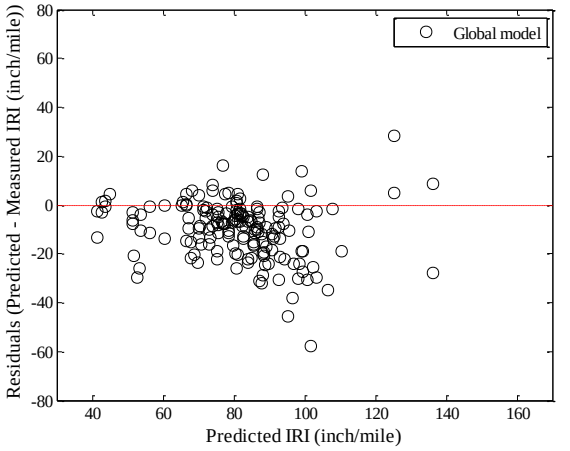

(a) Global model

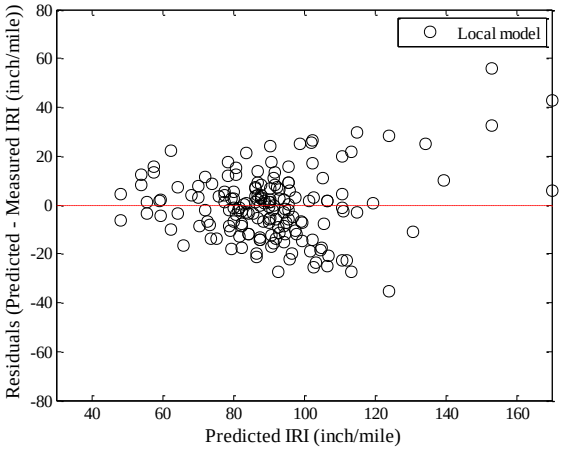

(b) Local model

Figure B-450 Option 2 IRI local calibration residual plots– no sampling

Reliability

The IRI reliability is internally estimated by the software, and uses an initial IRI standard deviation of 5.4 inch/mile.

Split sampling

Table B-190 Option 2 IRI local calibration results – split sampling

Parameter	Global model	Local model	Validation
SEE	16.433	14.847	12.641
Bias	-10.745	-1.109	1.212
R^2	0.716	0.597	0.630
t-test pvalue	0.000	0.418	0.486
Intercept = 0	0.000	0.000	0.015
Slope = 1	0.000	0.000	0.019
C1	0.820	1.301	1.301
C2	0.442	3.202	3.202
C3	1.493	1.493	1.493
C4	25.240	25.240	25.240

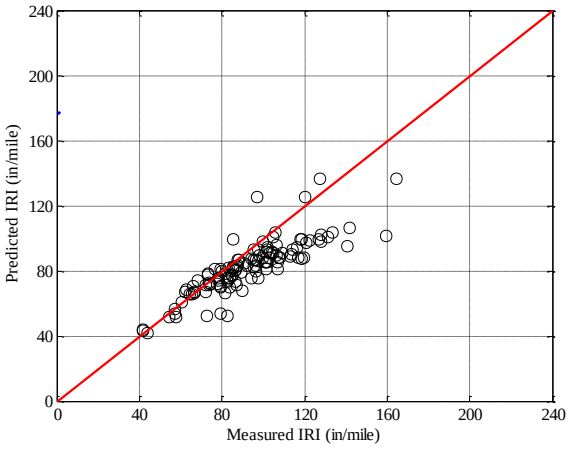

(a) Global model

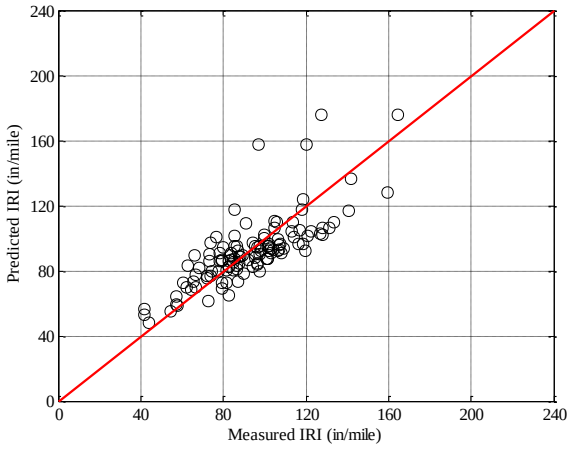

(b) Local model

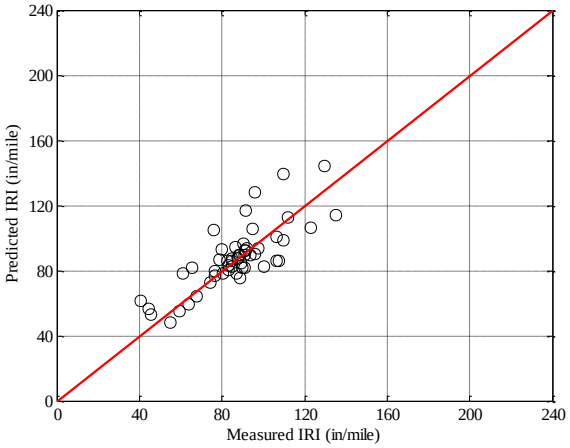

(c) Local model validation

Figure B-451 Option 2 IRI local calibration measured versus predicted – split sampling

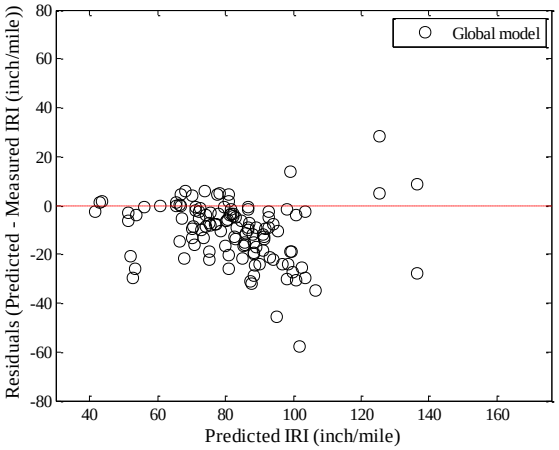

(a) Global model

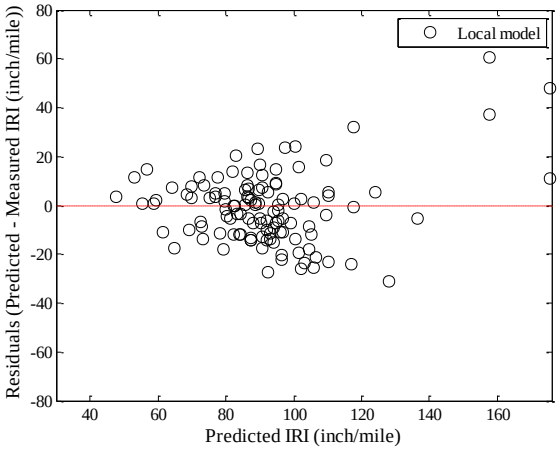

(b) Local model

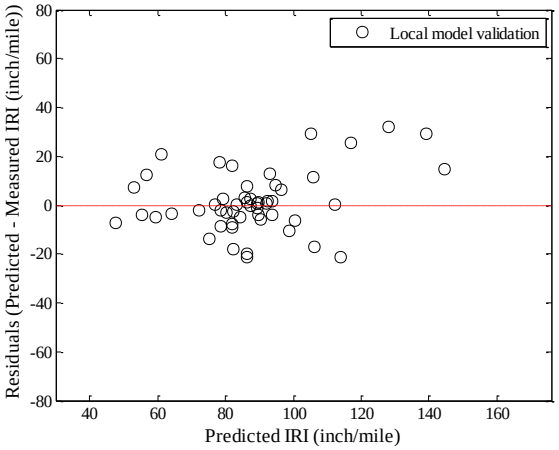

(c) Local model validation

Figure B-452 Option 2 IRI local calibration residual plots – split sampling

Reliability

The IRI reliability is internally estimated by the software, and uses an initial IRI standard deviation of 5.4 inch/mile.

Repeated split sampling

Table B-191 Option 2 IRI local calibration results – repeated split sampling

Global Model				
Parameter	Global Model Mean	Global Model Median	Global model lower CI	Global model upper CI
SEE	15.508	15.704	13.453	16.981
Bias	-10.038	-10.008	-11.764	-8.197
C1	0.820	0.820	-	-
C2	0.442	0.442	-	-
C3	1.492	1.492	-	-
C4	25.240	25.240	-	-
Local Model				
Parameter	Local Model Mean	Local Model Median	Local model lower CI	Local model upper CI
SEE	13.648	13.714	11.501	15.181
Bias	-0.415	-0.399	-1.543	0.704
C1	1.192	1.175	0.920	1.604
C2	3.512	3.467	2.701	4.610
C3	1.493	1.493	1.493	1.493
C4	25.240	25.240	25.240	25.240
Local Model validation				
Parameter	Local Model Mean	Local Model Median	Local model lower CI	Local model upper CI
SEE	14.954	14.644	9.934	22.917
Bias	-0.189	-0.436	-8.036	8.568
C1	1.192	1.175	0.920	1.604
C2	3.512	3.467	2.701	4.610
C3	1.493	1.493	1.493	1.493
C4	25.240	25.240	25.240	25.240

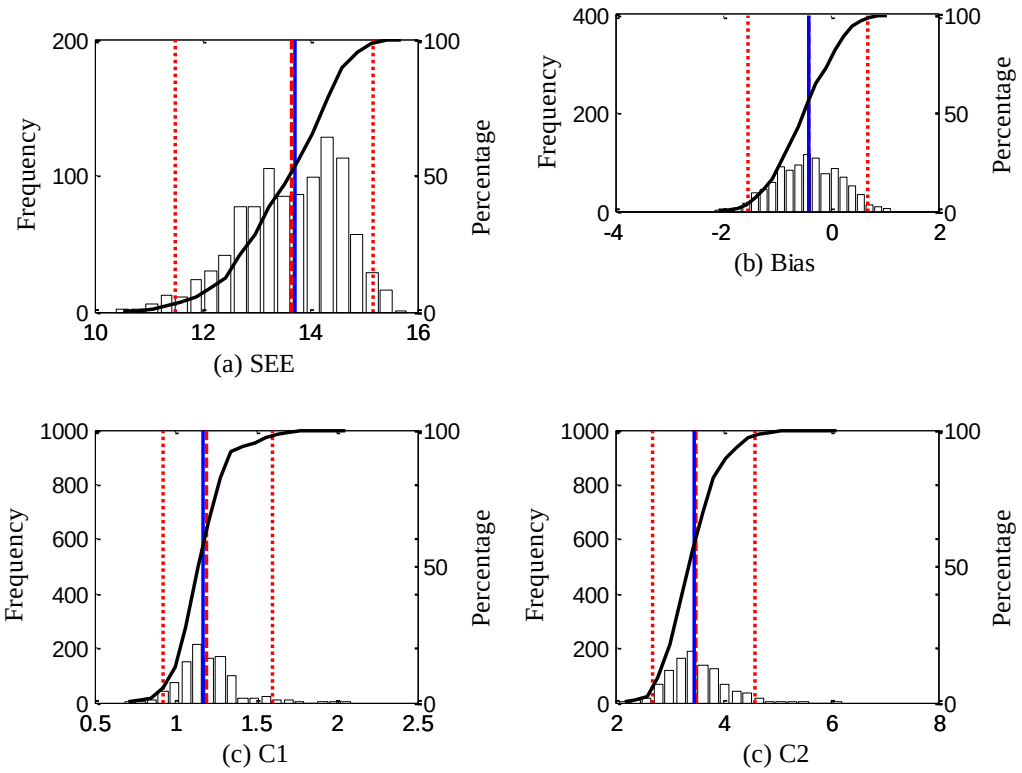

Figure B-453 Option 2 IRI repeated split sampling frequency distributions – calibration

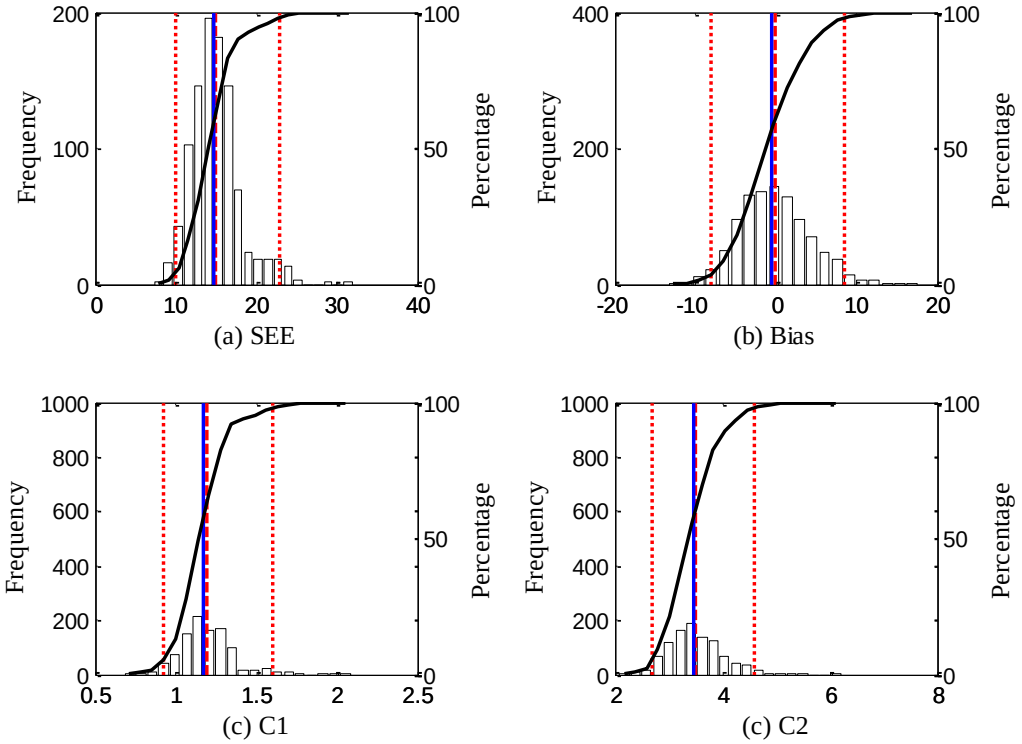

Figure B-454 Option 2 IRI repeated split sampling frequency distributions – validation

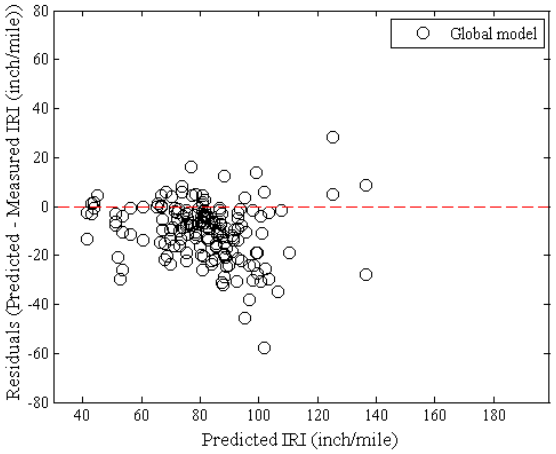

(a) Global model

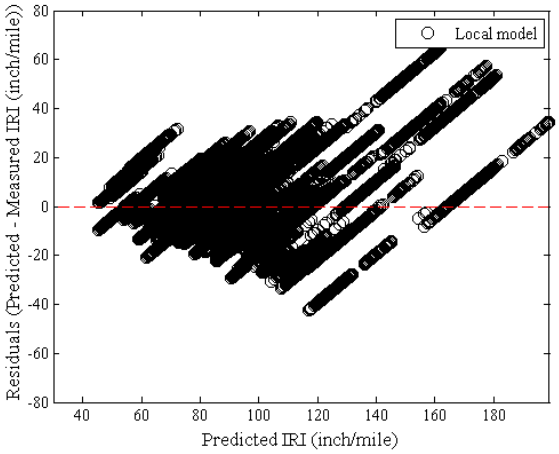

(b) Local model

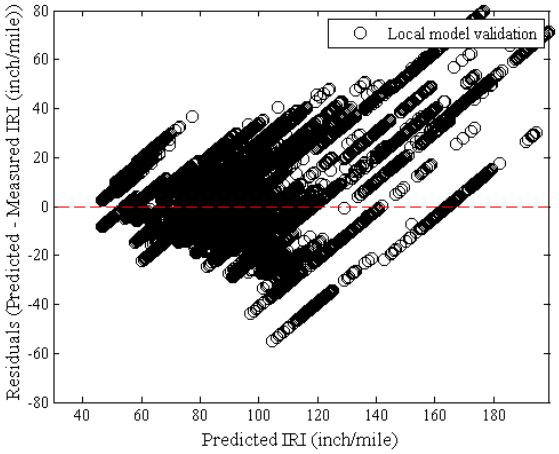

(c) Local model validation

Figure B-455 Option 2 IRI local calibration residual plots – repeated split sampling

Reliability

The IRI reliability is internally estimated by the software, and uses an initial IRI standard deviation of 5.4 inch/mile.

Bootstrapping

Table B-192 Option 2 IRI local calibration results – bootstrapping

Global Model				
Parameter	Global Model Mean	Global Model Median	Global model lower CI	Global model upper CI
SEE	15.390	15.341	12.704	18.146
Bias	-10.024	-10.025	-12.716	-7.403
C1	0.820	0.820	-	-
C2	0.442	0.442	-	-
C3	1.492	1.492	-	-
C4	25.240	25.240	-	-
Local Model				
Parameter	Local Model Mean	Local Model Median	Local model lower CI	Local model upper CI
SEE	13.424	13.451	10.963	15.932
Bias	-0.382	-0.407	-2.056	1.423
C1	1.198	1.171	0.829	1.686
C2	3.570	3.517	2.323	5.234
C3	1.492	1.492	1.492	1.492
C4	25.240	25.240	25.240	25.240

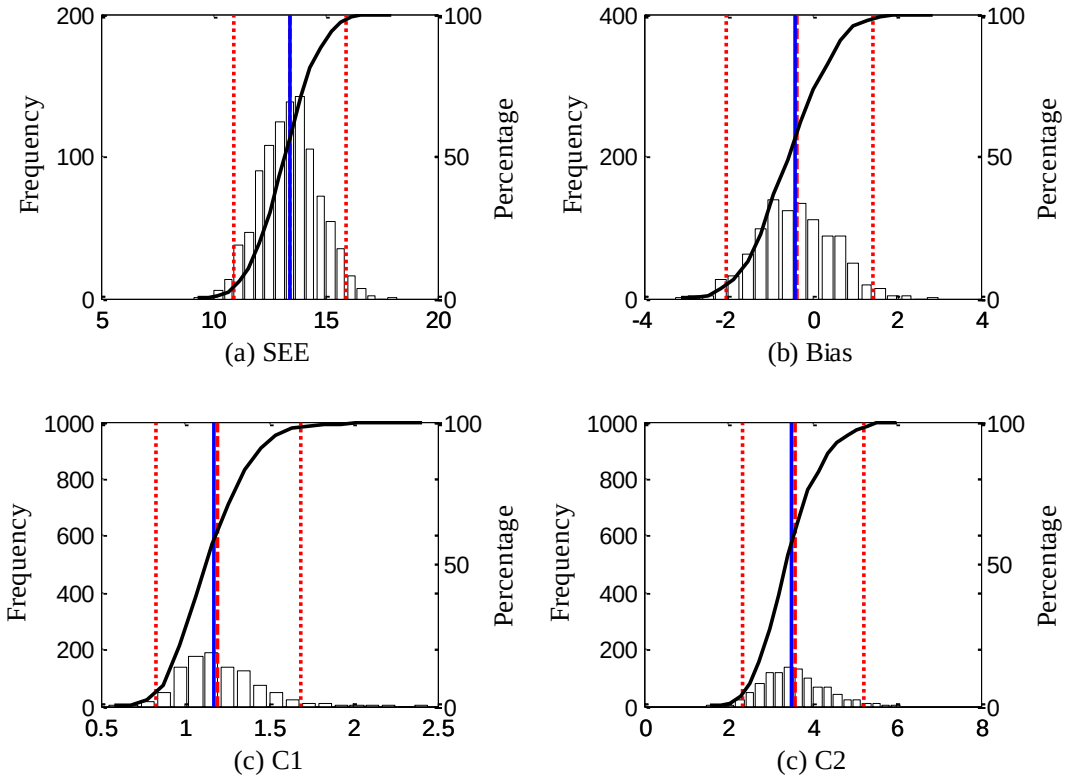

Figure B-456 Option 2 IRI bootstrapping frequency distributions

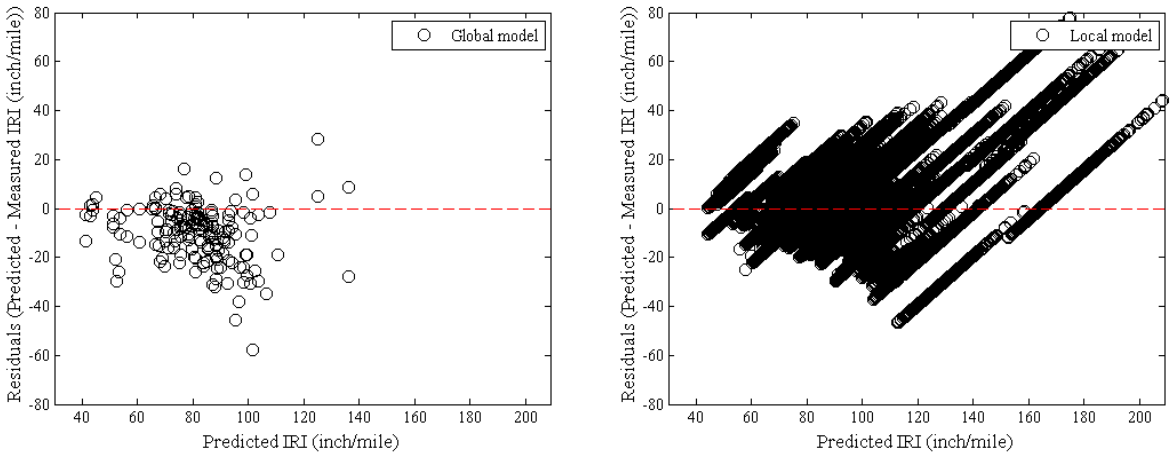

(a) Global model (b) Local model

Figure B-457 Option 2 IRI local calibration residual plots – bootstrapping

Reliability

The IRI reliability is internally estimated by the software, and uses an initial IRI standard deviation of 5.4 inch/mile.

B.2.3.3 Option 3

No sampling

Table B-193 Option 3 IRI local calibration results – no sampling

Parameter	Global	Local
SEE	23.056	21.471
Bias	-9.862	0.770
R^2	0.346	0.313
t-test pvalue	0.000	0.616
Intercept = 0	0.000	0.000
Slope = 1	0.000	0.000
C1	0.820	1.781
C2	0.442	2.028
C3	1.493	1.493
C4	25.240	25.240

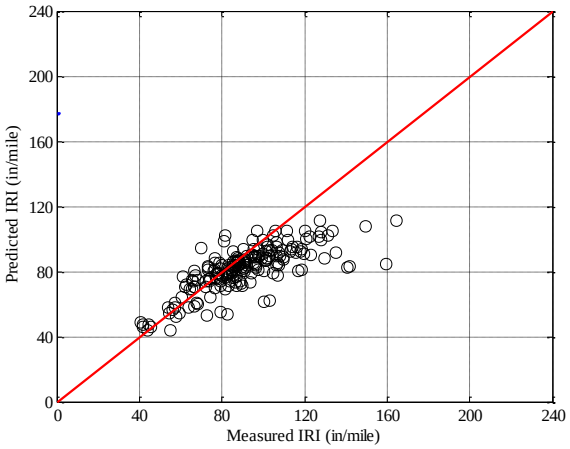

(a) Global model

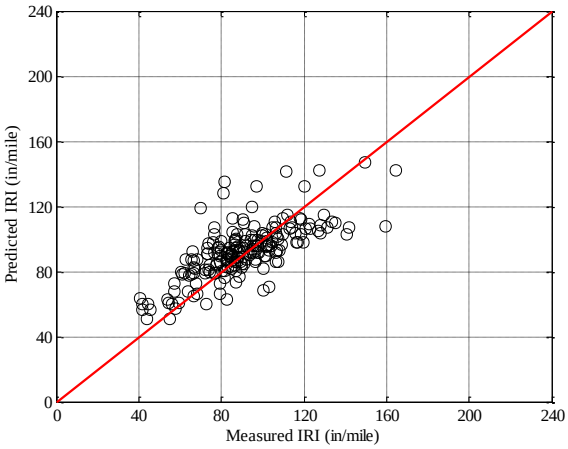

(b) Local model

Figure B-458 Option 3 IRI local calibration measured versus predicted – no sampling

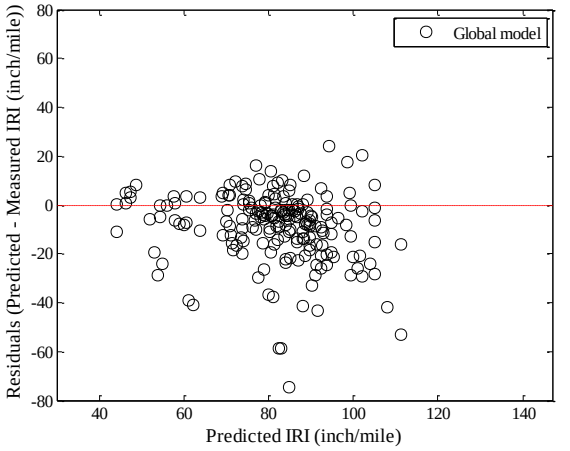

(a) Global model

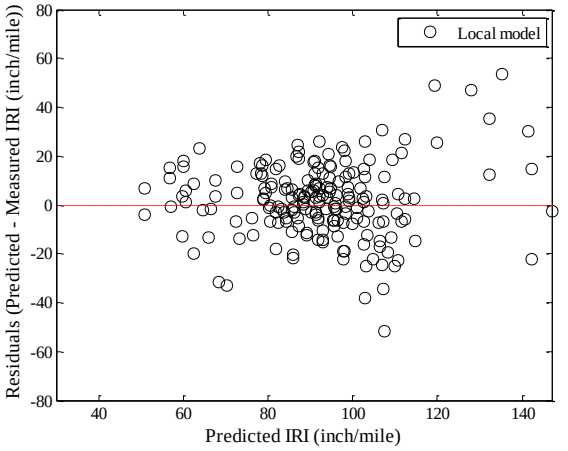

(b) Local model

Figure B-459 Option 3 IRI local calibration residual plots – no sampling

Reliability

The IRI reliability is internally estimated by the software, and uses an initial IRI standard deviation of 5.4 inch/mile.

Split sampling

Table B-194 Option 3 IRI local calibration results – split sampling

Parameter	Global model	Local model	Validation
SEE	24.611	23.889	14.764
Bias	-8.805	0.365	-4.996
R^2	0.274	0.230	0.686
t-test pvalue	0.000	0.862	0.004
Intercept = 0	0.000	0.000	0.000
Slope = 1	0.000	0.000	0.000
C1	0.820	1.562	1.562
C2	0.442	1.760	1.760
C3	1.493	1.493	1.493
C4	25.240	25.240	25.240

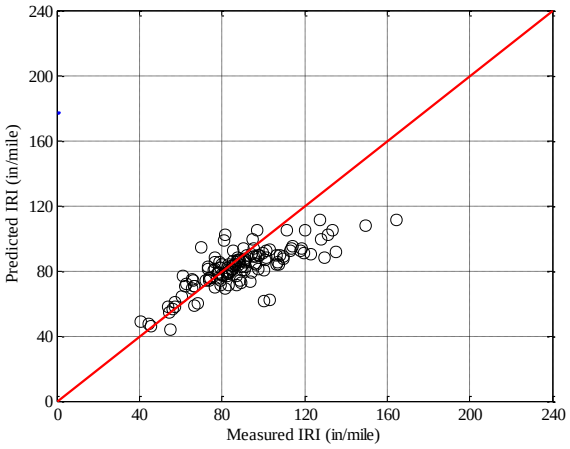

(a) Global model

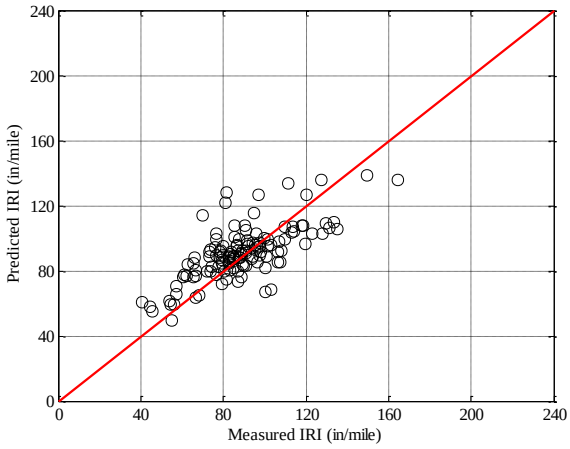

(b) Local model

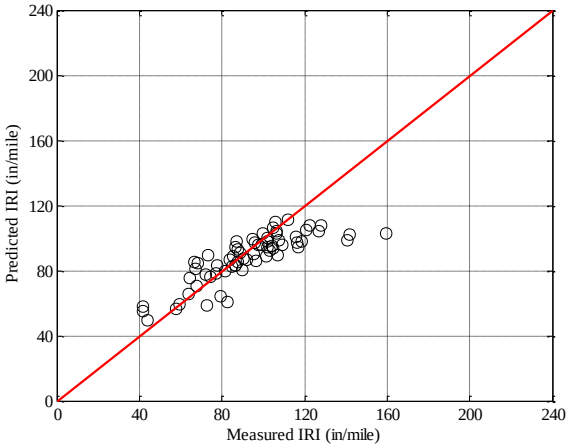

(c) Local model validation

Figure B-460 Option 3 IRI local calibration measured versus predicted – split sampling

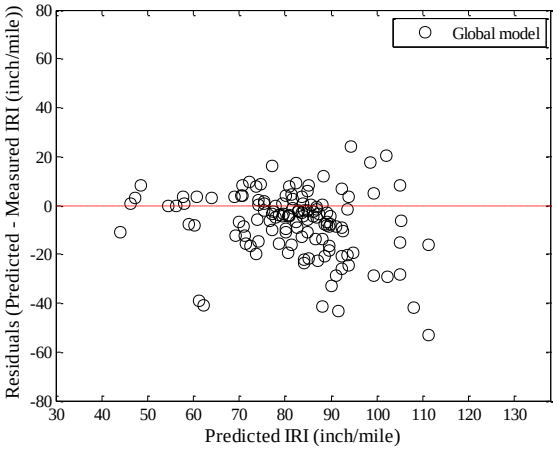

(a) Global model

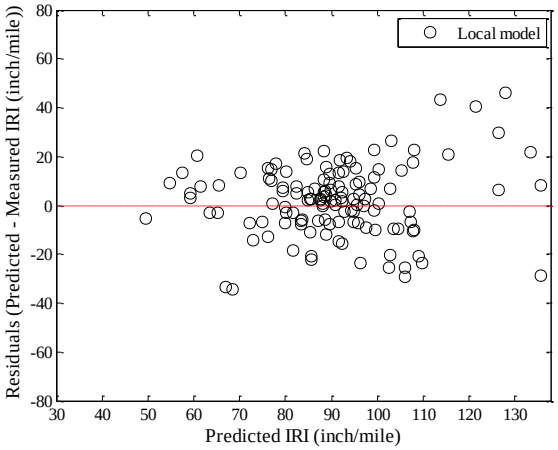

(b) Local model

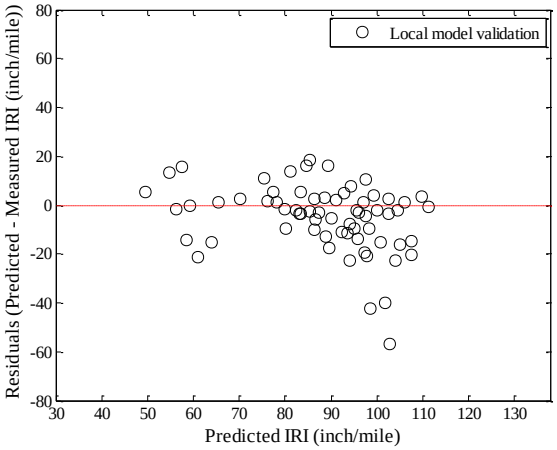

(c) Local model validation

Figure B-461 Option 3 IRI local calibration residual plots – split sampling

Reliability

The IRI reliability is internally estimated by the software, and uses an initial IRI standard deviation of 5.4 inch/mile.

Repeated split sampling

Table B-195 Option 3 IRI local calibration results – repeated split sampling

Global Model				
Parameter	Global Model Mean	Global Model Median	Global model lower CI	Global model upper CI
SEE	22.844	24.913	14.515	26.687
Bias	-9.897	-9.968	-12.087	-7.283
C1	0.820	0.820	-	-
C2	0.442	0.442	-	-
C3	1.492	1.492	-	-
C4	25.240	25.240	-	-
Local Model				
Parameter	Local Model Mean	Local Model Median	Local model lower CI	Local model upper CI
SEE	21.096	23.226	13.031	24.773
Bias	0.863	0.912	-0.883	2.445
C1	1.834	1.709	1.354	2.611
C2	1.993	2.027	0.292	3.670
C3	1.493	1.493	1.493	1.493
C4	25.240	25.240	25.240	25.240
Local Model validation				
Parameter	Local Model Mean	Local Model Median	Local model lower CI	Local model upper CI
SEE	21.177	18.866	11.079	34.851
Bias	1.535	0.722	-8.065	13.248
C1	1.834	1.709	1.354	2.611
C2	1.993	2.027	0.292	3.670
C3	1.493	1.493	1.493	1.493
C4	25.240	25.240	25.240	25.240

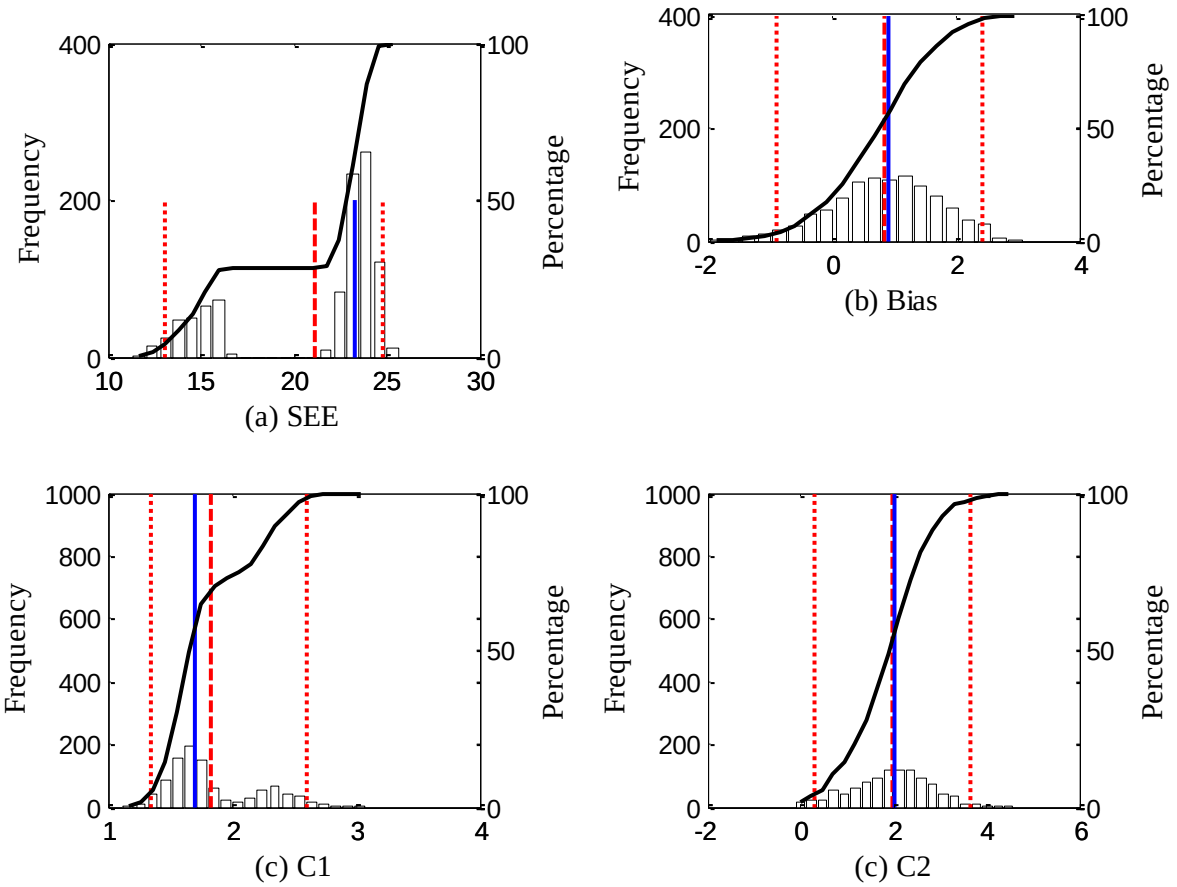

Figure B-462 Option 3 IRI repeated split sampling frequency distributions – calibration

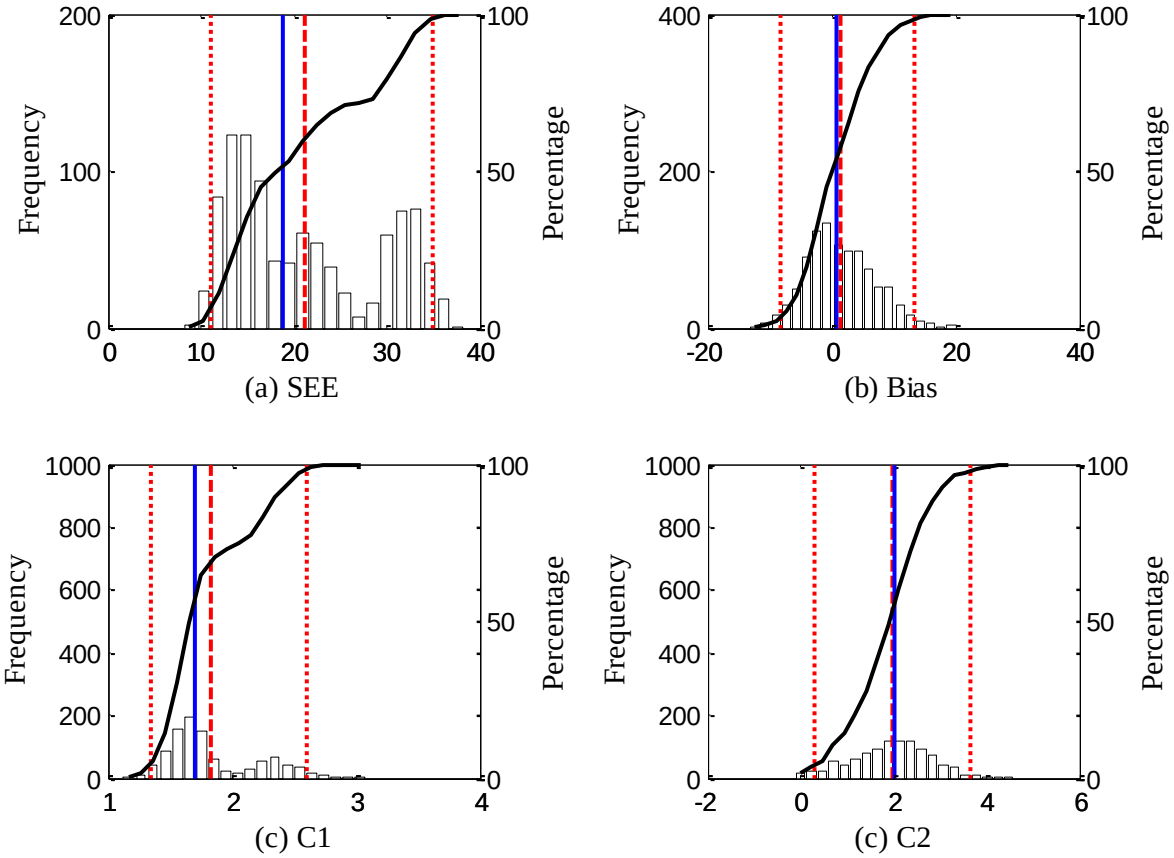

Figure B-463 Option 3 IRI repeated split sampling frequency distributions – validation

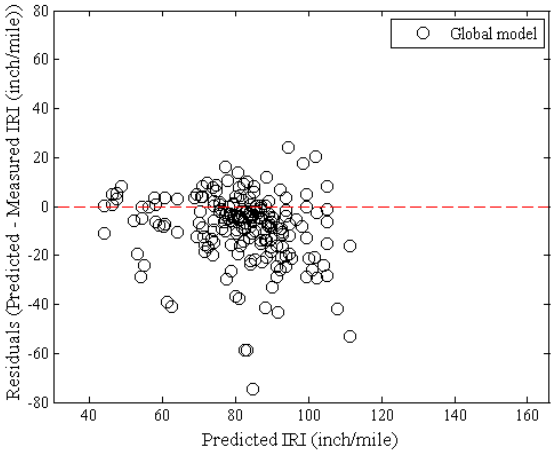

(a) Global model

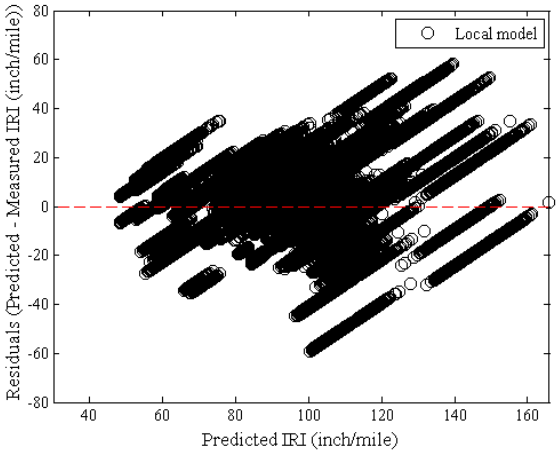

(b) Local model

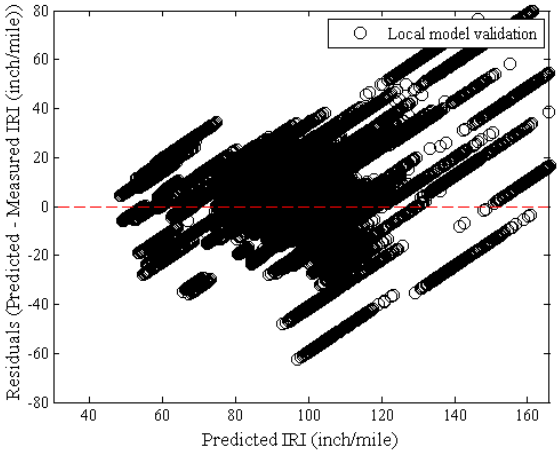

(c) Local model validation

Figure B-464 Option 3 IRI local calibration residual plots – repeated split sampling

Reliability

The IRI reliability is internally estimated by the software, and uses an initial IRI standard deviation of 5.4 inch/mile.

Bootstrapping

Table B-196 Option 1 IRI local calibration results – bootstrapping

Global Model				
Parameter	Global Model Mean	Global Model Median	Global model lower CI	Global model upper CI
SEE	21.999	21.994	13.546	32.976
Bias	-9.799	-9.654	-13.994	-6.247
C1	0.820	0.820	-	-
C2	0.442	0.442	-	-
C3	1.492	1.492	-	-
C4	25.240	25.240	-	-
Local Model				
Parameter	Local Model Mean	Local Model Median	Local model lower CI	Local model upper CI
SEE	20.099	20.566	12.371	31.016
Bias	0.996	0.939	-1.343	3.343
C1	1.855	1.799	1.096	2.785
C2	1.980	1.965	0.000	4.327
C3	1.493	1.493	1.493	1.493
C4	25.240	25.240	25.240	25.240

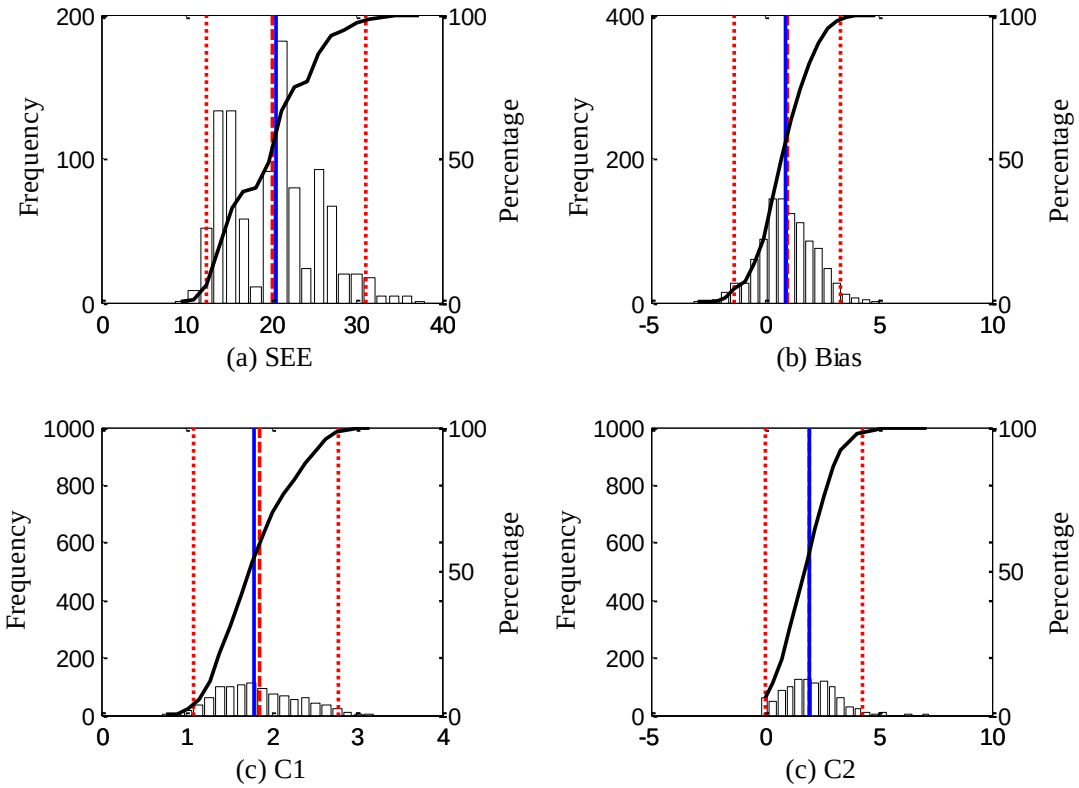

Figure B-465 Option 3 IRI bootstrapping frequency distributions

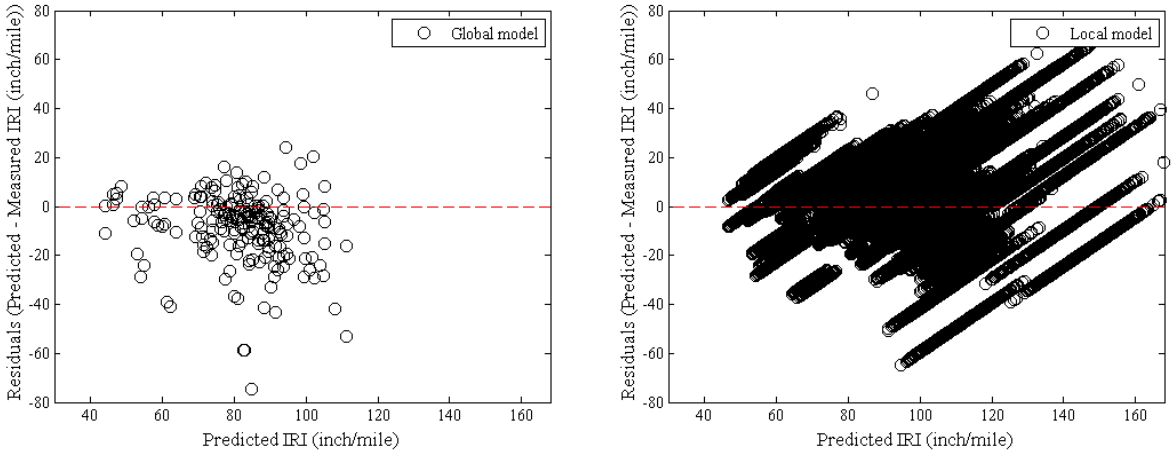

(a) Global model (b) Local model

Figure B-466 Option 3 IRI local calibration residual plots – bootstrapping

Reliability

The IRI reliability is internally estimated by the software, and uses an initial IRI standard deviation of 5.4 inch/mile.

B.2.3.4 Option 4

No sampling

Table B-197 Option 4 IRI local calibration results – no sampling

Parameter	Global	Local
SEE	11.339	7.949
Bias	-7.555	0.268
R^2	0.729	0.754
t-test pvalue	0.000	0.795
Intercept = 0	0.002	0.000
Slope = 1	0.000	0.000
C1	0.820	0.001
C2	0.442	2.541
C3	1.493	1.493
C4	25.240	25.240

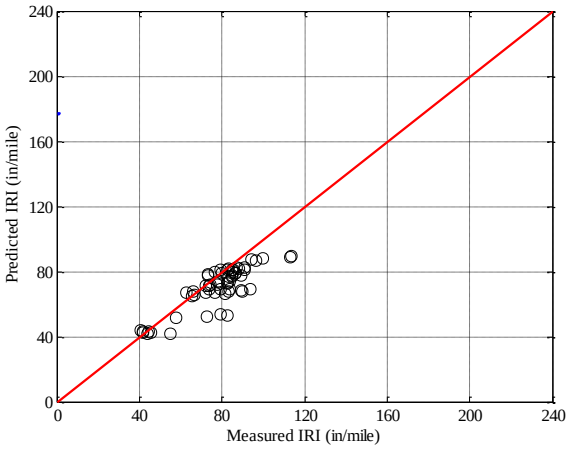

(a) Global model

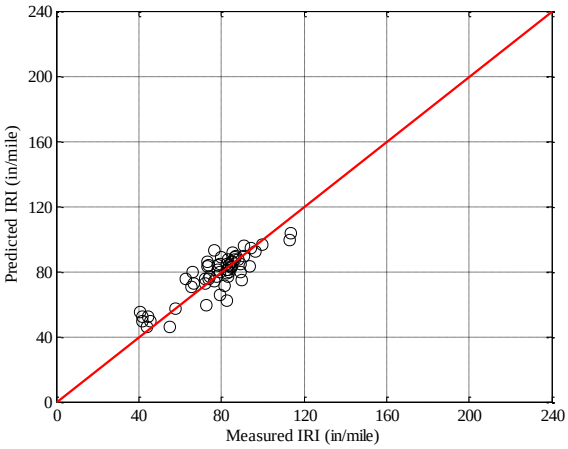

(b) Local model

Figure B-467 Option 4 IRI local calibration measured versus predicted – no sampling

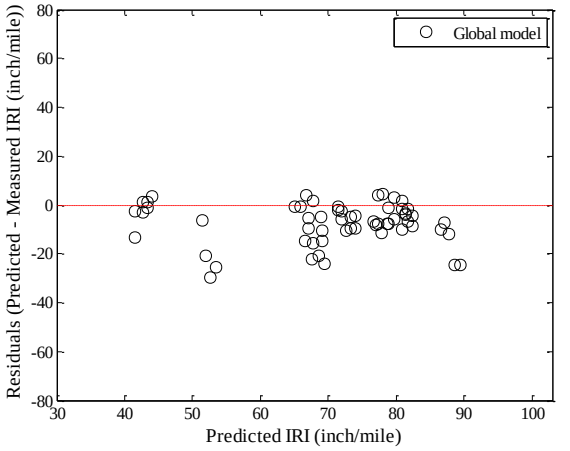

(a) Global model

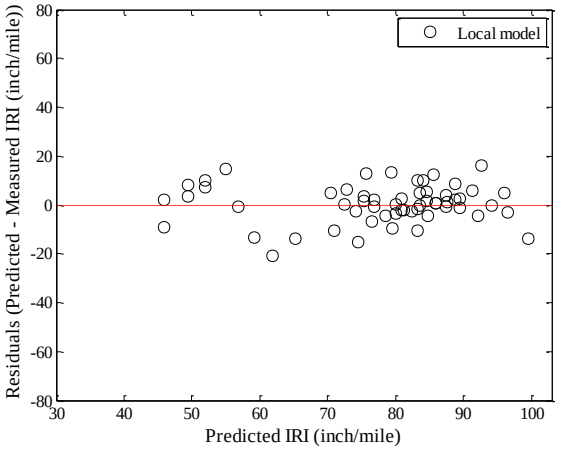

(b) Local model

Figure B-468 Option 4 IRI local calibration residual plots – no sampling

Reliability

The IRI reliability is internally estimated by the software, and uses an initial IRI standard deviation of 5.4 inch/mile.

Split sampling

Table B-198 Option 4 IRI local calibration results – split sampling

Parameter	Global model	Local model	Validation
SEE	10.872	7.128	10.483
Bias	-7.494	0.302	1.055
R^2	0.642	0.692	0.816
t-test pvalue	0.000	0.780	0.681
Intercept = 0	0.037	0.005	0.016
Slope = 1	0.002	0.005	0.017
C1	0.820	0.001	0.001
C2	0.442	2.601	2.601
C3	1.493	1.493	1.493
C4	25.240	25.240	25.240

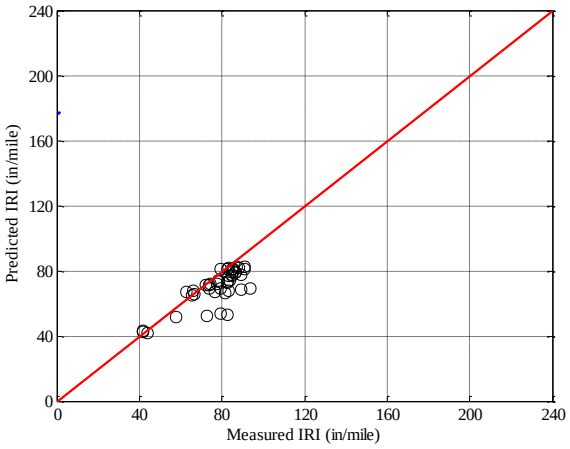

(a) Global model

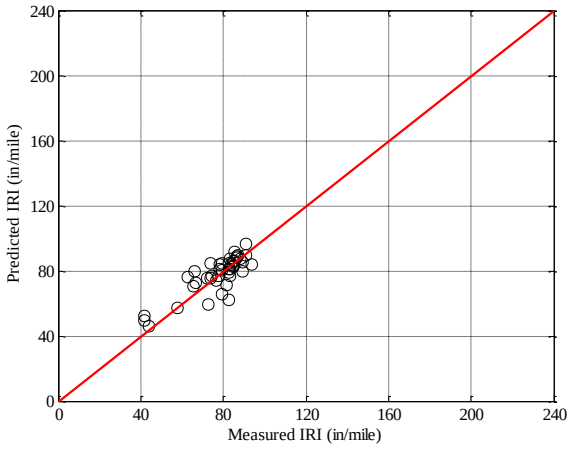

(b) Local model

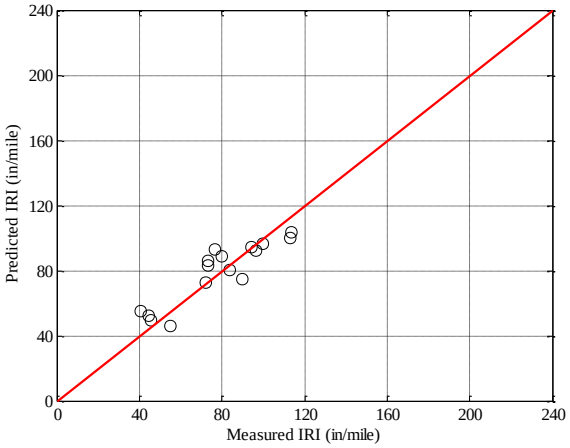

(c) Local model validation

Figure B-469 Option 4 IRI local calibration measured versus predicted – split sampling

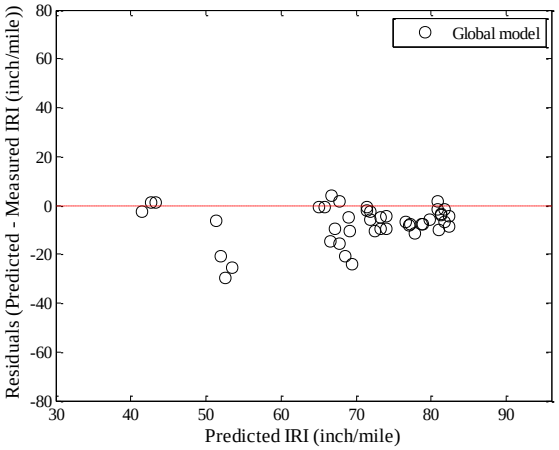

(a) Global model

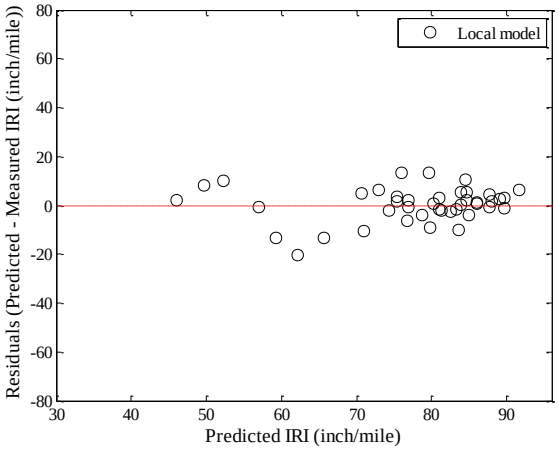

(b) Local model

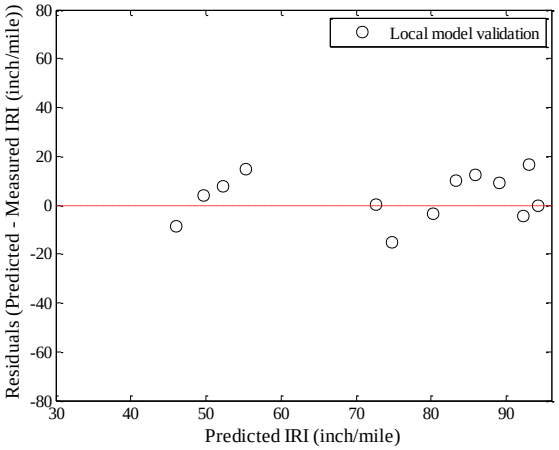

(c) Local model validation

Figure B-470 Option 4 IRI local calibration residual plots – split sampling

Reliability

The IRI reliability is internally estimated by the software, and uses an initial IRI standard deviation of 5.4 inch/mile.

Repeated split sampling

Table B-199 Option 4 IRI local calibration results – repeated split sampling

Global Model				
Parameter	Global Model Mean	Global Model Median	Global model lower CI	Global model upper CI
SEE	11.395	11.573	8.934	13.129
Bias	-7.575	-7.604	-9.768	-5.430
C1	0.820	0.820	-	-
C2	0.442	0.442	-	-
C3	1.492	1.492	-	-
C4	25.240	25.240	-	-
Local Model				
Parameter	Local Model Mean	Local Model Median	Local model lower CI	Local model upper CI
SEE	7.901	7.984	6.419	8.931
Bias	0.280	0.265	-0.085	0.686
C1	0.001	0.000	0.000	0.000
C2	2.554	2.551	2.003	3.164
C3	1.493	1.493	1.493	1.493
C4	25.240	25.240	25.240	25.240
Local Model validation				
Parameter	Local Model Mean	Local Model Median	Local model lower CI	Local model upper CI
SEE	8.754	8.740	4.798	12.622
Bias	0.393	0.352	-7.649	8.570
C1	0.001	0.000	0.000	0.000
C2	2.554	2.551	2.003	3.164
C3	1.493	1.493	1.493	1.493
C4	25.240	25.240	25.240	25.240

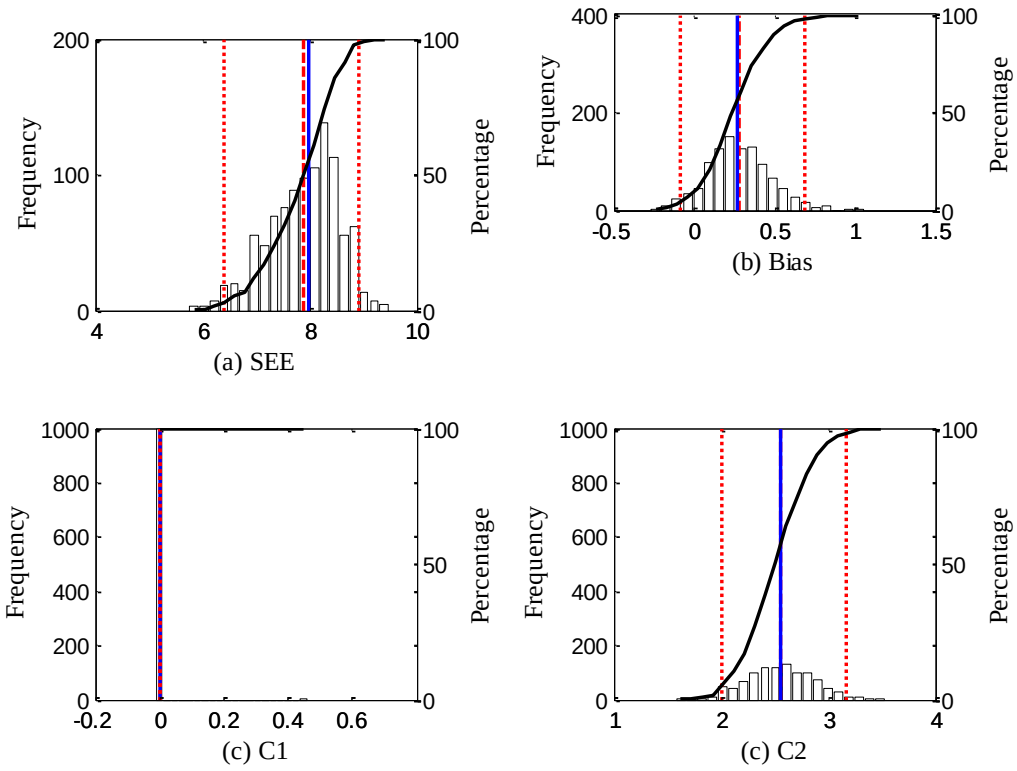

Figure B-471 Option 4 IRI repeated split sampling frequency distributions – calibration

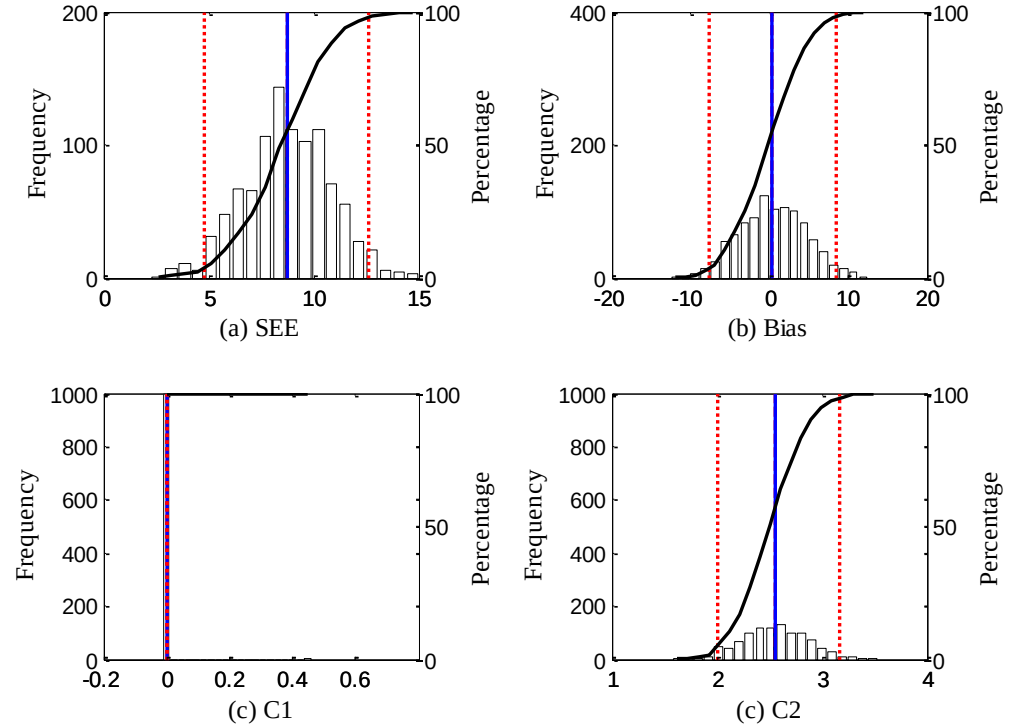

Figure B-472 Option 4 IRI repeated split sampling frequency distributions – validation

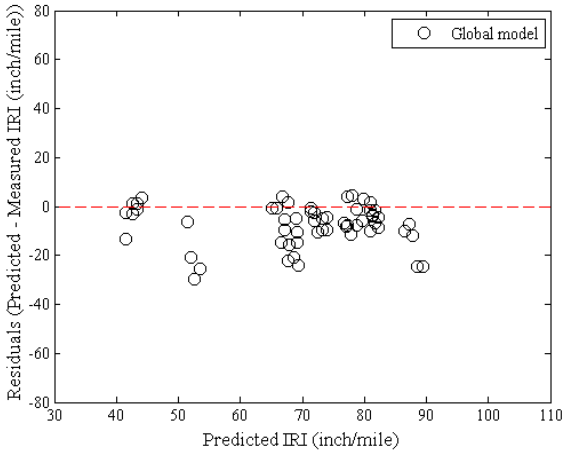

(a) Global model

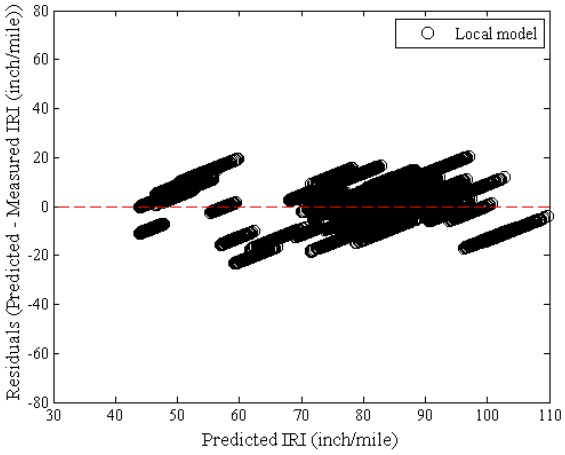

(b) Local model

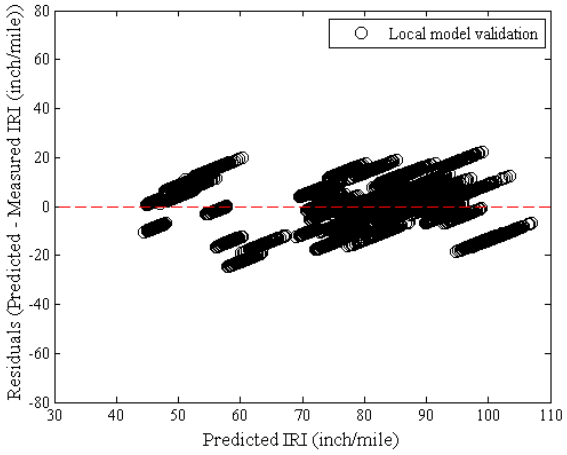

(c) Local model validation

Figure B-473 Option 4 IRI local calibration residual plots – repeated split sampling

Reliability

The IRI reliability is internally estimated by the software, and uses an initial IRI standard deviation of 5.4 inch/mile.

Bootstrapping

Table B-200 Option 4 IRI local calibration results – bootstrapping

Global Model				
Parameter	Global Model Mean	Global Model Median	Global model lower CI	Global model upper CI
SEE	11.179	11.203	7.518	14.591
Bias	-7.539	-7.501	-11.264	-4.032
C1	0.820	0.820	-	-
C2	0.442	0.442	-	-
C3	1.492	1.492	-	-
C4	25.240	25.240	-	-
Local Model				
Parameter	Local Model Mean	Local Model Median	Local model lower CI	Local model upper CI
SEE	7.602	7.613	5.470	9.510
Bias	0.295	0.281	-0.250	0.881
C1	0.041	0.000	0.000	0.000
C2	2.540	2.559	1.577	3.513
C3	1.493	1.493	1.493	1.493
C4	25.240	25.240	25.240	25.240

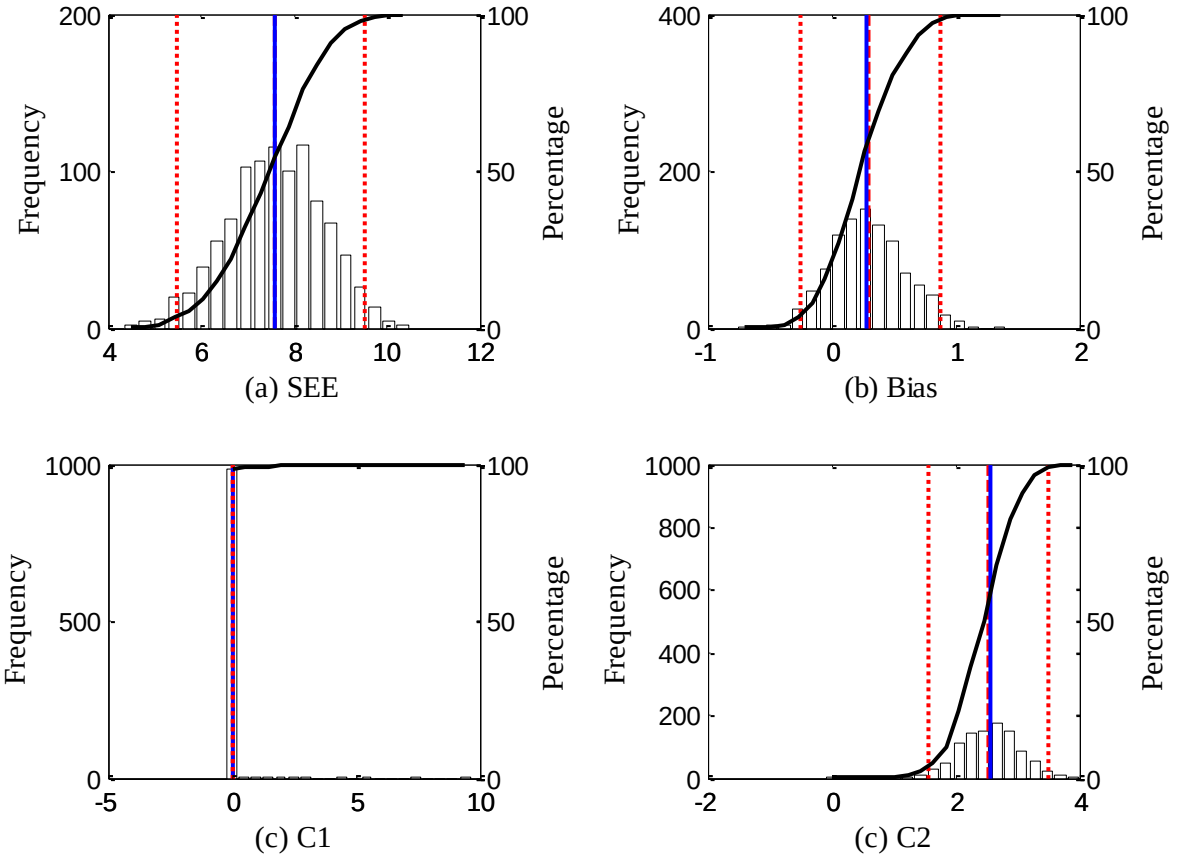

Figure B-474 Option 4 IRI bootstrapping frequency distributions

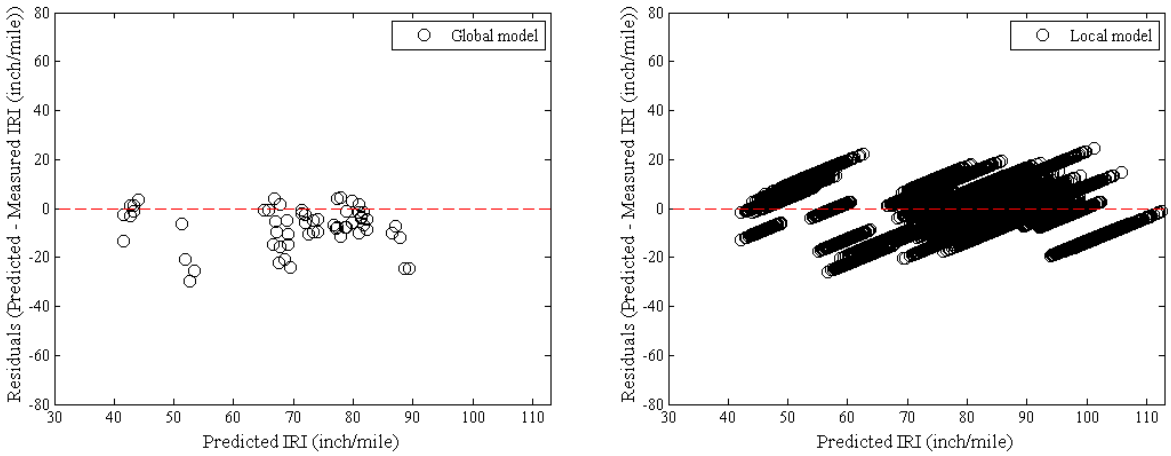

Figure B-475 Option 4 IRI local calibration residual plots – bootstrapping

Reliability

The IRI reliability is internally estimated by the software, and uses an initial IRI standard deviation of 5.4 inch/mile.

B.3 Validation

B.3.1 Fatigue cracking model – Bottom-up

B.3.1.1 Option 1a

Table B-201 Option 1a alligator cracking model validation

Parameter	Global Model	Local Model	Local model validation
SEE	7.447	6.269	6.946
Bias	-4.282	-0.716	-1.952
C1	1.000	0.496	0.496
C2	1.000	0.560	0.560

Table B-202: Option 1a hypothesis test results

Hypothesis test	*p*-value
Mean difference (paired *t*-test)	0.016
Intercept	0.000
Slope	0.000

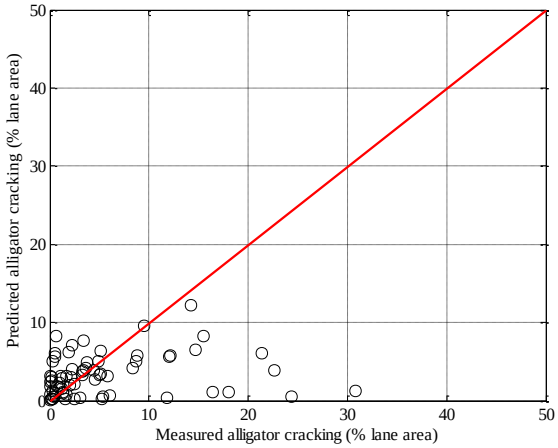

Figure B-476 Option 1a validation results

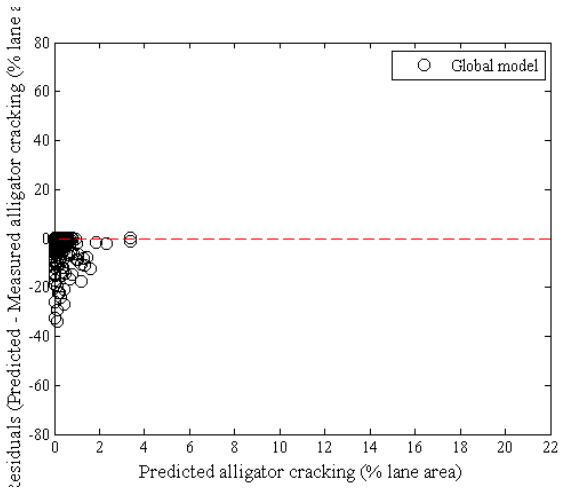

(a) Global model

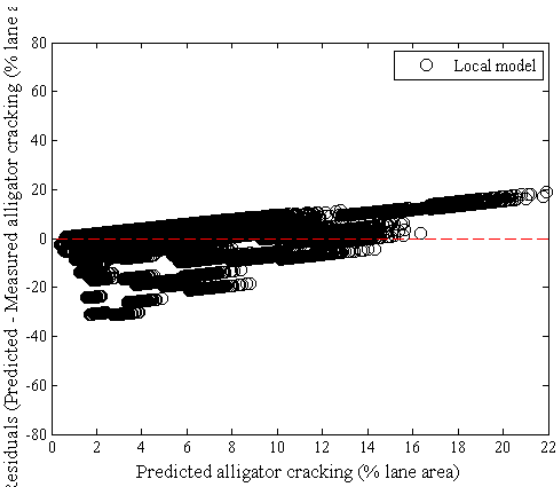

(a) Local model

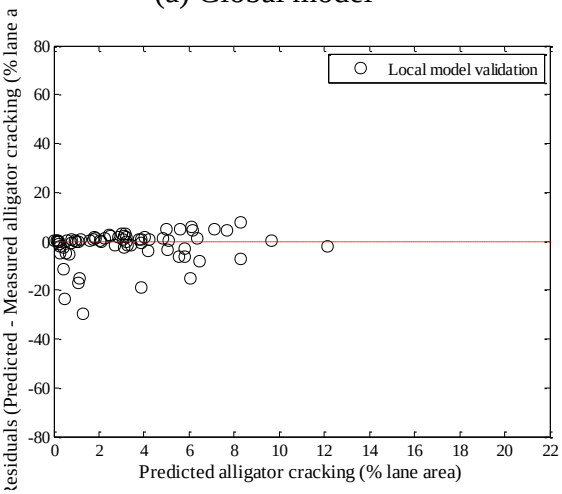

(a) Local model validation

Figure B-477 Option 1a residual plots

B.3.1.2 Option 1b

Table B-203 Option 1b alligator cracking model validation

Parameter	Global Model	Local Model	Local model validation
SEE	4.379	3.960	5.099
Bias	-2.366	-0.819	-1.558
C1	1.000	0.672	0.672
C2	1.000	0.560	0.560

Table B-204: Option 1b hypothesis test results

Hypothesis test	*p*-value
Mean difference (paired *t*-test)	0.283
Intercept	0.023
Slope	0.000

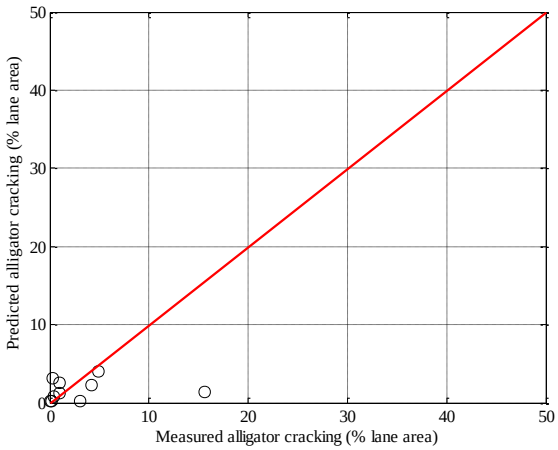

Figure B-478 Option 1b validation results

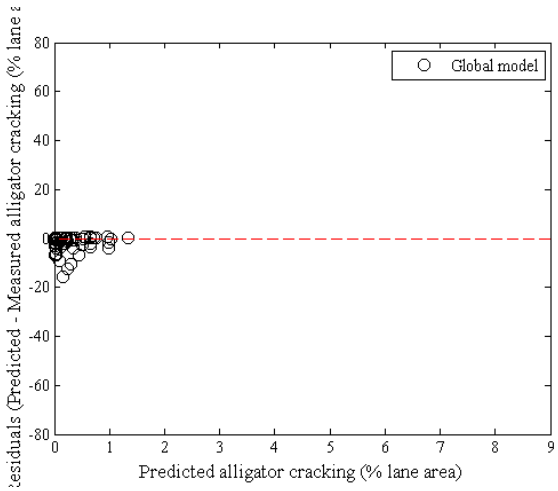

(a) Global model

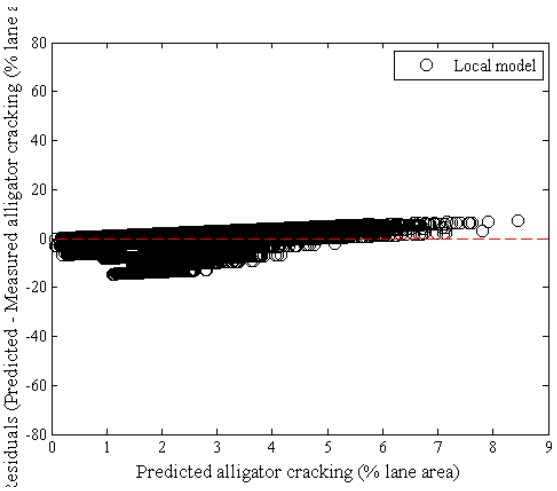

(a) Local model

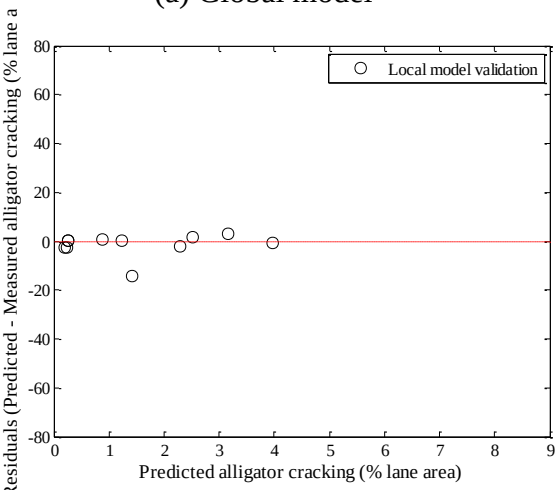

(a) Local model validation

Figure B-479 Option 1b residual plots

B.3.2 Fatigue cracking model – Top-down

B.3.2.1 Option 1

Table B-205 Option 1 longitudinal cracking model validation

Parameter	Global Model	Local Model	Local model validation
SEE	817.4715	696.8328	631.5130
Bias	-466.8421	-136.9143	-21.3558
C1	7.0000	3.1803	3.1803
C2	3.5000	1.2500	1.2500

Table B-206: Option 1 hypothesis test results

Hypothesis test	*p*-value
Mean difference (paired *t*-test)	0.7673
Intercept	0.0000
Slope	0.0000

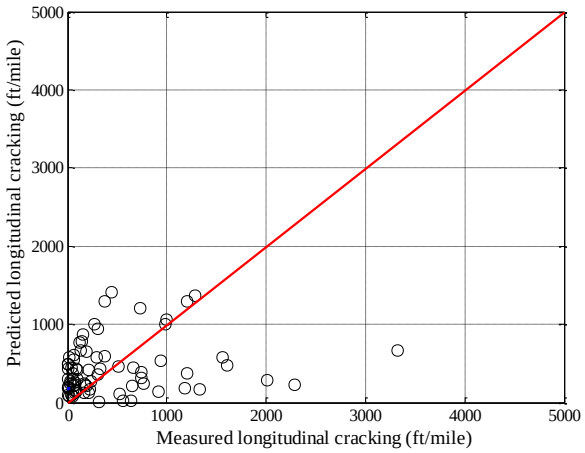

Figure B-480 Option 1 validation results

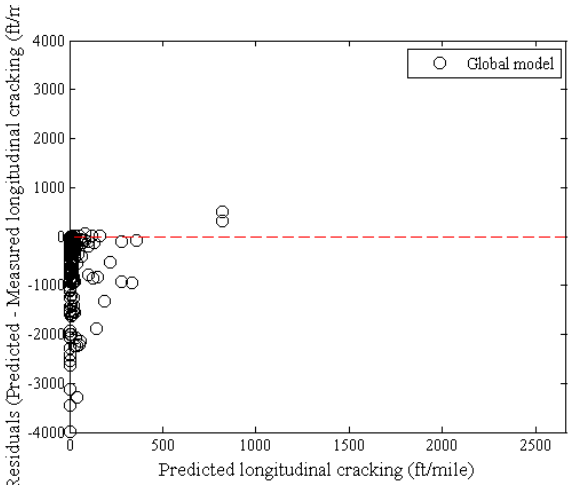

(a) Global model

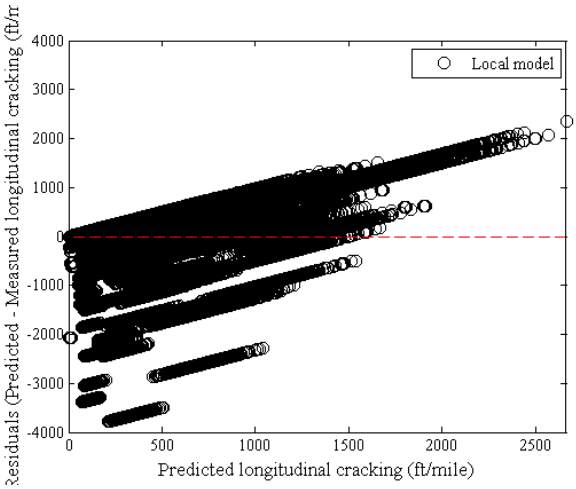

(a) Local model

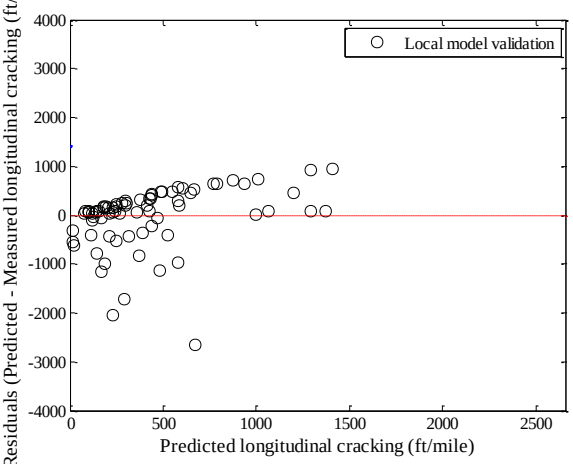

(a) Local model validation

Figure B-481 Option 1 residual plots

B.3.2.2 Option 2

Table B-207 Option 2 longitudinal cracking model validation

Parameter	Global Model	Local Model	Local model validation
SEE	729.1168	627.0209	892.3061
Bias	-405.5257	-111.3998	-439.1413
C1	7.0000	3.2846	3.2846
C2	3.5000	1.2000	1.2000

Table B-208: Option 2 hypothesis test results

Hypothesis test	*p*-value
Mean difference (paired *t*-test)	0.0000
Intercept	0.0000
Slope	0.0000

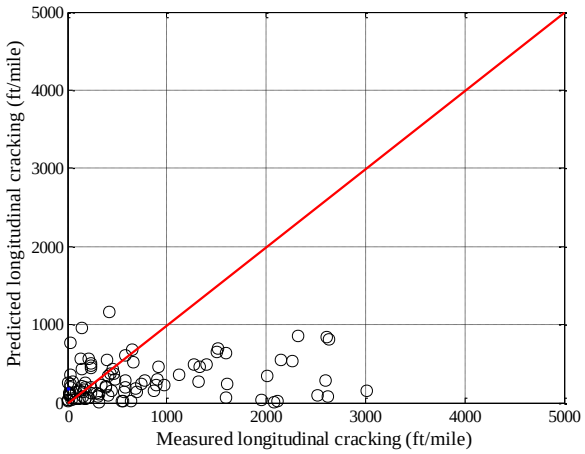

Figure B-482 Option 2 validation results

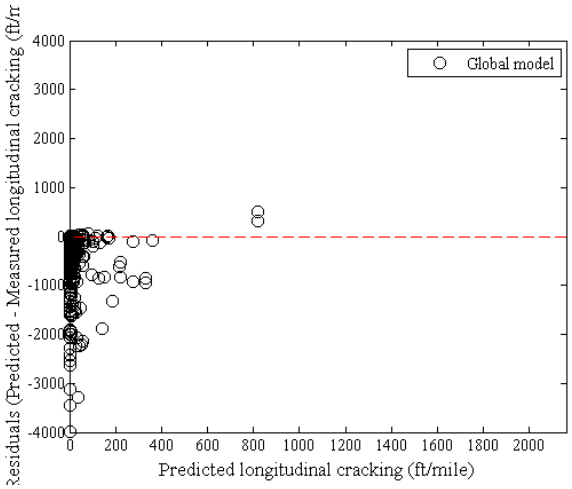

(a) Global model

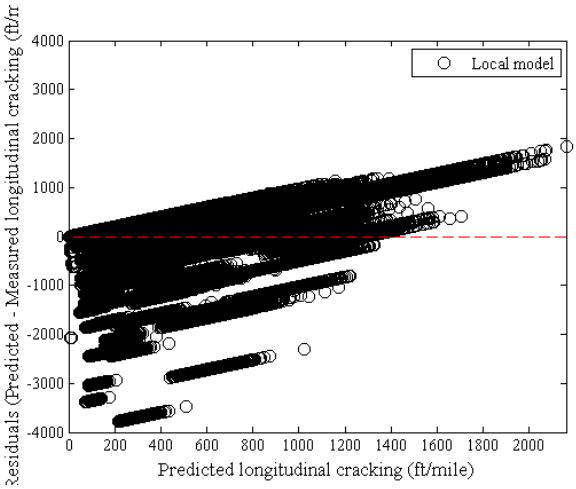

(a) Local model

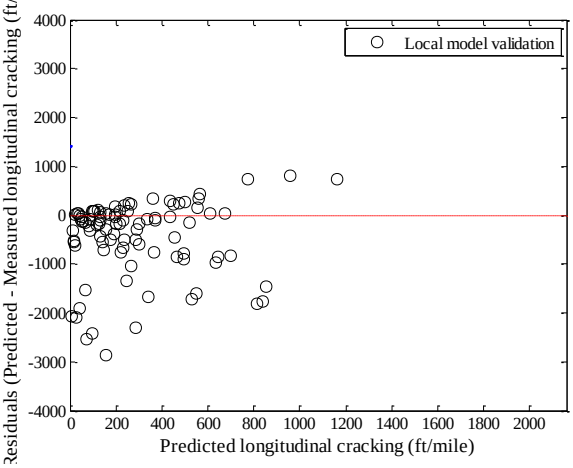

(a) Local model validation

Figure B-483 Option 2 residual plots

B.3.2.3 Option 4

Table B-209 Option 4 longitudinal cracking model validation

Parameter	Global Model	Local Model	Local model validation
SEE	1549.0513	1177.1581	629.3458
Bias	-1086.5433	-226.3333	201.7576
C1	7.0000	2.2118	2.2118
C2	3.5000	1.2114	1.2114

Table B-210: Option 4 hypothesis test results

Hypothesis test	*p*-value
Mean difference (paired *t*-test)	0.0952
Intercept	0.0001
Slope	0.0003

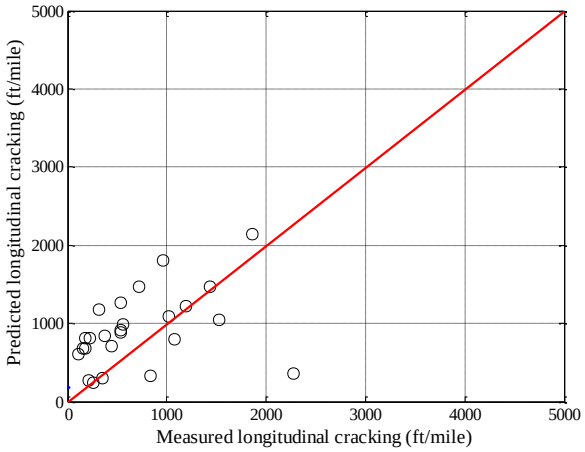

Figure B-484 Option 4 validation results

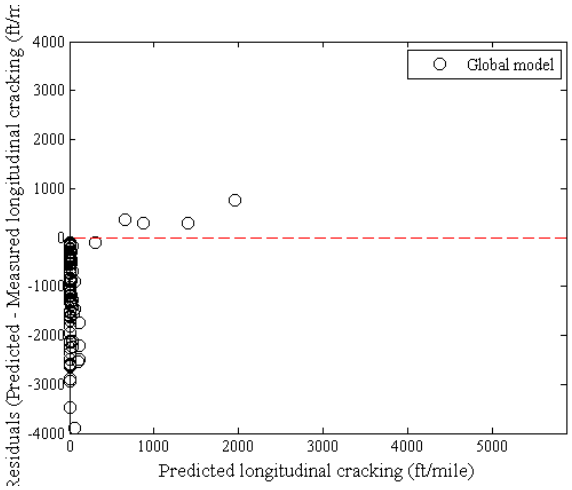

(a) Global model

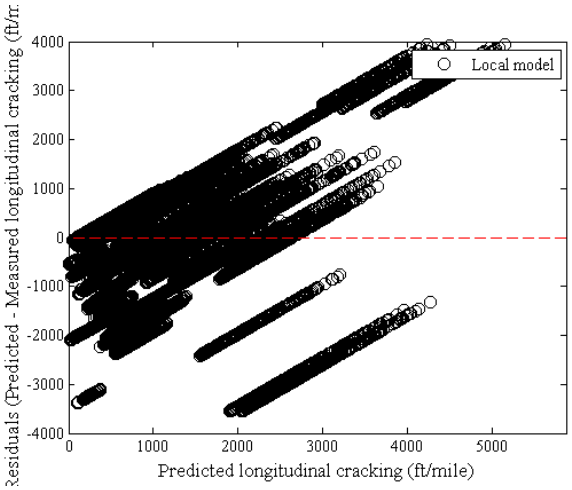

(a) Local model

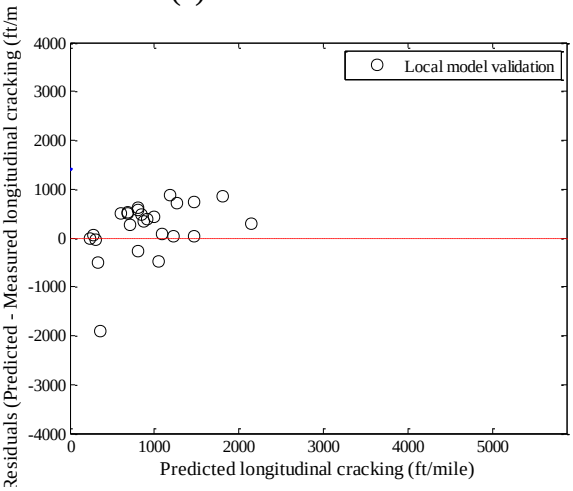

(a) Local model validation

Figure B-485 Option 4 residual plots

B.3.3 Rutting model

B.3.3.1 Option 1 Method 1

Table B-211 Option 1 Method 1 rutting model validation

HMA layer	SEE			Bias		
	Global Model	Local model	Validation	Global Model	Local model	Validation
AC rut	0.0779	0.0772	0.0958	-0.0020	-0.0068	-0.0030
Base rut	0.1186	0.0291	0.0457	0.1021	-0.0040	-0.0073
Subgrade	0.2235	0.0252	0.0381	0.2138	-0.0003	-0.0053
Total rut	0.3369	0.0849	0.1102	0.3139	-0.0111	-0.0155

Table B-212 Option 1 Method 1 rutting model validation hypothesis test results

HMA layer	AC rut	Base rut	Subgrade	Total rut
t-test p-value	0.7634	0.1205	0.1786	0.1704
Intercept p-value	0.0000	0.0000	0.0000	0.0000
Slope = 1 p-value	0.0000	0.0000	0.0000	0.0000

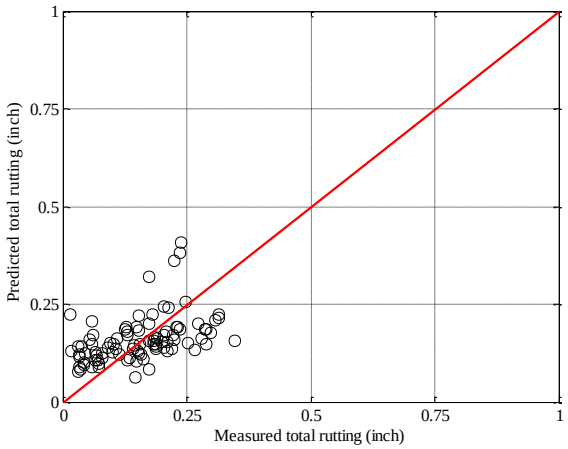

Figure B-486 Rutting model validation – option 1 method 1

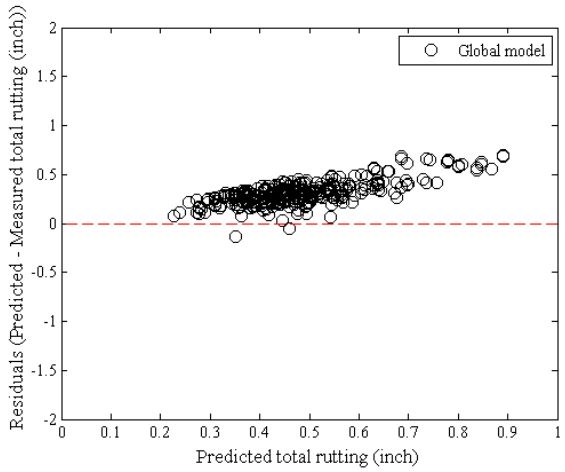

(a) Global model

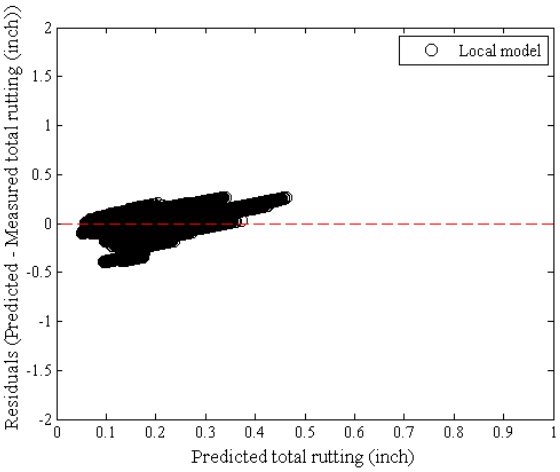

(a) Local model

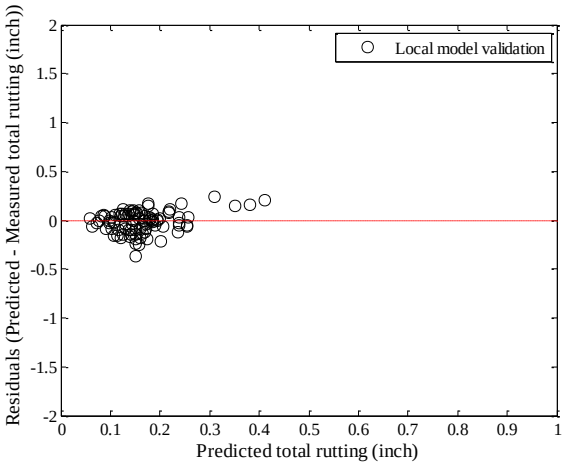

(a) Local model validation

Figure B-487 Rutting model residual plots – option 1 method 1

B.3.3.2 Option 1 Method 2

Table B-213 Option 1 Method 2 rutting model validation results

HMA layer	SEE			Bias		
	Global Model	Local model	Validation	Global Model	Local model	Validation
AC rut	0.0780	0.1160	0.1151	-0.0017	-0.0852	-0.0886
Base rut	0.1182	0.0341	0.0267	0.1019	0.0063	0.0120
Subgrade	0.2233	0.0855	0.0876	0.2136	0.0775	0.0797
Total rut	0.3368	0.0810	0.0745	0.3138	-0.0014	0.0031

Table B-214 Option 1 Method 2 rutting model validation hypothesis test results

HMA layer	AC rut	Base rut	Subgrade	Total rut
t-test p-value	0.0000	0.0000	0.0000	0.6904
Intercept p-value	0.0000	0.0000	0.0000	0.0000
Slope = 1 p-value	0.0000	0.0000	0.0000	0.0000

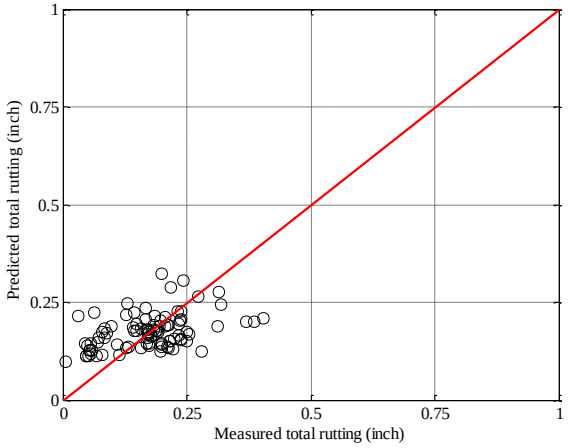

Figure B-488 Rutting model validation – option 1 method 2

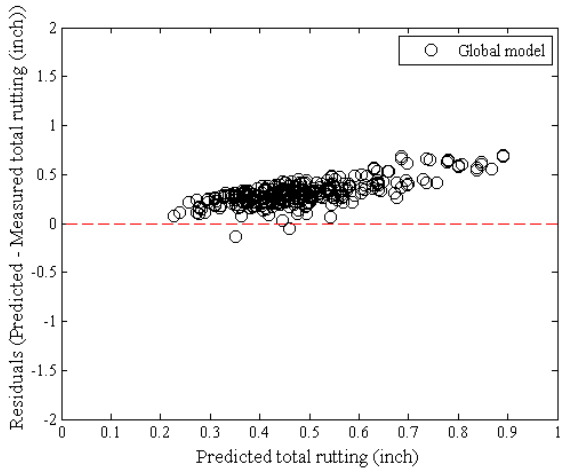

(a) Global model

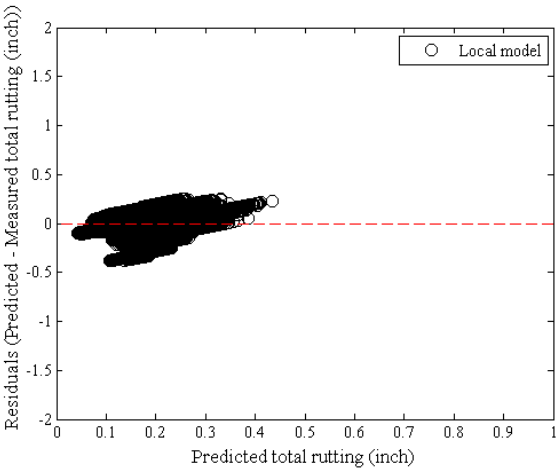

(a) Local model

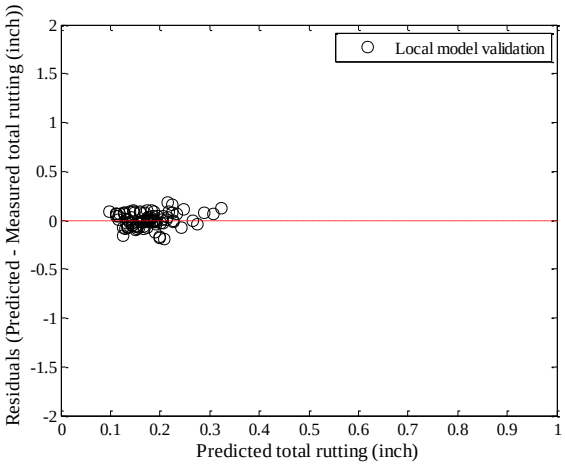

(a) Local model validation

Figure B-489 Rutting model residual plots – option 1 method 2

B.3.3.3 Option 2 Method 1

Table B-215 Option 2 Method 1 rutting model validation results

HMA layer	SEE			Bias		
	Global Model	Local model	Validation	Global Model	Local model	Validation
AC rut	0.0775	0.0768	0.0796	-0.0014	-0.0085	-0.0323
Base rut	0.1399	0.0272	0.0207	0.1118	-0.0059	-0.0013
Subgrade	0.2223	0.0226	0.0088	0.2076	-0.0006	0.0030
Total rut	0.3567	0.0858	0.0853	0.3180	-0.0151	-0.0306

Table B-216 Option 2 Method 1 rutting model validation hypothesis test results

HMA layer	AC rut	Base rut	Subgrade	Total rut
t-test p-value	0.0000	0.4968	0.0001	0.0001
Intercept p-value	0.0000	0.0000	0.0000	0.0000
Slope = 1 p-value	0.0000	0.0000	0.0000	0.0000

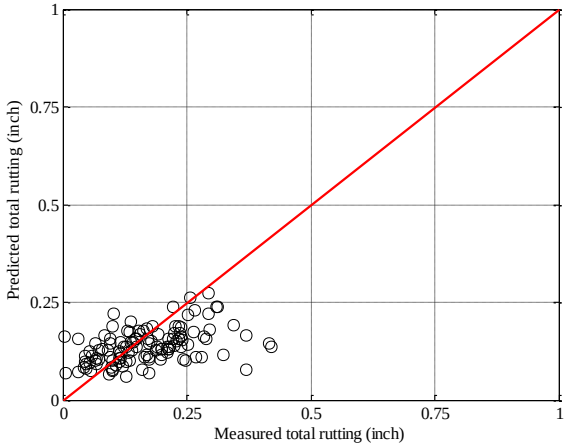

Figure B-490 Rutting model validation – option 2 method 1

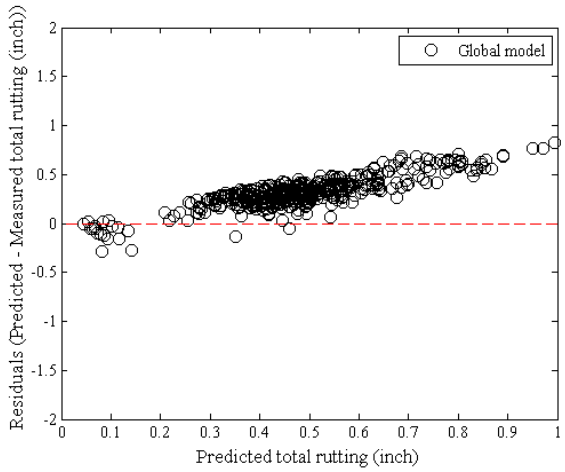

(a) Global model

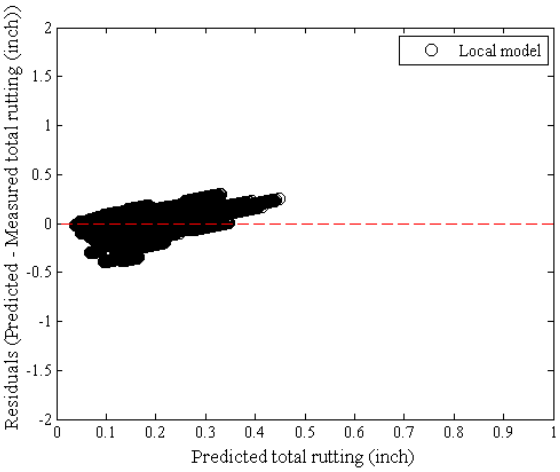

(a) Local model

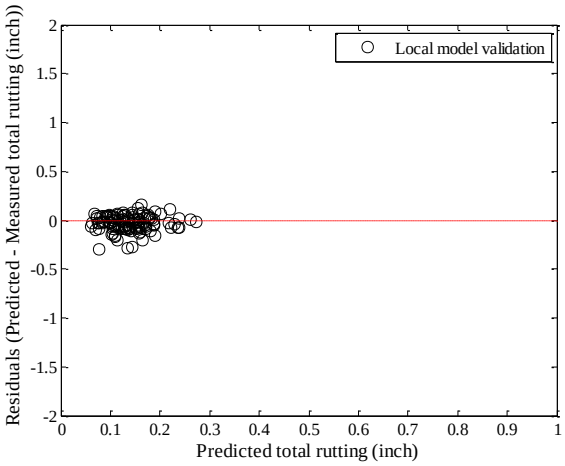

(a) Local model validation

Figure B-491 Rutting model residual plots – option 2 method 1

B.3.3.4 Option 2 Method 2

Table B-217 Option 2 Method 2 rutting model validation results

HMA layer	SEE			Bias		
	Global Model	Local model	Validation	Global Model	Local model	Validation
AC rut	0.0778	0.1147	0.1239	-0.0016	-0.0836	-0.0974
Base rut	0.1182	0.0345	0.0230	0.1019	0.0066	0.0172
Subgrade	0.2232	0.0837	0.0837	0.2136	0.0756	0.0796
Total rut	0.3368	0.0809	0.0808	0.3139	-0.0014	-0.0006

Table B-218 Option 2 Method 2 rutting model validation hypothesis test results

HMA layer	AC rut	Base rut	Subgrade	Total rut
t-test p-value	0.0000	0.0000	0.0000	0.9431
Intercept p-value	0.0000	0.0000	0.0000	0.0000
Slope = 1 p-value	0.0000	0.0000	0.0000	0.0000

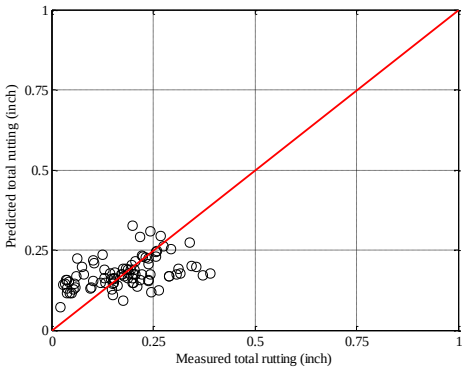

Figure B-492 Rutting model validation – option 2 method 2

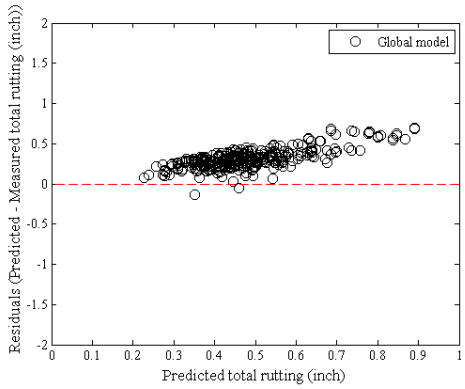

(a) Global model

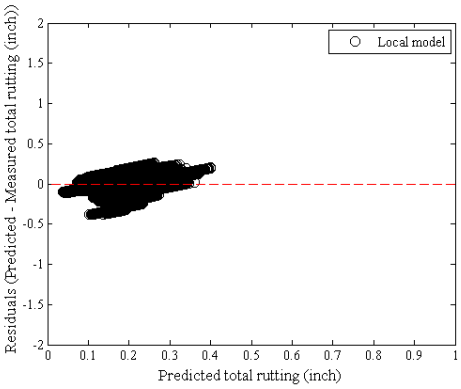

(a) Local model

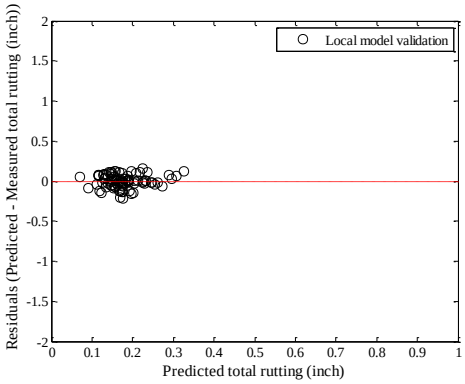

(a) Local model validation

Figure B-493 Rutting model residual plots – option 2 method 2

B.3.3.5 Option 4 Method 1

Table B-219 Option 4 Method 1 rutting model validation results

HMA layer	SEE			Bias		
	Global Model	Local model	Validation	Global Model	Local model	Validation
AC rut	0.0798	0.0757	0.0940	0.0059	-0.0129	-0.0428
Base rut	0.1421	0.0207	0.0197	0.0952	-0.0084	-0.0102
Subgrade	0.2143	0.0076	0.0062	0.1823	-0.0011	-0.0016
Total rut	0.3666	0.0865	0.1072	0.2833	-0.0224	-0.0546

Table B-220 Option 4 Method 1 rutting model validation hypothesis test results

HMA layer	AC rut	Base rut	Subgrade	Total rut
t-test p-value	0.0109	0.0033	0.1645	0.0038
Intercept p-value	0.0000	0.0039	0.0001	0.0000
Slope = 1 p-value	0.0000	0.0000	0.0000	0.0000

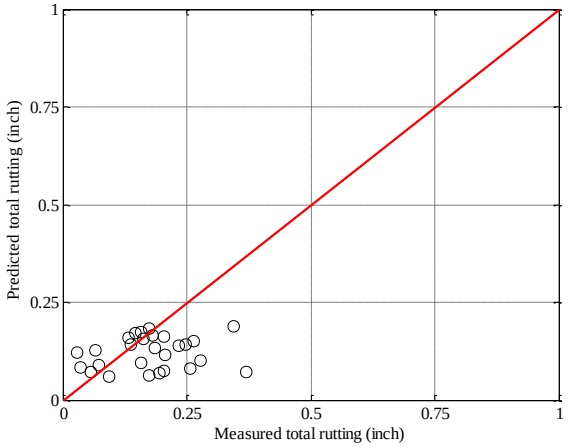

Figure B-494 Rutting model validation – option 4 method 1

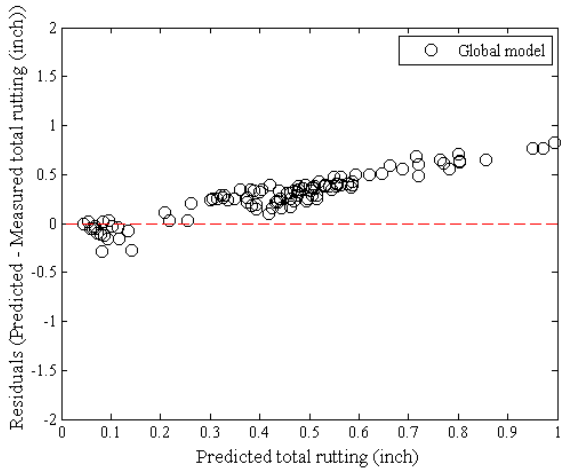

(a) Global model

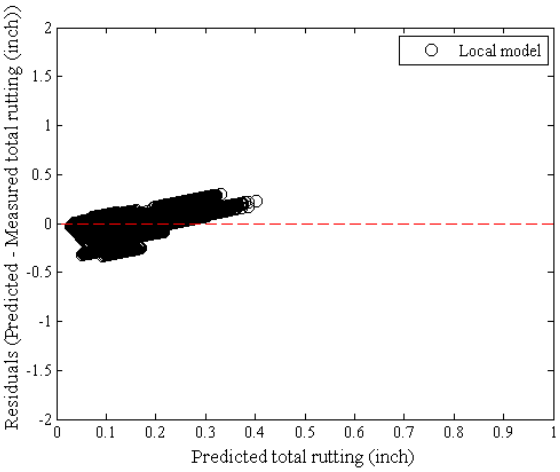

(a) Local model

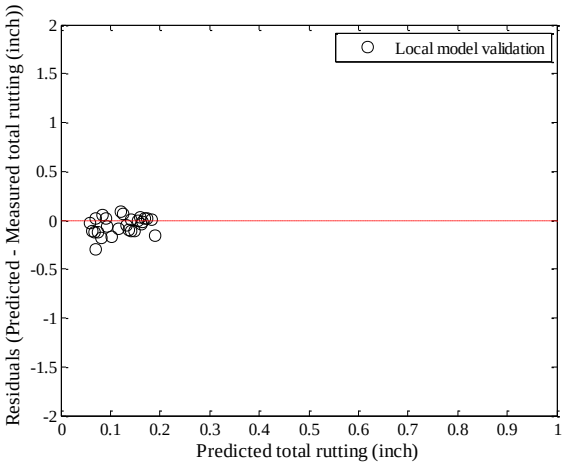

(a) Local model validation

Figure B-495 Rutting model residual plots – option 4 method 1

B.3.3.6 Option 4 Method 2

Table B-221 Option 4 Method 2 rutting model validation results

HMA layer	SEE			Bias		
	Global Model	Local model	Validation	Global Model	Local model	Validation
AC rut	0.0780	0.1148	0.1036	-0.0019	-0.0833	-0.0745
Base rut	0.1180	0.0342	0.0240	0.1016	0.0059	0.0056
Subgrade	0.2232	0.0842	0.0852	0.2136	0.0761	0.0777
Total rut	0.3361	0.0810	0.0774	0.3132	-0.0013	0.0088

Table B-222 Option 4 Method 2 rutting model validation hypothesis test results

HMA layer	AC rut	Base rut	Subgrade	Total rut
t-test p-value	0.0000	0.0192	0.0000	0.2585
Intercept p-value	0.0000	0.0000	0.0000	0.0000
Slope = 1 p-value	0.0000	0.0000	0.0000	0.0000

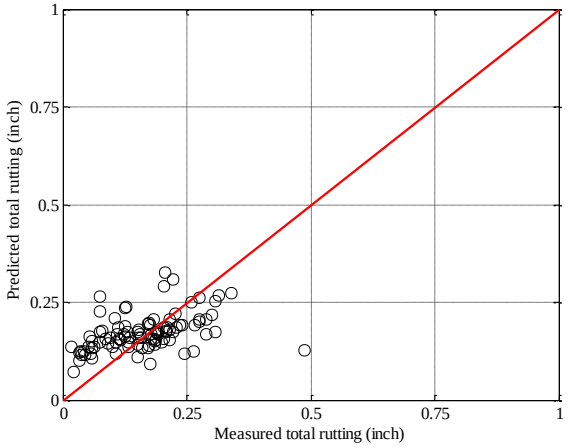

Figure B-496 Rutting model validation – option 4 method 2

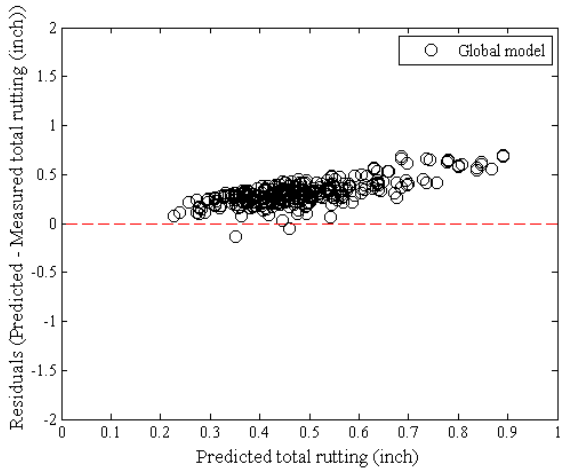

(a) Global model

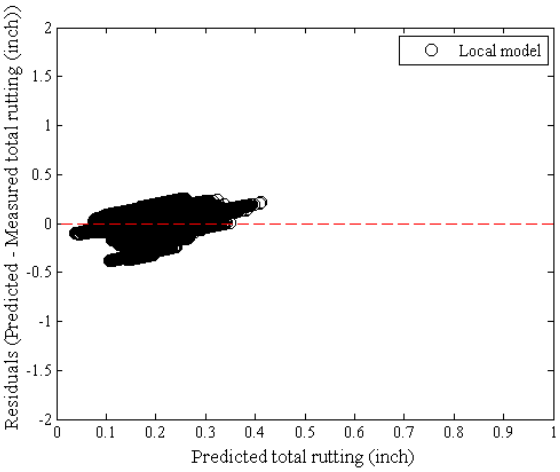

(a) Local model

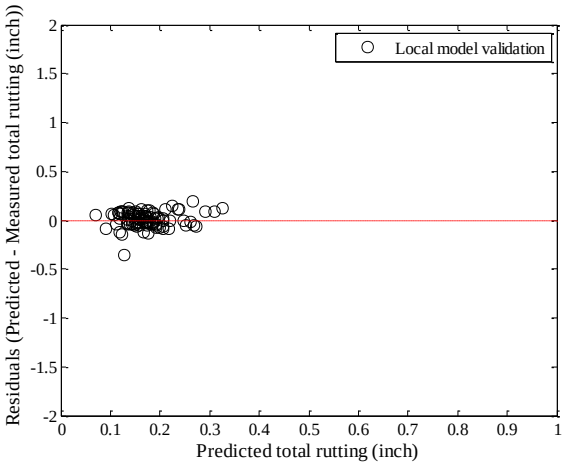

(a) Local model validation

Figure B-497 Rutting model residual plots – option 4 method 2

B.3.4 Flexible IRI model

B.3.4.1 Option 1

Table B-223 Option 1 IRI model validation results

Parameter	Global Model Mean	Local Model Mean	Local Model Validation
SEE	15.2543	15.1863	10.9135
Bias	0.6137	-0.7226	1.0022
C1	0.0150	0.0072	0.8178
C2	0.4000	0.3911	0.4462
C3	0.0080	0.0080	0.0000
C4	40.0000	54.2690	0.0000

Table B-224 Option 1 IRI model validation hypothesis test results

Hypothesis test	*p*-value
Mean difference (paired *t*-test)	0.4462
Intercept	0.0000
Slope	0.0000

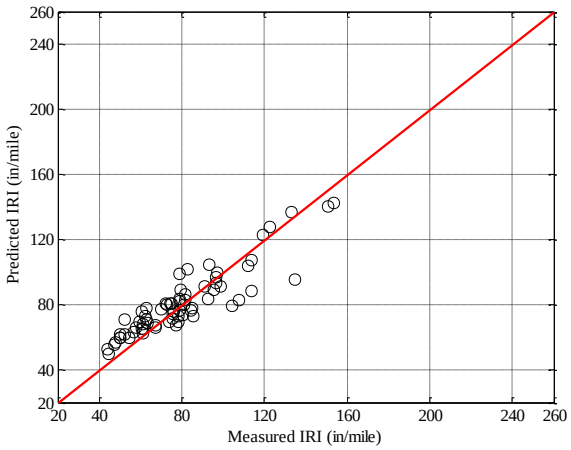

Figure B-498 IRI model validation – option 1

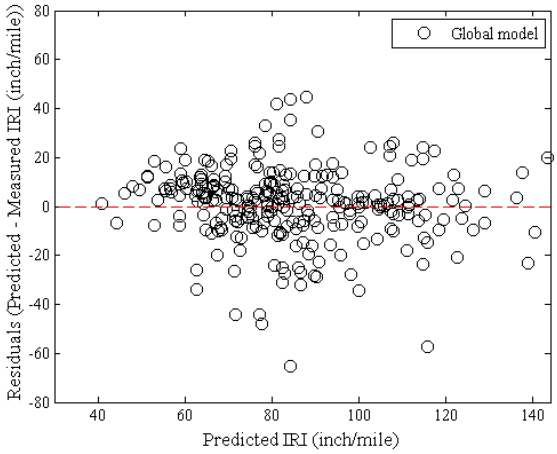

(a) Global model

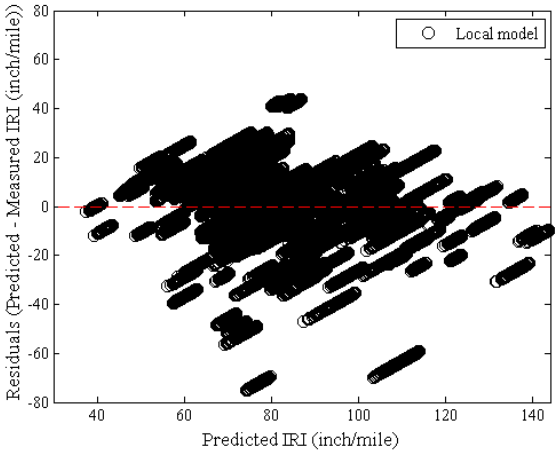

(a) Local model

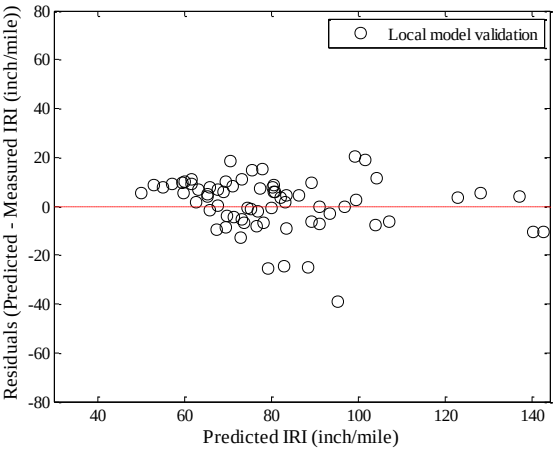

(a) Local model validation

Figure B-499 Option 1 residual plots

B.3.4.2 Option 2

Table B-225 Option 2 IRI model validation results

Parameter	Global Model Mean	Local Model Mean	Local Model Validation
SEE	15.2846	14.9275	18.2064
Bias	0.8357	-0.4715	0.0887
C1	0.0150	0.0157	0.0157
C2	0.4000	0.4043	0.4043
C3	0.0080	0.0064	0.0064
C4	40.0000	32.3044	32.3044

Table B-226 Option 2 IRI model validation hypothesis test results

Hypothesis test	*p*-value
Mean difference (paired *t*-test)	0.9603
Intercept	0.0000
Slope	0.0000

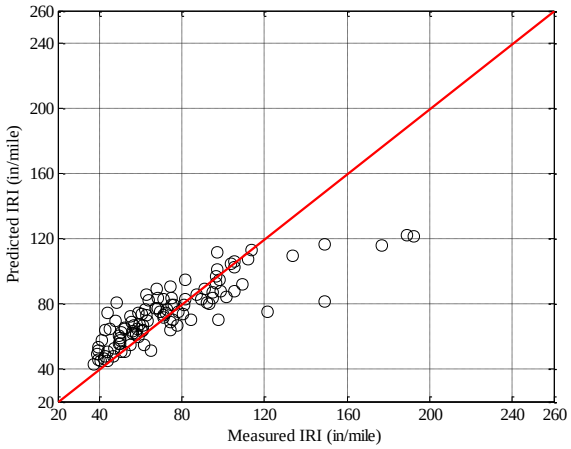

Figure B-500 IRI model validation – option 2

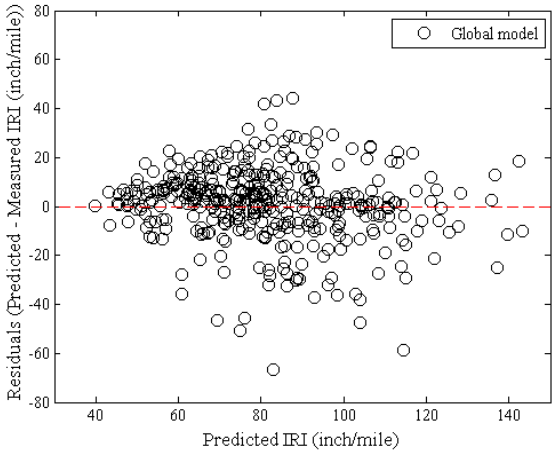

(a) Global model

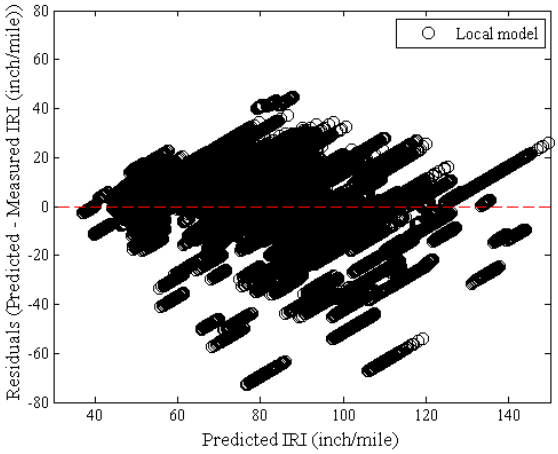

(a) Local model

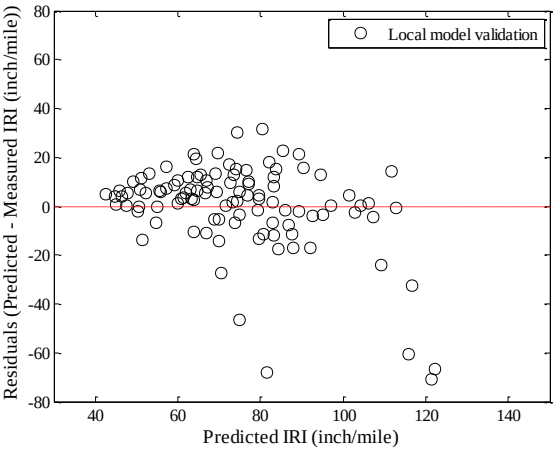

(a) Local model validation

Figure B-501 Option 2 residual plots

B.3.4.3 Option 4

Table B-227 Option 4 IRI model validation results

Parameter	Global Model Mean	Local Model Mean	Local Model Validation
SEE	22.6132	17.5204	14.0299
Bias	-9.4328	-0.4048	-1.8670
C1	0.0150	0.0294	0.0294
C2	0.4000	0.1606	0.1606
C3	0.0080	0.0052	0.0052
C4	40.0000	24.0057	24.0057

Table B-228 Option 4 IRI model validation hypothesis test results

Hypothesis test	*p*-value
Mean difference (paired *t*-test)	0.5750
Intercept	0.0362
Slope	0.0183

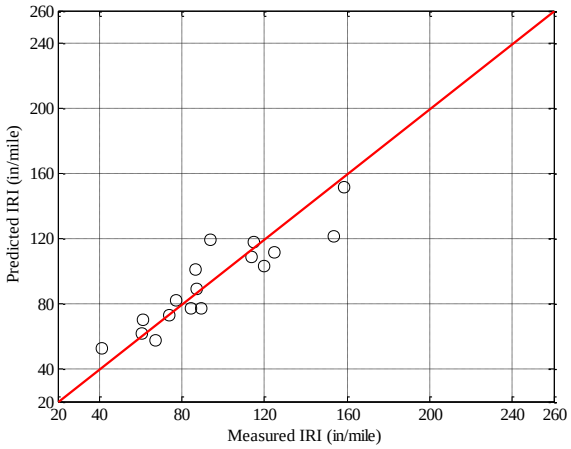

Figure B-502 IRI model validation – option 4

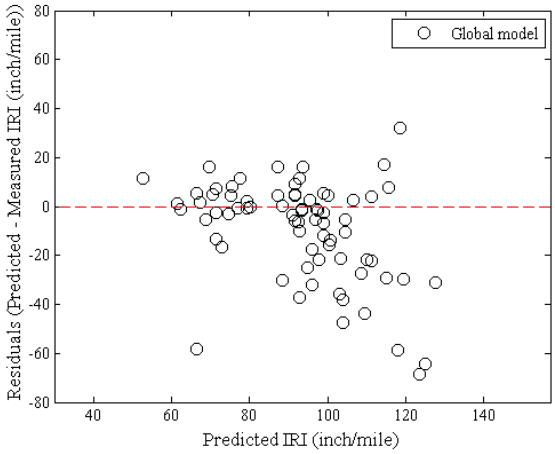

(a) Global model

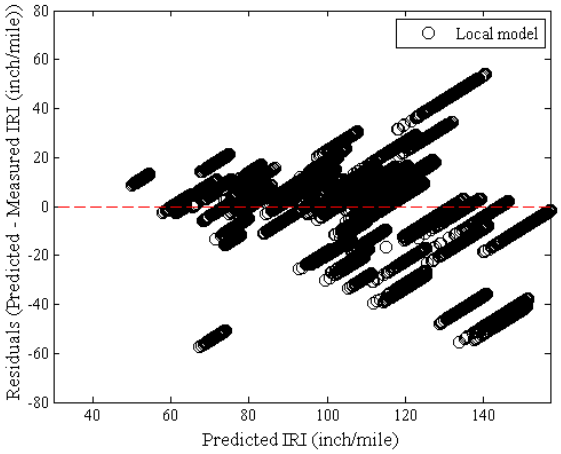

(a) Local model

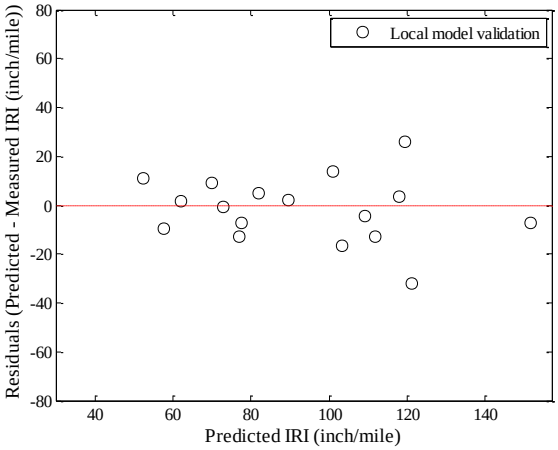

(a) Local model validation

Figure B-503 Option 4 residual plots

B.3.5 Transverse cracking model

B.3.5.1 Option 1

Table B-229 Option 1 transverse cracking model validation

Parameter	Global Model	Local Model	Local model validation
SEE	22.8853	12.6026	22.4378
Bias	-13.9244	0.3197	-8.9434
C1	1.0000	0.2612	0.2612
C2	-1.9800	-1.6662	-1.6662

Table B-230: Option 1 hypothesis test results

Hypothesis test	*p*-value
Mean difference (paired *t*-test)	0.1358
Intercept	0.2466
Slope	0.0073

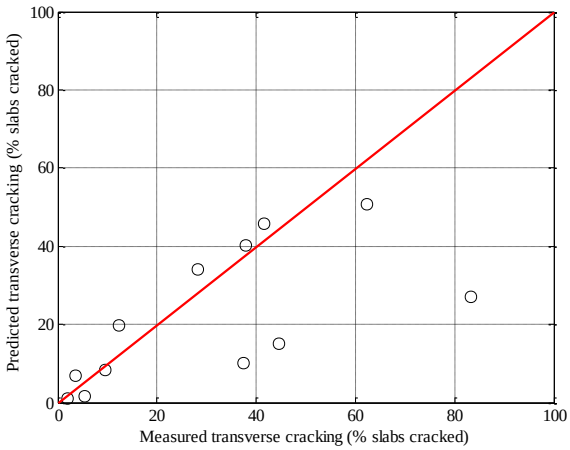

Figure B-504 Option 1 validation results

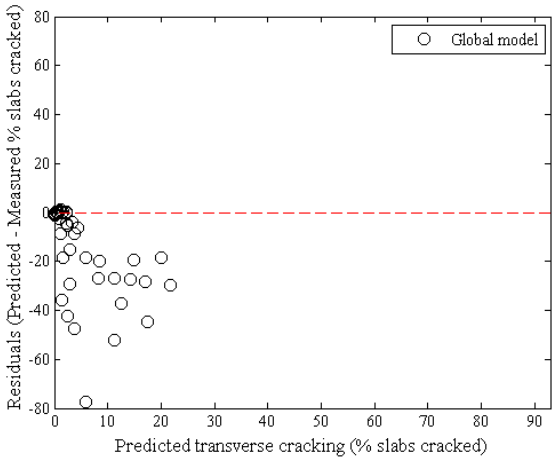

(a) Global model

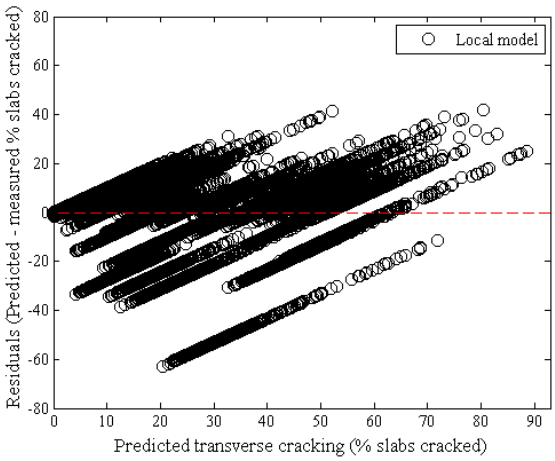

(a) Local model

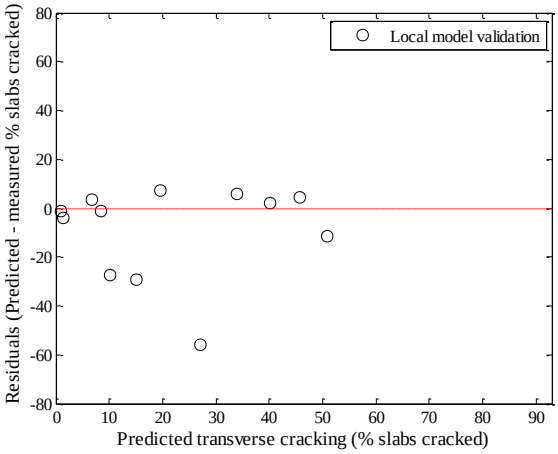

(a) Local model validation

Figure B-505 Option 1 residual plots

B.3.5.2 Option 2

Table B-231 Option 2 transverse cracking model validation

Parameter	Global Model	Local Model	Local model validation
SEE	16.0455	8.9093	12.2402
Bias	-7.5017	0.2667	-4.2322
C1	1.0000	0.2311	0.2311
C2	-1.9800	-1.7733	-1.7733

Table B-232: Option 2 hypothesis test results

Hypothesis test	*p*-value
Mean difference (paired *t*-test)	0.1225
Intercept	0.6342
Slope	0.0000

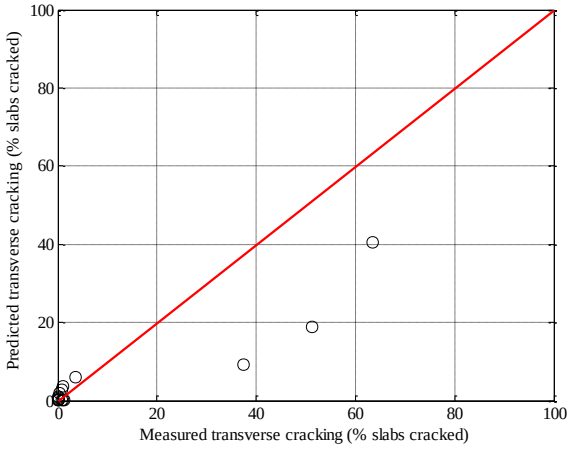

Figure B-506 Option 2 validation results

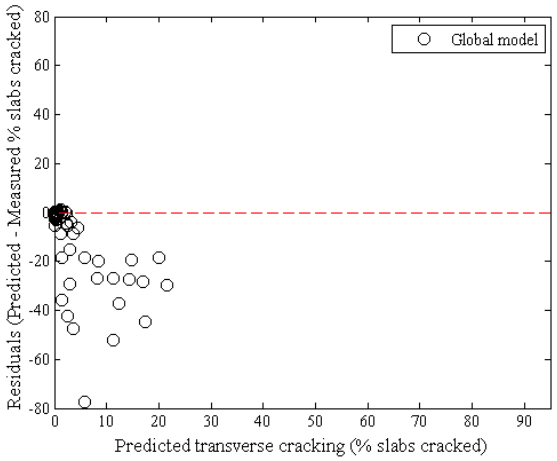

(a) Global model

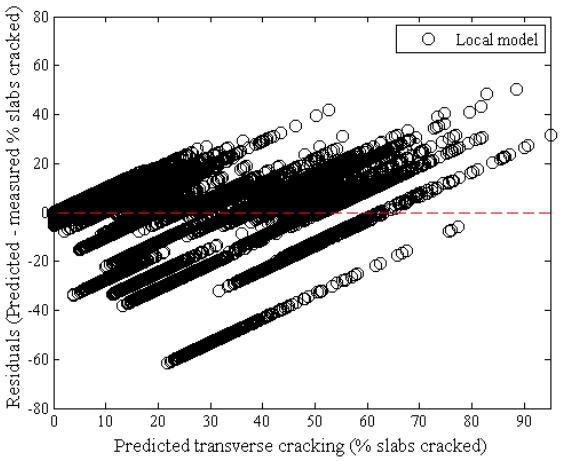

(a) Local model

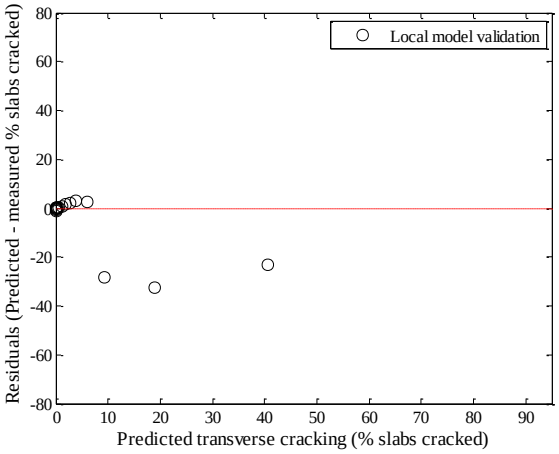

(a) Local model validation

Figure B-507 Option 2 residual plots

B.3.5.3 Option 3

Table B-233 Option 3 transverse cracking model validation

Parameter	Global Model	Local Model	Local model validation
SEE	14.0377	7.8001	13.7216
Bias	-5.9053	0.2924	-2.8180
C1	1.0000	0.2241	0.2241
C2	-1.9800	-1.8142	-1.8142

Table B-234: Option 3 hypothesis test results

Hypothesis test	*p*-value
Mean difference (paired *t*-test)	0.2032
Intercept	0.2231
Slope	0.0000

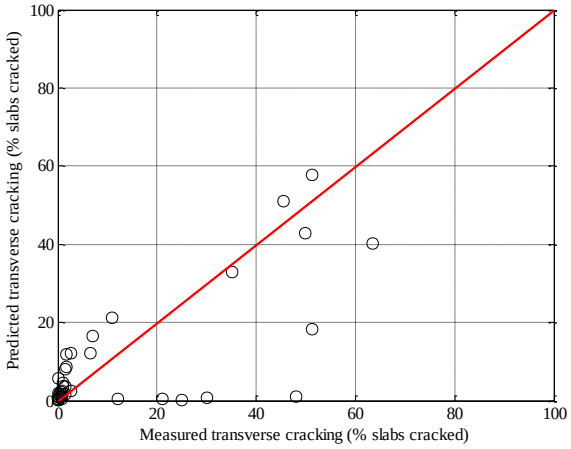

Figure B-508 Option 3 validation results

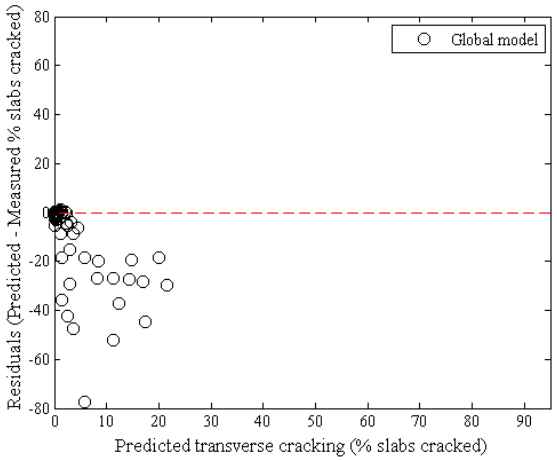

(a) Global model

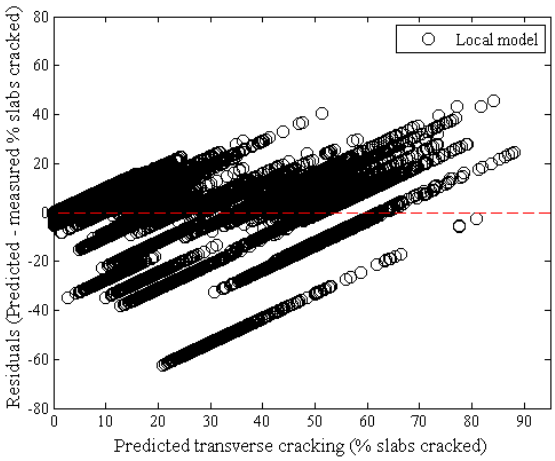

(a) Local model

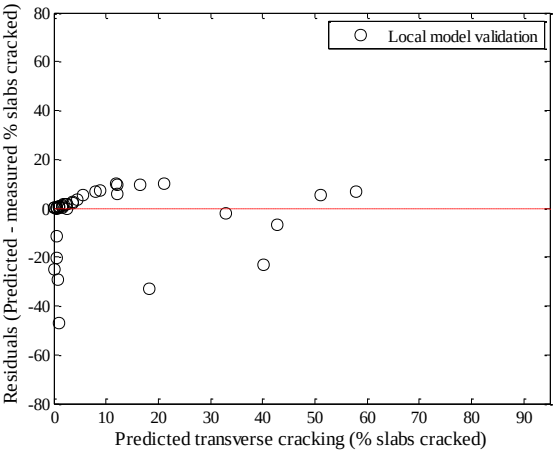

(a) Local model validation

Figure B-509 Option 3 residual plots

B.3.5.4 Option 4

Table B-235 Option 4 transverse cracking model validation

Parameter	Global Model	Local Model	Local model validation
SEE	0.9947	0.7029	0.5744
Bias	-0.6707	-0.0251	0.0776
C1	1.0000	4.9113	4.9113
C2	-1.9800	-0.9666	-0.9666

Table B-236: Option 4 hypothesis test results

Hypothesis test	*p*-value
Mean difference (paired *t*-test)	0.5917
Intercept	0.0005
Slope	0.0002

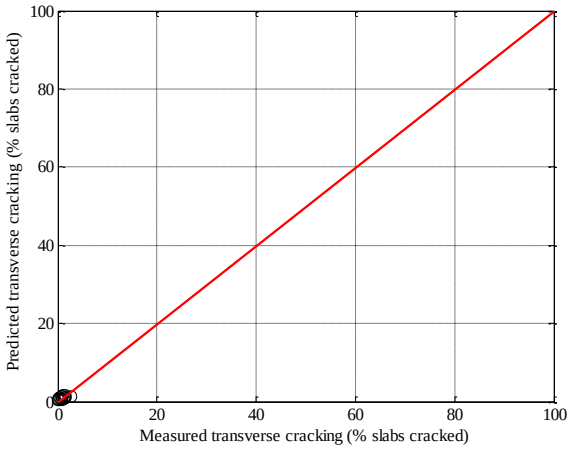

Figure B-510 Option 4 validation results

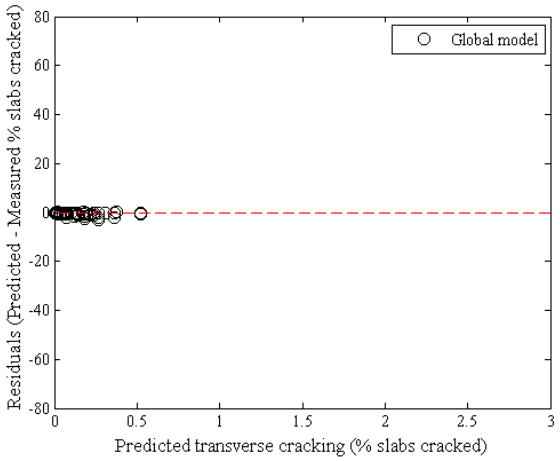

(a) Global model

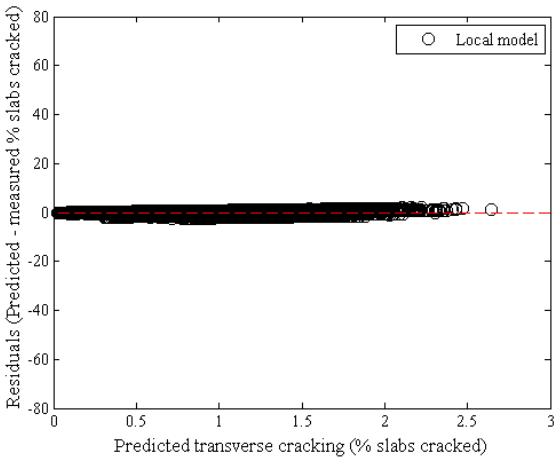

(a) Local model

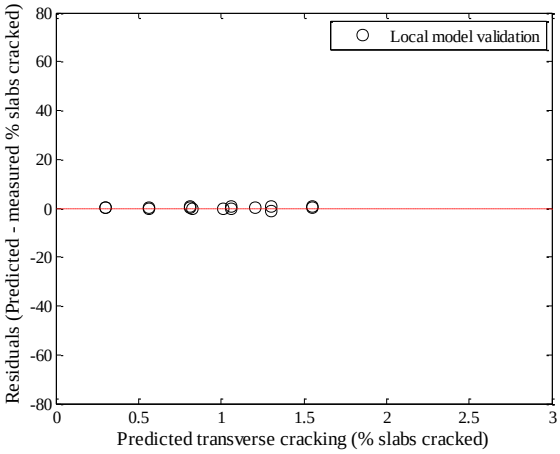

(a) Local model validation

Figure B-511 Option 4 residual plots

B.3.6 Rigid IRI model

B.3.6.1 Option 1

Table B-237 Option 1 IRI model validation results

Parameter	Global Model Mean	Local Model Mean	Local Model Validation
SEE	17.4759	15.2504	12.4435
Bias	-11.4262	4.3926	-2.4041
C1	0.8203	0.6059	0.6059
C2	0.4417	11.9325	11.9325
C3	1.4920	1.4929	1.4929
C4	25.2400	25.2400	25.2400

Table B-238 Option 1 IRI model validation hypothesis test results

Hypothesis test	*p*-value
Mean difference (paired *t*-test)	0.3334
Intercept	0.0007
Slope	0.0003

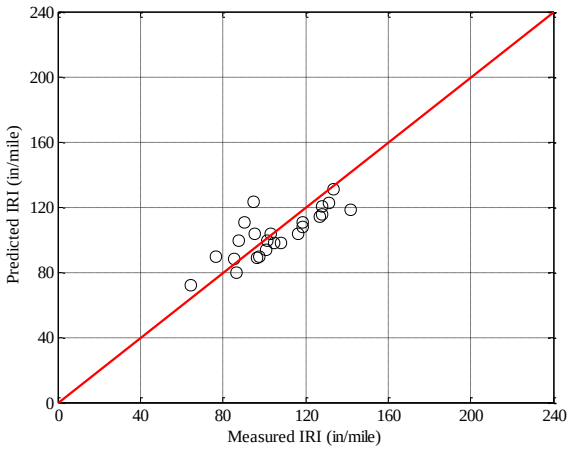

Figure B-512 IRI model validation – option 1

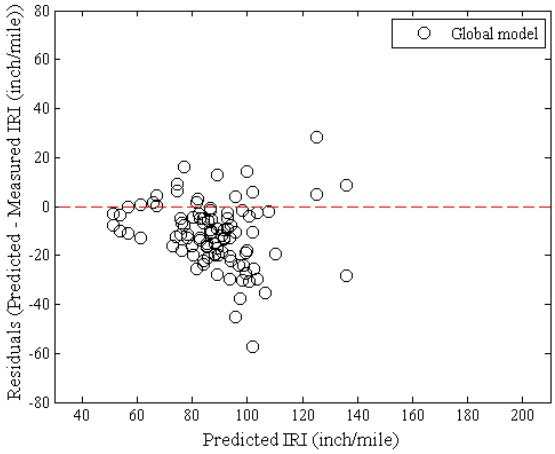

(a) Global model

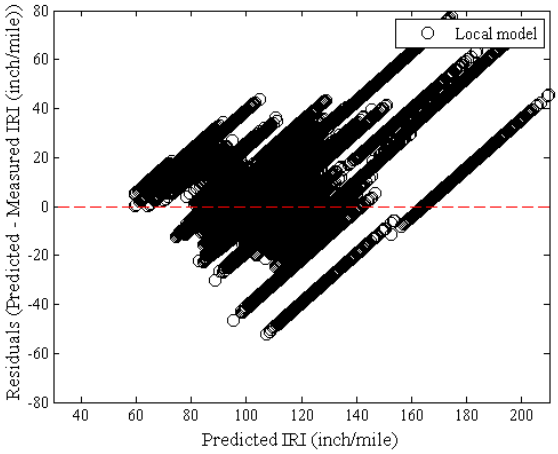

(a) Local model

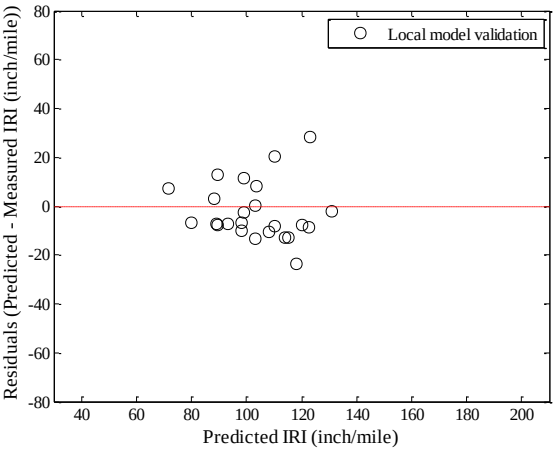

(a) Local model validation

Figure B-513 Option 1 residual plots

B.3.6.2 Option 2

Table B-239 Option 2 IRI model validation results

Parameter	Global Model Mean	Local Model Mean	Local Model Validation
SEE	16.3221	14.7545	14.4673
Bias	-10.5443	0.4799	7.5221
C1	0.8203	1.0704	1.0704
C2	0.4417	5.3282	5.3282
C3	1.4920	1.4929	1.4929
C4	25.2400	25.2400	25.2400

Table B-240 Option 2 IRI model validation hypothesis test results

Hypothesis test	*p*-value
Mean difference (paired *t*-test)	0.0002
Intercept	0.0001
Slope	0.0027

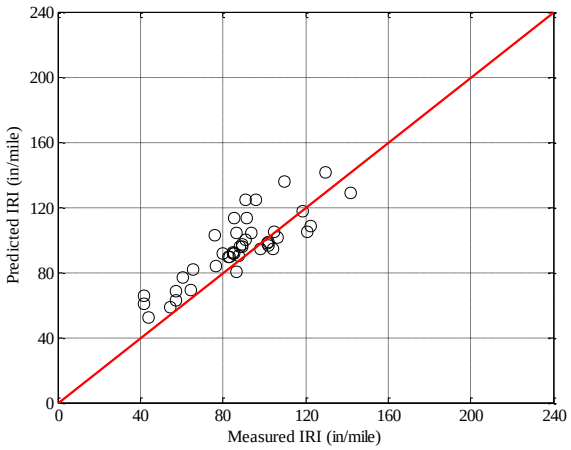

Figure B-514 IRI model validation – option 2

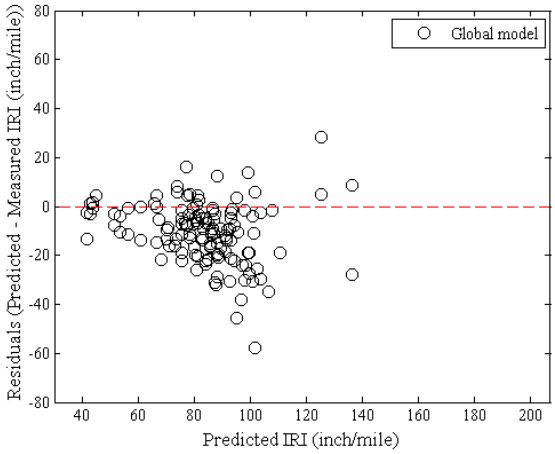

(a) Global model

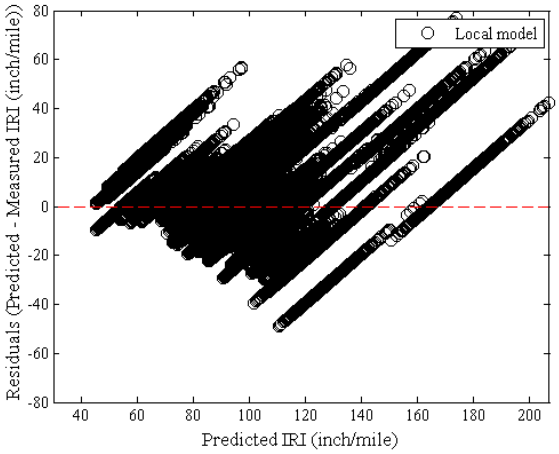

(a) Local model

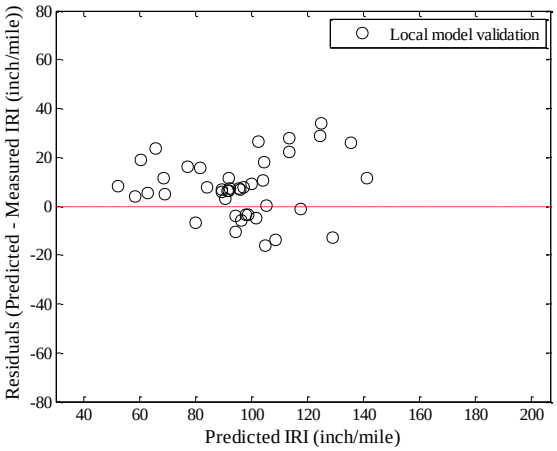

(a) Local model validation

Figure B-515 Option 2 residual plots

B.3.6.3 Option 3

Table B-241 Option 3 IRI model validation results

Parameter	Global Model Mean	Local Model Mean	Local Model Validation
SEE	17.4463	14.2258	16.9590
Bias	-10.3821	2.0902	-5.4326
C1	0.8203	2.2229	1.2656
C2	0.4417	1.6685	3.4776
C3	1.4920	1.4929	1.4929
C4	25.2400	25.2400	50.8002

Table B-242 Option 3 IRI model validation hypothesis test results

Hypothesis test	*p*-value
Mean difference (paired *t*-test)	0.2485
Intercept	0.0190
Slope	0.0285

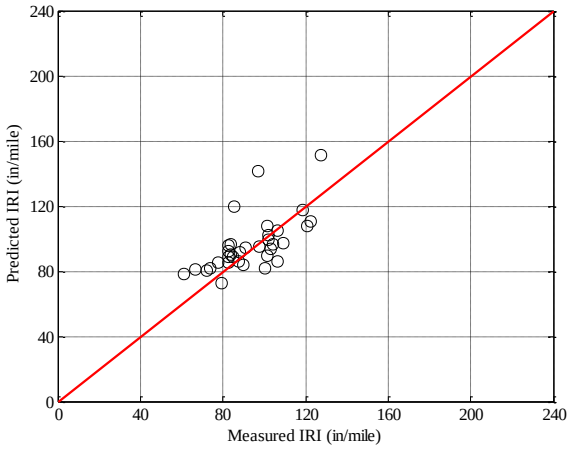

Figure B-516 IRI model validation – option 3

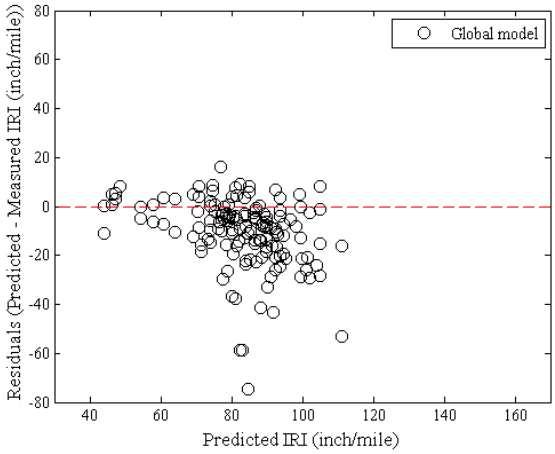

(a) Global model

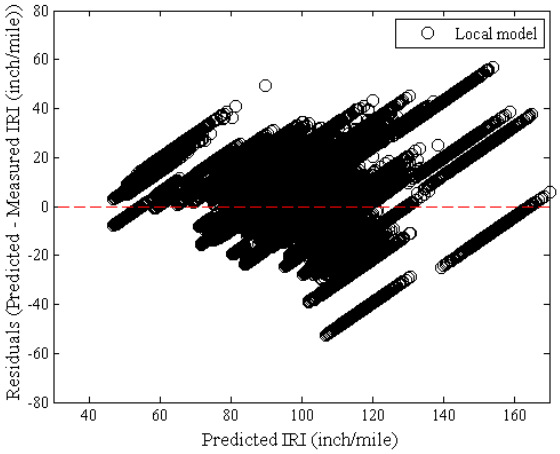

(a) Local model

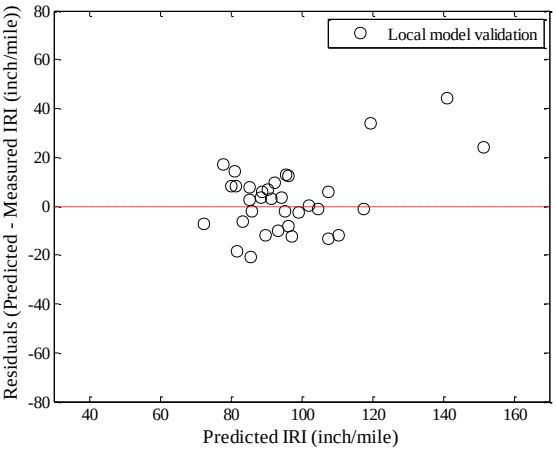

(a) Local model validation

Figure B-517 Option 3 residual plots

B.3.6.4 Option 4

Table B-243 Option 4 IRI model validation results

Parameter	Global Model Mean	Local Model Mean	Local Model Validation
SEE	10.5483	7.2943	11.2862
Bias	-7.1270	0.2066	1.4563
C1	0.8203	0.3637	2.1420
C2	0.4417	2.2600	2.6282
C3	1.4920	1.4929	1.4929
C4	25.2400	25.2400	5.7454

Table B-244 Option 4 IRI model validation hypothesis test results

Hypothesis test	*p*-value
Mean difference (paired *t*-test)	0.4266
Intercept	0.2262
Slope	0.2107

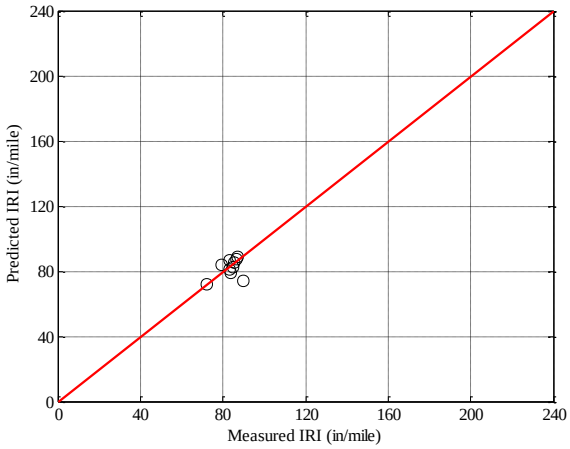

Figure B-518 IRI model validation – option 4

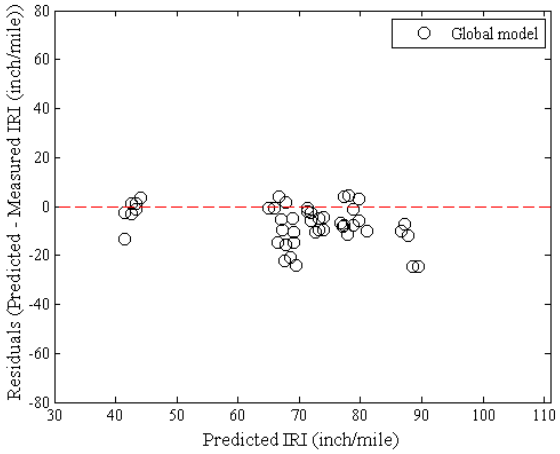

(a) Global model

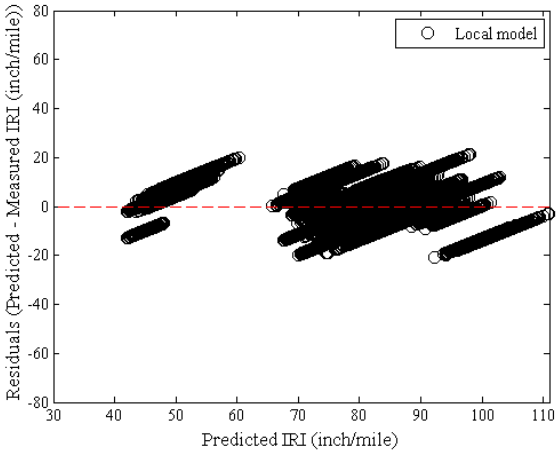

(a) Local model

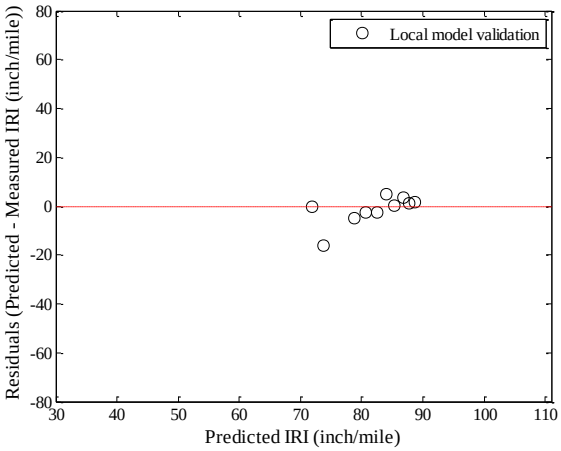

(a) Local model validation

Figure B-519 Option 4 residual plots

B.4 Use of local calibration coefficients

B.4.1 Flexible

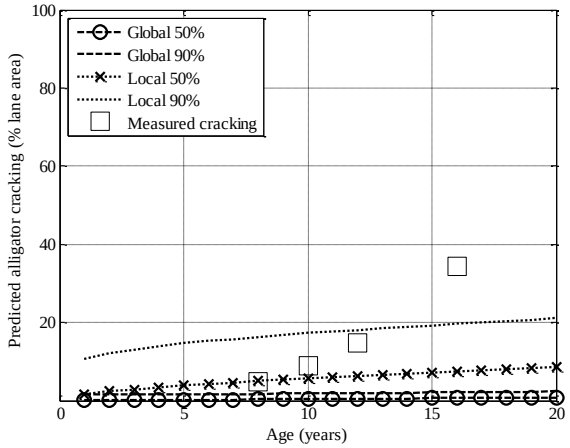

Figure B-520 Alligator cracking for Project 20046

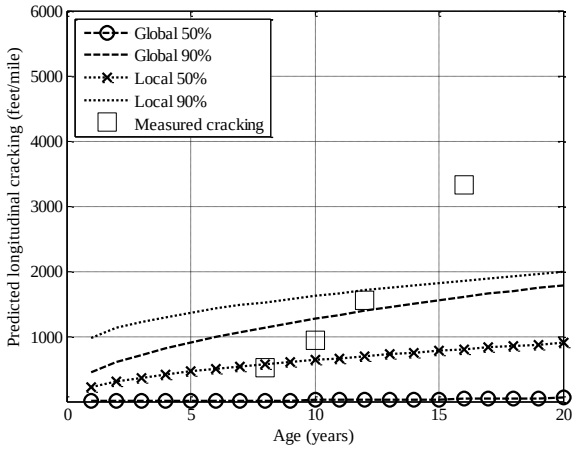

Figure B-521 Longitudinal cracking for Project 20046

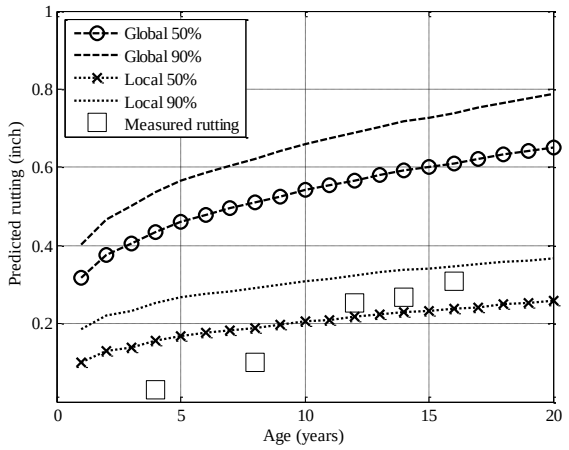

Figure B-522 Rutting for Project 20046

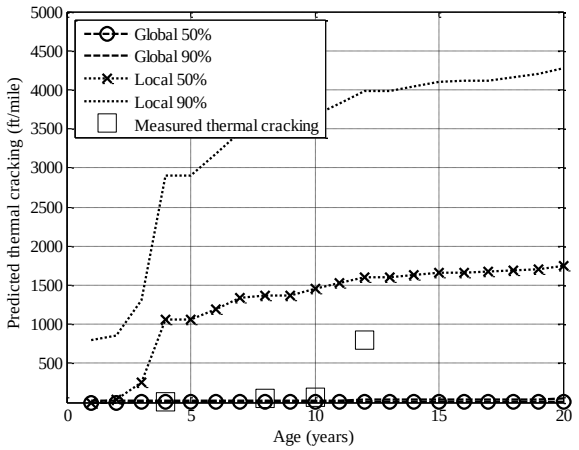

Figure B-523 Thermal cracking for Project 20046

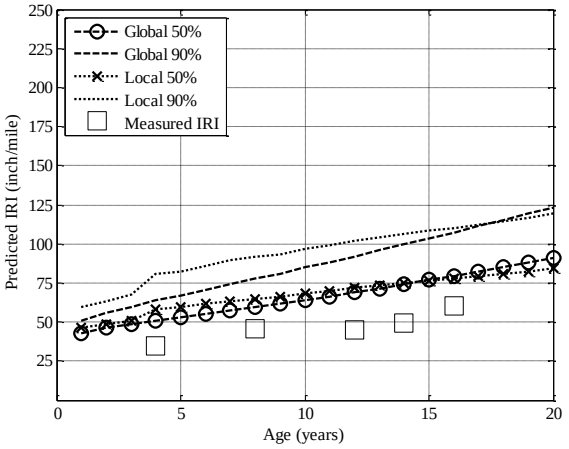

Figure B-524 IRI for Project 20046

B.4.2 Rigid

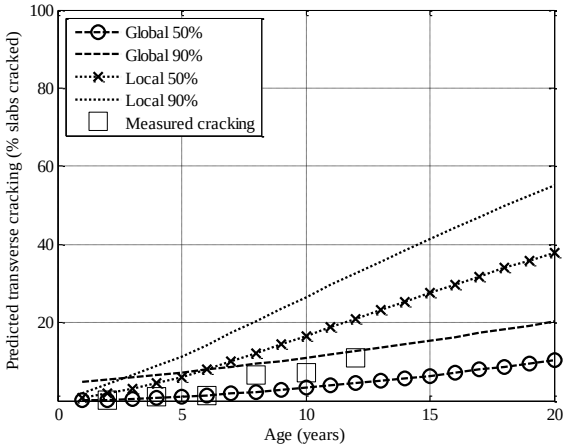

Figure B-525 Transverse cracking for Project 45855

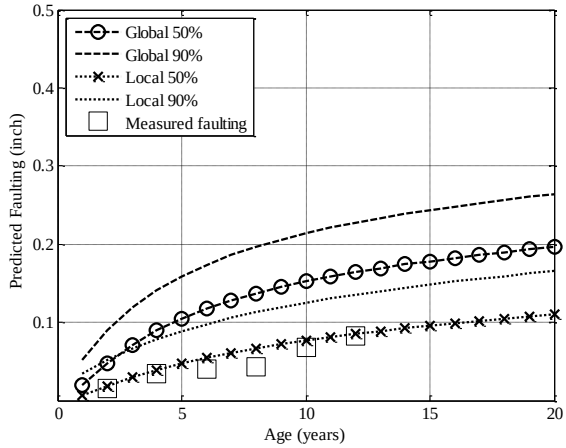

Figure B-526 Faulting for Project 45855

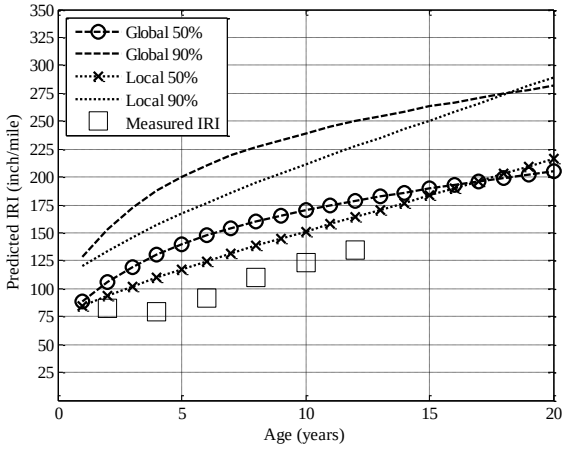

Figure B-527 IRI for Project 45855